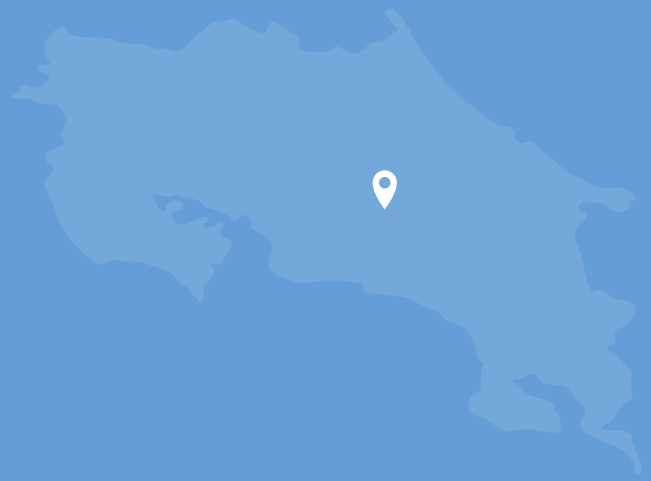


Proceedings of the III Ibero-American Conference on Smart Cities

(ICSC-CITIES2020)

*Hosted by the Costa Rica
Institute of Technology*
📅 *from November 9th to 11th*



Editors:

Carlos Meza

Luis Hernández-Callejo

Sergio Nesmachnow

Ângela Ferreira

Vicente Leite



CIUDADES INTELIGENTES TOTALMENTE INTEGRALES, EFICIENTES Y SOSTENIBLES

Con el apoyo de:



Elaborated by the organizing committee of the III Ibero-American Conference on Smart Cities (ICSC-CITIES 2020).

Cover design by Andrea Rojas

Disclaimer: The information in this book is true and complete to the best of the editor's knowledge. All recommendations are made without a guarantee on the part of the editors. The editors disclaim any liability in connection with the use of this information.

Editors: Carlos Meza, Luis Hernández-Callejo, Sergio Nesmachnow, Ângela Ferreira, Vicente Leite.

How to cite this book:

Meza, C., Hernandez-Callejo, L., Nesmachnow, S., Ferreira, A. & Leite, V. (Eds.). (2020). *Proceedings of the III Ibero-American Conference on Smart Cities*. Instituto Tecnológico de Costa Rica.

ISBN: 978-9930-541-79-1



This work is licensed under a Creative Commons Attribution 4.0 International License.

ABOUT THE EVENT

Smart Cities are the result of the increasingly urgent need to orient our lives towards sustainability. Infrastructure, innovation and technology for cities can be developed to minimize the environmental impact but still to foster life quality of citizens.

The Ibero-American Conference on Smart Cities (ICSC-CITIES) is a discussion forum that aims to create synergies among different research groups to promote the development of Smart Cities, and contribute to their knowledge and integration in different scenarios. The conference is held yearly since 2018 and is sponsored by the Ibero-American Program of Science and Technology for Development (CYTED). The two previous editions, i.e., 2018 and 2019, were celebrated in Soria, Spain.

The Third Ibero-American Conference on Smart Cities (ICSC-CITIES 2020) was hosted by the [Costa Rica Institute of Technology](#) from November 9th to 11th 2020 on-line. Fifty-nine technical presentations given by researchers from 12 different countries were presented during the ICSC-CITIES 2020. The aforementioned presentations were divided in four topics, i.e., Governance and Citizenship, Mobility and IoT, Infrastructures, Energy and the Environment and Energy Efficiency. Those contributions were selected from a pool of 99 submitted papers, yielding an acceptance rate of 60%.

ICSC-CITIES 2020 program also included the participation of government representatives from several American countries. More specifically, two panel discussion sessions were held. The first one was related to the role of national governments in the development of smart and sustainable cities. In this panel participated the First Lady of Costa Rica, Architect Claudia Dobles, the Minister of Science and Technology of Costa Rica, Dr. Paola Vega and the Vice minister of Digital Transformation of Colombia, Engineer German Rueda. A second discussion panel was held which was related to the role of local governments in the development of smart and sustainable cities. In this panel participated the former mayor of Quito, Ecuador, Mauricio Rodas, the first alderman of the City of Guatemala, Carlos Soberanis and the Director of Corporate Strategy of City of Vancouver, Canada, Bryan Buggley.

ICSC-CITIES 2020 was organized by the [Costa Rica Institute of Technology](#) with the collaboration of the [Colegio Federado de Ingenieros y Arquitectos](#), Costa Rica, the [University of Valladolid](#), Spain, [Universidad de la República](#), Uruguay and the [Polytechnic Institute of Bragança](#), Portugal.

COMMITTEE

The organizing committee of the Third Ibero-American Conference on Smart Cities was comprised by the following people:

- Dr. Luis Hernández-Callejo, Universidad de Valladolid, Spain, general co-chair and publication co-chair.
- Dr. Sergio Nesmachnow, Universidad de la República, Uruguay, general co-chair and publication co-chair.
- Dr. Carlos Meza, Instituto Tecnológico de Costa Rica, Costa Rica, local chair and program chair.
- Dr. Ângela Ferreira, Instituto Politécnico de Bragança, organizing committee
- Dr. Vicente Leite, Instituto Politécnico de Bragança, organizing committee
- Ing. Carlos Mauricio Segura, Instituto Tecnológico de Costa Rica, organizing committee
- Ing. José Alberto Díaz, Instituto Tecnológico de Costa Rica, organizing committee
- Ms. Grettel Moya, Instituto Tecnológico de Costa Rica, organizing committee

Professors, researches and experts that contributed as technical committee:

- ♦ Adolfo Ruelas Puente, Autonomous University of Baja California (Mexico)
- ♦ Adriana Correa, University of Valladolid (Spain)
- ♦ Albert Rego, Polytechnic University of Valencia (Spain)
- ♦ Alberto López Casillas, Diputación de Ávila (Spain)
- ♦ Alejandro Otero, Computational Simulation Center, COMICET (Argentina)
- ♦ Alejandro Paz Parra, Pontificia Universidad Javeriana Cali (Colombia)
- ♦ Ana Ruiz, San Jorge University (Spain)
- ♦ Andrei Tchernykh, CICESE Research Center (Mexico)
- ♦ Andrés Adolfo Navarro Newball, Pontificia Universidad Javeriana Cali (Colombia)
- ♦ Andres Felipe Fuentes Vasquez, Pontificia Universidad Javeriana Cali (Colombia)
- ♦ Ángel Zorita Lamadrid, University of Valladolid (Spain)
- ♦ Ângela Ferreira, Polytechnic Institute of Bragança (Portugal)
- ♦ Belén Carro, University of Valladolid (Spain)
- ♦ Carlos Meza, Costa Rica Institute of Technology (Costa Rica)
- ♦ Carlos Grande, Central American University "José Simeón Cañas" (El Salvador)
- ♦ Carmen Vasquez, UNEXPO University (Venezuela)
- ♦ Cristina Sáez Blázquez, University of Salamanca (Spain)
- ♦ Diego Arcos-Aviles, Armed Forces University - ESPE (Ecuador)
- ♦ Diego Loaiza, University of Santiago de Cali (Colombia)
- ♦ Diego Vilches Antao, National University of La Plata (Argentina)
- ♦ Diego Alberto Godoy, Gastón Dachary University (Argentina)
- ♦ Diego Gabriel Rossit, National University of South (Argentina)
- ♦ Edgardo Aníbal Belloni, Gastón Dachary University (Argentina)
- ♦ Eduardo Omar Sosa, National University of Misiones (Argentina)
- ♦ Emmanuel Luján, University of Buenos Aires (Argentina)
- ♦ Esteban Mocskos, University of Buenos Aires (Argentina)
- ♦ Fabian Castillo Peña, Free University of Cali (Colombia)
- ♦ Fernando Velez Varela, University of Santiago de Cali (Colombia)
- ♦ Francisco Moya Chaves, Francisco José de Caldas District University (Colombia)
- ♦ Gregorio López, Polytechnic University of Madrid (Spain)
- ♦ Hortensia Amaris, University Carlos III of Madrid (Spain)
- ♦ Irene Lebrusán, Harvard University (United States)
- ♦ Itziar Angulo, University of the Basque Country (Spain)
- ♦ Jaime Lloret, Polytechnic University of Valencia (Spain)
- ♦ Javier Prieto, University of Salamanca (Spain)
- ♦ Javier Rocher, Polytechnic University of Valencia (Spain)
- ♦ Jesús Vegas, University of Valladolid (Spain)
- ♦ Jorge Mírez, National University of Engineering (Peru)
- ♦ Jose Aguerre, Engineering Faculty, Udelar (Uruguay)
- ♦ José-Ramón Aira, University of Valladolid (Spain)
- ♦ Juan R. Coca, University of Valladolid (Spain)
- ♦ Juan Mauricio, Federal University of Paraíba (Brazil)
- ♦ Juan Espinoza, University of Cuenca (Ecuador)
- ♦ Lilian Johanna Obregón, University of Valladolid (Spain)
- ♦ Luis Hernández, University of Valladolid (Spain)
- ♦ Luis Garcia Santander, University of Concepción (Chile)
- ♦ Luis Marrone, National University of La Plata (Argentina)
- ♦ Luisena Fernandez, University of Zulia (Venezuela)
- ♦ Luiz Angelo Steffemel, University of Reims Champagne-Ardenne (France)
- ♦ Manuel Gonzalez, University of Valladolid (Spain)
- ♦ Manuel Alvarez-Campana, Polytechnic University of Madrid (Spain)
- ♦ Monica Alonso, University Carlos III of Madrid (Spain)
- ♦ Noelia Uribe-Pérez, Tecnalia Research & Innovation (Spain)
- ♦ Noelia Soledad Pinto, Technological College, Resistencia Regional Faculty (Argentina)
- ♦ Oscar Izquierdo, CEDER-CIEMAT (Spain)
- ♦ Oscar Duque-Perez, University of Valladolid (Spain)
- ♦ Pablo Monzon, Engineering Faculty, Udelar (Uruguay)
- ♦ Paul Ayala, Armed Forces University - ESPE (Ecuador)
- ♦ Paulo Gondim, University of Brasília (Brazil)
- ♦ Ponciano Jorge Escamilla-Ambrosio, Computing Research Center - IPN (Mexico)
- ♦ Rafael Asorey Cacheda, Polytechnic University of Cartagena (Spain)
- ♦ Renzo Massobrio, University of the Republic (Uruguay)
- ♦ Santiago Iturriaga, Engineering Faculty, Udelar (Uruguay)
- ♦ Santiago Hernan Bareiro, Gastón Dachary University (Argentina)
- ♦ Sara Gallardo-Saavedra, University of Valladolid (Spain)
- ♦ Sergio Nesmachnow, University of the Republic (Uruguay)
- ♦ Susana del Pozo, University of Salamanca (Spain)
- ♦ Vanessa Guimarães, CEFET/RJ (Brazil)
- ♦ Vicente Leite, Polytechnic Institute of Bragança (Portugal)
- ♦ Vicente Canals, University of the Balearic Islands (Spain)
- ♦ Yuri Molina, Federal University of Paraíba (Brazil)

PROGRAM

ICSC-CITIES 2020 took place simultaneously in more than 12 countries throughout Latin America, Spain and Portugal. To facilitate the attendance of students, researchers and professionals from these countries, the event was schedule in such a way that it was in a suitable period of the day for everyone. The conference program is shown below at the local time of the hosting institution (UTC-6).

Monday, November 9th

Hour (UTC-6)	Activity	Speakers	
8:00 a 8:30	Inauguration	Carlos Meza Benavides	Local Organizer
		Alejandra Morice Sandoval	President Federal Collegue of Engineers and Arquitects of Costa Rica
		Luis Hernández Callejo	Coordinator CITIES Cytcd
		Luis Paulino Méndez Badilla	President, Costa Rica Institute of Technology
8:30 a 10:00	Panel discussion: Perspective of national governments in the development of smart cities.	Introductory words from the First Lady of Costa Rica Claudia Dobles Camargo	
		Dra. Paola Vega, Minister of Science and Technology	Moderator: Dr. Luis Hernández Callejo
	Ing. Germán Camilo Rueda Jiménez, Vice minister of Digital Transformation, Colombia		
10:00 a 12:00	Public transportation and accessibility to education centers in Maldonado, Uruguay	R. Massobrio, S. Nesmachnow, E. Gómez, F. Sosa and S.Hipogrosso	S1. Governance and Citizenship Moderator: Dr. Carlos Meza Benavides
	Reimagining the Book ... Again! A New Framework for Smart Books Using Digital Twins Technology	H. Kolivand, E. C. Prakash, M.C. López Leal, D. Hernández Cárdenas, A. A. Navarro-Newball	
	Experimental Algorithmic Citizenship in the Policy and Design Sandbox as an Alternative to Ethical Frameworks and Governance-by-Design Interventions	D. Reshef Kera	
	Prototype system for remotely monitoring and managing second-hand clothing collection containers	I. Martin Martín, G. López López, S. González Jiménez, B. Corrieu.	
	Smart Fisheries, a key player in ocean sustainability and fair fish trade.	J. Carvajal, H. Sánchez, J.C. Martí	
	Smart city tools to evaluate healthy environments for the elderly	I. Lebrusán, J. Toutouh	
	Crowdsourcing and IoT Towards More Resilient Flooding Prone Cities	J. Ponciano, M. Escamilla-Ambrosio, I. Pulido-Navarro, V. Hernández-Gutiérrez, A. Rodríguez-Mota, M.A. Moreno-Ibarra.	
	Carbon regulation policies in transport: a review	V. de Almeida Guimarães, R. P. Correia Lima, M. de Azevedo-Ferreira, P.H. González.	

Monday, November 9th

Time (UTC-6)	Activity	Speakers	Session
12:00 a 14:00	A Prototype of Classroom Energetically Efficient	D. A. Godoy, S. H. Bareiro, F.E. Favret, J.P. Blariza, G. Colotti.	S2. Energy Efficiency and Sustainability Moderator: Dr. Vicente Leite
	Implementation of home energy management criteria for high school students in the city of Guayaquil-Ecuador	E. Delgado-Plaza, J. Peralta-Jaramillo, I. SosaTinoco, J. Guevara Saenz de Viteri, A.P. Ferreira.	
	REMOURBAN: Evaluation results after the implementation of actions for improving the energy efficiency in a district in Valladolid (Spain)	C. de Torre, J. Antolín, M.A. García-Fuentes, J Gómez-Tribeño, J.J Cubillo, M.L. Mirantes, I.- Tomé.	
	Analysis of residential electricity consumption by areas in Uruguay	J. Chavat, S. Nesmanchnow	
	Low-cost and real-time measurement system for electrical energy measuring of a smart microgrid	O. Izquierdo-Monge, P. Peña Carro, M. Martín Martínez, L. Hernández Callejo, O. Duque Pérez, A. Zorita Lamdarid	
	How the construction parameters influence the thermal loads of a building without internal gains	J.A. Díaz Angulo, S. Soutullo, E. Giancola, J.A. Ferrer Tevar.	
	A methodology for the conversion of a network section with generation sources, storage and loads into an electrical microgrid based on Raspberry Pi and Home Assistant	O. Izquierdo-Monge, L. Hernández Callejo, P. Peña Carro, O. Duque Pérez, A. Zorita Lamadrid, R. Villafafila Robles.	
	A data acquisition pipeline for home energy management systems	I. Munné-Collado, A. Bové-Salat, D. Montensinos-Miracle, R. Villafáfila-Robles	
	A novel algorithm for high compression rates focalized on electrical power quality signals	M. Ruiz, M. Jaramillo, S. Simani	

Tuesday, November 10th

Time (UTC-6)	Activity	Speakers	Session
08:00 a 10:00	Demand response control in electric waterheaters: evaluation of impact on thermal comfort	R. Porteiro, J. Chavat, S. Nesmanchnow, L.Hernández Callejo	S3. Energy Efficiency and Sustainability Moderador: Dra. Ángela Ferreira
	Computational intelligence for characterization and disaggregation of residential electricity consumption	M. Esteban, S. Nesmanchnow, M. Mujica, I. Fiori	
	Study and improvement of the efficiency of a hydraulic pumping system associated with a Pelton hydraulic turbine in a smart microgrid	O. Izquierdo-Monge, P. Peña-Carro, C. Barrera del Almo, L. Hernández-Callejo, A. Zorita-Lamadrid, O. Duque-Perez	
	Photovoltaic cell defect classifier: a model comparison	A. Pérez-Romero, L. Hernández-Callejo, S. Gallardo-Saavedra, V. Alonso Gpomez, M.C. Alonso García, H.F. Mateo Romero	
08:00 a 10:00	I-V tracers for PV panels, topologies and challenges: A Review	J. I. Morales-Aragonés, L. Hernández-Callejo, O. Duque-Pérez, A. Zorita Lamadrid.	S3. Energy Efficiency and Sustainability Moderator: Dra. Ángela Ferreira
	Embedded System for Hot Spots Characterization of Solar Panels	J. Carvajal-Godínez, J. Fonseca Cruz, D. Picado, F. Soto, C.E. Soto	
	The effect of clearance height, albedo, tilt and azimuth angle in bifacial PV energy estimation using different algorithms	H. Sánchez, C. Meza, S. Dittmann	
	Experimental comparison of visual inspection and infrared thermography for the detection of soiling and partial shading in photovoltaic arrays	L. Cardinale-Villalobos, C. Meza, L.D. Murillo	
10:00 a 12:00	Panel discussion: Perspective of local governments in the development of smart cities	Carlos Soberanis, first alderman of the City of Guatemala, Gutaemala	Moderator: Dr. Ricardo Sancho
		Mauricio Rodas, Former Major of Quito, Ecuador	
		Bryan Buggley, Director of Corporate Strategy, City of Vancouver, Canada	

Tuesday, November 10th

Time (UTC-6)	Activity	Speakers	Session
12:00 a 14:00	A Way to a Sustainable Universidad de Concepcion: Smart Parking	C. Ramírez-Rendón, I. Sanchez-Rangel, L. García-Santander	S4. Mobility and IoT
	Benefits of the integration of photovoltaic solar energy and electric mobility	M. Dávila-Sacoto, L. González, J. Espinoza, L. Hernández-Callejo	
	The role of the electrical vehicle in sustainable supply chains: a review	F.H. Amaro Verneque, P.H. González, M. Alonso Martinez, V. Almeida Guimaraes.	
	A comparative and exploratory case study of the concept of SDI applied to sustainable mobility. Exploring trends and divergences of SDIs in Ibero-American cities	C. Grande, T. Batista, C. Vázquez, L. Suarez, L. Navas, R. Ramírez-Pisco, R. Pérez	
	Computational intelligence for analysis of traffic data	H. Winter, J. Serra, S. Nesmachnow, A. Tchernykh, V. Shepelev	
	Exact and metaheuristic approach for bus timetable synchronization to maximize transfers	S. Nesmachnow, J. Muraña, C. Risso.	
	Plataforma de Movilidad Compartida Metropolitana (PMCM). Sistema tipo MaaS. Córdoba, Argentina. Ciencia y tecnología al servicio de los vecinos.	L. A. Giménez, C. J. Paz	
	Development of IoT Services Applied to a Photovoltaic Generation System Integrated with Vegetation	M. Camargo-Vila, G. Osma-Pinto, H. Ortega-Boada	
	Mapping the environmental criteria for facility location problems	V. de Almeida Guimarães, P.H. González, L. Hernández-Callejo, G. Mattos Ribeiro	

Wednesday, November 11th

Time (UTC-6)	Activity	Speaker	Session
08:00 a 10:00	Human-Computer Interfaces for Smart Bus Stops as Interconnected Public Spaces (IP-Spaces) elements in Smart Cities	D. Gachet, V. M. Padrón Nápoles, J. L. E. Penelas, F. Martín de Pablos, O. García Pérez, R. Muñoz Gil, J. García González, S. Escorial Santa Marina.	S5. Mobility and IoT
	Analysis of alternatives for the acceleration of a Hyperloop system	M. Lafoz, L. García-Tabarés, J. Torres, D. Orient, D. Fons and G. Navarro.	
	Smart Mobility in Cities: GIS analysis of solar PV potential for lighting in bus shelters in the city of Ávila	M. Sánchez-Aparicio, S. Lagüela, J.A. Martín-Jimenez, S. del Pozo, E. González-González and P. de Andrés Anaya.	
	Impact of the covid-19 pandemic on traffic congestion in Latin American cities: An updated five-month study	J. Ortego Osa, R. Andara, L.M. Navas, C.L. Vasquez and R. Ramirez.	
	Conditional Generative Adversarial Networks to Model Urban Outdoor Air Pollution	J. Toutouh	
	Towards a sustainable mobility plan for Engineering Faculty, Universidad de la República, Uruguay	S. Hipogrosso, S. Nesmachnow.	
	Performance assessment of the transport sustainability in the European Union	S. B. Gruetzmacher, C. B. Vaz, A. P. Ferreira.	
	Designing IoT services in smart cities through game-based knowledge acquisition	I. García-Magariño, J. J. Gómez-Sanz.	

Wednesday, November 11th

Time (UTC-6)	Activity	Speaker	Session
10:00 a 12:00	Integration of small wind turbines in a smart microgrid in a peri-urban environment	O. Izquierdo-Monge, L. Hernández-Callejo, P. Peña-Carro, C. Barrera del Amo, S. Soria Franco, G. Martín Jiménez.	S6. Infrastructure, environment and energy Moderator: Dr. Sergio Nesmanchnow
	Modeling of a Controlled Rectifier with Adaptive Control System for Vertical Axis Micro Wind Turbines	M. Aybar, M. Baldera Arvelo, L. León Viltre, D. Mariano Hernandez, M. Baldera Echavarria.	
	Detection of Wind System Faults using Analyze Current Rotor of Aerogenerator	B. Abdelkarim, L. Hernández-Callejo, B. Silmane	
	Study of a photovoltaic plant for the reduction of diesel consumption: case of Dominican Republic	M. E. Aybar Mejía, D. Mariano-Hernández, E. A. Jiménez Matos, A. I. Roa Arias, E. A. Geara Jimenez, G. Frias Lovera, E. Bido Cuello	
	Innovative Smart Microgrid Integrating Pico-hydro Systems: The Silk House Museum	V. Leite	
	Economic optimization of photovoltaic generation system with hydrogen storage	E. Alcover, R. Pujol-Nadal, V. Martínez-Moll, J. L. Rosselló and V. Canals.	
	INBAL Solar Photovoltaic Electricity Generation and Consumption Reduction Programme	J Escamilla-Ambrosio, M. Morales-Olea, O. Espinosa-Sosa, M. A. Ramírez-Salinas, A. Rodríguez-Mota, L. Hernández-Callejo	
	Optimization of the capacity of photovoltaic arrays and modification of the geometry of a turbine-generator system to minimize dependence on the electricity grid	R. López Meraz, L. Hernández Callejo, L.O. Jamed-Boza, J.A. Del Ángel-Ramos, J.J. Marín-Hernández, V. Alonso Gómez	
12:00 a 14:00	Preliminary evaluation of different underground hydrogen storage systems in Spain	C. Sáez Blázquez, I. Martín Nieto, M. Ángel Maté-González, A. Farfán Martín, D. González-Aguilera.	S7. Infrastructure, environment and energy Moderator: Dr. Carlos Meza
	Errors in the design and execution of the well field of low enthalpy geothermal systems.	C. Sáez Blázquez, I. Martín Nieto, M. Ángel Maté-González, A. Farfán Martín, D. González-Aguilera.	
	The Profile of Studies on Renewable Energy in Sustainable Supply Chain	E. Marques, M. de Azevedo-Ferreira, L. Hernández-Callejo, R. Boloy, V. de Almeida Guimarães.	
	Technological architecture for synchrophasor measurement in power systems: an application for Colombia	J. Molina-Castro, M. Alvarez-Alvarez, L. Buitrago-Arroyave, J. Zapata-Uribe.	
	New opportunities of Broadband Power Line Communications for the improvement of the Smart Grids	N. Uribe-Perez, I. Fernandez, D. De La Vega, A. Llano, I. Arechalde, A. Galarreta.	
	Solid Oxide Fuel Cell Electric Vehicle: Cost Reduction Based on Savings in Fixed Carbon by Sugarcane	D. Rodrigues de Moraes, V. de Almeida Guimarães, L. Hernández-Callejo, B. de Noronha Gonçalves, R. Arismel Mancebo Boloy.	
	Battery Energy Storage System Dimensioning for Reducing the Fixed Term of the Electricity Access Rate in Industrial Consumptions	J. Nájera, M. Blanco, G. Navarro, M. Santos.	
	Sizing of Autonomous Microgrid Considering Life Cycle Emissions	I. Jiménez Vargas, G. Osma Pinto and Juan M. Rey.	
	Methane emissions and energy density of reservoirs of hydroelectric plants in Venezuela	R. Pérez, C. Vásquez, L. Suárez, R. Vásquez, William Osal, R. Ramírez	

TABLE OF CONTENTS

Public transportation and accessibility to education centers in Maldonado, Uruguay	1
Reimagining the Book ... Again! A New Framework for Smart Books Using Digital Twins Technology	16
Experimental Algorithmic Citizenship in the Policy and Design Sandbox as an Alternative to Ethical Frameworks and Governance-by-Design Interventions	29
Prototype system for remotely monitoring and managing second-hand clothing collection containers	44
Smart Fisheries, a key player in ocean sustainability and fair fish trade.	57
Smart city tools to evaluate healthy environments for the elderly	68
Crowdsourcing and IoT Towards More Resilient Flooding Prone Cities	83
Carbon regulation policies in transport: a review	98
A Prototype of Classroom Energetically Efficient	113
REMOURBAN: Evaluation results after the implementation of actions for improving the energy efficiency in a district in Valladolid (Spain)	126
Analysis of residential electricity consumption by areas in Uruguay	137
Low-cost and real-time measurement system for electrical energy measuring of a smart microgrid	152
How the construction parameters influence the thermal loads of a building without internal gains	166
A methodology for the conversion of a network section with generation sources, storage and loads into an electrical microgrid based on Raspberry Pi and Home Assistant	181
A data acquisition pipeline for home energy management systems	195
Demand response control in electric waterheaters: evaluation of impact on thermal comfort	210
Computational intelligence for characterization and disaggregation of residential electricity consumption	225
Study and improvement of the efficiency of a hydraulic pumping system associated with a Pelton hydraulic turbine in a smart microgrid	240
Photovoltaic cell defect classifier: a model comparison	257
I-V tracers for PV panels, topologies and challenges: A Review	274
Embedded System for Hot Spots Characterization of Solar Panels	300
The effect of clearance height, albedo, tilt and azimuth angle in bifacial PV energy estimation using different algorithms	315
Experimental comparison of visual inspection and infrared thermography for the detection of soiling and partial shading in photovoltaic arrays	332
A Way to a Sustainable Universidad de Concepcion: Smart Parking	353
Benefits of the integration of photovoltaic solar energy and electric mobility	364
The role of the electrical vehicle in sustainable supply chains: a review	379
A comparative and exploratory case study of the concept of SDI applied to sustainable mobility. Exploring trends and divergences of SDIs in Ibero-American cities	392
Computational intelligence for analysis of traffic data	406
Exact and metaheuristic approach for bus timetable synchronization to maximize transfers	421

Plataforma de Movilidad Compartida Metropolitana (PMCM). Sistema tipo MaaS. Córdoba, Argentina. Ciencia y tecnología al servicio de los vecinos.	436
Development of IoT Services Applied to a Photovoltaic Generation System Integrated with Vegetation	448
Mapping the environmental criteria for facility location problems	463
Human-Computer Interfaces for Smart Bus Stops as Interconnected Public Spaces (IP-Spaces) elements in Smart Cities	478
Analysis of alternatives for the acceleration of a Hyperloop system	493
Smart Mobility in Cities: GIS analysis of solar PV potential for lighting in bus shelters in the city of Ávila	506
Impact of the covid-19 pandemic on traffic congestion in Latin American cities: An updated five-month study	519
Conditional Generative Adversarial Networks to Model Urban Outdoor Air Pollution	533
Designing IoT services in smart cities through game-based knowledge acquisition	548
Towards a sustainable mobility plan for Engineering Faculty, Universidad de la República, Uruguay	562
Performance assessment of the transport sustainability in the European Union	573
Integration of small wind turbines in a smart microgrid in a peri-urban environment	587
Modeling of a Controlled Rectifier with Adaptive Control System for Vertical Axis Micro Wind Turbines	603
Detection of Wind System Faults using Analyze Current Rotor of Aerogenerator	618
Study of a photovoltaic plant for the reduction of diesel consumption: case of Dominican Republic	630
Innovative Smart Microgrid Integrating Pico-hydro Systems: The Silk House Museum	641
Economic optimization of photovoltaic generation system with hydrogen storage	666
INBAL Solar Photovoltaic Electricity Generation and Consumption Reduction Programme	678
Optimization of the capacity of photovoltaic arrays and modification of the geometry of a turbine-generator system to minimize dependence on the electricity grid	690
Preliminary evaluation of different underground hydrogen storage systems in Spain	701
Errors in the design and execution of the well field of low enthalpy geothermal systems.	716
Methane emissions and energy density of reservoirs of hydroelectric plants in Venezuela	728
Technological architecture for synchrophasor measurement in power systems: an application for Colombia	740
New opportunities of Broadband Power Line Communications for the improvement of the Smart Grids	754
Solid Oxide Fuel Cell Electric Vehicle: Cost Reduction Based on Savings in Fixed Carbon by Sugarcane	774
Battery Energy Storage System Dimensioning for Reducing the Fixed Term of the Electricity Access Rate in Industrial Consumptions	790
Sizing of Autonomous Microgrid Considering Life Cycle Emissions	808
The Profile of Studies on Renewable Energy in Sustainable Supply Chain	823

Public transportation and accessibility to education centers in Maldonado, Uruguay

Renzo Massobrio, Sergio Nesmachnow, Emiliano Gómez,
Facundo Sosa, and Silvina Hipogrosso

Universidad de la República, Uruguay

Abstract. This article presents a study of public transportation and accessibility to public services in Maldonado, Uruguay. Accessibility is a crucial concept in nowadays smart cities, to guarantee a proper mobility, citizen participation in social, economic, and cultural activities, and an overall good quality of life. Several data sources are studied and processed to characterize the accessibility provided by the public transportation system of Maldonado to public services, specifically to education centers. A matrix of travel times by public transportation is computed and used to define a flexible accessibility indicator to reach destinations of interest. Finally, an interactive visualization tool is developed to graphically display the computed information. The accessibility indicator constitutes an input for the decision-making of the transportation authorities of the studied area, as well as it allows identifying potential inequity situations.

Keywords: smart cities, mobility, public transportation, accessibility, public services

1 Introduction

The characterization of urban accessibility is an important tool to determine the quality of transportation systems and their impact on the daily activities of citizens [5]. Several recent researches have studied different aspects of accessibility, e.g., regarding urban public facility spaces [13], urban planning [3], neighborhood retail [15], and other relevant issues.

Evaluating accessibility is a challenging task, even considering a simple definition of accessibility, related to the capability of reaching certain relevant destinations in the city. The challenges are consequence of the plethora of theoretical concepts to be considered (including land utilization, universal access, transportation modes, etc.), and also the lack of sound methodologies for empirical evaluation. Thus, accessibility is often considered as a poorly understood concept, which is not correctly evaluated, and rarely taken into account for elaborating policies for urban development, transportation design and operation, infrastructure investments, and other relevant actions for improving quality of life. Overall, knowledge about accessibility is very useful for assisting policy-makers and planners to evaluate different approaches to develop transportation with a special focus on inequities and phenomena with high social impact.

2 R. Massobrio, S. Nesmachnow, E. Gómez, F Sosa, S. Hipogrosso

This article presents a characterization of public transportation and accessibility to education centers in the metropolitan area of Maldonado, Uruguay. The case study is an important urban conglomeration in the Southeast of Uruguay, with more than 135.000 inhabitants. The proposed research focuses on public transportation, as it is understood to be the most efficient, sustainable, and socially fair transportation mode [4]. The distances and total travel times between different zones by using public transportation are studied via a data analysis approach [17] to identify areas with poor mobility provision that imply high travel times, and therefore impose restrictions on territorial accessibility.

In order to quantify the provision of the transportation system in the Maldonado metropolitan area, a matrix of travel times between different areas of the city is computed. Trips in different modes (walking, with a direct bus line, and trips involving transfers) are considered. Then, geolocated data about public services is used to compute the accessibility offered by the public transportation system. As a case study, the accessibility to education centers is computed, as it is a relevant public service for the Municipality of Maldonado. By incorporating the scope of different mobility options, the proposed methodology advances on a factor for the definition of indicators of inequity in intra-urban accessibility and their subsequent use for support and decision-making on urban planning.

The main contributions of the reported research include: i) a matrix of travel times on public transportation in the Maldonado metropolitan area, at the census segment level; ii) an accessibility indicator by public transportation to education centers located in the studied area; and iii) a web visualization tool that allows graphically displaying the accessibility indicator. The reported results are useful for transit and transportation authorities of the Municipality of Maldonado, since they constitute an important input when defining public policies, designing new transportation lines, or redesigning current ones in order to serve identified areas as of poor accessibility.

The article is organized as follows. Section 2 reviews relevant concepts and related works about accessibility and related initiatives in Uruguay. The proposed data analysis approach and the case study are described in Section 3. The implementation details are presented in Section 4, including the calculation of the matrix of travel times for public transportation and the accessibility indicator to education centers. The results of the analysis are shown and discussed in Section 5 along with a brief description of the web visualization tool. Finally, Section 6 presents the main conclusions and lines for future work.

2 Accessibility and related works

Citizen participation in social, economic, and cultural activities requires people to travel, sometimes long distances and involving long periods of time [8]. The ability of individuals to overcome limitations imposed by distances and other mobility-related difficulties is critical when actively participating in city life [2]. This measure of the ability of transportation systems to allow individuals to overcome distances is known under the concept of accessibility.

Public transportation and education centers in Maldonado, Uruguay 3

The term accessibility has been extensively studied in the literature, with the first definitions emerging from the area of geographical studies more than 60 years ago [6]. Although the term is widely disseminated, there are multiple (and complementary) definitions, which vary according to the area of study and the point of view from which its quantification is proposed. Generally speaking, accessibility can be defined as a measure of the effort (or ease) of overcoming spatial separation. Specifically, accessibility seeks to measure the spatial distribution of opportunities (e.g., jobs, study sites, hospitals) adjusted for people's ability or desire to overcome separation (e.g., distance, time, cost) to such opportunities. Within the classification established by Ingram [14], this project focuses on comprehensive accessibility, which contemplates the degree of interconnection of a point or area with all the others on the same surface.

Several indicators have been proposed to measure the separation between points/areas when evaluating accessibility, among them, travel time is one of the most intuitive, as it is strongly related to the perception of users of a transportation system. Lei and Church [16] presented a review on the use of travel time when quantifying the accessibility offered by public transportation systems. The authors show that various works in the literature focus on the physical characteristics offered by transportation systems (e.g., distance to the bus stop) rather than focusing on travel time. Furthermore, within the works that do focus on travel time, there are a number of assumptions that significantly affect the final measure, including considering fixed waiting and transfer times or a constant speed for vehicles. Salonen and Toivone [19] presented a comparison of different techniques for estimating travel times, both for private and public transport. The authors evaluated different travel time estimation models on a case study in the capital region of Finland. The results achieved show that those models that incorporate a greater amount of information regarding the transportation system are able to estimate travel times with greater precision, although the differences between models were less in the downtown areas.

In Uruguay, some studies have addressed the issue of accessibility, particularly using public transportation. Hansz [7] studied the disparity between public transportation supply and transportation needs in Montevideo. The author defined a public transportation provision index that combines the frequency of buses and the number of stops in a given area. The provision offered by the Montevideo public transportation system, measured according to this index, is strongly biased towards the city center. Hernández [9] studied inequities in access to employment and educational opportunities between different social classes as a consequence of the offer of public transport. This work used the travel time to compute accessibility, which was obtained through How to Go, a web application offered by the Municipality of Montevideo to estimate travel times by public transport. The study showed that there is an unequal distribution of mobility opportunities, particularly for access to job opportunities and access to higher level education. Later, Hernández et al. [10] built a matrix of travel times using theoretical timetables of buses in Montevideo, which was used as input to generate an index of accessibility to job opportunities in the city.

4 R. Massobrio, S. Nesmachnow, E. Gómez, F Sosa, S. Hipogrosso

Other research efforts developed within our research group include the socio-economic analysis of the transportation system in Montevideo using big data and distributed computing [18], the analysis of sustainable transportation initiatives in Montevideo [12] evaluating the accessibility index proposed by the World Business Council for Sustainable Development [20], and the empirical study performed in Parque Rodó neighborhood using face-to-face surveys [11].

3 Case study and data analysis approach

This section describes the studied area and the methodology applied for data analysis to characterize accessibility.

3.1 Maldonado metropolitan area

The metropolitan area of Maldonado includes the conurbation of the cities of Maldonado and Punta del Este, which progressively joined, including transportation routes. Maldonado is the administrative capital of the department and Punta del Este is considered the tourist capital at national level. The city of San Carlos is considered as part of this conurbation, although Maldonado and San Carlos are separated by a suburban space. These three cities are the arteries of an urban network that extends even west to Portezuelo and east to José Ignacio. The suburban area has specific mobility needs and the demand for public transportation, and currently has problems with traffic congestion and accessibility to important points. In addition, the cities of Piriápolis and Pan de Azúcar are less than 30 km from Maldonado and public transportation lines connect them frequently. More than 150.000 people live in the studied area, while about 20.000 live in Piriápolis and Pan de Azúcar.



Fig. 1: Metropolitan area of Maldonado

3.2 Data analysis approach

The Municipality of Maldonado granted access to a set of public transportation data, including lines, stops, and timetables of the different routes. Each dataset has specific features, which are described in the following paragraphs.

Bus lines and stops. This dataset includes the layout of routes lines and the location of the bus stops of the public transportation system. From a geographical point of view, the main difficulty with these data lies in the fact that the dataset of lines and stops are independent. Fig. 2 shows the set of stops and lines of the public transportation system, according to the provided data.

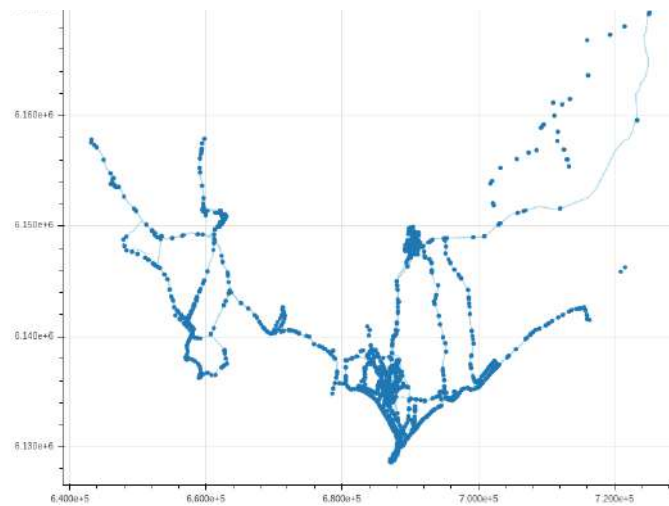


Fig. 2: Bus lines and stops of the public transportation system in Maldonado

Certain problems and particularities of the studied datasets pose challenges for building a matrix of travel times for public transportation to compute the accessibility indicator. Three main problems were identified: stops located in places without defined bus lines; stops located very close to each other (which clearly correspond to the same physical stop); and stops that do not coincide with the layout of the bus lines. This last point is the most challenging, since there is no direct association that indicates to which line(s) a certain stop corresponds.

An automated process was implemented to solve the aforementioned problems applying geospatial operations to associate lines and stops. The algorithm works as follows: i) for each bus line a *buffer* operation is performed to convert the line to a 10m wide polygon; ii) the polygon is intersected with the stop layer to obtain stops that are less than 10m from the line; and iii) the set of stops is traversed according to the direction of the line and consecutive stops that are less than 50m from each other are eliminated, on the understanding that it is the same physical stop. Fig. 3 shows the implemented correction process (stops in the original set are marked in red and the stops after applying the correction procedure are marked in green).

6 R. Massobrio, S. Nesmachnow, E. Gómez, .F Sosa, S. Hipogrosso

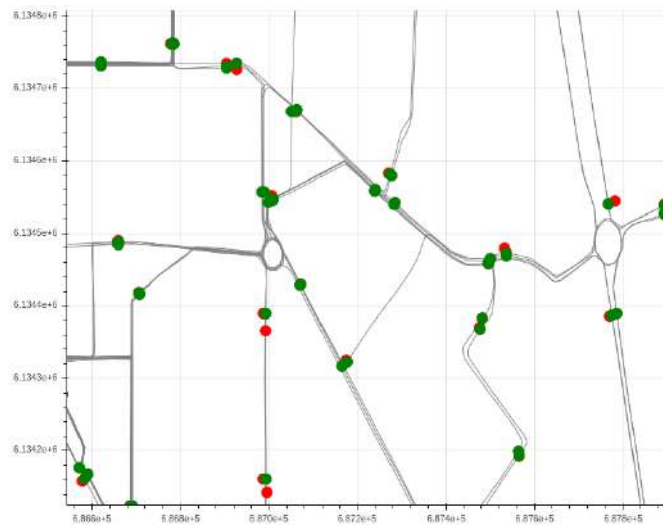


Fig. 3: Bus stop correction (red–original bus stops; green–corrected bus stops)

Timetables and trip times. The other provided dataset corresponds to the timetables of the different lines of the public transportation system. The data are separated according to the transportation company that operates the service. The provided dataset consist of Excel files that do not follow a standardized format, which makes its automated processing extremely difficult. Since it does not account for a large volume of data, the processing was carried out manually. For each line, departure times and passing times for some notable points along the route are reported. These notable points are identified by a name that does not necessarily match the name defined in the transportation system. Therefore, the procedure involved associating these points with their corresponding stops and associating the average travel time from the start of the route to that stop, based on the published timetables. Finally, for the rest of the stops on the line, travel times are interpolated from the known travel times.

Since the information of lines and stops is separated from the data of the timetables, there are differences between both datasets. In particular, timetable information is not available for a few lines (line 32 from Pan de Azúcar to Nueva Carrara, line 62 from/to Punta del Este, line 25 from San Carlos to José Ignacio, line 26 from Garzón to San Carlos, line 27 of Guscapar company, and direct line Punta del Este–San Carlos). In these cases, it is not possible to know the travel times between the stops on the route and, therefore, they were not considered within the model. Other lines were partially included in the model, according to the available data: e.g., line 34 from Las Flores (and not from Pan de Azúcar) to Piriápolis, line 55 from Manatiales (and not Buenos Aires) to Maldonado, and line 62 between Maldonado and La Capuera (and not from/to Punta del Este).

Overall, a total number of 66 lines/variants operated by six companies were included in the developed model.

4 Accessibility to education centers

This section describes the methodology for computing the proposed accessibility indicator to education centers, describing the studied area and the two needed inputs: the matrix of travel times and the location of education centers.

4.1 Definition of the studied area

The basic unit of the analysis is the census segment, defined by the National Institute of Statistics (INE). The file published by INE was corrected, since it had some invalid geometries that prevented the correct data processing.

The process used to define the studied area is graphically described in Fig. 4 and commented next. Initially, all census segments that have at least one stop of the transportation system within the polygon that defines them are considered (Figures 4a–4b). Then, neighboring towns that do not have stops are considered to avoid gaps in the studied area, computing the convex hull of the set of census segments (Fig. 4c) and intersecting with the total of census segments (Fig. 4d) to obtain all census segments to consider. The centroid of each census segment in the resulting set is computed, assuming that all trips from/to a certain segment begin (or end) at the centroid of that segment (Fig. 4e).

4.2 Matrix of travel times

The matrix of travel times for public transportation was built considering trips with up two legs (one transfer). Travel times include: i) the walking time from the centroid of the origin segment to the first bus stop; ii) the walking time from the descent stop of the last bus of the trip to the centroid of the destination segment; iii) the walking time between stops on those trips that involve transfers; and iv) the time traveling on each bus involved in the trip. Also, direct walks (up to 30 minutes) are considered between nearby centroids, since walking can be a more attractive option than public transportation. Walks from the origin centroids to the first bus stop and from the last bus stop to the destination centroids are limited to 30 minutes. Walks between transfer stops are limited to 20 minutes. The fastest travel connecting a pair of centroids is considered, assuming that people make optimal decisions to move within the city, within the rules imposed in the model regarding maximum walks and number of transfers allowed.

A directed and weighted multigraph is constructed to build the matrix. Nodes of the graph represent the centroids of census segments and the bus stops. Nodes can be connected by more than one edge. The weight of each edge represents the travel time between nodes (walking or by bus). A shorter path algorithm is applied to compute the fastest travel time between each pair of centroids.

Walking times between centroids, between centroids and stops, and between stops, are computed on the road network of the city. Each centroid/stop is moved to the nearest road and times are computed using Open Source Routing Machine, an engine implemented in C++ that combines routing algorithms with OpenStreetMap road network data to efficiently compute shorter paths. The table

8 R. Massobrio, S. Neschachnow, E. Gómez, F Sosa, S. Hipogrosso

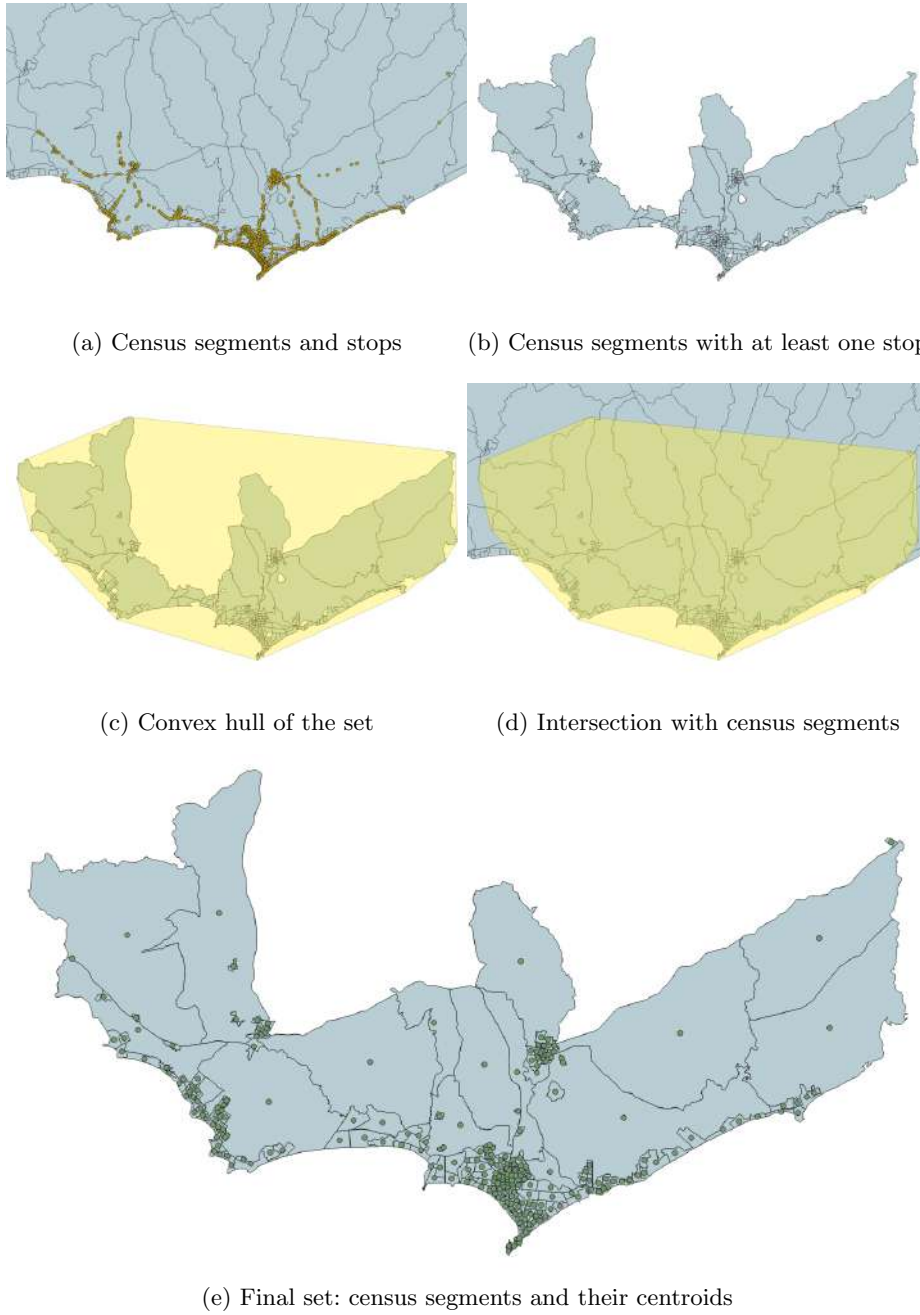


Fig. 4: Process for defining the studied area

method was used to compute the travel times between pairs in a list of geographic coordinates, using the average speed for each type of road and traffic rules imposes in the `foot.1ua` profile. Routes for a small subset of 41 nodes cannot be computed using this approach, as they were located in areas far from the road network. The travel times to/from these nodes was computed using the geographical distance and a walking speed of 5 km/h.

Bus travel edges are weighted according to the average travel time between the nodes they connect. To ensure that the shortest path does not have more than one transfer, two different nodes are used to represent each centroid (one when the centroid acts as the origin and the other when it acts as the destination) and four to represent each physical stop (which represent the stop when it is the origin or destination of the first or second trip within the total route). Origin centroids have only outgoing edges, while destination centroids have only inward edges. This allows routes to be modeled with a direct trip and even with a transfer, considering the walk between stops in the eventual transfer. A penalty of 15 minutes (added to the weight of the walking edges that connect stops) is considered on those roads that involve a transfer.

The NetworkX library of Python was used to represent the graph and compute the shortest paths. The generated graph includes a total number of 6382 nodes (253×2 centroids + 1469×4 stops) and 642 775 edges.

4.3 Location of education centers

The geographical location of education centers (initial, primary, secondary, and technical-professional education) are obtained from the Open Data Catalog [1]. Fig. 5 shows the location of these centers in the studied area.

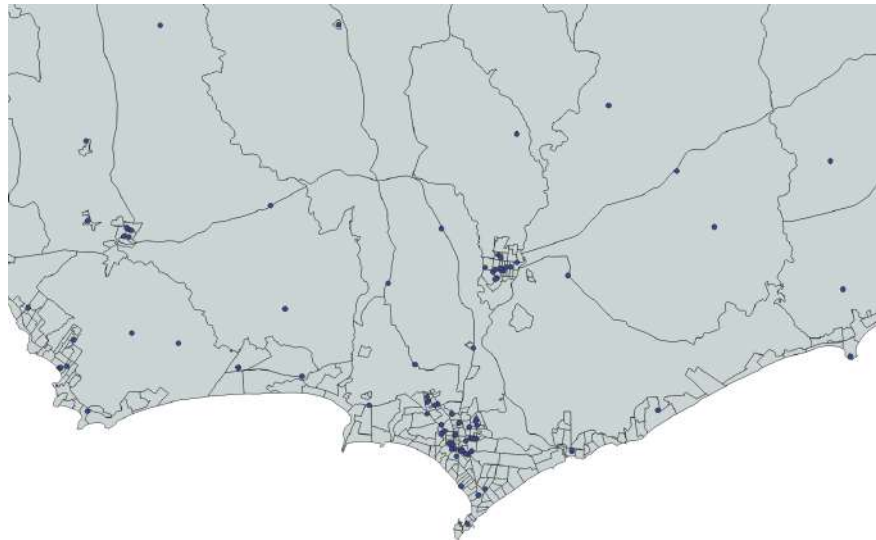


Fig. 5: Education centers in the metropolitan area of Maldonado

10 R. Massobrio, S. Neschachnow, E. Gómez, F. Sosa, S. Hipogrosso

4.4 Accessibility indicator

The matrix of travel times and the location of the education centers are used as input to compute the accessibility indicator to education centers by public transportation, using census segments as unit. The proposed indicator is based on the notion of accumulated opportunities, originally proposed by Hansen [6]. The method consists of characterizing the accessibility of every census segment by adding all education centers that are reachable from it, traveling for up to m minutes by public transportation. The threshold m is parameterizable, allowing to perform the accessibility study under different conditions. The proposed indicator is flexible, since it allows varying the travel time threshold, and can even be used to evaluate accessibility to other opportunities, provided that geolocated information of their location is available. An improved version of the proposed indicator could consider the opening hours of each education center computing the value for each hour of the day. However, opening hours is not included in the open dataset used in this study. The proposed indicator can be extended to contemplate the time dimension, if this information is published in the future.

5 Results and discussion

This section reports the main results achieved and presents the web tool developed to display the accessibility indicator.

5.1 Travel time matrix

The computed matrix of travel times for Maldonado metropolitan area is publicly available in CSV format at www.fing.edu.uy/~renzom/TTM.csv. The corresponding entry for each pair of census segments reports the travel time using public transportation, in minutes. The matrix is a relevant result in itself, since it is an important input to address various types of design and optimization problems related to public transportation in the studied area.

The matrix has dimension 253×253 . According to the implemented model, the travel time reflected in the matrix is the fastest option that connects each pair of census segments, considering direct walks, direct bus trips or even a transfer. Transfer trips add 15 minutes to walk between stops, transfer walks are limited to 20 minutes, and direct walks between centroids and entrance/exit to the transportation network are limited to 30 minutes. For this reason, some segments are disconnected, either due to the absence of lines connecting it with up to a transfer or because the stops are at a distance from the centroid that exceeds the limit allowed for walks. The results show that 13 021 origin-destination pairs (out of 64 009) are disconnected.

The average travel time between all pairs of connected census segments is 52.5 minutes. Fig. 6 shows a histogram with the frequency of each travel time value (in minutes), considering the total number of connected census segments. Regarding travel modes, 58.1% of the trips correspond to direct trips involving a single bus, 40.5% correspond to trips with a transfer, and 1.4% correspond to direct walks, without using the public transportation system.

Public transportation and education centers in Maldonado, Uruguay 11

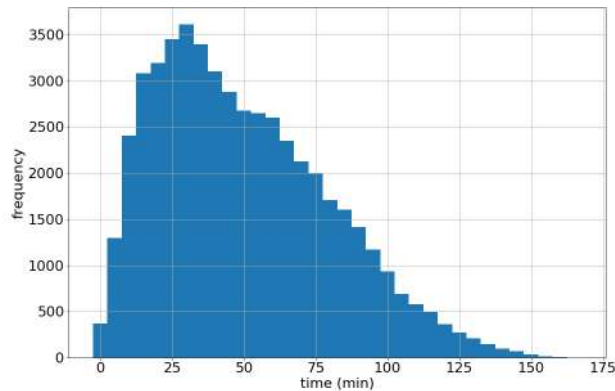


Fig. 6: Histogram with the frequency of travel times between census segments

5.2 Accessibility indicator

The accessibility indicator combines the matrix of travel times and the location of education centers. By definition, each census segment accesses all education centers in it and in census segments that can be accessed by public transportation on trips of up to m minutes. By varying the parameter m it is possible to study different situations, based on different assumptions. Using $m = 0$, each census segment only accesses the education centers that are located within the polygon that defines them. In the choropleth map in Fig. 7, the color of each segment indicates the percentage of education centers it contains, with respect to the total number of centers available. The figure shows that the rural census segments (those with the largest area) are mostly covered by at least one education center.

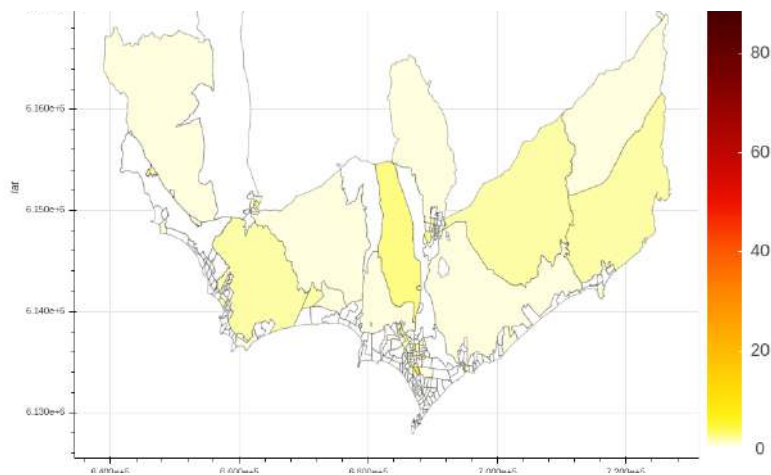


Fig. 7: Percentage of education centers located in each census segment

The accessibility of different scenarios can be studied varying the threshold m . Fig. 8 shows the accessibility indicator for $m = 10$ minutes. Results indicate that a small change in the threshold m implies a significant change on the spatial

12 R. Massobrio, S. Nasmachnow, E. Gómez, .F Sosa, S. Hipogrosso

distribution of the accessibility indicator. The census segments located in the central areas of Maldonado and San Carlos show higher accessibility values than the large census segments of the rural periphery. This effect occurs because census segments without an education center can access one in a neighboring segment through public transportation trips or short walks.

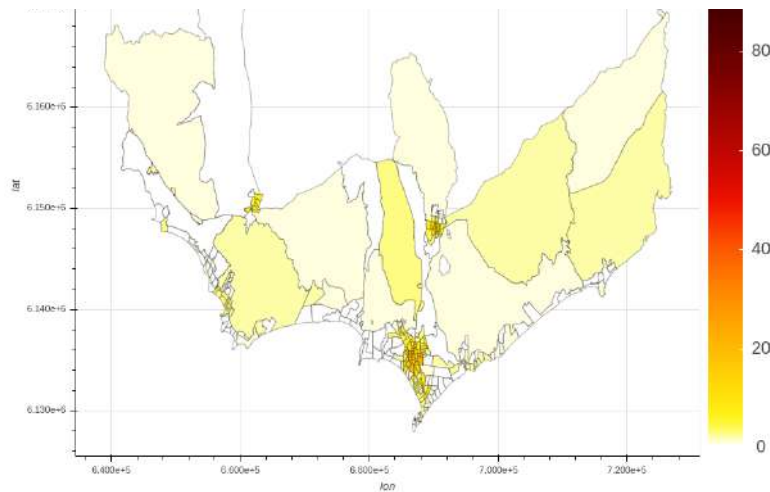


Fig. 8: Percentage of accessible education centers traveling up to 10 minutes

The coastal areas of Punta Ballena, Pinares, and Punta del Este still have low accessibility with low time thresholds. This phenomenon change when a slightly higher threshold is set. Fig. 9 shows the accessibility indicator with up to 20 minutes of travel ($m = 20$). In addition, accessibility continues improving both from the center of Maldonado and from San Carlos. In turn, it is observed that the coastal areas to the east (e.g., San Rafael, La Barra) present low accessibility indices when considering trips of up to 20 minutes.

Finally, Fig. 10 shows the accessibility indicator using a 40-minute threshold. In this case, good accessibility exists in most urban census segments. However, there is a clear stagnation in terms of accessibility in most rural segments, which only access to centers located in them and fail to access to centers in other areas. Likewise, an inequality phenomenon is observed in the coastal census segments, where the segments to the west of Punta del Este have better accessibility values than those located to the east of the peninsula.

5.3 Web visualization tool

A web visualization tool was developed to present the results of the accessibility indicator in a friendly and interactive way. The tool is publicly available at www.fing.edu.uy/~renzom/acc_maldonado. The tool shows the studied area on an interactive map, at the census segment level. The map has tools to zoom, scroll, and download the current image. A slider bar is provided to allow configuring the time threshold m considered for computing the accessibility index.

Public transportation and education centers in Maldonado, Uruguay

13

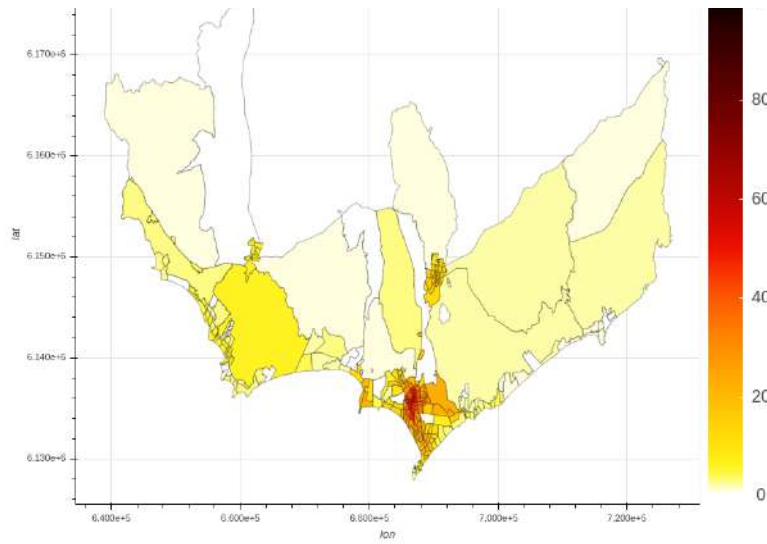


Fig. 9: Percentage of accessible education centers traveling up to 20 minutes

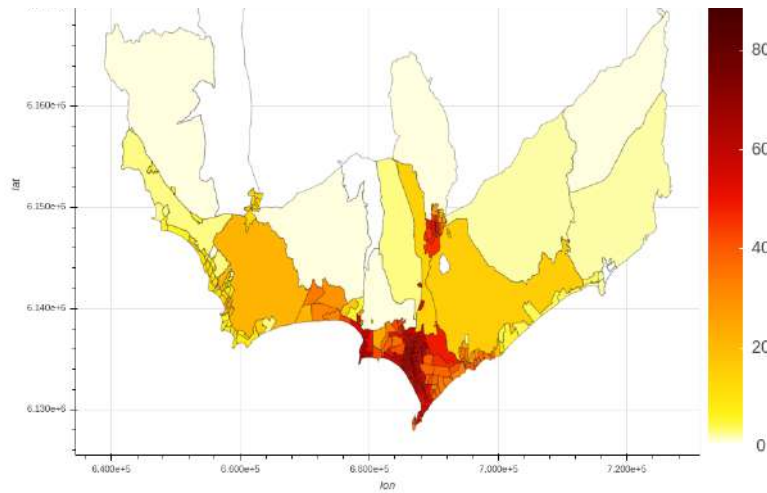


Fig. 10: Percentage of accessible education centers traveling up to 40 minutes

14 R. Massobrio, S. Neschachnow, E. Gómez, F. Sosa, S. Hipogrosso

Once a threshold is set, the map is updated to report the accessibility indicator to education centers. The result is shown through a choropleth map where each census segment is assigned a color based on its accessibility indicator value. Positioning the cursor on a specific census segment displays the code that identifies the census segment, the name of the city, the number of education centers reached, and the percentage of the total that they represent.

6 Conclusions and future work

This article presented a study of the accessibility to public services in Maldonado, Uruguay, when using the public transportation system. In order to compute an accessibility index a travel time matrix for the public transportation was built using open datasets and data provided by the local authorities, including bus lines, bus stops, and timetable information. With these data the public transportation was modeled as a graph, accounting for every alternative to connect origin and destination pairs in the studied scenario. A shortest-path algorithm was executed over this graph to compute the fastest travel time between each origin and destination. Computed travel times include walking times to/from the bus stop and in-vehicle time of both direct trips and multi-leg trips involving up to one bus transfer. The computed travel time matrix is publicly available and is a highly useful resource for authorities and researchers alike.

Then, the accessibility to education was studied combining the computed travel time matrix with the location of education centers in the studied area. Following the usual methodology in the field, accessibility was measured accumulating the opportunities (i.e., centers) that can be reached from a given origin when traveling up to a certain threshold of time via public transportation. An interactive web application was developed that outlines the accessibility measures of the studied zone when varying the travel time threshold. The application shows a map of the area and colors different zones according to their accessibility to education centers.

According to our review of the related works, this research is one of the first steps of studying the public transportation system of Maldonado, Uruguay. The results of this research (i.e., the travel time matrix, accessibility indicator, and web application) are valuable to transport and urban planning authorities and research interested in improving the public transport accessibility in the area.

The main lines of future work involve feeding the model with richer information including: up-to-date GPS bus location data, ticket-sale data from on-board smartcard readers present in the buses of the system, as well as historic passenger information to improve the travel time estimations and make recommendations to improve the quality of service of neglected areas with significant inequalities.

References

1. Administración Nacional de Educación Pública: Centros anep. Disponible en línea: <https://catalogodatos.gub.uy/dataset/anep-centros-anep> [12/2019] (2019)

Public transportation and education centers in Maldonado, Uruguay 15

2. Cardozo, O., Rey, C.: La vulnerabilidad en la movilidad urbana: aportes teóricos y metodológicos. In: Aportes conceptuales y empíricos de la vulnerabilidad global, pp. 398–423. Resistencia, Chaco: EUDENE (2007)
3. Duranton, G., Guerra, E.: Developing a common narrative on urban accessibility: An urban planning perspective. Tech. rep., Brookings, Moving to Access (2016)
4. Grava, S.: Urban Transportation Systems. McGraw-Hill Education (2002)
5. Hansen, H.: Analysing the role of accessibility in contemporary urban development. In: Computational Science and Its Applications, pp. 385–396. Springer Berlin Heidelberg (2009)
6. Hansen, W.: How accessibility shapes land use. *Journal of the American Institute of Planners* 25(2), 73–76 (1959)
7. Hansz, M.: Analysis of the spatial disparity in transport social needs and public transport provision in Montevideo. Master's thesis, University of Leeds (2016)
8. Harvey, D.: Social justice, postmodernism and the city. *International Journal of Urban and Regional Research* 16(4), 588–601 (1992)
9. Hernandez, D.: Uneven mobilities, uneven opportunities: Social distribution of public transport accessibility to jobs and education in montevideo. *Journal of Transport Geography* 67, 119 – 125 (2018)
10. Hernández, D., Hansz, M., Massobrio, R., Davyt, J.: Transporte público urbano y la accesibilidad a las oportunidades laborales. Disponible en línea: <https://ucu.edu.uy/es/node/47195>. [December 2019] (2019)
11. Hipogrosso, S., Nesmachnow, S.: Analysis of sustainable public transportation and mobility recommendations for montevideo and parque rodó neighborhood. *Smart Cities* 3(2), 479–510 (2020)
12. Hipogrosso, S., Nesmachnow, S.: Sustainable mobility in the public transportation of montevideo, uruguay. In: *Smart Cities*, pp. 93–108. Springer International Publishing (2020)
13. Huang, B., Chiou, S., Li, W.: Accessibility and street network characteristics of urban public facility spaces: Equity research on parks in fuzhou city based on GIS and space syntax model. *Sustainability* 12(9), 3618 (2020)
14. Ingram, D.: The concept of accessibility: A search for an operational form. *Regional Studies* 5(2), 101–107 (1971)
15. Krizek, K., Horning, J., El-Geneidy, A.: Perceptions of accessibility to neighbourhood retail and other public services. In: *Accessibility Analysis and Transport Planning*, pp. 96–117. Edward Elgar Publishing (2012)
16. Lei, T., Church, R.: Mapping transit-based access: Integrating gis, routes and schedules. *Int. J. Geogr. Inf. Sci.* 24(2), 283–304 (2010)
17. Massobrio, R., Nesmachnow, S.: Urban data analysis for the public transportation system of montevideo, uruguay. In: *Smart Cities*, pp. 199–214 (2020)
18. Nesmachnow, S., Baña, S., Massobrio, R.: A distributed platform for big data analysis in smart cities: combining intelligent transportation systems and socioeconomic data for montevideo, uruguay. *EAI Endorsed Transactions on Smart Cities* 2(5) (2017)
19. Salonen, M., Toivonen, T.: Modelling travel time in urban networks: comparable measures for private car and public transport. *Journal of Transport Geography* 31, 143–153 (2013)
20. World Business Council for Sustainable Development: Methodology and indicator calculation method for sustainable urban mobility. Tech. Rep. 978-2-940521-26-5 (2015)

Reimagining the Book ... Again! A New Framework for Smart Books Using Digital Twins Technology

H. Kolivand¹, E.C. Prakash², M.C. López³, D. Hernández³, and A.A. Navarro-Newball³

¹ Liverpool John Moores University, UK
h.kolivand@ljmu.ac.uk

² Cardiff Metropolitan University, UK
epakash@cardiffmet.ac.uk

³ Pontificia Universidad Javeriana Cali, Colombia
{mclopez09,davidher28,anavarro}@javerianacali.edu.co

Abstract. Technology enabled learning and communication are at the crossroads, which need flexible solutions. Flexible learning enables a learner to move seamlessly between the real and virtual world. We propose a novel flexible communication tool, “the smart book” to address these challenges. First, we review the role of the traditional book, its role in society today and the recent advances in augmented reality books. Next, we present a novel approach that integrates digital twins and mixed realities that is useful in communication, learning and for making decisions. We propose an initial vision of the architecture. Finally, we follow the Spiral of Creative Thought to create a first prototype with promising results. Our plan to further develop the architecture is to integrate this spiral with other software development methods. We need further iterations within the spiral to include final users and diverse applications.

Keywords: book, mixed reality, digital twin, augmented reality, virtual reality

1 Introduction

Humanity and books have a long relationship. Smart societies living in smart cities within a smart world demand innovative ways of communication and understanding of both traditional and new communication channels. Crisis such as the Covid-19 have evidenced the need and surge of novel interaction and collaboration mechanisms. This is evident from the authors own experience lecturing and researching during the crisis. This is only one of multiple examples that could come out. As we will discuss, the book in its multiple formats is still a current and versatile communication medium. Our goal is to create a smart book, an important communication tool in smart cities within a smart world to make reading, learning and teaching amusing and more efficient. We visualise the smart book as a tool that would be able to enhance the current state of the

2 Kolivand et al.

book, respecting its multiple formats and allowing different usages. Even though our examples and experience are mainly related to education; while we continue in the search for a smart education, we believe the book plays an important role in different sectors currently experiencing difficulties (for example, tourism, commerce, health care, maintenance, etc.).

1.1 About the Book and its Evolution

María Angélica Thumala Olave starts her paper questioning “why do people in the UK read and collect books when there are so many other sources of information and forms of story-telling available?” [1](p.1). In her qualitative analysis, she [1] highlights the powerful appeal of books due to the fusion of the act of reading, books iconic value as cultural goods and their surface material properties. In another study, James M. Donovan [2](p.1) “provide a reasonable basis to support an expectation that readers perform better on reading comprehension tasks performed in book-rich environments,” while challenging projects that remove print collections to provide space to other amenities and evidencing physical collections have a role in today’s digital society. Indeed, books also play an important role in education and are subject of diverse studies [3]. Evans et al. [3] present a study comparing pre-schoolers behaviour interacting with alphabet books in paper format and interactive alphabet books in an eBook. They [3] conclude that children spend less time on letter-related behaviour (e.g. saying object names) and more time oriented to the book. Potnis et al. [4] evidence difficulties in the adoption of e-books by millennials but highlights the potential benefit of available resources and strategies for their adoption. Learning books are diverse, for example, Reynolds [5] studies the role, limitations and possibilities of comic books in higher education. In another example, Gaylor et al. [6] claims the potential input for mathematics learning in children using counting books and study the impact of using tactile and narrative content within these books. Whatever the case, books seem to be important. Indeed, Beimorghhi, Hariri, Babalhavaeji [7] suggest that books play an important role in transforming knowledge to wisdom. Finally, a study from Bavishi, Slade and Levy [8] suggest that those who read books may acquire better survival skills. Of course, there is still a lot to study about books, however, the continuous interest in books is a strong evidence of their importance in humankind.

From the previous paragraph, it is evident that books have had an evolution too. The paragraph refers to paper books, eBooks, tactile books, and comic books, among others. Wikipedia [9], the modern version of the collection of books known as encyclopaedia, offers an effective summary of book evolution that goes from tablets and codex to eBooks and presents the type of content they can provide and multiple uses they can have. Following the evolution of the book, the pioneering work by Billinghamurst, et al. [10], the Magic Book, constituted the first book to include Augmented Reality (AR) and Virtual Reality (VR). The Magic Book project [10], presented in 2001 explored the concept of “how interfaces can be developed that allow for seamless transition between Physical Reality, Augmented Reality (AR), and immersive Virtual Reality (VR) in a collaborative

setting,” [10](p.25). As such, the Magic Book [10] was a book that could be read as a traditional book, without any technology; but the book could be read using a handheld device capable of displaying 3D virtual content. The reader could view AR scenes with 3D content overlaid on the pages from any perspective or they could fly into immersive VR scenes. A communication between the readers in AR and VR world could also be established [10].

1.2 Previous Work

According to Do and Lee [11] as cited by Navarro-Newball et al. [12] (p.3), “AR books enhance the reading experience, visualise products, tell stories and teach. They can provide other views of complex situations, increasing understanding and are an evolution of traditional books, the main medium of teaching and learning.” Then, in our previous work, Navarro-Newball et al. [12] identified some limitations in AR books. AR Books so far [12]: (1) did not mean to include contents using all major data types (e.g. 2D static, 2D dynamic, 3D content and sound); (2) apart from few cases [11], did not offer a usable authoring interface; (3) did not offer authoring tools to create pages and to introduce markers with related display elements such as virtual models, animations, videos, sounds, images and gestures in order to create any book; (4) limited reader interactions to flipping pages, and AR cards for additional content; (5) barely used natural features [13], but relied on abstract fiducial markers; (6) and, content creation possibilities from readers, although existent [14], were rare.

More recently, the work from Bischof et al. [15] overcome the problems of fiducial markers using Vuforia SDK, allowing the use of images of the book as AR markers; however, the kind of content displayed is still limited to video only and the work is focused on one book only. Leela, Chookeaw and Nilsook [16] presented a study to describe the effectiveness of mobile learning and AR books through the microlearning approach and concluded that books supported by technology increase interest and promote teamwork; however, they do not give details about the AR books. Kljun et al. [17] (p.103) state that “digital-augmentation of print-media can provide contextually relevant audio, visual, or haptic content to supplement the static text and images. The design of such augmentation - its medium, quantity, frequency, content, and access technique - can have a significant impact on the reading experience;” and provide evidence of this fact; however, their sample books only use video as the augmented media and falls short in testing other interactive possibilities. Yamamoto et al. [18] propose a method to integrate tactile sensation into an eBook using AR, reinforcing the importance of texture and physicality in a book. Mokhtar et al. [19] describe a framework which is reusable and allows the creation of new colouring content; however, the books display only 3D pop up images synthesized from the coloured pages, by visualizing them in 3D on a users view of the real world; and, the 3D models are still drawn by a modeller but texturized with the colours used by the user. Recently [20], researchers have presented the e-immersive Book, capable of assist readers relying on a HoloLens device. Moreover, users read in an inspectional way more than one book to find answers to questions [20].

4 Kolivand et al.

Finally, it is important to note that Gazcón and Castro [21] claimed back in 2015 an interactive and collaborative application for traditional books augmentation which allows the incorporation of AR content to any pre-existent traditional book and collaboration among readers.

The use of AR markers has evolved to using natural features taken from book pages thanks to SDKs such as Vuforia, but tools for content creation in AR books are still scarce. However, following the spirit of Gazcón and Castro [21], which allows the inclusion of AR content and collaboration; and, aware of the important role of books, we propose to develop further the book as it will be explained in the next sections. The book is widely presented in all its formats and requires a constant evolution so that new ways to convey information to readers, authors, teachers, students, guides and followers are discovered.

1.3 Problem Statement

There is a positive impact from VR and AR in formal and informal educational environments [22]; these technologies provide novel ways to learn, communicate and teach. Indeed, AR/VR may enhance the learning process in all content areas, are now more affordable and new user-oriented interfaces allow people from all over the world to connect in unique and exciting educational experiences [23]. One of these experiences is provided by AR books. AR books enhance the reading experience and can increase understanding by providing other interactive views of complex situations while visualising products, telling stories and teaching [12]. The first AR Book, the Magic Book [10], explored transitional interfaces between physical reality, AR and VR. In The Magic Book, readers could use AR to display content, but the interaction with the displayed content was limited to observing mostly.

AR book creation have had difficulties such as requiring complex image processing or relying on software configuration or scripting. Creation of multiple books and upload of diverse content; display of representative multimedia data such as video, text, image, animation and 3D and; integration of alternative interaction techniques which use game technology have also been limited in the AR book world. In a previous research described in a chapter by Praksh and Rao [24] (co-author of this paper) we proposed an AR book and we were able to overcome some of these problems. Firstly, we offered to include all major data types such as 2D static; 2D dynamic; 3D content and sound. Secondly, we offered an authoring interface in which the author could create pages and introduce AR markers with related elements such as virtual models, animations, videos, sounds, images and gestures in order to create his/her desired book. Thirdly, we explored a novel way of interaction, integrating body gestural interaction to the book, besides projecting 3D objects and animations with synchronised rotation and translation on pages. Figure 1A shows our previous book with a fiducial marker, video content displayed and, 3D content interaction through zooming. Our book was novel because:

- We provided a kind of flexibility to include major media data types (for example video and audio), while existing books focused on a subset of them. Focusing on a subset of media types is still common.
- We were able to create any book based on standard fiducial markers provided by the AR kit we used. In contrast, many existing AR book projects focused on the development of one single book, which is still a common practice.
- We included “take”, “move” or “zoom” gestures to virtual objects displayed in every page, while many books used additional AR cards for this. Also, with gestures we provided integration to basic VR scenarios.

However, our book had limitations:

- We could only create AR versions of books with no more than 48 pages, due to the limited set of fiducial markers offered by the SDK those days.
- We relied on fiducial markers and did not take advantage of natural features within the real book content to display AR content.
- We did not include mobile devices capabilities to the book.
- We did not allow the creation and sharing of content by readers.
- We did not take great advantage of gamification technologies to make reading more engaging.
- We did not implement a way to store book usage statistics; for instance, we did not know how the book was read and understood.

Therefore, we missed the chance to create more complex books, to utilise handier interaction strategies and to gather anonymous information about the reader’s learning, reading, authoring and sharing processes.

In his blog at IEEE’s Future Directions [25], Roberto Saracco answers to the question “what would education be like in 2050?”, with two words: “Digital Twins.” Saracco believes that VR Digital Twins are a new tool that will be key for education by 2050 [25]. We believe that the current Covid-19 crisis could accelerate their evolution in education. In essence, Saracco [25] explains that each person has several fragments of his/her own digital twin; these fragments can be used to represent both our skills and knowledge; and, Digital Twins offer the possibility to study in the digital representation rather than studying on the real thing. For instance, we believe we will have the chance to take advantage from the real world, the virtual world and the mixed world. As Saracco said more recently [26], Digital Twins bridge the physical space and the cyberspace. Digital Twins are a trend in the field of Mixed Reality (MR). “Digital Twin models are computerized clones of physical assets that can be used for in-depth analysis,” [27]. With current technology we see a chance to take the AR book beyond. That leads us to propose the research question: how to use Digital Twins to create a smart book which overcomes limitation from previous books?

To answer this and focusing on the learning applications of books first, we need to support complex contents in educational scenarios such as museums and classrooms using tools that favour learning and user’s entertainment. We expect to enhance flexibility, while staying independent of the technology used and taking care of not being disruptive with the real book. We believe the concept

6 Kolivand et al.

can be extended to any sustainable paper-based communication material such as brochures. Additionally, the content management model is fundamental to provide a flexible tool for the creation of content and narrative to entertain and educate. Finally, the digital twin approach can be useful to find out how the book is read and understood.

1.4 Objectives

Our main objective is to develop a smart book creation framework using the Digital Twins technology and taking advantage of MR. In order to achieve that we need to:

- Investigate how to integrate smart book content and interactions in a digital twin.
- Develop a digital twin architecture to support a smart books creation framework.
- Validate the resulting framework introducing a smart book.
- Validate the use of the smart book created using the framework

2 Methodology

After a continuous study of learning with children, Professor Mitchel Resnick [28], dedicated to helping children of all ages play, think and experiment with design and technology, came up with an approach with which students would engage in project analysis, implementation, and evaluation. To achieve this, Resnick gave life to the infinite Spiral of Creative Thought (SCT) specified below (1B). Basically, the projection of the future expressed in the spiral denotes the ability that everything that is imagined can become reality, through the repetition of five key steps [28]:

- Imagine: Visualize what you want to create without limit, detaching from value judgments such as the previous knowledge that binds imaginative capacity.
- Create: Make the thought or imagined a reality through compositions, drawings, or artifacts.
- Play: Explore, enjoy, listen, touch, and use all creations with an emphasis on recognizing that everything is upgradeable and that evolutions will arise at any time.
- Share: Teach or show the project to others taking into consideration their opinions.
- Reflect: Carry out a feedback process where the appropriate changes are made.

The iterative execution of the SCT leads to the creation of artifacts that promote research and experimental thinking. Therefore, for the realization of this project we will use SCT as the main source of the methodological process, at the

same time we will integrate the phases of the software engineering process into this research. Additionally we will need to realise a number of tasks to achieve our goals. To investigate how to integrate smart book content and interactions in a digital twin we need to:

- Implement the prototype of a smart book based on a real book and using MR.
- Identify potential interactions.
- Identify potential data of interest within a focus group.
- Identify requirements.

To develop a digital twin architecture to support a smart books creation framework we need to:

- Design the architecture.
- Design a data model to support the architecture.
- Design a way to measure books usage and understanding.
- Identify the most suitable technology for development.
- Implement the architecture.
- Design and implement a user interface for smart book creation.

To validate the resulting framework introducing a smart book we need to:

- Use the architecture to create one smart book inspired on a real book.
- Validate frameworks usability.

To validate the use of the smart book created using the framework we need to:

- Validate usability of the smart book within a focus group.
- Validate how the book is read and understood using statistics.

3 Proposed System

Figure 2 shows the proposed architecture and flow of smart book use. While in real books one author proposes content to the reads, AR, MR and VR technologies create a window that expands the book to the smart book allowing multiple readers become collaborative authors and the authors become collaborative readers. Users in both roles (readers and authors) can upload and download content that may come from different sources and media, such as text, 3D content, images and video, audio, interactions. This content is inspired in the real, imaginary, and virtual worlds. The smart book must be supported by an interconnected architecture based on the Digital Twins concept, which includes a layered model, a novel user interface, storage, and processing of data. This approach will integrate the real and virtual versions of the book allowing collaboration and allowing users to include their imaginary into the book.

8 Kolivand et al.

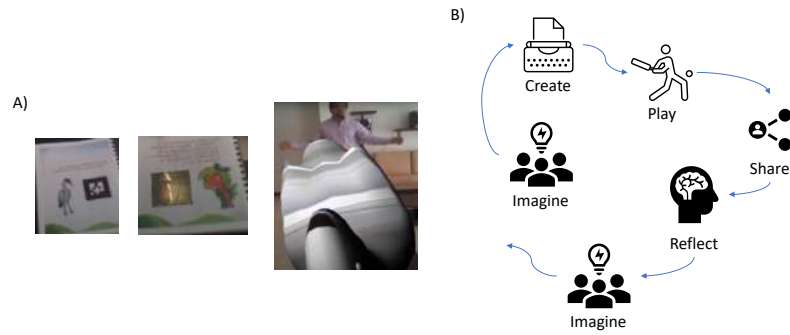


Fig. 1. Previous book and method. A) Previous AR book. B) SCT.

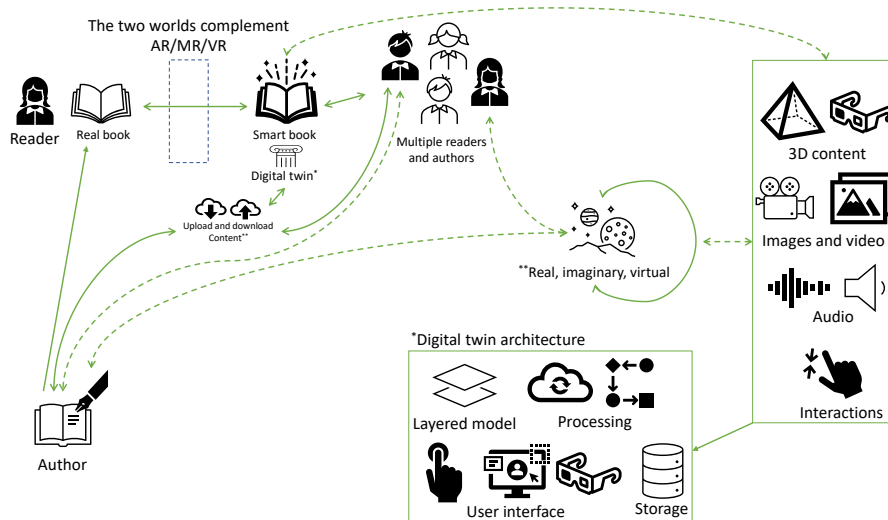


Fig. 2. Smart book's architecture.

4 Early Prototype

At the end of the year, we will have the prototype of a smart book and a list of feasible interaction oriented by the book. We chose “Journey of the Beetle” book [29] as a field test for the smart book early prototype. Following the idea of SCT, we started a creativity workshop with nine undergraduate students under the guidance of Miguel Fernando Caro, the author of the chosen book, who specialises in educational books and tales. During this workshop, the students had to: (1) write letter to their inner self (self-discovery) talking about their experiences in life and feelings; and, (2) write a short fictional story. In all cases, students were free to share their writings or not. This served to spark creativity and motivate story writing for video games and animation. Then, students had to study previous publications related to AR books and present a summary analysis of one paper to the rest of the group. These two activities were related to the “imagine phase” of the SCT. Finally, we had a brain storming session. Next, we started preparation for the “create phase” and all students participated in Unity, Unreal and Vuforia basic training and developed the first prototypes. Figure 3 shows “Journey of the Beetle.” Here, one example of the proposed interactions obtained from the first iteration displays and AR interactive game the first time the beetle is shown in the book. In the game the beetle must catch as many dung balls as possible. This game was played by two students who programmed the game (“play phase”) and then shared to the rest of the group (“share phase”). After the “reflect phase” we found that:

- There are many ways a the book can be used to interact. For example, you could go to the real word, photograph a beetle and upload it in new page of the book; you could expand the book by superimposing animation or videos as in previous books; or, you could write new pages in the digital twin.
- Some pages or chapters could contain video games. Particularly, the first video game implemented could be enhanced to include multiple players and collaboration mechanisms among a number of beetles.
- The book itself could be an interaction device for a narrative educational video game.
- Apart from the original game of the beetle making dung balls. Two other video game narratives for different sections of the book were proposed. The first one is about the illegal burning of fields versus the reforestation of the field to raise cattle in a sustainable way (the book explains the relationship between the beetle and the cattle). The second one is a survival game where beetles must avoid being caught by hungry birds. All proposed video game narratives can be a test field for AI (flocking and path finding for cattle), collaborative reading (reading/writing with other author-readers taking advantage of a digital twin), multiplayer interactive techniques (each reader becomes a beetle and compete to make the biggest dung ball), among others.
- Finally, different reading reward mechanisms were proposed, such as: access to books, documentaries and movies related to the book’s thematic and guided field visits where the situations explained on the book can be experienced in real life.



Fig. 3. Early prototype.

5 Discussion

We believe that if we manage to implement it, the smart book will become an important communication tool within a smart city environment supporting education, tourism, maintenance, training, health, environment, culture, etc. We expect our approach will respect and give relevance to other book formats while expanding those to different ways of interactions, collaborations and applications that may be used when required. The most important thing about the Digital Twins approach is that it will allow for a book that can not only be used to expand the real world but to take decisions from the data gathered during its usage, for example, to enhance learning or other processes that could be achieved through the book.

6 Conclusion

We finished the first iteration in the SCT. The process of the SCT has sparked initial ideas and interaction mechanism that will enrich the smart book and challenge the developer to create and architecture that supports such interactions. However, a few more iterations are needed to refine the prototype before we start implementing the architecture. Despite that, we dare to envision a possible basic architecture and work usage flow. Further iterations within the SCT should include reflection of the applications of the book in fields different from education and potential users. The completion of the smart book project will require funding and time to cause the desired impact.

We are aware that during the latest book evolution (the AR book), there have been advances which allow some content creation, inclusion of different data formats, introduction of new books and, the use of natural features of the book. However, we found no evidence of a book creation framework that takes advantages of all these features altogether; neither we found a vision of the book which takes advantage of the Digital Twins concept. Our previous project has now become obsolete because the software tools we used are no longer usable. We believe our Digital Twins approach is an opportunity for reimagining the book . . . again!

7 Acknowledgements

Authors would like to acknowledge:

- The thematic network from CYTED “CIUDADES INTELIGENTES TOTALMENTE INTEGRALES, EFICIENTES Y SOSTENIBLES (CITIES)” no 518RT0558.
- Carolina Giraldo Echeverry, Miguel Fernando Caro Gamboa, Fernando Uribe Trujillo authors of the “Journey of the Beetle”.
- CIPAV for freely distributing the book.

References

1. Mara Anglica Thumala Olave. Book love. a cultural sociological interpretation of the attachment to books. *Poetics*, page 101440, 2020.
2. James M. Donovan. Keep the books on the shelves: Library space as intrinsic facilitator of the reading experience. *The Journal of Academic Librarianship*, 46(2):102104, 2020.
3. Mary Ann Evans, Sarah Nowak, Brittany Burek, and David Willoughby. The effect of alphabet ebooks and paper books on preschoolers behavior: An analysis over repeated readings. *Early Childhood Research Quarterly*, 40:1 – 12, 2017.
4. Devendra Potnis, Kanchan Deosthali, Xiaohua Zhu, and Rebecca McCusker. Factors influencing undergraduate use of e-books: A mixed methods study. *Library & Information Science Research*, 40(2):106 – 117, 2018.
5. Pauline J. Reynolds. *From Superman to Squirrel Girl: Higher Education in Comic Books, 1938–2015*, pages 33–54. Palgrave Macmillan US, New York, 2017.
6. Shannon M. Gaylord, Connor D. ORear, Caroline Byrd Hornburg, and Nicole M. McNeil. Preferences for tactile and narrative counting books across parents with different education levels. *Early Childhood Research Quarterly*, 50:29 – 39, 2020. Parents supporting early mathematical thinking.
7. Alireza Atarodi, Nadjla Dr. Hariri, and Fahimeh Babalhavaeji. Transforming knowledge into wisdom: a grounded theory approach. *Library Philosophy and Practice (e-journal)*, (2955):1 – 13, 2019.
8. A. Bavishi, M. Slade, and B. Levy. The Survival Advantage of Reading Books. *Innovation in Aging*, 1(suppl 1):477–477, 06 2017.
9. Wikipedia. Book. <https://en.wikipedia.org/wiki/Book>, 2020. [Online; accessed 12-JAugust-2020].

- 12 Kolivand et al.
10. Mark Billingham, Hirkazu Kato, and Ivan Poupyrev. The magic-book moving seamlessly between reality and virtuality. *IEEE Comput. Graph. Appl.*, 21(3):6–8, May 2001.
 11. Trien V. Do and Jong Weon Lee. Creating 3d e-books with arbookcreator. In *Proceedings of the International Conference on Advances in Computer Entertainment Technology, ACE '09*, pages 429–430, New York, NY, USA, 2009. ACM.
 12. A. Navarro-Newball, I. Moreno-Sanchez, A. Arya, C. Prakash, E. Mike-Ifeta, and J. Mejia-Mena. An interactive modelling architecture for education and entertainment at museums. *Dyna*, 92(3):269–273, 2017.
 13. Camille Scherrer, Julien Pilet, Pascal Fua, and Vincent Lepetit. The haunted book. In *Proceedings of the 7th IEEE/ACM International Symposium on Mixed and Augmented Reality, ISMAR '08*, pages 163–164, Washington, DC, USA, 2008. IEEE Computer Society.
 14. Adrian Clark, Andreas Dünser, and Raphaël Grasset. An interactive augmented reality coloring book. In *SIGGRAPH Asia 2011 Emerging Technologies, SA '11*, pages 25:1–25:1, New York, NY, USA, 2011. ACM.
 15. Denise Bischof, Jürgen Sieck, Jacodia Fransman, Christian Kassung, and Eileen Klingner. Interactive recipe book - enhance your traditional recipe book: Showing cultural heritage through cooking. In *Proceedings of the Second African Conference for Human Computer Interaction: Thriving Communities, AfriCHI 18*, New York, NY, USA, 2018. Association for Computing Machinery.
 16. Soralak Leela, Sasithorn Chookeaw, and Prachyanun Nilsook. An effective microlearning approach using living book to promote vocational students computational thinking. In *Proceedings of the 2019 The 3rd International Conference on Digital Technology in Education, ICDTE 2019*, page 2529, New York, NY, USA, 2019. Association for Computing Machinery.
 17. Matjaž Kljun, Klen Čopič Pucihar, Jason Alexander, Maheshya Weerasinghe, Cuauhtli Campos, Julie Ducasse, Barbara Kopacin, Jens Grubert, Paul Coulton, and Miha Čelar. Augmentation not duplication: Considerations for the design of digitally-augmented comic books. In *Proceedings of the 2019 CHI Conference on Human Factors in Computing Systems, CHI 19*, page 112, New York, NY, USA, 2019. Association for Computing Machinery.
 18. T. Yamamoto, H. Aida, D. Yamashita, Y. Honda, and M. Miki. E-book browsing method by augmented reality considering paper shape. In *2017 International Symposium on Ubiquitous Virtual Reality (ISUVR)*, pages 30–33, 2017.
 19. M. K. Mokhtar, F. Mohamed, M. S. Sunar, M. A. M. Arshad, and M. K. Mohd Sidik. Development of mobile-based augmented reality colouring for preschool learning. In *2018 IEEE Conference on e-Learning, e-Management and e-Services (IC3e)*, pages 11–16, 2018.
 20. Shinhyo Kim, Jihyun Park, and Jusub Kim. E-immersive book: The ar book that assists the syntopical reading. In *Proceedings of the 9th Augmented Human International Conference, AH 18*, New York, NY, USA, 2018. Association for Computing Machinery.
 21. Nicolás Gazcón and Silvia Castro. Arbs: An interactive and collaborative system for augmented reality books. In Lucio Tommaso De Paolis and Antonio Mongelli, editors, *Augmented and Virtual Reality*, pages 89–108, Cham, 2015. Springer International Publishing.
 22. Barbara Mones. Before and after ar/vr: Empowering paradigm shifts in education. In *SIGGRAPH Asia 2017 Symposium on Education, SA 17*, New York, NY, USA, 2017. Association for Computing Machinery.

23. Shinhyo Kim, Jihyun Park, and Jusub Kim. E-mmersive book: The ar book that assists the syntopical reading. In *Proceedings of the 9th Augmented Human International Conference*, AH 18, New York, NY, USA, 2018. Association for Computing Machinery.
24. Edmond C. Prakash and Madhusudan Rao. *Gamification in Informal Education Environments: A Case Study*, pages 73–97. Springer International Publishing, Cham, 2015.
25. Roberto Saracco. What would education be like in 2050? Digital Twins. <https://cmte.ieee.org/futuredirections/2018/02/21/what-would-education-be-like-in-2050-digital-twins/>, 2018. [Online; accessed 12-JAugust-2020].
26. R. Saracco. Digital twins: Bridging physical space and cyberspace. *Computer*, 52(12):58–64, 2019.
27. Seok-Jin Song and Yong-Gu Jang. Construction of digital twin geotechnical resistance model for liquefaction risk evaluation. In *Proceedings of the 2nd International Symposium on Computer Science and Intelligent Control*, ISCSIC 18, New York, NY, USA, 2018. Association for Computing Machinery.
28. Mitchel Resnick. All I Really Need to Know (about Creative Thinking) I Learned (by Studying How Children Learn) in Kindergarten. In *Proceedings of the 6th ACM SIGCHI Conference on Creativity & Cognition*, page 16, New York, NY, USA, 2007. Association for Computing Machinery.
29. C. Giraldo, M.F. Caro, and F. Uribe. *La travesía del escarabajo*. Editorial CIPAV, 2019.

Experimental Algorithmic Citizenship in the Sandboxes: an Alternative to Ethical Frameworks and Governance- by-Design Interventions

Denisa Reshef Kera¹

¹ BISITE, University of Salamanca, Spain
denisa.kera@usal.es

Abstract. Various attempts to embed cultural, social, and legal norms directly into the design constraints and machine-readable code define the current ethical frameworks and interventions regulating algorithmic governance. The challenge is to balance the novelty and efficiency of automation with aspirational values of democracy, such as division of powers, political deliberation and inclusivity in decision making. To support these aspirations, we developed an experimental approach balancing regulation with code modeled after a regulatory sandbox. The Lithopy policy and design sandbox engaged stakeholders in blockchain smart contracts and regulations of an imaginary “smart village” using a simulated ledger on a server (testnet) in 2 – 4 hours long workshops. In 2019 we conducted five workshops with over 35 participants to design the sandbox. In 2020 we tested it with 59 participants in two workshops resulting in a structured feedback on how to regulate a biased and adversary code. The experimental form of algorithmic citizenship in the sandbox showed a preference for regulating code over audits and industry standards (rather than governments or markets).

Keywords: Blockchain, Distributed Ledger Technologies, Stakeholder Engagement, Policy and Design, Governance-by-design, Smart contracts.

1 Introduction

There is a democratic deficit in the present algorithmic services that support automated decision-making as a base for the future smart cities and governance [1]–[5]. Rather than supporting democratic institutions and procedures that define our off-line, non-digital institutions (norms, laws and regulations), these platforms and systems replace legitimacy with efficiency. They reinforce the existing biases and injustices translated into algorithms that promote efficiency but lead to “accountability gap” [6] and “de-responsibilisation of human actors” [7]. To support legitimacy along efficiency of the new infrastructures, we need governance over prototypes is reflective of the issues of power, stakes, interests, and ownership. We need a model of prototyping that balances the calls for innovation, disruption and technological change with participation, deliberation and legitimacy.

1.1 Frameworks, Interventions, Sandboxes

To address these structural challenges in the use of algorithms and new services for governance and decision-making, researchers proposed various interventions and frameworks. They try to increase the transparency [8]–[10], oversight [11], [12], accountability [8], [13], [14], but also participation and engagement [15], [16] with algorithms and data. Beyond these numerous interventions and frameworks regulating AIs, ML algorithms and blockchain systems, we can identify two strategies. One reduces and transforms the values and regulations into code and data [17], such as privacy-by-design [18], society-in-the-loop [19], [20], and adversarial public AI system proposals [21]. This “governance-by-design” strategy differs from the various aspirational ethical frameworks and tactics that try to separate the regulations from the code. This second strategy insists on an oversight by a public institution or independent body outside the platforms and systems through laws, regulatory oversight, audits, industry standards [22]–[25], but also “social licenses” in cooperation with communities [26] or even “people’s councils” [27].

The regulatory sandboxes [28], [29] present a third, experimental alternative to these aspirational ethical frameworks [30], [31] and equally popular “governance-by-design” [18], [32] and “value-sensitive design” initiatives [33]. Sandboxes address the structural challenges of algorithmic governance and automation [1] by connecting deliberation with experiments that work simultaneously with regulations and code without reducing one to another. Instead of reducing and transforming the various democratic values and regulations to code, such as privacy-by-design [18], society-in-the-loop [19], [20], adversarial public AI system proposals [21], or insisting on the oversight by a public body outside the infrastructure, the sandboxes support hybrid, tactical and situated engagements with automation and infrastructure [16], [34], [35].

1.2 Legitimacy and Efficiency: “Good Enough” Solutions with Friction

The sandbox alternative to the universalist models of regulating (with) algorithms leads to “good enough” solutions that are open for further iterations and modifications. The processes of negotiation and design reiterations do not separate nor reduce the regulations from/to code. They support friction by “slowing down” the technology and increasing participation and understanding of the issues involved in the technical decisions about the architecture of the system (open source, closed, in-house solutions, permissioned, permissionless etc.). Their main advantage is in giving a direct experience of the effects combining design and policy for a particular contexts and concrete community.

To support legitimacy along with efficiency in these new promissory infrastructures, we have to reflect upon the dichotomy between regulation and code, institutions and platforms and question whether it makes sense to develop them independently of each other. Instead of reducing and simulating the democratic processes to a level of code or strictly separating regulation from code and insisting on a more decisive role of the government institutions, we can actively support the hybrid and complex arrangements. The tensions between regulation and code in the sandboxes are produc-

tive and support experiments that challenge both, the institutions and platforms while emphasizing the issues of engagement, participation, and representation.

To tap into these hybrid opportunities of connecting regulation with code, we defined the algorithmic future as a problem of experimental and hybrid governance rather than a technical or governmental teleology of better Reg or Tech. In what follows, we will describe the process of designing such sandbox for supporting experimental and hybrid governance, including the mistakes which informed the final design. While we originally envisioned the sandbox as a space supporting collaborative work on the future scenarios of algorithmic governance, the 2019 workshops showed more urgent need for a tool gathering personal attitudes towards issues of code and regulation. Lithopy project was never a user study but a research into stakeholder engagements and we never collected any personal data on the participants except their self-identification in terms of their knowledge of blockchain technology and/or governance issues and interests.

2 Lithopy Sandbox

The critical engagements with algorithms via frameworks, interventions and sandboxes respond to various challenges in algorithmic governance (safety and security, bias, justice, participation, deliberation). The original focus of our research in 2019 was anticipatory governance of the emerging blockchain-based infrastructure for which we designed a “testnet” (running a simulated Hyperledger Fabric permissioned blockchain ledger) with a simulation game for 12 stakeholder roles [36]. In 2019 we organized five workshops with 35 participants that used a simulation game later formalized as a sandbox used in 2020 workshops.

The cards with the roles explored the various stakes in regulating algorithms and data in the near-future scenarios based on four functional smart contracts. The contract (becoming citizen, marriage, partnership, owning property) governed the life in the imaginary “smart village” of Lithopy consisting of functional permissioned blockchain services. To show how it feels to live under the extreme blockchain governance with automated contracts, we created a design fiction movie about a typical day in the village where people sing with 3D printers, move around their large coins, and perform various transactions in front of the satellites and drones. The artistic aspect of the project created an intentional ambiguity to support creative engagements with the code and regulations.

2.1 Surveillance, Automation, Deliberation in the Sandbox

The experience with the extreme forms of surveillance and automated governance over satellite and drone data in Lithopy informed the discussions but also the voting and decision-making processes in the workshops. In 2019, 35 participants took part in the 5 workshops with a questionnaires that also served as a training material for explaining the various tools of regulation of the emerging technologies (from governance-by-design to market incentives, codes of conduct, ISO norms, provision of ser-

vice, laws, moratoria etc.). The participants watched a design fiction movie about the life in the village and interacted with the blockchain services over a dashboard and templates documented on the GitHub to decide upon the future of their community¹.

While modifying the code for the testnet, the participants made decisions on the type of regulations of these future services through voting and deliberating. In 2019 most participants (16 out of the 18 that left feedback in a written form and majority in the group discussions) expressed a strong interest in hybrid, onchain and offchain combination of code and regulations but complained about a lack of skills to do this. Participants did not feel competent to decide on the future scenarios of their community. In the discussions, they would slip out of their stakeholder roles into personal opinions and issues with algorithmic governance in general.

2.2 Individual and Social Agency over Code and Regulations

The most important outcome from the 2019 workshops became a proposal for an environment or service that supports stakeholders in giving feedback in their natural languages about regulations, but also code. This led to the idea of a hybrid sandbox that uses the model of regulatory sandboxes [37] to support more participatory and public engagements in concrete scenarios of algorithmic services and governance.

Rather than a specific set of regulations, values or codes that make life in Lithopy safe and frictionless, participants demanded respect to their social and individual agency. We describe this demand as call for “experimental algorithmic citizenship” that we explored in 2020 over a hybrid and public sandbox. The experimental algorithmic citizenship involves continuous deliberation upon, but also prototyping and testing of blockchain services.

The failure of the original simulation game with stakeholders practicing anticipatory governance to agree upon scenario changed the goal of the data collection processes. From identifying scenarios for anticipatory governance of blockchain services, Lithopy became a tool for participatory and co-design-oriented engagements in regulatory sandbox and environment for mixing code and regulation.

2.3 Different Formats of Engagement

The several iterations of the Lithopy project followed different formats of public engagement in issues of algorithmic governance. The first iteration was the exhibition from March till November 2019 of Lithopy as an installation in two locations (Italy, Czech Republic) followed by five workshops on the stakeholder game (Germany, Israel, Bulgaria, USA, and the Czech Republic) in universities, museums, festivals, and hackerspace settings. In the installation, visitors interacted with the blockchain services over a dashboard by becoming citizens of Lithopy and offering imaginary assets and partnerships in the blockchain ruled village. In the workshops, participants used templates of functional smart contracts to learn the basics of Hyperledger Fabric

¹ Documentation of the code, forms and training material <https://github.com/anonette/lithopia>

permitted blockchain services and give feedback on the type of regulations they wish to see in their community.

The original hypothesis [36] that the primary purpose of this simulation is to enable stakeholder negotiation over blockchain futures as a form of anticipatory governance proved unrealistic. Participants expressed frustration with the simulation and their roles because of their strong personal opinions and attitudes towards intrusive technologies in general. Based on the 2019 workshops, we realized that the majority struggles to understand the infrastructure and there was never enough time to support the engagement between the stakeholders. Rather than learning code or regulations, participants expressed a wish for an interface or system that allows them to translate their personal views and feedback directly into both, the regulation and code. They felt overwhelmed by the impossibility of catching up with all the necessary skills to influence the future development of the blockchain services (in the questionnaire we had 5 explicit calls for improving code literacy).

3 Algorithmic Governance: Users and Stakeholders

To respond to this need for direct engagement with the blockchain services over natural language without becoming experts in programming or governance, we decided to transform the simulation into a sandbox. Regulatory sandboxes support stakeholder interactions over stakes and interests that directly influence the code and regulations. In this sense, they embody what one of the 2019 participants described as an actual interface that translates the natural language (values or goals) into regulations but also code (infrastructure) and enables the different stakeholders to give feedback in parallel about the algorithms, data, code and regulations. Based on the discussion and feedback, we modified the original emphasis on the future (anticipatory) blockchain governance and scenarios described in our early articles [36], [38]. We redefined the whole environment as a hybrid sandbox for experiencing citizenship and personal agency under one discriminatory contract that participants have to figure out how to regulate.

The contract that attracted attention and became central in the sandbox was the ownership of a property. We used this contract to include a discrimination that prevents selling and buying of property by anyone who identifies as “Czech”. Participants then followed a questionnaire on various strategies how to identify such bias and discrimination in the code and how to mitigate the problem on a level of regulations. While familiarizing with the regulations and the smart contracts, participants decided on which level to regulate it (blockchain architecture, community, industry, market, and government). The goal was to improve the blockchain governance in their imaginary village by providing feedback which we gathered in 2020 and visualized in the Tableau Story.

3.1 Stakeholder Cards

In the first three 2019 workshops, we assigned stakeholder roles to the participants (see Figure 1) to protect their privacy in the research, but also to simulate the potential conflicts that will lead to the collaborative future scenarios. The 12 stakeholder cards and roles described the different expectations and attitudes towards blockchain and Distributed Ledger Technologies (DLTs) broadly defined as “positive,” “negative,” and “neutral”.

The roles had ambiguous relations to technology and regulations even if their overall attitude was described as “positive” or “negative”. For example, the police chief interest in safety and security issues meant a positive attitude towards timestamping of the body camera content (prevention of tampering with data) but s/he was also worried about new types of cybercrimes. Similarly, the data regulator had a mission to audit how the new services fit the existing EU data protection framework, such as General Data Protection Regulation (GDPR). S/he experienced however a clash between the protection of fundamental rights and another government policy promoting innovation, transparency, and accountability (which the blockchain supports).

We recruited participants as volunteers during conferences, workshops, and symposia related to issues of technological art, design, algorithmic governance, and public engagements in science and technology. Since many of them shared interested in technology, they often refused to play the stakeholder role in some part of the simulation and voiced their personal opinion. There was also never enough time to collaborate on the scenarios with other stakeholders.



Fig. 1. One of the 12 stakeholder cards summarizing attitudes and issues related to blockchain governance.

Typical example of such conflict between a personal opinion and the stakeholder role is the following quote: *"My hacker identity would argue for the continuation of the Lithopy blockchain system as OK because I can hack it, but myself, I would discontinue the use because it is too easy to hack. I would maybe agree only with outside*

regulations and only for easy, low stakes transactions such as exchange food for value” (Hacker stakeholder in workshop 2). In the last two workshops, we abandoned the stakeholder roles. This improved the focus on the individual reactions, especially to the biased code in the contracts and made the experience more realistic. It generated more concrete ideas on how to combine code with regulations to prevent the biased and discriminatory smart contracts.

3.2 Principles and Rules

When facing the discriminatory contract, participants insisted on principle-based regulations that are aspirational rather than rule-based. They demanded a change of how code and regulations are designed and implemented (we interpreted this as a call for sandboxes) rather than only improve some rule (such as that the services should not include nationality as data point). In the discussions, this was often described as a need to level up the whole process of designing the new services to include more citizens and stakeholders in the process and not rely only upon experts.

Instead of concrete, code or policy-based interventions and rules, the participants demanded an environment, in which they will be heard and respected as stakeholders rather than only users of future services. Instead of frictionless design or software embedded with various values that reduce the citizens to users of future service, the participants demanded interfaces and environments, in which policy and design play an equal part. We decided to use the model of regulatory sandbox environments for their ability to engage the users as stakeholders in testing and auditing the services rather than insisting on the scenarios of common future [36].

3.3 Regulating Discriminatory Smart Contract

The purpose of the discriminatory smart contracts was to show how easy is to include a bias in the code and that often this remain invisible. We intentionally immersed the participants in the actual code of the smart contract written in JavaScript and Hyperledger Composer object-oriented modeling language to provoke the participants. The variables were readable (owner, newOwner, LithopyPlace) and the logic simple.

Most participants (28) in 2019 had not programming experience, and while they appreciated the readability, many felt uncertain about what they missed when reading the code and, and at various points, refused to engage with the code. After showing and explaining the blockchain system and the actual code of the application (smart contract for changing ownership of an asset), we asked the participants to create an adversary or evil “smart contract” that contains a bias. We used a simple example to show how easy is to introduce such bias in the managements of assets/properties in the village. Not one of the non-programmers in the workshop ever tried to work with the code even when we spend time and effort to explain the logic and tried to propose some help in influencing the code.

3.4 “newOwner.origin !== 'Czech'”

The command “newOwner.origin !== 'Czech'” excluded people based on their nationality from property transactions. It made structurally impossible to get a property in the “smart village” as Czech. Participants in all workshops reacted to this adversary code with lengthy group discussions about the dangers of data collection and personal information used in such future services. They became increasingly concerned that such bias is maybe difficult to spot, especially when the code of the service is not open source.

The discussion on making the contracts open-source and supporting transparency led to a new insight that it is unclear (at least in Lithuania) who is responsible for auditing the code of the services, to whom they should report and who makes the decision on the change on the level of code. Part of the participants (5) insisted that because of this uncertainty, smart contracts should be limited only to specific (less sensitive) domains, but not personal relations (marriage, property). Part of the participants also insisted on deploying contracts only after we clarify the regulations (3). Most reactions were less concrete in terms of steps and not very actionable in the case of the imaginary village.

Before playing with the template of the biased contract, most participants (25) feared surveillance and lack of privacy in front of the satellites (which they saw as a prominent scenario in the design fiction movie). The initial discussions were full of mistrust of both regulatory bodies and the developers of the services. After exploring the “evil” smart contract participants became more interested in the actual issue of auditing the code and data in the smart contracts, ledgers and databases.

We consider this sudden emphasis on auditing (by participants in 2019 and 2020) directly connected to the actual experience of prototyping and engaging with the code. The typical reaction at the start of the workshop after showing the design fiction movie would be: “No way! Privacy, costs that are not known, filming me all the time (the reasons for this refusal)” (stakeholder Mayor in workshop 2) or “No, it is very problematic to feel free or perform your own identity to be under control all the time” (stakeholder Editor in workshop 2). After prototyping, the reactions were typically less about the fear from a particular technology and more about the importance of preserving the democratic institutions and values: “I would argue for continuing with blockchain-based systems but only with outside regulations. A balancing act seems to be required. Government regulations, in a sense. Would depend on the type of government. I would desire less such a system if it was a fascist dictatorship that could push unethical regulation and design them into the code” (stakeholder Citizen in workshop 2).

The demand for an outside (offchain) regulation was particularly strong in the debates (and from 17 participants in the questionnaire). In one case this included a particular, concrete and restrictive clauses: “1. you can't fly your own drones, all drones need approval 2. contracts can't be overturned without outside approval 3. you can't make a contract to do something illegal” (stakeholder Policeman in workshop 2). This stakeholder also demanded that blockchain and satellites services in Lithuania are de-

signed by public institutions (or through a public-private partnership). If that is impossible, s/he would infiltrate the private companies as a security prevention: “The developers should work on the architecture with government officials to introduce very strict centralized blockchain system... in order to achieve control, I will choose to infiltrate the development group to have better understanding and influence, ability to report.”

The original question whether we should reduce all regulations to code or insist on institutions as safeguards from code turned into a search for more pragmatic and hybrid combinations of regulations and code that emphasized audits. The research transformed from understanding anticipatory governance of blockchain services via scenarios over simulated stakeholder roles to a blockchain sandbox for individual experiences with algorithmic governance and for gathering individual feedback.

4 Programming, Auditing, Regulating

The participants in the first three 2019 workshops questioned the sharp dichotomies of code (algorithms) and regulations (norms, laws), networks (infrastructure) and institutions and the whole idea of old and new forms of governance (without or with technology). They viewed the issue of governance as a problem of asymmetric control over both, the regulation and code, that gives too much power to the experts. The legitimacy as the primary purpose of regulation and law, meaning preventing the arbitrary decisions by influential stakeholders, was clearly failing in the case of regulation of new blockchain systems prone to numerous scandals around forks and forking.

Legitimacy is also an issue for the strict government interventions and regulations that ban certain technologies and try to protect the absolute state sovereignty in defining standards, norms, and rules. The regulations can create a different asymmetry of power and arbitrary decisions made by the policy “elites” that simply know how to tweak the governance system.

4.1 Independent Audits

In the five 2019 workshops, only 2 participants from the 18 that left some written feedback chose strict government interventions as a model for the anticipatory governance (in the group discussions this was a minority). One of the participants (number 13 who refused a stakeholder role in workshop 4) expressed this as a general preference for a “slow regulation” and neutrality: “*Automated contracts seem to be dangerous. As bad as non-automated bureaucratic systems go, their slowness and need for constant intervention can sometimes work as a check and balances system.*” The participant changed his/her opinion on the regulation after prototyping some of the contracts and emphasized the importance of non-government organizations and codes of conduct that can also slow down and “*introduce friction that ensures a proper review.*” The extreme call for strong government regulation was expressing a need for a process that creates friction and slows down the automation (like in blockchain mining) rather than insisting on the necessity of government institutions.

The majority (14 out of 18 that left written feedback in the questionnaire) preferred more hybrid arrangements between the onchain and offchain regulatory processes. Popular category in the questionnaire was on independent auditing of the code and data supported by certification processes to create public trust. The category of audits was also supported by the majority of the participants in the more structured 2020 workshops as we can see on Tableau story 4d “Future of RegTech Preferences” (31% consider it as a priority and 20% as very important)².

4.2 Audits as Hybrid Tools of Governance

Rather than preventing the interactions of code and regulations or reducing everything to one side, most participants called for hybrid, democratic and open design and policy processes that address both in parallel. In 2019, this led to discussions on how to involve non-experts and the natural language in the process of auditing the services without reducing this only to experts in the regulations or code.

The emphasis on involving non-experts was crucial for many participants in the discussions and while some viewed this as an issue of increasing literacy, most emphasized the “friendly” interfaces for influencing both code and regulations that also allows public audits. This “translation” of code and regulations into the natural language was viewed as the most important intervention that would make the blockchain futures in the Lithopy democratic.

In the final 2020 iteration of the Lithopy as a design and policy sandbox instead of only asking how many participants prefer audits, we also offered two forms of “auditing”: one happening ex post (lean model of development and regulation on the go after implementation of the code) and the other happening in a regulatory sandbox before implementation (with emphasis on defining algorithmic “accountability,” improving the system specifications and testing how it behaves under different conditions).

4.3 Audits Supporting Friction or Design Interventions

The two 2020 workshops provided more structured data from 59 participants visualized on Tableau and published as a dataset³. Majority (72%) demanded a sandbox (and 19% viewed this as priority) while only 12% expressed trust in the common “lean” model of implementation of new algorithmic services (Tableau story slide 6. “RegTech via Audits: overview”). The participants insisted (47% as a priority and 27% as very important) on audits that probe the “robustness of the algorithms (bugs, vulnerabilities)” via security and penetration testing methods or code reviews (software quality assurance). It was surprising that despite the calls for hybrid regulation and code interventions and support for the sandbox, regulation was perceived as a technical matter rather than a compliance intervention (the lowest number 31% views “regulatory compliance” as a priority in such audits).

² AlgoGov Research Data from Lithopy sandbox, Tableau story <https://tiny.cc/lithopy>

³ <https://tiny.cc/lithopy>

The participants who preferred the technocratic audits of the code also expressed strong preference for checking the transparency and quality of the data (54% of them) and the accountability of the governance structure of the platform (50%) (Tableau story slide 7. “What to audit and how?”). This emphasis on well-designed and transparent system that makes impossible attacks, misuses, and mistakes was surprising. Rather than friction and “slowness” (regulatory compliance), the participants seem to support the goals of frictionless and anticipatory design [39], [40]. Despite their experience with discrimination and bias, they still expected this to be solved on the level of code but under more public oversight.

4.4 Independent Audits or Institutional Oversight

Majority of participants in 2019 expressed a keen interest in the possibility of independent audits of the code and data before they are offered as a service to the public. While few imagined (9 responses) that this can be done by an independent institution (NGO) that is responsible to the Lithopy government, there were also proposals for a government agencies that use testnet (testing network for decentralized blockchain services), on which representatives of the smart village can explore and test the contracts before implementation (2 responses).

The public audit of the contracts conducted by government lead directly to the idea of a public sandbox for algorithmic governance. Few of the proposals (6) also advocated hybrid combination of technology and policy in the auditing process, AIs and humans following the inputs and outputs of data. The importance of auditing the code and data by independent institutions was expressed followingly: “*There should be an auditing body that follows the regulation and jurisdiction, in which the contract is operating. (In algo-governance) we need to insist on a democratic process and 360-degree feedback, the involvement of individuals... even in the code*” (stakeholder Hacker in workshop 2).

Others emphasized a more hybrid, technology and governance driven mechanism for auditing: “*I would prefer some auditing and certification requirements to e-incentivize industry to self-organize... as with most anything, I believe a multi-stakeholder action approach can result in the most balanced approach geared to support long terms capability*” (stakeholder Citizen in workshop 2). This participant also ticked auditing and “penetration testing,” a form of audit common in the security industry as an appropriate model for regulating Lithopy and emphasized the importance of government and industry agreements.

The importance of independent auditors as the translators of our natural languages concerns and hopes into laws and regulations but also code was most clearly expressed by the following participant: “*Perhaps the system should not allow access before you are 18 or 16? In the auditing, we need someone to translate what the coders make and explain it to the lawyers and some litigators invested in civil rights that will review the code.*” (stakeholder from an NGO in workshop 2). This participant also gave feedback about the workshop as “*ideal for coders who need to understand social ramifications of what they are building through code, but democratic future is*

ensured by involving public servants in it, they should be the one telling the coders what contracts to code."

In the two 2020 workshops (Tableau story 6d "Audit values and priorities") , the "independence of the auditing body" was a high priority (41%) followed closely by more technocratic attention to the "transparency of data" (44% consider it a priority) and security of the services (44% consider it a priority). The 2020 sandbox as a hybrid environment for improving both code and regulations and exploring algorithmic citizenship showed that the participants had low trust in government interventions in Lithuania. They demanded a better cooperation with the industry that would improve the services under the guidance of independent organizations.

5 Conclusions

The extremes of "governance by design" (code) and "policy by moratoria" (regulation) lead to arbitrary exercise of power and loss of legitimacy. To support transparent and just policies guiding the future services and algorithmic governance we need environments and services that engage the public with both, code and regulations and support independent audits that balance the principles with the implementation of the rules.

What the workshops in 2019 and 2020 show is the value of public engagement in these governance and regulation process that influence the code and future infrastructure. The current emphasis on ethical frameworks for algorithmic governance often supports only the aspirational values and principles and fails short in implementation or the design of the rules in code and regulation. The technocratic insistence of trustless networks or smart cities solving all policy issues on the level of code reduces everything to such issues of rules. The problem with rules without principles and aspirations is the emphasis on efficiency ignoring any issues of legitimacy. The workshop showed that there is a need for more hybrid approach that emphasizes public oversight and agency to influence and transform the code and regulations.

We need tools and environments that combine the aspiration value of the principles with the rules and pragmatic choices we make on the level of code and algorithms. The future of algorithmic governance is neither about inventing the ideal consensus mechanism nor about more stringent consumer privacy protection laws (such as US Federal Trade Commission or similar EU regulations related to GDPR). No consensus mechanism or service will ever prevent a future fork that will defraud part of the users. Neither will \$5.0 billion settlement with Facebook prevent future algorithmic scandals and excesses. The challenge we identified in our 2019 and 2020 workshops is to create a public space and environment (described as sandbox) where citizens can experience, understand, test, and improve such future infrastructure and policy in parallel.

Public sandboxes for connecting policy and design have the potential to improve the trust in public institutions but also technical infrastructure by allowing the participants to experience and identify the preferred form of algorithmic citizenship in near-

future scenarios. Such environments allow participants to anticipate and prevent problems and excesses rather than create ex-post or ex-ante regulations.

The main problem in the current attempts to combine regulations and code is their democratic deficit and ahistorical narrative (often inspired by game theory concepts or ideas of crowdsourcing or “crowd-pleasing” public sentiments as something that is constant). These deficits of algorithmic governance show the limits of all “rules-based systems” no matter if they use code or law. If our goal is to preserve a free and democratic society, it is not enough to concentrate only on the concrete regulations that fit the existing public sentiments, nor the technological solutions supported by powerful lobbies and platform owners.

This research identified the possibility of a public sandbox as an environment that enables stakeholders and citizens to influence how code and regulation are actually created and implemented. Rather than insisting on more security/penetration testing or more stringent laws (that are often impossible to implement), we need to increase the direct and public engagement with both, regulations and code, based on independent audits that support the division of powers.

The purpose of a hybrid and public sandbox is to support experimental forms of algorithmic citizenship. Only when we level the grounds for different stakeholders and citizens to engage over code and regulations, they can form a community or a future “smart village”. Whether we can achieve this by supporting more code and regulation literacy or by concealing them and translating them through interfaces, procedures, and intermediaries into natural languages remains a challenge.

ACKNOWLEDGMENTS

The design fiction work was supported by the Czech Ministry of Culture and the Czech Industrial Design Museum. The research into anticipatory prototyping, governance, and design is supported by Horizon 2020 Marie Curie Individual Fellowship (793059) “Anticipatory design and ethical framework for Distributed Ledger Technologies (blockchain or DAG) and applications (smart contracts, IoTs and supply chain)”.

References

- [1] J. Danaher *et al.*, “Algorithmic governance: Developing a research agenda through the power of collective intelligence,” *Big Data Soc.*, vol. 4, no. 2, p. 205395171772655, Dec. 2017.
- [2] S. Hassan and P. De Filippi, “The Expansion of Algorithmic Governance: From Code is Law to Law is Code,” *F. Actions Sci. Reports*, no. Special Issue 17, pp. 88–90, Dec. 2017.
- [3] M. Ziewitz, “Governing Algorithms: Myth, Mess, and Methods,” *Sci. Technol. Hum. Values*, vol. 41, no. 1, pp. 3–16, 2016.
- [4] A. Sinnreich, “Four Crises in Algorithmic Governance.” 2018.
- [5] K. Yeung, “‘Hypernudge’: Big Data as a mode of regulation by design,” *Information*,

- Commun. Soc.*, vol. 20, no. 1, pp. 118–136, Jan. 2017.
- [6] K. Crawford and J. Schultz, “AI systems as state actors,” *Columbia Law Rev.*, vol. 119, no. 7, 2020.
- [7] B. D. Mittelstadt, P. Allo, M. Taddeo, S. Wachter, and L. Floridi, “The ethics of algorithms: Mapping the debate,” *Big Data Soc.*, vol. 3, no. 2, p. 205395171667967, Dec. 2016.
- [8] J. A. Kroll *et al.*, “Accountable algorithms,” *University of Pennsylvania Law Review*, vol. 165, no. 3. University of Pennsylvania Law School, pp. 633–705, 01-Feb-2017.
- [9] L. D. Introna, “Algorithms, Governance, and Governmentality: On Governing Academic Writing,” *Sci. Technol. Hum. Values*, vol. 41, no. 1, pp. 17–49, Jan. 2016.
- [10] M. K. Lee, A. Jain, H. J. I. N. Cha, S. Ojha, and D. Kusbit, “Procedural justice in algorithmic fairness: Leveraging transparency and outcome control for fair algorithmic mediation,” *Proc. ACM Human-Computer Interact.*, vol. 3, no. CSCW, Nov. 2019.
- [11] B. Shneiderman, “The dangers of faulty, biased, or malicious algorithms requires independent oversight,” *Proceedings of the National Academy of Sciences of the United States of America*, vol. 113, no. 48. National Academy of Sciences, pp. 13538–13540, 29-Nov-2016.
- [12] D. L. Burk, “Algorithmic Fair Use,” *Univ. Chicago Law Rev.*, vol. 86, 2019.
- [13] R. Binns, “Algorithmic Accountability and Public Reason,” *Philos. Technol.*, vol. 31, no. 4, pp. 543–556, Dec. 2018.
- [14] N. Diakopoulos, “Accountability in algorithmic decision making,” *Commun. ACM*, vol. 59, no. 2, pp. 56–62, Feb. 2016.
- [15] M. K. Lee *et al.*, “Webuildai: Participatory framework for algorithmic governance,” *Proc. ACM Human-Computer Interact.*, vol. 3, no. CSCW, pp. 1–35, Nov. 2019.
- [16] M. Sloane, E. Moss, O. Awomolo, and L. Forlano, “Participation is not a Design Fix for Machine Learning,” Jul. 2020.
- [17] M. Hildebrandt, “Algorithmic regulation and the rule of law,” *Philos. Trans. R. Soc. A Math. Phys. Eng. Sci.*, vol. 376, no. 2128, 2018.
- [18] A. Cavoukian, “Privacy by Design - The 7 foundational principles - Implementation and mapping of fair information practices,” *Inf. Priv. Comm. Ontario, Canada*, p. 5, 2009.
- [19] I. Rahwan, “Society-in-the-Loop: Programming the Algorithmic Social Contract,” Jul. 2017.
- [20] I. Rahwan, “Society-in-the-loop: programming the algorithmic social contract,” *Ethics Inf. Technol.*, vol. 20, no. 1, pp. 5–14, Mar. 2018.
- [21] N. Elkin-Koren, “Contesting algorithms: Restoring the public interest in content filtering by artificial intelligence,” *Big Data Soc.*, vol. 7, no. 2, p. 205395172093229, Jul. 2020.
- [22] F. Fitsilis, *Imposing Regulation on Advanced Algorithms*. Cham: Springer International Publishing, 2019.
- [23] F. Fitsilis, “Administrative and Judicial Decisions on Advanced Algorithms,” 2019, pp. 25–53.
- [24] B. W. Wirtz, J. C. Weyerer, and C. Geyer, “Artificial Intelligence and the Public Sector — Applications and Challenges,” Jul. 2018.
- [25] L. Edwards and M. Veale, “Enslaving the algorithm: from a ‘right to an explanation’

- to a ‘right to better decisions’?”
- [26] M. Aitken, E. Toreini, P. Carmichael, K. Coopamootoo, K. Elliott, and A. van Moorsel, “Establishing a social licence for Financial Technology: Reflections on the role of the private sector in pursuing ethical data practices,” *Big Data Soc.*, vol. 7, no. 1, p. 205395172090889, Jan. 2020.
- [27] D. McQuillan, “People’s Councils for Ethical Machine Learning,” *Soc. Media + Soc.*, vol. 4, no. 2, p. 205630511876830, Apr. 2018.
- [28] D. W. Arner, J. N. Barberis, and R. P. Buckley, “FinTech and RegTech in a Nutshell, and the Future in a Sandbox,” *SSRN Electron. J.*, Jan. 2018.
- [29] E. Gromova and T. Ivanc, “Regulatory sandboxes (Experimental legal regimes) for digital innovations in brics,” *BRICS Law J.*, vol. 7, no. 2, pp. 10–36, 2020.
- [30] T. Hagendorff, “The Ethics of AI Ethics: An Evaluation of Guidelines,” *Minds Mach.*, vol. 30, no. 1, pp. 99–120, 2020.
- [31] J. Fjeld, N. Achten, H. Hilligoss, A. Nagy, and M. Srikumar, “Principled Artificial Intelligence: Mapping Consensus in Ethical and Rights-Based Approaches to Principles for AI,” *SSRN Electron. J.*, Feb. 2020.
- [32] D. K. Mulligan and K. A. Bamberger, “Saving governance-by-design,” *California Law Review*, vol. 106, no. 3, pp. 697–784, 2018.
- [33] B. Friedman and P. Kahn, “Value sensitive design: Theory and methods,” *Univ. Washingt. Tech.*, no. December, pp. 1–8, 2002.
- [34] J. Hee-jeong Choi, L. Forlano, and D. Kera, “Situated Automation,” in *Proceedings of the 16th Participatory Design Conference 2020 - Participation(s) Otherwise - Volume 2*, 2020, pp. 5–9.
- [35] K. Shilton, “Engaging Values Despite Neutrality,” *Sci. Technol. Hum. Values*, vol. 43, no. 2, pp. 247–269, Mar. 2018.
- [36] D. R. Kera, “Anticipatory policy as a design challenge: Experiments with stakeholders engagement in blockchain and distributed ledger technologies (bdlts),” in *Advances in Intelligent Systems and Computing*, 2020, vol. 1010, pp. 87–92.
- [37] D. Reshef Kera, “Sandboxes and Testnets as ‘Trading Zones’ for Blockchain Governance,” pp. 3–12, 2020.
- [38] D. R. Kera, P. Šourek, M. Kraiński, Y. Reshef, J. M. C. Rodríguez, and I. M. Knobloch, “Lithopia,” in *Extended Abstracts of the 2019 CHI Conference on Human Factors in Computing Systems - CHI '19*, 2019, pp. 1–6.
- [39] G. Lgd, “4. What’s going on in the design world: The Frictionless Cult,” *Medium*, 2016. [Online]. Available: <https://medium.com/re-introducing-frictions-in-design/4-what-s-going-on-in-the-design-world-the-frictionless-cult-21e527aa9abe>. [Accessed: 07-Feb-2019].
- [40] A. Monus, “Anticipatory Design: The Opportunities and Risks,” *Hongkiat*, Dec-2018.

Prototype system for remotely monitoring and managing second-hand clothing collection containers

Ismael Martin Martín¹, Gregorio López López¹, Sergio González Jiménez¹, and Brice Corrieu²

¹ Departament of Electronics, Automation and communications, Universidad Pontificia Comillas ICAI-ICADE

² Sigfox, Spain

Abstract. The current collection of second-hand clothes containers that Cáritas has distributed throughout the Community of Madrid presents some inefficiencies. Through the remotely monitoring of these containers, this project intends to address and reduce them. To do this, a study of the different alternatives on the market is carried out and a prototype is developed to check the functionality of the system. The system is composed of three different parts: a hardware or device composed of an ultrasound sensor that sends the free capacity of the container through the communications network of Sigfox to its own back-end. By creating a callback this message is redirected to the Microsoft Azure cloud platform where it is processed, stored and displayed. In addition, the user can know the capacity of the containers through a web application or front-end and create optimized routes based on this information.

Keywords Arduino MKRFox 1200, Azure IoT Hub, Azure Blob Storage, Azure Maps, Azure Time Series Insights, back-end, Cáritas, Digitalization, front-end, monitoring, Sigfox

1 Introduction

This study is part of the Moda Re- project of Cáritas Madrid, whose objective is the recycling of second-hand clothes through a network of containers distributed throughout the Community of Madrid.

Right now the clothes collection system has many inefficiencies caused mainly by the lack of knowledge about the real volume of the containers. This causes containers that are not yet full to be collected or others to get overflow, with bags of clothes accumulating on the outside. This creates a problem of clothing theft and bad image for the organization that can be solved by implementing a system to know the capacity of the containers in real time.

For this purpose, a collaboration project between Cáritas Madrid and the Fundación Ingenieros ICAI has been set up to monitor the free capacity of the containers. The aim is to provide the organization with a system to improve efficiencies through the optimization of the collection routes. The system will

2 Authors Suppressed Due to Excessive Length

consist of sensors placed in each container that will measure the space available. This data will be sent through an IoT communication network to a *back-end* platform where it will be processed and stored in order to be represented in a *front-end*.

This paper presents a first analysis of the system and the implementation of a prototype to validate results useful for future massive deployments. The developed system combines currently leader technologies such as Arduino, as hardware platform, Sigfox, as communication network, and Microsoft Azure, as Cloud platform.

The remainder of the paper is organized as follows. Section 2 presents the analysis of the different technologies and solutions available for this kind of systems and justify the technology selection in this case. Section 3 describes the design and development of a proof of concept for the target system. Section 4 presents the validation of the developed system. Finally, section 5 draws conclusions and discuss future works.

2 Analysis of the state of the art

Currently there are a large number of companies in Spain and around the world that are dedicated to the implementation of container monitoring systems. Although depending on the content and the application in particular there are many variations, all the systems are characterized by being supported by the three key pillars shown in Figure 1:

- a set of devices placed in each container that are in charge of evaluating the free capacity;
- a communications network that is used to send the data from each device to the back-end;
- a back-end where the data are processed, stored, analyzed, and represented through a dashboard.

A study of each of the parts of the system has been carried out, analysing which of the different options are optimal for the application of the project, considering both technological and economic parameters.

The first element to be decided is the communications network, since it will condition both the development of the device and the back-end. For the communication system, LPWAN (Low Power Wide Area Networks) technologies are chosen over others since they perfectly fit the application requirements (i.e., low data rates, very low consumption, high coverage) [1]. Emitting at fairly low frequency allows them to cover large areas, being able to reach all containers. On the contrary, there is a penalty in the bandwidth being able to send only a limited amount of information. Anyway, it is foreseen that one or two daily measurements will be made with very little weight each, so this would not be a restriction for the application of the containers.

Title Suppressed Due to Excessive Length 3

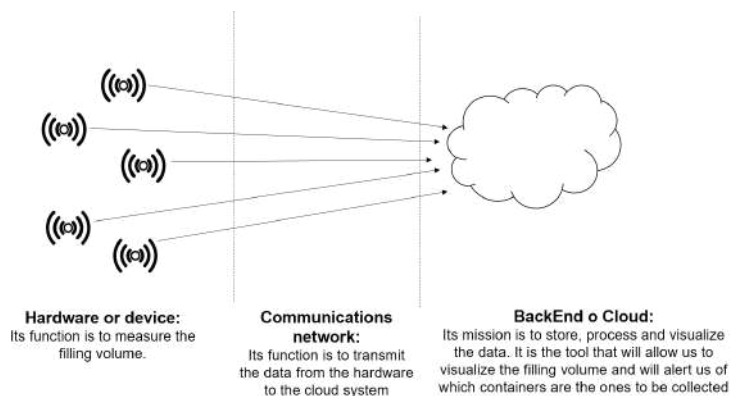


Fig. 1: Overview of the system operation

Within these networks there are two groups depending on whether the frequency band used has its use restricted or not. The MNO (Mobile Network Operator) networks use an existing telephony network and include NB-IoT and LTE-M. They provide security and reliability at the expense of higher cost [2]. On the other hand, the main non-MNO networks are Sigfox and LoRaWAN, which have cost advantages but lose reliability [3].

Despite the fact that the characteristics of all the networks are very similar for the development of the project, we have chosen the Sigfox network, which has advantages when it comes to implementation and development, since its operation is not based on SIM cards such as in the case of NB-IoT or LTE-M.

Once the communications network has been chosen, the Arduino platform was chosen for the development of the prototype due to its simplicity and cost. Among other options the purchase of a device that was too expensive for the prototype or the development of an ad-hoc board which would entail a high time and cost were considered. Therefore, the Arduino MKR 1200 was selected because it comes with a Sigfox communications chip, which facilitates communication without adding an extra communication module and is affordable. A measuring sensor is incorporated to fulfil the functionality of reading the capacity value. In addition, the battery consumption is quite low.

Finally, for the development of the visualization platform you can choose between an own development or the use of a cloud service. The latter option is chosen for its advantages in terms of cost, maintenance, commissioning time, reliability, security, and scalability. Most of the companies that sell these services have specialized services in IoT. Among the three main ones are Amazon Web Services, Microsoft Azure and Google Cloud, but the use of the Microsoft Azure platform is chosen for the development of the prototype due to its wide range of tools specialized in IoT [4].

3 Description of the developed system

After analyzing the different possibilities of implementation, it is determined that a prototype of the system based on the Sigfox communications network

4 Authors Suppressed Due to Excessive Length

will be developed. The objective is to send the free capacity data from a device to a backend where it is processed, stored, analyzed and represented in a web application.

To make a correct volume measurement it is necessary to analyze the type of sensor that best fits this application. Among the three evaluated ones (i.e., weight sensor, infrared, and ultrasound) the ultrasound sensor is chosen due to its good performance and robustness of the measurement. Its main advantage is the conical shape of the wave with which it is possible to sweep the entire volume of the container in a precise manner, as opposed to the infrared sensor which has a linear wave. For the design and development of the prototype, we have chosen to use the SRFO4 model [5]. This sensor has been connected to an Arduino MKRFox 1200 board whose function is to interpret the sensor reading and send it to the backend through the Sigfox communications network (the board itself includes a chip to facilitate communications with the network [6]).

Two tests are carried out to check the correct operation of the device. In the first one, the ultrasound sensor is calibrated by making different measurements at known distances. It is checked that the theoretical formula 1 to obtain the distance as a function of the time between sending and receiving the wave [7] fits the obtained results, with a small measurement error that can be considered negligible as it does not affect the application.

$$D(m) = \frac{t(s)}{2 \times 343 m/s} \quad (1)$$

In the second test the device is subjected to real conditions inside a container. The aim is to determine whether there is interference with the walls due to the conical shape of the wave. It is observed that there is a small maximum error margin of 6 cm when the distance is less than 70 cm. Despite this, the operation is considered correct for the application as no high accuracy is required.

For the communications part, the network used is Sigfox, as it has already been mentioned. This network is characterized by working in the ISM band at 868 MHz and being a UNB (Ultra Narrow Band) technology having low transfer speeds, of the order of 10 to 1000 bits per second, but being able to cover large areas (reaching 25 km in open field) [6].

Being in a free band one of the main problems that appear is the security and reliability. To guarantee this, each message is repeated three times with different serial numbers, thus ensuring its correct reception [8], and limiting the maximum number of messages sent to 144 per day. [9]. Another of the main advantages of the network is that it allows the location of the containers geographically by means of triangulation, obtaining approximate coordinates in the Sigfox backend. As it has been proved during the development of the prototype, the location is obtained with too much margin of error (around 1 kilometer) so the containers cannot be located based on Sigfox's triangulation.

The flow of information of the developed system is shown in Figure 2. The Arduino MKRFox 1200 sends the data to the Sigfox backend. Then, the information is forwarded to the Microsoft Azure cloud platform that allows processing and

visualization options. This will be done by means of a customised callback available in the Sigfox backend for connecting it to the Microsoft Azure IoT Hub. This callback is created by a HTTP Request of type 'text post' which sends a JSON file with the predefined variables to the IPs defined by the connection string of the previously created IoT Hub device [10].



Fig. 2: Flow of information of the system

The variables sent in this callback are the capacity value received from the device, the real coordinates obtained by triangulation of the signal on the Sigfox platform, and the assumed coordinates where the container has to be found.

Finally, this information has to be processed, stored and analyzed. To do this, the Microsoft Azure platform will be used, which has tools that allow the data to be processed in a simple, secure, and scalable way at different levels. In addition, it enables the creation of a web application in which the user is able to see the real state of the free capacity of the containers as well as their representation on a map.

Figure 3 shows the flow of information at the back-end, as well as the tools used within Azure for the development of the web app. The information is ingested in the Azure platform through the specialized tool Azure IoT Hub, from where the message is forwarded to the tool Azure Time Series Insight, which allows a temporary display and processing of information. In addition, the tool Azure Blob Storage is also used to perform cold storage (timeless but slow access) and hot storage (with a duration of 7 days but fast access) which is fed by Azure Time Series Insights. Finally, using an API, Azure Maps makes a request for the information stored and processed in Azure Time Series Insights which will then use the visualization app developed.

The Azure IoT Hub tool acts as a message center between the application and the devices, allowing the ingestion of large volumes of telemetry data from the devices [11]. Its operation is based on the creation of virtual devices with their IP address that will be connected to the real devices.

Two different devices are created for the prototype: a real device that corresponds to the device previously created by means of the Arduino board; and a simulated device that will be used to facilitate the testing tasks and that will be created by means of a virtual machine inside Azure.

This virtual machine has a Python file that simulates the operation of the container device, sending random capacity values and predefined geographic

6 Authors Suppressed Due to Excessive Length

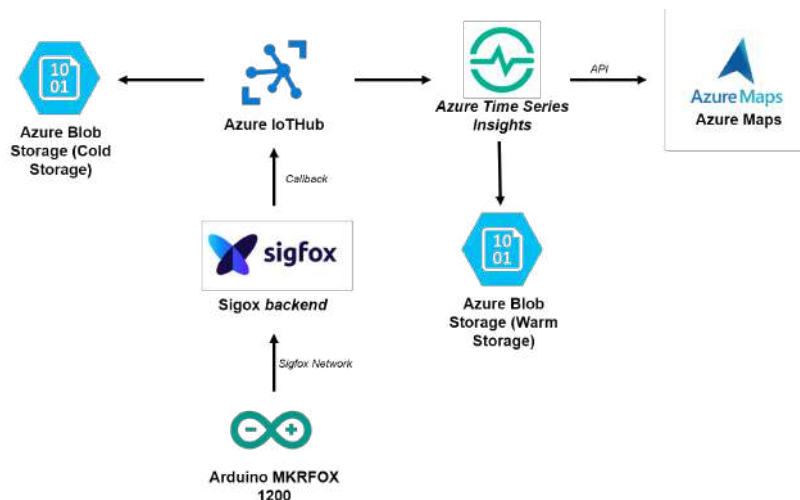


Fig. 3: Flow of information in the system

coordinates. Using the connection string of the device created in Azure IoT Hub, it is possible to send the data every time the file is executed, achieving an identical behaviour to the real device.

Once the information has been received in Azure, it has to be stored. To do this the platform has the tool Azure Blob Storage that stores the information in the form of so-called blobs (data structures that do not adhere to any particular data model or definition like text or binary data [12]). Within this tool, two types of storage will be used. On the one hand, a cold storage will be used, which allows a timeless use of the information, although it has a slower access to it. The routing of this information will be done by means of a text message brokering, which consists of assigning a text endpoint to the container for storing the information [13]. On the other hand, all the information is going to be stored in a hot storage for a period of 7 days, since the tool Azure Time Series Insights needs a quick access to the data that is only achieved with the hot storage.

To perform temporary processing and to be able to view the data, the use of another Azure tool is required: Azure Time Series Insights. This module is responsible for the collection, processing, analysis and consultation of data obtained from the containers. It is designed mainly for the needs of the industrial IoT, with tools such as multilayer storage, time series modelling, or low-cost queries [14].

For the configuration of this tool, it has been taken into account that the environment used is PAYG (Pay-as-you-go)[15], where the payment is based on the data input, the time series are identified based on the device ID of each device and a hot storage will be created to store the information so that it can be processed efficiently.

The last tool used is Azure Maps that provides geospatial functionalities by using maps with the objective of providing a geographic context for the

Title Suppressed Due to Excessive Length 7

application of the container [16]. The subscription is free and only has a cost when the number of requests is very high.

The final objective of the system is to be able to know the volume status of the containers in real time in order to optimize the collection routes. That is why it is necessary to develop a front-end or web application through which the user is able to visualize the information and manipulate it in a simple way. The development of it has been based on the Microsoft project Azure IoT Workshop: Real-Time Asset Tracking [17]. The web application is developed in an HTML environment to which several functionalities have been applied using Javascript. Many of these functionalities have been based on Azure Maps' Microsoft SDK examples' [18]. To obtain the data, both spatial and temporal, an API call to the Azure Time Series Insights and Azure Maps is used.

The main functionalities of the application are the obtaining of the capacity data, the location of the containers in a map, the visual representation of the state by means of a colour code, the representation of temporal graphics that show the evolution, and the creation of routes between the points that need to be collected.

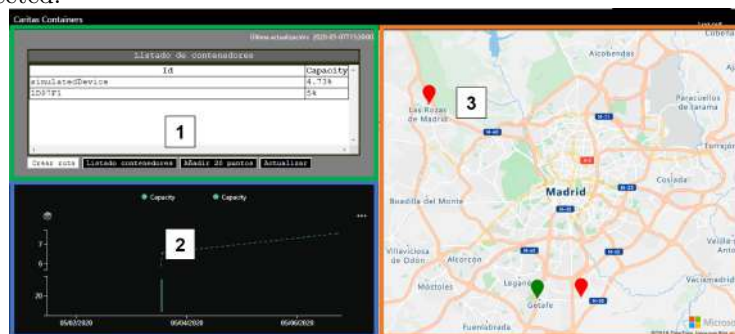


Fig. 4: Web application

In the web application shown in the Figure 3, three different areas can be distinguished:

- a user interface in which the containers and their capacity are visualised and some buttons that allow access to the different options of the application (zone 1 - green);
- a zone where the temporal evolution of the different containers is shown (zone 2 - blue);
- and a map in which the containers and their capacity are geographically represented based on a colour code (zone 3 - yellow).

The basic functioning of the application is shown in the diagram represented in Figure 5. When the application is executed, the capacity and location data are obtained from Azure Time Series Insights and with them the marks are created on the map, the values are written in the user interface table, and the time series are drawn. At this moment the program remains in a waiting position until a button is pressed in the user interface that executes some functionality of the application.

8 Authors Suppressed Due to Excessive Length

If the button 'Create route' is pressed, a route is created going through all those containers whose free capacity value is lower than 20 %, starting and ending in the Getafe base ship. This route is represented on a map and in the table of the user interface the containers appear in order of collection. Pressing the button 'container list' will return to the initial table showing all containers regardless of whether they have exceeded their capacity limit or not.

To check the correct operation of the application the option to 'Add 20 points' has been added which creates 20 bins with a random capacity. Finally, the 'Update' button repeats the reading process and executes the application with the last values obtained.

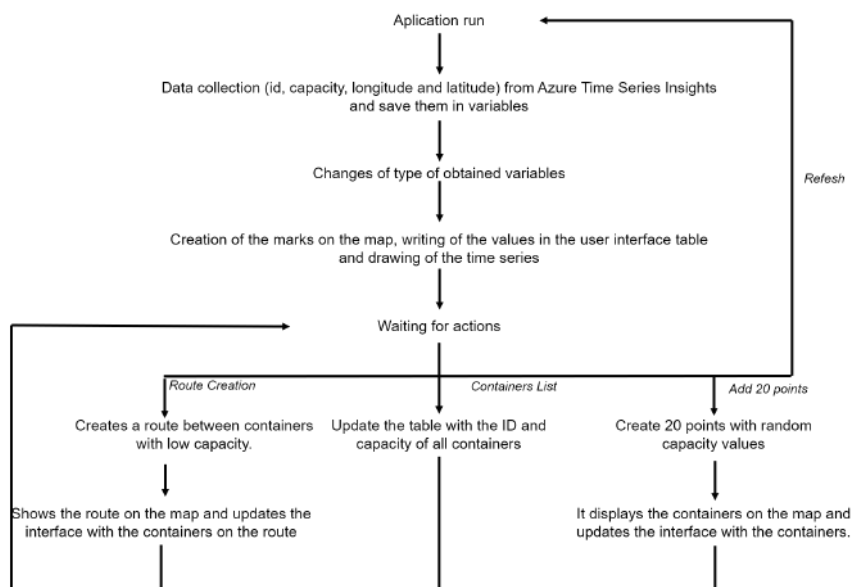


Fig. 5: Diagram of how the web application works

4 Validation of the developed system

The aim of this paper is to carry out an initial analysis of the viability of the Caritas project to monitor the clothing containers that are distributed throughout the Community of Madrid. The final objective is, therefore, to validate the future implementation of a system that will allow the organization to improve the efficiency in the collection of clothes from the containers through digitalization. In this section, a functional validation of the prototype will be carried out by analysing the possible areas of improvement for the different components of the system.

For the design of the hardware device, the choice of the ultrasound sensor is considered correct since it carries out measurements with sufficient precision and the conical geometry of the wave makes it ideal for the container. It has also been proven that the 3 m range of the sensor used [5] is sufficient for the

Title Suppressed Due to Excessive Length 9

2 m height of the container and in the tests carried out it has been shown that there is no negative influence of the container. There is a margin of error when the distance is less than 70% that can reach an absolute error of 6 cm. In order to improve the device, an ultrasonic sensor with better precision can be used, although this would increase the cost of the device.

As communication network we have chosen to use LPWAN networks that offer a long range at the cost of decreasing the bandwidth. For the application of the project, where it is intended to make one or two shipments per day of little weight, this is not an impediment. We have opted for the use of the LPWAN Sigfox network. The main problem found during the development has been the loss of messages. In areas where there is good coverage the message was sent and received, but in other trials where coverage has been reduced there has been loss of messages. This is a very serious error to be taken into account as it can cause serious problems for the organization by overlooking containers that are full on the collection routes, making the system unusable. To solve this problem there are several possible solutions. On the one hand, it is possible to opt for the creation of a downlink communication when a message is expected but not received, thus ensuring a re-sending of the data when it has not been sent correctly, ensuring the correct communication. Another option consists in the implementation of signal repeaters near the containers where the coverage is low in order to ensure a good communication.

On the other hand, it has also been purchased that the device coordinates obtained during the development of the prototype by the platform are very inaccurate in cases of good coverage (obtaining an error of more than 1 Km) and null in areas where coverage is low. This makes it impossible to use the location of the network to determine the position of the containers. As a solution to this problem, the prototype has been developed so that each container ID is associated with a geographic coordinate. In this way the location obtained by Sigfox is only used in case the container is stolen and the distance has been much higher.

Anyway, the network meets the system requirements in terms of bandwidth and coverage in all areas and has the advantage of allowing a two-way communication (although more limited[9]) in case it is necessary to communicate with the device. It also has a lower cost associated with the rest of the communication networks. The Sigfox back-end itself receives all the messages and is able to redirect them automatically to the Azure back-end. It has been verified that there is a certain delay of 1 minute between the sending of the Sigfox back-end and the Azure platform, which does not exist when the sending is done from the virtual machine with the simulated device. Anyway, this delay is not an important issue and during the tests carried out no message was lost.

For the storage and processing of the data, the use of a cloud platform has been chosen over the development of an own back-end because of its advantages in terms of reliability, maintenance, and scalability. The tools Azure IoT Hub, Azure Time Series Insights, Azure Blob Storage and Azure Maps from Microsoft Azure have been used and integrated to receive, process and store the capacity

10 Authors Suppressed Due to Excessive Length

data sent both from the developed device and from the device simulated with the virtual machine. The results obtained are very good as they are tools that allow easy integration at a low cost and high scalability.

The core of the project is the web application since it is the tool that the user is going to use to know the volume of the containers in real time and to be able to plan routes accordingly. To check the correct functioning, a test mode has been developed that creates 20 containers with a random capacity between 0 and 100 percent. In this mode the program is also capable of creating routes by selecting only those containers whose free capacity is less than 20%.

Among the necessary future extensions required by the application is the development of optimal routes. The routes obtained in this first version follow an order of creation based on a list that is not optimal, since this would need the algorithms that go beyond the scope of a first validation of the project.

Finally, it is checked that the prototype meets the project requirements of being able to provide the organization with a system to monitor the free capacity of the used clothing containers in order to create optimal routes and improve the efficiency of the collection system. This system has a low economic cost since the associated costs of the hardware, communication network and back-end have been optimized. It has a user-friendly user interface so that the application is accessible to staff in the organization with any type of qualification. In addition, it is highly adaptable and scalable thanks to the use of cloud platforms that allow modifications to be made easily without the need to alter the system.

5 Conclusions and future work

Cáritas Madrid currently has around 165 containers distributed throughout the Community of Madrid in which second-hand clothes are collected for people at risk of social exclusion. In order to achieve greater efficiency in the collection of these containers, a system has been developed to monitor the free capacity for the remaining clothes. In this paper an initial analysis of this system is carried out.

Two phases have been followed in order to carry out this analysis: from an analysis of the technological state of the system to the development of a small-scale prototype and its functional validation for the application.

At first, an exhaustive study has been made of the technological state of this type of technology. For this purpose, the different suppliers of this type of system have been compared, determining what characteristics they have in common (mainly battery power and the use of an ultrasonic sensor to measure the free capacity). An analysis has also been made of what the different technologies are, in the case of a system developed ad-hoc, which are suited to the project at the level of hardware, communications system and backend. Finally, the use of the ultrasound sensor and the Sigfox communications network is determined.

A prototype is developed that has the three functional parts of this system: a device that performs the measurement, a communications network through

Title Suppressed Due to Excessive Length 11

which to send this information, and a platform on which to process, store and display the information in real time.

The objective of the development of the prototype is the creation of a test environment in which to test the functionality of this system with a view to future massive deployment. It has been proven that the implementation of a technological system that allows the collection of clothing containers in a more efficient way can bring many advantages to a non-profit organization such as Cáritas.

On the one hand, the image of the organization would be improved. Currently one of the main problems they have is that the clothes are not collected in the containers and end up accumulating in bags on the outside of them. This creates a bad image of the organization and the theft of the best clothes. This system would prevent accumulation and improve the image of the NGO.

On the other hand, it would also make more efficient use of the organisation's resources. Another problem they have is collecting containers that are still empty. With the help of the system implemented, the routes could be optimized to collect only those containers whose capacity is equivalent to 80%, achieving a reduction in the number of them. This would imply an economic saving, since it would mean a lower expense in fuel and personnel that carry out the routes, and a redistribution of the human resources to tasks where they can contribute a greater value to the organization managing to create a greater impact to the society.

With this project we want to demonstrate that the impact of digitalization and technological development can be applied to all sectors of society. A non-profit organization can also benefit greatly by applying new technologies to its humanitarian work.

Among the main future works it is the implementation and development of the complete system. In addition, it will be important to develop an algorithm with which to achieve route optimization.

In the long term, it is necessary to study the viability of the project with the company and to begin the development with a pilot phase in which possible problems can be solved. This is when a large scale implementation will be made causing a great benefit for Cáritas.

6 Acknowledgements

This project has been carried out thanks to the collaboration between the NGO Cáritas Madrid that raises the problem, the Fundación Ingenieros ICAI that channels the problem and tries to give an answer to it and the Universidad Pontificia Comillas with which this master's final project is carried out to give a solution.

It could not have been possible to carry out this work without the support of the director of the Master thesis, Gregorio López López, who has assisted at all times by giving technological and creative support to the work. We also thank Sergio González Jiménez for his collaboration as co-director.

12 Authors Suppressed Due to Excessive Length

We would also like to thank Marta Reina, manager of Fundación Ingenieros ICAI, for her actions to achieve the project and her role as a mediator between the student and the NGO.

References

- [1] Frederic Chaxel Kais Mekki Eddy Bajic and Fernand Meyer. *A comparative study of LPWAN technologies for large-scale IoT deployment*. Tech. rep. The korean institute of communications and information sciences, 2018.
- [2] Raquel Ligeró. “Diferencias entre NB-IoT y LTE-M”. In: *accent systems* (May 2018). <https://accent-systems.com/es/blog/diferencias-nb-iot-lte-m/>.
- [3] Brian Ray. “Sigfox vs. LoRa: A comparison between technologies = Business models”. In: *Link Labs* (May 2018). <https://www.link-labs.com/blog/sigfox-vs-lora>.
- [4] José Miguel Álvarez Vañó. “Modelo Comparativo de Plataformas Cloud y Evaluación de Microsoft Azure, Google App Engine y Amazon EC2”. Trabajo de fin de grado, Grado en Ingeniería Informática. Escola Tècnica Superior d’Enginyeria Informàtica, Universitat Politècnica de València, 2018.
- [5] *Documentación del sensor de ultrasonidos SRF04*. SRF04 <http://www.robot-electronics.co.uk/htm/srf04tech.htm>.
- [6] *Aprendiendo Arduino: Sigfox*. <https://www.aprendiendoarduino.com/2018/03/05/arduino-y-sigfox/>. Aprendiendo con arduino. Mar. 2018.
- [7] Luis Llamas. “Medir distancia con Arduino y sensor de ultrasonidos HC-SR04”. In: (June 2015). <https://www.luisllamas.es/medir-distancia-con-arduino-y-sensor-de-ultrasonidos-hc-sr04/>.
- [8] *Todo lo que necesitas saber sobre la seguridad de Sigfox*. <https://www.wnd-group.io/2017/02/17/todo-lo-que-necesitas-saber-sobre-la-seguridad-de-sigfox/>. WND Group.
- [9] *Sigfox: Asses your project’s needs*. <https://build.sigfox.com/study>.
- [10] *Sigfox documentation: Callback Api*. <https://backend.sigfox.com/apidocs/callback>.
- [11] *Microsoft Azure Documentation. Azure IoT Hub: ¿Qué es Azure IoT Hub?* <https://docs.microsoft.com/es-es/azure/iot-hub/about-iot-hub>. Microsoft Azure. Aug. 2019.
- [12] *Microsoft Azure Documentation. Introducción a Azure Blob Storage*. <https://docs.microsoft.com/es-es/azure/storage/blobs/storage-blobs-introduction>. Microsoft Azure. Aug. 2019.
- [13] Sergio González Jiménez. *Azure IoT Hands on Lab*. Url: <https://github.com/SeryioGonzalez/azure-iot>. IoT - Universidad Pontificia Comillas ICAI. Madrid, Nov. 2020.
- [14] *Microsoft Azure Documentation. Azure Time Series Insights: ¿Qué es la versión preliminar de Azure Time Series Insights?* <https://docs.microsoft.com/es-es/azure/time-series-insights/time-series-insights-update-overview>. Microsoft Azure. Aug. 2019.

Title Suppressed Due to Excessive Length 13

- [15] *Documentación Microsoft Azure. Detalles de precios de Azure Time Series Insights.* <https://azure.microsoft.com/es-es/pricing/details/time-series-insights/>. Microsoft.
- [16] *Microsoft Azure Documentation. Azure Maps. ¿Qué es Azure Maps?* <https://docs.microsoft.com/es-es/azure/azure-maps/about-azure-maps>. Microsoft Azure. Jan. 2020.
- [17] *Microsoft Azure Documentation. Azure IoT Workshop. Real-Time Asset Tracking.* <https://github.com/Azure/iot-workshop-asset-tracking>. Microsoft Azure.
- [18] *Azure Maps Web SDK Samples.* <https://azuremapscodesamples.azurewebsites.net/>. Microsoft.

Smart Fisheries, a key player in ocean sustainability and fair fish trade.

Javier Carvajal¹, Hugo Sánchez¹ , and Juan Carlos Martí¹

Remora Fishing Traceability, San José, Costa Rica.

jcarvajal@remoraxyz.com

<https://www.remoraxyz.com>

Abstract. Historically, the ocean has played a role in the Earth's sustainability, the socio-economic progress of the cities, and human well-being. It is estimated that oceans generate USD\$1.5 trillion annually to the overall economy. From this revenue, 25% comes from fishing activities. However, 57% of the fish stocks are fully exploited, and another 30% are overexploited, depleted, or in recovery. Small fisheries catch around 50% of the fish that is consumed in the world. Along with this problem, there are other concerns related to fair-trade, equality, and decision making. Technology can become an essential tool to improve monitoring and enhance the decision-making process since it supports the generation of regulations and public policies that contribute to environmental health, economic prosperity, human well-being, equality, and justice. In this paper, we present the concept of Smart Fisheries, how these can contribute to sustainability and fair-trade, their role in *Smart Cities* and how societies could transition to this system. We also present the efforts made by *Remora Fishing Traceability* to achieve these goals

Keywords: Ocean Sustainability · Smart Fishery · Smart Cities · Fishing Traceability.

1 Introduction

One in every six people in the World depends on the Ocean for income, food, and protection [1]. The ocean provides food, jobs, and regulates the climate. From ancient times, the ocean has become an ally in the development of cities and countries, and it still is. The Organisation for Economic Co-operation and Development (OCDE) estimates that the oceans contribute USD\$1.5 trillion annually in value-added to the overall economy. [2]. This value represents 2.5 % of the world *GVA*¹ and almost 3 % of the *GDP*². But the non-economical benefits are invaluable. Oceans are the backbone of life on this planet.

A quarter of the economic production of the oceans comes from fishing activities. According to The United Nations (UN) Food and Agriculture Organization (FAO) [1], global fish production is estimated at 179 million tonnes in 2018,

¹ Gross Value Added

² Gross Domestic Product

2 Javier Carvajal et al.

with a total first sale value estimated at USD 401 billion. From this production, almost half (96.4 million tonnes) comes from capture. The marine capture represents 87.5% from the total. From the past three years, the marine fishing has sustained growth of 5.4 %. 50% of what is extracted from the ocean comes from small scale fisheries [3].

However, unsustainable human activities jeopardizes the marine biodiversity's natural ability to replenish. FAO estimates that 57% of fish stocks are fully exploited and another 30% are overexploited, depleted, or recovering. [4]. Due to the over-exploitation of marine resources some advances in innovation have been developed to collect data on where the boats are fishing and what they are fishing. These are relevant tools to protect the marine fauna; nevertheless, these technologies are usually implemented in industrial fishing and no cost-effective versions are available for the small-scale fisheries.

Small scale fisheries catch 50% of the fish that is consumed by the World [1]. According to experts there are approximately 3.2 million small artisan boats, which measure less than 12 meters in length. A fundamental problem is that they are getting very low margins for their catch, and in over-exploited oceans this makes them spend more resources to catch the same amount or less. This is a catastrophic cycle as they could be depleting the Oceans resources while entering poorer socio-economic conditions and food insecurity. It is imperative to find radical and more sustainable approaches to help small fisheries not to catch more, but to get better margins for what they are already catching. Consumers and technology are the key elements to help the small fisheries, using the market forces to address sustainability and social development. The technology can be used to prove fishers' compliance towards sustainable practices.

In the present paper we present a concept of *Small Fishery* and how can play a role in ocean sustainability and fair fish trade.

2 What is a Smart Fishery?

Fisheries play an important role in the development of coastal areas. In a very simplistic approximation, fisheries can be visualized from two perspectives. The first one corresponds to the coupled human-nature system.

A coupled human-nature system can define as integrated systems in which people interact with natural components and that exhibit nonlinear dynamics with thresholds, reciprocal feedback loops, time lags, resilience, heterogeneity, and surprises [5].

The second one, the fishery becomes an economical productive unit that allows commercializing the product with potential costumers. Also, it organizes the communities around fishing activities. In this line, an interesting approach about the Fishery System is provided by Charles [6]. Figure 1 shows the definition of a fishery system proposed by the author.

In a second perspective, fisheries become an economic productive unit that consist in the exploitation and commercialization of natural resources towards

Smart Fisheries, a key player in ocean sustainability and fair fish trade. 3

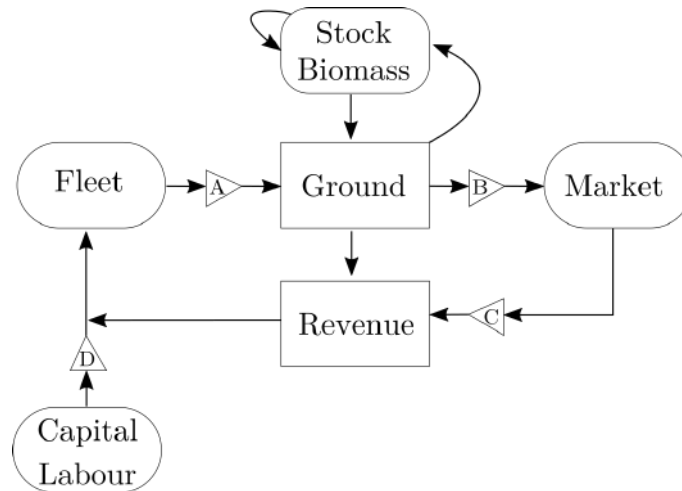


Fig. 1: Fishery System model [6]

potential customers. Mainly, it organizes the communities around fishing activities. In this line, an interesting approach about the Fishery System is provided by Charles [6] which is summarized in Figure 1 . The system includes three feedback loops, 1) the internal biological loop shows that we are dealing with renewable resources, 2) the harvest feedback loop shows that the harvest is affecting the fish stock and therefore it is affecting the future fishing possibilities, and 3) the market feedback loop where the fishing fleet is used to harvest a fishery resource. The catch brought to the market and sold is generating revenue which might be dissipated out of the system or recycled in the form of investments into the fishing fleet or fisheries. The system is simplified as it does not consider the fish processing elements that are taking their inputs from the market. Other key points in the system are the limited entry controls. There are indirect methods of fishing mortality control including restrictive licensing (*A*), catch limits control based on Total Allowable Catches (TACs)- represented by *B* - and *C*- monetary controls. The fourth regulatory position *D*, new fishing capacity entry controls, correspond to a new possibilities to integrate innovative elements into the system.

A simplification of the supply chain that complements Figure 1 is presented in Figure 2. The analysis of both schemes can contribute to the analysis and their future interventions, and also allows to find opportunities, in terms of conservation and equity. A complete analysis of these benefits and their respective interaction can be found in [7–10].

Figure 2 shows the main links of the supply chain, commonly referred to as “from the sea to the table”. The economic revenue is distributed to each segment; however, this distribution is not fair. Factors as informality, lack of financial and production information, and the participation of many actors in

4 Javier Carvajal et al.

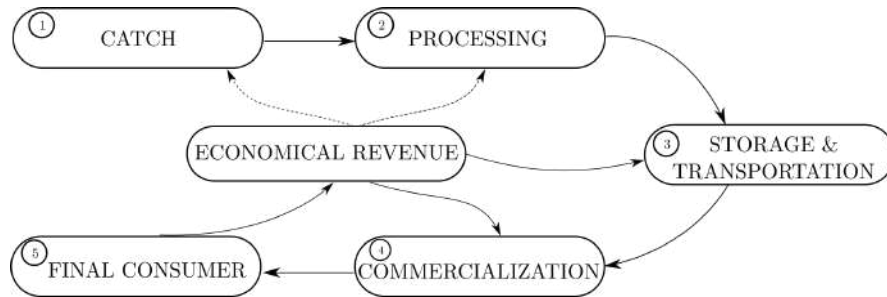


Fig. 2: Simplified supply chain for artisanal fishing activity.

the commercialization affect the distribution. The most affected by this situation are the fishers.

If the system cannot be measure, it will be not possible to control and enhance. This topic is the first of the aspects to consider a system *SMART*. The concept smart refers to five points: **S**pecific, **M**easurable, **A**greed upon, **R**ealistic and **T**ime-based [11]. In this case, the system is considered smart if its negative feedback loop is constantly working to reduce the difference between the actual and desired states (goals) of the system. An interesting approach of this principle in fishing system management is found in [12]

When the term *SMART* is mentioned, there is the misconception to think only about the adaptation of the technology in the process or system, which was the concept in the first days of Information Technology [13,14]. Nevertheless, the complexity of the systems requires more than technology to consider a system as *SMART*. It requires a synergy of economic, environmental, political, social, justice, and equity perspectives [15–17]. In this way, technology is only a tool to achieve its aim.

Enhancing a system with technology allows to obtain information that was not possible before. Technology trends such as *Internet of Things (IoT)*, *Big Data* and *Artificial Intelligence (AI)* are powerful tools to reach this purpose, but they are not the only step to consider a system as *SMART*. If there is more reliable and updated information about the real behavior of the system, it will be possible to generate better public policies and take decisions, that drive to an enhanced operation of the system. Achieving multiples aims in terms of sustainability, economics, and social progress. From this perspective it is possible to the term define *Smart Fishery*.

*A **Smart Fishery** can define as a coupled human-nature system enhanced with technology in charge of breeding, catching, or selling fish, using sustainable practices that contributes to economic prosperity, environmental health, the human well-being as well as the equity and justice.*

Figure 3 shows the smart fishery framework proposed, using as the base the framework for the smart city developed by [18]. The scheme illustrates the interaction for every component of a Smart Fishery. The first layer connects the

Smart Fisheries, a key player in ocean sustainability and fair fish trade. 5

fishermen’s communities and policies through technology in a bidirectional way. The technology can address fishermen to have sustainable practices and demonstrate that they are complying with the policies. On the other hand, it will get reliable and profitable data to the decision-makers, to get more accurate policies. The goal is not to displace fishermen, but rather to help them become more resilient by promoting efficient practices that guarantee ocean sustainability. In this way, the technology will also connect the fishermen with the final consumer, ensuring fair-trade schemes and the progression of economic prosperity and human well-being

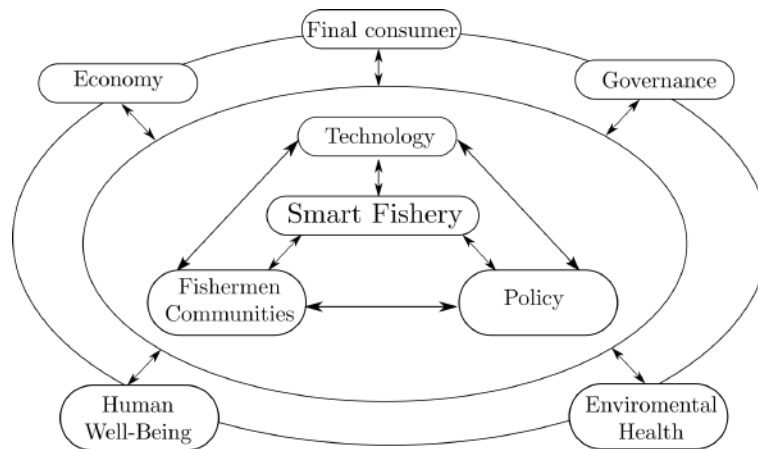


Fig. 3: Smart fishery framework.

In the next sections, there will be a review for the main points in the conceptualization of a Smart Fishery, the applications, and benefits for the implementation of this concept as well the effort made by *Remora Fishing Traceability*

3 Why a Smart Fishery could be a key player in ocean sustainability and fair fish trade?

The concept of Smart Fishery involves more than that, as it can be seen in Figure 4. As was previously exposed, the components for a *Smart Fishery* are holistic and the impact will enhance several areas. This integral approach needs to fulfill the necessities on different fronts, from the sustainability of the ocean to the socio-economic development in the fishers’ communities.

Punt and Smith [19] propose a paradigm about the extraction and sustainability in the long term. One of the problems in this paradigm is the acquisition of accurate data for these proposals. There is a lot of efforts to make biological control in fishing activities. However, this biological control is not well equipped with technology. This situation ends up in studies with small samples of the

6 Javier Carvajal et al.

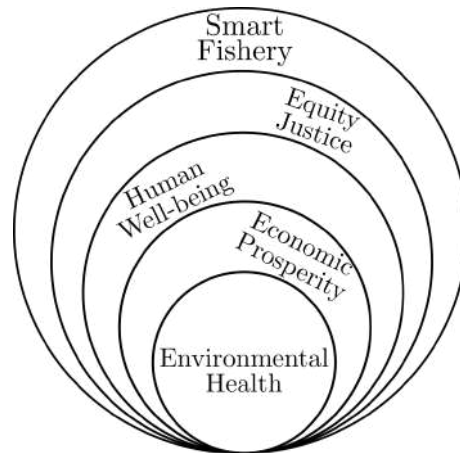


Fig. 4: Transverse axes that build a smart fishery.

data, that not reflects the real situation of the stock-fish. The lack of information becomes bigger in the small fisheries [10]. This situation is reflected in the generation of public policies, which are usually far and non updated from the real situation. Recent studies present the difficulties in the measurement for the fishery-ecosystems, due to practical challenges faced to study [20]. The use of technology trends such as *Iot* and *Big Data* can help with the problem of the data. And with this data, it will be possible to generate better studies which will provide information that supports the creation of better public policies in favor of sustainability and economic prosperity.

The second approach refers to economical revenue. As was presented in Figure 2, the simplified supply chains for a small fishery have several stakeholders. Inefficient management generates an unfair economic distribution. The disconnection between the final consumer and the fishers is significant, as most do not know where the product was caught and by whom. This reflects in the income received by the fishers, traditionally a small percentage of the final price of the product. But, the problem is not only about profit distribution. As is exposed by [21], the economic losses in marine fisheries add up to US\$50 billion per year. The study dictates: *"...Taken over the last three decades, these losses total over US\$2 trillion, a figure roughly equivalent to the GDP of Italy..."*. This because of poor management, inefficiencies, and overfishing. Well-managed fisheries can prevent more of these losses and transform into sustainable and economic benefits for the fishers and their communities.

The third point refers to the final consumer. Environmental awareness and responsible purchasing practices are becoming an important aspect to consider for the acquisition of goods. It should be a consumer's right to know the origin of the product that is being purchased. In this case, traceability would help the fulfillment of this right. Furthermore, technology facilitates a communication channel between fishermen and consumers, which could generate social interac-

Smart Fisheries, a key player in ocean sustainability and fair fish trade. 7

tion translating into opportunities and development for the coastal communities. The final consumer can choose a fish caught with sustainable practices or not. In economic terms, it is letting the market forces choose sustainable development. Market studies show an increasing interest in buying traceable fish, and even the intention of the consumer for paying more if the origin of the fish is known [22]. This can be addressed to the fishers to enhance the income that they received as an incentive about applying sustainable practices in their daily activities.

4 How to do a transition to a Smart Fishery?

As every technological transition, the transformation into a *Smart Fishery* cannot occur immediately. The problem is not just installing sensors, sending data through the internet, processing the large amount of data, and making efficient algorithms. Technology is one of many aspects to consider. Figure 5 shows the main elements involved in the transition for the *Smart Fishery*.

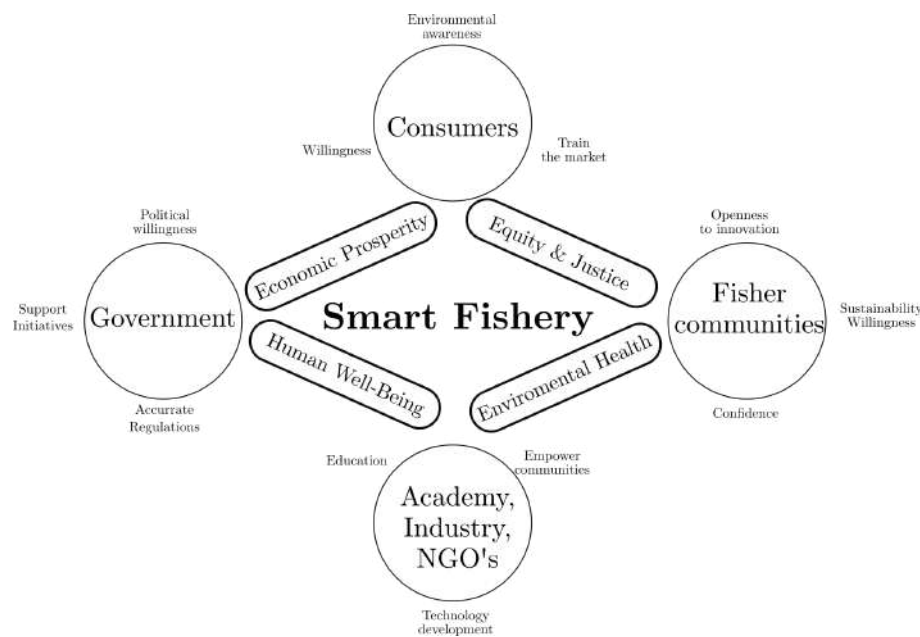


Fig. 5: Elements of a transition to Smart Fishery

There are four main sectors involved in the process. The first corresponds to academy, industry, and NGOs. In this case, they are responsible to generate knowledge, innovation, and technology for the operation of a Smart Fishery. At the same time, there are responsible to generate awareness in the fishermen communities, governments, and consumers. This is fundamental for the response

8 Javier Carvajal et al.

and cooperation of the other three elements. It is more than clear that the only way to make this possible is the establishment of collaborations between the different actors.

The second element in the transition scheme is the Government. First, it has to be concerned about the problem and show an interest for fishing sustainability. This will give the political commitment to support the innovative initiatives that the first group proposes. Also, the creation of public policies that aid in the creation and operation of Smart Fisheries. The third group corresponds to the consumers. In this case, they will have the environmental awareness and the Smart Fisheries will allow them to make better choices towards sustainably-caught fish. The final consumers are one of the most important actors as they provide financial sustainability to the model, usually covering the implementation cost of this system.

Finally, the last group corresponds to the fishers' communities. They play an important role in this transition and are the main beneficiary of the system. To achieve this, the communities must show commitment and responsibility to support this kind of initiative. They are the core of the project due to the operational functions. They are responsible to keep the Smart Fishery alive. Only the compromise of active collaboration if every group can guarantee success in the transition to a Smart Fishery.

5 Smart Fisheries as part of smart cities

As was well exposed, the term *smart* is more than just adding technology to any process. Technology by itself will not solve the problem in the small fisheries [18]. However, the opportunity to collect reliable and accurate data will help to reach the objective. Also, take appropriate decisions in many directions [16] from consumers (that buy fish captured with sustainable practices) to policy-makers (that design regulations and public policies). Smart Fisheries aim to transform one of the most ancient jobs in history into the new technological trends and getting multiple benefits in the process, including the conservation and sustainability of the ocean. A *Smart City* can be full of sensors, smart grids, autonomous cars, drones, algorithms, and other technology, but none of them will replace necessities like potable water, home, community, and food. In this way, it is also necessary to address efforts that guarantee the solvency of these necessities and efficient resource management

In ancient times, the ocean was the key to big and prosperous cities. But the modern development forgot to include coastal communities. Nowadays, most fisheries are still using the same techniques and management system that were used in ancient times, most have no management at all. This has generated the problems that were mentioned in the paper. It is time to bring the fisheries into the XXI century and with them, generate best practices in terms of sustainability, economic prosperity, equality, and justice. In a *Smart City* it is not hard to think about the possibility that when a consumer goes to the supermarket to buy seafood, this person can access the internet and see the data on when,

Smart Fisheries, a key player in ocean sustainability and fair fish trade. 9

where, how, and who caught that fish, know what percentage of the price is being distributed in the coastal communities, and if fishing practices assist in the conservation of the oceans. Even, there is evidence that the final consumers agree for paying more if they can get more information about the seafood, as is well explained by [22–24]

In this way, *Smart Fisheries* can be an integral part of *Smart Cities*. It would be an important aspect towards food security and job creation. More than that, Smart Fisheries will provide tracked food, guaranteeing efficient management of the fish stock and promoting the economic prosperity and human well-being for the fishing communities. The development of the cities, as well as the supply chains for their necessities, in this case, food, needs to contemplate how to make responsible management of the resources in an overexploited world. And in this case, the ocean.

6 Summary and future work

Smart Fisheries is a novel concept that can enhance the performance of artisanal fisheries. Also, the concept pretends to connect the final consumer with the fishing communities through technology, promoting the best practices regarding environmental health and fair-trade. The possibility to obtain accurate and time-based data will help decision-makers to take better and well-founded decisions and policies to drive into a real and sustainable blue economy. Making a transition into Smart Fisheries is not an easy task. It is trying to renew a model that has been broken for a long time. In this sense, there is a lot of political work and awareness that have to be included this process of transformation. Technology by itself will not solve the problem, it has to be implemented considering the social, environmental, emotional, economic, and political variables involved in the fisheries. It is imperative to developed cooperation between the main stakeholders involved in this ecosystem, as this will be the key to have success in the creation and operation of a Smart Fishery. In *Remora Fishing Traceability* we have been working hard in the development of powerful technologies to achieve sustainability in the small-scale fisheries, environmental awareness, fair-trade, and the integral progress of the fishermen and their communities. In this way, we will implement a pilot project on a Smart Fishery in three communities in the North Pacific coast of Costa Rica during 2021. The results and details about the implementation will be presented in future publications. With all this effort, we desire to bring sustainability back to the ocean.

7 Acknowledgments

All the work presented is possible thanks to the support for several private, public and NGO's organizations that provided support in the process. In the case, we will like to thank you *Mar Viva*, *Coopesolidar*, *Costa Rica por Siempre*, *SINAC* in Costa Rica. Also, we extend our gratitude to *Katapult Ocean Accelerator* in Norway. Not less important, the fishers communities that have trusted

10 Javier Carvajal et al.

our work: Cabuya, Tambor, Malpaís and Manzanillo in the North Pacific of Costa Rica.

References

1. F. Fisheries, *The state of world fisheries and aquaculture 2020*. Food and Agriculture Organization of the United Nations, 2020.
2. OECD, *The ocean economy in 2030*. OECD, 2016.
3. J. Zelasney, A. Ford, L. Westlund, A. Ward, and O. Riego Peñarubia, *Securing sustainable small-scale fisheries: Showcasing applied practices in value chains, post-harvest operations and trade*, vol. 652. Food and Agriculture Organization of the United Nations, 2020.
4. F. FAO, “General situation of world fish stocks,” 2018.
5. J. Liu, T. Dietz, S. R. Carpenter, M. Alberti, C. Folke, E. Moran, A. N. Pell, P. Deadman, T. Kratz, J. Lubchenco, *et al.*, “Complexity of coupled human and natural systems,” *science*, vol. 317, no. 5844, pp. 1513–1516, 2007.
6. C. Anthony, *Sustainable Fishery Systems: Fish and Aquatic Resources Series 5*. Blackwell Science, 2001.
7. J. N. Kittinger, L. T. Teneva, H. Koike, K. A. Stamoulis, D. S. Kittinger, K. L. Oleson, E. Conklin, M. Gomes, B. Wilcox, and A. M. Friedlander, “From reef to table: social and ecological factors affecting coral reef fisheries, artisanal seafood supply chains, and seafood security,” *PloS one*, vol. 10, no. 8, p. e0123856, 2015.
8. P. Howson, “Building trust and equity in marine conservation and fisheries supply chain management with blockchain,” *Marine Policy*, p. 103873, 2020.
9. M. Isaacs, “Small-scale fisheries governance and understanding the snoek (thyr-sites atun) supply chain in the ocean view fishing community, western cape, south africa,” *Ecology and Society*, vol. 18, no. 4, 2013.
10. D. J. Steenbergen, M. Fabinyi, K. Barclay, A. M. Song, P. J. Cohen, H. Eriksson, and D. J. Mills, “Governance interactions in small-scale fisheries market chains: Examples from the asia-pacific,” *Fish and Fisheries*, vol. 20, no. 4, pp. 697–714, 2019.
11. D. Draheim, “Smart business process management,” *BPM and Workflow Handbook, Digital Edition. Future Strategies, Workflow Management Coalition*, pp. 207–223, 2011.
12. R. Aps, M. Fetissof, and H. Lassen, “Smart management of the baltic sea fishery system: Myth or reality?,” in *2010 IEEE/OES Baltic International Symposium (BAL TIC)*, pp. 1–9, IEEE, 2010.
13. G. Salton, “The smart system,” *Retrieval Results and Future Plans*, 1971.
14. C. Buckley, “Implementation of the smart information retrieval system,” tech. rep., Cornell University, 1985.
15. G. Jucevičius and K. Grumadaitė, “Smart development of innovation ecosystem,” *Procedia-social and behavioral sciences*, vol. 156, pp. 125–129, 2014.
16. T. B. Rudolph, M. Ruckelshaus, M. Swilling, E. H. Allison, H. Österblom, S. Gelcich, and P. Mbatha, “A transition to sustainable ocean governance,” *Nature communications*, vol. 11, no. 1, pp. 1–14, 2020.
17. N. J. Bennett, A. M. Cisneros-Montemayor, J. Blythe, J. J. Silver, G. Singh, N. Andrews, A. Calò, P. Christie, A. Di Franco, E. M. Finkbeiner, *et al.*, “Towards a sustainable and equitable blue economy,” *Nature Sustainability*, pp. 1–3, 2019.

Smart Fisheries, a key player in ocean sustainability and fair fish trade. 11

18. H. Chourabi, T. Nam, S. Walker, J. R. Gil-Garcia, S. Mellouli, K. Nahon, T. A. Pardo, and H. J. Scholl, "Understanding smart cities: An integrative framework," in *2012 45th Hawaii international conference on system sciences*, pp. 2289–2297, IEEE, 2012.
19. A. E. Punt and A. D. Smith, "The gospel of maximum sustainable yield in fisheries management: birth, crucifixion and," *Conservation of exploited species*, vol. 6, p. 41, 2001.
20. S. Mackinson, B. Deas, D. Beveridge, and J. Casey, "Mixed-fishery or ecosystem conundrum? multispecies considerations inform thinking on long-term management of north sea demersal stocks," *Canadian Journal of Fisheries and Aquatic Sciences*, vol. 66, no. 7, pp. 1107–1129, 2009.
21. K. Kelleher, R. Willmann, and R. Arnason, *The sunken billions: the economic justification for fisheries reform*. The World Bank, 2009.
22. S. Ray, "Us consumer preferences for seafood traceability," 2019.
23. R. Mowla, "Adopting gender friendly climate smart fisheries technology in south west regions of bangladesh: Potentials and constraints," 2016.
24. B. Sterling, M. Gooch, B. Dent, N. Marenick, A. Miller, and G. Sylvia, "Assessing the value and role of seafood traceability from an entire value-chain perspective," *Comprehensive Reviews in Food Science and Food Safety*, vol. 14, no. 3, pp. 205–268, 2015.

Smart city tools to evaluate age-healthy environments

Irene Lebrusán¹ and Jamal Toutouh²

¹ Universidad Complutense de Madrid, TRANSOC, Spain
ilebrusa@ucm.es

² Massachusetts Institute of Technology, CSAIL, MA, USA
toutouh@mit.edu

Abstract. The urban population is aging and the elderly people desire to *age in place* and to continue in the environments chosen by them. Accordingly, the environment should be healthy-age orientated, improving health and fulfilling the United Nation Global Goals, including the aging-related ones. Using the case study of Madrid, the biggest city in Spain, this research analyzes the quality of the spaces to grow old in terms of environmental health. To do so, we have selected a number of variables, drawing on open data provided by the city council, using an age-oriented perspective. We propose a comparative analysis of the 21 districts in Madrid in terms of air pollution, noise, urban fitment adapted to moderate physical activity, and green spaces in the city, as those are very important aspects for healthy aging. According to our results, central areas of the downtown of Madrid offer a worse potential quality of life in terms of the environment than peripheral areas.

Keywords: smart governance · elderly · aging in place · environmental analysis

1 Introduction

The increase of life expectancy, along with a series of economic and social improvements, has led to changes in both the meaning and the manner of experiencing old age. Among the manifestations of these changes, one of the most relevant is the desire to remain independent in the known environment until a very advanced age [6, 9, 13]. The idea of *aging in place* comprises the continuity of the elderly in society, and more specifically, in the social environment known and chosen by them. However, for this to be possible, the environment has to fulfill several characteristics, allowing their participation into society, not posing barriers and, above all, in healthy conditions.

Ensuring an enabling and supportive environment to achieve the highest possible level of health and well-being for the elderly was pointed out in the **Madrid International Plan of Action on Aging** and in the Political Declaration adopted at the Second World Assembly on Aging in April 2002 [25]. More recently, specific attention to age in cities was taken as part of the **Sustainable Development Goal**. The *target 11.7* points that, by 2030, cities will provide

2 I. Lebrusán and J. Toutouh

universal access to safe, inclusive and accessible, green, and public spaces, for vulnerable population groups, specifically including the elderly among them. Besides, the *target 11.6* notes the commitment to reduce the adverse *per capita* environmental impact of cities by paying special attention to air quality by 2030, that, as we exposed before [11,12] is especially harmful to the elderly. This international commitment is a great advance, as the environment plays an important role in determining how we age and how we respond to disease, loss of function, and other forms of loss and adversity that we may experience at different stages of life, and particularly in later years [29].

But, could cities fulfill this road map? Are our cities a healthy space to grow old? And, how can we evaluate this? The use of digital technologies allow the design of smarter cities, addressing numerous challenges, such as environmental pressures, energy efficiency, and sustainability, or improving urban mobility, among others. But, besides, smart cities can provide a series of tools to advance knowledge of the well-being of the different age groups needs, and especially, the urban lacks as their inhabitants grow older, i.e., Open Data, Smart Governance, and the Internet of Things.

We selected Madrid as a case study to measure the capacity of Spain to achieve the referred international commitments. While it is not the most aged municipality in the country, it is the biggest city and so, it has the largest amount population over 65 years old. Since Madrid city has a greater number and amount of resources than other cities, it would be expected a high level of compliance with age-friendly environments. As there are not recognized specific guidelines of what an age-friendly environment should accomplish, or even explicit indicators with an age perspective to measure the quality of aging in cities, this research raises its own proposal. We use open data gathered by different sensors and other variables provided by the Council of Madrid to evaluate how adequate an environment is for aging, and thus, detect in which areas will be necessary to implement measures leading to healthy aging.

Thus, the main contributions of this work are: *i)* evaluating the possibility of using the provided open data to assess elderly people well-being in our cities, *ii)* assessing different variables that allow observing which districts are healthy for the elderly people; and *iii)* using such information to review the situation of Madrid in terms of age-friendly environments.

The rest of the paper is organized as follows: In the next section, we describe the importance of aging in place, paying especial attention to the effect of the environment for healthy aging. Section 3 introduces the context of our use case and the materials and methods used in this analysis. The evaluation of the air quality and noise based on the shared open data is shown in Section 4. Finally, Section 5 presents the conclusions and the main lines of future work.

2 Towards healthy and inclusive aging: spaces matters

Older adults' well-being is strongly linked to the residential environment, where the older population generally spend more time than the younger population [4]. Accordingly, cities should create healthy and age-friendly environments. A space

is age-friendly when they are accessible, equitable, inclusive, safe and secure, and supportive. Besides, we consider they should be healthy in terms of pollution and offering active mobility and moderate exercise possibilities.

2.1 The importance of *place* and place attachment while aging

Place attachment is explained as a set of feelings about a geographic location that emotionally binds a person to that place as a function of its role as a setting for the experience [21]. Attachment to space has a strong connection with the *identity of place*, which implies the incorporation of place into the broad concept of self [17].

The place and the known environment are fundamental in the processes of identity and self-definition of the self [17,26], becoming part of the social representation [14]. It acquires a great influence in old age, being a key element in the quality of life and well-being [15,20] that contributes to situate identity in old age [16,19]. This explains why elderly people desire and choose to live in their environment, where they feel they *belong*, as long as they can, and if it is possible, until their death. Thus, the environment has to provide minimum health conditions. Otherwise, problems such as the absence of green spaces or pollution will have an even more negative effect during old age, when the influence of the environment on well-being is greater [8].

2.2 Environment influence on a healthy aging

Older adults are often at risk for increased vulnerability to noise pollution due to slower mental processing and sensory changes that take place in the aging process [2]. They are also more vulnerable than other age groups to the exposure to air pollutants, which may even be fatal [22]. As we have pointed out in previous works, the elderly are more susceptible to suffer from urban pollution (as NO₂) and lack of public space [11,12]. Specifically, air pollution, which caused more than 400,000 premature deaths in 2016, is considered the top health hazard in the European Union (EU) [5] affecting all ages, but being some groups more vulnerable, as the older population. It is considered carcinogenic and causes infertility and diabetes Type 2 [18] and it is linked to obesity, systemic inflammation, aging, Alzheimer's disease, and dementia [5]. It affects the brain in the same way that Alzheimer's does as it causes changes in the structure of the brain [30].

Noise pollution, which causes annually at least 16,600 cases of premature death in Europe [28], is the major preventable cause of hearing loss [1]. It also affects the cardiovascular system and causes hypertension [1,23]. Finally, sound pollution can also cause a range of non-auditory problems, like annoyance, sleep disturbance, and cognitive performance [23].

In relation to this, nature can contribute both directly and indirectly to control pollutants, as the green infrastructure has a natural capacity to directly act as a barrier and remove air pollutants from the atmosphere through gaseous absorption or dry deposition. Vegetation can impede noise propagation by absorbing or diffracting [3]. Accordingly, a bigger presence of green areas would be positive for the elderly.

4 I. Lebrusán and J. Toutouh

2.3 The compromise with Sustainable Development Goals in terms of urban aging

The Sustainable Development Goals (SDGs) were adopted by all United Nations Member States in 2015 as a universal call to action to end poverty, protect the planet, and ensure that all people enjoy peace and prosperity by 2030. Preparing for an aging population is vital to the achievement of the integrated 2030 Agenda, with aging cutting across the goals on poverty eradication, good health, gender equality, economic growth and decent work, reduced inequalities, and sustainable cities [7]. Regarding the people aging in cities, the SDGs establish that: “By 2030, provide universal access to safe, inclusive and accessible public spaces and green areas, in particular for women and children, older persons and persons with disabilities”. More specifically, *target 11.7* focuses on access to green spaces and safe public spaces. Regarding the air quality, the *target 11.6* establish that, by 2030, reduce the adverse per capita environmental impact of cities, including by paying special attention to air quality, municipal and other waste management

These applications can make all the difference in the quality of life for elderly patients who want to continue living at home independently and provide peace of mind for their family members [27]

Finally, the consideration of the environment and urban space in terms of age is fundamental to evaluate the capacity of potential integration and adaptation of cities to the needs of their inhabitants.

3 Materials and methods

In this section, first, we introduce Madrid as our case study and, second, we present the methodology applied to evaluate the quality of the urban space in the city of Madrid to grow old in terms of environmental health. Since there are no specific guidelines to operationalize what an age-friendly environment should accomplish, we propose our definition of it. To do so, and after considering the theoretical definition summarized in Section 2 and the information available, we have selected different indicators applicable to the dimensions of environmental well-being from an old-age perspective.

3.1 Madrid information

The city of Madrid has 21 districts which are further subdivided into 131 neighborhoods. The districts are territorial divisions of the municipality, equipped with decentralized management bodies in order to facilitate the governance of such a big city. These administrative bodies have the purpose to promote and develop citizen participation in the management of municipal affairs. These districts are very different from an urban perspective (as a result of different construction stages) but also in terms of wealth and quality of life. We are specifically interested in analyzing if there is also a difference in the quality of the environment to age in place.

Table 1 summarizes some demographic information and the surface area data (in hectares) of the 21 districts of Madrid. Fig. 1 shows the territorial divisions

of the city of Madrid into districts. Regarding the distribution of the densities by districts, Madrid reflects a high dispersion (see Fig. 1 and Table 1) with a central area more densely populated and a peripheral area with lower population density. Specifically, the most densely populated districts are Chamberí, Tetuan, Salamanca, Centro, and Arganzuela. These districts are older and more consolidated in urban terms. The group of districts that present a density well below the Madrid average are Fuencarral-El Pardo, Moncloa-Aravaca (both including protected green areas) and Villa de Vallecas, Vicálvaro, and Barajas (spaces with growth expectations in terms of urbanization).

Table 1: Total population, population older than 65 years old, population older than 80, and district surface in ha. per district

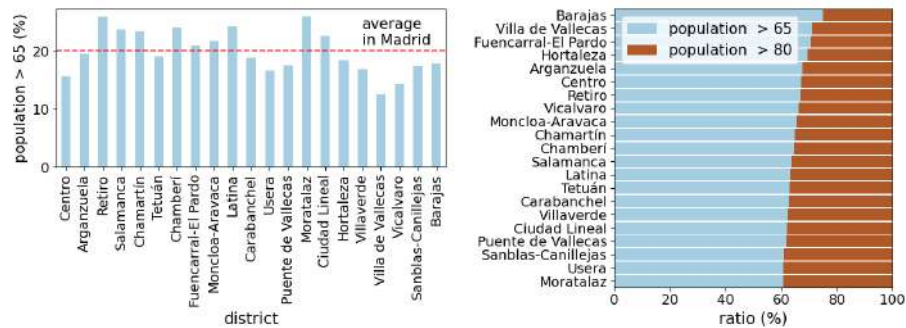
id.	district name	population	older than 65	older than 80	surface (ha)
1	Centro	140473	22006	7249	522.82
2	Arganzuela	155660	30411	9863	646.22
3	Retiro	120406	31227	10332	546.62
4	Salamanca	147854	35151	12707	539.24
5	Chamartín	147551	34443	12081	917.55
6	Tetuán	161313	30723	11365	537.47
7	Chamberí	140866	33855	12025	467.92
8	Fuencarral-El Pardo	249973	52164	1536	23783.84
9	Moncloa-Aravaca	121683	26543	9108	4653.11
10	Latina	242139	58967	2158	2542.72
11	Carabanchel	260196	48920	18149	1404.83
12	Usera	142894	23853	9352	777.77
13	Puente de Vallecas	240867	42270	16109	1496.86
14	Moratalaz	95614	24822	9768	610.32
15	Ciudad Lineal	219867	49803	18871	1142.57
16	Hortaleza	193264	35788	10926	2741.98
17	Villaverde	154318	26063	9805	2018.76
18	Villa de Vallecas	114512	14406	4139	5146.72
19	Vicalvaro	74048	10639	3594	3526.67
20	San Blas-Canillejas	161222	28034	10942	2229.24
21	Barajas	50010	8955	2231	4192.28
	Madrid	3334730	669043	235556	60445.51



Fig. 1: Map of Madrid with the districts ids.

Regarding the aging of districts, they are also clearly different (see Fig 2.a). In general terms, the core area and bordering zone is more aged (in some districts, as Retiro, almost 26% of population is over 65 years old, being Moratalaz the district with the highest percentage of people over 65 years old in the city). In the face of this, the districts in the periphery, less populated and with newer buildings, present a higher volume of young couples with children (Villa de Vallecas and Vicálvaro) and where, accordingly, the older population has a lower demographic weight. The case of the demographic pyramid of Centro is a deviation as is characterized by a young immigrant population. In each district, the older population is feminized, as womens life expectancy is higher (87.16 years).

When analyzing “the aging of the aging” or the over aging (the proportion of people older than 80 years over the total population older than 65 years) in Fig. 2, we can see that Moratalaz, Usera, and San Blas-Canillejas are the districts with a bigger percentage of “old-elderly”. In comparison, Barajas, Villa de Vallecas, and Fuencarral-El Pardo have a smaller proportion of people over 80 years old. In terms of needs and health frailty, the demographic composition can be important for our analysis, as the areas with the oldest population would have a greater need of an age-friendly environment.



a) Ratio of population older than 65 years old. b) Ratio of elderly older than 80 over the population older than 65 years old.

Fig. 2: Madrid main demographic information by district.

3.2 Methodology applied

One of the aims of this research is to prove how useful are Smart City tools, such as Smart Governance and open data, to assess how healthy are our cities to grow old. In this case, we use the data provided by the Open Data Portal (ODP) offered by the Madrid City Council (<https://datos.madrid.es/>). This data source has shown to be useful for different kinds of studies [10, 24].

To evaluate and compare the quality of the districts to grow old, and considering the aspects highlighted in Section 2, we have selected four key dimensions: the availability of green areas, the availability of urban fitment areas to optimize physical activity in old age, the air quality (considering NO₂) and the pollution in terms of noise.

Availability of the green areas The ODP provides the surface in hectares (ha) of the green spaces in the districts. Green spaces, including community gardens, allotments, and forests are an important factor in community identity and can strengthen people's attachment to their communities. Green infrastructure and accessible green space are important factors for individuals and communities to establish a 'sense of place' and 'ownership' of their local landscape [3]. Thus, we evaluated the number of ha per 10000 inhabitants and the number of ha per 10000 elderly people. This allows the analysis of whether there are a fair distribution and access to green areas for all age groups in the city.

Urban fitment for old age This refers to different facilities and furniture to practice moderate physical activity, as equipment to exercise fingers and wrists or arms, pedal, for waist movement, stairs, and ramp, among other fitments more complex. All those are adapted to different needs and to optimize mobility in later life. The data used for our analysis provide the number and the location of the urban fitment. Thus, we have evaluated the access to those urban elements as the number of urban facilities per 10000 elderly people.

Air quality OPD provides the hourly mean concentration of several air pollutants: sulfur dioxide (SO₂), nitrogen dioxide (NO₂), ozone (O₃), carbon monoxide (CO), particulate matter (PM₁₀ and PM_{2.5}). However, there is no information about all the pollutants in the 21 districts. The pollutant with information that covers more districts is the NO₂, there are sensors in 18 districts. The other pollutants have much less data, e.g., PM_{2.5} is sensed just in six locations of Madrid. Thus, as NO₂ has been proven the major health concern in our cities and it is the one that provides more spatial information, we evaluate NO₂ concentration as a metric of air quality.

Noise pollution WHO puts traffic-related noise as the second most harmful environmental factor in Europe, right after air pollution. Thus, we include it in our analysis. The noise pollution data provided by the OPD includes the daily mean of the equivalent sound pressure levels. These data are gathered by sound-meters installed in 31 locations covering 19 districts (excluding Ciudad Lineal and San Blas-Canillejas). Regarding the equivalent sound pressure levels (measured in A-weighted decibels, dBA), we take into account: L_{eq} , that averages the noise measured during the whole day (24 hours); L_d , which is evaluated during the day (from 7:00h to 19:00h); L_e , which assess the noise during the evening (from 19:00h to 23:00h); and L_n , which measures the noise at night (from 23:00h to 7:00h). We evaluated these noise levels because noise at different periods of time may have different impacts on the well-being of the elderly.

4 Results and discussion

This section evaluates the quality of the environment of the different districts of Madrid in terms of the availability of green areas, urban fitment for old age, air quality and, noise levels, based on the data available. These aspects cannot be ignored in the analysis of the individual well-being of the elderly.

4.1 Availability of the green areas

Table 2 ranks the evaluated districts according to the number of ha of green areas available per 10000 elderly (green area ratio). The third column takes into account the whole population. The second column express which proportion would be available for the elderly having in consideration the total potential green space users in the district. Fig. 3 illustrates the spatial evaluation of this metric. In this case, darker green indicates more ha per elderly (better districts according to that metric).

As we can see in Fig. 3, the *central almond* offers less green space to the elderly, while newer areas, less dense in terms of urbanization, offer a better rate. It is important to remark that the three best districts in terms of this metric are not the ones that provide the largest green area per inhabitant (see Table 2). Villa de Vallecas is the district that provides the largest green area per inhabitant, but the fifth if we take into account just the elderly. Finally, it is noticeable the differences between the best and the worst district, since Barajas provides about 20 times more green areas for the elderly than Chamberí.

Table 2: Ranking taking into account the availability of the green areas.

ranking	district	ha/10000 elderly	ha/10000 inhabitants
1	Barajas	3.54	19.76
2	Moncloa-Aravaca	3.45	15.80
3	Moratalaz	3.25	12.53
4	Vicálvaro	3.24	22.55
5	Villa de Vallecas	3.14	24.92
6	Hortaleza	3.02	16.30
7	Fuencarral-El Pardo	2.97	14.23
8	Latina	2.77	11.39
9	Villaverde	2.36	13.97
10	Puente de Vallecas	2.04	11.65
11	Usera	1.95	11.71
12	San Blas-Canillejas	1.74	10.00
13	Carabanchel	1.67	8.87
14	Ciudad Lineal	1.36	6.02
15	Arganzuela	1.12	5.74
16	Chamartín	0.87	3.73
17	Retiro	0.79	3.07
18	Tetuán	0.75	3.92
19	Salamanca	0.57	2.41
20	Centro	0.38	2.42
21	Chamberí	0.19	0.77

Madrid has a rich and extensive green heritage, highlighting its parks and gardens, both historical and advanced garden design. Central areas are not offering enough green areas to their (older) residents, while this lack of green spaces seems not to be a problem in the peripheral areas.

4.2 Urban fitment for old age

Table 3 ranks the evaluated districts according to the number of ha of fitment elements available per 10000 old people. Fig. 4 illustrates the spatial evaluation of this metric. In this case, darker blue indicates more (better) fitment equipment per old people.

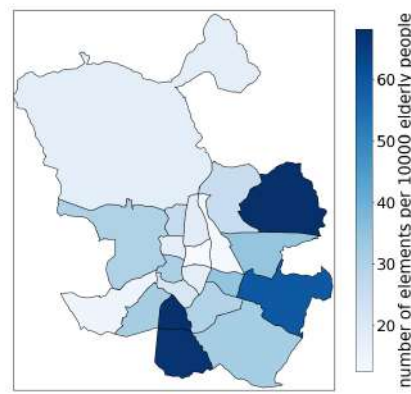
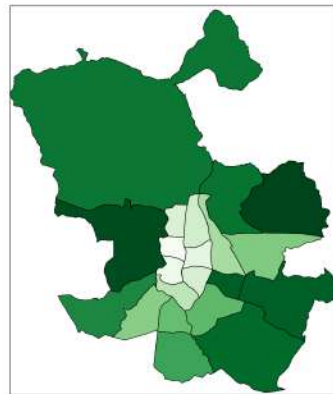


Fig. 3: Green areas availability map.

Fig. 4: Urban fitment map.

Table 3: Ranked according to the number of fitment elements per 10000 elderly.

ranking	district	number of urban fitment facilities per 10000 elderly
1	Barajas	68.12
2	Usera	67.50
3	Villaverde	67.14
4	Vicálvaro	59.22
5	Moratalaz	34.65
6	San Blas-Canillejas	34.60
7	Villa de Vallecas	31.93
8	Carabanchel	31.68
9	Centro	30.90
10	Moncloa-Aravaca	30.14
11	Puente de Vallecas	29.81
12	Tetuán	26.04
13	Hortaleza	25.71
14	Arganzuela	21.05
15	Chamartín	18.58
16	Fuencarral-El Pardo	17.83
17	Chamberí	17.72
18	Retiro	17.61
19	Latina	15.09
20	Ciudad Lineal	13.45
21	Salamanca	12.52

As it happens with the previous index (availability of the green areas) the peripheral districts are in better-compared position. Barajas, Usera, and Villaverde are in better positions, all over 67 facilities per 10000 older citizens. The difference between the best positioned and the worst positioned districts is noticeable because the first ones have about three times more elements than the worst ones. Salamanca, Ciudad Lineal, Latina, Retiro, Chamberí, Fuencarral-El Pardo, and Chamartín are all below 20 per 10000 people over 65 years old.

Given the importance of enhancing physical activity in old age, most districts should invest in this type of facility. There is a clear inequality in the number of fitment elements per elderly an in some districts are really scarce.

10 I. Lebrusán and J. Toutouh

4.3 Air quality

Table 4 ranks the evaluated districts regarding the air quality (less NO₂ concentration). Fig. 4 illustrates the spatial evaluation of this metric and the dots locate the sensors. NA in Table 4 and white shape in Fig. 5 indicates that there is not open data about pollution in that districts, i.e, Latina, and Vicálvaro .

Table 4: NO₂ concentration levels in terms of $\mu\text{g}/\text{m}^3$.

ranking	district	NO ₂ concentration
1	Moncloa-Aravaca	20.59
2	Retiro	24.85
3	Fuencarral-El Pardo	25.60
4	Hortaleza	31.00
5	Barajas	33.14
6	Arganzuela	33.65
7	San Blas-Canillejas	34.29
8	Ciudad Lineal	34.29
9	Puente de Vallecas	35.90
10	Moratalaz	35.99
11	Chamberí	36.16
12	Tetuán	36.82
13	Villa de Vallecas	36.83
14	Centro	37.95
15	Chamartín	38.04
16	Villaverde	39.23
17	Carabanchel	42.87
18	Salamanca	51.40
19	Usera	53.47
20	Latina	NA
21	Vicalvaro	NA

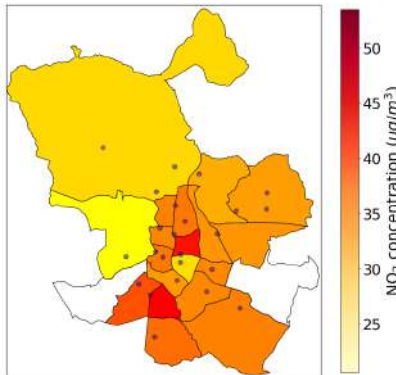


Fig. 5: NO₂ concentration levels map. The dots illustrate the sensors locations.

The results in Table 4 show that there is an important difference among districts. The best air quality is presented Moncloa-Aravaca, followed by Retiro, i.e., the north-west area (see Fig 5. This could be seen as the (comparatively) best districts to the elderly in terms of air quality. Those are coincident with the

presence of the so-called *lungs of Madrid* as *Parque del Retiro*, *Parque del Oeste* or the *Dehesa de la villa*, among others.

The south-east and the central area, as Usera, Salamanca, Carabanchel, or Villaverde districts, register a much worse air quality, with more than twice NO₂ concentration than Moncloa-Aravaca.

In general, Madrid presents a health problem regarding NO₂ concentration in the air [11]. Thus, measures should be taken to improve the air quality to avoid health problems for the population of that city.

4.4 Outdoor noise levels

Table 5 summarizes the information about the outdoor noise pollution gathered by the sensors installed in the city. Fig 6 a, b, and c illustrate the noise pollution by showing the L_d , L_e , and L_n levels, respectively. As there are no information about the levels of noise in Ciudad Lineal and San Blas-Canillejas, they are shown in the table as NA and in the maps, their shape is in white.

Table 5: Noise levels evaluated in terms of dBA. The districts are ranked according to the noise level (L_{eq}).

ranking	district	L_{eq}	L_d	L_e	L_n
1	Moncloa-Aravaca	53.54	54.81	53.82	48.68
2	Arganzuela	54.36	54.88	56.44	49.06
3	Vicalvaro	56.25	57.75	55.94	50.80
4	Villaverde	56.80	57.24	58.96	51.23
5	Fuencarral-El Pardo	57.60	58.89	58.19	51.83
6	Puente de Vallecas	58.35	59.33	58.20	52.32
7	Barajas	59.06	60.28	59.52	54.76
8	Carabanchel	60.14	61.20	61.06	55.17
9	Tetuán	60.17	61.06	61.90	54.34
10	Moratalaz	60.39	61.81	60.36	53.63
11	Hortaleza	61.38	62.83	62.92	52.64
12	Centro	61.67	62.68	62.66	56.88
13	Latina	62.57	63.95	63.19	57.18
14	Chamberí	62.80	63.92	63.43	58.70
15	Villa de Vallecas	62.90	64.05	63.55	59.04
16	Usera	63.35	64.36	64.23	59.79
17	Salamanca	64.31	65.12	65.12	60.58
18	Chamartín	65.84	66.94	66.46	61.88
19	Retiro	68.77	69.53	69.40	66.23
20	Ciudad Lineal	NA	NA	NA	NA
21	San Blas-Canillejas	NA	NA	NA	NA

As we can see in Table 5 and Fig. 6, noise levels during the day, evening, and night follow a pretty similar behavior in each district, with slight variations in some districts. This means that even at night inhabitants suffer from high levels of noise, which negatively affects their health. The noisiest areas are in the city center, with some exceptions (and some noisy districts) in the south area.

It is important to note that most of the evaluated districts suffer from noise levels higher than 55 dBA, which is the threshold of being considerate harmful for humans [28]. Thus, as it happens with air pollution, measures should be taken to improve such a hazardous situation [12].

12 I. Lebrusán and J. Toutouh

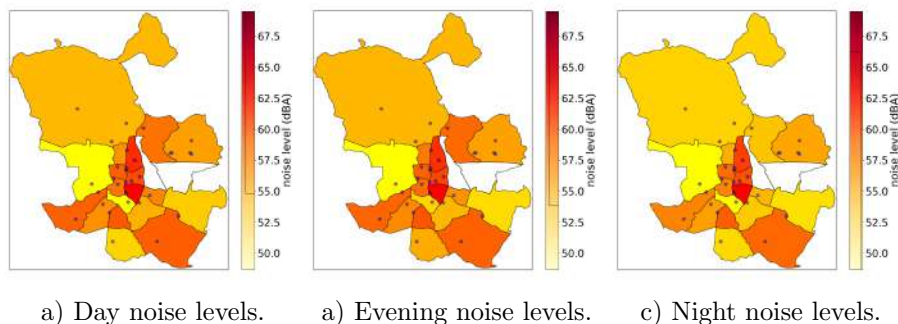


Fig. 6: Maps showing noise levels. The dots illustrate the locations of the sensors.

4.5 General overview

Table 6 shows the districts ranked according to the four index evaluated. Analyzing the positioning of each district in each of the rankings, we can clearly see that some are generally better positioned than others. While there is more variability regarding the better positions (most of them located at the peripheral areas of the city), it is clear that some districts are worse prepared to age in place, and according to our definition, they are not age-friendly areas. The central zone and the surrounding areas are more prone to offer an insufficient quality of life in terms of environmental health, with the worst punctuation’s in green areas, facilities, air quality, and noise pollution. It is also difficult that these districts can fulfill the measures promised before the UN in the SGDs. Other districts, such as Barajas, offer good quality in green areas and facilities. However, the location (in the airport area) contributes to a worsening of results in terms of pollution and noise.

Table 6: Districts sorted according to their ranks in the four variables evaluated.

green areas	fitment equipment	air quality	noise
Barajas	Barajas	Moncloa-Aravaca	Moncloa-Aravaca
Moncloa-Aravaca	Usera	Retiro	Arganzuela
Moratalaz	Villaverde	Fuencarral-El Pardo	Vicálvaro
Vicálvaro	Vicálvaro	Hortaleza	Villaverde
Villa de Vallecas	Moratalaz	Barajas	Fuencarral-El Pardo
Hortaleza	San Blas-Canillejas	Arganzuela	Puente de Vallecas
Fuencarral-El Pardo	Villa de Vallecas	San Blas-Canillejas	Barajas
Latina	Carabanchel	Ciudad Lineal	Carabanchel
Villaverde	Centro	Puente de Vallecas	Tetuán
Puente de Vallecas	Moncloa-Aravaca	Moratalaz	Moratalaz
Usera	Puente de Vallecas	Chamberí	Hortaleza
San Blas-Canillejas	Tetuán	Tetuán	Centro
Carabanchel	Hortaleza	Villa de Vallecas	Latina
Ciudad Lineal	Arganzuela	Centro	Chamberí
Arganzuela	Chamartín	Chamartín	Villa de Vallecas
Chamartín	Fuencarral-El Pardo	Villaverde	Usera
Retiro	Chamberí	Carabanchel	Salamanca
Tetuán	Retiro	Salamanca	Chamartín
Salamanca	Latina	Usera	Retiro
Centro	Ciudad Lineal	Latina	Ciudad Lineal
Chamberí	Salamanca	Vicálvaro	San Blas-Canillejas

Finally, it is important to remark that are districts that do not provide pollution data (air quality or noise). This hardness the evaluation of the quality of the health of the inhabitants of these districts. Thus, it would be important to install sensors to gather data from these districts. Besides, having a large number of sensors located in different areas would help to gather information with better resolution in this regard.

5 Conclusions and future work

Given the aging of the urban population, the challenge for cities lies in achieving a healthy and safe environment for the elderly. It means creating inclusive and accessible urban environments to benefit their aging population, enhancing health and well-being during old age. Environmental factors are interrelated and have a positive bearing on maintaining the capacities of the elderly.

In this work, we evaluate open data to assess the capacity of Madrid districts to offer a quality environment to age in place, as well as its capacity to accomplish with UN SDGs goals in terms of aging.

According to the evaluated data, we can see that central areas are less adequate to aging, meaning that they offer fewer possibilities for healthy aging in place. The elderly living there are exposed to more noise, more pollution, less green space, and in general, less urban facilities adapted for the elderly. This contrasts with the peripheral areas of Madrid that are (comparatively) more age-friendly. However, it seems difficult for this city to comply with the commitments referred to the UN if a large investment is not made from now to 2030.

Smart city tools proved their usefulness to analyze the environment quality. Smart cities can allow the elderly to age in society, preventing health frailty, and evaluating and foreseen needs and if there is a risk of not complying with an international agreement, as the UN commitments. Smart cities can be the tool to not leave vulnerable population behind.

Among the limitations of this paper, most important is data availability related. There is a shortage of information to evaluate other aspects of an age-friendly environment. The lack of use of open data standards in ODP and the poor documentation found hardness the analysis capacity for this type of studies. Obtaining and producing data with an age perspective is needed to reach an egalitarian society. For example, the lack of consistency in terms of urban fitment reduces the comparability of data.

The future research lines are: *i*) include socioeconomic aspects and housing new multivariable analysis taking into account new data (e.g., socioeconomic aspects, housing quality); *ii*) using machine learning approaches to evaluate more complex correlation of this results with health outcomes; and *iii*) assessing other cities in terms of comparison, considering new dimensions (such as, morbidity, economic impact, use of spaces).

Acknowledgements J. Toutouh research was partially funded by European Union's Horizon 2020 research and innovation program under the Marie Skłodowska-Curie grant agreement No 799078, by the Junta de Andalucía UMA18-FEDERJA-003, European Union H2020-ICT-2019-3, and the Systems that Learn Initiative at MIT CSAIL.

14 I. Lebrusán and J. Toutouh

References

1. Basner, M., Babisch, W., Davis, A., Brink, M., Clark, C., Janssen, S., Stansfeld, S.: Auditory and non-auditory effects of noise on health. *The lancet* **383**(9925), 1325–1332 (2014)
2. Brandom, P.: Noise Pollution and Older Adults – A Real Health Hazard. <http://www.ageucate.com/blog/?p=1377> (2018), Accessed: 2020-08-08
3. ten Brink, P., Mutafoğlu, K., Schweitzer, J.P., Kettunen, M., Twigger-Ross, C., Baker, J., Kuipers, Y., Emonts, M., Tyrväinen, L., Hujala, T., et al.: The health and social benefits of nature and biodiversity protection. A report for the European Commission (ENV. B. 3/ETU/2014/0039). London/Brussels: Institute for European Environmental Policy (2016)
4. De Keijzer, C. S.: Green Spaces and Healthy Ageing. <https://www.isglobal.org/en/healthisglobal/-/custom-blog-portal/green-spaces-and-healthy-ageing/6113078/0> (2019), Accessed: 2020
5. European Environment Agency: Air quality in Europe - 2018. <https://www.eea.europa.eu/publications/air-quality-in-europe-2018> (2018), Accessed: 2019-07-07
6. Fernández-Carro, C., Evandrou, M.: Staying put: Factors associated with ageing in one's 'lifetime home'. *insights from the european context. Research on Ageing and Social Policy* **2**(1), 28–56 (2014)
7. Help Age International: Ageing, Older Persons and the 2030 Agenda for Sustainable Development. <https://www.un.org/development/desa/ageing/news/2017/07/ageing-older-persons-and-the-2030-agenda-for-sustainable-development/> (2020), Accessed: 2020
8. Lawton, M.P., Nahemow, L.: Ecology and the aging process. (1973)
9. Lebrusán, I.: Las dificultades para habitar en la vejez. *Documentación Social* **6**(1) (2020)
10. Lebrusán, I., Toutouh, J.: Assessing the environmental impact of car restrictions policies: Madrid central case. In: *Ibero-American Congress on Information Management and Big Data*. pp. 9–24. Springer (2019)
11. Lebrusán, I., Toutouh, J.: Car restriction policies for better urban health: a low emission zone in madrid, spain. *Air Quality, Atmosphere & Health* pp. 1–10 (2020)
12. Lebrusán, I., Toutouh, J.: Using smart city tools to evaluate the effectiveness of a low emissions zone in spain: Madrid central. *Smart Cities* **3**(2), 456–478 (2020)
13. Lebrusán Murillo, I.: La vivienda en la vejez: problemas y estrategias para envejecer en sociedad. Consejo Superior de Investigaciones Científicas (2019)
14. Milgram, S.: Cities as social representations. *Social representations* pp. 289–309 (1984)
15. Oswald, F., Kaspar, R.: On the quantitative assessment of perceived housing in later life. *Journal of Housing for the Elderly* **26**(1-3), 72–93 (2012)
16. Peace, S., Holland, C., Kellaheer, L.: 'option recognition' in later life: variations in aging in place. *Ageing and society* **31**(5), 734 (2011)
17. Proshansky, H.M., Fabian, A.K., Kaminoff, R.: Place-identity: Physical world socialization of the self. *Journal of environmental psychology* (1983)
18. Raaschou-Nielsen, O., Andersen, Z.J., Beelen, R., Samoli, E., Stafoggia, M., Weinmayr, G., Hoffmann, B., Fischer, P., Nieuwenhuijsen, M.J., Brunekreef, B., et al.: Air pollution and lung cancer incidence in 17 european cohorts: prospective analyses from the european study of cohorts for air pollution effects (escape). *The lancet oncology* **14**(9), 813–822 (2013)

19. Rowles, G., Oswald, F., Hunter, E., Wahl, H., Scheidt, R., Windley, P.: Aging in context: Socio-physical environments. *annual review of gerontology and geriatrics* 2003 (2004)
20. Rowles, G.D.: Evolving images of place in aging and 'aging in place'. *Generations: Journal of the American Society on Aging* **17**(2), 65–70 (1993)
21. Rubinstein, R.I., Parmelee, P.A.: Attachment to place and the representation of the life course by the elderly. In: *Place attachment*, pp. 139–163. Springer (1992)
22. Simoni, M., Baldacci, S., Maio, S., Cerrai, S., Sarno, G., Viegi, G.: Adverse effects of outdoor pollution in the elderly. *Journal of thoracic disease* **7**(1), 34 (2015)
23. Stansfeld, S.A., Matheson, M.P.: Noise pollution: non-auditory effects on health. *British medical bulletin* **68**(1), 243–257 (2003)
24. Toutouh, J., Lebrusán, I., Nesmachnow, S.: Computational intelligence for evaluating the air quality in the center of madrid, spain. In: *International Conference on Optimization and Learning*, pp. 115–127. Springer (2020)
25. United Nations: Report of the Second World Assembly on Ageing: Madrid, 8-12 April 2002. Tech. rep., United Nations (April 2002)
26. Valera, S., Pol, E.: El concepto de identidad social urbana: una aproximación entre la psicología social y la psicología ambiental. *Anuario de psicología/The UB Journal of psychology* pp. 5–24 (1994)
27. Woetzel, J., Remes, J., Boland, B., Lv, K., Sinha, S., Strube, G., Means, J., Law, J., Cadena, A., Von der Tann, V.: Smart cities: Digital solutions for a more livable future. McKinsey Global Institute: New York, NY, USA pp. 1–152 (2018)
28. World Health Organization: Environmental noise guidelines for the European region. <http://www.euro.who.int/en/health-topics/environment-and-health/noise/publications/2018/environmental-noise-guidelines-for-the-european-region-2018> (2018), Accessed: 2019-07-07
29. World Health Organization: Age friendly environments. <https://www.who.int/ageing/projects/age-friendly-environments/en/b> (2020), Accessed: 2020-27-08
30. Younan, D., Petkus, A.J., Widaman, K.F., Wang, X., Casanova, R., Espeland, M.A., Gatz, M., Henderson, V.W., Manson, J.E., Rapp, S.R., et al.: Particulate matter and episodic memory decline mediated by early neuroanatomic biomarkers of alzheimer's disease. *Brain* **143**(1), 289–302 (2020)

Crowdsourcing and IoT Towards More Resilient Flooding Prone Cities

Ponciano J. Escamilla-Ambrosio^[0000-0003-3772-3651], Maria G. Pulido-Navarro,

Isabel V. Hernández-Gutiérrez, Abraham Rodríguez-Mota,

Marco A. Moreno-Ibarra

Instituto Politécnico Nacional
Centro de Investigación en Computación
Mexico City, Mexico.
pescamilla@cic.ipn.mx

Abstract. Crowdsourcing is a phenomenon where groups of persons sometimes from different backgrounds participate to accomplish a task by making use of technology. Internet of Things (IoT) is able to incorporate a large number of heterogeneous devices such as sensors, surveillance cameras, smartphones, home appliances, etc., all data generated by these devices is processed and analysed to incorporate applications that will make life easier for the end users. This article proposes that community members of a specific urban zone, prone to flooding, collaborate in sharing information about weather conditions using IoT techniques. The gathered information is sent to a cloudlet to be analysed together with information from weather forecast and a network of sensors and surveillance cameras installed in specific areas inside and surrounding the studied zone. Having members of the very community studied involved in the process will exploit the available IoT technologies and the use of crowdsourcing at a lower cost leading to the development of what is called Smart City. This paper revises the available technology and proposes a system that will help in collecting and evaluating information for prediction purposes as to whether the community involved is at risk of being flooded. It is being noted that this risk is getting higher every year due to overpopulation, bad urbanisation, and climate change. Results show that the use of this technology will improve weather forecast so the community could react in time in case of flooding threats.

Keywords: Crowdsourcing, Internet of Things, Smart Cities, Flooding Risk, Resiliency.

1 Introduction

Flooding risks in densely populated urban zones is becoming a big threat for its inhabitants; these cities are at danger not only for the material losses but for health hazards and even loss of lives. The problem arises principally from the lack of urban planning; it is possible that the urban services were initially designed for a number of houses and little by little were overpopulated leading to a disaster when the pluvial rain couldn't get its course through the normal planned way. Another situation that worsens this condition is the waste thrown at the drainage that clots it. Anyway, this circumstance

requires a preventive plan to give its residents enough time to react in case that flooding might occur. Thus, this paper reviews some already proposed systems and how they have helped distinct communities, in some cases information regarding flooding problems has been obtained through interviewing members of the affected communities. These investigations helped to identify communities' needs, concerns, and experiences about past flooding events, to finally propose a technology solution system to help attend these requirements. IoT and Crowdsourcing are techniques that support multiple data sources and are equipped with the latest technologies offering broader range of capabilities for enhanced connectivity, storage, real-time analytics, and cost-effective applications [1]. The system we are proposing consists in developing applications like flooding prediction and early warning system (EWS) with the help of incoming data from residents and data from surveillance cameras and sensors especially installed in specific points at the studied zone. These data will be helpful to predict the flooding phenomena. This is achieved by acquiring data in real time and being able to process it and present it in an easy way in order to support the residents in decision making in a fast manner.

Crowdsourcing is a concept where masses of the public get together to work in a specific task that otherwise would be done by employees or specialised persons. In our specific case the persons are members of the studied community that will help in reporting situations that they consider contribute to the flooding problem; reporting what they observe in their community and weather changes that will be of help to predict a possible flood event. This information is intended to be directed to the local authorities and, accordingly, they would have to attend the needs of the community. In this sense, utilising IoT leads to what is known as Smart City which constitutes a concentrated use of information and communications technologies (ICT) [2].

There are many projects that have integrated IoT with smart city environments such as the work of Zanella et al [3], where a complete review of the architectures, protocols and technologies for a web-centred service based IoT structure for a smart city project is presented. In [4] a framework for the development of a smart city by implementing IoT is proposed. Here the authors emphasise the need for intelligent cities as it mentions that by 2050, 70% of the world's population will live in cities and surrounding areas. In their work Mitton et al. [5] combine Cloud and sensors to develop a smart city and define the concept Cloud of Things (CoT) as more than just interconnecting things. It provides services by abstracting, virtualising, and managing things according to the specified needs of the end users. Hence, new and heterogeneous things can be aggregated and abstracted enabling things as a service known as CoT.

2 Crowdsourcing and IoT

Crowdsourcing [6] is the process by which streams of data are collected by a large number of people. These data are sent to a server to be analysed using different types of models. This data analysis task turns out to be high time consuming, so big-data techniques need to be included resulting in a more robust modelling approach. According to [7] IoT is nowadays present in all ways of life where global connection and big data applications are enabling innovation all around the world. It is seen as a possible

solution for many problems such as air pollution, transportation, weather changes, health monitoring, etc. There is also the fact that many people are living now in big cities, which means that the demand on services will increase exhibiting the reality that urban infrastructure is not meeting the needs of its citizens due to bad planning and overcrowding. Such needs can be and should be met using IoT technologies. Flooding prone cities would benefit from crowdsource flood reports combined with IoT and traditional detection data from forecast environmental monitoring stations as well as in site installed sensors. All these data could be of help in deciding whether a given community is at risk. According to Fenner et al. [8] crowdsourcing by itself has around 80% accuracy but combined with other techniques like weather forecast and in site sensing could reach an accuracy of 96%. From here, it is seen the importance of combining IoT and crowdsourcing; together will lead to an efficient preventive and warning method. In addition, as stated in [9] [10], smart cities depend on ICT solutions to improve our quality of life.

Today, daily used objects equipped with computing, storage and sensing abilities, enabled to communicate with other similar objects, can become part of an IoT system. In this case, citizens equipped with intelligent phones can generate data about environmental changes that both sensors in their smartphones and they themselves are seeing in their communities in real time. They can upload photos and text or voice messages to a collector. All this information together with the local weather forecast system could be analysed for mitigation and prediction purposes. A local network of surveillance cameras and sensors planned for a project like this is justified because the forecast environmental monitoring stations present high spatial and temporal variability inside urban areas. When sensors and cameras identify changes in the ambience, they could be compared to the other sources to identify if flooding is prone to occur. Sensors may be able, via an application, to request users nearby for more information such as description of ambience, images, videos, etc. This information together with weather forecast could help in evaluating and assessing if whether flooding is about to occur so citizens could decide what actions to take.

3 Technical Background

The applications required for this project will have to handle an enormous variety of data for the IoT system. Therefore, the need is for a communication infrastructure capable of unifying the heterogeneous technologies available to develop a smart city. This article presents a general reference background for the design of an urban IoT. IoT is the convergence of both sensing environments and the Cloud. The Cloud provides services by abstracting, virtualising, and managing things, its purpose is to implement services to provide indexing and querying methods applied to things such as sensors, actuators, computing, storage, and energy sources [11]. The huge amount of data and services that the Cloud must manage gives way to another concept: Edge Computing. Edge Computing attends the requirements of shorter response time, processing, bandwidth cost saving and data safety and privacy. Within Edge Computing there are basically three types: Fog computing, Mobile Edge Computing and Cloudlet computing.

Fog computing is an intermediate layer between edge and cloud that provides distributed computing, storage and networking services between end devices and cloud

computing data centres [12]. Mobile Edge Computing (MEC) focuses on mobile clients within the radio access network (RAN), works with edge servers at the RAN base stations [13]. Cloudlet Computing [5] is an evolution of Mobile Cloud Computing (MCC) which are small resource rich data centres that can be positioned strategically in close proximity to end users, it mimics the cloud allowing for intense computing closer to the data source. The proposal is the development of a system that analyses data coming from multiple sources in real time that will assist in the inquiry on whether the urban zone in question is at risk of flooding.

In crowdsourcing, participation from the very own inhabitants is crucial as the users share information from IoT mobile devices [14]. Under this scheme, it is inevitable to congest the actual computing service called the Cloud, getting a drop in the quality of service (QoS) that in this case is of critical importance when flooding might occur. The solution for this matter is the use of Edge Computing where resources are positioned at the Edge of the Network, so these resources can handle computational demanding tasks, reducing latency. This information is sent to a collector by a gateway where it is examined together with information from official weather forecast, surveillance cameras, and a network of sensors installed in specific areas surrounding the studied zone. As this information must be accurate and in real time, it cannot rely on cloud systems, there is the need for a private system (cloudlet). Efforts to concrete edge computing have been significant in recent years giving birth to Fog computing [15], where a virtualised platform for networking and computing services are distributed within the cloud to things continuum. Satya et al. [16] first defined cloudlet computing: a network of small data centres in a box (cloudlets) to act as an intermediate layer between user and cloud, this is a local processing unit used for temporary storage and processing.

The cloudlet evaluates the data coming from smartphones identifying spatiotemporal patterns; users can report weather changes such as temperature, humidity, and wind [17]. This information can be used by applications to infer to a certain degree of accuracy the severity of a possible rainfall. In this scenario, when there are enough data taken through time it is possible to observe patterns that as well will be useful in flooding prediction. Once patterns are available, it is probable to model how weather changes lead to strong rainfall flooding and then direct alerts to citizens. In this case, social media plays a big role when there is the need of exploring people's experiences such as how they describe their impressions about weather changes [18]. Considerations like different types of characterisation of land use such as buildings, green areas, areas that used to be unoccupied and now have been paved for private use, commercialisation, both fixed and itinerant, use of land with bad disposal of material residues, etc., have to be taken into account for design purposes.

4 Architecture

Architecture has been defined [19] as a set of functions, states, and objects together with their structure, composition and spatial-temporal distribution. The development of a smart city is usually based around a centralised architecture, where it must have the ability to work with a heterogeneous type of devices which generate different types of data. These data are sent via ICT to a control centre where will be stored, processed, and retrieved according to the needs of the end user. Hence, the integration of different

technologies is the main feature enabling this architecture to evolve if required, to allow for other devices to be connected to support new applications and services. In the development of this project the actual technology of the urban zone in question needs to be addressed, to make possible the monitoring and control for the weather prediction. Therefore, new IoT technology needs to be installed. Setting up this technology represents a huge challenge due to the considerable number of heterogeneous devices. Correspondingly, to be considered in this project is the IoT infrastructure maintenance to keep up with Smart Cities. Citizen participation sums up to IoT infrastructures by applications on their smartphones generating vast amounts of data. For these records, data models need to be created considering semantic descriptions of the urban atmosphere. This project proposes a platform to facilitate the services to the community members. In smart cities is important to adjust citizen's data streams to a data model that would facilitate its usage. The logic used will depend on the background of each community, as the model must take into consideration social, economic and idiosyncrasy to create new rules to integrate the community organisation into a decision model. Also, these data would be accessible to local authorities, making them aware of the situation in real time. Using these information/data the authorities could implement or improve the appropriate actions to control/prevent the flooding risk in the community.

Lots of issues need to be attended during the system designing, such as: how citizens can have easy access to the generated data, coming from heterogeneous sources? Is the proposed infrastructure robust enough for the collection of data from community members? How to use information coming from installed sensors and surveillance cameras? The proposed platform implements a directory that contains all data sources generated within the IoT infrastructures, from crowdsourcing data streams, data generated from the network of sensors and surveillance cameras. These data in time could also be of help when needed for statistical purposes as to detect whether climate change is worsening the flooding problem. To construct a model for weather prediction as in our case, variables such as temperature, wind, air pressure etc., must be established from theory like physical equations and from the empirical experience. These models are based on everyday language concepts. The relationship between different concepts should be automatically detected by a machine learning algorithm. This paper proposes the following architecture to show how an application would perform in analysing weather conditions for flooding prediction. The order is as follows: crowdsourcing and sensors, data transmission, data collection, data processing, and application.

Crowdsourcing and sensors. This layer consists of three types of data sources: smartphones, sensors and surveillance cameras. The users also can send voice or text messages as well as photos. The members of the community can send information daily or whenever they detect the environment is changing like air, wind, humidity etc. Additionally, they can co-operate giving information when they see situations like for example when they see that litter is clotting the drainage, or any other situation they consider might worsen flooding.

Transmission of data. All data coming from members of the community, sensors and surveillance cameras should be sent to a server for processing and analysing. At this point, forwarding and routing protocols must be well defined in advance as the nature of the heterogeneous data calls for enhanced nodes able to perform fine.

Data collection. Data is collected from selected nodes that can preserve privacy for all data contributors. This layer depends on both computing and human interaction, so its function has more weight over the other three layers.

Data processing. At this point what really is important is the fact that it is possible to singularise frequent data patterns that will be useful when it comes to compare how climate change is affecting or not the studied community. To solve this problem, a method is developed to transform the raw data that would allow clearly identifying patterns and measuring them.

Application. The function of this layer is multiple, such as data management, user interface, etc. It generates services for the crowd, so they can see results in a manner easily understood for them. A user interface is generated to enable communication between machines and humans. There should be an application that combines human interaction and electronic mechanisms. This layer has the task of integrating data streams with other events from lower layers to be stored in a common data storehouse.

5 Technological requirements for the community

People need to have access to an early warning system (EWS) in order to mitigate flood risk within communities including an evacuation or emergency plan. This EWS will help in taking measures of adaptation, preventive and reactive procedures by collaborating with neighbours and local authorities to build resilience. For the preventive plan, the community participation in detecting possible situations that worsens floods is of importance as well as acting upon it for alleviation purposes. Nowadays, many people are familiarised with the use of technology (being social media or web pages) to report or receive information they consider important about the issues that affect their community. Therefore, it would be interesting and important to take advantage of this matter by implementing a web page with an easy access and understanding of the information. This might be quite substantial to present it in a graphical way, so people that is not very technical can be informed in time when an event has a high probability to happen giving them as much time as possible to act appropriately. According to Alexander et al. [20], resilience includes the capacity to resist, to absorb and recover, and to adapt. Based on the work of Mees et al. [21] where the authors present an analysis on flooding in 5 different European countries, each country present different levels of flooding risk, and for all of them most of the responsibility in finding solutions depend on the state. Thus, being aware of this, in their work they start to consider the participation of citizens together with the authorities for a better understanding of the problem and ways of solving it. To accomplish this goal, they present an analysis of coproducing flood risk management through citizen involvement. They gathered information mainly from citizens, although analyse government documents as well. By analysing both kind of information, enhancement of the whole data was attained.

From the conclusions presented in [21], on every country studied there were stated that coproduction was an important issue about flood risk and for a suitable management of the problem. They developed coproduced practices on Flood Mitigation and Flood Preparation. As for mitigation in England, they analysed flood highs on the floodplain, took measures for property level protection (PLP) across the country. As for

Belgium they developed a project on flood-resilient building and PLP only in exceptional cases. In France there were limited PLP and implemented local programs for some buildings. Netherlands increased water retention in neighbourhoods, also had plot projects on flood-proof houses. Finally, Poland rarely have flood protection at property level. For the same countries, in respect to coproduction in flood preparation, England generates community flood action groups with voluntary schemes, as well as national and local awareness raising campaigns. Belgium presents only in very few cities voluntary emergency teams. In France local authorities are obliged to give information about risk and how to behave on an event by volunteers and civil servants. As for the Netherlands they have campaigns of awareness through volunteers and professional fire services. Finally, Poland works through local citizen initiatives with voluntary fire brigades along with professional fire services.

It is increasingly argued that a diversification, coordination and alignment of Flood Risk Management Strategies (FRMSs), including flood risk prevention through proactive spatial planning, flood defence, flood risk mitigation, flood preparation and flood recovery, will make urban agglomerations more resilient to flood risks [23].

In their paper, Mees et al. [21] conclude that co-participation of citizens in resolving the problem of flooding is important for resilient purposes. Also, they state that it really does not matter what country is under study and the differences in which they tackle flooding, the problematic is much alike and the main stages to deal with it are quite similar such as: mitigation, preparedness before and during the event, and continued work after the event. Therefore, for the project proposed in this article it is possible to adapt these data to some areas of Mexico, particularly in Mexico City where there are many communities prone to flooding. Accordingly, we have proposed in the following table the different stages and possible technology aids to the cocreation of smart cities. Later on, it is expected to corroborate this study in a small community within Mexico City, where it is expected to research the perception and adaptation of the communities to climate change-related risks, and in particular to understand people's perceptions and experiences on flooding events towards determining specific needs to mitigate such events. From the literature review and in order to adapt the technology to the community needs, it is observed that some of these needs are solved only with information supply, others with the combination of sensors, processing and communication technologies. Regarding to the use of technology, for a better management of a flood event, four stages have been identified: Mitigation, Before, During, and After flood. Hence, we propose technology requirements to attend each identified need in each stage of flood management. An example of these is described in Table 1.

An EWS needs data analysis, prediction models, and sensor fusion to forecast possible flood events based on data supplied by sensors and people. From the analysis in the literature of flooding events the technological aids requirements can be divided into three levels (see Figure 1):

First level technology aids (Informative). This consists of storage and communications technology to concentrate and supply information, about local reaction plans in a flood event, for example, to the community inhabitants, namely, a platform like a web page and/or a mobile application.

Table 1. Matching of needs and technology requirements for flood events management.

Stage	Aspect	Need	Possible technology aids
Mitigation	Infrastructure maintenance and adaptation.	Insufficient drainage.	Sensor Technology for monitoring the amount of rain. Processing Technology to analyse the data in a rainy season to evaluate the current drainage system. Communications Technology to report the results.
Before	Information for risk management for inhabitants.	Reduce damage to homes.	Communications Technology to send information to inhabitants about what they must do before, during and after suffering a flood.
During		Vehicular mobility problems to get to their houses.	Sensor Technology for monitoring avenues and/or streets. Processing Technology to analyse the sensors information. Communications Technology to present safe streets in a map.
After	Health risks.	To know about the health problems that the community faces after a flood and the stagnation of water. (Moreover, if they are sewage).	Communications Technology to issue prevention recommendations for health (cleaning, etc.).

Second level technology aids (Monitoring). Monitoring and situational awareness information on flood events in real-time. This can include the installation of sensors and crowdsourcing data from community inhabitants by means of text messages, social networks or from mobile apps; dashboard integrated with maps for real-time visualisation of information and registry of historical data and trends.

Third level technology aids (Analytics). Analytics of the captured data, prediction models, and sensor fusion algorithms to forecast future flood events, generate automated alerts, notifications, and data sharing.

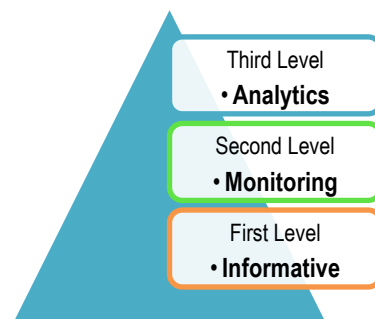


Fig. 1. Levels of technology aids for flood management.

The overall smart technology intervention will allow to go from a reactive to a proactive response to flooding events and ultimately to a predictive flood management. Furthermore, the overall aim of any technology aid is to increase community's resilience to flooding. IoT based smart cities depend on ICT, so the study of the main communication protocols is a must. IoT uses many short and wide range communication protocols with the purpose of transporting data between devices and servers. ZigBee, Bluetooth, Wi-Fi, WiMAX and IEEE 802.11p are the most used short-range wireless technologies. Within wide range technologies are Global System for Mobile Communication (GSM), General Packet Radio Service (GPRS), Long Term Evolution (LTE), Third Generation Partnership Project (3GPP). There is also Low Power Wide Area Network (LPWAN) technology which is a promising solution for long range and low power IoT and machine to machine (M2M) communication applications. The major proprietary and standards-based LPWAN technology solutions available in the market include Sigfox, LoRaWAN, Narrowband IoT (NB-IoT), and long-term evolution (LTE)-M, among others. For the development of this project the LoRaWAN, Wi-Fi and GPRS communications protocols are proposed to be explored for the monitoring of flooding prone areas.

6 Related issues

Another big problem is the fact that people need to have an incentive to participate, be economical or social. In this case a social benefit is the key. Community members need to know that they are part of the solution, highlighting this is the biggest incentive in overpopulated urban zones attracting and encouraging more involvement. An additional challenge is how to send data from members of the community to the server/cloud because these data can be text messages, voice or images. Accordingly, for example, in the case of text or voice messages, there is the need for analysis that depends a lot on language, culture or semantics. Also, characteristics of the server's devices must be considered, such as bandwidth, wireless communications, frequency of data sending from users, etc., all these problems should be addressed with data management and data processing. Data redundancy is another important issue as most of the time there are

data coming from multiple sources such as sensors systems, or multiple members of the community which causes what is called data redundancy. In this case, it is of importance to have a selection data system able to estimate the best approach. Especially when there is also the semantics problem involved, this represents a more intricate issue. Therefore, detection technology must be developed to guaranty the quality of the data. The proposed IoT architecture is the simplified three layers IoT model presented in Figure 2.

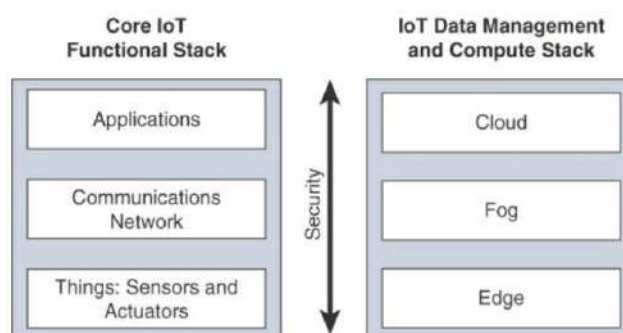


Fig. 2. Simplified three layers IoT architecture (adapted from (22)).

At the bottom layer are the sensors (and, if needed, actuators) nodes, which are proposed to be located at points in the studied zone where certain amount of rain flow comes into the zone, as for example, communities located at valleys which are surrounded by hills where it has been detected that in a matter of seconds huge amount of water may come into the urban zone. Therefore, a set of sensors could be used to measure rainfall, e.g. rain gauge sensors and/or water level measurement sensor (radar or ultrasonic sensors) are proposed to be installed at specific locations at these points at street level. Another set of sensors could be installed at street lights in the surrounding area of study with the purpose of sensing the level of rain fall on such streets so the locals could know if it is safe to walk or drive through these streets. Finally, and most importantly are the sensors that could be installed at street level in the actual community to detect the amount of rainfall that will lead to the decision on whether the community is at risk of flooding. Also, considering at this layer is the information gathered through smartphones and surveillance cameras.

The communications and network layer will collect measurements from sensors nodes, send these data together with the information from smartphones and cameras to gateways which then will send all collected data to the cloud (or to a private server) via Internet where these can be analysed, or alternatively edge computing technology can be used to perform data analytics closer to where the data are collected. The cloud has three basic types of services to offer: as infrastructure for storage of data, as platform for computing and as software for delivering IoT services.

At the application layer services can be provided such as data processing for analysing the data fetched from the devices (sensors, social networks, cameras, etc.) and transforming these into usable information, for example prediction of flooding, alarm

activation if thresholds are surpassed or statistical analysis and trending. Also, graphical user interfaces (GUI) can be provided for users, for example to use smartphones to provide users access to data or to other IoT applications. In addition, clouds can be used to analyse, sort out and store the data, and websites can be used as interfaces.

For the processing and management of data, a pre-processing and event detection must be performed in advance to convert it into knowledge. For this task it is essential to implement algorithms such as genetic algorithm or neural networks. As for data interpretation it is important to present to the end users' information that is easily understood. In this case visualisation is important for the residents so they can take decisions on whether flood is prone to occur. Visualisation for this project is expected to be through a web page where residents will have easy access by their phones or computers. It is proposed that data is going to be visualised using geo-spatial maps for a more friendly presentation for the end user being keyword based, semantic based and quality based.

7 Proposed technologies

At the first level a website is proposed and/or a mobile application to concentrate and make available diverse flood management relevant information. This information should be shown in a friendly form, especially for those citizens that have little knowledge of digital technologies. The proposed informative webpage could present sections as Memory Reinforcement to show past events, actions taken and which of them worked and/or failed; Risk Management to inhabitants; Days of waste collection information, Vulnerable areas map, Institutions information and a Health Risk consequences guideline. In figure 4 a proposed web page for informative needs about flooding events is shown.

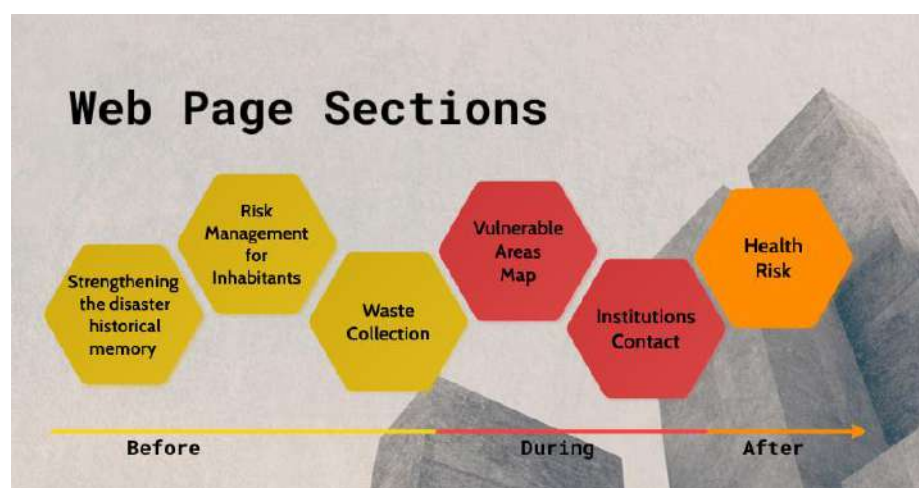


Fig. 4. Informative web page.

The second level considers monitoring and visualisation for situational awareness of flood events in real-time, which includes the installation of sensors and the use of communications technology using the three layers IoT architecture and crowdsourcing technology. Therefore, the first proposal to attend this need level is to integrate a minimum sensors kit by a block (street) to be monitored, which is scalable and modular; hence, can be scaled up to a suburb, town or even a city. Also, at this level a dashboard will be integrated with maps for real-time visualisation of information and registry of historical data and trends. This technology proposal is described as follows:

By Block:

- HD (High Definition) outdoor camera (powered with solar panel).

A camera designed to withstand rain, snow, and extreme temperatures, typically connected to a Wi-Fi network, which allow to view live video of the activities occurring outside. HD is defined by specific resolutions at specific frame rates with a specific aspect ratio. HD refers to cameras with a standardised resolution of 720p or 1080p (horizontal). This sensor could help in monitoring the streets and strainers.

- Water level sensor (radar or ultrasonic) for level monitoring in regulating streets.

A water level sensor is a device that is designed to monitor, maintain, and measure liquid (and sometimes solid) levels. Once the liquid level is detected, the sensor converts the perceived data into an electric signal. This sensor could help to monitor the water level on the streets.

- Smartphones for data collection. This device could help to send images and/or videos, texts and even voice messages.

By suburb:

- Disdrometer and / or weather station with rain gauge (powered with solar panel).

A disdrometer or rain spectrometer is a laser instrument that measures the drop size distribution falling hydrometeors. Based on the principle of optical laser active detection, the disdrometer can continuously observe the raindrops definition size, velocity, and quantity of raindrops. This device could help to monitoring the amount of precipitation and help to predict the trends in rain fall. Figure 5 shows an OTT Parsival² laser disdrometer.



Figure 5. OTT Parsival2 laser disdrometer (<https://www.ott.com/products/meteorological-sensors-26/ott-parsival2-laser-weather-sensor-2392/>).

A weather station is a facility with instruments and equipment for measuring atmospheric conditions to provide information for weather forecasts and to study the weather and climate. The measurements taken include temperature, atmospheric pressure, humidity, wind speed, wind direction, and the amount of liquid precipitation (rainfall).

Finally, the third level oversees the analytics. The data signals will be processed, therefore depend on the results, to send messages to inhabitants and/or institutions (using ICT). Besides, warning or announcements can be sent through a website and/or mobile applications. The processing could be done on the edge or in the cloud. Also, a deeper analysis could include neural networks to predict a hazard.

8 Conclusion

Building smart cities calls for the participation of its citizens defining strategies that involves them, getting their participation in discussions and proposals for the development of technologies that help them with the actual issues that affect the whole community. Implementation of IoT technologies in urban zones will enable the development of the concept of smart city, giving rise to a system able to help in dealing with the problematic that overpopulated urban zones generate by applying multidisciplinary strategies. By involving the residents in the problem-solving leads to the co-creation of a more resilient community implementing state of the art technological tools to communicate, monitor and mitigate flooding risk in vulnerable population. We have presented a system able to analyse heterogeneous data coming from crowdsourcing, surveillance cameras and a local network of sensors for an overpopulated urban zone. Many urban zones in Mexico suffer from severe flooding every year; this flooding may be the result of bad urban planning and climate change. The resulting information gather from these three sources is going to be used for statistical analysis to determine the probabilities of flooding in the studied zone. In this work a text analysis is proposed to be used to obtain information on ambience changes. Reported events will be computed by sampling different text messages which have been organised on type of event by determining a set of keywords indicating the weather state. The system we propose can be adapted for several applications to enhance community life (such as air pollution monitoring, health care, transport systems, etc.) as well as been adapted for other similar communities. Additionally, the development of this project highlights several challenges areas and research opportunities within communities. Investigation should be addressed on models and design patterns for crowdsensing systems using multidisciplinary sources of knowledge which should include social science, computing, sensor systems, community members etc.

9 Future work

This project will enable the implementation in the short time of a crowdsourcing and IoT system to collect, communicate, store, process and visualise data and information that is going to mitigate flooding risk, towards creating resilient communities facing these events. At the time of writing this paper, we already have identified some communities that present flooding problems in Mexico City and for mitigation purposes the

project is in the stage of technology identification, purchase, and integration of the overall system. This will enable future research and experimentation with smart city solutions as cities will, in time, depend more on technology to provide facilities to support solution to other worrying issues such as transportation, energy usage, waste management, health care, mobility, etc., in ever increasing overpopulated urban zones.

Acknowledgment

The authors would like to thank the Consejo Nacional de Ciencia y Tecnología (CONACYT) for its support in this research, under grant CONACYT-296528. We also acknowledge support from the UK Newton Fund and ESRC, under grant ES/S006761/1.

References

1. Shah, S., Seker, D., Hameed S., Draheim, D.: The Rising Role of Big Data Analytics and IoT in Disaster Management: Recent Advances, Taxonomy and Prospects. *IEEE Access* 7, (2019).
2. Mehmood, Y., Ahmad, F., Yaqoob, I., Adnane, A., Imran, M., Guizani, S.: Internet-of-Things-Based Smart Cities: Recent Advances and Challenges. *IEEE Communications Magazine*, 15-24 (2017).
3. Zanella, A., Bui, N., Castellani, A., Vangelista, L., Zorzi, M.: Internet of Things for Smart Cities. *IEEE INTERNET OF THINGS JOURNAL*, 1(1), 22-32 (2014).
4. Jin, J., Gubbi, J., Marusic, S., Palaniswami, M.: An Information Framework of Creating a Smart City through Internet of Things. *IEEE Journal*, (2013).
5. Mitton1, N., Papavassiliou, S., Puliafito, A., Trivedi, K.: Combining Cloud and sensors in a smart city environment. *Journal on Wireless Communications and Networking* 1, 1-10 (2012).
6. Caragliu, A., Del Bo, C., Nijkamp, P.: Smart cities in Europe. *Urban Technol* 18(2), 65– 82 (2011).
7. Zanella, A., Bui, N., Castellani, A., Vangelista, L., Zorzi, M.: Internet of Things for smart cities. *IEEE Internet Things J.* 1(1), 22–32 (2014).
8. Knüsel, B., Zumwald, M., Baumberger, C., Hadorn, G., Fischer, E., Bresch, D., Knutti, R.: Applying big data beyond small problems in climate research. *Nature Climate Change* 9, 196-202 (2018).
9. Gutiérrez, V., Amaxilatis, D., Mylonas, G., Muñoz, L.: Empowering Citizens Toward the Co-Creation of Sustainable Cities. *IEEE Internet Things J.* 5(2), (2018).
10. Fenner, D., Meier, F., Bechtel, B., Otto, M., Scherer, D.: Intra and inter 'local climate zone' variability of air temperature as observed by crowdsourced citizen weather stations in Berlin, Germany. *Meteorologische Zeitschrift* 26(5), 525-547 (2017).
11. Bonomi, F., Milito, R., Zhu, J., Addepalli, S.: Fog computing and its role in the internet of things. *Proceedings of the MCC workshop on Mobile cloud computing* 1, 13-16 (2012).
12. Sabella, D., Vaillant, A., Kuure, P., Rauschenbach, U., Giust, F.: Mobile-edge computing architecture: The role of mec in the internet of things. *IEEE Consumer Electronics Magazine* 5(4), 84–91 (2016).
13. Satyanarayanan, M., Bahl, P., Caceres, R., Davies, N.: The case for vm-based cloudlets in mobile computing. *IEEE Pervasive Computing* 8, 14–23 (2009).

14. Fiandrino, C., Anjomshoa, F., Kantarci, B., Kliazovich, D., Bouvry, P., Matthews, J.: Sociability-Driven Framework for Data Acquisition in Mobile Crowdsensing Over Fog Computing Platforms for Smart Cities. *IEEE transactions on sustainable computing* 2(4), 345-358 (2017).
15. Bonomi, F., Milito, R., Natarajan, P., Zhu, J.: Fog computing: A platform for internet of things and analytics, in *Big data and internet of things: A roadmap for smart environments*. Springer, 169-186 (2014).
16. Satyanarayanan, M. The emergence of edge computing. *Computer*, 50(1), 30–39 (2017).
17. Ganti, R., Ye, F., Lei, H.: Mobile Crowdsensing: Current State and Future Challenges. *IEEE Communications Magazine*, 32-39 (2011).
18. Ghermandi, A., Sinclair, M.: Passive crowdsourcing of social media in environmental research: A systematic map. *Global Environmental Change* 55, 36-47 (2019).
19. Zahariadis, T., Papadimitriou, D., Tschofenig H., Haller, S., Daras P., Stamoulis, D., Hauswirth, M.: Towards a Future Internet Architecture. *Future Internet Assembly*, 7-18 (2011).
20. Alexander, M.: *Constructions of flood vulnerability across an etic-emic spectrum*. Middlesex University, Flood Hazard Research Centre, London UK. (2014).
21. Mees, H., Crabbé, A., Alexander, M., Kaufmann, M., Bruzzone, S., Lévy, L., Lewandowski, J.: Coproducing flood risk management through citizen involvement: insights from cross-country comparison in Europe. *Ecology and Society* 21(3), 1-14 (2016).
22. Hanes, D., Salgueiro, G., Grossetete, P., Barton, R., & Henry, J.: *IoT fundamentals: Networking technologies, protocols, and use cases for the internet of things*. Cisco Press. (2017).
23. Hegger, D. L. T., Driessen, P. P. J., Bakker, M., Alexander, M., Beyers, J. C., Buijze, A. W. G. J., Dieperink, C.: A view on more resilient flood risk governance: key conclusions of the STAR-FLOOD project. STAR-FLOOD Consortium. (2016).

Carbon regulation policies in transport: a review

Vanessa de Almeida Guimarães¹[0000-0001-7662-3499], Rayssa Paula Correia Lima¹,
Maxwel de Azevedo-Ferreira² and Pedro Henrique González¹[0000-0003-0057-7670]

¹ Centro Federal de Educação Tecnológica Celso Suckow da Fonseca, Brazil

² Instituto Federal de Educação Ciência e Tecnologia do Rio de Janeiro, Resende/RJ, Brazil

vanessa.guimaraes@cefet-rj.br

rayssa.lima@aluno.cefet-rj.br

Abstract. Considering that climate change is one of the leading global concerns and the transport sector is one of the main global sources of CO₂ emission, this sector must be carefully considered when planning a low carbon economy. Therefore, this paper investigates how the scientific literature published in the Web of Science (WoS) database addresses the carbon policies in the transport sector, identifying the main collaboration network and the main interest topics. Besides, we have gathered some actions that could be implemented to reduce carbon emission and, consequently, help achieve the targets of carbon agreements. It was found that the interest on this subject is recent and the carbon tax is the policy addressed the most. The articles also point out actions aiming to reduce CO₂ emissions, such as improvements in urban mobility, use of biofuels, technological improvement of vehicles, incentives to electromobility, among others.

Keywords: Transport, Carbon Emission, Public Policy.

1 Introduction

Human activities such as industrialization, deforestation and soil cultivation methods emit pollutants and greenhouse gases (GHGs) into the atmosphere, causing climate change [1]. As a result of climate change, we have seen catastrophic effects, such as melting glaciers and rising sea levels. To reduce the effects of global warming, mitigation measures have been established for the most diverse sectors, from energy generation to transportation.

In this context, Conferences and International Agreements arise to discuss policies and actions to mitigate or stabilize GHGs' concentration in the atmosphere to prevent anthropic interference in climate change. For example, the Meeting of Conference of the Parties of the United Nations Framework Convention on Climate Change (UNFCCC) annually discusses climate change. Besides, the 2030 Agenda for Sustainable Development, proposed by the United Nations, has Sustainable Development Goals (SDGs) directly related to Climate Change (SDG 13) [21]. Besides, other SDGs are transversally related to it, as SDG 7 that verse on clean and accessible energy, SDG 14 about life below water, SDG 15 about life on land and SGG 9 that concerns Industry,

Innovation and Infrastructure, including here transport. Besides, the governments worldwide have developed carbon regulation policies, such as carbon cap, carbon trade and carbon tax [23], that will be addressed in this article.

The transport sector is one of the main elements of countries' infrastructure, fundamental to its economic development since transport activities allow the flow of people and goods. However, it causes environmental problems, as carbon dioxide (CO₂) emission. CO₂ is the main GHG, which emissions are associated with the growing use of motorized vehicles, especially those that use fossil fuels (such as gasoline and diesel). According to Energy Research Office (in Portuguese, *Empresa de Pesquisa Energética*), this sector was responsible for 45.4% of the total anthropogenic emissions of carbon dioxide equivalent (CO_{2-eq}) associated with the Brazilian energy matrix in 2019 [22].

Besides, among the transport modes, the road alternative corresponds to 72% of global emissions [20]. Thus, the transport sector must be carefully considered when planning a low carbon logistics sector. Based on this context, this paper is based on the following research question: how the carbon regulation policies are being implemented in the transport sector? This paper investigates how the scientific literature published in the Web of Science (WoS) database addresses the carbon policies in the transport sector, identifying the leading collaboration network and the main interest topics. Besides, we have gathered some actions that could be implemented to reduce carbon emission and help achieve carbon policy targets.

From this introduction, the article was divided into four sections: the theoretical framework about carbon regulation policies (Section 2); the methodological procedures (Section 3); the presentation of the main findings (Section 4) and the final considerations (Section 5). Finally, we have acknowledgments and references.

2 Carbon Regulation Policies

Although emissions from burning fossil fuels started before the industrial era, it became the dominant source of emissions, increasing CO₂ concentration in the atmosphere [1]. Aware of the adverse effects in climate change, different forums and agreements were developed to find alternatives to impact less the environment (as the United Nations Climate Change Conferences), and in a broader perspective, to promote sustainable development (as 2030 Agenda).

From 2000 to 2015, the United Nations Millennium Declaration was one of the main Sustainable Agreements that established 8 Millennium Development Goals (MDG) to reduce poverty. Among them, MDGs 7 was dedicated to deal with environmental issues [24]. Since 2016, the 2030 Agenda is the main Agreement committed to sustainable development, establishing 17 SGD and 169 targets. There are SGDs that concern with transport infrastructure (SGD 9) and environmental preservation (SGDs 13, 7, 14 and 15). [2] emphasize that agreements and protocols were created to enable a better world for future generations [2]. Figure 1 presents the main international agreements and climate conferences.

Vienna Convention set the basis for the Montreal Protocol's proposition, which proposes mechanisms to protect the ozone layer by progressively reducing the production

and consumption of Substances that Deplete the Ozone Layer (SDOs) [25]. United Nations Framework Convention on Climate Change proposed global agenda to minimize global environmental problems.

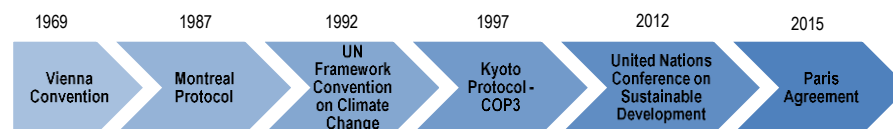


Figure 1 - Main International Agreements and Climate Conferences

Kyoto Protocol, by its turn, established targets for reduction/limitation of emissions. Besides, it implemented innovates mechanisms aiming at assisting the countries in reducing the emission and achieve their goals: Emissions Trading, Joint Implementation and Clean Development Mechanism - CDM. This Agreement is in its 2nd phase (2013 – 2020), aiming at reducing the emissions to, at least, 18% below the 1990s' levels (in Europe, the target is 20%) [26].

Developing countries, like Brazil (also called Non – Annex I Parts), can only participate in CDM mechanism. A developing country can obtain Certified Emission Reductions (CERs) from an MDL Project, which can be sold to a developed country (also known as Annex I Countries). Therefore, the Kyoto Protocol provides for the possibility of trading carbon offsets among the countries: by exchanging credits (or CERs), it would avoid an intense increase in global emissions [2].

As a result, interests in CDM projects in developing countries (which do not have mandatory targets) arise [3]. The costs or limits imposed by the increase in the concentration of GHGs in the atmosphere resulting from human activities are now reflected by the market, influencing investments in low carbon technologies. Table 1 presents the ten most recent CDM projects proposed and approved by UNFCCC related to the transport sector [28].

As a result of the Kyoto Protocol, Brazil developed CDM projects, benefiting from the carbon credits obtained and sold to other countries. There are incentives for investing in low-carbon technologies and financing for projects in the transport sector, such as the Taubaté Urban and Socio-Environmental Mobility Improvement Program, with the receipt of a loan of R\$ 60 million, made by the Development Bank of Latin America [29].

Regarding the United Nations Conference on Sustainable Development (also known as Rio+20), it discussed the renewal of the political commitment to sustainable development. It sets the basis for the proposition of the 2030 Agenda (already mentioned in this paper). Concerning to the Paris Agreement, it strengthened the global response to climate change by establishing a commitment to limit the increase of the global average temperature (equal or below to 2°C). It is considered the first-ever universal, legally binding global climate change agreement: the Katowice package adopted at the UN climate conference (COP24) in 2018 established the standard rules, procedures and guidelines that operationalize it [27].

According to the Nationally Determined Contribution (NDC), the European Union agreed to reduce, until 2030, the GHG emissions by, at least, 40% compared to 1990

[27]. By its turn, Brazil has committed to reducing GHG emissions by 37% and 43% below the level of 2005, by 2025 and 2030, respectively [4]. Regarding the transport sector emissions, the country committed to promote efficiency measures, improvements in transport infrastructure, and public transport in urban areas [4].

Table 1 – Ten most recent CDM projects proposed and approved by UNFCCC related to transport sector (Source: The authors based on [28])

Project	Objective	Country
Landfill Closure and Gas capture CDM project by GAIL at Ghazipur, India (2014)	To collect the landfill gas generated at Ghazipur landfill site in Delhi, India and upgrading it into enriched BTU Natural Gas to use it as a renewable source of energy as Compressed Natural Gas	India ¹
Guiyang MRTS Line I Project (2013)	To establish and operate an efficient, safe, rapid, convenient, comfortable and effective modern mass transit system	China ¹
Demonstration project for annual production 4,000,000 m ³ biogas from organic waste in Anyang City (2013)	To recover biogas to produce Bio-CNG to displace fossil fuel Compressed Natural Gas (CNG), reducing CO ₂ emissions and avoiding the air pollution	China ¹ , United Kingdom ² , Northern Ireland ²
LRT System in Tunisia (2012)	To establish and operate an efficient, safe, rapid, convenient, comfortable and effective modern mass transit system	Tunisia ¹
Mode-shift of passengers from private vehicles to MRTS for Gurgaon metro (2012)	The establishment and operation of an efficient, safe, rapid, convenient, comfortable and effective modern mass transit system with high ridership capacity	India ¹ , Switzerland ²
Lohia Auto Industries Electric Vehicles, India (2012)	To replace fossil fuel powered scooters and mopeds for electric 2-wheelers in India	India ¹ , Switzerland ²
Electrotherm Electric Vehicles, India (2012)	To replace fossil fuel powered 2-wheelers for electric ones in India	India ¹ , Switzerland ²
Nittsu Fuel Efficiency Improvement with Digital Tachograph Systems on Road Freight Transportation CDM Project in Malaysia (2012)	It seeks for various ways for disseminating Japan's knowledge, experience and technologies in the area of logistics services provision	Malaysia ¹
Hero Electric Vehicles, India (2012)	To replace fossil fuel powered scooters by electric scooters in India	India ¹
EKO electric vehicles, India (2012)	To replace fossil fuel powered scooters by electric scooters in India	India ¹

Note: (1) Hosts; (2) Other Parties

To achieve the emissions target, besides the technological improvements, the governments have developed carbon mitigation policies, such as: carbon tax, carbon cap and carbon cap-and-trade (as Figure 2). The carbon tax establishes a tax to be charged on CO₂ emissions (usually per ton of CO₂ emitted) [5], but there is not a maximum amount of emission pre-determined (as a cap). The carbon cap is the opposite: there is a limit of allowed emissions (cap) that cannot be exceeded for any reason. In this policy,

the tons of CO₂ emitted are not charged and there is no way of surpasses the imposed cap.

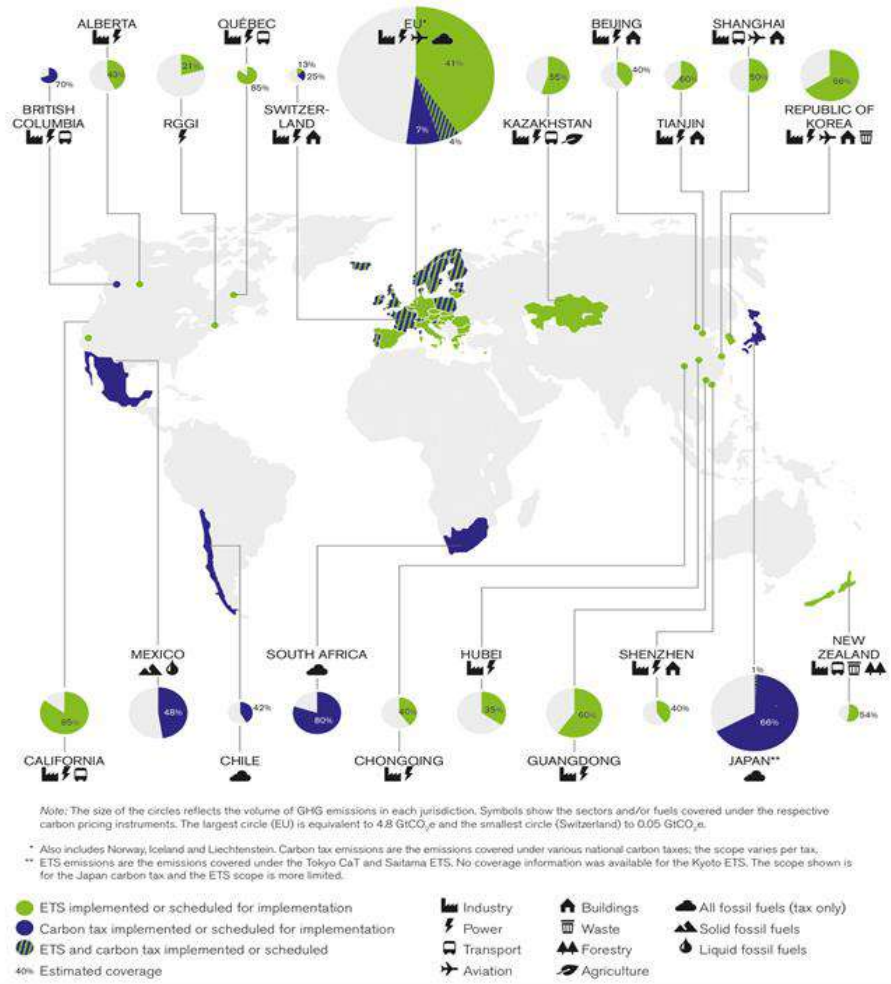


Figure 2 - Carbon pricing instruments implemented or scheduled for implementation, with sector coverage and covered GHG emissions. (Source: [23])

The carbon trading system (carbon cap-and-trade or carbon trade) is a combination of carbon cap and carbon tax policies: there is a maximum limited of CO₂ to be emitted, but a company or sector that need to surpasses this cap might buy carbon credits from another company or sector that emitted less than its cap in the same period. Thus, according to the established limit, the issuance volume will be fixed; what will happen is a rearrangement of credits between companies and sectors [5].

A carbon credit certificate is issued accordingly to the agreed limit for the allowed emissions (cap). These certificates can be traded in a market (called Emissions Trading System - ETS). A company that needs to emit over the cap must decide if it will develop

projects and/or cleaner production processes to reduce its emissions or buy credit certificates from other companies.

All the mitigation policies aim to reduce CO₂ emissions by encouraging companies to develop new low-carbon technologies. Besides, cap-and-trade might generate government revenue when assuming that emissions certificates are auctioned [5]. Another emission trade system is baseline-and-credit. The main difference from carbon cap-and-trade for the baseline-and-credit system is that there is no fixed limit on emissions in the latter. However, companies that reduce their emissions more than they are obliged to due to regulations can earn "credits" that might be sold to companies that need credits to comply with regulations they are subject to [29]. It is important to highlight that in baseline-and-credit' systems, it can be challenging to verify the policy's effectiveness in reducing carbon emission [29] since there is a maximum limit to the emission. At what extent emission reductions are 'additional' – i.e., to what extent they represent something different from what would have happened in any case. Therefore, these policy instruments will not be investigated in this paper.

Figure 2 also shows the carbon pricing instruments implemented or scheduled for implementation, segregated by sector (World Bank, 2016). It is observed that a few countries have adopted carbon policies, mostly in Europe. Among those that have implemented or scheduled pricing instruments, there is a balance between emission trading systems (in green), carbon tax (in blue) and both (hatched). However, the carbon pricing instruments are focused on specific sectors, mostly industry and energy. Initiatives in transport were found in the United States, Canada (British Columbia and Montreal), Kazakhstan, China, New Zealand. In addition, China, Korea and the European Union have policies related to aviation.

It should be noted that, if properly planned and implemented, emission mitigation policies could encourage the use of alternative energy sources, the adoption of cleaner technologies in industries, improvement of transport infrastructure, reduction of deforestation, among others. Those actions would help in achieving a low carbon global economy [5].

3 Methodological Procedures

To perform the review proposed in this paper, we selected the WoS database due to its good coverage, being used in papers with similar methodology [31]. The parameters of the search are detailed in Table 2.

Table 2 - WoS search description (Source: The authors, 2020)

Criterion	Description
Topic	“Transport*” AND (“carbon trade*” OR “carbon cap” OR “carbon tax*” OR “carbon regulation”)
Database	Web of Science (all areas)
Time	All years until 2019 (excluding 2020, as the current year)
Search date	March 2 nd , 2020 at 6:26 p.m.

After the search, we classified the articles, considering only those published in Journals and directly related to transportation. Papers about enhanced oil recovery and that

considered transport as one of many sectors to predict some economic or energetic matrix (macroeconomic forecasts) were removed from the database. The next step consisted of classifying and organizing the database and creating the collaboration networks with Vantage Point software's support. The search allowed us to find 426 documents published in WoS until 2019, 358 of them published in Journals. After the classification, it was found that only 279 articles published in Journals indexed in WoS deal with carbon policies in the transport sector. The main findings are discussed in Section 4.

4 Findings

Figure 3 shows the temporal evolution of publications that deal with some carbon mitigation policies in transport. The first paper was published in 1992, the same year that occurred the UNFCCC, held in Rio de Janeiro. Only in 1995, UNFCCC started to promote the annual meeting of the Conference of the Parties (COP) to discuss climate change. It is reflected in the low volume of publications that remain under five papers per year until 2006.

From 2007, there is a growth in the number of papers published year by year, until 2015. In 2015, we can see the first peak of publications (38 records) since 1992. This can be explained by the Paris Agreement, at COP21, where 195 countries that are part of the UNFCCC agree to develop actions and policies to reduce GHG emissions in the context of sustainable development. In 2016, however, the number of papers decreased to a lower level than in 2014 and 2015, for which we have not found any apparent reason.

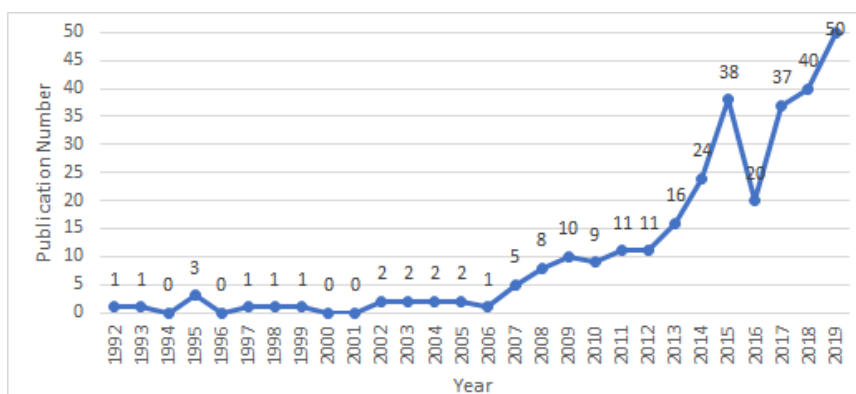


Figure 3 - Evolution of publications by year (Source: The authors, 2020)

After that, the volume of publications grew again, achieving the largest number of publications in 2019 (50 papers). From Figure 1, we can state that the interest in the subject is recent and tends to grow over the years.

Regarding the main authors who published about the subject, no one stands out, which can be explained by the recent interest in the area. The authors with higher

volume of articles are: Chaabane, A., Hassan, A., Leaver, JD., Liao, ZG., four papers each. Figure 4 presents the authors' collaboration network, highlighting in green those with the highest number of papers.

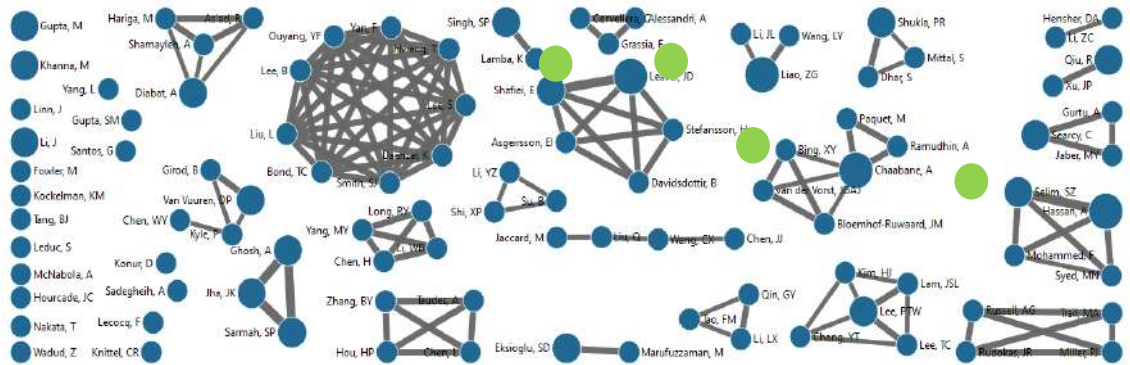


Figure 4 - Collaboration network between the authors (Source: Own elaboration with VantagePoint, 2020)

Figure 4 shows that the main authors are not part of the same collaboration network. Besides, there is a well-consolidated network fully connected, composed of 9 authors (each of them with only two publications). Besides, there are smaller networks, some fully connected, formed with 3, 4, or 5 authors.

Concerning the countries, China and the USA stand out with a higher number of papers (77 and 72 articles, respectively). The United Kingdom is in the 3rd position (with 37 records), followed by Canada with 29 papers and India with 25. Among the 41 countries published about the subject, Brazil is tied in the last position, with only 1 article. However, it is important to emphasize that Brazil is the only Latin American country in the database. Figure 5 presents the collaboration network among countries.

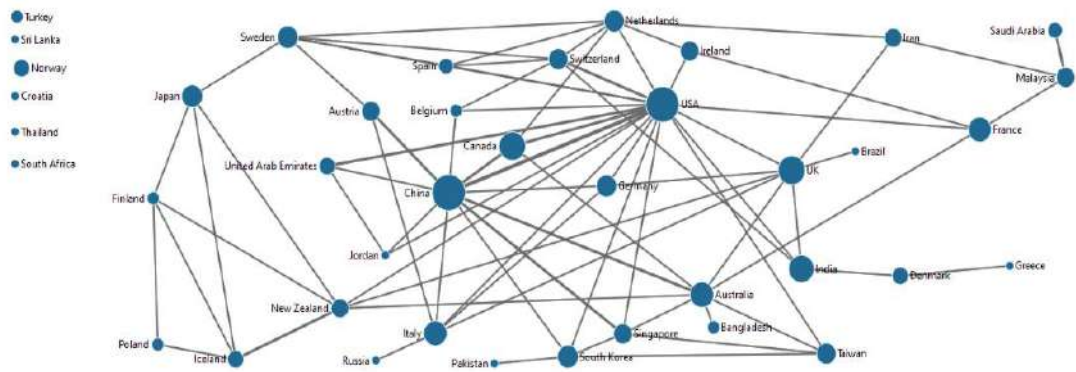


Figure 5 - Contribution network between countries (Source: Own elaboration with Vantage-Point)

USA and China are the countries that collaborate internationally the most, explaining their highest volume of publication. China collaborates the most with the USA (13 joint papers), Australia (6 papers), Canada (4 papers) and Singapore (4 papers), while the USA publishes the most with Canada (4 papers) and Switzerland (4 papers), besides China. Brazil, by its turn, has only one connection (with the United Kingdom). Note that countries with a higher number of publications tend to have more collaboration connections.

It was possible to map the research areas that publish about this subject. Among the 40 areas, the main are Environmental Sciences & Ecology (107 articles), Engineering (101), Business & Economic (95), Energy & Fuels (65), Transportation (55), Science & Technology - Other Topics (43), Operations Research & Management Science (35), Computer Science (19). Note that only the five main areas have published more than 50 papers about the subject. Figure 6 provides the intersection among the main areas.

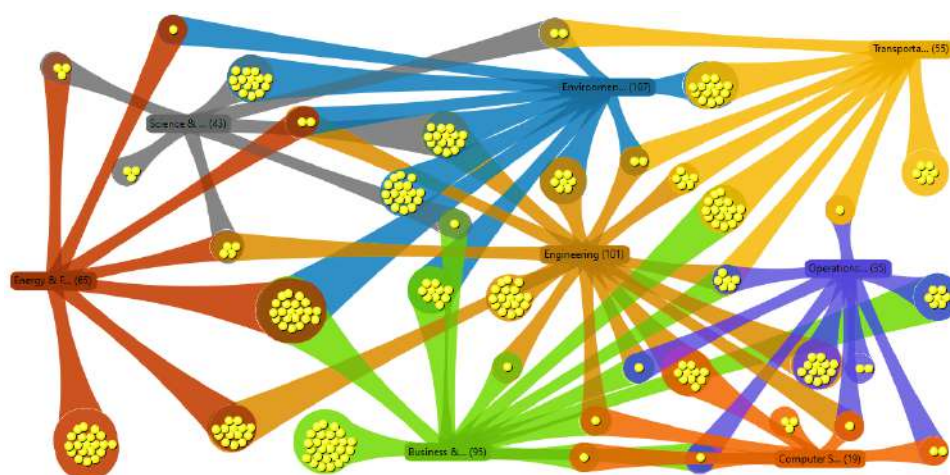


Figure 6 - Map of research area (Source: Own elaboration with VantagePoint)

The first paper, published in 1962, was indexed to the Engineering and Transportation areas. However, the areas did not keep constancy in their publications: both started publishing annually since 2007. We emphasize that Transport appears in the fifth position, with only 55 papers, despite its massive contribution to the emissions already discussed in this paper. In relation to the main journals, Table 3 shows that only four Journals have published more than ten papers about the subject.

Among the 161 journals, Energy Policy stands out with 18 papers, followed by the Journal of Cleaner Production and the Transportation Research Part D, with 14 papers. Likewise, it was possible to find the main keywords of the published articles (Figure 7). It appears that carbon tax, carbon emissions and transportation are the most frequent keywords, with 69, 46 and 21 records, respectively. When excluding the terms of search in the database, the more frequent keywords are carbon emission (46), carbon footprint (16) and climate change (12).

Table 3 - Main Journals (Source: Own elaboration, 2020)

Rank	Journal	Records	%
1°	Energy Policy	18	6.06
2°	Journal of Cleaner Production	14	4.71
3°	Transportation Research Part D (Transport and Environment)	14	4.71
4°	Sustainability	13	4.37
5°	Applied Energy	9	3.03
6°	International Journal of Production Economics	9	3.03
7°	Energy Economics	7	2.35
8°	Computers & Industrial Engineering	6	2.02
9°	Transport Policy	6	2.02
10°	Transportation Research Part A (Policy and Practice)	6	2.02



Figure 7 - Main keywords found in the database (Source: Own elaboration with World Cloud)

Among the policies, the carbon tax has 69 records, carbon trading (10), carbon cap-and-trade (8), personal carbon trade – which is focused on the level of the individual's choices (5), carbon price (4) and carbon cap (3). It can be explained that charging the emissions is easier than investigating a carbon trading market.

In a more detailed analysis of the keywords, they could be divided into ten categories: (i) carbon emission and carbon mitigation policies; (ii) transport alternatives; (ii) energy (e.g., renewable sources, alternative energies, policies related to low carbon fuel); (iii) green and reverse logistics; (iv) supply chain (closed loop or not); (vii) electric vehicles; (viii) smart cities; (ix) solution methods, often optimization methods; (x) other less frequent words, which are not included in the previous categories. The presence of variants of the word "sustainability" is also noteworthy (15 records). Figure 8 relates the most cited keywords with the most relevant country. Only the USA has published a paper with these keywords. China is the country with the largest volume of publications published with all of them, except by climate change.

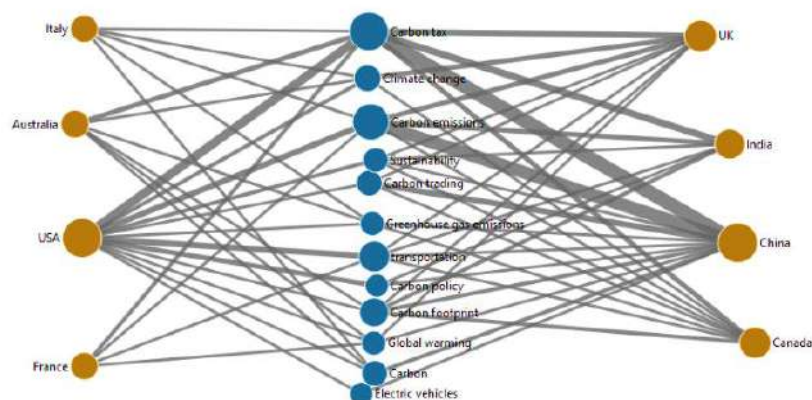


Figure 8 - Mapping of the most cited keywords by country (Source: Own elaboration with Vantage Point software).

Considering de 279 articles that compose our database, a systematic review showed that the carbon tax is present in 71% of the articles and 34% of the papers adopt more than one regulation policy. It was also observed that 46% of the articles deal with freight transportation, being the road mode the most frequent. The ten most cited papers are presented in Table 4.

Finally, it was analyzed the improvement actions proposed in the ten most cited papers. The production and use of low carbon fuels (biofuels) in the transport sector to reduce the use of fossil fuels [9, 15,16,17,18] is discussed the most. Besides, they also suggest: the use of electric vehicles [10,12], the improvement in public transport [13,14,18], a better management in transport logistics [11,13,15,18], the development of new engines [9], among others. There are also actions proposed in other areas, such as using renewable sources (installation of photovoltaic panels to recharge electric vehicles) and the improvement of energy efficiency [10,11,12,14,15] in the energy sector.

Some of the articles mention that individuals must collaborate to mitigate GHG by adopting actions as prioritizing public transport and avoiding the waste of energy [12,13,14,15].

Other improvements and technological innovations that could help in carbon mitigation are [6 - 8]: (1) incentives for the use of energy-efficient modes of transport; (2) incentives for the use of biofuels and electromobility; (3) incentives for non-motorized transportation (bicycle, pedestrian, among others) and public transportation; (4) optimization of logistics processes; (6) technological improvements aimed at energy efficiency; (7) changes in freight transport infrastructure and patterns; (8) home-office; (9) incentive to renew the fleet; (10) others.

It is worth mentioning that according to [7-8], Brazil has the potential to meet its transport commitments related to the NDC, with 13% cuts by 2030 (26MtCO₂-eq) achieved with intensive use of biofuels. However, this strategy's cost-benefit would not correspond to the mitigation potential, with financial losses above 1US\$ / tCO₂-eq. Therefore, the authors indicate that investments in electromobility and infrastructure would be most suitable.

Table 4 - Ten most cited articles (Source: Own elaboration 2020).

Rank	Author	Objective	Focus	Countries	Re-cords
1°	Scott et al. (2010)	It examines the GHG emission reduction goals postulated by various organizations and how the global tourism sector can achieve its participation in these goals	Passenger transport (tourism)	Canada Netherlands Norway Sweden	204
2°	Shiau et al. (2009)	It proposes a plug-in Hybrid Electric Vehicle simulation model to evaluate the effects of additional batteries on fuel consumption, cost and GHG emissions at variety of charging frequencies.	Battery and plug-in vehicle	USA	134
3°	Ramudhin et al. (2011)	It presents a methodology to address sustainable supply chain design problems.	Supply chain	Canada	110
4°	Tulpule et al. (2013)	It proposes a plug-in photovoltaic electric vehicle charging station during the day, located in a work garage.	EV charging station	USA	107
5°	Büchs and Schnepf (2013)	It provides an indication of the types of households that may be particularly affected by mitigation policies targeting of specific areas (as transport).	Passenger transport	UK	96
6°	Tiedemann et al. (2005)	It examines how people choose the technologies and incorporate this understanding of consumer choice in energy saving models.	Passenger transport	Canada	91
7°	Cachon (2013)	It presents a retail supply chain model that includes operating costs, as well as a cost for environmental externalities associated with carbon emissions.	Supply chain	USA	90
8°	Leduc et al. (2009)	It finds the ideal locations for polygeneration systems with simultaneous production of electricity, district heating, ethanol and biogas, with the aim of reducing the total cost of production and the environmental impact.	Biofuel refinery	Austria Sweden	88
9°	Giarola et al. (2011)	It determines the ideal configuration of the system that maximizes the expected financial profitability by assessing the influence of the volatility of raw material and carbon costs within an emission allowance trading scheme.	Biofuel supply chain	Italy UK	82
10°	Hensher (2008)	It evaluates instruments related to efficiency, sustainability and equity policies in passenger transport, focusing on cost-benefit ratio and the ability to reduce CO ₂ .	Passenger transport	Australia	78

5 Final considerations

This paper showed how the scientific literature published in the WoS database addresses the carbon policies in the transport sector, identifying the main collaboration network and the main interest topics. Besides, we have gathered some actions that could be implemented to reduce carbon emission and help achieve carbon policy targets.

Despite being one of the primary sources of carbon emission, there were few papers regarding the carbon policies in the transport sector. This can be explained by the research area: the first paper was published in 1992, but only from 2007 is observed an increase in the publication records. It might be related to the fact that the Climate Change Conferences are new: the first COP was in 1995, the Kyoto Protocol date from 1995 and the Paris Agreement was proposed in 2015. Besides, few carbon regulation policies are implemented or on schedule for implementation around the world, as shown in Figure 2.

China and the USA stand out as the countries with the highest level of publications. The five main areas of interest in this subject are Environmental Sciences & Ecology, Engineering, Business & Economic, Energy & Fuels and Transportation (55). Regarding the keywords, most of them are related to some environmental concerns. They were categorized into ten classes: (i) carbon emission and carbon mitigation policies; (ii) transport alternatives; (iii) energy; (iv) green and reverse logistics; (v) supply chain; (vi) electric vehicles; (vii) smart cities; (viii) solution methods; and, (ix) others.

Regarding the carbon policies, keywords related to the carbon tax, carbon trading, carbon cap-and-trade, personal carbon trade, carbon price and carbon cap were found. The carbon tax is the most addressed policy, which might be explained by the fact that it is easier to study a scenario where the emission is charged instead of trading carbon credits (especially due to the scarcity of real data).

Finally, we found as actions to mitigate carbon emission: use of energy-efficient modes of transport; use of biofuels and electromobility; use of non-motorized and public transportation; optimization of logistics processes; technological improvements; changes in freight transport infrastructure and patterns; home-office; fleet renewal; management improvements, among others.

As a limitation of this search, we point out that the results are directly related to the keywords and the database chosen. Also, there is a lack of consolidated data, mainly for the transport sector, since it is a recent interest area. For future studies, we suggest the assessment of the transport sector regarding emissions, the development of applied research considering the implementation of carbon policies (such as carbon trade), the evaluation of electric vehicles' role in the low carbon transport sector etc.

Acknowledgments

The authors thank CNPq for the scientific research scholarship granted and IFRJ for lending the Vantage Point software.

References

1. ONU e a mudança climática. Nações Unidas Brasil. Available in: <<https://nacoesunidas.org/acao/mudanca-climatica/>>.
2. Protocolo De Quioto. Ministério do Meio Ambiente. Available in: <<https://www.mma.gov.br/clima/convencao-das-nacoes-unidas/protocolo-de-quioto.html>>.
3. Araujo, João. Transporte Rodoviário de Cargas no Brasil Mercado Atual e Próximas Tendências. ILOS, 2011. Available in: <https://www.ilos.com.br/web/transporte-rodoviario-de-cargas-no-brasil-mercado-atual-e-proximas-tendencias/?utm_source=blog&utm_campaign=rc_blogpost>.
4. Acordo De Paris. Ministério do Meio Ambiente. Available in: <<https://www.mma.gov.br/clima/convencao-das-nacoes-unidas/acordo-de-paris>>.
5. Como Funcionam Os Créditos De Carbono. Bluevision. 2019. Available in: <<https://bluevisionbraskem.com/inteligencia/economia-florestal-como-funcionam-os-creditos-de-carbono/>>.
6. Guimarães, V. de A. Avaliação do desempenho sustentável das alternativas de transporte urbano de passageiros. Dissertação em Administração. Universidade Federal Fluminense, 2016.
7. Goes, G., Gonçalves, D., Agosto, M., Bandeira, R., Grottera, C. “transport-energy-environment modeling and investment requirements from brazilian commitments”, *Renawable Energy*, v.157, pp. 0960-1481, 2019. DOI: 10.1016/j.renene.2020.05.032
8. Goes, G., Gonçalves, D., Agosto, M., Rovere, E., Bandeira, R. “MRV framework and prospective scenarios to monitor and ratchet up Brazilian transport mitigation targets”, *Climatic Change*, 2019. DOI: 10.1007/s10584-020-02767-6
9. Scott, D., Peeters, P., GÖSSLING, S. ”Can tourism deliver its “aspirational” greenhouse gas emission reduction targets?”, *Journal of Sustainable Tourism*, v. 18, n. 3,pp. 393-408, 2010. DOI: 10.1080/09669581003653542.
10. Shiau, C., Samaras, C., Hauffe, R., et al. “Impact of battery weight and charging patterns on the economic and environmental benefits of plug-in hybrid vehicles”, *Energy Policy*, v. 37, pp. 0301-4215, 2009. DOI: 10.1016/j.enpol.2009.02.040.
11. Chaabane, A., Ramudhin, A., Paquet, M. “Designing supply chains with sustainability considerations”, *Production Planning & Control: The Management of Operations*, v. 22, n.8, pp. 727-741, 2011. DOI:10.1080/09537287.2010.543554.
12. Tulpule, P., Marano, V., Yurkovich, S., Rizzoni, G. “Economic and environmental impacts of a PV powered workplace parking garage charging station”. *Applied Energy*, v. 108, pp. 0306-2619,2013.
13. Büchs, M., Schnepf, S. “Who emits most? Associations between socio-economic factors and UK households' home energy, transport, indirect and total CO₂ emissions”. *Ecological Economics*, v. 90, pp.0921-8009, 2013.
14. Horne, M., Jaccard, M, Tiedemann, K. “Improving behavioral realism in hybrid energy-economy models using discrete choice studies of personal transportation decisions”, *Energy Economics*, v. 27, pp. 0140-9883, 2005. DOI: 10.1016/j.eneco.2004.11.003.
15. Cachon, G. “Retail Store Density and the Cost of Greenhouse Gas Emissions”. *ManagementScience*, pp. 1–19, 2014.
16. Leduc, S., Starfelt, F., Dotzauer, E. “Optimal location of lignocellulosic ethanol refineries with polygeneration in Sweden”. *Energy*, v. 35, pp. 0360-5442, 2010. DOI: 10.1016/j.energy.2009.07.018.

17. Giarola, S., Shah, N., Bezzo, F. “A comprehensive approach to the design of ethanol supply chains including carbon trading effects”, *Bioresource Technology*, v. 107, pp. 0960-8524, 2012. DOI:10.1016/j.biortech.2011.11.090.
18. Hensher, D. “Climate change, enhanced greenhouse gas emissions and passenger transport – What can we do to make a difference?”, *Transportation Research Part D-transport*, v. 13, pp. 1361-9209, 2008. DOI: 10.1016/j.trd.2007.12.003.
19. PROJETOS DE MDL. Educa Clima Ministério do Meio Ambiente. Available in: <<http://educaclima.mma.gov.br/transparencia/#roll3>>.
20. Análises Das Emissões Brasileiras De Gases De Efeito Estufa E Suas Implicações Para As Metas Do Brasil. Observatório do Clima. 2019. Available in: <http://www.observatoriodo-clima.eco.br/wpcontent/uploads/2019/11/OC_SEEG_Relatorio_2019pdf.pdf>
21. Objetivos e metas PNUD. Programa das Nações Unidas para o Desenvolvimento. Disponível em: <<http://www.pnud.org.br/ODS.aspx>>
22. RELATÓRIO SÍNTESE / ANO BASE 2019. Balanço Energético Nacional 2020, Empresa de Pesquisa Energética – EPE. 2019. Available in: https://www.epe.gov.br/sites-pt/publicacoes-dados-abertos/publicacoes/PublicacoesArquivos/publicacao479/topico521/Relato%CC%81rio%20Si%CC%81ntese%20BEN%202020-ab%202019_Final.pdf
23. GRZEGORZ PESZKO. Faster track to better carbon prices. World Bank. Available in: <<https://blogs.worldbank.org/climatechange/faster-track-better-carbon-prices>>
24. MILLENNIUM DEVELOPMENT GOALS. World Health Organization, 2020. Available in: <https://www.who.int/topics/millennium_development_goals/about/en/#:~:text=The%20United%20Nations%20Millennium%20Declaration,have%20specific%20targets%20and%20indicators.>>
25. CONVENÇÃO DE VIENA E PROTOCOLO DE MONTREAL. Ministério do Meio Ambiente. Available in: <<https://www.mma.gov.br/clima/protacao-da-camada-de-ozonio/convencao-de-viena-e-protocolo-de-montreal>>
26. KYOTO 2ND COMMITMENT PERIOD (2013-20). European Commission, 2013. Available in: <https://ec.europa.eu/clima/policies/strategies/progress/kyoto_2_en>
27. ACORDO DE PARIS. European Commission. Available in: <https://ec.europa.eu/clima/policies/international/negotiations/paris_en>
28. PROJECT SEARCH. United Nations Framework Convention on Climate Change. Available in: <<https://cdm.unfccc.int/Projects/projsearch.html>>
29. EMISSION TRADING SYSTEMS. Better Policies for Better Lives. Available in: <<https://www.oecd.org/environment/tools-evaluation/emissiontradingsystems.htm>>
30. RESULTADOS ALCANÇADOS. Educa Clima Ministério do Meio Ambiente. Available in: <<http://educaclima.mma.gov.br/transparencia/#roll4>>
31. Guimarães, V., Ribeiro, G.: Mapping of the Brazilian scientific publication on facility location. *Pesquisa Operacional* 38, 307–330 (2018)

A Prototype of Classroom Energetically Efficient

Diego A. Godoy^{1[0000-0002-7445-7375]}, Santiago H. Bareiro^{1[0000-0002-3060-5217]}, Fabián E. Favret^{1[0000-0002-3774-8982]}, Juan P. Blariza^{1[0000-0002-3291-5745]}, Guillermo Colotti^{1[0000-0001-5312-2165]}

¹Centro de Investigación en Tecnologías de la Información y Comunicaciones (CITIC).
Universidad Gastón Dachary, Av. López y Planes 6519, 3300 Posadas – Argentina
{diegodoy;hbareiro;efabianfavret}@citic.ugd.edu.ar
{juanblariza;gui.colotti}@gmail.com

Abstract. Various organizations have reported that buildings (among them, educational institutions) are responsible for the consumption of 40% or more of all the primary energy produced worldwide. The control of temperature and lighting in said institutions is carried out manually. That means that every time a classroom is used, people must turn on lights and air conditioners, and then take care of turning them off whenever they are not required. Faced with this scenario, the alternative proposed in this work allows efficient automatic control of lighting and temperature preferences for each professor and each class.

That is why a Prototype of Classroom Energetically Efficient was built in this paper. It has three modules: The one is the web application that was developed using the Laravel framework for the backend and Vuejs for the frontend. Its main function is to send commands to devices. The second is the IoT framework, which fulfills the function of communicating the web application with the hardware, providing the necessary endpoints, and making the registered data available. And finally, the hardware that was built using NodeMCU ESP8266 boards. Its function is to be an actuator i.e. receive the data from the IoT framework and executes commands. We also build a classroom mockup to show the prototype in action.

Also, the performance tests of different scenarios were carried out, being satisfactory, and allowing the development of the planned functionalities.

Keywords: Internet of Things, Smart Classrooms, Energy efficiency.

1 Introduction

A modern educational institution has a large number of classrooms, each with many lighting and cooling devices (air conditioners). "Various organizations, committed to the efficient use of energy and the conservation of our environment, have reported that buildings are responsible for the consumption of 40% or more of all the primary energy produced worldwide ..." [1]. For this reason, it is reasonable to say that the energy consumed in a school day during peak hours is very high.

That is normal (as well as in any, or most, educational institutions) considering the daily use and movement of students and professors. As well, it is also normal that the

temperature control (by turning on/off and regulation in air conditioners) and lighting (by turning on/off lights) in the classrooms, is carried out manually. This means that every time a classroom must be used, one person must take care of turning on the lights and air conditioners (if necessary), and turning them off when they are not required. And if we take into account that the people who perform these tasks are the same janitors and secretaries, responsible for many other tasks. Several devices may be turned on unnecessarily for several hours.

Likewise, it is observed that each professor usually has a lighting requirement in the classroom. For example, while there are professors who require the maximum possible lighting (all classroom lights on), others do not use the headlights (near the blackboard), since they use projectors with presentations and / or slides. In this way, the visualization of slides showed by projectors are more clear. So also other professors prefer all lights completely off for the same reason. The temperature will depend on the weather conditions. For example, days with extreme temperatures (hot or cold), will require more use of air conditioners.

Therefore, it is extremely important to find the method to manage efficiently the energy consumption, not only to reduce the institution's expenses but also to help preserve finite resources and thus mitigate the environmental impact due to its unnecessary use.

Consistently and because the technology advances it is necessary to design a solution to that problem through the use of an IoT Framework evaluated in [2], a Web application and specific hardware [3], which allows each professor to independently configure their desired lighting and temperature profile for the classroom to be used, and that this is applied automatically in the right time.

2 Related Works

Educational institutions are one of the main responsible for the amount of energy consumed, for the number of activities carried out in classrooms, offices, libraries, and also for the waste of energy due to the inefficient use of electricity [4], but also, by the mobilization of people using vehicles [5].

In [1] a line of action is established regarding customs and policies for the good use of energy that not only promotes the development, implementation, and adaptation of software and hardware. Instead, they serve as tools to save money at the National University of Misiones. In [6] the research process for the development of an IoT system is presented, which has been designed to promote an intelligent lighting service in an academic environment. The IoT system orchestrates a series of sensors, monitoring systems, and controlled actions, based on the principle of making available the functions of the system and the record of consumption in real-time through web services. Likewise, in [7] the design and implementation of an intelligent automated system based on Ethernet for the conservation of electrical energy using a second-generation INTEL GALILEO development board are proposed. The proposed system works on automation so that electrical devices and switches can be remotely controlled and monitored without any human intervention. The project developed in

[8] uses IoT-based technology to achieve automation in classrooms and proposes an approach to control and manage electrical equipment such as fans and lights based on the presence of people.

3 Methodology

This section presents the hardware and technology used in this research project

3.1 Used Hardware

The hardware used is the NodeMCU ESP8266(Figure 1). NodeMCU is an open source IoT platform. Includes firmware that runs on Espressif Systems ESP8266 WiFi SoC (System on Chip) and hardware that is based on the ESP-12 module [9].

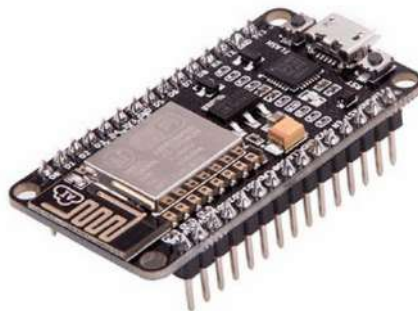


Figure 1. Node MCU ESP8266.

The ESP8266 is a low-cost WiFi chip with a full TCP / IP stack and a microcontroller. The firmware can be programmed using the Lua scripting language, although currently the Arduino IDE also supports programming in C language [10].

3.2 Used Web Applications Technologies

In the web application development, different frameworks were used such as Laravel, VueJs, and Postman.

Laravel is an open source PHP framework for developing web applications and services through layered architecture, providing multiple functionalities required for any web application.

VueJs is a progressive JavaScript framework for creating user interfaces. It is an alternative to frameworks like Angular or React [11].

Postman is a tool that allows you to make HTTP requests to any REST API, whether third-party or your own, to test the operation of the API through a graphical interface.

3.3 Framework IoT Ubidots

Ubidots [12] is a platform for building, developing, testing, learning, and exploring the future of applications and solutions connected to the Internet [12].

Regardless of whether one or one thousand devices are connected, the same effort is required with all types of Ubidots devices. The creation of the new device in Ubidots can be replicated by automatically setting the variables, the device properties, and the appearance each time a new piece of hardware is detected. Some of its characteristics can be seen in [13]. The Ubidots service stack can be seen in Fig. 2.

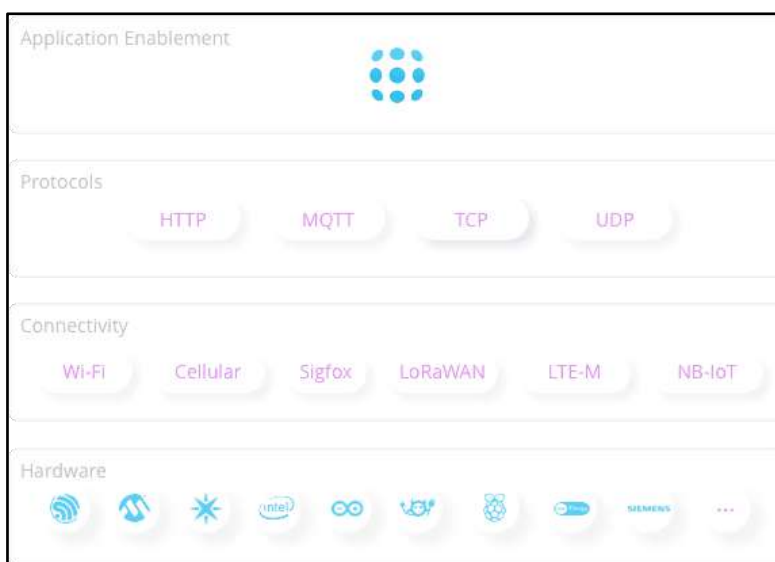


Fig. 2. Ubidots service stack

4 Proposed solution architecture

The technological solution to the problem consists of using an IoT framework that fulfills the function of carrying out communication between the parties (Web Application and Hardware), providing a method to store the information and make it available to read, to be consumed at the required time. The Web Application defines all the behavior to be followed and the hardware is only an executor of actions, ordered by the Web Application. Examples of this would be the web application reads the information from the temperature sensor sent by the hardware, and tells when to switch on or off an air conditioner. The proposed solution is shown in Fig. 3.

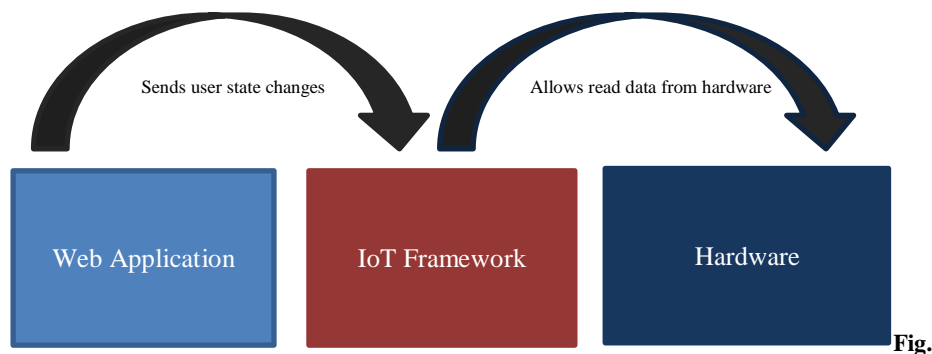


Fig.
3. Proposed solution architecture

Each arrow in the previous graphic represents an HTTP request performed by the web application and the hardware respectively. Based on this, we have four situations:

1. The web application sends state change data to the IoT framework. These changes of states refer to changes in the profiles according to the preferences of each professor. For example: If the air conditioning in classroom 1, at a certain time, should be turned on. The IoT framework stores this data and makes it available to be consumed. It should be noted that the IoT framework, in this case, does not handle the logic of when an air conditioning should be turned on or not, it simply receives the data. For example, "Air1: 1" data, already generated by the web application, and makes it available to be consumed by who requires it.
2. The available data is consumed by the hardware. The latter reads the data, through an HTTP Request, and just executes the action. For example, if the hardware read that the lights in classroom 1 should be on and they are off, it will turn them on.
3. There are certain times when the hardware needs to feed information to the system, for example, with the temperature sensor. In this case, it will take the ambient temperature and send it to the IoT framework, so that it is available to those who require it. As in previous cases, the IoT framework will only be in charge of storing and making the information available, without processing it.
4. Finally, there will be cases where the web application requires feedback from the system, such as, for example when the hardware reports the current temperature of a certain classroom. In this way, the Web Application will know what information to produce and send it to the IoT framework again.

5 Test Scenarios

The following scenarios will be used for testing the prototype.

1. A professor is far from the institution and has classes at that time.

2. A professor is at the institution and has classes at that time.
3. Functioning with different personalized professor profiles.

The activation condition of each profile includes the following three variables:

1. The professor is in the institution (position simulated by the marker on the map)
2. The professor has classes at that time.
3. The professor attends classes.

The actors involved are specified in each test. Also, if necessary, a different lighting and / or cooling profile is specified.

5.1.1 Scenario 1: A professor is far from the institution and has classes at that time

Actors involved: Web Application.

In this test, the framework did not participate, because the one who sends the orders to later be read by the hardware, is the web application. In this case, with any lighting and cooling profile activated, and being class time for the professor, no request was sent to the IoT framework since the professor was far from the institution. Fig. 4 shows in the "Network" tab how simulating any location of the professor on the map outside of the profile activation field, no request is sent.

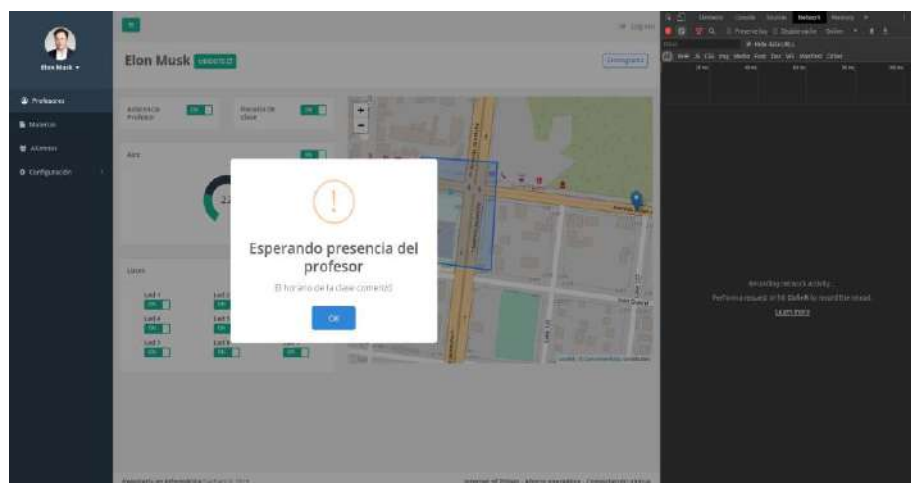


Fig. 4. Scenario 1

5.1.2 Escenario 2: A professor is at the institution and has classes at that time.

Actors involved: Web Application, IoT Framework and Hardware.

Test profile: All lights on and air conditioning on. Being the teacher's class schedule, the teacher being in the activation zone and marking that he attends classes

in Fig. 5 we can see how the Web Application sent 10 requests correctly, corresponding to the 10 variables used.

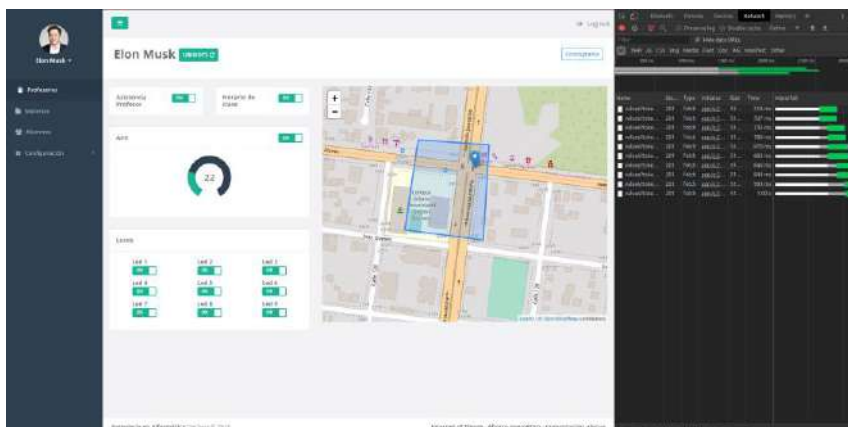


Fig. 5. Web application sending power signal for lights and air conditioning using Ubidots IoT Framework.

When clicking on the first request sent by the Web Application, corresponding to the first variable “led1” of Ubidots, the request details are observed in Fig. 6:

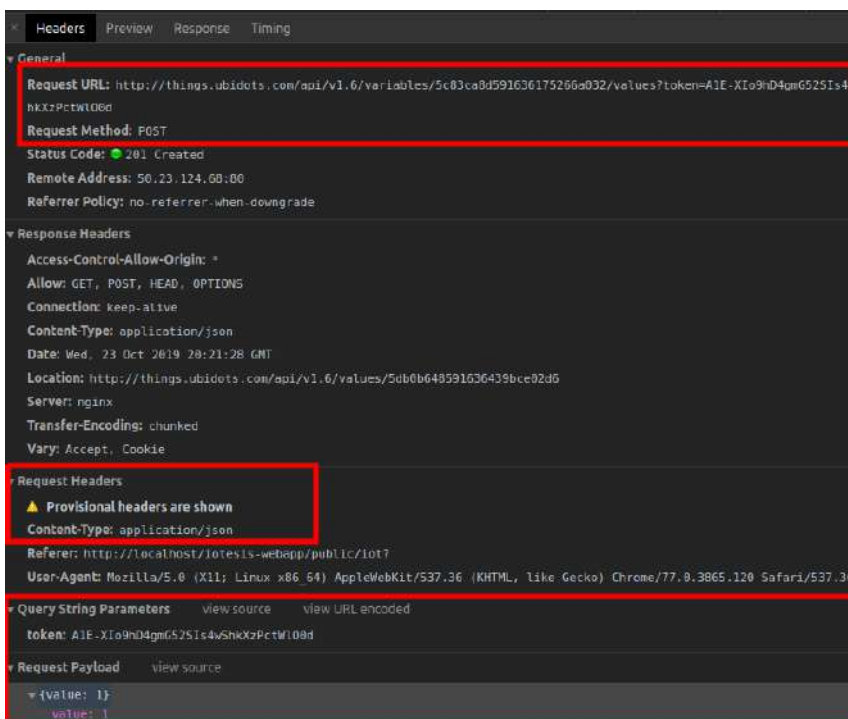


Fig. 6. first request sent by the Web Application.

The Request URL shows the endpoint to which the request was sent, corresponding to the first variable (“led1”). Other important data are observed, such as:

- Status Code 201: The request was successfully sent.
- Content-Type application / json: One of the headers required by the framework.
- Token
- Variable ID in the URL.

In the following requests corresponding to the other lights and air, the same results were obtained. As seen in Figura 7, it is verified that the data was written correctly in the Framework, using Ubidots Dashboard created for quick visualization.



Figura 7. Public Ubidots dashboard, showing widgets of all variables.

In the Classroom mockup where the hardware is installed, all the lights and the engine were turned on, as we can see in Fig. 8:

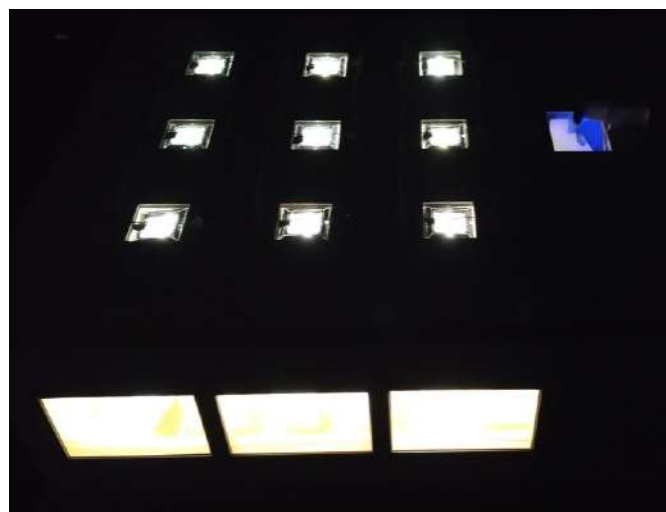


Fig. 8. A Classroom Mockup with all light and engines turned on.

5.1.3 Scenario 3: Functioning with different personalized professor profiles

Actors involved: Web Application, IoT Framework and Hardware.

Test profile: Only the last three lights turned on (in the classroom back) and air conditioning turned off.

The new profile with only the lights at the back of the classroom on (LEDs 7, 8, and 9) and the air conditioning off as we can see in Fig. 9.

The profile was configured, to leave only the lights in the background of the classroom on, and you can see how the web application sent ten requests correctly. For the lights that should be on, he sent “value”: 1, and for those that should be turned off, he sent “value”: 0. The air conditioning, with a temperature lower than 24°C, turns off.

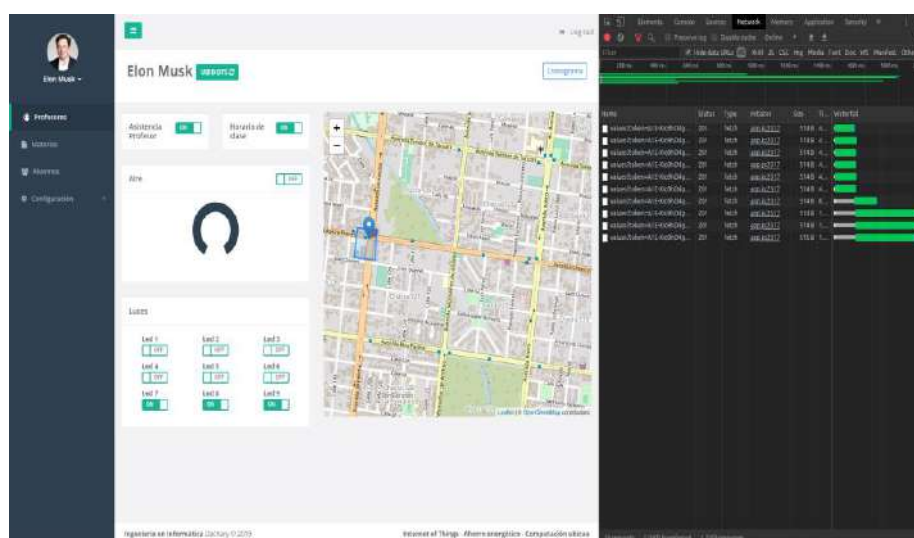


Fig. 9. Web Application sending on signal only for the last three lights and air conditioning off, using Ubidots.

In the first request, it is observed that the Request Payload has the value of false (Fig. 10)

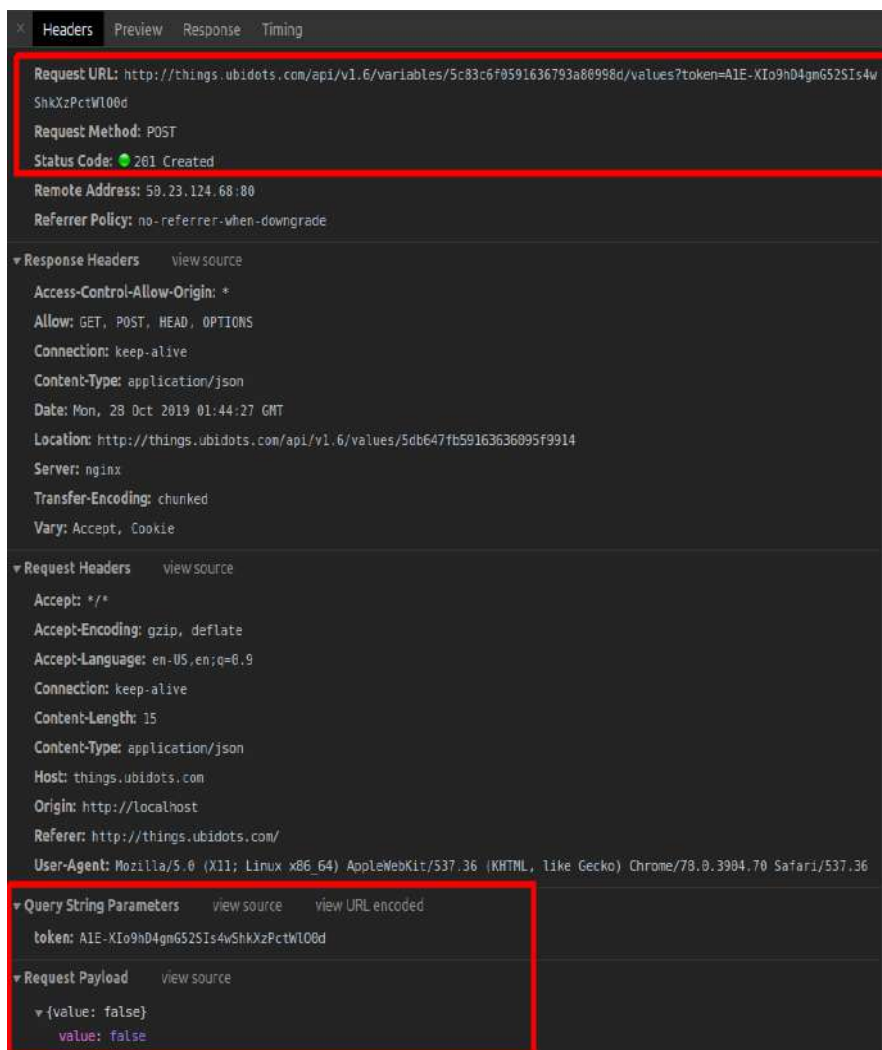


Fig. 10. Request with signal to turn off "led1" variable.

The same happens with the requests for all the lights in the first two rows. On the other hand, for the last row of lights, we can see light turned on. To do this, we observe the request, the variable "led9" and Request Payload has true value, as we can see in Fig. 11:

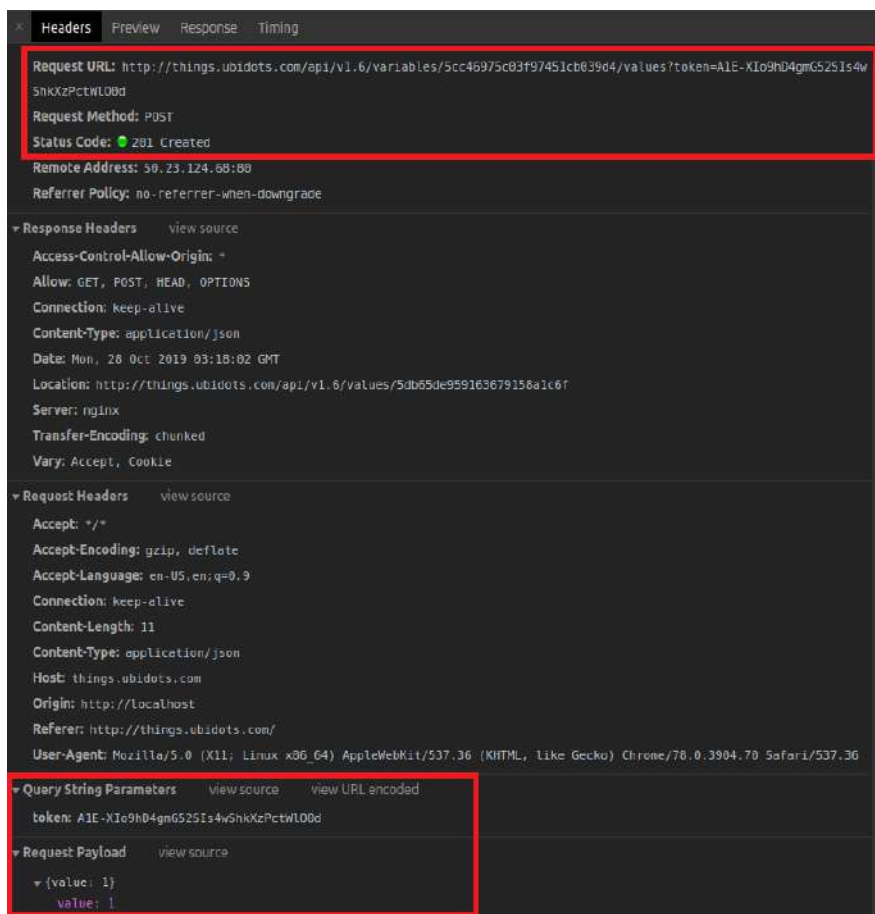


Fig. 11. Request with signal to turn on "led9" variable.

As seen in Fig. 12, everything worked as we expected in the Ubidots Dashboard.



Fig. 12. Ubidots Dashboard, showing the devices that must be turned on.

The hardware in the same way, it correctly read the framework data and executed the action(Fig. 13).



Fig. 13. The Classroom Mockup in the dark with only the last three lights are on.

6 Conclusions and Future Works

The use of the IoT Ubidots framework for the development of a Prototype of Classroom Energetically Efficient allowed to increase the implementation speed and the time saved in the construction of systems that need the interaction of devices connected to the internet. This is mainly due to the fact that it has the communication already resolved, having to focus only on the construction of the parts that must communicate.

Taking into account that all the packages that allow communication between the parties over the internet, using HTTP, the framework must guarantee the tools to give the necessary security to the packages, having SSL certificates and some method of authentication for the requests, either a token or an API_Key.

Finally, an efficient optimization in the time that lighting and cooling devices are on, avoiding idle time, translates into lower consumption, lower costs, and therefore less environmental pollution and greater energy efficiency.

Future work includes: Implement the prototypes with the MQTT protocol and later make the comparison against HTTP protocol used in this work.

Refactor the Ubidots firmware code for the NodeMCU ESP8266, improving the data reading and writing algorithms, to get better operations performance.

Design and implement fully functional versions of the web application which allow executing in a real way the change of teacher profiles as well as the dynamic configuration of the same, for each subject and schedule. Use the geo-positioning of a mobile device, for example, a cell phone, to locate the teacher, not just simulating the localization. Implement the prototype, in real classrooms of an educational institution to be used as a living laboratory.

7 References

1. Sosa, E. O., Godoy, D. A., Benítez, J., Sosa, M. E.: Eficiencia Energética y Ambientes Inteligentes. Investigación y Desarrollo Experimental en la UNaM., Posadas, Misiones, Argentina (2015)
2. Godoy, D., Bareiro, H., Fabret, F., et.al.: Propuesta de métricas para comparación de Frameworks IoT. In : Workshop de Investigadores en Ciencias de la Computación., El Calafate (2020)
3. Godoy, D., Bareiro, H., Fabret, F., et.al.: Análisis de componente de hardware para la utilización con Frameworks de IoT. In : Workshop de Investigadores en Ciencias de la Computación., El Calafate (2020)
4. Frimpong, , Appiah, : Energy efficiency awareness and preparedness among students. (2017)
5. Perez, J. A.: Proyectos de Eficiencia Energética para Instituciones de Educación Superior.
6. C.-A.González-Amarillo, C.-L. C.-G.-A.: Smart Lumini: A Smart Lighting System for Academic Environments Using IOT-Based Open-Source Hardware. Revista Facultad de Ingeniería 29(54) (2020)
7. Gupta, A., Gupta, P., Chhabra, J.: IoT based power efficient system design using automation for classrooms. In : Third International Conference on Image Information Processing (ICIIP), Wagnaghat, India (2015)
8. An Approach Towards Building an IoT Based Smart Classroom. In : 2018 International Conference on Advances in Computing, Communications and Informatics (ICACCI), Bangalore, India (R. Ani ; S. Krishna ; H. Akhil ; U Arun)
9. NodeMCU: Wikipedia. In: NodeMCU. (Accessed 2020) Available at: https://www.nodemcu.com/index_en.html
10. Programar facil. Available at: <https://www.programarfacil.com/esp8266/como-programar-nodemcu-ide-arduino/>
11. Vuejs. (Accessed August 2020) Available at: <https://vuejs.org/v2/guide/>
12. Ubidots. (Accessed August 2020) Available at: <https://ubidots.com/docs/>

REMOURBAN: Evaluation results after the implementation of actions for improving the energy efficiency in a district in Valladolid (Spain)

Cristina de Torre¹, Javier Antolín¹, Miguel Á. García-Fuentes¹, Jaime Gómez-Tribeño², José Cubillo³, María Luisa Mirantes⁴, Isabel Tome⁵

¹ Fundación CARTIF, Parque Tecnológico de Boecillo 205, 47151 Spain

²VEOLIA Servicios LECAM, Avenida del Euro 7, Ed B, OF312, 47009, Valladolid, Spain

³ACCIONA Ingeniería. c/Anabel Segura 11 Ed D 28108 Alcobendas, Spain

⁴Xeridia, Av del Padre Isla 16, 24002 León, Spain

⁵Iberdrola, C/Tomás Redondo 1, 28033 Madrid, Spain

critor@cartif.es

Abstract. REMOURBAN is a large-scale demonstration project whose main objective is to accelerate the urban transformation towards the smart city concept considering all aspects of sustainability. For this purpose, an Urban Regeneration Model has been developed and validated in the three lighthouse cities of the project (Valladolid-Spain, Nottingham-United Kingdom and Tepebaşı-Turkey). REMOURBAN has carried out different interventions in the city of Valladolid with the aim of transforming it in a more sustainable and smarter city. These actions have been evaluated using the evaluation framework developed within the project, to know the real impact of these interventions in the project area and to transfer the knowledge to other cities that want replicate these solutions for improving their sustainability and smartness. This paper is focused on showing the evaluation results after the application of the evaluation framework to the energy actions in a district in the city of Valladolid (Spain).

Keywords: Smart city, Near Zero Energy District, district heating, biomass, evaluation, sustainability, photovoltaic

1 Introduction

The sustainable development of urban areas is a key challenge for Europe where the retrofitting of its buildings and, more specifically, its thermal retrofitting takes on special importance. In Spain, more than half of the buildings are built without adequate thermal insulation, which means very high energy consumption and mostly from fossil fuels which exacerbates the problem of external energy dependence. In order to deal with this situation, projects such as REMOURBAN are demonstrating innovative, efficient and accessible technologies and processes in districts whose energy problems are evident in order to achieve Near Zero Energy Districts that serve as a reference and allow the replicability of this type of actions in other similar neighborhoods, improving the environment and the quality of life of citizens.

2

In order to help other cities to identify their needs and to establish the most suitable interventions for covering that demand and replicate the success of the project, REMOURBAN has designed a methodology, the Urban Regeneration Model, which covers all the phases of the transformation process. Within this model, the evaluation is sought as the main supporting mechanism throughout the deployment of this process. REMOURBAN evaluation framework considers two levels of evaluation: city level, to assess both sustainability and smartness of the city as a whole, from a comprehensive and integrated perspective, and project level, to provide a clear identification of the impact of implementation of technologies and solutions on the three key priority areas (sustainable districts and built environment, sustainable urban mobility and integrated infrastructures and processes) aimed at achieving the city high-level goals.

The objective of this paper is to present the evaluation framework at project level developed in REMOURBAN and to show the results of the final evaluation of the energy interventions implemented in the FASA district in Valladolid.

2 Description of the interventions implemented

In Valladolid, one of the lighthouse cities of the project, the FASA neighbourhood was selected for the implementation of a set of interventions designed in order to become a Near Zero Energy District and contribute to the city transformation to a more sustainable environment. This neighborhood was built during the 60s for the workers of the Renault factory in Valladolid, and it is composed by 19 blocks, a tower and a building that contains the thermal power station that supplies heating to the 398 homes that make up the neighborhood. These buildings presented severe deficiencies in their thermal insulation that resulted in lack of habitability and comfort, as well as low energy efficiency.

The heating system consisted of a district network supplied by two fossil fuel boilers (natural gas and gasoil) and it was divided into three different circuits that provided the 398 dwellings with space heating, whereas the domestic hot water (DHW) was individually produced in each dwelling with different technologies depending of the energy source in each particular case: natural gas, butane and electricity.

In REMOURBAN, with the aim of turning the neighbourhood into a Near Zero Energy District, a set of actions have been designed and those are described in following sub-sections:

2.1 Passive measures: Façade and roof insulation

One of the main objectives considered for the design of the interventions, was the reduction of the energy demand. For achieving the aim of decreasing it, it was needed to improvement the thermal isolation of the building envelope, including roof and façade.

For the thermal insulation of the façades, it was taken into account the least intrusive solution that could solve the thermal bridges completely. The external insulation was the final solution chosen, which consists of fixing an insulation board to the external side of the façade and later applying a finish over the board.

In FASA district, the installed insulation consisted of a four-layer scheme, based on a 60 mm expanded polystyrene (EPS) board fixed on the brick wall, a first layer of mortar, followed by a glass fiber mesh and a second layer of mortar. Finally, a surface finish was applied for aesthetical reasons.

Regarding the insulation of the blocks roofs, among the available options for their insulation, an intermediate insulation was chosen for the blocks and external insulation for the tower. The intermediate insulation offers a combination of best performance, easy installation and no disturbance on the tenants. 60 mm of sprayed foam (SPF) insulation were laid under the roof and over the last slab of the block.

The tower roof insulation was improved by adding an external insulation over the existing asphaltic layer. The scheme was an inverted roof system consisting of 60 mm of extruded polystyrene (XPS) insulation, a geotextile layer and gravel.

2.2 Active measures

Once the energy demand was reduced thanks to the passive measures implemented, the next step was to retrofit the thermal facilities in order to improve their energy efficiency and integrate renewable sources to the system.

The existing district heating system was renovated, on one hand the fossil fuel boilers were replaced by biomass ones with occasional support from natural gas and on the other hand the 20 substations of the district were renovated together with the distribution network which was updated with pre-insulated pipes to minimize heat losses.

With this new system, the dependence of the system on fossil fuels has decreased given that now the system depends fundamentally on a renewable energy source. Other relevant advantage is the decrease in the CO₂ emissions from the district heating to the environment because the CO₂ emissions factor for biomass is significantly lower than that for fossil fuels.

In addition to the new biomass boilers, with the aim of increasing the energy supply through renewable sources, a photovoltaic installation has been carried out. This new PV system was built on the south façade of the tower, which has a deviation of 12° and no shading obstacles, and the ventilation effect reduces overheating during summer improving the efficiency of the modules. The PV modules selected have a nominal power of 77.5 Wp. They were installed in two rows in the flat area of the façade avoiding interferences with the existing windows, finally adding up to a total aggregated capacity of 27.435 kWp.

The PV energy is fed into a circuit with 8 electrical resistors that heat up the water tank, which acts as a buffer. Then the hot water harnessed is used to preheat the DHW, and therefore reduce the biomass consumption.

Other intervention aiming to improve the energy efficiency of the district was the substitution of the incandescent lamps by LED in common areas of all buildings.

Last but not least, an Energy Management System (EMS) structured in three different levels has been implemented in the district. There are a District EMS that is responsible for managing the district heating as a whole, a Building EMS in charge of monitoring and controlling both the heating and DHW facilities in each of the 20 buildings and a Home EMS that has been installed in all 398 dwellings of the district. At this level there are two different kinds of devices: heat cost allocators installed in

4

each radiator to measure the individual consumption of the dwellings and thermostatic valves to allow the tenants to adjust the temperature inside each room.

3 REMOURBAN Evaluation Framework

REMOURBAN Evaluation Framework establishes the basis of the evaluation mechanisms for the REMOURBAN Project. The framework defines two levels of evaluation: Project Level, to provide a clear identification of the project impact regarding interventions, and City Level, to assess both sustainability and smartness of participating cities and the impact of the Sustainable Urban Regeneration Model developed in the project on the sustainability and smartness goals.

This paper is focused on the evaluation at project level and more specifically in the evaluation of energy actions in Valladolid. For the evaluation at project level, a specific index was defined; the Demo Site Index (Ds) that is used to evaluate the actions described in the previous section and others interventions related to urban mobility, ICT and non-technical actions.

Although the Ds index is used for the evaluation at project level, the specific actions in each city can be evaluated through one or various measurable objectives or sub-indexes to assist the evaluation of the project impacts and assess the progress of the lighthouse cities interventions.

The basis for the evaluation process are the KPIs (Key Performance Indicators) which are normalized, weighted and aggregated to calculate the Ds global index. Project level indicators (showed in Table 1) are weighted to estimate partial indexes defined for each of the areas of intervention (Buildings and District, Urban Mobility, integrated infrastructures through ICTs and Non-Technical actions). This framework of indicators, sub-indexes and project evaluation index constitute a valuable supporting tool for the evaluation of the impact and expected result of the REMOURBAN project.

Table 1. Project level indicators

Measurable Objective	Indicators	
Buildings and Districts	Energy Demand	CO ₂ Emissions
	Energy Consumption	Thermal Comfort
	Primary Energy Consumption	Indoor Air Quality Comfort
	Useful Energy	Energy Bill
	Renewable Energy Production	Investment
Urban Mobility	Energy Consumption (buses)	PM Emissions (buses)
	Energy Consumption (cars)	PM Emissions (cars)
	CO ₂ Emissions (buses)	EV Penetration Rate
	CO ₂ Emissions (cars)	EV Charging Points
	NO _x Emissions (buses)	Total KWh Recharged
	NO _x Emissions (cars)	Energy Bill (buses)

	HC Emissions (buses)	Energy Bill (cars)
	HC Emissions (cars)	Investment
ICT	Smart Electricity Meters	Indoor Sensors
	Visualising Real-time Information	Web Applications and Services
	Modes of Transport Integrated on Smart Cards	Visits/Access to Webs/Services
	Rate of Trips using Smart Cards	Registered Users
	Location Tracker Sensors	App Downloads
	Meteorological Sensors	Investment
	Air Quality Sensors	
Non-Technical	Initiatives of Public Incentives	Initiatives of Public Incentives
	Awareness Raising Campaigns	Marketable Products
	Learned solutions for Non-technical Barriers	Innovative/Green Public Procurement
	Channels Used for Citizen Engagement	Papers for Innovative Actions
	Visits to Project Information	Cities Interested to be Followers
	Social Media Accounts	Investment

4 Methodology for the Evaluation at Project level

This section presents the methodology of the project level assessment through the calculation of the Demo Site Index after the demonstration phase of the REMOURBAN project. This methodology requires of the following steps

- Scope definition: It is each of the three demo-sites (Valladolid, Nottingham and Tepebaşı) including the four areas of intervention (energy, mobility, ICT and Non-technical).
- Baseline period definition: it is the timeframe chosen to represent the initial status of the project level indicators that is used as reference for comparison in order to measure the impact due to the implementation of the project interventions.
- Reporting period definition: it should encompass at least one complete normal operating cycle, in order to fully characterize the effectiveness of the actions. Depending on the specific implementation timings for each of the actions in each demo-site a specific reporting period has been defined for each one. In REMOURBAN, the reporting periods of the energy and mobility actions implemented cover at least the last year of the project, but in most cases this period is longer, exceeding 24 months.
- Data collection and analysis: the collection of data is one of the most challenging tasks of the process and at the same time the quality and amount of data used for calculating the indicators is one of the most critical issues to

6

obtain a reliable index. Most of the data required for the calculation of the indicators at project level is gathered directly from direct measurement, statistical information and in some cases also from simulations. Data is collected and processed in each of the three Local ICT platforms deployed in each of the three lighthouse cities; and sent to the REMOURBAN Global ICT platform.

- Calculation of the index: the computer-based Evaluation Tool STILE has been defined and developed in the REMOURBAN framework to be used for the calculation of the established indices. STILE tool calculate and normalize the indicators, weights and aggregate them in order to calculate the Ds index in an automatic way based on the methodology and calculations implemented within the tool.
- Evaluation of the results. At this point it is possible to perform the comparison and detailed analysis of the reporting period index results and the baseline period index results.

5 Evaluation supporting tool: STILE

A valuable computer-based tool, named SmarTness and SustaInabiLity Evaluation Tool (STILE) has been developed as one of the core services that form part of the REMOURBAN ICT solutions. STILE was conceived as the service to support, automate and help to achieve the objectives set out in the Evaluation Framework. Therefore, in line with the Evaluation Framework, this tool allows for a quantified measurement of the cities' progress on the way to sustainability and smartness on one hand, and the performance of REMOURBAN project in terms of efficiency and effectiveness of its interventions on the other hand. This way, STILE arises as the cornerstone to reinforce the communication between stakeholders and decision-makers in the cities.

STILE enables to run evaluations for any of the REMOURBAN lighthouse cities at any moment. When an evaluation is launched, STILE takes the set of monitored variables stored in the Global ICT Platform for that city and the corresponding period of time.

The tool, at a first step, calculates a set of indicators taking those variables as inputs, by applying the formulas defined in the Evaluation Framework. Then, the set of formulas and calculations designed in the Evaluation Framework to obtain the Measurable Objectives from the indicators, were programmed as part of the tool and, finally, by implementing the corresponding formulas from the Measurable Objectives, the indices are obtained.

The key benefit of using STILE is not only the quantification of the indices, but a powerful presentation of the whole data set behind the final value of the index, that goes from the set of variables to an index value, with several intermediate calculation levels in between, all depicted in a graphical way, making it easier for the user to have full information at a glance.

The picture below let us find the direct relation of the general schema proposed by the Evaluation Framework for the Demo Site Index and its computer-based implementation:

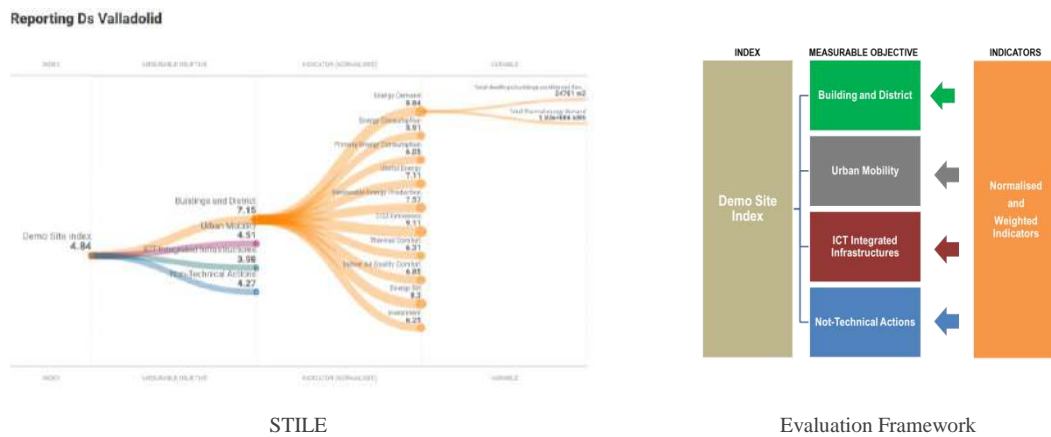


Fig. 1: Direct relation of the Evaluation framework and the computer based implementation

STILE visualization solution to represent the whole data set from variables to the final index makes it easier information understanding, having all figures in just one screen, quantified and depicted in a hierarchical way for a deeper insight into group-levels and dependencies.

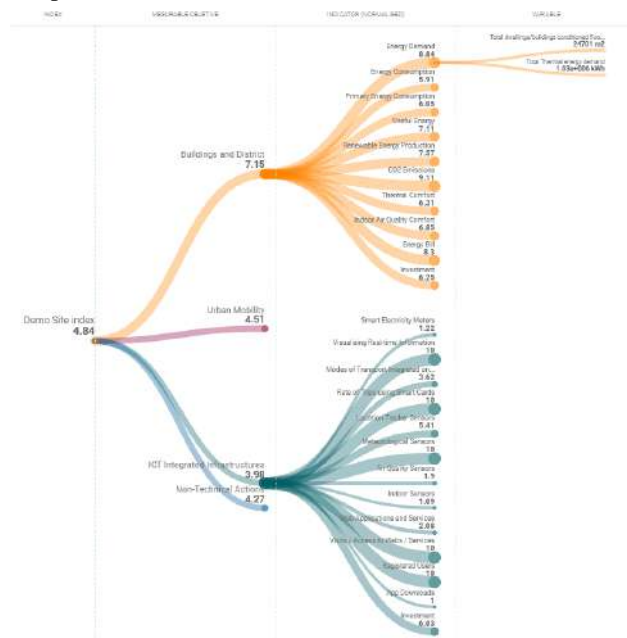


Fig. 2: Example of calculation and representation of Ds

8

Besides, the user can dig into any level or branch to get more information, just by clicking on each of the elements in a fully interactive way, which helps to better understand the final value of the indexes, based on its indicators and measurable objectives.

This way, the main objective of STILE tool implementing the Ds index is to help in the assessment of the effectiveness of the demo site interventions in cities, supporting decision-making when some new interventions or improvement of the existing ones is being under discussion or evaluation in the city.

6 Evaluation of Valladolid Demo Site

The Ds index is defined to assist on the assessment of the impacts of the overall project in each of the demo cities. This section presents the results of the calculation of the Demo Site Index (Ds) of the interventions in Valladolid.

The demo site index of Valladolid has increased from 1.89 to 4.84 showing the great impact of REMOURBAN interventions in the different areas of the city.



Fig. 3: Valladolid Ds Index (Baseline (Green) vs. Reporting 2019 (Blue))

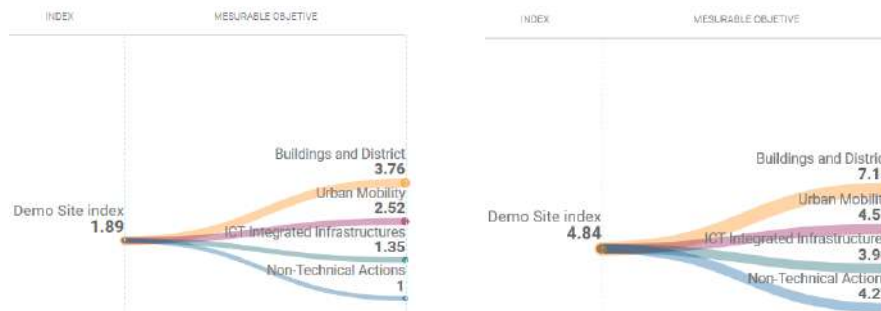


Fig. 4: Valladolid Ds Index. Baseline tree diagram (Left) vs. Reporting tree diagram (Right)

In Fig.4 can be appreciated as all the interventions areas (Buildings and District, Urban Mobility, ICT and non-technical) have increased their values. Since this paper is focused on Energy Interventions, looking at the Buildings and District sub-index it possible to conclude that both active (such as the new district heating system and PV panels) and passive (façade and roof insulation) interventions in the Valladolid district have had a positive impact, it is possible to see how these actions have allowed Build-

ings and District measurable objective to move from a baseline of 3.76 to 7.15 in the after retrofitting situation doubling practically the value.

6.1 Evaluation of Buildings and District Indicators for Valladolid demo site

The main aim of the REMOURBAN project within the scope of Buildings and District is to improve the efficiency in the use of energy and to change the current energy sources by decarbonising the energy supplies and increasing the share of renewable at the same time that improving the users comfort and reducing energy bill.

The Buildings and District Sub-Index it is composed by a group of indicators which allow to assess the impact of the specific actions and interventions of the project i.e., Energy demand, Energy consumption, Renewable energy production, Thermal comfort, etc., comparing the situation before and after the interventions.

Calculation algorithms have been implemented in STILE tool to calculate the buildings and district indicators according to their definition. These indicators are weighted to estimate the “Buildings and district sub-index” and to evaluate the impact of the area of the project related to buildings and district.

Fig.5 shows the comparison of the Valladolid demonstrator indicators’ results in the baseline and the reporting periods of Buildings and District. It shows an overall improvement in the district.

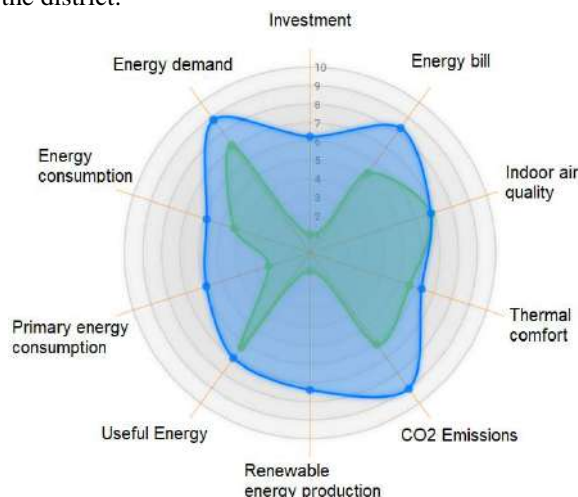


Fig. 5: Valladolid Ds Evaluation. Indicators related to the measurable objective “Building and Districts” Baseline (Green) vs Reporting 2019 (Blue)

The most affected indicator is the renewable energy production. In the baseline period, the energy produced for the heating and the domestic hot water came from non-renewable sources. The heating was produced with natural gas and diesel sources and the DHW with individual heaters fed with natural gas, butane and electricity. The intervention meant the replacement of one of the existing natural gas/diesel boilers with two new biomass boilers (renewable) and the centralization of the DHW in 46% of the dwellings. Furthermore, a new PV system was installed as support for the thermal plant. These measures implied that the renewable energy production was over

10

70% during the reporting period, making the value of the indicator increase up to 7.57.

Both energy demand and energy consumption improved almost in parallel. The energy demand was reduced due to the improvement in the insulation of the buildings carried out during the retrofiting. It was reported a reduction of 30% in “Thermal Energy Demand” (mainly due to the façade insulation carried out), and a 28% reduction in “Energy Consumption” (mainly also as improved efficiency in DH system). As buildings now have lower energy losses, the energy demand was reduced and the indicator improved. Together with this indicator goes the energy consumption. A reduction in the energy demand means also a reduction in the consumption, which considering also the higher increase of the systems efficiency implies the improvement on this parameter.

Furthermore, as buildings now have better thermal response to thermal fluctuations, the parameter “Thermal Comfort” increased a 12% showing a better thermal behaviour of insulated dwellings.

The primary energy consumption is also related to the energy consumption. However, it involves the typology of fuel too. The use of biomass boilers and PV system implied a variation on the fuel share and, thus, a variation on the primary energy factors, as the primary energy factor for biomass and PV are lower than the one for natural gas/diesel and electricity from grid respectively. The combination of a lower (better) primary energy factor together with lower energy consumption implied an important improvement in the primary energy consumption indicator.

A parameter that improved too is the useful energy. As the energy demand was reduced during the intervention, the useful energy necessary to heat the dwellings was also reduced, meaning that this indicator improved.

The energy bill for the tenants has also been reduced due to several factors. On one hand, the energy demand is lower, which means a lower consumption. On the other hand, the fuel changed from natural gas/diesel to biomass/natural gas. The cost of biomass is lower compared with the other two and the biomass share is close to 80%. Also the PV contribution to cover part of the heating needs of the district should be considered as it is reducing the use of biomass/natural gas and therefore reducing the operational costs. These two factors of energy consumption reduction and RES contribution justify the improvement on this indicator.

Important to highlight also the great reduction in CO₂ emissions, where a reduction of 70% was achieved, mainly due to high increase in renewable energy use, and efficiency achieved with dwellings insulation.

7 Conclusions

Evaluation is one of the key frameworks of the Urban Regeneration Model defined and developed in the REMOURBAN project. This evaluation framework defines metrics and standards for implementing the evaluation mechanisms in the project.

The evaluation of the results is key to assess the achievement of the expected impacts but also it brings an essential mechanism to foster replication of the solutions

developed which, indeed, is one of the strategic elements of the project. To ensure the replicability of the actions it is needed to create a consolidated and consistent reference of impacts.

For the evaluation of the actions, two levels have been considered within REMOURBAN evaluation framework: the Project Level, to provide a clear identification of the project impact regarding actions on the three key priority areas and the City Level, to assess both sustainability and smartness of participating cities.

The work presented in this paper is focused on the project level showing the Demo Site Index (Ds) which has been designed for this aim and more specifically the results achieved thanks to the actions implemented to reach a Near Zero Energy District in Valladolid.

The interventions carried out in the buildings (both passive and active) have reduced all forms of energy (demand, consumption, primary and useful). The increase of the use of renewable sources has considerably contributed to achieving a very low dependence on fossil fuels through the implementation of solutions such as biomass boilers and PV system. Interventions in buildings have not only reduced CO₂ emissions, but they have also improved indoor air quality and thermal comfort for people living in these buildings. From an economic perspective, the energy bill per household has been reduced considerably thanks to the combination of all the energy measures.

Acknowledgements

This research work has been partially funded by the EU through the European Union's Horizon 2020 Research and Innovation Programme under the research project REMOURBAN with grant agreement No 646511. The authors would like to thank the rest of the partners for their support. All related information to the project is available at www.remourban.eu.

References

1. REMOURBAN project Deliverable 2.2: Evaluation protocols and indicators. July 2016.
2. REMOURBAN project Deliverable 2.3: Implementation of the Methodology of Evaluation of Sustainability and Smartness in Cities. November 2016.
3. BOSCH, P., JONGENEEL, S. ET AL., 2016. D1.4 Smart city KPIs and related methodology. CITYkeys Project. Co-funded by the European Commission within the H2020 Programme. Grant Agreement no: 646440.
4. European Committee for Standardisation, 2007. Ventilation for non-residential buildings - Performance requirements for ventilation and room-conditioning systems. European Standard EN 13779.

Analysis of residential electricity consumption by areas in Uruguay

Juan Chavat^[0000–0001–9925–2651] and Sergio Nesmachnow^[0000–0002–8146–4012]

Universidad de la República, Montevideo, Uruguay,
{juan.pablo.chavat, sergion}@fing.edu.uy

Abstract. Home electricity demand has increased uninterrupted and is expected in 2050 to double the demanded in 2010. Making reasonable use of electricity is increasingly important and, in that way, different policies are carried out based on knowledge of how it is used. This article presents a procedure for measuring the potential electricity consumption in Uruguay. The study takes as main axis the appliance ownership information revealed by a national survey about severe socioeconomic aspects, and combines it with data on the characteristics of appliances, collected from local shops with an internet presence. Based on this data, an index of potential electricity consumption is performed for different census areas. To validate the analysis, it uses electricity consumption data from the ECD-UY (Electricity Consumption Data set of Uruguay) dataset and performs OLS linear regressions to evaluate real consumption and index correlation. The implementation uses Jupyter notebooks, language Python version 3, and utils libraries such as Pandas and Numpy. Results indicate that the departments with the highest index score are located on the West/Southwest coastlines. About census sections and segments in Montevideo, results show that the highest score areas are located in the South/Southeast coastlines, while lowest score ones are located in the outskirts. The validation process was limited by the lack of real consumption data.

1 Introduction

World Energy Outlook report, by the International Energy Agency [6], states that residential electricity demand has increased uninterrupted worldwide. It is expected to be double in 2050 than what it was in 2010 [7]. For that reason, it is important to make responsible use of electricity. In that way, multiple investigations have been carried on with the purpose of apply policies that motivate saving and reducing climate impact in factories, buildings, and homes [3, 5, 9, 12].

The population of Uruguay is 3.4 million inhabitants. Electricity in country is provided by the state-owned company, UTE. In 2020, the company provides electricity to a total of 1,498,164 customers throughout Uruguay, where 1,355,995 (90.5%) are residential customers. About 1.5 million people live in the capital city, Montevideo. The city presents an electrification rate of 99.8%, including urban and rural areas, according to data of 2018. In average, and according

2 J. Chavat and S. Nesmachnow

to 2017 stats, UTE serves per month 246 kWh to each residential customer in Montevideo.

Energy consumption data analysis and characterization are needed to apply demand management techniques oriented to a better use of energy resources. A possible approach for demand management is to motivate behavioral changes in customers that lead to electricity savings. Data analysis provides precise information on how customers consume electricity, which can be used to elaborate effective policies to consider for promotion of behavioral changes, elaboration of new plans and tariffs, etc.

In this line of work, this article presents an index of residential electricity consumption based on statistics about appliance ownership. The data of the 2017 National Continuous Household Survey (ECH, by its Spanish acronym) is used in combination with appliance characteristics information collected from local shops with a presence on the internet. The index is calculated to three census area levels: by departments, by sections and by segments. Real electricity consumption data, gathered from a subset of the ECD-UY dataset [2], is finally used to validate the correlation of the index results with real data.

The study applies a data analysis approach [10] over appliance ownership statistics, together with appliance characteristics information, to evaluate the potential electricity consumption by census area. Also, a validation method is proposed for the index, using real consumption data.

Results show that the departments with the highest index score are located on the West/Southwest coastlines, while the ones with the lowest scores are located in the East of Uruguay. Regarding census sections and segments in Montevideo, results show that the highest score areas are located in the South/Southeast coastlines of the city, decreasing progressively as it approaches the outskirts of the city. Score at the segment level shows great differences, up to six times, between the highest and lowest extreme. The index validation process was limited by the lack of more real consumption data.

This work is developed in the context of the project “Computational intelligence to characterize the use of electric energy in residential customers”, funded by the National Administration of Power Plants and Electrical Transmissions (Spanish: Administración Nacional de Usinas y Trasmisiones Eléctricas, UTE), and Universidad de la República, Uruguay. The project study how computational intelligence techniques can be used to process household electricity consumption data and characterize energy consumption. It also focuses on determining which appliances have the greatest impact on household electricity consumption and in the identification of patterns in residential consumption.

The article is structured as follows. Next section describes the problem of analyzing residential electricity consumption and reviews the main related work. The proposed approach for analyzing the electricity consumption in Uruguay is described in Section 3. The datasets and the processing are described in Section 4. The main results are reported and analyzed in Section 5. Finally, Section 6 presents the conclusions and the main lines of future work.

2 Analysis of residential electricity consumption

This section describes the problem addressed in this article and reviews relevant related works.

2.1 Main research question and hypothesis

This work analyzes the electricity consumption based on an index built from appliance ownership statistics. The statistics were obtained from a national survey implemented year by year by the National Statistics Institute (INE), Uruguay. The formulated question is: Can an index built from appliances ownership statistics model the electricity consumption per census area in Uruguay?

Some energy-intensive appliances, such as air conditioner or electric water heater, determine the electric consumption of a household. Some of these appliances are not a basic need, and therefore not every household count with them. If a degree of the appliances ownership is calculated for census areas, is expected to determine an average level of electricity consumption. From the previous question and considerations, and based on intuitive ideas, the following hypothesis was formulated to work on it.

Hypothesis: The more energy-intensive appliances owned, the higher the potential electricity consumption.

2.2 Related works

The analysis of the related literature allowed identifying several approaches for electricity consumption characterization in several countries. Most of the approaches have applied statistical tools (e.g., multilevel and logistic regression), such as in this article. Some relevant related works are reviewed next.

Chévez et al. studied the electricity consumption in Great La Plata, Argentina [4]. Two relevant problems of the Argentinean electricity sector were identified: i) consumption peaks, that increased 5% per year, could not be satisfied, and ii) a poor diversification of the electricity generation matrix. 1010 census areas with similar electricity consumption were identified and clustered in eight groups applying the k -means algorithm. Results were related to socio-demographic variables and its relevance in electricity consumption was studied. The article concluded that electricity demands grow quickly as the ratio of people per home and people per room increases. The greater the presence of flats in the area, the lower the electricity consumption. In turn, the more precarious the buildings, the greater the electricity consumption. Concerning unsatisfied basic needs, at higher the index level, proportionally higher is the electricity demand.

McLoughlin et al. [11] analyzed energy consumption data from 3941 smart meters in Ireland, and socio-economic, demographic, and dwelling characteristics. Four parameters were considered in the study: i) total electricity consumed, ii) maximum demand, iii) load factor (the lower, the more "peaky" of the consumption), and iv) time of use of maximum electricity consumption. Linear

4 J. Chavat and S. Nesmachnow

regression algorithms were developed to study how the dwelling/occupant characteristics and how the owned appliances affect on the electricity consumption. The analysis concluded that electricity consumption was negatively influenced by a higher number of bedrooms, head of households between 36–55 years, and a higher presence of professionals. On the other hand, it is positively influenced by dwelling type apartments and lower/middle social classes. About appliances, households using electricity for water heating or cooking consumed more electricity than the rest. Load factor, a measure of daily mean to daily maximum electricity demand, was sensible to the dwelling type and the number of bedrooms. Time length of maximum demand is more by the number of occupants than the dwelling type. It occurs during the morning for older heads of households, and late in the day for middle age heads of households.

Anderson et al. [1] explored inferring household characteristics of census areas from electricity consumption and number of residents for Ireland too. Data was limited to three days (Tuesday, Wednesday, and Thursday) of October 2009. Indicators were generated to describe household electricity consumption, considering load magnitude, summary statistics, and temporal properties. First, household characteristics were identified to infer profile indicators, applying multilevel regression considering several explanatory variables: income, employment status of the household response person (HRP), presence of children, and the number of residents. Then, the most likely profile indicators to reverse the direction of the prediction model were selected by logistic regression. Results showed an accuracy close to 60% to classify the employment status of the HRP. The work concluded that, despite the accuracy achieved, it is a feasible approach to infer household characteristics from the electricity consumption profiles.

Villareal and Moreira [13] studied residential electricity consumption in Brazil in 1985–2013. Residential consumption represented 26% of the electricity used in country, and the most demanding appliances were electric shower (19%), refrigerator (18%), lamps (15%), TV (11%), air conditioning and freezer (5%). Elasticity values were obtained from processing explanatory variables into linear regressions, and used to relate variables to consumption behaviours. The follow variables were used for the analysis: number of households on the country, available family income, electricity tariffs, appliances ownership, and social/economic policies that affect electricity consumption directly. About extra factors, the following three social policies were chosen: restraining of electricity consumption, facilitate access to electricity for low incoming families, and energy efficiency programs. Three models were developed to describe the consumption: i) considering variables represented by time series only, ii) considering electricity restraints, and iii) considering all the extra factors. Authors concluded that a rise of 1% in the number of residences increases electricity consumption by 1.53%, a rises of 1% in family income increase consumption in 0.19%, and a rise of 1% in the tariff cause a decrease of 0.23% in the consumption. The models presented high coefficients of determination (0.968 the first, 0.989 the rest), showing a strong relationship between explanatory variables and electricity consumption.

In Uruguay, Laureiro [8] analyzed residential electricity consumption based on socioeconomic characteristics, dwelling characteristics, energy uses, and temperature. Ordinary Least Square (OLS) and Quantile Regression (QR) were applied on data from 2994 houses. A cursory analysis yielded that income per capita is a relevant factor but not the unique, owning certain appliances (electric water heater/air conditioner) directly impacts over electricity consumption, and thermal comfort appliances are more common in dwellings with high electricity consumption. The OLS analysis concluded that: i) per capita income has high elasticity, ii) an increment of 1% in the square meters of a dwelling, increments 0.06% the electricity consumption, iii) houses consume 10.8% more than apartments, iv) electricity consumption increases 8.2% for each extra air conditioner and 17.2% for each extra electric water heater, and v) regional variables do not impact significantly in the consumption. The QR analysis concluded that: i) the impact of income per capita over consumption is lower in high quartiles than in low/medium ones, ii) dwelling size impact more in higher than in lower deciles iii) the dwelling type impacts only in medium/high deciles while building materials do not impact at all iv) air conditioners impact more in lower deciles and electric water heaters impact equally in all deciles, vi) the impact of cooking, washing/dryer machines, and sanitary heating have an inverted ‘U’ behaviour (low in extreme deciles, high in medium deciles). The work concluded that although the income per capita is a determining variable, it is not the only one that impacts on electricity consumption, and other characteristics must be taken into account (e.g., family composition, dwelling characteristics, and energy uses).

This article contributes by studying the electricity consumption based on appliance ownership data processed from national surveys in Uruguay.

3 Proposed approach for electricity consumption analysis

The proposed approach for the analysis consists of building an index that scores the electricity consumption degree, per census areas. For the construction, data provided by the ECH national survey from the year 2017 is used. ECH counts with several variables, described in the following section, that quantify the appliances ownership of the households. The surveyed households have geo-referenced information in at least three census levels: departments, census sections and census segments. Further details about the census areas are provided next.

Data is grouped by census area and the likelihood of owning the surveyed appliance is calculated. Besides, each appliance power consumption is collected from many local shops to weight the impact of each appliance in the final value. For example, owning an air conditioner affects more on electricity consumption than owning a flat TV. In the same way, each appliance is categorized by its frequency of use between low, medium or high. This represents a second weighting on the appliance consumption impact over the final result. Therefore, a fridge that is always on affects more than a notebook computer (sporadically used) on the final results. Frequencies are assigned as a rule of thumb guided by the authors own experience.

6 J. Chavat and S. Nesmachnow

The index scores are calculated as shown in Equation 1. Given a type of census area r with m different areas (e.g., $m = 19$ if $r =$ departments), $A^{(r)} \in \mathbb{R}^{m \times n}$ a matrix with one row per census area and one column per appliance likelihood information; $\mathbf{c}^{(r)} \in \mathbb{R}^n$ a vector with the consumption of the n appliances; and $\mathbf{f}^{(r)} \in \mathbb{R}^n$ a vector with quantified frequency of use for the n appliances. The result is a vector $index^{(r)} \in \mathbb{R}^m$ where each value in position i means the index score for the area i .

$$index^{(r)} = A_{m,n}^{(r)} \cdot \mathbf{c}^{(r)} \cdot \mathbf{f}^{(r)} \cdot \begin{bmatrix} 1 \\ \vdots \\ 1 \end{bmatrix} \quad (1)$$

4 Data collection and processing

This section describes the data used for the analysis and how it was prepared to be processed.

4.1 Census data

Used census data is provided by the National Institute of Statistics (INE, by its Spanish acronym). INE collect data of different index with monthly, quarterly, half-yearly and annual periodicity. The information is presented as a continuous household survey (ECH, by its Spanish acronym) every year. The ECH collects data about the labour market and income of households and individuals, from a representative set of households distributed around the country.

Information in ECH is georeferenced by, at least, the department, the census section, and the census segment. The definition of these georeferenced levels are provided next:

- *Department*: Coincides with the nineteen different political-administrative borders of the country.
- *Census section*: Corresponds to the first division level of the departments. Each section area can be cut into blocks or not. Its borders coincide with the ones used in the national census of 1963.
- *Census segment*: The segments are the subdivision of the sections. In census locations or areas cut into blocks, corresponds to a set of blocks, otherwise, the segments are a portion of territory that groups minor units with recognisable physical limits in the terrain and can include population centres.

Only a subset of the indexes in ECH was selected for the analysis. The selected indexes focus on georeferencing the data and quantifying appliance ownership. Table 1 list detailed information about the selected indexes.

Analysis of residential electricity consumption by areas in Uruguay 7

Table 1: Description of data from ECH (2017) used to build the index

name	description	type of value
dpto	Code of the department	Number (1-19)
nomdpto	Name of the department	String
secc	Census section	Number
segm	Census segment	Number
nombarrío	Name of the neighbourhood	String
d9	Number of residential rooms	Number
d18	Energy source for lighting	Number (1: electric; 2-4: other)
d260	Energy source for heating	Number (1: electric; 2-6: other)
d20	Energy source for cooking	Number (1: electric; 2-6: other)
d21.1	Electric water heater	Number (1: yes; 2: no)
d21.2	Shower water heater	Number (1: yes; 2: no)
d21.3	Fridge	Number (1: yes; 2: no)
d21.4	Tube TV	Number (1: yes; 2: no)
d21.4.1	Number of tube TVs	Number
d21.5	LCD/Plasma TV	Number (1: yes; 2: no)
d21.5.1	Number of LCD/Plasma TV	Number
d21.6	Radio	Number (1: yes; 2: no)
d21.8	videocassette player	Number (1: yes; 2: no)
d21.9	DVD player	Number (1: yes; 2: no)
d21.10	Washing machine	Number (1: yes; 2: no)
d21.11	Clothes dryer	Number (1: yes; 2: no)
d21.12	Dishwasher	Number (1: yes; 2: no)
d21.13	Microwave	Number (1: yes; 2: no)
d21.14	Air conditioner	Number (1: yes; 2: no)
d21.14.1	Number of air conditioners	Number
d21.15	Notebook computer	Number (1: yes; 2: no)
d21.15.2	'Plan Ceibal' laptops	Number
d21.15.4	Other Notebooks	Number

Data preparation. Preliminary analysis showed that records outside Montevideo do not have census section nor segment values set. Therefore, the index for these areas is evaluated only for Montevideo. The Yes/No columns were transformed from $\{1,2\}$ values to $\{0,1\}$ to facilitate the multiplication by the columns that indicate the number of appliances. Additionally, columns with common and 'Plan Ceibal' laptops were merged into one with the sum of both and the lighting columns was multiplied by the number of residential rooms to represents a light per room. Also, to discriminate between the air conditioner and other electric heating sources, the column indicating source was set to 'No' if the column of the air conditioners has a 'Yes' value. The final transformation consisted of multiplying all the columns that indicate the presence of an appliance by the corresponding column that indicates the number of appliances in the household.

Finally, several validations were processed to assure the integrity of the information. For example, columns that indicate the number of an appliance in a household were checked that if the value is greater than zero, then the column indicating the presence of this appliance have the corresponding "Yes" value. No integrity errors were found in this last step.

4.2 Appliance characteristics data

ECH surveys gather data about the ownership of certain household appliances. Based on these appliances and using the information of local shops with presence on the Internet, power consumption data was collected. Up to five different appliance models were gathered to define the median power consumption of each appliance. Table 2 lists the result of the data collection process, and Fig. 1 presents a bar graph of the mean power consumption together with its standard deviation measure. It can be observed how some appliances are more energy-intensive than others.

Table 2: List of appliances information used to build the index

appliance	Mean power (W)	Frequency of use	Power weighted by frequency of use
lighting	11.8	medium	8.85
heating	1200.0	high	1200.00
oven	1380.0	high	1380.00
electric water heater	1600.0	high	1600.00
shower heater	1810.0	medium	1357.50
fridge	199.4	high	199.40
tube TV	124.8	medium	93.60
flat TV	85.6	medium	64.20
radio	20.2	low	10.10
VHS player	10.0	low	5.00
DVD player	10.5	low	5.25
washing machine	740.0	medium	555.00
clothes dryer	3154.0	medium	2365.50
dishwasher	1409.6	medium	1057.20
microwave	1068.0	medium	801.00
air conditioner	1290.0	high	1290.00
notebook	57.0	medium	42.75

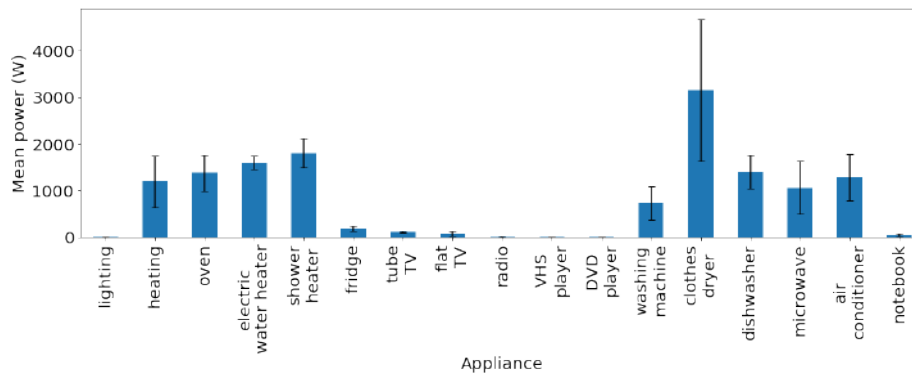


Fig. 1: Electricity consumption of the appliances used to build the index

4.3 Electricity consumption data

Real electricity consumption data is gathered from the ECD-UY dataset [2] and corresponds to the *electric water heater consumption* subset. The records originate from different clamp/meters installed by the National Electricity Company (UTE) in the households of their customers. The subset consists of mainly two parts, the records of the appliance consumption disaggregated and the total aggregated household consumption. The location of the households varies among the main Uruguayan cities. For this work, only the total aggregated consumption and the customer georeferenced information were used.

The subset contains the total consumption of 541 households on which only 242 are georeferenced. These georeferenced households are distributed into 6 departments. Households located in Montevideo are located along 12 census sections and 38 census segments. Fig. 2 shows three maps at different area level. The marked areas in each map correspond to those for which electricity consumption data is available in the ECD-UY dataset.

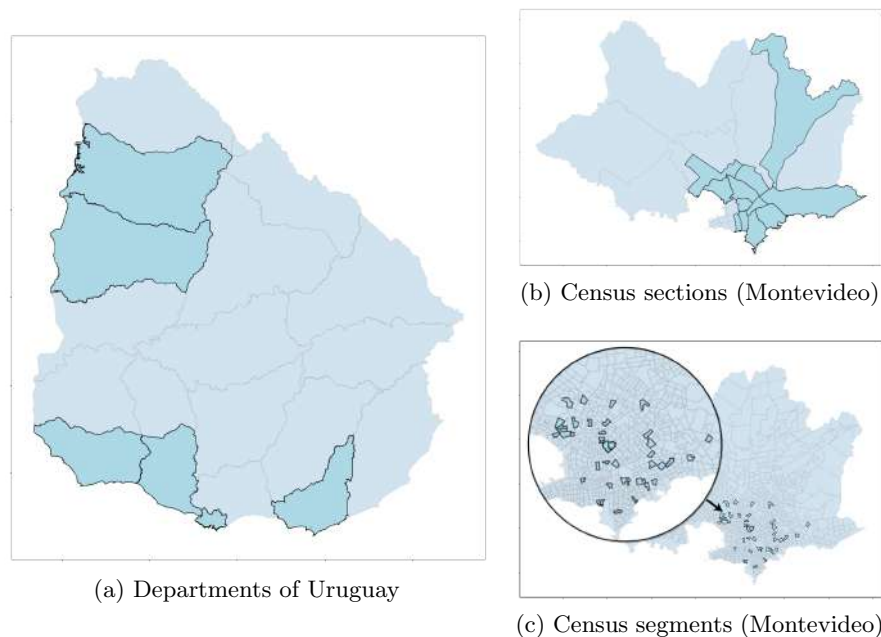


Fig. 2: Maps where the marked areas represents the one that counts with real electricity consumption data in the ECD-UY subset

The data preparation phase consisted of two steps. First, the electricity consumption of customers without georeferenced data was removed from the subset. Then, abnormal consumption values were filtered. For this task, the records with values lower than the 15th percentile and greater than the 85th percentile were removed.

10 J. Chavat and S. Nesmachnow

4.4 Implementation

The implementation consists of the next main steps: the load of the datasets, matrices construction for power demand by appliance and appliance ownership likelihood, processing of the index score per census area, visualization of results, and validation of the index scores.

The processing was executed on a personal computer with average processing power. Code was implemented in a Jupyter notebook using Python language version 3. For the data loading and the matrices construction, the utility libraries Pandas and Numpy were used, and the GeoPandas extension was applied for maps generation. The resulting notebook with its processing results is available for download at <https://bit.ly/3kGufV0>.

5 Results

This section present first the result of the proposed analysis by the three different census areas and then the results on the validation of the data using real consumption records.

5.1 Index scores by census areas

Results of the index by department areas show a difference up to 65% between the first and the last position. The department that results with the highest score is Montevideo, while the one with the lowest score was Cerro Largo. In general, the departments that present higher scores index are located on the west and south-west coastlines. A visual inspection of the departments in the Uruguayan map, starting from Colonia at the most southwest and pointing to the northeast, shows a progressive increase of the index score. That is observed at the map presented in Fig. 3. The complete list of departments together with its resulting index score is shown in the Table 3

Table 3: Index score by departments

score	department	score	department
4505.8	Montevideo	3725.7	Flores
4139.5	Colonia	3695.0	Florida
4097.9	Salto	3559.0	Durazno
4008.6	Maldonado	3543.8	Lavalleja
3964.9	Paysandu	3427.0	Rivera
3915.5	Rio Negro	3385.0	Treinta Y Tres
3894.8	Soriano	3373.8	Rocha
3821.7	Canelones	3322.9	Tacuarembó
3804.3	Artigas	2950.7	Cerro Largo
3792.1	San Jose		

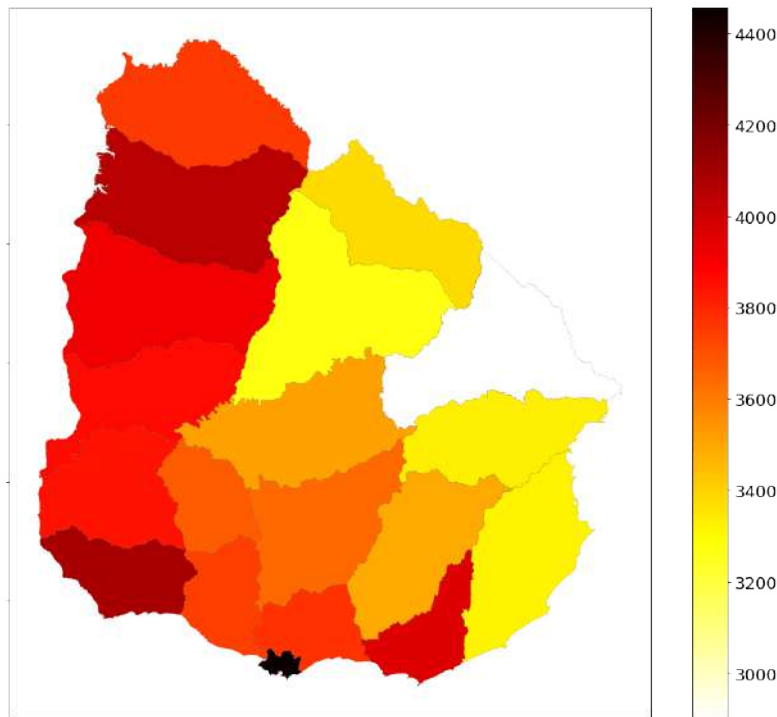


Fig. 3: Index scores calculated for departments of Uruguay

Results corresponding to the index score calculated by census section of Montevideo shows that the highest index score sections are located beside the south-east coastline of the city. The difference between the highest and the lowest index scores is up to 66%. The section with the highest score is number 10, and it covers the neighbourhoods Carrasco Norte, Buceo, Malvin, Malvin Norte, Punta Gorda, Union, Las Canteras and Carrasco. In the opposite side, the section with the lowest score is number 16, it covers the neighbourhoods Tres Ombues, Victoria, Nuevo Paris, Paso de la Arena, Casabó, and Pajas Blancas. A visual inspection on the map shown in Fig. 4 shows that starting from the southeast coastline and pointing to the northwest, the index score decrease progressively. Table 4 list the resulting scores by census section, together with the list of corresponding neighbourhoods of each section.

Finally, the index calculated by census segments shows an accumulation of segments with highest scores on the south and southeast area of Montevideo, while lowest scores segments are located mainly in the outskirts of the city. Fig. 5 shows a map of census segments in Montevideo, coloured by its index score. Results also reveal a big difference in the score among top and bottom scored segments, differing by more than six times in the most extreme cases. Table 5 shows a truncated list of the census segments ordered by its resulting index score.

Table 4: Index score by census sections

score	section	neighbourhoods
5444.1	10	Carrasco Norte, Buceo, Malvin, Malvin Norte, Punta Gorda, Union, Las Canteras, Carrasco
5297.3	18	Punta Carretas, Pocitos, Cordon, Tres Cruces, Parque Batlle, V. Dolores, Parque Rodo
5284.1	24	Pocitos, Pque. Batlle, Villa Dolores, Buceo
4981.8	14	Prado, Nueva Savona, Reducto, Capurro, Bella Vista
4898.2	23	Tres Cruces, La Blanqueada, Larrañaga
4795.5	6	Centro (Norte)
4710.5	12	Reducto, Atahualpa, La Figurita, Jacinto Vera, Larrañaga, Brazo Oriental, Mercado Modelo, Bolivar
4549.0	15	Cordon, Palermo, Parque Rodo
4432.7	7	Cordon, Palermo
4428.4	4	Centro (Suroeste), Ciudad Vieja (Sureste), Barrio Sur
4414.0	5	Centro (Sur), Barrio Sur
4358.1	21	Peñarol, Lavalleja, Conciliacion, Sayago, Nuevo Paris Paso de las Duranas, Belvedere
4322.9	22	Cerrito, Brazo Oriental, Villa Española, Bolivar, Mercado Modelo, Castro, P. Castellanos
4313.7	8	Aguada
4305.6	19	La Comercial, Villa Muñoz, Retiro
4211.6	20	Aires Puros, La Teja, Prado, Nueva Savona, Belvedere, Nuevo Paris
4162.1	3	Ciudad Vieja (Sur)
4143.9	1	Ciudad Vieja (Noreste), Centro
3907.3	13	Casabo, Pajas Blancas, Paso de la Arena, La Paloma, Tomkinson, Cerro
3867.4	9	Colon Centro y Noroeste, Colon Sureste, Abayuba, Lezica, Melilla
3842.9	99	Flor de Maroñas, Maroñas, Parque Guarani, Union Bañados de Carrasco, Villa Garcia, Manga Rural, Punta Rieles, Bella Italia, Las Canteras
3693.1	17	Casavalle, Manga, Las Acacias, Villa Española, Piedras Blancas, Castro, P. Castellanos, Manga, Toledo Chico
3663.9	11	Ituzaingo, Jardines del Hipodromo, Flor de Maroñas, P. Rieles, Bella Italia, Manga, Toledo Chico, Manga, Piedras Blancas, Villa Garcia, Villa Española, Union
3621.2	2	Ciudad Vieja (Norte)
3616.8	16	Tres Ombues, Victoria, Nuevo Paris, Paso de la Arena Casabo, Pajas Blancas

5.2 Validation of the proposed approach

For validating the proposed approach, the monthly average electricity consumption is calculated and compared with the index score results. Finally, the average consumption and the index scores are processed by an OLS linear regression to measure the correlation between real consumption and the index score.

Analysis of residential electricity consumption by areas in Uruguay 13

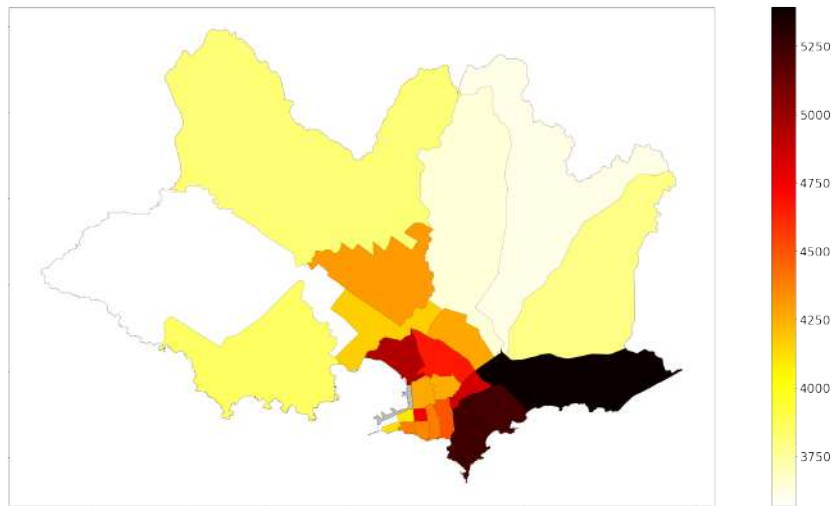


Fig. 4: Index score calculated by census sections of Montevideo

Table 5: Truncated list of index scores by census segment

score	section	segment	neighbourhoods
9249.1	10	67	Carrasco
9120.0	10	246	Malvín
9020.2	10	75	Carrasco
9013.0	10	74	Carrasco
8687.8	10	64	Carrasco
...
2322.6	9	1	Leizica, Melilla
2235.4	2	3	Ciudad Vieja
2164.1	99	208	Bañados de Carrasco
2141.0	13	9	Cerro
1450.4	13	113	Casabó, Pajas Blancas

Fig. 6 shows the average monthly electricity consumption of departments with available consumption data in the ECD-UY dataset. The calculation of the consumption is based on 242 georeferenced customers unequally distributed in departments. The comparison of the real consumption and the index score results shows that only two of the six departments, Montevideo (72 customers) and Paysandú (152), are in the same order. These two departments are the ones with more real data available, and therefore, its calculated average consumption is more reliable than the rest (which accounts for just six or less customers each).

OLS was performed with average real consumption and index score data. Results showed no correlation between the values but it should be taken into account the low number of samples that conform the calculation of average consumption. It is necessary to repeat the experiments with a more reliable calculation of real average monthly consumption.

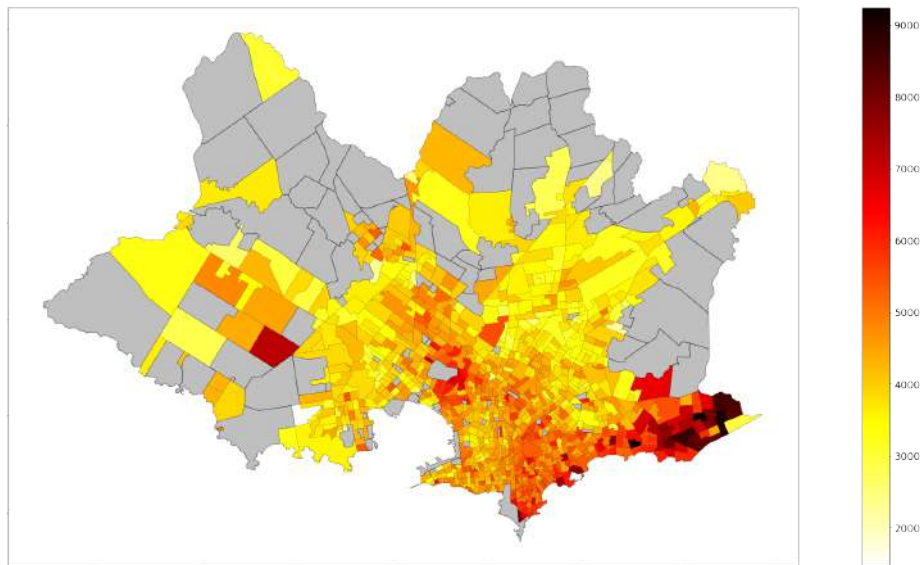


Fig. 5: Index score calculated by census segments of Montevideo

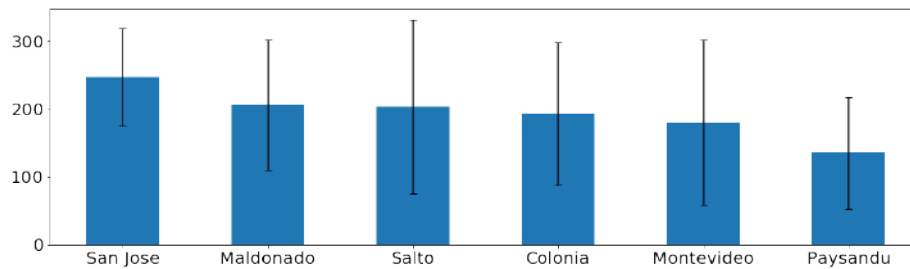


Fig. 6: Monthly average consumption from real data in ECD-UY dataset

Regarding the validation of the index by census section/census segment, the available real data is even more limited. For census sections, the available data is from 72 customers distributed in 12 sections, meaning an average ratio of 6 customers per section. For census segments, the 72 customers are distributed in 38 segments and its average ratio is lower than 2. Both cases are not statistically representative, and therefore, a full validation is not possible in this case.

6 Conclusions and future work

This article presented an electricity consumption analysis based on household appliance ownership data processed from national surveys in Uruguay. The proposed approach consists of building an index to score the potential electricity consumption in three different census areas: departments, sections, and segments.

Appliance information was collected from several sources and processed to build the proposed index. Results showed that departments located the South-eastern coastline have the highest index scores while departments in the north and northeast have the lowest ones. Regarding census sections and segments, the index was performed only for Montevideo and results show the highest scores in the south/southeast coastlines and lowest scores in the outskirts of the city. Census segments show great differences, up to six times, between extreme values. Validation of the index was limited by the lack of more real data.

The main lines for future work are related to study the relationship between the index and socioeconomic variables provided by the ECH, such as household incoming, education level, number of kids, among others. Also, updating the index to consider data from last and previous ECH versions, to study the index evolution along time.

References

1. Anderson, B., Lin, S., Newing, A., Bahaj, A.B., James, P.: Electricity consumption and household characteristics: Implications for census-taking in a smart metered future. *Computers, Environment and Urban Systems* 63, 58–67 (2017)
2. Chavat, J., Graneri, J., Alvez, G., Nesmachnow, S.: ECD-UY: Detailed household electricity consumption dataset of uruguay. *Scientific Data* (2020), (submitted)
3. Chavat, J., Nesmachnow, S., Graneri, J.: Non-intrusive energy disaggregation by detecting similarities in consumption patterns. *Revista Facultad de Ingeniería Universidad de Antioquia* (2020)
4. Chévez, P., Barbero, D., Martini, I., Discoli, C.: Application of the k-means clustering method for the detection and analysis of areas of homogeneous residential electricity consumption at the Great La Plata region, Buenos Aires, Argentina. *Sustainable Cities and Society* 32, 115–129 (2017)
5. Ford, R.: Reducing domestic energy consumption through behaviour modification. Ph.D. thesis, Oxford University (2009)
6. International Energy Agency: World Energy Outlook 2015. White paper (2015)
7. Larcher, D., Tarascon, J.: Towards greener and more sustainable batteries for electrical energy storage. *Nature Chemistry* 7(1), 19–29 (2015)
8. Laureiro, P.: Determinantes del consumo de energía eléctrica del sector residencial en Uruguay. *Serie Documentos de investigación estudiantil, DIE 05/18 FCS, Udela* (2018)
9. Luján, E., Otero, A., Valenzuela, S., Mocskos, E., Steffanel, L., Nesmachnow, S.: An integrated platform for smart energy management: the CC-SEM project. *Revista Facultad de Ingeniería Universidad de Antioquia* (2019)
10. Massobrio, R., Nesmachnow, S., Tchernykh, A., Avetisyan, A., Radchenko, G.: Towards a cloud computing paradigm for big data analysis in smart cities. *Programming and Computer Software* 44(3), 181–189 (2018)
11. McLoughlin, F., Duffy, A., Conlon, M.: Characterising domestic electricity consumption patterns by dwelling and occupant socio-economic variables: An Irish case study. *Energy and Buildings* 48(July 2009), 240–248 (2012)
12. Orsi, E., Nesmachnow, S.: Smart home energy planning using IoT and the cloud. In: *IEEE URUCON* (2017)
13. Villareal, M., Moreira, J.: Household consumption of electricity in Brazil between 1985 and 2013. *Energy Policy* 96, 251–259 (2016)

Low-cost and real-time measurement system for electrical energy measuring of a smart microgrid

Oscar Izquierdo-Monge¹, Paula Peña-Carro¹, Mariano Martín Martínez¹, Luis Hernández-Callejo², Oscar Duque-Perez³, Angel L. Zorita-Lamadrid³

¹ CEDER-CIEMAT, Autovía de Navarra A15 salida 56, 422290 Lobia (Soria), España, O.I.M.: oscar.izquierdo@ciemat.es; P.P.C.: paula.pena@ciemat.es; M.M.M: mariano.martin@ciemat.es

² University of Valladolid, Campus Universitario Duques de Soria, 42004 Soria, España. L.H-C: luis.hernandez.callejo@uva.es

³ University of Valladolid, Paseo del cauce 59, 47011 Valladolid, España. O.D.P.: oscar.duque@eii.uva.es; A.Z.L.: zorita@eii.uva.es

Abstract: One of the most important things in a microgrid is the real-time measurement of all its elements, whether they are consumers or energy producers so that at the end of an established period, the total balance of production-consumption is carried out. It is at this moment when the energy distribution company and its costs become important. Focusing on it, a measurement system based on an infrared sensor and Arduino has been developed, to which a specific software is installed that allows obtaining the value of the instantaneous power consumed by the microgrid from the reading of the LED indicator of metrology of the meter of the distribution company with an error less than 1% daily. This means an important improvement in the knowledge of the energy consumption of the microgrid and implies an advance in the understanding of the electric bill allowing reducing its cost in the contracted terms.

Keywords: Electric Smart microgrids, Arduino, Consumption, Measurement system.

1 Introduction

A microgrid is a concept used to define a group of interconnected loads and distributed energy resources within clearly defined electrical boundaries that act as a single controllable entity regarding the distribution network. A microgrid can be connected and disconnected from the grid to allow it to operate in grid-connected or island mode [1][2][3].

To manage a microgrid properly, it is essential to have a system of measurement, communication, and control in real-time. This remote monitoring will help in the management of the load and generation of the whole set, making it a semi-autonomous or autonomous microgrid and significantly reducing the response time to supply problems that may arise. With its implementation, an evolution from a microgrid to an intelligent network is achieved, providing the system with two-way communication

technologies, cyber-security, and intelligent software applications within its entire field of action.

In this way, greater security and knowledge of all the installed systems are achieved. After the study of the collected data, there is the possibility of modifying the management mode, to improve it [4][5].

There are various communication technologies within this context, some of which are copper conductors, optical fibre, power line communication, and wireless communication. Among them, the most outstanding and most used today is the wireless one, due to its high monitoring accuracy, its tolerance to failures, and the capacity to cover large areas thanks to the remote control without the need of civil works [6].

In turn, several standard communication protocols provide remote control and protection of the critical components that make up the microgrid, such as the Modbus, Profibus, or Fieldbus Foundation protocol.

For the total control of the microgrid, measurement mechanisms must be installed in each of the loads/generation systems, or group them by transformer stations. But if what is sought is the generation or total consumption of the entire microgrid the point of interest is the PCC (Point of common coupling) or meter of the distribution company. Point where the sum of energy generated/consumed by the entire microgrid is collected [7][8][9].

Thanks to the knowledge of these readings, different management strategies can be defined [10], such as storing energy in situations where production is greater than consumption, or providing energy at times when generation does not cover all the needs of the different centres of consumption.

The introduction of smart meters have provided detailed information on customer energy consumption [11]. In Spain, the National Commission for Markets and Competition (CNMC) has among its functions to ensure that customers have access to their consumption data in an understandable, harmonized and rapid manner [12][13]. However, at no time is indicated that access to data is in real-time.

The electricity distribution companies that own these smart meters allow access to the fifteen-minute average data used to prepare the electricity bill, which is not useful to carry out the real-time management of a smart microgrid.

The smart meters are technically prepared to perform instant queries [11] in real-time. However, communication can be slowed down by performing instant readings, generating a time lag that makes it difficult to perform in real-time on the microgrid.

In the case of the presented case study, after contacting the distribution company, they allowed access to this data for a brief period, less than a month, for testing purposes, but in no case did they grant access continuously. The only option to obtain the same measurements as the distribution company is to duplicate the measurement cell of the entrance substation or replace the current one with another double output measurement cell and in both cases install another meter. Either of these two options, apart from being costly (they can cost more than 3500€ between materials and installation work), are complex due to the reduced space available within the substation to install everything necessary.

For this reason, it is necessary to look for alternatives to know in real-time the value of the energy consumed by the microgrid or the energy injected into the distribution network from the microgrid.

This work aims to define an alternative measurement system for the intelligent meter of a microgrid, and of low cost that allows knowing in real-time the energy consumed from the distribution network or the one injected to it. The rest of the paper is as follows: section 2 explains the case study, showing the consumption of the microgrid and how it is currently measured. Section 3 presents the proposed new measurement system, the elements used and its installation. Section 4 details the results obtained. Finally, the conclusions obtained and the cited bibliography is presented.

2 Measurement of consumption in the CEDER microgrid.

The microgrid under study belongs to CEDER, which is the Centre for the Development of Renewable Energies. It is located in the municipality of Lobia, in the province of Soria and belongs to the Centre for Energy, Environmental and Technological Research (CIEMAT), which is a Public Research Organisation, currently dependent on the Ministry of Science and Innovation. It covers an area of 640 ha with more than 13000 m² built in three separate areas.

The CEDER microgrid starts from a 45 kV distribution line and serves a 45/15 kV (1000 kVA) substation. From this substation, it is distributed in medium voltage through an underground network to 8 transformer stations that adjust the voltage to 400 V three-phase low voltage. The network can be operated both in ring mode, which allows a medium voltage perimeter of 4,200 meters and in radial mode.

At CEDER, the loads are the elements that make up the centre, being the different buildings and their equipment (motors, lighting, boilers, laboratories, etc.) the energy demanders for its operation and thanks to which the daily activity of the centre is carried out. All these loads are connected to the low voltage network and have different consumption profiles, which are similar to those that can be found in an industrial environment, in the service sector, or even in domestic consumption.

To measure consumption, apart from the meter of the distribution company, CEDER has eight power grid/energy quality analysers (PQube). There is one in each transformer station, on the low voltage side. These analysers are also connected to the CEDER data network through an Ethernet card, so we can access their readings from any point of the centre.

To obtain the real power consumption of CEDER, besides the sum of the values measured by the PQube, we would have to add the consumption of the transformation centres (given that the PQube are on the low voltage side and therefore do not measure their consumption or losses) that we obtain from the test protocols of each of the CEDER transformation centres and that vary according to their load, and the possible losses due to the more than four kilometres of cabling that form the CEDER microgrid.

Figure 1 and Figure 2 show the comparison between the value obtained from the sum of the PQube and the value of CEDER consumption on April 5 and 25, 2020 respectively.

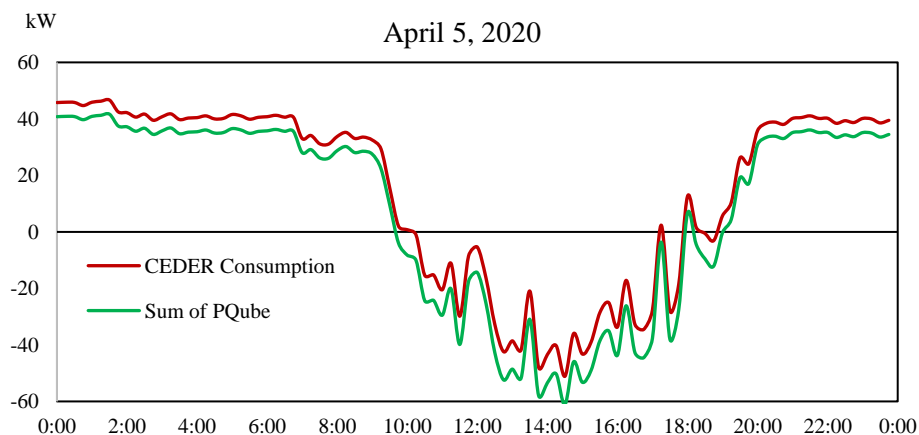


Fig. 1. Comparative CEDER consumption - Sum PQubes (05/04/2020).

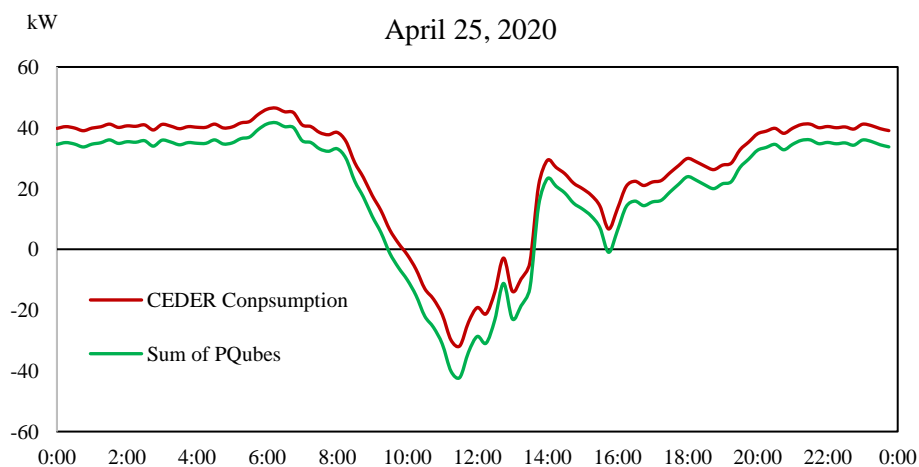


Fig. 2. Comparative CEDER consumption - Sum PQubes (25/04/2020).

The curves are parallel and the difference between both is due to the consumption of the transformer stations. It can also be observed that in low power values (close to zero), the curves are closer together.

If instead of one day, we see the data of a whole month, we get the results shown in Figure 3.

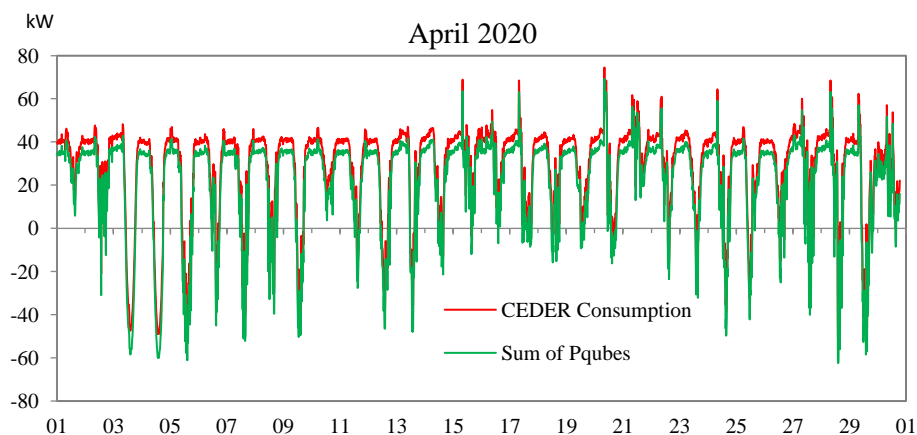


Fig. 3. Comparative CEDER consumption - Suma Pqubes (April 2020).

The PQube equipment is very complete and robust, but they also have a high cost (more than 2000 € each equipment), so we are going to look for an alternative measurement system that allows obtaining similar results to those obtained with the PQube with a much lower cost.

3 Proposed measurement system

To understand the measurement system to be used, it is necessary to know the smart meter installed by the distribution company. It is a meter model ACTARIS SL7000, it is a static meter, polyphase, in four quadrants, of multiple tariffs.

This counter has LED metrology indicators. The visible metrology pulses proportional to the active and reactive energy consumption are indicated by two LED indicators that blink according to the metrological constant marked on the front of the meter (imp/kWh or imp/kVAh).

This LED indicator is used by distribution companies to perform check readings in the field, in situations where automated reading fails, and temporarily perform manual readings through the optical reading port.

The direct connection specifications, as shown on the meter are nominal voltage 230 V, maximum voltage 400 V, nominal current 1 A, and maximum current 10 A.

Furthermore, the metrology constant for active energy is 10000 imp/kWh, that is to say, the LED light would flash 10000 times in an hour for every kWh imported or exported from the distribution network, provided that there was a direct voltage/current ratio.

In our case, there is no direct current-voltage ratio, but there is a transformation ratio for current 10/5 A and voltage 16500/120 V.

These three parameters, metrology constant, and the current and voltage transformation ratios will allow us to calculate, from the pulses of the LED light in a given period, the imported or exported active power recorded by the meter.

To measure these pulses, a measurement system based on an Arduino One will be used, with a microSD card where the operating system and software to be used are installed, connected to an optical sensor (an infrared meter that allows the measurement of the light pulses of the led light of the meter) and to an Ethernet card for Arduino. The cost of this equipment is less than 150 €.

Once the measurement system is installed, placing the optical sensor in front of the infrared communication port of the active power (see Figure 4), it is necessary to develop the software that allows calculating the active power from the number of light pulses of the meter using the three parameters of the meter that we have seen previously.



Fig. 4. Mounting the measuring system on the counter.

By default, Arduino stores the measured data on a microSD card, but this would not allow us to see it in real-time from the control system, which is why the Ethernet card is used to connect it to the CEDER data network and communicate with it.

Data transmission from the Arduino to the control centre can be done in two different ways:

- Arduino can be programmed to work as a web server and publish the measured values on a web page from which our control system will read them.
- Arduino can be programmed to have Modbus TCP communication and the

control system communicates directly with it, defining it in its configuration file.

After several tests with each of the two systems, it has been proven that Modbus communication is faster and more robust than the web server, so it will be the latter system that is used.

4 Results obtained

Once the Arduino based measurement equipment is installed and programmed, and the communication with the CEDER microgrid control system is established, the data acquisition begins.

Comparing the data obtained with this measurement system based on Arduino with the consumption of CEDER obtained from the measurements of the PQube network analyzers plus the consumption of the transformer stations, it can be seen in Figure 5 and Figure 6 (for the 5th and 25th of April respectively), that the results are practically the same.

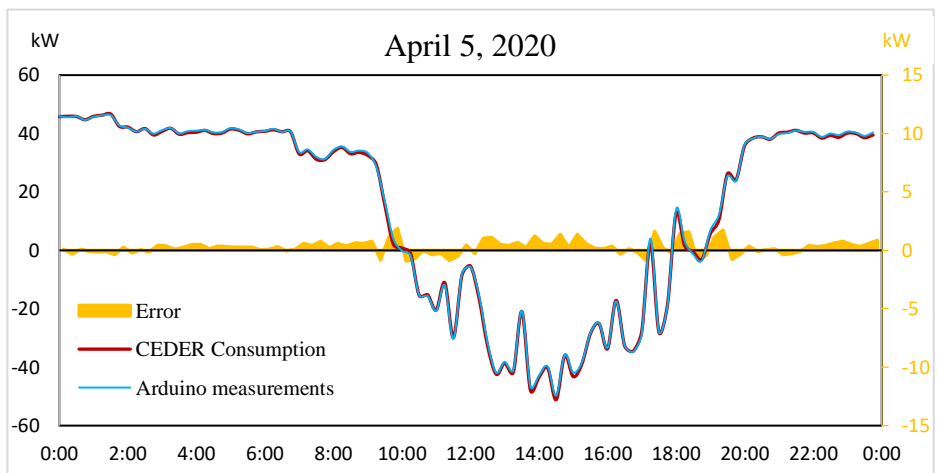


Fig. 5. Comparative CEDER consumption - Arduino measures (05/04/2020) and error

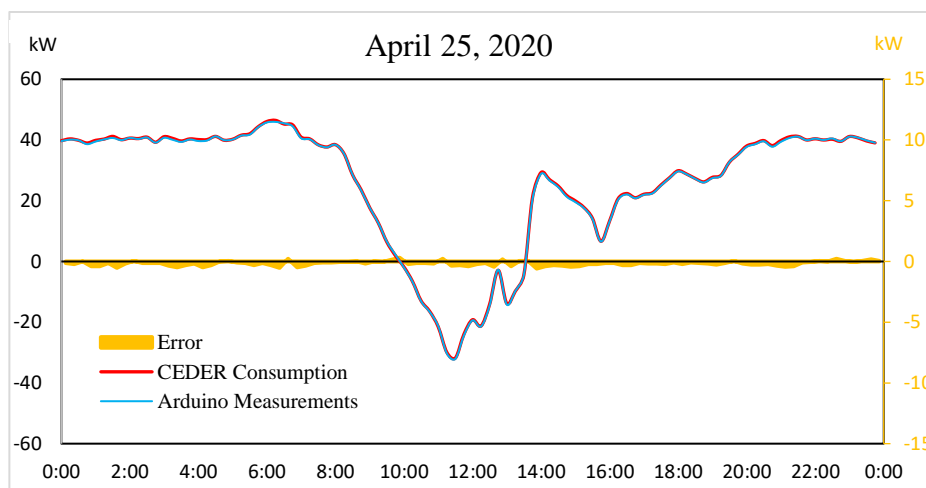


Fig. 6. Comparative CEDER consumption - Arduino measures (25/04/2020).

Graphically, it can be seen that the two curves are practically the same, there are hardly any differences between the two measurement systems. These variations can be somewhat higher in the proximity of zero kW and below -40 kW.

If we analyze the results numerically, averaging the measurements in real-time to periods of fifteen minutes, which is how the electricity distribution company accounts, we obtain the results shown in Table 1.

Table 1. PQube, Arduino and Real Consumption Data (25/04/2020).

Time	Measures PQube + consumption Transformer Substations		Arduino measures		Difference	
	CONSUMPTION (Wh)	INJECTED (Wh)	CONSUMPTION (Wh)	INJECTED (Wh)	CONSUMPTION (Wh)	INJECTED (Wh)
0:00	39641	0	39777	0	136	0
0:15	40128	0	40365	0	237	0
0:30	39909	0	39913	0	4	0
0:45	38639	0	39016	0	377	0
1:00	39492	0	39890	0	398	0
1:15	40203	0	40311	0	108	0
1:30	40671	0	41191	0	520	0
1:45	39959	0	40111	0	152	0
2:00	40690	0	40628	0	-62	0
2:15	40339	0	40470	0	131	0
2:30	40818	0	40945	0	127	0
2:45	39155	0	39267	0	112	0
3:00	40746	0	41103	0	357	0
3:15	40062	0	40522	0	460	0

Time	Measures PQube + consumption Transformer Substations		Arduino measures		Difference	
	CONSUMPTION (Wh)	INJECTED (Wh)	CONSUMPTION (Wh)	INJECTED (Wh)	CONSUMPTION (Wh)	INJECTED (Wh)
3:30	39377	0	39682	0	305	0
3:45	40174	0	40369	0	195	0
4:00	39659	0	40149	0	490	0
4:15	39822	0	40136	0	314	0
4:30	41201	0	41191	0	-10	0
4:45	39964	0	39931	0	-33	0
5:00	40171	0	40256	0	85	0
5:15	41457	0	41584	0	127	0
5:30	41772	0	42068	0	296	0
5:45	44279	0	44420	0	141	0
6:00	45794	0	46104	0	310	0
6:15	45960	0	46469	0	509	0
6:30	45489	0	45263	0	-226	0
6:45	44522	0	44996	0	474	0
7:00	40575	0	40940	0	365	0
7:15	40247	0	40377	0	130	0
7:30	38322	0	38414	0	92	0
7:45	37600	0	37691	0	91	0
8:00	38436	0	38464	0	28	0
8:15	35475	0	35507	0	32	0
8:30	28547	0	28538	0	-9	0
8:45	23425	0	23596	0	171	0
9:00	17699	0	17709	0	10	0
9:15	12697	0	12719	0	22	0
9:30	6564	0	6415	0	-149	0
9:45	2257	0	1944	0	-313	0
10:00	0	1999	0	1800	0	-199
10:15	0	6701	0	6586	0	-115
10:30	0	13096	0	12953	0	-143
10:45	0	16597	0	16421	0	-176
11:00	0	21312	0	21516	0	204
11:15	0	30239	0	29895	0	-344
11:30	0	32089	0	31797	0	-292
11:45	0	24370	0	23983	0	-387
12:00	0	19393	0	19192	0	-201
12:15	0	21409	0	21262	0	-147
12:30	0	14532	0	14105	0	-427
12:45	0	2726	0	2891	0	165
13:00	0	14188	0	13810	0	-378

Time	Measures PQube + consumption Transformer Substations		Arduino measures		Difference	
	CONSUMPTION (Wh)	INJECTED (Wh)	CONSUMPTION (Wh)	INJECTED (Wh)	CONSUMPTION (Wh)	INJECTED (Wh)
13:15	0	9719	0	9778	0	59
13:30	0	4406	0	4437	0	31
13:45	20396	0	20983	0	587	0
14:00	28862	0	29277	0	415	0
14:15	26628	0	26935	0	307	0
14:30	24526	0	24858	0	332	0
14:45	21314	0	21742	0	428	0
15:00	19569	0	19975	0	406	0
15:15	17618	0	17818	0	200	0
15:30	14034	0	14243	0	209	0
15:45	6539	0	6660	0	121	0
16:00	13150	0	13294	0	144	0
16:15	20361	0	20664	0	303	0
16:30	22077	0	22376	0	299	0
16:45	20838	0	20988	0	150	0
17:00	21962	0	22143	0	181	0
17:15	22431	0	22622	0	191	0
17:30	24965	0	25167	0	202	0
17:45	27476	0	27580	0	104	0
18:00	29664	0	29878	0	214	0
18:15	28709	0	28800	0	91	0
18:30	27227	0	27340	0	113	0
18:45	26031	0	26210	0	179	0
19:00	27460	0	27703	0	243	0
19:15	28202	0	28346	0	144	0
19:30	32758	0	32731	0	-27	0
19:45	35131	0	35304	0	173	0
20:00	37722	0	38001	0	279	0
20:15	38605	0	38879	0	274	0
20:30	39572	0	39810	0	238	0
20:45	37793	0	38157	0	364	0
21:00	39395	0	39820	0	425	0
21:15	40665	0	41043	0	378	0
21:30	41105	0	41193	0	88	0
21:45	39960	0	40021	0	61	0
22:00	40463	0	40408	0	-55	0
22:15	40014	0	40002	0	-12	0
22:30	40497	0	40266	0	-231	0
22:45	39595	0	39565	0	-30	0

Time	Measures PQube + consumption Transformer Substations		Arduino measures		Difference	
	CONSUMPTION (Wh)	INJECTED (Wh)	CONSUMPTION (Wh)	INJECTED (Wh)	CONSUMPTION (Wh)	INJECTED (Wh)
23:00	41101	0	41160	0	59	0
23:15	40762	0	40706	0	-56	0
23:30	39859	0	39700	0	-159	0
23:45	39103	0	39053	0	-50	0

The consumption of the distribution network by CEDER's microgrid on 25 April 2020, measured with PQube network analyzers is 677 kWh, while that obtained with the Arduino based measurement system is 674 kWh. The difference between both measurement systems is 3 kWh, which is 0.44%.

If we look at what CEDER's microgrid injects into the distribution network, with the PQube there is 57.6 kWh, while with the Arduino we have 58.1 kWh. The difference is only 0.5 kWh, which represents 0.86%.

If we look at each of the periods averaged individually, we see that the biggest differences when there is consumption, have a value of less than 600 Wh (587, 520 and 509). In the case of injection into the grid, the greatest differences are barely 400 Wh (427, 387 and 378).

It can also be seen that the measurement with the Arduino is not always higher than the measurement with the PQube, but it changes from one period to another, thus compensating for the total daily value. Thus, the average difference between the two measurement systems is 0.119 kWh in the 96 fifteen-minute periods that a day has.

The total energy measured by Arduino during the day is 615.8 kWh while the sum of the PQube plus the consumption of the transformation centres and the losses in the cabling is 619.8 kWh, which means an error of 3.97 kWh which represents 0.409% during the whole day.

If we analyze the data of the 5th of April 2020, they are similar, although the differences are slightly higher. In the case of distribution network consumption, measured with the PQube, 558.6 kWh are obtained, while with the Arduino based measurement system, 563.8 kWh are obtained. The difference between both measurement systems is 5.2 kWh, which is 0.93%.

In the injection to the distribution network, with the PQube, 212.5 kWh are obtained, while with the Arduino, 211.2 kWh are obtained. The difference is only 1.3 kWh, which represents 0.61%.

If we compare each of the periods averaged individually, the greatest differences occur for values close to zero (1.89, 1.63 and 1.58) and values below -40, that is to say when the microgrid injects more than 40 kW into the distribution network (1.39, 1.58 and 1.25). For all other values, the differences are less than 1 kWh.

If we do the study for a longer period, and instead of a day, we analyze a full month, we will have the results shown in Figure 7.

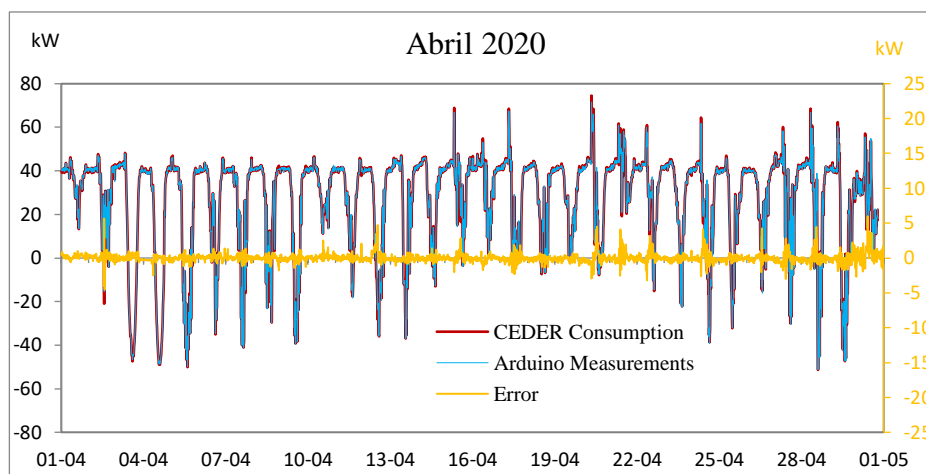


Fig. 7. Comparative CEDER consumption - Arduino measures (April 2020).

We see that the results obtained for one month are similar to the daily ones and no major differences are observed in Figure 7 between the two measurement systems studied. Generally, it is observed that the greatest differences occur for values around zero and values below -40 kWh.

If we analyze the data numerically, we get the following results:

- The consumption of the distribution network during April 2020 by CEDER's microgrid, measured with PQube network analyzers is 21808 kWh, while that measured with the Arduino based system is 21825 kWh. The difference between both measurement systems is only 17 kWh, which is 0.077%.
- If we look at the injection of CEDER's microgrid into the distribution network, with the PQube we get 1650 kWh, while with the Arduino we get 1658 kWh. The difference is 8 kWh, which represents 0.48%.

Table 2 shows the average daily differences between the two measurement systems used for all days in April 2020.

Table 2. Average daily differences between the two measurement systems (April 2020).

Day	Consumption obtained from PQubes (Wh)	Consumption obtained from Arduino (Wh)	Difference (Wh)	Error (%)
01/04/2020	879.96	874.43	5.53	0.63
02/04/2020	778.97	778.26	0.71	0.09
03/04/2020	356.10	355.30	0.80	0.22
04/04/2020	302.32	306.26	3.94	1.30
05/04/2020	351.37	353.50	2.13	0.61
06/04/2020	636.82	635.36	1.46	0.23
07/04/2020	576.65	575.91	0.74	0.13

08/04/2020	649.26	651.20	1.94	0.30
09/04/2020	538.90	541.08	2.18	0.41
10/04/2020	825.46	823.32	2.15	0.26
11/04/2020	694.97	694.81	0.16	0.02
12/04/2020	531.42	524.82	6.60	1.24
13/04/2020	679.33	681.49	2.16	0.32
14/04/2020	735.24	733.88	1.36	0.18
15/04/2020	865.15	860.49	4.67	0.54
16/04/2020	865.79	867.00	1.21	0.14
17/04/2020	721.74	719.97	1.76	0.24
18/04/2020	696.69	700.77	4.08	0.59
19/04/2020	710.01	713.65	3.63	0.51
20/04/2020	768.87	767.06	1.81	0.24
21/04/2020	976.49	968.50	7.99	0.82
22/04/2020	805.00	801.66	3.34	0.42
23/04/2020	723.40	726.33	2.93	0.40
24/04/2020	617.25	616.55	0.70	0.11
25/04/2020	615.83	619.86	4.03	0.66
26/04/2020	717.06	718.61	1.55	0.22
27/04/2020	753.97	756.22	2.25	0.30
28/04/2020	655.46	653.73	1.73	0.26
29/04/2020	434.16	439.81	5.65	1.30
30/04/2020	703.79	694.87	8.93	1.27

The average difference in April 2020 is 2.94 kW and represents a measurement error of 0.44%. The maximum difference between the two measurement systems occurs on April 30, 8.93 kW (error 1.28%) and the maximum error occurs on April 4 and 29, reaching a value of 1.3%.

5 Conclusions

This paper proposes a low-cost measurement system that allows real-time readings of any meter with active and reactive energy metrology LEDs to know the instantaneous power consumed or injected into the distribution network by a microgrid. This measurement system avoids having to duplicate the measurement cell at the entrance of a microgrid connected to the distribution network with the consequent cost savings.

Its operation has been tested on the CEDER electric microgrid for validation and has allowed knowing the energy measured by the meter in real-time, that is to say, the energy consumed or injected into the distribution network by the microgrid with an error of less than 1% in the worst case.

In this way, greater control of the production of the microgrid generation sources and their consumption is achieved, which translates into better management of the total invoice of the system with the distribution company, eliminating ranges of contracted power and their respective costs.

Besides, this low-cost measurement system, based on an Arduino and an infrared sensor, obtains measurements that are practically the same as those obtained with the previous system used at CEDER, based on PQube, significantly reducing the cost of the

system for recording the readings of the different generation and consumption elements of the microgrid.

References

1. Ton, D.T., Smith, M.A.: The U.S. Department of Energy's Microgrid Initiative. *Electr. J.* (2012). <https://doi.org/10.1016/j.tej.2012.09.013>
2. Lasseter, R., Akhil, A., Marnay, C., Stephens, J., Dagle, J., Guttromson, R., Meliopoulos, A., Yinger, R., Eto, J.: The CERTS microgrid concept, white paper on integration of distributed energy resources. *Calif. Energy Comm. Off. Power Technol. Dep. Energy, LBNL-50829*, <http://certs.lbl.gov>. 29 (2002)
3. Sachs, T., Gründler, A., Rusic, M., Fridgen, G.: Framing Microgrid Design from a Business and Information Systems Engineering Perspective. *Bus. Inf. Syst. Eng.* 61, 729–744 (2019). <https://doi.org/10.1007/s12599-018-00573-0>
4. Teufel, S., Teufel, B.: The Crowd Energy Concept. *J. Electron. Sci. Technol.* (2014). <https://doi.org/10.3969/j.issn.1674-862X.2014.03.006>
5. Gharavi, H., Ghafurian, R.: Smart grid: The electric energy system of the future. *Proc. IEEE.* 99, 917–921 (2011). <https://doi.org/10.1109/JPROC.2011.2124210>
6. van Leeuwen, G., AlSkaif, T., Gibescu, M., van Sark, W.: An integrated blockchain-based energy management platform with bilateral trading for microgrid communities. *Appl. Energy.* 263, 114613 (2020). <https://doi.org/10.1016/J.APENERGY.2020.114613>
7. Khavari, F., Badri, A., Zangeneh, A.: Energy management in multi-microgrids considering point of common coupling constraint. *Int. J. Electr. Power Energy Syst.* 115, 105465 (2020). <https://doi.org/https://doi.org/10.1016/j.ijepes.2019.105465>
8. Vargas-Salgado, C., Aguila-Leon, J., Chiñas-Palacios, C., Hurtado-Perez, E.: Low-cost web-based Supervisory Control and Data Acquisition system for a microgrid testbed: A case study in design and implementation for academic and research applications. *Heliyon.* 5, e02474 (2019). <https://doi.org/https://doi.org/10.1016/j.heliyon.2019.e02474>
9. Khan, K.R., Siddiqui, M.S., Saawy, Y. Al, Islam, N., Rahman, A.: Condition Monitoring of a Campus Microgrid Elements using Smart Sensors. *Procedia Comput. Sci.* 163, 109–116 (2019). <https://doi.org/https://doi.org/10.1016/j.procs.2019.12.092>
10. Hernández Callejo, L.: Microrredes eléctricas. Integración de generación renovable distribuida, almacenamiento distribuido e inteligencia. Publicaciones, Ibergarceta (2019)
11. Ministerio de Industria Turismo y Comercio: Reglamento de Puntos de Medida del Sistema Eléctrico 2007 Real Decreto 1110/2007, de 24 agosto. *ELECTRICIDAD.* Aprueba el Reglamento unificado de puntos de medida del sistema eléctrico. 28 (2007)
12. CNMC: DEL ÚLTIMO HITO DEL PLAN DE SUSTITUCIÓN DE CONTADORES. (2019)
13. CNMC: CONTADORES ELÉCTRICOS. (2016)w

How the construction parameters influence the thermal loads of a building without internal gains

Díaz J.A.¹, Soutullo S.¹, Giancola E.¹, Ferrer J.A.¹

¹ Energy Efficiency in Buildings Research Unit, CIEMAT, Av. Complutense 40, 28040 Madrid, Spain

alberto.diaz@ciemat.es

Abstract. The management of the building characteristics faces a series of uncertainties that influence its energy performance: climate, volumetry or operating conditions. It is important to have a low-cost system that performs this management by optimizing the coupling between production and consumption. The knowledge of the relationship between the annual thermal needs with different construction parameters can help to define this management system. This methodology will allow understanding the expected HVAC consumption based on easily available information.

In this work, a numerical methodology has been used to estimate the thermal loads of a building without internal gains. A simulation environment has been developed to execute a sensitivity analysis through the coupling between TRNSYS 16.1 and GenOpt. Volumetry, building materials according to the Spanish regulations and percentage of windows on the external façades are evaluated as analysis variables of the parametric study. Heating, cooling and total loads have been calculated to quantify the influence of the analysis variables. More annual loads are required for the oldest regulations. The increase of the number of plants and floor area reduces the annual thermal loads. Higher percentages of glass on the external façades lead to higher annual demands, being more marked in the east and west orientations. The variation of the building envelope is obtained as the most influential factor. Finally a statistical study has been performed to assess the annual trends reached for heating and cooling needs. Heating trends point to more stability with two defined intervals while cooling trends are more asymmetric.

Keywords: Energy Efficiency in Buildings, Sensitivity Analysis, Multivariable construction evaluation, Thermal Loads.

1 Introduction

Cities are one of the highest energy consumers in many industrial and high population countries so much research is underway to promote the development of “Low Carbon Cities”: This concept has primarily focused on ways to reduce the impacts of current energy consumption in transportation and buildings. In urban areas, increased population growth and energy demand in buildings have resulted in greater energy consumption thereby driving the global share (75%) of GHG emissions [1]. Inefficient build-

2

ing construction and equipment leads to an increased of GHG emissions, having a deep impact on the climate change. A building's operation is subject to several driving forces such as climate, site and location, geometry, façade and fenestration, architectural design, internal loads, ventilation systems, heating and cooling equipment, and control units. During its 50–100 years lifespan, a building may change its operational requirements [2]. Therefore, it is necessary to develop analytical methods to model building performance under future scenarios in response to climate change.

The operation of a building management system has many uncertainties that produce strong deviations from the real situation: representative climatology [3], volumetry or operating characteristics [4]. The main objective of this article is to establish a relationship between the thermal loads of a free-running building with different construction parameters that define it, such as height, envelope properties or ratio of windows on the external façades.

This work takes place under the SISGENER Project [5] that aims to develop a low-cost comprehensive energy management system. This system establishes, in an optimized way, the management of the energy generation and consumption that is carried out in buildings with centralized services, implementing new predictive techniques on simplified dynamic models [6], facilitating preventive maintenance tasks. One of its objectives is the development of simplified buildings models and energy systems with low computational cost to characterize their energy behaviour.

As the considered parameters are easy to obtain for any building, it is easy to extend the study to a district level, defining its building stock. The knowledge of the thermal load profile for one or a few reference buildings in a location make possible to estimate the overall needs of all the buildings in a district [7]. An estimation of the future demand allows optimizing the production and maximizing the use of renewable energies, reducing convectional energy consumption without losing comfort conditions, thus achieving an efficient production from an energy and economic point of view, complying with the principles that govern Smart Cities.

The optimized evaluation of a building management system requires an adequate characterization of heating and cooling loads. There are different methodologies to quantify the building energy performance, which can be differentiated in three categories: statistical models, numerical models and hybrid models [8]. The statistical models use mathematical correlations between the building constructive and operational properties and the environmental conditions to which they are subjected with their energy behaviour. These approximations usually do not require physical information of the building and are fed by real data [9-10]. The numerical models use physical principles to characterize energetically a building through the knowledge of its constructive, operational and functional characteristics [11]. These kind of approaches solve a set of mathematical equations that describe the energetic behaviour of the building [12-13]. The hybrid models use numerical models coupled with statistical models to characterize the energy behaviour of buildings. This methodology solves a set of mathematical equations defined by numerical models using real databases as inlet information [14-15].

In this work, a numerical methodology has been used to estimate the thermal loads of a building according to different inputs. The knowledge of the physical balance is a

key aspect to understand the sense of the constructive parameters influence. For this purpose, a sensitivity analysis has been carried out through a simulation environment that combines a dynamic simulation program with an optimization program. The coupling between these tools gives numerous simulation batteries that consider different options of a free-running building with constant temperature set points. Subsequently, a comparison between the obtained thermal loads has been made to determine the influence of the variables analysed in the sensitivity study. Finally, a statistical study has been carried out to identify the average, extreme values or the deviations obtained for the annual building thermal loads.

2 Methodology

Dynamic simulation programs are excellent tools to quantify the energy performance of multiple transitory systems such as conditioned buildings. These models consider the energy balances produced by external and internal fluctuations, solving the coupled and time-dependent equations based on its boundary conditions and input variables. The use of these tools allow the estimation of the building response when different variables are modified, assessing its influence on the annual energy loads [16]. In this framework, a simulation methodology has proposed to estimate the energy response of generic buildings when different constructive conditions are applied. This method solves a set of coupled mathematical equations with a time step of 1 hour and without real measurements.

In order to study the influence of geometry and construction variables on the building thermal loads, a local sensitivity analysis has been performed. This study has been carried out coupling a dynamic simulation program (TRNSYS) [17] with a parameterization program (GenOpt) [18], as shown in Figure 1.

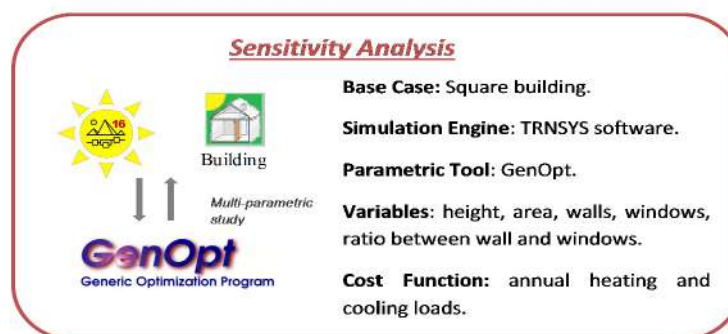


Fig. 1. Simulation environment to evaluate the energy performance of an unoccupied building

2.1 Base case

The dynamic simulation program TRNSYS has been used to assess the annual thermal loads required for conditioning the building.

The base case is a square floor plan building with a height between floors of 3 m, without internal gains (occupation, lighting and equipment). Seasonal temperature set

4

points have been fixed at 21°C for heating and 26°C for cooling, with 2°C oscillation. The reference building is located in Zamora, characterized by a cold and semi-arid climate with little annual rainfall. The summer season is short, hot and dry; while the winter season is cold and windy. The climate file provided by the Spanish Technical Building Code has been used [19].

2.2 Simulation environment

A sensitivity analysis has been carried out in a simulation environment coupling TRNSYS, as the simulation engine, with GenOpt, as the tool for the execution of different simulation batteries. Only one analysis variable is modified in each battery while the rest remains steady. The evaluated variables are: number of floors (2, 4 and 6), floor area (200, 400 and 600 m²), envelopes according to Spanish regulations for Zamora (NBE-CT79, CTE2006 and CTE2013) and percentage of the glass cover on the four main façades (25, 50 and 75%). The studied regulations correspond to the periods of 1979-2005 (NBE-CT79), 2006-2012 (CTE2006) and after 2013 (CTE2013). Table 1 shows the limit values of the global heat transfer coefficients defined for the envelope (exterior walls, ground and roof), windows and frames for these three standards. Finally, the annual building heating and cooling loads have been established as cost functions in the parametric evaluation, giving a total of 2187 simulations.

Table 1. Overall heat transfer coefficient of the building envelopes for the climatic zone D2.

Constructive element	U_{limit} (W/m ² K)		
	NBE-CT79	CTE2006	CTE2013
Exterior wall	1.40	0.66	0.27
Ground	1.00	0.66	0.27
Roof	0.90	0.38	0.22
Window	3.44	1.43	0.98
Frame	4.00	2.20	2.20

3 Results

The results provided by the simulation batteries are studied taking as a reference the average annual thermal load per m² of surface area, and the seasonal thermal loads (heating, cooling and total). In this way, the annual building needs with different volumes can be compared, attending to the compactness or the ratio between the volume of the building and the envelope area.

3.1 Global results

Once the thermal loads of the different studied options are calculated, the extreme cases of the series are identified for heating, cooling and total. Table 2 shows the ge-

ometric and constructive characteristics of these extreme cases (maximum and minimum values) obtained for the three series of annual loads.

Table 2. Geometrical and constructive characteristics of the extreme cases obtained for the annual total, heating and cooling loads.

Extreme Case	N° Floor	Surface Area (m ²)	Construction Normative	Window Ratio (%)			
				South	North	East	West
Minimum heat	6	600	CTE2013	75	25	75	25
Maximum heat	2	200	NBE-CT79	25	75	25	75
Minimum cool	6	600	NBE-CT79	25	25	25	25
Maximum cool	4	200	CTE2006	75	75	75	75
Minimum total	6	600	CTE2013	50	25	25	25
Maximum total	2	200	NBE-CT79	75	75	75	75

Figure 2 represents the annual values of heating loads (Q_{heat}, blue bars), cooling loads (Q_{cool}, brown bars) and total loads (Q_{tot}, green bars) identify for the six extreme cases. Higher differences are obtained for heating than cooling loads when comparing the maximum and minimum cases, reaching percentages of increase of 80% and 9% respectively.

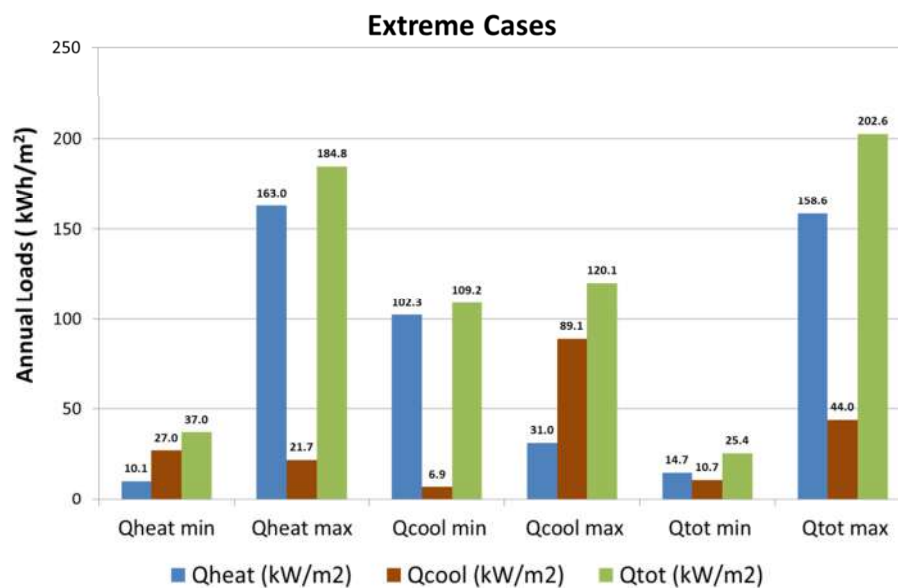


Fig. 2. Annual demands for heating, cooling and total for the 6 extreme cases

Analysing the results for heating, it is observed that higher constructive quality in the envelope provides lower values of annual thermal loads. This occurs with construction regulations after 2006. The greater the compactness the lower the thermal

6

loads. Finally, it highlights the strong influence obtained when the ratio of the glazed part to the opaque part of the façade differs depending on the orientation.

Large windows in the south and east façades are associated with higher overall solar gains and morning gains respectively, resulting in a reduction of heating loads. In these orientations the solar accumulation at first hours and during the day produces a positive balance in spite of the losses that are associated to bigger windows. On the contrary, lower percentage of windows in north and west orientations provide better results in thermal heating loads. In these orientations the losses produced by large windows give rise to a negative heat balance.

The global results obtained for cooling show that the increase of the window ratio to the façade leads to greater solar gains in summer, resulting in higher thermal loads. Therefore, in order to minimize the cooling loads, the size of windows in all orientations should be minimized. The construction quality of the envelope has a significant influence on the building cooling needs. A poorer quality of construction elements results in lower cooling loads. However, the maximum values are not produced for the most restrictive regulation (CTE2013), the peak is produced with the 2006 regulation. The greater the compactness, the lower the cooling loads.

The obtained results for the total loads are very similar to those obtained for heating. In these cases the greater annual contribution is produced during the winter period. The main difference between both series is reached for the optimization of the window ratio in the façades. This is due to the fact that the total annual balance must take into account both the heating and the cooling, trying to minimize the thermal loads in both periods. In the annual calculation, the best combination of the window percentage to minimize the total loads is 25% in the north, east and west façades and 50% in the south façade. This combination implies minimizing the annual losses for the most unfavourable orientations, minimizing the morning heat contributions and optimizing the heat contributions provided by the south façade throughout the year. The maximum values of total thermal loads are produced with the highest percentage of windows in all orientations.

In order to analyse the energy behaviour of the building under different constructive conditions, the annual thermal loads of four reference buildings have been evaluated: E1, E2, E3 and E4, whose geometric and constructive characteristics are shown in Table 3. Building E1 represents the maximum value of total annual load. Building E2 represents the minimum value of total annual load. Buildings E3 and E4 represent buildings with a total thermal load close to the intermediate value.

Table 3. Geometrical and constructive characteristics of the 4 representative buildings studied.

Building Case	N° Floor	Surface Area (m ²)	Construction Normative	Window Ratio (%)			
				South	North	East	West
E1	2	200	NBE-CT79	75	75	75	75
E2	6	600	CTE2013	50	25	25	25
E3	4	400	CTE2006	50	50	50	50
E4	4	600	NBE-CT79	50	25	25	25

The thermal loads obtained for the four representative buildings are shown in Figure 3, as well as the average value of the simulations battery. In this graph the annual values of heating loads (blue bars), cooling loads (brown bars) and total loads (green bars) are indicated.

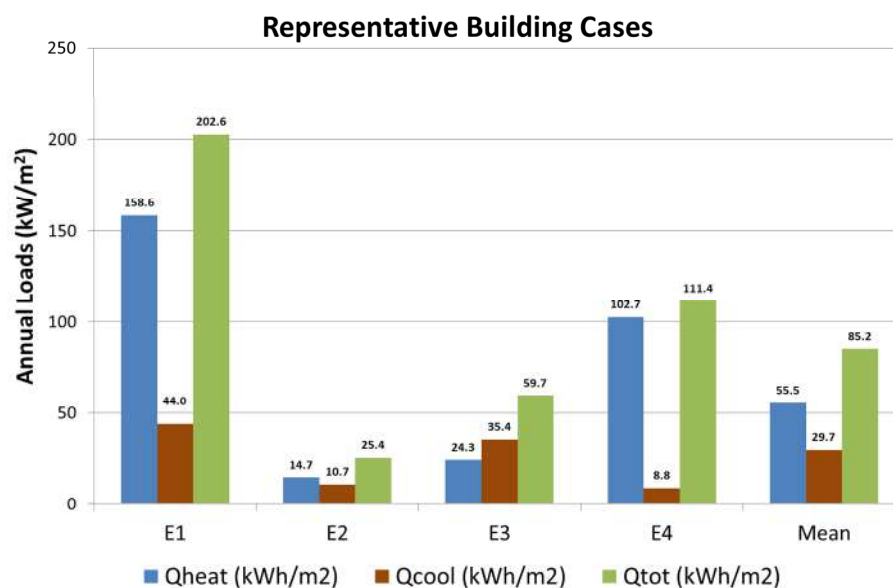


Fig. 3. Annual heating, cooling and total loads obtained for the 4 representative buildings and the average value of the studied series.

Comparing the two intermediate reference buildings with the complete series, E3 decreases 30% the total mean value while E4 increases 31%. In these buildings there is an opposite situation for heating and cooling. The heating need for E3 increases the average value by 56% while for E4 decreases by 85%, being the opposite situation for the cooling needs (reduction of 19% and increase of 70% respectively). The case E4 is slightly more compact, with an envelope built under less strict regulation and lower window ratio in all orientations (except in the south façade which is the same ratio). These characteristics result in less solar gains during the winter and more losses through the envelope, which leads to higher heating and total loads. This behaviour is due to the strong influence that winter loads produce on the annual calculation. As a result, the E3 building can be proposed for seasonal winter use and not be used in summer (schools). On the other side, the E4 building can be proposed for seasonal summer use (vacation housing or summer camps).

3.2 Influence of the analysis variables

The influence produced by height, envelope characteristics and window ratio in the four main façades (north, south, east and west) on the thermal loads of the base case

8

has been evaluated. The obtained results are shown in the following figures that represent the average values of annual loads for heating (blue columns), cooling (brown) and total (green).

Height. The first variable to be analysed is the number of building floors: 2, 4 and 6 floors. Evaluating the annual accumulated values, lower heating and total loads are observed as the building height increases (maximum decrease of 15% for heating and 9% for total loads). This effect is more marked when comparing buildings of 2 and 4 floors versus buildings of 4 and 6 (decreases for total loads of 6% and 3% respectively). However, the cooling values register very slight variations in spite of the height of the building (maximum increase of 3%). Figure 4 represents the accumulated thermal needs.

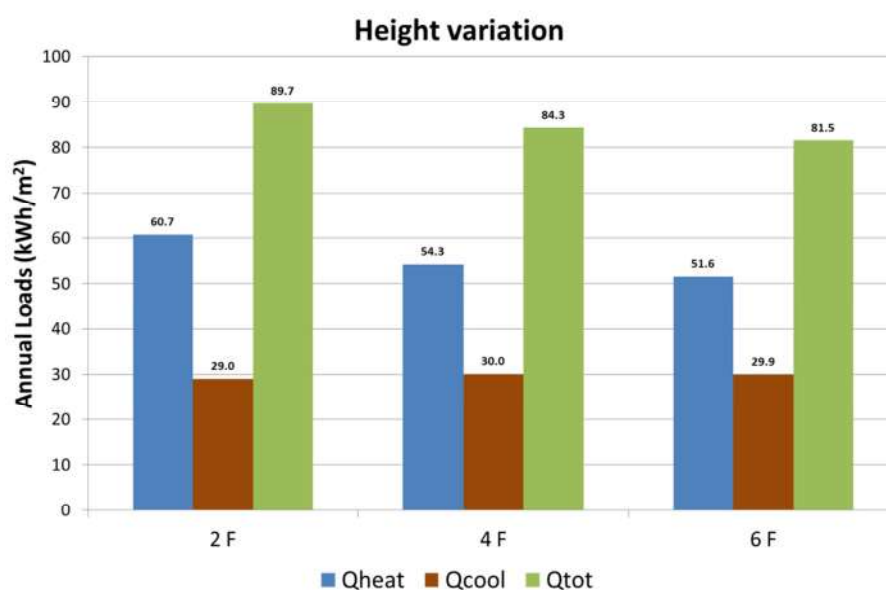


Fig. 4. Accumulated load averages obtained by varying the height (2, 4 and 6 floors)

Envelope. The influence of the building's construction parameters on the accumulated loads is analysed considering three regulatory periods. Figure 5 represents the accumulated needs for the standards NBE-CT79 (CT79), CTE2006 (CTE06) and CTE2013 (CTE13). As the construction regulations improve, the total annual and heating loads decrease (maximum decrease of 85% for heating and 68% for total loads). This reduction is being more marked for the regulations before 1979 (CT79) and the regulation 2006 (CTE06). On the other hand, the cooling loads increase for the regulations after 2006 (maximum increase of 22% comparing normative CT79 with CTE13).

Floor Area. Three floor areas of the building are evaluated: 200, 400 and 600 m². Figure 6 shows the influence of the floor area on the thermal loads. Each increase results in a reduction of the heating and cooling loads (maximum decrease of 21% for

heating and 46% for total cooling), decreasing the overall values (maximum decrease of 31%).

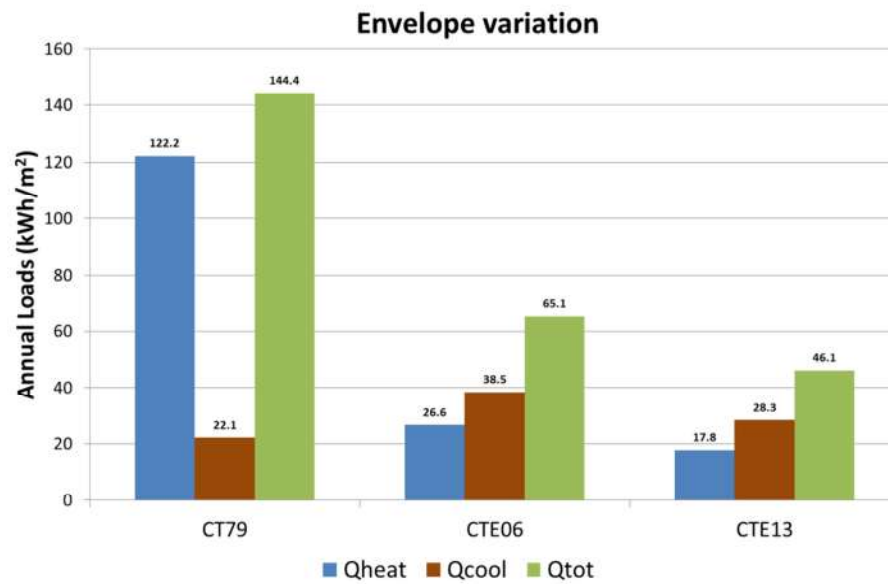


Fig. 5. Accumulated load averages obtained by varying the enclosures of the enclosure according to the three Spanish standards studied.

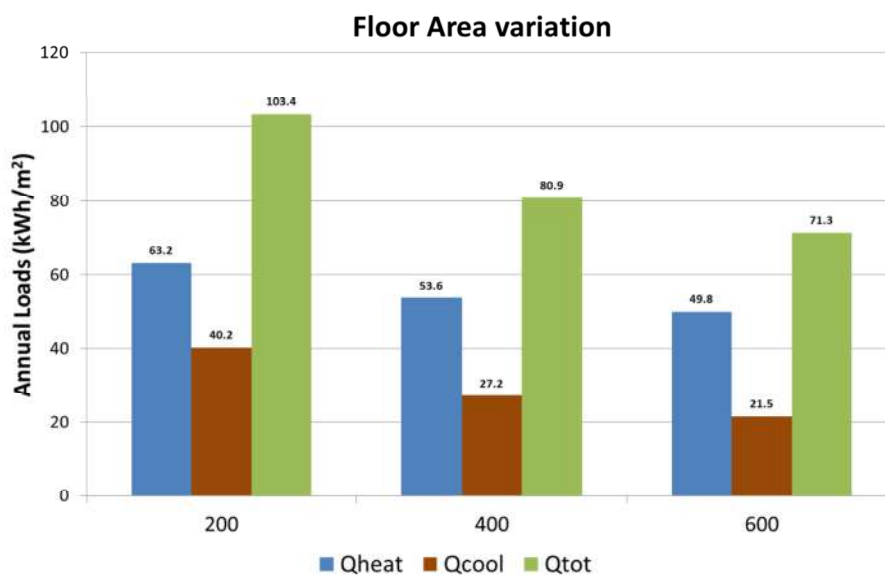


Fig. 6. Accumulated load averages obtained by varying the floor area (in m²).

Percentage of windows over the main façades. The influence produced by the ratio of glass versus the opaque wall in the exterior façades is shown in Figure 7. This figure represents the accumulated annual loads obtained by the building models with the three studied percentages of glass: 25, 50 and 75%, and the four main orientations; north (a), south (b), east (c) and west (d). The total annual needs increase as the percentage of glass elements increases, with maximum values of 9.5% for north, 5.3% for south, 18.9% for east and 11.9% for west orientations. The least marked effect is recorded in the south orientation. This orientation registers the highest heating load reduction when the percentage of windows increases, compensating the increase of cooling needs. On the opposite side is the east orientation. In this orientation the cooling loads significantly increase while the heating loads decrease with higher percentage of windows. The effect of increasing the percentage of glazing on the north and west façades is less extreme. In both cases the heating loads increase, contrary to the two previous orientations, but the increase of cooling loads is lower.

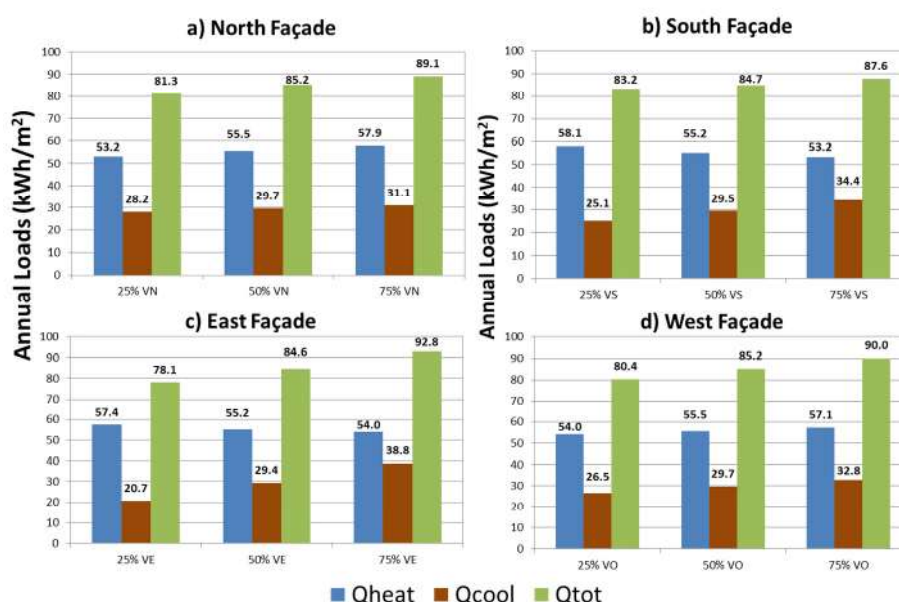


Fig. 7. Accumulated load averages obtained by varying the percentages of the glass ratio on the north (a), south (b), east (c) and west (d) façades.

3.3 Statistical study

A statistical study is carried out to observe the distribution of the annual thermal loads. This study is performed by setting the height analysis variable in the database, giving rise to three groups of 729 simulations. Due to the order of magnitude of the working values, the distribution of the heating and cooling loads is analysed in ranges of 10 and 5 kWh/m² respectively. The annual distribution of the cooling and heating needs, as well as their accumulated values is shown in Figures 8-10.

The most striking aspect of these graphs is that the higher the floor, the more concentrated the heating values seem to be. This fact is seen in the following table, which shows the loads obtained in the three cases (2, 4 and 6 floors).

Table 4. Most frequent heating load intervals.

Q _{heat} (kWh/m ²) 2 Floors	% Accumulated ordered	Q _{heat} (kWh/m ²)- 4 Floors	% Accumulated ordered	Q _{heat} (kWh/m ²) 6 Floors	% Accumulated ordered
30	32,92%	30	30,45%	20	39,09%
20	50,21%	20	59,53%	30	64,33%
40	65,71%	120	69,14%	110	75,45%
130	76,82%	110	78,46%	120	82,72%
120	83,95%	40	85,60%	140	88,34%

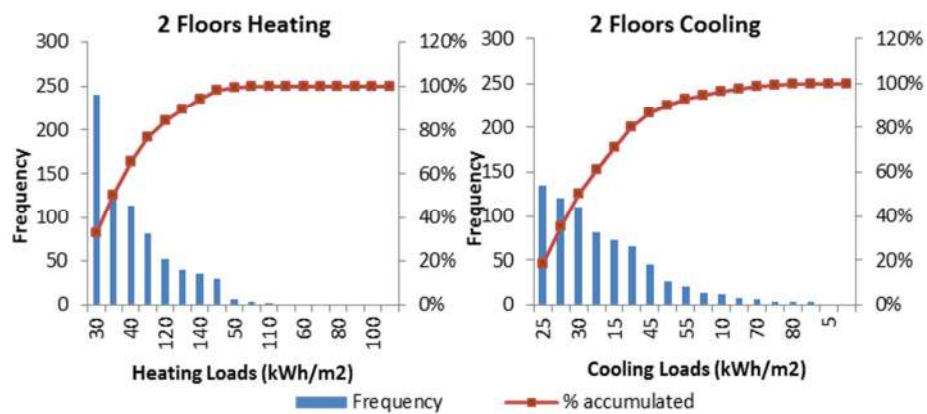


Fig. 8. Annual frequency and cumulative loads values for a 2-storey building

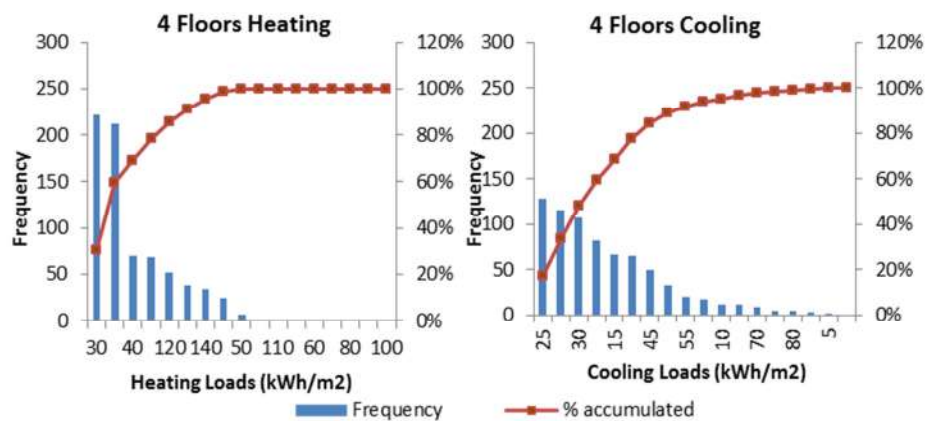


Fig. 9. Annual frequency and cumulative loads values for a 4-storey building

12

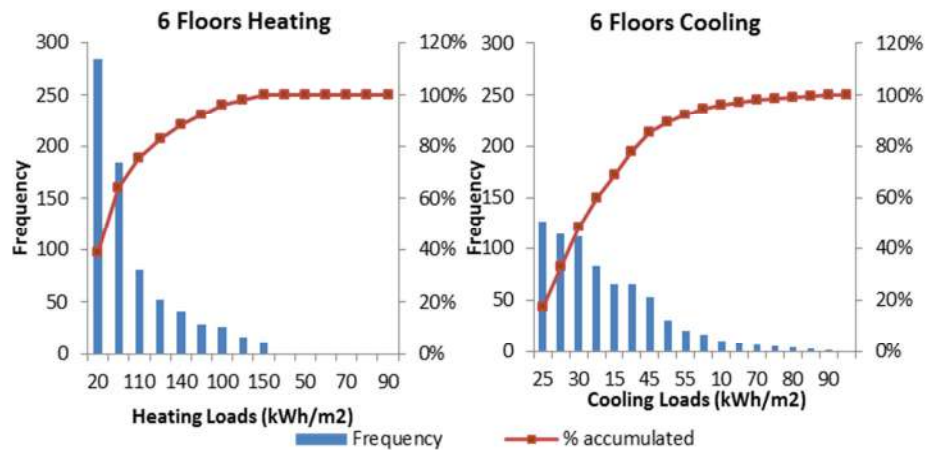


Fig. 10. Annual frequency and cumulative loads values for a 6-storey building

Figure 11 represents the distribution of the heating loads and cooling loads reached during the analysed period. It displays a tendency growing with height from the first two 10 kWh/m² periods, to concentrate thermal loads around some intervals. In the same way, in the heating series a range is seen (50-100 kWh/m²) in which only a few cases are obtained in the battery of 2 floors; and none in 4 and 6 floors.

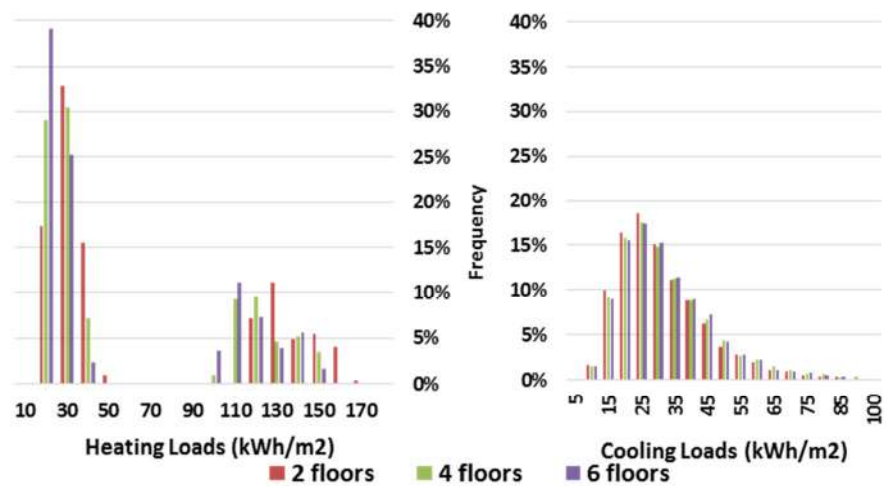


Fig. 11. Case distribution for increasing heating (left) and cooling (right) loads

The distribution of cooling values is very similar for the 3 heights, both in form and values. The summer distribution is less concentrated than the heating. In this fig-

ure it can be seen that the heat distribution has two clearly differentiated regions, mainly due to the strong influence of the envelope on the thermal loads.

The statistical values indicate that the heating loads are not only lower at higher heights; the error and deviation obtained are lower (Table 5). This trend points to more stability. The difference in height does not have such a marked effect on the cooling loads (Table 6).

Table 5. Statistical values of heating loads (kWh/m²).

Heating Loads (KWh/m ²)	2 floors	4 floors	6 floors
Media	60.74	54.27	51.60
Typical error	1.90	1.74	1.71
Medium	29.84	25.70	23.07
Standard deviation	51.18	46.96	46.13
Asymmetry Coefficient	0.75	0.77	0.78
Range	149.10	139.83	137.48
Minimum	13.92	11.41	10.05
Maximum	163.02	151.24	147.53

Table 6. Statistical values of cooling loads (kWh/m²).

Cooling Loads (KWh/m ²)	2 floors	4 floors	6 floors
Media	29.00	30.05	29.93
Typical error	0.51	0.54	0.53
Medium	26.05	26.86	26.97
Standard deviation	13.65	14.57	14.19
Asymmetry Coefficient	186.34	212.41	201.37
Range	1.17	1.18	1.13
Minimum	77.29	82.14	79.88
Maximum	7.23	6.94	6.88

4 Conclusions

Within the framework of the SIGGENER project, a sensitivity study has been carried out to evaluate the influence of different constructive factors on the building thermal loads. The base building analysed is a block without internal gains and located in a cold semi-arid climate (Zamora). As analysis variables, volumetry, materials of the envelope according to regulations and size of the windows in the main façades of the building (north, south, east and west) are considered. This study has been carried out through a dynamic simulation environment that gives rise to 2187 simulations.

The data series obtained for the heating loads generally shows higher values than those for the cooling loads. Evaluating the heating it is observed that the most influ-

ence factor is the variation of the materials that characterize the building envelope. This factor is followed by the variation in surface and height. Higher regulatory requirements for building envelopes (more recent regulations) lead to lower heating loads. The ratio of windows in the external façades is more influential in the South orientation, followed by East and North, with the least influence being on the West.

The composition of the building envelope is a very particular element when analysing cooling. Buildings built under the NBE-CT79 standard have less thermal needs while those built under the CTE2006 standard, which have more thermal needs. The buildings built under the CTE2013 standard correspond to intermediate cases.

The ratio of windows on east facing façades is almost as critical as the envelope. Surface and south facing windows have a noticeable effect, less so on west facing windows. The variation in the windows ratio in North orientation, and above all in the building height, point to less influence. The variations made on the parameters analysed, without counting the envelope, show that cooling is more sensitive to changes.

The element whose variation is most critical over the overall thermal load is the envelope, followed by the surface and the Eastern windows ratio. The number of floors, the windows ratio facing north and west achieve similar order of influence. The southern windows ratio seems to be less influential: beneficial in winter and harmful in summer.

The statistical analysis allows understanding the global building performance obtained from the simulation batteries. The distribution of the heating values highlights two quite defined intervals and shows more stability with a higher number of floors. The distribution of cooling values is asymmetric but more regular.

References

1. United Nations Human Settlements Programme: Global Report on Human Settlements 2011: Cities and Climate Change; Routledge: London, UK, 2011
2. Hallegatte, S. Strategies to adapt to an uncertain climate change. *Global Environmental Change*. 2009, 19, 240–247
3. Soutullo, S., Giancola, E., Jiménez, M.J., Ferrer, J.A., Sánchez, M.N.: How Climate Trends Impact on the Thermal Performance of a Typical Residential Building in Madrid. *Energies* 13, 237 (2020).
4. Van den Brom, P., Hansen A.R., Gram-Hanssen, K., Meijer, A., Visscher, H.: Variances in residential heating consumption – Importance of building characteristics and occupants analysed by movers and stayers, *Applied Energy* 250, 713-728 (2019).
5. SISGER homepage, <https://www.cartif.es/en/sisgener-en/> last accessed 2020/09/11.
6. Díaz, J.A., Soutullo, S., Bujedo, L.A., Castellanos, A., Heras, M.R., Samaniego, J., Ferrer J.A.: Modelo Reducido De Predicción De Demanda De Edificios Residenciales En Base A Parámetros Meteorológicos, Artículo aceptado para el XVII Congreso Ibérico e XIII Congreso Ibero-americano de Energía Solar, CIES 2020, 3-5 de Noviembre, Lisboa, Portugal.
7. Li, X., Li, W., Zhang, R., Jiang, T., Chen, H., Li, G.: Collaborative scheduling and flexibility assessment of integrated electricity and district heating systems utilizing

- thermal inertia of district heating network and aggregated buildings. *Applied Energy* 258, 114021 (2020)
8. Fouquier, A., Robert, S., Suard, F., Stéphan, L., Jay, A.: State of the art in Building modelling and energy performances prediction: A review. *Renewable and Sustainable Energy Reviews* 23, 272-288 (2013).
 9. Biswas, M.A.R., Robinson, M.D., Fumo, N.: Prediction of residential building energy consumption: A neural network approach. *Energy* 117 (1), 84-92 (2016).
 10. Giancola, E., Martin Chicott, I., Heras, M.R.: Desarrollo de un modelo de E-GIS DB (Environment and Energy Geographical Information System Database) para apoyar iniciativas de ciudades inteligentes. I Congreso de Ciudades Inteligentes 2015, Madrid, España.
 11. Crawley, D.B., Hand, J.W., Kummert, M., Griffith, B.T.: Contrasting the capabilities of building energy performance simulation programs. *Building and Environment* 43, 661-673 (2008).
 12. S. Soutullo, L.A. Bujedo, J. Samaniego, D. Borge, J.A. Ferrer, R. Carazo, M.R. Heras: Energy performance assessment of a polygeneration plant in different weather conditions through simulation tools, *Energy and Buildings* 124, 7-18 (2016).
 13. Zhang, R., Mirzaei, P.A., Jones, B.: Development of a dynamic external CFD and BES coupling framework for application of urban neighbourhoods energy modelling. *Building and Environment* 146, 37-49 (2018).
 14. Tronchin, L., Manfren, M., Tagliabue, L.C.: Optimization of building energy performance by means of multi-scale analysis – Lessons learned from case studies. *Sustainable Cities and Society* 27, 296-306 (2016).
 15. Enríquez, R., Jiménez, M.J., Heras, M.R.: Towards non-intrusive thermal load Monitoring of buildings: BES calibration. *Applied Energy* 191, 44-54 (2017).
 16. Soutullo S, Giancola E, Heras MR.: Dynamic energy assessment to analyze different refurbishment strategies of existing dwellings placed in Madrid. *Energy* 152,1011-1023 (2018).
 17. TRNSYS webpage, <http://www.trnsys.com/> , last accessed 2020/09/11
 18. GENOPT webpage, <https://simulationresearch.lbl.gov/GO/> , last accessed 2020/09/11.
 19. Ministerio de Fomento. Documento básico HE: Ahorro de Energía (CTE), Gobierno de España. (2020). <https://www.codigotecnico.org/>, last accessed 2020/09/10

A methodology for the conversion of a network section with generation sources, storage and loads into an electrical microgrid based on Raspberry Pi and Home Assistant

Oscar Izquierdo-Monge¹, Paula Peña-Carro¹, Luis Hernández-Callejo², Oscar Duque-Perez³, Angel Zorita-Lamadrid³, Roberto Villafafila-Robles⁴

¹ CEDER-CIEMAT, Autovía de Navarra A15 salida 56, 422290 Lobia (Soria), España, O.I.M.: oscar.izquierdo@ciemat.es; P.P.C.: paula.pena@ciemat.es

² University of Valladolid, Campus Universitario Duques de Soria, 42004 Soria, España. L.H-C: luis.hernandez.callejo@uva.es;

³ University of Valladolid, Paseo del cauce 59, 47011 Valladolid, España. O.D.P.: oscar.duque@eii.uva.es; A.Z.L.: zorita@eii.uva.es

⁴ Centre d'Innovació Tecnològica en Convertidors Estàtics i Accionaments (CITCEA-UPC), Departament d'Enginyeria Elèctrica, Universitat Politècnica de Catalunya, ETS d'Enginyeria Industrial de Barcelona, Av. Diagonal 647, 08028, Barcelona, Spain.
roberto.villafafila@citcea.upc.edu

Abstract: This paper presents a methodology to convert a network section with generation sources, storage, and loads into an electrical microgrid. This conversion will allow greater autonomy and efficiency in its management. Besides, after the analysis of the recorded data, a reduction in the consumption of the distribution network can be achieved, and therefore, a reduction in the costs of the electricity bill. To achieve this transformation it is necessary to provide the network with intelligence, proposing a methodology based on four steps: identification and description of the elements that form it, choice of hardware and software for monitoring and controlling the system, establishment of communication between the different elements and creation of a control network framework for visualization. As a case study, the microgrid of the Renewable Energy Development Centre (CEDER) located in the province of Soria (Spain) is shown, formed by different sources of generation, storage systems, and consumption. All the elements of this microgrid are integrated with single free software, Home Assistant, installed in a Raspberry Pi 4 to provide the network with basic intelligence, control and monitoring in real-time through different communication protocols.

Keywords: Smart electric microgrids, Home Assistant, monitoring and control system.

1 Introduction

The concept of a microgrid is a term that can be defined as the U.S. Department of Energy [1] proposes; "a group of interconnected loads and distributed energy resources within clearly defined electrical boundaries that act as a single controllable entity respect to the network. A microgrid can be connected and disconnected from the network to allow it to operate in grid or island mode. A remote microgrid is a variation of a microgrid operating in island conditions". Or define it more simply "Microgrids are decentralised distribution networks that integrate distributed energy resources and balance power generation and loads at the local level" [2].

This form of energy production, consumption, and management is becoming increasingly important today. It was born to reduce the different environmental problems that currently exist through a greater implementation of renewable energy sources. However, this proposal of management using microgrids is complex to implement and certain institutional changes are necessary to reach its maximum potential since at present the management of the network is monopolized by large generating companies and governments at different levels. The justification for the monopolies in the energy sector has weakened over time with the appearance of new companies, which, although smaller in size, are gaining more and more followers, betting on the purchase of clean energy from sources closer to the place of consumption.

The break-up of the monopoly will open up possibilities for intelligent local utility networks, microgrids, and automated building energy management. Their presence in the energy market, and the possibility of compensating for the surplus or deficit of power in the distribution network, makes the current energy system more resilient and efficient in terms of power quality, electricity costs and continuity of supply at critical loads in the event of prolonged outages [3].

But microgrids also have certain disadvantages, some relevant, such as temporary uncertainty, which can lead to some reluctance to implement them. This uncertainty is always associated with volatile load profiles and changes in climate conditions, which affect the uncontrollable generation and prevent the optimization of economic planning [4][5], making it challenging to make accurate forecasts about the future state of supply and demand [6][7][8].

To make the system more reliable and secure in terms of generation [9], storage systems such as batteries, flywheels or supercapacitors, are established as key elements within the microgrid system in slowing down power fluctuations and counteracting the energy imbalances produced [10] by matching the generation and total load of the microgrid [3][11].

To operate the whole microgrid more efficiently, it is necessary to have a measurement, communication, and data management system to allow the semi-autonomous or autonomous operation of the system, being able to solve the supply problems in the shortest time possible [12][13]. There are several communication technologies within this context, such as copper conductors, fibre optics, power line communication, and wireless communication.

Regardless of the communication technology selected, all microgrids must have the following elements at the communication level: local communication structure, hierarchical monitoring, control and management system, and intelligent controllers for the loads, consumptions and storage systems.

As mentioned above, a microgrid can operate either connected to the main distribution network through a common coupling point (PCC), or disconnected from it, on the island mode [14]. A stable and economically efficient way of operating is required [15].

The microgrid is managed by a central controller that is at the head of the hierarchical control system. This central controller (MGCC) provides the setpoints to the controllers of the rest of the equipment, such as generation sources, loads, and energy storage systems. The control system will be responsible for regulating the frequency and voltage in all modes of operation, as well as for distributing the load between the various elements of distributed generation (DG) and storage, managing the flow with the main network, and optimising operating costs.

To be able to control all the generation and consumption systems that make up the microgrid, it is necessary to have Smart Meters in each of the elements to be monitored. At present, Arduino devices are being used, which consist of a board with a microcontroller hardware and free software. For this case, they are configured for a real-time data collection of all the variables [16]. As for the software used, many microgrids are monitored and controlled by LabVIEW, a payment platform that allows the design of both real and virtual environments through visual programming [17].

The variations proposed respect to the software and hardware previously mentioned are the installation of a Raspberry, a computer with a reduced board with which greater versatility, calculation power, WiFi, or Ethernet connectivity integrated into the board is achieved. As for the software installed Home Assistant, it does not require a paid license for its use and its programming is simpler and more intuitive, which facilitates its integration into the microgrid and a significant reduction in monitoring costs.

With these implementations, we achieve the objective set out in this project, which is the transformation of a production and consumption microgrid into a smart microgrid that allows us to act autonomously thanks to the software and hardware configurations installed.

The rest of the paper is as follows: section 2 addresses the steps required to convert a network section into a microgrid, such as the identification and description of the passive network elements, the selection of the control hardware and software, the establishment of communication between the elements and finally the creation of a network control framework for the management of the microgrid; section 3 presents a case study. Finally, the conclusions obtained are presented.

2 Methodology to provide intelligence to the grid

As indicated in the introduction, this paper aims to describe a methodology that makes it possible to provide intelligence to an electricity network to which a set of generation, storage, and load elements are connected and to transform it into a smart microgrid that can operate as such, with high efficiency.

The steps to be able to convert an electrical network with independent elements of generation, storage and consumption that do not communicate with each other into a smart microgrid and that are developed in this article are shown in Figure 1.

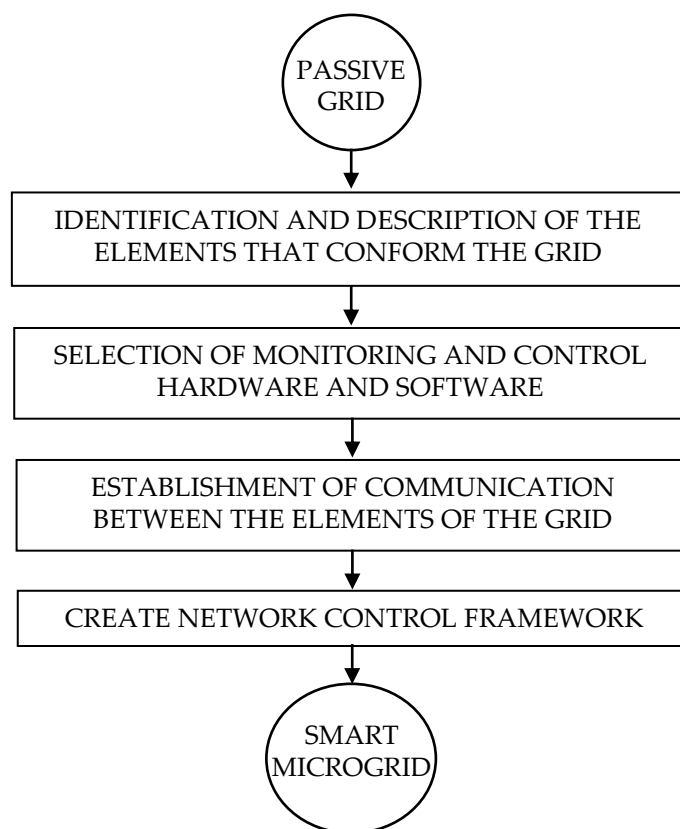


Fig. 1. The sequence of steps to convert passive network into a smart microgrid.

Step 1. Identification and description of the elements that make up the network: The first step in providing intelligence to an electricity network is to identify and describe all the connected elements of generation, storage, and consumption. It is essential to know at least the installed nominal power of each generation source, the capacity in the case of storage systems, the consumption of the most significant loads,

a ranking of loads by priority and influence of load profile. It is also necessary to know for each system if they allow direct communication with some of the equipment that composes it and the communication protocols that this equipment uses.

Step 2. Selection of the monitoring and control hardware and software: The hardware and software chosen will condition the human-machine interface (HMI) to be used as a microgrid management system. In this section lies the main novelty of this methodology and its main advantages. A Raspberry Pi is used, as will be shown later, together with the free software Home Assistant.

Step 3. Establishment of communication between the elements of the network: once the components of the network have been described, the forms and protocols of communication permitted by each of them are known, and the control software has been selected, communication must be established between all of them, so that they do not function independently, but as a whole in which there can be an interaction between them. This will allow the behaviour of each of the elements of the system to be subordinated to that of the others so that the operation of the microgrid can be optimized, with the consequent cost savings in the electricity bill. Besides, Home Assistant allows to establish communication with any element through the multiple communication protocols it has integrated, in a simple way.

Step 4. Creation of a control network framework: once the communication between all the elements has been established, a control network framework or interface (HMI) must be developed to observe, in a simple and as intuitive way as possible, the operation of each of the elements of the network, and to send them operation instructions to optimize the operation of the microgrid by increasing its efficiency as much as possible. It should also allow the recording of monitored data for subsequent analysis to define management strategies, and once implemented, to validate their effectiveness.

3 Case Study

The case study to apply the proposed methodology is the network of the Centre for the Development of Renewable Energy (CEDER), which belongs to the Centre for Energy, Environmental and Technological Research (CIEMAT), a Spanish Public Research Organisation, currently dependent on the Ministry of Science and Innovation. It is located in the town of Lobia, province of Soria (Spain), and has an area of 640 ha with more than 13000 m² built in three separate areas (see Figure 2).



Fig. 2. Location and buildings distribution at CEDER.

CEDER's grid is connected to a 45kV distribution network and carries out a transformation at its entrance to 15kV. The grid is made up of eight transformation centres that reduce voltage to 400V. The network has multiple renewable generation systems that are not controllable (wind and photovoltaic), controllable renewables (hydraulic turbine), non-renewable (diesel generator), different mechanical (pumping system with tanks at different levels) and electrochemical (lithium-ion and Pb-acid batteries) storage systems, as well as several consumption elements connected to each transformer station which are monitored with a network analyser (PQube) installed in the low voltage part of each transformer station.

Instead of considering the entire microgrid, only the elements connected to one of the transformer stations will be considered, to simplify the control system and not to repeat cases, since all the photovoltaic inverters are practically the same, the PQubes network analysers too, etc.

3.1. Identification and description of the network components

According to the previous section, the first step consists of identifying and describing all the elements connected to the network (see Figure 3). In this case study, they are the following:

- Photovoltaic generation system of 5 kW, consisting of 24 polycrystalline silicon panels of 210 W distributed in 4 series of 6 panels. The panels are assembled on a floor structure with a variable tilt angle and connected to an Ingeteam inverter model Ingecon Sun Lite.

To read photovoltaic generation values, it is necessary to communicate with the photovoltaic inverter, which has a network card to connect it to the CEDER data network (Ethernet) and allows communication using the Modbus TCP/IP protocol.

- Wind generation system consisting of a three-bladed wind turbine of 15 meters in diameter and 50 kW power. It is a horizontal axis and works leeward.

There was no connection to the wind turbine or its control panel, so it has been necessary to install some equipment that allows communication. In this

case, a National Instruments FieldPoint compact data acquisition system [18] has been installed, which allows variables such as power, wind speed, etc. to be measured and can be connected to the CEDER data network. This equipment allows communication under the Modbus TCP/IP protocol.

- Electrochemical storage system consisting of 120 Tudor Pb-acid 7EAN100T batteries of 2 V each. The capacity is 1080 Ah at 120 hours (C120). It is connected to a 50 kW inverter/charger/regulator developed by CEDER together CIRCE.

The inverter/charger is connected via an RS485 connector to the serial port of a computer with a SCADA (Supervisory Control and Data Acquisition) for battery control. Therefore, the control system of the microgrid to be developed will communicate locally with the inverter via Modbus RTU.

- Consumption: The loads are the different laboratory and workshop buildings that make up the part of CEDER considered and its equipment, which are connected to the low voltage side of the transformation centres. To measure consumption, a power quality/network analyser (PQube) has been installed. In this case study there are no critical loads to be powered in case of serious disturbances or microgrid failure. All of them have the same level of significant.

The PQube can be connected to the CEDER data network through Ethernet and allows Modbus TCP/IP communication.

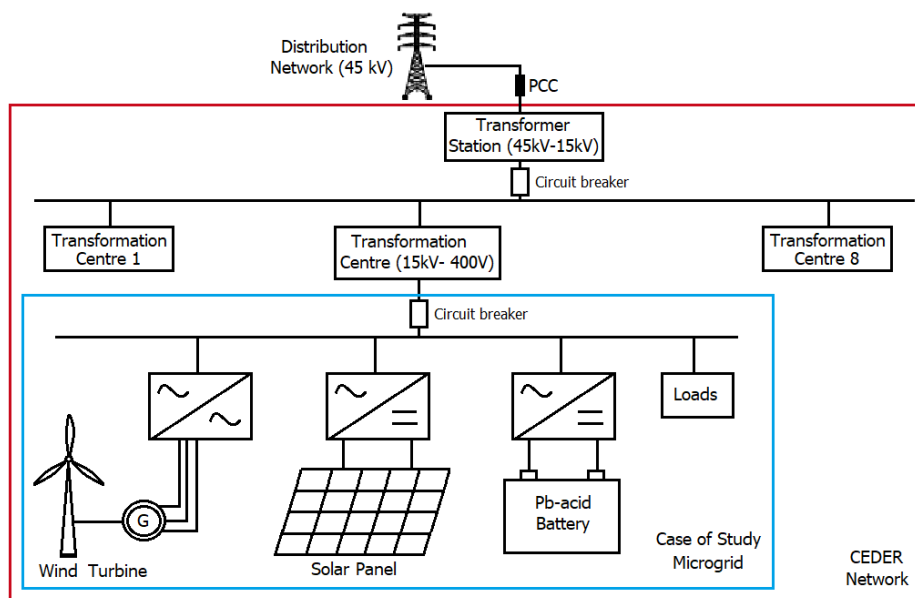


Fig. 3. Case of study microgrid.

3.2. Selection of monitoring and control hardware and software

Once all the elements of the microgrid have been described, and their characteristics and the form in which the communication with them is established, the following step is the election of the hardware and the software to carry out the control system.

There are several software packages available on the market for the analysis of energy systems, but not all of them allow the analysis and management of microgrids based on real-time data for the prediction and behaviour of the system [19], among which ETAP Real-Time 24 [20] is one of them. Another tool that allows this is Acciona's Microgrid Energy Management System – μ GEMS [21]. However, as seen in the introduction, the most common way is to use software such as Labview to design a specific program for the ad-hoc monitoring and control of each microgrid.

In this case, it is proposed to use a Raspberry Pi 4 Model B [22] [23], with a tool developed specifically for the management of microgrid such as CIRCE and its Energy Box [24]. The Raspberry Pi 4 Model B was introduced in June 2019 to replace the Raspberry Pi 3 B+, with a significant improvement in its specifications, which will increase the smoothness of operation of our control system. Raspberry Pi 4 B features a Broadcom BCM2711B0 quad-core ARM Cortex-A72 1.5 GHz processor, LPDDR4-3200 MHz SDRAM up to 4 GB, Gigabit Ethernet network connectivity (up to 1000 Mbps) and Wi-Fi 2.4 GHz/ 5 GHz wireless connectivity, IEEE 802.11 b/g/n/ac and Bluetooth 5.0, BLE. It works with a Raspbian operating system, which is the Linux (Debian) distribution prepared specifically for Raspberry.

As software, HomeAssistant is chosen [25] which is generally used for home automation applications but that is a robust solution, economically affordable (it is free software) and with great potential for monitoring and managing microgrids in real-time. This system allows communication with all the elements of generation, storage, and consumption of the network under study, through different communication protocols and their integration into a single HMI (Human Machine Interface). Home Assistant is a system developed in Python, free and open that allows to monitor all the elements connected to the microgrid, to control them from a unique interface (which allows its control from mobile devices), as well as to define advanced rules to control each one of the elements in a simple and intuitive form.

To store data collected by Home Assistant the best solution is to use MySQL [26], which is an open-source relational database management system. It can be installed on the same Raspberry, with a slight slowdown in the operation of the system, or on a different one exclusively for the database, achieving a higher system performance.

The use of MySQL is optional, although highly recommended whenever it is required to store the monitored data for later analysis, allowing to define much more efficient strategies for energy management of the microgrid.

The proposed control system of the microgrid is made up of three blocks:

- A communication block integrates the different communication protocols of the microgrid's generation, storage and consumption systems.
- A database: for information storage and subsequent analysis.

- A management block: with a user interface that allows real-time monitoring of all elements of the microgrid and programming of energy strategies to be defined.

3.3. Establishment of communication between the elements that make up the network

Next, the communication of each of the elements of the microgrid with Home Assistant has to be established. Different communication protocols allow the transmission of information, provided that all the equipment is connected to the same data network or other equipment in local mode and that they are in turn connected to this network.

Among the most common communication protocols, Modbus [27] stands out above all others. It allows us to control a network of devices (in our case, generation, storage, and consumption elements) and to communicate them with a control system (Raspberry Pi 4 with Home Assistant). It is the standard communication protocol in the industry since it is robust, easy to use, open-source and therefore free and, above all, reliable.

All elements of the CEDER network described in section 3.1 allow communication via the Modbus protocol, namely:

- RTU: It is based on master/slave architecture, to connect a control system to a Remote Terminal Unit (RTU) via a serial port. Typically, the master is a human-machine interface (HMI) or a supervisory and data acquisition (SCADA) system that sends a request and the slave is a sensor or a programmable logic controller (PLC) that returns a response. It uses a Cyclic Redundancy Checksum (CRC) to ensure the reliability of the data and as an error checking mechanism.
- TCP/IP (Transmission Control Protocol/Internet Protocol): It is based on a client/server architecture and allows communication over an Ethernet network. No CRC required.
- RTU over TCP: It is a combination of the two previous ones. It is based on client/server architecture for communications over Ethernet as Modbus TCP/IP but uses a CRC as Modbus RTU.

The microgrid scheme communications are shown in Figure 4.

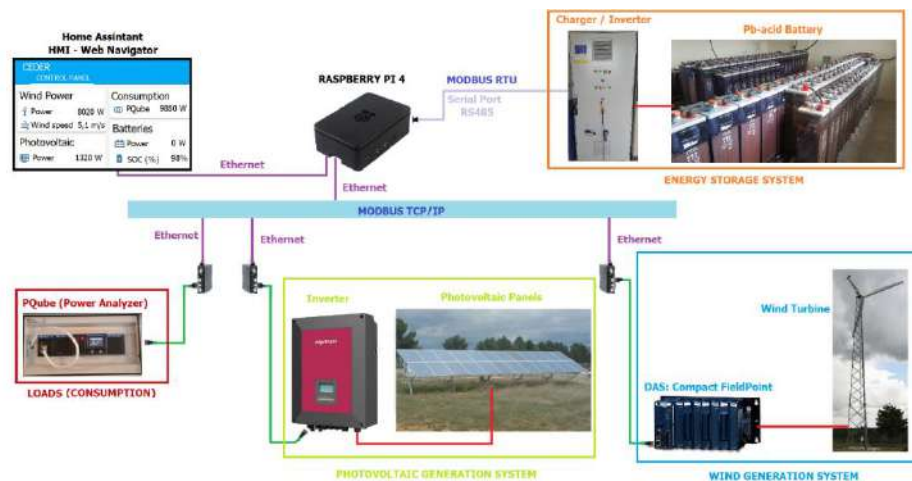


Fig. 4. Elements of the CEDER's microgrid.

To communicate each element with Home Assistant, first all the microgrid components must be defined in the configuration file, assigning them a name and indicating the type of communication, the IP, the port.

Once all the elements of the microgrid have been defined, the records with the desired information for each component must be read at the corresponding addresses. This is also done in the Home Assistant configuration file and it is necessary to have the Modbus frame of each unit (it should be in the manufacturer's manual, but many times it is not and it is necessary to contact the manufacturer to provide it) to know the addresses where the variables to be read are.

In the case of uncontrollable generation elements [11], such as the photovoltaic inverter and the wind generator, and loads (PQube network analyser), it is only necessary to read the instantaneous power since no action instructions can be sent to them. By contrast, in controllable generation elements and storage systems such as Pb-acid batteries in our case, it is necessary to read all the records to develop a SCADA that allows for control of their operation through the control panel, integrated with the rest of the elements.

3.4. Creation of a control network framework

Once communication has been established with all the equipment, an interface has to be created that allows the user to see in real-time the records collected from the elements that form part of the microgrid and to execute commands to give them instructions (start/stop of generation equipment, loading/unloading of storage systems, etc.).

Using Home Assistant, it is very intuitive to create a control network framework once communication has been established with each element of the microgrid and it has been defined in the configuration file. The starting point is a graphic interface that allows inserting cards with different functionalities. Default cards can be added with

maps or weather forecasts to help to estimate the production of the renewable generation systems available in the microgrid. It also allows adding cards with different values of all the registers read numerically (Entities) or to represent graphically those values (Historical graph), or to represent jointly (graphically and numerically) a value using the Sensor card. Home Assistant also allows inserting buttons to send instructions to the different elements that have been monitored.

Figure 5 shows the real-time power values of each of the elements connected to the microgrid under study, indicating a photovoltaic generation of 1320 W and a demand of 9880 W. Wind speed is 5.1 m/s and wind generation is 8020 W. The batteries are stopped, since there is no high demand to provide energy to the microgrid, nor is there a generation surplus to be able to charge them. Moreover, batteries are almost fully charged (SOC 98%).

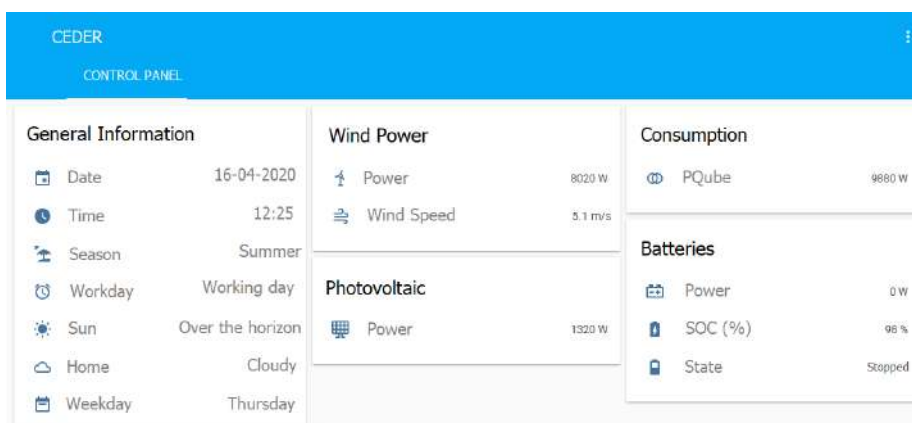


Fig. 5. Control network framework of the CEDER’s microgrid in Home Assistant.

The SCADA for the control of the batteries also has to be created, as can be seen in Figure 6. In figure 6 it can be observed how the batteries are in the process of normal charging, the microgrid is injecting them with 1780 W, they are at 96% of their capacity and with a voltage of 266 V.

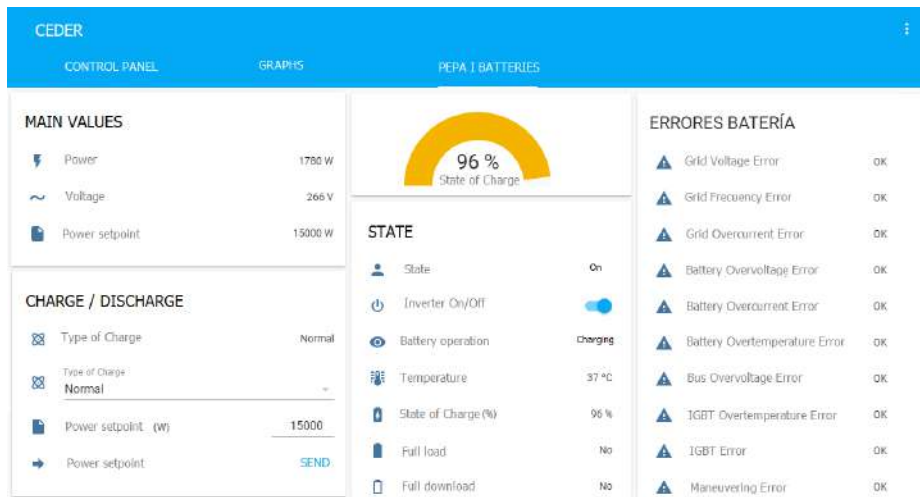


Fig. 6. SCADA of batteries at the CEDER’s microgrid in Home Assistant.

Home Assistant allows representing in real-time the value of the variables collected from each of the elements as can see in Figure 7.

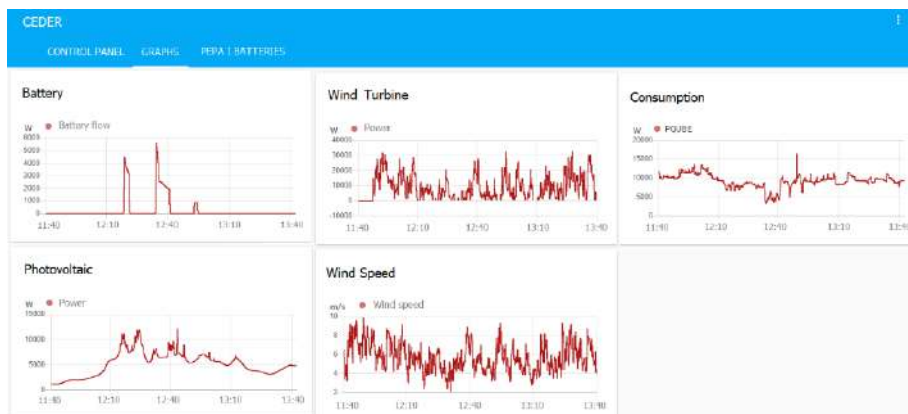


Fig. 7. Power time-series of the CEDER’s microgrid elements in Home Assistant.

4 Conclusions

In this paper, a methodology is proposed for the conversion of a network section with generation, storage and loads into a smart electricity microgrid that can be replicated in any network section, based on four steps: 1) identification and description of the elements that make up the network, 2) selection of the hardware and software for monitoring and control, 3) establishment of communication between the elements of

the network and 4) creation of a control network framework that allows the management of the electrical microgrid.

The main advantage of this methodology is the use of the free software Home Assistant, installed on a Raspberry Pi 4 to manage the microgrid. Although Home Assistant is a software whose widespread use is for home automation, it offers all the capabilities needed to monitor, manage and integrate into a single HMI and in real-time, all the elements of generation, storage, and consumption connected to a power network to turn it into a smart microgrid, simply and intuitively. It is worth mentioning the feature that this software offers us of unifying all the elements that form the microgrid only in one HMI. This is the main feature that differs from the most known way of monitoring, in which to know the current status of each of the elements it is necessary to access different connection points.

With the application of this methodology, it will be possible in the near future to establish strategies to optimize the operation of the microgrid by taking full advantage of the generation sources and reducing as much as possible the consumption of CEDER microgrid's from the distribution network with the help of storage systems. This could also lead to savings in the energy bill.

References

1. D. T. Ton and M. A. Smith, "The U.S. Department of Energy's Microgrid Initiative," *Electr. J.*, 2012.
2. T. Sachs, A. Gründler, M. Rusic, and G. Fridgen, "Framing Microgrid Design from a Business and Information Systems Engineering Perspective," *Bus. Inf. Syst. Eng.*, vol. 61, no. 6, pp. 729–744, Dec. 2019.
3. N. A. Warsi, A. S. Siddiqui, S. Kirmani, and M. Sarwar, "Impact Assessment of Microgrid in Smart Cities: Indian Perspective," *Technol. Econ. Smart Grids Sustain. Energy*, 2019.
4. J. Yang, B. Guo, and B. Qu, "Economic optimization on two time scales for a hybrid energy system based on virtual storage," *J. Mod. Power Syst. Clean Energy*, 2018.
5. B. Kroposki, "Integrating high levels of variable renewable energy into electric power systems," *J. Mod. Power Syst. Clean Energy*, 2017.
6. Q. LI, Z. XU, and L. YANG, "Recent advancements on the development of microgrids," *J. Mod. Power Syst. Clean Energy*, 2014.
7. Y. Jia, X. Lyu, C. S. Lai, Z. Xu, and M. Chen, "A retroactive approach to microgrid real-time scheduling in quest of perfect dispatch solution," *J. Mod. Power Syst. Clean Energy*, 2019.
8. A. Kaur, J. Kaushal, and P. Basak, "A review on microgrid central controller," *Renew. Sustain. Energy Rev.*, vol. 55, pp. 338–345, 2016.
9. S. Chandak, P. Bhowmik, and P. K. Rout, "Load shedding strategy coordinated with storage device and D-STATCOM to enhance the microgrid stability," *Prot. Control Mod. Power Syst.*, 2019.
10. K. C. Divya and J. Østergaard, "Battery energy storage technology for power systems- An overview," *Electric Power Systems Research*. 2009.

11. L. Hernández Callejo, *Microrredes eléctricas. Integración de generación renovable distribuida, almacenamiento distribuido e inteligencia*, Primera ed. Publicaciones, Ibergarceta, 2019.
12. H. Gharavi and R. Ghafurian, "Smart grid: The electric energy system of the future," *Proc. IEEE*, vol. 99, no. 6, pp. 917–921, 2011.
13. S. Teufel and B. Teufel, "The Crowd Energy Concept," *J. Electron. Sci. Technol.*, 2014.
14. R. Ortega, O. Carranza, J. C. Sosa, V. García, and R. Hernández, "Operando En Modo Isla Dentro De Una Microrred," *RIAI - Rev. Iberoam. Autom. e Inform. Ind.*, vol. 13, pp. 115–126, 2016.
15. Z. Shuai et al., "Microgrid stability: Classification and a review," *Renew. Sustain. Energy Rev.*, vol. 58, pp. 167–179, 2016.
16. V. Erice Carbonero, J. López Taberna, and J. Marcos Álvarez, "Monitorización del consumo eléctrico de un hogar : Procesado de datos mediante Arduino," *Universidad Pública de Navarra*, 2015.
17. L. Ariel, C. Francisco, J. Jorge, and C. María, "Algoritmo de control para la administración de una micro red," in *Congreso de Investigación y Transferencia Tecnológica en Ingeniería Eléctrica CITTIE*, 2019.
18. "Compact Fieldpoint." [Online]. Available: <http://sine.ni.com/nips/cds/view/p/lang/es/nid/1199>.
19. R. Franco-Manrique, E. Gómez-Luna, and C. A. Ramos-Sánchez, "Smart grid analysis and management in colombia towards ETAP real time solution," *Ingeniare*, vol. 26, no. 4, pp. 599–611, Dec. 2018.
20. Etap, "Model-Driven Real-Time Solutions for Power Systems SCADA & Monitoring Power Management Generation Management Transmission Management Advanced Distribution Management Microgrid Master Controller Intelligent Load Shedding Substation Automation."
21. "SOLUCIONES TECNOLÓGICAS PARA MICRORREDES." [Online]. Available: <https://www.accion-energia.com/es/sostenibilidad/proyectos-innovacion/microrredes/>. [Accessed: 06-Jun-2020].
22. "Raspberry Pi." [Online]. Available: <https://www.raspberrypi.org/>. [Accessed: 13-Dec-2019].
23. E. Tridianto, P. D. Permatasari, and I. R. Ali, "Experimental study of mini SCADA renewable energy management system on microgrid using Raspberry Pi," *J. Phys. Conf. Ser.*, vol. 983, no. 1, 2018.
24. Nerea Goitia-Zabaleta (IKERLAN) et al., "Rennaisance - Desarrollo de las comunidades energéticas locales y blockchain," 2019.
25. "Home Assistant." [Online]. Available: <https://www.home-assistant.io/>. [Accessed: 18-Dec-2019].
26. "MySQL." [Online]. Available: <https://www.mysql.com/>. [Accessed: 23-Dec-2019].
27. I. N. Fovino, A. Carcano, M. Maserà, and A. T. Betta, "Chapter 6 Design And Implementation of Software," pp. 107–121, 2009.

A data acquisition pipeline for home energy management systems

Íngrid Munné-Collado¹, Adrià Bové-Salat¹, Daniel Montesinos-Miracle¹, and Roberto Villafáfila-Robles¹

Centre d'Innovació Tecnològica en Convertidors Estàtics i Accionaments (CITCEA-UPC), Universitat Politècnica de Catalunya ETS d'Enginyeria Industrial de Barcelona, C. Avinguda Diagonal, 647, Pl. 2, 08028 Barcelona, Spain, ingrid.munne@upc.edu

Abstract. This paper presents a modular data acquisition pipeline to integrate flexible assets and distributed and renewable energy sources in households. This modular and general system's main aim is to enhance the data acquisition, data cleaning, and data storage steps of the different assets included in a Home Energy Management System, for the later scheduling of these resources based on economic optimization. The services that Home Energy Management Systems and data acquisition systems can provide to tackle the current distribution network challenges are identified. The data acquisition pipeline design is presented, being able to stock and collect data from many different real assets, as well as cloud-based data providers such as the electricity market price or the weather forecast. The description of the system is complemented by a study case, to validate the pipeline design and the data acquisition process.

Keywords: home energy management system, electric vehicle, distributed generation, renewable-based power plants, electricity markets, data acquisition, demand-side management

1 Introduction

The electricity grid is experiencing a profound transformation towards smart grids by including distributed energy resources (DERs) and the Internet of Things (IoT), in an effort to tackle climate change [1]. Renewable energy sources (RESs) help the energy transition by increasing its share in the energy mix. Furthermore, end-users have become more aware of their role in the energy transition. DERs, which are mainly renewable, have also been placed along the distribution network to decentralize the electricity generation and increase the local and renewable generation share. However, the increasing number of DERs leads to the need for flexibility services for distribution system operators (DSO), due to their variability, uncertainty, and often a mismatch between the time of generation and time of consumption [2]. According to Euroelectric [3], flexibility

is meant to be as the modification of generation injection and consumption patterns both on an individual and aggregated level, to provide a service within the power system. These flexibility services could be provided by several resources, from different nature, being centralized or decentralized. That includes centralized energy storage (CES), distributed energy storage (DES), electric vehicles (EV), solar panels (PV), or flexible loads such as water boilers (EWB) or space heaters (SH) [4], located in the distribution network, and owned and managed by end-users or third-parties. Flexibility is currently deployed by integrating energy storage systems, the activation of demand response (DR) mechanisms, and the development of flexibility markets [5].

Demand-Side Management activities (DSM), being the name for end-users' flexibility, are known by their numerous advantages, and can be essential for energy strategy and policy development [6]. First of all, it enhances the generation and consumption of locally-produced electricity [7]. In terms of the DSO benefits, this source of distributed flexibility can help the DSO in the congestion management of the network [8]. From the end-user perspective, there are several advantages, such as lowering the carbon footprint or achieving a cheaper electricity bill [9].

Several works in the literature have investigated how home energy management systems (HEMS) can help in the integration of DERs at a household level, as well as enhancing the implementation of DSM activities, see [9–12].

Research has tended to focus on a reduction of the energy bill rather than lowering the carbon footprint of the electricity consumption at household level. In [12], a HEMS has been designed to re-schedule electricity consumption from expensive to cheaper time-periods, also known as price-based programs. Related to economic savings, [13] proposes an incentive-based program, where the end-user is economically remunerated when providing flexibility by increasing or decreasing his or her electricity consumption at that specific time period. More recent evidence [9] proposes a novel DR mechanism, instead of the commonly known price-based programs. In that article, an environmental-based DR service is developed, and results show that significant reduction in terms of CO₂ can be achieved, compared to traditional schemes.

One of the requisites of HEMS is to improve the energy consumption at household level. These systems should be capable of communicating with the different home appliances to be monitored and controlled. Furthermore, this system needs some external communication as well to receive data from other sources, as Application Program Interfaces from the electricity market or from the aggregator. On top of that, HEMS require of some intelligence to handle the acquired data, store it in a general and useful way, as well as calculating energy consumption forecasts before feeding these data into the main optimization algorithm of the home energy management system. In that sense, some open source and private initiatives have been developed to create HEMS according to the prior requirements, see [14, 15]. Some of the most known initiatives are Building Energy Management Open-Source Software (BEMOSS), Open Energy Monitor and PowerMatcher [15]. These initiatives tend to focus on three objectives: data

acquisition, data visualization and asset scheduling. However, the main shortcoming of these systems is the lack of adaptability to assets coming from different manufacturers. Furthermore, none of them include the possibility to check the electricity market price, essential for scheduling the household assets based on the electricity tariff or the possibility to calculate asset forecasts, required for the HEMs optimization algorithm.

Implementing a HEMS can lead to some challenges and derived issues that the end-user should face. Some of them are the possible loss of comfort due to allowing third-parties to control and schedule his/hers resources [16, 17]; the lack of standardization, that adds more difficulties on the integration of the flexible assets under the same HEMS [18]; or the low value of savings that the end-users can achieve by participating in DSM programs [19].

HEMS require to have a stocked database with relevant data regarding electricity prices, weather forecast parameters, actual weather values, electricity consumption from smart meters and sub-meters, flexible assets parameters and real-time status, electricity grid parameters, and site self-generation and consumption values, as well as forecast algorithms for the load curve prediction of some of the flexible assets. In this study, a modular data acquisition pipeline is proposed, which consists of five different modules, covering from data extraction and storage to optimization and data visualization. This system's objective is to enhance the integration of different flexible assets, with different natures, data structure, and user-interface under the already existing and same HEMs, minimizing the difficulties in terms of integration and manually data integration processes. The developed data pipeline is flexible and versatile to store generated data in an automated way, coming from different sources, but also robust to ensure reliable data storage and pre-processing. The data-acquisition pipeline proposed in this paper comes along with the research developed in the INVADE H2020 Project (Grant agreement No 731148), as well as the FLEXRED Project (RTI2018-099540). Hence, the data acquisition pipeline is defined in such a way to allow the integration with the flexible devices installed under these projects, and for a later integration with the private HEMs designed under the development of these projects. However, and since the authors seek for the development of open-source initiatives, the data structure of this data acquisition system is ready to be integrated as well with the Open Energy Monitor initiatives for data visualization purposes, since the model developed in this paper is responsible for the data collection, cleaning, storing and asset forecasting.

The paper is structured as follows: Section 1 provided a literature review of all the services that HEMS can provide to distribution networks employing DSM programs. A case study in a residential household in Barcelona is explained in Section 2. Then, Section 3 defines the data acquisition system structure to integrate the already existing optimization module, as well as each flux in the data pipeline to achieve the previously mentioned objectives. Section 4 implements the previously defined data pipeline to the case study defined. Finally, conclusions are drawn in Section 5.

4 Munné-Collado et al.

2 Case Study: Household implementation

Section 1 has presented the challenges and benefits of HEMS for the development of DSM activities for flexibility provision. This section presents a real case study to test and validate the data acquisition pipeline. The case study is based on a residential household located in the province of Barcelona. It is based on one residence with flexible assets as an EV, EV charger, and PV panels. Furthermore, the household is equipped with a smart meter from which the main consumption of the household is recorded. Table 1 details the assets located in the house, as well as the electricity tariff of the end-user. The first step prior to implementing a HEMS in a specific household should be the calculation of the potential saving by activating DSM programs, to ensure that the activation of DSM activities results in some benefits for the end-user.

Table 1: Household assets overview

Asset type	Model	Specifications
EV	Nissan Leaf 2018	350 V, 62 kWh, 3.7 kW AC charging
PV panels	LONGi LR4-60HPH-360M	360 W Power Output at STC
PV Inverter	Fronius primo 4.0-1	4000 W Nominal Power Output 180-270 V Output voltage range
Electricity tariff	Endesa	PVPC 2.0 DHA 4.5 kW

To understand the optimization model for calculating the potential savings by implementing DSM activities, one should know the different available electricity tariffs in Spain, as shown in Figure 1. There are three possible tariffs for that chosen retailer contracted by the household: 2.0, 2.0 DHA, and 2.0 DHS. Also, in this figure, the actual scheduling and the optimal scheduling of the EV are shown. As can be observed, under the optimal scheduling, the EV charges its battery only when the lowest prices appear.

Hence, a batch of scenarios is defined, covering the worst scheduling, the current one, as well as the optimized one. From there, the possible savings and costs can be obtained, as shown in Figure 2. This figure shows all the possibilities between the scheduling strategy versus the contracted tariff. Summarizing the results from the table, the potential savings can be up to 400 € per year under the DHS tariff and the optimal scheduling. With the essential benefits of DSM in terms of decarbonization of the power system, together with the additional possibility of reducing costs, HEMS' implementation would be a feasible option for several households.

A data acquisition pipeline for home energy management systems 5

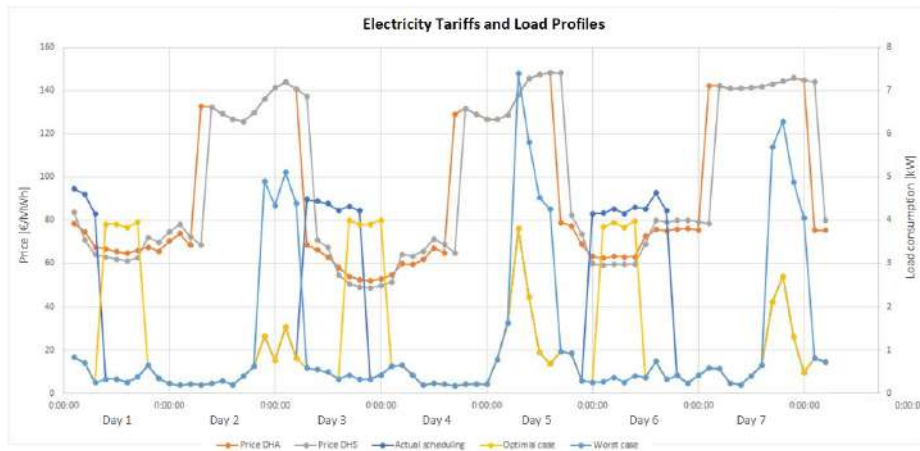


Figure 1: Spanish electricity market PVPC price structure

	Costs	1,005,42 €	692,71 €	713,92 €	1,041,67 €	1,064,39 €	1,064,37 €	988,92 €	675,71 €	665,59 €
Costs	Options	Actual with 2.0A	Actual with 2.0DHA	Actual with 2.0DHS	Worst case with 2.0A	Worst case with 2.0DHA	Worst case with 2.0DHS	Optimal case 2.0A	Optimal case 2.0DHA	Optimal case 2.0DHS
1,005,42 €	Actual with 2.0A		312,71 €	291,50 €	-36,26 €	-58,97 €	-58,95 €	16,50 €	329,71 €	339,83 €
692,71 €	Actual with 2.0 DHA	-312,71 €		-21,21 €	-348,96 €	-371,68 €	-371,66 €	-296,21 €	17,00 €	27,13 €
713,92 €	Actual with 2.0DHS	-291,50 €	21,21 €		-327,75 €	-350,47 €	-350,45 €	-275,00 €	38,21 €	48,34 €
1,041,67 €	Worst case with 2.0A	36,26 €	348,96 €	327,75 €		-22,72 €	-22,69 €	52,76 €	365,96 €	376,09 €
1,064,39 €	Worst case with 2.0DHA	58,97 €	371,68 €	350,47 €	22,72 €		0,02 €	75,47 €	388,68 €	398,81 €
1,064,37 €	Worst case with 2.0DHS	58,95 €	371,66 €	350,45 €	22,69 €	-0,02 €		75,45 €	388,66 €	398,78 €
988,92 €	Optimal case 2.0A	-16,50 €	296,21 €	275,00 €	-52,76 €	-75,47 €	-75,45 €		313,21 €	323,33 €
675,71 €	Optimal case 2.0DHA	-329,71 €	-17,00 €	-38,21 €	-365,96 €	-388,68 €	-388,66 €	-313,21 €		10,13 €
665,59 €	Optimal case 2.0DHS	-339,83 €	-27,13 €	-48,34 €	-376,09 €	-398,81 €	-398,78 €	-323,33 €	-10,13 €	

Figure 2: Potential savings and total costs

In this case study, as seen in Table 1, the integration of PV and EV is considered, as well with the household consumption and electricity tariff. It is important to know, apart of knowing the several benefits of the implementation of DSM activities, what the current consumption and generation profiles are. This can be seen in Figures 3, 4, 5, and 6, showing the consumption profiles for

6 Munné-Collado et al.

both a week day and a day in the weekend (Figures 3 and 4); as well as the combination of consumption and PV production (Figures 5, and 6). It can be noticed how the consumption patterns differ from weekdays to weekends, as well as how variable and uncertain the solar power output is based on the weather conditions. As can be noticed from the prior economic analysis and the data visualization plots of the current consumption and generation patterns, a HEMS is feasible and economic savings can be achieved. Hence, the development of a data acquisition pipeline is also feasible and necessary for achieving the HEMS implementation in a real case study.



Figure 3: Household consumption on a weekday

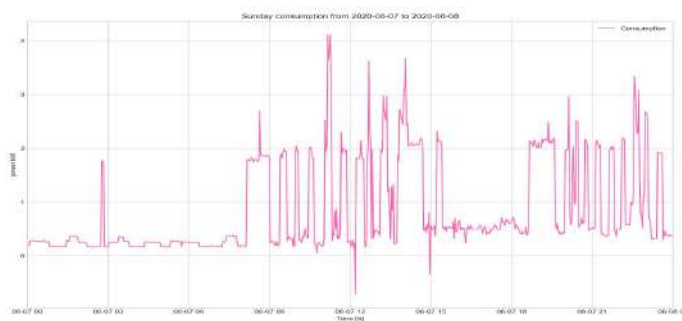


Figure 4: Household consumption on a weekend day

A data acquisition pipeline for home energy management systems

7

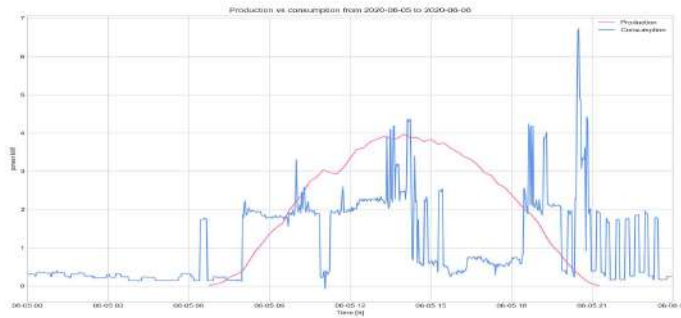


Figure 5: Household consumption and PV production on a sunny day

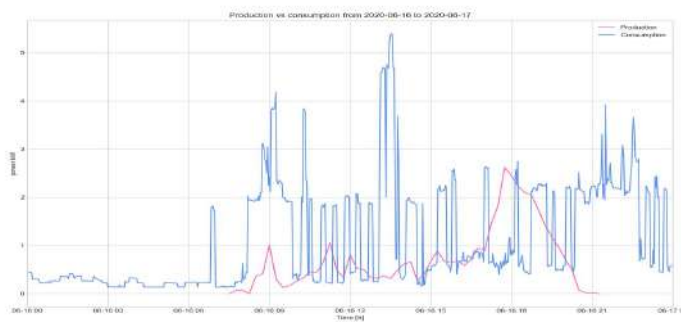


Figure 6: Household consumption and PV production on a cloudy day

3 Data acquisition pipeline design

According to [20], a Home Energy Management System (HEMS) is an interface of demand-side management programs used by the end-users. It assists the end-user and schedules the resources available in the household by solving an optimization problem, taking into consideration the available generation from the distributed and renewable energy sources in that household, other flexible assets such as water boilers or electric vehicles (EV), and market prices or even weather forecast. Figure 7 shows the current structure of the HEMS used for the current project and case study. There are five blocks, covering the following steps: Data extractors and treatment, asset modeling, optimization, actuators and controllers, and data analytics. This study addresses four out of five blocks, being the optimization block out of the scope of this paper. The aim of the presented data acquisition pipeline is to perform all the data pre-processing and data wrangling in a way that can easily be integrated with the already existing optimization modules in HEMS. An upstream layer collects useful data and results from each specific block, known as data storage. This module can include data required by one or many of the downstream blocks and data visualization figures for later analysis of the HEMs performance.

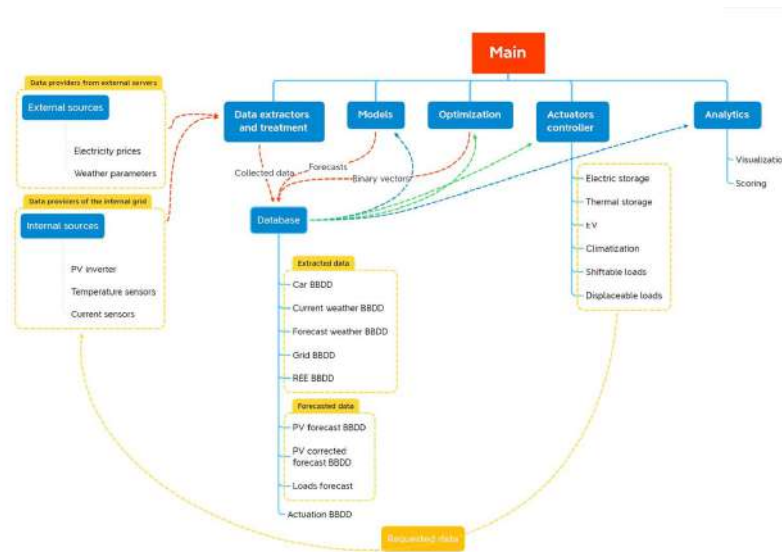


Figure 7: HEMS Structure

The data pipeline design is the main element for integrating different assets and data sources under the same data stream. According to [21], a data pipeline can be defined as a software that removes many manual steps from the process

A data acquisition pipeline for home energy management systems 9

and enables a smooth and automated flow of data. In a nutshell, it automates the processes involved in extracting, transforming, combining, validating, and loading data for further analysis and visualization. Figure 8 shows the data pipeline structure defined in this project.

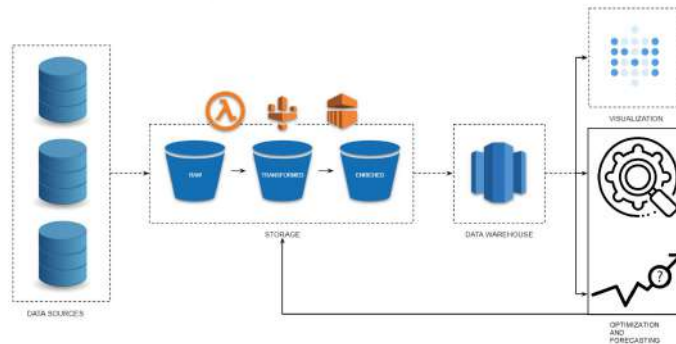


Figure 8: Data pipeline structure and flow

4 Data pipeline implementation

4.1 Data extractors and pre-processing

The first module that acts in this system is the data extractor and data pre-processing module. This module is responsible for requesting data from numerous Application Programming Interfaces (API), analyzing the data structure, dealing with missing values and errors in the data, and storing them using a standard format for each data source. Figure 9 shows in a more specific and detailed way how the data pipeline is applied for each data source and how the chosen protocol is used. Four data sources are covered: weather data, EV data, PV production, and electricity market prices. Table 2 shows each data source included in this model, the features obtained for each type of module, as well as the granularity of the data requests. As can be seen on the table, the request is made on a different time scale for each data source, depending on the source's nature and the frequency of new data generation. For example, the Spanish electricity market updates its PVPC prices once per day in the evening. Hence, the module called *PVPC_prices.py* will request new data for the data storage only once a day after the market-clearing time period is over (i.e., 20:00 CEST).

4.2 Assets and forecasting models

To provide the required information to the HEMS for the calculation of the optimal scheduling of the resources, two different time horizons have to be con-

10 Munné-Collado et al.

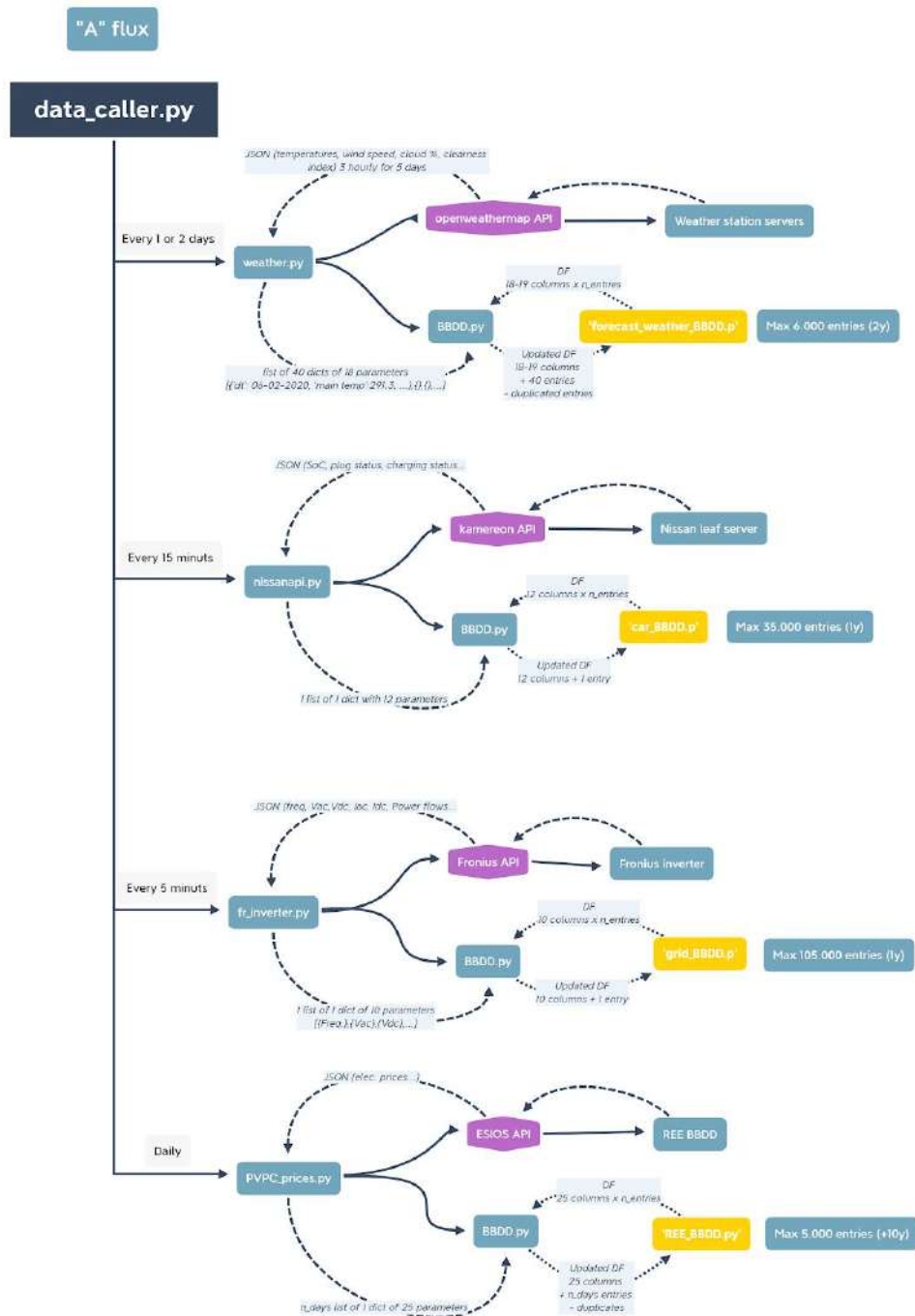


Figure 9: Data flow

A data acquisition pipeline for home energy management systems 11

Table 2: Data collection

Name	Data request granularity	Parameters
Weather data (weather.py)	every 1-2 days	Weather forecast and actual weather values Temperature: value, feels like, minimum, maximum Pressure Humidity Visibility index Wind: speed, direction Cloudiness index Rain index
EV Data (NissanAPI.py)	every 15 minutes	EV location Battery: SOC, temperature, capacity Plug: Status, charging speed, instant power EV: indoor temperature
PV production (fr_inverter.py)	every 5 minutes	Frequency AC Voltage / Current DC Voltage / Current Power Flows
Electricity market prices (PVPC_prices.py)	once a day	PVPC 2A hourly market price PVPC 2DHA hourly market price PVPC 2DHS hourly market price

sidered. Hence, different data sources will be required for each of them. As can be seen in Figure 10.

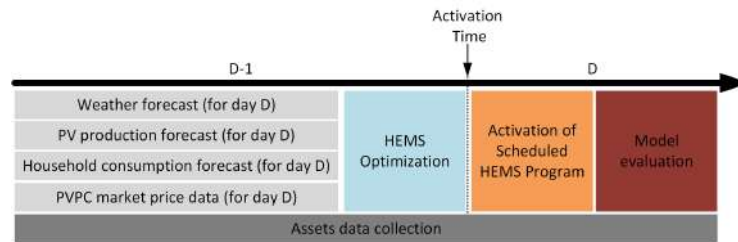


Figure 10: Modules Timeline

In this system, there are three forecasting models required:

- Weather forecast: provided by an API.
- PV production: calculated on a day-ahead basis.
- Household consumption: calculated on a day-ahead basis.

For the sake of clarification, the EV charging process is not forecast because it is considered as a fully controllable and shiftable load. Hence, its parameters are known, and the charging process’s scheduling will be regarded as an output of the optimization module. On the other hand, the PV panels installed in the household of study are considered as curtailable, meaning that their generation can be reduced if it is required. Since the curtailed power will output the optimization module, a prior forecast is necessary to feed the optimization module.

12 Munné-Collado et al.

In the case of the household total load consumption, no curtailable loads are considered. However, to evaluate the total load consumption and the total price of this electricity consumption, a forecast must initialize the optimization module for scheduling the resources.

4.2.1 PV production forecast

For the PV generation forecast, different PV system elements have to be forecast or modeled, being those as follows:

- Irradiance: obtained from the geographical location and weather conditions, employing an external API and the python library *pvlb*.
- PV panel model: Single diode model for each cell, based on [22] and the python library *pvlb*.

Figure 11 shows the PV production forecast from the developed model, compared to the actual value of the PV production for a time horizon of 16 days. In Figure 12 the PV array DC voltage forecast versus actual values is shown.

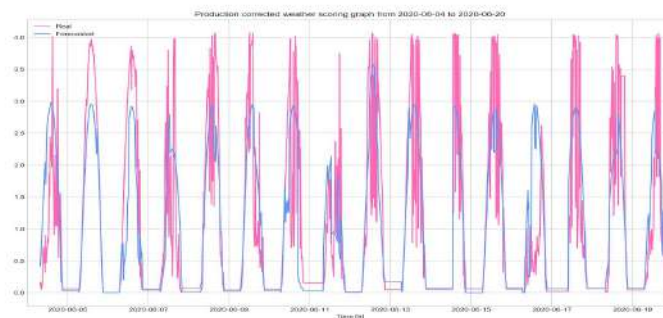


Figure 11: PV production for 16 days. Forecast and real value

4.2.2 Household consumption forecast

In the case of household consumption, the only available data is the historical household consumption of 1 year, with a time granularity of 1 hour, from the main smart meter. For the sake of simplicity, and to have a fast and straightforward forecasting tool for the household consumption curve, the climatology approach has been chosen. This approach is based on meteorologic forecasting tools and can be applied to many different techniques, as in [23]. The main objective of performing a climatology model is to define a benchmark of the

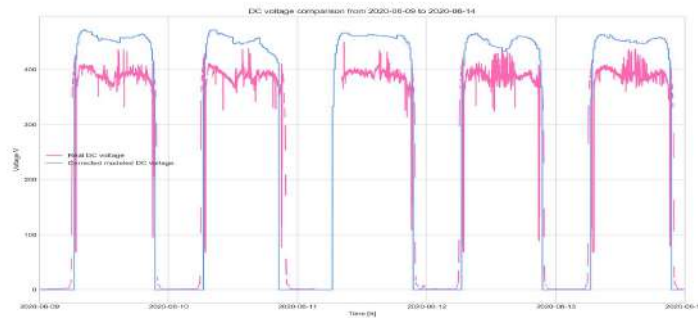


Figure 12: PV array DC Voltage. Forecast and real value

model, to compare advanced models against it in a later stage. In this project, the model is developed by calculating an average consumption model for each day of the week based on the historical data. Figure 13 shows the climatology model for a typical Monday of study, compared to the real consumption values. In this model, the RMSE score was 0.748 kW. Since this model is considered a benchmark, it cannot be compared to any previously existing model.

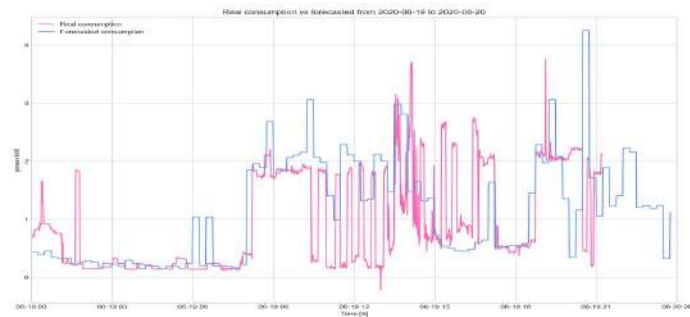


Figure 13: Household load consumption on Monday. Real value vs forecast.

5 Conclusions

This paper presented a modular data acquisition pipeline for the integration of different-nature assets into an existing HEMS. This system is robust and flexible since it can store data from different sources and different data structures in an

14 Munné-Collado et al.

automated way. Simultaneously, the proposed approach is robust and scalable, allowing integrating this system to already existing HEMS. To complement the data pipeline's technical definition and design, a case study has been developed to test and validate the system in a real scenario. Results derive that the model can integrate real flexible and controllable assets such as EV and PV panels, accurate metering data from the main smart meter, and data can be requested and extracted from cloud-sources, as it is the case for weather data and electricity market data. This performance validates the solution and its readiness for further integration with a HEMS.

6 Acknowledgments

This work was supported in part by the Ministerio de Economía, Industria y Competitividad (Spanish government), under the grant agreement number ENE2017-86493-R, and in part by Ministerio de Ciencia, Innovación y Universidades under the project RTI2018-099540.

References

1. European Commission, "Energy Roadmap 2050," *Publications Office of the European Union*, no. April, p. 5, 2012. [Online]. Available: <http://www.roadmap2050.eu/>
2. E. Netz, G. Germany, M. Schmidt, R. Knoll, E. Netz, G. Germany, P. Schegner, T. Darda, and E. A. G. Germany, "Providing Flexibility in the Distribution Network – Challenges and Solutions," *25 th International Conference on Electricity Distribution*, no. June, pp. 3–6, 2019.
3. CEDEC, EDSO, Eurelectric, and GEODE, "Flexibility in the Energy Transition: A Toolbox for Electricity DSOs." Tech. Rep., 2018. [Online]. Available: https://cdn.eurelectric.org/media/2395/flexibility_in_the_energy_transition_-_a_tool_for_electricity_dsos-2018-2018-oth-0002-01-e-h-503532B2.pdf
4. IRENA, *Power system flexibility for the energy transition. Part II: IRENA Flextool methodology*, 2018, no. December. [Online]. Available: <https://www.irena.org/publications/2018/Nov/Power-system-flexibility-for-the-energy-transition>
5. X. Jin, Q. Wu, and H. Jia, "Local flexibility markets: Literature review on concepts, models and clearing methods," *Applied Energy*, vol. 261, no. August 2019, p. 114387, 2020. [Online]. Available: <https://doi.org/10.1016/j.apenergy.2019.114387>
6. S. E. Reviews and P. S. Universit, "Demand response and smart grids - A survey," vol. 30, no. February 2014, pp. 461–478, 2016.
7. P. Olivella-Rosell, P. Lloret-Gallego, Í. Munné-Collado, R. Villafafila-Robles, A. Sumper, S. Ottessen, J. Rajasekharan, and B. Bremdal, "Local flexibility market design for aggregators providing multiple flexibility services at distribution network level," *Energies*, vol. 11, no. 4, 2018.
8. I. Munné-Collado, P. Lloret-Gallego, P. Olivella-Rosell, R. Villafafila-robles, V. Palma-costa, A. Sumper, and R. Gallart, "System Architecture for Managing Congestions in Distribution Grids Using Flexibility," *25 th International Conference on Electricity Distribution*, no. June, pp. 3–6, 2019.

9. S. Barja-Martinez, I. Munne-Collado, P. Lloret-Gallego, M. Aragiés-Peñalba, and R. Villafafila-Robles, "A Novel Home Energy Management System Environmental-based with LCA Minimization," in *20th International Conference on Environment and Electrical Engineering*, Madrid, Spain, 2020, p. 5.
10. M. Daneshvar, M. Pesaran, and B. Mohammadi-Ivatloo, "Transactive energy in future smart homes," pp. 153–179, jan 2018.
11. M. Ganji and M. Shahidepour, "Development of a residential microgrid using home energy management systems," pp. 173–192, jan 2018.
12. M. A. Fotouhi Ghazvini, J. Soares, O. Abrishambaf, R. Castro, and Z. Vale, "Demand response implementation in smart households," *Energy and Buildings*, vol. 143, pp. 129–148, may 2017.
13. Office of Gas and Electricity Markets (Ofgem), "Electricity system flexibility," 2019. [Online]. Available: <https://www.ofgem.gov.uk/electricity/retail-market/market-review-and-reform/electricity-system-flexibility>
14. M. Isshiki, M. Umejima, M. Hirahara, T. Minemura, T. Murakami, and S. Owada, "Case study of an ecological, smart home network: iZEUS-intelligent Zero Emission Urban System," pp. 91–111, apr 2015.
15. H. Zandi, M. Starke, and T. Kuruganti, *An Implementation for Transforming a Home Energy Management System to a Multi-agent System*. Syracuse University Libraries, 2018.
16. W. Zhang and Y. Xu, "Optimal energy management based on users' comfort degree in a microgrid," in *2017 IEEE International Conference on Energy Internet (ICEI)*, 2017, pp. 232–237.
17. H. Park, "Human comfort-based-home energy management for demand response participation," *Energies*, vol. 13, no. 10, 2020.
18. D. Egarter, A. Monacchi, T. Khatib, and W. Elmenreich, "Integration of legacy appliances into home energy management systems," *Journal of Ambient Intelligence and Humanized Computing*, vol. 7, no. 2, pp. 171–185, 2016.
19. S. van Dam, C. Bakker, and J. Buitter, "Do home energy management systems make sense? assessing their overall lifecycle impact," *Energy Policy*, vol. 63, pp. 398 – 407, 2013. [Online]. Available: <http://www.sciencedirect.com/science/article/pii/S0301421513009658>
20. H. Merdanoglu, E. Yakici, O. T. Dogan, S. Duran, and M. Karatas, "Finding optimal schedules in a home energy management system," *Electric Power Systems Research*, vol. 182, no. January, p. 106229, 2020. [Online]. Available: <https://doi.org/10.1016/j.epsr.2020.106229>
21. G. Alley, "What is a Data Pipeline," 2018. [Online]. Available: <https://www.alooma.com/blog/what-is-a-data-pipeline>
22. V. Tamrakar, S. Gupta, and Y. Sawle, "Single-diode pv cell modeling and study of characteristics of single and two-diode equivalent circuit," *Electrical and Electronics Engineering: An International Journal*, vol. 4, pp. 13–24, 08 2015.
23. P. Pinson and R. Hagedorn, "Verification of the ECMWF ensemble forecasts of wind speed against analyses and observations," *Meteorological Applications*, vol. 19, no. 4, pp. 484–500, 2012.

Demand response control in electric water heaters: evaluation of impact on thermal comfort

Rodrigo Porteiro¹[0000-0001-7793-1645], Juan Chavat²[0000-0001-9925-2651],
Sergio Nesmachnow²[0000-0002-8146-4012], and
Luis Hernández-Callejo³[0000-0002-8822-2948]

¹ Administración Nacional de Usinas y Transmisiones Eléctricas, Uruguay
rporteiro@ute.com.uy

² Universidad de la República, Uruguay
juan.pablo.chavat@fing.edu.uy, sergion@fing.edu.uy

³ Universidad de Valladolid, Spain
luis.hernandez.callejo@uva.es

Abstract. Energy demand management is an important technique for smart grids, under the paradigm of smart cities. Direct control of devices is useful for demand management, but it has the disadvantage of affecting user comfort. This article presents an approach for defining an index to estimate the discomfort associated with an active demand management consisting of the interruption of domestic electric water heaters to perform a load shifting. The index is defined based on estimations of water utilization and water temperature using continuous power consumption measurements of water heaters. A stochastic forecasting model is applied, including an Extra Trees Regressor and a linear model for water temperature. Monte Carlo simulations are performed to calculate the defined index. The evaluation of the proposed approach is performed using real data for both the forecasting model and the temperature model. The real effect of interruptions on the water temperature of two water heaters is compared to validate that the thermal discomfort index correctly models the impact on temperature. This result allows ordering devices by their thermal discomfort index and having a fair criterion to decide which ones should be interrupted.

1 Introduction

The concept of energy demand management is very relevant in nowadays smart cities, especially considering the smart grid paradigm [12]. Energy demand management refers to administering the energy consumption of end consumers of an electric grid, in order to promote better energy utilization. The most widely applied actions for demand management are load management (aimed at modifying/reducing/shifting the demand) and energy conservation (aimed at reducing the demand via technological improvements). Other actions applied for demand management include fuel substitution and load building [2]. Among load management techniques, the most used are peak reduction (reducing consumption

2 R. Porteiro, J. Chavat, S. Nesmachnow, L. Hernández-Callejo

in periods of maximum demand), valley filling (promoting energy utilization in off-peak periods), and load shifting (from peak to off-peak periods).

In daily operation, electricity generation and transmission systems may not always meet peak demand requirements. In these situations, various demand response and demand management tools can be used in order to mitigate overloads in the electrical system. One of the simplest methods for direct load control is allowing the electrical company to remotely control those devices with thermostat, especially those that have important thermal inertia. Remote control is a very effective technique to achieve peak reduction and load shifting at critical moments. However, the benefits of the reduction in the operating cost of the electrical system must be weighted against the loss of comfort that the users of the controlled devices may have. Assigning an economic value to the loss of comfort associated with an intervention requires quantifying such comfort in advance.

In the main Uruguayan cities, more than 90% of households have a thermostat-controlled electric water heater (according to the 2019 continuous household survey by National Statistics Institute, Uruguay [6]) Furthermore, electric water heater is one of the most energy-intensive household appliances (it represents 34% of residential energy consumption, in average). Thus, it is an ideal candidate to be considered for remote load control as demand management technique.

In this line of work, this article proposes a methodology to calculate a Thermal Discomfort Index (*TDI*), associated with a remote intervention for load management. The computed index evaluates the discomfort for users generated by the intervention of an electric water heater. *TDI* is computed from real data, a linear temperature model, and a forecasting model for water utilization applying artificial neural networks (ANN). The obtained *TDI* makes it possible to decide in which order the electric water heaters should be interrupted to minimize total discomfort. The key aspect of the proposed methodology is to know in advance the value of the *TDI*, in order to decide if it is economically profitable to carry out an intervention.

The experimental analysis is performed using data from real electric water heaters in Uruguay, gathered in the ECD-UY dataset [3]. ECD-UY includes power consumption utilization of water heaters installed with remote control and power measurement device in representative households in the main Uruguayan cities. Results reported for the considered case study demonstrate that the proposed index managed to capture the impact of thermal discomfort, fulfilling the objective of sorting electric water heaters to be properly managed by applying a direct control strategy.

The article is organized as follows. Section 2 presents the formulation of the demand management problem through direct control of devices and reviews related works. Section 3 describes the proposed approach to define a *TDI*. Details of the developed implementation are provided in Section 4. Section 5 reports the experimental validation of the water utilization forecasting, the temperature model, and the proposed index for a case study. Finally, section 6 formulates the main conclusions and lines for future work.

2 Demand management and direct control of electric water heaters

This section describes demand management strategies, direct load control applied to load shifting, and the problem of affecting comfort of the end user.

2.1 Demand management

The traditional model of an electric system feeds electricity to the end consumers through a unidirectional power flow. This flow is supplied by centrally controlled generators. With the development of energy markets and distributed energy resources, the concept of energy demand management has emerged. This concept includes a set of techniques oriented to modify the energy demand of consumers of an electric grid to fulfill specific goals [4]. The subset of these techniques that try to reduce the energy demand of consumers in the short term is known as demand response.

This article focuses on direct load control, a technique that is considered as an effective way to achieve immediate power reduction in a very short time. To handle this technique, the electricity utility must have permission to switch off the devices of end-users, which is usually obtained via specific agreements that grant users a monetary incentive. Among the main reasons for power reduction are implementing peak reduction [5], which allows obtaining a more stable grid, and providing frequency regulation services [22], which allows maintaining the system frequency very close to 60 Hz, preventing deviations that affect generators and also make the grid unstable. This article addresses some aspects related to the direct load control of electric water heaters, mainly focusing on the impact of using this tool in the thermal comfort of end-users.

2.2 Load shifting with direct control of electric water heaters

In most countries of the world, the profile of total electricity demand consumption shows a pronounced peak two hours after the return of workers to their homes. Usually, the power consumption of electric water heaters also presents a peak that coincides with the total consumption peak as shown in Fig. 1, which is explained by the showers that people take when they return from work. In addition, electric water heaters have the ability to accumulate energy in the form of heat inside the water tank. Thus, it is possible to switch off the device in a smart way, so that users thermal comfort is not affected.

According to the aforementioned correlation, in the presence of a demand peak, there is an amount of energy associated with the electric water heaters that can be deferred by turning off the devices in a moment, and turning them on in the future. Using this strategy, a load shifting on the demand curve is implemented, because the total amount of energy remains equal but the load profile is modified. Several studies have addressed the load shifting problem using direct control of devices, but few of them have focused on quantifying the thermal discomfort generated by the application of this technique.

4 R. Porteiro, J. Chavat, S. Nesmachnow, L. Hernández-Callejo

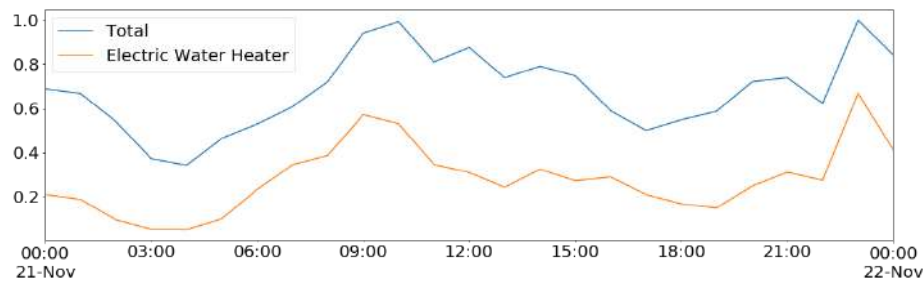


Fig. 1: (Normalized) total power and electric water heater demand in a weekday

2.3 Problem formulation and related works

Problem formulation. The problem proposes determining a *TDI* to evaluate quantitatively, the discomfort generated by the application of load shifting using a direct control of electric water heaters.

To address the problem, the first step consists in analyzing which variables are involved. In the case of electric water heaters, the variable that affects comfort is the temperature of the water in the tank. Installing a remote device to the water heater that allows measuring its power and switching it on/off is reasonable since it can be achieved without modifying its structure [15,16]. However, installing a remote thermometer to measure the temperature of the tank requires modifying structure of the water heater, which implies a large monetary investment.

The most important issue when analyzing comfort is comparing the same controlling action between several electric water heaters, in order to decide which of them can be affected while minimizing the probability of generating discomfort. Therefore, it is not crucial to determine the temperature exactly; computing a good approximation is enough to analyzing differences. Another aspect that seems trivial but worth to consider is that users perceives thermal discomfort only when they use water and its temperature is below a threshold. At any other time, users does not give relevance to the water temperature.

According to the considered aspects, to define an index of discomfort in the event of an intervention, the water utilization and the temperature of the water in the tank must be estimated. The proposed approach addresses these two lines of work and defines a discomfort index based on the corresponding findings.

Related works. Several works in the literature refer to peak load reduction strategies implemented in smart grids [5,25]. A special type of devices to perform load shifting are thermostatically-controlled appliances (TCA), due to the flexibility to select the thermostat set point [8,18]. Some TCA can store energy, providing a great advantage when performing load shifting strategies. This is the case of domestic electric water heaters, which are the focus of this article. Nehrir [13] analyzed an interactive demand side management strategy for electric water heaters, but without elaborating on specific aspects of thermal discomfort. Xi-ang [23] studied a complex strategy to minimize thermal discomfort related with electric water heater control. The proposed strategy required a large amount of information. Thus, the approach is difficult to apply in practice.

TCA demand response control strategies can be effectively implemented provided that thermal comfort is not compromised. This crucial issue has been the focus of several works. Kampelis [7] evaluated thermal discomfort in demand response control of heating, ventilation, and air conditioning, but the strategy used requires knowing the real temperature. Regarding electric water heaters, the study of the user hot water utilization profile is a key aspect for estimating discomfort. Seyed [21] studied whether a smart heating system can benefit from good predictions of the user behaviour. In turn, Pirow [19] proposed an algorithm for the estimation of domestic hot water utilization, but the technique requires the installation of temperature and vibration sensors.

The main factor that defines comfort is the water temperature. Thus, a model to estimate water temperature is crucial for the effectiveness of the comfort evaluation. Paull [17] proposed a water heater model to estimate the temperature of the water in the tank as a function of time and the related variables. The study by Lutz [10] provided a comprehensive empirical analysis of a simplified energy consumption model for water heaters considering the variation of the temperature of the water in the tank. Finally, comfort evaluation must be considered in the problem of controlling a subset of electric water heaters using a ranking that sorts the devices according to an appropriate criteria. Yin [24] proposed a scheduling strategy based on a temperature state priority list. In turn, Al-Jabery [1] analyzed a scheduling strategy for electric water heaters based on approximate dynamic programming techniques and q-learning.

The analysis of related works indicates that few articles have studied the thermal comfort effect when applying direct load control of electric water heaters. This article contributes in this line of work, by proposing an approach to evaluate the thermal discomfort of an intervention on electric water heaters, without requiring installing a thermometer to measure the water temperature.

3 The proposed approach for defining a discomfort index

This section describes the proposed approach for defining a discomfort index applying ideas described in the previous section and following a data analysis approach [9, 11] over a group of 140 remotely controlled electric water heaters located in Uruguay.

3.1 Data preparation

The data used in this article was provided by the Uruguayan National Electricity Company (UTE). It corresponds to “Electric water heater consumption”, one of the three subsets included in the EDC-UY dataset [3], which gathers data from 521 households located in the main Uruguayan cities.

Electric water heater consumption records has a sample period of one minute and cover a date range from 12th July 2017 to 26th June 2019. Customer records were filtered by the recording length, keeping only those that have more than 5 months of recording (i.e., at least 216.000 records).

6 R. Porteiro, J. Chavat, S. Neschachnow, L. Hernández-Callejo

The disaggregated electric water heater data have several gaps caused by different problems during the data collection process (e.g., misworking of the data transmission network, power failures, etc). The gaps were fixed using two techniques: resampling and refilling.

The resampling technique normalizes the sample period to an exact minute. First, the records are grouped by customers to build one-minute record containers. Then, records whose datetime match with the date range of the container, are assigned to it. In case one or more records match the same container, the minimum consumption value is set, otherwise, a null value is set. The resulting data is taken as the input of the refilling technique. First, data gaps (i.e., consecutive missed records) are detected and refilled according to the following criteria. Starting from both extremes of the gap up to seven minutes forward/backwards, the missing data is recreated by a linear interpolation method. Finally, if missing values are still present at the gap (i.e., gaps is larger than 14 minutes), zero values are assigned. The described process results in normalized time series of consumption values without gaps.

A Jupyter notebook was implemented for data preparation, based on scripts provided by ECD-UY, using Python (version 3) programming language, and libraries Pandas and Numpy. The resulting notebook is available to download from <https://bit.ly/2RN08SW>. The effects of refilling on electric water heater activation is observed in Fig. 2 (missing records) and Fig. 3 (after processing).

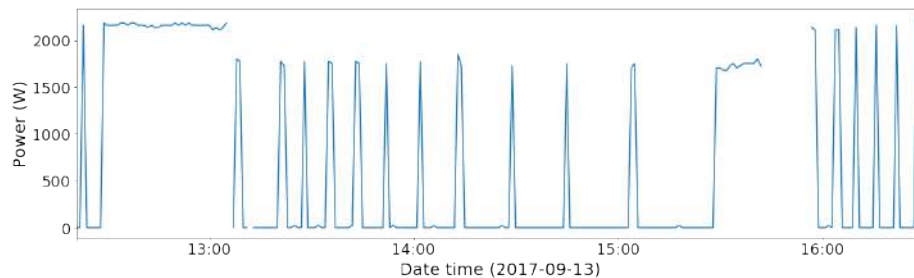


Fig. 2: A fragment of the electricity consumption of an electric water heater (meter id. 466147) before refilling the data gaps.

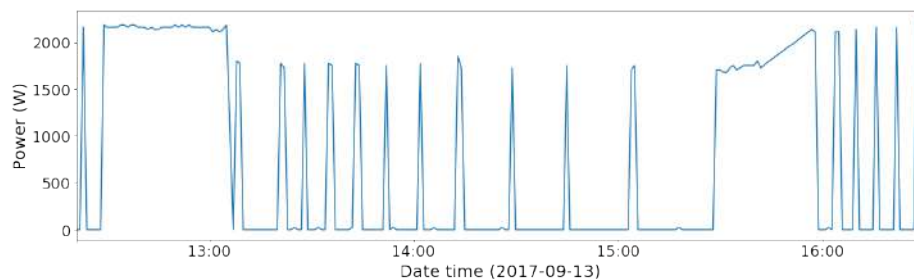


Fig. 3: A fragment of the electricity consumption of an electric water heater (meter id. 466147) after refilling the data gaps.

3.2 Water utilization forecasting model

Description. A particularity of electric water heaters is that when they are on, their power consumption has just slight variations, and it can be considered as constant. Therefore, the load curve can be represented in a binary format (0 when off and C when on). Lets consider a time interval in which the electric water heater is switched on continuously (defined as an *on block*). From the analysis of the power consumption time series, some of these blocks are associated with water utilization and other blocks correspond to thermal recoveries to maintain the target temperature of the water.

The proposed forecasting model is based on identifying the *on blocks* associated with water utilization and discarding those corresponding to thermal recoveries. In this regard, a threshold duration is defined, and any *on block* shorter than the threshold duration is considered to be a thermal recovery block and discarded. This is a robust approach, since discarding short blocks is not relevant for the main goal of identifying long-term utilization blocks, which are generally associated with showers. The analysis considers as a baseline an electric water heater with a capacity of 60l and an average water outlet flow rate, for which the duration of the *on block* is approximately eight times the duration of the utilization period. Applying this approximation, the information about *on blocks* can be converted into water utilization. Fig. 4 presents an example of *on blocks* and water utilization obtained with the aforementioned procedure.

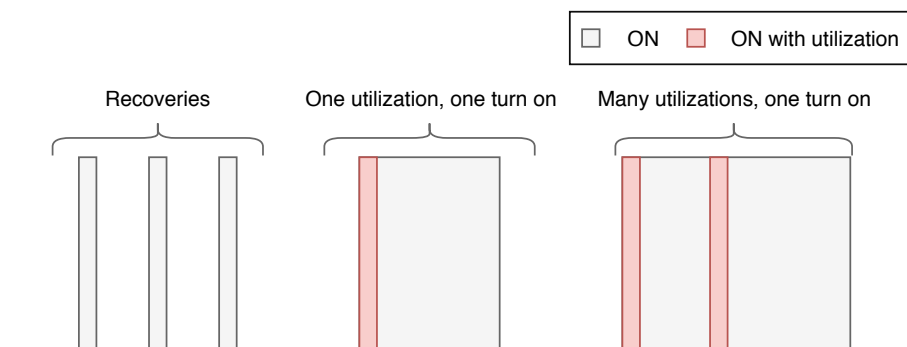


Fig. 4: Example of *on blocks* and water utilization patterns observed in the electric water heater consumption.

Features considered for training. An ExtraTrees Regressor model [20] was applied to train the forecasting model, considering the following input features:

- *Use* (120 Boolean values), indicating whether a water utilization occurs in the past 120 minutes.
- *Month* (integer), indicating the month of the horizon to forecast.
- *Day* (integer), indicating the day of the horizon to forecast.
- *Hour* (integer), indicating the hour of the horizon to forecast.
- *Dayofweek* (integer), indicating the day of the horizon to forecast.

8 R. Porteiro, J. Chavat, S. Nesmachnow, L. Hernández-Callejo

- *Workingday* (boolean), indicating whether the horizon to forecast is a working day or not.

The output of the model is a vector of 120 Boolean values, indicating the forecast of water utilization for the next two hours.

Evaluation. The standard mean absolute percentage error (*MAPE*) metric is applied for evaluating the proposed model. *MAPE* is defined in Eq. 1, where $actual_i$ represents the measured value for $t = i$, $pred_i$ represents the predicted value, and n is the predicted horizon length.

$$MAPE = 100 \times \frac{1}{n} \sum_{i=1}^n \left| \frac{actual_i - pred_i}{actual_i} \right| \quad (1)$$

3.3 Water temperature model

The equations for water heating and cooling in a water tank have exponential components and depend on several variables, including the insulation factor, the ambient temperature, the flow of water used, the time of use, the tank volume, among other factors [10]. However, the proposed model applying the *on blocks* and the estimation of water utilization makes it possible to define a linear temperature model, which provides a good approximation in order to estimate the *TDI*.

Five parameters are defined to build the temperature model from the data of *on blocks* and water utilization:

1. T_{min} : temperature at which the electric water heater is turned on by the action of the thermostat when the water is cooling.
2. T_{max} : temperature at which the electric water heater is turned off by the action of the thermostat when the water is heating.
3. c_{heat} : slope of the line when the electric water heater is turned on.
4. c_{cool} : slope of the line when the electric water heater is turned off and no water is being used.
5. c_{use} : slope of the line when using water, whether or not water is being used.

The considered parameters depend on several factors. This article proposes a specific approach to approximate their values, to assure that if a temperature approximation error occurs, it is always underestimated. This way, the proposed model is conservative about comfort estimation. It is assumed that the user sets the thermostat at a temperature value of 60° , with $T_{min} = 55^\circ$ and $T_{max} = 65^\circ$. The approximation model can be improved by considering more accurate values for T_{min} and T_{max} , which could be requested to the users, e.g., via a survey or web/mobile application. Fig. 5 presents a schema of the proposed model definition from *on blocks* and water utilization. Grey *on blocks* represents thermal recoveries, and *on blocks* caused by water utilization are marked in red.

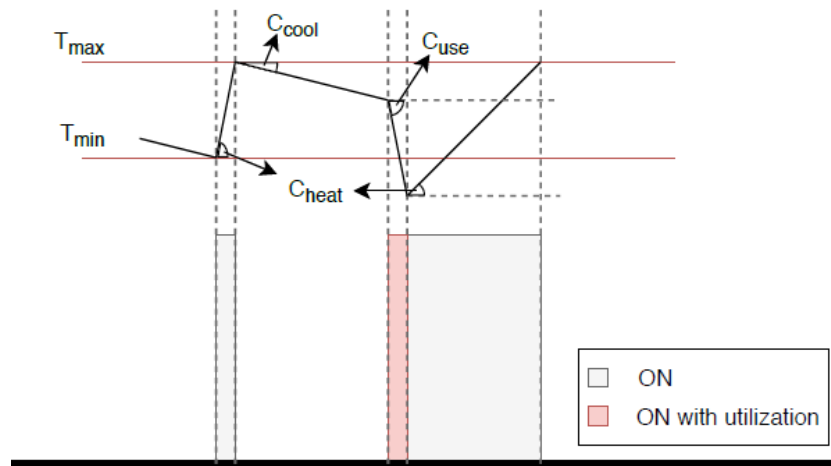


Fig. 5: Linear temperature model

The analysis of the temperature curve in Fig. 5 indicates that the water cools with a slope c_{cool} until it reaches T_{min} , and at that moment the electric water heater turns on. Heating phase starts with a slope c_{heat} until the temperature reaches T_{max} . Then, another cooling phase occurs until a water utilization causes a much faster cooling with a slope c_{use} . During the water utilization, the electric water heater turns on almost immediately after opening the water stream. After the utilization ends, the electric water heater remains on because the water temperature is below T_{min} , so it heats the water with a slope c_{heat} until T_{max} temperature is reached, where the gray *on block* ends. Assuming the described behaviour, the three slopes can be computed applying simple algebra.

The described procedure allows computing an approximation of the water temperature in a given interval from a set of *on blocks* and water utilization data in that interval. Therefore, a temperature forecast can be obtained from a set of *on blocks* predicted for a future time interval.

3.4 Defining the TDI

The proposed *TDI* aims at capturing the thermal impact that a user suffers due to an intervention by the electrical utility in the electric water heater, using the defined water utilization forecasting and the temperature model. Since every forecast has uncertainty, *TDI* is defined in terms of the expected value of the difference of the aforementioned temperatures, as expressed by Eqs. 2 and 3.

$$TDI(I) = E_w \left[\sum_{u \in U(w)} TDI(I, u, w) \right] \tag{2}$$

$$TDI(I, u, w) = \int_{t_{ini}(u)}^{t_{end}(u)} (T_n(t, w) - T_{int}(t, w)) dt + \rho \int_{t \in \tau} (T_{comf} - T_{int}(t, w)) dt \tag{3}$$

10 R. Porteiro, J. Chavat, S. Nesmachnow, L. Hernández-Callejo

In Eq. 2, I refers to the interruption of the electric water heater by the electric company, E_w represents the expected value of the indicator, considering all the forecasting realizations. $U(w)$ is the set of water utilization intervals in the analyzed time horizon (several of them can occur in the studied period).

In Eq. 3, $TDI(I, u, w)$ represents the discomfort index of an interruption, a water utilization, and a realization w that defines a single scenario of temperature evolution. $t_{ini}(u)$ and $t_{end}(u)$ are the starting and finishing time of utilization u . For realization w , $T_n(t, w)$ is the temperature curve without interruption and $T_{int}(t, w)$ is the temperature curve with interruption. Finally, T_{comf} is the water temperature below which the user feels discomfort, and τ represents the time interval in which $T_{int}(t, w) \leq T_{comf}$. The value ρ is a penalty attributed to the area below the comfort temperature.

Fig. 6 presents a visual representation of $TDI(I, u, w)$. The green area between the curve of temperature without interruption and the curve of temperature with interruption (defined by points PQRTU) is obtained from the integral $\int_{t_{ini}(u)}^{t_{end}(u)} (T_n(t, w) - T_{int}(t, w)) dt$, representing the loss of heat due to the interruption. Additionally, the area below the comfort temperature (defined by points RST and represented in red) is computed as $\int_{t \in \tau} (T_{comf} - T_{int}(t, w)) dt$, and weighted by the penalty ρ .

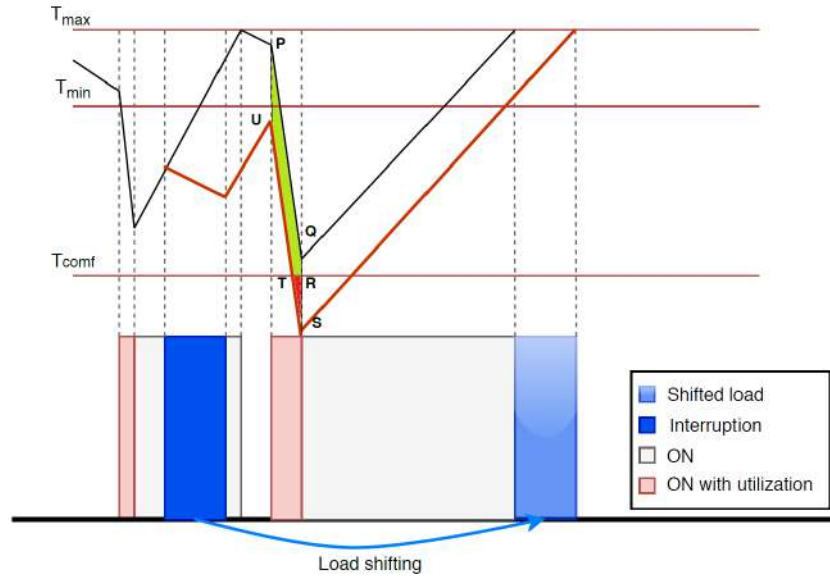


Fig. 6: Graphical representation of TDI

4 Implementation

This section describes the implementation of the proposed approach for defining TDI .

4.1 Development and execution platforms

The proposed models were implemented on Python. Several scientific libraries and packages were used to handle data, train models and visualize results, including Pandas, Numpy, and Tensorflow. The experimental analysis was performed on National Supercomputing Center (Cluster-UY), Uruguay [14].

4.2 Implementation details

Water utilization forecasting model. An Extratrees regression model was trained using input features and output described in subsection 3.2. Parameter search techniques were applied using a grid search implemented with GridSearchCV, the standard tool from `scikit-learn`. GridSearchCV uses it with an estimator using cross-validation and a predetermined metric to evaluate the models.

Linear temperature model. The implementation of the temperature model requires knowing values T_{min} and T_{max} . Then, using the information of *on blocks* and water utilization data, coefficients c_{cool} , c_{heat} and c_{use} are determined.

4.3 TDI calculation

A Monte Carlo simulation method is applied to compute the expected value of *TDI*, defined by Eq. 2. 100 realizations of w with distribution $N(0,1)$ are sampled. Then, for each value of w , the following procedure is applied:

- The next 12 hours are forecasted using the model described in Section 3.2.
- Using the temperature model described in Section 3.3 and the water utilization forecast for the next 12 hours, the water temperature is obtained for that period.
- An interruption of k minutes is simulated and the temperature for the next 12 hours is obtained using the proposed temperature model.
- Since T_{max} , T_{min} , T_{comf} are known, Eq. 3 is applied to compute $TDI(I, u, w)$ for all uses.
- An auxiliary variable $S_{uses}(w) = \sum_{u \in U(w)} TDI(I, u, w)$ is computed.

Finally, after computing $S_{uses}(w)$ for each realization, *TDI* is computed as the empirical expected value: $TDI(I) = \sum_{w=1}^{w=100} S_{uses}(w)/100$.

5 Experimental validation

This section presents the experimental validation of the proposed approach for defining a *TDI*.

12 R. Porteiro, J. Chavat, S. Nesmachnow, L. Hernández-Callejo

5.1 Water utilization forecasting

Metrics defined in Section 3.2 were applied to evaluate the implementation of the proposed two hours water utilization forecasting model. A subset of data in ECD-UY was used, consisting of ten electric water heaters with more than five consecutive months of measurements. The grid search procedure was performed on a two-dimensional grid to determine the best values for the number of trees in the forest and the maximum depth of the tree. The best parameter setting found by the grid search was $n_estimators = 50$, $max_depth = 200$.

Using the best parameter configuration, the ExtraTrees regressor achieved a *MAPE* value of 11.79 in just 4.09 s of execution time. This accuracy is adequate for the estimation purposes to compute *TDI*, considering the high variance in the water utilization of an individual electric water heater. The method provides a useful tool for generating scenarios to apply the Monte Carlo simulation approach, to estimate the empirical probability distribution of water utilization.

5.2 Water temperature model

The linear model described in Section 3.3 was determined for a real electric water heater having a thermometer to measure the temperature of the water in the tank. Values of $T_{min} = 55\text{ }^\circ\text{C}$ and $T_{max} = 65\text{ }^\circ\text{C}$ are known for this water heater, due to the setting of the thermostat. Parameters of the model are calculated as described in Section 5.1. Then, data of twelve hours *on blocks* of the electric water heater were used to estimate the temperature, and compared with the real temperature measured. Table 1 reports the comparison of the real and the estimated temperature, and the largest difference in the three long utilizations in the twelve hours analyzed.

Table 1: Accuracy of the water temperature model

	<i>1st utilization</i>	<i>2st utilization</i>	<i>3st utilization</i>
<i>Measured temperature</i>	59.09 °C	53.03 °C	58.34 °C
<i>Linear temperature</i>	59.88 °C	55.12 °C	59.41 °C
<i>Difference</i>	0.79 °C	2.09 °C	1.07 °C

The second utilization had the largest temperature difference (2.7 °C, marked in light blue in Table 1), which represents a percentage error of 4.5% in the worst case. The other utilizations had a significantly lower error. The accuracy of the temperature model is adequate for the purpose of estimating *TDI*.

5.3 TDI calculation

One of the main challenges related to the definition of *TDI* is modeling the differences of temperature (ΔT , quantitative factor) between performing an interruption in different moments. A relevant case is analyzing the ΔT values situations in the interruption affects the most to comfort.

As a relevant sample study, the comparison of the TDI for two different values of ρ and two particular electric water heaters (EWH_1 and EWH_2) is presented. The considered electric water heaters model two different utilization patterns from two different users. On weekdays, EWH_1 has two consecutive utilizations, and EWH_2 is only used once. The TDI associated with a 20-minute interruption between 20:10 and 20:30. Fig. 7 presents the empirical distribution of uses ($P(u)$) from 19:00 to 22:00 for EWH_1 (left) and EWH_2 (right). For each case, the interruption period is represented by the orange band.

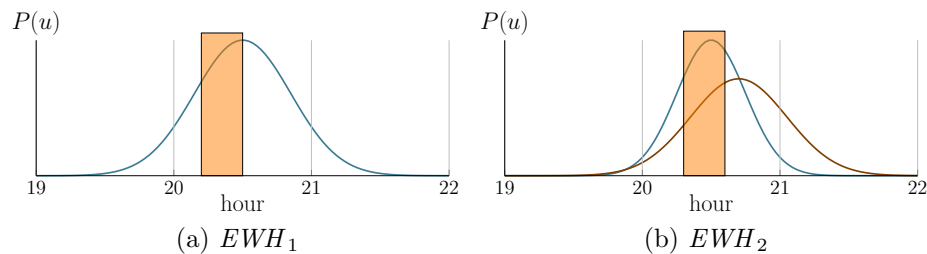


Fig. 7: Probability distribution for water utilization of two electric water heaters.

For the presented example, it is expected for the TDI value to be higher for EWH_2 than for EWH_1 , because in the hours immediately after the interruption analyzed, the average historical utilization is higher for EWH_2 . On the other hand, as the value of ρ increases, it is expected that the gap between the TDI of both electric water heaters became larger. Table 2 reports the TDI values computed for each electric water heater and ρ values.

Table 2: TDI applied for the interruption for EWH_1 and EWH_2 .

appliance	$\rho = 1$	$\rho = 2$
EWH_1	3362.3 °C s	4108.2 °C s
EWH_2	8109.6 °C s	11 041.7 °C s

Results in Table 2 confirms that the proposed index correctly models discomfort. The TDI value is higher for EWH_2 . Furthermore, the difference widens when considering larger penalty values (ρ). These results show that TDI properly models the differences of temperature between a scenario with an interruption and a scenario without interruption, as expected.

6 Conclusions and future work

This article presented an approach to evaluate the impact on the thermal comfort of direct demand response control using electric water heaters.

An index associated with the thermal discomfort is defined according to the following procedure. A water utilization forecasting model was built from real power data from a set of electric water heaters, using machine learning techniques. Then, applying the water utilization model, a linear model was developed to estimate the temperature of the water in the electric water heater tank.

14 R. Porteiro, J. Chavat, S. Nesmachnow, L. Hernández-Callejo

Finally, the *TDI* associated with an intervention on the electric water heater was defined stochastically, via Monte Carlo simulation.

The proposed models and the reliability of the proposed index were evaluated in a real case study considering two electric water heaters from different users, with different average historical utilization. The *TDI* values were analyzed for both electric water heaters for different penalization factors ρ . Results confirmed that the proposed index correctly models discomfort, since higher *TDI* values were computed for the electric water heater with the higher average historical utilization. The difference on *TDI* values increased when considering larger penalty values.

The main lines for future work are related to study the applicability of the proposed approach to perform load shifting when several electric water heaters are available, by properly adjusting the value of parameter ρ . In this scenario, the ranking of *TDI* values (from lowest to highest) provides useful information for decision-making when determining which electric water heaters should be interrupted. Another line of future work is to estimate an economic value of the *TDI* index. The economic value (in USD/MWh) would be useful to characterize the profit of reducing the energy demanded by a set of electric water heaters by applying the interruption action, in order to compare this strategy with other demand response techniques (e.g., using fuel generators).

7 Acknowledgements

This work was partly supported by CYTED Thematic Network “Fully Integral, Efficient And Sustainable Smart Cities (CITIES)”.

References

1. Al-Jabery, K., Xu, Z., Yu, W., Wunsch, D.C., Xiong, J., Shi, Y.: Demand-side management of domestic electric water heaters using approximate dynamic programming. *IEEE Transactions on Computer-Aided Design of Integrated Circuits and Systems* 36(5), 775–788 (2016)
2. Bhattacharyya, S.: Energy demand management. In: *Energy Economics*, pp. 135–160. Springer London (2011)
3. Chavat, J., Graneri, J., Alvez, G., Nesmachnow, S.: ECD-UY: Detailed household electricity consumption dataset of Uruguay. *Scientific Data* (2020), (submitted)
4. Deng, R., Yang, Z., Chow, M., Chen, J.: A survey on demand response in smart grids: Mathematical models and approaches. *IEEE Transactions on Industrial Informatics* 11(3), 570–582 (2015)
5. Hassan, N.U., Khalid, Y.I., Yuen, C., Tushar, W.: Customer engagement plans for peak load reduction in residential smart grids. *IEEE Transactions on Smart Grid* 6(6), 3029–3041 (2015)
6. Instituto Nacional de Estadística, Uruguay: Microdatos de la encuesta continua de hogares (2019), <http://www.ine.gub.uy/microdatos>, August 2020
7. Kampelis, N., Ferrante, A., Kolokotsa, D., Gobakis, K., Standardi, L., Crisalli, C.: Thermal comfort evaluation in hvac demand response control. *Energy Procedia* 134, 675–682 (2017)

8. Lu, N., Katipamula, S.: Control strategies of thermostatically controlled appliances in a competitive electricity market. In: IEEE Power Engineering Society General Meeting, 2005. pp. 202–207. IEEE (2005)
9. Luján, E., Otero, A., Valenzuela, S., Mocskos, E.E., Steffanel, L.A., Nesmachnow, S.: An integrated platform for smart energy management: the CC-SEM project. *Revista Facultad de Ingeniería Universidad de Antioquia* (2019)
10. Lutz, J., Whitehead, C., Lekov, A., Winiarski, D., Rosenquist, G.: WHAM: A simplified energy consumption equation for water heaters. In: ACEEE Summer Study on Energy Efficiency in Buildings (1998)
11. Massobrio, R., Nesmachnow, S., Tchernykh, A., Avetisyan, A., Radchenko, G.: Towards a cloud computing paradigm for big data analysis in smart cities. *Programming and Computer Software* 44(3), 181–189 (2018)
12. Momoh, J.: *Smart Grid: Fundamentals of Design and Analysis*. Wiley-IEEE Press (2012)
13. Nehrir, M., LaMeres, B., Gerez, V.: A customer-interactive electric water heater demand-side management strategy using fuzzy logic. In: Winter Meeting IEEE Power Engineering Society. vol. 1, pp. 433–436 (1999)
14. Nesmachnow, S., Iturriaga, S.: Cluster-UY: Collaborative Scientific High Performance Computing in Uruguay. In: *High Performance Computing*, pp. 188–202. Springer International Publishing (2019)
15. Orsi, E., Nesmachnow, S.: IoT for smart home energy planning. In: XXIII Congreso Argentino de Ciencias de la Computación. pp. 1091–1100 (2017)
16. Orsi, E., Nesmachnow, S.: Smart home energy planning using IoT and the cloud. In: IEEE URUCON. IEEE (2017)
17. Paul, L., MacKay, D., Li, H., Liuchen, C.: A water heater model for increased power system efficiency (2009)
18. Perfumo, C., Braslavsky, J.H., Ward, J.: Model-based estimation of energy savings in load control events for thermostatically controlled loads. *IEEE Transactions on Smart Grid* 5(3), 1410–1420 (2014)
19. Pirow, N., Louw, T., Booyesen, M.: Non-invasive estimation of domestic hot water usage with temperature and vibration sensors. *Flow Measurement and Instrumentation* 63, 1–7 (2018)
20. Porteiro, R., Nesmachnow, S., Hernández-Callejo, L.: Electricity demand forecasting in industrial and residential facilities using ensemble machine learning. *Revista Facultad de Ingeniería, Universidad de Antioquia* (2020)
21. Tabatabaei, S., Klein, M.: The role of knowledge about user behaviour in demand response management of domestic hot water usage. *Energy Efficiency* 11(7), 1797–1809 (2018)
22. Tang, R., Wang, S., Yan, C.: A direct load control strategy of centralized air-conditioning systems for building fast demand response to urgent requests of smart grids. *Automation in Construction* 87, 74–83 (2018)
23. Xiang, S., Chang, L., Cao, B., He, Y., Zhang, C.: A novel domestic electric water heater control method. *IEEE Transactions on Smart Grid* (2019)
24. Yin, Z., Che, Y., Li, D., Liu, H., Yu, D.: Optimal scheduling strategy for domestic electric water heaters based on the temperature state priority list. *Energies* 10(9), 1425 (2017)
25. Yoon, A., Kang, H., Moon, S.: Optimal price based demand response of HVAC systems in commercial buildings considering peak load reduction. *Energies* 13(4), 862 (2020)

Computational intelligence for analysis of traffic data

Hernán Winter¹[0000-0002-4075-3694], Juan Serra¹[0000-0002-4286-9316],
Sergio Nesmachnow¹[0000-0002-8146-4012],
Andrei Tchernykh^{2,3}[0000-0001-5029-5212], and Vladimir Shepelev³

¹ Universidad de la República, Montevideo, Uruguay
{hernan.winter, juan.serra, sergion}@fing.edu.uy

² CICESE, México
chernykh@cicese.mx

³ South Ural State University
shepelevvd@susu.ru

Abstract. This article presents a system developed for the collection and analysis of traffic data obtained from traffic camera videos using computational intelligence. The proposed system is developed using the modern object detection library Detectron2. A pipeline-type architecture is used for frame processing, where each step is an independent, configurable functional module, loosely coupled to the others. The validation of the proposed system is performed on real scenarios in Montevideo, Uruguay, under different conditions (daylight, nightlight, and different video qualities). Results demonstrate the effectiveness of the system in the considered scenarios.

Keywords: computational intelligence; neural networks; traffic data; smart cities

1 Introduction

The growth of cities and traffic density have led to an increased demand for surveillance systems capable of automating traffic monitoring and analysis. The main goal of these automatic systems is to aid or even remove the human labor for vision based tasks that can be performed by a computer, providing regulators and authorities the ability to respond quickly to diverse traffic issues and situations.

Tasks such as vehicle counting and infraction detection are of great importance for Intelligent Transportation Systems [23]. Recently, computer vision based detection and counting algorithms [22] have shown to be more effective and outperform traditional traffic surveillance methods, such as methods using different kinds of sensors [12]. However, there are still many challenges and open issues in computer vision based vehicle detection and counting processes, caused by illumination variation, shadows, occlusion, and other phenomena.

In this line of work, this article presents a system applying computational intelligence (based on Artificial Neural Networks, ANN) to solve traffic analysis

2 H. Winter, J. Serra, S. Nasmachnow, A. Tchernykh, V. Shepelev

problems using video recordings provided by surveillance cameras. The problems solved include vehicle detection, counting, classification, tracking, and detection of different types of traffic offenses, such as red light intersection crossing and parking vehicles in not allowed zones. The validation of the proposed system is developed using real traffic videos from the city of Montevideo, Uruguay.

The main contributions of the research reported in this article include: i) a methodology for the design of traffic analysis software systems using videos; ii) specific implementations of vehicle detection, counting, classification and tracking methods, and iii) the validation of the proposed methods on real scenarios.

The article is structured as follows. Section 2 presents a background on computational intelligence for image analysis. A review of the main related work is presented in Section 3. The technical aspects of the solution, including the proposed architecture, modules, and supporting libraries are described in Section 4. The experimental validation is reported and results are discussed in Section 5. Finally, Section 6 presents the conclusions and the main lines of future work.

2 Computational intelligence for image analysis

This section describes the main concepts about the analysis of traffic data using computational intelligence.

2.1 Detection

One of the fundamental problems in computer vision is the task of assigning a label from a fixed set of categories to an input image. This task is known as image classification and is divided into three subtasks: segmentation, location, and detection.

The goal of semantic segmentation is to obtain a category for each pixel given an input image. It does not differentiate instances of the same object because each pixel in the image is classified independently. The classification and location task consists of classifying an image with a label that describes an object and drawing the box within the image around the object. The output in this task are a label that identifies an object and a box that indicates where that object is located. Object detection takes as input a set of categories of interest and an image. The goal of this task is to draw a box around each one of these categories, each time they appear in the image, and also predict the category. This problem is different from classification and localization since there can be a variable number of outputs for each input image.

Another task to consider is instance segmentation. Given an input image, this task seeks to predict the locations and identities of the objects in that image. Additionally, instead of simply predicting a region for each of those objects, this task seeks to predict a segmentation mask for each of those objects and to predict which pixels in the image correspond to each object instance.

In the last few years, computational intelligence and deep learning have led to successful results on a variety of problems, including image classification.

Among different types of deep ANNs, Convolutional neural networks (CNN) have been extensively studied [8]. CNNs assume that the input to be classified is an image. This assumption allows the network to be more efficient and to design architectures that greatly reduce the number of network parameters.

Solving the object detection problem involves determining all the regions where objects to be classified can be located. Given an input image, a Region Proposal Network (RPN) uses signal processing techniques to create a list of proposed regions in which an object can exist. This architecture class is named R-CNN. Given an input image, an RPN is executed to obtain the proposals, also called Regions of Interest (RoI). The main drawback of this approach is its very high computational demands. In practice, the network training is slow and needs significant memory. Fast R-CNN was proposed to mitigate these problems, working in a similar way to R-CNN. In terms of speed, Fast R-CNN has proven to be nine times faster than CNN in training time [7]. However, the computation time is dominated by the calculation of the RoI, which turns out to be a bottleneck. This last problem is solved in Faster R-CNN [17].

Finally, one of the most recent methods to solve the instance segmentation task is the Mask R-CNN architecture. Similarly to Faster R-CNN, this method follows a multi-stage processing approach. It receives the complete image, which is executed through a convolutional network and a learned RPN. Once the RoIs are learned, they are projected onto the convolutional vector. Then, instead of simply performing the classification and the regression of the regions of each RoI, the method additionally predicts a segmentation mask for each region, solving a semantic segmentation problem within each of the regions proposed by the RPN. The RoI is finally wrapped to the proper shape.

2.2 Tracking

Object tracking consists in the process of accurately estimating the state of an object -position,identity,configuration- over time from observations [14], thus generating a trajectory given by the position of the object in each frame. When several objects are located at the same time, the problem is called Multiple Object Tracking. In this scenario, the difficulty of the task increases considerably due to the occlusion generated by the interaction of the objects, which in turn may have similar appearances. On the other hand, conditions such as the speed at which the objects move, the lighting or that these change their appearance depending on the position, require that the tracking system must be robust, maintaining the object identifier in such situations.

In classical tracking methods, object features are extracted in each frame and used to search for the same object in subsequent frames [25]. This causes errors to accumulate in the process and if occlusion or frame skipping occurs, tracking fails because of the rapid change of appearance features in local windows. Thus, modern tracking methods apply two steps: object detection and data association. First, objects are detected in each frame of the sequence and then, detected objects are matched across frames. This paradigm is called tracking by detection [10] and it relies on the performance of the detection algorithm. Detected

4 H. Winter, J. Serra, S. Nesmachnow, A. Tchernykh, V. Shepelev

objects are matched across frames using different approaches, including optical flow with mean shift of color signature, Earth mover's distance to compare color distributions, fragment-based features, and computational intelligence.

Another simple but effective method based on the tracking by detection approach is Intersection Over Union (IOU) [2]. This method requires a detection algorithm with a high rate of true positive results, as a detection is expected in each frame for each object to be tracked. It is also assumed that the detection of the same object in two consecutive frames present a great overlap of the intersection over the union (defined in Eq. 1), which is common for videos that present a high refresh rate.

$$IOU(a, b) = \frac{Area(a) \cap Area(b)}{Area(a) \cup Area(b)} \quad (1)$$

The advantage of the IoU method, in addition to its simplicity, is that it has lower computational cost than other methods. IoU can be integrated on other methods to achieve a more robust and accurate monitoring

3 Related work

Several articles have proposed automated systems for the analysis of traffic data applying image processing and computational intelligence techniques. The most related to the research reported in this article are reviewed next.

Zhou et al. [28] studied the vehicle detection and classification problem applying deep neural networks. The You Only Look Once (YOLO) architecture was used for vehicles detection and post-processing was performed to eliminate invalid results. The Alexnet architecture was applied for classification, feature extraction, and fine-tuning. The YOLO network obtained similar precision than a Deformable Parts Model, while the Alexnet network using Support Vector Machines (SVM) outperformed other methods such as Principal Component Analysis and Absolute Difference in a public dataset.

Uy et al. [20] studied methods for identifying traffic offenses using genetic algorithms (GA) and the recognition of offenders through ANN. GA were applied to detect vehicles obstructing pedestrian crossings and to identify the location of license plates in images, while a ANN is used to recognize the license plate number. The license plates recognition accuracy was high (91.6% on 47 test images), but some license plates were not properly located due to the vehicle position respect to the camera. Zhang et al. [26] applied a Fully CNN with Long Short Term Memory for the the vehicles counting problem. Compared to the state of the art, the proposed ANN architecture reduced the mean absolute error (MAE) from 2.74 to 1.53 on the WebCamT annotated dataset and from 5.31 to 4.21 on the TRANCOS dataset. In addition, the training time was accelerated by up to 5 times. However, the proposed ANN was not capable of handling long periods of information due to the large amount of memory required.

Dey et al. [5] applied CNN in a System-On-a-Programmable-Chip to analyze and categorize traffic, including the quality-of-experience variable to improve

predictions. A combination of transfer learning with re-training CNN models, allowed improving the prediction accuracy. Arinaldi et al. [1] applied computer vision techniques to automatically collect traffic statistics using Mixture of Gaussian (MoG) and Faster Recurrent CNN. Training and validation were developed on Indonesian road videos and a public dataset from MIT. Faster Recurrent CNN was best suited for detecting and classifying moving vehicles in a dynamic traffic scene, since MoG was weak for separating overlapping vehicles.

Chauhan et al. [3] studied CNN for real-time traffic analysis on Delhi, India. A YOLO network was used, pre-trained on the MS-COCO dataset and fitted with annotated datasets. The best trained model achieved a performance of 65–75% mean average precision, depending on the camera position and the vehicle class. This article provides the expected performance of YOLO models optimized using annotated data. The recent article by Zheng et al. [27] proposed TASP-CNN for predicting the severity of traffic accidents, considering relationships between accident features. The proposed method was successfully adapted to the representation of traffic accident severity features and deeper correlations of accident data. The performance of TASP-CNN was better than previous models when evaluated using data from an eight years period.

Our research group has developed research on detection on pedestrian movement patterns applying computational intelligence [4]. A flexible system was developed to process multiple image and video sources in real time applying a pipes and filters architecture to address different subproblems. The proposed system has two main stages: extracting relevant features of the input images, by applying image processing and object tracking, and patterns detection. The experimental analysis of the system was performed over more than 1450 problem instances, using PETS09-S2L1 videos and the results were compared with part of the MOTChallenge benchmark results. Results indicate that the proposed system is competitive, yet simpler, than other similar software methods.

4 The proposed system for traffic data analysis

This section presents the implemented system for traffic data analysis, describing the function of each module and the input and output parameters.

4.1 Overall description

The proposed approach is based on a modular architecture that implements an image processing pipeline [6]. The pipeline executes a set of tasks over input images (e.g., translation/rotation, resizing, etc.) to extract useful features. The modular architecture allowed for a progressive development process, starting from a few general modules and incorporating specific modules for relevant data.

Fig. 1 shows the final architecture of the pipeline for traffic video analysis, consisting of twelve modules. The pipeline has 40 parameters that allow controlling different aspects of the processing in each module.

6 H. Winter, J. Serra, S. Neschachnow, A. Tchernykh, V. Shepelev

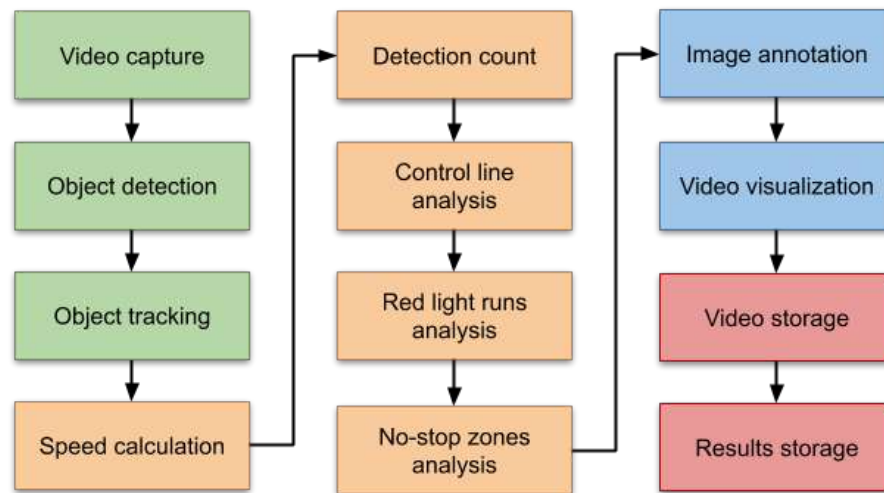


Fig. 1: The proposed pipeline for traffic video analysis

Four main stages are identified: i) video capture, object detection and tracking (in green in Fig. 1), detection data analysis (in orange), results visualization (in blue), results storage (in red). They are described in the following subsections.

4.2 Video capture and object detection

The goal of video capture is producing the frames used in the pipeline. A video stream (e.g., a local file or a webcam) is captured by a fast method using multi-threading parallel computing to read the video frames, using OpenCV utilities. Video capture initialize the cumulative data transfer object (DTO), used by all modules to read and write data, and stores several fields in the DTO, including *frame number*, *image* object, and *annotations*.

Then, the object detection process each frame to produce a bounding box, mask, score and class of the detected objects. This module is based on Detectron2 framework by Facebook [21], whose modular design allows using different state-of-the-art detection algorithms, such as Faster R-CNN, Mask R-CNN, or RetinaNet. The implemented module uses both synchronous and asynchronous detection, and adds different functionalities on top of the detection framework such as the possibility of defining regions of interest for the detection or filtering the classes of the detected objects. The output of the detection module is converted to the standard format used by the rest of the pipeline, so it might be replaced by other detection module without affecting the other modules in the pipeline. The output can contain bounding boxes or instance segmentation. The rest of the pipeline is compatible with both type of outputs and can take advantage of instance segmentation when available to compute more precise results when analyzing patterns.

4.3 Detection data analysis

Detection analysis includes five modules to extract information from data generated by previous modules in the pipeline.

The *speed calculation* module computes an estimation of the average speed of each detected object in recent frames, in pixels per frame (PPF) or pixels per second (PPS). The system stores the position of the center of each detected object in the last n frames (n is a parameter) and so the speed is given by the Euclidean norm of the first and last stored positions.

Detection count requires defining one or more counting lines on the video image. Based on a structure that keeps each detected vehicle as an object with several identifying properties, the counting module analyzes the vehicles that overlap with the counting lines. This analysis considers the intersection of the polygon of the mask or box with respect to the defined lines as an input parameter. If an overlapping is found, the vehicle information is updated with the lines it overlapped and the frame number in which it did so.

With *control lines analysis* it is possible to define a relationship between two lines, meaning that a vehicle should not cross both as doing so would be considered an infraction. This allows detecting different types of infractions that involves a vehicle circulating in a no-driving zone, e.g., a wrong turn or lane change near a corner. This module uses detected bounding boxes or masks to recognize if a vehicle overlaps with both lines in the relationship through the video.

The *red light runs analysis* module detects driving offenses of failing to comply with red light signal. The region where each semaphore is located is defined as an input parameter and each traffic light is associated with a line. The defined traffic lights are analyzed to determine their color frame by frame, applying an algorithm that transforms the cropped frame of the traffic light to Hue, Saturation, Value (HSV) color model.

The *no-stop zones analysis* considers zones, represented by polygons, in which vehicles should not stop (or park). The module analyzes the bounding box or mask of those vehicles that intersects with the defined non-stop zone. If an intersection greater than a certain value is detected, then the average speed of the vehicle in the last n frames (n is a parameter) is considered. When the average speed reaches a value lower than one, the vehicle is considered in infraction and labeled as stopped.

4.4 Annotation and results visualization

The *annotation* module is responsible of modifying frames to show information generated by the previous modules. The modified frames will be part of the output video. Additionally, this module is in charge of drawing the detected objects, boxes, or masks as appropriate. Fig. 2 presents an example of an annotated frame in one of the scenarios studied in this article.

The *video visualization* module is in charge of displaying the output frames as they are produced, using OpenCV to create a window and display the frames.

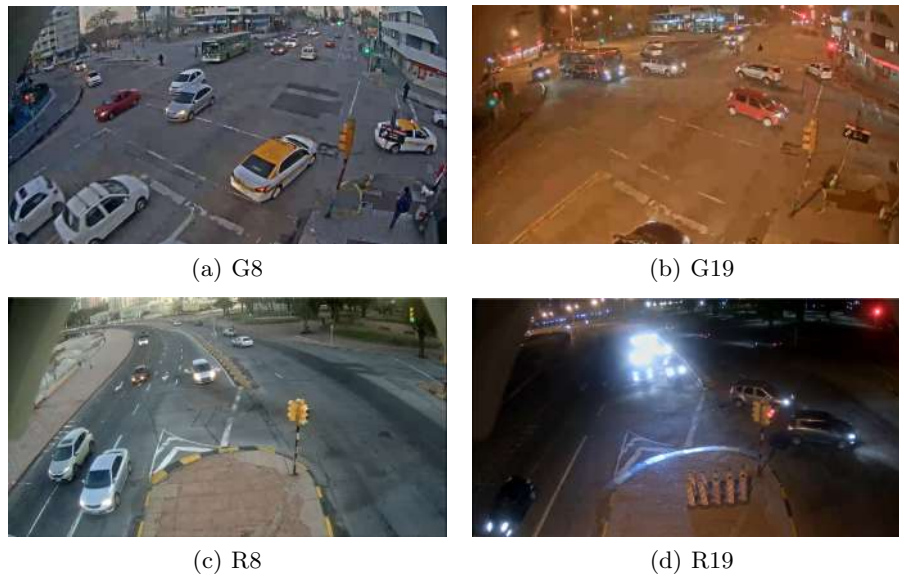


Fig. 3: Testing video scenarios

Table 1: Properties of the test videos

<i>reference</i>	<i>format</i>	<i>resolution</i>	<i># frames</i>	<i>rate</i>	<i>duration</i>
G8	MP4	1280×720 pixels	2393	8 FPS	5 minutes
G19	MP4	1280×720 pixels	2398	8 FPS	5 minutes
R8	MP4	1280×720 pixels	5998	20 FPS	5 minutes
R19	MP4	1280×720 pixels	5997	20 FPS	5 minutes

5.2 Development and execution platform

The proposed system was developed using Python and Anaconda for project environment management allowing to install and maintain the required libraries easily. For the implementation, training, and execution of the presented ANN models, the Detectron2 framework [21], based on pytorch, was used. The tracking service was provided by a Node.js server [19] running an implementation of the Node Moving Things Tracker [15] library. OpenCV [13] was used for image and video manipulation and processing.

The experimental evaluation was performed on a virtual environment defined on a high-end server with Xeon Gold 6138 processors (40 cores and 80 threads per core), 8 GB RAM, a NVIDIA P100 GPU and a 300 GB SSD, from National Supercomputing Center (ClusterUY) [16]. Using this high performance computing platform, it was possible to dynamically reserve the resources needed for the batch jobs for the system execution and validation.

10 H. Winter, J. Serra, S. Nasmachnow, A. Tchernykh, V. Shepelev

5.3 Metrics for evaluation

Statistical measures were considered for the evaluation of the developed system. To account for the performance of stages that involve a binary classification, the standard metrics were applied: True Positive (TP), which indicates the number of occurrences where the model correctly predicts the positive class; True Negative (TN) is the number of occurrences where the model correctly predicts the negative class; False Positive (FP) the number of occurrences where the model incorrectly predicts the positive class; and False Negative (FN) indicates the number of occurrences where the model incorrectly predicts the negative class.

Metrics proposed by Sokolova and Lapalme [18] were applied to evaluate the performance of detection and classification algorithms, including:

- *Average Accuracy*: indicates the overall effectiveness of a classifier (Eq. 2).
- *Error Rate*: indicates the average per-class classification error (Eq. 3).
- *Precision*: reflects the percentage of the results which are relevant (Eq. 4).
- *Recall*: refers to the percentage of total relevant results correctly classified (Eq. 5).

$$\frac{TP + TN}{\frac{TP + TN + FP + FN}{n}} \quad (2) \quad \frac{FP + FN}{TP + TN + FP + FN} \quad (3)$$

$$\frac{TP}{TP + FP} \quad (4) \quad \frac{TP}{TP + FN} \quad (5)$$

Metrics proposed by MOTChallenge [11] were used to evaluate the tracking method. Special metrics are required for evaluating multiple object tracking:

- Identity Switches ($IDSW$): indicates the number of occurrences where an already identified object is assigned a new identifier.
- Multiple Object Tracking Accuracy ($MOTA$): is a global performance indicator of the tracker combining three sources of error. (Eq. 6, where t represents the frame and G_t the number of objects in frame t).

$$MOTA = 1 - \frac{\sum_t (FN_t + FP_t + ID_{Sw})}{\sum_t G_t} \quad (6)$$

5.4 Results: object detection

For the evaluation of the object detection module, the configuration baseline of Detectron2 and the detection confidence threshold were taken into consideration.

The Detectron2 configuration baseline is a set of parameters which determines the type of ANN to be executed and the weight model. These baselines are part of the Model Zoo in Detectron2 [21]. The main properties of the selected baselines are presented in Table 2.

Table 2: Details of the configuration baselines of Detectron2 used in the experimental evaluation of object detection

	<i>R101-box</i>	<i>X101-box</i>	<i>R101-mask</i>	<i>X101-mask</i>
Backbone	R101-FPN	X101-FPN	R101-FPN	X101-FPN
Weights model	R101	X-101-32x8d	R101	X-101-32x8d
Using masks	no	no	yes	yes

The selected backbones used are ResNet-101+FPN (R101-FPN) which is a Faster R-CNN and ResNeXt-101+FPN (X101-FPN) which is a Mask R-CNN. The weight model R101 is an adaptation of the original ResNet-101 model [9] and X-101-32x8d is a ResNeXt-101-32x8d model trained with Caffe2 [24]. In turn, the detection confidence threshold allows discarding detected objects which classification score value is lower than a given value.

Tables 3 and 4 reports the results of the considered detection metrics for the G8 and G19 videos, respectively. These videos were selected as they account for a representative traffic flow of the city in rush hours in the morning (G8) and in the night (G19). In these videos the camera angle is such that the North to South flow of vehicles occasionally occludes the vehicles in the West to East flow. Additionally, this scenario has a crossing with multiple traffic lights which makes the vehicles stop and accumulate producing interesting detection situations.

Table 3: Classification metrics obtained with different settings in video G8

<i>configuration</i>	<i>average accuracy</i>	<i>error rate</i>	<i>precision</i>	<i>recall</i>
R101-box-t03	0.93	0.07	0.91	0.73
R101-box-t05	0.87	0.13	1.00	0.48
R101-box-t07	0.78	0.22	0.93	0.23
X101-box-t03	0.93	0.07	0.89	0.75
X101-box-t05	0.88	0.12	1.00	0.49
X101-box-t07	0.79	0.21	1.00	0.24
R101-mask-t03	0.94	0.06	0.90	0.80
R101-mask-t05	0.93	0.07	0.97	0.72
R101-mask-t07	0.90	0.10	0.96	0.58
X101-mask-t03	0.93	0.07	0.89	0.79
X101-mask-t05	0.91	0.09	0.96	0.66
X101-mask-t07	0.91	0.09	1.00	0.61

Results in Tables 3 and 4 indicate that the proposed system had an overall average accuracy of 85% and indicate that the mask configurations computed better results than the box configurations in most cases (10 out of 12 instances). No significant performance differences between R101 and X101 models on box nor segmentation mask prediction were detected, but X101 had slightly better results in the night cases for segmentation.

12 H. Winter, J. Serra, S. Nsmachnow, A. Tchernykh, V. Shepelev

Table 4: Classification metrics obtained with the different settings in video G19

<i>configuration</i>	<i>average accuracy</i>	<i>error rate</i>	<i>precision</i>	<i>recall</i>
R101-box-03	0.89	0.11	0.78	0.67
R101-box-05	0.82	0.18	0.89	0.40
R101-box-07	0.75	0.25	1.00	0.23
X101-box-03	0.84	0.16	0.70	0.53
X101-box-05	0.83	0.17	0.90	0.42
X101-box-07	0.73	0.27	1.00	0.21
R101-mask-03	0.87	0.13	0.67	0.67
R101-mask-05	0.85	0.15	0.67	0.60
R101-mask-07	0.86	0.14	1.00	0.49
X101-mask-03	0.89	0.11	0.77	0.70
X101-mask-05	0.87	0.13	0.92	0.56
X101-mask-07	0.87	0.13	0.96	0.53

5.5 Object tracking

The main parameter to consider is the *tolerance*, i.e. the number of frames before the algorithm concludes that a tracked object is no longer in the sequence. The tolerance value depends on the frame rate of the recording. Values corresponding to half, one, and two seconds were considered in the study, as they represent time windows in which the probability of a identity switch among detections is low. That is, 4, 8, and 16 frames for G8 and G19 videos, and 10, 20, and 40 frames for R8 and R19. The performance of the object tracking module depends on the detection module. The X101-mask-05 detection setting was defined as basis for all tracking tests as it was the best performing detection configuration.

Table 5: Tracking tests results

<i>configuration</i>	<i>MOTA</i>	<i>configuration</i>	<i>MOTA</i>
G8-t04	0.81	R8-t10	0.86
G8-t08	0.83	R8-t20	0.87
G8-t16	0.82	R8-t40	0.89
G19-t04	0.47	R19-t10	0.10
G19-t08	0.49	R19-t20	0.14
G19-t16	0.46	R19-t40	0.13

Results in Table 5 show average MOTA scores of 85% for the daylight cases and significantly lower (30%) for the cases in the night. This indicate that the module performs significantly better in daytime scenarios. In 3 out of 4 cases, the configurations with one second of tolerance (8 frames in G8 and G19, and 20 frames in R8 and R19) had slightly better results than for nighttime scenarios. *MOTA* was mainly affected by *FN* values. In the tracking evaluation this occurs when an existing vehicle is not detected in a given number of frames, therefore it is not tracked. Based on this observation, improving the detection module in bad lighting conditions would also improve the tracker performance.

5.6 Pattern analysis

For the evaluation of the counting module, the vehicle count resulting from the pipeline execution was compared to the number of vehicles obtained using manual counting. The performance of the method to count vehicles was measured using the detection and classification metrics presented above. To perform the evaluation, 30-second video segments were extracted from the four videos in the original test dataset. Four segments were considered for each video, thus having a total dataset of 16 segments from the two studied scenarios, eight taking place during the day and eight during the night.

Table 6 reports the results of the counting module evaluation, using the following configuration: the R101-mask-05 configuration was established for detection; the tracking module uses an IoU of 0.05, and a loss tolerance of eight frames for G8/G19 videos and 20 frames for R8/R19 videos.

Table 6: Counting test results

<i>reference</i>	<i>average accuracy</i>	<i>error rate</i>	<i>precision</i>	<i>recall</i>
G8	0.92	0.08	0.92	1.00
G19	0.52	0.48	0.62	0.76
R8	0.87	0.13	0.91	0.95
R19	0.19	0.81	0.27	0.33

Results in Table 6 show an average accuracy of 89% for the daylight cases and 36% for the cases in the night. This indicates that the counting module performs better under good lighting conditions. In this case there is still room to improve the classification of the counted vehicles as the comparison of *precision* and *recall* shows that the main source of error are the *FP*. This means that the counting algorithm correctly counts a vehicle, but classifies it in the wrong class. Under bad lighting conditions the performance is poor, this is also caused by the large number of *FP*, which in this case happens because the counting algorithm counts not existing vehicles. The performance of this module can be mainly improved by using a more precise classification model in the detection module, while a better detection under bad lighting conditions would also improve the performance of the counting module. Improving the classification under poor lighting conditions is one of the main lines for ongoing and future work.

6 Conclusions and future work

This article presented the design and implementation of a system for the analysis of traffic data using computational intelligence techniques.

The proposed system was developed following a flexible pipeline-type architecture built over the modern object detection library Detectron2. The proposed design provides an efficient frame processing, by using independent, configurable functional modules, loosely coupled between them. This feature allows including new methods, modifying existing ones, and evaluate different alternatives and configurations.

14 H. Winter, J. Serra, S. Nasmachnow, A. Tchernykh, V. Shepelev

The problems of object detection and tracking are solved using the Detectron2 framework and the Node Moving Things Tracker library, respectively. The information generated by these modules from the traffic videos allowed implementing a set of modules for the collection and analysis of traffic data.

The validation of the proposed system is carried out using real videos from two scenarios that include important streets of Montevideo, Uruguay, under different conditions (daylight, nightlight, and different video qualities). These recordings were taken in rush hours and show an interesting flow of vehicles.

Results demonstrate the effectiveness of the system in scenarios with proper lightning conditions. The detection results shown a overall average accuracy of 85%, and better performance using the mask models. In object tracking, the average MOTA scores were 85% in daylight. Results dropped to 30% in nighttime, indicating that improvements are required to deal with bad lightning conditions. Similarly, the counting module performed an average accuracy of 89% in daylight and 36% in nighttime.

The main lines for future work are related to improve the object detection module training the models with bad lightning conditions or bad weather annotated examples. In turn, the experimental evaluation of the proposed system can be extended to consider the analysis of red light runs and no-stop zones modules. Another interesting line of work is related to developing more sophisticated pattern detection methods to capture relevant events such as abrupt lane change or even traffic accidents. We are working on these topics right now.

References

1. Arinaldi, A., Pradana, J., Gurusinga, A.: Detection and classification of vehicles for traffic video analytics. *Procedia Computer Science* 144, 259–268 (2018)
2. Bochinski, E., Eiselein, V., Sikora, T.: High-speed tracking-by-detection without using image information. In: 14th IEEE International Conference on Advanced Video and Signal Based Surveillance. pp. 1–6 (2017)
3. Chauhan, M., Singh, A., Khemka, M., Prateek, A., Sen, R.: Embedded CNN based vehicle classification and counting in non-laned road traffic. In: 10th Int. Conf. on Information and Communication Technologies and Development (2019)
4. Chavat, J., Nasmachnow, S.: Computational intelligence for detecting pedestrian movement patterns. In: *Smart Cities*, pp. 148–163 (2019)
5. Dey, S., Kalliatakis, G., Saha, S., Kumar Singh, A., Ehsan, S., McDonald, K.: MAT-CNN-SOPC: Motionless analysis of traffic using convolutional neural networks on system-on-a-programmable-chip. In: *NASA/ESA Conference on Adaptive Hardware and Systems* (2018)
6. Gilewski, J.: detectron2-pipeline: Modular image processing pipeline using OpenCV and Python generators powered by Detectron2. <https://github.com/jagin/detectron2-pipeline> (2019), [2020-03-15]
7. Girshick, R.: Fast r-cnn. In: *Proceedings of the IEEE International Conference on Computer Vision* (December 2015)
8. Gu, J., Wang, Z., Kuen, J., Ma, L., Shahroudy, A., Shuai, B., Liu, T., Wang, X., Wang, G., Cai, J., Chen, T.: Recent advances in convolutional neural networks. *Pattern Recognition* 77, 354 – 377 (2018)

9. He, K., Zhang, X., Ren, S., Sun, J.: Deep residual learning for image recognition. arXiv preprint arXiv:1512.03385 (2015)
10. Leal-Taixé, L.: Multiple object tracking with context awareness. CoRR abs/1411.7935 (2014)
11. Leal-Taixé, L., Milan, A., Reid, I., Roth, S., Schindler, K.: MOTChallenge 2015: Towards a benchmark for multi-target tracking. arXiv:1504.01942 [cs] (2015)
12. Lou, L., Zhang, J., Jin, Y., Xiong, Y.: A novel vehicle detection method based on the fusion of radio received signal strength and geomagnetism. *Sensors* 19 (2019)
13. Mahankali, N., Vadivel, A.: OpenCV for computer vision applications (2015)
14. Moussy, E., Mekonnen, A.A., Marion, G., Lerasle, F.: A comparative view on exemplar ‘tracking-by-detection’ approaches. In: 2015 12th IEEE International Conference on Advanced Video and Signal Based Surveillance (AVSS). pp. 1–6 (2015)
15. Move-lab: Tracking things in object detection videos. <https://www.move-lab.com/blog/tracking-things-in-object-detection-videos> (2018), [2020-03-15]
16. Nesmachnow, S., Iturriaga, S.: Cluster-UY: Collaborative Scientific High Performance Computing in Uruguay. In: Communications in Computer and Information Science, pp. 188–202. Springer International Publishing (2019)
17. Ren, S., He, K., Girshick, R., Sun, J.: Faster R-CNN: Towards Real-Time Object Detection with Region Proposal Networks. In: Cortes, C., Lawrence, N.D., Lee, D.D., Sugiyama, M., Garnett, R. (eds.) *Advances in Neural Information Processing Systems* 28, pp. 91–99 (2015)
18. Sokolova, M., Lapalme, G.: A systematic analysis of performance measures for classification tasks. In: *Information Processing Management · July 2009* (2008)
19. Tilkov, S., Vinoski, S.: Node.js: Using javascript to build high-performance network programs. *IEEE Internet Computing* 14(6), 80–83 (2010)
20. Uy, A., Quiros, A., Bedruz, R., Abad, A., Bandala, A., Sybingco, E., Dadios, E.: Automated traffic violation apprehension system using genetic algorithm and artificial neural network. In: *IEEE Region 10 Technical Conference*. pp. 2094–2099 (2016)
21. Wu, Y., Kirillov, A., Massa, F., Lo, W., Girshick, R.: Detectron2. <https://github.com/facebookresearch/detectron2> (2019)
22. Yang, H., Qu, S.: Real-time vehicle detection and counting in complex traffic scenes using background subtraction model with low-rank decomposition. *IET Intelligent Transport Systems* 12, 75–85 (2018)
23. Yang, Z., Pun-Cheng, L.: Vehicle detection in intelligent transportation systems and its applications under varying environments: A review. *Image and Vision Computing* 69, 143 – 154 (2018)
24. Yangqing, J., Shelhamer, E., Donahue, J., Karayev, S., Long, J., Girshick, R., Guadarrama, S., Darrell, T.: Caffe: Convolutional architecture for fast feature embedding (2014)
25. Zhang, K., Zhang, L., Yang, M.: Real-time compressive tracking. In: *Computer Vision*. pp. 864–877. Springer Berlin Heidelberg (2012)
26. Zhang, S., Wu, G., Costeira, J., Moura, J.: Fcn-rlstm: Deep spatio-temporal neural networks for vehicle counting in city cameras. In: *International Conference on Computer Vision*. pp. 3687–3696 (10 2017)
27. Zheng, M., Li, T., Zhu, R., Chen, J., Ma, Z., Tang, M., Cui, Z., Wang, Z.: Traffic accident’s severity prediction: A deep-learning approach-based CNN network. *IEEE Access* 7, 39897–39910 (2019)
28. Zhou, Y., Nejati, H., Do, T., Cheung, N., Cheah, L.: Image-based vehicle analysis using deep neural network: A systematic study. In: *IEEE International Conference on Digital Signal Processing*. pp. 276–280 (2016)

Study and improvement of the efficiency of a hydraulic pumping system associated with a Pelton hydraulic turbine in a smart microgrid

Oscar Izquierdo-Monge¹, Paula Peña-Carro¹, Carlos Barrera del Amo¹, Luis Hernández-Callejo², Oscar Duque-Perez³, Angel L. Zorita-Lamadrid³

¹ CEDER-CIEMAT, Autovía de Navarra A15 salida 56, 422290 Lobia (Soria), España, O.I.M.: oscar.izquierdo@ciemat.es; P.P.C.: paula.pena@ciemat.es; C.B.A.: carlos.barrera@ciemat.es

² University of Valladolid, Campus Universitario Duques de Soria, 42004 Soria, España. L.H-C.: luis.hernandez.callejo@uva.es

³ University of Valladolid, Paseo del cauce 59, 47011 Valladolid, España. O.D.P.: oscar.duque@eii.uva.es; A.Z.L.: zorita@eii.uva.es

Abstract: The installation of a storage system on a microgrid is essential to achieve a balance between demand and generation. Within the diversity of storage systems that exist, it is hydraulic storage that presents the best characteristics for long-term storage. We are located in the smart microgrid of CEDER to improve the efficiency of your hydraulic storage system. Initially, the system is formed by three water tanks at different altitudes, two centrifugal hydraulic pumps of 23 kW each, and a Pelton-type hydraulic turbine. With the replacement of the pumping system by another one formed by 4 hydraulic pumps of a lesser power (7.5 kW each), it has been possible to have a more modular system that allows the set to be started up with less surplus energy and an improvement in the efficiency of 18.9 % concerning the previous installation.

Keywords: Electric Smart microgrids, hydraulic pumping system, hydraulic efficiency.

1 Introduction

Smart microgrids are locations where we can find a variety of power generation systems, where renewable generation systems predominate along with different storage and communications systems [1][2]. The correct control and monitoring of all the technologies provides the whole with a partial or total autonomy.

Within these sites, storage systems are of great importance as they are the ones that allow demand generation control to be as optimized as possible [3][4][5]. The development of these systems gives us the possibility of increasing the integration of renewable energy sources in the electricity generation sector [6][7].

It is common for there to be a high presence of uncontrollable generation systems within the microgrid. The intermittent nature of the resource associated with this type of generation source makes its production uncontrollable and random and, therefore,

requires the presence of storage systems when the uncontrollable systems are around 50-100% [8] of the total energy generation of the microgrid.

The most widely used and most efficient storage systems are batteries and hydraulic pumping systems. In this document we will develop the hydraulic pumping systems, which constitute 97% of the global stored power, assuming that about 160 GW at the end of 2019, and more than 99% of the stored energy thanks to the high efficiency that it presents being around 80% [9].

The hydraulic pumping systems can be river or non-river with the installation of water tanks at different heights. Conventional river installations are limited by water availability, flood control, and environmental considerations and therefore have limited potential. Non-river systems use artificial reservoirs at different altitudes to circulate water indefinitely in a closed circuit. The reservoirs are generally separated from several meters to several kilometres, connected by a pipe or a tunnel and the installation of a pumping and turbine system. Thanks to the installation of these reservoirs, together with the turbine and the pumping system, we can both store and generate. The system stores the excess electricity by pumping water to the upper reservoir and generating energy when the water flows to the lower level where the turbine is located, which will be in charge of transforming this gravitational energy into electrical energy.

This storage technology has a high potential being proportional to the volume of the upper reservoir, the section of the pipe or tunnel, and the efficiency of the return journey. This makes it one of the best large-scale, long-term storage systems with low evaporation losses. This is the most economical large scale storage technology [8].

This paper aims to characterize the existing hydraulic pumping system that is part of the smart microgrid located at CEDER and propose the improvement of efficiency by replacing the hydraulic pumps that compose it.

The rest of the paper is as follows: section 2 describes the CEDER microgrid power. Section 3 describes the hydraulic system, while section 4 characterizes its operation and calculates its efficiency. Section 5 presents the new pumping system, characterizing it, and calculating its efficiency. Finally, the conclusions obtained and the literature cited is presented.

2 Description of the CEDER electric microgrid.

CEDER is the Centre for the Development of Renewable Energies. It belongs to the Centre for Energy, Environmental and Technological Research (CIEMAT), which is a Public Research Organisation, currently dependent on the Ministry of Science and Innovation.

It is located in the town of Lubia, province of Soria (Spain), and has an area of 640 ha with more than 13,000 m² built in three separate areas (see Figure 1).



Fig. 1. Location and distribution of buildings in the CEDER.

CEDER-CIEMAT has a smart electric microgrid in operation on which you can act and make modifications for research purposes. The CEDER microgrid is fed by a 45 kV distribution network and carries out a transformation at its input to 15 kV.

Internally, there is an underground electrical network that feeds 8 transformer stations that adjust the voltage to 400 V low voltage, which is where all the elements of the microgrid are connected, as can be seen in Figure 2.

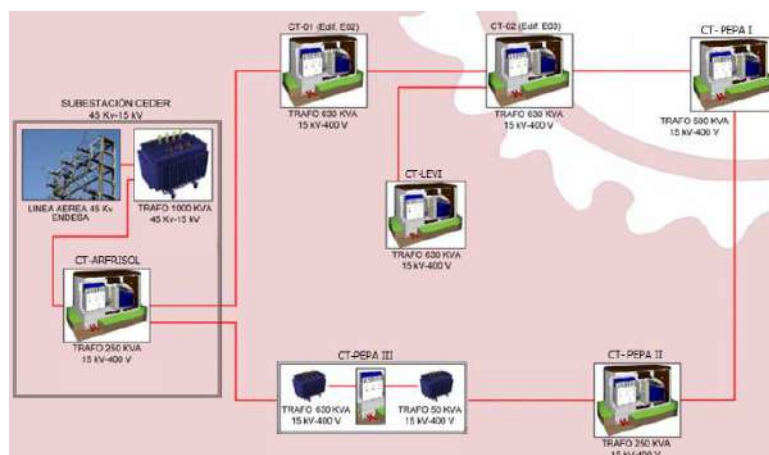


Fig. 2. Distribution of medium voltage between transformer stations.

The microgrid has a control system that monitors all components connected to it and allows it to be managed efficiently.

The components connected to the microgrid are as follows:

- **Distributed generation system:** Distributed generation consists of the production of electrical energy through many small energy sources in places as close as possible to the loads or points of demand. In this way, losses in the network are reduced by reducing the flow of energy through the network. In the electric microgrid of CEDER, there are different generation systems distributed by its 640 ha. and connected to the different transformation centres, always at low voltage.

Most of these generation systems are renewable and also uncontrollable, in other words, their primary energy source is neither controllable nor storable and their production cannot be controlled.

- Non-Controllable:
 - Photovoltaic: 8 photovoltaic systems with 116.6 kW installed
 - Wind: 1 wind turbine of 50 kW and 15 meters in diameter.
- Controllable:
 - From renewable origin:
 - **Turbine-pump system**
 - From non-renewable origin:
 - Diesel group: 100 kVA.
- Storage system: they are fundamental to achieve the balance between Distributed generation consists of the production of electrical energy through many small energy sources in places as close as possible to the loads or points of demand and generation. They allow for the accumulation of surplus energy at times when generation is exceeding Distributed generation consists of the production of electrical energy through many small energy sources in places as close as possible to the loads or points of demand, avoiding the injection of this energy into the distribution network, and making it possible to use it at those moments when it is most necessary, based on the microgrid control strategies defined from the analysis of generation, demand and storage data.
 - Mechanical:
 - **Hydraulic pumping system.**
 - Electrochemicals:
 - Pb-acid battery I: 120 glasses of 2 V with capacity 1080 Ah at 120 hours.
 - Pb-acid battery I: 120 glasses of 2 V with capacity 765 Ah at 120 hours.
 - Li-ion battery: 2 racks of 14 modules and 14 cells per module. Each cell has a nominal capacity of 50 Ah, a nominal voltage of 3.2 volts and a nominal power of 160 Wh (1 hour).
- Loads and demand: these are the elements that allow CEDER's daily operation, that is, the different buildings and equipment that demand energy for their operation. All loads are connected to the low voltage network. For monitoring demand, apart from the meter of the distribution company, CEDER has eight electrical network/energy quality analyzers (PQube), one for each transformation centre.

The purpose of this paper is to characterize the pumping system that is part of the reversible hydraulics and to improve its efficiency.

3 Description of the hydraulic system

CEDER has a hydraulic system of turbine-pumping, which besides transforming the potential power of the water into electricity through a turbine and an electric generator, can carry out the inverse process, that is, to increase the potential energy of the water by pumping it from a reservoir at the exit of the turbine to another at a higher level consuming electric power. It can, therefore, be considered a system of generation and a method of storing power at the same time.

This system is made up of:

- Pelton-type hydraulic turbine connected to a 60 kW asynchronous electric generator (Figure 3). The downstream pipe to the turbine from the main water storage tank has a significant pressure loss in its final section due to the ground conditions do not allow it to be carried in a straight line, which means that the maximum stable generation that can be achieved with it is 40 kW.



Fig. 3. Pelton-type hydraulic turbine and 60 kW asynchronous electric generator.

The installation is completed with a capacitor bank to compensate for the power factor of the asynchronous generator and a control system, as shown in Figure 4.



Fig. 4. Capacitor bank and turbine control panel.

- Three water storage tanks with a total capacity of 2000 m³ and an 86 meter total difference in level (Figure 5).
 The upper tank (LEVI) has a capacity of 500 m³ (25 meters in diameter and 0.5 meters high). The intermediate tank is 16 meters below the upper tank and has a capacity of 1500 m³ (25 meters in diameter and 3.5 meters in height). The lower tank has a capacity of 1900 m³ (25 meters in diameter and 3.5 meters in height) and is approximately 70 meters below the intermediate tank.

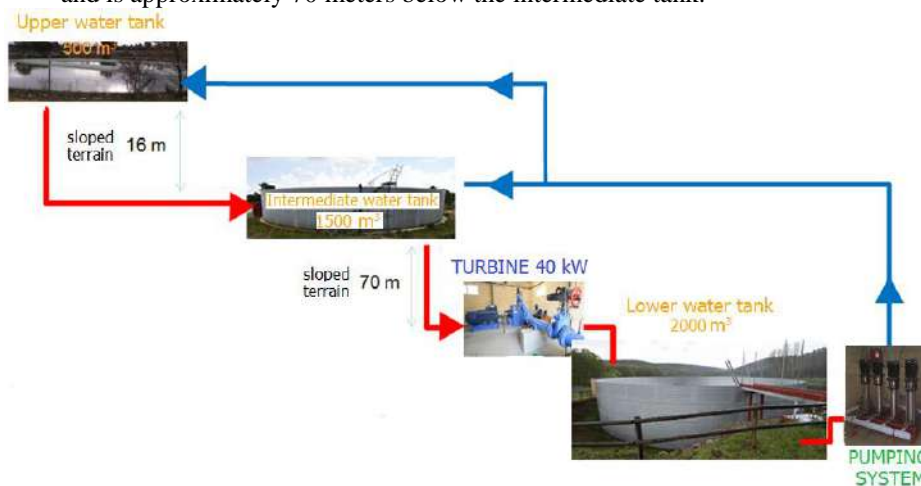


Fig. 5. Water storage tanks.

- Hydraulic pumping system consisting of two pumps of 23 kW each (Figure 6), with a soft starter to avoid demand peaks.



Fig. 6. Hydraulic pumping system consisting of two pumps of 23 kW each.

4 Characterization of the hydraulic pump-turbine system

4.1 Pelton-type hydraulic turbine

The turbine has hardly been used before starting this work so we do not have a detailed knowledge of its behaviour, therefore, the first task to develop will be its characterization to know its operation, and the amount of water it consumes according to the power it produces.

To know the amount of water in the main storage tank (intermediate tank), an ultrasonic sensor has been installed which monitors the height of the water in millimetres, so that to know the litres consumed, the volume of water must be calculated from the diameter of the tank, which as we saw in the description in the previous chapter, is 25 metres.

To characterize the turbine, a series of tests have been carried out, turbine at different powers and seeing the water demand for each of them, and the following results have been obtained:

- Turbine at 5 kW: Figure 7 shows water demand of the turbine operating at 5 kW.

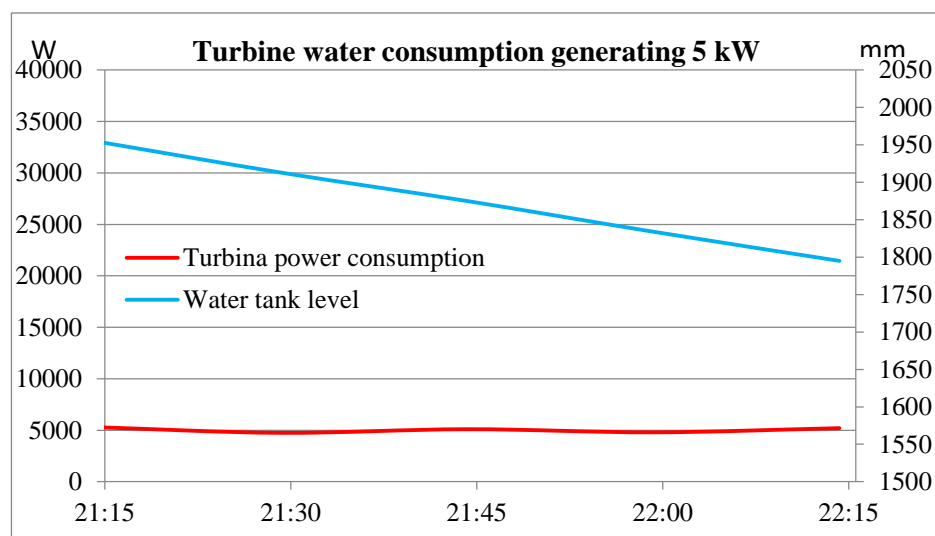


Fig. 7. Turbine demand graph at 5 kW.

With the turbine generating 5 kW for 1 hour, the water tank level decreases from 1955 mm high to 1795 mm, which means it consumes 160 mm of water every hour. As the tank is 25 metres in diameter, this is equivalent to a demand of 78540 litres of water per hour of operation.

Figure 7 shows data averaged over 15 minutes. If we look at the instantaneous data, we can see that it is difficult to maintain such a low power setting since its

nominal operation is around 30 kW, so we will always try to turbine at powers higher than 10 kW.

- Turbine at 10 kW: the water demand of the turbine operating at 10 kW is 220 mm water height in one hour that is 107992 litres of water.
- Turbine at 15 kW: the water demand of the turbine operating at 15 kW is 300 mm water height in one hour that is 147262 litres.
- Turbine at 20 kW: the water demand of the turbine operating at 20 kW is 370 mm of water per hour, which is equivalent to 181623 litres of water.
- Turbine at 25 kW: the turbine has a demand of 450 mm of water per hour, equivalent to 220893 litres of water.
- Turbine at 30 kW: in figure 8, it can be seen that at 30 kW the demand is 540 mm of water per hour, which is equal to 265072 litres of water.

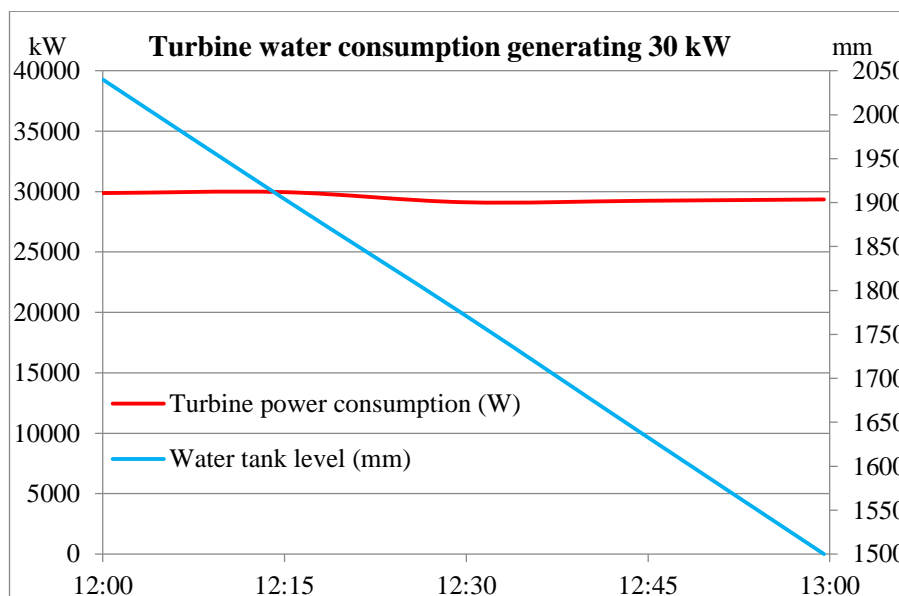


Fig. 8. Turbine demand graph at 30 kW.

If instead of data averaged over 15 minutes, we represent the instantaneous values, we get Figure 9.

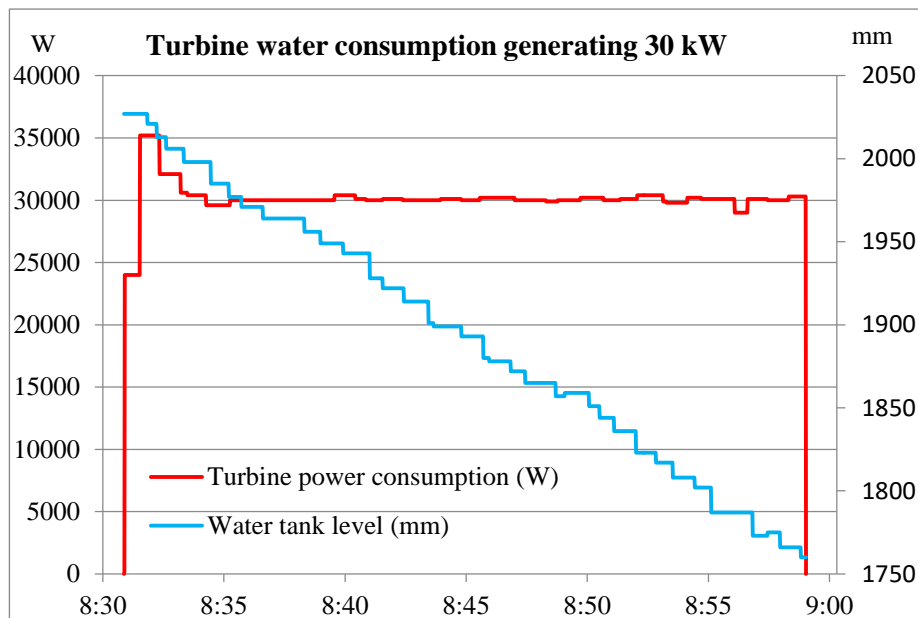


Fig. 9. Turbine demand graph at 30 kW. Instantaneous values.

Figure 9 shows how the turbine generates almost constantly at 30 kW for 30 minutes and the water tank level increases from 2030 mm high to 1760 mm, that is, it consumes 270 mm of water.

- Turbine at 35 kW: the water demand of the turbine operating at 35 kW is 700 mm per hour, that is, 343612 litres. Moreover, as it was at low power levels, it has difficulty in maintaining a constant and stable generation.
- Turbine at 40 kW: the behaviour is similar to the previous case, which means that there is no stable generation and the water demand is very high. Almost 900 mm of water is consumed per hour, which is equivalent to 441786 litres.

If we gather all these values in Figure 10, we can perfectly characterize the operation of the turbine.

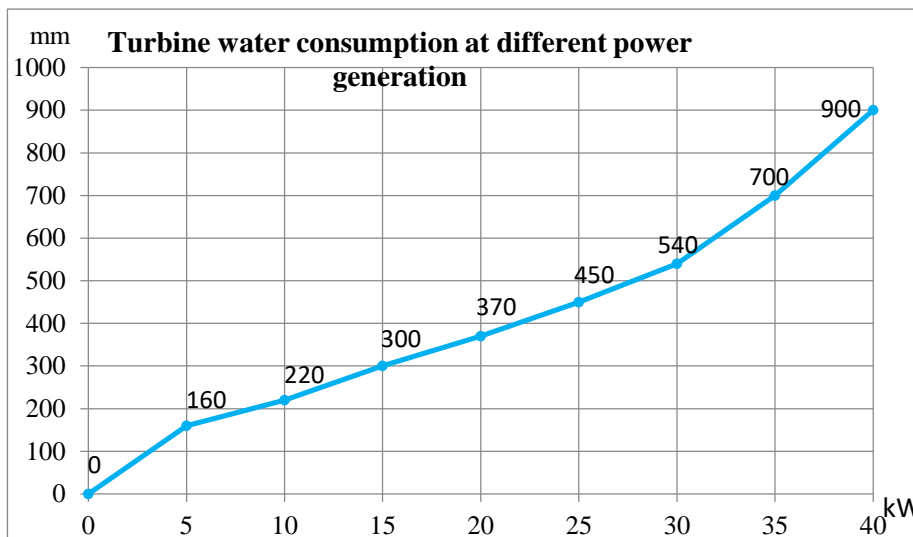


Fig. 10. Turbine demand-generation graph

In Figure 10 we can see how the amount of water consumed by the turbine increases in an almost linear way according to the power produced, up to 30 kW, and from then on the demand shoots up. Summarising the data for each power, we have:

Tabla. 1. Summary of turbine demand.

Power Generated (kW)	Water demand (mm/hour)	Water demand (litres/hour)	mm per kW
5	160	88357	32.0
10	220	117810	22.0
15	300	147262	20.0
20	370	181623	18.5
25	450	211076	18.0
30	540	265072	18.0
35	700	311705	20.0
40	900	441786	22.5

The lowest water demand per kW produced is in the 20-30 kW range, where only about 18 mm is needed for each kW of power generated by the turbine. Therefore, as far as possible, the turbine should ideally be operated in this power range.

4.2 Hydraulic pumping system

As was the case with the turbine, the hydraulic pumping system has also been used practically nothing before starting this work, so it is once again essential to carry out an initial characterisation task to define its operation.

In this case, it will be necessary to know the amount of water that the hydraulic pumps are capable of taking up to the upper tanks and their levels of electricity demand.

To characterize the hydraulic pumps, a series of tests have been carried out, similar to those carried out with the hydraulic turbine, but simpler, given that the demand of the pumps is practically constant, as can be seen in Table 2.

Table 2. Hydraulic pumping system demand.

Hour	Power demand (kW)	Pumped Water (mm height)	Pumped Water (litres)
12:00	23.58	11.20	5520
12:15	23.62	11.25	5522
12:30	23.77	11.18	5529
12:45	23.78	11.20	5530
13:00	22.29	11.15	5513
13:15	23.71	11.19	5528
13:30	23.76	11.25	5529
13:45	23.02	11.23	5498

Figure 11 shows the behaviour of one of the hydraulic pumps over three hours.

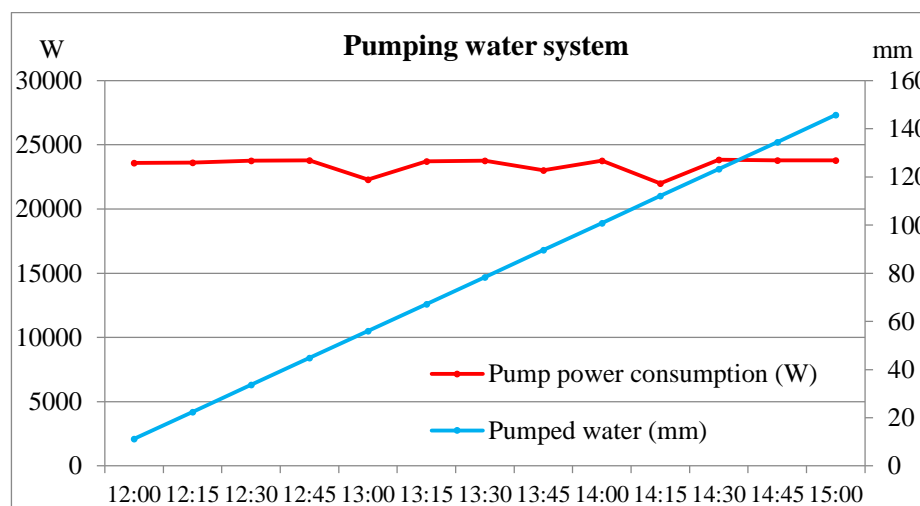


Fig. 11. Graphic of hydraulic pumping system (1 pump).

With this data, we can define the behaviour of the hydraulic pumping system which is shown in Table 3. The amount of water pumped every 15 minutes by each of the pumps is approximately 5520 litres, so in one hour 22100 litres are pumped up to the upper tanks and for this, the average demand of 23.69 kWh is required.

Table 3. Summary of hydraulic pumping system demand.

Power Demand (kW)	Pumped water (mm/hour)	Pumped water (litres/hour)	mm per kW
23.69	44.80	22100	1.89
47.41	89.70	44200	1.90

4.3 Efficiency of the hydraulic pump-turbine system

After an analysis of the data obtained from the pumping system and the turbine, we can determine the efficiency of the hydraulic pump-turbine system as a whole:

$$\eta = \frac{l_{pumped\ with\ 23,69\ kW}}{l_{consumed\ to\ generate\ 23,9\ kW}} = \frac{44,8\ mm}{426\ mm} = 0.105$$

The efficiency is 10.5%. This low efficiency is mainly due to the pumps used are not designed for this purpose but rather that some old pumps available at CEDER have been reused.

The demand of water for turbines indeed occurs at times of power demand by CEDER that could not be covered otherwise or a penalty would have to be paid to the electricity distribution company for the excess of the contracted power, while the pumping occurs in hours of excess power that if it were not pumped, would be given to the distribution company.

Another disadvantage of this pumping system is that since each pump consumes so much power in its operation, the surplus power needs to be very high for it to start and begin to store it. Thus, the monitoring that allows making the generation curve (see Figure 12 and Figure 13) is far from optimal.

For the first hydraulic pump to start there must be a surplus of 23 kW, and for both to start, there must be a surplus of more than 46 kW, which happens a few days a year on sunny summer days or with a lot of wind.

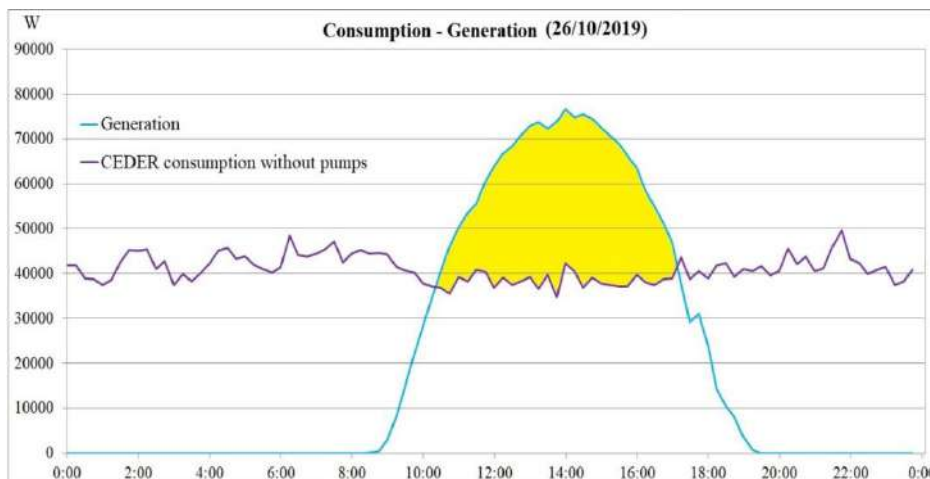


Fig. 12. Graph of power surplus in a day

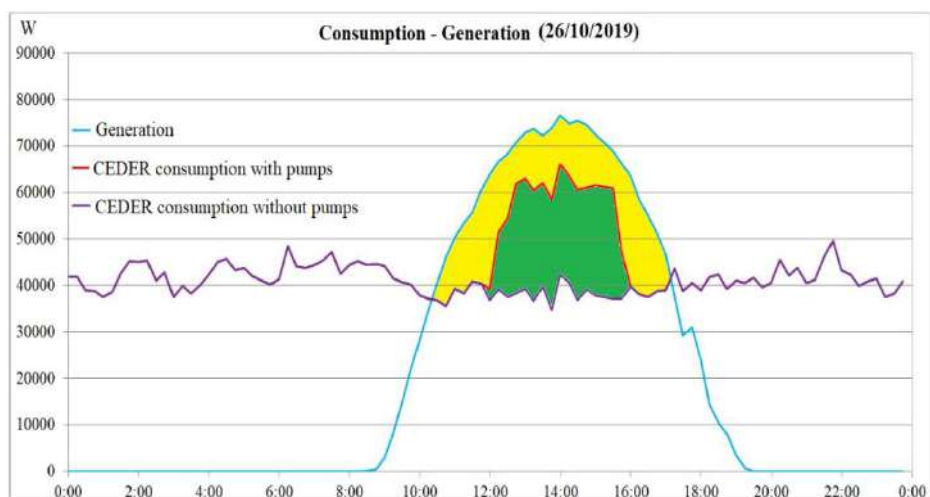


Fig. 13. Graph of stored power with pumping system

In Figure 12, the yellow area represents the power surplus of October 26, 2019, if the hydraulic pumps had been turned off since the production of CEDER's generation systems (blue line) is greater than its demand (purple line). Part of that power could be stored (as was done using the pumping system).

In Figure 13, we see the data from the same day (10/26/2019) but with the hydraulic pumps on to store the surplus power. The green area is the stored power (actually it is not the stored power, but the power spent by the pumps to bring water up to the upper tank) and the yellow area is the surplus power that could not be stored and therefore is injected into the distribution network.

As mentioned above, the fit between storage and generation is not very good, since a lot of surplus power is wasted as hydraulic pumps are very consumptive and cannot be started up except when there is a very high surplus power.

Moreover, as they are old hydraulic pumps, they cause many maintenance problems, water losses, etc. and the pumping system has to be stopped for a long time to solve them.

5 Characterization of the hydraulic pump-turbine system

After what was seen in the previous section, the first measure to be taken in this work is to replace the hydraulic pumping system formed by the two horizontal pumps of 23 kW each, with another system formed by four vertical hydraulic pumps of 7.5 kW each (see Figure 14) that are available in the centre after having dismantled an installation that was no longer in use.



Fig. 14. New pumping system

With this replacement several of the problems of the old pumping system are eliminated since the pumps are newer, so they give fewer maintenance problems; they are designed for a similar purpose to the one they are going to be used, not like the old ones and they consume a much lower amount of power so they can start longer periods and many more times, without the need of having a 23 kW surplus as we saw before with the old system. In Figure 15 and Figure 16 we see how the adjustment of storage and generation is much better with the new pumps than with the old ones.

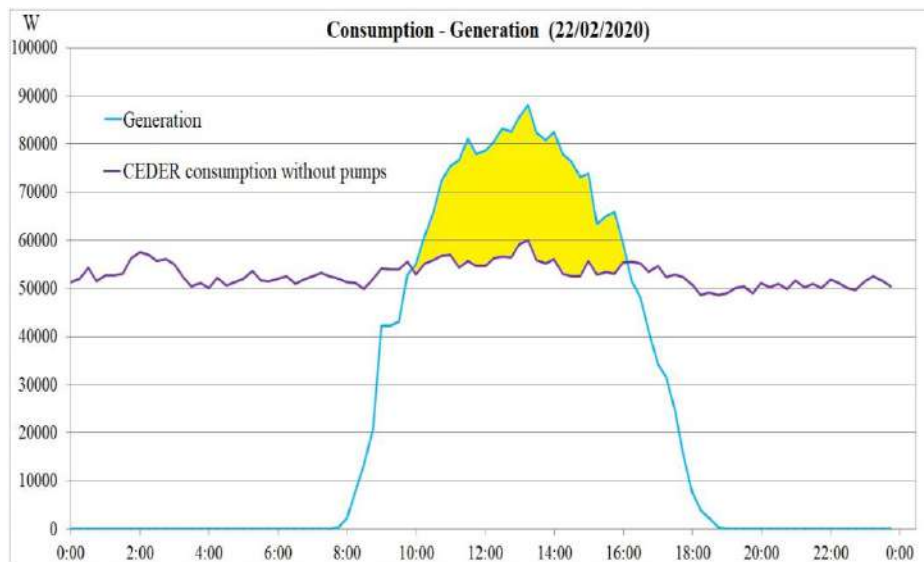


Fig. 15. Graph of power surplus in a day

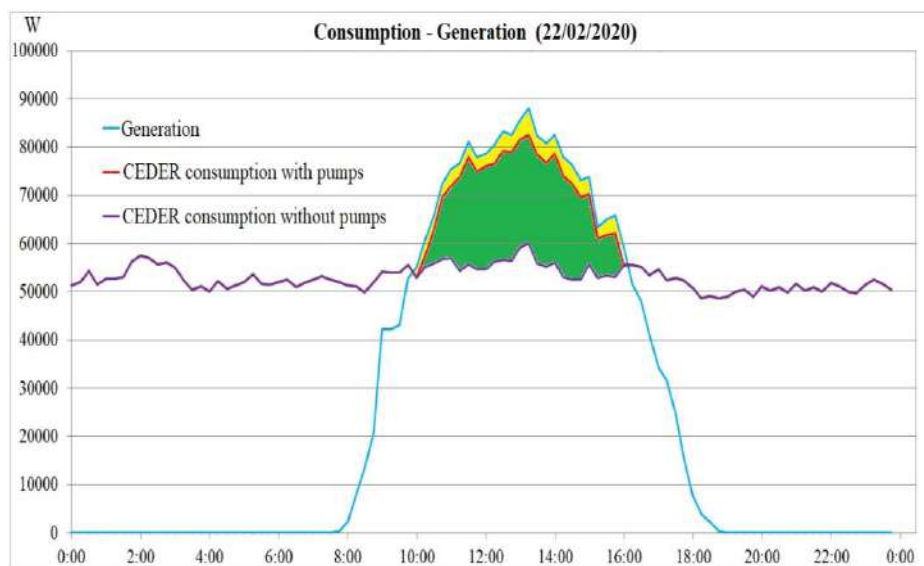


Fig. 16. Graph of stored power with the new pumping system

Once the pumps have been replaced, the pumping system must be re-characterized to know how it works (see Figure 17). It is summarized in Table 4.

Table 4. New pumping system demand.

Hour	Power demand (kW)	Pumped Water (mm)	Pumped Water (litres)
13:45	7.52	11.00	5399
14:00	7.49	11.03	5412
14:15	7.49	10.97	5387
14:30	7.51	11.01	5405
14:45	7.50	11.00	5399
15:00	7.51	11.01	5402

To see the joint efficiency of the reversible hydraulics we can compare the water raised to the upper tank using two pumps, which is equivalent to a demand of 15 kWh, with the water consumed by the turbine to produce the same power.

With two pumps in an hour 43308 litres of water are raised consuming 15 kWh, and water demand of the turbine for an hour producing 15 kW is 147262 litres.

$$\eta = \frac{E_{input}}{E_{consumed}} = \frac{43308}{147262} = 0.294$$

This gives us efficiency for the four-pump reversible hydraulic system of 29.4%, much higher than the 10.5% obtained with the old two-pump system.

6 Conclusions

In this paper, we have characterized the reversible hydraulics that is part of the CEDER smart microgrid and described the improvement of its efficiency by replacing a pumping system based on two horizontal pumps of 23 kW each, by another with four vertical pumps of 7.5 kW each.

By replacing the pumps, the efficiency of the hydraulic system has been improved from nearly 10% to over 29%, which means that three times less power is needed to pump the same amount of water to the upper tank and then to turbine it.

Besides, the new pumping system allows us to store much better the surplus of power by being much more modular, which allows us to go started up pumps as we have a surplus of power. The old system did not start up until the surplus was at least 23 kW, and all that power that could not be stored was wasted and injected into the distribution network. However, with the new system, power can be stored from 7.5 kW upwards, as the pumps start and stop depending on the surplus power to try and optimise the storage as shown in Figure 22.

References

1. H. Gharavi and R. Ghafurian, Smart grid: The electric energy system of the future, IEEE. 2011.
2. T. Sachs, A. Gründler, M. Rusic, and G. Fridgen, “Framing Microgrid Design from a Business and Information Systems Engineering Perspective,” *Bus. Inf. Syst. Eng.*, vol. 61, no. 6, pp. 729–744, Dec. 2019, doi: 10.1007/s12599-018-00573-0.
3. J. M. Aberilla, A. Gallego-Schmid, L. Stamford, and A. Azapagic, “Design and environmental sustainability assessment of small-scale off-grid energy systems for remote rural communities,” *Appl. Energy*, vol. 258, p. 114004, Jan. 2020, doi: 10.1016/J.APENERGY.2019.114004.
4. K. C. Divya and J. Østergaard, “Battery energy storage technology for power systems-An overview,” *Electric Power Systems Research*. 2009, doi: 10.1016/j.epr.2008.09.017.
5. S. Chandak, P. Bhowmik, and P. K. Rout, “Load shedding strategy coordinated with storage device and D-STATCOM to enhance the microgrid stability,” *Prot. Control Mod. Power Syst.*, 2019, doi: 10.1186/s41601-019-0138-0.
6. M. Guezgouz, J. Jurasz, B. Bekkouche, T. Ma, M. S. Javed, and A. Kies, “Optimal hybrid pumped hydro-battery storage scheme for off-grid renewable energy systems,” *Energy Convers. Manag.*, vol. 199, p. 112046, 2019, doi: <https://doi.org/10.1016/j.enconman.2019.112046>.
7. R. Lasseter et al., “The CERTS microgrid concept, white paper on integration of distributed energy resources,” *Calif. Energy Comm. Off. Power Technol. Dep. Energy*, LBNL-50829, <http://certs.lbl.gov>, p. 29, 2002.
8. A. Blakers, B. Lu, and M. Stocks, “100% renewable electricity in Australia,” *Energy*, vol. 133, pp. 471–482, Aug. 2017, doi: 10.1016/j.energy.2017.05.168.
9. C. Cheng, A. Blakers, M. Stocks, and B. Lu, “Pumped hydro energy storage and 100 % renewable electricity for East Asia,” *Glob. Energy Interconnect.*, vol. 2, no. 5, pp. 386–392, 2019, doi: <https://doi.org/10.1016/j.gloi.2019.11.013>.

Photovoltaic cell defect classifier: a model comparison

Álvaro Pérez-Romero¹[0000-0002-4292-6640], Luis Hernández-Callejo²[0000-0002-8822-2948], Sara Gallardo-Saavedra²[0000-0002-2834-5591], Víctor Alonso-Gómez²[0000-0001-5107-4892], María del Carmen Alonso-García³[0000-0002-4457-3551] and Héctor Felipe Mateo-Romero⁴[0000-0002-5569-3532]

¹ Universidad de Cantabria, Av. de los Castros, s/n, Santander 39005, Spain

² Universidad de Valladolid, Campus Universitario Duques de Soria, Soria 42004, Spain

³ Centro de Investigaciones Energéticas, Medioambientales y Tecnológicas (CIEMAT), Photovoltaic Solar Energy Unit, Energy Department, Madrid 28040, Spain

⁴ Universidad Politécnica de Madrid, Pº Juan XXIII 11, Madrid 28031, Spain

alvaro.pr470@gmail.com: A.P-R.; luis.hernandez.callejo@uva.es:

L.H-C.; s.gallardosaavedra@gmail.com: S.G-S.;

victor.alonso.gomez@uva.es: V.A-G.; carmen.alonso@ciemat.es:

M.C.A-G.; thehfmr2011@gmail.com: H.F.M-R.

Abstract. Advanced operation and maintenance of solar photovoltaic (*PV*) plants are necessary. With regard to maintenance, having defective cell sorting tools is important today. This work presents a methodology for the selection of variables important for the training of a defective cell classifier. To do this, the authors propose different classifiers and analyze their results, using electroluminescence images and I-V curves, at the level of a *PV* solar cell. In order to carry out the study, the authors use a *PV* solar module with accessible cells, in order to obtain I-V curves for each of the cells.

Keywords: photovoltaic cell defect, classifier, artificial intelligence.

1 Introduction

Renewable generation plants are being installed in the last decade. Among the renewables, photovoltaic (*PV*) solar plants are the most interesting in recent years, and it seems that they will be the most installed in the following years [1, 2].

The operation and maintenance (*O&M*) of *PV* solar plants are critical for industry players. The development of new equipment and methodologies for its application in *PV* solar plants are necessary, and in this sense, research and industry are evolving rapidly [3].

Some researchers have worked with real data from *PV* solar plants, and they have obtained important results of defects in them [4]. The *PV* inverter is a critical element in *PV* solar plants, but so is the *PV* solar module. A *PV* solar module is made up of *PV* solar cells, and these cells can present different problems or defects, as shown in the work presented in [5]. Although the knowledge at the *PV* solar cell level is interesting

for operators and maintainers of *PV* solar plants, the measurement level should be in the *PV* solar module.

The detection of faults in *PV* solar modules is subject to obtaining field data. The data obtained can be I-V curves, both from the *PV* solar cell (when the cell contacts can be accessed) or at the *PV* solar module level [5, 6].

Another way to obtain field data is by taking images. Classically, thermographic imaging (*IRT*) has been used for early detection of hot spots [7], and in recent years this *IRT* method has been carried out using drone flight [8, 9].

Artificial Intelligence (*AI*) is being applied in *PV* solar plants. *AI* application has long focused on energy production forecasting issues [10]. Some authors present a taxonomy study, which is a process to divide and classify the different forecasting methods, and the authors also present the trends in *AI* applied to generation forecasting in solar *PV* plants [11]. The use of artificial neural networks (*ANN*) has been successful in the last decade, some authors use *ANN* together with climatic variables to forecast generation in *PV* solar plants [12], while others use support vector machine (*SVM*) together with an optimization of the internal parameters of the model [13].

ANN have also been used for other tasks, such as for the detection of problems in energy production, as is the case of work [14], where the authors use radial basis function (*RBF*) to detect this type of failure in production. A similar goal is sought in [15], where this time an *SVM*-based model is employed.

Therefore, it is possible to affirm that the use of *AI* is common in *PV* solar plants. In this work, the authors present a comparison between *AI*-based models to classify *PV* solar cells. For this, the authors have a *PV* solar module manufactured in a special way, since *PV* solar cells have their back contacts accessible, with which their total characterization is possible [5]. With this situation, it is possible to have images (electroluminescence, *EL*) and their I-V curve, so it is feasible to label each cell (group 1: good, group 2: fair and group 3: bad) based on its production efficiency. The work makes a comparison between models to classify *PV* solar cells. The study is novel, since the cells are labeled based on their production efficiency, and this has been made possible thanks to the customized *PV* solar module. The document is as follows: section 2 presents the materials and methodology used, section 3 shows the results and section 4 deals the conclusions and future work.

2 Materials and methodology

This section is intended to explain the materials used, as well as the methodology followed to validate the classifier.

2.1 Materials

It has been used a 60-cells polycrystalline module composed of cells with and without defects. The front and back views of the module are presented in Figure 1, a) and b) respectively. The module has been ad-hoc manufactured with all cells accessible

from the backside of the module. Regarding the cell numbering, it has been used numbers from 0 to 59 to identify the cell, as detailed in Figure 2.

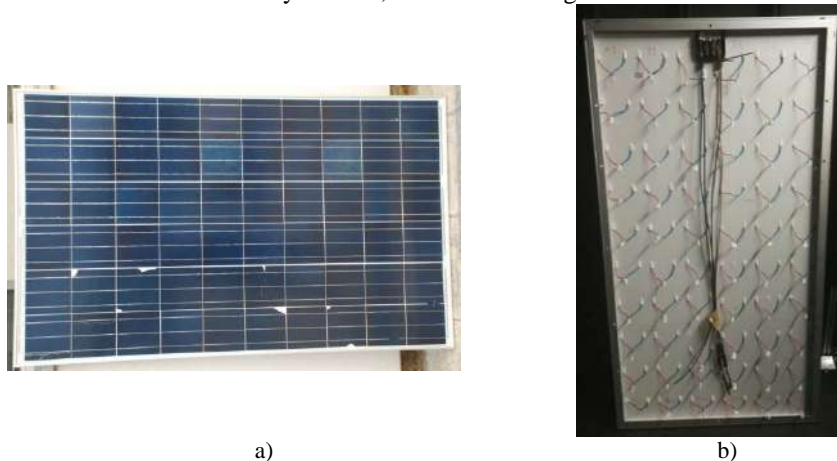


Figure 1. a) Front view of the module. b) Back view of the module.

The first string (first and second columns in the back view) contains manufacturing defects, the central string (third and fourth columns) contains soldering faults while the third string (fifth and sixth columns in the back view) contains breaking deficiencies. The low efficiency defects (cells 1 and 4) are due to manufacturing problems, but they do not correspond with breaking or short-circuited cells. Short-circuit cell (cell 6) has been generated by extending the cell connection tabs beyond the ordinary placement, short-circuiting the cell. In order to simulate the bad soldering defects, buses from the back of some cells have been left without soldering, either one bus (cell 22) or two buses (cell 34). Three buses have not been left without soldering in any case as it would have meant that this cell would not be series connected to the rest. The cell with only 1cm welded (cell 27) simulates a bad soldering, in which only 1 cm of the bus is welded instead of the typical 15 cm welded. When a piece of broken cell is placed on top of another cell (cells 49, 58 and 59), what it really generates is a partial shading. It could simulate an important permanent bird crap. These types of defects are analyzed as they ordinarily appear in commercial modules in operation, either in manufacturing, transport or operation. However, commercial modules are not accessible at the cell level. That is why an ad hoc module has been manufactured for the defects characterization.

The nominal characteristics of a standard module of this type are: nominal power (P) 250 W, efficiency 15.35%, maximum power point current (I_{mpp}) 8.45 A, maximum power point voltage (V_{mpp}) 29.53 V, short circuit current (I_{sc}) 8.91 A and open circuit voltage (V_{oc}) 37.6 V. Having 60 cells in series, the nominal values of a healthy cell have been considered: nominal power 4.17 W, I_{mpp} 8.45 A, V_{mpp} 0.49 V, I_{sc} 8.91 A and V_{oc} 0.63 V.

Table 1. Cells defects types and location per string.

String	Defect	Cell
First String – Manufacturing defects	Low efficiency cell (9% approx.)	1, 4
	Medium efficiency cell (16.4% approx.)	14, 17
	Short-circuited cell	6
Central String – Soldering defects	One bus without soldering	22
	Two buses without soldering	34
	Only 1cm of each bus welded	27
	All tabs loose (without soldering)	38
Third String– Breaking defects	Split cell (without cell area decrease)	50, 51
	Cracked cell (with cell area decrease)	41, 42, 55, 57
	Defects B-1 and B-2 in the same cell	45
	Piece of other broken cell over the cell surface	49, 58, 59

I-V curve measurement (at the cell level) and EL images have been carried out at CIEMAT’s facilities (Madrid, Spain). In summary, the facilities used are the following:

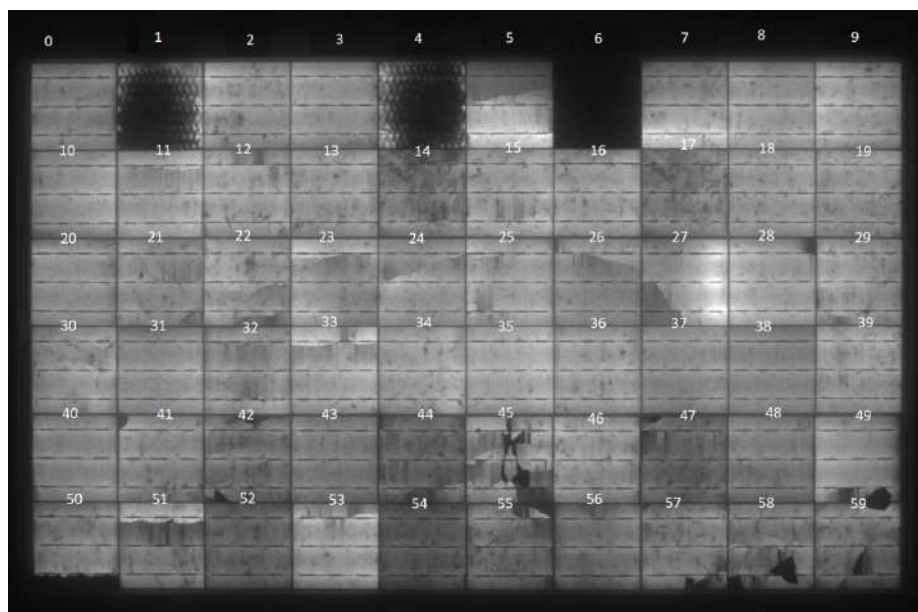
- The indoor measurements have been performed in the commercial system Pasan SunSim 3CM, that consists of a light pulse solar simulator class AAA according to IEC 60904-9 standard, which can perform I-V curve measurements at Standard Test conditions.
- The *EL* and indoor *IRT* tests simultaneously to the *EL* have also been taken in this chamber. The module is fed with a Delta power supply SM 70-22. A Fluke 189 multimeter connected to module terminals allow to register the exact module voltage. *EL* and *IR* images are captured with a PCO 1300 and a FLIR SC 640 camera, respectively.

In this way, the information of the *EL* image and I-V curve of each *PV* solar cell is obtained. This information will serve to validate the different models. In the training phase, the cells used will be labeled (group 1: good, group 2: fair and group 3: bad) according to the information obtained from their I-V curve, as explained in the following section.

2.2 Methodology

Since the *EL* image is taken from the entire module, the first thing is to cut out the cells, in order to have them individually. For this, a 115x115 pixel cropping window has been established, which has offered the best adjustment by superimposing it on each cell. It is necessary to zoom to the maximum to adjust the window optimally, thus ensuring that all the cropped images are aligned, and thus avoid including the black margins that separate (due to the natural structure of the panel) the cells. After that, with the objective of improving the edges, the images have been loaded in Python reducing each side by 1 pixel, finally resulting in 60 images of size 113x113.

Now, given the classification proposed in the work, in which the cells were grouped according to the power measured individually in each one, it is not possible to appreciate visible features (see Figure 2) that characterized the elements of the different groups, except perhaps the black spots in group 3.



Solar cells are classified as follows:

Group 1: 0,2,3,5,7,8,9,10,11,12,13,15,16,18,19,20,21,22,23,24,25,28,30,31,33,53

Group 2: 14,17,26,27,29,32,34,35,36,37,38,39,40,41,42,43,44,46,47,48,51,52,54,55,56,57,58

Group 3: 1,4,6,45,49,50,59

Figure 2. EL image and cell numbering for model training. Association of cells with each of the 3 groups.

Regarding the groups, the cells have been labeled according to their potency (measured through the I-V curve) and with the following criteria:

- Group 1: Power $\geq 95\%$.
- Group 2: $80\% \leq \text{Power} < 95\%$.
- Group 3: Power $< 80\%$.

To demonstrate the correctness of this classification, the authors have proposed using Self-Organizing Maps (*SOM*) to be able to observe the similarities detected between cells. *SOM* are a type of unsupervised neural network, and its purpose is to reduce the dimensionality of the data, as well as to preserve the topological properties of these [16]. It is made up of only 2 layers, the input and the output. The input layer has a number N of neurons equivalent to the dimension of the data. The output layer represents a two-dimensional array of neurons, each with an assigned N -dimension weight.

Each time the *SOM* map algorithm is executed, the weights are randomly initialized (once initialized, they are organized and distributed on the map based on their proximity) and compete with each other each time a data is entered in the input layer. The neuron whose weight most closely resembles the input information is the winner, which causes an update in the value of its weight, as well as that of its neighbors. Therefore, the algorithm consists of iterating enough times and each time choosing a random data in the training sample in order to progressively update the map until it is molded to the structure of the starting information. Furthermore, to study the similarity between the data, the Euclidean distance is used as the standard distance. In this study, a *SOM* network of 20 rows and 20 columns has been proposed, and the results will be shown in the results section.

Therefore, it has been necessary to decide which variables are the representative ones of the 60 members. Each image (in grayscale) is a matrix of 113 rows by 113 columns, where each coordinate or pixel takes values from 0 (black) to 255 (white). Therefore, each one has 12,769 pixels that take 256 possible values. From this information, 28 variable candidates have been calculated, thus obtaining a DataSet (D) of 60 rows by 30 columns, according to the procedure observed in Figure 3.

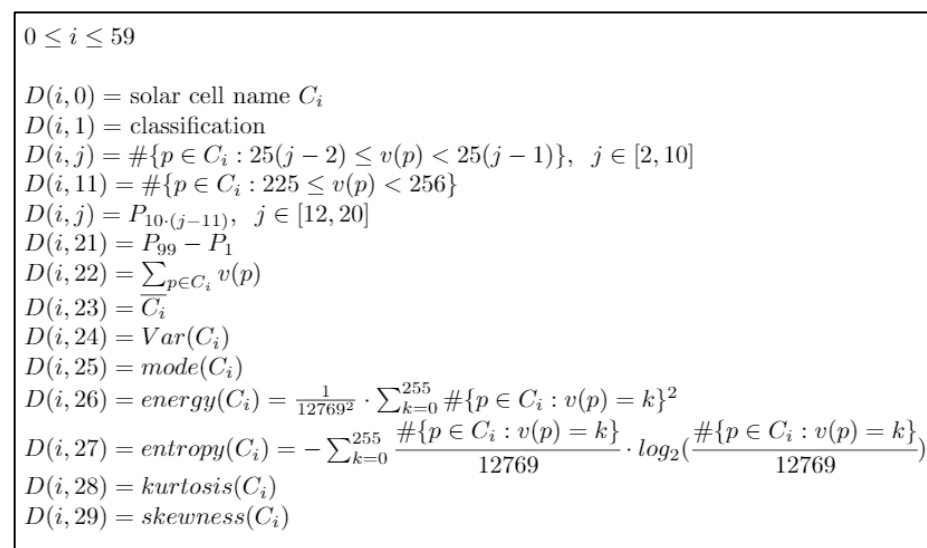


Figure 3. Pseudocode of the procedure for selecting the most significant variables.

Within the set of variables, the first 10 represented the number of pixels with values comprised in bands of length 25, except for the tenth variable that represented the number of pixels between 225 and 255. The next 9 variables represented 9 percentiles that ranged from the 10th percentile to the 90th percentile. The last 9 represented the range, the global sum of the 12769 pixels, the mean, the variance, the mode, the energy, the entropy, the kurtosis and the statistical skewness.

Before deciding the variables with which to start the study, some requirements that influence their choice must be taken into account. On the one hand, it has been sought to obtain the best global results, but it has been also tried to minimize the error in the classification of the elements related to group 3, that is, to avoid classifying elements from group 1 or 2 into group 3 and, vice versa. Furthermore, there is the possibility that there is more than one variable that returns similar values for cells of opposite groups, and therefore causes noise in the information. The above has been taken into account.

Given the difficulty of knowing which variables offer optimal results, the chosen strategy (previously standardizing all the data in mean 0 and variance 1) has consisted of repeating the method proposed in Figure 4 successively. For this, 55 random cells are chosen 20,000 times, as detailed in the following Figure 4.

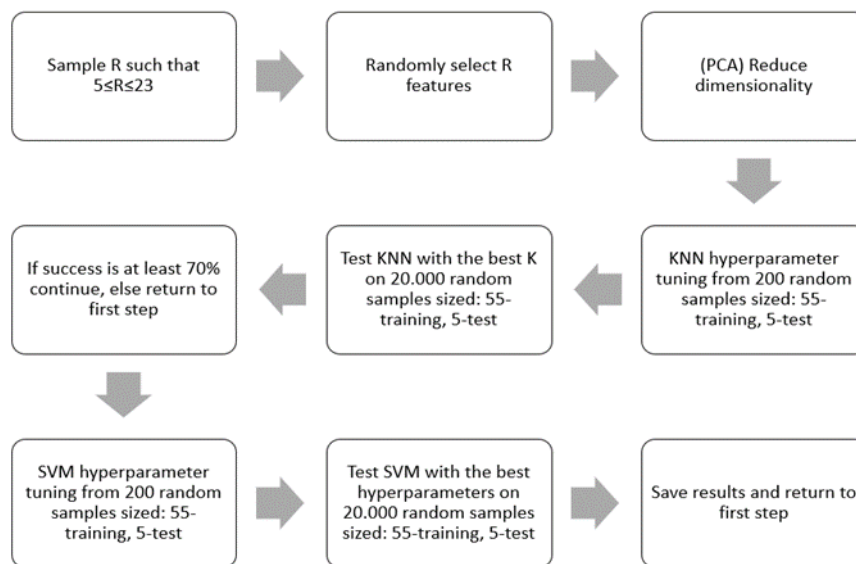


Figure 4. Proposed methodology for the selection of main variables.

Next, the method is explained:

1. A random number R is obtained between 5 and 23. Next, R variables are chosen at random from among the 28 possible ones.
2. Subsequently, principal component analysis is applied, saving the first variables that explain more than 99.5% of the variance of the data. Therefore, from now on, we work with 60 individuals explained in at most R new variables.
3. The next step is to apply k-nearest neighbors (*knn*). As we are interested in obtaining a good classification, the optimal number of neighbors *k* is sought, choosing between 1 and 10, starting from the one that offers the best results when applied in 200 random samples of size 55-training, 5-test. Once *k* has been obtained, the percentage of success with *knn* is now estimated from 20,000 random samples of size 55-training, 5-test. Finally, the

- proportion of bad classifications related to group 3 is noted. If the percentage of success with *knn* is less strict than 70%, step 1 becomes.
4. Now, exceeding 70% of success with *knn*, Support Vector Machines (*SVM*) is applied taking into account the following parameters:
 - a. Core: function in charge of transporting the data to a higher dimension where a better separation of the same can be achieved. Sigmoidal, polynomial, Gaussian and linear core are taken into account for the experiment.
 - b. Penalty parameter C: it is an indicator of the error that one is willing to tolerate. The values for C of 10, 50, 75 and 100 are taken into account for the experiment.
 - c. Gamma: indicates how far the points are taken into account when drawing up the separating boundary. The gamma values of 1, 0.8, 0.6, 0.4, 0.1, 0.01 and 0.001 are taken into account for the experiment.
 - d. Degree: degree of the function in the polynomial nucleus. Grades 1, 2, 3 and 4 are taken into account for the experiment.
 5. Based on these parameters, a search is made among all the possible combinations which one of them offers the best results applied to 200 random samples of size 55-training, 5-test. In Python there is a command called *GridSearchCV* that performs the above task.
 6. Once the ideal combination has been obtained, the efficacy of *SVM* is estimated running based on these parameters and applied to 20,000 random samples of size 55-training, 5-test. Hit and misclassification ratios related to group 3 are saved.
 7. Back to step 1.

For a sufficiently wide data collection, it has been necessary to run the previous process in Python for around 40 hours to obtain 1800 iterations, of which 250 corresponded to those cases where *knn* and *SVM* were calculated at the same time.

The number of data available is 60 (number of cells), which supposes very little information with which to carry out the study. This has influenced the search for the best parameters for *knn* and *SVM*, since *Cross Validation* has not been applied (the best parameters would hardly be obtained). Instead, a search based on 200 random samples of size 55-train, 5-test has been applied. However, an associated problem consists of the possibility of an undesirable phenomenon occurring within the world of machine learning such as *overfitting*, which is, obtaining a model that offers good results for the training data but bad results when applying unknown data.

Once the representative variables have been selected, then it has been made groups of 55 cells again to train each model and it has been validated with the 5 remaining cells in each case. The classifiers to be tested have been the following: *knn*, *SVM*, Random Forests (*RF*) and Multilayer Perceptron (*MLP*). These models have been chosen and compared, since they are the most used in classification [17–19].

Each classifier in *RF* has been built based on 500 trees. Additionally, *hyperparameter tuning* has been applied combining the following parameters:

1. **Maximum depth:** represents the maximum number of levels allowed in each decision tree. The values 20, 40, 60, 80 and 100 are taken into account.
2. **Minimum points per node:** this is the minimum number of data allowed in each partition. The values 1, 2, 3, 4 and 5 are taken into account.
3. **Maximum variables:** indicates the maximum number of variables (chosen at random) that are taken into consideration when partitioning a node. Usually \sqrt{n} is used as a standard parameter, where n is the number of total variables, but $\sqrt{n-1}$, \sqrt{n} and $\sqrt{n+1}$ are taken into account.

In the case of *MLP*, it has been built from an input layer made up of 7 neurons (coinciding with the dimensionality of the data), a first input layer made up of 128 neurons, a second hidden layer made up of 64 neurons and an output layer made up of only 3 neurons (matching the number of classifications). The neural network created is dense, that is, a network formed by neurons that are each connected to all possible neurons belonging to contiguous layers. The activator used in the process was the rectifier or *ReLU* activator, except in the last layer where the *softmax* function was used. In addition, *hyperparameter tuning* has been applied taking into account the following parameters:

1. **Epochs:** indicates the number of times that the neural network reads the data from the training sample in order to adjust to them (translated into a successive update of its parameters). The values 25, 50, 75, 100, 150 and 200 are taken into account.
2. **Batches:** indicates the speed with which the network parameters are updated as the epochs progress. The values 15, 25, 50, 75, 100, 150 and 200 are taken into account.

For the validation of the different models and obtaining the results, the methodology used with each of the 4 classifiers has been shown in Figure 5.

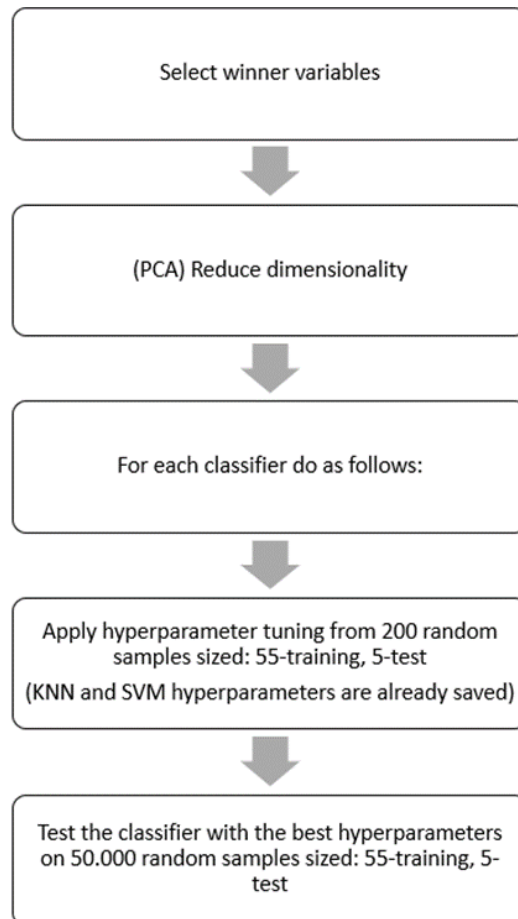


Figure 5. Methodology used with each of the 4 classifiers.

3 Results

3.1 Justification of the correct initial power rating

As already mentioned, *SOM* has been used to have some idea of whether the power classification has been correct.

Next, Figure 6 shows 4 maps obtained taking into account variables 5, 6, 9, 11, 14, 18, 20, 21 and 25 in the data. Each pixel represents one of the 400 possible output neurons. Nearby pixels with dark values reflect proximity to each other, while nearby pixels with contrast between light and dark represent distance. The elements of group 1 are represented in red, the elements of group 2 in green and the elements of group 3 in blue.

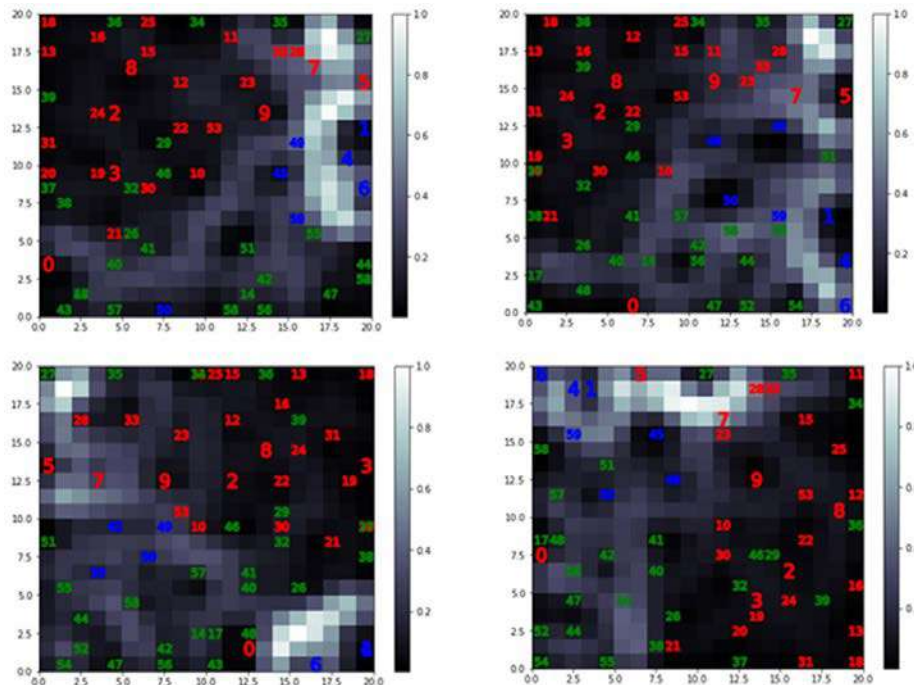


Figure 6. Result when applying SOM to the available data.

Observing the results it was possible to determine the existence of a certain grouping between the elements of the same color, and therefore of the same group. It is possible to conclude that the classification based on power was correct. Within group 3, it is deduced by the white border that the cells that are most distinguished from the rest of the groups are number 1, 4 and 6. Furthermore, comparing group 1 and 2 it can be concluded that it is easier to make a mistake when classifying cells from group 2 (green) in group 1 (red) than otherwise. This is due to the fact that some green points are mixed within the main mass of red points, which does not happen in the green group, where its elements have hardly any red elements inside them, except for element 0. Similarly, to Classifying elements of group 3 is possible to make a certain mistake, and they are identified as elements of group 2, or vice versa, due to their greater closeness (compared to group 1). This can be verified by observing the results of the classifications, which will be shown later.

3.2 Classification of variables

As already mentioned, the detection of the most important variables for the training of the models is crucial. To do this, it was necessary to run the previous process in Python for 40 hours to obtain 1800 iterations, of which 250 iterations correspond to those cases where *knn* and *SVM* were calculated at the same time.

Next, Figure 7 shows the best results obtained according to different criteria, such as the success in the classification with *knn* and *SVM* (columns 1 and 2), and proportion of bad classifications caused between groups 1 and 2 with respect to group 3, using *knn* and *SVM* respectively (columns 4 and 5). Therefore, the value 0.9331 in row 5 and column 5 is interpreted by associating 93.331% to the percentage of bad classifications (applying *SVM* with the indicated variables) that are not related to group 3, to which only 6.669% would correspond. Therefore, a high proportion represents a smaller error in the classification of elements related to group 3. The third column is the sum of the fourth and fifth columns. When observing the results, it can be concluded that variables 3, 5 and 11 are important.

	KNN success	SVM success	KNN+SVM success on group 3	KNN success on group 3	SVM success on group 3	variables
top 1 KNN success	0.745	0.756	1.425	0.734	0.691	3 5 6 8 11 14 17 18 23
top 1 SVM success	0.7077	0.7628	1.5973	0.6975	0.8998	5 6 9 11 14 18 20 21 25
top 1 KNN+SVM success on group 3	0.7005	0.7187	1.7646	0.9093	0.8552	3 5 7 9 11 21 24 25
top 1 KNN success on group 3	0.7005	0.7187	1.7646	0.9093	0.8552	3 5 7 9 11 21 24 25
top 1 SVM success on group 3	0.7099	0.7401	1.6371	0.704	0.9331	3 5 6 8 9 10 11 13 16 17 18 19 20 21 22

Figure 7. Relationship between success in classification and variables used.

In addition, Figure 8 shows the frequency of appearance of each of the 28 variables in all the iterations (1800 in total), based on 2 criteria: success with *knn* greater than 68.5% (75th percentile); proportion of bad classifications not related to group 3 higher than 79.4% (85th percentile). Observing both graphs it can be deduced that the good candidate variables are 3, 5, 6 and 8 (left figure) and the bad candidate variables are 2, 4, 7, 27, 28 and 29 (left figure). While the good candidate variables are 3, 5, 7, 24 and 29 (right figure) and the bad candidate variables are 2, 8, 26 and 28 (right figure). Comparing these results with those obtained in Figure 7, it is possible to conclude that there is a relationship between the importance of a variable and its proportion obtained in the graph.

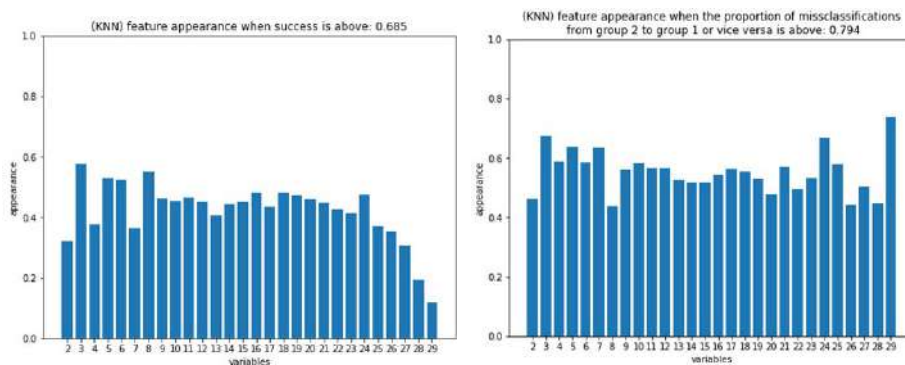


Figure 8. Frequency of appearance of each of the 28 variables in all the iterations for *knn*.

The same type of graphs have been obtained for *SVM* (Figure 9). However, it is possible that given the low number of iterations (250), the results are not entirely reliable.

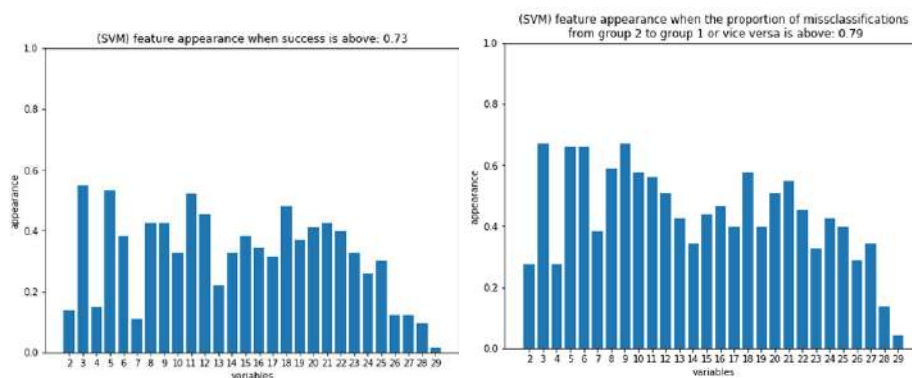


Figure 9. Frequency of appearance of each of the 28 variables in all the iterations for *SVM*.

3.3 Convergence and results of the models

An important aspect when working with AI is the convergence of the model. Next, Figure 10 shows the behavior of the hit obtained with each of the 4 classifiers, depending on the number of iterations performed. In the case of *MLP*, 50,000 iterations were not reached due to the high computational cost, although there was no loss of efficiency, as is well observed in all models, since there is some convergence in a lower number of iterations.

Table 2 shows the results (percentage of success) of the 4 models used, once the cells used for the validation phase are classified. The time (hours) required are also shown. With regard to time, the first column of times shows the time needed to locate the ideal parameters (*hyperparameter tuning*), while the second column of times indicates the time needed for the classifier training.

From the above results, the most successful model is *SVM*, closely followed by *MLP* and *RF*. The worst result is obtained by *knn*, however, the success rate is 70.61%, and it is possible to consider it as a high value.

Regarding the time spent in locating the main parameters, the fastest model is *knn*, then *SVM* follows, and with a time close to 1 hour is *MLF*. *RF* presents the worst time to locate these parameters, being necessary more than 2 hours.

Regarding the time spent for training, *SVM* is the fastest, closely followed by *knn*. At the other extreme, *RF* takes almost 9 hours, while the slowest model is *MLP*.

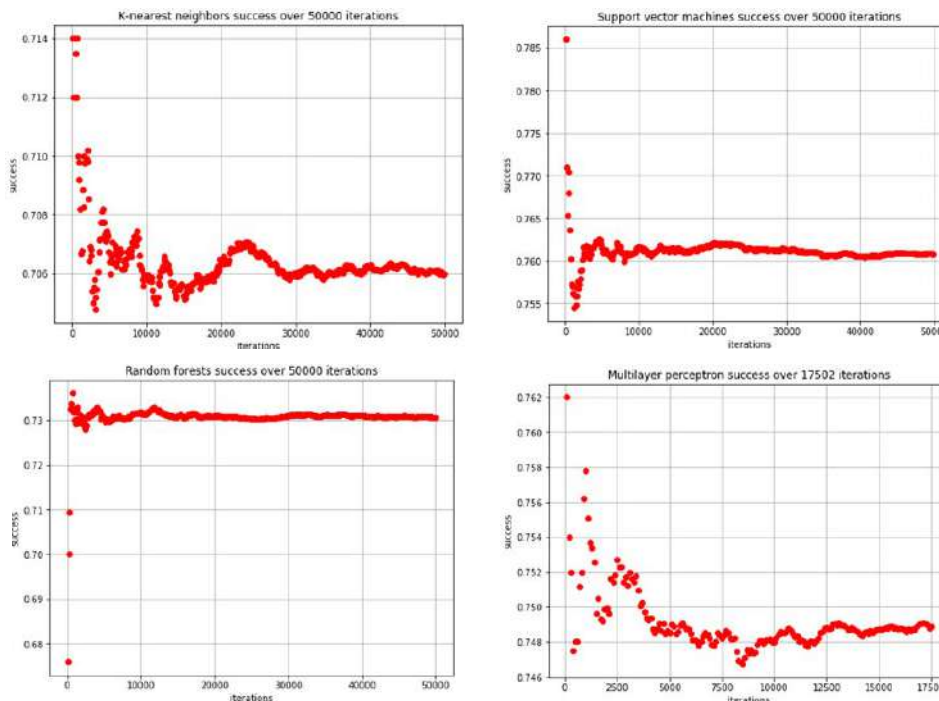


Figure 10. Comparison of classification success versus the number of iterations for the 4 models.

Table 2. Classification results in the 4 models.

	Classification success	Time spent on hyperparameter tuning (hr)	Time spent testing 50,000 (17,502 with MLP) samples (hr)
KNN	0.7061	0.0017	0.0267
SVM	0.7607	0.0223	0.0196
RF	0.7308	2.1552	8.8071
MLP	0.7488	0.9633	15.5442

Therefore, and in summary, *SVM* is the model that presents the highest efficiency (76.07%), and it is the model with reasonably lower times (search for parameters and training).

One of the main goals of sorting is to detect bad cells (group 3). In this sense, Table 3 shows the results of the classification of cells in group 3. In the same way, Table 3 shows the results of the misclassification between groups.

Table 3. Group 3 classification results, and results of misclassification between groups

	Success on group 3	1 miss-classified as 2	1 miss-classified as 3	2 miss-classified as 1	2 miss-classified as 3	3 miss-classified as 1	3 miss-classified as 2
KNN	0.7002	0.1017	0	0.5985	0.0117	0.0579	0.2302
SVM	0.9055	0.1377	0.0077	0.7678	0.0142	0.0044	0.0752
RF	0.7746	0.2525	0	0.5221	0.0142	0.0173	0.1939
MLP	0.8224	0.2166	0.0018	0.6058	0.0687	0.0073	0.0998

Focusing only on the classification of group 3, *SVM* obtains success results of 90.55%, while *MLP* obtains 82.24%, *RF* obtains 77.46% and the worst result is for *knn* with 70.02%.

It can also be observed that there is hardly any confusion between cells of group 1 with group 3, or cells of group 2 with group 3. In the first case, *knn* and *RF* do not present confusion (0%), while *SVM* and *MLP* present 0.77% and 0.18% respectively. In the second case, *knn*, *RF* and *SVM* present a value below 1.5%, and *MLP* 6.87%.

Greater confusion appears between groups 1 and 2. As can be seen, the misclassification of cells in group 1 as group 2 varies between 10.17% for *knn* and 25.25% for *RF*. Group 2 to group 1 varies between 52.21% for *RF* and 76.78% for *SVM*. This high confusion is due to the similarity between some cells, as can be seen in Figure 6.

4 Conclusions and future work

The work has presented different *PV* solar cell defect classifiers, using different classifier models. For all cases, the results have been optimal, and the classification has been carried out based on electroluminescence images and I-V curve, all of them at the level of a *PV* solar cell.

The classifier's biggest hit has been for bad *PV* solar cells. Furthermore, this group of cells is the one of greatest interest, since it is the group that contains cells with almost zero electrical production.

The work also presents the method to be used to select the variables of interest, which will serve to train the different models of the classifiers. This process is essential, since the use of variables without relevance can cause noise in training, and the consequent obtaining of bad results in the classification.

The study has focused on *PV* solar cells from a single *PV* solar module. The authors will extend this work, applying the classification to *PV* solar cells of other modules, but always of the same model of *PV* solar module.

The authors will also test thermography image-based classifiers, and thermography and *EL* image classifiers together. This work is interesting, since it is known that both techniques are complementary in certain aspects.

Another application of *AI*, and that these authors are going to develop, is the estimation of the I-V curve from *EL* images and *IRT*, this time at the level of the *PV* solar module.

Acknowledgments

The authors thank the CYTED Thematic Network “INTELLIGENT CITIES FULLY INTEGRAL, EFFICIENT AND SUSTAINABLE (CITIES)” n° 518RT0558. This work has been supported by Spanish national project [RTC-2017-6712-3] of the Spanish Ministry of Science.

References

1. Scholten, D., Bazilian, M., Overland, I., Westphal, K.: The geopolitics of renewables: New board, new game. *Energy Policy*. 138, 111059 (2020). <https://doi.org/10.1016/j.enpol.2019.111059>.
2. Gugler, K., Haxhimusa, A., Liebensteiner, M., Schindler, N.: Investment opportunities, uncertainty, and renewables in European electricity markets. *Energy Econ.* 85, 104575 (2020). <https://doi.org/10.1016/j.eneco.2019.104575>.
3. Hernández-Callejo, L., Gallardo-Saavedra, S., Alonso-Gómez, V.: A review of photovoltaic systems: Design, operation and maintenance. *Sol. Energy*. 188, 426–440 (2019). <https://doi.org/10.1016/j.solener.2019.06.017>.
4. Gallardo-Saavedra, S., Hernández-Callejo, L., Duque-Pérez, O.: Quantitative failure rates and modes analysis in photovoltaic plants. *Energy*. 183, 825–836 (2019). <https://doi.org/10.1016/j.energy.2019.06.185>.
5. Gallardo-Saavedra, S., Hernández-Callejo, L., Alonso-García, M. del C., Santos, J.D., Morales-Aragónés, J.I., Alonso-Gómez, V., Moretón-Fernández, Á., González-Rebollo, M.Á., Martínez-Sacristán, O.: Nondestructive characterization of solar PV cells defects by means of electroluminescence, infrared thermography, I–V curves and visual tests: Experimental study and comparison. *Energy*. 205, (2020). <https://doi.org/10.1016/j.energy.2020.117930>.
6. Blakesley, J.C., Castro, F.A., Koutsourakis, G., Laudani, A., Lozito, G.M., Riganti Fulginei, F.: Towards non-destructive individual cell I-V characteristic curve extraction from photovoltaic module measurements. *Sol. Energy*. 202, 342–357 (2020). <https://doi.org/10.1016/j.solener.2020.03.082>.
7. Jordan, D.C., Silverman, T.J., Wohlgemuth, J.H., Kurtz, S.R., VanSant, K.T.: Photovoltaic failure and degradation modes. *Prog. Photovoltaics Res. Appl.* 25, 318–326 (2017). <https://doi.org/10.1002/pip.2866>.
8. Gallardo-Saavedra, S., Hernández-Callejo, L., Duque-Pérez, O.: Technological review of the instrumentation used in aerial thermographic inspection of photovoltaic plants. *Renew. Sustain. Energy Rev.* 93, 566–579 (2018). <https://doi.org/10.1016/j.rser.2018.05.027>.
9. Gallardo-Saavedra, S., Hernandez-Callejo, L., Duque-Perez, O.: Image resolution influence in aerial thermographic inspections of photovoltaic plants. *IEEE Trans. Ind.*

- Informatics. 14, 5678–5686 (2018). <https://doi.org/10.1109/TII.2018.2865403>.
10. Gligor, A., Dumitru, C.D., Grif, H.S.: Artificial intelligence solution for managing a photovoltaic energy production unit. *Procedia Manuf.* 22, 626–633 (2018). <https://doi.org/10.1016/j.promfg.2018.03.091>.
 11. Wang, H., Liu, Y., Zhou, B., Li, C., Cao, G., Voropai, N., Barakhtenko, E.: Taxonomy research of artificial intelligence for deterministic solar power forecasting. *Energy Convers. Manag.* 214, 112909 (2020). <https://doi.org/10.1016/j.enconman.2020.112909>.
 12. Kayri, I., Gencoglu, M.T.: Predicting power production from a photovoltaic panel through artificial neural networks using atmospheric indicators. *Neural Comput. Appl.* 31, 3573–3586 (2019). <https://doi.org/10.1007/s00521-017-3271-6>.
 13. Li, L.L., Wen, S.Y., Tseng, M.L., Chiu, A.S.F.: Photovoltaic array prediction on short-term output power method in Centralized power generation system. *Ann. Oper. Res.* 290, 243–263 (2020). <https://doi.org/10.1007/s10479-018-2879-y>.
 14. Hussain, M., Dhimish, M., Titarenko, S., Mather, P.: Artificial neural network based photovoltaic fault detection algorithm integrating two bi-directional input parameters. *Renew. Energy.* 155, 1272–1292 (2020). <https://doi.org/10.1016/j.renene.2020.04.023>.
 15. Cho, K.H., Jo, H.C., Kim, E. sang, Park, H.A., Park, J.H.: Failure Diagnosis Method of Photovoltaic Generator Using Support Vector Machine. *J. Electr. Eng. Technol.* 15, 1669–1680 (2020). <https://doi.org/10.1007/s42835-020-00430-9>.
 16. Kohonen, T.: *Self-Organizing Maps*. Springer Berlin Heidelberg, Berlin, Heidelberg (2001). <https://doi.org/10.1007/978-3-642-56927-2>.
 17. Kothari, S.C., Oh, H.: *Neural Networks for Pattern Recognition*. *Adv. Comput.* 37, 119–166 (1993). [https://doi.org/10.1016/S0065-2458\(08\)60404-0](https://doi.org/10.1016/S0065-2458(08)60404-0).
 18. Clancey, W.J.: Heuristic classification. *Artif. Intell.* 27, 289–350 (1985). [https://doi.org/10.1016/0004-3702\(85\)90016-5](https://doi.org/10.1016/0004-3702(85)90016-5).
 19. Rodrigues, M.A.: *Invariants for Pattern Recognition and Classification*. WORLD SCIENTIFIC (2000). <https://doi.org/10.1142/4395>.

I-V tracers for PV panels, topologies and challenges: A Review

José Ignacio Morales-Aragón¹[0000-0002-9163-9357], Luis Hernández-Callejo¹[0000-0002-8822-2948], Miguel Dávila-Sacoto²[0000-0001-6318-2137], L. G. González³[0000-0001-9992-3494], Victor Alonso-Gómez¹[0000-0001-5107-4892]

¹ University of Valladolid, Duques de Soria University Campus, 42004 Soria, Spain

² Municipal Public Company of Mobility, Transit and Transportation of Cuenca EMOV EP, Technical Management of Mobility, Air Quality Department, 010104 Cuenca, Ecuador

³ Electrical, Electronics and Telecommunications Engineering Department, University of Cuenca, 010107, Cuenca, Ecuador

J.M-A. ziguratt@coit.es;
L.H-C. luis.hernandez.callejo@uva.es;
M.D-S. mdavila@emov.gob.ec;
L.G.G. luis.gonzalez@ucuenca.edu.ec;
V.A-G. victor.alonso.gomez@uva.es

Abstract. I-V tracers are equipment capable of forcing a photovoltaic (PV) generator to a set of current/voltage points and taking samples of them to obtain its electrical characteristics. The analysis of the I-V curves captured by this equipment can reveal different kind of failures in a PV generator, which allows the installation operator to take early actions in order to minimize power losses. I-V tracers are widely used in industry, and can be found with different topologies and configurations. This study presents a review of different types of I-V tracers, their advantages and disadvantages, and the possible challenges that the operator may encounter in their use and design.

Keywords: I-V tracer; variable resistor tracer; capacitive charge tracer; electronic load tracer; bipolar power amplifier tracer; four quadrant power source tracer; DC-DC converter tracer

1 Introduction

The demands of photovoltaic (PV) installations have become progressively important and minimizing power losses for a better efficiency in an optimal and economically viable way is a key point. The performance and adequate state of the system must be constantly evaluated to ensure that the panels that make up the installation are in optimal operating conditions and thus avoid energy losses. This performance is evaluated using current-voltage and power-voltage curve tracers (I-V and P-V), which provide the electrical characteristics of the panel or string under analysis [1]. These characteristics are compared from the data sheets supplied by the manufacturer, which

provide information on the panel parameters at standard test conditions (STC). Analysis of the I-V curve of a panel provides valuable information for the administrator of a PV installation as it allows the timely diagnosis of panel failure modes, leading to appropriate measures being taken to mitigate the failure or to replace the panel.

Globally, the PV power generation market in 2019 has installed 114.9GW, compared to 102.2GW in 2018 [2], that is, an increase of 12.43%, which indicates the important growth of this type power source. However, PV panels suffer degradation caused by aging, wear and tear, and their outdoor exposure [3], which causes their power to decrease and therefore affect the overall efficiency of the PV installation. Therefore, preventive maintenance is required to know the current status of each panel [4], and predictive maintenance to achieve comprehensive management [5]. In this way, the tracer is a device that allows the extraction of parameters from the panel to know exactly its current state [6].

This study presents a review of the different types of I-V tracers that exist in the bibliography, analyzing their advantages and disadvantages; The possible challenges that the operator may encounter in its use and design are also analyzed, focusing specifically on the power dissipated by the electronic components of the equipment.

2 I-V and P-V curves analysis

I-V and P-V curves allow characterizing a photovoltaic cell or panel, giving the electrical parameters that describe the operation of the device under test. I-V and P-V curve analysis is an usually invasive technique to detect the deterioration of photovoltaic panels that consists of applying a variable load on the panel terminals to obtain their current and voltage response. In this way, the analysis of the panel response curves gives us direct information on the electrical "state" of the panel, allowing the researcher to obtain data on the expected performance of the panel under different conditions of solar irradiation and panel load. However, it is an analysis that must be supported by other deterioration detection techniques to be able to give a conclusive answer [7], because in normal operating conditions photo-voltaic panels can develop several failure modes at the same time, which implies that the response of the characteristic curves is an addition of all the faults present in the panel.

2.1. I-V and P-V curves

The best-known way to characterize a photovoltaic cell or panel is to obtain its response curve to increases in voltage, current and power. These device responses are known as the IV (current-voltage) curve and the PV (Power-Voltage) curve as shown in Figure 1. These characteristic curves provide important information about the state of the cell or panel under analysis and are directly dependent on the temperature and radiation received by the panel or cell.

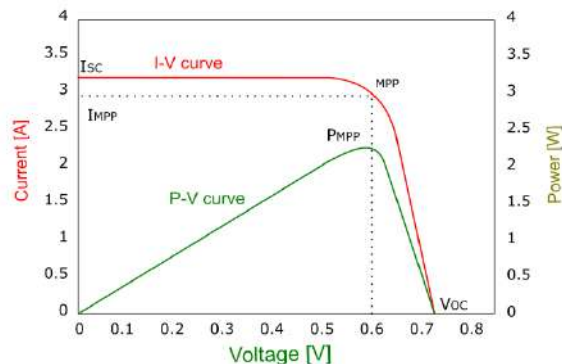


Figure 1. I-V and P-V characteristics of a solar cell [8].

An I-V curve indicates the response of the PV panel to different load conditions, at a known temperature and radiation. The radiation dependence of the PV characteristics is stronger than the temperature dependence, thus Figure 2a shows the response of a PV cell to different levels of radiation, where it is observed that the short-circuit current changes. Regarding its temperature dependence, Figure 2b shows the variation of the open circuit voltage at different temperatures.

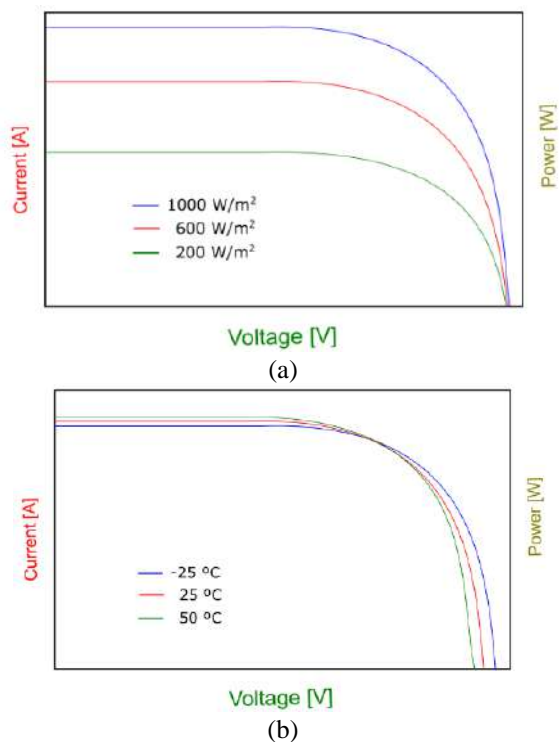


Figure 2. I-V curves of a PV panel at different levels of solar radiation [9] a) Irradiation dependence b) temperature dependence.

2.2. Deviations from the I-V curve

When a photovoltaic panel shows deterioration, the I-V curve also presents deviations compared to a curve of a faultless panel. Deviations in the IV curves correspond to different causes of deterioration and represents different type of failures in a photovoltaic generator. They can also be caused by errors at the time of the configuration of the curve sampling equipment, connection errors between the equipment and the panel, high cloudiness or radiation interference when taking the measurement, etc., so when capturing the curve these drawbacks should be avoided. Figure 3 shows the possible deviations that can be found in an I-V curve:

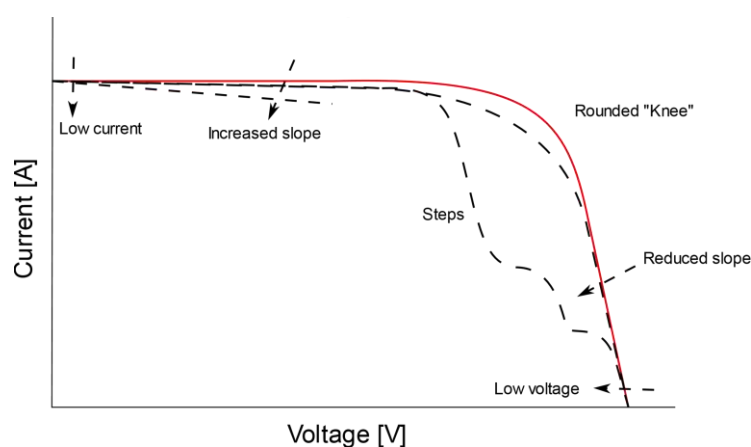


Figure 3. Common deviations of an I-V curve in a photovoltaic generator in deterioration mode.

The deviations of the I-V curve listed in Figure 3 and established in [10] are the following:

1. Steps or "ladder". - A deviation observed as steps or a "ladder" can be caused by partial shading, dust deposit, cracked cells or a short circuit in the bypass diode.
2. Low current. - An I_{SC} below the nominal can be caused by the uniform deposit of dust or the normal degradation of the module.
3. Low voltage. - A V_{OC} lower than nominal can be caused by thermal panel stress (hot spot or panel temperature above STC), completely shaded cells or bypass diode failure.
4. Rounder "knee". - If the inflection point of the curve or "knee" is rounder than that observed in a nominal curve it may be the cause of aging of the panel that can be evidenced by the change in the values of the series and parallel resistances of the model of a diode.
5. Slope reduction. - The reduction of the slope on the upper part or "horizontal leg" of curve IV can be caused by a dust deposit located on the edge of a cell, due to mismatch between the I_{SC} of the cells of a module (a reference to the quality of the cells), due to the presence of currents through the parallel branch

of the diode model (which appear as short circuits of cracked cells) or due to hot spots.

6. Increased slope. - The increase in the slope in the right side or "vertical leg" of the I-V curve can be caused by the increase in the serial resistance of the panel, or by excessive resistance of the connecting cables between panels.

2.3. Model of a photovoltaic cell

A photovoltaic module or cell can be modeled using its electrical characteristics like any electrical generator, considering that this model must predict the electrical output of the cell under different types of operating conditions. The commonly used model is the one that represents the cell as a diode in parallel with a current source dependent on solar radiation [11] as shown in Figure 4. Where the current delivered by the I_L photovoltaic generator is proportional to the solar radiation minus the currents flowing through the I_D diode and the R_{SH} parallel resistance.

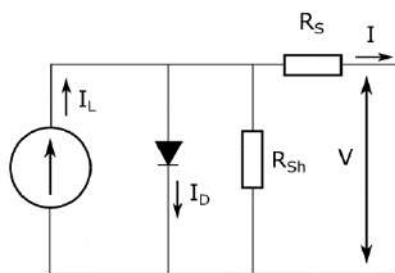


Figure 4. Equivalent model of a photovoltaic generator [11].

The equivalent circuit shown can be used as a single cell, a multi-cell module, or an array of multiple modules. This model is known as the "Diode Model" or "5-parameter Model", thus considering temperature and constant radiation, the characteristic I-V of the model is expressed by equations 1 and 2:

$$I = I_L - I_D - I_{SH} = I_L - I_o \left[\exp\left(\frac{V+IR_S}{a}\right) - 1 \right] - \frac{V+IR_S}{R_{SH}} \quad (\text{Eq. 1})$$

$$a = \frac{nN_s kT}{q} \quad (\text{Eq. 2})$$

Where:

I = current delivered by the photovoltaic generator;

I_L = current induced by solar radiation;

I_D = diode current;

I_{SH} = current flowing through the resistance in parallel;

I_o = reverse saturation diode current;

V = voltage at photovoltaic generator terminals;

R_S = series resistance;

R_{SH} = parallel resistance;

a = modified ideality factor;

k = Boltzmann constant (1.381×10^{-23} [J/K]);

T = cell temperature in degrees Kelvin;

N_S = number of cells connected in series;
 q = electron charge (1.602×10^{-19} [C]);
 n = diode ideality factor (1 for ideal diodes and 2 for real ones).

3. I-V tracers topologies

The drawing of I-V and P-V curves of a panel is carried out using equipment called a tracer, which is electronic equipment capable of varying the load on the panel or string terminals and taking measurements of corresponding voltages and currents. The equipment normally has a temperature sensor and a radiation sensor, so that with these data it is possible to perform the correction of the curve at STC. The correction is made following the standard IEC 60891: 2009 [12].

To obtain the I-V curve, different methods differ in their flexibility, fidelity and cost. Obtaining the I-V curve is based on the variation of the current consumed at the terminals of the photovoltaic generator and its voltage response, so both electrical parameters must be measured either by automatic or manual methods [13].

3.1.1. Variable resistor tracer or rheostat

A variable resistor tracer is a device that uses a variable resistor whose resistance can change in steps from zero to infinity (ideally) to capture points on the I-V curve (Figure 5). Normally this method is applicable in low power photovoltaic generators because high power resistors are rare in the market.

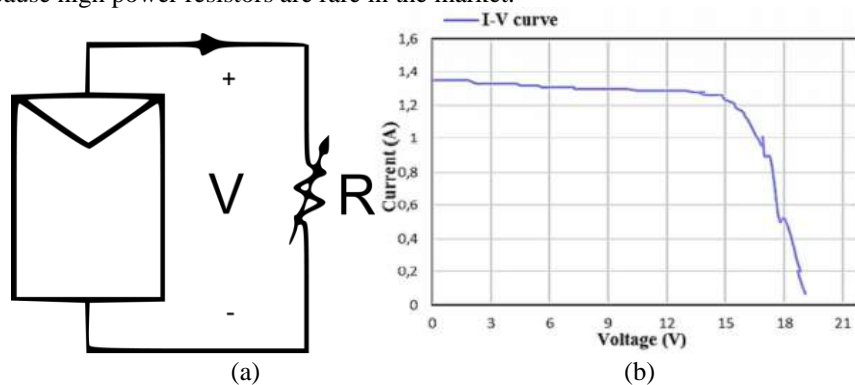


Figure 5. Schematic of a variable resistor tracer a) connection scheme [13] b) I-V curve obtained with a variable resistor tracer [14].

This topology is used in [14], [15], [16] and [17], but it has limitations due to the quality of the curve obtained and the variation of resistance is normally done manually. In [9] the author states that the precision of the method is not high since it is susceptible to the fact that the solar radiation and the temperature vary while the test is carried out, and that the IV curve does not have uniformity, and a high power rheostat is not common in the market, making this method applicable to low power PV generators (<1kW).

To improve the precision and fluidity of the curve in [14] a linear rheostat that is manually varied is used, in conjunction with a microcontroller with an external 12-bit analog-digital converter. In this way, the capture of current and voltage data is automated, increasing the number of points that can be obtained from the curve.

To improve the quality of the curve, in [18], [19], [20] and [21] diagrams of multiple resistors controlled by switches are presented to obtain curve IV (Figure 6), where its main limitation is the number of steps or points that can be obtained. In [18] a current and voltage sequencer is proposed, through the connection of resistors in parallel, automated by a computer, where the resistances must be selected appropriately to obtain a well-defined “knee”. In [19] a similar methodology is proposed, with the difference that the switches are MOSFETs, and the interface with the computer is an Arduino with a 12-bit external ADC. To increase the number of steps of this type of tracers, in [20] a binary scheme is proposed, where the resistors are in series and their activation depends on normally closed relays, thus, in the case of a tracer with 8 resistors 255 different resistance values could be obtained for the elaboration of the I-V curve. In [21] Lab-View is used to capture the curve and carry out previous analyzes.

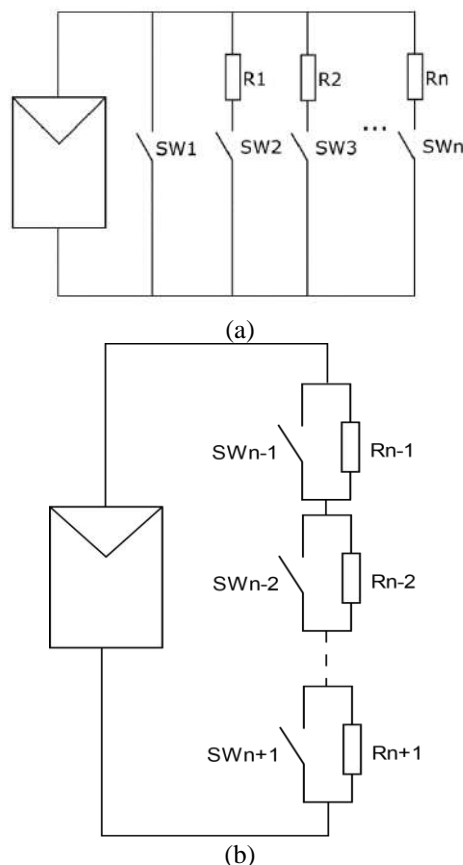


Figure 6. Variable Resistor Tracer Scheme (a) Conventional Scheme (b) Binary Tracer Scheme [20].

The use of variable resistors placed as a load in a photovoltaic generator to obtain IV curves is not recommended because with this method the I_{sc} is not exactly reached, and the manual change of resistors takes considerable time, so the solar radiation and thermal conditions may change during measurement [13], however, the cost advantages and ease of implementation and measurement automation of these types of tracers make them a viable alternative.

3.1.2. Capacitive load tracer

It is a capacitor-based method, where the capacitor is charged by the PV panel forcing it to go from a short circuit to an open circuit condition. It is a widely used tracer. In [16] it is stated that the value of the capacitor suitable for this type of tracer depends directly on the short circuit current and the open circuit voltage, and is given by (3), based on the time of establishment. of the capacitor (t_s).

$$C = \frac{t_s I_{sc}}{2 V_{oc}} \tag{3}$$

In [22] the plotting time of the I-V curve is indicated with this method, and it is given by (4). Besides, the use of the tracer is proposed as part of an MPPT controller to identify possible shading conditions of the panels, which is also considered in [17].

$$T_{sweep} = 1.261 \left(\frac{V_{oc} \cdot C}{I_{sc}} \right) \tag{4}$$

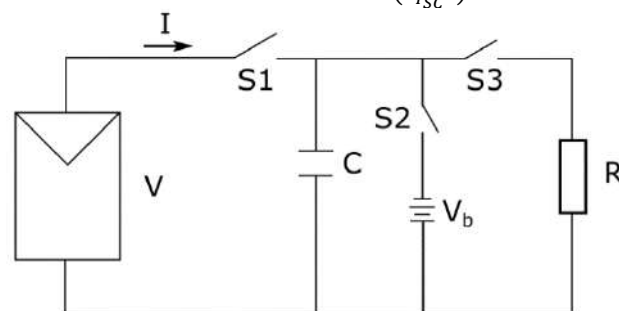


Figure 7. Schematic of a capacitive load tracer [13].

In Figure 7 the schematic of a capacitive tracer is shown, where before the measurement the capacitor begins unloaded by S3 and R. When the measurement is to be started, S3 opens and S1 closes, so the photovoltaic generator has a very low load, reaching short-circuit condition. As the capacitor charges, the current decreases and the voltage increases, so when the charge ends, the current delivered by the module becomes zero, reaching the open circuit condition. This scheme also allows to start the measurement with S2 closed, so that the capacitor would be charged to a negative voltage to reach I_{sc} exactly. There are simpler topologies such as that shown in Figure 8, where only the capacitor and a discharge resistor are used.

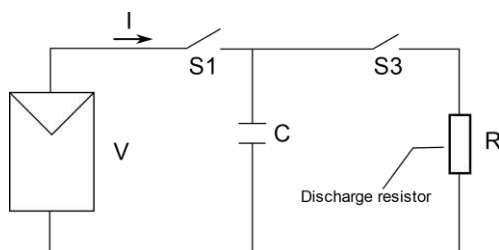


Figure 8. Schematic of a simpler capacitive load tracer [9].

For this type of tracer, the capacitors should be low ESR (equivalent series resistance) and low losses. The capacitance value depends on the required measurement time and has an impact on the measured voltage [23]. In this way, if you have short measurement times due to low capacitance values, the tracer design should consider voltage and current sensors that reach the required speed that may be in the order of milliseconds. Furthermore, depending on the current and voltage of the tracer, the use of IGBTs may be required for the proper triggering of the measurement stages, which increases implementation costs.

In [24] the effect of the arc produced by the connection of the capacitor is studied, which must be considered by the system converter. In [25] a genetic algorithm based on bee colony is used to obtain the parameters of a PV cell after plotting its I-V curve with a capacitive tracer. In [26], [27], [28] and [29] the operation of this type of tracer, and different methods of connecting the capacitor are discussed.

The low-cost advantage of this tracer has made it quite popular in the market, and it is even used in on-line tracers [30], that is, they are installed directly in the junction boxes of photovoltaic panels to measure their I-V curve regularly in a PV installation, constituting a semi-invasive measurement method as shown in Figure 9.

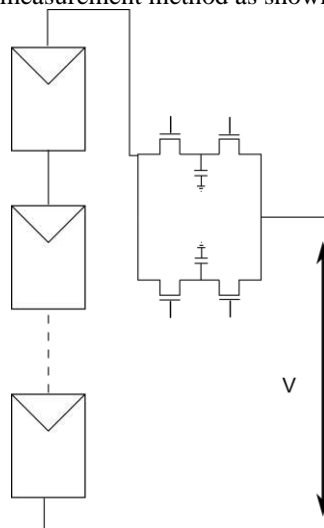


Figure 9. Electronic "semi-invasive" or "on-line" tracer installed in a junction box of a string of photovoltaic panels [30].

3.1.3. Electronic load tracer

An electronic load tracer is a device that uses a transistor (MOSFET or IGBT) as a controlled load (Figure 10). It takes advantage of the resistance variation between the transistor terminals by modulating its gate voltage, requiring its operation in cutoff modes, ohmic or linear region and saturation, so it could be considered as an electronic variable resistance tracer.

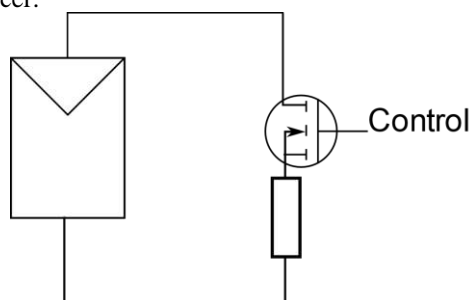


Figure 10. Schematic of an electronic load tracer with a MOSFET transistor [13].

These types of tracers use control circuits based on constant current loads and high-speed analog-digital converters. They have the advantage of being cheaper than the capacitive load for low voltages, with the limiting power that the transistors used in their design can handle, and they normally have noise in their measurement due to the transistor switching [31]. In [32] the use of a PWM control for the management of the MOSFET or an IGBT is proposed, and a structure for the galvanic isolation of the control circuit is exposed. In [33], this concept is extended, using a DAQ for the generation of a triangular signal as a control of the MOSFET. In [34] the characteristics of the MOSFET for its use in a tracer are studied.

In [35] the application of conventional tracers is expanded, adding an MQTT communication for the control of capacitive tracers. In [36] a low-cost tracer is designed, and information is gathered from studies to determine the characteristics of the MOSFET, specifically its characteristic curves, to properly select the transistor to be used based on the characteristics of the MOSFET (Figure 11) and the PV panel. In [37], [38], [39], [35] and [36] tracer designs with computer interfaces are carried out, both for the characterization of panels and for their use in solar farms.

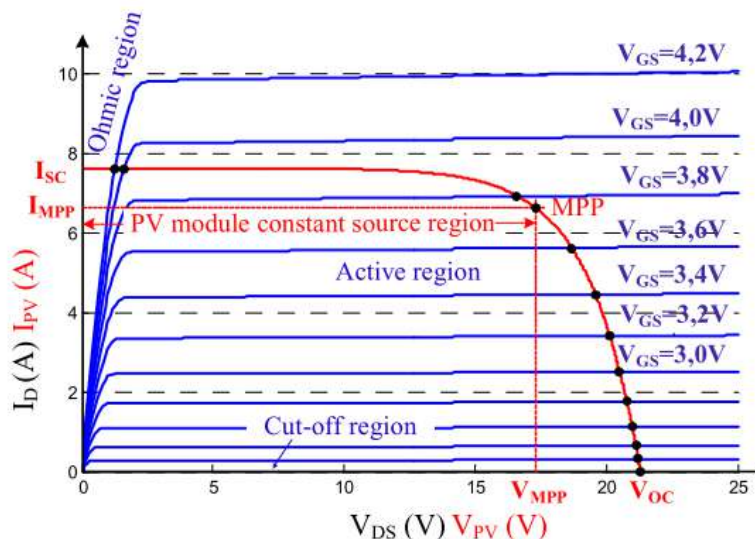


Figure 11. Characteristics of a PV panel and a MOSFET [36].

3.1.4. Bipolar power amplifier tracer

It is a type of tracer that uses a configuration of bipolar transistors as class B power amplifiers (Figure 12) to allow reversal of current and voltage for measurement of “dark” IV curves (simulation of an I-V curve of a module in conditions without lighting). In [39] this type of tracer is used as a reference for the design of a solar simulator.

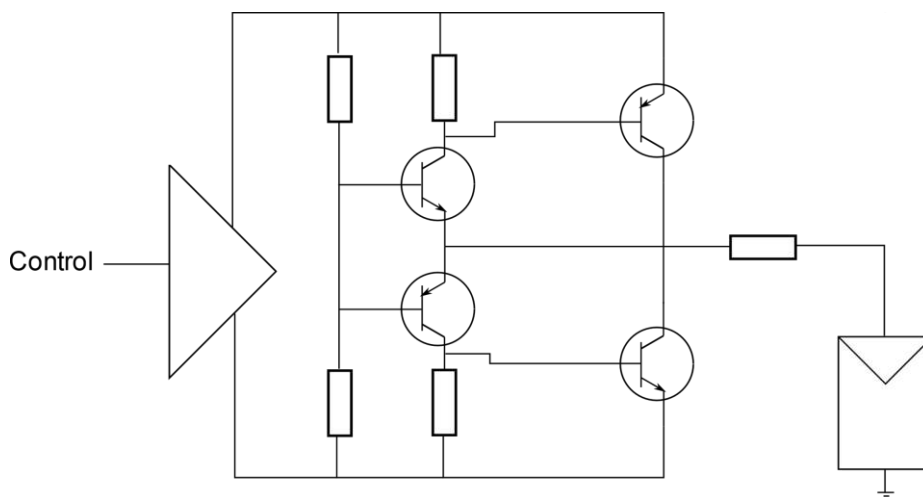


Figure 12. Bipolar Power Amplifier tracer [13].

These tracers have the limitation of the use of BJT transistors in the linear area, so they are limited to low powers.

3.1.5. Four Quadrant Power Supply tracer

It is a tracer based on a power source and transistors in H-bridge configuration that allows to deliver and consume energy from the photovoltaic generator to evaluate its performance in the four quadrants of an I-V curve (Figure 13).

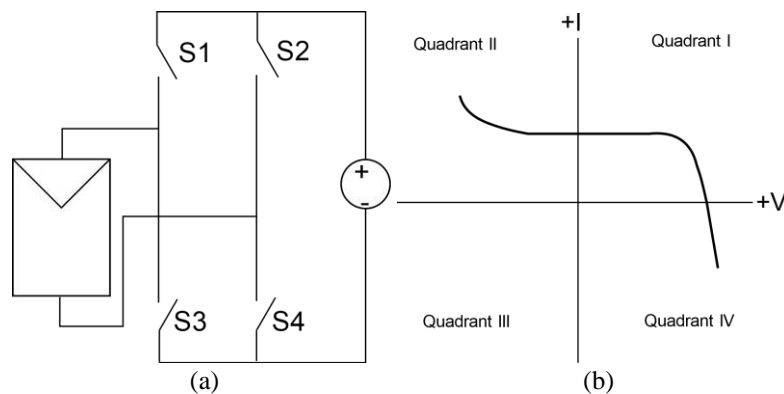


Figure 13. Four Quadrant Power Supply tracer [13].

Investigation of the operation of four quadrants on a solar panel allows the diagnosis of mismatches in partially shaded cells connected in series and is used for the generation of dark curves (dark I-V). The dark I-V curve is based as its name implies on plotting an I-V curve when the panel is unlit, and specifically on measuring current and voltage when the panel is powered by an external source. Figure 14 shows the dark IV curve of a solar panel, from which the values of the series and parallel resistances can be obtained, and the ideality factors for the diode model and I-V curve correction methods to STC. In studies carried out in [42] and in [43], methods for evaluating electrical panel parameters with this type of curve are reviewed.

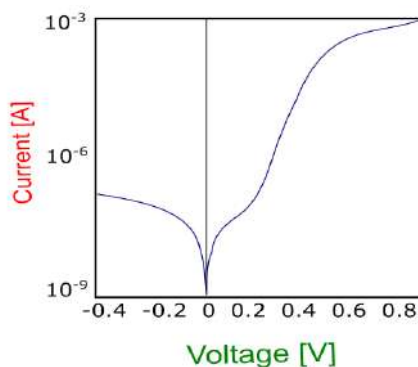


Figure 14. Dark I-V curve of a solar cell [44]

In [45] an experimental procedure is used to synchronize the measurement of two multimeters, to increase the precision of the measurement and reduce the uncertainty

of this method. In [46] such a tracer is used to analyze module parameter extraction methods, in [47] it is used for high-efficiency cell analysis and in [48] it is used to characterize modules and shading effects. Being a very precise method, in [49] is used to verify the effect of series resistances introduced by the internal connection bars in a PV cell.

3.1.6. DC-DC converter tracer

It is a tracer based on the ability of DC-DC converters to emulate a resistor by varying its duty cycle (Figure 15). A DC-DC converter can plot the I-V curve of a photovoltaic generator in Buck-boost, Cuk, or Single-ended primary inductor converter (SEPIC) configuration [9].

In [50] the use of DC-DC converters as I-V curve tracers is proposed and in [51] this concept is extended by an automatic capture system with LabView. In [52] and [53] bidirectional DC-DC converters are used to obtain the I-V curves and to emulate the real-time behavior of a PV generator, and in [54] they are applied to MPPT (Maximum Power Point Tracking). And in [55] the applications of DC-DC converters are analyzed as a variable electronic load. In [56] the control of DC-DC converters is studied by means of Switching-Frequency Modulation Scheme (SFMS) and its application in MPPTs.

As for the Buck-Boost converters, they need to be of this topology since the Buck structures do not allow the drawing of points of the curve close to I_{sc} and the Boost structures cannot reach points close to V_{oc} [13].

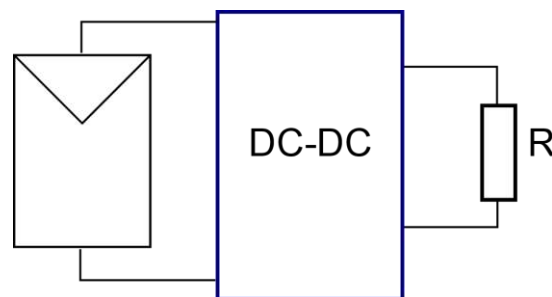


Figure 15. DC-DC converter tracer [13].

Buck-boost converters have the disadvantage of introducing noise into the measurement due to the commutation of their internal elements (transistor and inductor), which is why leads from this circuit are used (Figure 16), known as Cuk converters and SEPIC [57] which have a better frequency response and can be used as MPPTs as controllers for photovoltaic power generation. In [58] they use Cuk and SEPIC converters to decrease the ripple of the I-V curve caused by the commutation, and to reach the limits of I_{sc} and V_{oc} .

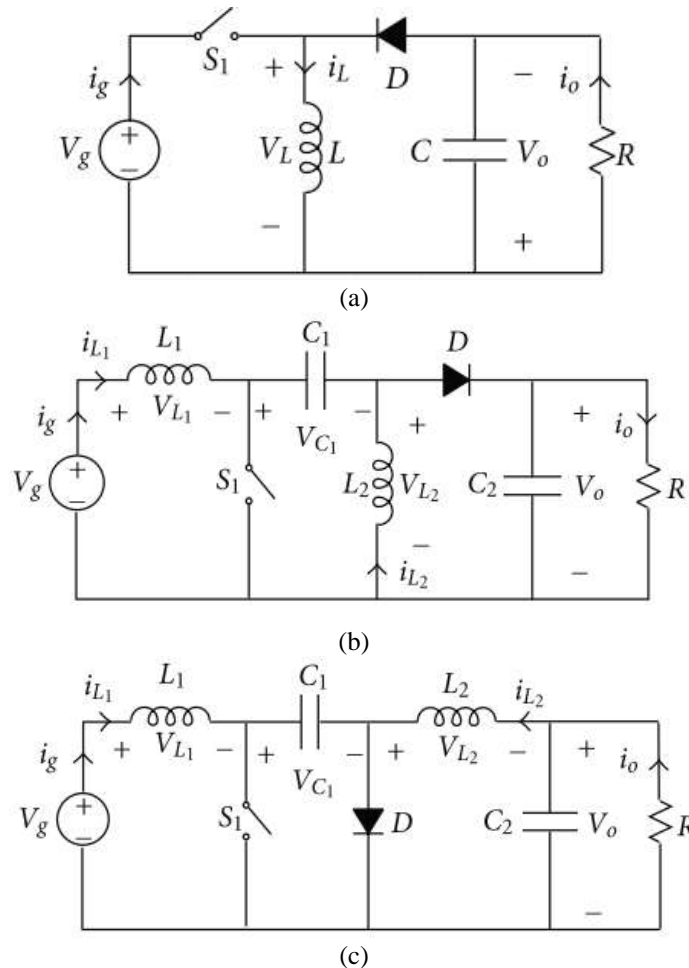


Figure 16. Derived DC-DC converters (a) Buck-boost (b) SEPIC (c) Cuk [59].

In [59] a SEPIC converter is used, with PWM control to generate the curve, and with Hall effect sensor for current measurement, and it is indicated that a four quadrant source can be used with this configuration. In [60] an adaptive control system is proposed, to ensure an optimal sampling rate.

In [61] two new methodologies are proposed, a voltage controlled sweep to obtain more information on the “flat” part of curve IV, and a current controlled sweep for the rest of the curve, that is, a hybrid sweep. In [62] converters are used to obtain characteristics of PV generation systems by analyzing their frequency response, and Nyquist diagrams. In [63] the authors propose the use of SEPIC converters installed in line with strings for automatic I-V curve tracing within a PV installation.

The application of a Cuk converter and a control method for plotting curves and MPPT is discussed in [64]. In [65] the mathematical analysis of the Cuk converter and

the details of its design are detailed. In [66] a digital control scheme of a Cuk converter is proposed for power factor correction, and its response to load variations.

3 Power dissipation considerations in I-V tracers

To select the appropriate topology when facing the design of an I-V tracer, it is of great importance to know the power to which the electronic elements that make up the equipment are exposed. Therefore, this section will carry out an analysis of the main types of topologies and the power dissipated by the electronic components in them.

With this aim, the model of one diode of a photovoltaic cell (Figure 17a) is taken as a reference, for which an $I_{SC}=3A$ and $V_{OC}=0.6239V$ are imposed, with an $M_{pp}=1.476W$. Figure 17b shows the I-V and P-V curves of the cell. Because the voltage of a single cell is limited, a 5-cell circuit in series was used, obtaining an $I_{SC}=3A$, $V_{OC}=3.1195V$ and $M_{pp}=7.38W$. Simulations were performed in LTSpice.

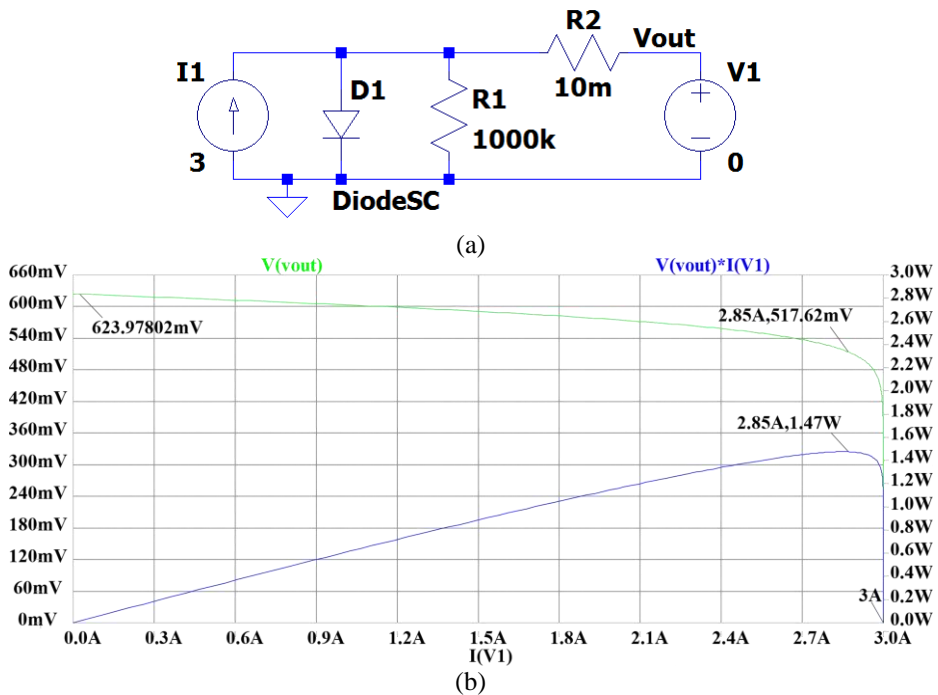


Figure 17. Simulation model of a PV cell: a) diode model circuit; b) I-V and P-V curves.

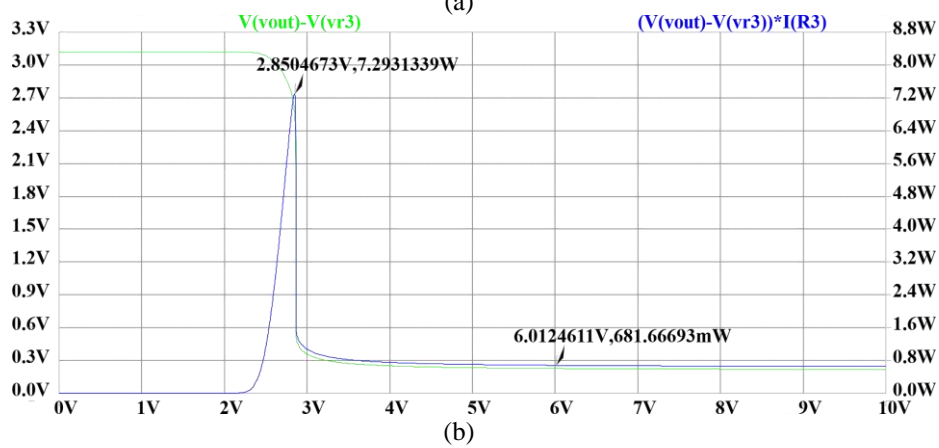
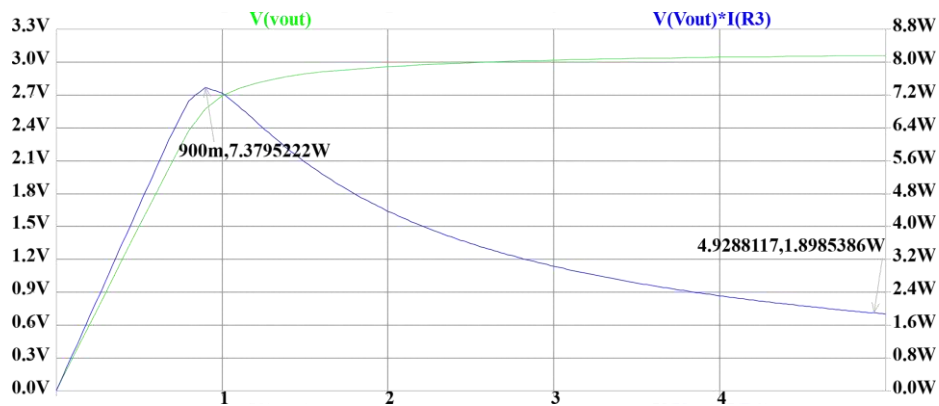
3.1 Variable resistance, electronic load and capacitive load tracers

These three tracers are analyzed for their similarity in their operating principle. Both the variable resistance and the switching element in an electronic load dissipate all the

energy when drawing the I-V curve. Also, the capacitive load tracer in the same way has a single element (resistor) that dissipates the total power of the circuit.

For the variable resistance tracer (Figure 18a) it is observed that the power dissipated by the resistance is the total power of the cells, that is, their power dissipation is 1p.u compared to the panel power. Similarly, for the MOSFET-based electronic load tracer (Figure 18b), the power dissipated by the device is the total power of the panel. However, in the electronic load there is an additional resistor for the current measurement, and the internal resistance of the MOSFET, which causes the device to dissipate 7.29W, that is, 0.98p.u., but for a shorter time.

In the case of the capacitive load tracer, the resistor dissipates all the power, i.e. 1p.u., during the charging time of the capacitor.



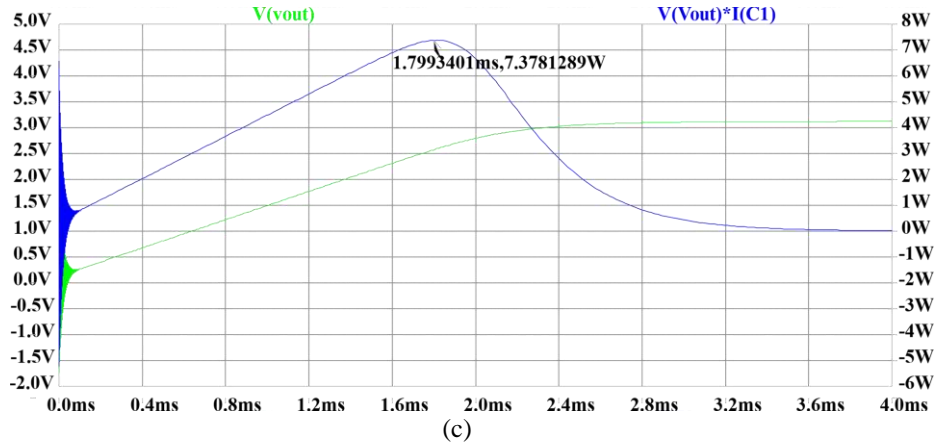


Figure 18. Power dissipation in elements of a tracer: a) variable resistance tracer; b) MOSFET in electronic load tracer; c) capacitive load tracer.

3.2 DC-DC converter tracers

Regarding the DC-DC converter-based tracers, Buck-Boost, SEPIC and Cuk converters are analyzed. For all these types of converters, elements with values that ensure an output voltage of 1p.u were used. of the set of cells, to find only the difference in power in each one (Figure 19).

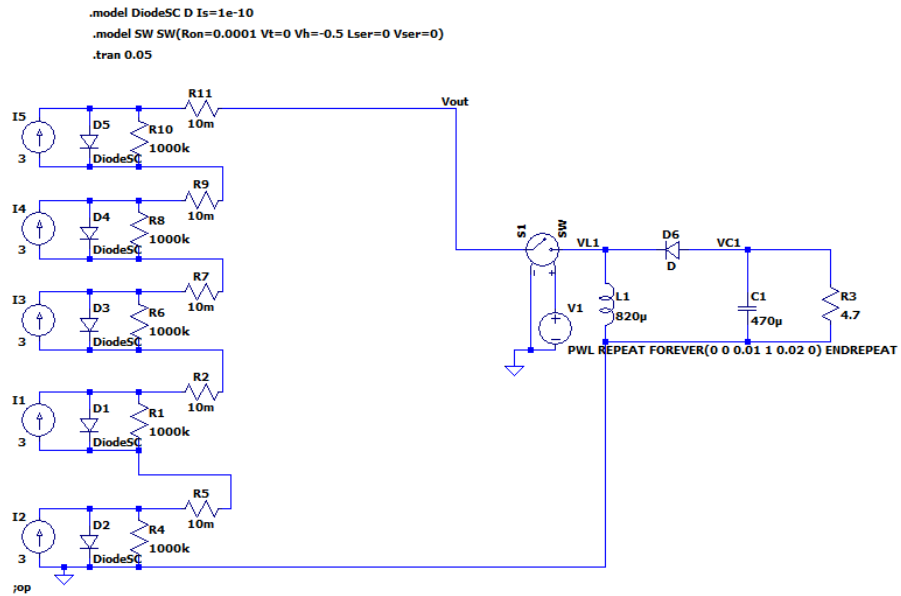
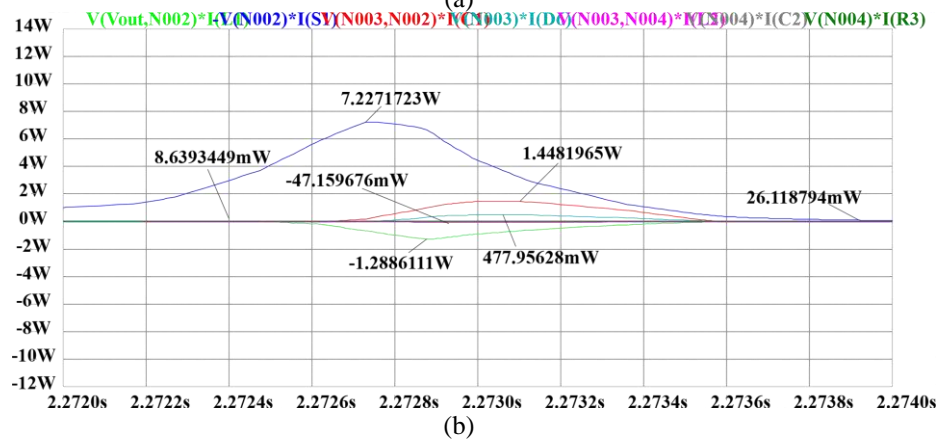
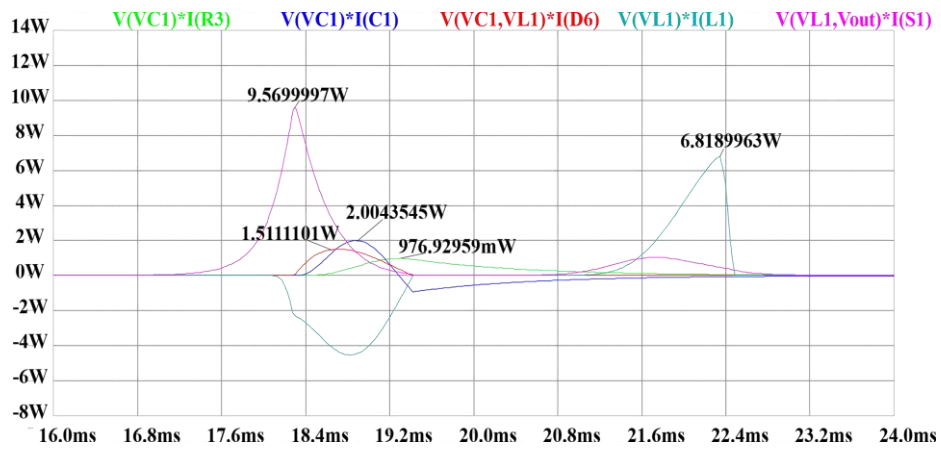


Figure 19. Circuit for simulating tracers based on DC-DC converters.

Thus, in the Buck-Boost converter (Figure 20a) it is obtained that the power in the resistance is 0.13 p.u., the diode 0.16 p.u., the inductor 0.92 p.u. and the switching element 1.29 p.u. In the Cuk converter (Figure 20b), it is observed that the element that dissipates the most power is the switch with 0.98 p.u., and in the case of SEPIC (Figure 20c), likewise the switch is the element that dissipates more power, in this case 1.2 p.u., and inductor L1 with 0.36 p.u.



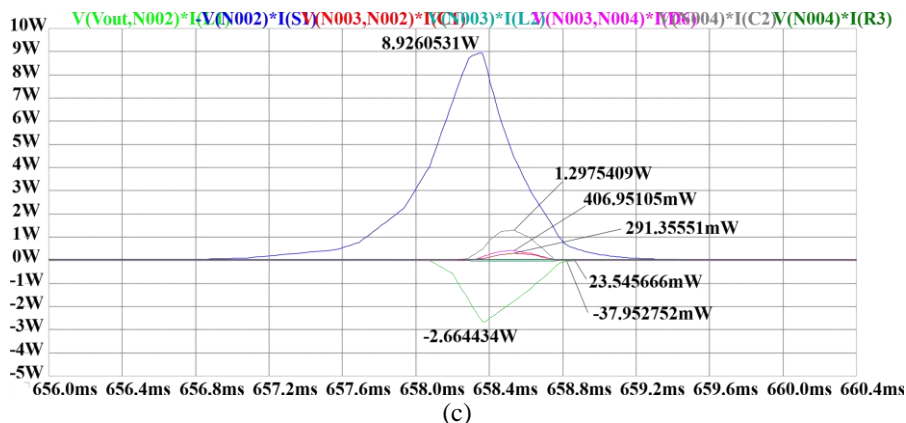


Figure 20. Power dissipation in elements of a tracer: a) Buck-Boost converter; b) Cuk converter; c) SEPIC converter.

4 Discussion

The topologies of the I-V tracers analyzed in this study are the most widely used in the industry and have evolved over the past 15 years. However, each has advantages and disadvantages that make them unique for specific applications and for studies that require obtaining certain electrical characteristics from PV generators (Table 1). To analyze the advantages and disadvantages of each topology, a study is carried out on the parameters that must be considered when choosing each topology.

One of the parameters that must be considered to analyze the application of the types of tracers studied, is the flexibility for the expansion of the equipment or its design, because the variation of its configuration allows coupling to different conditions of the PV system. In this aspect, the DC-DC converters allow the greatest flexibility since its control can be modified with different trip signals, their duty cycle and power direction, with which most of the curve areas IV can be addressed. On the other hand, the capacitive load tracer is the one that allows the least flexibility, since only the sweep time of the curve can be modified according to the capacitance value used.

Another parameter is modularity, which allows the tracer to be expanded. In this aspect, the electronic loads, the bipolar amplifier, and the DC-DC converters stand out, because more channels can be added, and the constituent elements can be modified. In this regard, the capacitive load, and the 4-quadrant source present difficulties for its expansion.

Regarding the fidelity of the analyzed methods, the ones that deliver the most reliable data are the DC-DC converters, the bipolar amplifier and the 4-quadrant source, because they are the only ones that can reach real I_{SC} values of the analyzed device.

Cost is a factor to consider in any tracer. Thus, the resistive load tracer is the least expensive, but is limited to low powers. On the other hand, both the electronic load and the DC-DC converter have high costs due to the switching elements and coils that are required for their operation.

The precision of the measurement is another parameter that must be considered, especially when working with cells and precise values of voltage and current are required. In this, the 4-quadrant source and the DC-DC converters stand out, due to the control that can be had over their operation and the algorithms existing in the bibliography. Electronic loads and capacitive loads are less accurate, but this can be improved with the use of robust ADCs.

Another important parameter is the sweep speed of the curve, in this the 4-quadrant source stands out for the ease of voltage control. In this aspect, capacitive loads can be very fast or very slow, depending on the charging time of the capacitor used.

The maximum power is another important parameter since the applicability of the tracer depends on different PV installations. In this, capacitive loads and DC-DC converters stand out, which can be modified according to the installation requirement easily and economically compared to other methods.

Finally, the resolution of the methods is important to have a greater number of analysis points of the curve. In this they emphasize the source of 4 quadrants and the DC-DC converter. A greater number of points allows detailed studies to be carried out on the state of the PV panel.

Table 1. Comparison of I-V tracers.

I-V Tracer method	Flexibility	Modularity	Fidelity	Cost	Accuracy	Sweep speed	Maximum rating	Resolution
<i>Resistive load</i>	Medium	Medium	Medium	Low	Low	Low	Low	Low
<i>Capacitive load</i>	Low	Low	Medium	High	Medium	Medium	High	Medium
<i>Electronic load</i>	High	High	Medium	High	Medium	Medium	Low	Medium
<i>Bipolar power amplifier</i>	High	High	High	High	Medium	Medium	Low	Medium
<i>4-Quadrant power supply</i>	Low	Low	High	High	High	High	Low	High
<i>DC-DC converter</i>	High	High	High	Low	High	Medium	High	High

Regarding DC-DC converters, it is necessary to analyze them separately and by their topologies for their correct use. For this, [9] in Table 2 presents a comparison of the converter topologies. It is observed that in the case of efficiency, the Cuk and SEPIC converters are better than the Buck-Boost, and this is inherent in their topology. In addition, it is observed that the SEPIC converter uses a lower current MOSFET than the other topologies, which translates into a lower cost of implementation.

Table 2. Characteristics of different DC-DC converter topologies [9].

Topology	Inductor	Input capacitor	Output capacitor	Power Mosfet	Efficiency
<i>Buck-Boost</i>	High RMS current	High capacitance	High capacitance	High current rating	Very low
<i>Cuk</i>	Low RMS current	Low capacitance	Low capacitance	High current rating	High
<i>SEPIC</i>	Low RMS current	Low capacitance	High capacitance	Low current rating	High

Regarding the analysis carried out of the powers in percentage of these converters, Table 3 shows the results of the powers in per unit of each element of the converters. It is observed that in the case of the Buck-boost and SEPIC the power of the switching element is greater than the Cuk. Furthermore, it is observed that in the Buck-Boost, the L1 inductance dissipates the highest power of the 3 topologies, which indicates that this element must be dimensioned considering this particular.

Table 3. Power per unit of the elements in DC-DC converters.

Elemento	Variable Resistance	Electronic Load	Capacitive Load	Buck-Boost	Cuk	SEPIC
<i>L1</i>	-	-	-	0.92	0.17	0.36
<i>MOSFET</i>	-	0.98	-	1.29	0.98	1.21
<i>C1</i>	-	-	-	-	-	-
<i>D</i>	-	-	-	0.16	0.06	0.01
<i>L2</i>	-	-	-	-	0.01	0.06
<i>C2</i>	-	-	-	-	0.00	0.18
<i>R</i>	1		1	0.13	0.00	0.00

5 Conclusions

A study is presented on the existing topologies of I-V and P-V tracers, analyzing parameters such as their flexibility, modularity, reliability, cost, precision, scanning speed and resolution. Also, an analysis is performed on the power that each element dissipates in different topologies, to have a reference for the selection of the elements within the circuit of a tracer.

It is observed that the tracers based on a capacitive load are widely used in the industry, due to their low cost and high sweep speed, so several commercial tracers can be found that use this topology. However, the use of tracers based on DC-DC converters is a trend due to their modularity, their precision, and the existence of these converters in MPPT systems integrated in inverters, which is a technical advantage that can be exploited in the future.

In the dissipated power analysis, it was observed that the variable resistance, electronic load and capacitive load tracers dissipate all the power of the panel under

analysis, so this should be considered when it is necessary to carry out the complete strings tracing. Regarding the DC-DC converter-based tracers, it was observed that the switching element dissipates the greatest amount of power in all the topologies studied. As for the Buck-boost converter, the second element to consider is the inductor, which dissipates a 0.92 p.u. panel power. The dissipated power has a direct impact on the tracer design, since it has a relationship with the equipment's cooling system, and limits the element's lifetime.

Acknowledgments

The authors thank the CYTED Thematic Network “INTELLIGENT CITIES FULLY INTEGRAL, EFFICIENT AND SUSTAINABLE (CITIES)” n° 518RT0558.

References

- [1] S. Sarikh, M. Raoufi, A. Bennouna, A. Benlarabi, and B. Ikken, “Implementation of a plug and play I-V curve tracer dedicated to characterization and diagnosis of PV modules under real operating conditions,” *Energy Convers. Manag.*, vol. 209, no. February, 2020.
- [2] International Energy Agency, “Snapshot of Global PV Markets 2020,” 2020.
- [3] M. Dhimish and A. Alrashidi, “Photovoltaic degradation rate affected by different weather conditions: A case study based on pv systems in the uk and australia,” *Electron.*, vol. 9, no. 4, 2020.
- [4] A. Baklouti, L. Mifdal, S. Dellagi, and A. Chelbi, “An optimal preventive maintenance policy for a solar photovoltaic system,” *Sustain.*, vol. 12, no. 10, 2020.
- [5] L. B. Bosman, W. D. Leon-Salas, W. Hutzler, and E. A. Soto, “PV system predictive maintenance: Challenges, current approaches, and opportunities,” *Energies*, vol. 16, no. 3, 2020.
- [6] M. Oulcaïd, H. El Fadil, L. Ammeh, A. Yahya, and F. Giri, “Parameter extraction of photovoltaic cell and module: Analysis and discussion of various combinations and test cases,” *Sustain. Energy Technol. Assessments*, vol. 40, no. February, p. 100736, 2020.
- [7] M. Davila-Sacoto, L. Hernandez-Callejo, V. Alonso-Gómez, S. Gallardo-Saavedra, and L. G. Gonzalez, “Low-cost infrared thermography in aid of photovoltaic panels degradation research,” *Rev. Fac. Ing. Universidad Antioquia*, pp. 7–9, 2020.
- [8] E. T. Hashim and A. A. Abbood, “Temperature Effect on Photovoltaic Modules Power Drop,” *Al-Khwarizmi Eng. J.*, vol. 11, no. 2, pp. 62–73, 2015.
- [9] Y. Zhu and W. Xiao, “A comprehensive review of topologies for photovoltaic I–V curve tracer,” *Sol. Energy*, vol. 196, pp. 346–357, 2020.
- [10] International Electrotechnical Commission, “IEC 62446,” 2006.
- [11] W. A. B. John A. Duffie, *Wiley: Solar Engineering of Thermal Processes, 4th Edition - John A. Duffie, William A. Beckman*. 2013.
- [12] IEC, “IEC 60891,” vol. 2016. pp. 2–7, 2016.
- [13] E. Duran, M. Piliouguine, M. Sidrach-De-Cardona, J. Galan, and J. M. Andujar, “Different methods to obtain the I-V curve of PV modules: A review,” *Conf. Rec. IEEE*

- Photovolt. Spec. Conf.*, no. May, 2008.
- [14] A. El Hammoui, S. Motahhir, A. Chalh, A. El Ghzizal, and A. Derouich, "Low-cost virtual instrumentation of PV panel characteristics using Excel and Arduino in comparison with traditional instrumentation," *Renewables Wind. Water, Sol.*, vol. 5, no. 1, 2018.
 - [15] A. Q. Malik and S. J. B. H. Damit, "Outdoor testing of single crystal silicon solar cells," *Renew. Energy*, vol. 28, no. 9, pp. 1433–1445, 2003.
 - [16] M. M. Mahmoud, "Transient analysis of a PV power generator charging a capacitor for measurement of the I-V characteristics," *Renew. Energy*, vol. 31, no. 13, pp. 2198–2206, 2006.
 - [17] A. Rivai and N. A. Rahim, "A low-cost photovoltaic (PV) array monitoring system," *CEAT 2013 - 2013 IEEE Conf. Clean Energy Technol.*, pp. 169–174, 2013.
 - [18] E. E. Van Dyk, A. R. Gxasheka, and E. L. Meyer, "Monitoring current-voltage characteristics and energy output of silicon photovoltaic modules," *Renew. Energy*, vol. 30, no. 3, pp. 399–411, 2005.
 - [19] H. Amiry *et al.*, "Design and implementation of a photovoltaic I-V curve tracer: Solar modules characterization under real operating conditions," *Energy Convers. Manag.*, vol. 169, pp. 206–216, 2018.
 - [20] N. A. Rahim and A. Rivai, "Binary-based tracer of photovoltaic array characteristics," *IET Renew. Power Gener.*, vol. 8, no. 6, pp. 621–628, 2014.
 - [21] A. K. Gupta, N. S. Chauhan, and R. Saxena, "Real time I-V and P-V curve tracer using LabVIEW," *2016 1st Int. Conf. Innov. Challenges Cyber Secur. ICICCS 2016*, no. Iccics, pp. 265–269, 2016.
 - [22] S. Bifaretti, V. Iacovone, L. Cina, and E. Buffone, "Global MPPT method for partially shaded photovoltaic modules," *2012 IEEE Energy Convers. Congr. Expo. ECCE 2012*, pp. 4768–4775, 2012.
 - [23] F. Spertino, J. Ahmad, A. Ciocia, P. Di Leo, A. F. Murtaza, and M. Chiaberge, "Capacitor charging method for I-V curve tracer and MPPT in photovoltaic systems," *Sol. Energy*, vol. 119, pp. 461–473, 2015.
 - [24] Q. Xiong *et al.*, "Detecting and localizing series arc fault in photovoltaic systems based on time and frequency characteristics of capacitor current," *Sol. Energy*, vol. 170, no. June, pp. 788–799, 2018.
 - [25] Z. Chen, W. Lin, L. Wu, C. Long, P. Lin, and S. Cheng, "A capacitor based fast I-V characteristics tester for photovoltaic arrays," *Energy Procedia*, vol. 145, pp. 381–387, 2018.
 - [26] F. Spertino, J. Sumaili, H. Andrei, and G. Chicco, "PV module parameter characterization from the transient charge of an external capacitor," *IEEE J. Photovoltaics*, vol. 3, no. 4, pp. 1325–1333, 2013.
 - [27] H. M. Aguilar, R. F. Maldonado, and L. B. Navarro, "Charging a capacitor with a photovoltaic module," *Phys. Educ.*, vol. 52, no. 4, 2017.
 - [28] F. Recart, H. Mäckel, A. Cuevas, and R. A. Sinton, "Simple data acquisition of the current-voltage and illumination-voltage curves of solar cells," *Conf. Rec. 2006 IEEE 4th World Conf. Photovolt. Energy Conversion, WCPEC-4*, vol. 1, pp. 1215–1218, 2007.
 - [29] J. Muñoz and E. Lorenzo, "Capacitive load based on IGBTs for on-site characterization of PV arrays," *Sol. Energy*, vol. 80, no. 11, pp. 1489–1497, 2006.

- [30] A. V. Joglekar and B. Hegde, "Online I-V Tracer for per string monitoring and maintenance of PV panels," *IECON 2018 - 44th Annu. Conf. IEEE Ind. Electron. Soc.*, vol. 1, pp. 1890–1894, 2019.
- [31] Y. Erkaya, I. Flory, and S. X. Marsillac, "Development of a string level I-V curve tracer," *2014 IEEE 40th Photovolt. Spec. Conf. PVSC 2014*, no. October 2014, pp. 3104–3107, 2014.
- [32] V. Leite, J. Batista, F. Chenlo, and J. L. Afonso, "Low-cost I-V tracer for photovoltaic modules and strings," *2014 Int. Symp. Power Electron. Electr. Drives, Autom. Motion, SPEEDAM 2014*, pp. 971–976, 2014.
- [33] A. Sahbel, N. Hassan, M. M. Abdelhameed, and A. Zekry, "Experimental performance characterization of photovoltaic modules using DAQ," *Energy Procedia*, vol. 36, pp. 323–332, 2013.
- [34] Y. Kuai and S. Yuvarajan, "An electronic load for testing photovoltaic panels," *J. Power Sources*, vol. 154, no. 1, pp. 308–313, 2006.
- [35] P. Papageorgas, D. Piromalis, T. Valavanis, S. Kambasis, T. Iliopoulou, and G. Vokas, "A low-cost and fast PV I-V curve tracer based on an open source platform with M2M communication capabilities for preventive monitoring," *Energy Procedia*, vol. 74, pp. 423–438, 2015.
- [36] A. A. Willoughby and M. O. Osinowo, "Development of an electronic load I-V curve tracer to investigate the impact of Harmattan aerosol loading on PV module performance in southwest Nigeria," *Sol. Energy*, vol. 166, no. March, pp. 171–180, 2018.
- [37] O. Henni, M. Belarbi, K. Haddouche, and E. H. Belarbi, "Design and Implementation of a Low-Cost Characterization System for Photovoltaic Solar Panels," *Int. J. Renew. Energy Res.*, vol. 7, no. 4, pp. 1586–1594, 2017.
- [38] V. Leite, J. Batista, F. Chenlo, and J. L. Afonso, "Low-cost instrument for tracing current-voltage characteristics of photovoltaic modules," *Renew. Energy Power Qual. J.*, vol. 1, no. 10, pp. 1012–1017, 2012.
- [39] M. G. Guvench, C. Gurcan, K. Durgin, and D. MacDonald, "Solar simulator and I-V measurement system for large area solar cell testing," *ASEE Annu. Conf. Proc.*, pp. 12747–12753, 2004.
- [40] N. Forero, J. Hernández, and G. Gordillo, "Development of a monitoring system for a PV solar plant," *Energy Convers. Manag.*, vol. 47, no. 15–16, pp. 2329–2336, 2006.
- [41] J. Salmon, R. Phelps, and S. Michael, "Solar Cell Measurement System for NPS Spacecraft Architecture and Technology Demonstration Satellite, NPSAT1," *Proc. 17th Annu.*, pp. 1–19, 2003.
- [42] A. Kaminski, J. J. Marchand, A. Fave, and A. Laugier, "New method of parameters extraction from dark I-V curve," *Conf. Rec. IEEE Photovolt. Spec. Conf.*, pp. 203–206, 1997.
- [43] A. Guechi, M. Chegaar, and M. Aillerie, "Environmental effects on the performance of nanocrystalline silicon solar cells," *Energy Procedia*, vol. 18, no. 1, pp. 1611–1623, 2012.
- [44] Z. Remes and J. Stuchlik, "Pulse measurements of small area thin film $\mu\text{-Si:H/ZnO:B}$ photodiodes," *IOP Conf. Ser. Mater. Sci. Eng.*, vol. 726, no. 1, pp. 0–8, 2020.
- [45] M. Piliouguine, J. Carretero, L. Mora-López, and M. Sidrach-de-Cardona, "Experimental

- system for current-voltage curve measurement of photovoltaic modules under outdoor conditions,” *Prog. Photovoltaics Res. Appl.*, vol. 19, no. 5, pp. 591–602, Aug. 2011.
- [46] M. A. De Blas, J. L. Torres, E. Prieto, and A. García, “Selecting a suitable model for characterizing photovoltaic devices,” *Renew. Energy*, vol. 25, no. 3, pp. 371–380, 2002.
- [47] J. Fernández-Reche *et al.*, “PSA Solar furnace: A facility for testing PV cells under concentrated solar radiation,” *Sol. Energy Mater. Sol. Cells*, vol. 90, no. 15, pp. 2480–2488, 2006.
- [48] L. A. Hecktheuer, A. Krenzinger, and C. W. M. Prieb, “Methodology for Photovoltaic Modules Characterization and Shading Effects Analysis,” *J. Brazilian Soc. Mech. Sci.*, vol. 24, no. 1, 2002.
- [49] F. Granek and T. Zdanowicz, “Advanced system for calibration and characterization of solar cells,” *Opto-electronics Rev.*, vol. 12, no. 1, pp. 57–67, 2004.
- [50] J. M. Enrique, E. Durán, M. Sidrach-De-Cardona, J. M. Andújar, M. A. Bohórquez, and J. Carretero, “A new approach to obtain I-V and P-V curves of photovoltaic modules by using DC-DC converters,” *Conf. Rec. IEEE Photovolt. Spec. Conf.*, no. 1, pp. 1769–1772, 2005.
- [51] M. A. Bohórquezb, J. M. Enrique, E. Durán, M. Sidrach-de-Cardona, J. Carretero, and J. M. Andújar, “ANALYSIS AND FAILURES MONITORING IN PV PANELS BY MEANS OF I-V AND P-V CURVES USING DC-DC CONVERTERS,” in *WREC 2005 (World Renewable Energy Congress)*, 2005, pp. 477–483.
- [52] P. Sanchis, I. Echeverría, A. Ursúa, O. Alonso, E. Gubía, and L. Marroyo, “Electronic converter for the analysis of photovoltaic arrays and inverters,” *PESC Rec. - IEEE Annu. Power Electron. Spec. Conf.*, vol. 4, pp. 1748–1753, 2003.
- [53] P. Sanchis, J. López, A. Ursúa, and L. Marroyo, “Electronic controlled device for the analysis and design of photovoltaic systems,” *IEEE Power Electron. Lett.*, vol. 3, no. 2, pp. 57–62, 2005.
- [54] L. Marroyo, P. Sanchis, J. López, A. Ursúa, R. González, and E. Gubía, “Equipment for the analysis of the maximum energy of real photovoltaic systems,” *IEEE Int. Symp. Ind. Electron.*, vol. III, pp. 1031–1036, 2005.
- [55] M. Kazerani, “A high-performance controllable DC load,” *IEEE Int. Symp. Ind. Electron.*, no. 1, pp. 1015–1020, 2007.
- [56] K. K. Tse, B. M. T. Ho, H. S. H. Chung, and S. Y. R. Hui, “A comparative study of maximum-power-point trackers for photovoltaic panels using switching-frequency modulation scheme,” *IEEE Trans. Ind. Electron.*, vol. 51, no. 2, pp. 410–418, 2004.
- [57] E. Durán, J. M. Enrique, M. A. Bohórquez, M. Sidrach-De-Cardona, J. E. Carretero, and J. M. Andújar, “A new Application of the Coupled-Inductors SEPIC Converter to obtain I-V and P-V Curves of Photovoltaic Modules,” in *2005 European Conference on Power Electronics and Applications*, 2005, p. 10.
- [58] E. Durán, J. Galán, J. M. Andújar, D. D. I. Electrónica, D. S. Infor, and U. De Huelva, “A New Application of the Buck-Boost Derived Converters to Obtain the I-V Curve of Photovoltaic Modules,” pp. 413–417, 2007.
- [59] E. Durán, J. M. Andújar, J. M. Enrique, and J. M. Pérez-Oria, “Determination of PV generator I-V/P-V characteristic curves using a DC-DC converter controlled by a virtual instrument,” *Int. J. Photoenergy*, vol. 2012, 2012.
- [60] Y. Zhu, “An Adaptive I-V Curve Detecting Method for Photovoltaic Modules,” *Proc.* -

- 2018 *IEEE Int. Power Electron. Appl. Conf. Expo. PEAC 2018*, pp. 1–6, 2018.
- [61] K. Spiliotis, G. H. Yordanov, G. Van den Broeck, H. Goverde, K. Baert, and J. Driesen, “Towards accurate, high-frequency I-V curve measurements of photovoltaic modules applying electronic loads,” p. 5.
- [62] W. Xiao, W. G. Dunford, P. R. Palmer, and A. Capel, “Regulation of photovoltaic voltage,” *IEEE Trans. Ind. Electron.*, vol. 54, no. 3, pp. 1365–1374, 2007.
- [63] C. W. Riley and L. M. Tolbert, “An Autonomous Online I-V Tracer for PV Monitoring Applications,” p. 102, 2014.
- [64] A. Safari and S. Mekhilef, “Simulation and hardware implementation of incremental conductance MPPT with direct control method using cuk converter,” *IEEE Trans. Ind. Electron.*, vol. 58, no. 4, pp. 1154–1161, 2011.
- [65] E. Babaei and M. E. Seyed Mahmoodieh, “Systematical method of designing the elements of the Cuk converter,” *Int. J. Electr. Power Energy Syst.*, vol. 55, pp. 351–361, 2014.
- [66] S. Dian, X. Wen, X. Deng, and S. Zhang, “Digital control of isolated Cuk power factor correction converter under wide range of load variation,” *IET Power Electron.*, vol. 8, no. 1, pp. 142–150, 2015.

Embedded System for Hot Spots Characterization of Solar Panels

Johan Carvajal-Godinez^{1,2}[0000-0003-1489-7894], José
Fonseca^{1,3}[0000-0002-9529-3576], David Picado^{1,4}[0000-0001-7371-3413], Felix
Soto^{1,5}[0000-0001-9306-8108], and Carlos E. Soto^{1,6}[0000-0002-1569-2199]

¹ Instituto Tecnológico de Costa Rica

² johcarvajal@itcr.ac.cr

³ josefonsecruz19@gmail.com

⁴ dpicadoa97@gmail.com

⁵ felixasr12@gmail.com

⁶ carlos97emilio18@gmail.com

Abstract. Smart cities require to have intelligent infrastructure that supports their efficient operations. Embedded systems technologies and computer vision techniques can be adapted to support the development of solar energy production by improving their solar panel efficiency. This paper presents a novel implementation of an algorithm for hot spot detection and characterization on solar panels. The paper describes the embedded systems design as well as its software development workflow. The fault algorithm showed its capability for stain detection as well as its size characterization with an 80% precision. These results can be used to develop maintenance strategies for solar generation farms to make them more efficient.

Keywords: Hots Spots Characterization · Smart Cities · Solar Panels · Fault Detection · Computer Vision

1 Introduction

The world is experiencing several challenges that endanger human existence [6]. For instance, global warming and the increase of the human population demand the availability of more resources and energy to satisfy the improvement of human life standards [11]. Also, the rapid spread of COVID-19 has accelerated the economic recession around the world, which threaten with increasing social inequality, and therefore poverty of developing countries [7]. It is for that reason that now, more than ever, Smart Cities needs to be engineered in order to cope with the challenges mentioned above.

One of the key elements of smart cities is its decentralized model for resource generation and management as discussed in [12]. It is imperative to develop and implement an intelligent infrastructure that supports their basic services, for example, transportation, and energy generation [1]. It is also very important to rely on renewable energy sources to power smart cities. That can help to reduce

2 C. Johan et al.

and mitigate the environmental footprint that is one of the major concerns of adopting the city model as a way of life.

This paper is intended to propose a mechanism to achieve greater energy efficiency in the generation of electricity grids in Smart Cities, specifically for solar energy farms. For that purpose, it takes advantage of increased computer miniaturization and computer vision techniques to implement an embedded algorithm aimed toward hot spot characterization on solar panels that causes efficiency issues on solar power plants. For instance, infrared thermography techniques are used for the detection and characterization of photovoltaic defects [2]. These methods can be described as embedded algorithms, and implemented in the field for speeding up the detection and recovery of faulty solar cells. These embedded algorithms can be also implemented using aerial vehicles to ease data collection and processing in open environments. One of the key challenges identified for the implementation of aerial thermographic inspections of photovoltaic plants is its image resolution, since it depends on the thermographic camera performance characteristics and lens configuration used to capture the image, as well as the image preprocessing techniques implemented. [3]

This paper describes the implementation aspects of the hot spot algorithms to mitigate their power loss using a similar approach as in [5]. For that purpose it uses commercial-off-the-shelf components and open-source software development tools. The system is synthesized as a remote surveillance application that takes advantage of the IoT services, such as the cloud and web services. This implementation can be replicated by others to improve their solar panel efficiency and also for proactive maintenance of solar power farms.

The paper is organized as follows. First, the design of the embedded system is presented, including its concept of operations, use case scenarios, and systems architecture. Then, the systems software and hot spot algorithm implementation are presented and described using the Yocto project toolset, to finish this part with a set of experimental results being shown and discussed. Finally, conclusions and recommendations for further implementation are presented and discussed.

2 Remote Surveillance Systems Design

This section presents and discusses the aspects considered for the hot spot algorithm implementation with the remote monitoring embedded application.

2.1 Concept of operations

The remote surveillance system considers a flow of operation so that the project is executed in the best way as shown in figure 1. This flow is composed by the following operation stages:

1. **Installation and verification:** A specialized technician goes to the desired location that will be monitored. The technician is in charge of installing the camera, the embedded module, and the necessary connections, like Ethernet and power supply. He turns on the device and checks that it works correctly.

Embedded System for Hot Spots Characterization of Solar Panels 3

2. **Link to cloud Services:** Communication via the internet is established. Enabling the use of sockets and a public server for the transmission of the image and the report. The service is enabled for any user with access to the URL.
3. **Access and requests:** The user can establish his connection to the monitoring service through the corresponding URL. She can access the image and a report on the status of the panel. The user can make requests for the current status of the panel through the interface, in this case, the image and the report are updated.
4. **Logout:** The user closes the web browser.

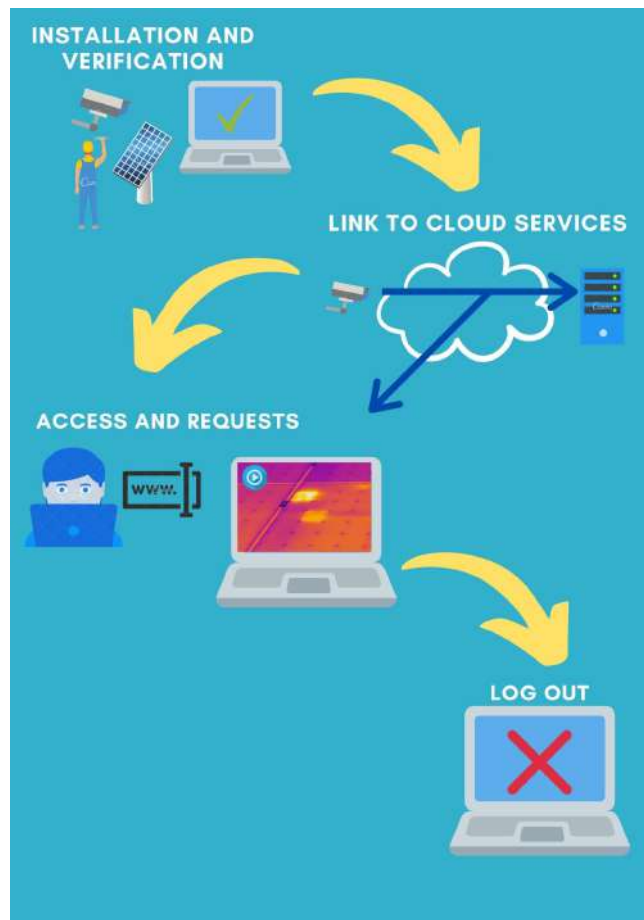


Fig. 1: Concept of operation for the remote surveillance system developed for hot spot characterization on solar panels.

4 C. Johan et al.

2.2 Use Cases Analysis

The use case analysis describes how the actors interact with the remote surveillance system. For that purpose, the use cases and 2 actors were identified as described in Figure 2. The actors correspond to the final user and the technician, the use cases identified were login, logout, the assembly, and finishing of the application.

The main actor for the assembly of the system is the technician which as pre-conditions requires a manual and to verify that the local network is active. The normal flow of operation includes powering the RaspberryPi 4, connecting the camera, verifying that the camera is recognized, and connecting to the router. The assembly includes verification of the operation of the system so the next use case described is the login and logout.

The login requires access to the local network on a web browser and the pre-defined IP address. The normal flow of operation includes accessing the web page and checking the last requested image, requesting an image, and changing the operation from automatic to manual. As for the logout closing, the web browser is enough.

To conclude with the operation of the system, terminating the web server and the disassembly are included.

2.3 Embedded Systems Architecture

The overall system architecture is represented in figure 3. This system is expected to work in a single place, as the web application was intended to be available on a local server. As one can see, the user (administrator or user) accesses the web application and is capable of managing the request of the image and state of the panel in real-time.

For the user interface, ReactJS will be used so that only the components of the image and the panel state are changed, in order to avoid rendering the entire page. The embedded system will not only process the image, it will contain a server written in NodeJS to handle requests from the User Interface and start the image capture and processing, and finally by sending back the results.

The integration diagram of software and hardware is shown in figure 4. The diagram describes the typical workflow and information that the “Hot Spots Monitoring System” has. The latter consists of remote access from a device with an internet connection to a local server through an URL address, enabling the possibility of observing the current state of the panel. Moreover, the current state of the panel is obtained by means of a thermal camera linked to a Raspberry Pi 4, that in return, processes and sends the image to the local server for its visualization. The AMG8833 thermal camera returns an array of 64 individual infrared temperature readings over I2C. It measures temperatures ranging from 0°C to 80°C with an accuracy of $\pm 2.5^\circ\text{C}$ and works at a maximum frame rate of 10 Hz.

The embedded system is equipped with a custom - Linux image developed with the Yocto Project tool. The Linux image optimizes the number of configurations and necessary packets for adequate functioning of the system without the

Embedded System for Hot Spots Characterization of Solar Panels 5

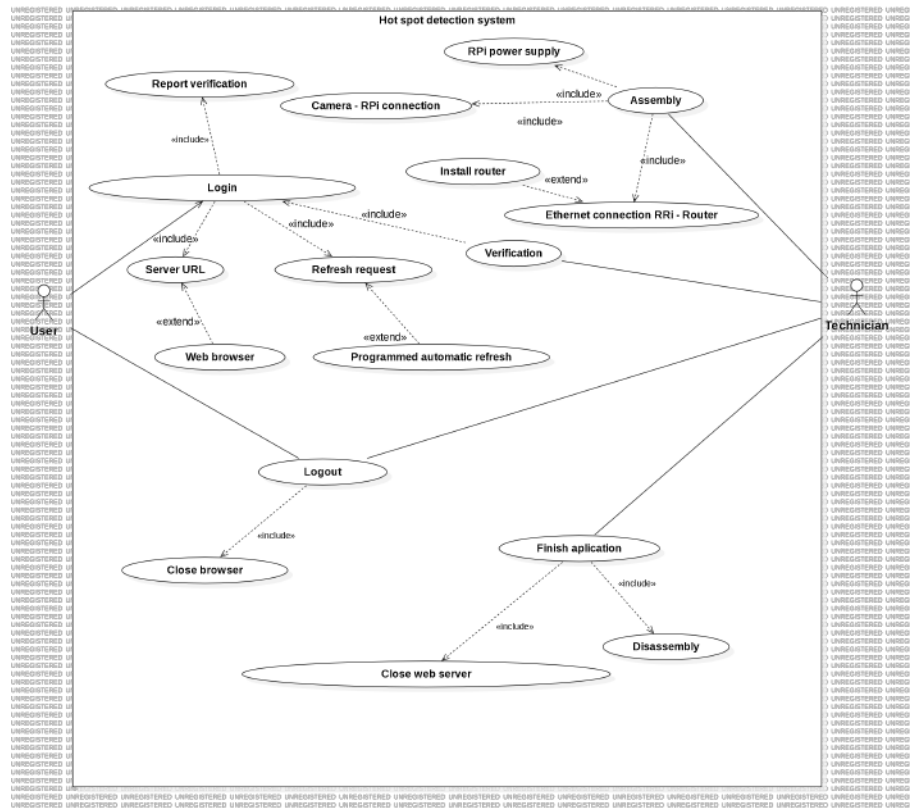


Fig. 2: Use cases diagram for the remote surveillance system developed for hot spot characterization on solar panels

6 C. Johan et al.

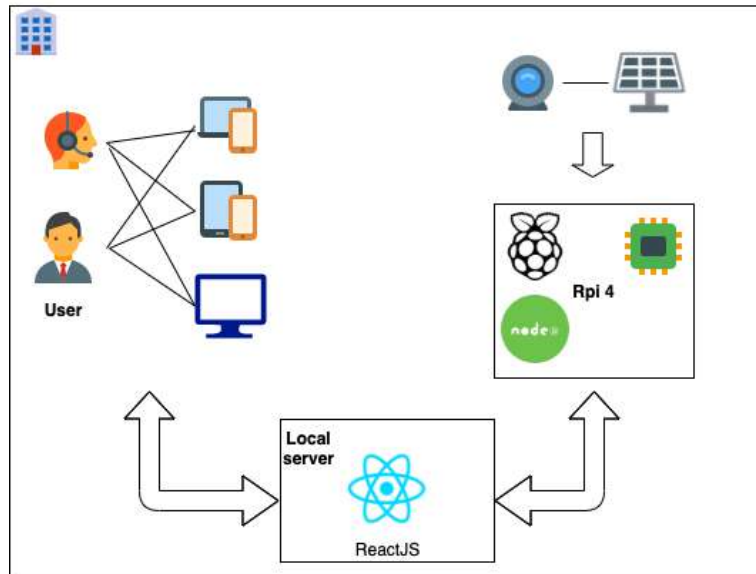


Fig. 3: General systems architecture for the remote surveillance system developed for hot spot characterization on solar panels

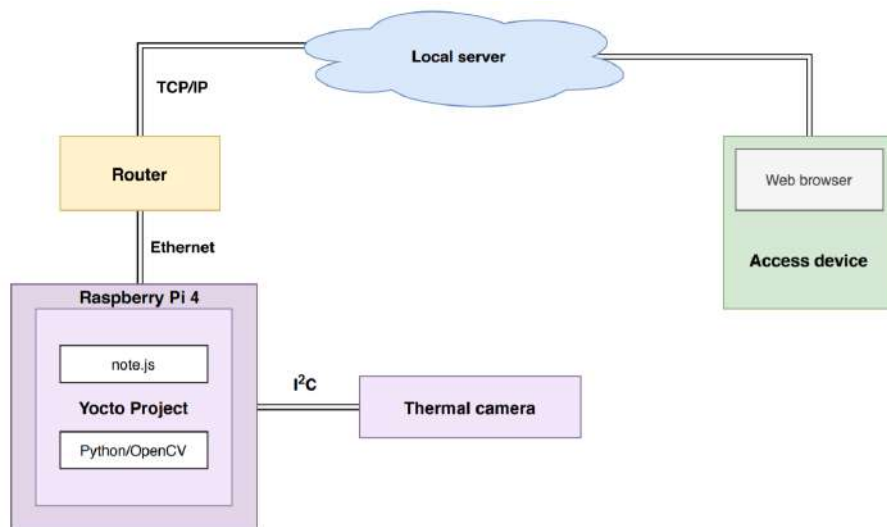


Fig. 4: Integration diagram of software and hardware in the hot spot characterization system

waste of resources. Furthermore, it is essential for the inclusion of two specific packets. Firstly, `note.js`, which serves to establish communication with the local server, and secondly, `Python/OpenCV`, which is in charge of the processing and analysis of the panel image.

The information flow of the system consists of the acquirement of an image in `.jpg` format from the thermal camera for its subsequent processing and analysis. Thereafter, a `.JSON` file is sent containing the current state and the image taken from the panel. Additionally, from the remote access device, it is possible to request the panel state through a `.JSON` file.

Figure 4 shows the interfaces/protocols between the Raspberry Pi 4 and the peripherals. The thermal camera employed is linked to the Raspberry employing an I2C (Inter-Integrated Circuit) protocol, which functions as a serial communication bus, synchronous, multi-master, and multi-slave. The protocol is widely utilized for attaching lower-speed peripheral ICs to processor and microcontrollers in short-distance, intra-board communication.

2.4 Systems Software Synthesis

The Yocto Project (YP) is an open-source collaboration project that helps developers create custom Linux-based systems regardless of the hardware architecture [13]. The project is built upon a series of tools which aide the embedded developers in the creation of these tailored operating system. The desired packages go through a building process which includes, fetching the source code, compiling, installing, and packaging. It allows multiple building schemes to be implemented at once such as `auto-tools` and `setup-tools` for python scripts. The building process is managed by the `Bitbake` which processes and schedules the packages, its dependencies, and the build itself. This process occurs within a cross-compilation scheme to take advantage of the processing capabilities of the host system.

Some limitations to this tool are the steep learning curve and the time required to build the first images depending on the host system processing capabilities.

The OpenEmbedded community metadata and layers are co-maintained by the Yocto Project and so most of the layers used within this project correspond to OpenEmbedded layers. All the layers used must be included in the `bblayers.conf` file.

The base layers included withing the `poky-zeus` distribution are:

- `meta`
- `meta-poky`

These layers contain basic configuration files to create some of the most common images like `minimal` or `sato`. The project is based on a minimal image so we are going to be using this basic configuration. This meta-layer also contains the necessary recipes to start an ssh server, graphics servers (X11, gnome, wayland, etc.) and other utilities useful to developers.

8 C. Johan et al.

The selected embedded device is the RaspberryPi 4 so we are going to need the meta-layer that contains the BSP for RaspberryPi and several configuration files to activate and control some of the hardware. The layer is:

- meta-raspberrypi

This meta-file also includes within the boot files the bcm2835-recipes-bb which gives support for the ARM processor for the newer RaspberryPi's. As for the OpenEmbedded layers we are going to be using:

- meta-networking
- meta-python
- meta-oe
- meta-multimedia
- meta-webserver

The OpenEmbedded layers give support for networking systems to configure systems as routers or switches as well as support for ftp/tftp servers. Most layers carry a dependency on meta-python to build some of the packages they include. It is important to note that including these layers does not mean that all the packages are going to be part of the final OS, but might be needed just for the building process. Meta-oe is the core layer and encloses recipes for various system features. Finally, meta-webserver provides the necessary recipes to use nodejs.

The last meta-layer included is going to be:

- meta-amg88xx

This meta-layer is of own elaboration and will contain all the necessary scripts for the server, image processing, and drivers needed to manage the thermal camera.

Most of the modifications to the basic minimal image are going to be made through the local.conf file. This allows reproducibility and portability. The variables which need to be modified are:

- MACHINE
- EXTRA_IMAGE_FEATURES
- DISTRO_FEATURES

With this we select the target machine we are building for, enable features like ssh server, x11 windows manager, and the package manager and activate communication protocols such as wifi and i2c. It is also through the local.conf that packages are installed. This is made using:

- IMAGE_INSTALL_append

If the name of the package exists within the layers included in the bblayers.conf file then Bitbake will build and install the package.

3 Results of the Implementation

3.1 Customized Operating System

Table 1 summarizes the installed packages and configurations for the customized operating system implemented for the remote surveillance application. The first section, RaspberryPi 4 support, states the target machine in this case raspberrypi4-64 because it is required for building a 64-bit system. The kernel modules are then loaded and the UART, i2c, and GPU memory are set to work.

For the thermal camera support and libraries, all the necessary libraries to command the camera are installed along with libraries needed for the image processing algorithm.

Python image processing englobes the scripts developed to process the image along with the Python interpreter for python3.

The OpenCV and python3 packages configurations are modified through the PACKAGECONFIG_append variable.

For the web server nodejs along with the Nodejs package manager nodejs-npm are installed. Finally, the license flag is set to commercial.

Table 1: Installed packages and configurations for the customized linux-based OS

RaspberryPi 4 support	Thermal Camera support + libraries
	IMAGE_INSTALL_append +=
	" adafruit-amg88xx"
	" python3-numpy"
	" opencv"
MACHINE ??= "raspberrypi4-64"	" imutils"
IMAGE_INSTALL_append +=	" adafruit-amg88xx"
" kernel-modules"	" python3-matplotlib"
" linux-firmware-bcm43455"	" python3-modules"
KERNEL_MODULE_AUTOLOAD_rpi +=	" cycler"
"i2c-dev i2c-bcm2708"	" kiwisolver"
ENABLE_UART = "1"	" python3-pillow"
ENABLE_I2C = "1"	" python3-pyparsing"
GPU_MEM = "120"	" python-dateutil"
	" python3-dateutil"
	" tk"
	" tcl"
	" colour"
Python image processing	Packages configurations
IMAGE_INSTALL_append +=	PACKAGECONFIG_append_pn-opencv =
" python3"	" dnn"
" python3-requests"	PACKAGECONFIG_append_pn-python3 =
" python-captura"	" tk"
" python-hotspot"	
Web Server	License
IMAGE_INSTALL_append +=	
" nodejs"	LICENSE_FLAGS_WHITELIST = 'commercial'
" nodejs-npm"	

3.2 Image Processing Algorithm

The hot spot characterization algorithm implemented consists of three different procedures: Gaussian filter, binarization, detection, and contour drawing. These steps were executed to determine and find the hot spot in the image of the solar panel acquired using the thermal camera connected to the system in the remote location. These procedures are explained in detail below. The algorithm is fed with thermal images as shown in Figure 5.

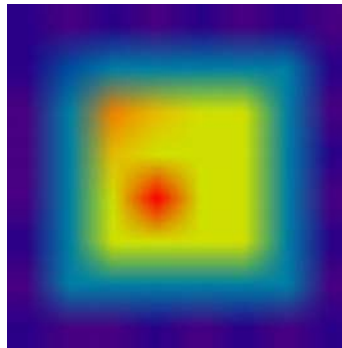


Fig. 5: Dirty solar panel image

Gaussian Filter: Gaussian filter (also known as Gaussian Blurring) is achieved by processing the input image of the panel through a low-pass filter. The blurring is applied for noise removal and softening of the image according to [10]. The function utilized is `cv2.GaussianBlur()`, which is part of the openCV library. The image with the filter applied is depicted in Figure 6a.

Binarization: Binarization or image thresholding assigns a fixed threshold value. Thereafter, each pixel is passed through this threshold. The pixel value is then compared to the threshold value, determining if the pixel is either black or white. To fulfill this procedure, the function utilized is `cv2.THRESH_BINARY` enclosed in the openCV library as it is shown in [9]. Moreover, the input image must be with a greyscale filter and the Gaussian Blurring already applied. The image with the binarization performed is presented in Figure 6b.

Detection and Contour Drawing: Once the image went through the Gaussian filter and the binarization process, the detection initiates together with the drawing in the original image of the found contours in the hot spots. To accomplish this process, it is employed the functions of detection and contour drawing, `cv2.findContours` and `cv2.drawContours`, respectively as it is shown in [8]. The final result of the complete image processing is presented in Figure 6c.

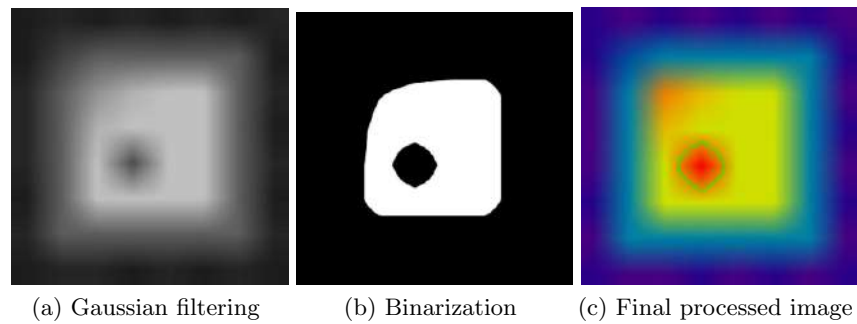


Fig. 6: Hot spot characterization algorithm

Finally, the system integration between the interface and the embedded system is completed. The user is able to type down the server ip and ports to initiate the request of solar panel data analysis. As depicted in figure 7, the image is fetched using get and post requests which are pointed to the RaspberryPi server, written in NodeJS, and the server handles the requests so that the application takes the picture, analyzes it and sends the data back to the page so that the user is able to corroborate the panel state using the image used to determine this state.

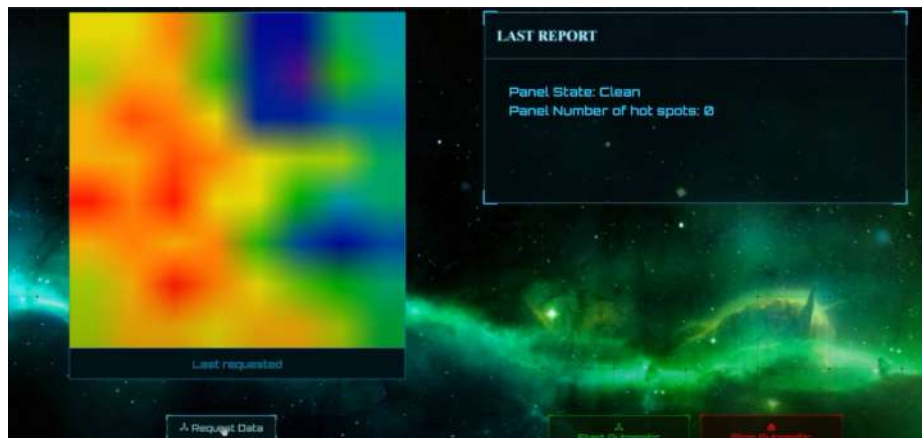


Fig. 7: Example of the integration of processed solar panel image with the user interface developed with remote surveillance system

3.3 Verification and validation

For the verification of the hot spot detection algorithm, two types of tests were carried out. The first one consisted of modifying the pixels value obtained from the thermal camera to generate an image that simulated the panel's surface with a hot spot and another without hot spots, these images are figures 8a and 8b, respectively.

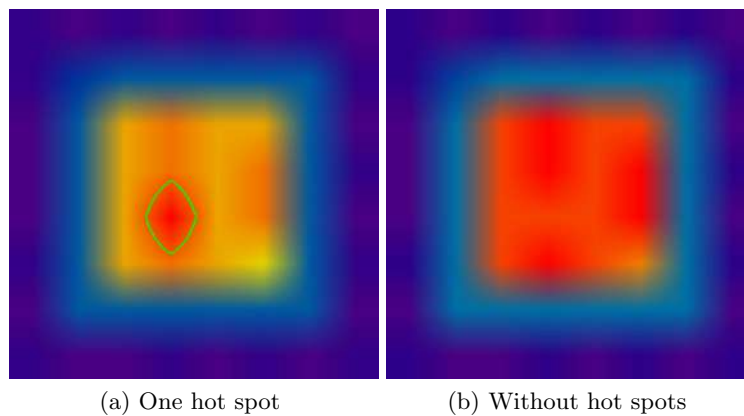


Fig. 8: Simulated images of the panel surface

The second test consisted of obtaining a thermal image of a single panel on the internet [4], which is shown already processed in the figure 9.

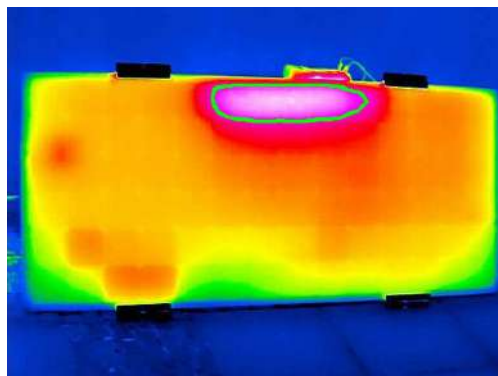


Fig. 9: Hot spot detection algorithm output

14 C. Johan et al.

For the validation of the system a Newpowa Off-Grid solar panel was used. It has a power output of 50 W at 12 V and dimensions of 58.6 x 50.5 x 30 cm. The test took place in Concepcion, Tres Rios, Costa Rica where the solar panel was set with an inclination of 0 °. To induce a hot spot a black A5 cardboard paper was placed in different places of the solar panel. The thermal camera was placed at a 30 cm distance from the solar panel. With this set up 5 images were taken and analyzed. From this set, up to 80% of them were consistent with input image containing a hot spot, the other 20% had trouble detecting the hot spots of the photo-voltaic surface.

4 Conclusions

For the development and implementation of the remote panel surveillance system, a concept of operation was developed that explains the general flow of the project. This concept of operation includes 5 stages, installation, and verification, link to cloud services, access and requests, and logout. There were 2 actors who defined the user and technician and 4 use cases login, logout, assembly and finishing the application.

The general architecture was designed and the embedded system along with the communication protocols was selected. A RaspberryPi 4 was selected as an embedded device, ReactJS as the front end, and NodeJS as the back end. The thermal camera selected was an Adafruit AMG8833 that uses i2c protocol to communicate with the RaspberryPi 4 embedded computer. For intra-network communication TCP/IP is used.

A prototype was implemented and a set of 5 images were taken and analyzed. From this set, 80% were effectively detected and the other 20% had trouble detecting the hot spots of the photo-voltaic surface due to image quality.

5 Future Work

To improve the overall system results, it is recommended the selection of a thermal camera with a better resolution. Another point to take into consideration is to study the time taken by each stage of execution, as this affects the timing between the requests. This becomes considerably important when changing the state of the system from manual requests to automatic requests, as there were collisions between different execution stages.





Further improvements to the hot spot detection algorithms are to be made to increment the efficiency of the detection system.

Another web server can be designed to work outside of the local network and improve the system reach.

References

1. Calvillo, C.F., Sánchez-Miralles, A., Villar, J.: Energy management and planning in smart cities. *Renewable and Sustainable Energy Reviews* **55**, 273–287 (2016)
2. Gallardo-Saavedra, S., Hernández-Callejo, L., Alonso-García, M.d.C., Muñoz-Cruzado-Alba, J., Ballestín-Fuertes, J.: Infrared thermography for the detection and characterization of photovoltaic defects: Comparison between illumination and dark conditions. *Sensors* **20**(16), 4395 (2020)
3. Gallardo-Saavedra, S., Hernández-Callejo, L., Duque-Perez, O.: Image resolution influence in aerial thermographic inspections of photovoltaic plants. *IEEE Transactions on Industrial Informatics* **14**(12), 5678–5686 (2018)
4. InfraTec: Thermographic inspection of photovoltaic installations, <https://www.infratec.eu/thermography/industries-applications/photovoltaic-inspection/>
5. Maghami, M.R., Hizam, H., Gomes, C., Radzi, M.A., Rezadad, M.I., Hajjighorbani, S.: Power loss due to soiling on solar panel: A review. *Renewable and Sustainable Energy Reviews* **59**, 1307–1316 (2016)
6. Meehl, G.A., Washington, W.M., Collins, W.D., Arblaster, J.M., Hu, A., Buja, L.E., Strand, W.G., Teng, H.: How much more global warming and sea level rise? *science* **307**(5716), 1769–1772 (2005)
7. Nicola, M., Alsafi, Z., Sohrabi, C., Kerwan, A., Al-Jabir, A., Iosifidis, C., Agha, M., Agha, R.: The socio-economic implications of the coronavirus pandemic (covid-19): A review. *International journal of surgery (London, England)* **78**, 185 (2020)
8. OpenCV: Contours : Getting started, https://docs.opencv.org/3.4/d4/d73/tutorial_py_contours_begin.html
9. OpenCV: Image thresholding, https://docs.opencv.org/master/d7/d4d/tutorial_py_thresholding.html
10. OpenCV: Smoothing images, https://docs.opencv.org/master/d4/d13/tutorial_py_filtering.html
11. Rode, P., Keim, C., Robazza, G., Viejo, P., Schofield, J.: Cities and energy: urban morphology and residential heat-energy demand. *Environment and Planning B: Planning and Design* **41**(1), 138–162 (2014)
12. Rumbach, A.: Decentralization and small cities: Towards more effective urban disaster governance? *Habitat International* **52**, 35–42 (2016)
13. Salvador, O., Angolini, D.: *Embedded Linux Development with Yocto Project*. Packt Publishing Ltd (2014)

The effect of clearance height, albedo, tilt and azimuth angle in bifacial PV energy estimation using different existing algorithms

Hugo Sánchez^{1,2} , Carlos Meza^{1,2} , Sebastian Dittmann^{2,3} , and Ralph Gottschalg^{2,3} 

¹ Electronics Engineering School, Costa Rica Institute of Technology, Costa Rica
husanchez@tec.ac.cr

² Anhalt University of Applied Sciences, Köthen, Germany

³ Fraunhofer-Center for Silicon Photovoltaics CSP, Halle, Germany

Abstract. Bifacial photovoltaic is a promising technology that is being considered more in solar installations worldwide. However, there is still a lot of open questions regarding the estimation of the energy generation for this technology. The present paper presents an analysis of the variables involved in the modelling of the energy yield, as well as a quantitative analysis for some of the most common models found in the literature. In this regard, a series of simulations were made in order to compare the bifacial PV model energy yield in Bernburg, Germany and Cartago, Costa Rica. A statistical comparison has been performed to analyse the accuracy and response for each variable. Also the algorithms are compared with respect to the computational resources they use. The work presented might serve as a base for validation with real data to contribute with the accuracy of the estimation for the energy yield in bifacial modules.

Keywords: bifacial PV · photovoltaic energy simulation, photovoltaic systems · Energy Rating

1 Introduction

It is well known that bifacial photovoltaic (PV) modules can utilise incident sunlight via front and rear side absorption. This allows higher energy production under various installation conditions such as large solar farms or roof-top installations. However, the bifacial energy gain depends highly on, e.g., module design, mounting method, and reflectivity of the background. However, the bifacial energy gain depends highly on, e.g., module design, mounting method, and reflectivity of the background. [1, 2, 4, 7, 12, 25]. Figure 1 shows a qualitative comparison between the monofacial and bifacial modules.

Nowadays, the PV bifacial technology has been getting much attention from stakeholders given the increased capacity of generation with practically the same amount of area and system costs as monofacial PV modules [13]. However, there is not yet a standard method to estimate the real energy output as it is the case in monofacial PV technologies. The energy estimation on bifacial PV modules

2 Hugo Sánchez et al.

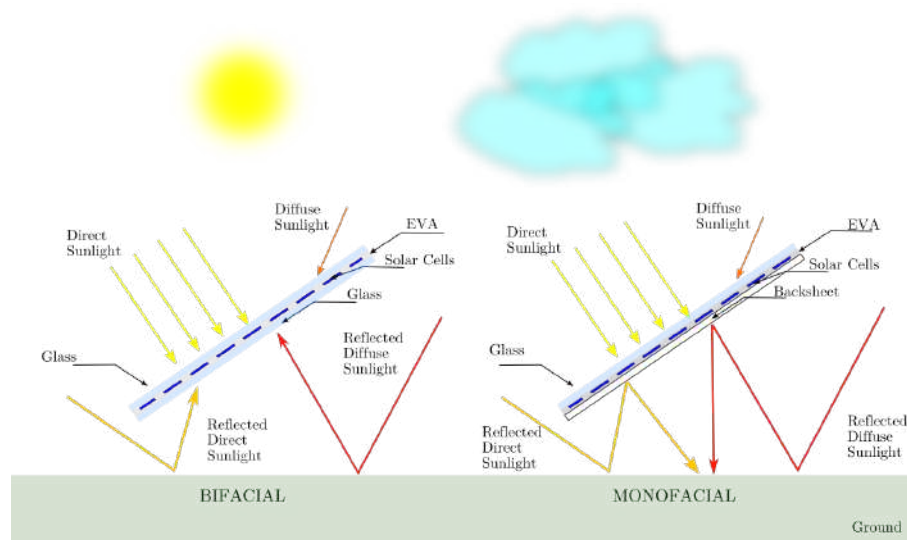


Fig. 1. Comparison between bifacial and monofacial module

presents even more challenges due to reflected rear side irradiance, which highly depends on the location and the design of the PV system. To reach confident estimations, it is necessary to consider several variables such as the height from the floor of the module, the tilt angle, the background reflectance, sun elevation, and diffuse irradiation [23]. The present paper compares different PV bifacial power estimation models located in two different climates, i.e., equatorial fully humid (Af) and warm temperate fully humid warm summer (Cfb) according to the Köppen-Geiger Climate Classification [14]. The comparative analysis is based on simulations executed with five different programs. The objective of the present paper is to determine the different results obtained and how that changes for different climates. The rest of the paper is structured as follows, first, a literature review about the methods for estimation of energy yield in bifacial modules as well as the main variables that affect the energy production in bifacial models are presented. Then, a description of the main simulation programs used in the comparison, methodology, and other considerations are shown. After that, the paper describes the simulation results for the two places selected (Bernburg, Germany, and Cartago, Costa Rica) and compares the energy yield between the models. Finally, the synthesis of the results and conclusions are shown.

2 Methods for estimation of Energy Yield in the Literature

Energy estimation model for bifacial modules have been studied by several authors and research groups developing diverse methods with its own considerations and assumptions ([1, 3, 4, 15–17, 22, 24]). However, it is possible to describe

a general approach when the different energy estimation methods are compared. Figure 2 shows a flow diagram of this general structure together with their tools founded in the literature, which is further detailed in Table 1.

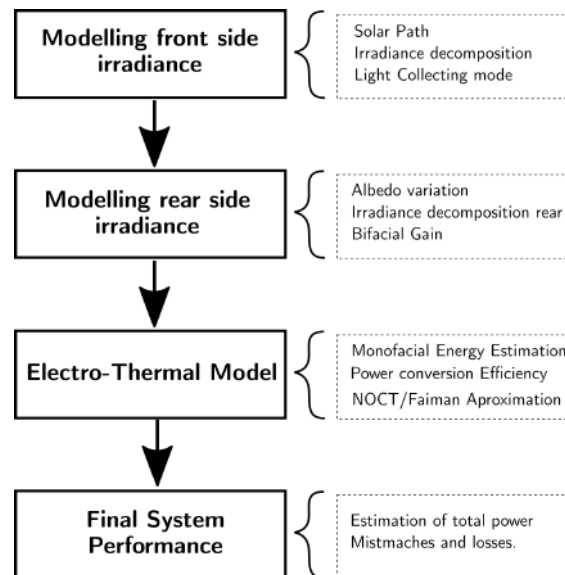


Fig. 2. General modelling flow for the estimation of energy in bifacial modules

Rear side irradiance analysis is a process that it is essential for the power estimation of bifacial modules, and that haven't been analysed in detailed until recently. The next section presents the main considerations that need to be taken into account for this case.

2.1 Estimation of the rear side irradiance

The front side irradiance estimation for bifacial PV modules can be adapted from monofacial PV modules, which is already standardised and validated in several models. [8]. However, the estimation of the rear side irradiance is relatively new and several approaches can be found in the literature. In addition to the variability of the solar resource during the day, the irradiance reflection on the surface generates a more complicated phenomenon to analyse. Several studies founded in the literature show that the energy output is dependent on the installation conditions (e.g. elevation, orientation, tilt angle), as well as the environment conditions (irradiance intensity, ground reflectivity of different substrates, seasonal variation) [9]. This situation opens the discussion about the optimisation in the energy estimation for a bifacial module.

Most of the models found in the literature can be classified in three categories: *Empirical models*, *View Factor Models* and *Ray Trace Models*. Figure 3

4 Hugo Sánchez et al.

Table 1. Description for the simulations steps in the energy estimation for bifacial modules

Stage	Description	Output Results
Modelling front side irradiance	This is the most common methods used because it is completely studied and analyzed for the estimation of energy in monofacial modules. Also it is standardized process.	<ul style="list-style-type: none"> – Sun Path – Direct Irradiance POA – Diffuse Irradiance POA – Albedo Irradiance POA
Modelling rear side irradiance	Then, the effects of the reflected irradiance is estimated. As a result, the the bifacial relatively gain is obtained.	<ul style="list-style-type: none"> – Direct Irradiance POA – Diffuse Irradiance POA – Albedo POA – Bifacial Gain
Electro-Thermal Model	In this step, the monofacial module energy is estimated. For this step the rules already analyzed and tested are used	<ul style="list-style-type: none"> – Power conversion – Efficiency – Thermal Losses – NOCT – Monofacial Energy Yield
Final System Performance	A final corrections are applied according the suppositions made in all the models. There is a difference in the methods used for every model found.	<ul style="list-style-type: none"> – Corrections – Electrical Losses – Mismatch

shows an overview and a classification of nine energy yield models for bifacial PV modules.

The *Empirical Models* corresponds to the group of models that were obtained using short or long term experimental data. The *View Factor Models* correspond to the utilisation of geometrical construction as a definition of thermodynamics. *Ray Tracing models* corresponds to the models that use software for the estimation of the light rays through a determined conditions in a 3D environment.

2.2 Variables that affects the energy production in bifacial models

Several variables affect the energy production of bifacial PV modules but also the energy yield estimation. The present section gives a primary definition of these variables. Figure 4 shows the main variables which affects the energy yield estimation of bifacial PV modules. Namely,

- **Albedo** (*albedo*): is the diffuse reflectivity of a horizontal surface which is defined as the ratio of the reflected irradiance by surface and the received irradiance. It is measured on a scale from 0 to 1.
- **Rear/front-side irradiance ratio** (α): is the diffuse reflectivity of a tilted surface which is defined as the ratio of the reflected irradiance by surface

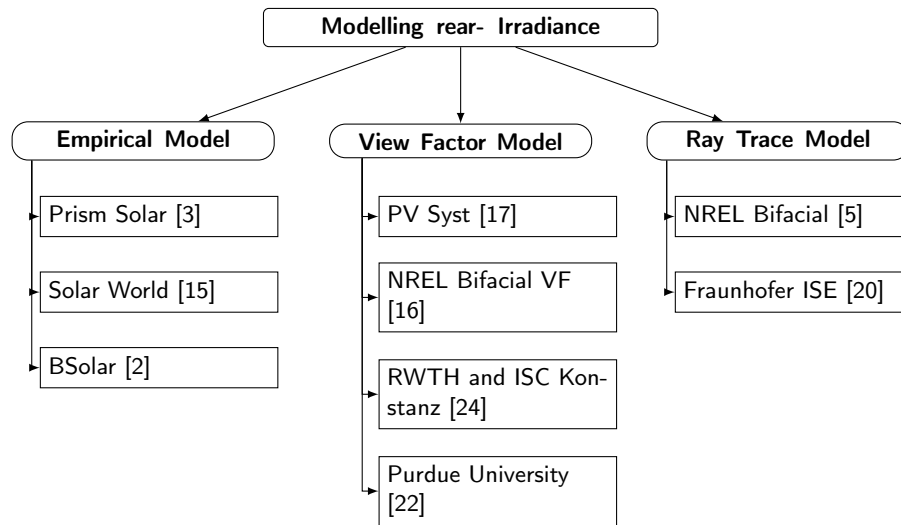


Fig. 3. Comparison for modelling rear-irradiance

and the received irradiance on the rear side of the bifacial PV module. It is measured on a scale from 0 to 1.

- **Clearance Height (CH):** is defined as the distance from the lowest point of the solar module to the ground. This influences the collection of the rear-side irradiance.
- **Tilt Angle (β):** refers to the inclination, measured in degrees, that the edge of the PV module forms with a parallel line to the ground. This factor will influence both front and rear side irradiance collection in the solar module.
- **Module Height (MH):** refers to the dimension of the PV module, seen in the lateral plane. It is dependent on the orientation of the module (landscape or portrait). This factor has an impact on the self-shadowing of the solar module and the possibility to collect rear-side irradiance.
- **Azimuth (γ):** refers to the compass direction in which the solar module or array is installed. It affects both front and rear side energy production due to the changing position of the sun during the day.
- **Ground Coverage Ratio (gcr):** it is defined as the ratio of the PV modules' area to the used land area. This is an important aspect when the analysis considers more than one array. It can be also defined as the ratio of array length to row-to-row pitch. A definition and discussion about this term can be found in [6, 7, 24]

3 Bifacial PV power estimation programs

The models considered for comparisons are listed next:

6 Hugo Sánchez et al.

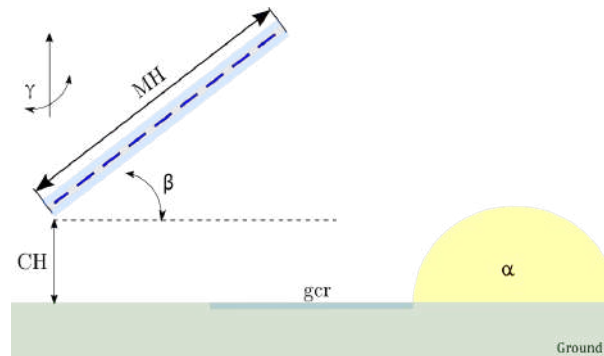


Fig. 4. Factors that affect the bifacial gain energy

- **Purdue University Bifacial:** this is a model that uses View Factor concept from thermodynamics developed by researchers at Purdue University for the estimation of bifacial energy generation. The information on the model can be found in [22]
- **Prism Solar:** This model was developed by the company Prism Solar. It consist in a general linear regression that allows predicting the behaviour of the solar bifacial tools. The linear regression was validated with real data for a small range of values. The model and its validation can be found in [3]
- **Solar World:** The model was developed by the company Solar World, using data analytic from three different systems installed and then obtaining a mathematical regression from the data. The description of model as well as the experiment can be found in [15]
- **NREL Radiance Bifacial:** It consists in a open source software that uses an integration of the back-end software *Radiance* for ray tracing estimation. The considerations for the software as well as the validation of the model can be found in [18].
- **PVSyst:** Since 2017 the software includes the feature for simulation for bifacial modules. The software uses the view factor geometry for the installation. The details of the models can be found in [17].

The models of *Prism Solar*, *Solar World* and *Purdue University Bifacial* were implemented in *Python v3.7* with the integration of the library *PVLib* [21]. For the case of *PV Syst*, the version used was the v6.8.6. In the case of *NREL Radiance Bifacial*, the release used was the 5.2 that is available in [5]. In the next section the simulation study and the comparison between the models are presented.

4 Simulation study

To compare the bifacial PV module power estimation results of the considered algorithms (*Purdue University Model*, *Prism Solar Model*, *Solar World Model*,

Variables involved in the generation of bifacial PV modules 7

Radiance Bifacial Model and *PVSyst Model*) a simulation case study has been designed. The places for study correspond to the location of the PV Outdoor Characterisation of Anhalt University of Applied Sciences at Bernburg, Germany, and the experimental PV plant from the Costa Rica Institute of Technology in Cartago, Costa Rica so that in the future it will be possible to run experiments to validate the simulated results. The parameters used in the simulation study are shown in Table 2.

Table 2. Main Parameters for the sites of analysis

Location	Latitude [°]	Longitude [°]	Tilt Angle [°]	Module	Module	Bifaciality [%]
				Landscape Height [m]	Portrait Height [m]	
Bernburg	51.773	11.763	35	1	2	90
Cartago	9.853	-83.912	15	1	2	90

The module height for both configurations (landscape and portrait) is assumed for the standard dimensions for a 72 solar cell PV module. The tilt angle is defined to maximise the power energy production of a monofacial PV modules in each site. The bifaciality is chosen in 90% as it is common to find in commercial modules. The 22 year meteorological database from NASA is used. Additional parameters used in the simulation are shown in Table 3.

Table 3. Main physical variables used in the

Parameter	Value	Unit
Azimuth Angle	180	°
Front Site Efficiency	18	%
Bifaciality	90	%
Temperature Coefficient	-0.4319	%/K
U_0 Constant heat transfer	22.7	$W/m^2/K$
U_1 Convective heat transfer	6.84	$W.s/m^3/K$

Only the landscape configuration was used given that this is the case from which more energy can be obtained. As a metric to compare the simulation results the same methodology for the analysis of the energy performance of the models in a *Round Robin* campaigns is used [8]. These metrics consider the deviation with respect to the average value. In this regards, for all the variables analysed the median value is calculated and then the Root Mean Square Deviation (RMSD) and the Mean Bias Deviation(MBD) are estimated using as a reference value the median for the all measurement.

5 Results

The results of the simulation study are shown in figures 5, 6, 7 and 8 and are discussed in the following sections.

5.1 Clearance Height

It is known that there is a dependence between the clearance height of the module and the reflected irradiance. The parameters used to evaluate the effect of the clearance height in the models are shown in Tables 2 and 3 and the following values have remained constant for all simulations:

- Rear/front-side irradiance ratio: 25%
- **GCR:** 50%
- **Clearance Height:** from 0.5m to 4m, in steps of 0.1m.

Figure 5 shows the results of the effect of the clearance height on the energy for the selected models, where it can be seen that as the height of the module increases the energy yield increases. The slope of the dependence is larger below 1,5 meters of height. Except for the *Prism Solar* model, the models follow the same trend for the height variation. The most conservative model for this variable is the *Solar World* model. The most optimistic model corresponds to the *Radiance Bifacial* for both locations. The curve from *Prism Solar* is expected because its authors stated that is only valid in a range from 0.5m and 1.2m. The calculation of RMSD and MBD gives a statistical comparison between modules. In this case, the average value of all models is estimated and this value is used as the reference for the estimation of the errors. Table 4 shows the calculation of RMSD and MBD.

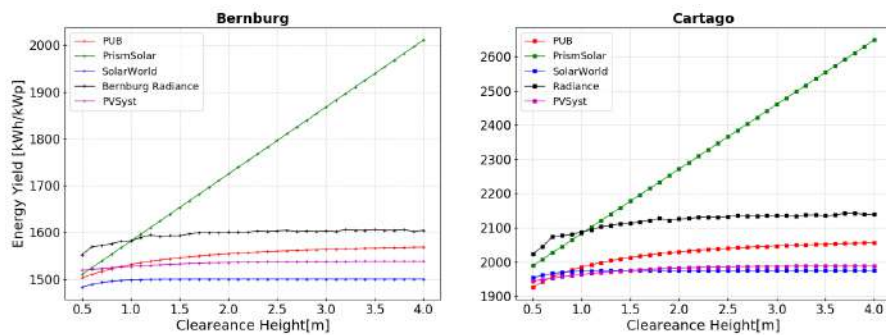


Fig. 5. Comparison height effects for different models Bernburg and Cartago

Based on the results shown in 4 the *Radiance* model has the closest approximation in the case of Bernburg. On the other hand, the *PUB* model has the closest approximation for the case of Cartago. The model of *Prism Solar* is the farthest approximation in both cases.

Table 4. Summary of comparison clearance height effects between different models

Site	Bernburg		Cartago	
Model	RMSD [%]	MBD [%]	RMSD [%]	MBD [%]
PUB	2.666	-2.331	2.2270	-1.935
Prism Solar	12.925	10.851	10.324	7.643
SolarWorld	6.019	-5.619	4.936	-4.2932
Radiance	1.748	0.505	3.923	3.890
PVSyst	3.938	-3.405	4.564	-4.087

5.2 Rear/front-side irradiance ratio

Rear/front-side irradiance ratio has an almost linear influence on the reflected irradiance and therefore in the bifacial energy estimation. In addition to the parameters given in Tables 2 and 3, the next values were set constant for all simulations:

- **Rear/front-side irradiance ratio:** from 10% to 70%, in 10% steps.
- **GCR:** 50%
- **Clearance Height:** 1.5m

Figure 6 shows the simulation results between the selected models.

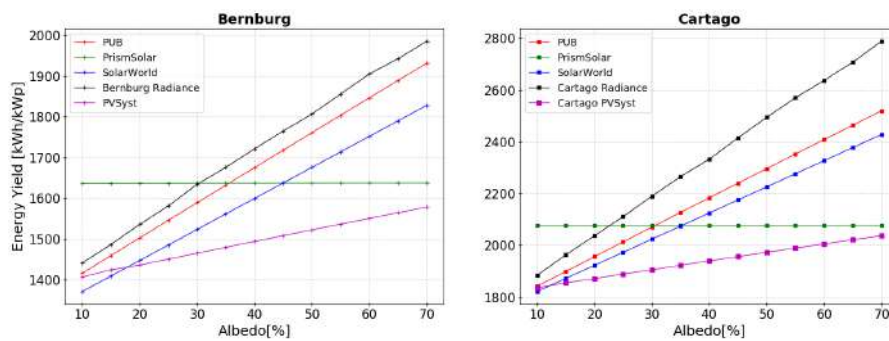


Fig. 6. Comparison Rear/front-side irradiance ratio effects for different models Bernburg and Cartago

In this case, it is possible to identify a linear relationship between the energy yield and the rear/front-side irradiance (RFI) value. For higher RFI more energy at the rear is expected. Except for the *Prism Solar* model, the models follow the same trend for the RFI variation. The most conservative model for this variable is the *Pv Syst* model. The most optimistic model corresponds to the *Radiance Bifacial* model for both locations. However the model from *Prism Solar* also has

a slope but it is too small that graphically looks like constant value. Using the same methodology from this analysis, the RMSD and MBD is estimated. Table 4 shows the calculation of RMSD and MBD.

Table 5. Summary of comparison rear/front-side irradiance ratio effects between different models

Site	Bernburg		Cartago	
Model	RMSD [%]	MBD [%]	RMSD [%]	MBD [%]
PUB	4.594	3.085	3.764	2.361
Prism Solar	6.517	0.787	7.439	-2.597
SolarWorld	2.749	-1.534	1.916	-0.343
Radiance	7.012	5.766	11.483	9.658
PVSyst	8.715	-8.104	9.944	-9.080

The obtained results shown that the *Prism Solar* model has the closest approximation for the case of Bernburg and for the *Solar World* model in the case of Cartago. On the other hand, the *PV Syst* is the farthest approximation in Bernburg and the *Radiance* model is the farthest approximation in Cartago.

5.3 Tilt Angle

Due to the movement of the Sun during the year the tilt angle has an influence on the performance of the installation. This situation is well analysed for monofacial PV modules. For the tilt angle analysis, in addition to the parameters given in Tables 2 and 3, the next values are maintain fixed for all simulations:

- **Rear/front-side irradiance ratio:** from 25%
- **GCR:** 50%
- **Clearance Height:** 1.5m
- **Tilt Angle:** from 20° to 50° in Bernburg. From 0° to 30° in Cartago.

Figure 7 shows the comparison between the selected models.

In contrast previous analysis all the models present more variability in the energy yield with respect to changes of the tilt angle. The most conservative model for this variable is the *Solar World* model in both sites. The most optimistic model corresponds to the *Prism Solar* model in Bernburg and the *Radiance* model in Cartago. Using the same methodology from this analysis, the RMSD and MBD are estimated. Table 6 shows the calculation of RMSD and MBD.

The *PUB* model has the closest approximation in the Bernburg case and the *PV Syst* model has the closest approximation for the case of Cartago. The *Prism Solar* model is the furthest in the case of Bernburg and the *Radiance* model is the furthest in the case of Cartago.

Variables involved in the generation of bifacial PV modules 11

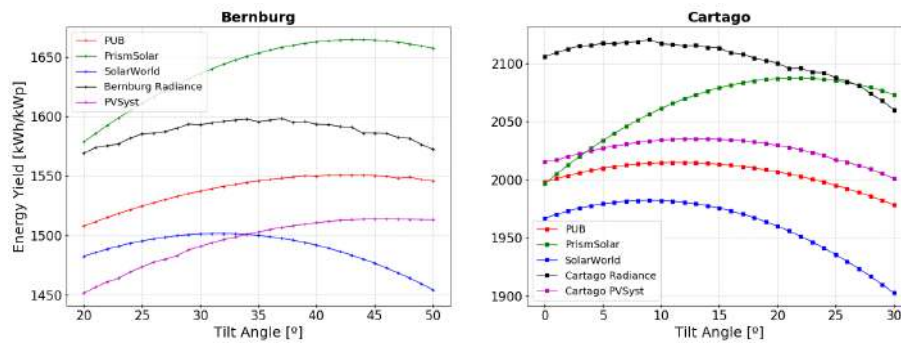


Fig. 7. Comparison tilt angle effects for different models Bernburg and Cartago

Table 6. Summary of comparison tilt angle effects between different models

Site	Bernburg		Cartago	
Model	RMSD [%]	MBD [%]	RMSD [%]	MBD [%]
PUB	0.756	-0.727	1.332	-1.332
Prism Solar	5.902	5.825	2.066	1.571
SolarWorld	4.130	-3.969	3.548	-3.463
Radiance	2.463	2.408	3.560	3.528
PVSyst	3.585	-3.536	0.326	-0.313

5.4 Azimuth

For the azimuth angle simulation the following variables are kept constant:

- **Rear/front-side irradiance ratio:** from 25%
- **GCR:** 50%
- **Clearance Height:** 1.5m
- **Azimuth:** from 90° to 270 °

Figure 8 shows the comparison between the selected models. It important to highlight that the response for this variable is similar than the monofacial modules. The models have the same trend of variation for both sites. However the sensibility to the azimuth angle is bigger in the case of Bernburg where the optimal angle is close to 180°. The most conservative model for this variable is the *PV Syst* model. The most optimistic model corresponds to the *Radiance Bifacial* model for both locations. However the model from *Prism Solar* also has a slope but it is so small that graphically looks like constant value. Using the same methodology from this analysis, the RMSD and MBD is estimated.

Table 4 shows the calculation of RMSD and MBD.

Compared to the average value, the *PV Syst* model has the closest approximation in both places. On the other hand, the *Solar World* has the farthest approximation in both places.

12 Hugo Sánchez et al.

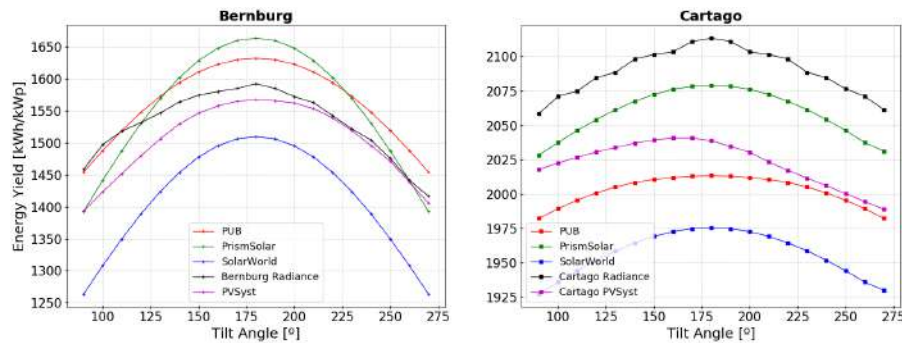


Fig. 8. Comparison azimuth effects for different models Bernburg and Cartago

Table 7. Summary of comparison azimuth effects between different models

Site	Bernburg		Cartago	
Model	RMSD [%]	MBD [%]	RMSD [%]	MBD [%]
PUB	3.367	3.321	1.189	-1.167
Prism Solar	3.260	2.8795	1.640	1.632
SolarWorld	6.722	-6.651	3.431	-3.428
Radiance	1.873	1.093	3.131	3.125
PVsyst	1.094	-0.642	0.473	-0.161

5.5 Computational Resources

In the previous section and analysis for different models under different variables was performed. This analysis gives an idea of the accuracy of the different models in every case. When simulation methods are compared, it is also necessary to have a look at the computational resources and performance for every algorithm. For this purpose, Table 8 shows a quantitative comparison for the result of every method available. The table is made using as a reference the work presented in [19].

From the previous table, the models from *PV Syst* and *Bifacial Radiance* from NREL that can estimate more features regarding the simulation. Looking for the time consuming aspect, the *Bifacial Radiance* model is the most time-consuming algorithm, due to the ray-tracing solving process. In the case of *Prism Solar* and *Solar World*, the running time is faster. These models are simplified for a simple equation. Nevertheless, these models are more liable to underfitting or overfitting the energy yield estimation in bifacial models.

A balance between accuracy and use of the computational resources has to be consider for the creation of suitable tool for the estimation of energy yield in bifacial models.

Table 8. Quantitative comparison between models for the energy estimation in bifacial models

Quantity	Prism Solar	Solar World	RTWH & ISC	PUB	PV Syst	Radiance
Albedo, tilt, h , gcr	✓ ¹	✓	✓	✓	✓	✓
Panel Size	X ²	✓ ³	✓ ³	✓ ³	✓	✓
BG _E resolution	Yearly	Yearly	Hourly	Monthly	Hourly	Hourly
Running time for yearly simulation ⁴	< 1s	< 1s	< 60s	< 60s	< 5s	< 60s
Irradiance profiles	-	-	-	✓	✓	✓
Ground incident irradiance	-	-	✓ ⁵	✓ ⁵	✓ ⁶	✓ ⁵
Glass-Air Transmission Loss	-	-	-	-	✓	-
Light transmitted between cells	-	-	-	-	✓	✓
Shading Losses	-	-	✓	-	✓ ⁶	✓
Specific nuMBDr & size rows	-	-	✓	1	✓	✓
Edge effects modelled	-	-	-	-	✓	✓
1-axis tracking	-	-	-	-	✓	✓

¹ Row spacing is assumed to be equal to or larger than the typical row spacing at noon on DeceMBDr 21st.

² The model is designed for a specific commercial modules.

³ Geometry is scaled relative to the collector width.

⁴ Simulations performed on a ASUS PREDATOR computer equipment with a Intel Core 17-7700HQ processor and 16 GB of RAM

⁵ Perez diffuse sky irradiance

⁶ Isotropic diffuse sky irradiance

⁷ Consider all the shadows with a shadow factor

6 Synthesis of results

The present paper contains an analysis of the influence of different variables in the energy yield estimation for bifacial modules. The factor analysed are clearance height, Rear/front-side irradiance ratio, tilt angle, and azimuth. The second part contains a comparison for every variable consider in the mathematical models found in the literature. Using *Round Robin* methodology presented in [8, 10, 11] a summary of the errors obtained are shown in Figure 9.

As was studied in the present chapter and making an analysis of Figure 9, Table 9 shows a summary of the comparison obtained.

The previous table shows the typical curve for every variable. Also, it shows which is the most accurate prediction as well as the less accurate prediction model for every variable. This accuracy is estimated compared to the mean val-

14 Hugo Sánchez et al.

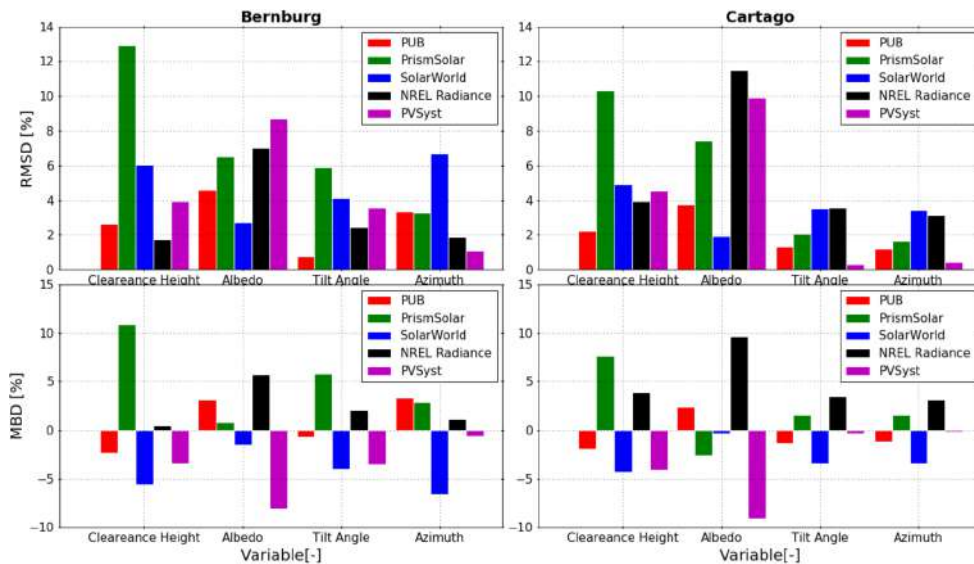


Fig. 9. Comparison albedo effects for different models Bernburg and Cartago

Table 9. Summary of the comparison in energy yield estimation models

Site		Bernburg		Cartago	
Variable	Curve	MAA ¹³	LAA ²³	MAA ¹³	LAA ²³
Clearance Height	Bounded Exponential	Radiance	Prism Solar	PUB	Prism Solar
	Linear increasing	Prism Solar	PV Syst	Solar World	Radiance
Tilt Angle	Polynomial	PUB	Prism Solar	PV Syst	Radiance
Azimuth	Parabola	PV Syst	Solar World	PV Syst	Solar World

¹ More Accurate Algorithm.

² Less Accurate Algorithm.

³ Compared to the mean value of the simulations.

ues for all models. When the RMSD and MBD are estimated, all the models report less than 10 % of error. This value indicates that all the models could fit the estimation. However, there are some atypical cases such as the *Prism Solar* model. This model has a different response when the clearance height and the albedo change. According to the error estimated, the more acceptable models for both places are *PUB* model and *PV Syst* model. In Bernburg, *Radiance* model has acceptable accuracy.

Another important point to consider is the computational performance of the algorithms. On this topic, it has to be considered the balance between the computational resources and the possible outputs obtained. Table 8 presents an

analysis for all the models used. From this table, the *PV Syst* model and the *Radiance* model give output variables and information. Nevertheless, the *Radiance* model is one of the most time-consuming algorithms to make an estimation along with the *PUB* model. Despite their differences in assumptions and complexity, there is a good agreement between all models.

7 Conclusions and outlook

The present work shows how the estimation of bifacial modules is affected by several factors such as Clearance Height, Albedo, Tilt Angle, and Azimuth. Also, the practical comparison of different models found in the literature. Due to the penetration in the market of bifacial modules it is necessary to elaborate on accurate tools for the process, planning and design. In the case of the *Ray Trace Models* it is still not clear the accuracy of the model compared to the *View Factor Models* (*PUB*, *PVSyst*), that present less deviation in the statistical analysis. On the other hand, the *Ray Trace Models* requires more time and more computational resources to converge into a result.

It is necessary to carry out analyses with field validation data to get a more realistic analysis, as well as considering the changes that the variables can present during the year. Bifacial technology offers interesting applications and benefits compare to the monofacial modules. For this reason, it is necessary to develop accurate tools to help other PV professionals and stakeholders in the making-decision process. And with that, contribute to the transition to a clean energy age.

References

1. Appelbaum, J.: Bifacial photovoltaic panels field. *Renewable Energy* **85**, 338–343 (2016)
2. Bsolar: Commercial test sites and outdoor field results. <http://www.b-solar.com/Technology.aspx?Sel=Field%20Results>, accessed: 2020-04-26
3. Castillo-Aguilella, J.E., Hauser, P.S.: Multi-variable bifacial photovoltaic module test results and best-fit annual bifacial energy yield model. *Ieee Access* **4**, 498–506 (2016)
4. Cuevas, A., Luque, A., Eguren, J., del Alamo, J.: 50 per cent more output power from an albedo-collecting flat panel using bifacial solar cells. *Solar Energy* **29**(5), 419–420 (1982)
5. Deline, C., Ayala, S.: Bifacial radiance. [Computer Software] <https://doi.org/10.11578/dc.20180530.16> (12 2017), <https://doi.org/10.11578/dc.20180530.16>
6. Deline, C., Dobos, A., Janzou, S., Meydbray, J., Donovan, M.: A simplified model of uniform shading in large photovoltaic arrays. *Solar Energy* **96**, 274–282 (2013)
7. Deline, C., MacAlpine, S., Marion, B., Toor, F., Asgharzadeh, A., Stein, J.S.: Evaluation and field assessment of bifacial photovoltaic module power rating methodologies. In: 2016 IEEE 43rd Photovoltaic Specialists Conference (PVSC). pp. 3698–3703. IEEE (2016)

16 Hugo Sánchez et al.

8. Dittmann, S., Friesen, G., Williams, S., Betts, T., Gottschalg, R., Beyer, H., de Montgareuil, A.G.: Results of the 3rd modelling round robin within the european project „performance”–comparison of module energy rating methods. In: Proceedings of the 25th European Photovoltaic Solar Energy Conference, Valencia, Spain. pp. 6–10 (2010)
9. Dittmann, S., Sanchez, H., Burnham, L., Gottschalg, R., Oh, S.Y., Benlarabi, A., Figgis, B., Abdallah, A., Rodriguez, C., Rütther, R., et al.: Comparative analysis of albedo measurements(plan-of-array and horizontal at multiple sites worldwide. In: 36th European Photovoltaic Solar Energy Conference (EU PVSEC). pp. 1388–1393 (2019)
10. Friesen, G., Gottschalg, R., Beyer, H., Williams, S., van Sark, W., Guérin de Montgareuil, A., Van Der Borg, N., Huld, T., Müller, B., De Keizer, A., et al.: Inter-comparison of different energy prediction methods within the european project" performance"-results of the 1st round robin. In: 22nd European Photovoltaic Solar Energy Conference. pp. 2659–2663. WIP-Renewable Energies (2007)
11. Friesen, G., Dittmann, S., Williams, S., Gottschalg, R., Beyer, H., de Montgareuil, A.G., Van Der Borg, N., Burgers, A.R., Kenny, R.P., Huld, T., et al.: Inter-comparison of different energy prediction methods within the european project „performance”-results of the 2nd round robin. In: Proceedings of the 24th European Photovoltaic Solar Energy Conference. pp. 3189–3197 (2009)
12. Guerrero-Lemus, R., Vega, R., Kim, T., Kimm, A., Shephard, L.: Bifacial solar photovoltaics—a technology review. *Renewable and sustainable energy reviews* **60**, 1533–1549 (2016)
13. ITRPV: International technology roadmap for photovoltaic (itrpv)-2019 results (2020)
14. Kottek, M., Grieser, J., Beck, C., Rudolf, B., Rubel, F.: World map of the köppen-geiger climate classification updated. *Meteorologische Zeitschrift* **15**(3), 259–263 (2006)
15. Kutzer, M., Fülle, A., Jahnke, A., Hahn, J., Wendt, S., Neuhaus, D., Witzig, A., Kutzer, K.: Ertragssteigerung durch bifaciale modultechnologie. In: Proc. 31st Symp. Photovolt. Sol. Energy. pp. 1–10 (2016)
16. Marion, B., MacAlpine, S., Deline, C., Asgharzadeh, A., Toor, F., Riley, D., Stein, J., Hansen, C.: A practical irradiance model for bifacial pv modules. In: 2017 IEEE 44th Photovoltaic Specialist Conference (PVSC). pp. 1537–1542. IEEE (2017)
17. Mermoud, A., Wittmer, B.: Bifacial shed simulation with pvsyst. In: Bifacial Workshop. pp. 25–26 (2017)
18. Pelaez, S.A., Deline, C., Greenberg, P., Stein, J.S., Kostuk, R.K.: Model and validation of single-axis tracking with bifacial pv. *IEEE Journal of Photovoltaics* **9**(3), 715–721 (2019)
19. Pelaez, S.A., Deline, C., MacAlpine, S.M., Marion, B., Stein, J.S., Kostuk, R.K.: Comparison of bifacial solar irradiance model predictions with field validation. *IEEE Journal of Photovoltaics* **9**(1), 82–88 (2018)
20. Reise, C., Schmid, A.: Realistic yield expectations for bifacial pv systems—an assessment of announced predicted and observed benefits. In: Proc. 31st Eur. Photovolt. Sol. Energy Conf. Exhib. pp. 1775–1779 (2015)
21. SANDIA Labs: Pvlib tool box. <https://pvlib-python.readthedocs.io/en/stable/>, accessed: 2020-03-15
22. Sun, X., Khan, M.R., Deline, C., Alam, M.A.: Optimization and performance of bifacial solar modules: A global perspective. *Applied energy* **212**, 1601–1610 (2018)

Variables involved in the generation of bifacial PV modules 17

23. Wang, S., Wilkie, O., Lam, J., Steeman, R., Zhang, W., Khoo, K.S., Siong, S.C., Rostan, H.: Bifacial photovoltaic systems energy yield modelling. *Energy Procedia* **77**, 428–433 (2015)
24. Yusufoglu, U.A., Pletzer, T.M., Koduvelikulathu, L.J., Comparotto, C., Kopecek, R., Kurz, H.: Analysis of the annual performance of bifacial modules and optimization methods. *IEEE Journal of Photovoltaics* **5**(1), 320–328 (2014)
25. Yusufoglu, U.A., Lee, T.H., Pletzer, T.M., Halm, A., Koduvelikulathu, L.J., Comparotto, C., Kopecek, R., Kurz, H.: Simulation of energy production by bifacial modules with revision of ground reflection. *Energy Procedia* **55**, 389–395 (2014)

Experimental comparison of visual inspection and infrared thermography for the detection of soiling and partial shading in photovoltaic arrays

Leonardo Cardinale-Villalobos¹ , Carlos Meza¹ , and Luis Murillo-Soto² 

¹ Electronics Engineering School, Instituto Tecnológico de Costa Rica, Costa Rica
lcardinale@tec.ac.cr

² Electromechanic Engineering School, Instituto Tecnológico de Costa Rica, Costa Rica

Abstract. Soiling and partial shading of solar panels are two of the most common conditions that affects the power yield of a photovoltaic (PV) installation. Even though human inspection can easily identify such situations, in the case of large power plants covering thousands of hectares it is not practical. In this regard, unmanned areal systems (UAS) represents a useful tool to gather images in a short time for the inspection of thousands of PV panels. Using RGB and infrared cameras, UAS can be used to perform visual inspection (VI) and infrared thermography (IRT) to detect failures in PV arrays. The present paper presents the results of an experiment designed to evaluate the effectiveness of VI and IRT for detecting soiling and partial shadowing. It has been found that for the aforementioned conditions VI are more effective. Also, the methodology presented can be used as a reference for future research for other techniques and other failures. The results provide technical-scientific information for those in charge of operation and maintenance to make an objective choice of failure detection techniques.

Keywords: Solar PV System · Fault detection performance · Partial shading · Soiling · Thermography

1 Introduction

A photovoltaic (PV) power plant is capable of operating for more than 25 years and due to its low energy density the installations can occupy thousands of hectares [37]. A group of PV panels are connected in series to form strings and, in some cases, in parallel to form arrays injecting the generated energy through a power inverter. Weather, soiling and obstacles that produces shadows yield suboptimal conditions in the PV array, i.e., the group of PV panels produces less power than expected. In the case of soiling or obstructing elements the suboptimal condition can be corrected if detected. In this regard, strategies related to the operation and maintenance of PV modules acquired greater importance. Even though such conditions can be identified by human operators, as reported in [11], expert visual inspection and fault analysis in a 3 MW installation take 60 days.

2 L. Cardinale-Villalobos, et. al

Thus, developing techniques that detects such suboptimal conditions in shorter time becomes a necessity.

There are several techniques to identify faults and suboptimal techniques, e.g. [36], [8], [32], [19], [22], [16], [20], [11], [4], [29], [28]. Two of the most promising are based on imaging, given that these techniques do not require to intervene the PV power plant circuit, does not require contact with the element of interest and generates a large amount of qualitative and quantitative information for each image. Such images can be taken in a relative short time if unmanned aerial systems (UAS) are used. UAS also known as drones with onboard thermal cameras enable inspections from the air and through digital photogrammetry techniques it is possible to detect failures in an agile way (e.g., [14], [35]).

The camera attached to the UAS can be of the type that captures the red, green, blue (RGB) band or the infrared band. With an infrared band detection camera it is possible to obtain thermal images of solar panels which allows the identification of temperature gradients or hot spots that can be associated with panel failures [2,23]. Such technique is referred as infrared thermography (IRT).

The present paper compares two drone image-based fault detection techniques: (1) visual inspection (VI) based on RGB images and (2) a strategy based on IRT through infrared images. An experiment has been designed to measure the performance of the aforementioned techniques for partial shadowing and soiling, which represents two of the most common suboptimal techniques. The rest of the paper is structured as follows: first the suboptimal conditions considered are described, then the material and methods are presented. Section 4 presents the main results and section 5 gathers the main conclusions.

2 Suboptimal conditions considered

For the comparative analysis we consider the following suboptimal conditions:

- Partial shadowing: The power generated by a series of solar panels will suffer a decrease in the power generated when they are partially shaded [26]. Partial shading can be caused by objects located in the surface on the panel or by objects not in contact with the panel. The power affectation depends on the portion of the module that is shaded and on the degree to which it is shaded [24,30]. An example of a shadowed panel is shown in Fig. 1.
- Soiling: can be caused due to the presence of a thin layer of particles such as soil, dust, leaves, pollen or bird droppings [24]. The PV power affectation is greater as the soiling increases. A dirty PV module is shown in Fig. 2. Soiling can be uniform or non-uniform. Dirt due to dust consists of particles of different sizes and materials that cover the entire PV module, which, over time, will form uniform layers of dust and regions with greater accumulation of dirt [17]. Non-uniform dirt covering only some cells of the PV module, due to leaves, bird droppings or patches of soil have a severe power loss effect, this type of failure is associated with both soiling and partial shading. PV cells that capture less irradiance have a lower short circuit current than the

Visual inspection and infrared thermography comparison 3

rest, causing the entire module to deliver less current. In addition, dirty cells will cause a hot spot that can be detected with IRT [24].



Fig. 1. Partial shadow on a PV panel (left) and strange object on a PV panel (right).



Fig. 2. Soiled PV module.

3 Materials and methods

3.1 The PV installation analyzed

The data used to compare VI and IRT suboptimal detection techniques consisted of images from a ground mounted PV installation located in Santa Clara, Costa Rica. The details of the PV installation are shown in Table 1.

4 L. Cardinale-Villalobos, et. al

Table 1. Information about the PV installation analyzed

Longitude	-84.51
Latitude	10.36
Azimuth angle	0° with respect to the South
Inclination angle	15°
Peak DC power	19.4
Number of PV panels	72
PV panel models	Canadian Solar CS6k-280M and HANWHA Q-Cells QPRO BFR G4.3
Total surface (m²)	125
Performance factor (%)	77.7
Annual Yield (MWh)	28.69
Date of commissioning	May 31st, 2017

Figure 3 shows an aerial view of the PV installation considered, where it can be seen that the site consists of six well distinguished sections. Each section has a string of 12 PV modules connected to an inverter SMA Sunny Boy 3000TL-US. In this analysis only strings 2, 4, and 6, shown in Fig. 3, were used. The aforementioned strings have a direct current STC power of 3380 W.



Fig. 3. Picture of the PV installation. Strings 2, 4 and 6 were used in this research.

3.2 Image capturing

The data used to determine the suboptimal conditions in the PV installation consisted of images taken from an (UAS). The following considerations have been considered to take the images:

- The drone is always flown at a height greater than 5 m to avoid that it causes shadows on the panels [20].

- The flight height depends on the detail that is necessary to observe in the PV modules for proper fault detection, thus, the size of the fault has been taken into account to determine the spatial resolution require for the images taken in a drone mission (ground sampling distance (GSD) [7]). A GSD of 3.0 ± 0.5 cm/px is required for deep inspections [8], allowing to detect possible hot spots at cell level [4].
- The measurements were made at a time with sufficient irradiance to allow the capture of thermal contrasts, with a correct angle and without wind currents that generate convection cooling [39], constant sunlight conditions with a clear sky are also desirable so that solar panels in good conditions have a homogeneous thermal distribution [35].
- The images were captured with an angle between 5° and 60° with respect to the perpendicular of the panel (see Fig. 4) [39] and the irradiance was always greater than $700\text{W}/\text{m}^2$ [15]. The camera's emissivity was set to 0.85 for crystalline cells as indicated in [16].
- The drone was set to consecutive image capture as recommended in [36,39] for fault detection in PV installations.

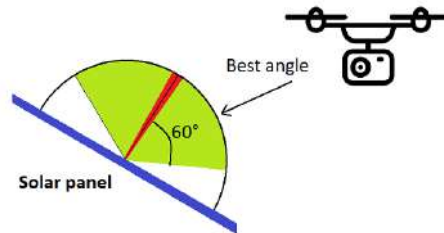


Fig. 4. Recommended orientation of the thermal camera with respect to the panel position.

A commercial Phantom 4 Pro multirotor drone was used as the UAS platform (see Fig. 5). The characteristics of the RGB and thermal infrared camera are shown in Table 2 and 3, respectively.

Table 2. Characteristics of the RGB camera used

Parameter	Value
Sensor	1" CMOS/ Effective pixels 20M
Lens	FOV 84° 8.8 mm/24mm
PIV Image Size	4096 x 2160
Photo	JPEG
Image Size	3:2, 4:3, 16:9
ISO Range	100-3200 (Auto)

6 L. Cardinale-Villalobos, et. al



Fig. 5. Drone with RGB and thermal camera used in this research.

Table 3. Characteristics of the FLIR VUE PRO R 336 thermal camera [9,10]

Parameter	Value
HFOV x VFOV	25°x 19°
Sensor (width x height)	5.764 mm x 4.351 mm
Focal length	13.00 mm
Image width x height	336 x 256
Frequency	9 Hz
Accuracy	+/- 5 °C o 5% from reading
Thermal sensitivity	40 mK
Sensor	Uncooled microbolometer

3.3 Other instruments and measurements

On-site irradiance was measured with a Spektron 210 sensor and the ambient temperature and relative humidity from a Vantage Pro 2 weather station. The power from the inverters was taken from the built-in SMA data logging system. A schematic of the system is shown in Fig. 6.

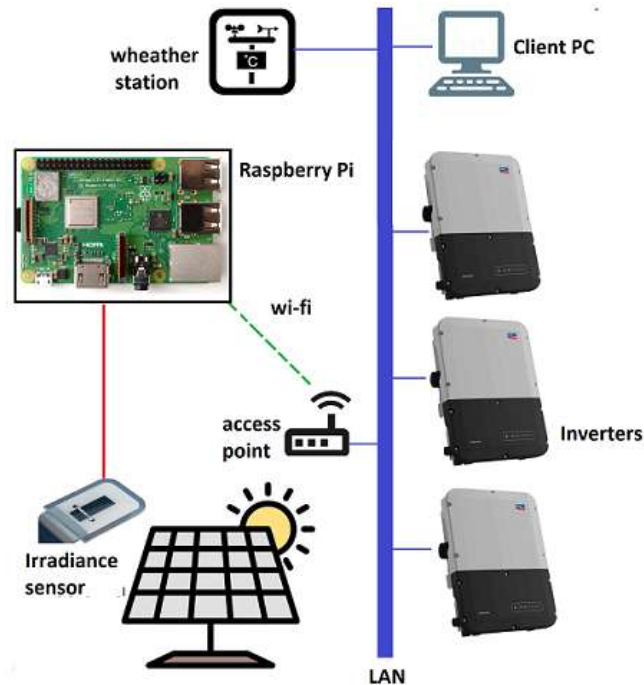


Fig. 6. Schematic diagram of communication links to information sources.

3.4 Experiments

The research was developed through a case study applying an experiment. Pre-defined temporary suboptimal conditions were induced to the PV installation in operation which allowed collecting and processing quantitative information to compare the IRT and VI techniques through statistical analysis. Taking as reference [13,38] the following stages were used:

- Selection of the sample and information sources.
- Design of the experiment.
- Definition of protocols and criteria for the interpretation of results.

8 L. Cardinale-Villalobos, et. al

The experiment used a repeated measurement design because multiple treatments had to be applied to the same subjects [34]. A total of 28 experimental units were analyzed from the 8 treatments applied to the 2 subjects (Strings 4 and 6). String 2 was used as a control subject to establish a reference condition in each experimental unit for the normal operation of the PV strings, i.e. without applying failures. The factors and levels evaluated are shown in Table 4.

Table 4. Factors and levels used in the experiment to generate the diverse treatments.

Failure	Factor	Level
S1	Soiling	10 months of natural soil
S2		30 months of natural soil
S3		12 cells with white spots
S4		12 cells with dry leaves from the site
S5		21 cells with white spots
S6		21 cells with dry leaves from the site
PS1	Partial shading	Shading of approximately 70% of a panel's area
PS2		2 shadows, each approximately 30% of the area of a panel

The treatments were applied to the subjects without interaction between factors. Each level was applied in both subjects making two repetitions in each one. The selection of the modules of each string to which the failure was applied was chosen at random. The partial shadows were limited to the modules on the right margin due to site conditions. It was considered that there is an independent relationship between the treatments, because they were randomized and do not generate a residual effect in the subject [12], i.e., the PV string return to their normal state once the treatment is removed.

3.5 Description of each factor and the levels of the experiment

– A. Soiling

Table 4 describes the dirt conditions used for faults S1 - S6. Faults S1 and S2 allowed the generation of soil conditions that cause weak shading [24]. Natural dirt accumulated in the solar panels over time was used as suggested in [17] which states that it is possible to take as an indicator of soiling the exposure time that the module has been under natural conditions.

Failures S3 and S5 were made to generate a strong obstruction of the irradiance due to some strange object on the solar panel. Samples of glass of 480 mm x 160 mm x 5 mm were prepared in which white paint was placed to simulate dirt on the PV module (see Fig. 7); this allowed to replicate the treatments in multiple moments in different positions of the PV array. The experiment took as a reference the methodology used in [33] to study the effects of dirt on solar modules.

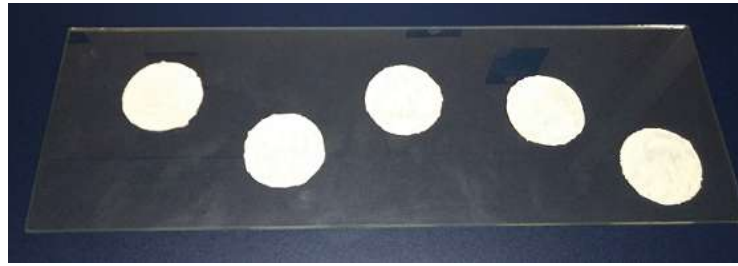


Fig. 7. Glass with white circles used to simulate dirt obstructing the path of radiation in three PV cells.

Faults S4 and S6 are a variation of S3 and S5 to evaluate soiling. In this case, dry leaves and seeds were used, where to achieve repeatability in the experiment the objects were adhered to the glass with cold silicon (see Fig. 8).



Fig. 8. Glass with dry leaves and seeds to simulate dirt obstructing the radiation path in three PV cells.

– B. Partial shading

The experiment was developed by applying shadows to the solar modules in operation. The methodology took as reference experiences of previous investigations, in which, they placed an object to obstruct the solar radiation of a portion of the solar module, allowing that it influences diffuse radiation [25]. The two partial shading levels (PS1 and PS2) applied were made by placing an object next to the PV string to create the shadow (Fig. 9).

3.6 Protocol for missions with UAS

As mentioned previously, for each treatment a flight was performed with the UAS capturing RGB and infrared images of the PV strings of interest ensuring



Fig. 9. Example of partial shadows generated on the PV modules.

that the requirements indicated in section 3.2 were met. The flight height was 25 m according to the GSD equation presented by [21] to obtain a maximum GSD of 3.0 cm/pixel in thermal images and even less in RGB images.

The thermal images were configured to contain the radiometric information in RJPEG format. Thermographs were taken every 1 s and RGB images every 2 s during each test. The orientation of the cameras with respect to the perpendicular plane of the module was around 20 °C.

For each test, the irradiance, ambient temperature and relative humidity were recorded. Each treatment was applied 15 minutes before the measurement was taken to ensure that thermal equilibrium existed [16].

3.7 Fault detection criteria

The temperature variation due to a hot spot is an indicator of the severity of the fault, where less than 10 °C is considered within the normal operation tolerance [15, 27] however, at lower irradiance, the temperature variation of a fault will decrease [6].

Fault detection in PV installations by VI can be done following the detailed guidance of [19]. For example, it is possible to identify soiling by evaluating the appearance of the solar modules so that it is classified as: clean, slightly dirty or very dirty. Furthermore, the dirt can be classified according to its location as: close to the frames or located somewhere on the glass (e.g. bird droppings). Partial shadows can be identified by observing the glass surface of the PV module.

According to the literature review, the criteria for the detection of the failures of interest for the applied techniques were determined. The criteria used are shown in the Table 5.

Table 5. Criteria used for the determination of failures

Technique	Criteria for fault detection
IRT	Hot spot with a delta ≥ 10 °C
VI	Presence of radiation attenuation on the panel due to shade
	Appearance of light or heavy soiling

3.8 Date and conditions of the experiment

All measurements were made between august 18 and september 2, 2020. The average ambient temperature was 30 °C, the relative humidity 60 % and the reflected temperature 22 °C.

3.9 Measurement normalizing

The three mono-crystalline strings are equivalent, however, their output power may vary slightly, so the power of the strings under test (String 4 and String 6) were compared with the control String 2 to set a reference level. Table 6 shows the variation in the average output power under non-fault conditions after two hours of operation with an irradiance greater than 700 W/m².

Table 6. Power comparison of the string under test with respect to the control string

String	Power (W)	Variation (%)
2 (control)	2549	-
4	2566	0.67
6	2534	-0.59

4 Results and discussion

The results of the induced suboptimal conditions are shown in Table 7. Each one of the induced condition was considered as a fault because it caused a decrease of at least 4 % in the power of the array [1].

Table 7. Power effect of the faults studied

Fault (String)	Power in control string (W)	Power in string under test (W)	Estimated power without fault (W)	Losses (%)
PS1 (4)	2224	1920	2239	14.2
PS2 (6)	3133	2746	3115	11.9
S1 (4)	2137	1879	2151	12.7
S2 (6)	2137	1461	2124	31.3
S3 (6)	2421	1994	2407	17.1
S4 (4)	2421	1749	2437	28.3
S5 (6)	2094	1648	2082	20.8
S6 (4)	2094	1573	2108	25.4

4.1 RGB and IR images analysis

The most representative images that identifies suboptimal conditions are shown in Fig. 10 to 15. For each experimental unit, a discrete output variable was generated to indicate whether or not the technique detected failure; the results are shown in Table 8.

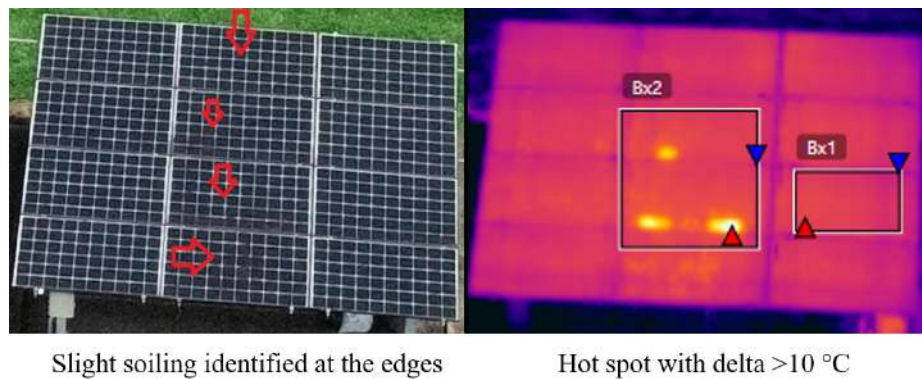


Fig. 10. RGB (left) and IR image (right) analyzed for experimental unit 1.

Figure 16 shows the summary of the failures detected with each of the techniques. It can be seen that VI identified more failures than IRT. The VI was able to detect all the failures, on the other hand, the IRT detected only 68% of the evaluated test, missing 45% of the cases of soiling.

The results of soiling failures for IRT are shown in the Fig. 17. IRT was not able to detect the 30 month natural soiling (S2). Also the types of soiling with white spots (S3 and S5) were the least detected. Finally, for the soiling with dry leaves (S4 and S6) there was one case of each that the failure could not be

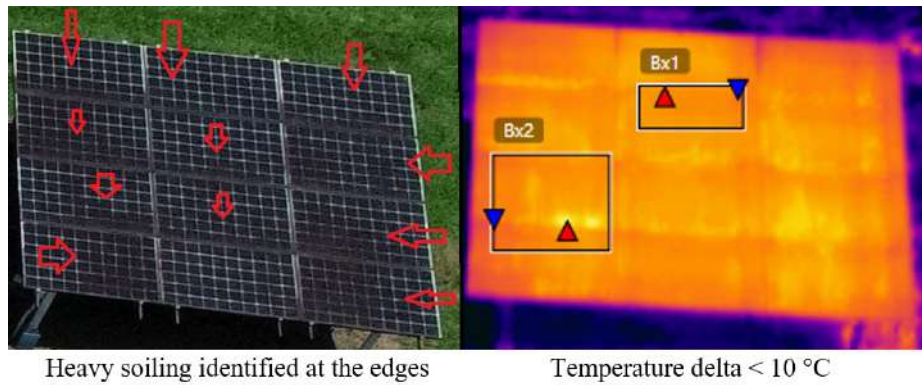


Fig. 11. RGB (left) and IR image (right) analyzed for experimental unit 2.

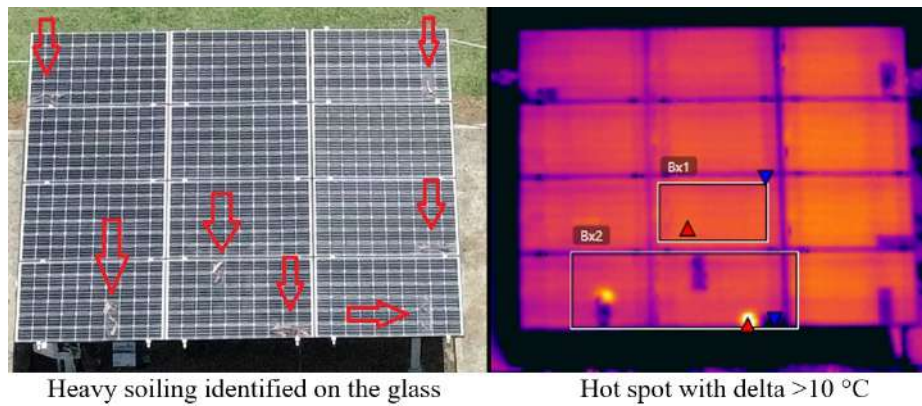


Fig. 12. RGB (left) and IR image (right) analyzed for experimental unit 6.

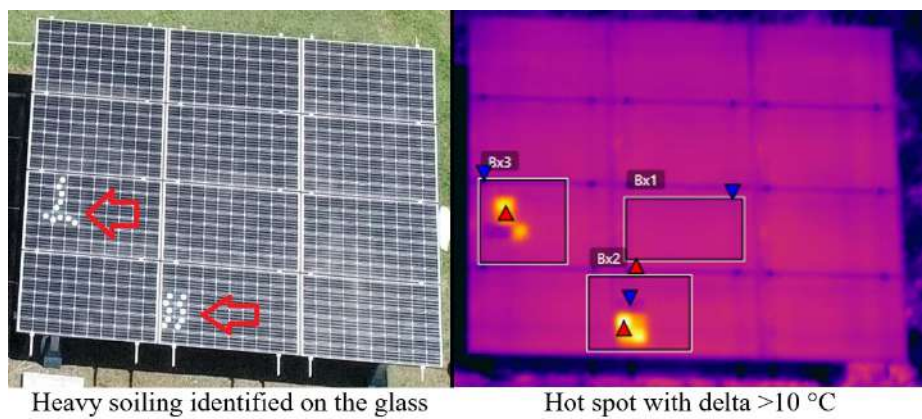


Fig. 13. RGB (left) and IR image (right) analyzed for experimental unit 18.

14 L. Cardinale-Villalobos, et. al

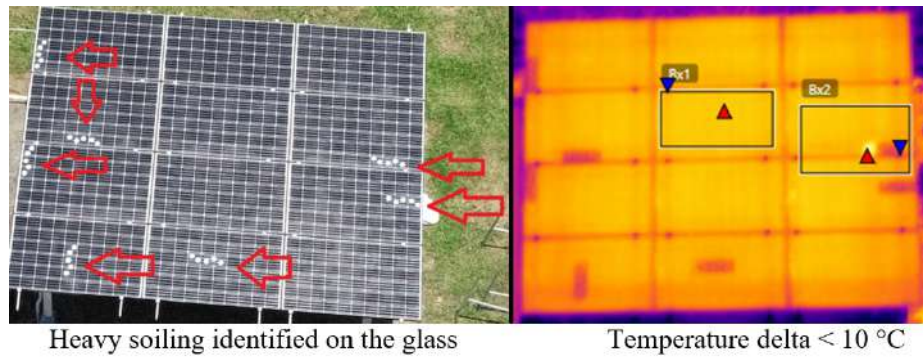


Fig. 14. RGB (left) and IR image (right) analyzed for experimental unit 19.

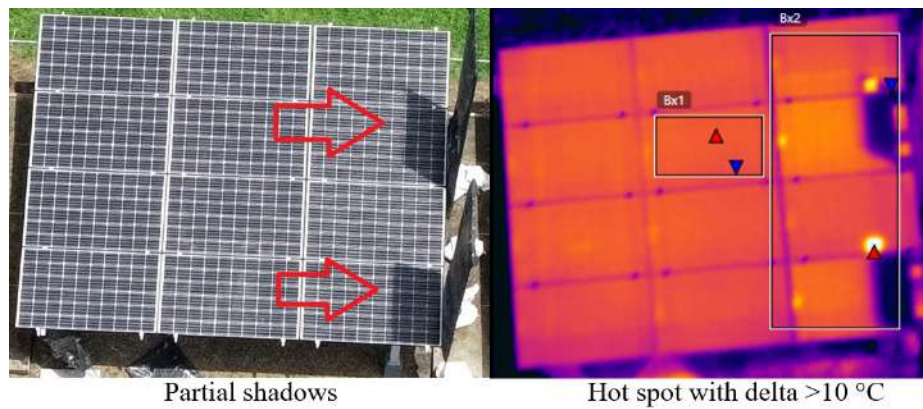


Fig. 15. RGB (left) and IR image (right) analyzed for experimental unit 22.

Visual inspection and infrared thermography comparison 15

Table 8. Output variable of the experiment for IRT and VI. D = Detected, ND = Not detected

Experimental unit	Treatment	IRT output	VI output
1	S1	D	D
2	S2	ND	D
3	S1	D	D
4	S2	ND	D
5	S4	ND	D
6	S6	D	D
7	S4	D	D
8	S6	D	D
9	S4	D	D
10	S6	ND	D
11	S4	D	D
12	S6	D	D
13	S5	ND	D
14	S3	ND	D
15	S5	ND	D
16	S3	D	D
17	S5	D	D
18	S3	D	D
19	S5	ND	D
20	S3	ND	D
21	PS1	D	D
22	PS2	D	D
23	PS1	D	D
24	PS2	D	D
25	PS1	D	D
26	PS2	D	D
27	PS1	D	D
28	PS2	D	D

16 L. Cardinale-Villalobos, et. al

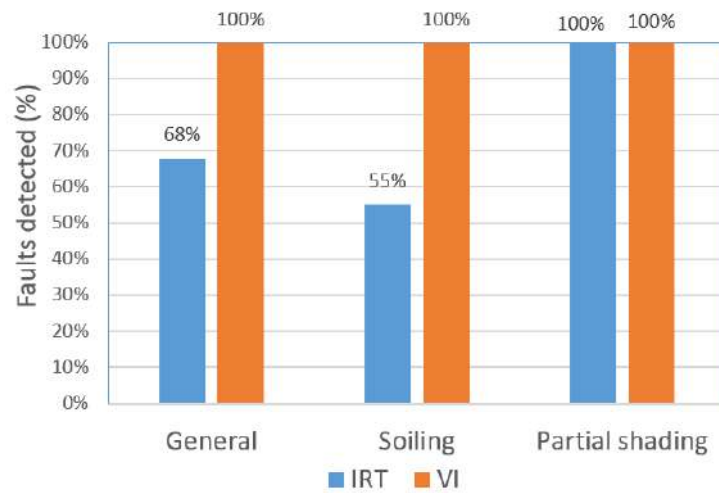


Fig. 16. Percentage of failures detected by each technique in the experiment.

detected. Therefore, IRT is able to detect all types of soiling evaluated, however, there are levels of soiling that were not detected in some cases.

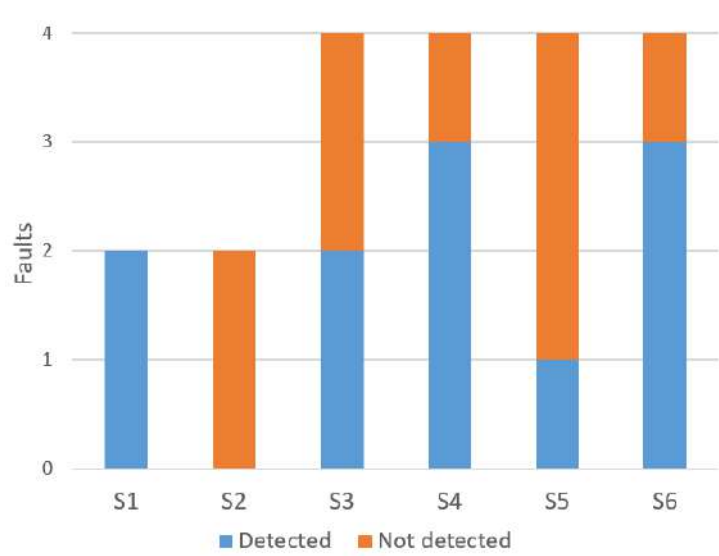


Fig. 17. Failures detected and not detected by the IRT under soiled conditions.

The detection of the failures was done strictly following the criteria of Table 5. However, in Fig. 11 it can be seen that through the IRT it was possible to appreciate a distortion in the thermal distribution of the PV array. In addition, in Fig. 14 it was possible to identify specific regions of lower temperature on the PV modules and temperature gradients lower than 10 °C, even though none of these cases met the requirement to be cataloged as failures, this suggests that, to detect soiling suboptimal conditions a lower threshold for the temperature gradient might be required.

4.2 Statistical analysis

To determine if one method performed significantly better than the other, a hypothesis test was done using Fisher’s exact test [3,18] as follows:

$$H_0 : N_i = N_j$$

$$H_a : N_i \neq N_j$$

$$\forall i \neq j$$

Where N is the number of identified failures, i and j are IRT and VI techniques respectively.

The test yields a p-value of $p = 0.002$ and odds ratio (OR) = 27.8, therefore, considering a significance level of $\alpha = 0.05$ it fulfills the alternative hypothesis ($p < \alpha$), i.e. significant differences were found between both methods [5]. In addition, when evaluating the hypothesis tests for each of the failure factors (soiling and partial shading) with the contingency tables shown in the Table 9, significant differences were obtained for soiling (S) with $p = 0.001$ and an OR = 33.87. The OR coefficient obtained in both cases indicate that there is a high probability that a fault will be not detect using IRT instead of VI, specifically detecting soiling. That is, the VI is associated with a greater capacity for dirt detection compared to the IRT.

Table 9. Contingency table separating the factors (types of failures) of the experiment

Factor	Technique	Result		Total
		Not Detected	Detected	
S	TI	9	11	20
	VI	0	20	20
	Total	9	31	40
PS	TI	0	8	8
	VI	0	8	8
	Total	0	16	16
Total	TI	9	19	40
	VI	0	28	40
	Total	9	47	56

18 L. Cardinale-Villalobos, et. al

Another way to compare both methods is by the sensitivity in the effectiveness of fault detection, this is based on the analysis of true positives achieved by each technique [31]. The results show that IRT had a sensitivity of 68% while VI had 100%.

5 Conclusions

The present paper has analyzed two image-based fault detection technique (IRT and VI) for photovoltaic arrays for two of the most common temporary faults or suboptimal conditions, i.e., soiling and shading. Partial shadows were correctly detected with both techniques, however, IRT did not perform as well as VI for the detection of soiling. Nevertheless, IRT did detect at least once all the types of faults evaluated. The results also suggest that soiling with IRT might be detectable if a temperature difference threshold smaller than 10 °C is used.

The methodology used allowed a quantitative comparison from experimental data between two techniques for failure detection in PV systems. This can be used for future experiments with other configurations of PV arrays and other types of failures, making it possible to validate theoretical models that are still being studied and to generate quantitative indicators of the effectiveness of each technique. Including treatments of conditions that are an apparent failure but without a significant affectation on power will allow studying the capacity of each technique to discriminate between true and false failures; this is pending for future research.

Acknowledgement

This paper is part of a project 5402-1360-4201 “Identificación de Fallas en Sistemas Fotovoltaicos” financed by the Costa Rica Institute of Technology. In addition, the first author is part of the Master of Science: Maestría en Ciencia y Tecnología para la Sostenibilidad of DOCINADE. Thanks to the Electronics students at ITCR Dalberth Alberto Corrales Alpizar and Jose Eduardo Zuñiga Ramirez for their contribution in the development of the data acquisition system and John Martin Chacon Zambrana for the support in the data collection of the experiment.

References

1. Acciani, G., Falcone, O., Vergura, S.: Typical defects of PV-cells. IEEE International Symposium on Industrial Electronics pp. 2745–2749 (2010). <https://doi.org/10.1109/ISIE.2010.5636901>
2. Alsafasfeh, M., Abdel-Qader, I., Bazuin, B.: Fault detection in photovoltaic system using SLIC and thermal images. In: 2017 8th International Conference on Information Technology (ICIT). IEEE (may 2017). <https://doi.org/10.1109/icitech.2017.8079925>, <https://doi.org/10.1109%2Ficitech.2017.8079925>

3. Bolboacă, S.D., Jäntschi, L., Sestras, A.F., Sestras, R.E., Pamfil, D.C.: Pearson-fisher chi-square statistic revisited. *Information* **2**(3), 528–545 (sep 2011). <https://doi.org/10.3390/info2030528>, <https://doi.org/10.3390%2Finfo2030528>
4. Cardinale-Villalobos, L., Rimolo-Donadio, R., Meza, C.: Solar panel failure detection by infrared uas digital photogrammetry: A case study. *International Journal of Renewable Energy Research (IJRER)* **10**(3), 1154–1164 (2020)
5. Cohen, H.W.: P values: Use and misuse in medical literature. *American Journal of Hypertension* **24**(1), 18–23 (jan 2011). <https://doi.org/10.1038/ajh.2010.205>, <https://doi.org/10.1038%2Fajh.2010.205>
6. Cubukcu, M., Akanalci, A.: Real-time inspection and determination methods of faults on photovoltaic power systems by thermal imaging in turkey. *Renewable Energy* **147**, 1231–1238 (mar 2020). <https://doi.org/10.1016/j.renene.2019.09.075>, <https://doi.org/10.1016%2Fj.renene.2019.09.075>
7. Felipe-García, B., Hernández-López, D., Lerma, J.L.: Analysis of the ground sample distance on large photogrammetric surveys. *Applied Geomatics* **4**(4), 231–244 (2012). <https://doi.org/10.1007/s12518-012-0084-2>
8. FLIR: A guide to inspecting solar fields with thermal imaging drones (2019), <https://thermalcapture.com/wp-content/uploads/2019/08/pv-system-inspection-thermal-drones-07-15-19.pdf>
9. Flir: Flir Vue Pro and Flir Vue Pro R (2019), <http://www.flir-vue-pro.com/wp-content/uploads/2016/10/FLIR-VUE-Pro-R-Datasheet-TeAx.pdf>
10. Flir.com: Adjusting Sensitivity & Gain On The FLIR Vue Pro R (2019), https://flir.custhelp.com/app/answers/detail/a_f_id/3134
11. Gallardo-Saavedra, S., Hernandez-Callejo, L., Duque-Perez, O.: Image resolution influence in aerial thermographic inspections of photovoltaic plants. *IEEE Transactions on Industrial Informatics* **14**(12), 5678–5686 (dec 2018). <https://doi.org/10.1109/tii.2018.2865403>, <https://doi.org/10.1109%2Ftii.2018.2865403>
12. Gutiérrez-Pulido, H., De la Vara-Salazar, R.: *Análisis y diseño de experimentos*. McGraw-Hill Interamericana, México D.F, second edn. (2008)
13. Hernández Sampieri, R., Fernández Collado, C., Baptista, L., Del Pilar, M.: *Metodología de la investigación*. Mc Graw Hill, México, fifth edn. (2010)
14. HIGUCHI, Y., BABASAKI, T.: Failure detection of solar panels using thermographic images captured by drone. In: 2018 7th International Conference on Renewable Energy Research and Applications (ICRERA). IEEE (oct 2018). <https://doi.org/10.1109/icrera.2018.8566833>, <https://doi.org/10.1109%2Ficrera.2018.8566833>
15. International Energy Agency: Review of Failures of Photovoltaic Modules. Tech. Rep. July, Performance and Reliability of Photovoltaic Systems (2014)
16. International Energy Agency: Review on Infrared and Electroluminescence Imaging for PV Field Applications. Tech. rep., PHOTOVOLTAIC POWER SYSTEMS PROGRAMME (2018)
17. Javed, W., Wubulikasimu, Y., Figgis, B., Guo, B.: Characterization of dust accumulated on photovoltaic panels in doha, qatar. *Solar Energy* **142**, 123–135 (jan 2017). <https://doi.org/10.1016/j.solener.2016.11.053>, <https://doi.org/10.1016%2Fj.solener.2016.11.053>
18. Jones, J.B., Schropp, M.A.: Research fundamentals: Statistical considerations in research design: A simple person's approach. *Academic Emergency Medicine* **7**(2), 194–199 (2000). <https://doi.org/10.1111/j.1553-2712.2000.tb00529.x>
19. renewable energy laboratory, N.: Development of a Visual Inspection Data Collection Tool for Evaluation of Fielded PV Module Condition. Tech. Rep. Au-

20 L. Cardinale-Villalobos, et. al

- gust, NREL, Denver, U.S (2012). <https://doi.org/10.2172/1050110>, <http://www.osti.gov/bridge>
20. Leva, S., Aghaei, M., Grimaccia, F.: PV power plant inspection by UAS: Correlation between altitude and detection of defects on PV modules. In: 2015 IEEE 15th International Conference on Environment and Electrical Engineering (EEEIC). IEEE (jun 2015). <https://doi.org/10.1109/eeeic.2015.7165466>, <https://doi.org/10.1109%2Feeeic.2015.7165466>
 21. Linder, W.: Introduction. In: Digital Photogrammetry, chap. Introduction, pp. 10–12. Springer-Verlag Berlin, 4 edn. (2016). <https://doi.org/10.1007/978-3-662-50463-5>
 22. M. Köntges: Reviewing the practicality and utility of electroluminescence and thermography (2014), https://www.nrel.gov/pv/assets/pdfs/2014_{_}pvmrw_{_}33_{_}kontges.pdf
 23. Madeti, S.R., Singh, S.: A comprehensive study on different types of faults and detection techniques for solar photovoltaic system. *Solar Energy* **158**, 161–185 (dec 2017). <https://doi.org/10.1016/j.solener.2017.08.069>, <https://doi.org/10.1016%2Fj.solener.2017.08.069>
 24. Maghami, M.R., Hizam, H., Gomes, C., Radzi, M.A., Rezadad, M.I., Hajjghorbani, S.: Power loss due to soiling on solar panel: A review. *Renewable and Sustainable Energy Reviews* **59**, 1307–1316 (jun 2016). <https://doi.org/10.1016/j.rser.2016.01.044>, <https://doi.org/10.1016%2Fj.rser.2016.01.044>
 25. Mekki, H., Mellit, A., Salhi, H.: Artificial neural network-based modelling and fault detection of partial shaded photovoltaic modules. *Simulation Modelling Practice and Theory* **67**, 1–13 (sep 2016). <https://doi.org/10.1016/j.simpat.2016.05.005>, <https://doi.org/10.1016%2Fj.simpat.2016.05.005>
 26. Mellit, A., Tina, G., Kalogirou, S.: Fault detection and diagnosis methods for photovoltaic systems: A review. *Renewable and Sustainable Energy Reviews* **91**, 1–17 (aug 2018). <https://doi.org/10.1016/j.rser.2018.03.062>, <https://doi.org/10.1016%2Fj.rser.2018.03.062>
 27. Moretón, R., Lorenzo, E., Narvarte, L.: Experimental observations on hot-spots and derived acceptance/rejection criteria. *Solar Energy* **118**, 28–40 (aug 2015). <https://doi.org/10.1016/j.solener.2015.05.009>, <https://doi.org/10.1016%2Fj.solener.2015.05.009>
 28. Murillo-Soto, L., Meza, C.: Fault detection in solar arrays based on an efficiency threshold. In: 2020 IEEE 11th Latin American Symposium on Circuits Systems (LASCAS). pp. 1–4 (2020). <https://doi.org/10.1109/LASCAS45839.2020.9069046>
 29. Murillo-Soto, L., Meza, C.: Photovoltaic array fault detection algorithm based on least significant difference test. In: Applied Computer Sciences in Engineering. WEA 2020. Communications in Computer and Information Science, vol. 1274. Springer-Verlag Berlin (2020). https://doi.org/https://doi.org/10.1007/978-3-030-61834-6_43
 30. Mäki, A., Valkealahti, S.: Power losses in long string and parallel-connected short strings of series-connected silicon-based photovoltaic modules due to partial shading conditions. *IEEE Transactions on Energy Conversion* **27**(1), 173–183 (mar 2012). <https://doi.org/10.1109/tec.2011.2175928>, <https://doi.org/10.1109%2Ftec.2011.2175928>
 31. Pinteá, S., Moldovan, R.: The Receiver-Operating Characteristic (ROC) analysis: Fundamentals and applications in clinical psychology. *Journal of Cognitive and Behavioral Psychotherapies* **9**(1), 49–66 (2009)

32. and Singh Chaudhary, A., Chaturvedi, D.: Thermal Image Analysis and Segmentation to Study Temperature Effects of Cement and Bird Deposition on Surface of Solar Panels. *International Journal of Image, Graphics and Signal Processing* **9**(12), 12–22 (2017). <https://doi.org/10.5815/ijigsp.2017.12.02>
33. Sisodia, A.K., kumar Mathur, R.: Impact of bird dropping deposition on solar photovoltaic module performance: a systematic study in western rajasthan. *Environmental Science and Pollution Research* **26**(30), 31119–31132 (aug 2019). <https://doi.org/10.1007/s11356-019-06100-2>, <https://doi.org/10.1007%2Fs11356-019-06100-2>
34. Tango, T.: *Repeated Measures Design with Generalized Linear Mixed Models for Randomized Controlled Trials*. Taylor & Francis Group, Tokyo Japan (2017)
35. Tsanakas, J.A., Ha, L., Buerhop, C.: Faults and infrared thermographic diagnosis in operating c-si photovoltaic modules: A review of research and future challenges. *Renewable and Sustainable Energy Reviews* **62**, 695–709 (sep 2016). <https://doi.org/10.1016/j.rser.2016.04.079>, <https://doi.org/10.1016%2Fj.rser.2016.04.079>
36. Tyutyundzhiev, N., Lovchinov, K., Martínez-Moreno, F., Leloux, J., Narvarte, L.: Advanced PV modules inspection using multirotor UAV. In: *31st European Photovoltaic Solar Energy Conference and Exhibition*. Hamburg (2015), <https://www.researchgate.net/publication/283087341>
37. Watson, J.J., Hudson, M.D.: Regional scale wind farm and solar farm suitability assessment using GIS-assisted multi-criteria evaluation. *Landscape and Urban Planning* **138**, 20–31 (jun 2015). <https://doi.org/10.1016/j.landurbplan.2015.02.001>, <https://doi.org/10.1016%2Fj.landurbplan.2015.02.001>
38. Wohlin, C., Runeson, P., Höst, M., Ohlsson, M.C., Regnell, B., Wesslén, A.: *No Title*. Springer, New York (2012). <https://doi.org/10.1007/978-3-642-29044-2>
39. Zefri, Y., ElKettani, A., Sebari, I., Lamallam, S.A.: Thermal infrared and visual inspection of photovoltaic installations by UAV photogrammetry—application case: Morocco. *Drones* **2**(4), 41 (nov 2018). <https://doi.org/10.3390/drones2040041>, <https://doi.org/10.3390%2Fdrones2040041>

A Way to a Sustainable Universidad de Concepción: Smart Parking

Carlos Ramírez-Rendón¹, Irving Sánchez-Rangel¹, Luis García-Santander²

¹Universidad de las Américas Puebla, Puebla, México

Carlos.ramirezrn@udlap.mx

Irving.sanchezrl@udlap.mx

²Universidad de Concepción, Concepción, Chile

Luis.garcia@udec.cl

Abstract. This paper proposes a Smart Parking Lot System based on computer vision technique. The application was implemented with OpenCV, an open source library for image classification and processing, an online database to store results. Both the information and the selection of available places are made through an Android application. The proposed system allows efficient management of both energy consumption and the use of place inside the parking lots, allowing users to know in real time which parking spaces are available. Additionally, provide information regarding the parking lot to which the users are going. This paper provides an explanation of the elements used during the test of the system considering the parking lots located inside the Universidad de Concepción, Concepción- Chile and adapting our proposal to the multiple characteristics of these parking lots.

Keywords: Smart Cities, Smart Parking, Computer Vision, Sustainability, Emission Reduction.

1 Introduction

In the last decade, there has been a great demographic growth around the world and therefore a significant change in multiple areas. One of them is the sustained increase in the number of cars for personal use, which implies difficulties in large cities to find places to park. Nowadays, we have to face traffic jams in streets or saturation of the spaces intended for parking, these new challenges causes a higher demand for fuel and energy by creating more fuel waste, instead of using it for a better purpose. It also brings multiple problems with the environment due to the greenhouse gas emission.

Within this ambit, we can relate this problem to universities due to the great concentration of students, professors and personal that need to go to these places. This concentration of people creates a saturation in parking lots where it's difficult to find free places in certain schedules making it a process of around 10 to 20 minutes where automobiles still produce greenhouse emissions but also a waste of energy and fuel, which could be used for better purposes. Thanks to the advances in technology, today we can

propose multiple systems that allows drivers reduce their greenhouse emissions while looking for a parking lot, in this case designated by the name of “smart parking lots”. According to [1] a smart parking system in London with a good user engagement can save up to 62.2 liters on fuel annually to drivers and also reduce carbon dioxide emissions by around 2300 kg per car per year, creating a significant change when this process is scaled to a bigger point of view like a university or even greater like a city, improving for the drivers their fuel consumption, time and greenhouse emissions.

To solve this problem, a Smart Parking system is proposed. For this, information is considered from smart parking projects developed by other researchers and companies, both in Chile and in other countries, proposing a better approach that adjusts to the specific characteristics of the Universidad de Concepción in Chile. The proposal allows us to manage outdoor parking lots and adapt to the current structures of those parking lots. The following document will explain our approach to the system proposed and will be conformed and distributed in the next way, in section 2 we will do a description of the place of implementation as well as a brief explanation of computer vision and multiple approaches to smart parking lots in Chile and internationally. Section 3 presents the architecture of the proposed model and describes each of its components. Section 4 shows the results obtained in the test carried out on the proposed system. Finally, section 5 shows the conclusions and future works.

2 Smart Parking

Smart parking is defined as the implementation of a set of techniques, tools, and devices to manage a parking in the most efficient way possible, using as few resources as possible, such as fuel, time, or space. Thanks to this, smart parking lots represent a strategic way to reduce vehicular congestion and therefore a convenient technique to fight against the emerging global challenges such as CO₂ emissions to the environment [2]. To achieve this there are several types of smart parking lots, among which we can distinguish mainly: Gaparking, Crowdensing, RFID, Wireless Sensor Network and Vision Based [3, 4].

The bibliographic review allowed us to find some projects that had already been implement in Chile, among which are the commercial application WeSmartPark or the prototype implemented by Entel and Urbiotika in Las Condes, Santiago. The aforementioned projects were applied to shopping centers or in areas/sectors that are very different from those on the campus of Universidad de Concepción, which is a very extensive public access space. The investment required to cover the entire area with sensors was too high in addition, visitors can easily damage the installed sensors. Thus, in this research, a system based on artificial vision has been proposed, since it allows the use of the infrastructure available inside the university campus, with minimal impact on the environment and significantly reducing the initial investment.

2.1 UdeC Campus

The Universidad de Concepción have 3 campuses distributed in Chile with a total extension of 1,195,261 m² which represents, for 2019, an academic center for 25,208 students of undergraduate level, 2,257 students of a postgraduate, 2,082 teachers and 2,613 nonacademic personal.

Our Smart Parking proposal considers the infrastructure available on the Concepción Campus. There are approximately 96 building and 45 parking lots with a total of 1500 places available for university employees and students from 07:00 to 19:00 from Monday to Friday and free for the citizens of Concepción at other times and periods of holidays/vacations. All the parking lots of campus Concepción present the same characteristics, all of them being outdoors and close to a building, the only difference we found between multiple parking lots was the entrance system that allows just certain people to enter an specific parking lot, per example a parking lot near the faculty of engineering allows only professors and personal to enter between 7 am to 7 pm, letting other users enter only after this schedule. Other parking lots had the same system but multiple of them did not had the same schedule therefore representing a space only available for the professors and the personal.

2.2 Computer Vision Algorithms

Nowadays, computer vision represents a huge area of study but for the purpose of this project, we will talk about some concepts of computer vision and image processing in which we can highlight the open source library OpenCV (Open Computer Vision Library), some classifiers, HAAR features, cascade detectors and border detection.

OpenCV is an open source library that includes several hundreds of computer vision algorithms. In this library we can find some useful utilities as for example image processing, video analysis, camera calibration and 3D reconstruction, 2D Features Framework, Object detection, High-level GUI and Video I/O [5]. In this project we use mainly three of these features:

- Image processing: We use these characteristics to scale the image obtained from the source, applying some Gaussian filters, Laplacian threshold, blur filter and the grayscale conversion.
- Object Detection: this feature allows us to use a pre-trained HAAR-cascade classifier to classify the cars in the smart parking lot
- Video I/O: We obtain the input video images captured from the parking lot cameras

Within the techniques we can find in computer vision for the detection of free spaces, we found multiple classifiers such as Y.O.L.O. (You Only Look Once), Fastest C.N.N. (Fastest Convolutional Neuronal Network) and Single Shot Detector (SDD), this classifiers have an high degree of reliability in the recognition of multiple objects but, in the case of real time detection, this classifiers still lack in speed. For us to have a faster recognition in real time it is necessary to have more processing power with dedicated

graphics cards that allow us to speed up the process. Due to the simplicity and the reliability these neuronal networks present, a Cascade Classifier was decided to be used with HAAR Detector.

HAAR descriptors are some of the most efficient classifiers that exist today due to their low computational cost. These characteristics are obtained after applying a set of filters throughout the image at different scales, these filters are known as HAAR filters, in this way a large numbers of characteristics of different images are obtained, positive and negative, creating a classifier capable of recognizing the desired object. This has the main advantages that it allows to analyze pixels directly. To achieve this, rectangles are used to define the structure of these characteristics, which allow coding data that is difficult to learn. The HAAR characteristics are calculated through the concept of integral image. The concept of cascade comes from the sequential application of different HAAR characteristics in the order established by the weights of the training stage, thus avoiding applying all the HAAR characteristics in all regions of the image. This is achieved by creating a decision tree to efficiently know if the object we are looking for exists in an image [6–8].

3 Proposed System

This section presents the system designed for our smart parking, considering the nature of the parking lots inside the campus and the multiple limitations we face, we decided to proceed using computer vision as our data collection method, as it allows us to reduce the costs in adapting the current structures of the parking lots and also take advantage of some of the current cameras located in the campus, as well as the creation of an android application which will help us display the data processed through our system to the users. The proposed system for a smart parking is illustrate in figure 1.

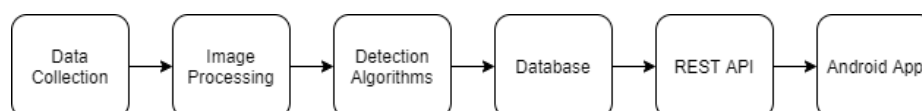


Fig. 1. Smart parking system.

Within our proposal, we decide to implement a computer vision based system in which the open source library OpenCV is been used for the classification and processing of images, also the Tkinter library in Python is been used for the design and creation of user interface for the visualization of the images obtained through the cameras and the result of the algorithm applied but also to create a friendly user interface for administration. For the database section, a hosting service is used as a backend where the data is stored and sent through the image processing algorithm in an online SQL database. This will communicate with a REST API created through PHP and receive the solicitudes from the Android app for data acquisition. Finally, for the Android application we will use the software Android Studio. We based our proposal on the related work of Ankit Khare [9].

Within our proposal we suggest the utilization of the security cameras that the campus has in the parking lots to obtain the image and a minimum investment for the processing devices that can be a Raspberry Pi.

3.1 Data Collection and Image Processing

First, the regions of interest (ROI) have to be delimited, these regions will cut the complete image into smaller squares that will indicate to the algorithm which portions of the image need to be processed, in other words it delimits each parking space to establish whether there is a car or not, we can see this process in figure 2. In this way, the scanning of the entire image is avoided to focus only on the parts that interest us and reduce the computational processing. The coordinates of these regions are saved in a file with a “.yml” extension that have a user-friendly format [10].



Fig. 2. Delimitation of the region of interest (ROI).

The next step is the video acquisition and data processing. For this, the open source “OpenCV” library is used, which allows capturing the image of a camera in an easier way with a method called “cv.VideoCapture” and also can be connected to the network via IP.

Once the image is captured, a grayscale conversion is applied, which allows to simplify the three-dimensional color space (R, G, B) to a single or monochrome dimensional representation as shown in figure 3. This significantly reduces the computational cost [10, 11].



Fig. 3. Grayscale conversion.

Once we have the image from the camera and the grayscale conversion, an image smoothing process is performed whose purpose is to eliminate the Gaussian noise in digital images, this procedure is performed with a Gaussian Blur, implemented in OpenCV as “cv.GaussianBlur” [12]. This blur is shown in figure 4.



Fig. 4. Gaussian Blur.

3.2 Image Processing and Detection Algorithms

Once the Gaussian filter is applied and the image is in black and white, two separate criteria are applied to each ROI for the decision of free parking places. The first criterion is an edge detection through a Laplacian threshold and the second criterion is a classifier cascade with HAAR features. If both criteria cannot coincide in the same result, a new criterion is applied, in this case a Canny border detector to determine more precisely if a parking lot is occupied or not. Also, thanks to the interface created with Tkinter we have the option to adjust the threshold of the edge subtractors allowing us to change that value without modify the source code.

Edge detections simplify the image analysis by reducing the amount of data to be processed, as well as keeping useful information about the boundaries of objects. This is done by identifying the points where the brightness of the image changes suddenly. This technique extracts the edges in the image by identifying pixels where the variation is very high [10]. We achieve this by using the Laplacian operator with the “cv.Laplacian”, we see this function in figure 5.



Fig. 5. Laplacian Operator.

The pre-trained HAAR cascade classifier is then used to determine if it detects a car. When the results of the classifier and the Laplacian are equal, the parking lot is marked with the corresponding status and the result is sent to the database. If the two results are different, then a third decision phase is applied with a Canny edge detection as shown in figure 5, this third process is carried out to obtain a new result that allows to guide the decision making of one of the other two previously obtained results. For the highest degree of certainty, Canny should be considered to have well-adjusted threshold values.



Fig. 6. Canny Edge Detector

3.3 Database and REST API

The creation of a database was essential part for the project to keep a communication between the detection algorithm phase and the android application we create. For this we use a free hosting service, a service that allow us to store all our data through a SQL database without the necessity of a server, allowing us to focus mainly during this test in the computer vision. During our exploration of the campus of Concepción, we recollected multiple information of the different parking lots that were important for the Android application like coordinates to let user know the parking lots ubicacion, the spaces available in every parking lot, entrance methods which as we say earlier not all the parking lots present the same schedules or access methods, as well as the special parking spots each parking lot presents, like disabled parking spots or load zones.

Within the hosting service and using our SQL database, we can store all the data recollected in our server and access, modify or check this data through the use of a PHP script and creating a REST API, an interface between HTTP systems that allow us to transfer data through JSON arrays or XML, this represents a safer way too keep communication between our database and the application but also a perfect way of separating the database from our application due to the limitations implemented on the users of not allowing them to have full access and control of the database, other benefits of this method is the prevention of overflowing our database with multiple calls, which allow us to connect multiple devices. In figure 7 a representation of the connection made with the online database, the REST API, and our Android application is shown.

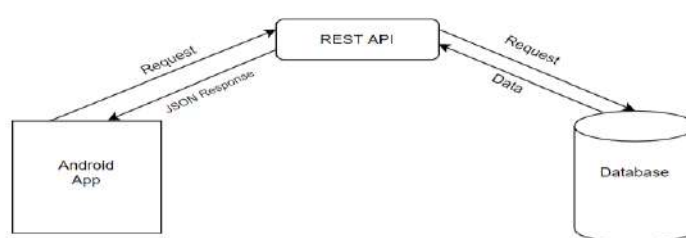


Fig. 7. Connection between Android app, REST API and database.

3.4 Android Application

Our android application was created thinking in an easy and friendly interface that allow the users to obtain the information they need as fast as possible. For the creation of

the application we made use of the Android Studio software, which allow us to design the interface and the inner algorithm the app will use to show the information. The application is designed to satisfy the following requirements:

- List of all the parking lots available inside the university sort by number of free spaces.
- Being able to find a parking lot near a destination.
- Know the type of parking lot, like “professors and personal only” or “guest parking spots”.
- “Map view” showing the actual entrance of the parking lots and the buildings this parking is near to.
- Information section, where the administrator can show multiple news, announcements or warnings related to the parking lots.

4 Results

Figure 8 shows the main screen of the desktop application performing the classification with a test video, since it was not possible for us to test the system directly with the university cameras. This application was made with the Python Tkinter library so that the configuration of the classifier and the visualization of the data were more direct and easier to understand and manipulate. We can see that the main window contains two tabs, in the first one the classifier image is displayed, it also contains some sliders to adjust the minimum threshold of the Laplace and Canny edge detectors, this serves to detect cars even if the sunlight or weather conditions that affect the camera image changes.

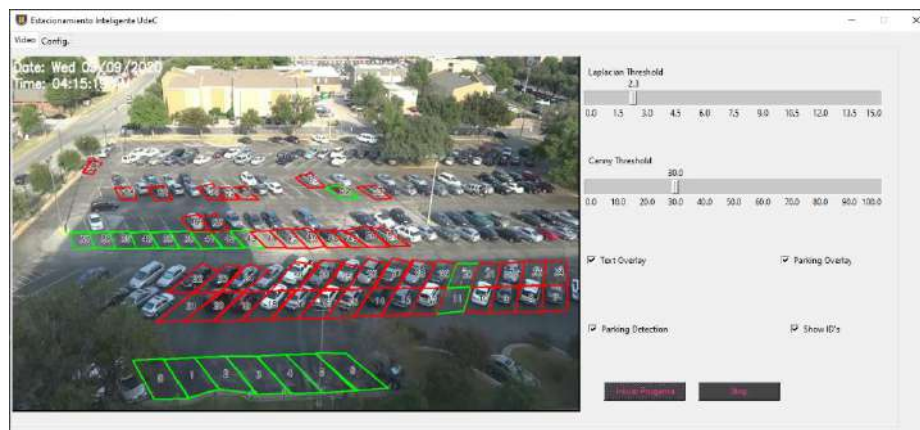


Fig. 8. Desktop Application Main Window.

The second Window represents a Configuration section where we can see that we have a configuration interface, this interface allows us change the file of the pre-trained model for car detection, we can also insert the file ".yml" where we have previously

stored the ROI coordinates. It also has a small algorithm application to create a new coordinate file by selecting them directly from the image, we just pass a pre-existing image of the parking lot and begin to delimit the spaces manually. Finally, this section has two selectors connected, they select the name or ID of the parking lot that we are viewing, this selection is used for the program to send the information on the places of the selected parking lot to the database.

To satisfy the requirements of the mobile application mentioned previously, 6 activity or user interfaces (UI) were designed where the user will have the option for a specific task, the first activity the user faces when the application is initialized is the login activity, which represents a future opportunity for a reservation system, that will allow the client to reserve an specific spot for certain time. Other activities for our mobile app are the preview activity, an activity designed before confirming the parking lot selected by the user and the help activity, a special activity designed to contain information of the administrator of the parking lot or the security inside the university.

The next activities represent the main interfaces of the application, where all the important data will be shown to the client, in this case, the application will have a bottom navigation menu which will allow us to switch between the three activities. The first activity is a list view of all the parking lots with available space, showing first the parking lot with most available places, also for a better use, a search bar was implemented in case the user needs to find an specific parking lot. The second activity represents a map view where the user can see exactly where the entrance of each parking lot is, showing them through an interactive map of the current university infrastructure. The third activity represents an information activity which will be used mainly as a news, alerts, or notification section so we can inform the client in case of an accident or maintenance in a parking lot (see figure 9).

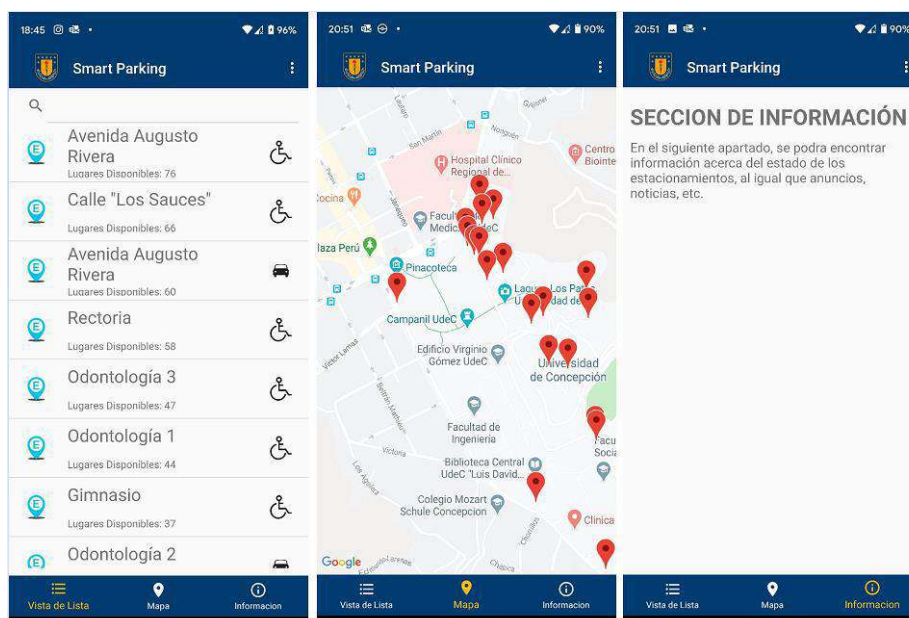


Fig. 9. List view, Map view and Information Activities.

During the project, the application was created as a validation to the system that allow us to proof the changes made inside the database, the application was tested through multiple calls to the database to prove the modification in the data collected and showing it in a list view so the user can check it, inside this list view the data was sorted showing the option with more free spaces at the top of the list and showing other important information like the name and the access method. Other options of the application were tested too, where we show the exact coordinates of the parking lot entrance in a real map of the campus, using the help of the Google Maps API, and proving the interaction the user can have with this option.

5 Conclusion and Future Work

In this paper a proposal for a smart parking lot system was presented, taking into consideration the characteristics the Universidad de Concepción presents and adapting it for it to be the best approach we can think of. Due to all the parking lots being outdoors the use of certain sensors where difficult to consider either by bad weather or the cost limitations like constant management or specific structures these sensors needed to work properly. This let us to the creation of a smart parking lot that presents the novelties of being cheaper and efficient outdoors by using a new method called computer vision, thanks to this we were allowed to use the cameras already located in certain parking lots and therefore keep the current structures inside the parking lots.

Finally to calculate the impact in the community we can do a simple calculation considering that a normal gasoline car emits approximately 2.3 kg of CO₂ per liter, we can determine that a search of at least 20 minutes in a parking lot can generate 230 kg of CO₂ for each person taking a school year as 10 months approximately. If the application reduce the search time in half, we could generate a saving of 130 kg of CO₂ per person, which translated into 10% of a total population of approximately 50,000 people in the three campuses we have a total saving of 575 tons of CO₂ per year.

It is necessary to mount the system within the proposed processor connected to the cameras that the university has, to obtain accurate results of the operation and to be able to carry the pertinent corrections and calibrations. As we mention early our proposed system was tested through multiple parking lot videos, in each case, all the parking lots present different characteristics in terms of lighting, contrast and angle view so we could proof if our algorithms can detect a car without the conditions the camera could present, thanks to the UI created we can change the threshold parameters and adapt the image obtained through the camera to obtain better results but still outdoors test are needed. We also hope to be able to expand the server to improve the current limitations with the request and test the system into a more real environment and allow more users to be able to use the application.

6 Acknowledgments

The authors thank the CYTED Thematic Network “INTELLIGENT CITIES FULLY INTEGRAL, EFFICIENT AND SUSTAINABLE (CITIES)” n° 518RT0558.

7 References

1. Peng, G.C.A., Nunes, M.B., Zheng, L.: Impacts of low citizen awareness and usage in smart city services: the case of London’s smart parking system. *Inf. Syst. E-Bus. Manag.* 15, 845–876 (2017). <https://doi.org/10.1007/s10257-016-0333-8>
2. Babic, M., Vekic, A., Stanojevic, M., Ostojic, G., Borocki, J., Stankovski, S.: Modern Parking Solutions for Smart Cities. *Ann. DAAAM Proc.* 30, 1075–1083 (2019). <https://doi.org/10.2507/30th.daaam.proceedings.150>
3. Carrasco Benavides, R.: Evaluación de sistemas de gestión para optimizar estacionamientos con IoT, https://www.mti.cl/wp-content/uploads/2019/01/Tesisna_2018_Carrasco-Ricardo.pdf, (2019)
4. Fraifer, M., Fernström, M.: Investigation of Smart Parking Systems and their technologies. Presentado en (2016)
5. OpenCV: Introduction, <https://docs.opencv.org/master/d1/dfb/intro.html>
6. Méndez Pelayo, F. de J.: Detección Visual de Vehículos Automotrices en Ambientes Reales, https://rei.iteso.mx/bitstream/handle/11117/5189/Tesis%20maestr%20c3%ada_rev_final.pdf?sequence=2&isAllowed=y, (2018)
7. Beaucamps Santofimia, E.: Implementación de software para la gestión de un parking mediante el uso de técnicas de visión artificial, <https://riunet.upv.es/bitstream/handle/10251/111197/Beaucamps%20-%20Implementaci%20c3%b3n%20de%20un%20soft-ware%20para%20la%20gesti%20c3%b3n%20de%20un%20parking%20mediante%20el%20uso%20de%20t%20c3%a9cnic....pdf?sequence=1&isAllowed=y>, (2018)
8. Navacerrada, J.: Sistema de detección de matrículas con OpenCV, http://oa.upm.es/51869/1/TFG_JORGE_NAVACERRADA.pdf, (2017)
9. Khare, A.: Automatic-Parking-Management, <https://github.com/ankit1khare/Automatic-Parking-Management>
10. Erazo Estrada, C.A.: Prototipo de detección de aparcamientos libres mediante visión artificial en un Parqueadero de la Universidad Tecnica del Norte, <http://repositorio.utn.edu.ec/handle/123456789/9075>, (2019)
11. Loong, D.N.C., Isaak, S., Yusof, Y.: Machine vision based smart parking system using Internet of Things. *TELKOMNIKA Telecommun. Comput. Electron. Control.* 17, 2098–2106 (2019). <https://doi.org/10.12928/telkomnika.v17i4.12772>
12. OpenCV: Smoothing Images, https://docs.opencv.org/master/d4/d13/tutorial_py_filtering.html

Benefits of the integration of photovoltaic solar energy and electric mobility

Miguel Dávila-Sacoto¹[0000-0001-6318-2137], L.G. González²[0000-0001-9992-3494],

J.L. Espinoza²[0000-0002-7450-2084], and Luis Hernández-Callejo³[0000-0002-8822-2948]

¹ Technical Management of Mobility, Air Quality Monitoring Department, Municipal Public Company for Mobility, Transit and Transportation of Cuenca EMOV EP, Ecuador

² Electrical, Electronics and Telecommunications Engineering Department, University of Cuenca, Ecuador

³ Agricultural and Forestry Engineering Department, University of Valladolid, Spain

M.D.S.:mdavila@emov.gob.ec

J.L.E.:juan.espinoza@ucuenca.edu.ec

L.H.C.:luis.hernandez.callejo@uva.es

corresponding author L.G.G.:luis.gonzalez@ucuenca.edu.ec

Abstract. The integration of electric vehicles to electricity grids is the key to the adoption of renewable energy. This study reviews the main benefits and challenges of integrating these technologies, considering the high variation of the photovoltaic resource. The use of an intelligent charging of electric vehicles based on the variation of solar radiation is shown to mitigate the voltage and power variations caused. A simulation of a feeder is performed to verify the benefit of an intelligent charging scheme, achieving an 8% decrease in the required power. In addition, a review of related studies is presented, and the types of communication systems used for the control of vehicle charging in an electrical grid are compared.

Keywords: Electric vehicle, photovoltaic generation, vehicle-grid integration.

1 Introduction

Today, renewable energies play an important role in societies, if environmental, social, and economic aspects are considered, which have allowed the proliferation of clean energy generation technologies. For approximately a decade, mobility systems based on Electric Vehicles (EV) have been considered to reduce the carbon footprint and improve the energy efficiency of transportation. These vehicles have improved in their autonomy and price competitiveness thanks to the advancement of their energy storage systems. Aspects such as decarbonization of the electric power system due to the inclusion of renewable sources and decarbonization of mobility due to the introduction of EV, must be articulated to multiply their individual benefits. The fluctuation of solar irradiance depends on climatic factors such as cloudiness in area, temperature, wind

speed, etc. Commonly these fluctuations are observed in the form of oscillations with a period that can be in the order of seconds up to several hours [1]. These variations in the photovoltaic (PV) resource are translated into fluctuations in the power delivered by the installation, which has a direct impact on the electrical grid. One of the impacts that causes the greatest interest in the scientific community is the fluctuation of the system voltage [2], since it can become a major problem in grids with a high penetration of PV generation [3].

PV generation in Ecuador is attractive due to the high PV resource with an average annual irradiance of 4574.99 Wh/m²/day [4], however, being in a mountainous area, the cloudiness causes fluctuations of the PV resource to be common and interfere with the solar radiation of the sector [5]. Studies determine that the months of higher solar radiation overlaps with the months of greater cloudiness [6]. It should also be considered that a significant number of the country's inhabitants are located in the mountainous region, thus in [7] it is observed that according to the last population census, the Andean region of the country has a 44.53 % of the population of Ecuador. This must be considered given the accelerated worldwide increase in penetration of residential PV energy systems, and it is necessary to be adequately prepared for the sizing and operation of the electrical distribution network within cities with high PV penetration.

2 PV resource fluctuations

Figure 1 shows the typical profile of the radiation and the power generated by a PV system located at the University of Cuenca-Ecuador (2°53'31.0"S, 79°02'18.7"W) during October 17, 2019, where the high radiation fluctuations and their respective power fluctuation can be observed. In [8] the dynamic behavior of radiation fluctuations in the PV installation of the University of Cuenca is analyzed, where the authors indicate that the rate of change in a 28-day sample, which can reach variations between $0.5\Delta P_{nom} < \Delta P < 0.7P_{nom}$ with intervals of $\Delta T \geq 15$ s.

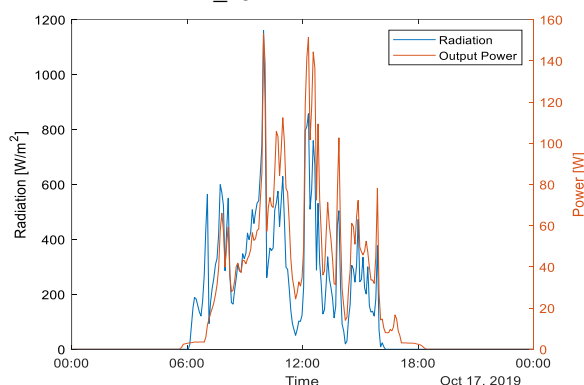


Fig. 1. Radiation and Output Power of a PV string

Former studies presents methods for predicting the fluctuation of PV generation with the use of Kalman filters [9], allowing early actions to be taken with these variations, in addition, methods have been studied for correcting these fluctuations avoiding the

effect in the voltage and power delivered to the PCC (Point of Common Connection). Other techniques analyze the use of supercapacitors [8], [10], and in [11] a method is suggested for the optimal selection of the battery bank to reduce the power fluctuation. Also in [12] a hybrid architecture of batteries and supercapacitors is proposed with centralized control by an EMS (Energy Management System), and in [13] a hierarchical control applied to EV charging stations is proposed, based on the combination of batteries and inertial wheels using dedicated storage systems to reduce the impact on the voltage in the PCC, which represents additional costs that can avoid the massification of PV generation. This study allows the use of additional elements with marginal costs that allow integrating renewable generation actors and private consumers that permit a synergy for the benefit of the environment.

3 Behavior of electric vehicles in public areas

Studies shown in [14] indicate that the average time of a car in the study area is 80% parked at the owner's residence, and another 16% parked on other place, so 96 % of the vehicle's useful life is unused, this important information makes it possible to establish that vehicles can spend a significant amount of time fulfilling functions that allow integrating actors that until now have not been foreseen. In addition, thanks to the massification of electric vehicles, in [15] and [16] idle time of connected EV in public charging stations is studied, finding that it presents a 61.4% of the total connected time, and it is given by equation 1.

$$T_{\text{connected}} = T_{\text{charging}} + T_{\text{idle}} \quad (1)$$

Although this result reduces the availability of chargers, it creates a very important opportunity to use the energy storage systems of vehicles for other uses, such as reducing demand peaks, improving energy quality, and reducing frequency variations. Regarding the behavior of the EVs connected in public stations, from the dataset of [16], it is obtained that the average connection time is 5.82 h, with an average charging time of 2.87 h and an average idle time of 2.94 h. Thus, Figure 2 shows the relationship between idle time and charging time. From there it is observed that the relationship is increasing, and it can be inferred that most vehicles are loaded at $T_{\text{charging}} < 1000$ min and $T_{\text{idle}} < 2000$ min, which indicates that vehicles tend to remain in idle longer.

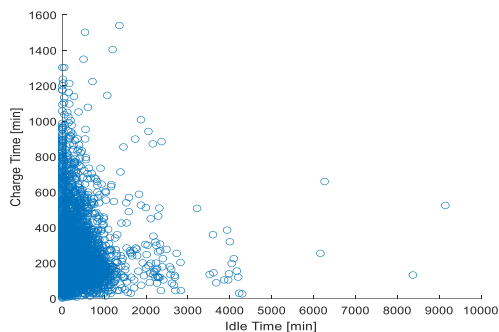
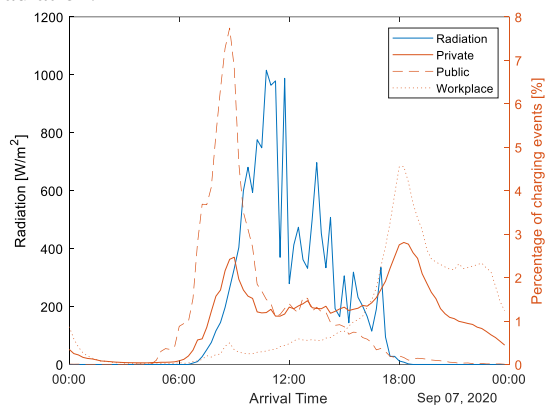


Fig. 2. Idle time and Charge time relationship

Regarding the behavior of EVs observed in [17] which analyzes the hours of arrival at the charging stations, Figure 3a indicates that during working days the vehicles are mostly connected at 9:00 in spaces intended for offices, while at 6:00 p.m. the predominant connection is at private charging points; and in Figure 3b, it is observed that during the weekends the predominance are private charging points, followed by public charging points, in a schedule between 12h00 and 21h00, which coincides mostly with the hours of solar radiation.



(a)

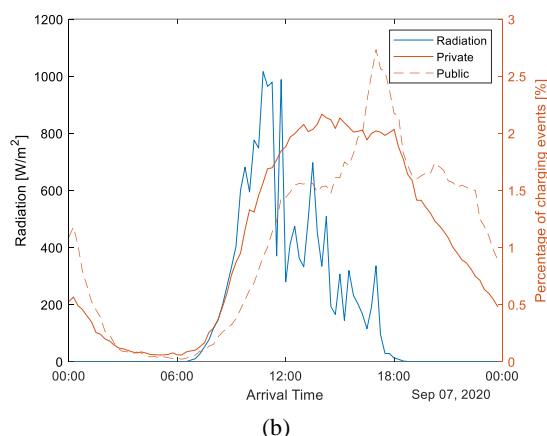


Fig. 3. Distribution of arrival times at charge stations a) workdays b) weekends [17]

4 Integration of electric vehicles to the electrical grid

The integration of vehicles to the electrical grid or VGI (vehicle-grid integration) encompasses the use of technologies allowing EVs to deliver services to the grid [18]. Grid compatibility is a requirement for VGI, for which vehicles must also be compliant with local guidelines and regulations [19]. According to [20] the levels of integration depend directly on the level of control over the load and the agents that intervene externally. Thus, Table 1 shows the levels of VGI and the control and regulations that need to be followed.

Table 1. VGI levels, controls and regulations

Level	VGI	Directionality	Control	Regulations
1	V1G	Unidirectional	Distribution System Operator (DSO), Charge Point Operator (CPO), EV user, EV, Hybrid energy Manager (HEM)	IEC 61851, DIN-SPEC 70121, OCPP 1.6
2	V1GH	Unidirectional	Internal or external	ISO/IEC15118, OCPP 1.6f
3	V2H	Bidirectional	Home or customer system	ISO/IEC15118, EEBus
4	V2G	Bidirectional	External (market)	Level 2 and level 3 regulations

The advantage of an intelligent charging scheme considering VGI lies in the impact it has on the distribution network, thus in [21] the authors show the application of intelligent charging to improve the frequency response of the electrical system. Unidirectional charging levels (V1G and V1H) are relatively simple, and depend on the technology present in the charger, where communication is limited between the vehicle and the charging system, while in bidirectional charging (V2G and V2H) a more complex communication is required, where energy management operators require equipment to perform this communication as well as a management system, in addition, it is required

that the charging station and the customer's meter are compatible with the bidirectionality of the energy flow. Both V1G and V2G represent significant savings compared to non-intelligent charging systems, thus, in [22] it is observed that V1G represents a saving of 62% compared to non-intelligent charging, however, V2G requires an additional investment, but it means a relative benefit of 407USD per vehicle.

5 Electric Vehicle Characterization

In recent years, interest in the use of EVs to compensate for variations in the electricity grid has grown, so it is necessary to know the response of EVs to variations in the charging setpoint in order to use the energy stored in their batteries as support for the grid. In this way, studies such as [23] analyze the dynamic response of EVs when they participate in a frequency control within an isolated system, the study uses an approach based on the use of V2G for the use of EVs in primary and secondary control of frequency in a 10kV single bus system with a 100kW synchronous generator, a transformer and a static load, with EVs connected for frequency compensation. Authors determine that for these disturbances the EVs can respond to the PFC (Primary Frequency Control) and LFC (Load Frequency Control) in an appropriate way, improving the maximum frequency drop in the event of disturbances with times less than 3 seconds. A similar study is performed in [24] with inter-area frequency variations, with improvements in frequency establishment time of up to 50%.

For this type of application, and for others such as voltage or power control, it is required that the variation of the vehicle's charging setpoint be achieved in a reduced time, thus in [25] the response times of a Nissan Leaf 2015, Peugeot Ion 2011 and Renault Kangoo 2012 vehicles are reviewed, all equipped with 3.3kW chargers that can be controlled between 6 to 16A, where it is found that average response times ranged from 0.3s up to 1s, which indicates that this response time depends on the EV under analysis. In this study, tests were carried out on EVs to check their response time to variations in charging setpoints. The vehicles analyzed were the Kia Soul EV, and the BYD E5 400. After the measurements, it was observed that the dynamic response of the vehicles are not the same, thus, it was obtained that for a load setpoint variation from 50% to 30%, an EV's response time is approximately 2 s, on the other hand a second EV showed a response time of 0.68 s (Figure 4), similar to the time found in [25]. Vehicle charging starts at 5.5kW / 25A in fast charge, then the setpoint is changed to a 2.8kW / 12.7A slow charge state and the time when the vehicle's charge controller reaches the required setpoint is measured.

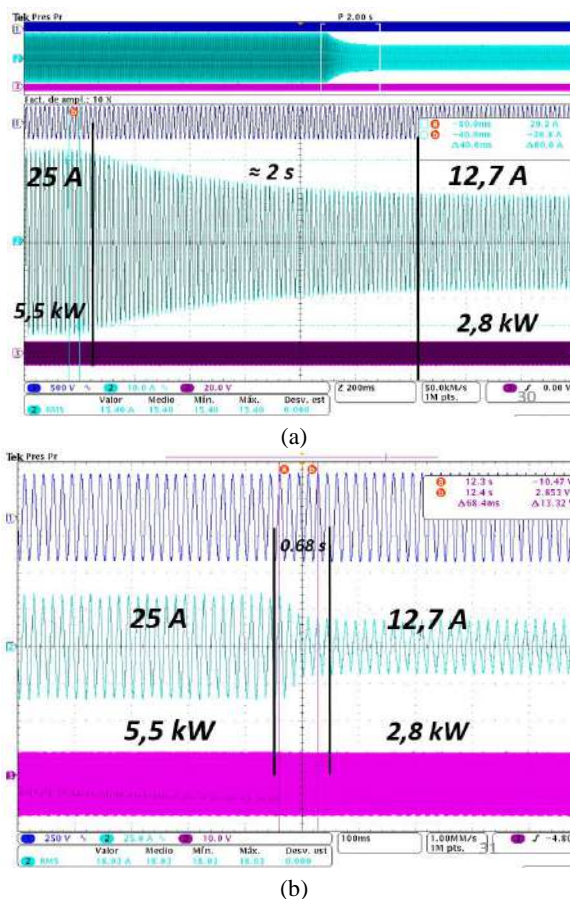


Fig. 4. Dynamic behavior of charging setpoint changes a) EV No.1 b) EV No. 2

6 Integration of smart charging electric vehicles to a grid with high photovoltaic generation

Given the high variation of the PV resource, which causes among other inconveniences the decrease in the voltage in the grid’s feeders, the intelligent charging of EVs constitutes a very important alternative to reduce these variations. In this way, figure 5 shows a day with PV power variations. For the charging setpoint delivered to the vehicle, a low pass filter based on the Tustin bilinear transformation is used [26]. The filter basically removes the high frequency component of the PV radiation variations (Figure 5a) and the control is carried out with the remaining high frequency component (Figure 5b), which is taken as the load command for the EVs, limiting the maximum charge to 7.2kW.

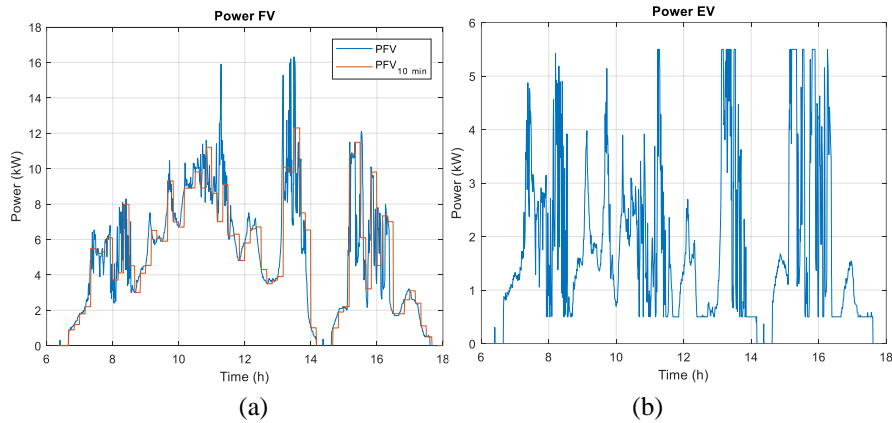


Fig. 5. Compensation of PV resource variations with EVs a) solar radiation b) charging setpoint after applying the Tustin bilinear filter

Extending the concept to a distribution system (Figure 6), the grid is considered to have a high penetration of PV generation, assuming that all customers have 1kW to 3kW of PV generation installed, and all customers have EVs connected to the grid from 06h00 to 18h00. All PV generators deliver normalized power (Figure 8a), and vehicle powers are limited to 7.2kW.

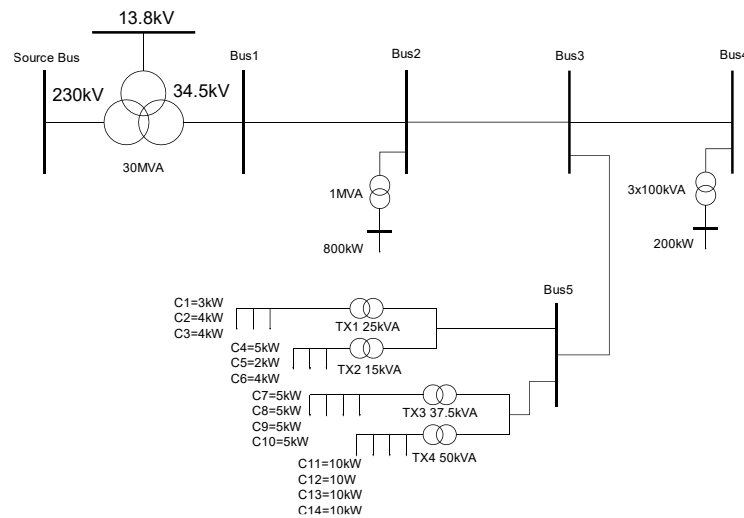
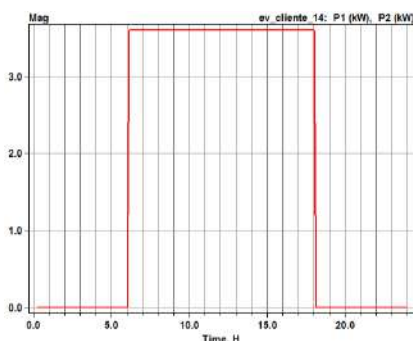


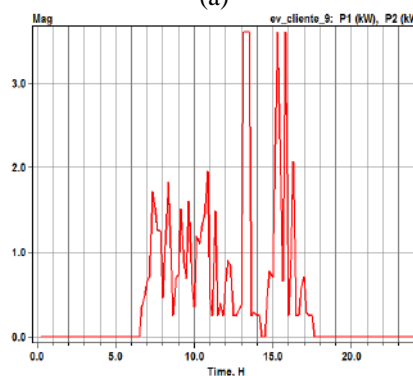
Fig. 6. Feeder with loads (EV) and PV generation

In the case of an installation without intelligent charging control, all vehicles are connected and disconnected at the same time, consuming constant power (Figure 7a). In this case, the voltage at TX1, varies from 119.6VAC to a minimum of 115.9VAC (Figure 7c), that is a decrease of 3.09%. In the main transformer of the feeder, the load curve (Figure 7e) indicates a maximum of 1124kW. In the case of an installation that considers intelligent control of EV charging, all vehicles are connected and

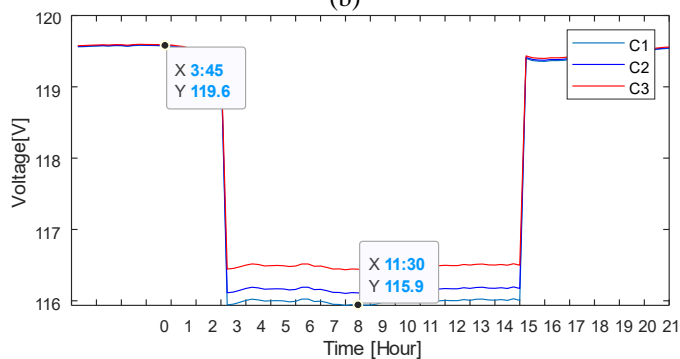
disconnected at the same time, but they consume a power depending on the variations of the PV generators (Figure 7b). In this case, the voltage at TX1, although it varies from 119.6VAC to a minimum of 116VAC (Figure 7d), that is, a decrease of 3.01%, considering the same time as the minimum of the case without control of the load, this value is 119.2VAC that is a decrease of 0.33%. In the main transformer of the feeder, the load curve (Figure 7f) indicates a maximum of 1122kW at 13:30, but at 11h00 from the peak of the previous case, with an intelligent control it reaches 1032kW, which means 8.19% of decrease in load.



(a)



(b)



(c)

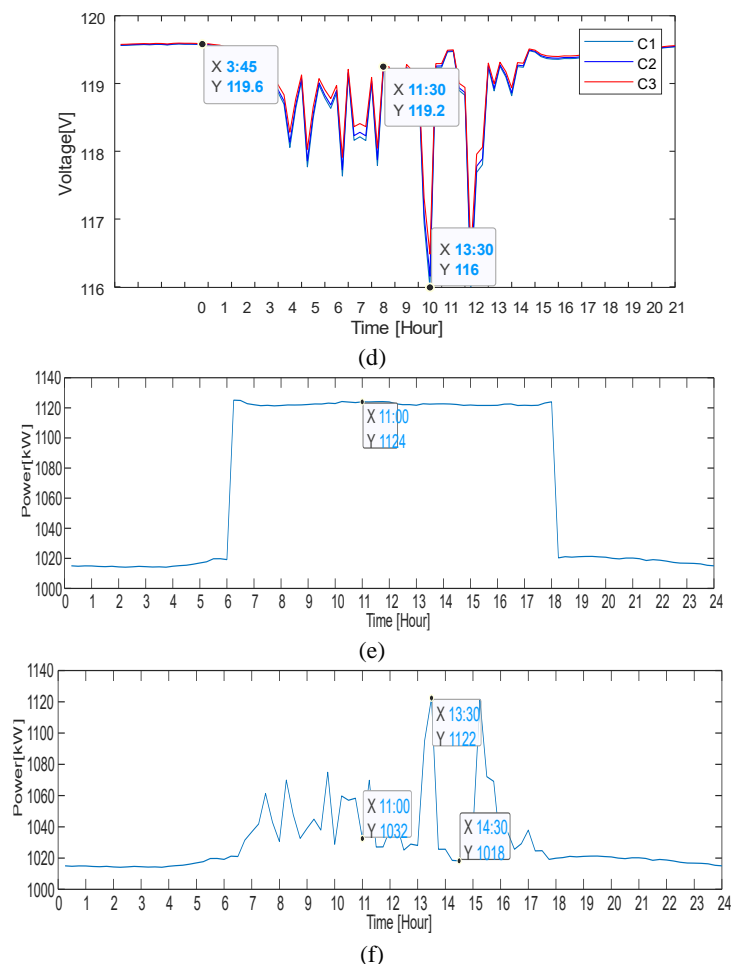


Fig. 7. Feeder simulation results: a) constant power charging setpoint, b) intelligent charging setpoint, c) voltage on TX1 without charging control, d) voltage on TX1 with charging control, e) Power on the feeder without charging control, f) Power at feeder with charging control

7 Benefits and challenges of integrating electric vehicles to photovoltaic generation systems

The integration of EVs to distributed generation systems with the incorporation of PV presents benefits, which have been studied during the last decade. Thus, in [27] some benefits of VGI are listed as auxiliary services for the balance of generation and demand, voltage and frequency regulation, load leveling, and management of power peaks, where the authors mention scenarios where the economic benefits reach the 4000USD per year per vehicle connected to the grid and that provides a power regulation service. This should be considered in networks with high penetration of PV generation. In more current studies such as [28] through interviews with experts in the area,

authors identify 25 categories of benefits of V2G, where integration to renewable energies, controlled charging and the connection between the EV and the home are the three main benefits of VGI, PV power intermittence and fluctuations being the benefit most discussed by experts. Specifically, the use of EV services as a tool to reduce the fluctuation of PV generation has been validated in studies such as [29], [30] and [31], from which it can be observed that the adequate management of VGI has a potential for reduce typical storage systems such as supercapacitors, inertial wheels and batteries, both in their capacity and number.

However, the main challenge of VGI consists in the implementation of charging strategies, since EV charging events usually overlaps with demand peaks [32]. There are also economic challenges such as the implementation of the required technology both on the consumer side and on the energy distributor, requiring both chargers with the necessary technology, as well as bidirectional energy meters. But, perhaps one of the most important challenges is the communication platform that encompasses all these aspects [33], and this is more drastic in systems that have PV generation due to the high intermittency of the resource, and its variations in very short times . Therefore, a communication infrastructure capable of responding to these fluctuations in the required time is required. As previously observed, in the case of frequency control, the system can respond in several minutes, however, voltage variations are faster, and in small-scale cases such as local distribution systems, if there are several PV generators, the variations can be significant and with dynamics in the order of milliseconds. To overcome this drawback, various communication technologies have been proposed. Thus, in [34] Industrial Internet is used as a communication channel between the dispatch center and the vehicles, in [35] the LoRaWAN radio frequency system is used, and in [36] they use a hybrid alternative, with the 5G network as main hub and wireless communication between the EV and the distribution company, but on the condition that the 5G network is properly configured for sending messages with low latency. Table 2 shows a comparison of the most used communication systems in VGI.

Table 2. Main characteristics of communication systems used in VGI

Communication system	LoRa-WAN	Zigbee	4G	5G	Industrial Ethernet	FO
Type	Wireless	Wireless	Wireless	Wireless	Cable	Cable
Data rate	50kbps	250kbps	1Mbps	100Mbps	100Mbps	10Gbps
Sensitivity	-142dBm	-126dBm	-117dBm	-113dBm	-31dBm	-19dBm
Range	3km	300m	2.5km	45km	100m	100km (single mode)
Average response time	22.95ms	10ms	50ms	5ms	100ms	0.1ms per 10km

Considering that the primary control of voltage in electrical grids can be carried out between 2 and 20 seconds, the limitation of the communication technologies for VGI

have sufficient characteristics to deliver the control messages, however, the time of EV response, which, as mentioned, depends on the EV and can also take a few seconds. Therefore, although the response time of the communication systems are high, the vehicle must be able to respond adequately to the control signal and adjust its power appropriately, thus, the system must know the time in advance. response of the vehicle to dispatch the energy in the required time.

8 Conclusions

This study presents the main advantages and challenges of the integration of electric vehicles and photovoltaic generation, with an emphasis on mitigating voltage variations caused by the high variability of the photovoltaic resource. A bibliographic verification of studies on the subject was carried out, rescuing the main findings that highlight the importance of considering smart charging for the integration of electric vehicles to the grid.

Through a simulation of a feeder circuit, it was shown that a charging control based on filtering the high frequency variations of solar radiation can mean a reduction of 8.19% of the power in the main transformer of the feeder, and a decrease in voltage variations in distribution transformers was observed.

For an adequate management of the services that EVs can provide to the grid, it is necessary to know the response time to charging setpoint changes, and this information should be delivered by the manufacturers, or the EVSE (Electric Vehicle Supply Equipment) should be able to measure it, in order to have an appropriate database for use by the energy distribution company and thus achieve an efficient integration between renewable energies and EVs.

Acknowledgments

The authors thank the CYTED Thematic Network “INTELLIGENT CITIES FULLY INTEGRAL, EFFICIENT AND SUSTAINABLE (CITIES)” nº 518RT0558. This work has been supported by Spanish national project [RTC-2017-6712-3] of the Spanish Ministry of Science.

References

- [1] W. A. Omran, M. Kazerani, and M. M. A. Salama, “A study of the impacts of power fluctuations generated from large PV systems,” in *2009 IEEE PES/IAS Conference on Sustainable Alternative Energy (SAE)*, Sep. 2009, pp. 1–6, doi: 10.1109/SAE.2009.5534823.
- [2] A. Ali, D. Raisz, and K. Mahmoud, “Voltage fluctuation smoothing in distribution systems with RES considering degradation and charging plan of EV batteries,” *Electr.*

- Power Syst. Res.*, vol. 176, no. April, p. 105933, Nov. 2019, doi: 10.1016/j.epsr.2019.105933.
- [3] S. A. Aleem, S. M. S. Hussain, and T. S. Ustun, "A Review of Strategies to Increase PV Penetration Level in Smart Grids," *Energies*, vol. 13, no. 3, p. 636, Feb. 2020, doi: 10.3390/en13030636.
- [4] Consejo Nacional de Electricidad (CONELEC), "Atlas Solar Del Ecuador Con Fines De Generación Eléctrica," *Corporación para la Investig. Energética*, 2016, [Online]. Available: <http://energia.org.ec/cie/wp-content/uploads/2017/09/AtlasSolar.pdf>.
- [5] O. H. Á. Hernández, T. Montaña, and E. Quentin, "La radiación solar global en las provincias El Oro , Loja y Zamora Chinchipe , Ecuador . Utilización de datos de reanálisis de la nubosidad diurna .," *Rev. Climatol.*, vol. 14, no. April, pp. 25–33, 2014.
- [6] Ma. J. Alvares Orlando, Quentin Emmanuelle, Montano Thuesman, "La radiación solar global en la región sur del Ecuador . Reanálisis de la nubosidad diurna," no. November, 2013, doi: 10.13140/RG.2.1.4101.9282.
- [7] B. Villacís and D. Carrillo, "País atrevido: la nueva cara socio-demográfica del Ecuador," *Analitika*, p. 52, 2012, [Online]. Available: http://www.inec.gob.ec/publicaciones_libros/Nuevacarademograficadeecuador.pdf.
- [8] L. G. González, R. Chacon, B. Delgado, D. Benavides, and J. Espinoza, "Study of Energy Compensation Techniques in Photovoltaic Solar Systems with the Use of Supercapacitors in Low-Voltage Networks," *Energies*, vol. 13, no. 15, p. 3755, Jul. 2020, doi: 10.3390/en13153755.
- [9] J. Dong *et al.*, "Novel stochastic methods to predict short-term solar radiation and photovoltaic power," *Renew. Energy*, vol. 145, pp. 333–346, Jan. 2020, doi: 10.1016/j.renene.2019.05.073.
- [10] H. B. Wang, X. Yang, J. Liu, and J. Chen, "Control Strategy of the Hybrid Energy Storage System for Leveling Off Fluctuating Power Output of Stand-Alone Photovoltaic System," *Adv. Mater. Res.*, vol. 860–863, pp. 608–612, Dec. 2013, doi: 10.4028/www.scientific.net/AMR.860-863.608.
- [11] F. Ferdowsi, A. Sadeghi Yazdankhah, and B. Abbasi, "Declining power fluctuation velocity in large PV systems by optimal battery selection," in *2012 11th International Conference on Environment and Electrical Engineering*, May 2012, pp. 983–988, doi: 10.1109/EEEIC.2012.6221520.
- [12] W. Ma, W. Wang, X. Wu, R. Hu, F. Tang, and W. Zhang, "Control Strategy of a Hybrid Energy Storage System to Smooth Photovoltaic Power Fluctuations Considering Photovoltaic Output Power Curtailment," *Sustainability*, vol. 11, no. 5, p. 1324, Mar. 2019, doi: 10.3390/su11051324.
- [13] L. Shen, Q. Cheng, Y. Cheng, L. Wei, and Y. Wang, "Hierarchical control of DC micro-grid for photovoltaic EV charging station based on flywheel and battery energy storage system," *Electr. Power Syst. Res.*, vol. 179, no. November 2018, p. 106079, Feb. 2020, doi: 10.1016/j.epsr.2019.106079.
- [14] J. Bates and D. Leibling, "Spaced Out Perspectives on parking policy," 2012. doi: 10.1109/CMD.2008.4580239.
- [15] A. Lucas, G. Pretico, M. G. Flammini, E. Kotsakis, G. Fulli, and M. Masera, "Indicator-based methodology for assessing EV charging infrastructure using exploratory data analysis," *Energies*, vol. 11, no. 7, 2018, doi: 10.3390/en11071869.

- [16] Elaad NL, "Elaad NL data sets," 2019. <https://platform.elaad.io/download-data/> (accessed Jul. 30, 2020).
- [17] Elaad NL, "ElaadNL Open Datasets for Electric Mobility Research Update April 2020." https://platform.elaad.io/analyses/ElaadNL_opendata.php (accessed Aug. 03, 2020).
- [18] V. Integration, "California Vehicle-Grid Integration (VGI) Roadmap : Enabling vehicle-based grid services," no. February, 2014.
- [19] International Electrotechnical Commission, "IEC 60364-7-722 Low-voltage electrical installations Part 7-722: Requirements for special installations or locations - Supplies for electric vehicles," *61010-1* © *Iec:2001*. p. 13, 2018.
- [20] CHARIN, "Grid Integration Levels," 2018. [Online]. Available: https://www.charinev.org/fileadmin/Downloads/Papers_and_Regulations/CharIN_Levels_Grid_Integration.pdf.
- [21] W. Wei *et al.*, "The effect of different charging strategies on EV load frequency control," *2016 Int. Conf. Smart Grid Clean Energy Technol. ICSGCE 2016*, no. October, pp. 161–165, 2017, doi: 10.1109/ICSGCE.2016.7876045.
- [22] California Energy Commission, "Distribution System Constrained Vehicle-to- Grid Services for Improved Grid Stability and Reliability California Energy Commission," no. March, p. 92, 2019.
- [23] A. Zargiannis, M. Marinelli, C. Traholt, K. Knezovic, and P. B. Andersen, "A dynamic behaviour analysis on the frequency control capability of electric vehicles," *Proc. Univ. Power Eng. Conf.*, no. 2013, 2014, doi: 10.1109/UPEC.2014.6934763.
- [24] Y. R. Prajapati, V. N. Kamat, and J. Patel, "Load Frequency Control Under Restructured Power System Using Electrical Vehicle as Distributed Energy Source," *J. Inst. Eng. Ser. B*, 2020, doi: 10.1007/s40031-020-00458-5.
- [25] S. Martinenas, M. Marinelli, P. B. Andersen, and C. Træholt, "Evaluation of electric vehicle charging controllability for provision of time critical grid services," *Proc. - 2016 51st Int. Univ. Power Eng. Conf. UPEC 2016*, vol. 2017-Janua, pp. 1–5, 2016, doi: 10.1109/UPEC.2016.8113989.
- [26] A. Tustin, "A method of analysing the behaviour of linear systems in terms of time series," *J. Inst. Electr. Eng. - Part IIA Autom. Regul. Servo Mech.*, vol. 94, no. 1, pp. 130–142, 1947, doi: 10.1049/ji-2a.1947.0020.
- [27] M. Yilmaz and P. T. Krein, "Review of benefits and challenges of vehicle-to-grid technology," *2012 IEEE Energy Convers. Congr. Expo. ECCE 2012*, pp. 3082–3089, 2012, doi: 10.1109/ECCE.2012.6342356.
- [28] L. Noel, G. Zarazua de Rubens, J. Kester, and B. K. Sovacool, "Beyond emissions and economics: Rethinking the co-benefits of electric vehicles (EVs) and vehicle-to-grid (V2G)," *Transp. Policy*, vol. 71, pp. 130–137, 2018, doi: 10.1016/j.tranpol.2018.08.004.
- [29] A. K. Verma, O. Elma, Y. Wang, H. R. Pota, R. Gadh, and M. Srivastava, "Smoothing PV Power Fluctuations with Electric Vehicle and its Grid Interaction," in *2020 IEEE International Conference on Power Electronics, Smart Grid and Renewable Energy (PESGRE2020)*, Jan. 2020, pp. 1–6, doi: 10.1109/PESGRE45664.2020.9070501.
- [30] Y. Kobayashi, M. Hamanaka, K. Niimi, K. Yukita, T. Matsumura, and Y. Goto, "Power Quality Improvement Method Using EV for PV Output Fluctuation," in *2018 International Conference on Smart Grid (icSmartGrid)*, Dec. 2018, pp. 272–275, doi: 10.1109/ISGWCP.2018.8634448.

- [31] N. B. G. Brinkel *et al.*, “Impact of rapid PV fluctuations on power quality in the low-voltage grid and mitigation strategies using electric vehicles,” *Int. J. Electr. Power Energy Syst.*, vol. 118, no. November 2019, p. 105741, Jun. 2020, doi: 10.1016/j.ijepes.2019.105741.
- [32] N. Daina, A. Sivakumar, and J. W. Polak, “Electric vehicle charging choices: Modelling and implications for smart charging services,” *Transp. Res. Part C Emerg. Technol.*, vol. 81, pp. 36–56, 2017, doi: 10.1016/j.trc.2017.05.006.
- [33] B. C. Liu, M. Ieee, K. T. Chau, F. Ieee, D. Wu, and S. M. Ieee, “Opportunities and Challenges of Vehicle-to-Home , Vehicle-to-Grid Technologies,” pp. 1–19, 2013.
- [34] Y. Zhang, C. Dong, Q. Xiao, M. Wang, K. Hou, and H. Jia, “Discrete Spectrum Iteration Based Comprehensive Stability Assessment Method for the Delayed Cyber-Physical System with Electric-Vehicle Frequency Regulation,” *IEEE Access*, pp. 1–1, 2020, doi: 10.1109/access.2020.3011832.
- [35] H. Klaina *et al.*, “Aggregator to Electric Vehicle LoRaWAN Based Communication Analysis in Vehicle-to-Grid Systems in Smart Cities,” *IEEE Access*, vol. 8, pp. 124688–124701, 2020, doi: 10.1109/ACCESS.2020.3007597.
- [36] M. Tao, K. Ota, and M. Dong, “Foud: Integrating Fog and Cloud for 5G-Enabled V2G Networks,” *IEEE Netw.*, vol. 31, no. 2, pp. 8–13, 2017, doi: 10.1109/MNET.2017.1600213NM.

The role of the electrical vehicle in sustainable supply chains: a review

Fernanda Helena Amaro Verneque¹, Pedro Henrique González²[0000-0003-0057-7670],
Monica Alonso Martinez³[0000-0001-9006-8196] and Vanessa de Almeida Guimarães¹[0000-
0001-7662-3499]

¹ Centro Federal de Educação Tecnológica Celso Suckow da Fonseca, Angra dos Reis/RJ,
Brazil

² Centro Federal de Educação Tecnológica Celso Suckow da Fonseca, Rio de Janeiro/RJ, Brazil

³ Universidad Carlos III de Madrid, Leganés, Spain

fernanda.verneque@aluno.cefet-rj.br

pegonzalez@eic.cefet-rj.br

monica.alonso@uc3m.es

vanessa.guimaraes@cefet-rj.br

Abstract. Environmental concerns, such as global warming and scarcity of natural resources, pressure companies to develop and adopt cleaner technologies and production processes. Besides, the search for sustainable development (as recommended by Agenda 2030 from the United Nations) has made companies rethink their whole supply chain, including transport activities. Besides, governments have been proposing public policies to obtain positive impacts in the economic, social and environmental dimensions. In this context, many studies have pointed out that electric mobility is a sustainable alternative to the transport sector and, in many EU countries, the government has bet on subsidies to attract manufacturers and customers to this market. Therefore, this paper aims to identify the role of electric vehicles (EV) in sustainable supply chains, considering the articles published in the Web of Science (WoS) database. We realize that there is a low quantity of papers dedicated to investigating the EV in this context. Many papers claim to perform sustainable analysis but do not evaluate the triple bottom line's three dimensions. Nevertheless, we identified that governments had developed policies to incentivize the introduction of electric vehicles in the market.

Keywords: electric vehicle, sustainability, supply chain.

1 Introduction

The last decades have been marked by growing concerns about energy usage and other environmental impacts [1], so we have experienced the development of policies to mitigate climate change, the proposition of actions to reduce the environmental impact and the discussion of renewable resources for energy sources in different sectors.

With the exponential growth of the population, the natural resources are being increasingly consumed and, therefore, the raw materials are becoming scarce and

expensive [2]. In this context, companies have been pressured to act according to the sustainable development concept, which is understood as the development that meets the present's needs without compromising future generations [3]. This concern is not restricted to the company but extends to the entire supply chain and its activities [4].

Supply chains correspond to the entire management of a product useful life, from the extraction of raw material to its final disposal [4]. Therefore, the introduction of sustainability concept requires that the entire supply chain seeks more than the efficient management of processes, also considering innovative alternatives that improve environmental, social and economic conditions [5].

At this point, it is important to emphasize that, among the logistic activities performed in a supply chain, the transport is one of the most important, being responsible for the greater part of the costs, up to $\frac{1}{3}$ of the logistic costs [6].

From the environmental point of view, the transportation sector accounted for 45.4% of greenhouse gas (GHG) emissions and consumed about 32.7% of energy in Brazil in 2019, surpassing the industrial sector [7]. So, the transport sector contributes to the increase in global warming potential (GWP) and the scarcity of natural resources [8]. For this reason, this sector has been increasingly pressured to implement eco-friendly and sustainable strategies [9]. Sustainable strategies focused in this sector can be seen in [10-11].

In this context, many manufacturers of vehicles have sought to improve the technologies of internal combustion engines (ICE) to decrease GHG and pollutant emissions [12]. However, due to the increasing demand for vehicles and all the mentioned environmental problems, replacing ICE for electric vehicles (EV) have been raising as a possible solution [12], aiming to reduce both carbon emissions and dependency on fossil fuels.

It is important to emphasize that the concept of sustainability requires the triple bottom line, in other words, the assumption of the equal importance of the economic, social and environmental aspects. Only the joint analysis of these is possible to get sustainable strategies of energy resources [12].

Therefore, this paper aims to identify the role of the electric vehicle in sustainable supply chains, considering the articles published in the Web of Science (WoS) database. Assuming that electromobility is pointed by the literature to reduce the environmental impacts of the transportation sector, especially energy consumption of fossil fuels and carbon emission, we aim to understand if and how the discussion about sustainable supply chains is related to electromobility.

From this introduction, the article was divided into four sections: the theoretical framework about electric vehicles and sustainability (Section 2); the methodological procedures (Section 3); the presentation of the main findings (Section 4) and final considerations (Section 5). Finally, we have acknowledgments and references.

2 Theoretical Framework

There has been an increasing worry about sustainable development in order to reduce the impact in the environment in which we live and, thus, ensure the quality of life for future generations [13], and this is a main challenge in mobility sector. On the other

hand, the concept of sustainability is not always used correctly, as will be discussed in this paper. Many studies claim to analyze the sustainability of a certain product, process, or operation, but the social analysis is left aside, being performed only environmental and/or economic assessments [12, 14, 15, 16]. Nevertheless, to be considered sustainable, there must be a balance between the three pillars: economic, social and environmental [17].

Focusing on transport sector, sustainable transport has been an important challenge for many countries [10 - 11] to reduce air pollution, climate change, negative impacts on population life, energy consumption, material use, and provide better service with less cost. Papers concerned with improving sustainability in transport operations can be found in the literature, focusing in many countries, in Europe [18 – 19], in Brazil [15 – 16] and so on. In this context, many studies have bet on EVs as a sustainable alternative to ICE [20, 21, 17], although some of them emphasize the environmental pillar aiming at reducing the dependence on oil and carbon emissions [22].

In order to have greater acceptance of electric vehicles, it is necessary to provide information about their sustainability performance, because the impacts of increasing their use are unknown, especially regarding the materials and technologies used [8]. For example, many studies have pointed out the need for government interventions to provide renewable energy sources to maximize the potential environmental benefits [2, 13, 14, 22, 23] of EVs since the level of environmental benefits are highly dependent on the main source of electricity used as fuel for the EVs.

Authors in [12] state that adopting these EVs in regions in which the energy matrix relies primarily on coal or oil could have worse environmental effects than internal combustion vehicles (ICV). Therefore, the development of policies to incentivize electric vehicles' adoption requires further analysis of the impacts. In that sense, reference [23] states that the decisions should be based on the sustainability assessment of the EV's entire life, from the raw material's extraction to its disposal.

When evaluating the life cycle of a vehicle (cradle-to-grate), [1] realized that lithium batteries production (the most used in EVs) accounts for 13% of the energy consumption and 20% of GHG related to the vehicle [1]. Besides, the increase in the lithium use for batteries would lead to its depletion if no recycling program of lithium battery is established. From the social point of view, this paper's systematic review shows that cobalt as raw material for producing batteries might cause a political crisis in the countries that export it [as in 24].

Section 4 will present how the papers about electric vehicles in sustainable supply chains are dealing with the environmental, social and economic concerns in their studies.

3 Methodological Procedures

To perform the review proposed in this paper, at first, we performed a generic search related to sustainable supply chain. We have not included any keyword related to electric vehicles since we decided to gather all the papers published about the subject and select our frame of analysis. By doing this, we reduced the error associated with the elimination of papers that could be related to the theme but does not use a specific keyword as its indexation terms.

In the approach adopted, we could select those papers that had any keyword related to electromobility among all the papers published. We believed that it was the widest procedure to review precisely the papers published in the selected database. Therefore, the parameters of the search are listed in Table 1. Web of Sciences (WoS) repository was chosen due to its satisfactory coverage, being used in papers with similar methodology as [25]. We highlight that the papers published in 2020 were not considered since it is the current year.

Table 1: WoS database search description

Criteria	Description
Topic	TS = (“supply chain*” OR “supply network”) AND (“sustainab*”)
Database	Web of Science
Refinement	All areas of WoS until 2019.
Search	20/03/2020 at 16:20 GMT-3

Among the papers gathered, the only keywords related to electric vehicles or electromobility was: “electric vehicles”, “battery electric trucks” and “electrification of mobility”. Therefore, a systematic review of the papers indexed with at least one of these keywords was performed.

4 Results and Discussion

Performing the search described in Table 1, it was found 9.558 about sustainable supply chain. Thus, we identified 11,333 keywords related to those publications, highlighting: Sustainability (1118 records), Supply Chain (467), Supply Chain Management (382), Life cycle assessment (LCA) (276), Sustainable Supply Chain (SSC) (253), Sustainable Development (243), Sustainable supply chain management (158), Green Supply Chain Management (156), Circular Economy (CE) (127) and Closed-Loop Supply Chain (CLSC) (126). Note that none of them are directly indicating any kind of electromobility.

As mentioned in the previous section, only three words directly related to electromobility were found: “electric vehicles” (with 22 records), “battery electric trucks” (1 paper) and “electrification of mobility” (1 paper). It suggests that the studies about sustainable supply chain published in the WoS database do not focus on electric vehicles, since only 24 papers among 9.558 study this subject.

We performed a literature review of these papers and the main findings are presented in the following subsections. We provided a brief contextualization of the articles and the analysis was divided according to the study object, emphasizing if they adopt (or not) sustainability indicators. Therefore, Section 4.1 analysis the papers that have the battery as the main object of study, Section 4.2 evaluates those that are focused on the supply chain design and Section 4.3 presents the articles that compare the performance of EVs e ICEVs.

Although papers [24] and [21] are listed among the papers found in the search, they are out of this search scope and, therefore, will not present in the tables. In [24], authors explore how the decision to exclude the use of Congolese cobalt in supply chains

interferes in the political stability and corruption in the Democratic Republic of Congo. Reference [21] focuses on policy strategies for the insertion of renewable energy sources in households in the north of the United Kingdom, considering the use of solar panels and electric vehicles.

Besides, article [13] is not in the tables since it performs a literature review of lithium's supply chain dedicated to producing batteries for EV, identifying safety problems and the suppliers' risks.

4.1 Battery as study object

Only 5 of the 22 articles are dedicated to studying EV batteries (as presented in Table 2). There is a more significant concern with battery disposal [17, 23], since the cathode material is harmful to the environment and human health [23]. Besides, it is responsible for 20% of the GHG emission, when considering EVs' life cycle [1]. Nevertheless, [8] is dedicated to the evaluation of the EVs' charges.

Reference [20] proposes a battery management model in which EVs' users would be registered in a monitoring system. Instead of recharging their batteries, the users would go to a service point and exchange their discharged batteries for a charged one. The optimization model finds the shortest route to the service point. The authors also analyze the savings that this method would bring compared to fuel vehicles, about 37.4% of the expenses.

In [17] a model to compare two kinds of batteries' sustainable performance is proposed: nickel-manganese-cobalt (Li-NMC) and iron-phosphate (LiFeP) batteries. The results do not point to an explicit recommendation of which battery technology is the best, but have important insights: for example, Li-NMC batteries emit less GHG, while LiFeP batteries have more benefits in relation to natural resource depletion).

[23] studies reverse logistics, especially the recycling process of EVs' batteries. The authors analyze some scenarios (with penalties and/or governmental incentives) to evaluate how it would impact the manufacturers' behavior regarding batteries' correct disposal.

With a slightly different perspective, [26] aims to identify the risks to the electricity grid's operation and reliability that arise from the integration of transport and energy supply chains in the Netherlands. The results show that in densely populated areas, such as the city of Amsterdam, the additional demand for energy (from EVs) might exceed the capacity of the local network in the short term, due to the rapid adoption of EVs and old distribution network.

4.2 Supply chain management as study object

Among the 22 articles analyzed, eight are focused on supply chain management, as presented in Table 2. It is observed that although the EVs' market has not achieved its production peak, there are studies concerned with the long-term risks of raw material supplies [1, 17, 23], mainly for batteries that must be replaced before their charging potential drops to 20% (approximately after eight years of use) [1 – 23].

Among the supply chains studied, one of the papers is focused in the usage of biomass for generating bioelectricity [27] and others is dedicated to evaluating the risk

of disruption in the supply of the minerals used in the EV and ICEV production (as copper, nickel, zinc) [28, 29]. Reference [30] also, analyze the risks of raw material supply in the supply chain of EVs but include the forward flows (e.g., recycling).

Authors in [14] study the design of the automotive supply chain (including EV and ICEV), with emphasis to long term planning to attend the 2030 Agenda considering the EV insertion in the fleet and [31] evaluates how governmental incentives might encourage the supply and the demand of EVs [31].

One of the articles studies the possibility of inserting EVs in a food supply chain, investigating if the local farmers are willing to use EVs to deliver the cargo to local producers [32].

A model to maximize profit related to the lithium batteries' remanufacture used in the EVs is proposed in [1]. The model deals with a closed-loop supply chain considering the quality levels of lithium-ion batteries in the decision to recycle it or not. Using the proposed model, a 30.93% increase in profit can be achieved if the remanufacturing infrastructure is integrated into the lithium-ion battery manufacturing network.

4.3 Papers that compare the performance of EVs and ICEVs

Table 2 shows that three papers compare the performance between the types of EV: Battery Electric Vehicles (BEV), Hybrid Electric Vehicles (HEV), Plug-In Hybrid Electric Vehicles (PHEV) and ICEVs, especially in relation to GHG emission/reduction and cost analysis.

Authors in [12] make a comparative analysis of the three pillars of sustainability in relation to the use of BEV, PHV, HEV with ICEV. By introducing 10% of EVs in the fleet (individually), they found that: the BEVs have a higher potential for reducing the Global Warming Potential (GWP), achieving 12% while the HEVs and PHVs have 4% and 8%, respectively. On the other hand, the water consumption would increase by 1.3 times due to the withdrawal of water for electricity generation, which is higher than ICEVs.

[33] shows that all kinds of EVs would reduce CO₂ emissions compared to ICEV (by petrol and diesel), but only if renewable energy sources were used to generate electricity for the EVs. Although HEVs do not have zero emission, this type of vehicle has a higher energy efficiency level.

There is also one reference that studies the adoption of EVs in a taxi fleet in New York [34]. The findings show that adopting EVs only for fuel savings is not feasible due to the limited capacity of EVs' batteries under assessment. There would be questions related to recharge times and routes. The New York pilot project showed that the taxi driver would achieve a 10% reduction in his income because he had to refuse some trips when the battery level was low [34].

Table 2: Main features of the analyzed papers regarding the role of electric vehicle in a sustainable approach

Study object	Paper	Objective	Environmental	Social	Economic
Battery	[8]	Compare the energy consumption and GHG of four types of EVs chargers throughout the life cycle and assess the environmental impacts of future EV infrastructure.	Energy consumption; GHG; GWP; Cumulative energy demand (CED)	None	None
	[20]	Design an intelligent battery information management system (IBIS) for effective EV battery management.	*	None	Fuel price compared to changing batteries
	[17]	Develop a procedure to analyze the sustainability performance of an EV, with emphases in comparing two types of lithium-ion batteries: Li-NMC and LiFeP.	GHG; Depletion of natural resources	Social risks along supply chain (child and forced labor)	Raw materials supply; Life cycle costs (LCC) for consumer; external costs for society
	[23]	Investigate the socioeconomic and environmental impacts of recycling EV batteries under reward-penalty mechanisms.	Recycling of materials; Environmental Benefit	Social welfare	Governmental incentives
	[26]	Identify and analyze the risks to the operation of the electricity grid due to the insertion of electric vehicles in the transmission network.	*	None	Risk of failure and reliability in the supply of the network
Supply chain	[1]	Propose a model to maximize the profit of battery remanufacturing, considering the quality levels of lithium batteries.	Depletion of natural resources; Recycling of materials	None	Profit
	[27]	Propose a model to optimize the economic and environmental performance of a supply chain.	GHG	None	Global net present value (NPV)
	[14]	Address the long-term dynamics in the supply chain, along with the development of powertrain fleets by 2030.	Equivalent carbon dioxide emission	Unemployment number	Costs of supply chain
	[28]	Develop a MRIO-based life cycle assessment approach to estimate the material footprint of each vehicle alternative considering regional and global supply chains.	Material footprint	None	None

	[32]	Explore the intention of entrepreneurs operating in the food supply chain to introduce EVs to deliver their products aiming at achieving sustainability.	*	None	None
Supply chain	[31]	Analyze the effects of government subsidies on a supply chain, considering an EV manufacturer and consumer.	None	Social welfare	Demand impacts
	[30]	Identify the risk factors of the EV supply chain and help related companies prevent risks.	Environmental risks ¹	None	Technical risk ² and market risk ³
	[29]	Propose model to quantify the product supply risk considering the Life Cycle Sustainable Assessment framework (the case study focus on EV and ICEVs).	Impacts of Life Cycle Analysis (LCA)	Supply chain resilience, socioeconomic and geopolitical risk	Own indicator: economic importance (EI)
EVs and ICEs	[12]	Evaluate and compare the impacts of electric and gasoline vehicles in the environmental, social and economic dimensions.	GWP; Particulate Matter Formation; Photochemical Ozone Formation; Land use	Human Health; Total Tax; Compensation; Employment	Operating Surplus; Gross Domestic Product (GDP); LCC
	[33]	Analyze the environmental benefits of EVs in relation to ICEVs; identify how the emission savings depend on the source of electricity and the efficiency of the plant.	CO ₂ emission; Depletion of natural resources	None	Comparison with current and future EVs and ICEVs costs
	[34]	Study the impact of adopting an EV fleet for taxicabs and the factors that might influence this adoption.	*	None	Comparison of EVs and ICEVs costs
	[22]	Present a study on the effectiveness of government subsidies for EV consumers and manufactures, finding the ideal subsidy to maximize social welfare.	None	Social welfare	Demand impacts
	[35]	Assess the performance of EV to support EV manufacturers and customers in their decision of produce or buy it, respectively.	*	None	Operational characteristics of the vehicle (as price,battery)
	[36]	Examine the impacts of governmental incentive schemes in EV adoption and in the consumer's buying behavior.	None	Social welfare	Demand impacts

Note: (1) Risks of force majeure, air pollution, insufficient funds and change of government subsidy; (2) Node information sharing, product launch cycle and battery manufacturing risk; (3) Parts quality, inventory and product supply delay risk.

Besides, four papers in Table 2 compare the performance of different types of EVs. Among them, we highlight the [35]. Based on experts' opinions (representatives of manufacturers, customers, researchers and academics), [35] raised a list of 22 criteria of performance for EVs. Besides, they performed an analysis of Pareto to identify the nine most significant criteria: price, battery capacity, torque, charging time, overall weight, seating capacity, driving range, top speed and acceleration. These criteria were used to feed the model proposed in FAHP-EVAMIX and evaluate the performance of 12 types of EVs available in the market.

4.4 Governmental subsidies

Due to the initial stage of EVs' insertion in the market, many gaps still need to be filled, such as low autonomy, high purchase price, long charging time and insufficient charging infrastructure [12 - 22]. Therefore, [22], [31] and [36] analyze the impact of a subsidy scheme on EVs' demand and production.

[22] analyzes the effectiveness of the government subsidy for manufacturers to migrate from ICEVs to EVs. The results show that an increase in government subsidies would not always increase the EVs production, since the cost of EV production is still higher than conventional vehicles. Consumer acceptance depends directly on the purchase price, available infrastructure, battery disposal and the need to change it. In contrast, when the subsidy is higher than a pre-defined limit, it becomes profitable for the manufacturer to enter the EV market, although EV production results in a decrease in the profits of ICEVs.

To address these obstacles, countries like China have implemented several subsidies policies, credit taxes and infrastructure improvements to motivate consumers and new manufacturers to adopt/invest in this technology [22]. Similarly, [16] and [22] show that, since 2010, USA has offered a tax credit of \$2,500 to \$7,500 as an incentive to purchase PHEVs and BEVs. Besides, [36] present a discount scheme adopted in Romania and Spain (MOVELE plans): the governments offer a 25% discount rate on EV's purchase price. The UK government has also implemented a similar discount scheme since January 2011.

[37] show that the USA federal, state and local governments have implemented, since 2000, a broad set of incentives to encourage consumer adoption of hybrid vehicle technologies, including credits and income tax deductions as well as exemption of state sales tax, registration fees, emissions testing, excise duties and parking [37].

It is important to highlight that although the mentioned papers showed that the government subsidies had attracted an increasing number of manufactures, there are still doubts about the impact of these subsidies in the demand. So, [22, 31, 36] performed scenarios analysis to evaluate the governmental subsidies' impact on the demand.

As seen in Table 2, papers [22], [31] and [36] deal with the same "sustainability" indicators, investigating the impacts of governmental subsidies in social welfare and in demand and production of EV. However, none of them evaluates the environmental dimension.

4.5 Sustainability analysis

Among the papers analyzed, only five papers evaluate and quantify at least one indicator of each sustainable pillars (economic, social and environmental). Concerning the environmental indicator, some papers of Table 2 are marked with "*", because they made only a theoretical investigation, highlighting the possible benefits of using EVs to the environment and people.

From the 11 papers that quantify the environmental aspect, the indicators used the most are: GHG and/or CO₂ emissions, raw material depletion, recycling of materials. From the eight papers that quantify the social aspect, the indicator evaluated the most is social welfare.

Regarding the economic indicator, the indicators used the most in the 17 papers that deal with this dimension are: Impacts on demand, costs comparing ICEVs with EVs and risks of failure in supply chains.

At the end, we emphasize that many countries have encouraged the use of EVs, setting goals for carbon reduction and the use of renewable energy sources [21], implementing incentives as subsidy and price discounts [22, 31, 36]. However, most of the papers investigated are dedicated to analyzing the environmental and economic impacts related to the EV insertion in the transport sector. Besides, even if EVs are claimed as a sustainable alternative, hardly ever the studies consider the three sustainability pillars [8].

5 Final considerations

Given the growing concerns about the environment and the scarcity of natural resources, many studies have pointed to EVs as an eco-friendly solution. These papers show that some countries in Europe have proposed government subsidies to attract more manufacturers and consumers to this market, as the MOVELE Spanish plan.

Nevertheless, this paper showed that there is a gap when investigating the role of electric vehicles in sustainable supply chain. Only 22 among almost 9,000 papers published at the WoS database about sustainable supply chain deals with some aspect of electromobility (battery, vehicles and so on). It must be emphasize that: (i) transport is one of the main logistic activities that play an essential role whole in the supply chain [25]; (ii) there is increasing pressure for sustainable process and activities since Agenda 2030 established goals and targets for achieving a sustainable living [38]; (iii) electric mobility is recognized as an important public policy aiming at reducing environmental impacts of transport sectors, as can be seen in [1, 12, 20, 27, 22].

Besides, this research also showed that although some studies claim to be about EVs in the context of sustainability, some of them do not analyze the three pillars of sustainability. Many of them are focused on the environmental aspects, studying material footprint, material depletion, life cycle and battery exchange management projects.

In addition, the literature review arises that there are still doubts about the potential effects of inserting EVs in the transport sector, as there is no past data from purely

electrified vehicle fleets, but there are strong environmental advantages compared to conventional vehicles.

As a limitation, the results found in this paper are limited by the methodological procedures adopted, specifically the keywords and the database. Besides, it is focused on the role of the electric vehicles in the supply chain, but a broader search must be interesting to evaluate the electromobility role from other standpoints.

As suggestions, future studies might try to evaluate the electric vehicles' role in the low carbon economy, approaching different kinds of vehicles and technologies, the optimal location of recharge stations, the management and planning of the transport sector and so on.

Acknowledgement

The authors thank CNPq for the scientific initiation scholarship and IFRJ for lending the software Vantage Point. CYTED Thematic Network “Ciudades Inteligentes Totalmente Integrales, Eficientes Y Sostenibles (CITIES)” no 518RT0558.

References

1. Lin, L., Fadwa, D., Jing, Z.: Cost-effective supply chain for electric vehicle battery remanufacturing. *Applied Energy* 226, 227-286 (2018).
2. Abrantes, N., Gandolpho, A.: Cadeias de suprimentos sustentáveis: como o conceito de sustentabilidade aplicado nos diversos níveis da cadeia pode gerar valor para as empresas. Congresso Nacional de excelência em gestão (2015)
3. Carvalho, A.: Gestão Sustentável de cadeia de suprimento: análise da indução e implementação de práticas socioambientais por uma empresa brasileira do setor de cosméticos. Tese em Administração de Empresas: Fundação Getúlio Vargas. (2011)
4. Jr Green, K., Zelbst, P., Meacham, J., Bhadauria, V.: Supply Chain Management: An International Journal Emerald Article: Green supply chain management practices: impact on performance. *Emerald* 17(3), 290-305 (2012)
5. Silva, M., Neutzling, D., Alves, A., Dias, P., Santos, C., Nascimento, L.: Gestão da cadeia de suprimentos sustentável: entendendo o discurso brasileiro. *EnANPAD* (2013)
6. Ballou, R. H. (2010): “Gerenciamento da cadeia de suprimentos/logística empresarial”. 5ª Edição, Porto Alegre: Bookman.
7. EPE (Empresa de Planejamento Energético): Balaço Energético Nacional. Relatório. (2020) Disponível em: < <https://www.epe.gov.br/pt/publicacoes-dados-abertos/publicacoes/balanco-energetico-nacional-2020>> . Acessado em 19/09/2020
8. Zhan, Z., Sun, X., Ding, N., Yang, J.: Life cycle environmental assessment of charging infrastructure for electric vehicles in China. *Journal of Cleaner Production* 227, 932-941 (2019)
9. Krishna, P., Krishna, K., Kuladeep, M., Kumar, G.: The Importance of Transport and Logistics Services in Green Supply Chain Management. *International Journal of Innovative Technology and Exploring Engineering* 1(6), (2012)
10. Litman, T.: Well Measured: Developing Indicators for Sustainable and Livable Transport Planning. Victoria Transport Policy Institute, 10–15 (2015).
11. Litman, T., Burwell, D.: Issues in sustainable transportation. *International Journal of Global Environmental Issues*, 6(4), 331–347 (2006).

12. Onata, N., Kucukvarb, M., Aboushaqraha, N., Jabbara, R.: How sustainable is electric mobility? A comprehensive sustainability assessment approach for the case of Qatar. *Applied Energy* 250, 461-477 (2019).
13. Egbue, O., Long, S.: Critical Issues in the Supply Chain of Lithium for Electric Vehicle Batteries. *Engineering Management Journal* 3(24), 52-62 (2012)
14. Günther, H., Kannegiesser, M., Autenrieb, N.: The role of electric vehicles for supply chain sustainability in the automotive industry. *Journal of Cleaner Production* 90, 220-233 (2015)
15. Guimarães, V., Leal, J., Silva, M.: Evaluating the sustainability of urban passenger transportation by Monte Carlo simulation. *Renewable and Sustainable Energy Reviews*, 93, 732-752 (2018)
16. Guimarães, V., Leal, J.: Performance assessment and evaluation method for passenger transportation: a step toward sustainability. *Journal of Cleaner Production*, 142, 297-307 (2017)
17. Reuter, B.: Assessment of sustainability issues for the selection of materials and technologies during product design: a case study of lithium-ion batteries for electric vehicles. *Int J Interact Des Manuf* (10), 217- 227 (2016)
18. Alonso, A., Monzón, A., Cascajo, R.: Comparative analysis of passenger transport sustainability in European cities. *Ecological Indicators*, 48, 578-592 (2014).
19. Bojkovi, N., Macura, D., Pej, S.: A Comparative Assessment of Transport- Sustainability in Central and Eastern European Countries with a Brief Reference to the Republic of Serbia. *International Journal of Sustainable Transportation*, 5(6), 319-344 (2015)
20. Wong, D., Choy, K., Lin, C., Lam, H., Lee, C.: An intelligent battery information management system to support information sharing and vehicle routing planning for battery distribution in Hong Kong. *Int. J. Innovation and Sustainable Development* 1(9), 1-27 (2015).
21. Strielkowski, W., Volkova, E., Pushkareva, L., Streimikiene, D.: Innovative Policies for Energy Efficiency and the Use of Renewables in Households. *Energy*, 1-17 (2019)
22. Zheng, X., Lin, H., Liu, Z., Li, D., Llopis-Albert, C., Zeng, S.: Manufacturing Decisions and Government Subsidies for Electric Vehicles in China: A Maximal Social Welfare Perspective. *Sustainability*, 1-38 (2018)
23. Tanga, Y., Zhanga, Q, Li, Y., Li, H., Pan, X., Mclellane, B.: The social-economic-environmental impacts of recycling retired EV batteries under reward-penalty mechanism. *Applied Energy* 251, 1-16 (2019)
24. Zeuner, B.: An Obsolescing Bargain in a Rentier State: Multinationals, Artisanal Miners, and Cobalt in the Democratic Republic of Congo. *Frontiers in Energy Research* 123(6), 1-6 (2018)
25. Guimarães, V., Ribeiro, G.: Mapping of the Brazilian scientific publication on facility location. *Pesquisa Operacional* 38, 307-330 (2018)
26. Eising, J., Onna, T., Alkemade, F.: Towards smart grids: Identifying the risks that arise from the integration of energy and transport supply chains. *Applied Energy* 123, 448-455 (2014)
27. Ascenso, L., d'Amore, F., Carvalho, A., Bezzo, F.: Assessing multiple biomass-feedstock in the optimization of power and fuel supply chains for sustainable mobility. *Chemical Engineering Research and Design* (2017).
28. Sena, B., Onat, N., Kucukvarc, M., Tataria, O.: Material Footprint of Electric Vehicles: A Multiregional Life Cycle Assessment. *Journal of Cleaner Production*, (2018)
29. Cimprich, A., Young, S., Helbig, C., Gemechu, E., Thorenz, A., Tuma, A., Sonnemann, G.: Extension of geopolitical supply risk methodology: Characterization model applied to conventional and electric vehicles. *Journal of Cleaner Production* 162, 754-763 (2017)
30. Wu, Y., Jia, W., Li, L., Song, Z., Xu, C., Liu, F.: Risk assessment of electric vehicle supply chain based on fuzzy synthetic evaluation. *Energy* 182, 397-411 (2019)
31. Fu, J., Chen, X., Hu, Q.: Subsidizing strategies in a sustainable supply chain. *Journal of the Operational Research Society* (2017)

32. Giacomarra, M., Tulone, A., Crescimanno, M., Galato, A.: Electric mobility in the Sicilian short food supply chain. *Studies in Agricultural Economics* 121, 84-93
33. Ajanovic, A., Haas, R.: Driving with the sun: Why environmentally benign electric vehicles must plug in at renewables. *Solar Energy*, 1-12 (2015)
34. Kuppusamy, S., Magazine, K., Rao, U.: Electric Vehicle Adoption Decisions in a Fleet Environment. *European Journal of Operational Research*, (2017)
35. Das, M., Pandey, A., Mahato, A., Singh, R.: Comparative performance of electric vehicles using evaluation of mixed data. *Operational Research Society of India* (2019)
36. Shao, L., Yang, J., Zhang, M.: Subsidy scheme or price discount scheme? Mass adoption of electric vehicles under different market structures. *European Journal of Operational Research*, 1-37 (2017)
37. Gallagher KS and Muehlegger E. Giving green to get green? Incentives and consumer adoption of hybrid vehicle technology. *Journal of Environmental Economics and Management* 61(1), 1–15 (2011).
38. ONU (Organização das Nações Unidas): Agenda 2030. Disponível: http://www.pnud.org.br/Docs/genda2030_completo_PtBR.pdf

A comparative and exploratory case study of the concept of SDI applied to sustainable mobility

Exploring trends and divergences of SDIs in Ibero-American cities

Carlos Grande¹[0000-0003-0406-3538]; Teresa Batista²[0000-0002-1055-6841], Carmen Vásquez³[0000-0002-0657-3470]; Leonardo Suarez-Matarrita⁴[0000-0002-6835-8362]; Luis Manuel Navas⁵[0000-0002-7895-925X]; Rodrigo Ramírez-Pisco⁶[0000-0001-8648-3805] and Rhonmer Pérez³[0000-0003-4343-0935]

¹ Universidad Centroamericana José Simeón Cañas (UCA), San Salvador, El Salvador, y Doctorando en Desarrollo Inclusivo y Sostenible Universidad Loyola Andalucía, España

² Universidade de Évora - CIMAC, Évora, Portugal

³ Universidad Nacional Experimental Politécnica Antonio José de Sucre, Barquisimeto, Venezuela

⁴ Universidad Técnica Nacional, San José, Costa Rica

⁵ Universidad de Valladolid, Valladolid, España

⁶ Universidad de Barcelona (UNIBA) y Universidad Politécnica de Cataluña (UPC), Barcelona, España

cgrande@uca.edu.sv

Abstract. The Spatial Data Infrastructures (SDI) can be defined as the set of data, technologies, policies, and institutional arrangements aimed at facilitating the availability and access to spatial information. These allow us to synthesize, calculate, and analyze spatial data through interoperable web services. It is also the most effective way to have a distributed and flexible system based on standards (OGC, W3C & ISO) and open source technology. They consist of three components: a data viewer (map viewer), a metadata catalog, a Toponym catalog. Local geographic information systems are available through Web Map Services (WMS), Catalog Service Web (CSW), and Web Feature Services (WFS). Geographical information is essential for mobility planning, management, and monitoring. Indicators such as the number of vehicles per unit area, the concentration of gaseous emissions, or the resident population are basic geographic indicators for planning sustainable mobility. However, establishing good practices in the use of these protocols has not been successful in all countries, the objective of this paper is to establish the main points of trends and divergent aspects between the implementation of SDIs both in Europe and in Latin America used for this, the cases of Alentejo-Extremadura, Colombia and Cuba, mainly in intermediate cities, from a systematic review of the literature, which will allow finding future lines of study to strengthen the experiences between both regions.

Keywords: Urban Mobility, Spatial Data Infrastructure, Latin America, Iberoamerica.

1 Spatial data infrastructure and urban mobility, backgrounds about its implementation in Ibero-America.

In the Iberian Peninsula, there are various processes for the implementation of spatial data infrastructures at national (i.e Portugal [1] and Spain [2]), regional (i.e. Extremadura [3]), and local levels (i.e. Sevilla [4]). These SDI are mainly oriented to the systematization of territorial information, to generate the necessary knowledge to develop several studies to support decision-making. These are supported by robust regulations arising from the European Union, like the INSPIRE Directive 2007/2/EC [5] and the preferential use of standards data formats to exchange information. These information systems, technologies, and policies to share data, offer an important source of experience that by contrasting them to Latin America (LA), allows establishing common ground and challenges.

In order to be accurate about geographical context, this paper proposes as an initial case study one particular case of cross border SDI between Portugal and Spain. This project called OTALEX C [6] is the Territorial and Environmental Observatory of the cross-border region composed by Alentejo and Centro regions of Portugal and the Extremadura region of Spain. It was built on the cooperation of several locals, regional, and national entities of Portugal and Spain to monitor and analyses the territorial, environmental changes and human pressures on both sides of the Spanish-Portuguese border, covering about 92.200 km² [7].

Among the several results achieved, highlights the compatibility of cartography with the creation of common cross border continuous cartography [8], indicators [9], and the creation of the first cross border in 2007, non-pilot, multilingual, SDI between contiguous Portuguese (Alentejo and Centro) and Spanish (Extremadura) regions IDE-OTALEX [10]. This was developed in open source technology, using standards and the guidelines of INSPIRE EU Directive Among the several research developed it was created an indicator system – SIOTALEX, composed by more than 60 indicators (territorial, environmental, social and economic), which permitted to understand better the dynamic of these three regions. Although it was built with a broader purpose of characterizing the different pillars of sustainability in a territory, IDE-OTALEX integrates several important information related to accessibility and mobility like road and train networks, human settlements (villages and cities), with human density, socioeconomic indicators: total population, population by ages, education level, income *per capita*, localization of services and equipment's (schools, public services, hospitals); which allow the development of accessibility studies and several others in the context of sustainable development [11] [12] [13].

This step was the first to share information for the sustainable development of this area. The results lead to the publication of several result books among them the Alentejo Extremadura ATLAS and the Alentejo Centro Extremadura ATLAS [14] [15].

In contrast in Latin America, most of the data required for urban mobility planning and management are captured and managed in several ways by central and local governments like in Europe case, but the main difference is there is not a regional entity

that provides guidelines that homogenise the generation and exchange of information through SDI, however, the most recent IDB report [16, pp. 47–48] about open data, offers a panoramic look at the situation in Latin America and the first comparison with various regions of the planet, through its proposal of four indicators for assessing the global open data situation, these are: (1) the Open Data Barometer (ODB); (2) the Global Open Data Index (GODI); (2) the Open Data Inventory (ODIN); (4) and the OECD OURdata Index [16].

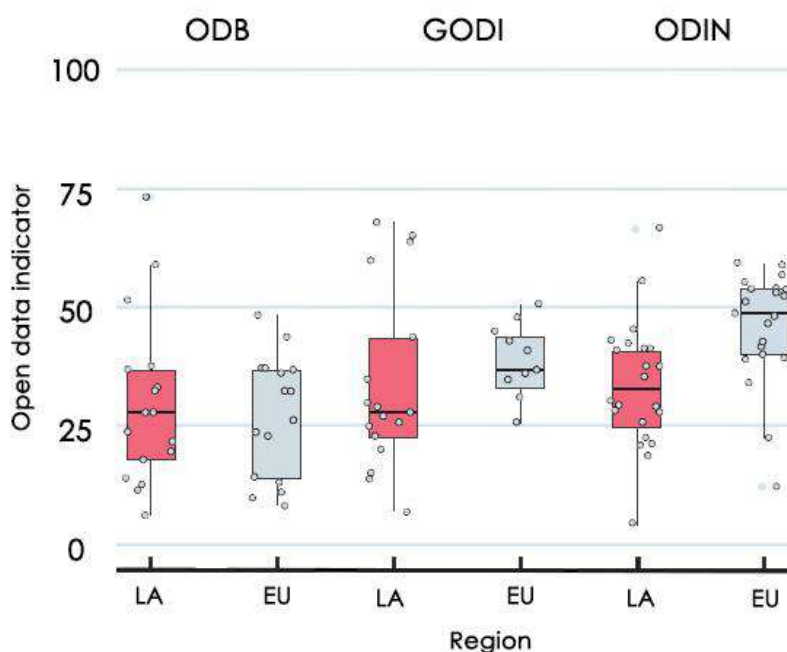


Fig. 1. Open data indicator contrast between Latina America (LA) and Europe (EU)*
Source: Edited from the original version [16, p. 49]

As can be seen in Fig. 1, all AL indicators are always below the European indicators. Moreover, Vilches and Ballari advise [17] about the heterogeneity of the situation within AL in contrast to the strongest block that is Europe¹, this result of assuming more rigorously standards such as the INSPIRE initiative, ISO 19100, and ISO 19115 of Europe in contrast to LA. However, in both studies, it stands out Mexico, Brazil, Chile, and Colombia that are well above the average of the LA region. Examples of implementation of SDI for urban mobility such as the implemented in Chile can be a highlight in the first instance, but a specific case in Concepción de Chile that, while considering aspects of data collection protocols, it uses SDI at the national level to enhance the functioning of the local SDI [18].

¹ The IDB report cited above put together European and Central Asia countries.

After this brief outline of the SDI situation among Iberian countries and LA, it would be possible to specify in more detail the comparison between the two (2) regions situation regarding the use of SDI in urban mobility? Is it possible to identify continuities, adaptations, and ruptures between these regions concerning the practice of implementing SDIs? To what extent is the implementation of SDI for urban mobility in the context of LA can be fed by the EU experience? And which of those EU experience elements can be suitable for the AL situation?

2 State of the art

Similar to other types of services, users of transport systems are eager for information, before, during, and after use, which has generated a whole information management process and has proven to be a strategic advantage in improving the efficiency of public transport systems [19]. Becoming a profitable investment, the use of quality integrated information systems has positive impacts on the demand for transport systems.

According to Vasconcellos [20], to ensure sustainable and equitable urban management and mobility in LA and the Caribbean, it is necessary to analyze the different uses of transport modes, their impacts, and the conditions of public policies and organizations, among others, depending on the country where they are implemented. Where public policies must be "clear, coherent and continuous" (p.9). This means that they must remain in time, adapting to changes and new user needs.

UNDP 2019 Human Development Report [21] states, despite achievements in the fight against poverty, hunger, and inequalities, a new gap is opening up for future generations. This is based on two (2) radical transformations, climate change, and technological transformations, which must be planned at present to break the existing trend. Technological ones include those that support urban mobility and could serve its proper management and planning. From here the importance of studies that seek, among other purposes, the transfer of results between two (2) regions with differentiated technological characteristics in urban mobility: LA vs Spain and Portugal. This comparison allows for obtaining the similarities and differences of the SDI (both technological and government action, in terms of urban mobility) and establishes best practices for their management and planning.

Technologies impact people and their displacement, but it is also these technologies that allow recording these dynamics so it is necessary to establish the policies that will allow these technologies to be approved in such a way that the information they produce is useful for their analysis. Hence, these two (2) levels of categorization of the technologies used were established to achieve the comparison of the SDI, i.e. type of technology used and data-sharing policy. This will reduce the bias of analyzing the information in the selected document set.

The second categorization corresponds to the urban mobility approaches used to implement SDI, in addition to a brief description of the types of cities and the technology used to develop establish the SDI, and the transport guiding institution is also incorporated as relevant data to identify whether it is a local or central government that takes

the initiative and in this way contrast the progress of decentralization especially in LA; and overall because are these institution that defines the policies to exchange data, finally, general characteristics of the urban transport system (presence of systems meters, BRT, railways, trams or trolleybuses) and the city (metropolitan area or type, among others).

To better understand the concepts exposed about the diversity of the SDI implemented in the study areas and their relation with urban mobility data requirements it was established the following variable to analyze: 1) the overall application of SDI concept; 2)types of data shared; 3) technology used; 4) data sharing policies; 5) type of institution that share the data; 6) urban mobility focus; 7) type of cities involved; 8) transport authority and 9) main characteristics of the city and transport systems.

These variables can be utilized to develop a systematic literature review of the implementation of SDI that supports urban mobility to become more sustainable, equitable, and inclusive, and so identify points of trends and divergent aspects in these cases of study.

3 Methodology

It is appropriate to emphasize that a comparative case study methodology is used in an exploratory manner between two (2) regions: the Iberian Peninsula and AL through a systematic literature review. It is emphasized that these regions are diverse in terms of population, type of cities, and a wide diversity of transport systems focused on sustainable mobility.

Moreover it important to define this study as a descriptive study, which is based on identifying relevant properties of groups, communities, people, and other elements such as technology, conceptual approaches, participating institutions, subject to the research approach, allowing to evaluate aspects or different dimensions of the event under study [22]. In this case, the variables have been defined in the previous section, and in the subsequent paragraphs, the methodology design will be presented.

The steps considered in this study as a research procedure, as well as the identification of data collection sources are as follows:

Exploratory study cases from two regions such as the Iberian Peninsula and AL through a Systematic Literature Review to obtain an analysis in the two main categories in question.

Regarding the concept of SDI , how data is shared, the type of technology to be used in IDEs, whether there is evidence of policies to share data, and those characteristics of institutions involved in IDE participation or as a secondary information provision, all set out in Table 1.

Table 1. Analysis categories for SDI in selected cases

Author & Year	SDI Concept	Data characteristics to share	Technology type	Policy to share data	Characteristics of participant institutions
---------------	-------------	-------------------------------	-----------------	----------------------	---

Concerning Urban Mobility. , the approach of urban mobility is detailed, the city(s) involved in the systematic study, the type of technology used to get and manage the data, Identify main characteristics of the transport governing institution in the city under study, and the general characteristics of the city and the existing transport system. This information is reflected in Table 2.

Table 2. Analysis categories for urban mobility approach in selected cases.

Author & year	Urban Mobility approach	Type of cities studied.	Technology Type	Institution responsible for transport	General features of the city and transport system
---------------	-------------------------	-------------------------	-----------------	---------------------------------------	---

To obtain the scientific papers, a guide to doing the same search on Ebsco-host was accorded between the research team. “Urban mobility”, “SDI”, “Transport”, “Spatial Data Infrastructure” were the keywords. Each member of the team selects two or three scientific papers in the first ten pages of the results, then it is proceeded to share that paper with the team to avoid duplicates and starting to fill table 1 and Table 2. It is important to mention that the papers wrote in Spanish or the English language was admitted.

After filling the Tables 1 and 2 it was proceed to union results of each member in only one matrix that is shown in table 3.

Once the literature review was organized in Table 3 a Delphi technique [23] is developed with a group of members of the research team composed of the RITMUS² network. This technic organizes each idea of the research team members and establishes a very interesting consensus dynamic about the deducted results of the contingency matrix composed by the preliminary results of Table 1 and Table 2 as mentioned initially.

The Systematization of the summaries of papers under review and de transdisciplinary discussion allowing to identify in this exploratory study the trends and contrasts of the implementation of SDI to develop an analysis of results and discussion in order to improve urban mobility.

² Red Iberoamericana de Transporte y Movilidad Urbana Sostenible (RITMUS) is a research network funded by Ibeoramerican Program of technology and research. (CYTED)

Table 3. Data analysis contingency matrix

Author & year	SDI concept	Data characteristics to share	Type of Technology	Policy to share data	Characteristics of participants institutions	Urban mobility scope	Type of cities studied	Institution responsible for transport	General features of the city and transport system
Díaz-Muñoz, Cantergiani, Salado-García, Rojas-Quezada, Gutiérrez-Martínez, 2007 [24]	Do not mention the concept of SDI but of GIS to provide precision in geospatial information.	Provide mobility information based on indicators and correlation matrix.	GIS, Mobility Indicators.	No data sharing policy	Institute of Statistics of the Community of Madrid for access to digital cartography and demographic data; Regional Transport Consortium which offers Intra and inter Cuban transport zona maps.	Mobility patterns, public transport system, urban model.	Intermediate city, Alcalá de Henares (Spain)	Madrid Regional Transport Consortium.	The city with building typology of blocks, residential in open order, neighborhoods. The transport signals the railway and urban public.
J. Castillo and D. Grajales, 2012[25]	Public information access tool to improve citizen participation.	Multiple sources, government offices, transport operations, and users.	Integration between IDE's, GIS, and mobile devices.	Management of IDE's that integrate information from multiple databases and users with relevant information for daily mobility	Cadaster, Ministry of Mobility.	Intermodal urban mobility and public participation.	Metropolis, Bogotá (Colombia)	Ministry of Mobility of the central district.	A diverse metropolis with sophisticated urban planning, BRT mass transport is articulated with non-motorized mobility and plans for other modalities.

Author & year	SDI concept	Data characteristics to share	Type of Technology	Policy to share data	Characteristics of participants institutions	Urban mobility scope	Type of cities studied	Institution responsible for transport	General features of the city and transport system
Sánchez-Ansola, Sánchez-Jimenez & Armas-García, 2013[26]	Tools that support society information, decisions, and problem-solving from spatial data.	Free database services like Open Street Map.	GIS and spatial database managers: Oracle, PostgreSQL, SQLite, ArcGIS.	There are no sharing policies and it is exposed that the data structure makes interoperability difficult even with software such as QGIS or ArcGIS.	The private company provides data collection and analysis services.	Focused on road infrastructure and private vehicles.	Intermediate city, La Habana (Cuba)	There is no reference to the governing institution of transport.	A city with road infrastructure and transport systems is limited mainly to conventional bus transport.
Aubrecht, C., Özceylan Aubrecht, D., Ungar, J., Freire, S., & Steinnocher, K., 2017 [27]	The IDE concept is not used, the analysis is based on retrieving data from social networks to determine patterns of individual activity.	Data voluntarily shared by social network users.	Volunteered Geo-Dynamic Information (VGDI) was applied to explain the variations in space-time human activity.	There is no data sharing policy, only application requirements and restrictions to extract data.	Social networks developing companies.	Determination of activity patterns on land uses.	Metropoli, Lisbon (Portugal)	There is no reference to the institution responsible for transport	A robust transport system including metro, streetcars, and bus
Calvo-Poyo, Moya-Gómez, García-Palomes,	The concept of GIS is used instead of SDI. It integrates data collection, calculation of	Maps to visualize changes in accessibility and indicators to	GIS, Accessibility Indicators.	There are no policies for sharing data.	Ministry of Development and Housing of the Andalucía Board for the planning and evaluation of the	Transport infrastructures in peripheral regions to	Andalucía City (Spain-territorial study)	There is no reference to the institution responsible	Andalucía is a peripheral region of Spain with an extra-urban bus system.

Author & year	SDI concept	Data characteristics to share	Type of Technology	Policy to share data	Characteristics of participants institutions	Urban mobility scope	Type of cities studied	Institution responsible for transport	General features of the city and transport system
Gutiérrez-Puebla, 2018[28]	indicators, and cartographic representation. The IDE allows a more detailed analysis of land use planning, mobility, land use, and operations.	improve efficiency and equity. Data managed by the municipal administration.	ArcMap, Microsoft Excel, TransCad	They do not indicate policies for sharing data.	territorial impacts on road transport. Quibdó Mayor's Office, in charge of public administration and establishment of plans in the city.	improve accessibility. A direct relationship between the uses and articulation of soils and the location of current and future equipment in a transportation system.	Quibdó (Colombia)	for transport There is no reference to the institution responsible for transport	Functional city, central city, and dependence on its environment. The mode of transport most used by the population is the motorcycle.
Montoya, Escobar & Moncada, 2019[29]									

3.1 Trends

The levels of territory, institutions, and scale of cities. As can be seen in Table 3, LA like EU regions has been developed SDI in a different level of territorial scale and different levels of the institution (i.e. local and central governments) this is an interesting trend among those region, but those scale in the LA case do not have the integration between different levels and territories like EU. In this case, a bottom-up process to get aligned with those SDI is probably the most appropriate way to follow. Chiefly when to assess and forecast analysis of urban mobility is need to be compared with different cities and region.

Citizen participation to generate and share data. According to Ronzhin et al. [30], the need for geospatial data integration across national borders [and into the cities too] raises questions about how to overcome technical and organizational barriers between national mapping agencies. This is because the first efforts used heterogeneous technologies and developed a certain culture among users, which has changed over time. That is why the technical capabilities of the user community along with the way data is provided from a technical perspective is crucial for the potential (re) usability of data at any level. In LA this is a huge challenge because there is a digital gap as have been mentioned above. In contrast, the EU has an important issue about the normative that control that process.

The extended use of Geographical Information Systems open source version. Not only how people share their information is been influenced by open data, but the way that data is also managed too. There is an economic and financial reason to take that way, but it is a way to link with similar initiatives that are looking to improve urban mobility especially in developing countries.

Improve accessibility instead of managing the congestion. As can be seen in the literature review the paradigm of manage the congestion does not appear, instead of improving the accessibility is the main objective in different researches and projects, this is a continuity in both regions, it is possible because the accessibility measure is a complex activity that requires an exhaustive and high data quality in order to conduct the best way to measure this important indicator of sustainable urban mobility (i.e. infrastructure-oriented, person-oriented, utility-oriented and so on [31])

Measure the level of sustainability of urban transport systems. Different initiatives try to build indicators to measure the sustainability of the public transport system, which is another trend that identifies the change of paradigm which puts at the top the public transit instead of private vehicle use.

The absence of a smart mobility concept. Here there is an interesting finding that is necessary to confirm with other deepest research process, but it seems that the smart mobility concept is not the engine that moves the digitalization process of urban mobility, rather there is a basic necessity to assess the progress of implementation of projects and policies, more than become in technologies services by itself. Probably the huge diversity of concepts about Smart Mobility, i.e. Albino cited by Uteng et al. [32, p. 65] identify 26 definition concepts about Smart Mobility, and a compromising with a privative software can be several of answers in this interesting trend.

3.2 Divergences

The region guideline. Although it is obvious the sturdiness of European Union specify the INSPIRE initiative give to the European countries there are not reference in the case of LA, but this divergence can be straightness because the different initiatives of SDIs implementation have been built considering the specifics necessities of each LA countries, here there is an interesting line of research in order to give a key step to start a bottom-up process that gives to LA a policy and technical aspects that guide to develop a Latin America Structure of Spatial Data.

The cross-border initiative. There is not registered initiative in LA like different projects of cross-border SDI like *Alentejo -Extremadura* for instance. Nonetheless, the cross-border initiative SDI projects in LA should be seen as an opportunity to build an SDI project implementation that outlined step by step a more widely SDI implementation project at a regional level.

4 Final remarks

Although the EU is well supported in data sharing legislation and standards implementation there is still a need to promote cooperation between institutions at the different levels of administration. Sustainable mobility needs this cooperation, among not only public administration but also with private transport enterprises and operators. This is a trend also with AL, where this gap of cooperation between organizations can be highlighted.

Another final remark to add is that in LA and, in general in developing countries the coverage of internet services, access to a smartphone and, the reduced digital literacy [32] is a reality, the role of governments to encourage the SDI's establishment is fundamental but to obtain better results is necessary to promote interaction between SDI and people that could be beneficiaries, for instance, information and communication technologies can readily permit the capture and harnessing of physical access data for transport and travel systems which would better service to the people with limited physical mobility[33] but this only is possible if the gap former mentioned it is reduced.

5 Acknowledgment

The authors of this article are grateful for the effort and support of the Ibero-American Network for Sustainable Urban Transportation and Mobility (RITMUS / CYTED for its acronym in Spanish) for facilitating the establishment of this work network, which allowed the development of the research that led to this paper. The authors of this paper.

References

- [1] D.-G. do Território, “SNIG | SNIG,” 2019. <https://snig.dgterritorio.gov.pt/> (accessed Sep. 17, 2020).
- [2] C. S. Geográfico, “Geoportal IDEE,” 2020. <https://www.idee.es/> (accessed Sep. 17, 2020).
- [3] D. R. P. y T. D. G. de U. y O. del T. Concejería de Agricultura, “Geoportal IDEEX -,” 2020. <http://ideextremadura.com/Geoportal/> (accessed Sep. 17, 2020).
- [4] G. de U. / A. de Sevilla, “ide.SEVILLA,” 2020. <https://sig.urbanismosevilla.org/InicioIDE.aspx> (accessed Sep. 17, 2020).
- [5] European Union, “Directive 2007/2/EC of the European Parliament and of the council of 14 March 2007 establishing an Infrastructure for Spatial Information in the European Community (INSPIRE),” *Off. J. Eur. Union*, vol. 50, no. January 2006, pp. 1–14, 2007, Accessed: Sep. 17, 2020. [Online]. Available: <http://eur-lex.europa.eu/LexUriServ/LexUriServ.do?uri=OJ:L:2007:108:0001:0014:EN:PDF>.
- [6] E. centro Observatorio Territorial Alentejo, “OTALEX C,” 2009. <http://www.ideotalex.eu/OtalexC/> (accessed Sep. 17, 2020).
- [7] T. Batista and C. Caballero, “OTALEXC-15 anos de cooperação transfronteiriça em Território e SIG,” 2013. Accessed: Sep. 09, 2020. [Online]. Available: www.ideotalex.eu.
- [8] T. Batista and F. C. Rodriguez, “GeoALEX–cartografia comum Alentejo-Extremadura,” Évora, 2006.
- [9] C. Carriço, T. Batista, M. Duran, H. Lopes, and A. Garrido, “O sistema de Indicadores do Projecto OTALEX II,” 2011, Accessed: Sep. 09, 2020. [Online]. Available: <https://dspace.uevora.pt/rdpc/handle/10174/4979>.
- [10] T. Batista *et al.*, “IDE-OTALEX C. The First Crossborder SDI between Portugal and Spain: Background and Development Grande Rota do Montado View project IDE-OTALEX C. The First Crossborder SDI between Portugal and Spain: Background and Development,” *J. Earth Sci. Eng.*, vol. 3, pp. 393–400, 2013, doi: 10.17265/2159-581X/2013.06.006.
- [11] T. Batista *et al.*, “Benefits of a Spatial Data Infrastructure on the Sustainability of a Southwestern European Territory,” in *Cross-Border Cooperation (CBC) Strategies for Sustainable Development*, Rui Alexandre Castanho, Ed. IGI Global, 2020, pp. 1–29.
- [12] R. Castanho, B. Ramirez, ... J. C.-... and C. for, and U. 2017, “Sustainability Indicators in the Southwest of Iberian Peninsula. Highlighting the Euro-region EUROACE: The OTALEX-C Project.,” in *repositorio.ipcb.pt*, 2017, p. 32, Accessed: Sep. 09, 2020. [Online]. Available: <http://repositorio.ipcb.pt/handle/10400.11/5639>.
- [13] T. Batista, “Can a SDI act as a Sustainability Observatory in a Certain Territory?,” 2015.
- [14] F. Ceballos, M. Puerto, T. Batista, and C. Carriço, “OTALEX C: Resultados del Proyecto,” 2013. Accessed: Sep. 09, 2020. [Online]. Available: <https://dspace.uevora.pt/rdpc/handle/10174/10045>.
- [15] T. B. e C. C. Ceballos, F., M. Puerto, “Atlas OTALEX C,” 2013. Accessed: Sep. 09, 2020. [Online]. Available: <https://dspace.uevora.pt/rdpc/handle/10174/10350>.
- [16] A. Munte-Kunigami and F. Serale, *Los datos abiertos en América Latina y el Caribe*. New York, 2018.

- [17] L. M. Vilches-Blázquez and D. Ballari, “Unveiling the diversity of spatial data infrastructures in Latin America: evidence from an exploratory inquiry,” *Cartogr. Geogr. Inf. Sci.*, vol. 00, no. 00, pp. 1–16, 2020, doi: 10.1080/15230406.2020.1772113.
- [18] M. Martínez, C. Rojas, J. Gutiérrez, and C. Borjas, “Diseño de una plataforma sig-web para la gestión integral del sistema de transporte-gesitran biobío,” in *Análisis Territoriales mediante tecnologías de la información geográfica*, 2018, pp. 375–397.
- [19] J. Sánchez Hernández, “Ante las necesidades de información de los usuarios del transporte público urbano en Murcia, se propone la creación de un canal de comunicación,” *Cuad. gestión Inf.*, vol. 6, no. 1, pp. 1–12, 2016.
- [20] E. A. Vasconcellos, “Contribuciones a un gran impulso ambiental para América Latina y el Caribe, movilidad urbana sostenible,” Santiago de Chile, 2019. doi: LC/TS.2019/2.
- [21] P. Conceição, “Informe Sobre Desarrollo Humano 2019,” New York, 2019. [Online]. Available: http://hdr.undp.org/sites/default/files/hdr_2019_overview_-_spanish.pdf.
- [22] J. Hurtado, *Metodología de la investigación holística. 3ra*, Fundación. Caracas, Venezuela, 2000.
- [23] A. Peñalva, E. de los Rios, S. Aguilera, and L. Eraso, “Manual de Participación en Políticas de Movilidad y Desarrollo Urbano,” ITPD, Ciudad de México, 2014. [Online]. Available: <https://3gozaa3xxbpb499ejp30lxc8-wpengine.netdna-ssl.com/wp-content/uploads/2014/07/manual-de-participacion.pdf>.
- [24] M. A. Díaz, C. C. Cantergiani, M. J. Salado, C. Rojas, and S. Gutiérrez, “Propuesta de un sistema de indicadores de sostenibilidad para la movilidad y el transporte urbanos. Aplicación mediante SIG a la ciudad de Alcalá de Henares.” Accessed: Sep. 19, 2020. [Online]. Available: <https://dialnet.unirioja.es/descarga/articulo/2596372.pdf>.
- [25] J. Castillo and D. Grajales, “Propuesta para el sistema de información al usuario de transporte público de Bogotá combinando preferencias y datos espaciales básicos,” *repository.udistrital.edu.co*, Accessed: Sep. 19, 2020. [Online]. Available: <http://repository.udistrital.edu.co/handle/11349/21220>.
- [26] E. Sánchez-Ansola *et al.*, “UNA MIRADA AL ANÁLISIS DE REDES DE TRANSPORTE EN CUBA DESDE EL PUNTO DE VISTA DE LOS DATOS A GLANCE AT THE TRANSPORTATION NETWORK ANALYSIS IN CUBA FROM THE DATA POINT OF VIEW,” *funlam.edu.co*, Accessed: Sep. 19, 2020. [Online]. Available: <https://www.funlam.edu.co/revistas/index.php/lampsakos/article/view/918>.
- [27] C. Aubrecht, D. Özceylan Aubrecht, J. Ungar, S. Freire, and K. Steinnocher, “VGDI – Advancing the Concept: Volunteered Geo-Dynamic Information and its Benefits for Population Dynamics Modeling,” *Trans. GIS*, vol. 21, no. 2, pp. 253–276, 2017, doi: 10.1111/tgis.12203.
- [28] F. J. Calvo-Poyo, B. Moya-Gómez, J. C. G. Palomares, and J. G. Puebla, “Effects on the accessibility of the highways network planned in the infrastructure plan for the sustainability of transport in andalusia (Spain),” *Cuad. Geogr.*, vol. 58, no. 1, pp. 229–252, 2019, doi: 10.30827/cuadgeo.v58i1.6732.
- [29] D. Escobar, J. Montoya, C. M.-I. tecnológica, and undefined 2019, “Estudio de la Localización Espacial de Universidades mediante un Análisis de Accesibilidad Geográfica. El Caso de Manizales y Villamaría, en Colombia,” *scielo.conicyt.cl*, Accessed: Sep. 19, 2020. [Online]. Available: <https://scielo.conicyt.cl/scielo.php?pid=S0718->

- 07642019000600325&script=sci_arttext.
- [30] S. Ronzhin *et al.*, “Next Generation of Spatial Data Infrastructure: Lessons from Linked Data implementations across Europe,” *Int. J. Spat. Data Infrastructures Res.*, vol. 14, pp. 83–107, 2019, doi: 10.2902/1725-0463.2019.14.art4.
 - [31] K. T. Geurs and B. Van Wee, “Accessibility evaluation of land-use and transport strategies: review and research directions,” *J. Transp. Geogr.*, vol. 12, no. 2, pp. 127–140, 2004, [Online]. Available: [http://files/360/Geurs y Van Wee - 2004 - Accessibility evaluation of land-use and transport.pdf](http://files/360/Geurs%20y%20Van%20Wee%20-%202004%20-%20Accessibility%20evaluation%20of%20land-use%20and%20transport.pdf).
 - [32] T. P. Uteng, Y. J. Singh, and O. H. Hagen, “Social sustainability and transport: Making ‘smart mobility’ socially sustainable,” in *Urban Social Sustainability: Theory, Policy and Practice*, 1st ed., R. Shirazi and R. Keivani, Eds. Springer, 2019, pp. 59–77.
 - [33] J. Turner, “Urban Mass Transit and Social Sustainability in Jakarta , Indonesia,” *Case study Prep. Glob. Rep. Hum. Settlements 2013*, p. 15, 2013, [Online]. Available: <http://www.unhabitat.org/grhs/2013>.

Computational intelligence for analysis of traffic data

Hernán Winter¹[0000–0002–4075–3694], Juan Serra¹[0000–0002–4286–9316],
Sergio Nesmachnow¹[0000–0002–8146–4012],
Andrei Tchernykh^{2,3}[0000–0001–5029–5212], and Vladimir Shepelev³

¹ Universidad de la República, Montevideo, Uruguay
{hernan.winter, juan.serra, sergion}@fing.edu.uy

² CICESE, México
chernykh@cicese.mx

³ South Ural State University
shepelevvd@susu.ru

Abstract. This article presents a system developed for the collection and analysis of traffic data obtained from traffic camera videos using computational intelligence. The proposed system is developed using the modern object detection library Detectron2. A pipeline-type architecture is used for frame processing, where each step is an independent, configurable functional module, loosely coupled to the others. The validation of the proposed system is performed on real scenarios in Montevideo, Uruguay, under different conditions (daylight, nightlight, and different video qualities). Results demonstrate the effectiveness of the system in the considered scenarios.

Keywords: computational intelligence; neural networks; traffic data; smart cities

1 Introduction

The growth of cities and traffic density have led to an increased demand for surveillance systems capable of automating traffic monitoring and analysis. The main goal of these automatic systems is to aid or even remove the human labor for vision based tasks that can be performed by a computer, providing regulators and authorities the ability to respond quickly to diverse traffic issues and situations.

Tasks such as vehicle counting and infraction detection are of great importance for Intelligent Transportation Systems [23]. Recently, computer vision based detection and counting algorithms [22] have shown to be more effective and outperform traditional traffic surveillance methods, such as methods using different kinds of sensors [12]. However, there are still many challenges and open issues in computer vision based vehicle detection and counting processes, caused by illumination variation, shadows, occlusion, and other phenomena.

In this line of work, this article presents a system applying computational intelligence (based on Artificial Neural Networks, ANN) to solve traffic analysis

2 H. Winter, J. Serra, S. Nasmachnow, A. Tchernykh, V. Shepelev

problems using video recordings provided by surveillance cameras. The problems solved include vehicle detection, counting, classification, tracking, and detection of different types of traffic offenses, such as red light intersection crossing and parking vehicles in not allowed zones. The validation of the proposed system is developed using real traffic videos from the city of Montevideo, Uruguay.

The main contributions of the research reported in this article include: i) a methodology for the design of traffic analysis software systems using videos; ii) specific implementations of vehicle detection, counting, classification and tracking methods, and iii) the validation of the proposed methods on real scenarios.

The article is structured as follows. Section 2 presents a background on computational intelligence for image analysis. A review of the main related work is presented in Section 3. The technical aspects of the solution, including the proposed architecture, modules, and supporting libraries are described in Section 4. The experimental validation is reported and results are discussed in Section 5. Finally, Section 6 presents the conclusions and the main lines of future work.

2 Computational intelligence for image analysis

This section describes the main concepts about the analysis of traffic data using computational intelligence.

2.1 Detection

One of the fundamental problems in computer vision is the task of assigning a label from a fixed set of categories to an input image. This task is known as image classification and is divided into three subtasks: segmentation, location, and detection.

The goal of semantic segmentation is to obtain a category for each pixel given an input image. It does not differentiate instances of the same object because each pixel in the image is classified independently. The classification and location task consists of classifying an image with a label that describes an object and drawing the box within the image around the object. The output in this task are a label that identifies an object and a box that indicates where that object is located. Object detection takes as input a set of categories of interest and an image. The goal of this task is to draw a box around each one of these categories, each time they appear in the image, and also predict the category. This problem is different from classification and localization since there can be a variable number of outputs for each input image.

Another task to consider is instance segmentation. Given an input image, this task seeks to predict the locations and identities of the objects in that image. Additionally, instead of simply predicting a region for each of those objects, this task seeks to predict a segmentation mask for each of those objects and to predict which pixels in the image correspond to each object instance.

In the last few years, computational intelligence and deep learning have led to successful results on a variety of problems, including image classification.

Among different types of deep ANNs, Convolutional neural networks (CNN) have been extensively studied [8]. CNNs assume that the input to be classified is an image. This assumption allows the network to be more efficient and to design architectures that greatly reduce the number of network parameters.

Solving the object detection problem involves determining all the regions where objects to be classified can be located. Given an input image, a Region Proposal Network (RPN) uses signal processing techniques to create a list of proposed regions in which an object can exist. This architecture class is named R-CNN. Given an input image, an RPN is executed to obtain the proposals, also called Regions of Interest (RoI). The main drawback of this approach is its very high computational demands. In practice, the network training is slow and needs significant memory. Fast R-CNN was proposed to mitigate these problems, working in a similar way to R-CNN. In terms of speed, Fast R-CNN has proven to be nine times faster than CNN in training time [7]. However, the computation time is dominated by the calculation of the RoI, which turns out to be a bottleneck. This last problem is solved in Faster R-CNN [17].

Finally, one of the most recent methods to solve the instance segmentation task is the Mask R-CNN architecture. Similarly to Faster R-CNN, this method follows a multi-stage processing approach. It receives the complete image, which is executed through a convolutional network and a learned RPN. Once the RoIs are learned, they are projected onto the convolutional vector. Then, instead of simply performing the classification and the regression of the regions of each RoI, the method additionally predicts a segmentation mask for each region, solving a semantic segmentation problem within each of the regions proposed by the RPN. The RoI is finally wrapped to the proper shape.

2.2 Tracking

Object tracking consists in the process of accurately estimating the state of an object -position,identity,configuration- over time from observations [14], thus generating a trajectory given by the position of the object in each frame. When several objects are located at the same time, the problem is called Multiple Object Tracking. In this scenario, the difficulty of the task increases considerably due to the occlusion generated by the interaction of the objects, which in turn may have similar appearances. On the other hand, conditions such as the speed at which the objects move, the lighting or that these change their appearance depending on the position, require that the tracking system must be robust, maintaining the object identifier in such situations.

In classical tracking methods, object features are extracted in each frame and used to search for the same object in subsequent frames [25]. This causes errors to accumulate in the process and if occlusion or frame skipping occurs, tracking fails because of the rapid change of appearance features in local windows. Thus, modern tracking methods apply two steps: object detection and data association. First, objects are detected in each frame of the sequence and then, detected objects are matched across frames. This paradigm is called tracking by detection [10] and it relies on the performance of the detection algorithm. Detected

4 H. Winter, J. Serra, S. Nesmachnow, A. Tchernykh, V. Shepelev

objects are matched across frames using different approaches, including optical flow with mean shift of color signature, Earth mover's distance to compare color distributions, fragment-based features, and computational intelligence.

Another simple but effective method based on the tracking by detection approach is Intersection Over Union (IOU) [2]. This method requires a detection algorithm with a high rate of true positive results, as a detection is expected in each frame for each object to be tracked. It is also assumed that the detection of the same object in two consecutive frames present a great overlap of the intersection over the union (defined in Eq. 1), which is common for videos that present a high refresh rate.

$$IOU(a, b) = \frac{Area(a) \cap Area(b)}{Area(a) \cup Area(b)} \quad (1)$$

The advantage of the IoU method, in addition to its simplicity, is that it has lower computational cost than other methods. IoU can be integrated on other methods to achieve a more robust and accurate monitoring

3 Related work

Several articles have proposed automated systems for the analysis of traffic data applying image processing and computational intelligence techniques. The most related to the research reported in this article are reviewed next.

Zhou et al. [28] studied the vehicle detection and classification problem applying deep neural networks. The You Only Look Once (YOLO) architecture was used for vehicles detection and post-processing was performed to eliminate invalid results. The Alexnet architecture was applied for classification, feature extraction, and fine-tuning. The YOLO network obtained similar precision than a Deformable Parts Model, while the Alexnet network using Support Vector Machines (SVM) outperformed other methods such as Principal Component Analysis and Absolute Difference in a public dataset.

Uy et al. [20] studied methods for identifying traffic offenses using genetic algorithms (GA) and the recognition of offenders through ANN. GA were applied to detect vehicles obstructing pedestrian crossings and to identify the location of license plates in images, while a ANN is used to recognize the license plate number. The license plates recognition accuracy was high (91.6% on 47 test images), but some license plates were not properly located due to the vehicle position respect to the camera. Zhang et al. [26] applied a Fully CNN with Long Short Term Memory for the the vehicles counting problem. Compared to the state of the art, the proposed ANN architecture reduced the mean absolute error (MAE) from 2.74 to 1.53 on the WebCamT annotated dataset and from 5.31 to 4.21 on the TRANCOS dataset. In addition, the training time was accelerated by up to 5 times. However, the proposed ANN was not capable of handling long periods of information due to the large amount of memory required.

Dey et al. [5] applied CNN in a System-On-a-Programmable-Chip to analyze and categorize traffic, including the quality-of-experience variable to improve

predictions. A combination of transfer learning with re-training CNN models, allowed improving the prediction accuracy. Arinaldi et al. [1] applied computer vision techniques to automatically collect traffic statistics using Mixture of Gaussian (MoG) and Faster Recurrent CNN. Training and validation were developed on Indonesian road videos and a public dataset from MIT. Faster Recurrent CNN was best suited for detecting and classifying moving vehicles in a dynamic traffic scene, since MoG was weak for separating overlapping vehicles.

Chauhan et al. [3] studied CNN for real-time traffic analysis on Delhi, India. A YOLO network was used, pre-trained on the MS-COCO dataset and fitted with annotated datasets. The best trained model achieved a performance of 65–75% mean average precision, depending on the camera position and the vehicle class. This article provides the expected performance of YOLO models optimized using annotated data. The recent article by Zheng et al. [27] proposed TASP-CNN for predicting the severity of traffic accidents, considering relationships between accident features. The proposed method was successfully adapted to the representation of traffic accident severity features and deeper correlations of accident data. The performance of TASP-CNN was better than previous models when evaluated using data from an eight years period.

Our research group has developed research on detection on pedestrian movement patterns applying computational intelligence [4]. A flexible system was developed to process multiple image and video sources in real time applying a pipes and filters architecture to address different subproblems. The proposed system has two main stages: extracting relevant features of the input images, by applying image processing and object tracking, and patterns detection. The experimental analysis of the system was performed over more than 1450 problem instances, using PETS09-S2L1 videos and the results were compared with part of the MOTChallenge benchmark results. Results indicate that the proposed system is competitive, yet simpler, than other similar software methods.

4 The proposed system for traffic data analysis

This section presents the implemented system for traffic data analysis, describing the function of each module and the input and output parameters.

4.1 Overall description

The proposed approach is based on a modular architecture that implements an image processing pipeline [6]. The pipeline executes a set of tasks over input images (e.g., translation/rotation, resizing, etc.) to extract useful features. The modular architecture allowed for a progressive development process, starting from a few general modules and incorporating specific modules for relevant data.

Fig. 1 shows the final architecture of the pipeline for traffic video analysis, consisting of twelve modules. The pipeline has 40 parameters that allow controlling different aspects of the processing in each module.

6 H. Winter, J. Serra, S. Neschachnow, A. Tchernykh, V. Shepelev

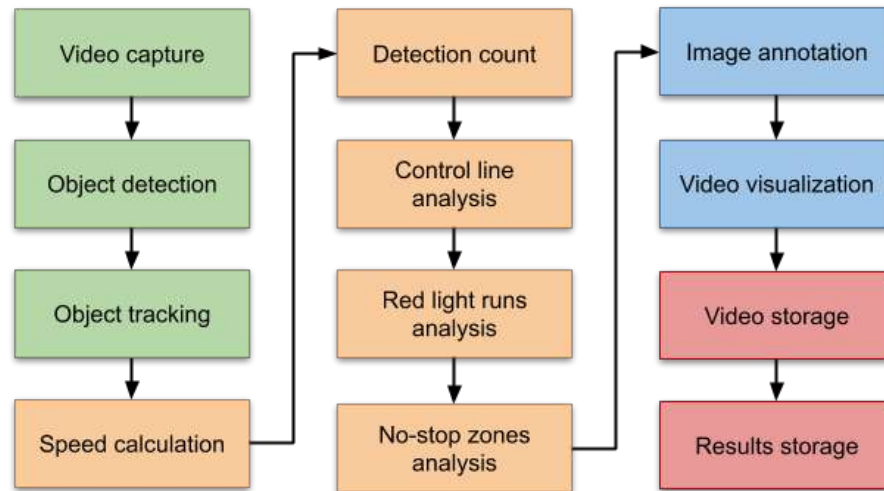


Fig. 1: The proposed pipeline for traffic video análisis

Four main stages are identified: i) video capture, object detection and tracking (in green in Fig. 1), detection data analysis (in orange), results visualization (in blue), results storage (in red). They are described in the following subsections.

4.2 Video capture and object detection

The goal of video capture is producing the frames used in the pipeline. A video stream (e.g., a local file or a webcam) is captured by a fast method using multi-threading parallel computing to read the video frames, using OpenCV utilities. Video capture initialize the cumulative data transfer object (DTO), used by all modules to read and write data, and stores several fields in the DTO, including *frame number*, *image* object, and *annotations*.

Then, the object detection process each frame to produce a bounding box, mask, score and class of the detected objects. This module is based on Detectron2 framework by Facebook [21], whose modular design allows using different state-of-the-art detection algorithms, such as Faster R-CNN, Mask R-CNN, or RetinaNet. The implemented module uses both synchronous and asynchronous detection, and adds different functionalities on top of the detection framework such as the possibility of defining regions of interest for the detection or filtering the classes of the detected objects. The output of the detection module is converted to the standard format used by the rest of the pipeline, so it might be replaced by other detection module without affecting the other modules in the pipeline. The output can contain bounding boxes or instance segmentation. The rest of the pipeline is compatible with both type of outputs and can take advantage of instance segmentation when available to compute more precise results when analyzing patterns.

4.3 Detection data analysis

Detection analysis includes five modules to extract information from data generated by previous modules in the pipeline.

The *speed calculation* module computes an estimation of the average speed of each detected object in recent frames, in pixels per frame (PPF) or pixels per second (PPS). The system stores the position of the center of each detected object in the last n frames (n is a parameter) and so the speed is given by the Euclidean norm of the first and last stored positions.

Detection count requires defining one or more counting lines on the video image. Based on a structure that keeps each detected vehicle as an object with several identifying properties, the counting module analyzes the vehicles that overlap with the counting lines. This analysis considers the intersection of the polygon of the mask or box with respect to the defined lines as an input parameter. If an overlapping is found, the vehicle information is updated with the lines it overlapped and the frame number in which it did so.

With *control lines analysis* it is possible to define a relationship between two lines, meaning that a vehicle should not cross both as doing so would be considered an infraction. This allows detecting different types of infractions that involves a vehicle circulating in a no-driving zone, e.g., a wrong turn or lane change near a corner. This module uses detected bounding boxes or masks to recognize if a vehicle overlaps with both lines in the relationship through the video.

The *red light runs analysis* module detects driving offenses of failing to comply with red light signal. The region where each semaphore is located is defined as an input parameter and each traffic light is associated with a line. The defined traffic lights are analyzed to determine their color frame by frame, applying an algorithm that transforms the cropped frame of the traffic light to Hue, Saturation, Value (HSV) color model.

The *no-stop zones analysis* considers zones, represented by polygons, in which vehicles should not stop (or park). The module analyzes the bounding box or mask of those vehicles that intersects with the defined non-stop zone. If an intersection greater than a certain value is detected, then the average speed of the vehicle in the last n frames (n is a parameter) is considered. When the average speed reaches a value lower than one, the vehicle is considered in infraction and labeled as stopped.

4.4 Annotation and results visualization

The *annotation* module is responsible of modifying frames to show information generated by the previous modules. The modified frames will be part of the output video. Additionally, this module is in charge of drawing the detected objects, boxes, or masks as appropriate. Fig. 2 presents an example of an annotated frame in one of the scenarios studied in this article.

The *video visualization* module is in charge of displaying the output frames as they are produced, using OpenCV to create a window and display the frames.

8 H. Winter, J. Serra, S. Nesmachnow, A. Tchernykh, V. Shepelev

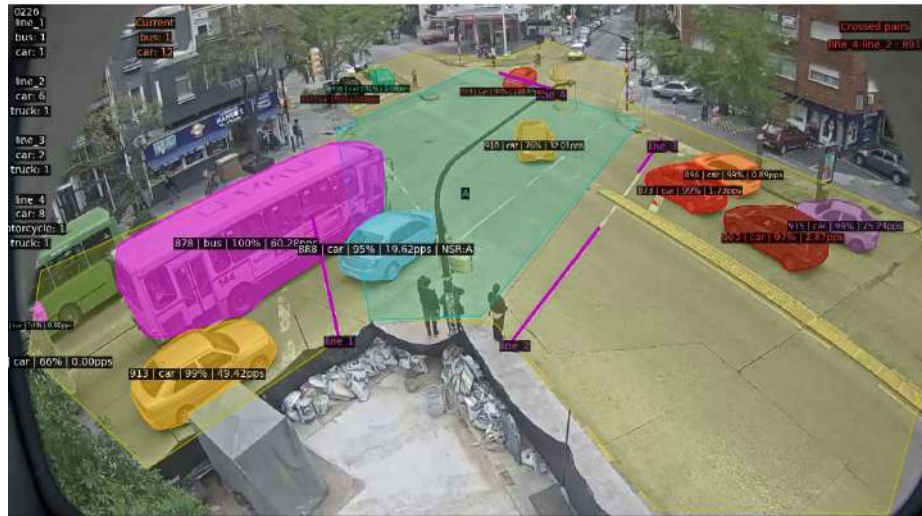


Fig. 2: Frame annotated with object masks, labels, text, lines, and polygons

4.5 Storage

The *video storage* module saves the frames in a file in a given path, considering the output format and FPS rate specified as parameters. Finally, the *results storage* module shows the information generated in each frame and the cumulative one, using a JSON-based logging system.

5 Validation experiments

This section reports the validation experiments of the proposed system.

5.1 Case studies in Montevideo, Uruguay

The experimental evaluation considered two case studies in Montevideo, Uruguay. The first case study corresponds to the intersection of 8 de Octubre and Garibaldi avenues, representing a classic intersection between two avenues in Montevideo. The second case study corresponds to the intersection between Rambla Wilson and Sarmiento Avenue. This case is relevant because it involves the avenue considered as the main traffic lane during rush hour.

The test dataset used consists of four videos taken by video surveillance cameras from the two studied locations. The cameras model is AXIS P1365 Mk II and record up to 60 frames per second. Recordings were taken at two different times of the day, in the morning (8:00 AM) and in the evening (7:00 PM) to analyze the efficacy of the proposed system under different lighting conditions. Fig. 3 presents sample images of the considered scenarios. In turn, Table 1 summarizes the main properties of the analyzed videos.

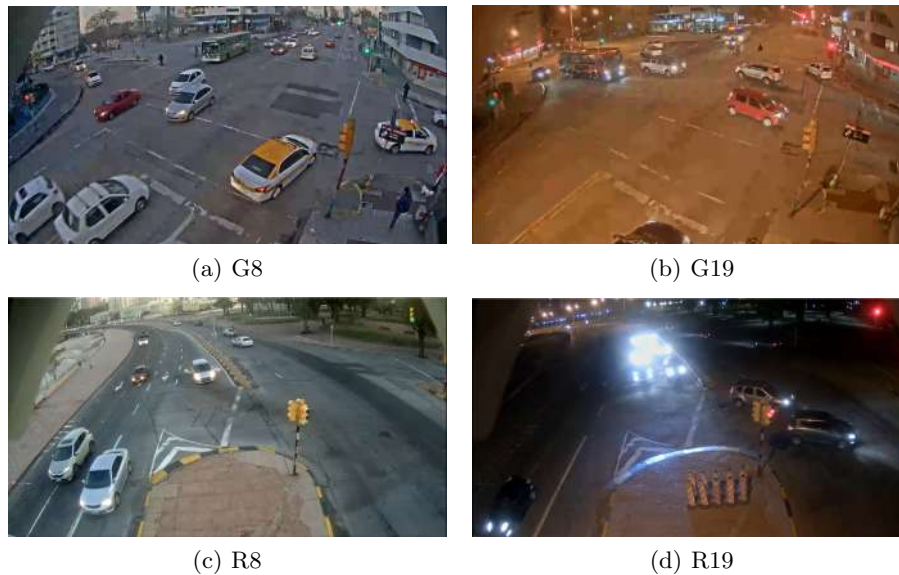


Fig. 3: Testing video scenarios

Table 1: Properties of the test videos

<i>reference</i>	<i>format</i>	<i>resolution</i>	<i># frames</i>	<i>rate</i>	<i>duration</i>
G8	MP4	1280×720 pixels	2393	8 FPS	5 minutes
G19	MP4	1280×720 pixels	2398	8 FPS	5 minutes
R8	MP4	1280×720 pixels	5998	20 FPS	5 minutes
R19	MP4	1280×720 pixels	5997	20 FPS	5 minutes

5.2 Development and execution platform

The proposed system was developed using Python and Anaconda for project environment management allowing to install and maintain the required libraries easily. For the implementation, training, and execution of the presented ANN models, the Detectron2 framework [21], based on pytorch, was used. The tracking service was provided by a Node.js server [19] running an implementation of the Node Moving Things Tracker [15] library. OpenCV [13] was used for image and video manipulation and processing.

The experimental evaluation was performed on a virtual environment defined on a high-end server with Xeon Gold 6138 processors (40 cores and 80 threads per core), 8 GB RAM, a NVIDIA P100 GPU and a 300 GB SSD, from National Supercomputing Center (ClusterUY) [16]. Using this high performance computing platform, it was possible to dynamically reserve the resources needed for the batch jobs for the system execution and validation.

10 H. Winter, J. Serra, S. Nasmachnow, A. Tchernykh, V. Shepelev

5.3 Metrics for evaluation

Statistical measures were considered for the evaluation of the developed system. To account for the performance of stages that involve a binary classification, the standard metrics were applied: True Positive (TP), which indicates the number of occurrences where the model correctly predicts the positive class; True Negative (TN) is the number of occurrences where the model correctly predicts the negative class; False Positive (FP) the number of occurrences where the model incorrectly predicts the positive class; and False Negative (FN) indicates the number of occurrences where the model incorrectly predicts the negative class.

Metrics proposed by Sokolova and Lapalme [18] were applied to evaluate the performance of detection and classification algorithms, including:

- *Average Accuracy*: indicates the overall effectiveness of a classifier (Eq. 2).
- *Error Rate*: indicates the average per-class classification error (Eq. 3).
- *Precision*: reflects the percentage of the results which are relevant (Eq. 4).
- *Recall*: refers to the percentage of total relevant results correctly classified (Eq. 5).

$$\frac{TP + TN}{\frac{TP + TN + FP + FN}{n}} \quad (2) \quad \frac{FP + FN}{TP + TN + FP + FN} \quad (3)$$

$$\frac{TP}{TP + FP} \quad (4) \quad \frac{TP}{TP + FN} \quad (5)$$

Metrics proposed by MOTChallenge [11] were used to evaluate the tracking method. Special metrics are required for evaluating multiple object tracking:

- Identity Switches ($IDSW$): indicates the number of occurrences where an already identified object is assigned a new identifier.
- Multiple Object Tracking Accuracy ($MOTA$): is a global performance indicator of the tracker combining three sources of error. (Eq. 6, where t represents the frame and G_t the number of objects in frame t).

$$MOTA = 1 - \frac{\sum_t (FN_t + FP_t + ID_{Sw})}{\sum_t G_t} \quad (6)$$

5.4 Results: object detection

For the evaluation of the object detection module, the configuration baseline of Detectron2 and the detection confidence threshold were taken into consideration.

The Detectron2 configuration baseline is a set of parameters which determines the type of ANN to be executed and the weight model. These baselines are part of the Model Zoo in Detectron2 [21]. The main properties of the selected baselines are presented in Table 2.

Table 2: Details of the configuration baselines of Detectron2 used in the experimental evaluation of object detection

	<i>R101-box</i>	<i>X101-box</i>	<i>R101-mask</i>	<i>X101-mask</i>
Backbone	R101-FPN	X101-FPN	R101-FPN	X101-FPN
Weights model	R101	X-101-32x8d	R101	X-101-32x8d
Using masks	no	no	yes	yes

The selected backbones used are ResNet-101+FPN (R101-FPN) which is a Faster R-CNN and ResNeXt-101+FPN (X101-FPN) which is a Mask R-CNN. The weight model R101 is an adaptation of the original ResNet-101 model [9] and X-101-32x8d is a ResNeXt-101-32x8d model trained with Caffe2 [24]. In turn, the detection confidence threshold allows discarding detected objects which classification score value is lower than a given value.

Tables 3 and 4 reports the results of the considered detection metrics for the G8 and G19 videos, respectively. These videos were selected as they account for a representative traffic flow of the city in rush hours in the morning (G8) and in the night (G19). In these videos the camera angle is such that the North to South flow of vehicles occasionally occludes the vehicles in the West to East flow. Additionally, this scenario has a crossing with multiple traffic lights which makes the vehicles stop and accumulate producing interesting detection situations.

Table 3: Classification metrics obtained with different settings in video G8

<i>configuration</i>	<i>average accuracy</i>	<i>error rate</i>	<i>precision</i>	<i>recall</i>
R101-box-t03	0.93	0.07	0.91	0.73
R101-box-t05	0.87	0.13	1.00	0.48
R101-box-t07	0.78	0.22	0.93	0.23
X101-box-t03	0.93	0.07	0.89	0.75
X101-box-t05	0.88	0.12	1.00	0.49
X101-box-t07	0.79	0.21	1.00	0.24
R101-mask-t03	0.94	0.06	0.90	0.80
R101-mask-t05	0.93	0.07	0.97	0.72
R101-mask-t07	0.90	0.10	0.96	0.58
X101-mask-t03	0.93	0.07	0.89	0.79
X101-mask-t05	0.91	0.09	0.96	0.66
X101-mask-t07	0.91	0.09	1.00	0.61

Results in Tables 3 and 4 indicate that the proposed system had an overall average accuracy of 85% and indicate that the mask configurations computed better results than the box configurations in most cases (10 out of 12 instances). No significant performance differences between R101 and X101 models on box nor segmentation mask prediction were detected, but X101 had slightly better results in the night cases for segmentation.

12 H. Winter, J. Serra, S. Nsmachnow, A. Tchernykh, V. Shepelev

Table 4: Classification metrics obtained with the different settings in video G19

<i>configuration</i>	<i>average accuracy</i>	<i>error rate</i>	<i>precision</i>	<i>recall</i>
R101-box-03	0.89	0.11	0.78	0.67
R101-box-05	0.82	0.18	0.89	0.40
R101-box-07	0.75	0.25	1.00	0.23
X101-box-03	0.84	0.16	0.70	0.53
X101-box-05	0.83	0.17	0.90	0.42
X101-box-07	0.73	0.27	1.00	0.21
R101-mask-03	0.87	0.13	0.67	0.67
R101-mask-05	0.85	0.15	0.67	0.60
R101-mask-07	0.86	0.14	1.00	0.49
X101-mask-03	0.89	0.11	0.77	0.70
X101-mask-05	0.87	0.13	0.92	0.56
X101-mask-07	0.87	0.13	0.96	0.53

5.5 Object tracking

The main parameter to consider is the *tolerance*, i.e. the number of frames before the algorithm concludes that a tracked object is no longer in the sequence. The tolerance value depends on the frame rate of the recording. Values corresponding to half, one, and two seconds were considered in the study, as they represent time windows in which the probability of a identity switch among detections is low. That is, 4, 8, and 16 frames for G8 and G19 videos, and 10, 20, and 40 frames for R8 and R19. The performance of the object tracking module depends on the detection module. The X101-mask-05 detection setting was defined as basis for all tracking tests as it was the best performing detection configuration.

Table 5: Tracking tests results

<i>configuration</i>	<i>MOTA</i>	<i>configuration</i>	<i>MOTA</i>
G8-t04	0.81	R8-t10	0.86
G8-t08	0.83	R8-t20	0.87
G8-t16	0.82	R8-t40	0.89
G19-t04	0.47	R19-t10	0.10
G19-t08	0.49	R19-t20	0.14
G19-t16	0.46	R19-t40	0.13

Results in Table 5 show average MOTA scores of 85% for the daylight cases and significantly lower (30%) for the cases in the night. This indicate that the module performs significantly better in daytime scenarios. In 3 out of 4 cases, the configurations with one second of tolerance (8 frames in G8 and G19, and 20 frames in R8 and R19) had slightly better results than for nighttime scenarios. *MOTA* was mainly affected by *FN* values. In the tracking evaluation this occurs when an existing vehicle is not detected in a given number of frames, therefore it is not tracked. Based on this observation, improving the detection module in bad lighting conditions would also improve the tracker performance.

5.6 Pattern analysis

For the evaluation of the counting module, the vehicle count resulting from the pipeline execution was compared to the number of vehicles obtained using manual counting. The performance of the method to count vehicles was measured using the detection and classification metrics presented above. To perform the evaluation, 30-second video segments were extracted from the four videos in the original test dataset. Four segments were considered for each video, thus having a total dataset of 16 segments from the two studied scenarios, eight taking place during the day and eight during the night.

Table 6 reports the results of the counting module evaluation, using the following configuration: the R101-mask-05 configuration was established for detection; the tracking module uses an IoU of 0.05, and a loss tolerance of eight frames for G8/G19 videos and 20 frames for R8/R19 videos.

Table 6: Counting test results

<i>reference</i>	<i>average accuracy</i>	<i>error rate</i>	<i>precision</i>	<i>recall</i>
G8	0.92	0.08	0.92	1.00
G19	0.52	0.48	0.62	0.76
R8	0.87	0.13	0.91	0.95
R19	0.19	0.81	0.27	0.33

Results in Table 6 show an average accuracy of 89% for the daylight cases and 36% for the cases in the night. This indicates that the counting module performs better under good lighting conditions. In this case there is still room to improve the classification of the counted vehicles as the comparison of *precision* and *recall* shows that the main source of error are the *FP*. This means that the counting algorithm correctly counts a vehicle, but classifies it in the wrong class. Under bad lighting conditions the performance is poor, this is also caused by the large number of *FP*, which in this case happens because the counting algorithm counts not existing vehicles. The performance of this module can be mainly improved by using a more precise classification model in the detection module, while a better detection under bad lighting conditions would also improve the performance of the counting module. Improving the classification under poor lighting conditions is one of the main lines for ongoing and future work.

6 Conclusions and future work

This article presented the design and implementation of a system for the analysis of traffic data using computational intelligence techniques.

The proposed system was developed following a flexible pipeline-type architecture built over the modern object detection library Detectron2. The proposed design provides an efficient frame processing, by using independent, configurable functional modules, loosely coupled between them. This feature allows including new methods, modifying existing ones, and evaluate different alternatives and configurations.

14 H. Winter, J. Serra, S. Nasmachnow, A. Tchernykh, V. Shepelev

The problems of object detection and tracking are solved using the Detectron2 framework and the Node Moving Things Tracker library, respectively. The information generated by these modules from the traffic videos allowed implementing a set of modules for the collection and analysis of traffic data.

The validation of the proposed system is carried out using real videos from two scenarios that include important streets of Montevideo, Uruguay, under different conditions (daylight, nightlight, and different video qualities). These recordings were taken in rush hours and show an interesting flow of vehicles.

Results demonstrate the effectiveness of the system in scenarios with proper lightning conditions. The detection results shown a overall average accuracy of 85%, and better performance using the mask models. In object tracking, the average MOTA scores were 85% in daylight. Results dropped to 30% in nighttime, indicating that improvements are required to deal with bad lightning conditions. Similarly, the counting module performed an average accuracy of 89% in daylight and 36% in nighttime.

The main lines for future work are related to improve the object detection module training the models with bad lightning conditions or bad weather annotated examples. In turn, the experimental evaluation of the proposed system can be extended to consider the analysis of red light runs and no-stop zones modules. Another interesting line of work is related to developing more sophisticated pattern detection methods to capture relevant events such as abrupt lane change or even traffic accidents. We are working on these topics right now.

References

1. Arinaldi, A., Pradana, J., Gurusinga, A.: Detection and classification of vehicles for traffic video analytics. *Procedia Computer Science* 144, 259–268 (2018)
2. Bochinski, E., Eiselein, V., Sikora, T.: High-speed tracking-by-detection without using image information. In: 14th IEEE International Conference on Advanced Video and Signal Based Surveillance. pp. 1–6 (2017)
3. Chauhan, M., Singh, A., Khemka, M., Prateek, A., Sen, R.: Embedded CNN based vehicle classification and counting in non-laned road traffic. In: 10th Int. Conf. on Information and Communication Technologies and Development (2019)
4. Chavat, J., Nasmachnow, S.: Computational intelligence for detecting pedestrian movement patterns. In: *Smart Cities*, pp. 148–163 (2019)
5. Dey, S., Kalliatakis, G., Saha, S., Kumar Singh, A., Ehsan, S., McDonald, K.: MAT-CNN-SOPC: Motionless analysis of traffic using convolutional neural networks on system-on-a-programmable-chip. In: *NASA/ESA Conference on Adaptive Hardware and Systems* (2018)
6. Gilewski, J.: detectron2-pipeline: Modular image processing pipeline using OpenCV and Python generators powered by Detectron2. <https://github.com/jagin/detectron2-pipeline> (2019), [2020-03-15]
7. Girshick, R.: Fast r-cnn. In: *Proceedings of the IEEE International Conference on Computer Vision* (December 2015)
8. Gu, J., Wang, Z., Kuen, J., Ma, L., Shahroudy, A., Shuai, B., Liu, T., Wang, X., Wang, G., Cai, J., Chen, T.: Recent advances in convolutional neural networks. *Pattern Recognition* 77, 354 – 377 (2018)

9. He, K., Zhang, X., Ren, S., Sun, J.: Deep residual learning for image recognition. arXiv preprint arXiv:1512.03385 (2015)
10. Leal-Taixé, L.: Multiple object tracking with context awareness. CoRR abs/1411.7935 (2014)
11. Leal-Taixé, L., Milan, A., Reid, I., Roth, S., Schindler, K.: MOTChallenge 2015: Towards a benchmark for multi-target tracking. arXiv:1504.01942 [cs] (2015)
12. Lou, L., Zhang, J., Jin, Y., Xiong, Y.: A novel vehicle detection method based on the fusion of radio received signal strength and geomagnetism. *Sensors* 19 (2019)
13. Mahankali, N., Vadivel, A.: OpenCV for computer vision applications (2015)
14. Moussy, E., Mekonnen, A.A., Marion, G., Lerasle, F.: A comparative view on exemplar ‘tracking-by-detection’ approaches. In: 2015 12th IEEE International Conference on Advanced Video and Signal Based Surveillance (AVSS). pp. 1–6 (2015)
15. Move-lab: Tracking things in object detection videos. <https://www.move-lab.com/blog/tracking-things-in-object-detection-videos> (2018), [2020-03-15]
16. Nesmachnow, S., Iturriaga, S.: Cluster-UY: Collaborative Scientific High Performance Computing in Uruguay. In: Communications in Computer and Information Science, pp. 188–202. Springer International Publishing (2019)
17. Ren, S., He, K., Girshick, R., Sun, J.: Faster R-CNN: Towards Real-Time Object Detection with Region Proposal Networks. In: Cortes, C., Lawrence, N.D., Lee, D.D., Sugiyama, M., Garnett, R. (eds.) *Advances in Neural Information Processing Systems* 28, pp. 91–99 (2015)
18. Sokolova, M., Lapalme, G.: A systematic analysis of performance measures for classification tasks. In: *Information Processing Management · July 2009* (2008)
19. Tilkov, S., Vinoski, S.: Node.js: Using javascript to build high-performance network programs. *IEEE Internet Computing* 14(6), 80–83 (2010)
20. Uy, A., Quiros, A., Bedruz, R., Abad, A., Bandala, A., Sybingco, E., Dadios, E.: Automated traffic violation apprehension system using genetic algorithm and artificial neural network. In: *IEEE Region 10 Technical Conference*. pp. 2094–2099 (2016)
21. Wu, Y., Kirillov, A., Massa, F., Lo, W., Girshick, R.: Detectron2. <https://github.com/facebookresearch/detectron2> (2019)
22. Yang, H., Qu, S.: Real-time vehicle detection and counting in complex traffic scenes using background subtraction model with low-rank decomposition. *IET Intelligent Transport Systems* 12, 75–85 (2018)
23. Yang, Z., Pun-Cheng, L.: Vehicle detection in intelligent transportation systems and its applications under varying environments: A review. *Image and Vision Computing* 69, 143 – 154 (2018)
24. Yangqing, J., Shelhamer, E., Donahue, J., Karayev, S., Long, J., Girshick, R., Guadarrama, S., Darrell, T.: Caffe: Convolutional architecture for fast feature embedding (2014)
25. Zhang, K., Zhang, L., Yang, M.: Real-time compressive tracking. In: *Computer Vision*. pp. 864–877. Springer Berlin Heidelberg (2012)
26. Zhang, S., Wu, G., Costeira, J., Moura, J.: Fcn-rlstm: Deep spatio-temporal neural networks for vehicle counting in city cameras. In: *International Conference on Computer Vision*. pp. 3687–3696 (10 2017)
27. Zheng, M., Li, T., Zhu, R., Chen, J., Ma, Z., Tang, M., Cui, Z., Wang, Z.: Traffic accident’s severity prediction: A deep-learning approach-based CNN network. *IEEE Access* 7, 39897–39910 (2019)
28. Zhou, Y., Nejati, H., Do, T., Cheung, N., Cheah, L.: Image-based vehicle analysis using deep neural network: A systematic study. In: *IEEE International Conference on Digital Signal Processing*. pp. 276–280 (2016)

Exact and metaheuristic approach for bus timetable synchronization to maximize transfers

Sergio Nesmachnow^[0000-0002-8146-4012],
Jonathan Muraña^[0000-0002-9328-2320], and
Claudio Risso^[0000-0003-0580-3083]

Universidad de la República, Uruguay

Abstract. This article presents the application of mathematical programming and evolutionary algorithms to solve a variant of the Bus Timetabling Synchronization Problem. A new problem model is proposed to include extended synchronization points, accounting for every pair of bus stops in a city, the transfer demands for each pair of lines, and the offset for lines in the considered scenario. Mixed Integer Programming and evolutionary algorithm are proposed to efficiently solve the problem. A relevant real case study is solved, for the public transportation system of Montevideo, Uruguay. Several scenarios are solved and results are compared with the no-synchronization solution and the current planning of such transportation system too. Experimental results indicate that the proposed approaches are able to significantly improve the current plannings. The Mixed Integer Programming algorithm computed the optimum solution for all scenarios, accounting for an improvement of up to 95% in successful synchronizations when compared with the actual timetable in Montevideo. The evolutionary algorithm is efficient too, improving up to 68% the synchronizations with respect to the current planning and systematically outperforming the baseline solutions. Waiting times for users are significantly improved too, up to 33% in tight problem instances.

Keywords: smart cities, mobility, public transportation, timetabling, synchronization

1 Introduction

Transportation systems are a crucial component of modern society, and they are one of the most important services to improve efficiency of activities in nowadays smart cities [6,10]. Transportation systems include a wide range of logistic activities related to transporting passengers and goods. One of the main goals of transportation systems is coordinating the movement of people, providing efficient mobility at reasonable fares. In this regard, public transportation is the most efficient and environmental friendly mean for mobility of citizens. However, the efficacy of public transportation systems in large cities requires a proper planning of several issues that affect the quality of service, including routes design and management, timetabling, drivers assignment, and others [3].

2 S. Nesmachnow, J. Muraña, C. Risso

A transportation system usually includes timetables accounting for reporting the expected location of vehicles during a day. Timetables are closely related to the transportation network design, and they are usually built to account for specific origin-destination demands. Synchronization of multi-leg trips or *transfers* is usually a secondary goal of the timetabling problem, although it is important for providing an adequate quality-of-service, allowing passengers to wait reasonable times for transfers from one route to another.

The proposed problem is very relevant for the case study proposed: the transportation system of Montevideo, Uruguay [13]. Montevideo has a rather uniform public transportation system, operated by buses with similar capacities and service provision. Many users of the system manage to complete their end-to-end journey using only one line, but several other users rely on connections between different lines to make their trips, using transfers. Transfers can be made between different (geographically separated) bus stops. They are allowed without additional charge and are controlled by the intelligent Metropolitan Transportation System (STM), which identifies users using personal smart cards.

The STM also maintains historical records of the mobility of users. From these data, time periods in the day are identified during which the use of the system is regular, that is, where the utilization numbers have little dispersion and their average values are known. These numbers include: number of passengers boarding or alighting, number of transfers between lines and combinations of stops, bus circulation times at stops on their routes, and transfer times between stops for passengers seeking to transfer. These data are the main inputs used by the local administration to plan the frequency of each line within the uniform periods. Even knowing the frequency of each line, that is, the number of buses to use in the service period to satisfy the demand of the system (including direct and transfer trips), and knowing the circulation times between stops, there is room to adjust the departure time of each bus, which in turn determines the arrival time of that bus at each stop on its route.

Considering the case study described above, the main goal of this article is to optimize the number of successful transfers allowed by a timetable realization. The types of transfer are identified, and for each one a maximum threshold is established for the time that a passenger waits for their connection. If the passenger manages to transfer within a waiting time below that threshold, the transfer is successfully timed. The variant of the transfer synchronization problem elaborated here studies how to coordinate the departure schedule of buses—and therefore of arrivals at stops on their routes—, in order to maximize the number of successful transfers during a uniform time period, for which all previous data are known and fixed.

The article is organized as follows. Section 2 introduces the bus synchronization problem and the variant solved in this article. Section 3 reviews related works. The proposed approaches for bus synchronization are described in Section 4. The experimental evaluation of the proposed methods over realistic instances in Montevideo is reported in Section 5. Finally, the conclusions and the main lines for future work are formulated in Section 6.

2 Bus timetable synchronization to maximize transfers

This section describes the bus timetable synchronization problem to maximize transfers.

2.1 Problem model

The problem accounts for the main goals of a modern transportation system: providing a fast and reliable way for the movement of citizens, while maintaining reasonable fares. The problem model mainly focuses on the quality of service provided to the users, i.e., a better traveling experience with reduced waiting times when using more than one bus for consecutive trips.

In the proposed model, the events of favoring passenger transfers with limited waiting times are called *synchronization* events. The study is aimed at solving real scenarios, based on real data from urban transit systems that accounts for the number of passengers that perform transfers between lines on each bus stop.

The main idea of the problem model is to divide any day into several planning periods on the basis of demand and travel time behavior of passengers. This way, the analysis of historical data allows obtaining similar accurate and almost deterministic information to build the problem scenarios.

2.2 Problem formulation

The mathematical formulation of the bus timetable synchronization problem to maximize transfers is presented next.

Problem data. The set of data that defines an instance of the bus synchronization problem includes the following elements:

- A planning period $[0, T]$.
- A set of lines of the bus network $I = \{i_1, i_2, \dots, i_n\}$, with predefined routes, and the number of trips f_i needed to fulfill the demand for each line i within the planning period $[0, T]$, accounting for both direct trips and transfers.
- A set of *synchronization nodes*, or *transfer zones*, $B = \{b_1, b_2, \dots, b_m\}$. Each synchronization node $b \in B$ is a triplet $\langle i, j, d_b^{i,j} \rangle$ indicating that lines i and j may synchronize in b , and that the bus stops for lines i and j are separated by a distance $d_b^{i,j}$. Each synchronization node represents a pair of bus stops for which regular transfers between lines i and j are registered. The value of $d_b^{i,j}$ defines the time needed for a passenger that transfers from line i to line j to walk from one stop to another in the transfer zone (see next item).
- A *traveling time function* $TT : I \times B \rightarrow \mathbf{Z}$. $TT_b^i = TT(i, b)$ indicates the time needed to reach the synchronization node b for buses in line i (from the origin of the line). Generally, this value depends on several features, including the bus type, bus velocity, traffic in roads, passengers' demand, etc.

4 S. Nasmachnow, J. Muraña, C. Risso

- A demand function $P : I \times I \times B \rightarrow \mathbf{Z}$. $P_b^{ij} = P(i, j, b)$ indicates the number of passengers that transfer from line i to line j in synchronization node b , in the planning period. Assuming a uniform demand hypothesis in the planning period, the number of passengers that transfer from a given trip of line i to a given trip of line j is P_b^{ij}/f_i . This is a realistic assumption for planning periods where demand does not vary significantly, such as in the case study presented in this article.
- A maximum waiting time W_b^{ij} for each transfer zone, indicating the maximum time that passengers are willing to wait for line j , after alighting from line i and walking to the stop of line j , in a synchronization node b . Trips of line i and j are considered synchronized for transfers if and only if the waiting time of passengers that transfers is lower or equal to W_b^{ij} .
- The departing time of the first trip of each line i (the *offset* of the line) must be lower than a maximum headway time H_i , which is defined by the bus system operator. Subsequent trips depart at a fixed frequency ΔX^i . All trips of each line must start within the planning period $[0, T]$.

Mathematical model. The bus synchronization problem proposes finding appropriate values for the departure time of the first trip of each line to guarantee the maximum number of synchronizations for all lines with transfer demands in the planning period T .

The control variables of the problem are the offset of each line (X_1^i), which define the whole set of departing times for all trips of each line. Auxiliary variables are needed to capture the synchronization events in each transfer zone. Binary variables Z_{rsb}^{ij} takes value 1 when trip r of line i and trip s of line j are synchronized in node b (i.e., trip r of line i arrives before trip s of line j and allows passengers to complete the transfer, i.e., walk between the corresponding bus stops and wait less than the waiting threshold for that transfer, W_b^{ij}).

The mathematical model of the bus synchronization problem as Mixed Integer Programming (MIP) problem is formulated in Eq. 1.

$$\text{maximize} \quad \sum_{b \in B} \left(\sum_{r=1}^{f_i} \sum_{s=1}^{f_j} Z_{rsb}^{ij} \right) \cdot \frac{P_b^{ij}}{f_i} \tag{1a}$$

$$\text{subject to} \quad Z_{rsb}^{ij} \leq 1 + \frac{(A_{rb}^i + d_b^{ij} + W_b^{ij}) - A_{sb}^j}{M} \quad \forall b \in B \tag{1b}$$

$$Z_{rsb}^{ij} \leq 1 + \frac{A_{sb}^j - (A_{rb}^i + d_b^{ij})}{M} \quad \forall b \in B \tag{1c}$$

$$\text{with } A_{sb}^j = X_1^j + (s-1)\Delta X^j + TT_b^j$$

$$A_{rb}^i = X_1^i + (r-1)\Delta X^i + TT_b^i$$

$$Z_{rsb}^{ij} \in \{0, 1\}, 0 \leq X_1^i \leq H_i, \quad \forall i \in I \tag{1d}$$

The objective function of the optimization problem (Equation 1a) proposes maximizing the number of passengers that successfully complete a transfer in the planning period in every synchronization point. The value $\sum_{r=1}^{f_i} \sum_{s=1}^{f_j} Z_{rsb}^{ij}$ is the total number of successful connections between trips of each pair of lines i and j involved in each synchronization point b , while P_b^{ij}/f_i is the demand for each transfer.

Equations 1b–1d specify the constraints of the problem. According to Equation 1a, the optimization will seek to activate as many variables Z_{rsb}^{ij} as possible. Constraints for variables Z_{rsb}^{ij} prevent them from taking the value 1 if the corresponding transfer is not synchronized. In both, Equations 1b and 1c, A_{rb}^i denotes the arrival time of trip r of line i to transfer zone b and A_{sb}^j denotes the arrival time of trip s of line j to transfer zone b . For an interpretation of constraint 1b, consider the maximum time passengers from trip r of line i are willing to wait for a transfer with trip s of line j at transfer zone b . This value defines the limit time $A_r^i + d_b^{ij} + W_b^{ij}$. Whenever the arrival time of trip s of line j does not surpass that limit, the right-hand side of Equation 1b is greater or equal to 1, so the synchronization variable Z_{rsb}^{ij} is allowed to be 1. In addition, it is also necessary for passengers alighting from trip r of line i to walk to the transfer point (arriving at time $A_{rb}^i + d_b^{ij}$) before the arrival time of the corresponding trip s of line j (A_{sb}^j). Otherwise, those passengers would lose the connection. Whenever this second condition is met, the right-hand side of constraints Equation 1c also allow Z_{rsb}^{ij} to take the value 1. So far, there is a potential issue when non-synchronized trips lead to values lower than 0 on the right-hand side of Equation 1c, which derives into unfeasible constraints sets. The proposed model only needs that either $(A_{rb}^i + d_b^{ij} + W_b^{ij}) - A_{sb}^j$ or $A_{sb}^j - (A_{rb}^i + d_b^{ij})$ to be negative to deactivate synchronization variables Z_{rsb}^{ij} . Hence, suffices to get a constant value M , large enough to guarantee that both Equations 1b and 1c are always feasible. However, using extremely large values for M might cause numerical stability problems when the model is implemented in a solver. The procedure applied in this article to find compliant and relatively low values for M consisted in computing the maximum value within the union of sets $\{(H_i(j) + (f_i(j) - 1) \times \Delta X^j + TT_b^j) - (TT_b^i + d_b^{ij} + W_b^{ij})\}$ and $\{(H_i(i) + (f_i(i) - 1) \times \Delta X^i + TT_b^i + d_b^{ij}) - TT_b^j\}$, for all synchronization points $b \in B$. These values of M can be easily calculated during the process of crafting the MIP formulation before using a specific solver, so the problem of finding M is of polynomial complexity. Finally, Equation 1d defines the domain for decision variables Z_{rsb}^{ij} (binary variables).

The problem formulation assumes, without loss of generality, that $\Delta X^j > W_b^{ij}, \forall j \in I$, i.e., headways of bus lines are larger than the waiting time thresholds for users. The case where $\Delta X^j \leq W_b^{ij}$ correspond to a scenario in which the headway of line j is lower than the time users are willing to wait, thus all transfer with line j would be synchronized and they would not be part of the problem to solve.

3 Related work

The bus timetable synchronization problem was recognized as a relevant issue for modern public transportation systems in early works by Ceder [3]. One of the first approaches for schedule synchronization on bus network systems was presented by Daduna and Voß [4], studying several objective functions (e.g., weighted sum considering transfers and the maximum waiting time at a transfer zone). Metaheuristic algorithms were evaluated for simple versions of the problem with uniform frequencies, using data from the Berlin Underground network and other German cities. Tabu Search computed better solutions than Simulated Annealing over randomly generated examples, and a trade-off between operational costs and user efficiency was concluded.

Ceder et al. [2] studied the Transit Network Timetabling problem to optimize the number of synchronization events between bus lines at shared stops, by maximizing the number of simultaneous arrivals. A greedy algorithm was proposed to solve the problem, based on selecting specific nodes from the bus network to define custom timetables. The article focused on simultaneous bus arrivals, and just some examples to illustrate synchronizations on small instances with few nodes and few lines were reported.

Fleurent et al. [5] proposed a subjective metric to evaluate synchronizations, using weights defined by experts and public transport authorities. The authors solved an optimization problem to minimize variable (vehicle) operation costs. A heuristic method was proposed for optimization, using the defined synchronization metric. Several timetables were computed for small scenarios from Montréal, Canada, using different weights for costs.

Ibarra and Ríos [8] studied a flexible variant of the the synchronization problem, considering time windows between travel times. A Multi-start Iterated Local Search (MILS) algorithm was applied to solve eight instances modeling the bus network in Monterrey, Mexico with between three and 40 synchronization points. MILS was able to compute efficient solutions for medium-size instances in less than one minute, when compared with a simple upper bound and a Branch & Bound exact method. Later, Ibarra et al. [7] applied MILS to solve the multi-period bus synchronization problem, to optimize multiple trips of a given set of lines. MILS was able to compute similar results than a Variable Neighborhood Search and a simple population-based algorithm on synthetic instances with few synchronization points. Results for a sample case study using data for a single line of Monterrey demonstrated that maximizing synchronizations for a specific node usually reduces the number of synchronizations for other nodes.

Our previous article [12] proposed an evolutionary approach for a specific variant of the bus synchronization problem. Results for realistic case studies in Montevideo demonstrated that the evolutionary approach outperformed real timetables by the city administrator and other heuristic methods. This article extends our previous research, accounting for a different variant of the bus synchronization problem aimed at determining the optimal offset values while keeping the headways and number of trips as indicated by the real timetable, in order to not impact in the quality of service offered to direct passengers.

4 Proposed resolution approaches

This section describes the exact and metaheuristic approaches developed to solve the bustimetable synchronization problem to maximize transfers.

4.1 Exact Mathematical Programming

The exact resolution of the proposed MIP model was developed using AMPL.

IBM ILOG CPLEX was used as the optimization tool, over the environment defined by ptimization Studio 12.8. Optimal solutions are computed applying a branch-and-cut heuristic, considering the following stop conditions for the execution:

- The time limit for the execution (parameter CPX_PARAM_TILIM) was set to ... (explicar: not relevant)
- The GAP tolerance in CPLEX (parameter CPX_PARAM_EPGAP) was set to the default value of 0.01% (0.0001). It is considered the default value since, the main goal is to compare with previous solutions obtained with that specific limit. The GAP represents, in percentage terms, the distance between the solution found and the best achievable solution. It is defined as $(f(x) - bestBound)/f(x)$, where x is the solution found and $bestBound$ is the best value achievable by the objective function.

4.2 Evolutionary algorithm

The proposed EA was implemented in C++, using the Malva library (github.com/themalvaproject).

Solution encoding. Candidate solutions to the problem are represented using integer vectors. In a solution representation, each integer value represents the offset (in minutes) of each bus line, i.e., the time between the start of the planning period and the depart of the first trip of each line. Formally, a candidate solution to the problem is represented by $X = X_0^1, X_0^2, \dots, X_0^n$, where n is the number of bus lines in the problem instance, $X_0^i \in \mathbf{Z}^+$, and $0 \leq X_0^i \leq H^i$.

Evolution model. The $(\mu + \lambda)$ evolution model [1] is applied in the proposed EA: μ parents generate λ offsprings, which compete between them and with their parents, to determine the individuals that will be part of the new population on the next generation. Preliminary experiments demonstrated that $(\mu + \lambda)$ evolution was able to provide better solutions and more diversity than a traditional generational model.

Initialization operator. A random initialization operator is applied. Randomly generated solutions are included in the initial population, accounting for the constraints defined for the offset of each line. This initialization procedure intends to provide diversity to the evolutionary search.

8 S. Neschachnow, J. Muraña, C. Risso

Selection operator. A tournament selection is applied. The tournament size is three individuals, and one individual survives. Tournament selection computed better results than proportional selection in preliminary calibration experiments, mainly due to the appropriate level of selection pressure for the evolution.

Recombination operator. The recombination operator is a specific variant of two-point crossover. It defines two crossover points randomly in $[1, n-1]$ and exchanges the information encoded in both parents between the crossover points. This operator was conceived to preserve specific features of lines already synchronized in parent solutions, trying to keep useful information in the offspring generation process. The recombination operator is applied to individuals returned by the selection operator, with a probability p_R .

Mutation operator. The mutation operator applied is a specific variant of Gaussian mutation. Specific position(s) in a solution are modified according to a Gaussian distribution, and taking into account the thresholds defined by the minimum and maximum frequencies for each line. The mutation operator is applied to every gene in the proposed representation with a probability p_M .

5 Experimental evaluation

This section reports the experimental evaluation of the proposed methods for the bus synchronization problem.

5.1 Methodology

Problem instances. The experimental evaluation of the proposed methods for bus synchronization is performed in problem instances built using real data from the Metropolitan Transportation System in Montevideo, Uruguay.

Several sources of data from the National Open Catalog were considered to gather information about bus lines description, routes, timetables, and bus stops location in the city. The information about transfers was provided by Intendencia de Montevideo and processed applying a urban data analysis approach [9].

The key elements of the scenario and problem instances are described next: the period is the interval of hours considered for the schedule; the demand function is computed from transfers information registered by smart cards used to sell tickets; the synchronization points are chosen according to their demand, i.e., the pairs of bus stops with the largest number of registered transfers for the period are selected; the bus lines correspond to the lines passing by the synchronization points; the time traveling function TT for each line is computed empirically by using GPS data; the walking time function is the estimated walking speed of a person (assumed constant at $ws = 6$ km/h) multiplied by the distance between bus stops in each transfer zone computed using geospatial information about stops. The maximum waiting time is equal to λH , with $\lambda \in [0.3, 0.5, 0.7, 0.9]$, to allow configuring instances with different levels of tolerance/quality of service.

Sixty problem instances were defined, accounting for three different dimensions (including 30, 70, and 110 synchronization points), using real information about bus operating in Montevideo, Uruguay. The synchronization points of each instance were chosen randomly from the most demanded transfer zones for the considered period in the city (a total number of 170 zones).

Each defined problem instance is identified by the following name convention: [NP].[NL].[λ].[id], where NP = n is the number of synchronization points, NL = m is the of bus lines, λ is the coefficient applied to W_b (percentage) and id is a relative identifier for instances with the same values of NL, NP, and λ . Scenarios are available at <https://www.fing.edu.uy/inco/grupos/cecal/hpc/bus-sync/>.

Execution platform. The experimental evaluation was performed on a Quad-core Xeon E5430 at 2.66GHz, 8 GB RAM, from National Supercomputing Center (Cluster-UY), Uruguay [11].

Baseline solutions for the comparison. Two main baseline solutions were considered for the comparison of the solutions computed by the proposed methods. A relevant baseline for comparison is the current timetable applied in the transportation system of Montevideo (the *real* timetable), which provides the actual level of service regarding direct travels and transfers. In turn, another relevant baseline for comparison is the solution without applying any explicit approach for synchronization of transfers, i.e., a solution where the first trip of each line departs at the beginning of the planning period (time 0, the *zeros* timetable). This solution provides a number of synchronized transfers according to the predefined headways for each line.

Metrics. The metrics applied for the evaluation include: i) the number of synchronized trips for passengers, as proposed in the summatory that defines the objective function of the problem; ii) the improvements over the baseline solutions, iii) the average waiting time each passenger wait for the connection (bus of line j) in a synchronization point.

Parameter setting. EAs are stochastic methods, thus parameter setting analysis are needed to determine the parameter configuration that allows computing the best results. The values of stopping criterion ($\#gen$), population size (ps), recombination probability (p_R), and mutation probability (p_M) were studied for the proposed EA on three instances, different from the ones used in validation experiments, in order to avoid bias. The best results were obtained with the configuration $\#gen = 10000$, $ps = 20$, $p_R = 0.9$ and $p_M = 0.01$.

5.2 Numerical results

Table 1 reports the objective function values computed by EA and the exact resolution approach for the considered problem instances. In turn, the relative improvements over the baseline solutions are reported: Δ_r is the relative improvement over the real timetable and Δ_z is the relative improvement over the zeros solution.

10 S. Nesmachnow, J. Muraña, C. Risso

<i>scenario</i>	<i>real</i>	<i>zeros</i>	<i>EA</i>			<i>exact</i>		
			<i>obj</i>	Δ_r	Δ_z	<i>obj</i>	Δ_r	Δ_z
30.37.90.0	276.08	286.89	302.09	0.09	0.05	302.09	0.09	0.05
30.37.70.0	224.62	232.79	271.75	0.21	0.17	271.75	0.21	0.17
30.37.50.0	162.41	151.99	208.65	0.28	0.37	208.99	0.29	0.38
30.37.30.0	111.58	107.85	154.49	0.38	0.43	154.62	0.39	0.43
30.40.90.0	218.61	229.78	237.05	0.08	0.03	243.02	0.11	0.06
30.40.70.0	163.64	175.85	199.40	0.22	0.13	219.97	0.34	0.25
30.40.50.0	126.11	127.07	146.39	0.16	0.15	173.24	0.37	0.36
30.40.30.0	92.28	90.97	101.18	0.10	0.11	127.08	0.38	0.40
30.40.90.1	227.36	248.57	252.45	0.11	0.02	262.36	0.15	0.06
30.40.70.1	178.07	193.32	219.92	0.24	0.14	238.19	0.34	0.23
30.40.50.1	129.80	140.22	163.30	0.26	0.16	190.16	0.47	0.36
30.40.30.1	80.24	108.97	117.42	0.46	0.08	156.44	0.95	0.44
30.41.90.0	246.99	260.32	279.49	0.13	0.07	279.49	0.13	0.07
30.41.70.0	197.16	201.00	248.29	0.26	0.24	248.42	0.26	0.24
30.41.50.0	141.93	136.07	186.27	0.31	0.37	186.36	0.31	0.37
30.41.30.0	93.79	98.26	141.87	0.51	0.44	142.63	0.52	0.45
30.42.90.0	241.44	241.45	255.78	0.06	0.06	255.78	0.06	0.06
30.42.70.0	195.96	191.28	228.08	0.16	0.19	228.08	0.16	0.19
30.42.50.0	145.01	140.28	172.52	0.19	0.23	172.52	0.19	0.23
30.42.30.0	95.81	93.08	124.88	0.30	0.34	125.74	0.31	0.35
70.60.90.0	568.51	579.73	609.29	0.07	0.05	609.68	0.07	0.05
70.60.70.0	463.02	454.24	545.02	0.18	0.20	546.03	0.18	0.20
70.60.50.0	339.70	296.11	414.29	0.22	0.40	415.80	0.22	0.40
70.60.30.0	218.71	213.86	301.34	0.38	0.41	304.07	0.39	0.42
70.62.90.0	543.67	560.98	590.80	0.09	0.05	591.17	0.09	0.05
70.62.70.0	443.22	443.89	524.86	0.18	0.18	525.81	0.19	0.18
70.62.50.0	325.70	317.75	393.66	0.21	0.24	394.13	0.21	0.24
70.62.30.0	212.04	215.66	295.31	0.39	0.37	298.68	0.41	0.38
70.63.90.0	550.17	575.71	609.44	0.11	0.06	609.68	0.11	0.06
70.63.70.0	441.71	455.92	546.46	0.24	0.20	547.61	0.24	0.20
70.63.50.0	316.46	300.67	427.58	0.35	0.42	429.74	0.36	0.43
70.63.30.0	208.82	202.82	324.20	0.55	0.60	328.02	0.57	0.62
70.67.90.0	510.16	535.04	567.09	0.11	0.06	567.43	0.11	0.06
70.67.70.0	409.57	418.35	512.30	0.25	0.22	513.00	0.25	0.23
70.67.50.0	302.15	299.78	400.06	0.32	0.33	402.49	0.33	0.34
70.67.30.0	194.05	201.63	298.87	0.54	0.48	302.55	0.56	0.50

Continue on next page

Table 1 – *Continued from previous page*

scenario	real	zeros	EA			exact		
			obj	Δ_r	Δ_z	obj	Δ_r	Δ_z
70.69.90.0	522.36	550.33	583.61	0.12	0.06	583.85	0.12	0.06
70.69.70.0	406.63	435.12	529.19	0.30	0.22	531.05	0.31	0.22
70.69.50.0	298.53	292.98	416.07	0.39	0.42	418.24	0.40	0.43
70.69.30.0	193.05	205.18	324.08	0.68	0.58	328.15	0.70	0.60
110.76.90.0	815.78	843.26	894.86	0.10	0.06	895.72	0.10	0.06
110.76.70.0	656.63	669.18	798.41	0.22	0.19	799.61	0.22	0.19
110.76.50.0	479.29	451.85	622.49	0.30	0.38	627.71	0.31	0.39
110.76.30.0	333.66	294.90	467.28	0.40	0.58	474.09	0.42	0.61
110.78.90.0	847.33	879.90	900.09	0.06	0.02	931.35	0.10	0.06
110.78.70.0	699.49	667.77	763.71	0.09	0.14	835.26	0.19	0.25
110.78.50.0	507.05	453.87	551.42	0.09	0.21	644.97	0.27	0.42
110.78.30.0	324.79	317.42	379.43	0.17	0.20	477.47	0.47	0.50
110.78.90.1	867.23	895.99	910.82	0.05	0.02	941.85	0.09	0.05
110.78.70.1	708.89	689.30	780.93	0.10	0.13	845.71	0.19	0.23
110.78.50.1	525.85	460.71	567.71	0.08	0.23	654.75	0.25	0.42
110.78.30.1	338.42	319.33	390.82	0.15	0.22	489.02	0.45	0.53
110.78.90.2	848.47	872.66	894.37	0.05	0.02	932.92	0.10	0.07
110.78.70.2	681.46	676.82	765.56	0.12	0.13	836.45	0.23	0.24
110.78.50.2	494.80	449.03	571.35	0.15	0.27	654.02	0.32	0.46
110.78.30.2	333.19	309.13	397.57	0.19	0.29	492.76	0.48	0.59
110.83.90.0	810.76	850.69	897.02	0.11	0.05	897.65	0.11	0.06
110.83.70.0	624.94	674.88	803.28	0.29	0.19	806.25	0.29	0.19
110.83.50.0	463.61	460.48	634.77	0.37	0.38	639.36	0.38	0.39
110.83.30.0	299.88	300.96	490.14	0.63	0.63	498.28	0.66	0.66

Table 1: Objective function results of exact and EA

Results reported in Table 1 indicate that exact and EA methods significantly outperform the baseline solutions in all studied scenarios. The improvements of EA over the real solution were up to 68% in instance 70.69.30.0 and the improvements of the exact method over the real solution were up to 95% in instance 30.40.30.1. Regarding the comparison with the zeros solution, the improvements of EA were up to 63% and the improvements of the exact method were up to 66%, both in instance 110.83.30.0. Average improvements over the real timetable were 20% for EA and 25% for the exact solution.

In turn, the proposed EA was able to compute solutions close to the exact method (i.e., the optimal value) in low dimension and high tolerance scenarios, computing the optimal solution in six scenarios.

12 S. Neschachnow, J. Muraña, C. Risso

Table 2 reports the average improvements of exact and EA over the baseline solutions, grouped by scenario size and tolerance. Improvements of the exact method are up to 52% over the real timetable (in scenarios with NP=70 and $\lambda=30$) and up to 52% over zeros (in scenarios with NP=100 and $\lambda=30$). In turn, the EA improved up to 50% over the real timetable and up to 49% over zeros, both in scenarios with NP=70 and $\lambda=30$. The values grouped by tolerance allow concluding that for all sizes sizes, the improvements increase as user tolerance decreases. This result indicates that the proposed methods scale with the complexity of the problem, effectively increasing the quality of service. Improvements of the exact method also increase with the size of the scenario.

NP	λ	EA		exact	
		Δ_r	Δ_z	Δ_r	Δ_z
30	90	0.10	0.05	0.11	0.06
30	70	0.22	0.17	0.26	0.21
30	50	0.24	0.26	0.32	0.34
30	30	0.35	0.28	0.49	0.42
70	90	0.10	0.06	0.10	0.06
70	70	0.23	0.20	0.23	0.21
70	50	0.30	0.36	0.30	0.37
70	30	0.50	0.49	0.52	0.50
110	90	0.07	0.04	0.10	0.06
110	70	0.16	0.16	0.22	0.22
110	50	0.19	0.30	0.30	0.42
110	30	0.30	0.38	0.49	0.58

Table 2: Improvements of exact and EA over baseline solutions, grouped by dimension and tolerance

Fig. 1 shows the average objective values (normalized by NP) for all scenarios, grouped by tolerance. The largest difference in objective values is 1.51 (4.53 – 3.02), between the exact approach and the real timetable in scenarios with low user tolerance ($\lambda=30$). The lowest difference is 0.37, between EA and zeros, when $\lambda=90$. As for results in Table 2, the graphic clearly shows that improvements of the proposed approaches increase for tight scenarios.

Table 3 reports three values ($r-l_s/l_n$) for the considered solutions, grouped by NP and λ . The value r is the ratio of the average waiting time results over the maximum waiting time for each synchronization point, which evaluates the number of successful synchronized trips and the relative waiting time for each synchronization point. Successful synchronization are represented by $r \leq 1.0$, and unsuccessful synchronization are represented by $r > 1.0$. In turn, l_s is the average number of lines successfully synchronized and l_n is the average number of lines not synchronized.

Maximum transfers bus timetable synchronizations 13

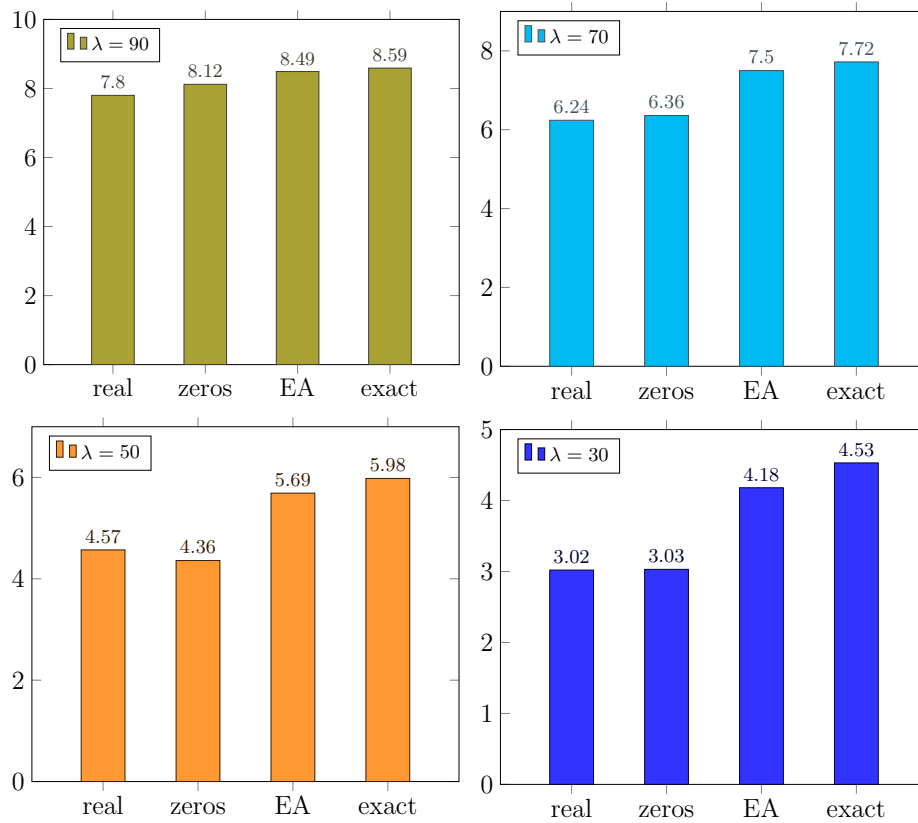


Fig. 1: Objective function comparison grouped by tolerance

<i>NP</i>	λ	<i>real</i>	<i>zeros</i>	<i>EA</i>	<i>exact</i>
30	90	0.47 – 22/0	0.48 – 22/0	0.46 – 22/0	0.47 – 22/0
30	70	0.59 – 22/0	0.61 – 21/1	0.54 – 22/0	0.53 – 22/0
30	50	0.85 – 16/6	0.87 – 16/6	0.76 – 19/3	0.75 – 19/3
30	30	1.33 – 3/19	1.37 – 3/19	1.19 – 5/16	1.12 – 7/15
70	90	0.47 – 39/0	0.49 – 39/0	0.46 – 39/0	0.47 – 39/0
70	70	0.59 – 38/1	0.62 – 38/1	0.54 – 39/0	0.52 – 39/0
70	50	0.85 – 28/10	0.88 – 28/10	0.74 – 35/3	0.73 – 35/4
70	30	1.35 – 5/33	1.40 – 4/35	1.14 – 11/28	1.13 – 12/27
110	90	0.49 – 49/0	0.50 – 49/0	0.48 – 49/0	0.46 – 49/0
110	70	0.61 – 46/2	0.64 – 47/2	0.57 – 48/1	0.53 – 49/0
110	50	0.87 – 34/14	0.91 – 34/15	0.79 – 41/8	0.72 – 44/5
110	30	1.38 – 7/42	1.43 – 4/45	1.24 – 11/38	1.10 – 17/32

Table 3: Average waiting time results for the considered solutions

Results in Table 3 indicate that the proposed approaches significantly improve the quality of service with respect to the baseline solutions, accounting for lower values of the waiting time metric for all scenarios. Largest improvement of EA over baseline solutions occur where NP=70 and $\lambda=30$ (0.26 over zeros solution and 0.21 over real solution). Largest improvements of the exact method occur where NP=110 and $\lambda=30$ (0.33 over zeros solution and 0.28 over real solution). The proposed approaches achieve better waiting time values in lower tolerance scenarios, with respect to baseline solutions.

Fig. 2 presents a histogram comparison of the waiting times (normalized by W_b) for bus lines of a sample scenario (70.63.30.2) for a baseline solution (left) and the exact solution (right). The graphic shows that the exact solution manages to reduce the waiting time in a significant percentage of lines in the scenario. The exact solution has more bus lines with a waiting time less than or equal to 1 (16 vs. 6). Also, the exact solution has two lines with wait less than 0.5 while the baseline solution has none. Regarding higher waiting times, in the exact solution only 6 lines are higher than 1.5 of the expected value, while the baseline solution has 13 bus lines where users wait more than 1.5 of the expected value. The histogram comparison clearly indicates that the proposed solution improves the QoS, by synchronizing a larger number of lines of the system.

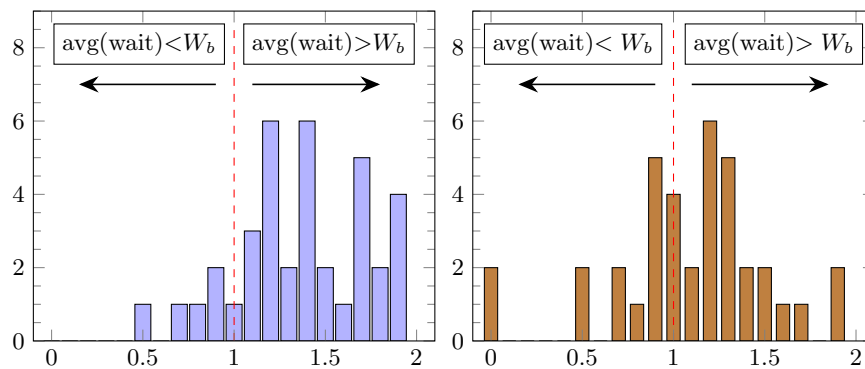


Fig. 2: Histogram comparison of the waiting time metric for baseline (left) and exact solutions (right) in scenario 70.63.30.2

6 Conclusions and future work

This article presented exact and evolutionary approaches to solve a variant of the Bus Timetabling Synchronization Problem considering extended synchronization points for every pair of bus stops in a city, transfer demands, and the line offsets.

A Mixed Integer Programming approach and an evolutionary algorithm were proposed to efficiently solve the problem. Results were compared with the no-synchronization solution and also with real timetables for a real case study in Montevideo, Uruguay.

Experimental results indicate that the proposed approaches significantly improve over current timetable. The exact method computed the optimum solution for all scenarios, improving successful synchronizations up to 95% (25% in average) over the real timetable in Montevideo. The EA is efficient too, improving up to 68% the synchronizations (20% in average) over the current timetable and systematically outperforming other baseline solutions. The proposed EA can be useful for addressing larger scenarios of the considered problem. Waiting times for users are significantly improved too, up to 33% in tight problem instances.

The main lines of future work include solving different variants of the bus timetable synchronization problem, accounting for different headways in the planning period, and modeling the real demand for direct trips too. Multiobjective version of the problem must be included too, by considering other relevant functions: cost and quality of service.

References

1. Bäck, T., Fogel, D., Michalewicz, Z. (eds.): Handbook of evolutionary computation. Oxford University Press (1997)
2. Ceder, A., Golany, B., Tal, O.: Creating bus timetables with maximal synchronization. *Transportation Research Part A: Policy and Practice* 35(10), 913–928 (2001)
3. Ceder, A., Wilson, N.: Bus network design. *Transportation Research Part B: Methodological* 20(4), 331–344 (1986)
4. Daduna, J., Voß, S.: Practical experiences in schedule synchronization. In: *Lecture Notes in Economics and Mathematical Systems*, vol. 430, pp. 39–55. Springer Berlin Heidelberg (1995)
5. Fleurent, C., Lessard, R., Séguin, L.: Transit timetable synchronization: Evaluation and optimization. In: *9th International Conference on Computer-aided Scheduling of Public Transport* (2004)
6. Grava, S.: *Urban Transportation Systems*. McGraw-Hill (2002)
7. Ibarra-Rojas, O., López-Irarragorri, F., Rios-Solis, Y.: Multiperiod bus timetabling. *Transportation Science* 50(3), 805–822 (2016)
8. Ibarra-Rojas, O., Rios-Solis, Y.: Synchronization of bus timetabling. *Transportation Research Part B: Methodological* 46(5), 599–614 (2012)
9. Massobrio, R., Nesmachnow, S.: Urban Mobility Data Analysis for Public Transportation Systems: A Case Study in Montevideo, Uruguay. *Applied Sciences* 10(16), 5400 (2020)
10. Nesmachnow, S., Baña, S., Massobrio, R.: A distributed platform for big data analysis in smart cities: combining intelligent transportation systems and socioeconomic data for Montevideo, Uruguay. *EAI Endorsed Transactions on Smart Cities* 2(5), 1–18 (2017)
11. Nesmachnow, S., Iturriaga, S.: Cluster-UY: Collaborative Scientific High Performance Computing in Uruguay. In: *Communications in Computer and Information Science*, pp. 188–202. Springer (2019)
12. Nesmachnow, S., Muraña, J., Goñi, G., Massobrio, R., Tchernykh, A.: Evolutionary approach for bus synchronization. In: *High Performance Computing*, pp. 320–336. Springer (2020)
13. Risso, C., Nesmachnow, S.: Designing a Backbone Trunk for the Public Transportation Network in Montevideo, Uruguay. In: *Smart Cities*, pp. 228–243. Springer (2020)

Plataforma de Movilidad Compartida Metropolitana (PMCM). Sistema tipo MaaS. Córdoba, Argentina. Ciencia y tecnología al servicio de los vecinos.

Leandro Alberto Giménez¹
Claudio José Paz²

¹ Facultad de Arquitectura Urbanismo y Diseño. Universidad Nacional de Córdoba, Haya de la Torre s/n, Córdoba, Argentina.

leandro_gimenez@live.com

² Centro de Investigación en Informática para la Ingeniería. Universidad Tecnológica Nacional, Regional Córdoba, Maestro M. López esq. Cruz Roja, Córdoba, Argentina.

cpaz@frc.utn.edu.ar

Resumen. Desde hace décadas el éxodo constante de la población rural a centros urbanos y especialmente a grandes urbes en busca de mejores condiciones de vida y laborales han generado un cambio de paradigma en las ciudades actuales con retos a futuro cada vez más complejos a resolver. Dentro de estos uno no menos importante es la movilidad urbana.

En la actualidad, según la revisión de 2018 del informe “Perspectivas Mundiales de Urbanización” elaborado por la Organización de Naciones Unidas (ONU), el 55% de la población mundial vive en áreas urbanas y nuestra realidad latinoamericana no escapa a esa tendencia. Por el contrario, lleva adelante crecimientos poblacionales exponenciales en diversos casos. Este proceso de urbanización constante genera grandes planteos y desafíos a nivel social, económico y político.

La movilidad urbana plantea retos que antiguamente se abordaban con perspectivas muy diferentes a lo que actualmente se requiere para generar soluciones íntegras de mediano y largo plazo. En la actualidad el estado necesita de una sinergia público-privada para atacar las diversas problemáticas que surgen de las nuevas formas de desplazamiento dentro de una ciudad.

El presente trabajo aborda la problemática actual de la movilidad urbana en el ámbito del área metropolitana de la ciudad de Córdoba, Argentina proponiendo luego de indagar el presente una solución sustentable en el tiempo. La misma se materializa en una Plataforma de Movilidad Compartida Metropolitana (PMCM) de tipo MaaS (Mobility as a Service) que posibilite la sinergia del conjunto de actores presentes y un cambio desde los modos de transporte de propiedad personal hacia la movilidad que se desarrolle como servicio (SM).

El proyecto no tiene razón de ser si no se apoya en la ciencia y la tecnología. Sin embargo el éxito del mismo depende del aporte social, de la sinergia colectiva, el aporte de conocimiento dado por vecinos, usuarios, organizaciones, instituciones, estado; en fin, el común de la sociedad involucrada puede lograr un cambio de paradigma en beneficio propio y las generaciones futuras.

Palabras claves: Movilidad Urbana Sustentable, Smart City, Córdoba Argentina Sustentable, MaaS, Movilidad Compartida.

2

1 Introducción

1.1 Contexto

La realidad latinoamericana actual de las grandes áreas metropolitanas y más precisamente dentro del territorio nacional argentino se encuentra atravesada en su mayoría por la falta de planificación estratégica a corto, mediano y largo plazo. Esto conlleva el constante deterioro de la calidad de vida de sus habitantes, la falta de previsión, la contaminación medio ambiental y la utilización de recursos de manera no eficiente.

En la actualidad, según la revisión de 2018 del informe “Perspectivas Mundiales de Urbanización” elaborado por la Organización de Naciones Unidas (ONU), el 55% de la población mundial vive en áreas urbanas [1]. La ciudad de Córdoba, con aproximadamente 1.329.604 habitantes [2], y una importante área metropolitana, no ha escapado a esta tendencia de las grandes urbes y no es ajena a los principales problemas de movilidad urbana que presentan la mayoría de las grandes ciudades de América Latina, e inclusive de algunos países desarrollados.

El problema de la movilidad urbana, está totalmente ligada al proceso de urbanización sin planificación previa [3]. Por eso, la industrialización y el crecimiento económico del país, tuvieron como efecto el crecimiento acelerado de las ciudades sin el desarrollo de la correspondiente infraestructura y equipamiento, entre ellas, las del transporte [4].

El problema de la movilidad puede ser entendido como la necesidad de comunicación, movilidad de bienes, personas y servicios, originada por las actividades urbanas de producción, provisión, recreación, etc [5]. Las personas viven en un lugar y necesitan realizar sus actividades productivas, de servicios, de consumo y recreación en sitios diversos. Se entiende a la movilidad como los diferentes modos de desplazamientos que permiten la realización de las actividades humanas.

Por otro lado, el alto costo de la tierra urbana y la concentración de actividades, hace que las ciudades se densifiquen y con ello sea crítica la generación de nuevos espacios físicos e infraestructura para la movilidad. De esta manera, surge la necesidad de desarrollar e incentivar formas de movilidad masiva por sobre los modos individuales para proveer más oferta y una mejor utilización del sistema y del espacio público ya existente. Se trata de mejorar el sistema de transporte masivo, adecuándolo a la demanda presente y prevista, de manera de lograr una movilidad urbana segura, fluida y confiable que permita mejorar la calidad de vida de los habitantes de la ciudad [6].

1.2 Conceptualización

Actualmente las grandes urbes en su búsqueda de eficiencia y sustentabilidad indagan entre otros campos en las economías colaborativas y proyectan a partir de ellas planteos tanto a presente como a futuro y articulan esquemas de sinergia con el fin de dotar al ámbito urbano de herramientas que permitan dar soluciones tangibles al cúmulo de actores que en ella interactúan. Esta tendencia persigue la optimización de los costos de transporte individual, reducción de contaminación ambiental, introducción de tecnología entre otros impactos positivos. En este contexto actualmente los denominados sistemas de Movilidad Compartida (SM) han tenido en los últimos años crecimientos exponenciales [7].

La evolución actual de las plataformas digitales, la geo localización de dispositivos y con estos de usuarios, el concepto de *big data*, la tecnología IoT y el blockchain potencian estos desarrollos, pero también se considera que las mismas no son suficientes para resolver de manera integral la complejidad de la movilidad urbana y sus casos puntuales según los ámbitos de aplicación y realidades [8]. A futuro el reto es aún mayor y es allí donde la intención de esta propuesta pretende centrarse e indagar en busca de nuevos sistemas de movilidad urbana de tipo MaaS (Mobility as a Service) vinculados de manera estratégica a la Agenda 2030 de ODS ONU para el Desarrollo Sostenible y en particular los Objetivos 3, 6,7, 9, 11, 12, 13 y 16 [9] todos vinculados a los ODS ARGENTINA Agenda 2030 [10].

La Movilidad como Servicio (MaaS) describe un cambio desde los modos de transporte de propiedad personal hacia la movilidad que se brinda como servicio [11]. Esto se materializa combinando servicios de proveedores de transporte públicos y/o privados a través de una plataforma de enlace única que articula y gestiona viajes en la que los usuarios pueden acceder para solicitar, abonar, gestionar y tomar beneficios por dichos viajes desde una cuenta virtual y/o e-wallet.

Así, los usuarios pueden acceder a un abono por viaje único o una tarifa mensual por una distancia limitada. El concepto clave detrás de MaaS es ofrecer a los viajeros soluciones de movilidad basadas en sus necesidades de viaje reales optimizando la respuesta con un servicio ajustado a demanda, pero también deben articular beneficios a los actores involucrados como descuentos en tasas e impuestos, accesos a exenciones fiscales, descuentos en programas de fidelización y fomento, en fin, brindar herramientas que permitan la aceptación, masificación y fidelización de usuarios dentro de un ecosistema de movilidad urbana sustentable ampliando sus ofertas para persuadir a mayor cantidad de actores a futuro.

Los sistemas MaaS (Mobility as a Service) permiten desarrollar marcos de interoperabilidad necesarios para diversas plataformas de transporte. Interoperabilidad es la clave en el desarrollo de las ciudades inteligentes para poder gestionar mejor el flujo de viajeros. Y con ella, también son decisivos tanto las forma de pago como la gestión, monitoreo y control de los datos generados.

4

Las entidades públicas requieren poner a disposición de los *ecosistemas* que se generen a futuro la explotación de los datos y crear organismos de control, de forma que todos los actores colaboren de forma pro activa en la movilidad. Por ejemplo, una plataforma en la nube permite intercambiar y consumir información entre sistemas, servicios y proveedores de transporte de manera interoperable. Esto, a su vez, permite a los proveedores integrarse en el ecosistema, con mínimo esfuerzo y costo, y poner sus datos a disposición de servicios y usuarios de forma transparente.

1.3 Área metropolitana de Córdoba y su realidad actual.

La provincia de Córdoba es una de las 24 jurisdicciones que componen la República Argentina. Se encuentra localizada en la zona central del país con un área de 165,321 km² dividida en 26 departamentos que representan el 4.4% del territorio nacional. Según el censo de 2010, la provincia de Córdoba cuenta con 3.308.876 habitantes, con una densidad de 20 hab/km² y un crecimiento inter censal de la población (2001 – 2010) de 7.9% [12].

El departamento Capital integrado por la ciudad de Córdoba es la principal ciudad de la provincia. El 83% de la población del Área Metropolitana de Córdoba (AMC) vive en la ciudad de Córdoba [13]. Córdoba es una ciudad de más de 400 años de antigüedad con un centro histórico importante, y una fuerte identidad, con una alta calidad educativa que la posiciona como receptora de estudiantes universitarios de todo el país y del mundo.

La ciudad de Córdoba, capital de la provincia homónima y segunda urbe en importancia de Argentina, representa el 0,35% de la superficie de la provincia, el 40,18% de la población provincial y el 3,31% de la población nacional [14]. Su ubicación en el área central productiva del país es estratégica dentro de la región que comprende el tratado del Mercosur y el corredor bioceánico por lo que sirve de nexo entre ciudades, provincias y países [15]. La configuración actual de la ciudad de Córdoba responde a un complejo conjunto de factores históricos, económicos, políticos, sociales, geográficos y culturales.

Desde una visión integral del concepto de Movilidad Urbana Sustentable y para interpretar su realidad local hay que referirse a la ciudad de Córdoba como un área metropolitana en la cual interactúan un conjunto de poblaciones satélites, las cuales están atadas a la dinámica diaria de la metrópolis [16]. Con este enfoque se tienen en cuenta los flujos de viajes en la ciudad de Córdoba y en su área metropolitana (Villa Carlos Paz, Alta Gracia, Malagueño y Bouwer, La Calera-Dumesnil, Saldan, Villa Allende, Mendiolaza, Unquillo, Río Ceballos, Juarez Celman, Malvinas Argentinas, Mi Granja, Montecristo y Toledo). En la Fig. 1 se aprecia la distribución geográfica del Área Metropolitana de Córdoba y la distancia en kilómetros que abarca.

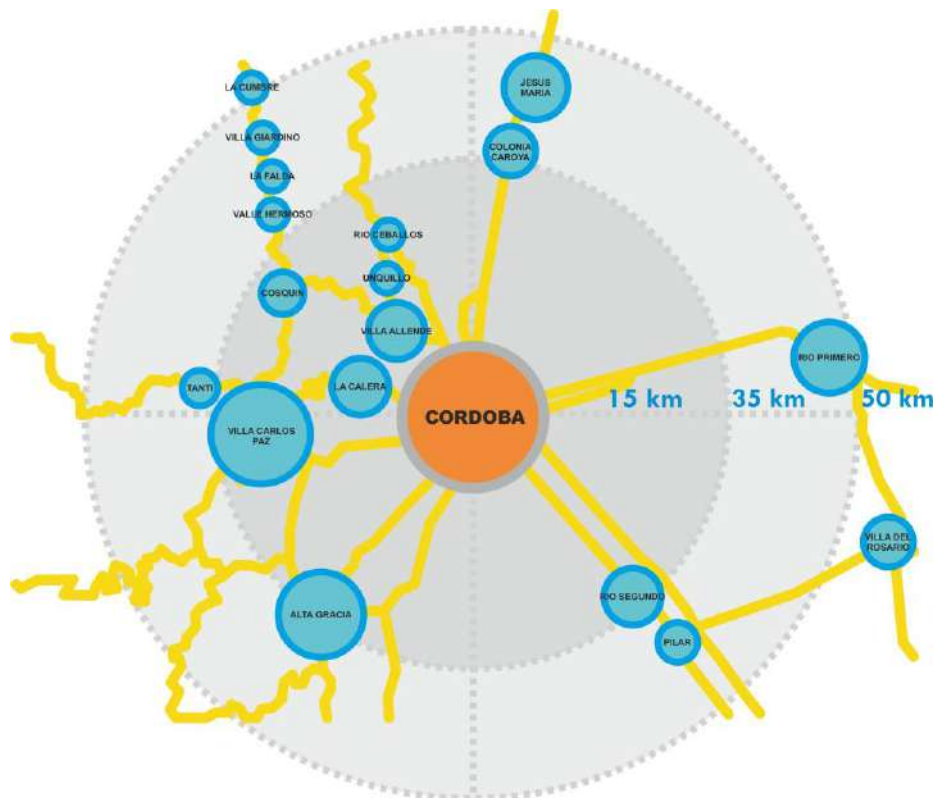


Fig 1. Esquema referencia. Área metropolitana Córdoba (AMC).

Según la Encuesta Origen-Destino del año 2009/2010 la población estimada para el Área Metropolitana (AMC) [9], en conjunto con la Ciudad de Córdoba es de **1.581.113 individuos** que habitan **479.780 hogares**, los que realizan **2.705.310 viajes diarios**. Del mismo estudio surge que el promedio de viajes por día hábil/persona es de 2,47 considerando el grupo de personas que realiza al menos un traslado al día. Si se tiene en cuenta la totalidad de la población este promedio desciende a 1,84 viajes por persona. (Fig 2)

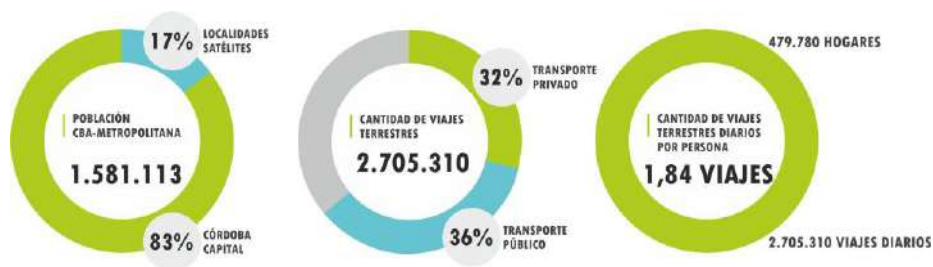


Fig 2. Encuesta Origen-Destino del año 2009/2010. PTUMA.

6

La movilidad en la ciudad de Córdoba, tal como se la conoce en la actualidad, adolece de serias deficiencias estructurales, que se materializan en problemáticas como las siguientes:

- La congestión de tránsito y con ello la pérdida de tiempo de los usuarios.
- La contaminación del medio ambiente, y el deterioro en la calidad de vida, con sus costos asociados.
- El sobre consumo energético de combustibles de origen fósil no renovable.
- Infraestructura vial deficiente, desactualizada y escasa para el parque automotor actual.
- Los accidentes causados por la falta de observancia de las normas de tránsito.
- El deterioro de los vehículos, el estrés de los conductores y las consecuencias psico-físicas en su salud [18].

La situación actual del transporte público masivo de pasajeros ofrece un único servicio a través de ómnibus y trolebuses teniendo para esto una red de servicio anacrónica, deficiente y obsoleta. Además, debido a la magnitud en superficie y las distancias de recorridos dentro de la ciudad no logra ofrecer una solución satisfactoria para los actores afectados (usuarios, empresarios, organismos públicos, y trabajadores relacionados con la actividad). Esto genera efectos de ineficiencia los cuales se agudizan ante factores tales como:

- Un crecimiento explosivo de la ciudad, que escapa a todo intento de planificación, genera mayores necesidades de desplazamientos por una nueva redistribución de las actividades ya existentes, y la incorporación de nuevos orígenes y destinos para los movimientos en la ciudad. Estas dos últimas son las fuentes de la demanda de transporte y cada una de ellas con diferentes dinámicas de exigencias y crecimiento en el tiempo.
- La no elasticidad física en la oferta de la infraestructura necesaria y del equipamiento vial urbano.
- El explosivo crecimiento del parque vehicular en los últimos años. Esto sumado a lo indicado en los puntos anteriores impacta en situaciones cada vez más frecuentes de congestión.

2 Propuesta piloto Plataforma Movilidad Compartida Metropolitana (PMCM)

2.1 Objetivos generales.

El concepto de servicio de movilidad compartida tipo MaaS (Mobility as a Service) tiene como eje principal el cambio de paradigma en la percepción actual del vehículo de transporte automotor como un bien privado, por una nueva perspectiva de horizonte donde el mismo debe transformarse indefectiblemente en una pieza dentro de un servicio integral de movilidad a nivel urbano. Esto permitirá la multiplicidad de elementos combinados dentro de una red multimodal [19].

Dicho esto es importante manifestar que la presente propuesta pretende articular un espacio de consenso donde el principal resultado que se persigue es dotar a la ciudad de una estrategia sustentable en el tiempo dando claros indicios de transformación a corto, mediano y largo plazo. Para esto es necesario un cambio de paradigma y una transformación profunda y novedosa en la forma de abordar un problema anacrónico que a futuro se torna insostenible en el ámbito de la ciudad de Córdoba y su área metropolitana. Es por esto que la principal meta es materializar los siguientes objetivos generales:

- **Promover** espacios de articulación, investigación, y gestión pública privada con el fin de llevar adelante análisis de casos actuales de movilidad urbana sustentable mediante la implementación de sistemas MaaS en grandes urbes a nivel mundial mediante la promoción de sitios piloto o *living labs* dentro del ámbito metropolitano de Córdoba.
- **Investigar** casos testigos de Smart City tomados como ejemplo a nivel latinoamericano y global y reconocer en ellas los factores que llevaron a esos resultados. Reconocer planes estratégicos, iniciativas público-privadas, aportes normativos, regulaciones y soluciones de escala micro, macro región y de escala global.
- **Indagar** en los conceptos de economía colaborativa y movilidad urbana sustentable mediante la implementación de sistemas MaaS a fin de detectar herramientas, estrategias y casos que permitan apoyar la investigación y dar bases sólidas a futuros desarrollos de Plataformas de Movilidad Compartida Metropolitana.
- **Estructurar** una plataforma física-virtual en la cual se condense toda la información recolectada, aprendida, ensayada, transferida y aplicada en políticas públicas, desarrollos privados, modelos comerciales, inteligencia artificial, plataformas colaborativas, experiencias de usuarios, blockchain y criptomonedas a fin de poder procesarla y volcarla luego en futuros proyectos referidos a la materia.

2.2 Objetivos específicos.

Dentro de esta amplia red de vinculaciones generales la idea de negocio que se pretende explotar es la de Vehículos Públicos y/o Privados hacedores de una Plataforma de Movilidad Compartida Metropolitana (PMCM). El usuario propietario o arrendatario de un vehículo particular y/o público tiene la posibilidad de articular la movilidad de usuarios de manera rentable y eficiente en la modalidad “hogar al trabajo”, “hogar a recreación” y/o “hogar a obligaciones” mediante la utilización de flotas de vehículos con conductor asignado utilizando para su funcionamiento una plataforma en la cual se vinculen usuarios, vehículos, gestores y controladores.

Los objetivos específicos de la propuesta piloto es desarrollar dicha plataforma materializando una aplicación de usuario, un servicio de back-office, equipos de abordaje para vehículos intervinientes, sistema de pago de última generación, etc. Todo esto integrando tecnologías ya mencionadas como sistemas de posicionamiento global, big data, IoT, blockchain, e-wallets, criptomonedas, etc.

Los componentes en desarrollo dentro del piloto son los siguientes:

- **Consumidor:** aplicación móvil, sitio web y también dispositivos móviles (vehículos).
- **Back-office:** gestión de solicitudes de viajes, algoritmos de enrutamiento óptimos, recopilación de datos de viajes de pasajeros y vehículos, trazado de recorridos virtuales, gestión de incidentes, alta, baja o bloqueo de usuarios.
- **Equipo a bordo en vehículos:** dispositivo móvil para la interacción del conductor designado con la plataforma, conectada a una central de despacho *inteligente*.
- **Pagos:** un sistema de blockchain vinculado a un entorno de criptomonedas permite procesar las solicitudes de viaje a usuarios por el uso de e-wallets, tarjetas sin contacto, etc. El vehículo de transporte puede estar equipado con un elemento para validar reservas de viajes e identidades de usuarios al momento de tomar las solicitudes. Existe la posibilidad de efectivizar las transacciones por medio de tarjetas sin contacto y/o móviles como medio de pago menos complejos de resolver en cuanto a desarrollo, validación y aplicación.

Las entidades públicas deberán poner a disposición del ecosistema la explotación de los datos y crear organismos de control, de forma que todos los actores colaboren de manera colectiva en la movilidad urbana resultante. Gracias a modelos como el *cloud* esto ya es posible (la sangre del transporte); una plataforma en la nube permite intercambiar y consumir información entre sistemas, servicios y proveedores de transporte de manera interoperable [20]. Esto, a su vez, permite a los proveedores integrarse en el ecosistema, con mínimo esfuerzo y coste, y poner sus datos a disposición de servicios y usuarios de forma transparente [21].

3 Conclusiones

En este trabajo se presentó un sistema innovador en un ámbito tan complejo y poco planificado como el de la ciudad de Córdoba. En él, se involucran actores públicos y privados persiguiendo metas en común y aplicando desde el campo de la ciencia y la tecnología conocimiento, herramientas y desarrollos para materializar soluciones de Movilidad Urbana Sustentable. Actualmente están implementándose en gran cantidad de prototipos y pilotos, en diversas partes del planeta [22], soluciones similares atendiendo a necesidades de movilidad urbana mediante living labs [23].

El ecosistema de desarrolladores tecnológicos locales no presenta empresas que estén trabajando en un servicio idéntico, es por esto lo importante de la vinculación y puesta en práctica de concertaciones público-privadas capaces de articular de manera urgente estrategias escalables y replicables en el área metropolitana mediante pilotos o living labs.

Pueden sumarse a la iniciativa empresas que actualmente brindan servicio de transporte tradicional de ómnibus, taxis, remises y transfers en carácter de prestatarios de servicios, empresas desarrolladoras de software y hardware, vehículos eléctricos autónomos, inteligencia artificial, desarrollo aeroespacial y/o geo posicionamiento, instituciones públicas o privadas, educativas, organismos de gobierno todas afines para dar soporte en etapas de investigación, validación y puesta en funcionamiento experimental. Es importante mencionar que el ámbito nacional e internacional presenta plataformas como Uber, Cabify, Whimm, Ubigo o similares que tienen una génesis similar a la que se propone en este proyecto pero que no son necesariamente idénticas por naturaleza, funcionalidad, servicio y finalidad.

La propuesta también depende de la financiación para su desarrollo y materialización es por esto que un dato no menor es la estrategia de escala y captación de fondos desde su origen. Los ingresos van a proceder de varias fuentes dependiendo la etapa en desarrollo. El principal es a través del financiamiento privado para el desarrollo, posicionamiento y puesta en funcionamiento. Luego una vez funcionando el sistema se monetizan los ingresos mediante los pagos efectuados por los usuarios por medio del uso de una aplicación, el licenciamiento del servicio a prestatarios y el cobro de un canon al estado donde tenga aplicación el sistema. Por último pero no menos importante es la inyección de capitales por medio de inversiones públicas o privadas en fases críticas de desarrollo del proyecto.

La implementación de sistemas de blockchain e e-wallets permite además, vincular la monetización del sistema entre los actores y ofrece la posibilidad de articular y efectivizar beneficios extras como exenciones impositivas, reducción de tasas, alianzas promocionales entre actores del ecosistema. Todos y cada uno materializados

10

en el uso de criptomonedas, dando seguridad en las transacciones y controlando que los usuarios sean los beneficiarios finales de dichos programas.

Los resultados financieros que el proyecto muestre por su naturaleza y el medio donde se desarrolla requiere además de trabajo de promoción y validación para atraer usuarios y actores interesados en sumarse al ecosistema. El plan de acción de comunicación debe centrarse en persuadir a usuarios potenciales a que abandonen su automóvil privado y cambien por un modo de transporte más ecológico y de carácter público/privado compartido. El poder y la influencia de las redes sociales e internet son indiscutibles. De esta manera, la promoción a través de redes sociales, plataformas virtuales de estados, organismos u otros sitios web locales será vital para persuadir a los propietarios de automóviles privados. Rompiendo el paradigma actual el proyecto conseguiría aceptación y por consiguiente funcionamiento. Trayendo consigo las fuentes de financiamiento para darle sustento económico a la propuesta.

El proyecto no tiene razón de ser si no se apoya en la internet de las cosas, inteligencia artificial, machine learning, big data, geo posicionamiento satelital, blockchain, criptomonedas, e-wallets, etc. Pero también el éxito del mismo depende de la conciencia social, de la sinergia colectiva, del aporte de conocimiento dado por usuarios, los cuales en conjunto deben tomar partida e involucrarse. Por todo lo antes mencionado es una propuesta atada a una realidad actual de desigualdades y deberá recurrir a la ciencia y la tecnología para dar soluciones al conjunto de actores involucrados, en especial a los vecinos de la ciudad de Córdoba, los cuales sufren a diario la falta de planificación y respuestas sustentables dentro de un área metropolitana que se encuentra atravesada por todas las variables antes mencionadas.

4 Agradecimientos

Los agradecimientos se hacen extensivos a cada uno de los participantes que mediante su asesoramiento, consejos, enseñanzas, aportes profesionales y personales permitieron dar forma a este proyecto, el cual a la fecha sigue nutriéndose del conocimiento, capacidad y generosidad de ellos. En especial al Ing. Cristian Senyk por sus aportes referidos a la factibilidad técnica.

Referencias

1. ONU: Perspectivas Mundiales de Urbanización. 2018. <https://www.un.org/development/desa/publications/2018-revision-of-world-urbanization-prospects>. Julio 2020.
2. INDEC, Instituto Nacional de Estadística y Censos. República Argentina. Censo Nacional de Población, Hogares y Viviendas 2010. Agosto 2020.
3. Comisión de Elaboración del Plan Integral de Movilidad CEPIM, Municipalidad de Córdoba, Argentina. 2018. Julio 2020.
4. Pre diagnóstico, Plan de Movilidad Urbana Ciudad de Córdoba, mayo del 2012. Julio 2020.
5. Líneas estratégicas para el desarrollo de Córdoba. IPLAM Ciudad. Municipalidad de Córdoba, Argentina. Año 2015.
6. Comisión de Elaboración del Plan Integral de Movilidad CEPIM, Municipalidad de Córdoba, Argentina. 2018.
7. RACC Blog. Movilidad colaborativa: 4 formas de compartir coche. <http://blog.racc.es/category/nueva-movilidad>. Julio 2020.
8. The promises of big data and small data for travel behavior. Cynthia Chen, Jingtao Mab, Yusak Susilo, Yu Liu, Menglin Wange. Traffic Technology Services, Portland, USA Royal Institute of Technology, KTH, Sweden Institute of Remote Sensing and Geographical Information Systems, Peking University, China. Cambridge Systematics, Chicago, USA. 23 April 2016.
9. UNESCO ODS, <https://es.unesco.org/sdgs/> Julio 2020.
10. ODS ARGENTINA, <https://www.odsargentina.gob.ar/> Julio 2020.
11. Galileo from mobility. The technology <http://www.galileo4mobility.eu/the-technology/> Julio 2020.
12. INDEC, Instituto Nacional de Estadística y Censos. República Argentina. Censo Nacional de Población, Hogares y Viviendas 2010.
13. Encuesta Origen Destino 2009, Municipalidad de Córdoba, provincia de Córdoba.
14. INDEC, Instituto Nacional de Estadística y Censos. República Argentina. Censo Nacional de Población, Hogares y Viviendas 2010.
15. Córdoba una Ciudad en cifras 2012. Municipalidad de Córdoba, provincial de Córdoba.
16. Galileo from mobility. The technology <http://www.galileo4mobility.eu/the-technology/> . Julio 2020.
17. Encuesta Origen-Destino del año 2009/2010. PTUMA. Agosto 2020.
18. Pre diagnóstico, Plan de Movilidad Urbana Ciudad de Córdoba, mayo del 2012. Agosto 2020.
19. Aplicación de Movilidad Compartida en la ULPGC. M. Roger-Hernández, J. J. Sánchez-Medina y J. A. Herrera-Melián. Centro de Innovación para la Sociedad de la Información (CICEI), Instituto Universitario de Ciencias y Tecnologías Cibernéticas (IUCTC), Campus

12

- de Tafira, 35017, ULPGC. Oficina de Sostenibilidad de la ULPGC, Mediateca, Campus de Tafira, 35017.
20. W. Lam y M. Bell. *Advanced Modeling for Transit Operations and Service Planning*, Emerald Group, Bingley, UK (2002).
 21. L. Figueiredo, I. Jesus, J. Machado, J. Ferreira y J. De Carvalho. *Towards the development of intelligent transportation systems*. In *Intelligent Transportation Systems* (2001).
 22. *Planificación de transporte urbano en ciudades inteligentes*. Sergio Nesmachnow, Renzo Massobrio, Alfredo Cristóbal, Andrei Tchernykh. Universidad de la República, Uruguay. Universidad de Cádiz, España. Universidad Veracruzana, México. Centro de Investigación Científica y de Educación Superior de Ensenada, México.
 23. *Paris Cité Descartes (Car and bike-sharing) – Galileo For Mobility*. Descartes Vallée de la Marne, Francia.

Development of IoT Services Applied to a Photovoltaic Generation System Integrated with Vegetation

Maria Camargo-Vila¹, German Osma-Pinto¹, and Homero Ortega-Boada¹

¹Universidad Industrial de Santander, Bucaramanga, COL,
alejandravila.2232@hotmail.com

Abstract. The Internet of Things (IoT) has been transforming different sectors of society, facilitating the integration of technologies to offer various types of services that meet the needs of the world. Renewable energy sector has been involved in this new paradigm. Specifically, this work focuses on green roof integrated photovoltaic system. These types of systems offer a scenario of heterogeneous objects that are responsible for sensing different variables that serve as support for their maintenance, operation, control and study. Due to the diversity of technologies used, challenges appear in relation to the integration, storage and processing of information. In some cases, it is not easy to achieve these processes due to the connectivity and interconnectivity limitations of the equipment, associated with the manufacturing family. Therefore, this document aims to present the design and implementation of a prototype of an IoT service platform for monitoring a photovoltaic generation system integrated with vegetation. In this context, the first challenges of these systems are addressed from the perspective of IoT and under the enterprise architecture approach.

Keywords: IoT, Enterprise architecture, Photovoltaic system, Green roof

1 Introduction

The Internet of Things (IoT) is an emerging architecture based on the global Internet. It facilitates the exchange of goods and services between networks that belong to a supply chain and ensures the security and privacy of the stakeholders. It has become a trend in different sectors of industry, engineering, medicine and society, providing new opportunities for data access, services in education, healthcare, transportation, etc. Additionally, it has become a key element to increase productivity in companies through local networks and smart devices that meet customer needs [1].

The International Telecommunications Union (ITU) indicates that the IoT is a “global infrastructure at the service of the information society. The IoT propitiates the provision of advanced services through the interconnection (physical

2 Maria Camargo-Vila et al.

and virtual) of things thanks to the interworking of information and communication technologies (existing and evolving)” [2, 3]. Under this concept, the reference model of IoT was defined, which was used as a fundamental basis for the development of this work.

This model is made up of four layers: the application layer contains all the IoT applications; The services and applications support layer consists of generic capabilities that can be used by different IoT applications and specific capabilities that meet the particular needs of each of these; the network layer that offers network and transport capabilities; and finally the device layer that has device and gateway capabilities. Besides this, this model also associates each one of the layers, management and security capabilities in a transversal way [4].

Within this context, a sector involved in the world of IoT is energy. Specifically, this work deals with Green Roof Integrated Photovoltaic systems (GRIPV). Photovoltaic (PV) panels embedded in green roofs are green technologies that provide environmental benefits. On one side, PVs are a low-carbon renewable energy source; and green roofs mitigate the heat island effect in the cities, improving air quality, regulating temperature and providing protection to the building cover, among others [5, 6]. A growing number of studies have shown that their combination is an interesting option for the use of the roof of buildings. This configuration jointly takes advantage of the previous mentioned benefits and in addition the possible synergic effects between plants and PV [7, 8].

GRIPV systems monitoring provides the necessary information for their maintenance, operation and control, as well as for their study for academic or industrial purposes. This monitoring involves sensing different types of electrical and environmental variables, related to PV, the vegetation of the green roof and the climatic conditions of the site where the system is located. This monitoring involves a great variety of equipment and technologies and this means dealing with the incompatibilities and differences that may happen between them. For example, some equipment is tied to the software and certain functionalities of the manufacturer. This limits its storage capacity for variables, interconnectivity with other devices and the integration of information in a database. There are also other devices that do not have internet connectivity. This always makes difficult the access to information, the monitoring and off-site controlling.

From this situation arises this work which has as purpose designing and implementing a prototype of a service platform based on IoT for monitoring, control and study of GRIPV systems, integrating heterogeneous components from various manufacturers, that allow users and enterprises to select components from different providers according its availability, devices features and budget or even local development of them. All this combining the IoT reference model with the enterprise architecture (EA) under the TOGAF framework. EA is a new component that was decided to include to take advantage of the benefits and achieve an entrepreneurial vision design. This is intended to facilitate decision-making that may come up for the most diverse reasons [9].

EA dates back to the late 1980s, from which multiple methodologies have emerged for its development, with a common goal, to put technology at the

service of the business [10]. The ISO / IEEE defines EA as “The fundamental organization of a system, included in its components, the relationships between them and the principles that govern their design and evolution”. In this way, it becomes a tool capable of aligning the business with information technologies, going from being a theoretical concept to one applicable for the organization [11].

Consequently, the platform prototype was proposed from the EA approach under the TOGAF framework. This framework offers a methodology that allows continuous improvement of the organization, through the alignment of processes, data, applications and technological infrastructure. Facilitates and supports design decisions. Finally, it creates a transferable abstraction of the system description for everyone involved [12].

Thus, the platform is mainly composed of three layers, the business layer, the application layer, and the technological and physical infrastructure layer. Each of them is responsible for attacking specific problems. As a result, a whole is obtained that adjusts to the needs of the stakeholders, from the capture of information, its processing and storage, to its visualization.

The rest of the document is organized as follows: Section 2 presents the literature related to this document. Section 3 describes the case study for which the platform was designed and implemented. Section 4 shows the methodology developed together with the deployment of the platform. Finally, section 5 presents the conclusions.

2 Related literature

GRIPV systems seek to harmonize the use of green roofs in buildings with the use of PV, which will be each time more essential in green buildings. These two technologies are recognized in the American system of certification of sustainability of buildings LEED (Leadership in Energy Environmental Design).

In the literature, there are different works that are dedicated to studying the green roof-PV interaction [5, 6, 8, 13–26]. To this they analyze different electrical and meteorological variables; but they do not give information about the data acquisition process and/or the devices used. On the other hand, studies such as [7, 27–31] allow us to review some details about obtaining the information and the equipment used.

In general, regarding the device layer, there are sensors and devices with the capacity to measure electrical and climatic variables. Each of these belonging to a particular manufacturing family, which facilitates the communication and data sending to dataloggers compatible with them. In the case of using external information, for example, that coming from meteorological stations on site or from microinverters directly connected to the PVs, the integration process is not referred. Communication technology is mostly wired and there is only one case of WiFi use and one of Ethernet. Finally, the monitoring center is concentrated in a computer and there were no specifications on the software for the acquisition of

4 Maria Camargo-Vila et al.

information, storage and visualization. Excepting cases where Excel and Logger Net software were used.

On the other hand, there are also studies that only include the monitoring of PV systems, some make use of IoT solutions [32–35], and others do not [36–39]. In monitoring solutions that are not associated with the IoT, it is observed that specific sensors are used in the acquisition and communication layer. These can be easily connected to a microcontroller and this through an electronic board transmits the information to a SCADA software. This software is responsible for the management and processing of information and its display online. The most common communication technology is ZigBee and wired based, in addition to the introduction of the Modbus protocol. Finally, in relation to storage, use is made of specific devices, such as ROM-EEPROM or the online server.

Moreover, there are studies that implement monitoring and control solutions for PV systems supported by IoT. In these, the layer of devices for sensing variables and the layer of communication technologies, do not differ much from the previous works presented. The difference appears in the development of their own SCADA software and the inclusion of databases for storing information. And in relation to access to information, it can be consulted directly online.

In summary, according to the works found in the literature that specify details about the monitoring of GRIPV and PV systems, sensors and devices are used that allow an easy process of acquisition and sending of data. In general, all of these belong to the same manufacturer or are compatible with each other through common communication protocols. Therefore, in cases like these, the centralization of information is simpler. The data is sent by all the equipment to a data acquisition card that oversees communicating with the monitoring center and with the SCADA software. At this point, it is stored and displayed, generally online.

Consequently, the systems found do not present great challenges in terms of technology integration. In general, the devices used belong to the same family of manufacturers or, at worst, they are compatible with each other. This facilitates the tasks of sending and receiving information, processing and storing data, and viewing. Therefore, this work focuses on a system made up of various technologies. The objective was to achieve the connectivity and interconnectivity of the devices to the IoT network and with it the offer of different services that meet the needs of the stakeholders.

3 Case of Study

At the Universidad Industrial de Santander, the line of GRIPV systems has been developed. For the deployment of this type of research, the conditions for experimentation have been created on the terrace of the Electrical Engineering building of this institution. The GRIPV system, case of study of this research, is installed in this building. Figure 1.

The GRIPV system (at the date of this work) has a photovoltaic system with a capacity of 9,63 kW, associated with 37 panels. Each of these panels

has an associated M250 Microinverter from the manufacturer Enphase Energy, whose functionality is to deliver information on the photovoltaic injection to the electrical system.



Fig. 1. GRIPV system of the Electrical Engineering building

Enphase microinverters make use of the Enlighten platform, provided by their manufacturers, to supply information on the power delivered by each PV panel. This task is carried out with a time window of 15 minutes, allowing remote monitoring of the system. These teams are connected to a device called Envoy through AC power lines and this in turn with the router in situ, to transmit the data to the platform.

There are also two types of advanced energy meters. The AcuRev2020 meter performs measurements in real time, supports the open RS485 communication protocol (Modbus RTU) and has proprietary software. This allows you to configure it, monitor some of the variables in real time and download the information. And on the other hand, the Acuvim IIR multifunction digital power meter, which also supports the Modbus RS485 communication protocol (or optional Ethernet port) and all its power and energy parameters are visible through the software provided by the manufacturer.

In addition to this, there is an intelligent irrigation system for the green areas of the roof. The control of this system is carried out based on the level of soil moisture in each area. In addition, the soil temperature of each zone, the ambient temperature and the interior temperature of the boxes where the automation system is located are monitored. All this is done through humidity and soil temperature sensors, ambient temperature sensors and temperature sensors inside the control boxes. The control system is based on a core module (Arduino development board) and four sub modules (Arduino NANO board). These boards are responsible for receiving the data directly from the sensors and sending them to the central module through the XBee S2 module. In this

6 Maria Camargo-Vila et al.

last module, the necessary control actions are carried out, associated with each irrigation technique. The communication protocol used is ZigBee.

In this scenario are the initial challenges that are presented in GRIPV systems from the point of view of ICT. For the development of the different research works carried out on this type of system, a variety of devices are used, which makes the processes of data integration and the storage, processing and visualization of information more complex. All of this as a result of the connectivity and interconnectivity limitations of each of the components used for sensing variables, derived from the manufacturer or the technology they use.

In this context, we sought to resolve this type of conflict through the IoT, which precisely provides space for practically anything. The solution is proposed through a support platform open to different types of sensing and control technologies. And also, to those that take advantage of the cloud and offer the possibility of developing their own applications for end users with different needs.

4 Development of IoT services

This new horizon offered by the IoT brings with it various challenges. In this work it has been decided to address the modeling of the connectivity and interconnectivity of the devices to the IoT network. And in addition to that, their interaction with the services they will offer to achieve applications that are adapted to needs.

The solution proposed in this work for the interconnection of heterogeneous and ubiquitous objects, within the context of a photovoltaic generation system integrated with vegetation, is an IoT platform. This is responsible for supporting the unidirectional and/or bidirectional communication of the different devices. This seeks to meet the requirements of the stakeholders through the services developed.

This platform is designed in a modular way so that it can be extended by incorporating different modules. In addition to allowing a centralization of information acquisition, storage, processing and visualization services, through a web application that facilitates all these tasks.

In this way, the design and implementation of this prototype of an IoT service platform is developed under a methodology that combines the enterprise architecture approach and the IoT reference model. With this, it is possible to systematize the processes associated with the monitoring and control of this type of systems that use different sensing, measurement, control and communication technologies.

The methodology developed is briefly presented below, followed by a description of the design and implementation of the IoT service platform.

4.1 Methodology for the Development of IoT Services

The proposed methodology is part of the EA approach integrated with the IoT reference model. The TOGAF framework is taken as a reference because it allows

the generic development of architectures through its ADM method. These architectures can be modified and adapted to the changing needs of all stakeholders. In Figure 2 it is possible to see the general vision of the proposed methodology.

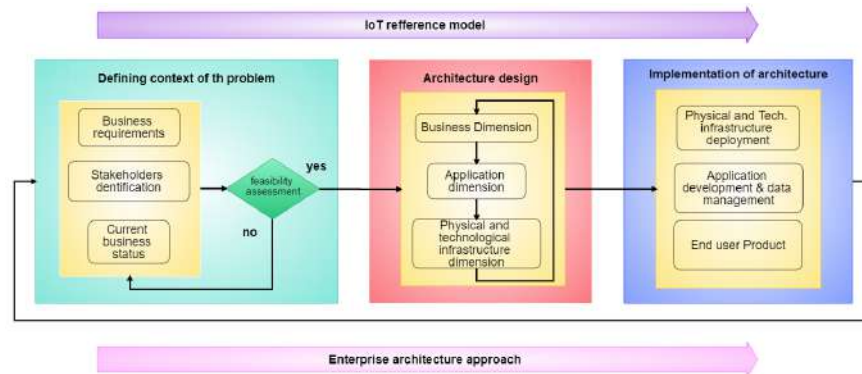


Fig. 2. Overview of the proposed methodology stages

The methodology has three main stages: Definition of the context of the problem, Design of the architecture and Implementation of the architecture. These stages feedback each other in order to carry out a continuous evaluation of the results of each process, so that they can be contrasted with the requirements set by all stakeholders.

The first stage of the methodology (Defining context of the problem) refers to the global vision of the business. This is understood as any activity, occupation, system or method whose main objective is to obtain an economic benefit [40]. But this definition is also extended to also include the value of academic productivity and research. This achieves the development of services that are useful for society in general and may in the future be a source of income for the same sector.

Clarifying this concept, this stage, fundamental basis for the design of the IoT service platform, consists of four steps: current state of business, identification of stakeholders, business requirements and feasibility evaluation.

The next stage (Architecture design) is attacked from an EA approach, with the purpose of approaching the development of IoT services from another point of view. It aims to guide the transformation of systems into intelligent environments, aligning the interests of stakeholders with the new paradigm of IoT. Putting this vision into an architecture that responds to the agility and flexibility needs that the digital world today demands.

EA is developed around three dimensions, the business dimension, the applications dimension, and the technological and physical infrastructure dimension. Each of these dimensions make up the layers of the architecture shown in Figure 3. The layers are composed of reusable architectural building blocks through which the creation of more specific architectures is possible. The architecture de-

8 Maria Camargo-Vila et al.

sign is developed under the open and independent modeling language ArchiMate for enterprise architectures [41].

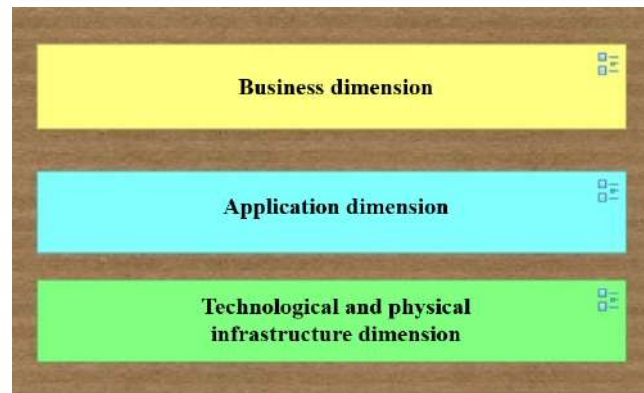


Fig. 3. Layers of the architectural model

Finally, the last stage (Architecture implementation) consists of modeling and prototyping the system. These must be approved by all stakeholders, in an iterative evaluation process that leads to the desired final product.

4.2 Design and Implementation of the IoT Services Platform

This section presents the design and implementation of the IoT service platform for the use case system. The platform prototype implemented through the proposed methodology is responsible for the centralization of all the data from the different devices and sensors and/or actuators. As a result, interaction and communication between them is possible through the creation of a ubiquitous network. This network solves the problem of interconnection of heterogeneous objects. This platform supports object registration, sending, receiving and processing of data and information management of the entire GRIPV system.

Definition of Problem Context In this first stage of the methodology, the current state of the business is described. In this case, reference is made to the GRIPV system installed on the terrace of the Electrical Engineering Building of the Universidad Industrial de Santander. The monitoring of this system is carried out thanks to various equipment and devices, which make use of different communication, storage and data download technologies.

The information from all the equipment in the system is managed in a decentralized way. This implies that data must be manually integrated for further analysis. This is time consuming work that requires constant human supervision and long periods of work.

This problem is the starting point to envision a service platform that meets this initial need for the GRIPV system. Achieving centralized management of the information from the different devices that make up the system is the basis of the challenges to be faced. The first one is the connectivity of all computers to the internet. Then, centralized and remote access to information. Finally, the processing and visualization of the information.

Once the current state of the business was described, the stakeholders were identified, they are represented by the members of the GISEL and RadioGIS research groups, attached to the institution. After the layers of the architecture had been explored, the functional and non-functional requirements that platform prototype must meet were formally established with each of the research groups. This is an essential task that allows to technically capture the needs detected for the efficient management of the GRIPV system.

Finally, in the last step of this stage, the functionality and needs presented by all stakeholders and future users were inspected by the designer with the support of experts in each of the relevant areas. Their analysis showed that the development of the prototype of a service platform based on IoT for the monitoring of a photovoltaic generation system integrated with vegetation is technically feasible and achievable. In addition, the interconnection of the heterogeneous objects of the system is recognized as a challenge, which goes hand in hand with the current challenges of the IoT.

Architecture Design The architecture design modeled with the Archi tool, under the three dimensions proposed in the methodology, can be seen in Figure 4.

The business dimension represents the final product that is delivered to the client, a website that allows access and administration of the entire system. This is made up of two components, the IoT service user and the access interface to the IoT service.

The applications dimension is responsible for establishing a bridge between the applications that the user uses and the subjacent layer that supports the transmitted information. This dimension is made up of two main elements, the database server and the application server. These two components share an application collaboration element, which represents precisely the joint work they carry out to support the services that are delivered to the end user.

The last dimension of the architectural model is the technological and physical infrastructure, mainly made up of the IoT terminal node, the server node, the development devices node and a component for connecting external platforms through the network.

Each of the nodes represent both computational and physical resources. They are the basis of the entire system, as they are responsible for supporting sending and receiving of information, storage and processing data and application development.

In this way, the modeling of each of the dimensions of the architecture results in the architectural model of the prototype of the platform. The overview of all

10 Maria Camargo-Vila et al.

the layers allows to appreciate each single components of the architecture. In addition, it shows how these are related to each other within their own layer and outside of it and with the components of the other layers.

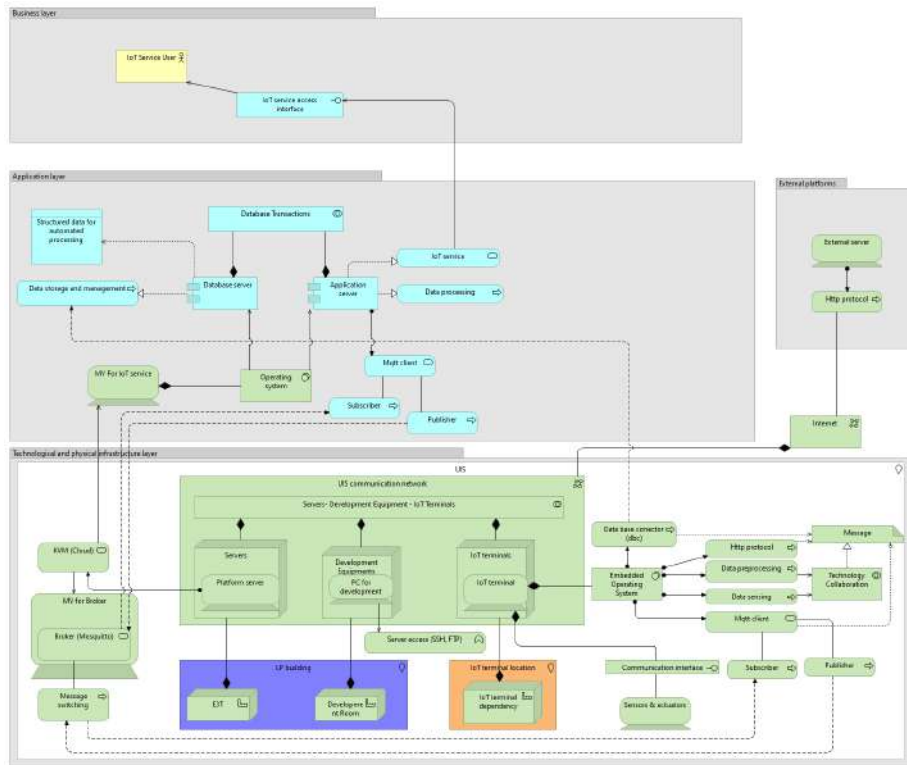


Fig. 4. Architectural model of the IoT services platform

Architecture Implementation It presents the implementation of the architectural model developed. At this point it is important to clarify that each of the layers of the architecture can be developed in parallel, since all the specifications and mapping of each of the components are available.

Technological and Physical Infrastructure Layer

The implementation of this layer covers the entire technological and physical infrastructure. These components are responsible for capturing and collecting data that will be used as input from the upper layers.

Each of the equipment, sensors and/or actuators of the system was mainly identified. All the objects that will be connected and from which the data will be obtained, in order to identify those that are IoT terminals and those that

are not. Once the differentiation of the system equipment has been carried out, there is an inspection for the first group of the information transfer process they offer, to connect them to the IoT network. And in the case of the second group, the devices are equipped with the capabilities of an IoT terminal, represented in the architectural model of this layer. Internet connectivity has main priority.

Once each of the system devices were adjusted to the IoT terminal model, the equipment that supports the server node and development equipment were reviewed to complete this layer.

Application Layer

In this layer are all the components in charge of supporting the interface between the underlying network that contains all the transmitted data and the applications of which the end user works with. The data storage and processing tasks oversee the server with Linux Mint operating system and a GNU / Linux community distribution. This is located within the facilities of the Electrical Engineering Building.

The installed database server corresponds to MySQL. The database was created subject to the requirements of the GRIPV system and supports the intelligent irrigation system and the energy meters of the entire photovoltaic system. On the other hand, the application server refers to an Apache Tomcat, which oversees the IoT service, under the client-server model.

Business Layer The business layer is the final product, a website (see Figures 5, 6 and 7) . It runs within the application server and can be accessed from any browser or web device. This application handles two types of access, one public where it is only possible to consult the information that does not handle any confidentiality restriction. And another type of private access that grants permissions to consult and download information from the system.

Finally, this effort results on a fully integrated GRIPV system along with an IoT platform which website allow users to access public and private information to monitor, storage and control the system using electrical variables of the building, generation and injection variables from solar panels and micro-inverters, meteorological variables (humidity and temperature) and irrigation variables (soil moisture and temperature).

5 Conclusions

The synergistic sum achieved with the inclusion of EA in the development of IoT services, provides concepts, models and instruments to face the challenges represented by the articulation of stakeholder requirements and business processes with ICT areas. Consequently, it is possible to generate greater value, improve performance, communication and integration in the alignment of technology with the business. In addition, it was proven how EA can also be adapted to the development needs of IoT services for GRIPV systems.

In this work, it has been demonstrated by construction that it was possible to develop an architecture for GRIPV systems, with an EA approach and based on the IoT reference model. The architecture presented in this work is a contribution

12 Maria Camargo-Vila et al.



Fig. 5. View of the variables associated with the microinverters of the photovoltaic system



Fig. 6. View of variables associated with advanced energy meters



Fig. 7. View of Management of smart irrigation system

to existing architectures in the Internet of Things community. At the time of development of this work, no works have been found that cover the structure that a GRIPV system must have.

Additionally, the implemented prototype achieves the integration of data from the different equipment and sensors that make up the GRIPV system. This becomes a breakthrough for the field which works on connectivity and interconnectivity of heterogeneous objects. Likewise, the platform prototype under the developed architectural model facilitates the integration of new and varied devices to the system.

Acknowledgments The authors wish to thank the Department Of Electrical, Electronics, and Telecommunications Engineering (Escuela de Ingenierías Eléctrica, Electrónica y de Telecomunicaciones); the Vice-Rectorate for Research and Extension (Vicerrectoría de Investigación y Extensión) from the Universidad Industrial de Santander (Project 8593 and Project 2525); and the Ministry of Science, Technology, and Innovation (Ministerio de Ciencia, Tecnología e Innovación)—MINCIENCIAS (Project - Contract No. 80740-191-2019 - Funding source).

References

1. Jordi Salazar and Santiago Silvestre. Internet de las Cosas. *PMQuality*, pages 1–27, 2014.
2. K. Rose, S. Eldridge, and C. Lyman. The Internet of Things: an overview. *Internet Society*, (October):53, 2015.
3. Bruno Baccino. Internet of Things - Oportunidades y desafíos. (August), 2015.
4. UIT. Descripción general de Internet de los objetos (Recomendación UIT-T Y.2060). page 20, 2012.
5. Bracha Y. Schindler, Lior Blank, Shay Levy, Gyongyver Kadas, David Pearlmutter, and Leon Blaustein. Integration of photovoltaic panels and green roofs: review and predictions of effects on electricity production and plant communities. *Israel Journal of Ecology and Evolution*, 62(1-2):68–73, 2016.
6. German Osma-Pinto and Gabriel Ordóñez-Plata. Measuring factors influencing performance of rooftop pv panels in warm tropical climates. *Solar Energy*, 185:112 – 123, 2019.
7. D. Chemisana and Chr Lamnatou. Photovoltaic-green roofs: An experimental evaluation of system performance. *Applied Energy*, 119:246–256, 2014.
8. Chr Lamnatou and D. Chemisana. Photovoltaic-green roofs: a life cycle assessment approach with emphasis on warm months of Mediterranean climate. *Journal of Cleaner Production*, 72:57–75, 2014.
9. Maria Camargo-Vila, German Osma-Pinto, and Homero Ortega-Boada. Enterprise architecture an approach to the development of iot services oriented to building management. In *Applied Technologies*, pages 207–221, Cham, 2020. Springer International Publishing.
10. Daniel Ricardo Cerinza Mejia. Modelo Para Medir Los Beneficios De Una Arquitectura Empresarial. 2015.

- 14 Maria Camargo-Vila et al.
11. Rafael Castillo Santos and Hernando Castillo García. *Arquitectura Empresarial y las Organizaciones Estatales*. 1(1):1–9, 2014.
 12. Hugo Fernando Sarasty España. *Documentación y análisis de los principales frameworks de arquitectura de software en aplicaciones empresariales*. PhD thesis, 2015.
 13. Chr Lamnatou and D. Chemisana. A critical analysis of factors affecting photovoltaic-green roof performance. *Renewable and Sustainable Energy Reviews*, 43:264–280, 2015.
 14. Xueping Li, Mohammad Ramshani, Anahita Khojandi, Olufemi Omitaomu, and Jon Michael Hathaway. AN AGENT BASED MODEL FOR JOINT PLACEMENT OF PV PANELS AND GREEN ROOFS. (Administration 2015):1133–1144, 2017.
 15. Jinlin Xue. Economic assessment of photovoltaic greenhouses in China. *Journal of Renewable and Sustainable Energy*, 9(3), 2017.
 16. Mohammad Ramshani, Anahita Khojandi, Xueping Li, and Olufemi Omitaomu. Optimal Planning of the Joint Placement of Photovoltaic Panels and Green Roofs Under Climate Change Uncertainty. (August), 2018.
 17. Adam Scherba, David J Sailor, Todd N Rosenstiel, and Carl C Wamser. Modeling impacts of roof reflectivity , integrated photovoltaic panels and green roof systems on sensible heat flux into the urban environment. 46:2542–2551, 2011.
 18. Amy Nagengast, Chris Hendrickson, and H Scott Matthews. Variations in photovoltaic performance due to climate and low-slope roof choice. 64:493–502, 2013.
 19. T. Nacer, A. Hamidat, and O. Nadjemi. Feasibility study and electric power flow of grid connected photovoltaic dairy farm in Mitidja (Algeria). *Energy Procedia*, 50:581–588, 2014.
 20. Chr Lamnatou and D. Chemisana. Evaluation of photovoltaic-green and other roofing systems by means of ReCiPe and multiple life cycle-based environmental indicators. *Building and Environment*, 93(P2):376–384, 2015.
 21. C. Nash, J. Clough, D. Gedge, R. Lindsay, D. Newport, M. A. Ciupala, and S. Connop. Initial insights on the biodiversity potential of biosolar roofs: a London Olympic Park green roof case study. *Israel Journal of Ecology and Evolution*, 62(1-2):74–87, 2015.
 22. Mohammed Alshayeb and Jae D. Chang. Photovoltaic Energy Variations Due to Roofing Choice. *Procedia Engineering*, 145(May):1104–1109, 2016.
 23. Dalia El Helow, Jennifer Drake, and Liat Margolis. Testing the Potential Synergy of Green Roof-Integrated Photovoltaics at the University of Toronto Green Roof Innovation Testing (GRIT) Laboratory. pages 0–8, 2017.
 24. German Osma-Pinto, G. Ordóñez, Emmanuel Hernandez, L. Quintero, and M. Torres. The impact of height installation on the performance of pv panels integrated into a green roof in tropical conditions. pages 147–156, 09 2016.
 25. German Osma-Pinto and Gabriel Ordóñez-Plata. Measuring the effect of forced irrigation on the front surface of pv panels for warm tropical conditions. *Energy Reports*, 5:501 – 514, 2019.
 26. German Osma-Pinto and Gabriel Ordóñez-Plata. Dynamic thermal modelling for the prediction of the operating temperature of a pv panel with an integrated cooling system. *Renewable Energy*, 152:1041 – 1054, 2020.
 27. Hamid Ogaili and David J. Sailor. Measuring the Effect of Vegetated Roofs on the Performance of Photovoltaic Panels in a Combined System. *Journal of Solar Energy Engineering*, 138(6):061009, 2016.
 28. Andrea F. Tosi. *Green roofs and solar panels as a single assembly system in Austin , Texas*. PhD thesis, 2016.

29. Souradeep Gupta, Prashant Anand, Suveera Kakkar, Pratyusha Sagar, and Akanksha Dubey. Effect of evapotranspiration on performance improvement of photovoltaic-green roof integrated system, 2017.
30. Mohammed J. Alshayeb and Jae D. Chang. Variations of PV panel performance installed over a vegetated roof and a conventional black roof. *Energies*, 11(5), 2018.
31. Dalia El Helou. *Performance of Green Roof Integrated Solar Photovoltaics in Toronto*. PhD thesis, 2018.
32. Soham Adhya, Dipak Saha, Abhijit Das, Joydip Jana, and Hiranmay Saha. An IoT Based Smart Solar Photovoltaic Remote Monitoring and Control unit. *2016 2nd International Conference on Control, Instrumentation, Energy & Communication (CIEC)*, pages 432–436, 2016.
33. Jesús Israel Guamán, Carlos Vargas, Alberto Rios Villacorta, and Rubén Nogales. Solar Manager : Acquisition , Treatment and Isolated Photovoltaic System Information Visualization Cloud Platform. (March), 2017.
34. Renata I S Pereira, Ivonne M Dupont, Paulo C M Carvalho, and Sandro C S Jicá. IoT Embedded Linux System based on Raspberry Pi applied to Real-Time Cloud Monitoring of a decentralized Photovoltaic plant. *Measurement*, 2017.
35. M Suresh, R Meenakumari, R Ashok Kumar, T Alex Stanley Raja, K. Mahendran, and A. Pradeep. Fault Detection and Monitoring of Solar PV Panels using Internet of Things. (August), 2018.
36. Miguel J Prieto, Alberto M Pernía, Fernando Nuño, Juan Díaz, and Pedro J Villegas. Development of a Wireless Sensor Network for Individual Monitoring of Panels in a Photovoltaic Plant. pages 2379–2396, 2014.
37. Jinsoo Han, Chang-sic Choi, Wan-ki Park, Ilwoo Lee, and Sang-ha Kim. PLC-Based Photovoltaic System Management for Smart Home Energy Management System. 60(2):184–189, 2014.
38. Fariyah Shariff, Nasrudin Abd Rahim, and Hew Wooi Ping. Zigbee-based data acquisition system for online monitoring of grid-connected photovoltaic system. 42:1730–1742, 2015.
39. Farid Touati, M.A. Al-Hitmi, Noor Alam Chowdhury, Jehan Abu Hamad, and Antonio J R San Pedro Gonzales. Investigation of solar PV performance under Doha weather using a customized measurement and monitoring system. *Renewable Energy*, 89:564–577, 2016.
40. Arturo Rosas. ¿Qué es un negocio? (definición, tipos y diferencia con una empresa), 2019.
41. Andrew Josey, Marc Lankhorst, Iver Band, Henk Jonkers, and Dick Quartel. *An Introduction to the ArchiMate® 3.0 Specification*. Number June. 2016.

Mapping the environmental criteria for facility location problems

Vanessa de Almeida Guimarães^[0000-0001-7662-3499]¹, Pedro Henrique González Silva¹,
Luis Hernandez-Callejo² and Glaydston Mattos Ribeiro³

¹ Federal Centre of Technological Education Celso Suckow da Fonseca, Brasil

² Agricultural and Forestry Engineering Department, University of Valladolid, Spain

³ Federal University of Rio de Janeiro, Brasil

vanessa.guimaraes@cefet-rj.br

Abstract. Facility location mathematical models deal with different kinds of issues (from telecommunication to transportation), mostly focused on economic criteria. However, there is increasing pressure for including environmental aspects in the decision-making process, either at corporate or governmental sectors. Then, this paper aims to identify whether (and how) the literature about facility location in logistics, published in the Web of Science database, has been dealing with the environmental concerns in the mathematical models. We performed a systematic review to propose a framework of the environmental criteria and the main features of the investigated mathematical models. In the end, it can be noted an increase in the studies considering environmental aspects, although they still represent a small number of papers published about the subject (6.6%). Besides, the most evaluated environmental aspect is CO₂, which can be explained by international agreements and legislation. We emphasize that there are still gaps to be filled, especially with concerns to models for strategic governmental planning.

Keywords: facility location, carbon emission, optimization

1. Introduction

Facility location is a critical decision to the strategic design and planning of logistics networks [1-3], since it can influence in the operational aspects of a corporate and in the success of the whole supply chain (and the transversal chains). Besides, it is also crucial for the planning of the public sector [2]. Nevertheless, the design of logistic networks (involving facility location, allocation of "customers" to be served from the facilities and their operations) have substantial economic, environmental and social impacts. Different kinds of facility location problems have been covered by relevant papers as [1; 4-20]. However, none of them deals with environmental and/or social concerns.

Despite all the evolution of the Operational Research (OR) area, the main criteria considered in mathematical models are still the cost, time and/or distance between the

points of production and consumption [2, 21-25]. Traditionally, the mathematical models aimed at minimizing cost or maximizing profit, while environmental and social effects have attracted limited attention of the facility location literature [3; 26-27]. It can be explained by the difficulty in measuring the social and environmental dimensions [14,17,28,29]. Therefore, considering them has been identified by [15,17,20,30,31] as a challenge for the new models in OR. [26] agreed that this area should focus on more comprehensive aspects of eco-efficiency and the carbon footprint, while [32] defend the need to introduce and investigate the environmental policy instruments in the supply chain planning.

In this sense, we realized that the companies and government have been pressured by public opinion to propose actions aiming to reduce the environmental impacts of different kinds of operations. As a result, there had been developed stringent legislation and regulatory mechanisms, especially, aiming to reduce greenhouse gas (GHG) emissions worldwide, in an attempt to tackle climate change [2,32-37].

Then, this paper aims to answer the following question: how is the scientific literature about facility location in logistics dealing with environmental concerns? Therefore, we aim to identify whether and how the scientific literature about facility location in logistics has been dealing with the environmental concerns in the mathematical models published in Web of Science (WoS) from 1968 to 2017. Based on that, this study presents a framework of environmental indicators found in the papers evaluated and the main features of the investigated mathematical models.

We highlight that the coverage of this research includes only the papers published in the Web of Science database until 2017 and the results are directly influenced by the keywords selected to the review. Although the main objective of this paper is not to evaluate the social aspects, during the proposition of the environmental framework, we discussed the social aspects found in the database, especially those that perform sustainable analysis of facility location.

We emphasize that, although comprehending the environmental aspect does not fulfill the existent gaps to develop sustainable mathematical models on facility location, we believe that understanding how to deal with the environmental concerns is a step toward the desired sustainable development.

From this Introduction, this paper presents the methodological procedures (Section 2), followed by the main findings (Section 3) and, finally, the final considerations.

2. Methodological Procedures

Based on relevant papers in OR area that deals with facility location, we selected the most relevant keywords to perform the survey. WoS repository was chosen due to its satisfactory coverage, being used in papers with similar methodology as [38]. The parameters of the search are listed in Table 1.

We have not included any environmental keyword since we decided to gather all the papers published about the subject and, then, select our frame of analysis. By doing it, we reduced the error associated with the elimination of papers that could be related to the theme but does not use a specific environmental word as its indexation terms. In the

approach adopted, we could select those who had any environmental keyword among all the papers published. Considering that we did not know, a priori, how the scientific literature is dealing with the environmental aspects, we believed that it was the widest procedure to review precisely the papers published in the database select.

Table 1. Description of the search in Web of Science (WoS) database

Criteria	Description
Topic	TS = (“facilit* locatio*” OR “hub* locatio*” OR “p-median” OR “set covering proble*” OR “p-cent*” OR “maximal cover*”)
Database	Web of Science
Indexes	All the database indexes, except for books indexes
Temporal coverage	All years until 2017
Refinement	None, the search included papers of all areas registered in WoS
Search date	25 of April, 2018, at 2:25 p.m. GTM -3

Once the data was gathered, we removed those papers that were not related to logistics or transportation. Then, from 8.328 papers reported in the search, we considered 7,773 that was related somehow to the subject. Among them, only 217 had keywords related to environmental concerns (2.8% of the paper). Those keywords were categorized into ten classes: (i) emissions and its policies; (ii) energy; (iii) solid; (iv) green logistics; (v) land use; (vi) water; (vii) biodiversity; (viii) Life Cycle Analysis (LCA); (ix) climate change; and (x) performance (eco-efficiency). Then, the data were treated by using descriptive statistical analysis and considering the systematic review techniques. Therefore, from the 217 papers with environmental keywords, we had open access to 129. After reading each of them, we selected for the systematic review, only those applying environmental criteria in the mathematical optimization models. The main findings are described in Section 3.

3. Main Findings

Among the 217 papers indexed by environmental keywords, we realized that interest of the scientific community (universities, governmental agencies and companies - with emphasis to the first) in including environmental concerns in the mathematical models is recent. The first paper about facility location was published in 1968, but only in 1995 (27 years later), we found the 1st paper mention to environmental keywords (Figure 1).

From 2012, it can be noted an increase in the studies considering environmental aspects. Nevertheless, they still represent a small number of papers published about the subject (6.6% in 2017, e.g.). In Figure 1, the line represents the accumulated growth of the publications that have, at least, one environmental keyword, revealing an increasing tendency. It could be explained by the intensification in the researches and forums dedicated to the environmental preservation (as Paris Agreement) and by the recognition that adopting environmental criteria in the operations (manufacture, transport, supply chain design etc.) is a step toward the sustainable development. We also emphasize that the 1st paper mentioning specifically the term "sustainability" was published in 2010.

Regarding the 129 papers with open access, we proceed with a systematic review aiming to find which environmental criteria were dealt the most in the papers published and how they were included in the mathematical models. Among them, we verified that some papers do not apply nor develop mathematical models of optimization, adopting multi-criteria techniques, as Analytic Hierarchy Process (AHP).

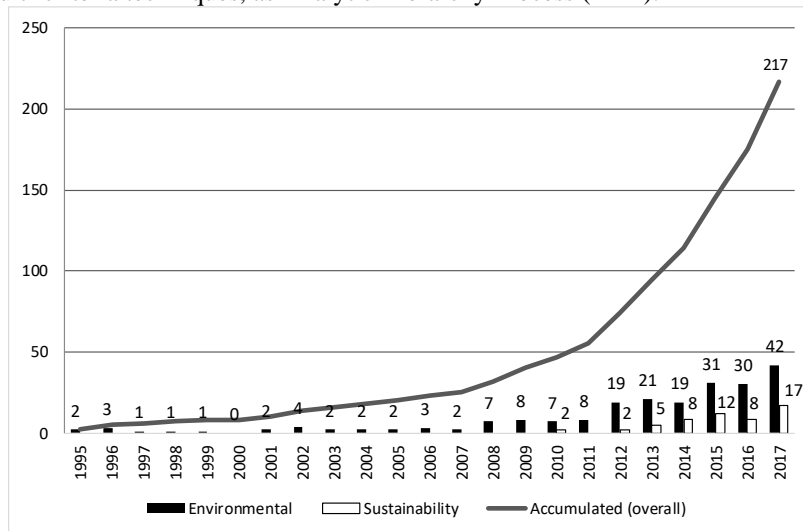


Fig. 1. Temporal evolution of publications about facility location and environmental criteria

Some of them do not investigate the facility location and others are focused in different areas than logistic, especially, telecommunications. Besides, the analysis involves different areas, although the bias is mainly from the corporate standpoint, focusing on the supply chain. Then, from the 129 papers, we selected only those that deal, somehow, with the green facility location problem (resulting in 47 papers).

Among them, [39] and [3] are not in Table 2, because present literature reviews. The former conducted a survey from 1990 to 2011, aiming to understand what sustainable aspects are involved in the facility location decisions of the manufacturing process. The latter makes a survey of papers that included social and/or environmental criteria in the methods and models dedicated to design and planning of the supply chains.

Table 2 summarizes the features of the analyzed papers. There are models with a single objective function (aiming to minimize the total cost, including the environmental cost, for example), bi-objective (most of the time, one economic and other environmental) or multi-objective. Although most of them are multi-echelon (76%), they are dedicated to a single product (58%) in a specific period (82%), not considering the possibility of intermodality (87%). Besides, it is verified the chosen for deterministic variables (76%) and scenarios or sensitivities analysis are performed to deal with the randomness of the data (80%). About the types of facilities to be located, they vary in complexity and number of echelons. Most of the papers are dedicated to the design of a closed-loop supply chain aiming to identify the optimal location of manufacture (or remanufacture) centers and/or distributions centers (or warehouses).

Table 2. Main features of the analyzed papers

Paper	Features of the mathematical model						Features of the case in study			
	Model	Optimization objective	Product	Period	Echelon	Variables	Environmental criteria	Transport	Inter-modal?	Sensitivity
[40]	O, B	Cost, CO ₂ emission, LCA	M	S	M	D	CO ₂ emission and dimensions of LCA	R	No	Yes
[41]	B	Cost, including those related to CO ₂ emissions	M	S	M	D	CO ₂ emission	R, F, Me	Yes	Yes
[30]	B	Cost and customer satisfaction	M	M	M	D	Recycled spare parts	None	No	Yes
[27]	Mt	Cost, environmental impact (carbon emission, waste and water consumption), social impact	S	S	S	E	Carbon emission, waste generation, water consumption and land use	R, F, Me, Ar	No	Yes
[33]	Mt	Net present value - NPV, LCA	M	M	M	D	CO ₂ emission and dimensions of LCA	None	No	Yes
[26]	Mt	LCA, service level, carbon emission	M	M	M	D, E	Carbon emission	R, Me, Ar	No	Yes
[42]	Mt	Revenue, costs, CO ₂ emission, social incidents	M	M	M	D	CO ₂ emission	R	No	Yes
[43]	O	Cost	S	S	M	E	CO ₂ emission	None	No	Yes
[44]	O	Cost, including those related to CO ₂ emissions	M	S	M	D	CO ₂ emission	None	No	Yes
[45]	O	Cost, including those related to CO ₂ emissions	S	S	M	D	CO ₂ emission	None	No	Yes
[46]	Mt	Cost, GHG emission, energy and material recovering	S	S	M	D	GHG emission (CO ₂ and CH ₄)	None	No	No
[32]	Mt	Cost, environmental score, social score	M	S	M	D	Environmental score	R, F e Me	No	Yes
[34]	O	Cost, including those related to CO ₂ emissions	M	S	M	D	Carbon emission	R, F, Me	No	No
[35]	B	Profit, number of trucks	S	S	M	D	Carbon footprint	R	No	No
[47]	O	Cost and carbon credit	S	S	S	D	CO ₂ emission	None	No	Yes
[48]	O	Cost, emission, acceptance of community	S	S	S	D	Emission of pollutants	R	No	No
[49]	Mt	Noise, coverage, trip time	N/A	S	S	D	Noise	Ar	No	No
[50]	B	Cost and CO ₂ emission	S	S	S	D	CO ₂ emission	None	No	Yes
[51]	B	Profit and carbon footprint	M	S	M	E	CO ₂ emission	None	No	Yes
[52]	O	Cost, including environmental	S	S	S	D	None	R	No	Yes
[53]	B	Categories of impact of LCA and NPV	S	S	M	D	Midpoint impact of LCA	None	No	Yes
[54]	O	Cost and CO ₂ emission	M	S	M	E	CO ₂ emission	D, R, F	No	Yes
[29]	Mt	Cost, involving emissions, noise and network	S	S	M	D, E	Energy consumption and noise	R	No	No
[55]	B	Profit and environmental impact	M	M	M	D	Midpoint impacts of LCA	R, Ar, Me	Yes	Yes
[56]	Mt	Profit, LCA, number of jobs created	M	M	M	D	Midpoint impacts of LCA	R, Ar	Yes	No
[57]	Mt	Cost, responsiveness, CO ₂ emissions	S	S	M	D	CO ₂ emission	R	No	Yes
[58]	B	Cost of network, operator and CO ₂ emissions	S	S	M	D	CO ₂ emission	R	No	Yes
[59]	O	Cost	M	S	M	D	Recycling	None	No	Yes
[60]	Mt	Profit, LCA, jobs created	M	M	M	D	Impact of LCA	R, D	No	No
[61]	B	Cost and energy consumption	S	S	M	D	Energy consumption	None	None	Yes
[62]	O	Total cost, including carbon emission	S	S	M	E	CO ₂ emission	None	No	Yes
[63]	B	Profit and carbon emission	S	S	M	D	Carbon emission	R, Ar, Me	No	Yes
[37]	B	Cost and CO ₂ emission	M	S	M	D	CO ₂ emission	None	No	Yes

Table 2. Main features of the analyzed papers

Paper	Features of the mathematical model						Features of the case in study			
	Model	Optimization objective	Product	Period	Echelon	Variables	Environmental criteria	Transport	Inter-modal?	Sensitivity
[64]	Mt	Cost, CO ₂ emission, service level	S	S	S	D	CO ₂ emission	R	No	Yes
[65]	O	Energy consumption	S	S	S	D	Energy consumption and CO ₂ emission	R	No	No
[66]	Mt	Cost, CO ₂ -eq emission, service level and social impact	S	S	M	D	CO ₂ -eq emission	R, F, Me	Yes	Yes
[67]	Mt	Cost, CO ₂ emission, waste generation	S	S	M	D	CO ₂ emission and waste generation	None	No	Yes
[68]	Mt	Cost, CO ₂ emission, waste generation	S	S	M	D	CO ₂ emission and waste generation	None	No	Yes
[69]	O	Cost, including those related to CO ₂ emissions	S	S	M	D, E	CO ₂ emission	R, F	No	Yes
[70]	Mt	Cost, emission of CO ₂ , service level	S	S	S	D	CO ₂ emission	R	No	Yes
[71]	Mt	Cost, CO ₂ -eq emission, jobs created	M	S	M	D	CO ₂ -eq emission	R, F	Yes	Yes
[72]	B	Cost and carbon trade	M	S	M	E	CO ₂ emission	None	No	Yes
[36]	Mt	Cost, environmental and social impacts	M	M	M	E	CO ₂ emission, fuel consumption and energy waste	R	No	Yes
[73]	O	Disutility (risk aversion)	S	S	S	D,E	CO ₂ emission	F, R, Me	Yes	Yes
[74]	O	Cost, including those related to CO ₂ emissions	S	S	S	D	CO ₂ emission	None	No	No

Note: It presents the type of the model (O – single objective, B - bi-objective and M -multi-objective), the optimization objectives, the kind of decisions covered and if the variables are deterministic (D) or stochastic (E). It also presents if the model is multi-period, multi-product and multi-echelon (where S and M represent, respectively, single and multiples) and specific features of the case in the study: modes of transport (R - Roadway, F - Rail, Me - Maritime, Ar - Air), if the intermodality is considered in the transport network and if scenario or sensitivity analysis are performed.

About the optimization objective, minimizing costs was the most common goal of economic dimension, with 33 records, while minimizing CO₂ emissions (cost and/or credit) stands out in the environmental dimension with 28 records. When the social dimension is evaluated, the most recurrent indicator is the "number of jobs created".

Regarding specifically the environmental aspect, we identified the following concerns: emissions (CO, CO₂, CO_{2-eq}, GHG and pollutants), carbon policies (carbon cap, carbon tax, carbon cap-and-trade), carbon footprint, application of LCA, fuels consumption, consumption and recovering of energy, noise, waste generation, recycling and recovering of materials and use of recycled materials. Besides, one of the papers [32] attributed environmental scores, in their mathematical model, according to experts' opinion. However, the most recurrent criterion in the models is carbon emission.

About the sensitivity analysis, there are different of approaches. [30], for instance, allocate different weights in the Objective Functions of their bi-objective model, while [32] and [73] propose different scenarios changing the parameters adopted in their case studies [29] and [51] deal with uncertainty in the decision process by applying Fuzzy Logic. In a specific environmental approach, [40] adopt different carbon costs as a parameter of the mathematical model in the three scenarios established. Similarly, [43] propose five scenarios: one deals with the carbon cap policy; another varies that social index and the other three evaluate changes in the probability parameters of the model.

We highlight that there are still gaps to be filled, especially with concerns to models for strategic governmental planning. Most of the time, the analysis is performed from a business standpoint, seeking a design that reduces the cost or increases the supply chain's profit. Once presented the mapping of the papers, Sections 4.1 to 4.5 are dedicated to present how they deal with the environmental aspect.

3.1 Indirectly Approaches

Among the papers of Table 2, we verified that some papers deal with the environmental concerns indirectly, which means that there is no environmental parameter or variable in the mathematical models [30,35,49,52]. For example, [30] consider that the collection and the reuse of material, as well as the proper disposal of waste, are eco-friendly actions. The authors assume that by determining the number of items for recycling, their model can be considered eco-friendly, although it should be adequately assessed since the activities involved in recycling can cause environmental impacts.

[35] also assumes that recycling is a green action that should be encouraged. Then, they study the reverse flows in a closed-loop supply chain, considering that the users have financial incentives to return the product, at the end of its useful life. So, it would be designated to reuse, recycling or final disposal. About the CO₂ emission, they consider that reducing the number of trucks used in the transport of the products in the forward supply chain reduces the environmental impact (but it is not measured).

In a similar approach, [52] consider that the use of remanufactured products could reduce some environmental impact (as natural resources depletion), but it is not directed treated in the mathematical model. Analogously, [59] assume that recycling consumes less energy than the traditional process of producing paper so that it would reduce the

consumption of natural resources and pollution; but it is not measured. Then, their model aims to maximize the amount of paper collected and assigned to recycling.

The approaches of these papers might not be the most appropriate since they do not measure the environmental impacts or the results of the proposed actions. Nevertheless, the papers show interest in the international literature in considering the environmental impacts in the optimization models that design supply chains.

3.2 LCA Assessment

Although [3] state that LCA is the most used technique to evaluate the environmental aspect in the decision-making, the literature review showed few papers that apply this technique in the optimization models related to facility location [33,40,51,55,56,60,71]. It can be justified by the fact that obtaining environmental data and modeling the whole supply chain is a challenge. Therefore, it is easier to deal with some environmental objectives, constraints, or parameters instead of evaluating the whole supply chain [3].

It is relevant to emphasize that the optimization models that adopt LCA to measure the environmental impacts, usually, has its application restricted to the context under assessment [3], hardly ever being applicable to other realities since the results of LCA are highly dependent of the system's boundaries and the functional unit chosen.

3.3 Sustainable Evaluation

Among the papers of Table 2, seven perform a sustainable analysis considering social, environmental and economic parameters in the mathematical models. Besides dealing with the traditional economic impact (supply chain's cost), [32] assign scores to the environmental and social impacts of the suppliers, which were defined based on experts' opinions. Regarding the environmental dimension, the most relevant aspects are "alternatives sources of energy", "water consumption" and "GHG emission".

[36] propose a model to support the strategic and operational planning of a closed-loop supply chain (e.g., location-allocation decisions jointly with inventory management and routing). The social aspects are measured in terms of "number of jobs created" and "balanced economic development", while the environmental ones are "CO₂ emissions" and "energy consumption".

[60] and [71] study the fuel supply chain, the former focus on biorefinery and the latter plan the design of lignocellulose ethanol supply chain. In both, the economic dimension is measured in terms of profit, the environmental impact is evaluated by applying LCA and the social impact is related to the number of jobs created.

The model proposed by [27] aims to minimize the costs and environmental impacts and, at the same time, maximize the social utility. The authors deal with the environmental impacts in two ways: (i) an environmental Objective Function that measures the CO₂ emission and waste generation; and (ii) a constraint that restricts the water and land consumption. The social utility is measured in a specific social Objective Function that sums the values related to job equity distribution, development equity, security level and medical access level.

[66] and [43] apply multi-criteria techniques to evaluate the social impact. [66] perform a sustainable analysis by proposing a multi-objective model to determine the design of a wine supply chain. The first objective evaluates the total costs (transportation, building and operating facilities and so on), the second evaluates CO_{2-eq} emission from transport activities in all echelons of the supply chain and the third measures the social impact of suppliers and facilities. The social impact is generic measured by a score and the authors state that they are related to employment or regional impact, but the calculations are not detailed in the paper. In the case study, the assigned score to the social dimension is based on an adaptation of AHP.

In [43] model, the environmental (CO₂ emission) and social (related to suppliers' performance) impacts are treated on specific constraints. The differential of this proposal is how the social dimension is treated: they transform qualitative factors in a social index, by applying a combination of TOPSIS and AHP multi-criteria techniques.

We highlight that some papers appeal as a sustainable proposal, but the model developed does not incorporate the three dimensions that compose the sustainability concept (economic, social and environmental). It is related to a conceptual confusion that remains in the scientific fields: the process or activity is considered sustainable when including the environmental aspect in the planning or evaluation, even if it does not consider the social impact. [73] and [29], for example, claim to be sustainable but do not include any social indicator in their model.

3.4 Carbon Emission and Regulatory Policies

Since CO₂ emission is the major concern of the papers found in Table 2 (31 of 45), Table 3 summarizes how the papers surveyed dealt with carbon emission, highlighting some features of the mathematical models and indicating if any carbon policy is considered. According to Table 3, CO₂ is mostly treated as an emission (in 29 papers), but it is also measured as cost in 13 papers. Five papers considered both: CO₂ in terms of tons emitted and as cost. The papers are mainly concerned with the emissions from transport (29 records). Nevertheless, since a significant amount of papers are focused on supply chain (closed loop or not), the emissions from operation (forward, as manufacture, or reverse, as recycling) are also accounted for in 15 articles. Besides, 13 papers consider the facility's emissions during the construction and opening and/or operation.

However, most papers do not explicitly consider the carbon policy, even if some of them (papers marked with $x^{(1)}$ in Table 3) deal with carbon tax in the analysis, by proposing models where carbon emission is charged. The policy addressed the most is carbon trade (in 9 papers), followed by carbon cap (in 8 papers). The scarcity in models involving those policies can be explained by Figure 1 (that indicates the recent interest of the scientific community for this subject) and to the youth of these initiatives. For instance, the Paris Agreement was launched in 2015 and ratified in 2017. It is important to highlight that Paris Agreement (Article 6), established the basis for the operation of international carbon markets, reinforcing targets, transparency and accountability. It raised the relevance of carbon trade (or carbon cap-and-trade) as a tool to help the parties involved in the agreement achieve the emission reduction targets, by using the carbon trading market. For further information, see United Nations (2019).

Table 3. Treatments given to CO₂ in the papers surveyed

Paper	Measuring of CO ₂		CO ₂ in the Mathematical Model			Emission Sources				Carbon Policies			
	As emission	As cost	Objective Function	Constraints	Both	Supplier	Operations	Transport	Facility	Carbon cap	Carbon tax	Carbon trade	None
[40]	x	x			x	x	x	x	Operation	x		x	
[41]	x		x			x	x	x	Opening, Operation				x
[27]	x		x					x					x
[33]	x	x			x	Not specified				x		x	
[26]	x				x		x	x	Operation				x
[42]	x	x	x			x	x	x				x	
[43]	x			x		x	x	x	Operation	x			
[44]		x	x			x	x	x	Operation			x	
[45]		x	x					x		x		x	
[46]	x		x						Operation				x
[34]	x	x			x		x	x	Operation	x	x	x	
[47]	x	x			x		x	x		x		x	
[48]		x	x					x	Operation				x ⁽¹⁾
[50]	x		x					x	Operation				x
[51]	x		x					x					x
[54]		x	x				x	x			x		
[57]	x		x					x					x
[58]		x			x			x					x ⁽¹⁾
[62]		x	x				x	x	Opening, Operation	x		x	
[63]	x		x				x	x					x
[37]	x		x				x	x	Opening, Operation				x
[64]	x		x					x					x
[66]	x		x					x					x
[67]	x		x				x	x					x
[68]	x		x				x	x					x
[69]	x		x					x					x
[70]	x		x					x					x
[71]	x		x			x	x	x	Operation				x
[72]	x	x			x		x	x	Opening, Operation	x		x	
[73]	x			x				x					x ⁽¹⁾
[36]	x		x					x					x
[74]		x	x					x					x ⁽¹⁾

3.5 Solution Techniques

Regarding the main solution techniques, Table 4 shows that Branch-and-Bound is used in 11 papers, mostly combined with weighted objective functions (multi-objective problems), as well as e-constraint, which also appears in 11 articles. Genetic Algorithms are also recurrent, appearing combined (or not) with other techniques in 5 papers.

Table 4. Solution Techniques applied in the surveyed papers

Paper	Solution technique
[40]	Branch-and-Bound
[41]	Weighted objective functions + Branch-and-Bound
[30]	Weighted objective functions + Branch-and-Bound
[27]	e-constraint
[33]	e-constraint
[26]	Goal Programming
[42]	Goal Programming
[43]	Combined AHP and fuzzy TOPSIS methods + Nonlinear Solver SNOPT
[44]	Branch-and-Bound
[45]	Lagrangean Heuristic
[46]	Lexicographic Minimax
[32]	Stochastic Fuzzy Goal Programming
[34]	Branch-and-Bound
[35]	Weighted objective functions + Branch-and-Bound
[47]	Generalized Reduced Gradient
[48]	Weighted objective functions + Branch-and-Bound
[49]	e-constraint
[50]	SEAMO2 + Lagrangean Relaxation
[51]	e-constraint
[52]	Branch-and-Bound
[53]	Weighted objective functions + Branch-and-Bound
[54]	Weighted objective functions + Branch-and-Bound
[29]	Simulated Annealing + Imperialist Competitive Algorithm
[55]	Branch-and-Bound + Lexicographic Optimization
[56]	e-constraint
[57]	Non-dominated Sorting Genetic Algorithm-II (NSGA-II)
[58]	Dual lexicographic max–min approach
[59]	Goal Programming
[60]	e-constraint
[61]	Multi-objective Imperialist Competitive Algorithm (MOICA) + NSGA-II
[62]	Chance Constraint Programming + Benders' Decomposition
[63]	e-constraint
[37]	e-constraint
[64]	Non-dominated Sorting Genetic Algorithm-II (NSGA-II) + Greedy Algorithm
[65]	Artificial Fish Swarm Algorithm
[66]	e-constraint
[67]	Iterative Pareto Frontier
[68]	Iterative Pareto Frontier
[69]	Nonlinear Solver + Lipschitz-continuous Global Optimizer
[70]	Hybrid Algorithm (e-constraint + greedy heuristic)
[71]	e-constraint
[72]	Multi-Criteria Scenario-Based Solution Method
[36]	Hybrid Algorithm (Self-adaptive Genetic Algorithm + Variable Neighborhood Search)
[73]	Hybrid Algorithm Penalty Function Method + Genetic Algorithm + Gauss-Seidel Decomposition

Paper	Solution technique
[74]	Multi-Angles Analysis

4 Final Considerations

Throughout this paper, it was possible to identify which environmental impact is treated the most and how the papers incorporate them in the facility location mathematical models. We believe that understanding the evolution of the researches in this field help to develop models following the new trends.

Although [27] state the facility location problem cannot be treated from a purely economic perspective, due to strong environmental and social effects of establishing facilities and interconnections among them, we saw that a small number of papers published in the WoS up to 2017 deals with these effects in the mathematical model (less than 7%). Regarding the features of the mathematical models, most of them are multi-echelon (76%), dedicated to a single product (58%) in a specific period (82%), not considering the possibility of intermodality (87%). Besides, they use deterministic variables (76%) and perform scenarios or sensitivities analysis to deal with the randomness of the data (80%). The analysis is mostly performed from a business standpoint, seeking a design that reduces the cost or increases the profit of the supply chain.

Then, we emphasize that there are still gaps to be filled, especially with concerns to models for strategic governmental planning. We also could realize that carbon emission (and its variants) is the impact considered the most in the evaluations, which can be explained by international agreements and public pressure. Although in a less proportion, regulatory policies have also been included in the analysis, especially carbon trade. Besides, there is not a consensual way to deal with the environmental dimension in the mathematical models.

It was shown that sustainable analysis has also been performed, even if there is a recognized difficulty in dealing and measuring social impacts. It is in consonance with [15,17,20,28,30] that point out the inclusion of environmental and social aspects in the mathematical models as future trends in OR. As limitations of this paper, the results are directly related to the chosen keywords, the database and the temporal coverage. Then, new researches could include (or compare) other databases and keywords. Besides, it would be relevant to develop papers focused on governmental strategic planning, since it was not explicitly founded among the surveyed papers.

Acknowledgment

The authors thank CNPq, CAPES - 001 and FAPERJ for the financial support. We also thank the CYTED Thematic Network “Ciudades Inteligentes Totalmente Integrales, Eficientes Y Sostenibles (CITIES)” no 518RT0558.

References

1. Melo, M.T., Nickel, S., Saldanha-da-Gama, F., 2009. Facility location and supply chain management – A review. *Eur. J. Oper. Res.* 196, 401–412 (2009).
2. Das, S.K., Roy, S.K. Effect of variable carbon emission in a multi-objective transportation-p-facility location problem under neutrosophic environment. *Comput. Ind. Eng.* 132, 311–324 (2019).
3. Eskandarpour, M., Dejax, P., Miemczyk, J., Péton, O. Sustainable supply chain network design: An optimization-oriented review. *Omega*, 54, 11–32 (2015).

4. ReVelle, C.S., Swain, R.W. Central facilities location. *Geogr. Anal.* 2, 30–42 (1970).
5. Geoffrion, A.M., Graves, G.W. Multicommodity Distribution System Design by Benders Decomposition. *Manage. Sci.* 20, 822–844 (1974).
6. Erlenkotter, D. A Dual-Based Procedure for Uncapacitated Facility Location. *Oper. Res.* 26, 992–1009 (1978).
7. Feo, T.A., Resende, M.G.C. A probabilistic heuristic for a computationally difficult set covering problem. *Oper. Res. Lett.* 8, 67–71 (1989).
8. Campbell, J.F. Theory and Methodology Integer programming formulations of discrete hub location problems. *Eur. J. Oper. Res.* 72, 387–405 (1994).
9. Beasley, J.E., Chu, P.C. A genetic algorithm for the set covering problem. *Eur. J. Oper. Res.* 94, 392–404 (1996).
10. Owen, S.H., Daskin, M.S. Strategic facility location: A review. *Eur. J. Oper. Res.* 111, 423–447 (1998).
11. Klöse, A., Drexl, A. Facility location models for distribution system design. *Eur. J. Oper. Res.* 162, 4–29 (2005).
12. Alumur, S., Kara, B.Y. Network hub location problems: The state of the art. *Eur. J. Oper. Res.* 190, 1–21 (2008).
13. Campbell, J.F., O’Kelly, M.E. Twenty-Five Years of Hub Location Research. *Transp. Sci.* 46, 153–169 (2012).
14. Farahani, R.Z., SteadieSeifi, M., Asgari, N. Multiple criteria facility location problems: A survey. *Appl. Math. Model.* 34, 1689–1709 (2010).
15. Arabani, A., Farahani, R.Z. Facility location dynamics: An overview of classifications and applications. *Comput. Ind. Eng.* 62, 408–420 (2012).
16. Farahani, R.Z., Asgari, N., Heidari, N., Hosseini, M., Goh, M. Covering problems in facility location: A review. *Comput. Ind. Eng.* 62, 368–407 (2012).
17. Farahani, R.Z., Hekmatfar, M., Arabani, A.B., Nikbakhsh, E. Hub location problems: A review of models, classification, solution and applications. *Comput. Ind. Eng.* 64, 1096–1109 (2013).
18. Farahani, R.Z., Hekmatfar, M., Fahimnia, B., Kazemzadeh, N. Hierarchical facility location problem: Models, classifications, techniques, and applications. *Comput. Ind. Eng.* 68, 104–117 (2014).
19. Ortiz-Astorquiza, C., Contreras, I., Laporte, G. Multi-level facility location problems. *Eur. J. Oper. Res.* 267, 791–805 (2018).
20. Farahani, R.Z., Fallah, S., Ruiz, R., Hosseini, S., Asgari, N. OR models in urban service facility location: A review of applications and future developments. *Eur. J. Oper. Res.* 276, 1–27 (2019).
21. Crainic, T.G., Laporte, G. Planning models for freight transportation. *Eur. J. Oper. Res.* 97, 409–438 (1997).
22. Ishfaq, R., Sox, C.R. Hub location-allocation in intermodal logistic networks. *Eur. J. Oper. Res.* 210, 213–230 (2011).
23. Meisel, F., Kirschstein, T., Bierwirth, C. Integrated production and intermodal transportation planning in large scale production-distribution-networks. *Transp. Res. Part E* 60, 62–78 (2013).
24. Bhattacharya, A., Kumar, S.A., Tiwari, M., Talluri, S. An intermodal freight transport system for optimal supply chain logistics. *Transp. Res. Part C Emerg. Technol.* 38, 73–84 (2014).
25. Guimarães, V. de A., Ribeiro, G.M., Forte, V.L., Lucena, A., 2017. A location-allocation model for logistics integration centers. *Int. J. Transp. Econ.* XLIV, 273–291.
26. Brandenburg, M. Low carbon supply chain configuration for a new product – a goal programming approach. *Int. J. Prod. Res.* 53, 1–23 (2015).
27. Anvari, S., Turkay, M. The facility location problem from the perspective of triple bottom line accounting of sustainability. *Int. J. Prod. Res.* 55, 6266–6287 (2017).
28. Barbosa-Povoa, A.P., Mota, B., Carvalho, A. How to design and plan sustainable supply chains through optimization models? *Pesqui. Operacional* 38, 363–388 (2018).

29. Mohammadi, M., Torabi, S.A., Tavakkoli-Moghaddam, R.. Sustainable hub location under mixed uncertainty. *Transp. Res. Part E Logist. Transp. Rev.* 62, 89–115 (2014).
30. Afshari, H., Sharafi, M., ElMekkawy, T., Peng, Q. Optimizing multi-objective dynamic facility location decisions within green distribution network design. *Procedia CIRP* 17, 675–679 (2014).
31. Govindan, K., Soleimani, H., Kannan, D. Reverse logistics and closed-loop supply chain: A comprehensive review to explore the future. *Eur. J. of Oper. Res.*, 240(3), 603–626 (2015)
32. Fahimnia, B., Jabbarzadeh, A. Marrying supply chain sustainability and resilience: A match made in heaven. *Transp. Res. Part E Logist. Transp. Rev.* 91, 306–324 (2016).
33. Bojarski, A.D., Laínez, J.M., Espuña, A., Puigjaner, L. Incorporating environmental impacts and regulations in a holistic supply chains modeling: An LCA approach. *Comput. Chem. Eng.* 33, 1747–1759 (2009).
34. Fareeduddin, M., Hassan, A., Syed, M.N., Selim, S.Z. The impact of carbon policies on closed-loop supply chain network design. *Procedia CIRP* 26, 335–340 (2015).
35. Garg, K., Kannan, D., Diabat, A., Jha, P.C. A multi-criteria optimization approach to manage environmental issues in closed loop supply chain network design. *J. Clean. Prod.* 100, 297–314 (2015).
36. Zhalechian, M., Tavakkoli-Moghaddam, R., Zahiri, B., Mohammadi, M. Sustainable design of a closed-loop location-routing-inventory supply chain network under mixed uncertainty. *Transp. Res. Part E Logist. Transp. Rev.* 89, 182–214 (2016).
37. Talaei, M., Farhang Moghaddam, B., Pishvae, M.S., Bozorgi-Amiri, A., Gholamnejad, S. A robust fuzzy optimization model for carbon-efficient closed-loop supply chain network design problem: A numerical illustration in electronics industry. *J. Clean. Prod.* 113, 662–673 (2016).
38. Guimarães, V. de A., Ribeiro, G.M., de Azevedo-Ferreira, M. Mapping of the Brazilian scientific publication on facility location. *Pes. Operacional* 38, 307–330 (2018).
39. Chen, L., Olhager, J., Tang, O. Manufacturing facility location and sustainability: A literature review and research agenda. *Int. J. Prod. Econ.* 149, 154–163 (2014).
40. Abdallah, T., Farhat, A., Diabat, A., Kennedy, S. Green supply chains with carbon trading and environmental: Formulation and life cycle assessment. *Appl. Math. Model.* 36, 4271–4285 (2012).
41. Accorsi, R., Manzini, R., Pini, C., Penazzi, S. On the design of closed-loop networks for product life cycle management: Economic, environmental and geography. *J. Transp. Geogr.* 48, 121–134 (2015).
42. Costa, Y., Duarte, A., Sarache, W. A decisional simulation-optimization framework for sustainable facility location of a biodiesel plant in Colombia. *J. Clean. Prod.* 167, 174–191 (2017).
43. Das, R., Shaw, K. Uncertain supply chain network design considering carbon footprint and social factors using two-stage approach. *Clean Technol. Environ. Policy* 19, 2491–2519 (2017)
44. Diabat, A., Abdallah, T., Al-refaie, A., Svetinovic, D., Govindan, K. Strategic Closed-Loop Facility Location Problem. *IEEE Trans. Eng. Manag.* 60, 398–408 (2013).
45. Elhedhli, S., Merrick, R., 2012. Green supply chain network design to reduce carbon emissions. *Transp. Res. Part D Transp. Environ.* 17, 370–379.
46. Erkut, E., Karagiannidis, A., Perkoulidis, G., Tjandra, S.A. A multicriteria facility location model for municipal solid waste management in Greece. *Eur. J. Oper. Res.* 187, 1402–1421 (2008).
47. Ghaddar, B., Naoum-Sawaya, J., 2011. Environmentally friendly facility location with market competition. *J. Oper. Res. Soc.* 63, 899–908 (2011).
48. Guyon, O., Absi, N., Feillet, D., Garaix, T. A Modeling Approach for Locating Logistics Platforms for Fast Parcels Delivery in Urban Areas. *Procedia - Soc. Behav. Sci.* 39, 360–368 (2012).
49. Hammad, A.W.A., Akbarnezhad, A., Rey, D. Bilevel Mixed-Integer Linear Programming Model for Solving the Single Airport Location Problem 31, 3–7 (2017).
50. Harris, I., Mumford, C.L., Naim, M.M. A hybrid multi-objective approach to capacitated facility location with flexible store allocation for green logistics modeling. *Transp. Res. Part E Logist. Transp. Rev.* 66, 1–22 (2014).
51. Jindal, A., Sangwan, K.S. Multi-objective fuzzy mathematical modelling of closed-loop supply chain considering economical and environmental factors. *Ann. Oper. Res.* 257, 95–120 (2017).

52. Kizilboga, G., Mandil, G., Genevois, M.E., Zwolinski, P. Remanufacturing network design modeling: A case of diesel particulate filter. *Procedia CIRP* 11, 163–168 (2013).
53. Laínez, J.M., Bojarski, A., Espuña, A., Puigjaner, L. Mapping environmental issues within supply chains: a LCA based approach. *Comput. Aided Chem. Eng.* 25, 1131–1136 (2008)
54. Liqiang, H., Guoxin, W. Two-stage Stochastic Model for Petroleum Supply Chain from the Perspective of Carbon Emission. *Proceedings of ICLEMCS*, 117, 926–930 (2015).
55. Mota, B., Carvalho, A., Barbosa-Povoa, A., Gomes, M.I. Green supply chain design and planning. *2015 Int. Conf. Ind. Eng. Syst. Manag.* 537–545 (2015).
56. Mota, B., Carvalho, A., Isabel, M., Barbosa-póvoa, A. Supply chain design and planning accounting for the Triple Bottom Line, in: *12th Intern. Symp.on Process Systems Engineering* (2015)
57. Musavi, M.M., Bozorgi-Amiri, A. A multi-objective sustainable hub location-scheduling problem for perishable food supply chain. *Comput. Ind. Eng.* 113, 766–778 (2017)
58. Niknamfar, A.H., Niaki, S.T.A. Fair profit contract for a carrier collaboration framework in a green hub network under soft time-windows: Dual lexicographic max–min approach. *Transp. Res. Part E* 91, 129–151 (2016).
59. Pati, R.K., Vrat, P., Kumar, P. A goal programming model for paper recycling system. *Omega* 36, 405–417 (2008)
60. Santibañez-Aguilar, J.E., González-Campos, J.B., Ponce-Ortega, J.M., Serna-González, M., El-Halwagi, M.M. Optimal planning and site selection for distributed multiproduct biorefineries involving economic, environmental and social objectives. *J. Clean. Prod.* 65, 270–294 (2014).
61. Sedehzadeh, S., Tavakkoli-Moghaddam, R., Baboli, A., Mohammadi, M. Optimization of a multimodal tree hub location network with transportation energy consumption: A fuzzy approach. *J. Intell. Fuzzy Syst.* 30, 43–60 (2016).
62. Shaw, K., Irfan, M., Shankar, R., Yadav, S.S. Low carbon chance constrained supply chain network design problem: Benders decomposition based approach. *Comput. Ind. Eng.* 98, 483–497 (2016).
63. Smith, N.R., Manzano, M.G., Castillo-Villar, K., Rivera-Morales, L.A. A bi-objective model for local and global green supply chain. *IEEE Symp. Comput. Intell. Prod. Logist. Syst.* 83–90(2014).
64. Tang, X., Zhang, J., The multi-objective capacitated facility location problem for green logistics, in: *2015 4th IEEE Intern.Conference on Advanced Logistics and Transport*, 163–168 (2015)
65. Tian, G., Liu, Y. Energy-efficient models of sustainable location for a vehicle inspection station with emission constraints. *IEEE Trans. Autom. Sci. Eng.* 12, 238–243 (2015).
66. Varsei, M., Polyakovskiy, S. Sustainable supply chain network design: A case of the wine industry in Australia. *Omega* 66, 236–247 (2017).
67. Wang, Y., Lu, T., Gao, C., Zhang, C., Chen, C. Research on Remanufacturing Closed-loop Logistics Network Design under Low-carbon Restriction. *Adv. Manuf. Technol. Syst.* 159, 224–234 (2012).
68. Wang, Y., Zhu, X., Lu, T., Jeeva, A.S. Eco-efficient based logistics network design in hybrid manufacturing/remanufacturing system in low-carbon economy. *J. Ind. Eng. Manag.* 6, 200–214 (2013).
69. Wanke, P., Correa, H., Jacob, J., Santos, T. Including carbon emissions in the planning of logistic networks: a Brazilian case. *Int. J. Shipp. Transp. Logist.* 7, 655 (2015).
70. Xifeng, T., Ji, Z., Peng, X. A multi-objective optimization model for sustainable logistics facility location. *Transportation Research Part D*, 22,45–48 (2013).
71. You, F., Tao, L., Graziano, D.J., Snyder, S.W. Optimal Design of Sustainable Cellulosic Biofuel Supply Chains: Multiobj.Optimization with LCA and Input–Output. *AIChE J.* 58, 1157–1180 (2012).
72. Yu, H., Solvang, W.D. A stochastic programming approach with improved multi-criteria scenario-based solution method for sustainable reverse logistics design of waste electrical and electronic equipment. *Sustain.* 8 (2016)
73. Zhang, D., Li, X., Huang, Y., Li, S., Qian, Q. A robust optimization model for green regional logistics network design with uncertainty in future logistics demand. *Adv. Mech. Eng.* 7 (2015)
74. Zheng, S., Zhou, J. Research on Multi-Facility Weber Problem to Reduce Carbon Emissions, In: *Proceedings of Inter. Conf. on Low-Carbon Transport., Logis. and Green Build.* 735–742 (2012).

Human-Computer Interfaces for Smart Bus Stops as Interconnected Public Spaces (IP-Spaces) elements in Smart Cities

Fernando Martín de Pablos¹, Víctor Manuel Padrón Nápoles¹, Diego Gachet Páez¹, José Luis Esteban Penelas¹, Olalla García Pérez¹, Rafael Muñoz Gil¹, Jorge García González¹, Sonia Escorial Santa Marina²

¹Escuela de Arquitectura, Ingeniería y Diseño

²Facultad de Ciencias Sociales y de la Comunicación

Universidad Europea de Madrid. c/ Tajo s/n, Villaviciosa de Odón, Madrid

fernando.martin2@universidadeuropea.es, vic-

tor.padron@universidadeuropea.es, die-

go.gachet@universidadeuropea.es,

jluis.esteban@universidadeuropea.es, olalla.garpe@gmail.com,

Rafael.munoz@universidadeuropea.es, geosm524@outlook.com, so-

nia.escorial@universidadeuropea.es

Abstract. As Smart City concept evolves, it necessarily incorporates more sustainability and inclusiveness features. Smart Cities and digital inclusion efforts are moving rapidly and multiple initiatives are taking place all around the world using different technologies to address accessibility, safety (especially for women) and social inclusion of vulnerable groups as minorities, disabled people or the elderly. In this context, the mobility of people is still one of the major challenges for cities due vulnerable groups demand special requirements in the design of smart mobility, but at the same time, smart cities' technologies could be used to maintain their quality of life. From architectural and sociological point of view, smart cities change the meaning and the use of public spaces, from physical meeting places to relational public spaces, in which humans use interposed technological means and information flows. This leads to the concept of Interconnected Public Spaces (IP-Spaces). A mixture of physical and virtual environments, generating interconnections at a planetary scale, that can be used to attract elderly and minorities for collectively sharing outdoor experiences in public spaces (parks, squares or bus stops, in any city on our planet), increasing their physical form and stimulating them mentally, socially and emotionally. This paper describes the Human-Computer Interfaces design for IP-Spaces and their implementation in a smart bus stop.

Keywords: Smart Cities, inclusive transport, quality of life, interconnected public spaces.

2

1 Introduction

The lexicon that describes the characteristics of a Smart City has been changing, largely due to the different stakeholders that have taken part in the concept of Smart City, adapting it to their priorities and interests. The term "Sustainable Cities" gained momentum in the 1950s, being widely used in English-speaking countries, as well as those facing climate problems and looking for solutions to mitigate them. In the 90s, the term "Digital Cities" took center stage, as a consequence of the exponential growth that technology had been experiencing since the late 1980s. The European Commission created the program called "European Digital Cities" (1996-1999), with the intention to rely on the digitization of cities to help their complex growth and sustainability, making citizens increasing their participation for decision-making. Towards the end of first decade of the 2000s, the term "Smart City" emerged strongly, with connotations of sustainability and social inclusion, but without forgetting its bases supported by new technologies emerging from the Internet age. This last term has a branch called "Inclusive Smart Cities".

Taking into account the mobility of citizens as a key aspect in a Smart City, in April 2018, European Commission published the document "Transport in the European Union. Current Trends and Issues", which highlights the importance of social aspects in the development of an advanced European transport system: "From a social perspective, affordability, reliability and accessibility of transport are key. However, this has not been achieved across the board. Addressing these challenges will help pursue sustainable growth in the EU" [1].

The concepts of social inclusion and the digitalization of transport have to be harmonized in terms of accessibility, affordability, reliability and inclusiveness. Public transport plays a crucial role for mitigating the social exclusion of vulnerable and disadvantaged groups, affecting their access to basic services and their social and employment relationships. In order to achieve the above mentioned functionalities, elements that conform a smart transport system as for example bus stops, should include information about all the stages of the journey, including the walking environment, so that people with mobility impairment can reach and use transport services, addressing the specific needs of vulnerable groups and also considerer people's safety and security.

A transportation system element with a high level of smartness as the bus stop or inter-modal station then will be part of an "Interconnected Public Space", IP-Spaces is a novel concept. It is a mixture of physical and virtual environments that can be used to attract the elderly and minorities for collectively sharing mostly outdoor experiences in public spaces (parks, transport stations or bus stops), generating interconnections at a planetary scale, in order to increase their physical form and stimulate them mentally, socially and emotionally. The IP-Spaces accomplish their functions using a vast amount of technological interfaces providing the information and interactivity with the users.

Thus following sections of this paper describe the state of the art in relation with the IP-Spaces, the technological interfaces suitable for using in their implementa-

tion, an example of smart bus stop that take into account those concepts and finally the conclusions and future work.

2 Related Work and Background

Currently, in our cities, there are groups of citizens who are especially vulnerable to exclusion, including persons with disabilities and elderly (many of whom live alone), as well as persons on low incomes and the unemployed. Special attention deserves the situation of women, as some studies reveal that women have different travel patterns from men and that public transportation plays a crucial role in empowerment, access to opportunities and independence [2], enable people at risk of poverty or social exclusion to have the opportunity to participate fully in social life, and thus enjoy an adequate standard of living considered normal in the society in which they live [3].

Elderly people are one of the most vulnerable group of citizens. There were 703 million persons aged 65 years or over in the world in 2019. The number of elderly is estimated to double to 1.5 billion in 2050, growing from current 9% to 16% of population [4]. This growing sector of population have special needs to maintain a good physical and mental wellbeing. These needs include physical exercise, social interaction and mental stimulation. Research into ageing and cognition has demonstrated the close relationship of sensory functioning and social communication to maintaining cognitive performance and mood in the elderly, yet in modern societies elderly people are increasingly isolated and under stimulated, both physically and psychosocially [5]. This situation results in accelerated cognitive decline and the suffering associated with loneliness and confusion. Social interaction and intellectual stimulation may be relevant to preserving mental functioning in the elderly [6]. Some studies reports that subjects, who participated in senior citizen clubs or senior centers, can a lower risk of cognitive decline, specially is this interaction id realized with young adults [7]. Other studies highlight the potential of video games for developing of physical skills, creating mental and social interactions for elderly people. Particularly if these video or computer games are designed with an engaging content and provided through, an easy and pleasurable interface [8].

2.1 Stop Buses as Interconnected public spaces

An “Interconnected Public Space” or IP-Space [9] i.e. an outdoor space provided with an ICT equipment that can connect only with a similar space in other part of the world. Therefore, an IP-Space becomes a node in a network of IP-Spaces. An IP-Space node can be establish in an bus stop, in a park, in a square or any other outdoor spot in the city, in which a group of persons could potentially interact with it. Therefore, IP-Spaces allow the sharing of collective experiences.

These nodes can be used to connect with persons from other regions or countries, using the same or different languages. They can be used to participate remotely in different sport, physical, cultural and playful activities (such as intellectual games or

4

video games, physical exercises, dancing competition and many more) engaging elderly people in remote communities and stimulating them physically, socially and intellectually.

For groups in risk of social exclusion and specifically for elderly, promoting participation in cultural and sport activities contributes to emotional, physical health and social cohesion [10]. The positive impact of participation in cultural activities –no matter what the level of ‘artistic competence’ of the people involved –on the perception of one’s own psycho-physic wellbeing has been acknowledged for around 40 years and confirmed by a scientific measurement scale, the psychological general wellbeing index. As conclusion, the connection between culture and subjective wellbeing may often seem obvious although scientific evidence is much harder to get [11]. Interconnected public spaces can help create the conditions under which well-being is more likely to improve. As mentioned before, the implementation of the IP-Space can take place on a smart bus stop or in other elements forming part of a transportation system as well in public places as parks, squares, etc. Good examples of how smart urban furniture can evolve to interconnected public spaces may be the outdoor bus ticket-kiosk (Portuguese OEMKIOSK) or information providing smart furniture adapted to people with disabilities as Portuguese TOMI as shown in Fig. 1.



Fig. 1. Outdoor TOMI accessible information kiosk (Courtesy TOMI World).

2.2 Human-Computer interfaces for Smart Bus Stops

The variability of possible locations of IP-Spaces within Smart Cities and the diversity of the people who interact with them require the inclusion of user interfaces that allow adequate communication and interaction at all times and for each user, meeting the criteria of Design for All [13] for human diversity, social inclusion and equality. Multimodality [14] is a fundamental aspect in the design of IP-Spaces interfaces to promote a larger adoption among the community.

Based on different levels of information to be provided to specific groups of users, several human computer interfaces can be used as for example, tactile, pressure or sound based. The basic information like maps, numbers of approaching buses, their detailed route, type of buses and timing according to their live location can be provided by a tactile screen forming part of the physical structure of the bus stop, more detailed information can be collected by connecting the phone to the stop with wireless technology. Use of mobile phones ensures quick and personalized information. It also

avoids users to use the bus stop screen for a long time and also, many users are shy to use a screen in public as they are afraid of something going wrong. Use of mobile phone avoids such cases.

The NFC (Near Field communication) technology has been used in many countries as for example Finland for connecting the phone to the bus stop as it is brought in close proximity to the screen, although a Bluetooth connection is possible [15].

For more sophisticated services provided by the bus stop, as for example entertainment or special services for disabled people, possible solutions are based on ultra-directional sound projection systems that allow the user to cleanly hear the sound coming from the IP-Spaces in noisy environments as well as user interfaces based on gesture recognition, allows interaction with the IP-Spaces at distance, without touching any screen or panel. The recent develop of new artificial vision techniques combining convolutional neural networks and cloud computing will allow the recognition of gestures to go one-step further and be can be used by all people as well as by deaf persons using sign language.

3 Technological Interfaces for Smart Stops used as IP-Spaces

In this section introduces some of the most advanced and inclusive Human-Computer Interfaces (HCI) that can be used in the IP-Spaces. These HCI not only should ensure accessibility, but also allow the development of recreational and educational applications.

3.1 Audiovisual Accessibility

If the application that implements the IP-Spaces incorporates a screen where videos are played, in addition to the audio associated to the video, it is necessary to include, based on the specific needs of people with sensory disabilities, the following services, each one in one or more languages:

- Sign language interpretation
- Subtitles
- Audio description



Fig. 2. Live Streaming including Subtitles and Sign Language. [CEAPAT: <https://youtu.be/Y3mI27IRCKw?t=2316>]

The image shown in Fig. 2 corresponds to one frame captured from a live streaming that includes accessibility for persons with sensorial disabilities. A hearing impaired or deaf person may prefer to display subtitles only, while another person, also hearing impaired or deaf, would prefer to use subtitles and sign language interpretation at the same time. Meanwhile, a visually impaired person will need the use of the audio description in order to follow of the videos, images or presentations that are being shown. Audio description is a voice service that requires an independent audio channel from the main audio of the video. In live events, individual headphones with wireless sound reception systems are normally used by the blind, similar to those used for simultaneous multilingual translation in international congresses.

In this specific event’s speakers are talking in English and the majority public is Spanish, so, in that case, it was mandatory to include some kind of translation in real time. Instead of using audio receptors, congress organizers decided to use subtitles to include translation. In this way, this accessibility service has been used by people with or without disabilities, whenever we consider that not knowing a foreign language is not considered a disability.

One of the main issues using videos with audio in noisy environments, where IP-Spaces are normally located, such as transport stations or parks, is the loss of sound intelligibility. The following proposal can be a valid solution, both for people who follow the main audio channel of the video on the IP-Spaces screen, and for those who are using the audio description service on a separate channel. To allow the correct transmission of sound signals, the use of a new kind of speakers, known as of ultra-directional speakers is proposed. These devices allow the concentration of the sound in a specific and narrow area which significantly enhances the intelligibility of the signal and avoids discomfort caused by excessive volume to other people passing by nearby.

Traditionally, sound propagation theory and the study of loudspeakers demonstrate that loudspeaker directivity is conditioned by the size of the speaker related to the size of the wavelength produced: “A large loudspeaker will be more directive than a small loudspeaker, or a loudspeaker specified at higher frequency (smaller wavelength) will also have more directivity” [16].

The Holosonic® technique used by Audio Spotlight uses a different approach (Fig. 3).

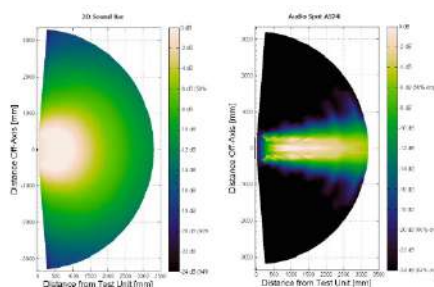


Fig. 3. Comparison of Directivity: Traditional 2D directional Array (Left) and Audio Spot Speaker (Right) [<https://www.holosonics.com/>]

Their “speakers” modulate the audio input to higher and inaudible frequencies (ultrasound waves around 60 kHz). Due to certain nonlinear characteristics of the ultrasound propagation through air, the volume of air in front of the ultrasound generator (Audio Spotlight speaker) acts as a “virtual loudspeaker”. The result of this technique is a source of directional audio able to be pointed as the same way than a concentrated light, (like a “Spot Light”) where the demodulation part is naturally created by thin air. The listener inside the Sweetspot hears a fully focused sound that cannot be localized when moving the head (feeling as hearing a monophonic source).

Another remarkable feature of this system is that the sound is concentrated in a relatively small space, which can go from half a meter to a meter and a half, depending on the distance from the speaker to the listener and the speaker power. If the listener leaves the area where the sound is concentrated, the sound disappears completely. This allows different sound spaces to be created near each other without any interferences between them.

The comparison shown in the Fig. 3 shows, on the left, the directivity pattern of a 2D loudspeaker array, generally considered directive, whose graph shows a semicircular pattern, without clear directivity in any direction. The image on the right shows the directivity pattern corresponding to the Audio Spotlight AS24i model, where a directive and concentrated beam is shown in the propagation axis.

The technology described above has been consolidated for more than 10 years and is being used worldwide, mainly in museums. In addition, a motion detector is integrated in the system to sense the presence of a visitor in front of a painting or sculpture and triggers a recorded narration explaining, for example, its technique, details or history. The playback can only be heard by the person standing within a specific physical space (Sweetspot) but not by the other visitors. Currently, due to the hygienic measures necessary to avoid virus contagion, this alternative is preferred because is much safer than audio guides, which must be disinfected after individual use.



Fig. 4. Bus Stops using Directional Sound
[<https://www.holosonics.com/applications-1>]

The pictures shown in Fig. 4 have been taken from a real installation at a Bus Stop in Disneyland Hong Kong to promote the film Star Wars: Tomorrowland Takeover. Floor indicators help people to know where the audio beam can be audible (Sweetspot). Each of these beams, associated with the holograms and the screens can

8

play the demonstration loop in a different part of the video because the audios are not mixing in the air. If other people are watching the screens out of the Sweetspots, they cannot hear it. The rectangular black speakers are installed on the ledge of the bus stop, pointing to the designated spaces on the floor.

The technology and its installation in the IP-Spaces would be similar to that described previously for bus stops when the IP-Spaces play audio videos with audio but without an extra track for the audio description service. One or more points can be set in front of the screen to indicate where the sound is audible.

If audio description accessibility service is being included, podotactile (Fig. 5) tiles should be installed to determine the location where the blind person should stand in order to hear the audio description track (Audio description-Sweetspot). In general, an audio description channel usually contains only the voice of a speaker with the description of what is happening on the screen because the main audio, from the main speakers, can be heard at the same time. In this case, if the main audio is also using Audio Spotlight speakers the audio description track must mix the main audio (at a lower volume), as it is not audible at the location of the audio description, and audio description voice.



Fig. 5. Podotactile floor [<https://www.tododisca.com/pavimento-podotactil/>]

3.2 Gestural interfaces for IP-Spaces

User interfaces using modalities such as touch, gestures or voice are referred to as Natural User Interfaces (NUI). These interfaces are easy to use because they are adapted to the way humans naturally communicate. Gesture recognition is one of them and is being applied to consumer electronics, automobiles or medical systems. These emerging technologies are opening new ways to control devices without contact and are becoming very popular. Gesture capture is conditioned by the needs of the specific control application. The interface has to be designed based on interaction range (close or distant/far), the resolution of gestures (hands movement or full-bodied movements), duration of gestures (short or long) and conditions of the environment in which the interaction takes place (indoor or outdoor).

Recently, due to the global pandemic caused by COVID-19, the adoption of touchless systems has increased considerably. Many manufacturers have launched touchless interfaces in their electronic kiosks for access to work centers or to manage tickets at transport stations. For some developers, and on certain web pages, the concepts

of hand tracking and gesture recognition are separated. In these cases, gesture recognition is a limited set of movements and positions of hands and arms while a hand tracking system has a greater number of interactions to capture finger movement and recreate it in a virtual environment. “A gesture-based system is usually limited to a specific number of gestures, since people have a hard time remembering more than a few gestures, but for those limited number of hand poses, the gesture system will usually recognize them fairly robustly” [17].

Some parallelism can be established with another type of interface: voice commands. In general, people do not usually remember a high number of voice commands and the same happens with gestures. Moreover, a detection system for a limited number of voice commands or gestures is going to be a robust recognition system. On the other hand, continuing with the parallelism, the processing of natural language equivalent to hands tracking requires a high computational power and is based mainly on artificial intelligence techniques. Voice recognition results are usually not as accurate as command detection. It is quite common to have experienced (with voice assistant or mobile device) a very precise recognition in quiet environments and quite the opposite in noisy environments.

As previously mentioned, the IP-Spaces (Interconnected Public Spaces) are located in outdoor areas that are normally exposed to high levels of ambient noise that cause loss of quality in sound capture or voice recognition. This limitation can be avoided by use of other data entry interfaces, such as gesture recognition (Fig. 6). The variability of light during the day, the incidence of direct sun on the IP-Spaces or the lack of light at night are undesirable in image capture in the same way high noise levels are in sound capture. Therefore, a preliminary study of the exact location of the IP-Spaces, its position with respect to the sun, the design and installation of protective panels or artificial lights are recommended. In this way, capture and inference processes of the artificial vision system will work correctly and will make it usable. Otherwise, any kind of gesture recognition will not work, with the consequent frustration of the IP-Spaces user.



Fig. 6. Console based game controlled using gestures [Pop Culture Geek taken by Doug Kline [https://commons.wikimedia.org/wiki/File:CES_2012_-_Microsoft_Kinect_Star_Wars_Episode_1_Podrace\(6764013293\).jpg](https://commons.wikimedia.org/wiki/File:CES_2012_-_Microsoft_Kinect_Star_Wars_Episode_1_Podrace(6764013293).jpg)].

Among the two alternative solutions introduced above, hand tracking is ruled out due to its difficult implementation without the use of sensors in fingers or special gloves, something that goes against the current trend of not touching or sharing any

object with other users. If gesture recognition in IP-Spaces should not have any additional elements, there is no point in using 3D models based on skeletal or volumetric structures. Therefore, the model to be used will be appearance-based type, where the input information will come from image sequences from a stereoscopic camera, also called depth camera. Since IP-Spaces must include a webcam for video conferencing applications, in order to take advantage of the same hardware for various applications, this camera will be used to gesture recognition.

Among the options available on the market for depth cameras, a new product that is prepared for outdoor installation is the Intel RealSense Depth Camera D455. The advantages of this device are that the development environment is cross-platform, its SDK is Open Source and is prepared to be used with multiple programming languages and software development environments: NodeJS, Python, C, C++, C#, LabVIEW, MATLAB, Unity, Unreal, OpenCV, etc. A video demonstration of the possibilities of using a gestural interface that can be implemented in IP-Spaces using a depth camera is shown in [18].

There is still a lot of work to be done in this area to achieve full integration of gesture recognition in IP-Spaces where the possibilities of interaction based on human skills and the way of expressing oneself through movement opens the door not only to communicative but recreational and educational applications in open spaces.

4 MUSA Smart Stop Architecture. One example of an IP-Space

MUSA (Advanced Sustainable Urban Furniture – Mobiliario Urbano Sostenible y Avanzado) is the smart bus stop under development in the city of Madrid that will also host an IP-Space [19] [20]. Its main characteristic is the provision of information services with focus on inclusive and social driven transport aspects.

The smart bus stop, from inclusiveness point of view, is:

- a) An interactive bus stop available to the whole population. This public point to a DTS allows access to persons without apps or even without a smart phone.
- b) Improving the accessibility to DTS through customization of interfaces and reduction of cognitive demand.
- c) Working as a travel assistant for low-income or disadvantaged groups of users.
- d) Improving service in real time considering and warning about unexpected events that can improve or disrupt transport operations.
- e) Through an attractive and customized interface, fostering the penetration of travel planning apps and its use by different users' segments.
- f) Implemented as "small" smart furniture providing a robust, essential electronic equipment, they can convert traditional stops into accessible Smart-Stops minimizing costs and having a wide use in cities and rural areas.
- g) It can help to introduce Interconnected Public Space spots. This is very suitable when the smart bus stop is in a park or square, where people can be involved in sports, physical and cultural activities. Sharing the same ICT infrastructure makes the system aesthetically and economically attractive.

4.1 Smart stop services.

MUSA architecture is shown in Fig. 7. Research about possible smart stop services are being performed.

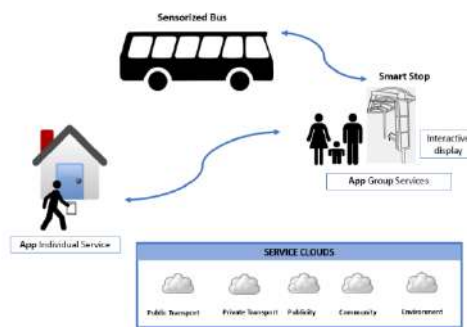


Fig. 7. Main components of MUSA architecture.

The smart bus stop is being designed as a smart furniture, which provides different services: information about public and private transport, reservation of trips, as well as publicity services, community communication services, environment awareness information and delivering point for e-commerce [19]. These services can be accessed from a screen which will connect passengers to a set of cloud services. The works on smart stop are currently in progress. Designed as a special software layer, it can run on a commercial travel planner, such as Google Maps. This has two advantages; it allows the customization of interfaces for different users' segments and the collection of traveling data, which can be used anonymously for building mobility models and develop social innovation solutions. In addition, it can be adapted to different commercial planners.

The prototype of the Smart Stop and its interface are shown in Fig. 8.



Fig. 8. Main interface of the smart bus stop prototype.

Advertisement is running on the background (in this case for musicals in the center of Madrid), different services are available in the lower carousel. To intuitively attract user to different interfaces, two type of icons are available. A traditional picture is used to attract more serious and direct users. Let's call it the "conservative inter-

12

face”. And, a more playful icon is used to attract more skillful and playful users. Let’s call this the “playful interface”. Other future special services for assisting traveler with special needs (elder, reduced mobility, easier travel with kids or pregnant women) are also included in the interface. IP-Space services will be available following the already mentioned two icons policy.

The “conservative interface” of the public transport app is shown in Fig. 9. A box with the most frequently used destination from current stop is shown on top right corners, increasing the probabilities of reducing the interaction to minimum. Below, a box shows time and duration of the selected trip (cost will be available soon). Also, there is an option to select private or other type of alternative transport without leaving conservative mode of interaction. A third box allows user to select any origin and destination, using a tactile keyboard on the screen. Finally, information about nearest bus stops can be searched. Typical interactive features of Google Maps are disabled, so conservative user cannot be distracted from their simple, direct interaction with the app.

Transport app includes a mode for fostering physical exercises by means of walking. In this case, time and duration of a trip walking and using public transport are similar, so the option of walking can be healthier for the user. This feature can be very interesting for elder people.



Fig. 9. Multimodal planner using public transport.

4.2 Interconnected Public Space service in MUSA.

The new functionality of the Interconnected Public Space (IP-Space) is being developed in the current prototype of MUSA smart bus stop.

From the stop, which is an IP-Space node, a user or set of users can connect to persons from other regions or countries present in another IP-Space node, using the same or different languages. All they can participate remotely in different sport, physical, cultural and playful activities (e.g. interesting games or video games, physical exercises, dancing competition and many more). Interface can transmit audio or video using cameras and microphones, although this can be restricted in accordance with current local privacy laws. This also will depend on whether the IP-Space is physically enclosed or it is a completely open public location. However, in all cases the inter-

face will allow the transmission of images, graphics and text as basic means of communication.

In a first approach to the design of the prototype, the high-level operation of this service consists in three steps (Fig. 10):

- a) Map. Users request the realization of a given activity to other people in a remote IP-Space. They can start the activity immediately or schedule it at a given date.
- b) Menu. They select the desired or scheduled activity from the repository and access to it.
- c) Activity. They proceed to realize the desired activity. They will have a language assistance application, so people from different countries and culture can communicate.



Fig. 10. IP-Space users' interaction sequence.

Another important aspect of IP-Space design are human-computer interfaces including interactive electronic surfaces i.e. displays with gestural or tactile interfaces, cameras (or image systems) and audio systems. Interactive video walls, floors and tables will allow a rich communication of local and remote groups (Fig. 11). These interfaces jointly with advanced algorithms and AI techniques will ensure accessibility and the development of a rich set of activities.



Fig. 11. IP-Space users' interactions.

5 Conclusions

This work describes the first steps of development of a smart stop and an IP-Space designed to increase social inclusiveness and quality of life of elder people. The paper is focused on the inclusive advanced Human-Computer Interfaces that not only should ensure accessibility, but also allow the development of rich recreational and educational applications. Following the legal framework in the European Union [21], some measures must to be applied to ensure that a video call or conversational interaction

14

system at Smart Bus Stops safeguard the privacy rights of people who use it actively, such as those who are within the area of vision of the cameras.

Real-time image processing technology can be used to blur image background or to remove part of the images that may be capturing private properties. It is also necessary to determine and justify the categories of processed data (image, audio, video, text) and the duration of the retention of the data. Finally, it is necessary to have an accessible information process to advice the user in detail on the use and treatment of the application's data. After the detailed report, there must be a decision point in the application event that does not allow its use without user's consent. In this way, individual rights of users and other people who may be passing nearby are safeguarded.

Acknowledgments: This research was funded by Universidad Europea de Madrid grant number 2019/UEM19.

References

1. Transport in the European Union: Current Trends and Issues, <https://ec.europa.eu/transport/sites/transport/files/2018-transport-in-the-cu-current-trends-and-issues.pdf>, last accessed July 2019.
2. Kenyon, K., Lyons G., Rafferty, J. (2003), Transport and social exclusion: investigating the possibility of promoting social exclusion through virtual mobility, *Journal of Transport Geography*, Vol. 10, pp. 207-
3. Manuela Samek, Flavia Pesce, Patrizia Malgieri, Silvia Maffi and Caterina Rosa. The Role of Women in the Green Economy. The Issue of Mobility, [http://www.europarl.europa.eu/RegData/etudes/note/join/2012/462453/IPOL-FEMM_NT\(2012\)462453_EN.pdf](http://www.europarl.europa.eu/RegData/etudes/note/join/2012/462453/IPOL-FEMM_NT(2012)462453_EN.pdf), last accessed July 2019.
4. Department of Economic and Social Affairs, United Nations. World Population Ageing 2019: Highlights; United Nations: New York, NY, USA, 2019; pp. 1–2.
5. Waterworth, J.; Ballesteros, S.; Christian, P.; Bieber, G.; Kreiner, A.; Wiratanaya, A.; Polymenakos, L.; Wanhe-Politis, S.; Capobianco, M.; Etxeberria, I.; et al. Ageing in a networked society—Social inclusion and mental stimulation. In *Proceedings of the 2nd International Conference on Pervasive Technologies Related to Assistive Environments (PETRA 2009)*, Corfu, Greece, 9–13 June 2009.
6. Wang, H.; Karp, A.; Winblad, B.; Fratiglioni, L. Late-Life Engagement in Social and Leisure Activities Is Associated with a Decreased Risk of Dementia: A Longitudinal Study from the Kungsholmen Project. *Am. J. Epidemiol.* 2002, 155, 1081–1087.
7. Lee, S.H.; Kim, Y.B. Which type of social activities may reduce cognitive decline in the elderly?: A longitudinal population-based study. *BMC Geriatr.* 2016, 16, 165.
8. IJsselsteijn, W.; Nap, H.H.; de Kort, Y.; Poels, K. Digital Game Design for Elderly Users. In *Proceedings of the Conference on Future Play—Future Play '07*, Toronto, ON, Canada, 15–17 November 2007.
9. Padrón Nápoles, Víctor M.; Gachet Páez, Diego; Esteban Penelas, José L.; García Pérez, Olalla; García Santacruz, María J.; Martín de Pablos, Fernando. 2020. Smart Bus Stops as Interconnected Public Spaces for Increasing Social Inclusiveness and Quality of Life of Elder Users. *Smart Cities* 3, no. 2: 430-443
10. Bacon, N.; M. Brophy, N. Mguni, G. Mulgan and A. Shandro. The State of Happiness: Can Public Policy Shape People's Wellbeing and Resilience? The Young Foundation:

- London, UK, 2010. Available online: <https://youngfoundation.org/wp-content/uploads/2012/10/The-State-of-Happiness.pdf> (accessed on 8 September 2020).
11. Diener, E. *The Science of Well-Being: The Collected Works of Ed Diener*; Social Indicators Research Series; Springer: London, UK, 2009; Volume 37.
 12. Social Inclusion in EU Public Transport, [http://www.docutren.com/pdf/boletin/\[IIIA%201440\].pdf](http://www.docutren.com/pdf/boletin/[IIIA%201440].pdf), last accessed 8 September.
 13. Design For All Criteria. <https://designforall.org>, last accessed 2020/9/7.
 14. Multimodal. (2020). Multimodal Access Interfaces. <https://www.w3.org/standards/webofdevices/multimodal>. Accessed 20 June 2020.
 15. Sumit Arora. Designing a Smart Bus Stop for Metropolitans and Tier-1 Cities of India. In *Proceedings of the India HCI 2014 Conference on Human Computer Interaction (IndiaHCI '14)*. Association for Computing Machinery, New York, NY, USA, 122–125. DOI:<https://doi.org/10.1145/2676702.2676722>
 16. Audio Spot Light. Fundamental limitations of loudspeaker directivity <https://www.holosonics.com/fundamental-limitations-of-loudspeaker-directivity>. Accessed 7 September 2020.
 17. Hand Tracking. Hand Tracking and Gesture Recognition. <https://www.intelrealsense.com/hand-tracking-overview/>, last accessed 2020/9/7.
 18. Project Prague. Project Prague. Demos. <https://youtu.be/k38ygfIAqVg>, last accessed 2020/9/7.
 19. Nápoles V.M.P., Páez D.G., Penelas J.L.E., García G.G., Santacruz M.J.G. Bus Stops as a Tool for Increasing Social Inclusiveness in Smart Cities. In: Nesmachnow S., Hernández Callejo L. (eds) *Smart Cities. ICSC-CITIES 2019. Communications in Computer and Information Science*, vol 1152. Springer, Cham. https://doi.org/10.1007/978-3-030-38889-8_17.
 20. Nápoles, V.M.P.; Rodríguez, M.B.; Páez, D.G.; Penelas, J.L.E.; García-Ochoa, A.G.; Pérez, A.L. MUSA-I. towards New Social Tools for Advanced Multi-Modal Transportation in Smart Cities. *Proceedings 2018*, 2, 1215.
 21. EDPB. Guidelines 3/2019 on processing of personal data through video devices. 10 July 2019 EDPB plenary meeting, 09-10 July 2019. https://edpb.europa.eu/our-work-tools/our-documents/guidelines/guidelines-32019-processing-personal-data-through-video_es, last accessed 2020/9/7.

Analysis of alternatives for the acceleration of a Hyperloop system

Luis García-Tabarés¹[0000-0003-2732-9108], Marcos Lafoz¹[0000-0001-9613-1280], Jorge Torres¹[0000-0001-7524-9925], Gustavo Soriano¹[0000-0002-5169-9080], Daniel Orient², Daniel Fons²

¹ CIEMAT. Av. Complutense, 40. 28040 Madrid (Spain)

² ZELEROS. Muelle de Nazaret sn, 46024 Valencia (Spain)

marcos.lafoz@ciemat.es

Abstract. The paper introduces the Hyperloop inspired system by the company ZELEROS and provides a discussion about the alternatives for the acceleration. The ZELEROS system comprises a named propulsion system, based on an air turbine, and an acceleration system based on a linear motor. Different options have been discussed for the linear motor: induction machines, permanent magnet machines and switched reluctance machine, among some other hybrid solutions. Advantages and drawbacks are presented for all of them. For this particular application, where the length of the active side and the speed are really significant, the option of a linear switched reluctance motor results convenient both from the technical and economic points of view. A further discussion about the type of linear switched reluctance motor (LSRM) preferred is also accomplished during the paper, taking into account a particular model of the machine as well as its operation conditions regarding the frequency, dimensions and operation parameters. Three options are compared during the analysis: a single-side horizontal LSRM, a N-side vertical LSRM and a cylindrical LSRM. Qualitative and quantitative (based on the model) arguments are given in favour and against each alternative. Finally, the two-sided vertical switched reluctance machine has been considered as the most adequate for the development of the Zeleros Acceleration System.

Keywords: Railway transportation, linear motor, switched reluctance machine.

1 Operation of the ZELEROS Hyperloop system

Hyperloop is the commercial name for an ultrahigh speed railway transportation system [1], used both for passengers and cargo, through a tube where the air pressure has been reduced in order to reach speeds up to 1000 km/h. Many technologies have been developed during the last years and one of them belongs to the Spanish company ZELEROS.

The system Zeleros, presented in Fig 1, is envisioned as suitable for the transportation of passengers and cargo; it aims at being strongly competitive at distances between 500 and 1500 km, still maintaining the ability to be used for shorter distances, and for much longer distances as well, so long the business case works [2]. Therefore,

its tactical range falls in the intercity connection, what in the case of Western Europe will mostly mean state capital cities, and large cities such as Barcelona, Frankfurt, or Marseille [3]. The station can be potentially brought to the city center, despite this feature is optional, since arriving at an airport or other type of hub can be potentially equally efficient. A case by case analysis needs to be set up. Vehicles will depart and arrive at a minimum interval around of two minutes and a half, keeping this headway during the whole route. Cruise speed will be between 600 and 750 km/h. The pressure level inside the tube will be around 100 mbar, or 1/10th of atmosphere pressure. This is a pressure value similar to that of air at the flight level where the Concorde used to cruise. All the energy needed to fulfill the mission will be carried onboard. Fleets can be composed by vehicles of between 50 and up to 200 passengers. The goods only vehicle equivalent to the 200 passengers vehicle will have a maximum payload of 30 metric tons. In terms of passengers, this means up to 4.800 passenger per hour and per direction per one tube. The capacity can be scaled up by adding further tubes per direction. In case sufficient demand exist and this expansion is deemed necessary, the increment on the infrastructure cost will represent only a fraction of the cost of the works needed to put in place the first tube, especially in the case the tube is placed over pylons, additional cost that what will be largely compensated by the additional traffic.



Fig. 1. Technology of the Hyperloop inspired system from ZELEROS.

The system targets a niche of distance that are currently being served by medium size airplanes, since traditional high-speed rails are not fast enough to compete, while maglev solutions seem to be too expensive. The system can be seen as an expansion of the operational envelope of the traditional land transportation, whose current limit is the service provided by high speed rail for well established and densely travelled corridors/routes, and can also be seen as a green alternative to airplanes, since the vehicles are fully electrical driven, and the overall energy consumption is substantially lower than that of aircrafts in the above mentioned range.

From a passenger perspective, the user will board as he will normally do on a high-speed rail car. Once inside, a door similar to that of an airplane will close. The vehicle will start motion as driverless people mover. Once the platform deck has been left behind, the vehicle will ingress on an airlock. The vehicle will be quickly depressurized, same as fighter jet on a vertical climb. Then the vehicle will reach the acceleration system. It will provide thrust enough to achieve cruise speed. Once cruise speed is achieved, the compressed air propulsion system will take over and will take care of sustaining the speed.

2 The propulsion of the ZELEROS system

There are two main propulsion systems included in the solution:

a) The cruise speed system:

A compressed air propulsion system, where the air at high pressure is used to generate enough thrust to compensate the overall drag. It can be used to some extent to accelerate it too, particularly for small speed adjustments during the run. This is a system onboard the vehicle. The requirements are: a turbofan like that of airplanes, trained by one or several electrical drives. Depending on the vehicle capacity, mission range, speed profile, and specific pressure value, among others, the electric power needed will be between 7 and 13 MW.

b) The acceleration system:

A linear motor commissioned to accelerate from zero speed to cruise speed. It will have a length of between 6 and 15 km that will be placed at the start of the route. This is a system that is placed primarily on the track, with some elements placed on the vehicle, depending on the specific type of motor used. The acceleration system can be used at the stations to regenerate the kinetic energy of the moving vehicle, in order to use this energy for the launch of the next vehicle. The requirements are: to be able to provide the power needed to achieve a maximum acceleration of 3 m/s² to the heaviest vehicle on the fleet, to have adjustable power for vehicles of different mass, a standard acceleration request between 1.5 and 2.5 m/s², and a jerk (m/s³) limitation in accordance with passenger comfort needs.

3 Options for the Acceleration Systems

As commented in the previous point, the main propulsion system of the vehicle is unable to produce the required force to drive the vehicle below a certain speed and this is the reason why an auxiliary propulsion system is needed.

Different alternatives may be considered for this purpose, some of which are based on electrical devices while others use catapults, rockets or any other mechanical system.

While these last options have been used for accelerating different devices in experimental facilities [4], a solution based on an electrical machine for a future commercial ultra high-speed vehicle seems to be much more adequate for different reasons, including controllability, cost, regenerative braking capability, simultaneous operation of different vehicles, etc. Particularly, electrical Linear Machines (LM) are especially suitable and advantageous over rotary ones with gears, because they allow smoother operation with less noise and absence of slipping if the rotational movement is transmitted to a wheel (besides the challenges associated to the use of wheels at very high speeds). So, the first decision was to use a Linear Electrical Machine to accelerate the vehicle.

The second decision was to decide the configuration of that LM. Besides the type of machine to be used (which will be commented in the next paragraphs), the most critical point to consider is whether the Active Side of the LM (the side which in-

cludes those coils contributing with the required active power and in some cases with both, the active and reactive power) is stationary (Stator) or moving (Translator).

In order to continue with the decision process, let us consider just as a very simple example, a vehicle with a mass of 10 t, which needs to be accelerated at 700 km/h with an acceleration of $g \text{ m/s}^2$ (which is well above a commercial value). The required length of the machine should be in the range of 2,000 m, needing a force of 100,000 N.

Common sense advices to choose a moving Active Side located in the vehicle, in order to avoid having a 2 km long Stationary Active Side full of coils. For accelerations closer to commercial values, the length of this Active Side could still increase one order of magnitude.

Nevertheless, having a moving Active Side implies two options with their corresponding challenges:

- a) Coils are fed from ground using feedthroughs, catenaries or whatever system requiring physical contact and the corresponding wear. So far, there is no reliable off the shelf system able to be used at affordable conditions of cost and maintenance.
- b) Coils are fed from the vehicle, which includes an energy storage system based on batteries (any other would not be able to store the required levels of energy). Coming back to our previous example, the overall amount of energy needed to accelerate the vehicle would be 52,500 kWh. Considering the highest available energy density batteries (in the range of 160 Wh/kg) an extra mass of 328 t would be required, becoming fully inadmissible.

Previous situation leads to choose undoubtedly a stationary Active Side, which will be fixed to the ground as part of the track.

Next decision would concern the type of LM to be selected, taking into consideration that the Active Side must be long (extremely long in many cases) and stationary, while the Passive Side must be as light and simple as possible in order to maximize the payload of the transport system.

In principle, there are many types of LMs [5] but only a reduced number may be envisaged for this application. The main options that can be considered are [6,7]:

- 1) **Linear Induction Machines (LIM)**, the rotary version of the most popular electrical machine (Induction Machine) which is based on the interaction of two travelling magnetic fields, one created by the Active Side and other induced in the Passive Side. In the Linear version, the Passive Side is usually a solid aluminum plate, although a ladder-slit can also be used. There is a conceptual important difference with the rotary version: The existence of “end effects”: two additional induced fields at each end of the Passive Side, producing a net reduction of the force and the efficiency. As for other LMs, the machine can be single-sided (one Active Side) or doubled-sided (two Active Sides) but, in any case, there is only one aluminum plate. In the first case, there is a back iron behind the plate to close the field, while in the second one the magnetic flux is closed through both Active Sides.

The main advantages of LIMs are its simplicity and robustness, while the drawbacks are related with the low power factor and medium efficiency, as well as the power which is induced in the Passive Side in the form of Joule losses. End effects can also be very negative.

- 2) **Linear Switched Reluctance Machines (LSRM)** based on the sequential commutation of coils located in the Active Side creating a magnetic circuit that closes through the Passive Side trying to minimize its reluctance to produce mechanical work from electric power (motoring operation) or to maximize the reluctance to produce electrical power from mechanical work (generating operation). Each group of coils, which are fed in series simultaneously, constitute a phase of the machine. Coils are wound around iron poles forming the Active Side. Passive Side has only iron poles with no coils. Only certain combinations of Active and Passive Side number of poles are allowed in a LSRM. As for the case of the LIM, LSRMs can be either single-sided or double-sided. Since attraction force between both sides of the machine (normal force) can be much higher than propulsion force, the choice of a double-sided machine is mandatory to avoid non-compensated forces perpendicular to the machine displacement. In this regard, some of the authors participated in the past in the development of the so called Linear Multitranslator Switched Reluctance Machine (LMSRM) [8], a machine with two lateral Active Sides and one or more central Active Sides in between the lateral ones. Between the Active Sides are placed the Passive Sides in an arrangement, which is balanced from the normal force point of view. While lateral Active Sides need back iron to close the magnetic circuit, central Active Sides do not, so as the number of these elements grow, the traction force density (force per unit mass) of the machine increases. Recently, new configurations of LSRMs have been developed like the Mutually Coupled LSRM [9] in which more than one phase are excited simultaneously achieving more force density and less noise and vibrations levels. The main advantages of the LSRMs are its robustness and the low cost derived from its simplicity: Passive Side are simply laminated iron poles while Active Side include simple flat coils that can be manufactured independently and after mounted and connected in their position. In the list of drawbacks, the noise and vibrations due to the big normal force.
- 3) **Linear Permanent Magnet Machines (LPMM)**, linear machines that include permanent magnets in any of their two Sides. When the magnets are included in the Passive Side, they are in charge of creating the excitation field and the machines are Linear Permanent Magnet Synchronous Machines (LPMSM). Like for the case of the LIMs, this machine presents end effects which cause force ripple. There are also other sources of ripple like the cogging force, a tendency of the two sides of the machine to align due to the presence of the permanent magnets in one side that are attracted by the iron poles in the other side. In a conventional LPMSM, permanent magnets are located in the passive side: they provide the excitation magnetic field but they do not exchange active power.
Active Side only has coils which really deal with the active power of the system, converting mechanical work into electricity or the other way around. It is

usual to name “the Primary” the Active Side with the Coils and “the Secondary” the Passive Side.

Besides LPMSMs, there are a number of Synchronous Machines which have Permanent Magnets in the Primary Side (LPPMM) [6] coexisting with the coils, while the Secondary Side is purely Passive like for the case of LSRMs. There are basically four sub-categories of LPPMMs: Linear Switched-Flux Permanent Magnet Machines, Linear Flux-Reversed Permanent Magnet Machines, Linear Doubly-Salient Permanent Magnet Machines and Linear Vernier Permanent Magnet Machines.

The main advantage of LPMM in general, is their high force density and controllability as well as the good power factor while in the side of drawbacks, the most significant is the need of expensive and relative delicate NdFeB magnets and also the presence of ripple in the force and the higher complexity of the coil manufacturing. Other drawback is the existing cogging force due to the permanent magnets.

As a kind of summary, Table 1 shows the advantages and drawbacks for the three previously described families of linear electrical machines, for the particular application that we are considering which is basically characterized by the extremely long Active Side (Primary), a high commutation frequency, low cost requirement and robustness.

Table 1. Comparison of alternatives of Electrical Linear Machine for the Zeleros Hyperloop Impulsion System

Type of Machine	Advantages	Drawbacks
LIMs Linear Induction Machines	- Simple & robust	- Induced currents & heat dissipation in the moving Side
	- Absence of Permanent Magnets	- Relatively complex windings
		- Poor Power Factor
		- End Effects
		- Medium Efficiency
LSRMs Linear Switched Reluctance Machines	- Very simple & robust	- Noise & Vibration
	- Low Cost	- High lateral forces
	- Absence of Permanent Magnets	- Force Ripple
	- Very simple & cheap coils	
LPMMs Linear Permanent Magnet Machines	- High controllability & efficiency	- High or extremely high number of needed Permanent Magnets
	- Good Power Factor	- Force Ripple and cogging force
		- More complex windings

After this analysis, the selected candidate was the Linear Switched Reluctance Machine since some of the drawbacks could be overcome with an adequate drive system while advantages make it especially suitable for this application, especially in real scale systems where the impact of the cost in the overall solution can be decisive. In

this regard, Permanent Magnet Machines have to be discarded, especially LPPMMs since they would use this type of magnets along the full accelerating track.

4 Modeling and Selection of a Switched Reluctance Machine Type

Before coming into details regarding the specific type of LSRM that has been selected, we present a short introduction to the working principle of this kind of machine for a better understanding of the methodology, which has been used for its selection and calculation [10]. This introduction is based on Fig. 2, which represent a 3-phase one-sided LSRM with one Active Side with coils and one Passive one with only iron poles.

When working as a motor, one phase (green one for instance) is activated in the moment the iron pole P is entering that phase (fully misaligned, Fig 2.1.a). The pole tries to fully align the phase (Fig 2.3.a) to minimize the reluctance of the circuit and generates a force in the same sense as the pole moves (motoring operation). When the alignment is achieved, the phase is switched off and the next one comes into operation (the yellow one).

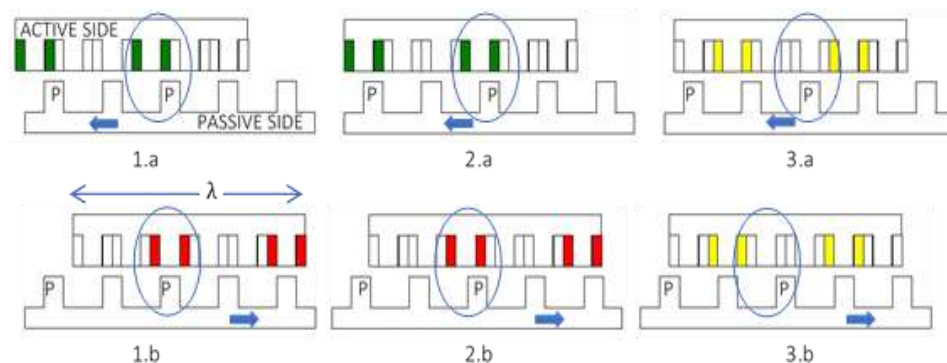


Fig. 2. Working principle of the LSRM: a) Motor Mode b) Generator Mode

When working as a generator, one phase is activated in the moment the pole P is fully aligned with that phase (Fig 2.1.b). Then, an external force pulls the pole and tries to take it to the fully misaligned position (Fig 2.3.b), a force that acts in the opposite sense as the pole moves (generating operation) to maximize the reluctance of the circuit. When misalignment is achieved, the phase is switched off and the next one is switched on (the yellow one).

Switched reluctance machines may present different configurations in terms of number of phases in the active side (m) and number of poles per machine period either in the Active (N_A) and Passive (N_P) Sides. If λ is the length of a machine period (see Fig. 2), in every commutation the machine advances one stroke (s), given as:

$$s = \lambda / (m \cdot N_p) \tag{1}$$

Since high speeds required high commutation frequencies, “s” must be high in order to minimize that frequency and hence m and NP must be as small as possible.

Calculating the force that the machine is able to produce, requires some knowledge on how it is fed [11, 12]. Fig. 3 shows one pole of the Passive Side and the corresponding coil of the Active Side acting over it. The coil is connected to a so-called H-Bridge which is connected to a DC Voltage Source. Positive voltage is applied to the coil when both switches are closed, while negative voltage is applied when the diodes of the bridge are conducting. By closing and opening the switches, the polarity can be reversed and the current controlled. When the switches are conducting, the current goes out the power supply extracting energy from it. When the diodes are conducting the current goes in the power supply injecting energy in it. These two situations are presented in Fig. 3.

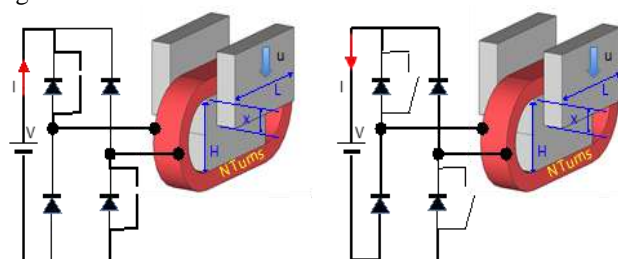


Fig. 3. H-Bridge topology to feed the SRM Coils: a) Conduction of the Switches b) Conduction of the Diodes

The net energy conversion from mechanical into electrical or vice versa is the power flowing through the battery along one period T. If the electrical resistance of the coil is neglected, we can express the total energy W, as a function of the current I and the flux ϕ :

$$W = \int_0^T V \cdot I \cdot dt = \int_0^T \frac{d\phi}{dt} I \cdot dt = \oint I \cdot d\phi \tag{2}$$

Representing the area enclosed by the closed Flux-Current curve. According to the nomenclature of Fig. 3 and for the pre-dimensioning of the different alternatives of LSRM, the force can be calculated as:

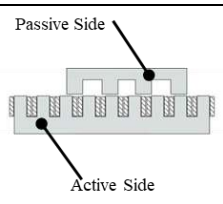
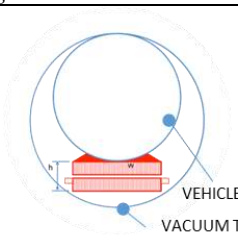
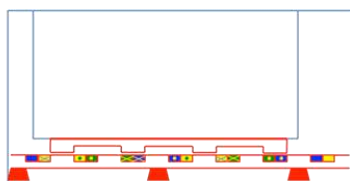
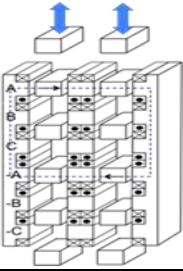
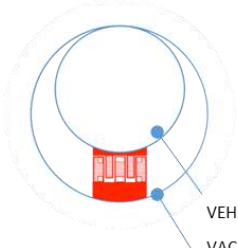

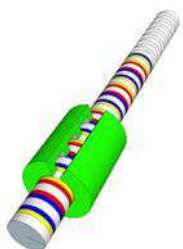
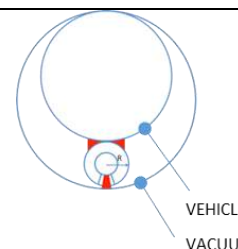
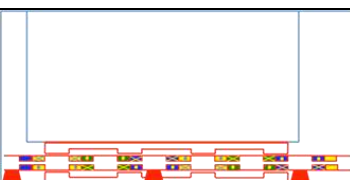
$$F = \frac{W}{T \cdot U} = \frac{K_{mag} \cdot \phi_{max} \cdot I_{max}}{H} = K_{mag} \cdot B_{max} \cdot I_{max} \cdot L \tag{3}$$

Assuming the simplification that the value of $\oint I \cdot d\phi$ is proportional to the product of the maximum values of the current and flux, respectively. The proportionality coefficients are derived from some analytical considerations and also from FEM calculations performed over some benchmark cases.

Equations (1), (2) and (3), along with purely geometrical considerations allowed us to develop a simple universal model to perform the selection of the optimum machine for a given vehicle. These geometrical considerations are based on easy relationships like imposing that the pole width must be twice the width of the coil, or that the pole

area must be the same as the return yoke area to avoid saturation in that yoke and obviously from the overall dimensions of the machine to fit in the available space.

Table 2. Analyzed topologies of LSRMs for impelling the vehicle

<p>Single-Sided Horizontal LSRM (ISH) <i>One Active Side all along the track and one Passive Side attached to the vehicle</i></p>		
 <p>Passive Side</p> <p>Active Side</p>	 <p>VEHICLE</p> <p>VACUUM TUBE</p>	
<p>N-Sided Vertical LSRM (NSV) <i>N Active Sides (2 lat. & (N-2) cent.) along the track. N-1 Passive Sides at the vehicle</i></p>		
	 <p>VEHICLE</p> <p>VACUUM TUBE</p>	
<p>Cylindrical LSRM (CYL) <i>One tubular Active Sides all along the track and one Tubular Passive Side at the vehicle</i></p>		
	 <p>VEHICLE</p> <p>VACUUM TUBE</p>	

In this application, we can define a so-called Unit Machine consisting of the portion of machine, which repeats sequentially every λ meters and the Traction Modulus, which comprises the number of Unit Machines to produce the required force.

Regarding the optimization criteria, the first approach has been to choose a Unit Machine that maximizes the electromagnetic force produced in it. Once it is defined, the number of Units Machines of the Traction Modulus is decided according to the overall forced requirements.

4.1 Three configurations of LSRMs

The next step is to choose the most suitable machine topology for this application. In this regard, we have concluded that there are three possible options, which a priori, would fulfil the requirements. Table 2 summarizes these three options in terms of their description, appearance and situation in the vehicle. Left hand side column shows the configuration of the machine while the right hand side corresponds to its location in the vehicle.

Single-Sided Horizontal LSRMs seem to be more adequate to the shape of the available room. They are also simple and easy to adjust with only one airgap but they present the tremendous disadvantage of the non-compensated transversal forces tending to attract the vehicle to the Active Side.

N-Sided Vertical LSRMs present a much higher force density, but they have the drawback of the adjustment of the several airgaps. When $N=2$ we have the case of the conventional Double-Sided LSRM.

Cylindrical LSRMs are fully compensated and have the great advantage of avoiding the coil ends so that every meter of the coil is producing thrust. The major drawback when working at high frequency is the difficulty for laminating the iron in the convenient direction all along the magnetic circuit.

4.2 Comparison and Selection of the three configurations of LSRMs

The previously described model was adapted to three options of LSRMs to perform individual optimizations for each solution and especially a comparison between the three configurations to select the most appropriate for this application.

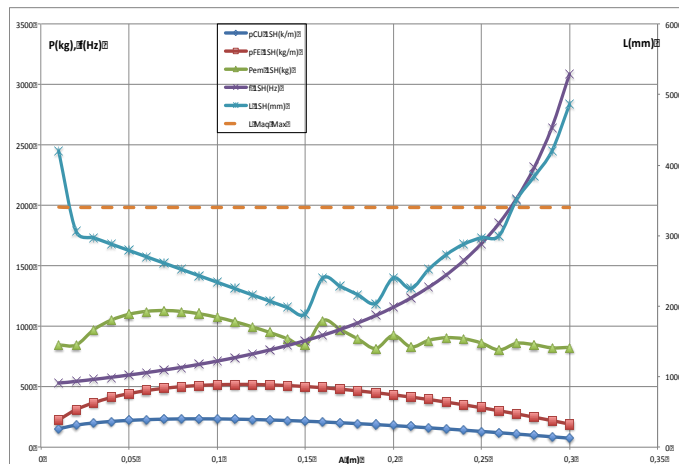


Fig. 4. Results for the 1SH Option

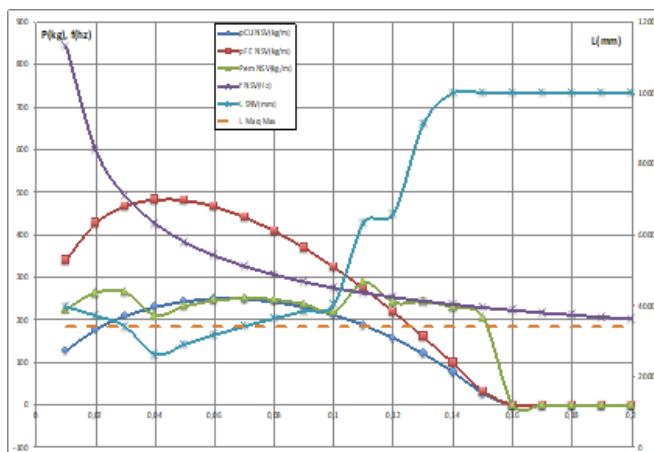


Fig. 5. Results for the NSV Option

Fig. 4. and Fig. 5 show some of these results for the Single-Sided Horizontal and the N-Sided Vertical options. X-axis represents the geometrical parameter “A” related to the machine enveloping dimensions, while Y-axes show: the Conductor weight per unit length of Active Side, the same for the iron, the weight of the Passive Side on board, the commutation frequency, the required length of the machine and, as a dotted line, the maximum available length to place the machine (machine length must be bigger than that value). Intersection of the Active Side length curve with the dotted line provides the two limits for parameter “A”. Working at low values of “A” imply higher conductor weights but much lower commutation frequencies. Although not shown, results for the Cylindrical machine are similar: there is a limit value for the parameter “A” but the smaller its value, the smaller the commutation frequency.

Table 3. Comparison of the topologies of LSRMs

1SH Option	2SV	SRM Ci
Advantages		
<ul style="list-style-type: none"> - Lower weight/meter of conductor & Iron - Reduced onboard weight 	<ul style="list-style-type: none"> - Reduced weight /meter of conductor & iron - Min. weight onboard - Min. commutation frequency - High force density - Balanced lateral forces 	<ul style="list-style-type: none"> - Moderate weight/meter of conductor - Easy coils manufacturing - No coil ends (all the coil length contributes to generate force)
Drawbacks		
<ul style="list-style-type: none"> - Very high commutation frequency - Non-balanced vertical force higher than the traction force 	<ul style="list-style-type: none"> - Worse fitting to the available space. - Need for precise adjustment of the two airgaps 	<ul style="list-style-type: none"> - High weight/meter of Iron - High onboard weight - Difficulty for laminating the iron in the adequate directions

Finally, Table 3 summarizes the qualitative and quantitative (given by the model) arguments in favour and against each alternative. For the case of the N-Sided Vertical machine, and for the sake of simplification, “N” has been set to two.

According to the previous considerations, the two-sided vertical switched reluctance machine has been considered as the most adequate for the development of the Zeleros Acceleration System.

5 Conclusions

The paper describes the concept of the ZELEROS Hyperloop Inspired system and the impelling system which is required to accelerate the vehicle up to the needed speed for operating the main propulsion system, which is based on a turbine driven by an electric motor.

Clearly, the option of an electric linear motor is preferred for this application to any other mechanical system due to its better controllability, capability of simultaneous operation for various vehicles, efficiency, etc.

A decision sequence is described along the paper: First, the choice of a Linear Electrical Machine, second to place the Active Side stationary on ground in spite its big length, as supplying the required power and energy to a moving Active Side would be unfeasible. The third decision is to choose the type of Linear Electric Machine among realistic candidates which have been identified and reduced to the following three options: The Linear Induction Machine, the Linear Switched Reluctance Machine and the Linear Permanent Magnet Machine. A justified rationale leads to choose for this application the Linear Switched Machine, basically for cost and robustness reasons.

In the category of Switched Reluctances Machines, three topologies have been identified as potential candidates: The singled-sided horizontal arrangement, the N-sided vertical one (with particular attention to $N=2$) and the cylindrical configuration. In order to evaluate and compare the three of them, an analytical model based on simplified equations and geometrical relationships, has been developed and run. Considering both, qualitative and quantitative arguments, we have concluded that a double-sided vertical switched reluctance machine represents the best option for this application.

The selection of the linear motor type for the acceleration system can be complemented with the analysis of the power supply of the motor, already accomplished in a previous publication [13].

References

1. Musk, E. Hyperloop Alpha. 2013. Available online: Available online: http://www.spacex.com/sites/spacex/files/hyperloop_alpha-20130812.pdf (accessed on 1 November 2019).

2. Kale, S.R.; Laghane, Y.N.; Kharade, A.K.; Kadus, S.B. Hyperloop: Advance Mode of Transportation System and Optimize Solution on Traffic Congestion. *Int. J. Res. Appl. Sci. Eng. Technol. (IJRASET)* **2019**, *7*; ISSN 2321-9653
3. <https://en.wikipedia.org/wiki/Hyperloop> (accessed on 18 January 2020).
4. Factor Lambda. Holloman High Speed Test Track Design Manual. Research Summary, 2005, vol. 1, p. 2.
5. Chevailler S. Comparative Study and Selection Criteria of Linear Motors. DOI:10.5075/epfl-thesis-3569. Jan 2006.
6. Eguren I., Almandoz G., Egea A., Ugalde G., Escalada J.A. Linear Machines for Long Stroke Applications-A Review. DOI:10.1109/ACCESS.2019.2961758, IEEE Access.
7. Kumar P., Geetha K., Madhavi K. Design, Modeling and Analysis of Linear Switched Reluctance Motor for Ground Transit Applications. *IOSR Journal of Electrical and Electronics Engineering*. Vol 10. Issue 1. 2015.
8. "Switched Reluctance Linear Motor/Generator P200602943(OPEM).
9. Azer P., Berker B., Ali E. Mutually Coupled Switching Reluctance Motor: Fundamentals, Control, Modeling, State of the Art and Future Trends. DOI:10.1109/ACCESS.2019.2930895, IEEE Access.
10. Miller T.J. Switched Reluctance Motors and Their Control. Magna Physics Publishing and Clarendon Press. Oxford 1993.
11. L. Kolomeitsev L., et al., Control of a Linear Switched Reluctance Motor as a Propulsion System for Autonomous Railway Vehicles. 2008 13th International Power Electronics and Motion Control Conference, Poznan, 2008, pp. 1598-1603. DOI: 10.1109/EPEPEMC.2008.4635495.
12. Torres, P.M.; Lafoz, M.; Blanco, M.; Navarro, G.; Torres, J.; García-Tabarés, L. Switched Reluctance Drives with Degraded Mode for Electric Vehicles. Modeling & Simulation for Electric Vehicle Applications. Chapter 5. *INTECH* **2016**, 97–124, doi:10.5772/64431.
13. Lafoz, M.; Navarro, Gustavo; Torres, Jorge; Santiago, Álvaro; Nájera, Jorge; Santos-Herrán, Miguel; Blanco, Marcos. Power Supply Solution for Ultrahigh Speed Hyperloop Trains. *Smart Cities*. 3. 642-656. DOI 10.3390/smartcities3030033. July 2020.

Smart Mobility in Cities: GIS analysis of solar PV potential for lighting in bus shelters in the city of Ávila

M. Sánchez-Aparicio¹[0000-0002-7931-9561], S. Lagüela¹[0000-0002-9427-3864], J. Martín-Jiménez¹[0000-0003-4383-9386], S. Del Pozo¹[0000-0003-4869-3742], E. González-González¹[0000-0002-8025-2464] and P. Andrés-Anaya¹[0000-0001-7708-3260]

¹ University of Salamanca, Ávila 05003, Spain
sulaguela@usal.es

Abstract. The reduction of CO₂ emissions in cities implies the generation of clean energy for the supply of the municipal energy demand. In the conversion to Smart Cities, the consumption sources and the generation possibilities should be considered as a whole, in such a way that all the urban elements can be integrated in the energy mix. In this study, bus shelters are evaluated as potential energy generators. The installation of PV panels with the optimal configuration can contribute to the supply of the energy needed in the bus shelter, but also to the generation of surplus energy. The analysis of the possibilities and the definition of the recommendable configuration of PV installations in bus shelters are performed using the city of Ávila (Spain) as case study. In this city, the PV generation reached with the optimal configuration (3500 kWh/year) can cover the energy demand of the bus shelters, including their role as lighting points in the city, and being able to contribute to other energy demands. For this study, geospatial information and a solar radiation model are incorporated in a Geospatial Information System (GIS) tool, specially developed to replicate this study in other cities.

Keywords: solar energy, bus shelters, municipal self-consumption.

1 Introduction

The Sustainable Development Goals (SDG) [1], and the goals established by the European Union [2] at urban level regarding the reduction of CO₂ emissions in the automotive sector focus on electrical mobility, mainly applied to cars and buses. In addition, the conversion to a more sustainable society in terms of mobility includes promoting the use of alternative individual transport, such as bicycles and scooters, also electrical, which allow a more agile mobility and a better management to be within the reach of most users [3, 4].

The integration of electrical transport, both public and private, incorporates a new component to the municipal energy demand, which is spatially distributed throughout the city [5]. This transport energy demand is added to others with the same characteristics, such as public lighting demand [6]. Thus, in the context of decarbonization of the municipal energy consumption through its electrification, the reduction of CO₂

emissions needs the inclusion of clean energies for the energy supply [7]. Among the existing clean energies, solar energy is the energy source more evenly distributed in space and with the more versatile technology to be used at different scales and from different locations [8].

The implementation of self-consumption strategies associated to the use of natural resources implies a reduction in municipal spending on services such as public lighting and transport [9]. This reduction could affect the economy of the citizens through a reduction in public taxes and could expand the supply of public transport [10], more adapted to the real needs and economic resources of the users. Consequently, the gap caused by energy poverty can be minimized thanks to the fact that the facilitation of transport can imply the removal of barriers to employment [11]. In addition, the supply of energy from renewable energy sources, together with the improvement in the public transport service, would lead to an improvement in the habitability of municipalities facing problems of depopulation [12, 13]. In this way, renewable energy for the energy supply of public services would be a solution to the depopulation of rural areas, acting as an incentive for the incorporation of new inhabitants and for the return of the original ones [14].

For a proper planning, distribution and design of solar installations to supply the municipal energy consumption, a prior knowledge of the characteristics of each individual consumption, as well as the possibilities of combined consumption among several components is required.

An example of a combined service is the incorporation of the bus shelters as part of the public lighting, with the dual purpose of increasing the level of lighting with street furniture already in use and the consequent increase in the sense of security for citizens. It has been proved that higher levels of lighting provide a higher sense of security and, consequently, a higher willingness towards mobility [15]. Another example is the equipment of bus shelters as connectivity points, with WiFi stations, USB chargers and Air Control Quality stations, also supplied with solar energy for their contribution to smart cities [16].

For these reasons, the main objective of this work is to analyze the viability of incorporating PV solar installations in bus shelters that serve for the energy supply of municipal services towards their decarbonization. The work is aligned with many SDGs, such as SDG 1 (end of poverty), 7 (clean and affordable energy) and 11 (sustainable cities and communities) [1]. Similar works have been published for the incorporation of the bus shelters as energy providers of an electric system of public transport with PV panels [17], as well as for the combined installation of solar and wind energy systems in the bus shelters in order to maximize their contribution to the supply of municipal services [18].

The analysis of municipal energy demand and the availability of solar energy has an important geospatial component. In addition, the three dimensions of space should be analyzed, provided that the height component is key regarding the intensity of the incoming solar radiation and the shadow projection [19]. Thus, the study is based on the development of a 3D-GIS that, together with numerical analysis of energy needs of the municipal services in terms of public lighting and transport, will be the basis for the design of solar installations in bus shelters.

2 GIS of bus shelters in the city of Ávila

Spain is one of the European countries with highest number of solar hours along the year [20], due to its climate conditions and geographic situation. This results in a greater potential of PV solar energy. Within the territory of the Iberian Peninsula, Ávila is the city that receives the second higher solar insolation (2700 h/year) as the highest city (1132 m above sea level) of the Iberian Peninsula [21]. For these reasons, Ávila has been chosen as pilot case study.

The first step for the analysis of the spatial distribution of street furniture and for the incorporation of bus shelters as a solar energy resource is to perform an inventory of the existing urban furniture related to public transport. This inventory includes the geospatial location of each element and information about its connection to the electrical grid. The connection to the electrical grid allows the possibility to exchange energy from the solar installation to the grid in those hours when production is higher than consumption, and vice versa.

The inventory of urban furniture related to public transport resulted in 64 bus shelters and 131 bus stops, respectively (Fig. 1). Among bus shelters, 41 of them are 4 meters long, and 23 are 5 meters long.

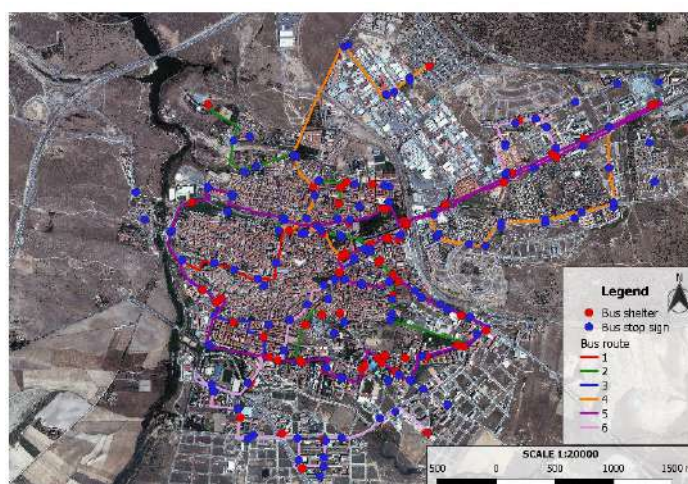


Fig. 1. GIS of the bus shelters (in red) and the bus stops (in blue) of the city of Ávila (plan view). Color lines represent the different bus routes in the city.

Thus, the GIS for street furniture related to public transport includes the geospatial distribution of the bus shelters and bus stops. This can be associated with the different bus routes to manage the number of passengers in each stretch of the tour and for each tour schedule to size the lighting requirements and the possible energy demand regarding some services of the bus shelters such as the use of interactive screens.

In addition, the environment of the bus shelters is modelled in 3D, so that the tool can provide information on the shadow cast on each bus shelter throughout the year.

The modelling is performed using as a basis the LiDAR data of the city freely offered by the Spanish Geographic Institute (IGN), as in [22]. The 3D modelling includes the buildings that can cast shadows over the bus shelters (those located East, South or West with respect to the bus shelter), as well as the trees that are taller than the shelters in those orientations.

2.1 Energy demand in shelters

In order to assess whether the solar potential of bus shelters meets their supply needs, it is key to determine the main consumption sources in bus shelters.

In the context of digitalization and Smart Cities, the objective of giving a double use to bus shelters as furniture for public transport and as public lighting elements determines the sources of energy in bus shelters. Regarding the first condition of Smart Cities, the bus shelter should be equipped with: (i) a LED panel that offers information on the incoming buses and their estimated arrival times, (ii) an interactive screen for the user to obtain information about the city and the public transport, and (iii) a digital advertising panel that minimizes the consumption of paper billboards. These elements should work 24 hours a day in order to cover the public transport service hours (mainly during the day) and to reinforce the lighting in the bus shelters during non-service hours, at night. With respect to the integration of the bus shelters as part of the public lighting system, LED lighting would be included with operating hours that match with that of the street lamps, which are adapted to the duration of the night along the year (Table 1). To estimate the total energy demand for lighting, an average operation of 11.8 hours has been considered (Table 2).

Table 1. Summary of possible sources of energy consumption in bus shelters.

Element	Power (W)	Average daily usage time (h)	Daily demand (W)
LED panel	18	24	432
Interactive screen	7	24	168
Digital advertising panel	350	24	8400
Lighting	40	11.8	473

According to the average value of hours of sun per month, the total energy demand required per bus shelter in the City of Ávila would be that detailed in Table 2. This table distinguishes between the energy demand required if the complete equipment is installed and if only the basic equipment (information LED panel, interactive screen and lighting) is installed. This distinction is made because the high consumption of the digital advertising panels can limit the efficiency of the PV solar installation, and also because of the commercial value of the panels, which makes their energy supply with municipal services arguable.

The main source of variability on consumption shelters is lighting. Therefore, the energy demand decreases in summer, when the length of the day is longer, and increases gradually until winter, when there is a greater need for lighting.

Table 2. Daily energy demand on the bus shelters.

Month	Street lighting daily usage time (h)	Demand with a complete equipment (W)	Demand without digital advertising panels (W)
Jan.	14.21	9568	1168
Feb.	13.41	9536	1136
Mar.	12.02	9481	1081
Apr.	10.65	9426	1026
May	9.54	9382	982
June	8.98	9359	959
July	9.39	9376	976
Aug.	10.22	9409	1009
Sep.	11.55	9462	1062
Oct.	12.93	9517	1117
Nov.	14.11	9564	1164
Dec.	14.77	9591	1191

3 Analysis of PV solar potential in bus shelters

3.1 Shadow analysis

The analysis of shadows cast on the bus shelters has been performed using the NOAA Solar Calculator [23] and the 3D modelling and geospatial information from the GIS created for the street furniture related to public transport (and presented in Section 2).

The NOAA Solar Calculator determines the azimuth and altitude coordinates of the Sun for specific times, considering the position under study. With these azimuth and altitude values, the NOAA Solar Calculator determines the Sun position for each hour, and consequently the sunrise, sunset, and solar noon through the year. The calculations of solar position and incoming solar radiation are based on [24], including the computation of the refraction effect on the incoming solar radiation, increasing the precision of the results.

The shadow analysis is based on the tracing of rays from the Sun to the position of the bus shelter, and the determination of an obstacle (building, tree) within the path of the rays. If an obstacle is present, it would cast a shadow on the bus shelter, consequently reducing the generation of energy of the solar installation on the shelter. The size of the obstacle determines the size of the shadow projected on the bus shelter.

In order to include the loss of energy generation caused by the shadows cast on each bus shelter, the hourly position of the Sun was calculated for one representative day of each month. In this pilot case study, the day 15th of each month was considered.

In addition to the visual analysis shown in Fig. 2, which shows the results of the presence of obstacles (shadow projectors) within the rays between the Sun position and the bus shelter, a summary table has been created for each bus shelter (Fig. 3). The summary table shows in which hours the bus shelter is covered by shadows, and therefore for what times the total PV solar production initially calculated is minimized. As a criterion established for this pilot case study, a bus shelter is considered as “overshadowed” if more than 50% of its surface is covered by shade. In the GIS tool developed, this percentage can be adapted to the characteristics of each case also, the reduction in production can be proportional to the percentage of surface in the shade.

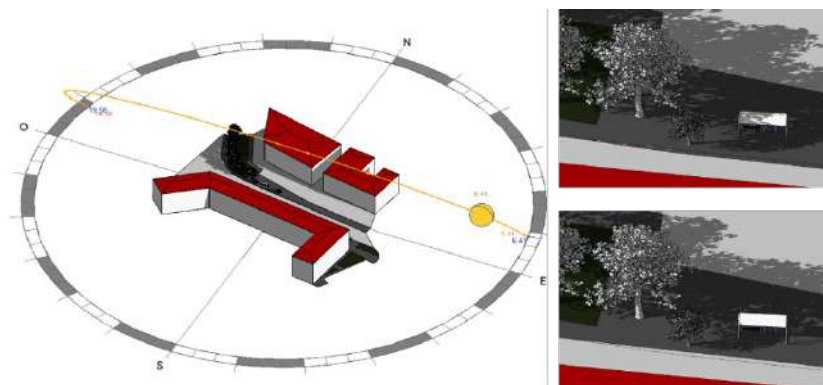


Fig. 2. Example of the simulation of shadow projection on a bus shelter, 4 meters long. Left: Sun path; right: detail of shadow projected at two different times.

Hour	Months											
	January	February	March	April	May	June	July	August	September	October	November	December
6.00					YES	YES	YES					
7.00				YES	YES	YES	YES	YES	YES			
8.00		YES	NO	NO	NO	NO	NO	NO	NO	YES	YES	
9.00	YES	YES	NO	NO	NO	NO	NO	NO	NO	NO	YES	YES
10.00	YES	NO	NO	NO	NO	NO	NO	NO	NO	NO	YES	YES
11.00	YES	NO	NO	NO	NO	NO	NO	NO	NO	NO	YES	YES
12.00	YES	NO	NO	NO	NO	NO	NO	NO	NO	NO	YES	YES
13.00	YES	NO	NO	NO	NO	NO	NO	NO	NO	NO	YES	YES
14.00	YES	NO	NO	NO	NO	NO	NO	NO	NO	NO	YES	YES
15.00	YES	YES	NO	NO	NO	NO	NO	NO	NO	NO	YES	YES
16.00	YES	YES	NO	NO	NO	NO	NO	NO	NO	YES	YES	YES
17.00	YES	NO	NO	NO	NO	NO	NO	NO	NO	NO	NO	YES
18.00	NO	NO	NO	YES	YES	YES	YES	YES	NO	YES		
19.00				YES	YES	YES	YES	YES	YES			
20.00					YES	YES	YES	YES				

NO The bus shelter is **NOT** overshadowed
 YES The bus shelter **IS** overshadowed

Fig. 3. Summary of the presence of shadows in the bus shelter of Fig.2, for each month and with hourly resolution.

3.2 Optimal PV panels design

The bus shelters are structures that can be open to different designs for PV solar installations. The key to an optimal design is to analyze the different options available,

calculate the total energy production for each option and decide which production regime is best suited to each case. In turn, there is a criterion of generating the maximum amount of energy or generating energy for the longest possible time each day.

In the case of Spain, the energy production in bus shelters can benefit from the possibility of discharging the surplus of energy to the electricity grid and proportionally reduce the cost of the energy consumed from the grid when there is no generation. In other countries, where discharging the surplus of energy to the electricity grid is not possible, there is the possibility of installing batteries to store the surplus of energy and make it available in non-generation hours.

Among the design possibilities contemplated in the study, the following are included: (i) maximum annual production, consisting on panels oriented to the south (northern hemisphere) and optimal inclination (35° for the city of Ávila); (ii) energy production for the longest period per day, which consists on the horizontal position of the panels that guarantees that the panels receive solar radiation from the sunrise to the sunset; and (iii) highest level of geometrical integration of the panels, with flexible panels following the curved shape of the shelter.

For the three possibilities, the computation of energy production includes the subtraction of the energy that is not generated due to the presence of shadows cast over the shelter. For this reason, in the case study of Ávila, the months with zero energy production are those in which the bus shelter is in the shade during the entire day.

PV panels with south orientation and optimal inclination

The installation of PV panels on orientable supports is a common strategy in order to adapt the position of the panels to the desired design of the PV installation. In the case of cities located in the northern hemisphere, the panels must be oriented towards the south in order to receive the incoming solar radiation from the most perpendicular angle. The opposite orientation (north) is recommended in the south hemisphere. In the case of Ávila, the optimal inclination of the panels is 35° . This is the inclination that guarantees the capture of Sun rays as perpendicular as possible throughout the year, allowing the generation of the maximum energy possible.

Table 3 shows the estimated energy production of the bus shelter of Fig. 2 with PV panels facing south and inclined 35° . As shown in Fig. 3, there is only one hour in which the shelter is not covered by shadows for the months of January and November, while the solar radiation never reaches the bus shelter in December. This is the reason why low or no energy generation is obtained during those months.

Table 3. Daily maximum power production per month, in watts, for the bus shelter of Fig. 2 with a PV installation facing south and inclined 35° .

Jan.	Feb.	Mar.	Apr.	May.	Jun.	Jul.	Aug.	Sep.	Oct.	Nov.	Dec.
60	3038	5264	5462	6021	6493	7077	6966	6366	4436	199	0

By analyzing the energy demands, the percentages of self-consumption and the possible energy surplus can be computed. Table 4 shows an example of the self-consumption level achieved for the example shown in Fig. 2.

In addition to the energy production, another criterion to be considered is the structural and visual integration of the panels on the bus shelter. In the case of establishing a design with south orientation and 35° inclination, the panels would require the installation of an additional support to facilitate the installation in this position. This support would imply: (i) an additional weight for the shelter, which may have not been designed to support such load and that caused by the resistance offered against the wind; and (ii) an over-height that would not favor either the visual integration nor the conservation of the panels (possibility of vandalism).

Table 4. Daily percentage of self-consumption and energy surplus for solar panels facing south and with an inclination of 35° on bus shelters in Ávila.

	Self-consumption (%) with all sources of consumption (Table 1)	Self-consumption (%) with no digital adver- tising panels	Energy discharged to the electricity grid with no digital advertising panels (Wh/day)
Jan.	1	5	0
Feb.	32	267	1902
Mar.	56	487	4183
Apr.	58	532	4436
May	64	613	5040
June	69	677	5534
July	75	725	6102
Aug.	74	691	5958
Sep.	67	599	5304
Oct.	47	397	3322
Nov.	2	17	0
Dec.	0	0	0

Horizontal PV panels

The PV panels can be installed horizontally directly on the top of the bus shelters or using a support in case the shelter has a pronounced curvy design. Table 5 shows an example of the energy production of horizontal panels for the bus shelter of Fig. 2.

Table 5. Daily maximum production per month, in watts, for the bus shelter of Fig. 2 when installing PV panels horizontally.

Jan.	Feb.	Mar.	Apr.	May	Jun.	Jul.	Aug.	Sep.	Oct.	Nov.	Dec.
30	2126	4217	5037	6064	6813	6813	6529	4592	3165	107	0

As in the case of south orientation and 35° inclination panels, the percentages of self-consumption and the generation of surplus energy can be computed in the case of horizontal panels. Table 6 shows an example of the self-consumption level achieved for the example of Fig. 2.

Regarding the analysis of integration of horizontal panels and the need of supports for the panels, both depend on the specific design of the bus shelters. In the case of the

bus shelters of the city of Ávila, these have a curved shape of 30° (angle formed by the horizontal plane and the shelter), in such a way that supports would be necessary to stabilize the panels in a horizontal position. This position, closer to the shelter, implies a reduction of the wind loads regarding the load caused by the 35° panels. A higher level of integration also decreases the risk of damage caused by vandalism. On the other hand, horizontal panels are easily damaged by natural causes such as snow or hail, which are typical in Ávila in winter and summer. In addition, the panels are more susceptible to accumulating dust, reducing their performance.

Table 6. Daily percentage of self-consumption and energy surplus for bus shelters with a horizontal PV panel configuration.

	Self-consumption (%) with all sources of consumption (Table 1)	Self-consumption (%) with no digital adver- tising panels	Energy discharged to the electricity grid with no digital advertising panels (Wh/day)
Jan.	0.3	3	0
Feb.	22	187	989
Mar.	44	390	3136
Apr.	53	491	4011
May	65	618	5082
June	73	710	5854
July	73	698	5838
Aug.	69	647	5520
Sep.	49	432	3529
Oct.	33	283	2048
Nov.	1	9	0
Dec.	0	0	0

Flexible PV panels integrated on the shelter

The latest advances in adaptable materials have allowed the generation of flexible PV panels. The position of these panels can be adjusted to the geometry of the bus shelters, which mostly present curved shelters. The main limitation of flexible panels is that their curvature must not exceed 30°.

The average curvature value of the shelters in Ávila is 30°, which is exceeded in some parts of the shelters. Therefore, and in order to satisfy the curvature requirement, the proposal was to install flexible panels in the middle of the shelter, in such a way that each panel had half of its surface facing towards one orientation and half towards the opposite orientation.

For the bus shelter in Fig. 2, 50% of the panel faces south and 50% of the panel faces north. With this configuration, the average degree of curvature is 25°, which is within the technical requirements of the flexible panels. The maximum monthly production obtained with this PV solar design is shown in Table 7.

Table 7. Daily maximum production per month, in watts, for the bus shelter of Fig. 2 when installing flexible PV panels.

Jan.	Feb.	Mar.	Apr.	May	Jun.	Jul.	Aug.	Sep.	Oct.	Nov.	Dec.
14	715	1526	1825	2190	2453	2601	2341	1901	1142	45	0

Again, the percentages of self-consumption and the generation of surplus energy were computed as shown in Table 8.

In terms of structural and visual integration, flexible PV panels are the best configuration. On the one hand, their position, parallel to the bus shelter, eliminates the need for additional support and reduces the visual impact. On the other hand, the lightness of the flexible material reduces the additional weight on the shelter, also reducing the structural demand and possibility of being damaged by the wind or other meteorological phenomena. In addition to minimizing the visual impact, the integrated panels reduce the possibility of vandalism due to the unawareness of their presence.

Table 8. Daily percentage of self-consumption and energy surplus for bus shelters with flexible PV panels.

	Self-consumption (%) with all sources of consumption (Table 1)	Self-consumption (%) with no digital adver- tising panels	Energy discharged to the electricity grid with no digital advertising panels (Wh/day)
Jan.	0.2	1	0
Feb.	7	63	0
Mar.	16	141	445
Apr.	19	178	799
May	23	223	1208
Jun.	26	256	1493
Jul.	28	267	1625
Aug.	25	232	1333
Sep.	20	179	839
Oct.	12	102	25
Nov.	0.5	4	0
Dec.	0	0	0

4 Discussion

Applying the methodology proposed in Section 3 and making use of the GIS of bus shelters, it is possible to know the PV solar potential in all the bus shelters of the city of Ávila. The average annual production for the different PV designs considering all the bus shelters in Avila (and their different dimensions) is shown in Table 9.

Table 9. Annual average production, in gigawatts-hour, for the city of Ávila and the different configurations of the panels.

Inclination	Conventional PV panels		Flexible PV panels
	0°	35°	25°
Annual average production for the bus shelters in Ávila (GWh)	122	132	52

For all the configurations, the highest production was obtained for PV panels with the optimal inclination (35°), followed by the configuration with a 0° inclination.

Although the flexible panels have an inclination (25°) closer to the optimal in this pilot case study, the energy production was reduced by half for two reasons:

- Maximum power. Conventional solar panels can reach high production power (330W has been used for computation of this work) while flexible solar panels are currently limited to 200W (for the computations of this work, 170W panels have been considered).
- Available radiation. Although the incident radiation on solar panels with an inclination of 25° is greater than on a horizontal surface, the available radiation is practically the same. This is due to the limitation of the curvature of the flexible panels on the shelter, which means that the entire panel cannot be oriented optimally.

Table 10 sums up the percentage of self- consumption considering (i) all consumption sources considered in Table 1, and (ii) without considering the digital advertising panels. For the first case, with conventional PV panels, the self-consumption percentages were between 55% and 59% while for flexible panels the self-consumption did not reach 25 %. For the second case, without the digital advertising panels, the percentage of self-consumption was always more than 100%. Specifically, for conventional panels with 35° inclination, self-consumption reaches 527%, while 487% of the demand was covered with the energy generated with horizontal panels (0° inclination). For flexible panels, the percentage was reduced in a half (208%). As a result, the energy discharged to the electricity grid was 107 GWh/year, 97 GWh/year and 27 kWh/year when using a 35°, 0° and 25° inclination, respectively. With the current average price of the energy in Spain (0.09€/kWh), savings will be around 9630€, 8730€ and 2430€, respectively.

Table 10. Annual percentage of self-consumption and energy surplus for bus shelters depending on the inclination of the solar PV panels.

	Self-consumption (%) with all sources of consumption (Table 1)	Self-consumption (%) with no digital advertising panels	Energy discharged to the electricity grid with no digital advertising panels (GW)
0°	55	487	97
25°	24	208	27
35°	60	527	107

5 Conclusions

This work presents the development of a tool based on geospatial data with the aim of analyzing the PV potential of bus shelters. With this tool, bus shelters could play a dual role: (i) serve as street furniture, and (ii) contribute to the energy supply of the municipal demand with clean resources. In addition, the analysis of energy capabilities of bus shelters has been performed seeking the integration of the bus shelters in the street lighting, and in the public transport system.

Taking this into account, an analysis of the solar PV potential in bus shelters has been performed with two combined approaches: the presence of shadows, and the configuration of the panels.

The presence of shadows in the bus shelters reduces energy production during certain months and depend on the location of the bus shelters. Due to the greater intensity of solar radiation in summer, if shadows cannot be avoided, it is possible to reduce their influence in the annual energy production if their presence occurs mainly in winter.

The results of the analysis of the configuration of the panels have shown that the maximum production occurred when the panels are installed on the shelters with their optimal inclination (determined by the location of the city under study, 35° in the city of Ávila). A 7% reduction of the production was obtained when the panels are horizontally installed, while the installation of flexible panels resulted in a 60% loss of energy production. Thus, considering other criteria such as the visual and structural integration level as well as the safety of the panels, the most recommended configuration for the panels would be that with horizontal position.

References

1. United Nations: Transforming our world: the 2030 Agenda for Sustainable Development A/RES/70/1. United Nations (2020).
2. European Commission: The European Green Deal. COM (2019), Brussels (2019).
3. Bortoli, A., Christoforou, Z.: Consequential LCA for territorial and multimodal transportation policies: method and application to the free-floating e-scooter disruption in Paris. *Journal of Cleaner Production* 273, 122898 (2020).
4. Maas, S., Attard, M., Caruana, M.A.: Assessing spatial and social dimensions of shared bicycle use in a Southern European island context: The case of Las Palmas de Gran Canaria. *Transportation Research Part A: Policy and Practice* 140, 81-97 (2020).
5. Sierpinski, G., Staniek, M., Klos, M.J.: Decision making support for local authorities choosing the method for siting of in-city ev charging stations. *Energies* 13(18), 4682 (2020).
6. Yao, J., Zhang, Y., Yan, Z., Li, L.: A group approach of smart hybrid poles with renewable energy, street lighting and EV charging based on DC micro-grid. *Energies* 11(12), 3445 (2018).
7. Dong, K., Dong, X., Jiang, Q.: How renewable energy consumption lower global CO2 emissions? Evidence from countries with different income levels. *The World Economy* 43(6), 1665-1698 (2020).
8. Guangul, F.M., Chala, G.T.: Solar energy as renewable energy source: SWOT analysis. In: 4th MEC International Conference on Big Data and Smart City, IEEE, Muscat (Oman) (2019).

9. Arcos-Vargas, A., Núñez, F., Román-Collado, R.: Short-term effects of PV integration of global welfare and CO2 emissions; An application to the Iberian electricity market. *Energy* 200, 117504 (2020).
10. Pestana, C., Prieto-Rodríguez, J.: A revenue-neutral tax reform to increase demand for public transport services. *Transportation Research Part A: Policy and Practice* 42(4), 659-672 (2008).
11. Mohammadi, A., Elsaid, F., Amador-Jiménez, L., Nasiri, F.: Optimizing public transport for reducing employment barriers and fighting poverty. *International Journal of Sustainable Development and Planning* 13(69), 861-871 (2018).
12. Heras, J., Martín, M.: Social issues in the energy transition: effect on the design of the new power system. *Applied Energy* 278, 115654 (2020).
13. Stastná, M., Vaishar, A.: The relationship between public transport and the progressive development of rural areas. *Land Use Policy* 67, 107-114 (2017).
14. García, A.V., Muñoz, V.L.: Actions from public administration to avoid depopulation of rural areas. What can be done by provincial government and local councils? *Revista Galega de Economía* 29(2), 1-14 (2020).
15. Markvica, K., Richter, G., Lenz, G.: Impact of urban street lighting on road users' perception of public space and mobility behavior. *Building and Environment* 154, 32-43 (2019).
16. Mutani, G., Vodano, A., Pastorelli, M.: Photovoltaic solar systems for smart bus shelters in the urban environment of Turin (Italy). *INTELEC 2017-October*, 20-25 (2017).
17. Santos, T., Lobato, K., Rocha, J., Tenedório, J.A.: Modeling photovoltaic potential for bus shelters on a city-scale: a case study in Lisbon. *Applied Sciences* 10(14), 4801 (2020).
18. Ashwin, M., Mounika, V., Kommineni, M., Swetha, K.: Secure design for smart bus shelter using renewable energy. *Journal of Critical Reviews* 7(1), 387-394 (2020).
19. Sánchez-Aparicio, M., Martín-Jiménez, J., Del Pozo, S., González-González, E., Lagüela, S.: Ener3DMap-SolarWeb roofs: a geospatial web-based platform to compute photovoltaic potential. *Renewable and Sustainable Energy Reviews* 135, 110203 (2021).
20. Suri, M., Huld, T.A., Dunlop, E.D., Ossenbrink, H.A.: Potential of solar electricity generation in the European Union member states and candidate countries. *Solar Energy* 81(10), 1295-1305 (2007).
21. Sancho, J.M., Riesco, J., Jiménez, C., Sánchez, M.C., Montero, J., López, M.: Atlas de Radiación Solar en España utilizando datos del SAF de Clima de EUMETSAT. AEMET, Madrid (Spain) (2012).
22. Martín-Jiménez, J.A., Del Pozo, S., Sánchez-Aparicio, M., Lagüela, S.: Multi-scale roof characterization from LiDAR data and aerial orthoimagery: automatic computation of building photovoltaic capacity. *Automation in Construction* 109, 102965 (2020).
23. NOAA Solar Calculator – Global Monitoring Laboratory, Earth System Research Laboratories, <https://www.esrl.noaa.gov/gmd/grad/solcalc/>, last accessed 2020/09/10.
24. Meeus, J.: *Astronomical algorithms*. 2nd edn. Atlantic Books, London (1998).

Impact of the covid-19 pandemic on traffic congestion in Latin American cities: An updated five-month study

Jesús Ortego¹[0000-0001-6173-2940], Renato Andara²[0000-0002-6706-1567], Luis Manuel Navas¹
[0000-0002-7895-925X], Carmen Luisa Vásquez²[0000-0002-0657-3470], Rodrigo Ramírez-
Pisco³[0000-0001-8648-3805]

¹ Universidad de Valladolid, Valladolid, España

² Universidad Nacional Experimental Politécnica Antonio José de Sucre, Barquisimeto, Venezuela

³ Universidad de Barcelona y Universitat Politècnica de Catalunya, Barcelona, España
jesus.ortego@uva.es

Abstract. This study analyzes the impact of the COVID-19 pandemic on traffic congestion in 15 metropolitan areas of 13 Latin American countries. The database of the Traffic Congestion Intensity (TCI) of the IDB Invest Dashboard is used, it was developed from the alliance between the IDB and Waze and it is correlated with the contagions of the population published by Johns Hopkins Hospital University, for the period from March 9 to July 31, 2020, approximately five (5) months. For the analysis, the areas have been categorized into four (4) clusters, based on the Coefficient of Variation and the TCI / WHO ratio. For each cluster, the graphs of the variation of the Δ TCI, the contagion cases, and the mobility recovery rate are analyzed. Among the conclusions include that the decrease in the number of infections and the flexibility of social distancing measures can be related to a recovery from congestion and that this can be measured as a function to the rate of recovery of mobility. In addition, the pandemic has revealed less collective and more agile forms of mobility, being this an important opportunity for the region to develop new forms of transport.

Keywords: Traffic congestion, COVID-19 infections, IDB Invest Dashboard, Intensity of traffic congestion, mobility recovery rate.

1 Introduction

The global pandemic due to SARS-CoV-2 or COVID-19 has been public since its appearance in Wuhan, China, in 2019 [1]. Latin America comes to suffer it later, compared to other regions such as Asia and Europe. The first case of contagion officially detected in the region was on February 26, 2020 in Brazil [2] and the first death, announced in Argentina, the following March 7 [3]. This situation has led to the implementation of sanitary measures to try to understand and stop its spread, according to sociodemographic characteristics, mobility and reports on the number of infections and deaths by country and region of the world [4]. Among the sanitary measures are social distancing based on measures such as quarantine and mandatory, total or partial confinement. These measures have been heterogeneous among the countries of the

region [5] and have directly impacted the mobility of people, among other effects [6] [7] [8] [9].

The direct measures that affect mobility are the closure of regional and international borders, suspension or restrictions on the use of urban transport systems, reduction of their levels of occupation, enabling of bicycle lanes and location of medical equipment in transport stations for monitor the temperature of the users or request their identification to guarantee traceability in case of contagion, among others [7] [10] [11] [12] [8].

Currently, the conception of mobility goes beyond just the transport of people and goods, being the reflection of a social expression by interrelating in different ways, giving rise to patterns of behavior due to different social experiences, to guarantee communication to different distances, and influencing the regional and world economy [13]. This is in a constant process of change, being a basic need for people in the world. It is part of urban life and an important cultural component and of political, economic and sociocultural development, being essential for its analysis to consider the phenomenon of traffic congestion [14].

Latin America is a flourishing region, whose urban growth has accelerated dramatically in recent decades in an uncontrolled manner [15]. According to [16], it is the second region in the world with the highest urban growth and, with this, its service needs, including mobility and transportation. Traffic congestion problems are evident in the region [17] and, especially, in cities such as Bogotá [18], Cali [19], Mexico City [20], Santiago de Chile [15] and Buenos Aires [21], among others. Accelerating the need for higher levels of urban infrastructure, transportation and investment modalities, representing in expenses up to 3.5% of the region's GDP [13] and, for families, one significant cost to achieve mobilization [22].

Mostly, traffic congestion is an incident problem in capital cities, where its root is due to a complex context, in which political, economic, social, cultural and historical heritage variables are articulated [19]. In this framework, Table 1 shows the number of hours that a driver remains detained during the year due to congestion and the average speed of advance of vehicles in some of the cities of Brazil, Colombia, Ecuador and Mexico during 2019, according to the INRIX Global Traffic Scorecard [23]. In this ranking, 975 cities and 43 countries in the world regions are analyzed and positioned, based on traffic congestion.

Table 1. Congestion Time and Average Vehicle Speed for 2019 [23]

Country	City	Number of Peak Congestion Hours	Variation of the average Congestion Rate with respect to the previous year (%)	Average vehicle speed (mph)
Brasil	Rio de Janeiro	190	-5	11
	Sao Paulo	152	+5	13
Colombia	Bogotá	191	+3	9
	Cali	94	-8	12
Ecuador	Quito	144	0	10
	Guayaquil	130	+4	13
México	Mexico City	158	+2	12
	Guadalajara	85	-10	13

Among other variables, congestion depends on the motorization of travel in cities, where Latin America is one of the highest in the world, along with Asia and the Middle East [24]. The number of vehicles per area (km^2) is higher in Costa Rica (21), Mexico (19) and Guatemala (17) than in European countries. This motorization is reflected in the modal share of travel in the city and in the performance of public transport. This has brought problems and impacts to the accessibility of the population to jobs and education, public health and also, to recreational and cultural activities, in addition the consumption of fuel and other resources.

Currently, as a result of the global pandemic COVID-19, congestion levels have been reduced in Latin America [5] [4]. This decrease has been significant in the first days of the implementation of various social distancing measures. Which indicates that this distancing can be analyzed through mobility patterns. Platforms of the Interamerican Development Bank (IDB) [25], Moovit [26] and Google [27], among others, have published their databases and comparisons with months prior to the pandemic, to be used for the different studies on COVID-19.

The IDB has published the IDB Invest Dashboard [25] which allows monitoring the distancing measures in the region based on its mobility, in real time, with the purpose of tracking the variables so that they serve as input for the public policy-making in the countries. The traffic data published in this Dashboard [25] comes from the alliance between the IDB and Waze [28], with these the Traffic Congestion Intensity indicator (TCI) can be estimated. According to this Index, in the first weeks of the implementation of the distancing measures, congestion in 69 metropolitan areas in Latin America fell significantly. The most extreme case being the city of Lima [29] where a decrease of up to 88% of the TCI is registered.

The purpose of this article is to analyze the TCI of 15 Latin American areas belonging to 13 countries, for the period from March 9 to July 31, 2020, approximately five (5) months. In addition to the data published in the IDB Invest Dashboard [25], the information from Johns Hopkins Hospital University [30], has been used for the COVID19 number of infections. The 15 metropolitan areas have been grouped into four (4) clusters, to serve for the analysis. As shown in the methodology, descriptive statistical measures were estimated for each area from the graphs, based on observing the recovery of traffic congestion, once the contagions decrease. From this analysis, the mobility recovery rate (MRR) is defined, which in most cases is positive and distinctive of the analyzed area. For each case, the dispersion and correlation of the data is estimated for the period of increase of the ΔTCI , after the maximum decrease.

2 Methodology

The data used in this article are obtained from the IDB Invest Dashboard [25], according to the Methodological Note [2], from the agreement of this institution with Waze [28]. This data comes from the information of the mobile phones of Waze users [28], which is aggregated and geocoded in real time every two (2) minutes. The Dashboard [25] uses as the reference or comparison period the week of March 1 to 7, 2020, because traffic patterns were not affected by regional holidays and there were still very few reported cases of contagion in the region. Additionally, governments had not yet issued restrictions or recommendations for social distancing.

It is difficult to compare different cities, with different administrative, legal and historical limits [2] [30] and that do not necessarily reflect their functional and economic reach. In this sense, using IDB's methodology to create urban centers as adjacent grid groups (with more than 1,500 inhabitants / grid and more than 100,000 inhabitants), the IDB Invest Dashboard [25] limits its publication to urban centers with more 750,000 inhabitants. That is, it restricts the analysis to centers with sufficient activity and historical information from Waze [28], remaining in only 64 metropolitan areas in 19 countries. Using the TCI as indicator for the analysis.

According to [2], the TCI is the sum of the total times and lengths of congestion for periods of 24 hours compared to those carried out on the days of March 1 to 7, 2020. With this, a Δ TCI is estimated, which allows the percentage comparison between the same days of the week, called the ratio-20.

In [25] the information of 64 metropolitan areas is published, however for the present study are considered the cities of Buenos Aires (AR-BA), Santa Cruz de la Sierra (BO-SC), Brasilia (BR -BR), Sao Paulo (BR-SP), Rio de Janeiro (BR-RJ), Santiago de Chile (CL-ST), Bogotá (CO-BO), San José (CR-SJ), Quito (EC-QU), San Salvador (SV-SS), Tegucigalpa (HN-TE), Guatemala City (GT-GT), Mexico City (MX-MX), Panama City (PA-PA) and Lima (PE-LI). The analysis period comprises from March 9 to July 31 of this year, approximately five (5) months. Only for Bogotá, Colombia, the start date is taken from March 9, since the data from the IDB Invest Dashboard [25] started from that day. This country announces the start of its closure on March 2 [29].

The areas were grouped into four (4) clusters, based on the Coefficient of Variation (CV) (which is an indicator developed by the IDB) and the TCI / WHO ratio, published in [2] as a methodological guide. For each cluster, the Δ TCI variation graphs are analyzed, as a function of time and, in turn, of the daily cases of contagions detected for the same day. The contagion data is taken directly from those published by the Center for Systems Engineering and Sciences (CSSE) of the Johns Hopkins Hospital University (JHU) [31].

For each area, graphic analyzes were carried out and descriptive statistical measures were estimated, based on observing the recovery of traffic congestion, once contagions decrease. These graphs show the lowest point of the Δ TCI and, from this moment, the recovery of traffic congestion in the area, as a line product of the linear regression. With these, the MRR is estimated as the slope of this line, which in most cases is positive and distinctive of the analyzed area. For each case, the dispersion and correlation of the data is estimated for the period of increase of the Δ TCI, after the maximum decrease.

3 Results and their analysis

Figure 1 shows the conformation of the clusters of the 15 cities under study, according to the Coefficient of Variation (CV) and the TCI / WHO ratio, published in [2]. Additionally, Table 2 shows the description of each of these clusters. Next, the graphs of TCI [25] and daily contagions [30]. Are shown for each group of clusters. Subsequently, the cluster analysis shows the general statistical analysis of the areas in summarized in Table 3.

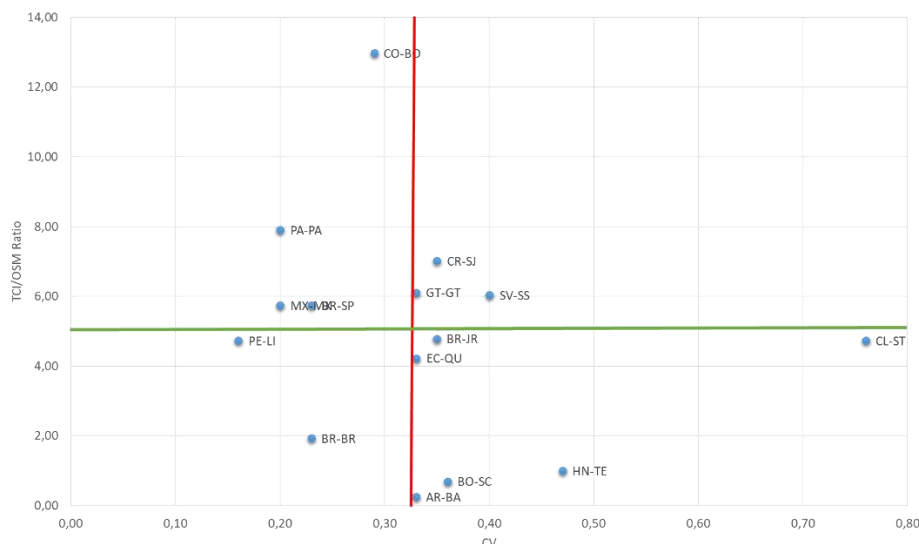


Fig. 1. Distribution of the clusters of the cities (CV, Coefficient of Variation; TCI/WHO, Traffic Congestion Intensity indicator)

Table 2. Definition of the clusters

Group	Definition ⁽¹⁾	Number of cities	Percentage (%)	Member Cities
A	0,33 < CV TCI/WHO < 4,93	2	13,3	Brasilia, Lima
B	0,33 < CV TCI/WHO ≥ 4,93	4	26,6	Bogotá, Mexico City, Panamá City, Sao Paulo
C	CV ≥ 0,33 TCI/WHO < 4,93	6	40,0	Buenos Aires, Quito, Santa Cruz de la Sierra, Tegucigalpa, Rio de Janeiro, Santiago de Chile
D	CV ≥ 0,33 TCI/WHO ≥ 4,93	3	20,0	Guatemala City, San José, San Salvador

⁽¹⁾ Definition: CV, Coefficient of Variation; TCI/WHO, Traffic Congestion Intensity indicator

3.1 Cluster A

Cluster A is made up of the cities of Brasilia and Lima. Figures 2 and 3 show their graphs of ΔTCI and number of infections for the same day, as expressed in the methodology, respectively. In these figures, it is observed that as the number of contagion decreases, there is a relaxation from the point of view that there is a recovery of the TCI. As discussed in the methodology, the MRR for both cities has a positive slope of 30.9 and 44.94%, with a dispersion of 0.1661 and 0.7261, respectively.

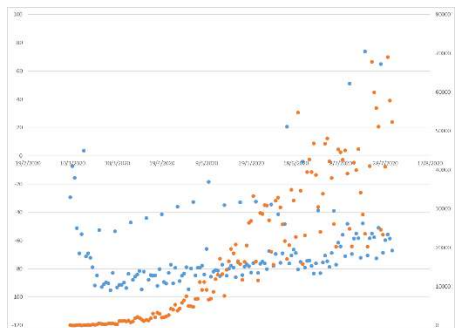


Fig. 2.Recovery of Traffic Congestion (Axis Y₁, blue) for Brasilia and COVID19 Infections (Axis Y₂, red)



Fig. 3. Recovery of Traffic Congestion (Axis Y₁, blue) for Lima and COVID19 Infections (Axis Y₂, red)

3.2 Cluster B

Cluster B is made up of the cities of Bogotá, Mexico City, Panama City and Sao Paulo. Figures 4 to 7 show their graphs of ΔTCI and number of infections for the same day, as expressed in the methodology, respectively. During 2019, Bogotá has been ranked number 1 among the cities with the highest traffic congestion, thanks to its high levels of motorization and other variables. Additionally, Mexico City and Sao Paulo are within the top ten (10). In this sense, this grouping is to be expected. The MRR of the cities is 40; 43.89; 23.2; 54.57%, respectively, with dispersions above 0.5455. This shows that the recovery from congestion is one of the fastest in the region.



Fig. 4. Recovery of Bogota Traffic Congestion (Axis Y₁, blue) and COVID19 Infections (Axis Y₂, red)

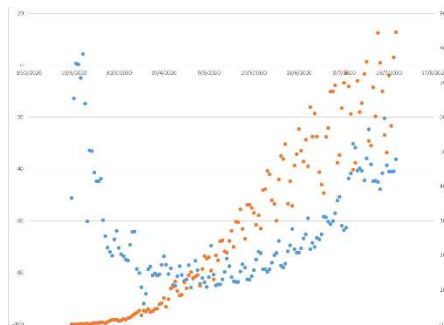


Fig. 5. Recovery of Mexico City Traffic Congestion (Axis Y₁, blue) and COVID19 infections (Axis Y₂, red)

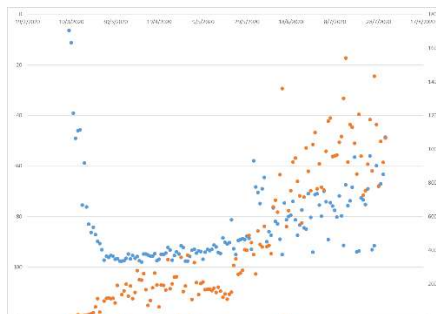


Fig. 6. Recovery of Panama City Traffic Congestion (Axis Y₁, blue) and COVID19 Infections (Axis Y₂, red)

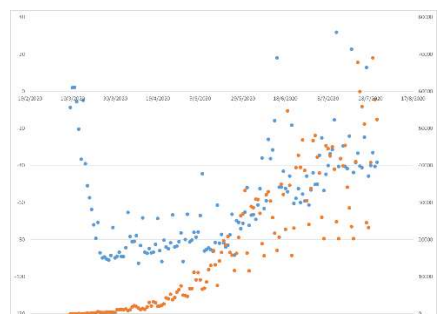


Fig. 7. Recovery of Sao Paulo Traffic Congestion (Axis Y₁, blue) and COVID19 Infections (Axis Y₂, red)

3.3 Cluster C

Cluster C is made up of the cities of Buenos Aires, Quito, Santa Cruz de la Sierra, Tegucigalpa, Rio de Janeiro and Santiago de Chile. Figures 8 to 13 show their graphs of ΔTCI and number of infections for the same day, as expressed in the methodology, respectively. In this conglomerate, unlike the previous ones, it is observed that the MRR is 16.7; 29.9; 11.6; 10.4; 51.1 and 5.4%, respectively, with dispersions ranging from 0.013 to 0.8217. Of this group, Rio de Janeiro stands out, for having the highest MRR in the group, comparable to conglomerate B, and Santiago de Chile. The latter, unlike all the others, stands out by a recovery in the number of infections from the week XX and in this sense, a correlation of its data close to zero (0.013).

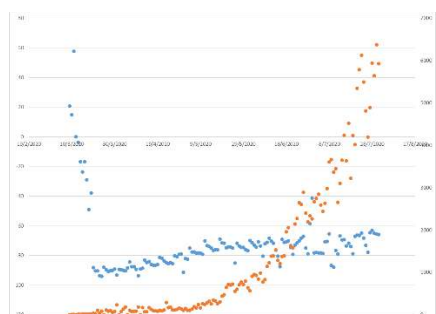


Fig. 8. Recovery of Buenos Aires Traffic Congestion (Axis Y₁, blue) and COVID19 Infections (Axis Y₂, red)

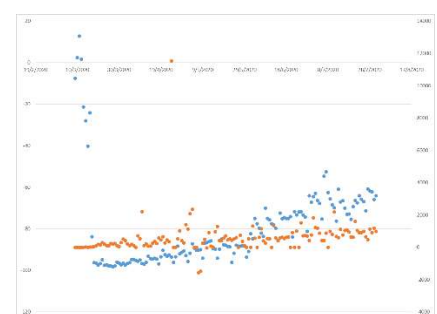


Fig. 9. Recovery of Quito Traffic Congestion (Axis Y₁, blue) and COVID19 Infections (Axis Y₂, red)

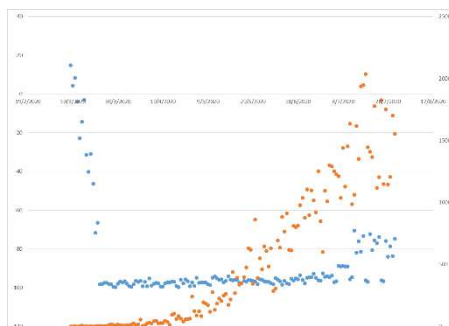


Fig. 10. Recovery of Santa Cruz de la Sierra Traffic Congestion (Axis Y₁, blue) and COVID19 Infections (Axis Y₂, red)

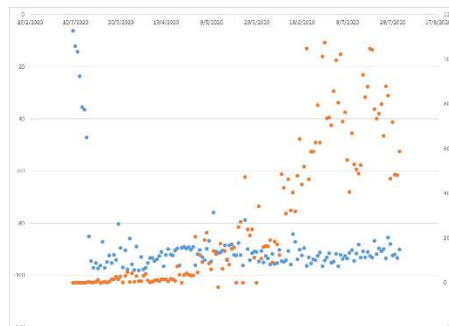


Fig. 11. Recovery of Tegucigalpa Traffic Congestion (Axis Y₁, blue) and COVID19 Infections (Axis Y₂, red)



Fig. 12. Recovery of Rio de Janeiro Traffic Congestion (Axis Y₁, blue) and COVID19 Infections (Axis Y₂, red)

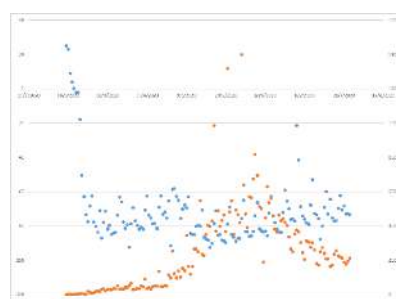


Fig. 13. Recovery of Santiago de Chile Traffic Congestion (Axis Y₁, blue) and COVID19 Infections (Axis Y₂, red)

3.4 Cluster D

El Cluster D is made up of the cities of Guatemala City, San José and San Salvador. Figures 14 to 16 show their graphs of ΔTCI and number of infections for the same day, as expressed in the methodology, respectively. In this group, it is observed that the measures implemented for social distancing were aimed at restricting the use of private vehicles or public transport. Their MRR is 2.12; 14.6 and 28.87%, respectively, with dispersions from 0.0017 to 0.6413. The highest dispersion is for Guatemala City and the lowest for San Salvador.



Fig. 14. Recovery of City of Guatemala Traffic Congestion (Axis Y₁, blue) and COVID19 Infections (Axis Y₂, red)

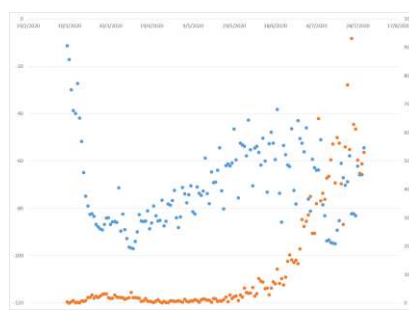


Fig. 15. Recovery of San Jose Traffic Congestion (Axis Y₁, blue) and COVID19 Infections (Axis Y₂, red)



Fig. 16. Recovery of San Salvador Traffic Congestion (Axis Y₁, blue) and COVID19 Infections (Axis Y₂, red)

Table 3. Statistical data per area

Country	Argentina	Bolivia	Brazil	Brazil	Brazil	Chile	Colombia	Costa Rica
City	Buenos Aires	Santa Cruz de la Sierra	Brasilia	Rio de Janeiro	Sao Paulo	Santiago	Bogotá	San José
Average Variation in Congestion	-72,41	-87,93	-66,79	-64,58	-59,02	-70,93	-68,04	-70,49
Maximum value	57,64	14,75	73,93	3,05	31,93	25,11	1,38	-11,28
Minimum value	-94,08	-99,74	-95,04	-94,22	-92,74	-92,52	-97,00	-96,99
Standard deviation	21,93	22,74	28,26	23,80	26,99	21,14	23,58	16,94
Median	-76,10	-96,23	-76,14	-73,90	-65,30	-75,81	-68,44	-73,65
Country	Ecuador	El Salvador	Guatemala	Honduras	Mexico	Panamá	Perú	
City	Quito	San Salvador	Guatemala City	Tegucigalpa	Mexico City	Panamá City	Lima	
Average Variation in Congestion	-79,33	-79,50	-66,35	-88,89	-64,54	-83,42	-71,85	
Maximum value	12,75	6,38	18,65	-6,28	4,44	-6,30	2,72	
Minimum value	-98,26	-98,33	-98,38	-98,06	-92,05	-97,97	-97,24	
Standard deviation	20,32	19,41	22,80	15,16	20,42	15,73	24,71	
Median	-86,26	-88,46	-69,23	-92,22	-71,86	-89,17	-84,20	

4 Analysis of Results

In order to understand how the pandemic will affect in the future and, above all, the different changes that may occur from this health emergency, it is necessary to review the transformations that occurred, especially from the 12th and 19th centuries. Fundamentally, these pandemics highlight the health problems associated with overcrowding and industrial development. According to [32] it indicates the rezoning and ordering of the city as a space for “social reproduction” in order to solve the problems derived from unhealthy conditions and overcrowding of people.

If in previous centuries, the bubonic plague in Florence in 1348, which of 1665 in London or the diseases in the city of Seville in 1786, motivated the processes of transformation of the cities. At the beginning of this 21st century, practically the same reasons plague cities globally, with inequality in said social reproduction, health and the environment being a matter of concern for the United Nations System. It is estimated that approximately 828 million people live in slums. In addition, the levels of energy consumption and pollution in urban areas are also considered worrisome, although cities occupy only 3% of the earth's surface, they represent between 60 and 80% of energy consumption and 75 % of carbon emissions [33] and nine (9) out of ten (10) people suffer from health problems derived from poor air quality and 7 million people die each year from respiratory diseases of contaminated air particles [34].

The main recommendations of the WHO for the transformation of transport in cities establish lines of concrete actions for its future in cities:

“Adoption of clean electricity generation methods; prioritization of rapid urban transport, pedestrian and bicycle paths in cities, and interurban freight and passenger transport by rail; use of cleaner heavy duty diesel engine vehicles and low emission vehicles and fuels, especially low sulfur fuels” [34].

An indicator of the change in the behavior model associated with mobility in this period of restrictions is the increase in Internet data traffic BID 2020 [35]. According to an IDB report during the first months of the application of mobility restrictions, the Internet pressure index (KASPR) was affected in some cities up to 40%, as shown in Table 4. Which can be inferred as the reduction of face-to-face activities and its substitution to virtual ways of work and communications. Since the selected cities are the major cities of each country (Table 2), we assume a proportionality between the behavior of the country and the corresponding behavior of its major cities and capitals.

Table 4. Increase in data traffic on the Internet, according to data in [35]

Country	Percentage (%)
Argentina	22 y 25
Brazil	10 y 20
Ecuador	30 (fixed networks) y 8 (mobile networks)
Colombia	40 (fixed networks) y 12 (mobile networks)

Another indicator of behavior changes in the pandemic has been the impact of restrictions, this time on people's mobility behavior (5). As it can be seen in Table 5, only trips to second homes increased perhaps as a way to flee from areas with more

demographic density, and it can be noted the decrease in movements associated with areas with close personal contact such as leisure and parks.

The pandemic and the different mobility restrictions have shown the need for more agile and less collective forms of transport services. Already in 2014, at the ITS Conference in Helsinki, the concept of MaaS appeared as a set of subscription mobility services [36]. This is defined as the integration of various forms of accessible transport services based on demand for individual mobility. MaaS services provide various menus of transport options, both public, bicycle, taxis, shared or rental car and combinations of both. COVID-19 represents an opportunity for the development of new public-private transport services that would contribute to sustainability, resilience, mitigation of so-called climate change and the health of the population.

For the case of Latin America and the study cities, there are several challenges that must be addressed [37]. To the low quality in time cost of public transport, are added the road insecurity for the most vulnerable (pedestrians), the high level of polluting emissions, its impact on health, as well as the high traffic congestion and a very limited management that prevents the optimization of road infrastructure, as well as the effective prioritization for buses, pedestrians and cyclists. COVID-19 highlights the importance of health when facing these challenges in the future.

Table 5. Mobility in the face of COVID-19 in Latin America [27]

Contry	Stores and Leisure (%)	Supermarkets and Drugstores (%)	Parks (%)	Transport Stations (%)	Work (%)	Second residences (%)
Argentina	-61	-21	-83	-54	-28	17
Bolivia	-53	-31	-42	-56	-43	23
Brazil	-40	-2	-39	-38	-22	14
Chile	-66	-46	-67	-66	-50	28
Colombia	-47	-24	-38	-48	-35	20
Costa Rica	-36	-23	-46	-46	-30	15
Ecuador	-36	-20	-38	-47	-45	23
Guatemala	-48	-32	-40	-63	-42	24
Honduras	-56	-32	-39	-65	-46	20
Mexico	-46	-18	-39	-52	-39	17
Panamá	-60	-36	-50	-61	-53	30
Perú	-67	-35	-46	-58	-54	28
El Salvador	-51	-28	-50	-60	-52	24
Venezuela	46	-27	41	56	-38	19

Conclusions

This study begins with the analysis of the impact of the COVID-19 pandemic on traffic congestion in 15 metropolitan areas of 13 Latin American countries. The database of the Intensity of traffic congestion of the IDB Invest Dashboard and the number of infections in the population published by Johns Hopkins Hospital University were used, for the period from March 9 to July 31, 2020, approximately five (5) months. From the categorization of four (4) clusters, the graphs of the variation of the ΔTCI , the cases of contagion and the rate of recovery of mobility are analyzed. It should be noted that the decrease in the number of infections brings flexibility of social distancing measures and the recovery of congestion, which is observed based on the rate of recovery of mobility.

It is observed that the mobility recovery rate for conglomerates A and B is higher than for the rest, coinciding with the areas of the cities with the greatest traffic congestion. In cluster D, this rate is lower, however, they present greater dispersion (seen from the point of view that their correlation is not very significant), coinciding with the areas where the distancing measures were related to restrictions on the use of vehicles individuals or public transport.

Similar to what happens with pandemics of the twelfth and nineteenth centuries, this brings as evidence that social inequality, health and the environment are reasons for concern. Non-negligible effects for citizens, especially in large urban centers, are evident: the rapid recovery of pollution levels and traffic congestion as the economic recovery becomes more pressing

Finally, the COVID-19 pandemic has revealed that less collective and more agile forms of mobility are needed, being an important opportunity for the region to develop new forms of transport in the face of a pandemic which has required people to have physical distance and yet they need to move from one place to another.

However, if the problems associated with the pandemic continue, a review of the World Health Organization recommendations regarding the use of public transport will be necessary. This fact raises a dilemma between maintaining state-of-the-art urban mobility policies (mitigation of climate change), versus public health and the well-being of citizens.

Acknowledgments

The authors of this article would like to thank the *Programa Iberoamericano de Ciencia y Tecnología para el Desarrollo (CYTED)*, since it was carried out within the framework of the *Red Iberoamericana de Transporte y Movilidad Urbana Sostenible (RITMUS, 718RT0566)*.

References

1. N. Chen, N. Zhou, X. Dong, J. Qu, F. Gong, Y. Q. Y. Han, J. Wang, Y. Liu, Y. Jia'an y T. Yu, «Epidemiological and clinical characteristics of 99 cases of 2019 novel coronavirus pneumonia in Wuhan, China: a descriptive study,» *The Lancet*, vol. 365, pp. 507-513, 2020.

2. I. Invest, «Coronavirus Impact Dashboard Methodological Note,» IDB, 2020.
3. R. Pierre y P. Harris, «COVID-19 en América Latina: Retos y oportunidades,» *Revista Chilena de Pediatría*, vol. 91, n° 2, pp. 179-182, 2020.
4. M. Ribeiro-Dantas, G. Alves, R. Gomes, L. Bezerra, L. Lima y I. Silva, «Dataset for country profile and mobility analysis in the assessment of COVID-19 pandemic,» *Data in Brief*, vol. 31, p. 4, 2020.
5. IDB, «Del Confinamiento a la reapertura: Consideraciones estratégicas para el reinicio de actividades en América Latina y el Caribe en el marco del Covid-19,» IDB, New York, 2020.
6. A. Iranzo, «COVID-19: ¿(in)seguridad sin (in)movilidad? Acercando la política de la movilidad a los Estudios Críticos de Seguridad,» *Geopolítica(s) Revista de estudios sobre espacio y poder*, vol. 11, pp. 61-68, 2020.
7. M. Kraeme, C. Yang, B. Gutierrez, C. Wu, B. Klein, D. Pigott, L. Plesiss, N. Faria, R. Li, W. Hanage, J. Brownstein, M. Layan, A. Vespignani, H. Tian, H. Dye, O. Pybus y S. Scarpino, «CORONAVIRUS. The effect of human mobility and control measures on the COVID-19 epidemic in China,» *Science*, vol. 368, p. 493-497, 2020.
8. I. Sirkeci y M. Murat, «Coronavirus and Migration: Analysis of Human Mobility and the Spread of COVID-19,» *Migration Letters*, vol. 17, n° 2, p. 379 – 398, 2020.
9. L. Peñafiel-Chang, G. Camelli y P. Peñafiel-Chang, «Pandemia COVID-19: Situación política - económica y consecuencias sanitarias en América Latina,» *Revista Ciencia UNEMI*, vol. 13, n° 33, pp. 120-128, 2020.
10. A. Lasry, D. Kidder, M. Hast, J. Poovey, G. Sunshine y K. Winglee, «Timing of Community Mitigation and Changes in Reported COVID-19 and Community Mobility — Four U.S. Metropolitan Areas, February 26–April 1, 2020,» *Morbidity and Mortality Weekly Report.*, vol. 69, pp. 451-457, 2020.
11. S. Lokhandwala y P. Gautam, «Indirect impact of COVID-19 on environment: A brief study in Indian context,» *Environmental Research*, vol. 188, pp. 1-10, 2020.
12. Shezen, «Combating COVID-19,» Shezen Bus Group, 2020.
13. R. Alonso y D. Lugo-Morin, «El estado del arte de la movilidad del transporte en la vida urbana en ciudades latinoamericanas,» *Revista Transporte y Territorio*, vol. 19, pp. 133-157, 2018.
14. G. Alonso, «El estado del arte de la movilidad del transporte en la vida urbana en ciudades latinoamericanas,» *Revista Transporte y Territorio*, vol. 19, pp. 133-157, 2018.
15. M. Jans, «Movilidad Urbana: En Caminos a sistemas de transporte Colectivos Integrados,» *Artículo*, pp. 6-11, 2018.
16. H. Terraza, D. Rubio y F. Vera, «De ciudades emergentes a ciudades sostenibles. Comprendiendo y Proyectando las ciudades del Siglo XXI,» BID, 2016.
17. C. Rivasplata, «Congestion pricing for Latin America: Prospects and constraints,» *Research in Transportation Economics*, vol. 40, pp. 56-65, 2013.
18. R. Alirio, R. Escobar y D. Liberona, «Government and governance in intelligent cities, smart transportation study case in Bogotá Colombia,» *Ain Shams Engineering Journal*, vol. 11, pp. 25-34, 2020.
19. R. Vergara, J. Arias y M. Rodríguez, «Congestión urbana en Santiago de Cali, un estudio de caso de política pública,» *Territorios 42*, pp. 1-29, 2020.
20. J. Luyando y J. Herrera, «Propuesta vial para atacar el problema de contaminación en la Ciudad de México,» *Revista de Direito da Cidade*, vol. 11, n° 2, pp. 316-336, 2019.
21. C. Mauricio y M. Pilar, «Planificación Multiescalar. Las desigualdades territoriales. Volumen II,» CEPAL, 2017.

22. N. Gandelman, T. Serebrisky y A. Suárez-Alemán, «Household spending on transport in Latin America and the Caribbean: A dimension of transport affordability in the region,» *Journal of Transport Geography*, vol. 79, pp. 1-14, 2019.
23. INRIX, «INRIX Global Traffic Scorecard,» INRIX, 2020. [En línea]. Available: <https://inrix.com/scorecard/>.
24. M. Rivas, A. Suárez-Aleman y T. Serebrisky, «Hechos estilizados de transporte urbano en América Latina y el Caribe,» BID, 2019.
25. IDB, «Tablero de Impacto del Coronavirus,» 2020. [En línea]. Available: <https://www.iadb.org/es/topics-effectiveness-improving-lives/coronavirus-impact-dashboard>.
26. Moovit, «Moovit Public Transit Index,» 2020. [En línea]. Available: https://moovitapp.com/insights/en/Moovit_Insights_Public_Transit_Index-countries.
27. GOOGLE, «Informes de Movilidad Local sobre el COVID-19,» 2020. [En línea]. Available: <https://www.google.com/covid19/mobility/>.
28. Waze, «WAZE for Cities,» 2020. [En línea]. Available: <https://www.waze.com/es/ccp>.
29. IADB, «IDB Mejorando Vidas,» IDB, 2020. [En línea]. Available: <https://blogs.iadb.org/efectividad-desarrollo/es/tablero-de-impacto-del-coronavirus-midiendo-los-efectos-del-distanciamiento-social-en-la-movilidad-de-america-latina-y-el-caribe/>.
30. L. Dijkstra y H. Poelma, «Cities in Europe: The New OECD-EC Defintion. Regional Focus 1/2012,» European Commission, https://ec.europa.eu/regional_policy/sources/docgener/focus/2012_01_city.pdf, 2012.
31. JHU, «Coronavirus Research Center,» John Hopskin Hospital, 2020. [En línea]. Available: <https://coronavirus.jhu.edu/map.html>.
32. A. Álvarez, «La ciudad como productor versus la ciudad como obra, o la realidad urbana entre el espacio de la renta y el espacio social,» Universidad de Valladolid, Valladolid, 2015.
33. ONU, «17 Objetivos que transforman el mundo,» [En línea]. Available: <https://www.un.org/sustainabledevelopment/es/>. [Último acceso: 03 04 2020].
34. OMS, «Calidad del aire y salud,» 2 5 2018. [En línea]. Available: [https://www.who.int/es/news-room/fact-sheets/detail/ambient-\(outdoor\)-air-quality-and-health](https://www.who.int/es/news-room/fact-sheets/detail/ambient-(outdoor)-air-quality-and-health). [Último acceso: 03 04 2020].
35. IDB, «Coronavirus: generando nuevo tráfico en América Latina,» 1 4 2020. [En línea]. Available: <https://blogs.iadb.org/transporte/es/coronavirus-generando-nuevo-traffic-en-america-latina/>. [Último acceso: 6 5 2020].
36. T. Serafimova, «Covid-19: An opportunity to Redesign Mobility Towards great Sustainability and Resilience?,» European University Institute, 2020.
37. CAF, «Transpote y Desarrollo en América Latina. Vol. 1. No.1,» 2018.

Conditional Generative Adversarial Networks to Model Urban Outdoor Air Pollution

Jamal Toutouh

Massachusetts Institute of Technology, CSAIL, MA, USA
toutouh@mit.edu

Abstract. Modeling, predicting, and forecasting ambient air pollution is an important way to deal with the degradation of the air quality in our cities because it would be helpful for decision-makers and urban city planners to understand the phenomena and to take solutions. In general, data-driven modeling, predicting, and forecasting outdoor pollution methods require an important amount of data, which may limit their accuracy. To deal with such a lack of data, we propose to train generative models, specifically conditional generative adversarial networks, to create synthetic nitrogen dioxide daily time series that will allow an unlimited generation of realistic data. The experimental results indicate that the proposed approach is able to generate accurate and diverse pollution daily time series, while requiring reduced computational time.

Keywords: urban outdoor pollution modeling · machine learning · generative adversarial networks · data augmentation

1 Introduction

Artificial intelligence, computational intelligence, and automated learning are already coping with different areas in our daily life due to their success in a wide range of applications [5]. In this study, we focus on generative models, which have shown success on tasks related to learning and gaining knowledge about data, data distributions, and other valuable information [24].

In particular, generative adversarial networks (GANs) is a powerful method to train generative models [6]. GANs take a training set drawn from a specific distribution and learn to represent an estimate of that distribution by using unsupervised learning. The output of this method is a generative model that produces new information units that approximate the original training set.

In general, GANs consist of two artificial neural networks (ANN), a generator and a discriminator, that apply adversarial learning to optimize their parameters (weights). The discriminator learns how to distinguish between the “natural/real” data samples coming from the training dataset and the “artificial/fake” data samples produced by the generator. The generator is trained to deceive the discriminator by transforming its inputs from a random latent space into “artificial/fake” data samples. GAN training is formulated as a minimax optimization problem by the definitions of generator and discriminator loss [6].

2 J. Toutouh

GANs have been successfully applied to generate realistic, complex, and multivariate distributions. This has motivated a growing body of applications, especially those concerning multimedia information (e.g., images, sound, and video), in science, design, art, games, and other areas [14, 20].

Urban design has traditionally prioritized motorized mobility (the use of the individual or collective vehicles), with the growth of the cities this is having an undesired negative effect over safety and reducing the quality of life of the inhabitants. A major concern derived from the rapid development of car-oriented cities is the high generation of air pollutants and their impacts on the citizens' health [17]. Thus, air pollution is the top health hazard in the European Union because it reduces life expectancy and diminishes the quality of health [9, 18].

In the urban areas, one of the major sources of pollutants, such as nitrogen dioxide (NO₂), is road traffic [18]. Thus, reducing it would be an effective strategy to improve urban livability and their inhabitants' health. However, it is not easy to understand the different phenomena that may have implications for the production or dissipation of pollutants. For this reason, there have been different approaches to evaluate the real impact of mobility policies in the air quality [8, 10, 23].

The interest in modeling, predicting, and forecasting ambient air pollution has also been growing during the last years. Getting in advance accurate quality air values would allow policy-makers and urban city planners to provide rapid solutions to prevent human risk situations [13].

Traditionally, physics-based and deterministic approaches have been applied to address air pollution modeling [3,4]. These approaches are sensitive to several factors, including the scale and quality of the parameters involved, computationally expensive, and dependent on large databases of several input parameters, of which some may not be available [3].

With the rapid development of ANNs and their successful application to many different short-term and long-term forecasting applications, several researchers have proposed the use of such a data-driven methodology to deal with air outdoor pollution modeling, prediction, and forecasting [3]. On the one hand, the main advantage of this approach is that the use of ANNs does not require an in-depth understanding of the physics and dynamics between air pollution concentration levels and other explanatory variables [3, 11, 15]. On the other hand, it is an open question the selection of the appropriate ANN model, the interpretation of the results of that kind of black-box methods, and the results are problem specific. Besides, as the deterministic models, this kind of machine learning and deep learning methods require a vast amount of data to be trained.

In this research, we want to propose the use of a specific type of GANs, conditional GANs (CGANs) [12], to train generators able to create synthesized data, as a data augmentation approach, to feed data-driven methodologies for modeling, forecasting, and predicting outdoor pollution. The data samples generated are the daily time series of a given pollutant from a given area of a city according to a given condition (class). As a use case, we deal with the generation of daily NO₂ concentration time series at the *Plaza the España* in Madrid

(Spain). The real dataset provided used to train the CGAN is build by collecting the levels of NO₂ gathered by a sensor located there. It is important to remark that we are not trying to create a pollution forecasting method, but a modeling one from training the generative models.

The main contributions of this research are: a) proposing a new approach based on CGANs to create pollution time series, and b) generating new data samples to be used by data-driven pollution modeling approaches. Thus, we want to answer the following research question: **RQ**: Is it possible to apply generative modeling to produce new daily time series to improve our understanding of the phenomena related to the pollution in our cities?

The paper is organized as follows: The next section introduces the main concepts to understand CGANs and how they are applied to generate air pollution data. Section 3 introduces the research methodology applied in this research. The experimental analysis is presented in Section 4. Finally, Section 5 draws the conclusions and the main lines of future work.

2 CGANs for pollution data augmentation

The CGANs are an extension of a GAN for conditional settings (labeled data). This section introduces the main concepts in GANs and CGANs training and presents how CGANs are applied to generate pollution daily series to address pollution data augmentation.

2.1 Conditional generative adversarial networks training

GANs are unsupervised learning methods that learn the specific distribution of a given (real) training dataset, to produce samples using the estimated distribution. Generally, GANs consist of a generator and a discriminator that apply adversarial learning to optimize their parameters.

During the training process, the discriminator updates its parameters to learn how to differentiate between the natural/real samples from the training data set and the artificial/fake samples synthesized by the generator.

The GAN training problem is formulated as a minimax optimization problem by the definitions of generator and discriminator. Let $\mathcal{G} = \{G_g, g \in \mathbb{G}\}$ and $\mathcal{D} = \{D_d, d \in \mathbb{D}\}$ denote the class of generators and discriminators, where G_g and D_d are functions parameterized by g and d . $\mathbb{G}, \mathbb{D} \subseteq \mathbb{R}^p$ represent the respective parameters space of the generators and discriminators. The generators G_g map a noise variable from a latent space $z \sim P_z(z)$ to data space $x = G_g(z)$. The discriminators D_d assign a probability $p = D_d(x) \in [0, 1]$ to represent the likelihood that x belongs to the real training data set. In order to do so, $\phi : [0, 1] \rightarrow \mathbb{R}$, which is concave *measuring function*, is used. The $P_z(z)$ is a prior on z (a uniform $[-1, 1]$ distribution is typically chosen). The goal of GAN training is to find d and g parameters to optimize the objective function $\mathcal{L}(g, d)$.

$$\min_{g \in \mathbb{G}} \max_{d \in \mathbb{D}} \mathcal{L}(g, d), \text{ where} \\ \mathcal{L}(g, d) = \mathbb{E}_{x \sim P_{data}(x)}[\phi(D_d(x))] + \mathbb{E}_{z \sim P_z(z)}[\phi(1 - D_d(G_g(z)))] , \quad (1)$$

This provokes that D_d becomes into a binary classifier providing the best possible discrimination between real and fake data. Simultaneously, it encourages G_g to fit the real data distribution. In general, both ANN are trained by applying backpropagation

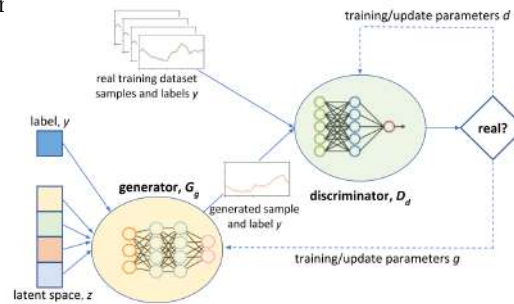


Fig. 1: Most commonly used CGANs training setups.

CGANs are an extension of GANs to deal with labeled training datasets (structured in classes). The idea is to train generative models able to create samples of a given class given according to a given label. Thus G_g and D_d receive an additional variable y as input, which represents the label of the class (see Fig 1). The CGANs objective function can be rewritten it is shown in Eq 2.

$$\min_{g \in \mathbb{G}} \max_{d \in \mathbb{D}} \mathcal{L}(g, d), \text{ where} \quad (2)$$

$$\mathcal{L}(g, d) = \mathbb{E}_{x, y \sim P_{data}(x, y)} [\phi(D_d(x, y))] + \mathbb{E}_{z \sim P_z(z), y \sim P_y(y)} [\phi(1 - D_d(G_g(z, y), y))],$$

2.2 GANs applied to urban sciences

There is a consistent body of evidence that GANs excel at implicitly sampling from highly complex, analytically-unknown distributions in a great number of contexts [24]. Thus, nowadays, researchers are using such a machine learning approach to generate data across a variety of disciplines.

However, there is a lack of studies on applying GANs to problems related to our cities. Some examples of this type of research are: a generative model trained by an unconditional GAN was trained to create realistic built land use maps, i.e., the model was able to generate cities (maps of built land use). These maps showed a high degree of realism and they provided realistic values on several statistics used in the urban modeling literature with real cities [2]. Later, the same authors proposed the use of CGANs to add new levels of realism to the generated maps and the ability to predict land use maps from underlying socio-economic factors. These new maps take into account, for example, physical constraints such as water areas [1]. Physics-informed GAN (PIGAN) was proposed to enhance the performance of GANs by incorporating both constraints of covariance structure and physical laws. The idea es to improve the robustness of GANs when dealing with problems related to remote sensing [25]. This is important for applications that require the use of satellite data and could suffer from phenomena like the appearance of clouds. In turn, we could include in this class of urban sciences research by applying GANs, the study of applying GANs

to create synthetic data about building energy consumption in order to be used together with real data to train a data-driven forecasting model to predict energy consumption [19]. The idea was to overcome the issues of having a lack of data to train the model to predict with enough accuracy.

2.3 Pollution daily time series generation

Dealing with the problem of not having enough data to analyze pollution in our cities, we proposed an approach for data augmentation to create synthetic daily time series of given pollutant. The approach consists in sampling from an existing dataset of real daily time series of given pollutant labeled according to different classes to train the discriminator, while the generator reads a vector z (from the latent space) and a label y to generate a fake daily time series (see Fig. 1). The generator and discriminator are trained against each other. Fig. 2 illustrates samples of the real training dataset.

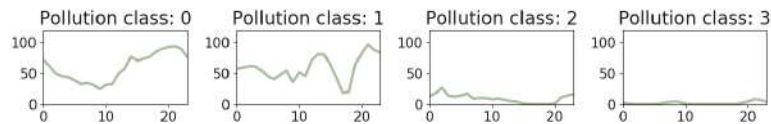


Fig. 2: Some samples of the real dataset, i.e., NO₂ pollution daily series.

3 Materials and methods

This section presents the applied methodology for training generative models by using GANs to create synthetic pollution data.

3.1 Training dataset description

The training dataset studied here is provided by the Open Data Portal (ODP) offered by the Madrid City Council¹. Specifically, the training dataset is the NO₂ concentration gathered by a sensor located at *Plaza de España*, which is in the downtown of the city. The dataset is built considering a temporal frame of five years, from January 2015 to December 2019. A given data sample is a time series that represents the NO₂ concentration of a given day which is averaged every hour. (Fig. 2). Therefore, it could be seen as a vector of 24 continuous values.

Following previous research about the pollution in Madrid, the daily NO₂ concentration is classified into eight classes according to the season (winter, spring, summer, and autumn) and the type of day (i.e., working days, from Mondays to Fridays, and weekends, Saturdays and Sundays) [9, 10]. This classification follows the idea that warmer seasons have lower NO₂ concentration due to meteorological reasons and weekends have better air quality because the road traffic is lower than in working days. Table 1 presents this pollution classification and the number of samples per class.

¹ Madrid Open data Portal web - <https://datos.madrid.es/>

6 J. Toutouh

Table 1: NO₂ pollution classification and number of samples per class.

season	type of day	class	number of samples
winter	weekend	0	439
winter	working day	1	1082
spring	weekend	2	439
spring	working day	3	1119
summer	weekend	4	445
summer	working day	5	1116
autumn	weekend	6	420
autumn	working day	7	1045

The classes are highly unbalanced (see Table 1), i.e., autumn-weekend (class 6) has 420 samples (the minimum) and spring-working day (3) has 1119 (the maximum). For our experiments, we randomly sampled over the classes to select 420 samples of each class to balance the dataset to avoid training biases. Thus, the training dataset size is 3360 (420×8).

Fig 3 illustrates the training dataset. The green line shows the mean value, i.e., it contains the mean pollution values for the whole data of the class (we named it as the representative time series of a given class c , i.e., rep_c). The dark green area represents the values between the border defined by the mean minus the standard deviation and the mean plus the standard deviation (mean \pm the standard deviation). Finally, the lighter green area represents the values between the minimum and maximum pollution measured in a given time.

3.2 CGAN design details

In our research, both ANNs, the generator and the discriminator, are implemented as multilayer perceptrons (MLP) [7]. MLP are comprised of perceptrons or neurons, organized on layers. The minimum setup is formed by an input layer, which receives the problem data as input, and an output layer, which produces the results. In between, one or more hidden layers can be included to provide different levels of abstraction to help with the learning goal. The main difference between linear perceptrons and MLP is that all the neurons on the hidden and output layer apply a nonlinear activation function. MLP have shown competitive results when dealing with different kinds of machine learning, such as classification/prediction problems with labeled inputs, regression problems, etc.

Our approach explores the use of a four-layer MLP to build the generator and the discriminator. The input of the generator has a size of 64 (size of z) plus eight (size of y) to specify the label of the class of the data sample to be generated, i.e., the total input size is 72. The output of the generator has the same input of the discriminator, which in this case is 24 (the size of the generated sample) plus eight (size of y) to identify the label of the sample, i.e., the total size is 32. Both types of MLP use linear layers. Hidden layers apply the leaky version of a rectified linear unit (LeakyRelu) as activation function, and the discriminator output layer the sigmoid function. The output of the generator applies a linear function since the output is in the range of real values, \mathbb{R} . The two hidden layers have 256 units for both trained ANN models.

Title Suppressed Due to Excessive Length 7

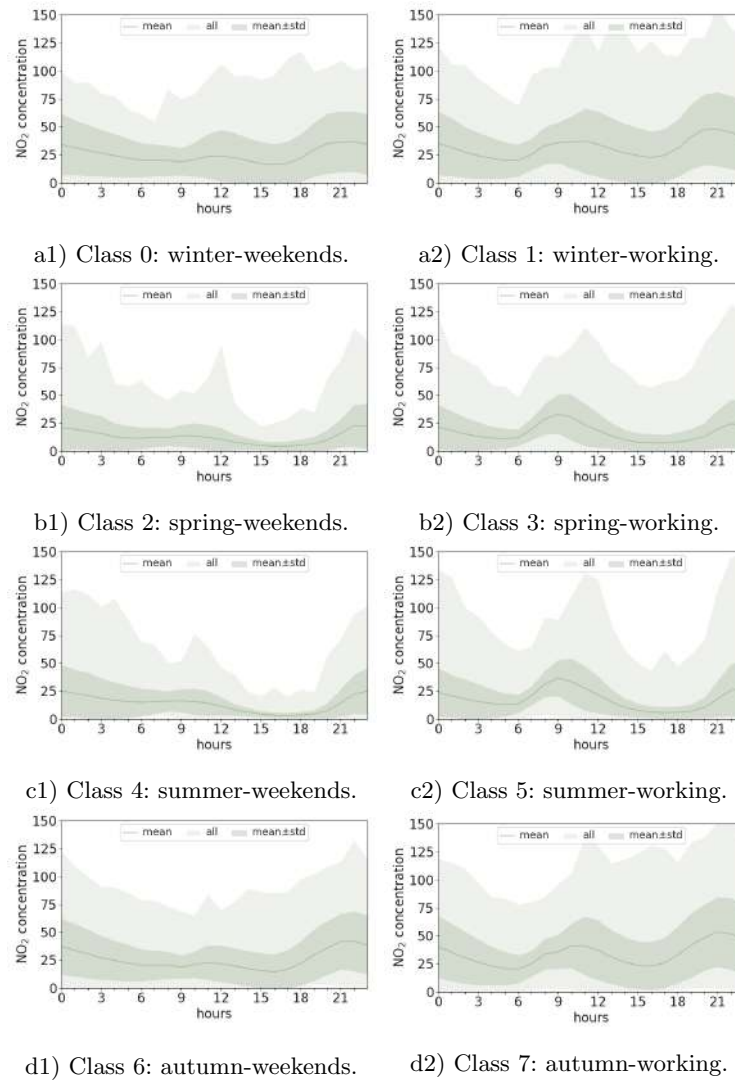


Fig. 3: NO₂ hourly values for the seven classes defined in our study (real data).

3.3 Metrics evaluated

As we are dealing with GAN training, we evaluate the loss values computed for the generator and the discriminator during the training process. The function applied to compute the loss is the binary cross-entropy (BCE) [6] (\mathcal{L}_d and \mathcal{L}_g).

$$\mathcal{L}_d = \frac{1}{2} \mathbb{E}_{x,y \sim P_{data}(x,y)} [\log(D_d(x,y))] - \frac{1}{2} \mathbb{E}_{z \sim P_z(z), y \sim P_y(y)} [\log(1 - D_d(G_g(z,y), y))], \tag{3}$$

$$\mathcal{L}_g = \mathbb{E}_{z \sim P_z(z), y \sim P_y(y)} [\log(1 - D_d(G_g(z,y), y))] \tag{4}$$

8 J. Toutouh

When working with GANs it is important to assess the quality of the generated samples. In our problem, the aim is to generate accurate daily time series of pollution that follow the same distribution as the real pollution in *Plaza de España*. We propose the use of the root mean squared error (RMSE) between the fake samples produced and the time series that represents the mean (rep_c). Thus, given a fake sample of a given class c , i.e., f_c , the quality of the sample is given by the $RMSE(rep_c, f_c)$ shown in Eq. 5, where $rep_c(t)$ and $f_c(t)$ represent the pollution level at a given time t of the representative time series c and the fake sample f_c , respectively. Thus, lower values indicate better sample quality.

$$RMSE(rep_c, f_c) = \sqrt{\frac{1}{24} \sum_{t \in [0, 23]} (rep_c(t) - f_c(t))^2} \quad (5)$$

Finally, we also take into account the computational time in order to evaluate the cost of the proposed generative method.

4 Experimental analysis

This section presents the numerical analysis of the proposed approach.

4.1 Development, training configuration, and execution platform

The proposed generative approach is implemented in Python3 using Pytorch as the main library to deal with ANNs (pytorch.org). The GAN training has configured with a learning rate of 0.0002, batch size of 16 samples (210 batches per training epoch), and 2000 iterations (training epochs).

The experiments have been performed on a workstation equipped with an Intel Core i7-7850H processor, 32GB of RAM memory, 100 GB of SSD storage for temporary files, and a Nvidia Tesla P100 GPUs with 12 GB of memory.

4.2 Experimental results

This subsection reports the experimental results. The training process has been performed 10 times. Thus this section studies: *a)* the accuracy of the generators is analyze, *b)* the evolution of the loss during the training process, *c)* the samples synthesized by the generators, and *d)* the computational time.

Accuracy of the trained generators The accuracy of the generators is evaluated according to the RMSE between the created samples of a given class c and the daily time series that represents the mean of that c class. Thus, after training each generator, we create 40,000 samples (5,000 samples of each class) as fake datasets. Table 2 shows the minimum, mean, standard deviation (stdev), and maximum of the calculated RMSE. The first row includes the same values obtained when computed the RMSE taking into account real samples. The fake datasets in the table are ranked according to their mean RMSE, thus *fake-1* dataset contains the samples with the best quality (lowest RMSE) and *fake-10* the samples with the highest RMSE.

All the fake datasets present lower mean RMSE than the samples of the real dataset. This is mainly due that the training process converges to a generator

Table 2: RMSE results for each dataset.

dataset	minimum	mean±stdev	maximum
real	3.6	17.3±8.5	67.0
fake-1	4.0	15.3±7.8	75.8
fake-2	4.2	15.4±8.1	82.1
fake-3	3.7	15.4±7.7	71.0
fake-4	3.5	15.5±8.3	91.7
fake-5	3.8	15.5±7.9	75.6
fake-6	3.3	15.5±8.2	77.3
fake-7	4.3	15.6±7.9	68.3
fake-8	3.8	15.7±8.3	81.4
fake-9	3.3	15.7±8.4	80.2
fake-10	4.0	15.7±8.2	83.7

that creates samples with limited diversity (real data shows the highest standard deviation). Even the results shown by our approach are competitive, it would be desirable to add diversity to the produced samples. This is still an open question that some authors are facing by providing generative models as a mixture of several generators [22].

Table 3 shows the mean and standard deviation (stdev) of the computed RMSE taking into account the classes. Real data samples show the highest differences for the eight classes. Besides, it can be seen that the classes that represent working days (classes represented by odd numbers) show the highest differences, for both real and fake datasets. This mainly indicates that there is not a general behavior that defines all the working days and therefore, we should take into account different kinds of classification to deal with working days (maybe taking into account the day itself).

Table 3: RMSE per class for each dataset.

dataset	0	1	2	3	4	5	6	7
real	20.2±7.1	23.8±8.3	10.7±5.6	13.2±5.9	11.5±6.3	13.4±6.6	18.3±6.4	22.4±7.6
fake-1	17.6±9.1	20.1±9.0	10.5±5.4	11.2±5.1	10.1±4.1	11.1±3.9	15.3±6.5	19.3±7.2
fake-2	17.6±9.8	19.8±8.8	10.1±4.7	10.7±4.3	9.5±3.3	11.1±4.2	15.9±7.6	19.5±7.7
fake-3	17.7±8.7	20.7±9.0	9.7±4.5	10.7±4.0	9.7±3.4	10.8±3.4	15.7±6.1	19.9±6.9
fake-4	18.6±9.3	20.6±9.5	9.9±5.1	10.6±3.9	9.4±3.8	10.7±3.6	15.6±7.3	20.1±7.9
fake-5	17.9±8.6	20.2±9.1	9.8±4.2	11.0±4.4	10.0±3.7	11.2±4.1	15.3±6.6	19.9±7.3
fake-6	18.6±9.9	20.5±8.7	9.3±5.1	10.9±5.0	9.1±3.0	11.0±3.8	15.4±6.6	20.1±7.8
fake-7	18.1±9.7	20.3±8.2	10.4±4.7	11.4±5.6	10.0±3.7	11.8±4.5	15.5±6.4	19.4±7.3
fake-8	18.4±10.0	20.9±9.5	10.2±5.2	11.5±5.6	10.0±3.9	11.4±4.2	15.9±6.6	19.6±8.0
fake-9	18.5±10.7	20.0±9.0	9.7±5.1	11.3±4.8	9.6±3.6	11.1±4.4	15.6±6.8	19.3±7.7
fake-10	18.0±8.9	20.8±9.6	10.7±5.1	11.3±4.9	9.8±4.1	11.4±4.3	15.7±6.5	19.7±8.0

Training process In this section, we evaluate the behavior of the training process by showing the losses of the generator and the discriminator. In turn, we show the mean RMSE of the generated data at the end of each training epoch. The mean RMSE score is computed by creating 10,000 samples. Fig. 4 illustrates these metrics for the best, median, and worst run, i.e., *fake-1*, *fake-5*, and *fake-10*, respectively.

10 J. Toutouh

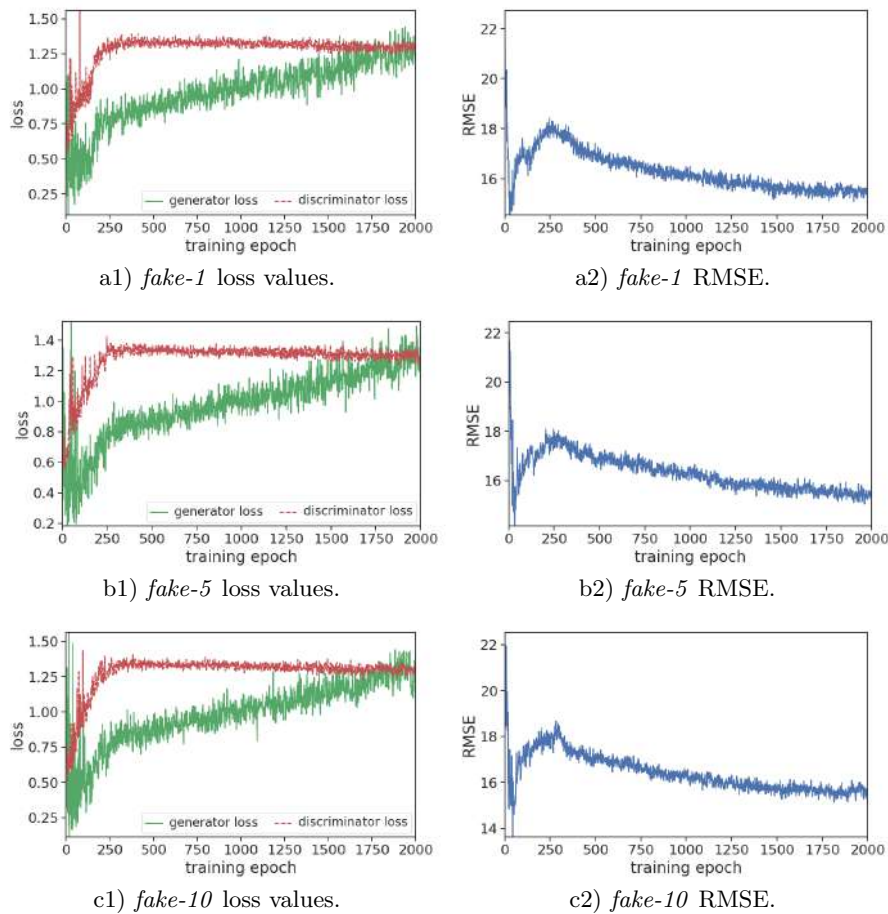


Fig. 4: Discriminator and generator loss values and RMSE for three runs.

Focusing on the evolution of the losses in Fig. 4 a1, b1, and c1, we observe that the general behavior is very similar for the three evaluated runs. At the beginning (about the first 200-300 training epochs) the discriminator and the generator losses oscillate without showing a clear trend. This is mainly due to the discriminator has not been trained enough yet, and it is not able to discriminate anyhow between fake and real samples and it randomly assigns a loss value (i.e., it basically flips a coin). Thus, the generator can easily get low losses values that do not give the feedback required to learn (to update its parameters) property. For this reason, the samples produced provide increasing and oscillating RMSE (Fig. 4 a2, b2, and c2).

After that, the discriminator starts becoming stronger and reduces the loss values. Thus, it is harder for the generator to deceive the discriminator. For this reason, the generator starts increasing the computed loss values, allowing the generator to learn how to create more accurate samples. Therefore, the RMSE values start being reduced in an almost monotonically decreasing way.

Title Suppressed Due to Excessive Length 11

After the 2,000 iterations, the generator and the discriminator seem to be in an equilibrium in which both loss values are similar. However, long runs will be able to give more insights into this concern.

It is important to remark that none of the runs shows typical GAN training pathologies, such as mode collapse, vanishing gradient, and oscillation; which would require to use more advanced GAN training methods, e.g., Lipizzaner [16] or Mustangs [21].

Synthetic daily pollution time series generated The robustness shown by the GAN training when addressing the problem studied here allows the generation of realistic synthetic daily pollution time series. Here, we illustrate the 40,000 samples generated that belong to *fake-1* and *fake-10* datasets, the fake datasets with the best and the worst RMSE. Figs. 5 and 6 summarizes the samples by showing the mean values (the orange line), the values between the mean \pm the standard deviation (the dark orange area), and all other values, i.e., between the minimum and maximum (the lighter orange area). In turn, the dotted black line presents the mean value of the real training data set (see Fig 3).

As can be seen in both figures, the mean values of the fake data and the mean values of the real data are very close. However, the distance between the orange line and the dark line increases for *fake-10*.

The shape of the dark orange areas are different depending on the class, but similar among the different datasets, i.e., the three generators studied produce samples with similar general trends. However, the shapes are less wide for the *fake-1* dataset (it shows the lowest standard deviation in Table 2). This is mainly because it tends to generate less diverse samples than the other evaluated generators. Notice, that the fake datasets are ranked taking into account the RMSE against the mean curves of the real data set.

Thus, according to the insights got from the datasets illustrated in Figs. 5 and 6 and the results in tables 2 and 3, we can see the effectiveness of the methodology proposed to augment the pollution daily time series; and therefore the answer to **RQ**: Is it possible to apply generative modeling to produce new daily time series to improve our understanding of the phenomena related to the pollution in our cities? is yes.

Computational time One of the main drawbacks of applying ANNs and deep learning approaches, as CGANs, is the computational effort (time and memory) required to train the models. As the size of the data samples and the ANN models used are not significant, the memory is not an issue et all. Regarding the computational times, the minimum, mean, and maximum times were 67.68, 69.64, and 72.04 minutes, respectively. That represents a non-very-high time-consuming investment, mainly because once the generators are trained, they create the new samples instantaneously.

12 J. Toutouh

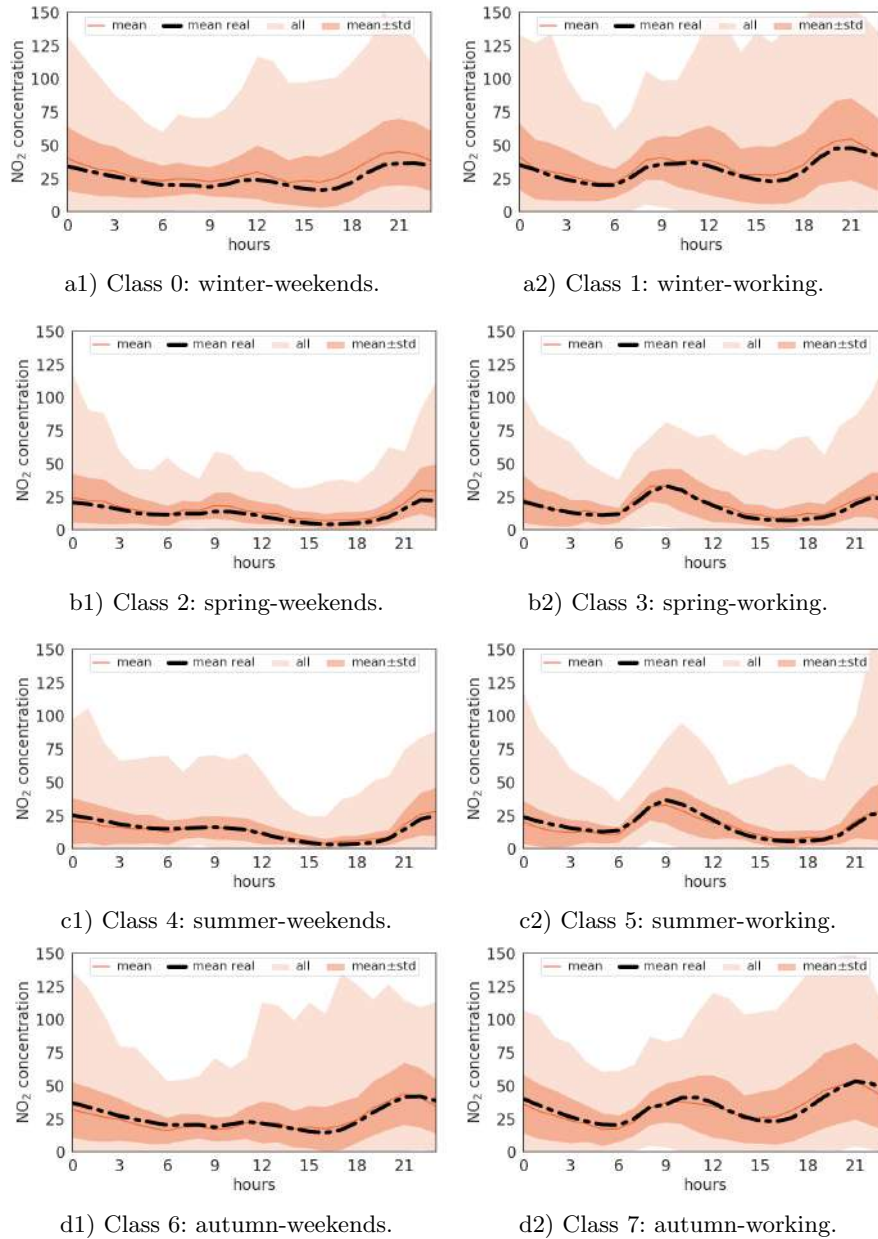


Fig. 5: Synthesized data samples created by *fake-1*.

Title Suppressed Due to Excessive Length 13

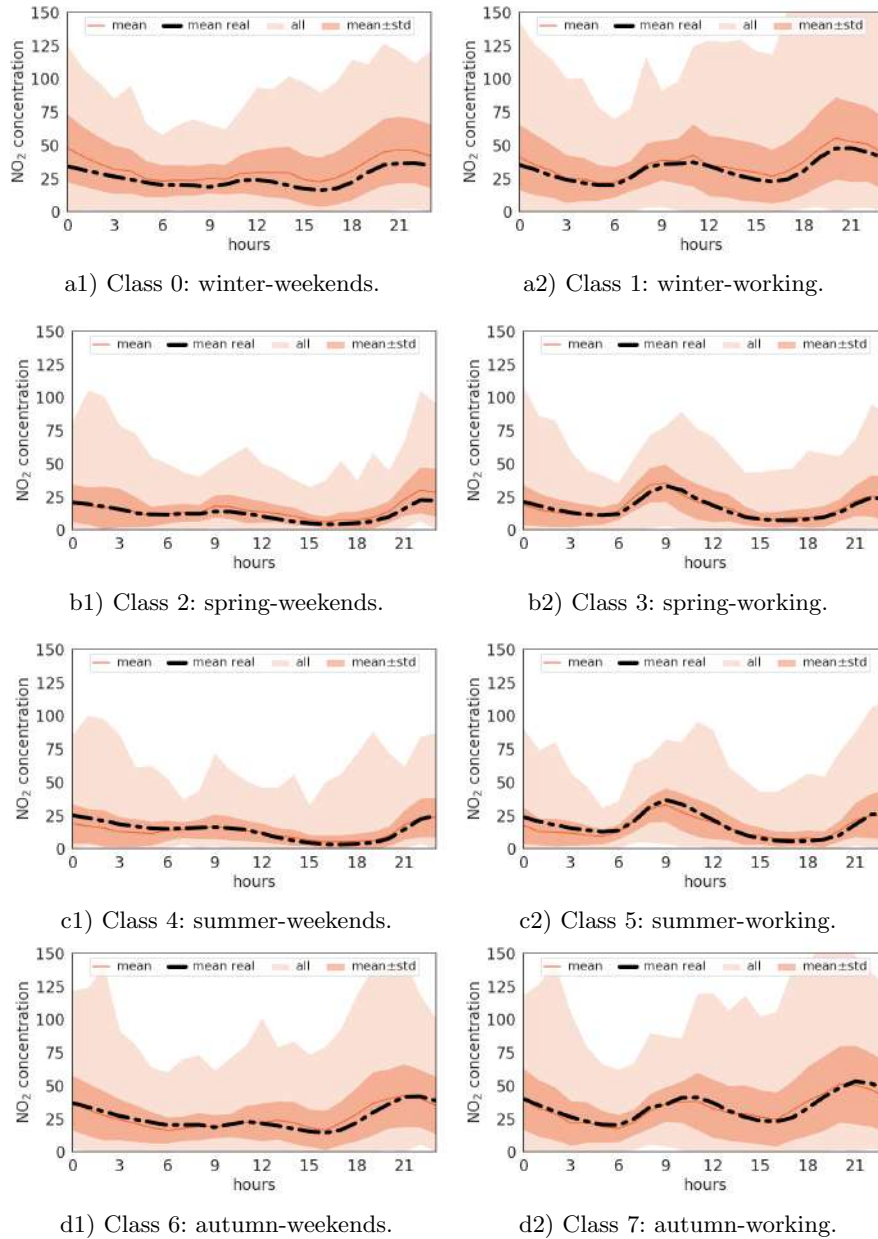


Fig. 6: Synthesized data samples created by *fake-10*.

14 J. Toutouh

5 Conclusions and future work

The interest in modeling, predicting, and forecasting ambient air pollution has been growing during the last years. Data-driven methods suffer from a lack of data to provide more accurate results. Thus, we propose the use of CGANs to train generative models able to create synthesized daily time series of a given pollutant from a given area of a city according to a given label. In this research, we have modeled NO₂ concentration at the downtown of Madrid as a use case.

The main results indicate that the proposed model is able to generate accurate NO₂ pollution daily time series while requiring a reduced computational time. CGANs have shown robustness on the training because all the experiments converged to accurate generators. Thus, we are optimistic that this is the first step to develop more complex generative models to produce synthetic pollution of a whole city taking into account information as the weather or the road traffic.

The main lines for future work are related to extend the proposed model to generate the pollution of the whole city of Madrid by taking into account information from different sensors, propose other classification that will allow including road traffic density and the weather (it will require the definition of more classes), and applying the generated data to feed data-driven models to prove that they are able to improve their accuracy after including fake samples.

Acknowledgements J. Toutouh research was partially funded by European Union's Horizon 2020 research and innovation program under the Marie Skłodowska-Curie grant agreement No 799078, by the Junta de Andalucía UMA18-FEDERJA-003, European Union H2020-ICT-2019-3, and the Systems that Learn Initiative at MIT CSAIL.

References

1. Albert, A., Kaur, J., Strano, E., Gonzalez, M.: Spatial sensitivity analysis for urban land use prediction with physics-constrained conditional generative adversarial networks. arXiv preprint arXiv:1907.09543 (2019)
2. Albert, A., Strano, E., Kaur, J., González, M.: Modeling urbanization patterns with generative adversarial networks. In: IGARSS 2018-2018 IEEE International Geoscience and Remote Sensing Symposium. pp. 2095–2098. IEEE (2018)
3. Cabaneros, S.M., Calautit, J.K., Hughes, B.R.: A review of artificial neural network models for ambient air pollution prediction. *Environmental Modelling & Software* **119**, 285–304 (2019)
4. Chuang, M.T., Zhang, Y., Kang, D.: Application of WRF/Chem-MADRID for real-time air quality forecasting over the Southeastern United States. *Atmospheric environment* **45**(34), 6241–6250 (2011)
5. Engelbrecht, A.: *Computational Intelligence: An Introduction*. John Wiley & Sons (2007)
6. Goodfellow, I., Pouget-Abadie, J., Mirza, M., Xu, B., Warde-Farley, D., Ozair, S., Courville, A., Bengio, Y.: Generative adversarial nets. In: *Advances in neural information processing systems*. pp. 2672–2680 (2014)
7. Hastie, T., Tibshirani, R., Friedman, J.: *The Elements of Statistical Learning*. Springer New York (2009)

Title Suppressed Due to Excessive Length 15

8. Lebrusán, I., Toutouh, J.: Assessing the Environmental Impact of Car Restrictions Policies: Madrid Central Case. In: Ibero-American Congress on Information Management and Big Data. pp. 9–24. Springer (2019)
9. Lebrusán, I., Toutouh, J.: Car restriction policies for better urban health: a low emission zone in Madrid, Spain. *Air Quality, Atmosphere & Health* pp. 1–10 (2020). <https://doi.org/https://doi.org/10.1007/s11869-020-00938-z>
10. Lebrusán, I., Toutouh, J.: Using Smart City Tools to Evaluate the Effectiveness of a Low Emissions Zone in Spain: Madrid Central. *Smart Cities* **3**(2), 456–478 (2020)
11. Liu, H., Wu, H., Lv, X., Ren, Z., Liu, M., Li, Y., Shi, H.: An intelligent hybrid model for air pollutant concentrations forecasting: Case of Beijing in China. *Sustainable Cities and Society* **47**, 101471 (2019)
12. Mirza, M., Osindero, S.: Conditional generative adversarial nets. arXiv preprint arXiv:1411.1784 (2014)
13. Moustris, K.P., Ziomas, I.C., Paliatsos, A.G.: 3-Day-ahead forecasting of regional pollution index for the pollutants NO₂, CO, SO₂, and O₃ using artificial neural networks in Athens, Greece. *Water, Air, & Soil Pollution* **209**(1-4), 29–43 (2010)
14. Pan, Z., Yu, W., Yi, X., Khan, A., Yuan, F., Zheng, Y.: Recent progress on generative adversarial networks (GANs): A survey. *IEEE Access* **7**, 36322–36333 (2019)
15. Qi, Y., Li, Q., Karimian, H., Liu, D.: A hybrid model for spatiotemporal forecasting of PM_{2.5} based on graph convolutional neural network and long short-term memory. *Science of the Total Environment* **664**, 1–10 (2019)
16. Schmiechlechner, T., Yong, I., Al-Dujaili, A., Hemberg, E., O'Reilly, U.: Lipizzaner: A System That Scales Robust Generative Adversarial Network Training. In: 32nd Conference on Neural Information Processing Systems (2018)
17. Soni, N., Soni, N.: Benefits of pedestrianization and warrants to pedestrianize an area. *Land Use Policy* **57**, 139 – 150 (2016)
18. Steele, C.: A critical review of some traffic noise prediction models. *Applied acoustics* **62**(3), 271–287 (2001)
19. Tian, C., Li, C., Zhang, G., Lv, Y.: Data driven parallel prediction of building energy consumption using generative adversarial nets. *Energy and Buildings* **186**, 230 – 243 (2019)
20. Toutouh, J., Esteban, M., Nesmachnow, S.: Parallel/distributed generative adversarial neural networks for data augmentation of covid-19 training images. In: Latin America High Performance Computing Conference (CARLA 2020). p. 10 (2020)
21. Toutouh, J., Hemberg, E., O'Reilly, U.: Spatial evolutionary generative adversarial networks. In: Auger, A., Stützle, T. (eds.) Proceedings of the Genetic and Evolutionary Computation Conference, GECCO 2019. pp. 472–480. ACM (2019)
22. Toutouh, J., Hemberg, E., O'Reilly, U.M.: Re-purposing heterogeneous generative ensembles with evolutionary computation. In: Proceedings of the 2020 Genetic and Evolutionary Computation Conference, GECCO '20. p. 425–434. Association for Computing Machinery (2020)
23. Toutouh, J., Lebrusán, I., Nesmachnow, S.: Computational Intelligence for Evaluating the Air Quality in the Center of Madrid, Spain. In: International Conference on Optimization and Learning. pp. 115–127. Springer (2020)
24. Wang, Z., She, Q., Ward, T.: Generative adversarial networks: A survey and taxonomy. preprint arXiv:1906.01529 (2019)
25. Wu, J., Kashinanth, K., Albert, A., Chirila, D.B., Xiao, H.: Generative learning to emulate pde-governed systems by preserving high-order statistics. In: Workshop on Climate Informatics. pp. 1–2 (2018)

Designing IoT services in smart cities through game-based knowledge acquisition

Iván García-Magariño and Jorge J. Gómez-Sanz

GRASIA Research Group
Department of Software Engineering and Artificial Intelligence,
Complutense University of Madrid,
Madrid 28040, Spain
igarciam@ucm.es, jjgomez@ucm.es
Website: <http://grasia.fdi.ucm.es/>

Abstract. Designing IoT services for smart cities adapted for satisfying the most relevant citizens' needs is not a trivial task. Not all interplays of technology would be accepted or considered natural. Evaluating the reaction of people towards these systems in advance is a necessary step that it is usually performed using surveys or focus group meetings. However, surveys have low response rates and focus groups meetings are expensive. In order to overcome this problem, this work proposes an online game-based approach so that potential users experience the interplay before the actual deployment. The decisions of players are analyzed to extract the most relevant requirements of IoT services and the most desired interaction patterns to guide the development of IoT services.

Keywords: IoT service design, requirements engineering, game-based knowledge acquisition, smart city service specification

1 Introduction

Developing IoT services for smart cities usually requires considerably high costs, specially if it involves the installation of large IoT devices in a large scale. In fact, the high cost of some IoT services has been considered as an obstruction or a barrier for the appropriate progress of smart cities, as one can observe in the critical study with empirical insights from India in this topic [6].

Also, the fact that the trained professionals in smart cities have usually a technological background rather than a social sciences background may be negative towards having more inclusive smart cities [7].

Simulations can help to foresee problems, but they will not reveal issues related with user preferences or human behavior. For instance, a research on traffic lights control system [10] simulates the effect of having a fuzzy control over the lights. However, they do not discuss the effect on human drivers who are used to fixed duration of lights rather than varying ones.

In our previous experience, we built a smart cupboard for measuring memory [9], and we designed an experiment for assessing its accuracy in measuring mem-

2 Iván García-Magariño & Jorge J. Gómez-Sanz

ory. However, we did not analyzed the users' opinions until the smart cupboard was already built.

These uncertainties can be at the core of smart cities failures. Unfortunately, failures in smart cities are rarely subject of academy papers. Digital press covers this gap and identifies side effects such as segregation, loneliness, or privacy [1] because the human factor matters [16].

Prior, less expensive, exploration of these issues could help determining what works and what does not. Rather than surveys (which traditionally have low response rate and many times low quality response) or focus groups (which are expensive), this work follows previous results [8] and proposes using text-based online games.

This work proposes a novel mechanism for rapidly extracting citizens' opinion before developing an IoT service. In particular, it proposes a framework to develop text-based brief games that are both easy-to-build and easy-to-play in any short spare time by casual users. This approach has been illustrated in the context of designing IoT services for avoiding drunk people driving on the streets of a smart city.

2 Related work

The related work considers the problem of how to know in advance with a low investment what is the opinion of users with respect a planned intervention in a city. This approach discards views were more traditional co-creation approaches, such as living labs method, because of their inherent costs.

The problem of advancing user opinion with respect to some urban development has many previous results in the area of Public Participation Geographic Information Systems (PPGIS). PPGIS are about performing online surveys using renderings of maps or other means to explain better what is the expected outcome of the modification. Despite expectations, the PPGIS have 13% average respond rate though greater reach, while paper based surveys have 30% though smaller reach [4].

3D recreations of the environment have been tested as well as a mean to gather information. There are several works in the intersection of human-computer interaction (HCI) and IoT. Mixed reality [15] can be used as well to analyse user and IoT devices interaction. However, the hardware cost for this kind of solutions is not always a low cost one. A cheaper way is to produce 3D simulations which are then coded into videos that others can check and have an opinion about [5]. Nevertheless, videos are not interaction and the reaction of users is hard to record without an important effort.

Some works highlight the need of considering people in the development of IoT services. In particular, [3] identified the main challenges, approaches and enabling technologies to conform people-centered IoT. One of the main challenges they identified was the user-centered requirement analysis. They stated that IoT systems were mainly focused on technical level like performance, interoperability

and integration, at the time. Most works missed following a user-centered approach, maybe because the lack of interactive e-assessment technologies. In this gap of the literature, we propose a game-based approach for the user-centered design of IoT services.

The systematic mapping study by [2] reviews the existing works that combine IoT and gamification. They showed that in this line of research, the most relevant application domains were energy, health, learning and sustainability in the last three years. In fact, in these domains, IoT applications usually interact with humans. Therefore, users should be considered in the development.

Game-based applications are recently related with IoT services. In particular, serious games have been used in environments with IoT devices for improving personalized healthcare [12]. In addition, [11] proposed a framework for using serious games through users' mobile devices and several sensors from the IoT environments. However, none of these games were designed for extracting the most preferred requirements of IoT services, as the current work proposes.

Therefore, the literature lacks a framework-supported approach for using text-based brief games for rapidly extracting IoT service requirements that are well-accepted by citizens. The presented approach addresses this gap of the literature.

3 Designing games for acquiring user-centric requirements of IoT services in smart cities

3.1 Technique for designing IoT services with a user-centered design

This work proposes to use agile development of games to make users identify their problems in a friendly environment. In this way, the requirements extracted from users are related to their immersion in a story, and these requirements are considered to be relevant, according to the common principles of requirements engineering [14].

This technique proposes to use text-based games because of their agile development. In these games, the player reads a story, and they can express preferences, indicate actions or mention their emotions, among others, by clicking on the links within the text or at the end. In this way, readers can continue the story by deciding on which action to focus in a smooth way. At the beginning of the games developed with this technique, the game instructions encourage players to read all the text of each scene before clicking in any link. In this way, the player is aware of all the options before taking any decision.

This technique recommends IoT-service designers to follow the steps below:

1. *Brainstorming*: The designers should discuss in group about which smart-city IoT service to develop and all the possible options and factors to consider. In case there is only one designer, then they should make notes of all these possible ideas.

4 Iván García-Magariño & Jorge J. Gómez-Sanz

2. *Identification of the key factors*: The designer(s) should select which are the key factors in their IoT services concerning the users.
3. *Determining options for each factor*: The most relevant options will be associated with each factor to analyze which option(s) users generally prefer.
4. *Design the storyboard of a game*: The storyboard should consider all the necessary steps to make players feel identified with a certain problem. In addition, the storyboard should include scenes that cover all the key factors of step 2. In addition, each game scene associated with a key factor should provide the proper links for all the associated options from step 3 for extracting the player's preference about these.
5. *Write the game script*: In order to extract the user preferences, it is necessary that the story is enough detailed to make the player engaged with the game and identify their problems in the game scenarios. It should be enough brief to avoid making the game boring or excessively long. This script associates each storyboard element with some text to be presented to the user.
6. *Develop the game*. The user can develop the game from the script thanks to the proposed software framework for developing text-based for prototyping IoT service options.

3.2 Software support for developing games for facilitating the user-centered design

We have developed a framework in the PHP programming language for facilitating the development of text-based games for facilitating the prototyping of IoT services for smart cities. This framework includes the following components:

- *Header template*: This header is designed to be include in all the scene files. It gathers all the functionality regarding the registering of information through URL parameters.
- *Footer template*: This is designed to be included in all the scene files, and complements the header file.
- *Main Functions file*: This includes the necessary function for storing the information in both the logs files and the MySQL database.
- *Game example*: This includes an example of game so the framework users have an example to understand how to define a game with this framework.
- *Style template*: This CSS file provides a default style for the framework and can be adapted for each game.
- *Database script*: This file contains the necessary queries for creating the database.

In order to develop a game from the storyboard and the script, the developer has to perform the following steps:

1. *Create a scene for each storyboard element*: Each scene is a PHP file with a name representative of the storyboard element. It includes both the header and the footer files at the beginning and end of the file respectively.

2. *Include the text of the script*: The text of the script associated with each storyboard element will be included in the corresponding scene, by just including the text in the corresponding PHP file.
3. *Include the transitions of the storyboard*: Each transition of the storyboard will be represented with an HTML link to the relative path of the file that represents the corresponding scene. If this transition corresponds to an option of a key factor, the link will include URL parameters with the names “factor” and “msg” to represent the corresponding option selected. Some transitions may not be related to any key factor, and in these cases only the “msg” parameter is used.

The generated game will record the transitions in a table called “events” in the database, indicating the factor if any, and the preferred option or message in the column “msg”. This information will be analyzed to detect the most common preferences of users regarding the corresponding factors. The database table includes “none” for the factor column and the corresponding message, if a recorded transition is not related with any key factor. All the events are associated with the date and the time, in the “datetime” column.

4 Case study: user-centered design of a IoT service for avoiding drunk drivers based on the collaboration of citizens

Figure 1 shows the storyboard of the game for designing and IoT service for avoiding drunk drivers. Figure 2 presents an example of the information stored in the events table of the database, after player several times to the game for testing. One can observe the names of factors and the corresponding message options selected. Table 1 shows the key factors, their brief descriptions and the options for each factor.

Figure 3 shows the initial screen of the game after the instructions. This screen introduces the user in the situation of being in a party in the Complutense University of Madrid. Then, the player starts dreaming that Madrid smart city can help in avoiding this situation. They have to select the preferred system, which can be a mobile app (a device very commonly used for accessing other IoT services), a smart traffic light (a ground-breaking device at least in Madrid, in which the user can interact with the traffic light), or a hand gesture (representing an advanced computer-vision software using common traffic cameras). This online game can be visualized in different kinds of devices properly, including smartphones, tablets, PCs and laptops, for include a wide range of players including the casual ones. In particular, this game snapshot was taken from a smartphone. This game was written in Spanish to facilitate the participation of Spanish participants. The game is available from a website¹ dedicated for the experiments.

¹ <http://igarciam/epizy.com/instead/>

6 Iván García-Magariño & Jorge J. Gómez-Sanz

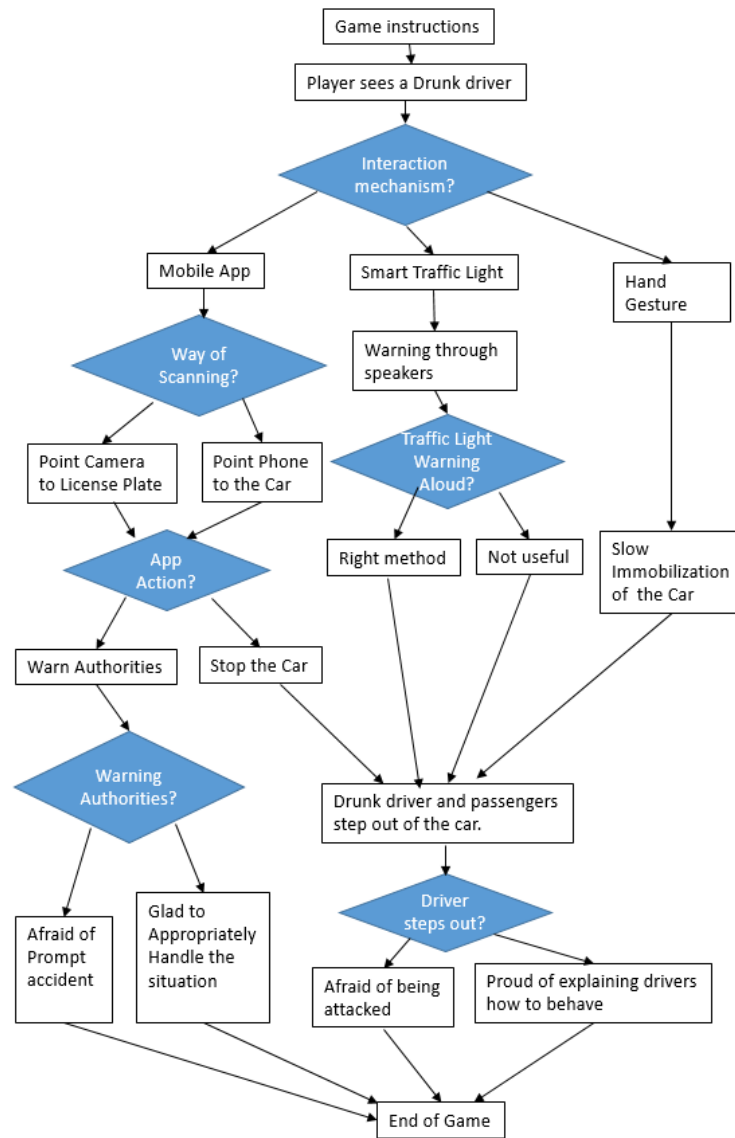


Fig. 1. Storyboard of the game-based case study for designing IoT service for avoiding drunk drivers

5 Experiments

5.1 Protocol

In order to assess the utility of the game-based extraction of requirements of the presented case study, we asked some of our contacts through What-

Designing IoT services in smart cities through games 7

datetime	factor	msg
2019-11-27 09:23:35	none	begin
2019-11-27 09:23:38	interactionMechanism	app
2019-11-27 09:23:39	wayOfScanning	scanNumberPlate
2019-11-27 09:23:41	appAction	stopVehicle
2019-11-27 09:23:45	driverStepsOut	scareOfDrivers
2019-11-27 09:23:47	none	restart
2019-11-27 09:23:51	interactionMechanism	trafficLight
2019-11-27 09:23:53	trafficLightAloudWarning	OkTrafficLightFunctioning
2019-11-27 09:23:56	driverStepsOut	possibilityToExplain
2019-11-27 09:23:58	none	restart
2019-11-27 09:24:04	interactionMechanism	handGesture
2019-11-27 09:24:08	driverStepsOut	scareOfDrivers
2019-11-27 09:24:10	none	restart
2019-11-27 09:24:14	interactionMechanism	trafficLight
2019-11-27 09:24:17	trafficLightAloudWarning	NotOkTrafficLightFunctioning
2019-11-27 09:24:18	driverStepsOut	possibilityToExplain
2019-11-27 09:24:20	none	restart
2019-11-27 09:24:23	interactionMechanism	trafficLight
2019-11-27 09:24:25	trafficLightAloudWarning	NotOkTrafficLightFunctioning
2019-11-27 09:24:28	driverStepsOut	possibilityToExplain
2019-11-27 09:24:30	none	restart
2019-11-27 09:24:33	interactionMechanism	trafficLight
2019-11-27 09:24:36	trafficLightAloudWarning	OkTrafficLightFunctioning
2019-11-27 09:24:38	driverStepsOut	possibilityToExplain
2019-11-27 09:24:40	none	restart
2019-11-27 09:24:43	interactionMechanism	app
2019-11-27 09:24:44	wayOfScanning	pointWithPhone
2019-11-27 09:24:51	appAction	warnAuthorities
2019-11-27 09:25:00	authorities	authoritiesFine
2019-11-27 09:25:02	none	restart
2019-11-27 09:25:05	interactionMechanism	app
2019-11-27 09:25:07	wayOfScanning	pointWithPhone
2019-11-27 09:25:09	appAction	stopVehicle
2019-11-27 09:25:23	driverStepsOut	possibilityToExplain
2019-11-27 09:25:27	none	restart
2019-11-27 09:25:32	interactionMechanism	trafficLight
2019-11-27 09:25:34	trafficLightAloudWarning	OkTrafficLightFunctioning

Fig. 2. Events stored in the database

sApp to participate in this experimentation with just the following instructions (translated to Spanish): “Try this game, which only takes half minute, and you will help us in our research about avoiding traffic accidents in smart cities: <http://igarciam/epizy.com/instead/> Thank you very much!”. No other instructions were given, as we have designed a easy-to-play game with the appropriate brief self-contained instructions. The game did not stored any personal information such as names, emails, telephones or postal addresses to ensure the privacy rights of participants, and consequently all stored data were anonymous. The participation was completely voluntarily and had no economic compensation or any other compensation. Participants may have been driven by the desire of having fun playing the game, curiosity or the willing of helping our research.

We started contacting people at 17:25 on Wednesday November 27, 2019. We selected this hour, as some people may stop working around this time and

Table 1. Key factors of IoT services for avoiding drunk drivers based on the collaboration of citizens

Factor	Description	Options
Interaction Mechanism	It determines the preferred way of citizens fo communication with smart city	(1) A mobile app, (2) a smart traffic light, and (3) hand gesture detected by cameras.
Way of scanning	It determines how a mobile app could identify a car	(1) Scan the number plate and (2) point with the phone to the car
App action	It indicates the preferred action from the mobile app	(1) Stop the vehicle, (2) warn authorities
Warn authorities	It determines whether warning authorities is perceived as a feasible solution for urgent matters. For example, users could wonder whether it would be better to stop the car immediately	(1) Afraid of prompt accident, (2) glad because warning authorities is fast enough for handling the situation properly.
Traffic light warning aloud through speakers	It determines whether asking drivers through speakers to stop is perceived as an appropriate method or not	(1) right solution, (2) not useful
Driver steps out	It determines whether people identifying drunk drivers want to keep anonymous	(1) Afraid of being attacked by the drivers, (2) proud of having the possibility explaining the driver the risks of their behavior.

they may have some spare time for this casual playing and contributing to the research about this social problem. We analyzed the results with all the data collected this day and the next one.

5.2 Sample of participants

We sent the request to groups of friends, family, former and current PhD students, and parents of some children from the School “Colegio La Purísima y Santos Mártires” of Teruel. We only contacted adults (i.e. above 18 years old) in Spain. We received WhatsApp messages of 10 participants confirming that they have played the game, although more participants played the game as we observed in the database. Out of the 10 confirmed participants, six of them lived in Madrid, while the other four lived in Teruel. The database registered the game was started 31 times from the beginning (this excludes the ones that restarted the game, registered through a different event). Thus, we assume that we had 31 participants.

5.3 Results

From all the game matches of all the participants, we received 122 events. The database registered that the game was started from the beginning 31 times, and

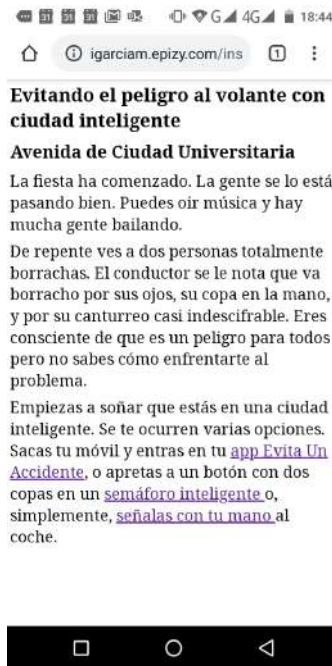


Fig. 3. Initial screen of the game after the instructions

the first decision was taken only 27 times. Thus, 87.1% of the users were probably enough engaged to take the first decision (i.e. the one about the preferred interaction mechanism).

Figure 4 shows the participation of players in the decisions related to each key factor. Notice that the participation in the decisions about each factor varies, since depending on the storyboard and the decisions taken, each player only reaches to the scenes related to some key factors.

Table 2 provides information about each key factor, indicating (a) the number of participants that took each particular decision regarding a key factor (column “# decisions”), and (b) the percentage of each preference about each factor considering all the decisions taken concerning the corresponding factor (column “% preference”). Figure 5 graphically presents these percentages of preferences about each factor.

Figure 6 shows the hours in which participants had interactions with the presented game.

6 Discussions

In only 30h of experimentation without any compensation, we achieved experiments from 27 users. This reveals the potential of our approach of very-quick game-based approach for extracting requirements, as a promising tool. We think

10 Iván García-Magariño & Jorge J. Gómez-Sanz

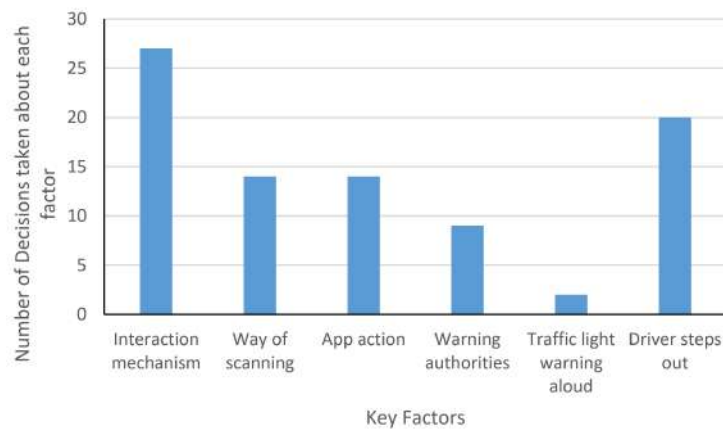


Fig. 4. Participation in decisions related to each key factor

Table 2. Numbers of decisions and percentage of preferences for each factor

Factor	Decision	# decisions	% of preference
Interaction mechanism	App	15	55.6
	Hand Gesture	11	40.7
	Traffic Light	2	7.4
Way of scanning	Point with phone	7	50.0
	Scan number plate	7	50.0
App action	Stop Vehicle	8	57.1
	Warn Authorities	6	42.9
Warning authorities	Authorities Fine	8	88.9
	Authorities Not Fast Enough	1	11.1
Traffic light warning aloud	Not Ok traffic light functioning	2	100.0
	Ok traffic light functioning	0	0.0
Driver steps out	Possibility to explain	12	60.0
	Scare of driver	8	40.0

that just letting the user play without any questionnaire afterwards made the experiments attractive enough to easily enroll users. Most other user studies require much more time [13].

It is worth highlighting that the text-based nature of the proposed kind of games with the presented framework makes this approach quick enough to design requirements extractions. The proposed case study only took 5h and 33min in being designed and written, once the topic of the IoT system knowledge extraction was conceptualized. The development work of the framework is excluded

Designing IoT services in smart cities through games 11

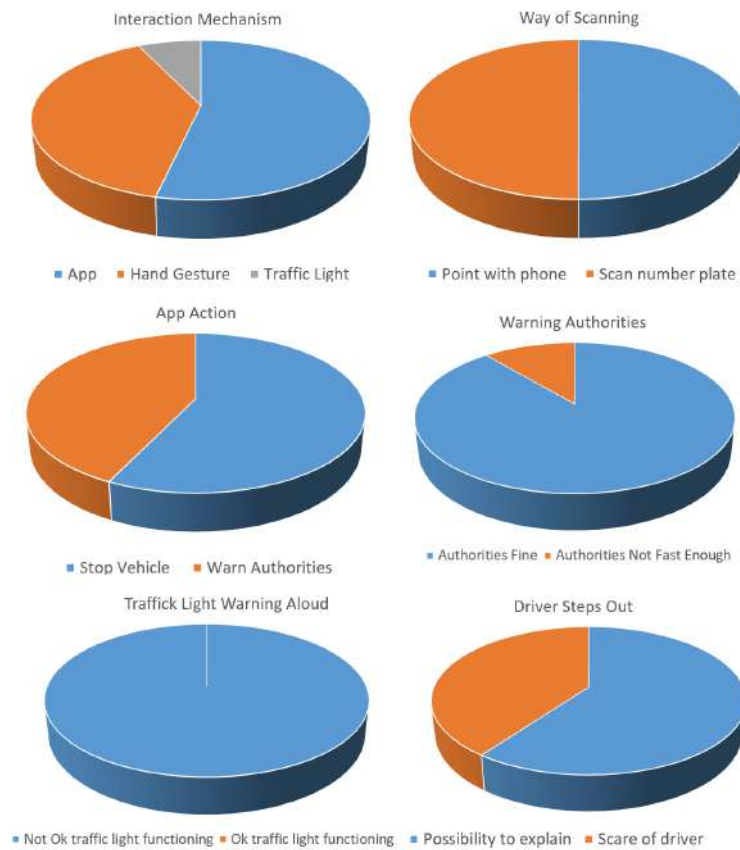


Fig. 5. Percentage of different decisions for each factor

from this measurement, given that this framework can be reused in other case studies.

Considering the experiment results regarding the key factor of interaction mechanism, a mobile app is the most preferred one (56% of preferences). Maybe the reasons might be that (a) the citizens are familiar with these devices, and (b) they may think that this solution is the most realistic and easy to be implemented soon. The usage of computer vision with the existing cameras for detecting hand gestures is also selected by a high number of participants (41% of preferences).

Only 7% of participants selected novel smart traffic lights as the preferred interaction mechanism. In addition, the proposed behavior of the smart traffic lights (i.e. stopping the car and inform the driver aloud) was not considered appropriate, although the number of players reaching to the corresponding scene of the storyboard may not be representative (only 2 clicks registered in this scene). This quick requirement extraction can save a lot of investment of novel smart devices if they are not accepted by citizens. In addition, this case reveals

12 Iván García-Magariño & Jorge J. Gómez-Sanz

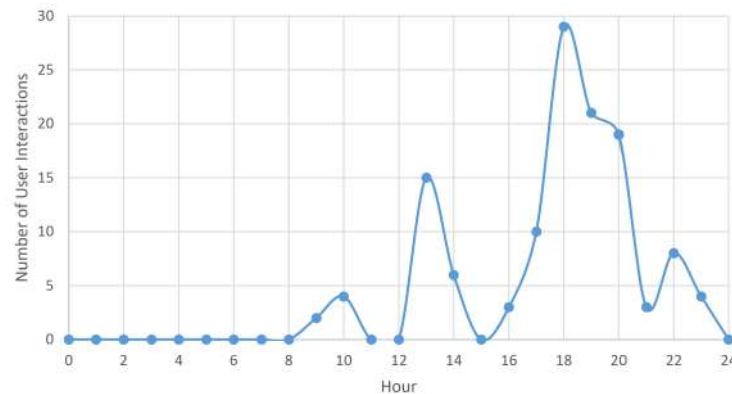


Fig. 6. Number of user interactions per hour

that this approach has the limitation that the factor analyzed in some branches may not be representative when very few participants get to a branch of the storyboard. This can be ameliorated by either (1) increasing the participants sample size or (2) making more branches get to the most relevant key factor. The latter was applied for the key factor of whether the citizens can feel afraid of drunk drivers if they notice who is the one reporting their action.

These experiments revealed that a great ratio of users (40%) may feel afraid of the drunk drivers if they find out who is accusing them. This shows that privacy of citizens reporting drivers is relevant for achieving well-accepted IoT systems in this context. From this study about requirements, developers could for example consider adding some random delay before taking actions after some citizens reported drunk drivers in the IoT services, so that the drivers cannot notice by whom they are reported.

In the distribution of day hours for playing the game, one can observe that most participants selected the evening (i.e. between 17:00 to 20:00) time for doing the participants and also around the Spanish lunch time (i.e around 13:00). These hours usually coincide with the spare time of people that work in office hours. Notice that the tests were performed on Wednesday and Thursday, which are commonly working days. Thus, the extraction of requirements is compatible with the spare time of participants without barely interrupting their daily activities. Notice that the experiments took only about one minute for each user, and was integrated in the context of a game, so participants were motivated for participating in this study.

This case study was useful to detect the most preferred whole interaction mechanism considering the path of the storyboard with the most frequent decisions. In particular, the experimentation revealed that the most accepted path was to use a mobile app to indicate that a car driver was drunk. They would either scan the license plate or just point to the car with their smartphone, to

immediate stop the car, feeling proud of being able to explain the driver the risks of driving under the alcohol effects.

7 Conclusions and future work

This work has presented a new approach for analyzing possible new IoT services with a light-weight mechanism or requirements extraction, which needs low effort from both the developers and the potential users. This approach has been illustrated for exploring which options are well-accepted by citizens in IoT services for avoiding drunk drivers based on real-time collaboration of citizens.

In the future, we plan to compare the proposed requirements technique with other requirements techniques to quantify the improvement of the proposed approach over them. We also plan to further develop the tool by giving users the opportunity to explain their reasons for taking the decisions. The proposed approach will also be tested in more case studies.

Acknowledgment

We also acknowledge “CITIES: Ciudades inteligentes totalmente integrales, eficientes y sostenibles” (ref. 518RT0558) funded by CYTED (“Programa Iberoamericano de Ciencia y Tecnología para el Desarrollo”) and “Diseño colaborativo para la promoción del bienestar en ciudades inteligentes inclusivas” (TIN2017-88327-R) funded by the Spanish council of Science, Innovation and Universities from the Spanish Government.

References

1. Albert, S.: Smart cities: The promises and failures of utopian technological planning. *The Conversation* (digital media) (April 2019), <http://theconversation.com/smart-cities-the-promises-and-failures-of-utopian-technological-planning-114405>
2. Alla, A., Nafil, K.: Gamification in IoT Application: A Systematic Mapping Study. *Procedia Computer Science* 151, 455–462 (2019)
3. Boavida, F., Kliem, A., Renner, T., Riekkki, J., Jouvray, C., Jacovi, M., Ivanov, S., Guadagni, F., Gil, P., Triviño, A.: People-centric internet of things—challenges, approach, and enabling technologies. In: *Intelligent Distributed Computing IX, Studies in Computational Intelligence*, vol. 616, pp. 463–474. Springer (2016)
4. Brown, G., Kytta, M.: Key issues and research priorities for public participation gis (ppgis): A synthesis based on empirical research. *Applied geography* 46, 122–136 (2014)
5. Castillo, N., Pérez, J., Gómez-Sanz, J.: A computational approach to improve the gathering of ambient assisted living requirements. In: *Multidisciplinary Digital Publishing Institute Proceedings*, vol. 2, p. 1246 (2018)
6. Fromhold-Eisebith, M., Eisebith, G.: What can smart city policies in emerging economies actually achieve? conceptual considerations and empirical insights from india. *World Development* 123, 104614 (2019)

14 Iván García-Magariño & Jorge J. Gómez-Sanz

7. Gomez-Sanz, J.J., Alba, E., Fernandez-Guell, J.M.: Teaching experiences in academia to understand the impact of smart cities. *IEEE Internet of Things Magazine* 2(2), 20–24 (June 2019)
8. Gomez-Sanz, J.J., Cubillos, C., Pavon, J.: Citizen participation in the context of smart cities (2019)
9. González-Landero, F., García-Magariño, I., Amariglio, R., Lacuesta, R.: Smart cupboard for assessing memory in home environment. *Sensors* 19(11), 2552 (2019)
10. Karakuzu, C., Demirci, O.: Fuzzy logic based smart traffic light simulator design and hardware implementation. *Applied Soft Computing* 10(1), 66–73 (2010)
11. Kim, H.Y.: A design and implementation of a framework for games in IoT. *The Journal of Supercomputing* 74(12), 6516–6528 (2018)
12. Konstantinidis, E.I., Billis, A.S., Paraskevopoulos, I.T., Bamidis, P.D.: The interplay between IoT and serious games towards personalised healthcare. In: 2017 9th International Conference on Virtual Worlds and Games for Serious Applications (VS-Games). pp. 249–252. IEEE (2017)
13. Malinen, S.: Understanding user participation in online communities: A systematic literature review of empirical studies. *Computers in human behavior* 46, 228–238 (2015)
14. Pohl, K.: Requirements engineering: fundamentals, principles, and techniques. Springer Publishing Company, Incorporated (2010)
15. Shao, Y., Lessio, N., Morris, A.: IoT Avatars: Mixed Reality Hybrid Objects for CoRe Ambient Intelligent Environments. *Procedia Computer Science* 155, 433–440 (2019)
16. Smart Cities World Team: Three-quarters of iot projects are failing. *The Smart Cities World (digital media)* (May 2017), <https://www.smartcitiesworld.net/news/news/three-quarters-of-iot-projects-are-failing-1729>

Towards a Sustainable Universidad de Concepción: Feasibility of Solar and Energy management projects

Erick David Rodriguez¹, Gerardo Montero-Mejia², Luis García-Santander³

¹ Universidad de las Américas Puebla, Puebla, México, erick.rodriguezao@udlap.mx

² Universidad de las Américas Puebla, Puebla, México, Gerardo.monteroma@udlap.mx

³ Universidad de Concepción, Chile, luis.garcia@udec.cl

Abstract. The Region of Bio-Bio is one of the multiple regions in Chile that have Irradiance levels that permit the constant production of electrical energy using PV Systems. This generation is considered globally as a clean production of energy because of the reduction of carbon footprint it represents. The Universidad de Concepcion (UdeC) is involved in several global projects that have the objective of implement fully efficient and sustainable Smart Campuses around the world. For this specific case we consider that the implementation of a solar generation project is within the goals of these Smart Campuses. But every infrastructure project needs to be feasible in all aspects, for this paper we developed a methodology that considers Social, Technological, Economical, and Environmental Aspects.

In this paper we present the results of these aspects that demonstrated that doing such as an investment like this will not only cover an important part of the generation it will also add value to the UdeC itself that will lead to a campus attractive to possible investor and more students in the future.

Keywords: Solar Panel, Feasibility Analysis, Social Perception, Sustainable Campus

1 Introduction

The Universidad de Concepción (UdeC) is an important university in Chile. The Concepción Campus has approximately 100 building, with more than 25,000 people between employees and undergraduate and graduate students. [1]

The amount of energy required to power all the Concepcion campus at the UdeC is massive. supplying more than one hundred buildings, which include classrooms, laboratories, professors and administrative offices, student residences, museums, etc.. Therefore, the costs of the energy consumed by the campus are excessive and that is the main purpose of the project, to reduce the amount of billing by analyzing the incorporation of photovoltaic systems in some strategic buildings and performing a management of the electrical energy to obtain the most efficient system. In addition, the carbon footprint must be reduced as well, intending to become an environmentally responsible University.

The UdeC campus and surroundings do not have the capacity to implement large scale distributed generation sources, main reason to search for different alternatives, a possible solution is to use the roof of the buildings as solar generators, nevertheless not all building roofs are eligible for implementation of PV systems, so an analysis of the best buildings needs to be done in order to place PV systems in the near future, among economic situations the university is trying to become a Smart Campus so it needs to be sustainable and efficient about energetics, for this reason a renewable system to generate electricity needs to be implemented, the label of Smart Campus, requires major implementations and one of them is the renewable generation, so, an analysis of the whole campus looking for the best building roofs to place PV systems will be done.

The document contains the following sections: The technical preliminaries about the energy capacities of the campus and where geography is described. The proposed Methodology that considers social, environmental, technical, and economic aspects. The results are presents in the last section.

1.1 Social Importance

Within the develop of the social study, it was demonstrated that the UdeC is not considered by the community as an environmentally friendly university.

According to a survey made to students and workers at the university and to external people at Concepción, the UdeC is barely considered to be “Sustainable”, as only 50% of the surveyed people thinks that the university has policies for the care of the environment. In addition, in the Fig. 1, we can see a problem for the UdeC, we asked the community to put in order from 1 to 5, their perception about the University, and obtained that the option “Responsible of the environment” was in the last place.

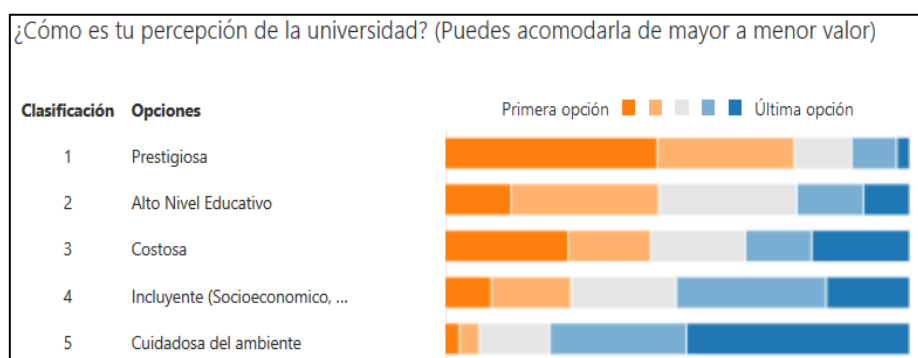


Fig. 1.Social Perception of UdeC.

2 About the Project

In this section we will talk about some the fundamentals toward applying the methodology for the feasibility analysis, here we will discuss about the solar characteristics of the site, then we will present the billings aspects that motivate the project.

2.1 Solar Capacities

We obtained the solar capacities of UdeC from the platform of the solar explorer [2], and the optimal angles for maximum power generation were calculated, obtaining an elevation of 30° and an azimuth of -8° . This platform is reliable because was developed by the Chilean Government and several aspects are analyzes such as wind, cloudiness among others.

2.2 Electrical Capacities

The electrical service of the UdeC is distributed in 8 points of connection with the electricity generator company these connections are placed in different areas of the campus. Fig. 2 shows the connection areas and existing buildings on the Concepción campus UdeC.

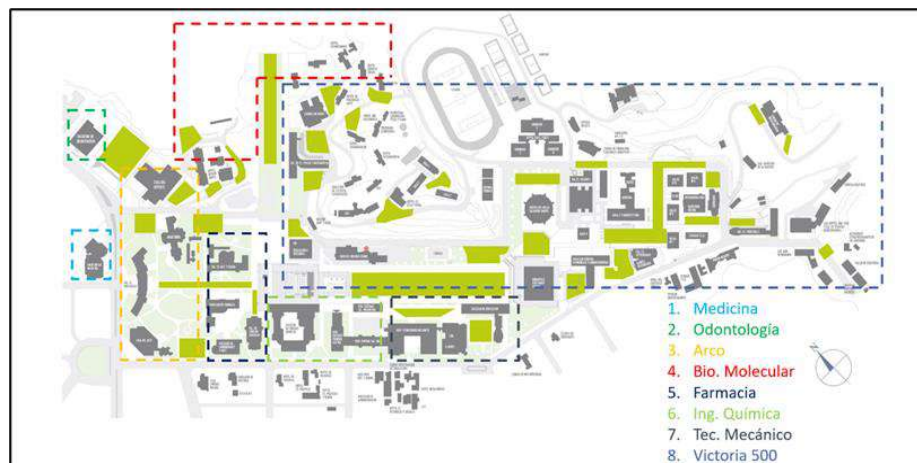


Fig. 2. Lay-Out Electrical connections Campus Concepción, Universidad de Concepción.

2.3 Billing

In the Table 1 we can observe the different charges and tariffs for the connections. Each junction has different types of tariffs, where some buy the energy from CGE (Compañía General de Electricidad) with the type of tariff AT4.3 [3] and others, when meeting the requirements to be free customers [4], pay a lower rate for energy to ENEL, and only the toll to CGE.

The AT4.3 tariff allows us to obtain a breakdown of the types of payment we have, a fixed charge, one for leasing for measuring equipment, one for transportation and the most significant, which are: the energy charge, which is the consumption in kWh for the whole month; the maximum demand charge supplied, which compares the highest value of power required by the junction in the current month with the average of the two highest values of the last 12 months, and the higher of both is charged; and the maximum demand read at peak time charge, which is the highest value read power of the month for the HP (Hora Punta; Peak Hour) period from April to September from 18:00 to 23:00, and for the rest of the year it is it charges the average of the two highest values of the previous peak hour period.

For the free customer rate, of the 3 main charges, only the energy supplied, and the demand read in HP are charged. Although, in turn, the toll must be paid, which is based on maximum demand energy and demand at HP.

Table 1. Billing points and Billing Campus Concepción, Universidad de Concepción.

	Junction Name	Company	Tariff
1	Medicina	CGE	AT 4.3
2	Odontología	ENEL + CGE	Free Client
3	Arco	CGE	AT 4.3 – LV Measurement
4	Bio Molecular	ENEL + CGE	Free Client
5	Farmacia	CGE	AT 4.3 – LV Measurement
6	Tec Químico	ENEL + CGE	Free Client
7	TecMecánico	ENEL + CGE	Free Client
8	Victoria 500	ENEL + CGE	Free Client

3 Methodology

A solar project is a high investment so, a full feasibility analysis is required to avoid money loss or an inefficient implementation. The UdeC is a huge university with more than 100 buildings placed inside the campus and other near the campus in the city of Concepcion. Although the University has 3 campuses in the region of “Bio-Bio” for this project only the campus Concepcion will be analyzed.

We are considering that there are four mains aspects of this kind of infrastructure projects, these are, Technical, Social, Economic and Environmental, for each of these aspects we develop a section to explain it as easy as possible.

For the technical aspect we have two proposal, one is to use the solar panels to produce energy and it's expected to be at a lower price that the consumed by the companies, but we have a second proposal that is the energy management, in this case we

consider to use an Electrical Storage System to reduce the price of the peak hours, this cost is greater than the cost for demand and energy.

3.1 Technical

Traditional System

To implement our proposal, we analyzed multiple solar modules and inverters to determine the most suitable for our case. We considered price per generation, or per kW for inverters, area, prices, compatibility, and the most important, that the component was accepted by the “Ministerio de Energía” because in Chile every object that can connect to the grid needs to fulfill several requirements. [5]

The solar module which suited more to our project was *the Trina Solar TSM-300* and the inverter selected for the analysis was the Solis 40kW/50kW-HV-5G. It is also very important to consider the warranties offered by every provider, to determine the convenience of each option.

Energy Management

For the energy management section, we reviewed similar projects in the world and one of necessities of the companies is to reduce the charge of peak-demand because it is considerably bigger than others, in perspective 1kW for Peak Demand is charged 3.8 USD and 1kW during Peak Hour is Billed 9.2 USD, the peak hour is considered from April to September from 18:00 to 23:00.

A control Technique is necessary because the charge in the batteries is limited and needs to be manage during the hour period, commonly, a threshold for demand is set but if the supply is beyond the setup configuration the battery discharges early and the peak is still charged. For the proposal of the peak reduction we are based ins a paper presented by CHUA [6], the proposal is to use a Fuzzy control based algorithm that considers and lower and an upper threshold, this to set when to charge batteries and when to discharge them. For this task we consider charging the batteries with our solar panels or the grid, and discharging when the price can be significant, at peak hours, results are in the next section

To implement our peak reduction proposal, we analyzed multiple batteries and storage inverters to determine the most suitable for our case. We decided to use the Ax-storage li 10S and the Battey Inverter Sunny Island 8.0H, because of its price and capacity. Currently there is no specific regulation for this system.

3.2 Economical

Every infrastructure project needs to be feasible otherwise no investor would be interested, to calculate how feasible it is, the most practical theory is the Net Present Value Analysis) (see equation 1).

$$NPV = \sum_{t=1}^n \left[\frac{FutureValue_t}{(1+r)^t} \right] - II \quad (1)$$

For all the economic equations r represents discount rate, it could be inflation or a fixed quantity according to the project. While t represents time in years.

The net present value analysis will let us know if the project its feasible, all values above 0 is a gain, now, Investors like the percentage of gain, this value is calculated by doing the equality of NPV to 0 and finding the value of r, this value is the maximum discount rate where the project its feasible. This calculation is known as Internal Rate of Return, and it's convenient to analyze by doing iterations of r (The Discount Rate).

The most important analysis we will do is the LCOE (Levelized Cost of Energy) (see Eq. 2) and LCOS (Levelized Cost of Storage: Power).[7][8]

The LCOE, that is the value in money for every kWh of energy produced for the lifetime of the project considering investment, Operation, Maintenance, rated Energy, discount rate and degradation of the system

$$LCOE \left[\frac{\$}{kWh_{year}} \right] = \frac{I_0 + \sum_{t=1}^n \frac{O_t + M_t}{(1+r)^t}}{\sum_{t=1}^n \frac{(E_r)(1-deg)^t}{(1+r)^t}} \quad (2)$$

For the LCOS:P (\$/kW) (Eq. 3) is a value that determines for the lifetime of the project how much money is required to reduce 1kW of peak demand in bill. It considers investment, operation and maintenance, cost of charging the battery, including effect of time in batteries, it does not consider the value of energy, because energy used to charge battery will be returned to system and because the prize of energy does not change over time, demand of cumulative consumed energy, it is based in the LCOS that is the price of every kW stored and returned to the system.

$$LCOS:P \left[\frac{\$}{kW_{year}} \right] = \frac{I_0 + \sum_{t=1}^n \frac{O_t + M_t + CC_t}{(1+r)^t}}{\sum_{t=1}^n \frac{DS_t}{(1+r)^t}} \quad (3)$$

3.3 Social

Possibly the most important analysis is the social implication and acceptance from the people to the project, we did a survey for the UdeC community, the survey is the next, it is in Spanish because was presented to Chilean People.

The survey considered several aspects like:

- Relation with UdeC
- Knowledge of Solar energy
- Perception of the university
- Importance of the sustainable implementations.
- Perception of UdeC considering panels in the roof of emblematic buildings

The representative sample was calculated using statistical principles and it was determined that 202 people will be the ideal, in reality the survey reached 299 people 48% more than the minimum ideal.

3.4 Environmental

This project is trying to be friendly with environment so we decided to calculate how many CO₂ we will avoid producing by using traditional methods for generating electricity, we also decided to do the equivalent of how many trees were planted, we did the calculation based in other projects in the region and data from the “Ministerio de energía” because this values change for regions. We considered to do a linear interpolation because is the approximation that this entity is currently using. [5]

4 Results

In this section we will talk about the results we obtained for the different analysis.

4.1 Technical

The proposal of the most suitable buildings was the following:

1. Ingeniería Química
2. Tecnológico Mecánico
3. Arquitectura + Ciencias Sociales
4. Biblioteca

For a precise calculation of the surface available for the panels, we simulated the selected buildings, using a software called SketchUp with a plugin called Skelion. Few simulations can be seen in Fig. 3.

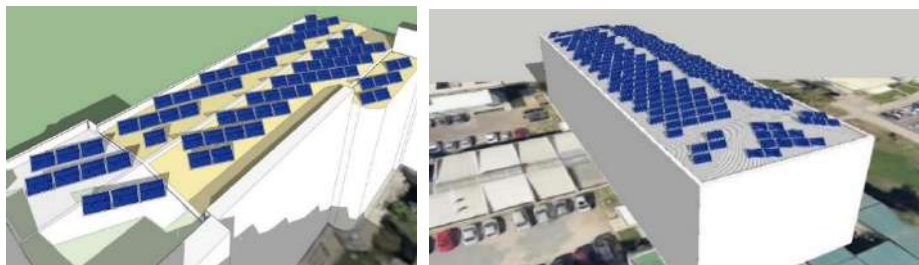


Fig. 3. Simulation of solar panels on Buildings. Campus Concepción, Universidad de Concepción.

For the peak shaving system, we simulated the results in Table. In the Fig 4, the expected load profile can be seen, with the storage and grid consumption of the Cs. Químicas building after performing the peak reduction.

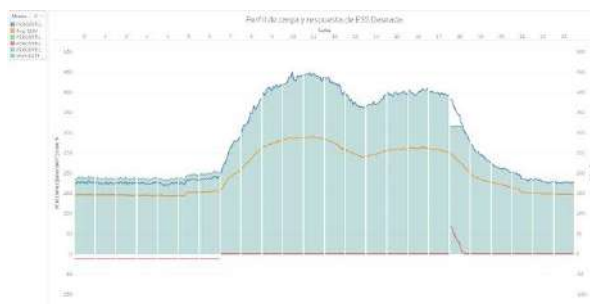


Fig. 4. Simulation of Load Profile after Peak Shaving of Cs Químicas Building, Campus Concepción Universidad de Concepción.

4.2 Economical

We simulated the earnings with a discount rate of 3% and obtained the results in Table 2

Table 2. Economical Results of Solar Panels Implementation.

Analysis/Buildings	Cs Químicas	Tec Mecanico	Arq Cs Sociales	Biblioteca
Total Investment (USD)	127,920	154,182	122,704	123,588
Number of Panels	376	476	381	384
Max Power(kW)	112.8	142.8	114.30	115.2
Yearly Generation (kWh)	178,534	225,905	180,291	182,169
Discount Rate	3%	3%	3%	3%
LCOE (USD/kWh)	0.0439	0.0798	0.070	0.075
Monthly earnings (USD)	1,569.8	706.6	563	576
Payback period (years)	7.12	15.58	15.52	15.21
Total earnings (USD)	204,138.8	57,813	46,485	49,392

PEAK REDUCTION

Afterwards we analyzed the IRR and PRI for each threshold for the peak reduction for Cs Quimicas proposal and obtained the ideal one at 315 kW. With a maximum peak reduction of 48 kW, because it requires less investment. Then we simulated the same reduction of 48kW with Tec Mecanico building. Results are presented in table 3

Table 3. Simulations of Peak Reduction system.

Analysis/Buildings	Result (Cs Quimicas)	Result (Tec-Mecanico)
Total Investment (Inverter, Batteries, Cable) (USD)	43,483	43,483
Discount Rate	3%	3%
LCOS:P (USD/kWh)	5.79	5.79
Monthly earnings (USD)	388	322
Payback period (years)	9.32	9.328
Internal Rate of Return	10.43%	10.6%
Total earnings (USD)	\$ 33,454.96	\$ 33,908

4.3 Social

With the results of our survey we can clearly see that the 62.24% of the surveyed would choose the university above others if it generates its energy through clean energies, also up to 89.24% of the UdeC students and workers agree with the implementation of solar panels at the campus and only 18.47% would be affected by an alteration of the façade of the buildings (Fig. 5).

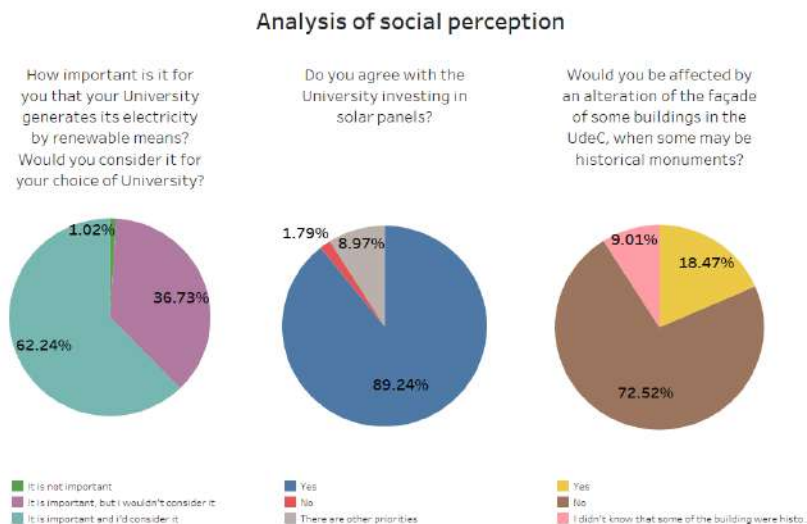


Fig. 5. Results of Survey. Campus Concepción Universidad de Concepción.

4.4 Environmental

And for the environmental impact we obtained the CO₂ avoided and the equivalent trees planted is showed in Table 4.

Table 4. Environmental Results for Solar Project.

	kWh per year	CO ₂ total (ton)	Trees planted
Ing. Química	178,534	1,543	35,948
Tec. Mecánico	225,905	1,952	45,486
Arq + CS	180,291	1,558	36,301
Biblioteca	182,169	1,574	36,679
Total	766,899	6,627	154,414

5 Discussion

We can conclude that the objectives were reached because we were able to make a feasible proposal to place solar panels at the UdeC campus, we considered the best places according to solar generation, the best economical option in which the invest can be returned in a considerable time and also that generates income for the university in the future, we also made an estimate of how good for the environment is the project, this project is a good choice because it reduces more than 5 thousand Tons of CO₂ and is equivalent to plant more than 150 thousand trees, this results can express how necessary it is to try to be sustainable, UdeC is trying to be sustainable but also to be a model for another universities. The social results express that the population is ready to do a change in habits to be careful with the environment.

The most important result of this project is the social aspects, because the population is concerned about the social aspects we live in and is ready for a change, obviously with exceptions, among this results we want to do an emphasis that UdeC has campaigns about the environment but they are not well informed to the population, also the monument category is not known by all the community, so a marketing strategy needs to be done in the future. To finalize we can say that the project is feasible in all aspects, that were analyzed. With this we can say that the objectives were reached.

6 References

1. Universidad de Concepción Chile, en Cifras <http://www6.udec.cl/pexterno/node/16>
2. Explorador de Energía Solar para autoconsumo. <http://walker.dgf.uchile.cl/Explorador/Solar3/>.
3. Tarifas Compañía general de Electricidad. <https://www.cge.cl/informacion-comercial/tarifas-y-procesos-tarifarios/>
4. Clientes Libres y Clientes Regulados en el Sistema Eléctrico. https://obtienearchivo.bcn.cl/obtienearchivo?id=repositorio/10221/27799/1/Clientes_regulados_y_clientes_no_regulados_en_el_mercado_electrico.pdf
5. Ministerio de energía (2016) Guía de Evaluación inicial de edificios para la instalación de sistemas fotovoltaicos.
6. Chua, K H, et al. (2017) Peak Reduction for Commercial Buildings Using Energy Storage. IOP Conference Series: Earth and Environmental Science, vol. 93, 2017, p. 012008., doi:10.1088/1755-1315/93/1/012008.
7. Branker, K., et al. (2011) A Review of Solar Photovoltaic Levelized Cost of Electricity. *Renewable and Sustainable Energy Reviews*, vol. 15, no. 9, pp. 4470–4482., doi:10.1016/j.rser.2011.07.104.
8. EL-Shimy, M. (2017) Economics of Variable Renewable Sources for Electric Power Production. doi: 10.6084/m9.figshare.6168899

Performance assessment of the transport sustainability in the European Union

Sarah B. Gruetzmacher^{1,2}[0000-0002-1193-4461], Clara B. Vaz^{2,3}[0000-0001-9862-6068] and Ângela P. Ferreira²[0000-0002-1912-2556]

¹ Universidade Tecnológica Federal do Paraná, Av. Sete de Setembro, 3165 - 80230-901 Curitiba, Brazil

sarah.gruetz@gmail.com

² Research Center in Digitalization and Intelligent Robotics (CeDRI), Instituto Politécnico de Bragança, Campus de Santa Apolónia, 5300-253 Bragança, Portugal

³ Center for Management and Industrial Engineering (CEGI/INESC TEC)
{clvaz,apf}@ipb.pt

Abstract. Based in the current growth rate of metropolitan areas, providing infrastructures and services to allow the safe, quick and sustainable mobility of people and goods, is increasingly challenging. The European Union has been promoting diverse initiatives towards sustainable transport development and environment protection by setting targets for changes in the sector, as those proposed in the 2011 White Paper on transport. Under this context, this study aims at evaluating the environmental performance of the transport sector in the 28 European Union countries, from 2015 to 2017, towards the policy agenda established in strategic documents. The assessment of the transport environmental performance was made through the aggregation of seven sub-indicators into a composite indicator using a Data Envelopment Analysis approach. The model used to determine the weights to aggregate the sub-indicators is based on a variant of the Benefit of the Doubt model with virtual proportional weights restrictions. The results indicate that, overall, the European Union countries had almost no variation on its transport environmental performance during the time span under analysis. The inefficient countries can improve the transport sustainability mainly by drastically reducing the greenhouse gas emissions from fossil fuels combustion, increasing the share of freight transport that uses rail and waterways and also the share of transport energy from renewable sources.

Keywords: Transport environmental performance · Data Envelopment Analysis · Sustainable Development.

1 Introduction

The interest in sustainability and sustainable development has been increasing in the past decades [1]. The rapidly growing population of the cities, their aging infrastructure and the environmental concerns continue to challenge and pressure policymakers. Providing the infrastructure and services to allow safe, quick and

2 Gruetzmacher, S. et al.

sustainable mobility of people and goods is increasingly challenging [2]. Investing in improving the quality and sustainability of the transport system will improve the productivity, attractiveness and quality of life of the cities. Therefore, the transport sector has become one of the main subjects with regards to sustainable development.

In the European Union (EU), the transport sector employs more than 11 million people and accounts for about 5% of Europe's Gross Domestic Product (GDP). Between 2010 and 2050, passenger transport activity is expected to grow by 42% and freight transport activity by 60% [3]. An effective transportation system should contribute positively to the economic growth, to social development through the fair use of the natural resources and to environmental protection [4].

Under this scenario, the European Commission's, 2011, White Paper on transport - Roadmap to a Single European Transport Area – Towards a competitive and resource efficient transport system [5] proposed strategies for deep changes in the European transport sector aiming at a more sustainable and efficient system.

The adoption of the United Nations' Sustainable Development Goals (SDG) also provided new targets to address the transport sustainability. These goals address global challenges in several areas such as poverty, inequality and climate change, in a total of 17 goals to be achieved in 2030 [6]. Some SDG targets are related directly to transport sustainability and others to areas where transport has an important impact, such as energy consumption and pollutant emissions.

The sustainable development of the transport sector has been put on the agenda of EU countries, making it clear the necessity of measuring and assessing the current transport performance towards achieving these targets. It is also evident the importance of analysing sustainable transport planning, as transport policy and planning decisions can have diverse and long-term impacts on sustainable development. A critical component of transport planning is the development of a comprehensive evaluation program that assesses the transport performance based on an appropriate set of sub-indicators.

In order to fulfill this objective, this study aimed at developing a composite indicator (CI) to measure the environmental performance of the transport sector in the EU countries, from 2015 until 2017, towards a more sustainable mobility. The CI is a practical approach that allows to summarize, compare and track the performance of the countries. It allows the measurement of complex and multi-faceted issues that cannot be captured completely by analysing individual sub-indicators [7]. To aggregate the different sub-indicators into the CI, a variant of the Benefit of the Doubt model, as proposed by Färe et al. in [8], was used.

This paper is organized as follows: the second section presents a literature review on the construction of composite indicator and the the variant of Benefit of the Doubt model proposed by Fare et al. [8]. Section 3 describes the sub-indicators selected to compose the CI. Section 4 analyses the data used and the results obtained. Finally, the conclusions from this work are presented in Section 5.

2 Literature review

2.1 Composite indicators

Composite indicators have been proven to be a useful method to synthesize masses of data, benchmark countries performance in relation to desirable states, demonstrate progress towards goals and to communicate current status to stakeholders leading to effective management decisions towards the established targets [9]. It is also a recognized tool for public communication, since they provide a big picture of a subject and often make it easier for the general public to interpret its results rather than having to identify common trends across many sub-indicators [10].

The essential purposes of the CI is to summarize a complex, multi-faceted phenomena in wide-ranging fields, e.g. environment, economy, society or technological development, enabling the performance comparison of several countries or the evolution of a country over time [11]. The CI comprises of several individual sub-indicators that measures different aspects with usually no unit of measurement in common. The sub-indicators are compiled into a single index on the basis of an underlying model [10].

The subjective judgment about the relative worth of each sub-indicator is modelled through the weight assigned to it [11]. The weight reflects the significance of the sub-indicator and assigns a value to it in relation to the others, and it has, usually, a great impact on the aggregation results [12]. The weights attributed to the sub-indicators can be derived through different methods. They can be based on opinions, such as expert judgment or public opinion poll results. When these information are unavailable, the easiest and most common approach is to use equal weights [13]. However, not all evaluated units will agree to be evaluated with equal weights, since each of them has different characteristics and preferences. Finally, to avoid the subjectivity in determination of the sub-indicators' weights, the preferred tools are the statistical methods that derive the weights endogenously, such as the Principal Component Analysis/Factor Analysis and the Data Envelopment Analysis [14].

2.2 Data Envelopment Analysis

The DEA is a linear programming method, proposed by Charnes et al. [15], that assesses the relative efficiency of several decision making units (DMU) that use multiple inputs to produce multiple outputs. Therefore, DEA measures the efficiency of each DMU, given observations on input and output values in a set of similar entities, without knowledge of the production or cost function [11]. By comparison with the best practices frontier, the DEA model enables the selection of weights that are the most advantageous for the DMU under assessment [7]. This means that the weights are derived from the data itself, avoiding *a priori* assumptions and computations involved in fixed weight choices [16]. Thus, DEA is a popular method in the CI literature as it can solve the problem of subjectivity in the weighting procedure. Another well-known property of the original DEA

4 Gruetzmacher, S. et al.

model is its unit invariance. This is very interesting for the construction of CI as its final value is independent of the measurement units of the sub-indicators which in turn makes the normalization stage redundant and unnecessary [17].

The application of DEA to the construction of CI, referred to as the Benefit of the Doubt model (BoD), was originally proposed by Melyn and Moesen in 1991 [18]. The BoD is equivalent to the original DEA input oriented model, with all sub-indicators considered as outputs and a single dummy input equal to one for all countries. The dummy input can be understood intuitively by regarding the model as a tool for aggregating several sub-indicators of performance, without referencing the inputs that are used to obtain this performance [19]. Since the BoD model only includes outputs it measures the country's performance rather than its efficiency.

In fact, the conventional BoD model derives the composite indicator, aggregating forward sub-indicators, which capture the positive aspect of a performance, where their increasing values are desirable. Frequently, the performance assessment has to manipulate anti-isotonic sub-indicators, which capture the negative aspect of a performance, where their increasing values are undesirable. There are many sub-indicators that fall in this category, for example, emission of a pollutant, traffic accidents, crime rate, etc. The data of these sub-indicator needs to be transformed, to allow them to be incorporated in the conventional BoD model and treated as the forward sub-indicators [8]. Previous approaches used to deal with these anti-isotonic sub-indicators were the use of data transformation techniques and of directional distance function models. One of the most common data transformation technique is the inversion of the value of the reverse sub-indicator [20]. The subtraction of the sub-indicator from a sufficiently large constant and the rescaling normalization using the maximum-minimum method are also approaches that can be found in the literature. Some of these techniques are presented and compared in [21] and [22]. Even though these transformation are simple, they can be problematic. Since the BoD model is derived from an input-oriented DEA model with constant returns to scale, it is not translation invariant for the output values. This means that, the use of translated or rescaled data will affect the CI results and, consequently, the ranking of the DMUs [8].

Färe et al. [8] proposed a new BoD model (FKHM), which directly incorporates the anti-isotonic sub-indicators without using any transformation. The model treats the anti-isotonic sub-indicators as reverse rather than as undesirable. This means that the model assumes that the reverse sub-indicators values can decrease or increase independently from the values of forward sub-indicators.

Given a cross-section of M sub-indicators and S countries, y_{ij} is the value of sub-indicator i for the country j , and w_i is the weight attributed to the i -th sub-indicator. The formulation for the FKH model is presented in Eq.(1), where y_{ij} ($j = 1, \dots, m$) are the forward sub-indicators (i.e., capturing positive aspect) and y_{ij} ($j = m + 1, \dots, M$) are the reverse sub-indicators (i.e., capturing negative aspect).

$$\begin{aligned}
 CI_{j_o} &= \max \sum_{i=1}^m w_i y_{ij_o} - \sum_{i=m+1}^M w_i y_{ij_o} \\
 \text{s.t.} \quad & \sum_{i=1}^m w_i y_{ij} - \sum_{i=m+1}^M w_i y_{ij} \leq 1 \quad \forall j = 1, \dots, S \\
 & w_i \geq 0 \quad \forall i = 1, \dots, M \\
 & \frac{w_i y_{ij_o}}{\sum_{i=1}^m w_i y_{ij_o} + \sum_{i=m+1}^M w_i y_{ij_o}} \geq 0.05 \quad \forall i = 1, \dots, M
 \end{aligned} \tag{1}$$

The main difference from the FKHM model to the conventional BoD model is that Eq.(1) maximizes the difference between the weighted average of forward sub-indicators and the weighted average of reverse sub-indicators. Additionally, the presence of forward sub-indicators does not imply the presence of reverse ones and, when there are no anti-isotonic indicators, model FKHM can be reduced to the formulation of the conventional BoD model [8].

The formulation given by Eq.(1) has three kinds of restrictions. The first restriction imposes that no country can have a CI value greater than one, to ensure an intuitive interpretation of the indicator. The second restriction imposes that each weight attributed to the sub-indicators should be non-negative, which implies that the CI is a non-decreasing function of the sub-indicators. The third restriction prevents the model from assigning zero weights to some sub-indicators, since zero weight means that the sub-indicator associated has no influence in the global performance. By adding a virtual proportional weight restrictions, as proposed by [23], each sub-indicator is required to have a minimum percentage of contribution in the assessed composite indicator. The value of 0.05 (or 5%) was chosen as it is sufficient to prevent the attribution of zero weights to any sub-indicator, thus, guaranteeing the contribution of all sub-indicators in the final composite indicator and have a higher countries' discrimination in the performance assessment. Consequently, the CI value obtained varies between zero and one for each assessed country j_o , where higher values indicate a better relative performance [17].

3 Methodology

This paper intends to assess the transport environmental performance of EU countries through the aggregation of sub-indicators into a CI using the Fare et al [8] (FKHM) model. Therefore, the selection of these sub-indicators is of crucial importance to compute the countries overall performance while encompassing all the important subjects.

3.1 Data and variables

The selection of the sub-indicators was based on a literature review of CI with similar conceptual framework, the goals of transport sustainability mentioned in

6 Gruetzmacher, S. et al.

the Roadmap (EU's White Paper [5]) and the SDG [6], while also taking into consideration the data that was available for all the EU countries in the time span under analysis. Besides, each sub-indicator must be of easy interpretation and should measure a specific area of the performance, ensuring a minimal number of sub-indicators that assures that all dimensions are reflected in the calculation of the CI. All the data used in this work were gathered from the Eurostat database [24].

To assess the transport environmental performance of EU countries, the CI was constructed based in three forward sub-indicators (i.e., capturing positive aspect) and four reverse sub-indicators (i.e., capturing negative aspect). The forward sub-indicators are the share of buses and trains in total passengers transport, the share of energy from renewable sources in transport and the share of rail and inland waterways in total freight transport. The reverse sub-indicators are people dead in road accidents, GHG emissions by fuel combustion in transport, the average CO₂ emissions per kilometer from new passenger cars and the energy dependency on oil and petroleum products. These sub-indicators are described hereinafter.

The share of collective transport in total passengers transport (*public transport*) is expressed in percentage and measures the share of passenger's transport made by collective transport in the total inland transport. Collective transport refers to buses (including coaches and trolleybuses) and trains, while the total inland transport includes these facilities and also passenger cars. Trams and metros are not included due to the lack of harmonised data. The public transport sub-indicator is related to two Sustainable Development Goals, in which it is highlighted the importance of building resilient and sustainable infrastructure and the necessity to renew and plan cities so they offer access to basic services for all. This sub-indicator also relates to the necessity of improving the transport quality, accessibility and reliability, as discussed in the Roadmap.

The share of energy from renewable sources in transport (*renewable fuels*) is expressed as the percentage of renewable fuels in the total transport fuels. Energy by renewable sources consumed in transport is given by the sum of sustainable biofuels, renewable electricity, hydrogen and synthetic fuels of renewable origin and other reported forms of renewable energy [25]. With this sub-indicator it is possible to understand how extensive is the use of renewable energy in the transport sector and how much it has been replacing fossil fuels. The Renewable Energy Directive promotes policies for the production and promotion of energy from renewable sources in the EU, which states, in the revised version from 2018, the target of 32% share of renewable energy in the transport sector for 2030 [26]. The Roadmap also suggests a regular phase out of conventionally-fuelled vehicles from urban environments by halving their number in 2030 and phasing them out of the cities by 2050.

The share of rail and inland waterways in total freight transport (*freight transport*) is expressed in percentage. The total inland transport in the denominator of the sub-indicator includes freight on national territory made by road, rail and inland waterways transport. Sea and air freight transport are not represented

in the sub-indicator. The freight transport sub-indicator was not applicable for Cyprus and Malta since these countries did not present values for railways or inland waterways. As an effort to have a complete database without excluding these countries from the evaluation in this work the lowest values observed on the dataset were used for Cyprus and Malta for every year. This method avoid that these countries become unintended benchmarks, and therefore, it will not affect the location of the best practice frontier. This method has been suggested by Morais et al. [27]. The Roadmap mentions the objective of shifting 30% of the road freight to other modes, such as rail and waterways, by 2030 and more than 50% by 2050. This sub-indicator also reflects the progress toward the Sustainable Development Goals focused on innovation and on building resilient and sustainable infrastructure.

The people dead in road accidents (*road deaths*) sub-indicator measures the number of fatalities in road accidents per hundred thousand inhabitants. This sub-indicator includes passengers and drivers of motorized vehicles and pedal cycles, as well as pedestrians, that have died up to 30 days after the accident. This sub-indicator is aligned with two Sustainable Development Goals aiming at safer cities, health and well-being status. As highlighted in the Roadmap, EU aims to reduce fatalities close to zero by 2050 with initiatives in the areas of technology, enforcement and education.

The GHG emissions by fuel combustion in transport (*GHG emissions*) measures the transport's fuel combustion contribution in the total greenhouse gas emissions inventory. The values are originally expressed in thousand tonnes and were normalized using the countries' population on 1st January of each year, to take into consideration their dimension. Therefore, the sub-indicator's data is expressed in thousand tonnes per hundred thousand inhabitants for each country. The GHG emissions from the transport by road and inland waterways accounted for 22% of the total European Union emissions in 2017 and reached 27% when including international aviation and maritime emissions [28]. The Roadmap sets out a target of 60% reduction in the GHG emissions by 2050 compared to 1990 levels.

The average carbon dioxide (CO₂) emissions per kilometer from new passenger cars (*new car emissions*) is defined as the average CO₂ emissions per kilometer in a given year for new passenger cars and expressed in grams of CO₂ per kilometer. This is a target for the average of the manufacturer's overall fleet, meaning that cars above the limit are allowed in the market as long as they are offset by the production of lighter cars. The Regulation (EU) 2019/631 sets a mandatory target for emission reduction for new cars of 95 grams of CO₂ per kilometer by 2021 [29]. This sub-indicator reflects three Sustainable Development Goals related to ensuring environmentally aware consumption, to innovation in search of lasting solutions to environmental challenges and the call for climate action. The Roadmap also highlights the importance of the research and innovation on vehicle propulsion technologies and the improvement of energy efficiency performance of vehicles across all modes.

8 Gruetzmacher, S. et al.

The energy dependency on oil and petroleum products (*energy dependency*) sub-indicator monitors to which extent the countries economy relies on imports of oil and petroleum products to meet its energy needs. It is calculated by dividing the net imports by the gross available energy and it is used in a percentage basis. The net imports are the difference between the total imports and the total exports. The gross available energy is the sum of primary products, recovered and recycled products and imports, minus the sum of exports and stock changes. Regarding its metrics, energy dependency may be higher than 100% with regard to countries creating a stock in a given year or it can be negative, for oil exporter countries. A negative value occurred only once in the dataset, and the value was close to zero (-4.701%) for the exporter country. To achieve the best relative position of that energy exporter country regarding the other countries, the best score of 1% for this forward sub-indicator was assigned to the exporter country, to avoid handling negative data in the model. This sub-indicator shows how the EU countries progress toward more resource efficient policies. As oil becomes scarcer each year, the necessity of reducing EU dependency on oil imports, without reducing the transport system efficiency, is one of the objectives mentioned in the Roadmap. Imports exposes the economy to volatile world market prices and the risk of supply shortages.

These seven sub-indicators are used to assess the transport environmental performance of EU countries, as presented in the next section.

4 Results and discussion

4.1 Descriptive analysis of the variables

The transport environmental performance was assessed for the 28 EU countries, from 2015 to 2017. It was chosen to use the United Kingdom data, since during the time span of the assessment the country still integrated the European Union. Table 1 shows two descriptive statistics for the sub-indicators under analysis across countries for each year. The mean of the sub-indicators was calculated for each year, as well as the dispersion coefficient (DC). The DC measures the dispersion of the data around the mean and is given by the ratio between the standard deviation and the mean. It was calculated in order to facilitate the analysis among sub-indicators, since it allows the comparison of the degree of variation between different data sets even if they have different measurement units.

Analysing the forward sub-indicators in Table 1, it can be seen that the share of public transport in total passenger transport has constantly decreased in the time span under study, by 2017 it was more than 2% lower compared to 2015 levels. The share of renewable energy in transport decreased in 2016 but by 2017 its average had increased more than 5% above 2015 value. And the share of freight transport decreased between 2015 and 2017 staying 3.7% lower than 2015 levels.

Regarding the reverse sub-indicators, the average of road deaths for all countries has decreased more than 9% from 2015 to 2017. The average of GHG

Table 1. Mean and DC of the indicators data used in the construction of the CI.

Indicator	2015		2016		2017	
	Mean	DC	Mean	DC	Mean	DC
Public transport	18.175	0.241	18.011	0.238	17.768	0.246
Freight transport	27.979	0.731	26.982	0.728	26.936	0.724
Renewable energy	6.544	0.795	6.191	0.746	6.884	0.733
Road deaths	5.800	0.366	5.625	0.325	5.325	0.358
GHG emissions	208.670	0.771	211.493	0.714	213.696	0.696
New car emissions	120.946	0.078	118.757	0.066	119.168	0.064
Energy dependency	92.605	0.245	90.736	0.248	89.935	0.250

emissions for all countries has increased more than 2.4% during the time span studied. The mean of CO₂ emissions from new passengers cars has increased from 2016 to 2017 but still remained 1.5% below 2015 levels. And the average energy dependency of the EU countries decreased almost 3% between the years under analyse.

The highest data dispersion relative to the mean was observed in the share of renewable energy, which translates the difference among countries in available renewable energy. Another high DC value was obtained by the GHG emissions sub-indicator, reflecting the different policies of EU countries for reducing emissions. The share of freight transport also had a high DC, since some countries have geographical locations and environmental conditions that facilitate the utilization of rail and inland waterways. The DC for these three sub-indicators, however, have been constantly decreasing during the time span of the data, reflecting a tendency to increase the homogeneity among EU countries.

The lowest variability relative to the mean was observed for the CO₂ emissions from new passengers cars. This can be reflecting a higher homogeneity in the energy efficiency performance of vehicles engines among car manufacturers.

4.2 Performance assessment of the EU countries

The transport environmental performance for each country in a given year was computed by aggregating the seven chosen sub-indicators using the FKHM model, presented in Eq.(1).

The CI of the transport environmental performance was calculated using the data from the time span of three years, from 2015 to 2017 and it is assessed by comparison to the best practices observed during this time period. The results are summarized in Table 2. The countries are ranked based on their 2017 CI results from the highest to the lowest.

The average of the CI results in the three years analysed was around 0.591 and had only slight variations through the years. The average decreased by almost 3% in 2016 when compared to 2015, increased again in 2017 but still kept slightly below 2015 levels, by 1.17%. The standard deviation of the CI results was similar in the three year, showing that the results variability was kept the same during this period.

Table 2. Transport environmental performance results.

Country	2015	2016	2017
Denmark	0.972	0.937	1.000
Hungary	1.000	1.000	1.000
Netherlands	1.000	0.906	1.000
Sweden	0.878	0.960	1.000
Romania	1.000	0.977	0.948
Slovakia	0.886	0.927	0.895
Latvia	1.000	0.918	0.856
Austria	0.826	0.821	0.803
Czechia	0.761	0.773	0.800
Lithuania	0.790	0.763	0.784
Finland	0.842	0.620	0.759
Bulgaria	0.700	0.693	0.662
Poland	0.633	0.600	0.594
Belgium	0.548	0.570	0.583
France	0.540	0.522	0.542
Germany	0.531	0.550	0.538
Italy	0.539	0.550	0.525
Slovenia	0.488	0.416	0.494
Luxembourg	0.491	0.469	0.489
UK	0.420	0.410	0.416
Portugal	0.378	0.395	0.395
Spain	0.312	0.442	0.381
Croatia	0.463	0.348	0.341
Greece	0.189	0.162	0.216
Estonia	0.161	0.165	0.164
Ireland	0.141	0.125	0.131
Malta	0.139	0.126	0.130
Cyprus	0.131	0.120	0.120
Mean	0.599	0.581	0.592
St. Dev.	0.290	0.283	0.286

This assessment identifies nine efficient units: Denmark (in 2017), Latvia (in 2015), Hungary (in 2015, 2016 and 2017), Netherlands (in 2015 and 2017), Romania (in 2015) and Sweden (in 2017). From 2015 to 2017, half of the countries followed a small improvement and half of the country had a slight decrease in their overall performance. The highest improvement in the CI score between 2015 and 2017 were observed in Greece, Spain and Sweden, which increased in 2017 by 14%, 22% and 13% above 2015 levels, respectively.

The highest decrease during this time frame were observed for Croatia (26.4%) and Latvia (14.4%). The highest improvement in the time-span of one year was observed in Greece, that had a large decrease in its CI score between 2015 and 2016, but between 2016 and 2017 its CI value increased more than 33%. Estonia, Ireland, Cyprus and Malta were the most inefficient countries in this analysis

Assessment of the transport sector in the EU. 11

with almost no improvement in the considered years. Besides Estonia, all these countries also had a decrease in their CI value in 2017 when compared to 2015.

This study also compares the forward and reverse sub-indicators of the benchmark countries, which obtained a CI score of 1, with the inefficient ones. The mean for each sub-indicator is calculated for both groups (benchmarks and inefficient countries). Figure 1 shows a comparison for each sub-indicator between the benchmark countries and the inefficient ones.

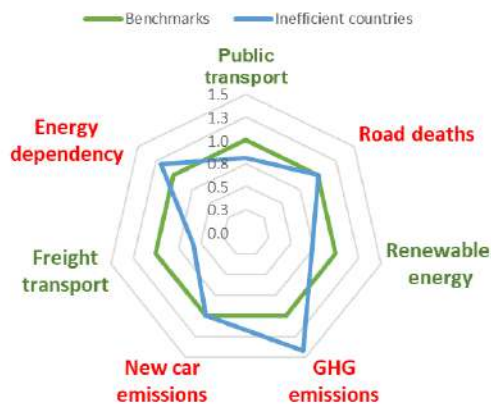


Fig. 1. Comparison between benchmarks and inefficient countries.

Analysing Figure 1, it is possible to notice the areas where the inefficient countries need improvement, for instance, by setting out policies and/or redefine output standards. Except for the number of road deaths and the new car emissions indicators, in which both groups had a very similar performance, the inefficient countries were always outperformed by the benchmarks. The inefficient countries have 80% of the share of public transport presented by the benchmarks and almost 75% of the renewable energy share presented by the benchmark group. In the freight transports sub-indicator, the inefficient countries have less than 60% of the value presented for the benchmarks. Considering the reverse sub-indicators, with regard to the GHG emissions, the inefficient countries had a value more than 40% higher than the benchmarks. The average of energy dependency sub-indicator of the inefficient countries was almost 20% higher than the average for the benchmarks.

Most of the work to improve transport sustainability should be done in reducing the GHG emissions from fossil fuel, improving the infrastructure and promote policies to increase the share of freight transport that uses rail and waterways and also increasing the share of transport energy from renewable sources. The public transport of the inefficient countries also needs improvements in its accessibility and quality to allow a larger share of passenger to benefit from it.

12 Gruetzmacher, S. et al.

There is still also margin to reduce the oil and petroleum dependency through changes in the transport energy consumption.

5 Conclusions

The assessment of the transport environmental performance was made through the aggregation of seven transport sub-indicators. The model used to obtain the CI values was derived from a variant BoD model with virtual proportional weights restrictions. Based on the results achieved, it is possible to conclude that, in general, the EU countries had almost no variation on their transport environmental performance and by 2017 were, on average, 1.17% lower than 2015 values. This result points out that EU countries should make efforts to enable them to develop and strengthen their ability towards sustainability.

The performance assessment identified that only nine units were efficient: Denmark (in 2017), Latvia (in 2015), Hungary (in 2015, 2016 and 2017), Netherlands (in 2015 and 2017), Romania (in 2015) and Sweden (in 2017). By using these units as benchmarks and comparing their performance in each sub-indicator with the remaining units (the inefficient ones), it was possible to identify the areas that need improvement. Most of the work to improve transport sustainability should be done by drastically reducing the GHG from fossil fuel, increasing the share of freight transport that uses rail and waterways and also the share of transport energy from renewable sources.

Future works should explore other models for treating anti-isotonic sub-indicators in order to allow results comparison among those different models. Furthermore, some other sub-indicators can be taken into account, to calculate the composite indicator for each country.

6 Acknowledgements

This work has been supported by FCT – Fundação para a Ciência e Tecnologia within the Project Scope: UIDB/05757/2020.

References

1. Litman, Todd.: Well measured. Victoria Transport Policy Institute (2016)
2. Sustainable Mobility Project 2.0. Integrated sustainable mobility in cities - a practical guide. World Business Council for Sustainable Development (2016)
3. European Commission: EU mobility package: Europe on the move briefing note, <http://nws.euocities.eu/MediaShell/media/EuropeonthemoveBriefingnote.pdf>. Last accessed 10 Mar 2020
4. Dobranskyte-Niskota, A., Perujo, A., Pregl, M.: Indicators to assess sustainability of transport activities. European Commission, Joint Research Centre (2007)
5. European Commission: White Paper on Transport: Roadmap to a Single European Transport Area: Towards a Competitive and Resource-efficient Transport System. Publications Office of the European Union (2011)

Assessment of the transport sector in the EU. 13

6. About the Sustainable Development Goals, <https://www.un.org/sustainabledevelopment/sustainable-development-goals/>. Last accessed 13 Mar 2020
7. Reisi, M., Aye, L., Rajabifard, A., Ngo, T.: Transport sustainability index: Melbourne case study. *Ecological Indicators*, 43, 288-296 (2014)
8. Färe, R., Karagiannis, G., Hasannasab, M., Margaritis, D.: A benefit-of-the-doubt model with reverse indicators. *European Journal of Operational Research*, 278(2), 394-400 (2019)
9. Mitchell, G., May, A., McDonald, A.: PICABUE: a methodological framework for the development of indicators of sustainable development. *The International Journal of Sustainable Development and World Ecology*, 2(2), 104-123 (1995)
10. Joint Research Centre-European Commission: Handbook on constructing composite indicators: methodology and user guide. OECD publishing (2008)
11. Cherchye, L., Moesen, W., Rogge, N., Van Puyenbroeck, T.: An introduction to 'benefit of the doubt' composite indicators. *Social indicators research*, 82(1), 111-145 (2007)
12. Kunicina, N., Waeger, P., Calderon, E., Arce, R., Joumard, R., Nicolas, J. P., Quintana, S. M.: Indicators of environmental sustainability in transport. An interdisciplinary approach to methods. (2010)
13. Gudmundsson, H., Regmi, M. B.: Developing the sustainable urban transport index. *Transport and Sustainable Development Goals*, 35. (2017)
14. Zhou, P., Ang, B. W., Poh, K. L.: A mathematical programming approach to constructing composite indicators. *Ecological economics*, 62(2), 291-297. (2007)
15. Charnes, A., Cooper, W. W., Rhodes, E.: Measuring the efficiency of decision making units. *European journal of operational research*, 2(6), 429-444 (1978)
16. Cooper, W. W., Seiford, L. M., Tone, K.: Data envelopment analysis: A comprehensive text with models, applications, references and DEA-solver software. *Journal-Operational Research Society*, 52(12), 1408-1409. (2001)
17. Cherchye, L., Moesen, W., Rogge, N., Van Puyenbroeck, T., Saisana, M., Saltelli, A., Tarantola, S.: Creating composite indicators with DEA and robustness analysis: the case of the Technology Achievement Index. *Journal of the Operational Research Society*, 59(2), 239-251 (2008)
18. Melyn, W., Moesen, W.: Towards a synthetic indicator of macroeconomic performance: unequal weighting when limited information is available. *Public economics research papers*, 1-24. (1991)
19. Chung, W.: Using DEA model without input and with negative input to develop composite indicators. *International Conference on Industrial Engineering and Engineering Management (IEEM)*, IEEE, pp. 2010-2013 (2017)
20. Lovell, C. K., Pastor, J. T., Turner, J. A.: Measuring macroeconomic performance in the OECD: A comparison of European and non-European countries. *European journal of operational research*, 87(3), 507-518. (1995)
21. Dyson, R. G., Allen, R., Camanho, A. S., Podinovski, V. V., Sarrico, C. S., Shale, E. A.: Pitfalls and protocols in DEA. *European Journal of operational research*, 132(2), 245-259 (2001)
22. Scheel, H.: Undesirable outputs in efficiency valuations. *European journal of operational research*, 132(2), 400-410. (2001).
23. Wong, Y. H., Beasley, J. E.: Restricting weight flexibility in data envelopment analysis. *Journal of the Operational Research Society*, 41(9), 829-835 (1990)
24. Eurostat Database, <https://ec.europa.eu/eurostat/data/database>. Last accessed 20 Mar 2020

14 Gruetzmacher, S. et al.

25. European Commission: SHARES Tool Manual. Directorate E: Sectoral and regional statistics. Unit E.5: Energy. (2018)
26. European Commission: DIRECTIVE 2018/2001 of the European parliament and of the council. Official Journal of the European Union. (2018)
27. Morais, P., Camanho, A. S.: Evaluation of performance of European cities with the aim to promote quality of life improvements. *Omega*, 39 (4), 398–409. (2011)
28. European Commission: Proposal for a Regulation of the European Parliament and of the Council setting CO2 emission performance standards for new heavy duty vehicles (2011).
29. European Commission: Regulation (EU) 2019/631 of the European parliament and of the council. Official Journal of the European Union. (2019)

Integration of small wind turbines in a Microgrid in a peri-urban environment

Oscar Izquierdo-Monge¹, Paula Peña-Carro¹, Carlos Barrera del Amo¹, Siro Soria Franco¹, Gonzalo Martín Jiménez¹, Luis Hernández-Callejo²

¹ CEDER-CIEMAT, Autovía de Navarra A15 salida 56, 422290 Lobia (Soria), España, O.I.M.: oscar.izquierdo@ciemat.es; P.P.C.: paula.pena@ciemat.es; C.B.A.: carlos.barrera@ciemat.es; S.S.F.: siro.soria@ciemat.es; G.M.J.: 100333375@alumnos.uc3m.es

² University of Valladolid, Campus Universitario Duques de Soria, 42004 Soria, España. L.H-C: luis.hernandez.callejo@uva.es

Abstract: The use of wind resources has always gone hand in hand with high wind speeds. This paper develops the decisions to be taken for the installation of small wind turbines in peri-urban environments where wind speeds are medium or low, as well as their instantaneous monitoring for their integration into a power microgrid. In this way, we favour the installation of small wind energy technology in locations as close as possible to the place of demand, achieving a reduction in the cost of the electricity bill with real-time control without added costs through the Home Assistant software.

Keywords: Microgrids, small wind turbine, wind resource, peri-urban environment, monitoring and control, Home Assistant.

1 Introduction

The implementation of renewable sources of energy generation is increasing, increasing the percentage of non-fossil energy in the energy market. The most mature technologies are large-scale solar photovoltaic and wind energy [1], but the current trend is towards generating as close as possible to the source of demand, which means generating near or within urban centres. For years we have seen how the installation of solar panels on buildings has been increasing in new buildings to reduce the demand bill, but we must not forget other possibilities such as the installation of small wind turbines on the roofs of buildings and the potential that this technology has.

Traditionally, small wind turbines were used for pumping and in systems isolated from the electricity grid (rural electrification and telecommunications). However, in recent years their applications have grown in systems connected to the electricity grid, coinciding with the development of electrical microgrids based on distributed generation systems [2].

In this way, we extrapolate the use of wind energy to locations with low or medium winds where previously there was no installation of this technology having the possibility to take advantage of this resource [3].

This allows the production of green energy in a decentralized way, promoting energy independence, saving fossil fuels, reducing CO₂ emissions, and saving energy costs by avoiding losses in transport [4].

It must be taken into account that when connecting a small wind turbine to an electrical microgrid, it is just as important to select a model suitable for the characteristics of the site, as its exact location to maximize its production.

This paper explains how two small wind turbines have been integrated into CEDER's electric microgrid, with special emphasis on their monitoring and integration into the microgrid's control system, to allow efficient controlled of the microgrid. The rest of the paper is as follows: section 2 describes the microgrid and the wind turbines under study, section 3 presents the different criteria for the location of wind turbines in peri-urban environments. Section 4 discusses the selection of wind turbines for peri-urban environments. Section 5 explains the installation and connection of a small wind turbine to the power grid. In section 6 the integration of the wind turbines into the CEDER microgrid is presented. Finally, the conclusions obtained and the cited bibliography are shown.

2 Case of Study: CEDER microgrid

CEDER's microgrid is formed by eight transformation centres with multiple distributed generation systems, different mechanical and electrochemical storage systems, as well as several demand components connected to each transformation centre. All of this is monitored and controlled with a controlled system developed by CEDER based on the HomeAssistant software [5] installed on a Raspberry Pi 4 Model B [6] [7], which is a robust and affordable solution with great potential that allows communication with the different components of generation, storage, and demand of CEDER, through different communication protocols and their integration into a single interface.

This study will focus on the integration of two small wind turbines into this microgrid.

2.1 Wind turbines description

The Wind Energy Unit carries out different tests on small wind turbines so at CEDER there are always multiple wind turbines installed, some connected to the grid and others to batteries. Currently there are two wind turbines connected to the microgrid:

- ATLANTIC AOC: It is a three-bladed wind turbine of 50 kW, with a diameter of 15 meters. It has a horizontal axis and works downwind. It is installed on the site of the small wind turbine test plant number I (PEPA I) (see Figure 1).



Figure 1. Atlantic AOC Wind Turbine in PEPA I.

- ENAIR EPRO70: It is a three-bladed wind turbine of 3.5 kW, 4.3 meters in diameter. It has a horizontal axis and works upwind. It is located on the roof of the Wind Component Testing Laboratory (LECA) building (see Figure 2).



Figure 2. Enair EPRO70 Wind Turbine on the roof of LECA building.

As will be seen in the following sections, the selection of a wind turbine suitable for the site, as well as the exact location of the wind turbine, are keys to achieving optimum efficiency. In peri-urban environments, the selection of the wind turbine is a complex decision due to all the parameters to be considered: type of wind turbine, nominal power, operating regime, weight, rotor diameter, tower height, etc.

The best wind turbine to install can vary from one location to another depending on the characteristics of the wind in each one of them (speed, laminar or turbulent regime, etc.) within the same location.

3 Criteria for the location of wind turbines in peri-urban environments

At CEDER, the installation of wind turbines is done for research purposes and to carry out different tests, and therefore its main objective is not production. In fact, in general terms, it is not a good location since the wind resource is not particularly good since the annual average wind speed is relatively low.

Therefore, although general considerations have been considered (as we will see below) for the selection of the specific location of each wind turbine, these were chosen based on other criteria in addition to the purely productive ones.

Before installing a wind turbine it is necessary to evaluate and characterize the wind resource of the site and this is especially important in peri-urban environments given the peculiarities of wind in these environments [2] [8]. To do this, it is necessary to have wind measurements for at least one year, to avoid seasonal variations.

To characterize the wind resource it is necessary to carry out measurements of different wind variables such as speed, direction, and a series of meteorological variables that have a great impact on the production of power by a wind turbine such as atmospheric pressure, ambient temperature and relative humidity. To carry out these measurements, a meteorological mast is installed with all the necessary sensors (cup anemometer, vane, thermo-hygrometer and atmospheric pressure sensor) to measure these variables.

Wind speed sensor should be at the same height than the wind turbine rotor. If not possible, measured values must be extrapolated to rotor height, according to the vertical wind profile, which varies according to the roughness of the terrain:

$$\frac{V_2}{V_1} = \frac{\ln\left(\frac{h_2}{Z_0}\right)}{\ln\left(\frac{h_1}{Z_0}\right)} \quad (1)$$

Where:

V1: is the wind speed at altitude 1.

V2: is the wind speed at altitude 2.

h1: is the height 1.

h2: is the height 2.

Z0: is the roughness of the terrain.

As can be seen in Figure 3, the height at which 100% of the wind resource is obtained increases in peri-urban environments respect to open fields, as the roughness increases. Thus, in an urban area, 100% of the resource is not obtained until more than 350 meters high, while in a rustic area it is reached at just over 250 meters.

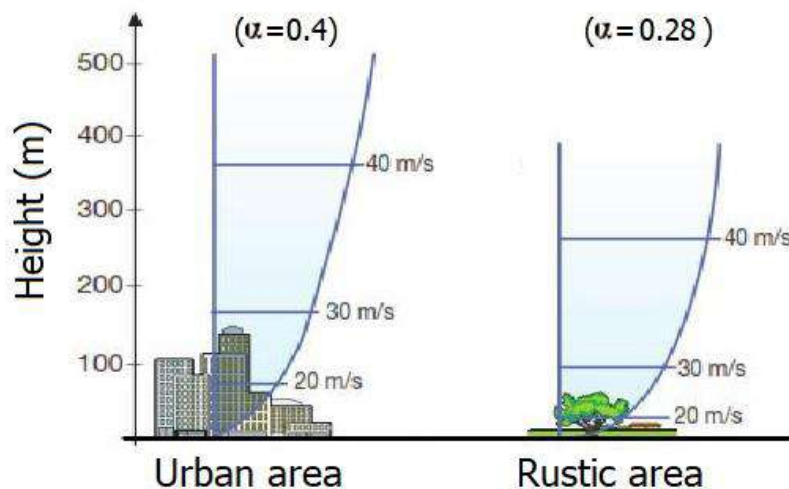


Figure 3. Vertical wind profile (rustic area $\alpha=0.28$ and urban area $\alpha=0.4$).

For the position, this extrapolation is much more complicated in peri-urban environments than in open country because, as already mentioned, the wind characteristics vary significantly from one point to another, even on the same roof, depending on whether the location is closer to the building wall or more indoors, on one side of the building with one shape or another with a different shape, so that the vertical component of the wind changes or turbulence is generated, etc. All this makes it very difficult to choose an optimal location for the installation of a wind turbine in a peri-urban environment, the installation of a wind turbine in an incorrect location can cause the power output to decrease to zero even when the wind is high [9].

Before installing the EPRO70 wind turbine on the roof cover of the LECA building, weather towers with sonic anemometers were mounted in different positions of the building to know the wind in each position. This type of sonic anemometers allows the measurement of the three components of the wind speed, which makes it especially interesting in this location given the vertical component of the wind on the roof of a building after it hits the walls of the building.

This measurement procedure is expensive, which means that it cannot always be carried out in peri-urban environments. When wind cannot be monitored, it is advisable to carry out a study using Computational Fluid Dynamics (CFD) techniques [2] [9] which simulate the behaviour of the wind using numerical methods and allow the wind resource on the site to be estimated (see Figure 4).

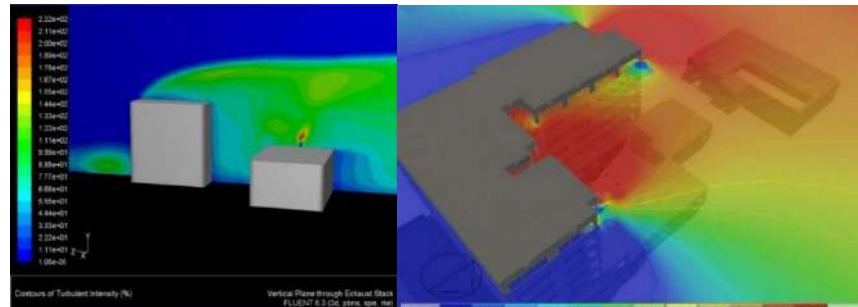


Figure 4. CFD example.

Finally, we must take into account a series of considerations regarding the wind resource that do not occur in open fields but in peri-urban environments, which will be more notable the higher the density of buildings and the greater the height:

- The wind flow in open country is practically laminar, while in peri-urban environments it is mostly turbulent. This means that there is a significant change over relatively short distance.
- Obstacles can change the wind speed:
 - Increasing it: the streets can serve as air ducts that by Venturi effect increase the wind speed.
 - Decreasing it: The wind when it hits the buildings slows down.
- The wind flow around the perimeter of a building's roof has a turbulent behaviour (different for each building) due to the collision with the façade. For this reason, a wind turbine should not be placed near the perimeter of the building. Exceptionally, buildings with a certain geometry can improve wind behaviour.

For all these reasons, from a wind energy point of view, peri-urban sites are complex and difficult to evaluate as they depend on the shape, distance, and height of the nearby buildings. It is necessary to make a detailed study of each site where a wind turbine is to be installed.

Besides, cities have not been built in such a way that they have a good orientation to the prevailing wind, but generally try to protect themselves from it. This causes significant problems of access to an undisturbed wind component suitable for the placement of wind turbines.

3.1 Wind turbine efficiency in peri-urban and open field environments

We have seen that the conditions of the wind resource change significantly between peri-urban environments and open fields, which means that the efficiency of the same wind turbine will change from one environment to another [2] [3].

The CEDER wind energy unit has performed two power curve tests according to the IEC 61400-12-1 Annex H standard on the Enair EPRO70 wind turbine (see Figure 5), to see how conditions in peri-urban environments affect the efficiency of the wind turbine.



Figure 5. Enair EPRO70 Wind Turbine in an open field and peri-urban environment.

The results obtained are shown in Figure 6, where it can be seen how at low wind speeds (up to 5 m/s) the wind turbine behaves similarly, but as the speed increases, much more power is obtained in open field.

It can also be seen how in open field speeds higher than 15 m/s are obtained, while in the peri-urban environment during the test no values above 12 m/s was obtained.

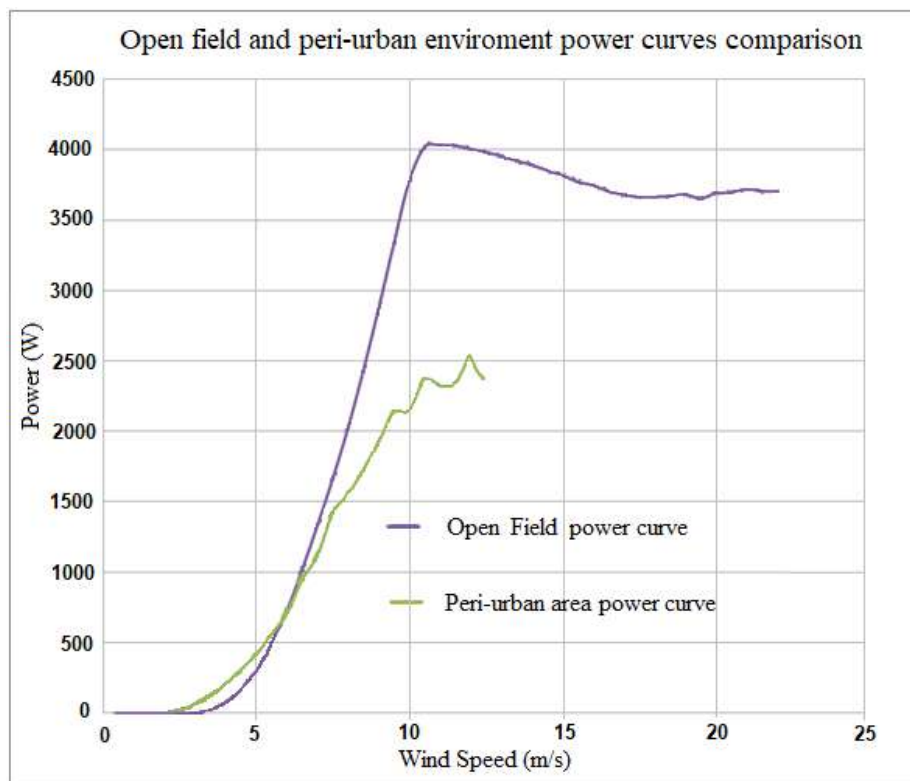


Figure 6. Comparison of the power curve in the open field and on deck in peri-urban environment.

With these differences in the power curve, annual power production will be of the order of 40% less in the peri-urban environment.

It is important to note that this is only valid for the exact location of the wind turbine in the peri-urban environment where the power curve test was carried out, as when changing location the wind conditions can change and the power curve can be modified. In the open field as the power curve is standardized it is always the same.

4 Selection of small wind turbines

There are several definitions of mini wind turbines, but the most widely used is the one established by the International Electrotechnical Commission (IEC) [10] in its Standard IEC 61400-2:2013 *Small wind turbines*. It considers a wind turbine to be of small power when the area swept by its rotor is less than 200 m². This is equivalent to approximately 16 meters in diameter and a power of 65 kW.

The selection of the wind turbine must go hand in hand with the selection of the location. There is no single best wind turbine for every location, but depending on the

characteristics of the wind, one model or another may be better suited. Also, factors such as the installed power must be considered, which is closely related to the dimensions of the wind turbine. The height of the tower in which the wind turbine is to be installed will also have an important influence.


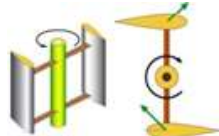

The requirements for a wind turbine to be integrated into a microgrid in a peri-urban environment are different from those in the open:

- High efficiency in low and turbulent winds: The average wind speed in an optimal location for a wind turbine in the open field can be higher than 10 m/s, while in a peri-urban environment it barely reaches 4 m/s, so it is necessary to choose wind turbines that are designed to maximize their production with low wind levels.
- Safe operation: The risk to people is greater than in the open, so machines must be designed to be safe.
- Low noise and vibration emission. The TSR (Tip speed rate) should be between three and five. If it is less than three, a blade design with a large area leads to low efficiency and if it is more than five it produces a lot of acoustic noise.
- Robust and reliable machines with low maintenance.

At present, there are numerous models of small wind turbines to choose the one that best suits our specific needs. Table 1 shows a summary of the characteristics of the different types of small wind turbines on the market, which can be classified into three main groups:

- HAWT (Horizontal Axis Wind Turbine): the axis of rotation is parallel to the ground and its principle of operation is to support.
- VAWT (Vertical Axis Wind Turbine) Darrieus type: the axis of rotation is perpendicular to the ground and its principle of operation is sustentance.
- VAWT (Vertical Axis Wind Turbine) Savonius type: the axis of rotation is perpendicular to the ground and its principle of operation is to drag.

Table 1. Summary of characteristics types of wind turbines.

	HWAT 	VAWT Darrieus 	VAWT Savonius 
Efficiency	High	Low	Very low
Visual impact	Low	Medium	High
Level of development	High	Low	Low
Noise and Vibrations	High	Low	Low
Reliability	Medium	Low	High
Orientation	Presents problems	No need for orientation	No need for orientation
Starting speed	High	Low	Low
Operation with turbulent wind	Bad	Good	Good
Use of the vertical wind component	Unusable	Usable	Usable

5 Installation of the wind turbine and connection to the electricity grid

Once the location and model of the wind turbine has been decided, it must be installed and connected to the electricity grid.

When installing on the ground, no special installation precautions should be taken, but when installing on the roof of a building, care should be taken to reinforce the roof structure if necessary, before starting installation work.

To connect a small wind turbine to a microgrid, there are generally two possibilities depending on the type of electric generator. If it is an induction generator, it can be connected directly or through an AC/DC converter. If it is a permanent magnet synchronous generator (PMG), it is connected via a rectifier and a DC/AC converter.

In Europe, the EN 50438 standard defines the tests required for the DC/AC converter. Some countries do allow the connection directly such as the United Kingdom, Denmark, Greece, Ireland, or Portugal; and other countries that do not allow it (the distribution

grid operator must give prior permission for the connection) such as Spain, Germany, France, Italy, etc.

Besides, there are a set of international standards for small wind turbines. Standard IEC 61400 is an international standard published by the International Electrotechnical Commission [10] that aims to ensure the safety and efficiency of each wind turbine.

However, these rules are not compulsory for the installation of a wind turbine in all countries. Furthermore, each country has its own rules or criteria. For example, in Spain, there are no mandatory rules for the installation of a small wind turbine beyond the CE (Conformité Européenne) mark, while in other countries such as Great Britain, the United States, Japan or Denmark, certification is required.

6 Integration of wind turbines into the microgrid control system

Once the wind turbine is installed and connected to the grid, it is necessary to monitor it with the control software that manages the microgrid in which it is incorporated, to see its production in real-time and to be able to define the most appropriate strategies for the controlled of the microgrid together with the rest of its components.

As wind turbines are unmanageable generating components, that is, their primary energy source is neither controllable nor storable, their integration into any microgrid is particularly complex, as their variability makes it difficult to maintain a balance between electricity generation and demand. This variability is because its operation depends exclusively on the meteorological conditions existing at each site, which implies uncertainty in the prediction of production.

However, from the point of view of monitoring, the work is made easier, since reading the instantaneous power variable would be sufficient, since it is not necessary to communicate with them to give them work instructions.

In the CEDER case study, in addition to recording the instantaneous power, the wind speed will also be recorded.

In neither of the two wind turbines there is the possibility of directly communicating the CEDER microgrid controlled system (based on Home Assistant) with their control panels as they allow local communication (RS485) but not remote communication via Ethernet as they do not have a network card. However, the National Instruments data acquisition system [11] used to record multiple variables from each wind turbine and its meteorological towers (power, voltage, wind speed, wind direction, etc.) for different tests does allow communication via Ethernet. Using the Modbus TCP/IP protocol we can communicate both wind turbines with the microgrid control centre. In the case of Enair EPRO70, the SAD is a FieldPoint model, while the Atlantic AOC wind turbine uses the compact FieldPoint model [12].

The communications scheme of the microgrid with the two wind turbines under study is presented in Figure 7.

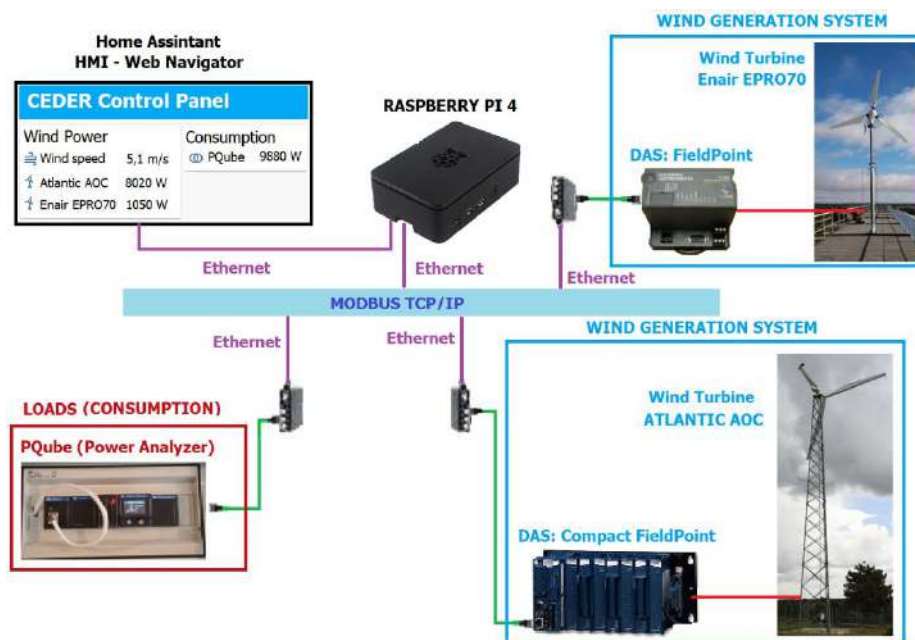


Figure 7. Scheme for monitoring wind turbines using Modbus TCP/IP.

To communicate each wind turbine with Home Assistant, first of all, each SAD must be defined in the configuration file by assigning it a name and indicating the type of communication to be used (in both cases it is Modbus TCP/IP), the IP of each one and the port (by default, Modbus TC/IP uses port 502).

Once defined, we must read the records that contain the desired information of each one of them in their corresponding directions (monitor), that is, the power of each wind turbine and the wind speed. This is also done in the Home Assistant configuration file and for this, it is necessary to have the address where each SAD stores the variables that we want to read.

Once monitored, all that remains is to incorporate them into the control panel in Home Assistant to see all the values collected in real-time. Figure 8 shows the real-time values of the power of each wind turbine, the wind speed, as well as the demand in each of the eight transformer centres that make up the CEDER microgrid. The Atlantic wind turbine is producing 16205 W and the Enair 1610 W for a wind of 8.9 m/s. The total demand of CEDER is 41668 W, of which 21853 W is consumed by the distribution network since the remaining 19815 W is produced by the wind systems incorporated into the microgrid.

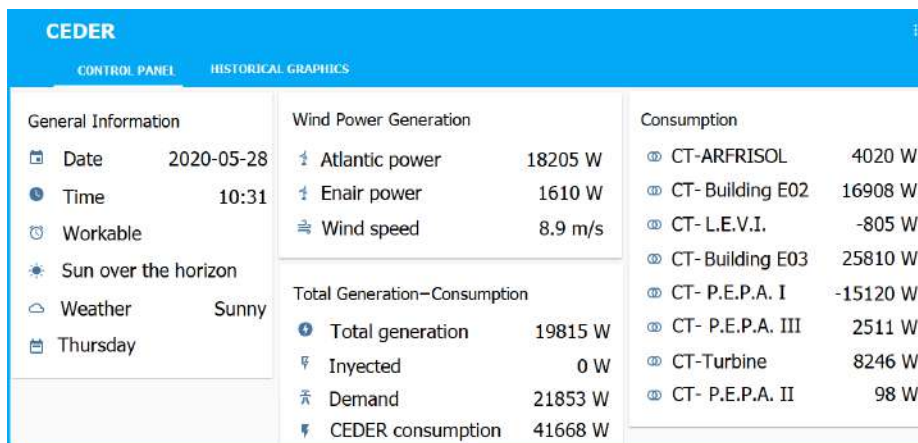


Figure 8. Control panel in Home Assistant.

The values obtained for each variable can also be represented graphically, as shown in Figure 9.

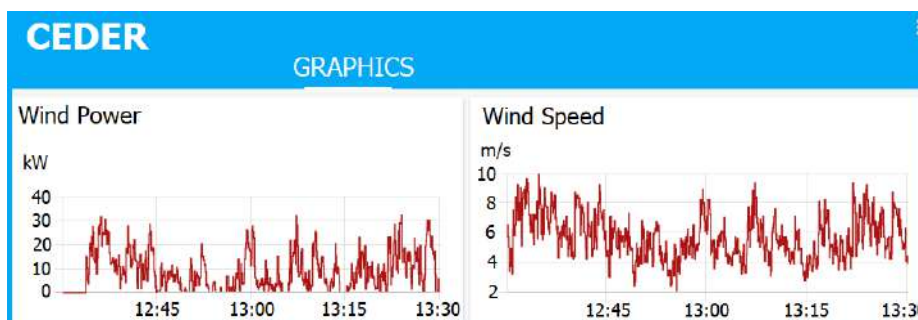


Figure 9. Graphic representation in Home Assistant.

Home Assistant has the disadvantage of storing data, it only records each variable when there is a change in value, which from a space-saving point of view is very efficient. However, it makes subsequent analysis of the data difficult. To solve this, the CEDER microgrid control system uses an open-source relational database controlled system based on MySQL [13].

The use of MySQL is optional, although highly recommended whenever it is desired to store the monitored data for later analysis, which will allow the definition of much more efficient power controlled strategies for the microgrid and facilitate the graphical representation as can be seen in Figure 10 and Figure 11.

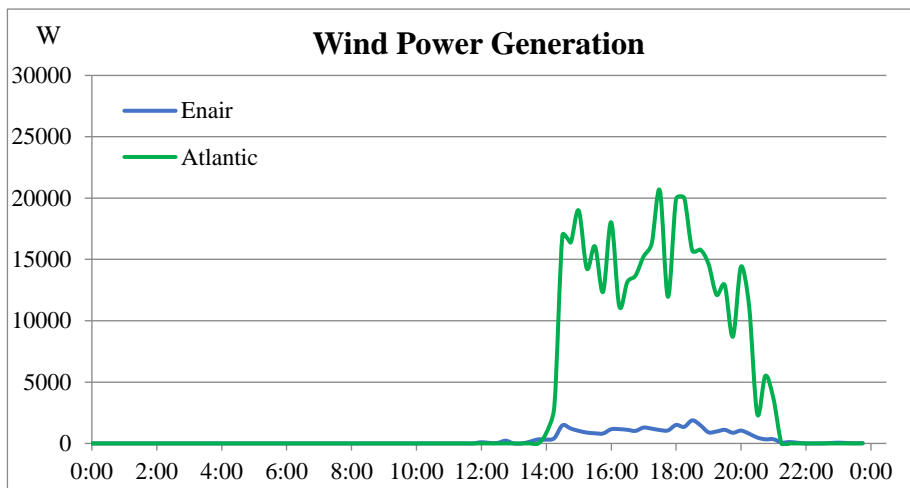


Figure 10. Daily graph of wind power generation at CEDER (15 minutes average).

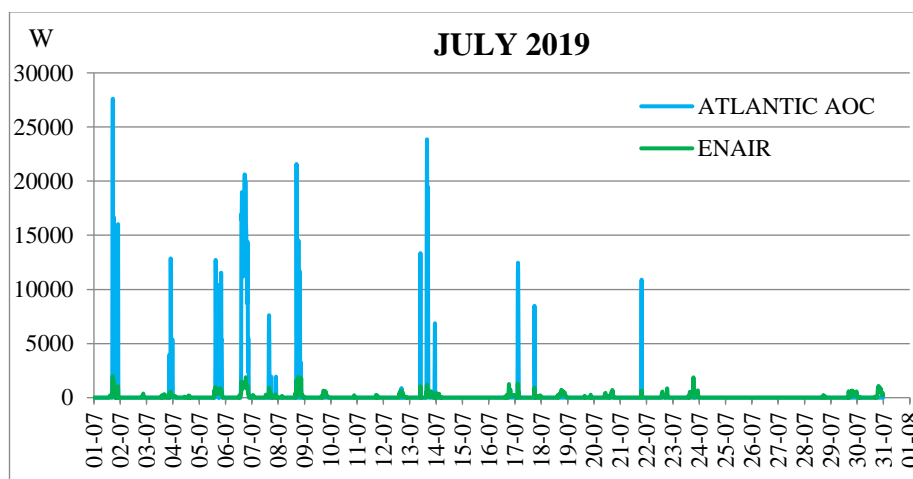


Figure 11. Monthly graph of wind power generation in CEDER (15 minutes average).

7 Conclusions

This paper has explained how to integrate small wind turbines into a microgrid, taking into account all aspects related to the assessment of the wind resource, with special emphasis on its peculiarities in peri-urban environments, the selection of the wind turbine best suited to the site, its connection to the electricity grid and its monitoring and incorporation into the microgrid controlled system to see its operation in real-time.

The integration of wind turbines into electrical microgrids is of great interest as distributed generation systems that allow the generation to be brought closer to the points of demand. However, it presents certain difficulties that are not easy to solve.

On the one hand, they are unmanageable generation systems, since they depend on the wind at any given time, and this makes the controlled of generation-demand difficult and makes storage systems necessary to optimize it.

On the other hand, the great variability of the wind resource further complicates the controlled of the microgrid, as significant changes in wind speed can occur in two consecutive seconds.

It should also be taken into account that most microgrids are located in urban or peri-urban environments, which makes it very difficult to determine exactly the ideal location for each wind turbine to be incorporated into them, given the peculiarities of the wind in these types of environments. Besides, most wind turbines are designed to operate in open fields and the more specific designs for urban environments are in the process of maturing, trying to improve their efficiency, noise levels, and safety.


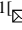
Once a solution has been found to these problems and a series of standards have been established to ensure the technical quality of wind turbines, they will make it possible to produce "green" energy in a decentralized manner with a high efficiency that will improve the efficiency of the microgrid to which they are integrated.

References

1. Hernández Callejo, L.: Microrredes eléctricas. Integración de generación renovable distribuida, almacenamiento distribuido e inteligencia. Publicaciones, Ibergarceta (2019)
2. Ramenah, H., Tanougast, C.: Reliably model of microwind power energy output under real conditions in France suburban area. *Renew. Energy*. 91, (2016).
<https://doi.org/10.1016/j.renene.2015.11.019>
3. Sinha, S., Chandel, S.S.: Prospects of solar photovoltaic-micro-wind based hybrid power systems in western Himalayan state of Himachal Pradesh in India. *Energy Convers. Manag.* 105, (2015). <https://doi.org/10.1016/j.enconman.2015.08.078>
4. Karthikeyan, N., Kalidasa Murugavel, K., Arun Kumar, S., Rajakumar, S.: Review of aerodynamic developments on small horizontal axis wind turbine blade, (2015)
5. Home Assistant, <https://www.home-assistant.io/>
6. Raspberry Pi, <https://www.raspberrypi.org/>
7. Tridianto, E., Permatasari, P.D., Ali, I.R.: Experimental study of mini SCADA renewable energy management system on microgrid using Raspberry Pi. *J. Phys. Conf. Ser.* 983, (2018). <https://doi.org/10.1088/1742-6596/983/1/012061>
8. van Bussel, G.J.W., Mertens, S.M.: Small wind turbines for the built environment. *Fourth Eur. African Conf. Wind Eng.* 1–9 (2005).
<https://doi.org/10.1109/PES.2005.1489306>
9. Abohela, I., Hamza, N., Dudek, S.: Effect of roof shape, wind direction, building height and urban configuration on the energy yield and positioning of roof mounted wind turbines. *Renew. Energy*. 50, (2013).

- |
- <https://doi.org/10.1016/j.renene.2012.08.068>
10. IEC. International Electrotechnical Commission, <https://collections.iec.ch/std/catalog.nsf/collection.xsp?open&col=IEC 61400>
 11. National Instruments, <https://www.ni.com/es-es.html>
 12. Compact Fieldpoint, <http://sine.ni.com/nips/cds/view/p/lang/es/nid/1199>
 13. MySQL, <https://www.mysql.com/>

Modeling of a Controlled Rectifier with Adaptive Control System for Vertical Axis Micro Wind Turbines

Miguel Baldera Arvelo¹^[0000-0001-9842-6402], Lesyani León Viltre^{2,3}^[0000-0002-6829-5285], Miguel Baldera Echavarría¹^[0000-0001-6038-1894], Deyslen Mariano-Hernández¹^[0000-0002-4255-3450], Miguel Euclides Aybar Mejía¹^[0000-0002-4715-3499]

¹ Área de Ingeniería, Instituto Tecnológico de Santo Domingo, INTEC, Distrito Nacional, Dominican Republic

miguel.aybar@intec.edu.do

baldera_arvelo@siemens.com

² Department of electrical engineering, Universidad Central “Marta Abreu” de las Villas, Santa Clara, Cuba

³ Área de Ciencias Básicas y Ambientales, Instituto Tecnológico de Santo Domingo, INTEC, Distrito Nacional, Dominican Republic.

Abstract. The development of power electronics and intelligent control systems plays an essential role in their essential presence in all types of modern design for the renewable energy area, seeking to convert energy efficiently to maximize its utility and integrate with smart cities. Wind energy production from a vertical axis wind turbine becomes interesting when used to maximize the energy produced from improving its conversion with the power electronics and the control system. This paper aims to integrate the turbine model and an adaptive control loop-controlled rectifier using Simulink, which proved to have a considerable and useful performance in capturing wind energy compared to passive rectification or non-controlled rectifier.

Keywords: Power Electronics, Adaptive Control System, Bode stability, Boost converter, Micro Wind Turbine, Vertical Axis Wind Turbine, Permanent Magnetic Synchronous Generator, MATLAB, Simulink.

1 Introduction

Distributed generation has experienced rapid growth today, among the different energy consumption sectors such as small industry, housing, and public services. It is greater efficiency and a lower level of toxic emissions [1][2] and is an essential element to develop in the Smart city concept [3]. The integration of distributed generation is being developed in smart cities due to global warming and implementing energy policies that encourage sustainability [4]. It is essential to consider the adequate intelligent integration of renewable energy sources in smart cities with control elements and converters that allow their use [5].

Like other cities in Latin America, the city of Santo Domingo has begun to develop projects to become smart cities. However, they have focused on transportation projects, infrastructure projects [6], and smart equipment [7].

Among the technologies of distributed generation of small power, the small wind turbine (SWT) is an attractive candidate in the users connected on the grid networks or in an independent energy producer way, because it has a utility factor of high capacity and the reasonable cost of capital [8]. One of the most widely used DC-DC converter topologies for SWT consists of a diode rectifier and a boost topology DC-DC converter [9]. A passive rectifier without control could allow the electric load to decrease the revolutions and reduce the energy production in the turbine by representing an electro-magnetic brake, contrary to the movement of the shaft developed by the turbine. From the load, the standard passive rectifier is not stable; this would, in effect, cause opposition to the natural movement of the turbine due to the difference established between the mechanical torque and the electrical torque [10] and, as a consequence, complications in the inertial moments for the mechanical movement of the turbine and the considerable decrease in the energy produced.

It is possible to stabilize the direct current from the alternating current produced by the vertical axis turbine and the permanent magnet generator, maximizing useful energy production through controlled rectification. Controlled rectifier through a Boost topology step-up DC-DC converter, handling by pulse width modulation (PWM) based on an adaptive feedback loop, which can be adjusted to the behavior and dynamic electrical power conditions of the turbine wind power, it will be able to adapt to the dynamic variations of the nature of the wind and improve energy capture given the wind potential of the urban scenario.

The implementation of this type of controlled rectifier could be considered a high-cost application concerning the benefit or energy return in urban micro-production of fewer than 400 Watts. However, a controlled rectification guarantees multiple influencing factors in general, such as controlling the load current at the optimum power point, controlling useful loads for accumulation systems, speed control to maximize micro wind generation; which are factors of considerable impact on the return on investment and also on the acceptance of the cost of this type of technology in the market [11]. This article's objective is the evaluation using computer modeling of a controlled rectifier with a feedback loop through the implementation of an adaptive control system, which guarantees the stability and the best use conversion of the energy produced by a vertical axis micro wind turbine in the conditions of urban environments.

2 Wind Turbine Model

Wind turbines can transform energy kinetic into electrical. The rotary movement originated from the wind flow, and the pressure difference present in the blades, whose vector-shaped components, both dragging and support, can produce the energy conversion described.

In our case, the vertical axis turbine will be directly coupled to the generator; we will neglect the implications of a speed multiplication arrangement.

The mechanical power capable of being extracted from the wind by the turbine will depend on the power coefficient and the specific speed ratio; parameters define any wind turbine [12].

Since the wind potential is not entirely usable, understood in effect by the Betz limits, the ideal coefficient is limited to a maximum value of 59.3%; according to the limit of the useful potential to extract the wind [13] [14].

Considering in a general manner, the characteristics and dynamic behavior of the diversity of vertical axis turbines' designs will be similar between the Savonius and Darreius type [15]. This experiment has considered the modeling to use the characteristics and power coefficient of the Savonius type of turbine, which means that it will be favorable for the start of energy production from a lower wind speed condition.

For the turbine type selected for modeling, the power coefficient (C_p) is obtained from equation (1) [11]. The value of the tip-speed ratio (λ) is represented by equation (2), where ω_m is the rotor angular speed (rad/s), R is the radius of the turbine (m), and V is the wind speed (m/s) [7]. To obtain the maximum possible C_p value for the selected turbine, λ will be equal to 1 ($\lambda = 1$); therefore, the power coefficient obtained will be $C_p = 0.17$.

$$C_p = -0.12\lambda^3 + 0.0856\lambda^2 + 0.20\lambda \tag{1}$$

$$\lambda = \frac{\omega_m R}{V} \tag{2}$$

For the different wind energy conversion systems (WECS), which have different C_p characteristics, dependent on the specific speed λ [16], the mechanical power by the wind turbine is represented by equation (3), where ρ is the air density ($1,225 \text{ kg/m}^3$), A is the turbine swept area ($2RL, m^2$) and V is the wind speed (m/s).

$$P_m = 0.5\rho(C_p)AV^3 \tag{3}$$

Because the wind potential is not entirely usable, the reason for maintaining the rotational movement of the wind turbine through the flow, it is by the coefficient, limited to a maximum value of 59.3%; according to the limit of the useful potential to extract the wind [13] [14]. Considering that the diversity of vertical axis turbine designs' characteristics and behavior will generally be similar to those of the Savonius and Darreius types [15]. The equation defines the relationship between torque T_m and mechanical power P_m (4), equation (6) represent mechanical torque T_m , as a function of the variables and input parameters that define the vertical axis wind turbine, and the torque coefficient C_t is defined by equation (5).

$$T_m = \frac{P_m}{\omega_m} \tag{4}$$

$$C_t = \frac{C_p}{\lambda} \tag{5}$$

$$T_m = 0.5\rho(Ct)ARV^2 \tag{6}$$

To relate the equations found with the electrical part corresponding to the three-phase permanent magnet generator, the differential equation (7) is established. The moment of inertia J (kgm^2), the mechanical torque T_m (Nm) produced by the wind turbine, the angular speed of the rotor ω_m (rad/s), the torque resulting from differential acceleration T_a (Nm) and the electromagnetic torque resulting from the permanent magnet generator T_e (Nm). It is fundamental and necessary to start the mechanical movement, modeling the turbine's rotational dynamic changes as a function of the variations in wind speed and electrical load, greatly impacting the permanent magnet generator (PMSG).

$$J \frac{d^2\theta_m}{dt^2} = J \frac{d\omega_m}{dt} = T_a = T_m - T_e \tag{7}$$

The differential equation (7) of torque and moment of inertia will be fundamental for our modeling since the equation is a tool that allows to dynamically study the accelerating rotational movement of the turbine by depending on the evolution of the wind speed and the electromagnetic effects induced as a consequence of the electrical load, which will be necessary to evaluate the adaptive control system.

3 Permanent Magnet Generator Model.

The permanent magnet generator's dynamic model is based on the three-phase permanent magnet electrical machine library represented in a block in the SIMULINK tool. The model is based on equations (8), (9), and (10), which describe the dynamic operation of the electrical machine through the d and q axis (direct axis and quadrature axis flux) and also the currents represented in the same manner i_d, i_q .

Also, by applying the Park and inverse Park transforms, it is possible to obtain the dynamic evolution of the rotational and electrical system as a function of the angular speed ω_m as an input variable and then obtain the torque expression.

$$\frac{d}{dt} i_d = \frac{1}{L_d} v_d - \frac{R}{L_d} i_d + \frac{L_q}{L_d} p \omega_m i_q \tag{8}$$

$$\frac{d}{dt} i_q = \frac{1}{L_q} v_q - \frac{R}{L_q} i_q + \frac{L_d}{L_q} p \omega_m i_d - \frac{\lambda_o P \omega_m}{L_q} \tag{9}$$

$$T_e = 1.5 p [\lambda_o i_q + (L_d - L_q) i_d i_q] \tag{7}$$

The equations of the permanent magnet electrical machine describe the behavior of the generator as a function of the stator inductance in the direct and quadrature axis flux, L_d and L_q , R the resistance of the stator coils, p the number of pairs of poles, λ_o the magnetic flux of the permanent magnets of the rotor and ω_m the angular speed. The permanent magnet generator model based on the SIMULINK tool library also has the properties of dynamically generating three-phase electric current and frequency in a torque dependent, as an input variable, depending on the angular position θ . For the

experiment have basic parameter for configuration in SIMULINK, $L_d=L_q= 6mH$, $R= 2.15$ Ohms, $p = 4$ and $\lambda_o= 0.1$ Wb. This model is based on the transforms of Park (8), (10) and inverse Park (9) and (11); it is beneficial to make a representation of all electrical changes in current, voltage, and frequency in the order of the modeling of the system, before the variations in torque and angular speed ω_m , produced by the evolution of the movement of the wind turbine.

$$\begin{bmatrix} f_q \\ f_d \\ f_0 \end{bmatrix} = [T_{qdo}] \begin{bmatrix} f_a \\ f_b \\ f_c \end{bmatrix} \tag{8}$$

$$\begin{bmatrix} f_a \\ f_b \\ f_c \end{bmatrix} = [T_{qdo}]^{-1} \begin{bmatrix} f_q \\ f_d \\ f_0 \end{bmatrix} \tag{9}$$

$$[T_{qdo}(\theta_e)] = \frac{2}{3} \begin{bmatrix} \cos \theta_e & \cos(\theta_e - \frac{2\pi}{3}) & \cos(\theta_e + \frac{2\pi}{3}) \\ -\sin \theta_e & -\sin(\theta_e - \frac{2\pi}{3}) & -\sin(\theta_e + \frac{2\pi}{3}) \\ \frac{1}{2} & \frac{1}{2} & \frac{1}{2} \end{bmatrix} \tag{10}$$

$$[T_{qdo}(\theta_e)]^{-1} = \begin{bmatrix} \cos \theta_e & -\sin \theta_e & 1 \\ \cos(\theta_e - \frac{2\pi}{3}) & -\sin(\theta_e - \frac{2\pi}{3}) & 1 \\ \cos(\theta_e + \frac{2\pi}{3}) & -\sin(\theta_e + \frac{2\pi}{3}) & 1 \end{bmatrix} \tag{11}$$

In Figure 1, we have the SIMULINK modeling of the turbine with the PMSG, the input variable of wind speed, and the generator's three-phase output.

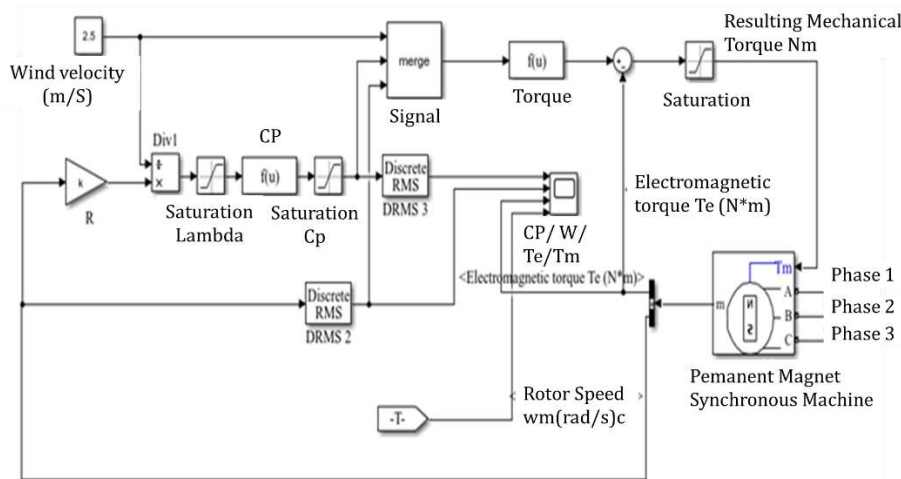


Figure 1. Wind turbine model with Permanent Magnet Generator in SIMULINK.

4 Adaptive Controlled Rectifier Model

For the conversion of three-phase electrical energy with variable frequency and voltage in wind energy applications, semiconductor rectifiers are commonly used to obtain direct current and facilitate its use. Current rectification can be passive or without a control system controlled like active rectification [17][18].

Passive rectifiers are currently used in typical applications globally for microturbines because they are considered relatively robust and low cost [19]. Also, do not require a control system, and the switching frequency is low [20], in addition to having a low electrical efficiency compared to fully controlled thyristor or transistor rectifiers called active rectification [21]. In general, the passive rectifier used for wind applications lacks stable control of the output voltage and stability in the power produced to the electrical load [17].

This type of passive configuration has an unfavorable impact on energy production. While an active rectifier, it could adapt to the real conditions of generation and electrical power. That control stage consists of a booster DC-DC converter topology. This active rectification technique integrated into our modeling has the advantage that the output current and power can be regulated under the wind turbine's generation conditions and the permanent magnet generator, maintaining stable output voltage [22].

The experimental adaptive control system shown in Figure 2 was implemented to control the DC-DC converter and rectifier circuit. It has a primary electrical power control loop and another feedback control loop work with the angular speed ω_m of the turbine, which is also the adaptive function block's input variable.

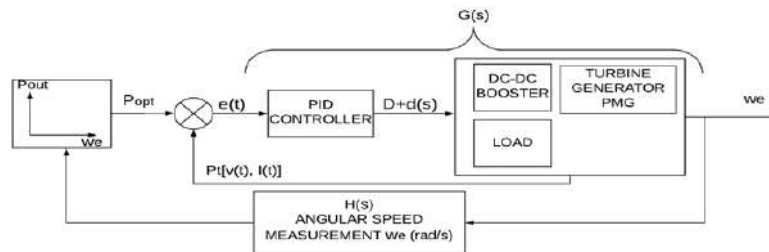


Figure 2. Adaptive control system with a double closed loop.

The adaptive function contains a table that depends on the power curve of the selected turbine, with which the input variable ω_m will serve as an index to dynamically select the desired electrical power generation related to direct the corresponding loop and adjust the output power as a setpoint to get zero error, $e(t) = 0$.

The error function $e(t)$ is the input variable for the controller/compensator, from which the controller responds will generate a pulse modulation signal, specifically the PWM. The modulated signal will perform the switched activation of the gate of the MOSFET transistor of the DC-DC boost converter stage as a secondary part of the same controlled rectifier. According to its theoretical power curve, the adaptive control loop will maintain the maximum possible power production related to the turbine's dynamic

conditions. The power to be extracted from the wind turbine will not be more than what the wind's nature can generate.

4.1 DC-DC Converter Boost Topology

The DC-DC converter type boost can increase the voltage output as a PWM function by controlling the MOSFET Q1 transistor (see Figure 2). This topology allows high conversion; the losses in the semiconductors will be lower [23]. In general, the boost converter consists of an arrangement of a single transistor Q1 (MOSFET), a semiconductor diode D1, an inductor L, and an output capacitor C [22]. For the design of the converter; the following expressions were used:

$$\int_0^{Ts} V_L(t) dt = (V_g)DTs + (V_g - V)(D' Ts) = 0 \tag{12}$$

$$M(D) = \frac{V}{V_g} = \frac{1}{D'} = \frac{1}{1-D} \tag{13}$$

The expression of the current through the converter is obtained with the expression from the capacitor's load balance and deriving it in the steady-state:

$$\int_0^{Ts} i_c(t) dt = (-V/R)DTs + (I_L - V/R)(D' TS) = 0 \tag{14}$$

$$I_L = \frac{V}{D'R} \tag{15}$$

From where $V = \frac{V_g}{D}$ we have:

$$I_L = \frac{V_g}{D'^2 R} \tag{16}$$

The value of the inductance L depends on the switching frequency and the period Ts. A design criterion will be used from the required inductance (Equations 17 and 18); the peak current could reach 15% above the current IL's nominal value, controlled by the control system.

$$\Delta i_L = \frac{V_g}{2L} DTs \tag{17}$$

$$L = \frac{V_g}{2L} DTs \tag{18}$$

The value of capacitance will be obtained from the output voltage ripple level. Depending on the switching, it will be considered an acceptable ripple voltage of 0.1Volts. From equations (19) and (20), we obtain the required value of output capacitance for the boost converter circuit [22].

$$\Delta V_c = \frac{V}{2RC} DTs \tag{19}$$

$$C = \frac{V}{2\Delta V_c} DTs \tag{20}$$

4.2 DC-DC Boost Converter Transfer Function

To obtain the complete expression of the $G_c(S)$ controller, the closed-loop expression of the system to be controlled must be established first, in our case, the boost type DC-DC converter. The stability of the power loop will also depend on the boost transfer function. The Transfer function is obtained [22] by the following expression (21).

$$G_{vd}(S) = G_{go} \frac{\left(1 - \frac{S}{\omega_z}\right)}{1 + \frac{S}{Q\omega_o} + \left(\frac{S}{\omega_o}\right)^2} \tag{21}$$

The expression $G_{vd}(S)$ is the frequency domain transfer function of the boost converter. Also, the expression $T_o(S)$ is the complete function of the control open-loop, including the controller $G_c(S)$, as a factor of the system transfer function, V_m is the gain expression for the PWM control. The converter's transfer function's expression will be used to model and study the frequency response through a Bode diagram, allowing to validate the system's stability.

$$T_o(S) = G_c(S) * \frac{1}{V_m} * G_{vd}(S) \tag{22}$$

4.3 Control System Model and Stability

To achieve the modeling of the proportional, integral, and derivative (PID) type controller $G_c(S)$, it will be necessary to define the system's transfer function's coefficients to be controlled $G_{vd}(S)$, in this case, the boost type DC-DC converter.

Through expressions (23), (24), (25), and (26), it will be possible to obtain the corresponding values to introduce in the Transfer function [22].

$$G_{go} = \frac{1}{D} \tag{23}$$

$$\omega_o = \frac{D'}{\sqrt{LC}} \tag{24}$$

$$Q = \frac{RD'}{\sqrt{\frac{C}{L}}} \tag{25}$$

$$\omega_z = \frac{RD'^2}{L} \tag{26}$$

Using the design parameters established in Table 1 is possible to obtain the necessary values to complete the expression representing the transfer function $G_{vd}(S)$, which will be used to obtain the controller $G_c(S)$, using the Ziegler and Nichols methodology.

Table 1. Design parameters for the DC-DC (Boost) controller

Design Parameters (Boost)	Value	Unit
L (Inductor)	100	μH
RL (Inductor Series Resistance)	0.011	Ohms
C (Output Capacitance)	47	μF
Rc (Capacitance Resistance)	0.04	Ohms
Rload (Load Resistance)	8	Ohms
fo (Frequency)	15	kHz
Ts (Period)	66.7	μs
Vg (Input Voltage)	16.8	Volts
V (Output Voltage)	24	Volts
$\Delta I_L\%$ (Inductor Current)	0.1	%
ΔV_c (Capacitor Ripple Voltage)	20	mVolts
I_n (Nominal Output Current)	11.6	Amperes
I_p (Peak Output Current)	13	Amperes
D (Duty Cycle ON)	0.35	%
D' (Duty Cycle OFF)	0.65	%

According to the values proposed for the boost converter's design, we have the coefficients of G_{d0} is 37, ω_o is 9677, Q is 3.56, V_m is 4, and $H(S)$ is 0.0125 to establish the transfer function. The expression $G_{vd}(S)$ is the transfer function of the boost type DC-DC converter.

$$G_{vd}(S) = \frac{37 - 0.001 s}{1 + 0.000029 s + 0.00000001 s^2} \tag{27}$$

In Figure 3, the Bode plot is presented, representing the behavior in the frequency domain of the plant or process of the system. It can be seen that the system is not stable and that it requires compensation for the phase margin φ_m .

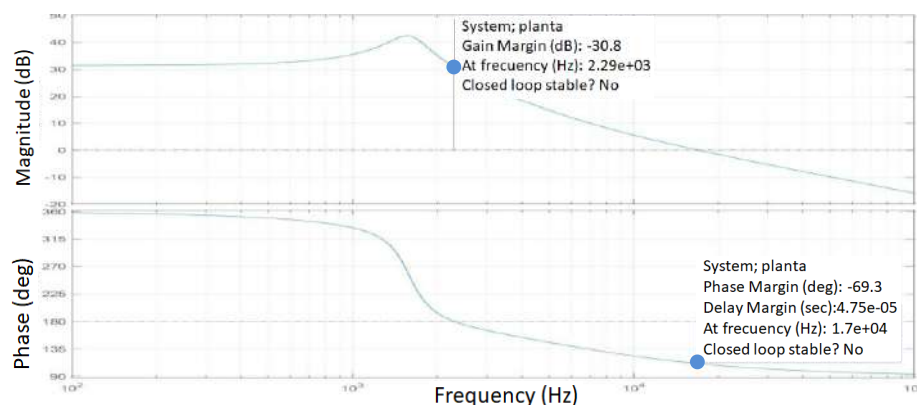


Figure 3. Bode Plot of the plant or process $G_{vd}(S)$.

To apply the Ziegler and Nichols methodology, the closed-loop control expression $T_c(S)$ is obtained. The initial conditions $G_c(S) = 1$, with $H(S)$ being the feedback function with the established gain value from Table 2.

$$T_c(S) = \frac{T_o(s)}{1 + T_o(s)} \tag{28}$$

The function representing the closed control loop is $T_c(S)$, for $G_c(S) = 1$, which will be used to apply the Ziegler and Nichols methodology and determine the controller. The closed-loop expression $T_c(S)$ is shown in equation (29).

$$T_c(S) = \frac{0.1156 - 0.00000031 s}{1.11 + 0.000029 s + 0.00000001 s^2} \tag{29}$$

The resulting coefficients for applying the Ziegler and Nichols method for tuning the controller and achieving system stability [24] was ω_u (2900), P_u (0.0022), and K_u (1). Applying the Ziegler and Nichols methodology and introducing the values of P_u and K_u , the resulting values corresponding to the proportional, integral, and derivative gains, K_p , K_i y K_d , are obtained.

Table 2. Coefficients of gain and time constants for the design and tuning of the $G_c(S)$ controller.

Controller Type	K_p	T_i	K_i	T_d	K_d
Proportional (P)	0.5	-	-	-	-
PI (Proportional-Integrative)	0.45	0.00183	245	-	-
PID	1	0.0011	544	0.00028	0.00017

According to the results in Table 2, the derivative action represents very minimal gain value for using a PID type controller; it is considered only to use the proportional and integral gains (PI).

After obtaining these coefficients in expression (30), we have the controller $G_c(S)$. The expression (31) is also equivalent to $G_c(S)$ by rearranging the elements in the function.

$$G_c(S) = 1 + \frac{544}{s} \tag{30}$$

$$G_c(S) = \frac{s + 544}{s} \tag{31}$$

Through the control open-loop expression (32) $T_o(S)$, the system's stability is evaluated after implementing the controller.

$$T_o(S) = \frac{1}{4} * G_{vd}(S) * G_c(S) * H(S) \tag{32}$$

The expression $T_{oc}(S)$ represents the open-loop system compensated with the controller $G_c(S)$.

$$T_{oc}(S) = \frac{-0.0000125 s^2 + 0.4557 s + 251.6}{0.00000004 s^3 + 0.000116 s^2 + 4s} \tag{33}$$

Figure 4 shows the Bode plot for the expression $T_{oc}(S)$ after tuning the control system. It is observed that the system is stable and that the phase margin has been corrected, compensated to $\varphi_m = 96.4^\circ$. The gain margin is -18.5 dB, which indicates a rejection of the possibility of oscillation and system instability.

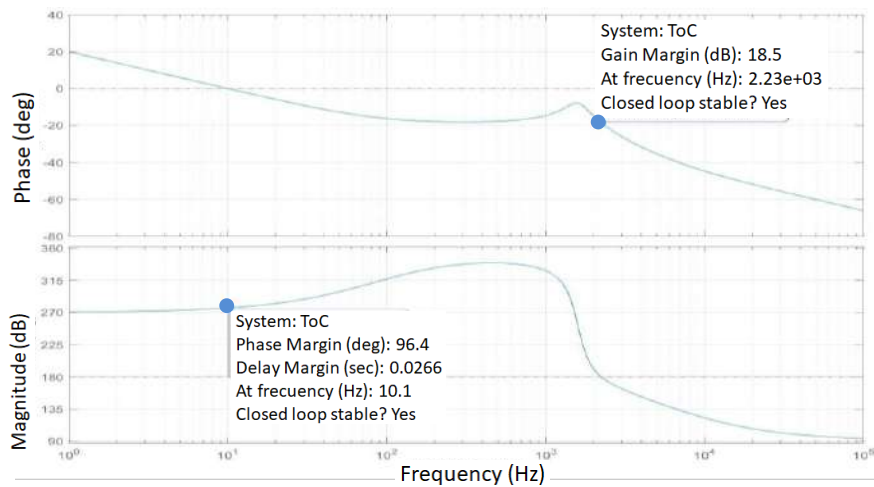


Figure 4. Bode Plot of the expression $T_{oc}(S)$ representing the open-loop system compensated with the controller $G_c(S)$.

4.4 Implementation of the adaptive control system

A table of corresponding electrical power values must be incorporated into the system to achieve the adaptive controller's implementation. Each input angular speed value has a value of the power according to the wind turbine model.

In figure 5, the adaptive function can be seen, which will represent an index of reference value corresponding to the measured value of the angular speed, obtaining for each angular speed value, the reference that the control system will have for each wind speed scenario, and maintaining optimal power production.

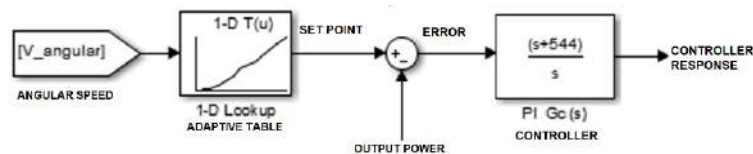


Figure 5. Adaptive function in SIMULINK for the control system.

5 Experiment Methodology

For the experimental process, the modeling of both rectifiers, passive rectifiers (without controller), and the controlled rectifier with adaptive control and regulation system has been carried out under the same test conditions and wind speed characteristics. Two similar experiments were carried out, one for each type of rectifier using the SIMULINK tool.

We work with a 24V battery and an 8 Ohms resistance in parallel for each test, connected to each rectifier's output, to maintain a fixed electrical charge during the experiment. We use the wind speed from 1 to 8 meters per second (m/s) for each test, typical for urban environments.

5.1 System Modeling

For the experiment with the passive rectifier, it is made up of the wind turbine model, the PMSG, the passive rectifier, and the 24V battery with a resistive load of 8 Ohms.

Similarly, the experiment with the adaptive controlled rectification system includes the wind turbine model, the PMSG, the passive rectifier, and a 24V battery with the resistive load of 8 Ohms.

6 Analysis of the results and discussion.

The two experiments were realized and completed. Table 3 shows the value of wind speed and according to the range established in the methodology for its evaluation.

According to the data resulting from the experiment, the controlled rectifier's voltage is stable, and the electric power generated is at the optimum point of possible power that the turbine will produce according to the wind conditions and its angular speed. On the other hand, for the passive rectifier, the situation is different; the voltage varies according to the power production and the wind speed variation, that the energy production would not be according to its optimum point of power produced.

To carry out a comparative study of the energy contribution with both technologies to rectify and convert energy into a useful form. The urban location is taken in a central area of the city of Santo Domingo. The Weibull probability distribution shows that the annual hours of wind potential are estimated for the selected urban area. The wind data related to generated electrical power and energy production in kWh/year are presented for each rectifier in Table 3. The total energy produced adaptive rectifier was 155 kWh and for the passive rectifier was 96 kWh.

Table 3. Comparative data of wind energy production produced by both rectifiers according to the Weibull distribution of probabilities of annual hours for wind speeds (*m/s*).

Wind Speed (m/s)	Distribution hours/year	Pe (W) Adaptive rectifier	Pe (W) passive rectifier	Energy produced Adaptive rectifier (kWh/year)	Energy produced Passive rectifier (kWh/year)
0	0	0	0	0	0
1	2012	1.68	0	3.4	0
2	2744	2.3	2.6	6.3	7.1
3	2174	14.8	10.3	32.2	22.3
4	1186	22.8	19.2	27.0	22.8
5	470	103.6	50.1	48.6	23.5
6	138	194.6	97.4	26.9	13.5
7	31	278.4	110.2	8.5	3.4
8	6	410	142.3	2.5	0.9

The experiment verified that the passive rectifier in the face of low wind speed, the electric current is very little or null for the battery because the voltage level is not stable. It will be less than the battery voltage level of 24 Vdc; it will not capture power and energy from the wind source.

7 Conclusions & Future Works

The results obtained in the tests carried out show that the controlled rectifier's adaptive control shows satisfactory results. By modeling the system of an adaptively controlled rectifier, for micro wind turbines, maximizing power capture and increasing energy production is by 65% in kWh/year. The development of all kinds of technology, similar to the adaptively controlled rectifier, will improve renewable energy production.

The production of wind energy from a smaller scale of power is currently being projected to integrate into a smart city. Future work proposes building a real test bench with a data acquisition system that can perform electrical and mechanical parameters to validate rectifiers' characteristics in real-time, under physical conditions, and real thermodynamics scenario. Also, implement the adaptive control system in a microcontroller or ARM processor to achieve a low-cost and straightforward electronic controller.

8 References

- [1] Y. Yang, C. Zhang, and X. Zhu, "Economic and Feasibility Analysis of Planning a Community-connected Micro-grid," 2020, pp. 1–6, doi: 10.1109/icpes47639.2019.9105552.
- [2] V. Kouloumpis, R. A. Sobolewski, and X. Yan, "Performance and life cycle assessment of a small scale vertical axis wind turbine," *J. Clean. Prod.*, vol. 247, p. 119520, Feb. 2020, doi: 10.1016/j.jclepro.2019.119520.
- [3] D. Menniti, N. Sorrentino, A. Pinnarelli, A. Burgio, G. Brusco, and G. Belli,

- “In the future Smart Cities: Coordination of micro Smart Grids in a Virtual Energy District,” in *2014 International Symposium on Power Electronics, Electrical Drives, Automation and Motion*, 2014, pp. 676–682, doi: 10.1109/SPEEDAM.2014.6872123.
- [4] M. Ghasemian, Z. N. Ashrafi, and A. Sedaghat, “A review on computational fluid dynamic simulation techniques for Darrieus vertical axis wind turbines,” *Energy Convers. Manag.*, vol. 149, pp. 87–100, 2017, doi: <https://doi.org/10.1016/j.enconman.2017.07.016>.
- [5] A. Nishimura *et al.*, “Wind Turbine Power Output Assessment in Built Environment,” *Smart Grid Renew. Energy*, vol. 04, no. 01, pp. 1–10, Feb. 2013, doi: 10.4236/sgre.2013.41001.
- [6] M. Calderón, G. López, and G. Marín, “Smart cities in Latin America: Realities and technical readiness,” in *Lecture Notes in Computer Science (including subseries Lecture Notes in Artificial Intelligence and Lecture Notes in Bioinformatics)*, 2017, vol. 10586 LNCS, pp. 15–26, doi: 10.1007/978-3-319-67585-5_2.
- [7] Silverio-Fernandez, Manuel Renukappa, Suresh, and S. Suresh, “Utilisation of Smart Devices in the Construction Industry: An Empirical Study in the Dominican Republic,” *Int. J. 3-D Inf. Model.*, no. 1, 2018, doi: 10.4018/IJ3DIM.2018010102.
- [8] R. Khezri, A. Mahmoudi, and M. H. Haque, “SWT and BES optimization for grid-connected households in South Australia,” in *2019 IEEE Energy Conversion Congress and Exposition, ECCE 2019*, 2019, pp. 418–425, doi: 10.1109/ECCE.2019.8912767.
- [9] C. Lumbreras, J. M. Guerrero, P. García, F. Briz, and D. Díaz, “Control of a small wind turbine in the high wind speed region,” in *2014 IEEE Energy Conversion Congress and Exposition, ECCE 2014*, 2014, pp. 4896–4903, doi: 10.1109/ECCE.2014.6954072.
- [10] S. Keshavarz, “Design and Evaluation of an Active Rectifier for a 4.1 MW Off-Shore Wind Turbine,” Göteborg, 2011.
- [11] M. Mayouf and R. Abdessemed, “Comparative study of a small size wind generation system efficiency for battery charging,” *Serbian J. Electr. Eng.*, vol. 10, no. 2, pp. 261–274, 2013, doi: 10.2298/sjee120707003m.
- [12] O. Anaya-Lara, N. Jenkins, J. B. Ekanayake, P. Cartwright, and M. Hughes, *Wind Energy Generation: Modelling and Control*. Wiley, 2011.
- [13] J. Fadil, Soedibyo, and M. Ashari, “Performance comparison of vertical axis and horizontal axis wind turbines to get optimum power output,” in *2017 15th International Conference on Quality in Research (QiR): International Symposium on Electrical and Computer Engineering*, 2017, pp. 429–433, doi: 10.1109/QIR.2017.8168524.
- [14] M. De Lellis, R. Reginatto, R. Saraiva, and A. Trofino, “The Betz limit applied to Airborne Wind Energy,” *Renew. Energy*, vol. 127, pp. 32–40, Nov. 2018, doi: 10.1016/j.renene.2018.04.034.
- [15] F. R. Eldridge and N. S. F. (U. S.). R. A. to N. N. Program, *Wind Machines*. U.S. Government Printing Office, 1976.

- [16] T. Shanker and R. K. Singh, "Wind energy conversion system: A review," in *2012 Students Conference on Engineering and Systems*, 2012, pp. 1–6, doi: 10.1109/SCES.2012.6199044.
- [17] M. Rossander, A. Goude, and S. Eriksson, "Mechanical Torque Ripple From a Passive Diode Rectifier in a 12 kW Vertical Axis Wind Turbine," *IEEE Trans. Energy Convers.*, vol. 32, no. 1, pp. 164–171, 2017, doi: 10.1109/TEC.2016.2626783.
- [18] M. H. Rashid, *Power Electronics Handbook*. Elsevier Science, 2011.
- [19] A. Van den Bossche, A. S. Marinov, P. V Yankov, and E. B. Bekov, "Automated methodology for adjustment of component values in passive converter circuit for wind turbine generators," in *2012 15th International Power Electronics and Motion Control Conference (EPE/PEMC)*, 2012, p. DS2d.4-1-DS2d.4-4, doi: 10.1109/EPEPEMC.2012.6397307.
- [20] A. Goude and F. Bülow, "Aerodynamic and electrical evaluation of a VAWT farm control system with passive rectifiers and mutual DC-bus," *Renew. Energy*, vol. 60, pp. 284–292, 2013, doi: <https://doi.org/10.1016/j.renene.2013.05.028>.
- [21] M. Gupta, S. Kumar, and V. Karthik, "Design and Implementation of Cosine Control Firing Scheme for Single Phase Fully Controlled Bridge Rectifier," 2013.
- [22] R. W. Erickson and D. Maksimovic, *Fundamentals of Power Electronics*. Springer US, 2007.
- [23] D. Brunelli, "A High-Efficiency Wind Energy Harvester for Autonomous Embedded Systems," *Sensors*, vol. 16, no. 3, 2016, doi: 10.3390/s16030327.
- [24] J. G. Ziegler and N. B. Nichols, "Optimum Settings for Automatic Controllers," *J. Dyn. Syst. Meas. Control*, vol. 115, no. 2B, pp. 220–222, Jun. 1993, doi: 10.1115/1.2899060.

Detection of Wind Generator Systems Faults Using Current Signature Analysis

Abdelkarim Bouras¹, Luis Hernández-Callejo² and Slimane Bouras³

¹ Electromechanical Systems Laboratory, Badji Mokhtar University Annaba, Algeria

² Department of Agricultural Engineering and Forestry, University of Valladolid (UVA). C. P. 42004. Soria, Spain

³ The industrial risks, C.N.D, S.O.M.M Laboratory, Badji Mokhtar University Annaba, Algeria

karim.bouras@hotmail.com

Abstract. In recent years, different types of generators have been used in the conversion of wind energy namely the wound rotor synchronous generator (WRSG) and the doubly-fed asynchronous generator (DFAG). In order to ensure energy efficiency and satisfactory sustainability of electricity production, it is necessary to ensure that these generators are protected from any untimely shutdown.

This article focuses on the predictive detection of mechanical and electrical faults that affect wind turbines, such as unbalance which is cited as one of the main causes of degradation of rolling elements. As well as the brush faults causing electrical asymmetries and consequently overheating with serious consequences for the WRSG and DFAG generator.

Many methods for detecting and diagnosing electrical and mechanical faults have been developed to date. Among these techniques, we cite the spectral analysis of the current by the fast Fourier transform (FFT), which seems to be very affordable, reliable and less expensive to implement than other techniques. Its application to the processing of the rotor or stator current signal, depending on the type of generator, aims at early detection of faults affecting the wind power system.

An experimental validation was carried out on a WRSG generator linked to the utility network by the rotor and on a 3 kW DFAG delivering its electrical energy by the stator. The results obtained by this fault detection technique are satisfactory and interesting because they allow the prediction and detection of the unbalance fault at the level of the wind generator (or turbine) and the wear of the brushes or the bad contacts affecting the electric generators.

Keywords: Wind Energy, Current Analysis, Generator Fault, Electrical Sliding Contacts Faults, Diagnosis, FFT.

1 Introduction

As a result of global warming and the depletion of fossil fuels, wind renewable energy production systems are expanding rapidly across the world [1–4] Due to the reduction in the price of this technology and its technical mastery, wind power sys-

2

tems will expand further over time. However, compared to the various traditional electric drives, the maintenance of wind systems is difficult and more expensive, it is even more so if they are offshore wind turbines or tidal turbines. Most medium and high power wind power systems are equipped with wound rotor synchronous generator (WRSG) and doubly-fed asynchronous generator (DFAG) [5, 6]. In order for the power generation capacity to be satisfied, care must be taken to keep these generators running smoothly and to be free from mechanical or electrical breakdown [7–10].

Only, in the long run, the generators that we are talking about can be affected by mechanical degradation, among the most frequent faults we can mention the mass unbalance caused by the deposit of dusty material on the turbine blades, the degradation of the blades or turbine and generator shaft alignment problems. This mechanical defect is cited as one of the main causes of the degradation of the bearing components. As for electrical degradations mainly concerning WRSG and DFAG, the electrical switching fault caused by poor contact between brushes and rings is very common, involving wear of the rings and electrical asymmetries in the rotor and stator electrical circuits [11–15].

The appearance of these anomalies is translated by a significant vibratory impact, but this information is often very late. Failing to process the stator current for the purpose of detecting faults altering the wind power system based on WRSG and DFAG, we refer to the analysis of the rotor current given that the current delivered by the stator of the generator can also contain information on mechanical load and power electronic interfacing faults. As the rotor current strength is also a magnitude derived from the electromagnetic torque, therefore, its exploitation for the extraction of characteristics affecting the wind power system represents a simple, reliable and inexpensive solution. The WRSG or DFAG generator rotor current signature analysis approach can be applied as a periodic monitoring and predictive diagnostic technique for maintenance purposes for wind power systems [16–19].

The spectral analysis of the current using the FFT tells us about the nature of the fault. The results obtained are satisfactory and can be used effectively to predict mass unbalance, electrical unbalance and poor switching faults of the wind generator and the electric generator [20, 21].

This diagnostic methodology allows sufficient time to be given to prepare for the operation in the context of balancing the system and changing the brushes or their brush holder if necessary.

2 Theoretical Background

Fourier transform is one of the simplest and most used techniques for signal analysis and processing for the purpose of detecting mechanical and electrical faults [22], the Fourier transform (TF) of a signal $x(t)$ any is defined by:

$$\hat{x}(f) = \int_{-\infty}^{+\infty} x(t) e^{-j2\pi ft} dt \quad (1)$$

3

Degradation due to unbalance or misalignment affects certain characteristic frequencies, so frequency analysis will detect the increase in the energy of these harmonics. Generally, the characteristic frequencies of mechanical defects obtained by spectral analysis (FFT) are given by the following formula:

$$f_d = f_1 \left(k \mp \frac{n}{p(1-s)} \right) \quad (2)$$

Where: p is pole pairs, s is the slip, it is the difference between the speed of the rotating field n_s in the air gap and the speed of rotation of the rotor n_r , f_1 is the fundamental frequency (Hz), f_d is the related fault frequency in (Hz), $k = 1, 3, 5, \dots$ and $n = 1, 2, 3, \dots$

The monitoring and diagnostic of mechanical unbalance based on current signature analysis used as non-invasive method to detect sidebands harmonics around the fundamental supply frequency expressed by:

$$f_{mass\ unbalance} = f_s \pm 1 f_r \quad (3)$$

Where: f_s is the source frequency and f_r is the rotation frequency (Hz)

With regard to the monitoring and diagnosis of electrical asymmetry based on the analysis of the rotor current signature of the WRSG or DFAG generator, the detection of harmonics of multiple bands of the fundamental supply frequency is expressed as:

$$f_{electrical\ unbalance} = n f_s \quad (4)$$

It should be noted that if we want to use the stator current delivered by the generator, the detection of the fault are not correct because the current will concern the load and the generator, unless active loads are used to detect the mechanical defects.

Regarding the detection of electrical faults of the generator, it is necessary to ensure that the electrical load is symmetrical and perfect and the same for the power electronic interfacing (PEI).

3 Experimental Tests

The test bench shows two aggregates of electrical machines, the first consisting of a variable speed DC motor coupled to an WRSG and for the second a variable speed DC motor coupled to a DFAG (Fig. 1).

4

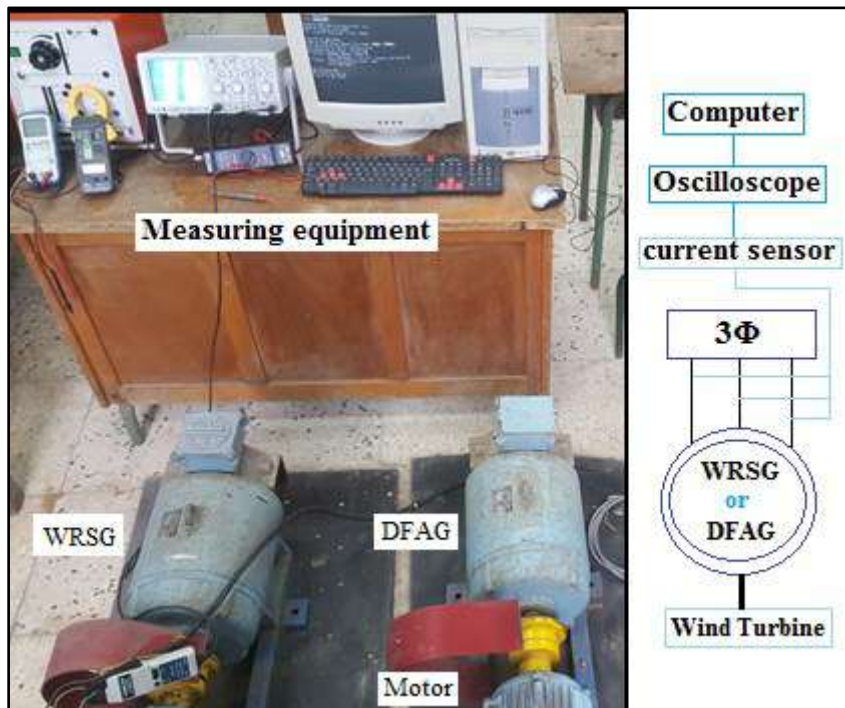


Fig. 1. Test bench.

Only in our work all the tests were carried out at a speed of 1500 RPM to meet the frequency 50 Hz comparable to that of the electrical grid. The Wind System required (Table 1):

Table 1. Characteristics of electrical machines of the wind power system.

Machines	DC Motor	DFAG	WRSG
Power	3 kW	3 kVA	3 kVA
Voltage	220 V	220 V	220 V / 380 V
Speed	1500 RPM	1500 RPM	1500 RPM

The AC generator is coupled to a 3 kW DC motor simulating the turbine. In order to create an unbalance fault in the engine - generator system, a mass was attached to the fin of the cooling fan of this drive motor.

As for the electrical fault, the analysis of the electrical switching was intentionally created by loosening the spring of the brush holder, the disturbance of the pressing force of the spring will automatically lead to poor contact of the brushes on the corresponding ring of the rotor wound generator.

At the end, the current signal is analyzed and compared in the healthy and degraded case of systems; an appearance of new harmonics in the spectrum is synonymous of a degradation of the machine, the severity of the failure or its evolution is signified by increasing the amplitude of the signal, the acquisition of the signals for the diagnosis was carried out by means of a HAMEG507 oscilloscope connected to a Chauvin Arnoux brand current sensor; caliber 0.01-10 A and type: PAC 12.

The current acquisition was carried out by a digital oscilloscope equipped with software SP107 E, in order to read the acquisition data and control the oscilloscope. The measured current data were downloaded to a PC. The representation of the different spectra was obtained using programs written in the Matlab 2011 environment.

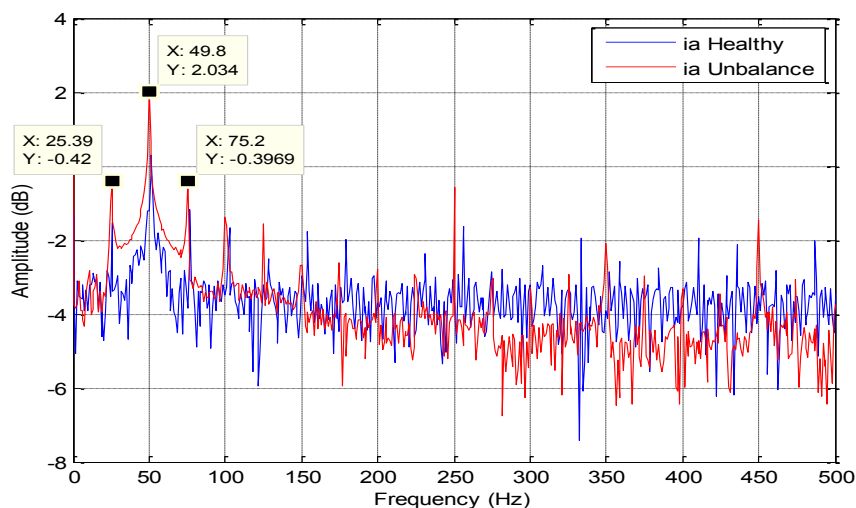
4 Discussions of Experimental Results

4.1 Healthy Wind System and in the Presence of an Unbalance: Spectral Analysis of the Rotor Current of The WRSG Generator

The characteristic frequency of the unbalance defect is present on each side of the fundamental at 50 Hz (Fig. 2). These results are in accordance with what was obtained in the theoretical context concerning the unbalance (Equation. 3).

The measured speed Generator is $n_{rot} = 1500$ RPM, thus $f_r = 25$ Hz. The line around the fundamental $f_s = 50$ Hz, which has the greatest amplitude in the frequency ranges below, is then searched on the spectrum of the current:

$$\begin{cases} f_{unbalance} = 50 - 25 = 25 \text{ Hz} \\ f_{unbalance} = 50 + 25 = 75 \text{ Hz} \end{cases} \quad (5)$$



6

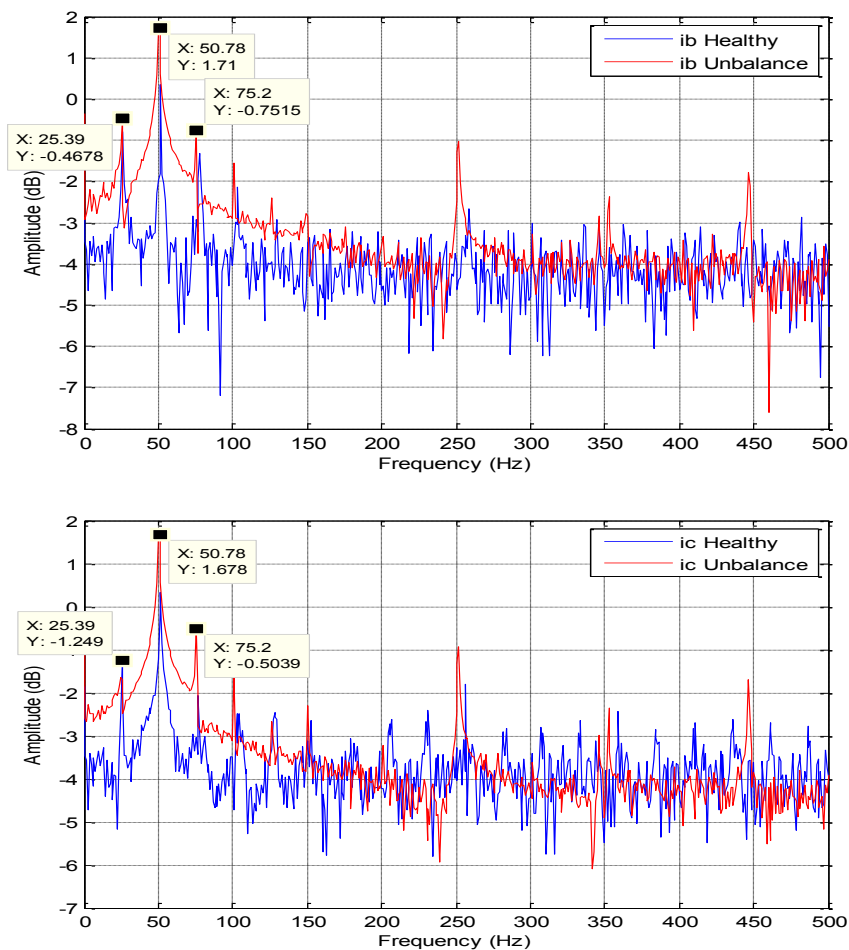


Fig. 2. Spectrum of the Rotor Current I (a, b, c): healthy and degraded wind system.

4.2 Healthy Wind System and in the Presence of an Electrical Unbalance: Spectral Analysis of the Rotor Current of The WRSB Generator

Figure 3 shows the signature of the rotor current of the WRSB generator, the signature of the electrical imbalance fault is expressed in the spectrum of the rotor current through the appearance of harmonic peaks corresponding to odd frequencies multiple of the fundamental frequency 50 Hz.

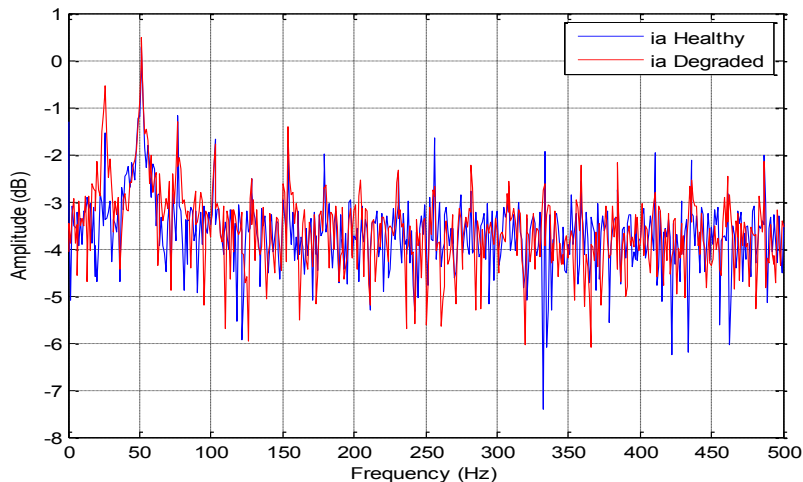


Fig. 3. Wind turbine system healthy and in the presence of a brush-ring contact fault: I_{rotor} spectrum.

4.3 Spectral Analysis of the Rotor Current of the Wind Power System Equipped with DFAG Generator

Just by referring to the temporal characteristics of the rotor current represented by Figures 4 and 5, it can be seen that the amplitude of the current of the rotor phase has greatly increased as soon as the DFAG generator of the wind power system is in the presence of the fault of electrical switching.

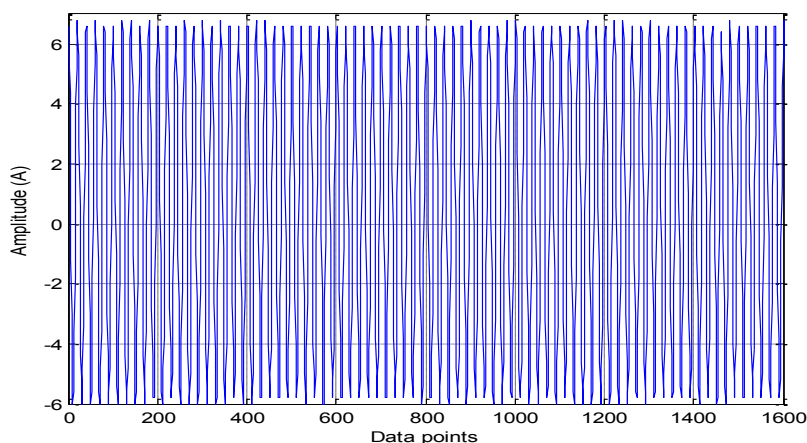


Fig. 4. Temporal characteristic of the rotor current of the healthy wind system.

8

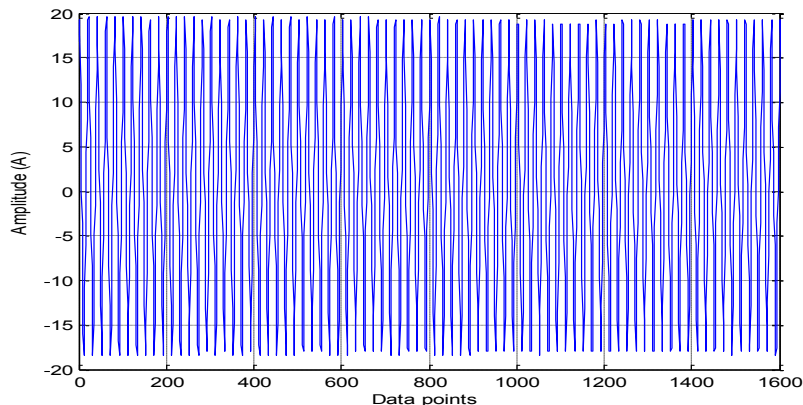


Fig. 5. Temporal characteristic of the rotor current with a brush-ring contact fault.

Figures 6 and 7 show the current spectrum of the rotor of the DFAG generator in healthy operation and during the appearance of poor contact between the rotor rings and the brushes.

Analysis of the rotor current spectrum indicates the presence of degradation in the functioning of the wind power system. The presence of a switching fault between the rings and the brushes is reflected in the spectrum by an increase in the amplitude of the rotor currents in the different phases of the wound rotor of the DFAG. This increase in current is proportional to the severity of the electrical switching fault which will increase as the load on the wind power system increases.

This justifies the observation of the increase in amplitude at the characteristic frequency of the fault coinciding with the fundamental harmonic $f_s = 50$ Hz and the peaks of harmonics at odd frequencies multiple of 50 Hz.

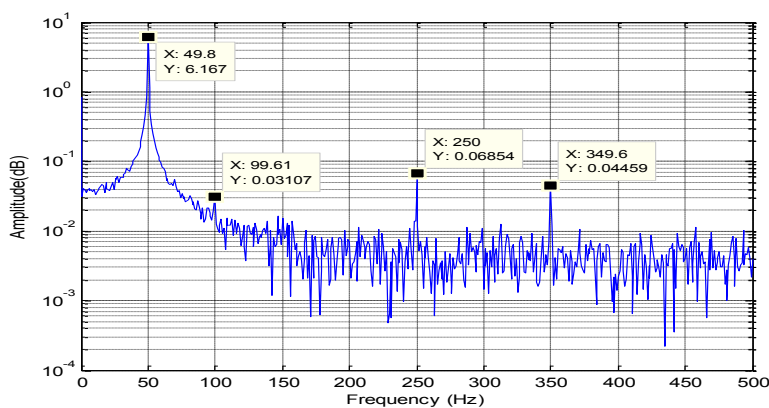


Fig. 6. I_{rotor} spectrum of the healthy wind system based on DFAG.

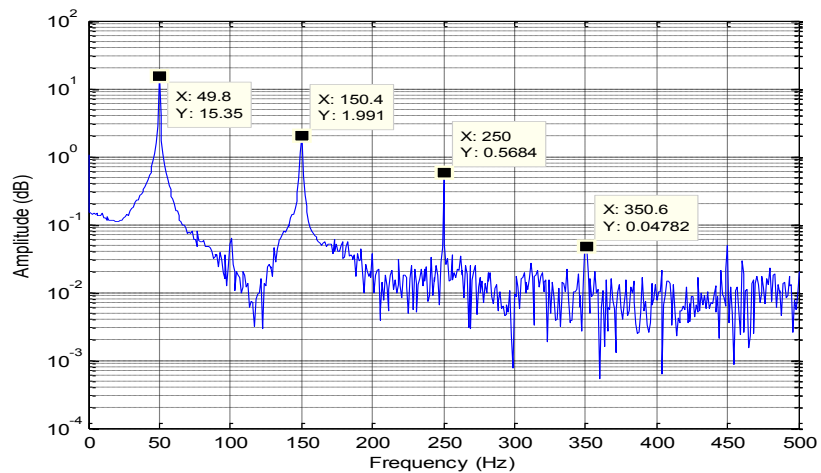


Fig. 7. I_{rotor} spectrum of the wind system based on DFAG with a brush-ring contact fault.

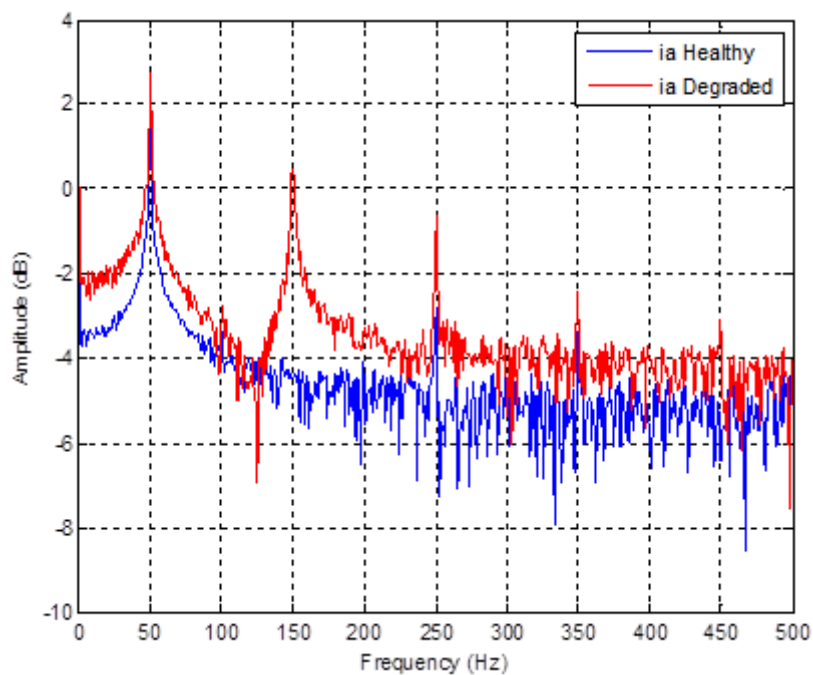


Fig. 8. Spectrum of a rotor phase (I_a rotor) of the healthy DFAG-based wind system and with a brush-ring contact fault.

We notice a comb of lines (red color) around the fundamental frequency (Fig. 8). This justifies the observation of frequencies characteristic of the harmonics of the notch where the turns corresponding to the winding of the phase are directly impacted by the poor contact of the brush-ring system.

4.4 Spectral Analysis of the Stator Current of the Wind Power System Equipped with DFAG Generator

Figure 9 shows the spectrum of the stator current of the healthy DFAG generator and in the presence of the electrical switching fault.

It should be noted that the emergence of peaks of harmonics of multiple bands of the fundamental supply frequency (nf_s) well justifies the presence of electrical asymmetry (electrical unbalance) and this responds to the aforementioned theoretical context.

This current is delivered by the stator of the generator in a purely active load in order to avoid any interference from the reaction of the load which would influence the spectrum of the stator current

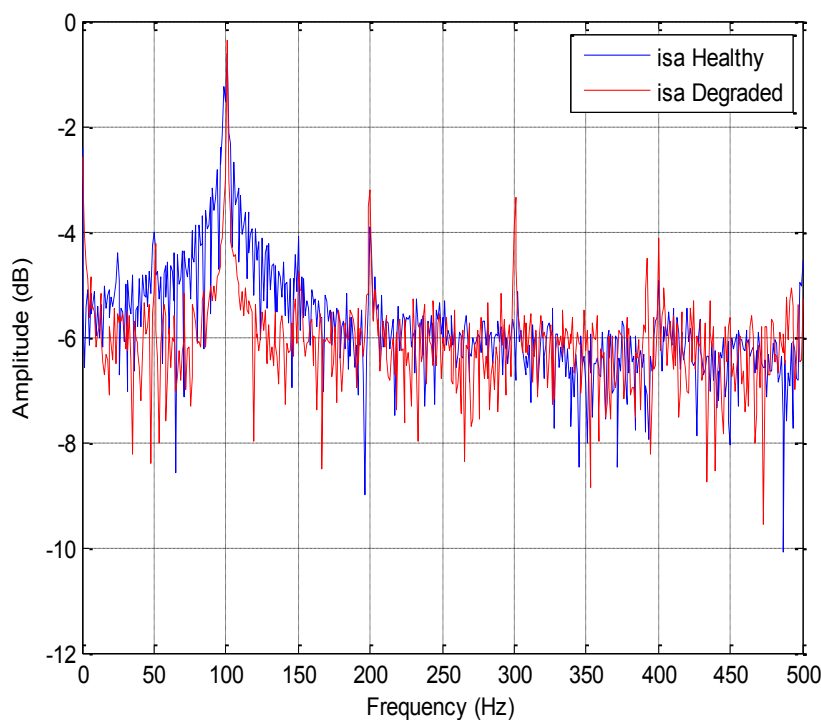


Fig. 9. Spectrum of a stator phase (I_a sotor) of the healthy DFAG-based wind system and with a brush-ring contact fault.

5 Conclusion

This article focuses on an experimental study conducted on the detection of the defect of mass unbalance and electrical asymmetry that affects wind systems based on synchronous generators (SG) and doubly-fed asynchronous generator (DFAG). The aforementioned faults are the most frequent and vulnerable because their impact can spread to other elements of the wind system if they are not detected in time.

For this purpose we have in this experimental work applied the technique of analysis of the signature of the rotor current by the FFT, the signal is picked up at the level of the generator when it is possible, this is in our opinion more reliable and correct than that. stator current for the detection of mechanical or electrical faults affecting wind power systems.

The spectral analysis of the rotor current clearly revealed the unbalance defect affecting the mechanical axis of the wind power system and the electrical unbalance affecting the phases of the WRSG and DFAG generator.

The theoretical consideration was validated by the experimental results. Thus, it has been shown that the analysis of the rotor current signal by the FFT represents a useful tool for the monitoring of the state of the wind power system. It can extend to the detection of other mechanical and electrical faults that may be experienced by the wind power system. The proposed approach can be combined with other signal processing techniques and allow higher diagnostic accuracy and low cost enrichment in favor of predictive maintenance.

References

1. Baroudi, J., Dinavahi, V., Knight, A.: A review of power converter topologies for wind generators. IEEE International Conference on Electric Machines and Drives. San Antonio, TX, USA, pp. 458–465, (2005).
2. Chen, Z., Blaabjerg, F.: Wind energy-the world's fastest growing energy source. IEEE Power Electronics Society Newsletter 18(3), 15–19 (2006).
3. Shipurkar, U., Ma, K., Polinder, H., Blaabjerg, F., Ferreira, J.A.: A review of failure mechanisms in wind turbine generator systems. 17th European Conference on Power Electronics and Applications, pp. 1–10 (2015).
4. Rouabhia, C.E., Bouras, A., Bouras, S., Haouem, N.E.: Contribution of the wind turbine based on a special alternative current generator to the production of positive energy. II Ibero-American Congress of Smart Cities (ICSC-CITIES), Soria, Spain, pp. 471–481, (2019).
5. Lipo, T.A.: Introduction to AC Machine Design. IEEE Press Series on Power Engineering. John Wiley & Sons, Inc., Hoboken, NJ, USA (2017).
6. Li, H., Chen, Z.: Overview of different wind generator systems and their comparisons. IET Renewable Power Generation 2 (2), 123–138 (2008).
7. Rahab, A., Senani, F., Benalla, H.: Direct Power Control of Brushless Doubly-Fed Induction Generator Used in Wind Energy Conversion System. International Journal of Power Electronics and Drive System (IJPEDS) 8(1), 417–433 (2017).
8. Alewine, K., Chen, W.: A review of electrical winding failures in wind turbine generators. Electrical Insulation Conference (EIC-IEEE), pp. 392–397, (2011).

12

9. Lyding, P., Faulstich, S., Hahn, B., Tavner, P.: Reliability of the Electrical Parts of Wind Energy Systems - a Statistical Evaluation of Practical Experiences. EPE Wind Energy Chapter Symposium, (2010).
10. Brutsch, R., Tari, M., Frohlich, K., Weiers, T., Vogelsang, R.: Insulation Failure Mechanisms of Power Generators. IEEE Electrical Insulation Magazine 24(4), 17–25 (2008).
11. Polinder, H., Lendenmann, H., Chin, R., Arshad, W.: Fault tolerant generator systems for wind turbines. IEEE International Electric Machines and Drives Conference, (2009).
12. Keskes, S., Sallem, S., Nouha Bouchiba, N., Kammoun, N., Chrifi-Alaoui, L., Drid, S.: Experimental Analysis for enhancement of unbalanced standalone Wind Energy Conversion System. 16th International Multi-Conference on Systems, Signals & Devices (SSD), (2019).
13. Yongchang, Z., Jian, J., Donglin, X., Dong, J., Zhankuo, W., Chaonan, T.: Model Predictive Direct Power Control of Doubly Fed Induction Generator, Under Balanced and Unbalanced Network Conditions. IEEE Transactions on Industry Applications 56(1), 771–786 (2020).
14. Chen, X.F., Li, J.M., Cheng, H.: Research and Application of Condition Monitoring and Fault Diagnosis Technology in Wind Turbines. Journal of mechanical engineering 47(9), 45–52 (2011).
15. Sun, D., Wang, X.: Low-complexity model predictive direct power control for DFIG under both balanced and unbalanced grid conditions. IEEE Trans. Ind. Electron 63(8), 5186–5196 (2016).
16. Pan, H.X., Gao, Y.: Study of remote fault diagnosis system to wind generator gearbox based on DSP. International Conference on Machine Design and Manufacturing Engineering, (ICMDME), pp. 568–571, (2012).
17. Cheng, C., Cheng, P., Nian, H., Sun, D.: Model predictive stator current control of doubly fed induction generator during network unbalance. IET Power Electron 11(1), 120–128 (2018).
18. Prabhakar, N., Pinjia, Z., Manoj, S., and al.: Electrical Signature Analysis Based Online Monitoring of Drive-trains for Doubly-fed Wind Generators. The 38th IEEE Annual Conference on Industrial Electronics Society (IECON), pp. 1746–1769, (2012).
19. Tan, Y., Zhang, H., Zhou, Y.: Fault Detection Method for Permanent Magnet Synchronous Generator Wind Energy Converters Using Correlation Features Among Three-phase Currents. Journal of Modern Power Systems and Clean Energy 8(1), 168–178 (2020).
20. Bouras, A., Bouras, S., Kerfali, S.: Prediction of the mass unbalance of a variable speed induction motor by stator current multiple approaches. Turkish Journal of Electrical Engineering & Computer Sciences 26(2), 1056–1068 (2018).
21. Li, X., Lu, Y.: Improved Amplitude Differential Protection Scheme Based on the Frequency Spectrum Index for Distribution Networks With DFIG-Based Wind DGs. IEEE Power & Energy Society Section 8, 64225–64237 (2020).
22. Haouem, N.E., Bouras, S., Bouras, A., Rouabhia, C.E.: Experimental investigation for the detection of high-risk external electrical faults through stator current analysis. Australian Journal of Electrical and Electronics Engineering 16(2), 86–95 (2019).

STUDY OF A PHOTOVOLTAIC PLANT FOR THE REDUCTION OF DIESEL CONSUMPTION: CASE OF DOMINICAN REPUBLIC

Miguel Euclides Aybar Mejía ^{1[0000-0002-4715-3499]}, Elvin Arnaldo Jiménez Matos ^{1[0000-0002-0031-6772]}, Deyslen Mariano-Hernández ^{1[0000-0002-4255-3450]} Ángel Isaac Roa Arias ^{1[0000-0002-4380-1348]}, Eduardo Geara ^{1[0000-0002-0599-9816]}, Gerardo Fría ^{1[0000-0001-5832-8322]}]
Ezequias Bido Cuello, ^{1[0000-0001-8692-3524]}

¹ Área de Ingeniería, Instituto Tecnológico de Santo Domingo. Santo Domingo, Dominican Republic
miguel.aybar@intec.edu.do

Abstract. A microgrid is a small part of a given electrical distribution system with distributed generators for storing energy and loads that can be controlled to achieve a self-sufficient energy system integrated with fossil fuel generation technologies if they can reduce their operating costs. Pedernales municipality in the Dominican Republic currently operates in an isolated microgrid of the National Interconnected Electric System (SENI) with three diesel generators, which incur high operating costs, large emissions of carbon dioxide (CO₂) and sulfuric acid (SO₂). This paper aims to propose a photovoltaic (PV) system with a battery energy storage system (BESS) for the decrease of diesel consumption. To achieve this objective, an analysis of load profiles, market exploration of the energy storage, sudden entries and exits of charge and generation, photovoltaic penetration capacity, and establishing a comparison between the system with and without energy storage. DIGSILENT and HOMER Pro were chosen to analyze and optimize the design of the PV system. For the financial analysis, Net Present Value (NPV), Internal Rate of Return (IRR), and payback period were used. The cost-benefit method of production and reduction of greenhouse gases was chosen for the environmental analysis.

Keywords: Photovoltaic, renewable energy, energy storage, solar energy.

1 Introduction

Microgrids are low-voltage power systems isolated from the primary power system, which have distributed generation sources, storage systems, distributed loads, and monitoring and control systems for each of these parts. Due to the challenges faced by power systems around the world (including drastic increases in demand, deterioration of the environment, low energy efficiency, among others) [1], microgrids have become increasingly most used worldwide because they allow the control of distributed generation sources effectively and flexibly [2].

Currently, most microgrids work with diesel generation [3], which frequently increases operating costs and polluting emissions; thus, more and more microgrids are changing to renewable energy such as wind and solar energy [4]. Electrical power systems have very delicate characteristics affected by the use of this type of technology [5]. The high penetration of unmanageable energy increases the risk and instability of microgrids due to intermittent production. Therefore, the percentage in the generation matrix of photovoltaic systems is limited [6].

BESS is an energy storage system with smart batteries that regulate the system's frequency and optimize it, improving the reliability and quality of the system's energy [7]. Coordinating BESS in a power system offers enormous advantages. BESS is appropriate to help distribution system operators, conveniently beating the difficulties of expanding distributed, fluctuating, and questionable generation from sustainable power sources [8].

In the Dominican Republic, Pedernales municipality has an isolated system that worked with the generation of fossil fuels, which have resulted in high operating costs and high CO₂ emission. To achieve a reduction in diesel consumption, this paper proposes a change in the generation matrix by implementing a PV system with BESS.

2 Methodology

A research methodology was developed, dividing it into literature review stages, raw data collection, data analysis, design and sizing of a photovoltaic power station with storage system, simulations, and analysis of results.

Literature review: consisted of a review of the state of the art to determine the advances and information of other authors regarding the subject worldwide, obtaining a knowledge of the parameters and tools currently being used.

Raw data collection: Technical information was collected from the selected microgrid, such as type of fuels used for power plants, electrical circuits that are energized, electrical demand of the system, electrical losses, current operating costs of the system (OPEX), projection of demand, and climatological information of the area to see the renewable potential it has.

Data analysis: Using spreadsheets, the data obtained was analyzed, and the possible equipment that would be needed for the integration of the photovoltaic system and energy storage.

Design and sizing: The projection of the current system's demand for up to 25 years and the current state of the electrical distribution networks were evaluated for the sizing of the proposed system.

Simulations: The behavior of the microgrid was evaluated using two software. HOMER PRO allowed simulating different types of scenarios and configurations between conventional generation technologies and configurations of photovoltaic and storage systems considering technical-economic factors used to evaluate a project DIgSILENT, a group of events that could affect the microgrid's electrical stability response was simulated.

Analysis of results: The response of the microgrid with and without the proposed system was evaluated for all the scenarios to see how the proposed configuration improves the electrical, economic, environmental, and social indicators of the selected area.

3 Case of Study

The Pedernales municipality, which is the head of the province of its name, is located in the southwest of the country. The annual average temperature is 29 °C, and it is one of the driest towns in the Dominican Republic. It has a generation matrix that operates entirely with three generators with a maximum capacity of 5.1 MW, which use Heavy Fuel Oil (HFO) and Low Fuel Oil (LFO). The main characteristics of the electricity distribution system are shown in *Table 1*.

Table 1. The current state of the electricity distribution system.

Circuit Distribution	Clients	Installed Power (kVA)	Demand Factor	Maximum Demand (kW)	Maximum Demand (kVA)	Power Factor
PEDE501	1.463	2.528	0.3819	906	965	0.9386
PEDE502	1.131	3.550	0.3001	1.020	1.065	0.9573
PEDE503	1.234	1.843	0.5977	1.065	1.101	0.9671
Total	3.828	7.920	0.3954	2.991	3.132	0.9550

The load curve corresponding to the previous year (2019) was obtained for the annual load profile. The annual energy consumption is presented in *Fig. 1*.

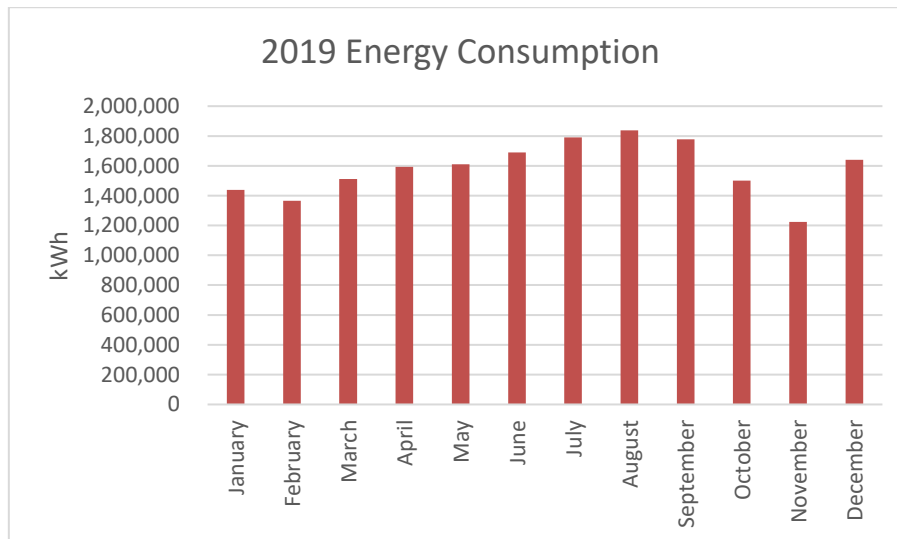


Fig. 1. Energy consumption for 2019.

The total energy consumption for the year 2019 was 18,979,497 kWh, while the total equivalent to CO₂ emissions was 13,599 metric tons.

4 Design and Sizing of the Photovoltaic Power Station

4.1 PV System Nominal Power

For the dimensioning of the solar plant's power, the specific photovoltaic performance of the Pedernales region is used, it is 1,753 kWh / kWp; this data was recovered from the "Global Solar Data" of the World Bank Group. It is starting from an energy requirement of 18,979,497 kWh. The minimum peak power ($P_{minimum}$) is obtained using *Equation 1*. This power is subject to a fully renewable generation matrix. To verify that an 11 MWp plant is supplying the demand, it is necessary to use simulation software [9].

$$P_{minimum} = \frac{18.979.497 \text{ kWh}}{1.753 \text{ kWh/kWp}} = 10.826,86 \text{ kWp} \approx 10,83 \text{ MWp} \quad (1)$$

4.2 PV Module Selection

The performance of photovoltaic cells depends on the internal design of the silicon sheets inside [10]. Within the PV module manufacturing companies, a select group is made up of the most renowned companies called Tier 1. For selecting the manufacturer of the photovoltaic modules of this project, a verification of the companies that make up this group was made, listed in reference [11]. PERC Canadian Solar technol-

ogy PV modules were chosen due to their high efficiency and good profitability (price-durability).

4.3 BESS Selection

The lithium-ion and lead-acid batteries are the ones with the best characteristics [12]. Lead-acid batteries are the safest type of energy storage technology; however, their useful lives are considerably short (approximately 3 to 10 years) and have an intermediate energy density [13]. In contrast, lithium-ion batteries have a longer life, a high energy density, and are smaller in size [14]. Given the power required for this case, the use of lithium-ion batteries for its development has been decided. For the BESS selection, Tesla Megapack has been chosen, which is a large-scale lithium-ion energy storage system capable of storing up to 3 Megawatt-hours (MWh) of electricity, designed to store energy generated by intermittent renewable sources.

Some of the reasons why this pack was selected are because it is a competitive solution in terms of quality and cost [15], the investment cost decreases with the advancement of technology [16], it has a high density of charge and a longer useful life [17], a more significant amount of energy in smaller space [18] and designed to improve the quality of the frequency [19].

4.4 PV Inverter Selection

There are different types of photovoltaic inverter technologies used in solar installations such as, microinverter that must be installed one for each panel having a power range of 0,4kW to 2kW [20], a central inverter that has high efficiency and low cost per installed watt with a power range of 250kW to 870kW [21] and string inverter that offers flexibility and higher performance with a power range of 1000kW to 1GW [22]. A string inverter was selected since the PV system will have an installed 11 MWp and belongs to an isolated system.

5 Photovoltaic Power Station Simulations

The steps carried out for the simulations of scenarios and the system proposed for the case study are presented in *Fig. 2*.

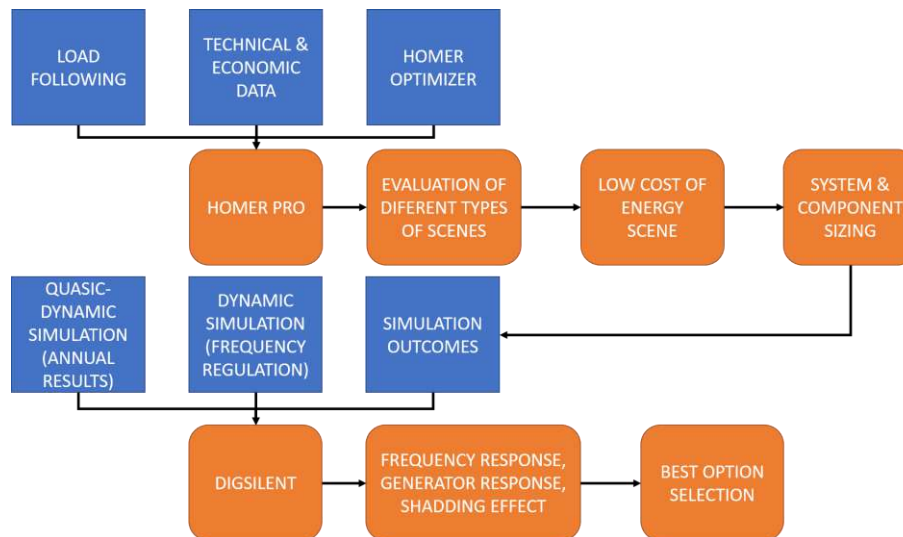


Fig. 2. Flowchart of the simulation process.

The simulation used the technical data related to the current generation system, inverter features, PV modules, and storage systems, which are presented in *Table 2*.

Table 2. Summary of the input data for the case of study.

Description	Current Generation	Inverter Features	PV Modules	Storage System
Capacity (kW)	1.700	*1	*1	-
Capital (USD)	\$1.800.000	\$300	\$800	\$438,43
Replacement (USD)	\$1.800.000	\$300	\$700	\$438,43
O&M (USD/hr)	\$5,70	0,00	1,20	\$0,27
Minimum Load (%)	25	-	-	-
Lifecycle (years)	20	15	25	15
Fuel Price (USD/L)	\$0,57	-	-	-
Efficiency (%)	-	95	-	-
Relative Capacity (%)	-	100	-	-
Performance (kWh)	-	-	-	21.081.851
DC Voltage (V)	-	-	-	600
Initial Charge Status	-	-	-	100
Minimum Charge Status	-	-	-	20

* Default value of a unit recommended by the software for analysis

The cost information presented in *Table 2* was obtained from the electric company in the area. As for the technical data, the data recommended by the HOMER PRO were used.

6 Discussion

In the simulation of the circuit opening with the highest demand, it was obtained that the proposed system with primary frequency regulation and secondary frequency regulation manages to decrease the response time from 2,88s to 0,06s. The same happens in the simulation of a three-phase short circuit 300m from the main bus; the results showed a frequency disturbance time of 0,066s for the proposed system compared to a frequency disturbance time of 4,7s for the current system. The result of the current system's full load output was a curve that tends to 0 Hz indicating a blackout, as observed in *Fig. 3*.

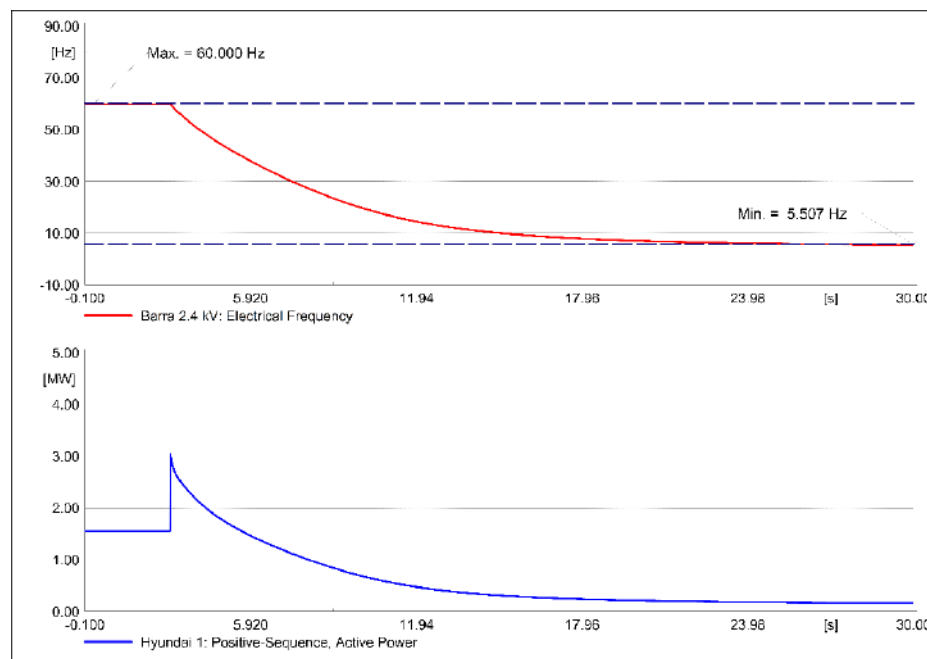


Fig. 3. The output of the current system at full load.

However, with the proposed system, a blackout does not occur due to the contribution provided by the BESS, keeping the frequency between 59,9992 and 60,0003 Hz, as shown in *Fig. 4*.

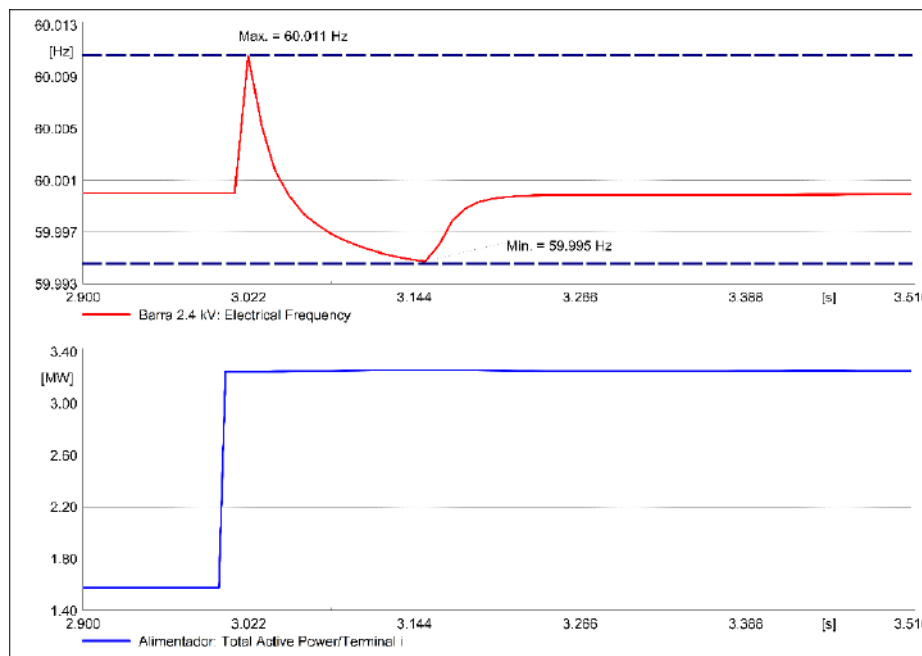


Fig. 4. The output of the proposed system at full load.

The results obtained in the simulation of circuit closure with the highest demand show that the frequency with the current system decreases to 58,027 Hz, and it took 5s to resume stability. In comparison, with the proposed system, the frequency decreases to 59.997 Hz, and the recovery time also with 0,0480s. Finally, a simulation of the shading effect was performed on the PV system with a duration of 29s, which caused the frequency to drop to only 59,999 Hz. After the 29s, the system returned to the nominal frequency in just 1.2s, showing that the BESS manages to maintain the frequency without problems.

The different scenarios and events that simulated to affect the voltage and frequency stability of the current microgrid (with combustion engines) versus the proposed hybrid microgrid (diesel-FV-BESS) are presented in Table 3.

Table 3. Summary of the events carried out and their response in the current system and the proposed system.

Case	Event	Frequency stability	Voltage Stability	Maximum frequency [Hz]	Minimum frequency [Hz]	Stability recovery time [s]	Minimum voltage [p.u.]
Current microgrid with combustion engines	1	yes	yes	61,9270	no	2,8800	no
	2	no	no	no	no	no	0,236
	3	yes	yes	no	58,0270	5,000	no
	4	no	no	no	57,0000	no	no
Hybrid microgrid proposal (diesel-FV-BESS)	1	yes	yes	60,0100	no	0,0600	no
	2	no	no	no	no	no	0,433
	3	yes	yes	60,0040	59,9970	0,0480	no
	4	yes	yes	60,0003	59,9992	0,2000	no
	5	yes	yes	60,0100	59,9990	1,2000	no

Event 1: Opening of the circuit with the highest demand

Event 2: Failure in the circuit with the largest installed capacity

Event 3: Closing of the maximum demand circuit

Event 4: Triggering a generating unit

Event 5: Cloud effect (shadow) on the solar plant

The current power generation system is composed of diesel generators, which have an excellent response to the inertia of the system and produce CO₂ emissions that affect the environment, the proposal to integrate photovoltaic generation systems to the grid reduce greenhouse gases produced by using fossil fuels.

The social impact of implementing the proposed system in the case of study leads to a decrease in the cost of electric energy and the reduction of blackouts to improve the quality of life of residents. In addition to improving the supply and stability of energy, new employment sources will be generated in the province and an increase in tourism. Regarding the environmental impact, we have greenhouse gases, harmful chemical substances, polluting chemical substances, and vegetation degradation. This can be solved by improving production efficiency, optimizing battery disposal, reuse of metal components, and minimizing the impact on the ground.

7 Conclusions and Future Works

This paper proposed a microgrid, which consisted of a PV system with BESS to reduce diesel consumption in the current electrical system of the municipality of Pedernales in the Dominican Republic. The results show that the proposed system is much more robust, reliable, and of higher energy quality than the current system, as demonstrated by the simulations carried out in HOMER PRO, which shows that the project's implementation manages to reduce diesel consumption by up to 80%. The Levelized Cost of energy analysis shows that a reduction in the price of electricity of USD 0,04 is obtained compared to the current system.

Different scenarios in DIgSILENT where the operating variables that represented disturbance problems in the grid were evaluated. The most critical case being the output of the system at full load, showed that the proposed system has a better performance to maintain the frequency. By implementing the proposed system, an annual reduction of 11,248 metric tons of CO₂ can be obtained. In future work, the proposed system could be improved with the consideration of a wind system or even a solar-thermal hybrid system to reduce the dependence on gas to use hot water.

Acknowledgment

EGE Haina for the information from the Pedernales microgrid, the technical and economic data of the electric generation system, in addition to the support during the simulations of network stability in the Digsilent Software, also to EDESUR Dominicana for the information on the behavior of the electrical demand of the distribution circuits of the analyzed area. This research was supported by FONDOCYT 2018-2019-3C1-160 (055-2019 INTEC) in the Dominican Republic.

References

- [1] L. Fusheng, L. Ruisheng, and Z. Fengquan, "Overview of microgrid," in *Microgrid Technology and Engineering Application*, Elsevier, 2016, pp. 1–10.
- [2] M. A. Hossain, H. R. Pota, M. J. Hossain, and F. Blaabjerg, "Evolution of microgrids with converter-interfaced generations: Challenges and opportunities," *International Journal of Electrical Power and Energy Systems*, vol. 109. Elsevier Ltd, pp. 160–186, 01-Jul-2019.
- [3] P. Pérez Fernández, "Descripción e infraestructura de una microrred para un entorno residencial," Universidad de Valladolid, 2017.
- [4] D. Ribó-Pérez, P. Bastida-Molina, T. Gómez-Navarro, and E. Hurtado-Pérez, "Hybrid assessment for a hybrid microgrid: A novel methodology to critically analyze generation technologies for hybrid microgrids," *Renew. Energy*, vol. 157, pp. 874–887, Sep. 2020.
- [5] K. J. Nam, S. Hwangbo, and C. K. Yoo, "A deep learning-based forecasting model for renewable energy scenarios to guide sustainable energy policy: A case study of Korea," *Renew. Sustain. Energy Rev.*, vol. 122, p. 109725, Apr. 2020.
- [6] S. Mishra, K. Anderson, B. Miller, K. Boyer, and A. Warren, "Microgrid resilience: A holistic approach for assessing threats, identifying vulnerabilities, and designing corresponding mitigation strategies," *Appl. Energy*, vol. 264, p. 114726, Apr. 2020.
- [7] Y. Jiang, L. Kang, and Y. Liu, "Optimal configuration of battery energy storage system with multiple types of batteries based on supply-demand characteristics," *Energy*, vol. 206, p. 118093, Sep. 2020.
- [8] R. Hidalgo-León *et al.*, "A survey of battery energy storage system (BESS), applications and environmental impacts in power systems," in *2017 IEEE Second Ecuador Technical Chapters Meeting (ETCM)*, 2017, pp. 1–6.

- [9] M. K. Deshmukh and A. B. Singh, "Modeling of Energy Performance of Stand-Alone SPV System Using HOMER Pro," *Energy Procedia*, vol. 156, pp. 90–94, 2019.
- [10] K. Ramalingam and C. Indulkar, "Solar Energy and Photovoltaic Technology," in *Distributed Generation Systems: Design, Operation and Grid Integration*, Elsevier, 2017, pp. 69–147.
- [11] Thomas Edison, "Latest Tier 1 Solar Panels List 2019 (Q1, Q2, Q3 update). Solar Review.," *Solar Review*, 2019. [Online]. Available: <https://review.solar/latest-tier-1-solar-panels-list-2019/>. [Accessed: 01-Aug-2020].
- [12] D. W. Gao, "Chapter 5 - Sizing of Energy Storage Systems for Microgrids," D. W. B. T.-E. S. for S. M. Gao, Ed. Oxford: Academic Press, 2015, pp. 125–142.
- [13] H. Keshan, J. Thornburg, and T. S. Ustun, "Comparison of lead-Acid and lithium-ion batteries for stationary storage in off-grid energy systems," *IET Conference Publications*, 2016, vol. 2016, no. CP688, pp. 30 (7 .)-30 (7 .).
- [14] Y. Zhang and W. Wei, "Model construction and energy management system of lithium battery, PV generator, hydrogen production unit and fuel cell in islanded AC microgrid," *Int. J. Hydrogen Energy*, May 2020.
- [15] M. Barbaro and R. Castro, "Design optimization for a hybrid renewable microgrid: Application to the case of Faial island, Azores archipelago," *Renew. Energy*, vol. 151, pp. 434–445, May 2020.
- [16] T. Weitzel, M. Schneider, C. H. Glock, F. Löber, and S. Rinderknecht, "Operating a storage-augmented hybrid microgrid considering battery aging costs," *J. Clean. Prod.*, vol. 188, pp. 638–654, Jul. 2018.
- [17] M. Pourbehzadi, T. Niknam, J. Aghaei, G. Mokryani, M. Shafie-khah, and J. P. S. Catalão, "Optimal operation of hybrid AC/DC microgrids under uncertainty of renewable energy resources: A comprehensive review," *International Journal of Electrical Power and Energy Systems*, vol. 109. Elsevier Ltd, pp. 139–159, 01-Jul-2019.
- [18] M. Jayachandran and G. Ravi, "Predictive power management strategy for PV/battery hybrid unit based islanded AC microgrid," *Int. J. Electr. Power Energy Syst.*, vol. 110, pp. 487–496, Sep. 2019.
- [19] S. S. Fazlhashemi, M. Sedighzadeh, and M. E. Khodayar, "Day-ahead energy management and feeder reconfiguration for microgrids with CCHP and energy storage systems," *J. Energy Storage*, vol. 29, p. 101301, Jun. 2020.
- [20] K. Misbrener, "How to choose between string and microinverters in residential solar projects," *Solar Power World*, 2019. [Online]. Available: <https://www.solarpowerworldonline.com/2019/08/string-versus-microinverters-residential-solar/>. [Accessed: 02-Aug-2020].
- [21] G. Balaji and B. Priyadarshini, "A Review of Grid Connected Inverters for Photovoltaic System," *Int. J. Adv. Res. Electr. Electron. Instrum. Eng.*, vol. 6, no. 8, pp. 6243–6253, 2017.
- [22] C. Warren, "From Energy Storage to Microgrids, String Inverters Are the Key to Expanding Solar's Capabilities | Greentech Media," *Green Tech Media*, 2016. [Online]. Available: <https://www.greentechmedia.com/articles/read/string-inverters-are-the-key-to-expanding-solar-capabilities>. [Accessed: 02-Aug-2020].

Innovative Smart Microgrid Integrating Pico-hydro Systems: The Silk House Museum

Vicente Leite¹[000000028790519X]

Research Centre in Digitalization and Intelligent Robotics (CeDRI),
Instituto Politécnico de Bragança, Campus Santa Apolónia, Bragança, Portugal
avt1@ipb.pt
<http://cedri.ipb.pt>

Abstract. Smart microgrids are local electric grids integrating distributed generation (renewable or not) and consumers, energy storage, power control and energy management. They are an emerging alternative for the energy supply of a house, a building, a small village, or a wider region. Furthermore, they can be connected to the utility grid or operate in stand-alone mode. This paper presents a smart microgrid implemented in a small museum dedicated to the dissemination of science: the House of Silk (Casa da Seda). The renewable generation sources are three photovoltaic systems and two pico-hydro systems – a low-head propeller turbine and a water wheel. The energy storage system is implemented with a battery bank. The power control and energy management consists of the SMA Flexible Storage System based on three Sunny Island inverters and the Sunny Home Manager. The microgrid is in full operation and feeds the House of Silk loads. It can operate in both grid-connected and islanded modes. This paper also presents innovative approaches, based on photovoltaic inverters, to connect small-scale hydro turbines to the (micro)grid.

Keywords: Microgrids · Pico-hydro Systems · Photovoltaic.

1 Introduction

Global societal challenges, such as climate change, combined with the recent economic and health crises, create the opportunity to accelerate the paradigm shift towards a more sustainable world. To pursue this goal, according to IRENA's report [1], by 2050, the energy-related CO₂ emissions would have to reduce 70%, compared to nowadays levels. Fortunately, the continued growth of renewables is encouraging, with an increase of over 40% in primary energy growth in 2019 [2]. Under this scenario, a 60% reduction of CO₂ can be achieved with a large-scale shift to electricity from renewable sources. It can be even higher, 75%, if renewables for heating and transport are considered. Moreover, renewable sources could supply 86% of power demand [1]. Photovoltaic (PV) and hydropower are important distributed renewable sources. Grid-connected small-scale PV systems are widely spread. However, small-scale hydropower generation from small

2 Vicente Leite

reservoirs or small heads (without requiring massive dams) are very promising [3]. In particular, very small-scale hydropower (pico-hydro) has an enormous untapped potential [4]. Pico-hydro is the classification for power plants under 5 kW [5]. They are an emerging renewable power source available from flowing water in small rivers, canals and streams, or even in water supply systems [6–8]. Recently, innovative strategies have been developed to connect these systems to the grid [4, 9, 10]. Distributed generation (DG) from renewables, combined with energy storage, are becoming a promising solution to produce on-site highly reliable and good quality electrical power [11] with environmental, technical, and economic advantages for consumers and utility grid. Furthermore, the integration of DG, such as PV and pico-hydro, into microgrids is an emerging solution either for electrification of remote regions or making buildings more sustainable [12]. In general terms, microgrids are local electric grids integrating DG (renewable or not) and dispersed loads, energy storage systems, power control and energy management, which may operate in both grid-connected or islanded modes [11]. They are an emerging alternative to supply a wide region, a small village, a building or even a house. Energy sustainable buildings are being under continued development and, according to Bernard Looney [2], “the technologies required to reach net zero exist today – the challenge is to use them at pace and scale, and I remain optimistic that we can make this happen”. The SilkHouse project – Development of a smart microgrid based on renewable energy sources and a monitoring system for the House of Silk – was developed under this spirit. It was funded by FCT - Portuguese Foundation of Science and Technology, the Municipality of Bragança, and the Polytechnic Institute of Bragança, Portugal. Nowadays, the House of Silk (Casa da Seda) is a small museum dedicated to the science dissemination. This museum was restored in 2006 and maintained the original constructive characteristics, including all infrastructures of a former mill (two galleries and a water channel between them). The description and implementation of the Silk House microgrid was firstly presented in [12]. This paper presents the full development of the project and its contribution for the “state of the art” is twofold. First, it describes a real and complete case study of a smart house of future smart cities, with a microgrid integrating PV and pico-hydro systems, energy storage system, energy management and monitoring system. Second, it presents innovative strategies to connect two pico-hydro systems to the microgrid – a water wheel and a low-head propeller turbine.

2 Description of the Silk House museum microgrid

2.1 Context of the project

The House of Silk (Casa da Seda) is a small museum in the heart of the city of Bragança, Portugal. It is an interactive space that belongs to the Bragança Ciência Viva (Live Science) Centre (CCVB), which is part of the European Network of Science Centres and Museums (www.ecsite.eu). This is aimed to inspire and empower science centres, museums and other organisations to engage people with science. CCVB also belongs to the Portuguese Network of Science



Fig. 1. The House of Silk museum.

Centres of Ciência Viva (www.cienciaviva.pt). Its mission is to promote scientific and technological education for the Portuguese society, with special emphasis on the younger generation. The House of Silk is located on the left bank of the Fervença River, as shown in Fig. 1. In the 18th Century, people used that place to dyed silks. During the 19th and 20th centuries, it functioned as a mill. The Municipality bought this former Mill in 1990 and recovered it in 2006. Nowadays, the House of Silk is an interactive museum that offers a course on the history of silk. It gives an overview of the various stages of silk production and tells the story of silk based on people's interaction. This is a space of experimentation and playful learning, encouraging the discovery of the stories of silk. It is also a place for exhibitions, lectures and courses about several themes.

2.2 On-site renewable energy sources

By analysing the place where the House of Silk is located, two endogenous resources emerged immediately: hydro and photovoltaic.

Hydro. The reconstruction of the House of Silk by the Municipality, in 2006, conserved the historical architecture of the building as well as the former mill infrastructures: two galleries and the water channel between them, as shown in Fig. 2. By the same time, the riverside area upstream of the Silk House was re-qualified. In order to create "water mirrors", they built several small dams. The downstream dam of all is next to the House of Silk, as can be seen in Fig. 1. Figure 3 presents an overview of the Silk House framework. As can be seen, the dam is less than 10 m from the entrance of the upper gallery.

From a land surveying carried out, the maximum head from the dam water level to pavement of lower gallery is 4 m. This gallery, in the lower level of the museum, is the place where there was a former mill. To conserve this historic heritage, an horizontal water wheel was planned. From the top of the lower gallery to the river level is about 6 m (under normal water flow conditions). Taking advantage of this head, and to make better use of the available infrastructures it was planned to install a low-head propeller turbine [13]. Figure 4 shows some details of hydro implementation in the lower gallery.

4 Vicente Leite



Fig. 2. Former mill infrastructures: two galleries and the water channel between them.

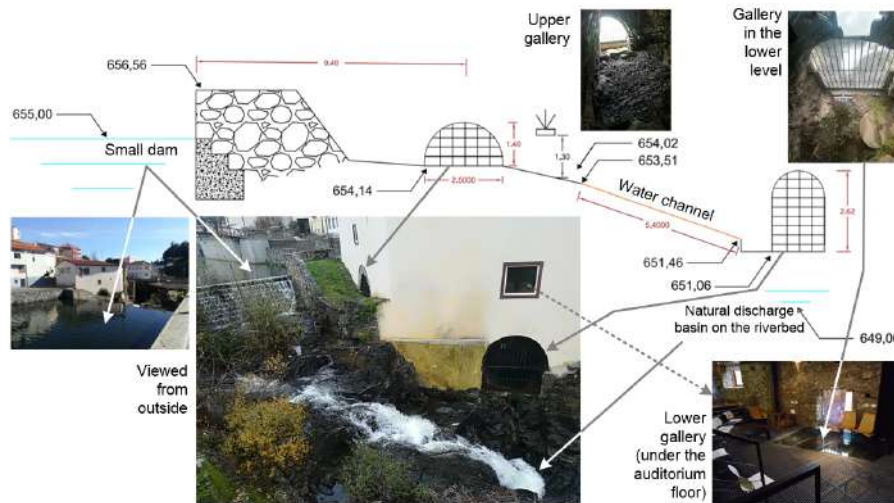


Fig. 3. Illustration of the hydro on-site implementation.

The water wheel was designed specifically for the site, considering a maximum water flow of 30 l/s and a head of approximately 3.8 m (disregarding the height of the jets in relation to the pavement). It was designed with 4 jets, 20 buckets and an external diameter of 1.2 m (85 cm between the outlets of each pair of jets). Initial tests were carried out in the laboratory emulating the installation in the House of Silk. Several jet diameters were used to optimize the water wheel speed and, therefore, the output power.

Figure 5 illustrates the scheme for capturing water from the dam to the lower gallery, passing through the channel between both galleries. Considering this figure, the water flow can be estimated from the Bernoulli equation [14] as follows:

$$p_1 + \rho \times g \times h_1 + \frac{1}{2} \times \rho \times v_1^2 = p_2 + \rho \times g \times h_2 + \frac{1}{2} \times \rho \times v_2^2 \quad (1)$$

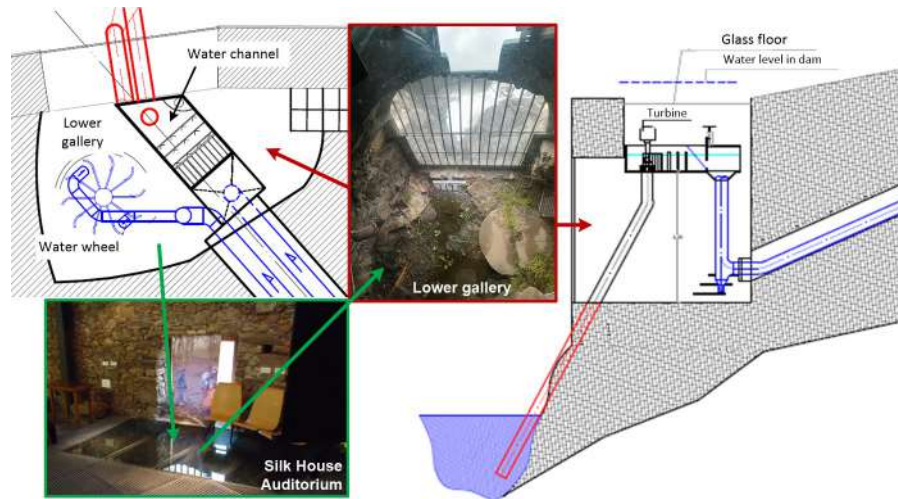


Fig. 4. Illustration of the hydro implementation in the lower gallery.

where p_1 and p_2 are the pressure at points 1 and 2, respectively, ρ is the water density ($=1000 \text{ kg/m}^3$) and g is the gravitational acceleration.

Since $p_1 = p_2 =$ the atmospheric pressure and the water velocity in the dam (v_1) is zero, it gives:

$$g \times (h_1 - h_2) = \frac{1}{2} \times v_2^2 \tag{2}$$

As v_2 is the waterjet velocity and $h_1 - h_2$ is the head, results:

$$v_{wjet} = \sqrt{2 \times g \times head} \tag{3}$$

It gives a waterjet velocity of 8.63 m/s. Thus, the water flow (l/s) is calculated multiplying this speed by the jet hose exit area A (m^2):

$$Q_{jet} = v_{wjet} \times A = v_{wjet} \times \frac{\pi}{4} \times D_{jet}^2 \tag{4}$$

D_{jet} is the jet hose exit diameter (m), which is 2.5 cm. This gives a total water flow of $Q = 4 \times Q_{jet} = 17 \text{ l/s}$. The power available from a hydro system is obtained as follows [15]:

$$P = \eta \times \rho \times g \times Q \times H \tag{5}$$

In the above equation, P is the generated mechanical power at the turbine shaft (W), η is the turbine hydraulic efficiency, Q is the water flow in the turbine (l/s), and H is the gross head (m) of water available on site.

The hydropower systems are usually classified according to their powers. In [15] they are classified as pico-hydro plants for a power range up to 10 kW and as micro-hydro for the range 10-500 kW. In [5, 16], these power ranges are 0-5 kW

6 Vicente Leite

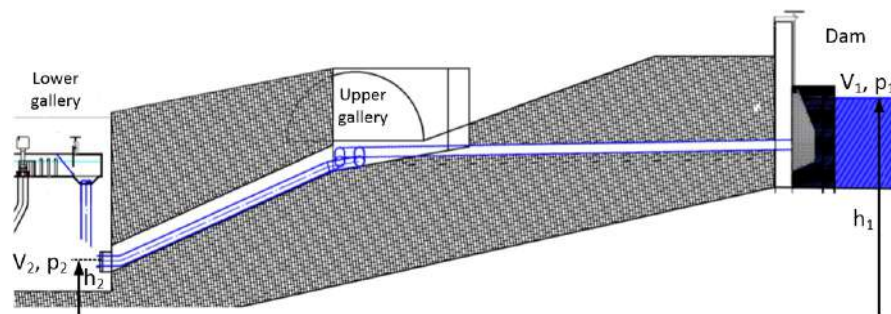


Fig. 5. Scheme for capturing water from the dam to the lower gallery.

and 5-100 kW, respectively. The hydraulic efficiency of the best turbines is in the range of 80% to over 90% but it reduces with size. For micro-hydro systems it is in the range of 60% to 80% [15]. For pico-hydro systems, the efficiency is expected to be lower. For the low-head propeller turbine selected for this project an efficiency of 50% is expected [13]. The efficiency of an horizontal water wheel is even lower. Indeed, for a well-optimized wheel, the efficiency should not exceed 50% and values in the range of 20-30% can be expected [17]. Assuming an efficiency of 25% and from equation (5), the power generated by the horizontal water will be about 158.3 W.

To increase the hydro potential, taking advantage of a useful quota of 5 m from the gallery to the river, a low-head propeller turbine was planned as illustrated in Fig. 4. This turbine is designed for a head of 5 m and a water flow of 56 l/s [13]. However, the head varies slightly throughout the year depending on the amount of water flowing in the river. As a result, the water level in the discharge basin varies.

Considering the analysis above and from (5), assuming an efficiency of 50% [13], the power generated by the turbine will be 1.4 kW. Due to the physical conditions of the place, the draft tube could not be vertical. Thus, it was necessary to create a curve and, furthermore, the tube was a little longer, but with larger diameter. Therefore, according to [13], losses of around 15-25% were expected for a 90° curve, which is not the case in the House of Silk, as can be seen in Fig. 4. However, assuming additional losses of 10%, the expected power will be about 1260 W.

Unfortunately, either through knowledge of the site or previous studies [18], the period of operation of these hydro systems will not exceed 7-8 months due to the reduced flow in the summer months. In any case, this is an interesting renewable energy source because, in the months when there is water, it produces energy 24 hours a day. The lack of hydro energy in the summer period is complemented by solar irradiance as described in the next section.

Photovoltaic. Another endogenous resource is the solar photovoltaic. According to solar radiation database PVGIS-SARAH (year 2016) [19], the monthly

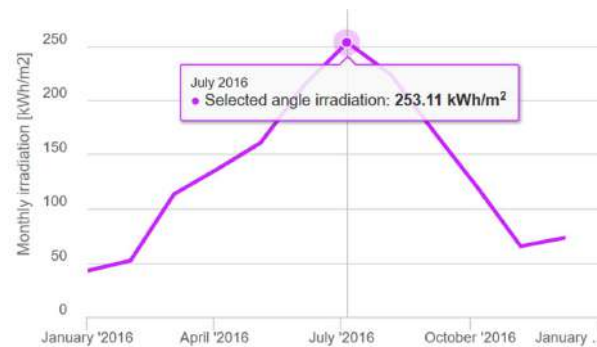


Fig. 6. Monthly solar irradiation estimates, slope 12 degrees, latitude 41.804, longitude -6.756, solar radiation database PVGIS-SARAH (year 2016) [19].

solar irradiation estimates for the Silk House (roof slope of 12 degrees, latitude 41.804 and longitude -6.756) is maximum in summer, as shown in Fig. 6, when hydro energy is rarely available. The House of Silk roof is illustrated in Fig. 7. It has three suitable areas, by only considering the orientation. However, the leftmost area is shaded during the first hours in the morning. Thus, two suitable areas are available: One South oriented and the other Southwest oriented. Both have a slope of approximately 12 degrees. According to [19], for the House of Silk conditions, the expected annual photovoltaic yield is approximately 1343 kWh/kWp, per year. These data were obtained for crystalline silicon, slope of 12 degrees, azimuth 0 degrees and system losses of 14%. According to real data from PV systems installed 2 km away, also close to the river, energy production is 1466.9 kWh/kWp, per year. In this case the slope is 35° and the modules were installed in 2010. For new PV modules with higher efficiency, but not with the optimum slope, it will be used 1500 kWh/kWp per year.

3 Design of the microgrid

A preliminary design of a smart microgrid based on renewable energy sources and a monitoring system for the House of Silk was described in [20]. The implementation of the microgrid is described in [12] with preliminary results, but without the integration of the pico-hydro systems. The implementation of the microgrid is now finished with the integration of two pico-hydro turbines. This section summarizes the complete design of the implemented microgrid, which it is now in full operation.

As previously mentioned, a microgrid is a local electric grid integrating distributed generation and consumption, power control and energy storage and management, which may operate in both grid-connected or islanded modes [11]. They can supply a wide region, a small village, a building or even a house. Next, these items are described for the Silk House museum microgrid.

8 Vicente Leite

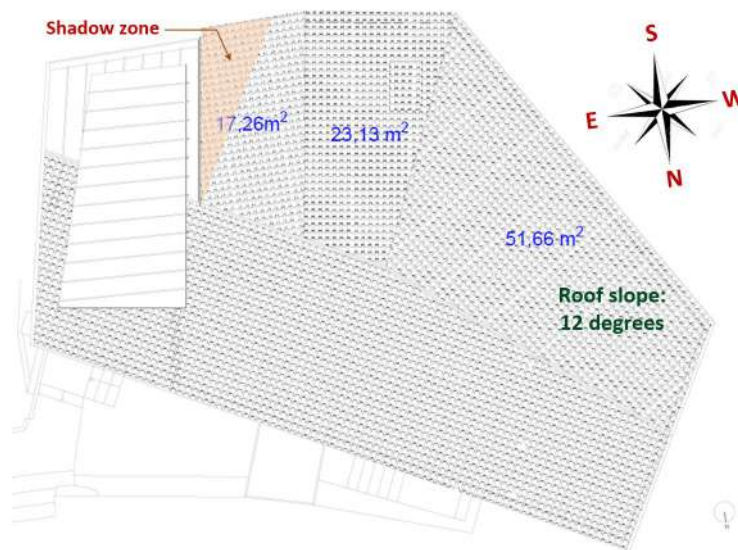


Fig. 7. The Silk House roof with two suitable areas (South and Southwest oriented and slope of 12 degrees).

3.1 The energy consumption and project goal

Initially, the electricity bills of the building, for three years, were analysed (2014-2016). The energy demand results from the following loads: heating, ventilation and air conditioning system; some electrical heaters in offices; computers and monitors; multimedia projectors; a stereo system and lighting. The building is powered by a three-phase electrical system (400 V, 50 Hz) with a contracted power of 13.8 kW and its energy profile was initially characterised in [20].

The museum's opening hours are from 10 a.m. to 6 p.m. from Tuesday to Fridays and 11 a.m. to 7 p.m. on Saturdays and Sundays. It is closed on Mondays. Sometimes, especially on Fridays, there are activities that last until midnight. The average daily consumption is 45 kWh in normal working days, and the annual average is about 16000 kWh [20].

The implementation of the Silk House microgrid was funded by the Foundation for Science and Technology of Portugal under the SilkHouse Project. The goal was to transform the House of Silk in a self-sustainable building. In this way, this small museum should contribute to the dissemination of renewable sources and new technologies for future buildings in smart cities [12]. The main goal of this project was to promote the self-sustainability of the museum, in annual average terms. The first task was to analyse the energy consumption and usage profile of the building. The underlying idea was that, annually, the production of electricity should be equal to the consumption to transform the Silk House in a net zero energy museum.

3.2 Energy savings and generation

In order to reduce the energy consumption, an annual reduction of around 1900 kWh/year was expected (12.3%), through the promotion of new organizational behaviours and the replacement of loads, namely halogen lamps [20]. The remaining energy demand would be generated by the local endogenous resources (hydro and PV), as described next.

The hydro energy generation was estimated by considering the equivalent of 7 months of operation and a total generation power of approximately 1.4 kW (158 W plus 1260 W, respectively from the water wheel and propeller turbine). Therefore, the annual hydro generation is $1.4 \times 24 \times 365 \times 7/12 = 7200$ kWh. Thus, the required annual PV energy would be $16271 - (1900 + 7200) = 7171$ kWh. Table 1 resumes the Silk House energy consumption, expected energy savings by improving energy efficiency, and required energy generation (hydro plus PV) for a net zero energy building. Let us consider the expected annual PV generation of 1500 kWh/kWp/year, as explained before, and the annual required PV generation of 7171 kWh/year. Thus, the required PV power is $7171/1500 = 4.8$ kWp.

The implemented PV system consists of 18 PV modules divided by three strings of 6 modules. One string is oriented South and two are oriented Southwest. The selected modules are from Panasonic, model VBHN325SJ47, series HIT, with 325 Wp and 19.7% efficiency. So, the maximum power of the system is 5.85 kWp and the expected annual PV yield is about $1500 \text{ kWh/Wp} \times 5.85 \text{ kWp} = 8775$ kWh. The three PV strings are connected to each phase of the Silk House electrical system, using three SMA Sunny Boy 1.5-1 VL 40 (SB) PV inverters [12]. This configuration is important because the slightly different roof orientations. Fortunately, it allows to distribute the energy over the three phases and to extend, a little more, the generation throughout the day [12].

There is not a specific technology for connecting very small-scale (pico-) hydro turbines to the grid. The strategy developed in this project will be presented later.

Table 1. Energy consumption, savings in energy efficiency and generation for a net zero energy building.

Annual demand (kWh)				Annual savings and generation (kWh)		
2014	2015	2016	Average	Savings	Hydro	Required PV
18102	14008	16703	16271	1900	7200	7171

3.3 Energy storage

In addition to the analysis of the energy invoices, the energy consumption of the building was also monitored using the PEL 103 energy analyzer. Monitoring took

10 Vicente Leite

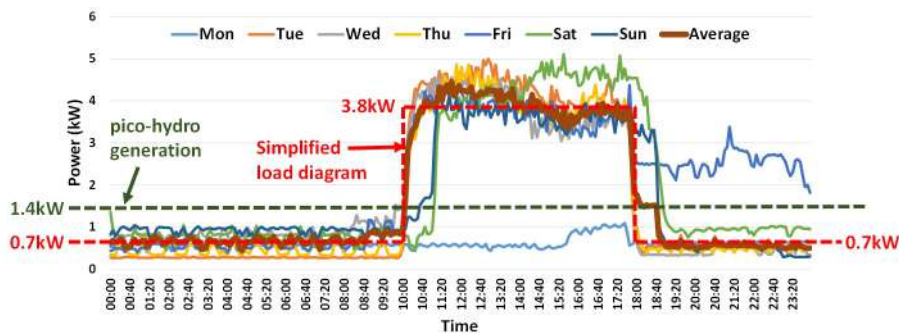


Fig. 8. Average power of loads per day of the week (during February and March 2017).

place over 7 weeks, specifically from February 6 to April 2, 2017. Fig. 8 shows the loads’ diagram with the average power of each day of the week, during the monitoring period. In this graph, the expected hydro generation and a simplified average load diagram were overlapped with dashed lines, with dark green and the red colors, respectively.

From Fig. 8 it appears that, on average, during the hours when the museum is closed (16 hours), the excess power is approximately $0.7 \text{ kW} = 1.4 \text{ kW}$ (hydro generation) minus 0.7 kW (the average load power). This is equivalent to an average power generation of 0.7 kW . This gives $0.7 \text{ kW} \times 16 \text{ h} = 11.2 \text{ kWh} \approx 11.2 \text{ kVAh}$. This energy must be stored in the battery bank. Thus, the capacity can be estimated dividing this energy by the battery voltage, which is 48 V , as will be described later. This gives a battery capacity of 233 Ah . In general, the number of battery charging cycles reduces exponentially with increasing discharge depth [21]. Considering a depth of discharge (DOD) of 50%, at least a 400 Ah battery bank is required.

In the summer months there is no hydro generation but the photovoltaic generation will be maximum. Figure 9 overlaps the average daily power demand of the building and the PV power generation for a clean day. Both were obtained from real data. The PV curve was obtained by multiplying the known data of the 15 kW (ac) PV system, mentioned above, by the factor $4.5/15$. In this ratio, 4.5 is the (ac) PV power of the Silk House PV system.

From Fig. 9 it is possible to estimate the excess energy produced by the photovoltaic system that must be stored. This energy can be estimated by the area of the triangle shown in the figure. Thus, it gives approximately $(2.75 \text{ h} \times 3 \text{ kW})/2=4.125 \text{ kWh}$. Dividing this value by the voltage of the battery bank it gives about 86 Ah . This would require a capacity of about 180 Ah for a 50% DOD. Thus, the capacity required for the batteries is determined by the hydro generation. Even if the consumption is considerably lower, as on days when heaters or air conditioning is not necessary, the capacity of 400 Ah seems to be high enough. Furthermore, the PV generation curve will shift slightly to the right due to the layout of the PV modules. Luckily, the PV strings orientations

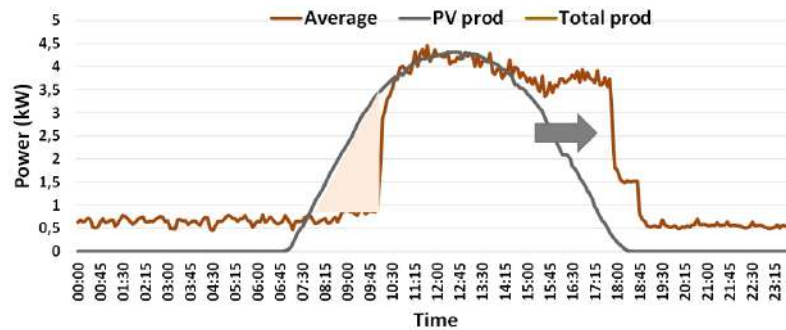


Fig. 9. Daily average power of loads in the building and estimated PV power.

make possible to improve the distribution of PV generation throughout the day, adjusting it to the opening hours of the museum (from 10 a.m. to 6 p.m. or from 11 a.m. to 7 p.m.) [12].

The implemented 48 V battery bank consists of twenty four VRLA 2 V battery's blocks, Sonnenschein's A602/625 Solar, $C_{10}=455$ Ah. These gel technology blocks can have more than 3000 cycles at 60% DOD C_{10} [21].

4 Grid connection of the pico-hydro system

The connection of conventional hydro systems to the utility grid is made by making the generator run at constant speed. This speed must be as close as possible to the nominal speed of the generator. In these cases, speed regulation requires complex mechanical devices [22].

In recent years, there has been a growing interest in the development of pico-hydro systems [23–30], including water wheels [14, 17, 31–35]. New approaches have also been investigated for grid connection of pico-hydro systems [4, 36]. Recently, under the context of the Silk House project, a grid connection approach was investigated for very small-scale pico-hydro systems using PV microinverters [9, 10]. Unlike conventional systems, the new approaches allow systems to be operated at variable speed. The solution consists of conveniently integrating a low speed permanent magnet synchronous generator, used in wind systems, with PV inverters. Both are widely available on the market and competitively priced. However, the solution is not straightforward and may require a protection circuit [4, 10]. This was the strategy developed, within the scope of the House of Silk project, to connect the low-head turbine and the water wheel to the microgrid as described next.

Grid-connection of the water wheel. The solution to connect the water wheel to the grid was found after an extensive research, using different wind generators and PV microinverters [9, 10, 14]. However, the details that led to

the implemented scheme are outside the scope of this paper. Basically, the solution consists of the integration of the water wheel with the wind generator TGET280-I-0.2KW-150R, a 18:40 pulley system for speed multiplication, a three-phase rectifying bridge and the Solis-mini-700-4G PV inverter. The most relevant technical characteristics, regarding their connection, are on Table 2 and Table 3, respectively.

Table 2. Technical characteristics of the water wheel generator.

Technical characteristics	PMSG TGET280
Rated power	200 W
Rated speed	150 rpm
Rated voltage	24 V_{AC}
Rated line current	4.81 A
Efficiency	> 85 %
Stator	Three-phase
Rotor	PM inner rotor
Axis	Vertical

Table 3. Technical characteristics of Solis-mini-700 and Solax X1-1.5 PV inverters.

Technical characteristics	Solis 700	Solax X1-1.5
Maximum DC input power (W)	900	1650
Maximum DC input voltage (V)	450	400
MPPT voltage range (V)	50-400	70-380
Maximum input current (A)	10	10
Rated AC output power (W)	700	1500

Initially, two tests were performed with the generator connected to the water wheel. The first with no load and the second with a variable power resistor. With the 4 jets open, the open circuit voltage was 112 V_{DC} and the speed $40/18 \times 122 = 271.1$ rpm (104 V_{DC} and the speed $40/18 \times 114 = 253.3$ rpm, respectively, if only two jets are open).

The results of the test with variable load are shown in Fig. 10. Each point of the power curve was obtained by the average of three measurements. From the analysis of the curve, it should be noted that, unlike PV modules, the power curve is quite flat around the maximum power point. This fact makes the search for the maximum power point in a wide voltage range. By analyzing the graph, it is possible to verify that, for a power variation of less than 2%, it is expected that the voltage may vary in a range of approximately 45 to 62V.

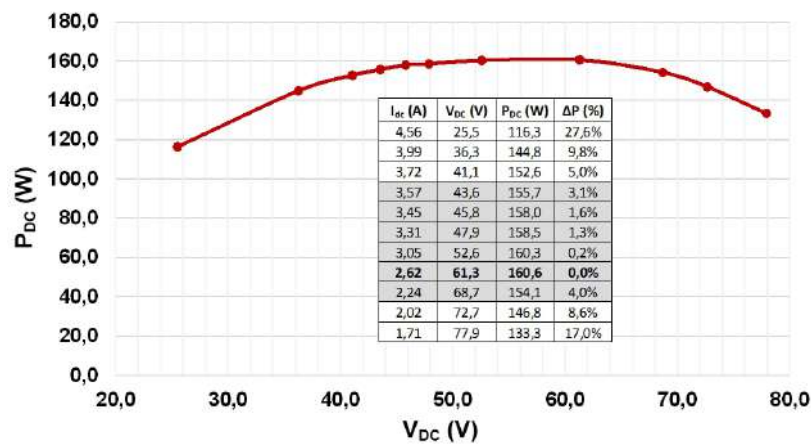


Fig. 10. P-V curve of the water wheel with variable power resistor.

A more detailed analysis is outside the scope of this paper. However, when using a PV microinverter, to connect the generator to the grid, it would be necessary to reduce the speed transmission ratio in order to obtain a lower voltage. Furthermore, the voltage range, around the maximum power point, would cover almost the entire MPP range of the PV microinverter. Thus, the PV inverter Solis-mini-700-4G was chosen, whose MPP voltage lower limit is 50 V. Therefore, it is expected that the voltage of the inverter can oscillate around this value. Moreover, the maximum input voltage of this inverter is 450 V, which is well above the open circuit voltage of the generator. Thus, no over-voltage protection circuit is necessary.

Grid connection of the low-head propeller turbine. Important information was previously available about the LH propeller turbine [13]. Anyway, the grid connection of the turbine was previously studied in laboratory [4, 36]. Many tests were done with several PV inverters for grid connection. The operating point of the turbine was previously well characterized. The only doubt was the losses associated with the curve and the longer length of the draft tube. In order to obtain the maximum power curve available on site, tests were carried out with the turbine already installed in the Silk House’s gallery. The tests were carried out with the generator 60R110-4S-3P-S-HP [13], connected to a variable resistance and with the maximum available head (5 meters). The results are shown in Fig. 11. The current and voltage values correspond to the average of five measurements. From the analysis of the figure, as verified with the water wheel, the power curve is quite flat around the maximum power point, and with some oscillation. Also here, this makes the search for the maximum power point in a wide voltage range. By analyzing the graph of Fig. 11, it is possible to verify that, for a power variation of less than 4%, the voltage can vary, approximately, in the range of 125 to 190V.

14 Vicente Leite

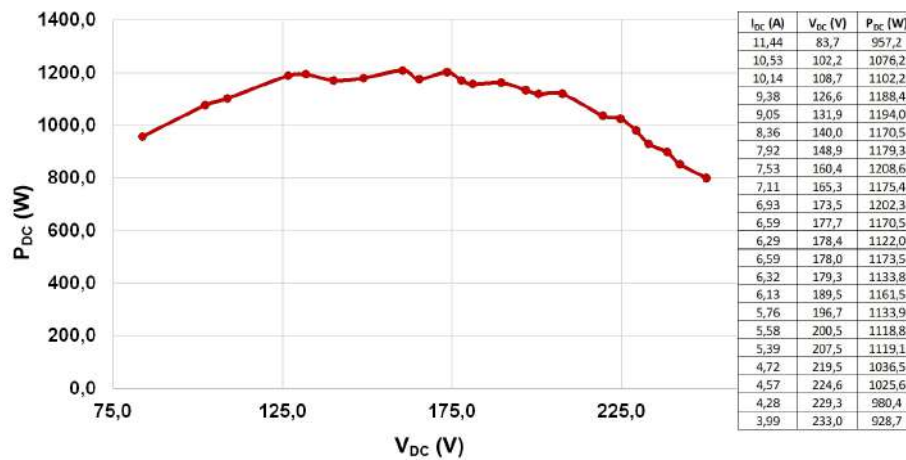


Fig. 11. P-V curve of the LH turbine with variable power resistor.

For the connection of the LH400 turbine to the microgrid, the PV inverter Solax X1-1.5 was used, which technical characteristics are shown in Table 3. Its MPPT voltage range is 70 to 380 V, which means it covers the operating voltage range of the LH400 turbine generator shown in Fig. 11. The open circuit average voltage is 390 V. As this value is very close to the maximum DC input voltage of the PV inverter (400V), an over-voltage protection circuit was used, which limits the voltage to 350 V. This prevents the PV inverter from being damaged, in case it goes out of operation. It can happen, for example, when the utility grid fails, until the microgrid starts operating in islanded mode. This transition takes only 5 to 7 seconds, but the PV inverter, typically, takes more than a minute to reconnect to the microgrid.

5 Description of the implemented microgrid

A general diagram of the microgrid implemented in the House of Silk is presented in Fig. 12. Figure 13 shows some photos of the galleries taken from the upper floors of the House of Silk. The photos on the left and center show the lower gallery, where pico-hydro turbines are installed. On the right is the upper gallery where the microgrid is installed. Both windows on the floors existed before the project was started.

The microgrid was designed for these spaces and the original three-phase electrical system (400V, 50Hz) with a contracted power of 13.8 kW. It is based on the SMA Flexible Storage System with battery-backup and increased of self-consumption [37, 38].

General description. It is a smart microgrid connected to the utility grid and integrates PV and pico-hydro generation, energy storage with a battery bank,

energy consumption of electric loads, power control, energy management and monitoring. It is based on three Sunny Island 4.4M battery inverters in a master-slave configuration to establish a three-phase system. PV generation consists of three PV strings connected to different phases using three Sunny Boy 1.5 PV inverters, which are compatible with the power control by frequency required for limiting of their active power [12]. Each PV string consists of six VBHN325SJ47 PV modules from Panasonic. Hydro generation is based on an horizontal water wheel designed on demand and one LH400 low-head turbine from PowerSpout, as described before. These two pico-hydro turbines were connected to the microgrid using the PV inverters Solis-mini-7 and Solax X1-1, respectively. The later requires an over-voltage protection circuit [4, 36]. It was used the power clamp and air resistor AC4-350/400 from PowerSpout. The energy storage system consists of twenty-four VRLA 2 V Sonnenschein Solar A602/625 blocks and a battery fuse box for protection. Control and monitoring is based on the Sunny Home Manager 2.0 and Sunny Portal. An automatic transfer switch, as shown in Fig. 12, is required to disconnect the utility grid and the microgrid operates in off-grid mode.

As for operation, the microgrid is the utility grid whenever it is available. In case of utility grid failure, the microgrid is formed by the three Sunny Island connected in a master-slave configuration. The automatic transfer switch disconnects the utility grid in case of grid failure. Then, in 5 to 7 seconds the microgrid starts the operation in islanded mode. Now, generated energy - PV and hydro - is injected into the microgrid. If the generation is higher than the consumption, the excess of energy is stored in the battery bank. If the generation is less than the consumption the batteries provide the necessary energy. When the state of charge of the batteries is less than a pre-defined value, the microgrid goes into standby mode. When the utility grid is available again, and connection requirements are accomplished, the utility grid is reconnected.

Sunny Island inverters use the battery bank to control the power flow and improve self-consumption [12, 40]. The active power generated by the PV inverters is limited by frequency control [37]. There is no power limitation in the case of inverters connected to the pico-hydro turbines.

Energy management and monitoring. The operation of the microgrid can be monitored remotely, by analysing several data and graphs obtained through Sunny Portal. Errors, alerts and operation reports are also available. The monitoring includes several features such as: system overview; current state; prognosis and recommendations; energetic balance; system diary; daily and monthly system reports; overview of each device. The system overview also includes many information: current PV power, consumption, battery and system status, and generated PV energy, among other information.

The power control and energy management is carried on by Sunny Island battery inverters and Sunny Home Manager (SHM). The SHM is a central energy manager for self-consumption systems with PV generation [39]. It gives an overview of all relevant power flows in the House of Silk and optimizes the gener-

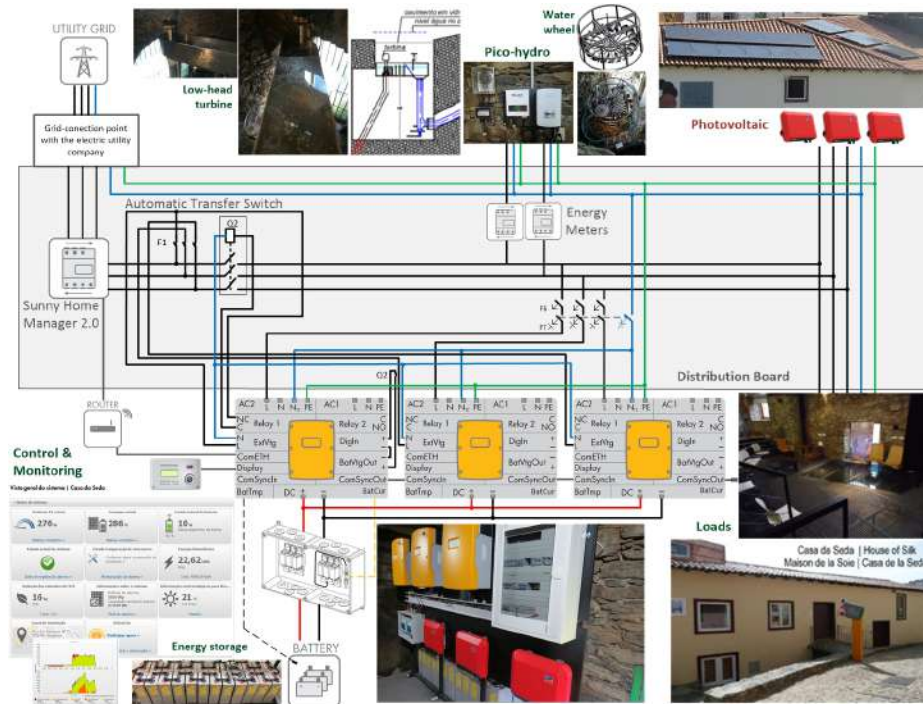


Fig. 12. Illustration of the microgrid implemented in the House of Silk.

ation self-consumption. SHM has an integrated measuring device and measures the energy flow at the grid-connection point. It measures the PV generation power, purchased electricity and grid feed-in. The PV generation data is given directly by the three connected PV inverters. If the PV generation power is higher than loads' power, SHM uses this excess of active power to charge the battery bank. But if, even so, the PV power is excessive, it performs the dynamic limiting of the active power feed-in. This enables the microgrid to limit the active power fed into the utility grid to a fixed limit or a percentage of the installed PV power. SHM monitors the active power injected into the utility grid. If the active power feed-in exceeds the prescribed limit, it limits the PV generation of the inverters accordingly [38]. This is possible with PV inverters from SMA as it happens with the PV generation in the House of Silk. However, the hydro generation systems - the LH turbine and water wheel - are connected to the microgrid through PV inverters from other manufacturers. In these hybrid systems, with SMA inverters and inverters from other manufacturers, the generation meter should measure the joint power of all inverters taken together. Thus, monitoring of the PV system and the dynamic limitation of the active power fed into the utility grid would not be possible with inverters from other manufacturers [39]. On the other hand, two of the five inverters in the House of Silk, are connected to the pico-hydro turbines, not to PV strings. Therefore, limiting of their active



Fig. 13. House of Silk galleries seen from the upper floors.

power is not like in PV generation, since the energy excess must be dissipated anyway. By this reason, the three PV string inverters are directly connected to the three phases and dynamic limiting of the active power is possible. After limiting the PV power to zero, excess power from the two hydro (PV) inverters is preferably used to charge the batteries. If the power is still excessive, it is injected into the utility grid, but for free.

6 Results and discussion

The smart microgrid with PV generation is in operation since July 31, 2019 [12]. The low-head propeller turbine started its normal operation on February 14, 2020 and was operating continuously until on March 23 when it was stopped because the House of Silk museum was temporarily closed due to the COVID-19 pandemic. The water wheel was finished later, on July 7, 2020. Several tests have already been carried out but normal operation (24 hours a day) will only be possible from autumn, when the river starts to have water enough. The turbine, which needs a higher water flow, will also start working again at that time.

The results of the LH turbine connected to the microgrid with Solax X1-1.5 PV inverter and the over-voltage protection circuit are shown in Fig. 14. The current and voltage values correspond to the average of five measurements. The test was carried out on August 21, 2020. Initially, the over-voltage protection circuit limited the DC voltage, before the PV inverter started to inject energy into the grid. The time elapsed between consecutive measurements was not constant.

The operation of the turbine was monitored for about one hour after starting until achieve the MPP. As it was expectable, around this value, the power curve is quite flat. Thus, it can be seen that, for a power variation of less than 4,2%, the voltage vary from about 137 V to 189 V and current from 6 to 8.6 A. By observing in loco the operation of the turbine, it was possible to verify that the operating point oscillates in the range of 150-160 V.

The observation of the water wheel operation, when connected to the microgrid through the Solis700 PV inverter, gave similar results, as shown in Fig. 15.

18 Vicente Leite

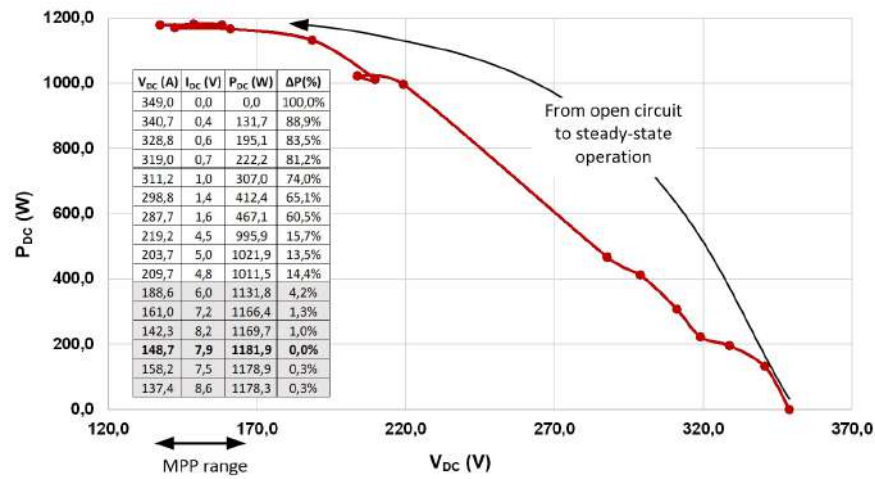


Fig. 14. P-V curve of LH turbine connected to the microgrid with Solax X1-1.5 PV inverter and the over-voltage protection circuit.

This test was carried out on September 7, 2020. In this case, the power varies between 147 W and 156 W. The average value is about 153 W. The generator’s DC voltage fluctuated between about 55 V and 65 V. It is worth noting that this variation is within the MPPT range of the PV inverter, which is 50-400 V, according to Table 3.

Monitoring the hydro generation is not straightforward because the inverters are not from SMA company and do not have power control by frequency. Even if they did, it would not be so advantageous because the turbines would have to dissipate the power generated, in order to avoid operating under no load. Anyway, indirect monitoring of the hydro generation is possible using the energy balance given by the Sunny Home Manager 2.0 and Sunny Portal. Figure 16 shows the energy balance of March 23, 2020, when the LH turbine was stopped and Fig. 17 shows the energy balance of September 7, when tests were carried out with the water wheel. By analyzing both diagrams, the influence of the power generated by the turbines can be verified. When the LH turbine was stopped, on March 23 (Fig. 16), the House of Silk was already temporarily closed. Therefore, the battery bank was fully charged and the excess energy was being injected into the utility grid. After stopping the turbine, the loads started to be supplied with energy from batteries and PV generation, as can be seen in Fig. 16. At that time, there was no energy consumption from the utility grid.

September 7 was a Monday. The day was chosen because the museum closes on Mondays and in the early afternoon the batteries were already charged. Thus, from Fig. 17, it is possible to monitor the generation of the water wheel in the portal, despite the low power generated. By this time of the year, the LH turbine cannot operate for more than 1 to 2 hours, otherwise, the water level in the small dam would drop too much.

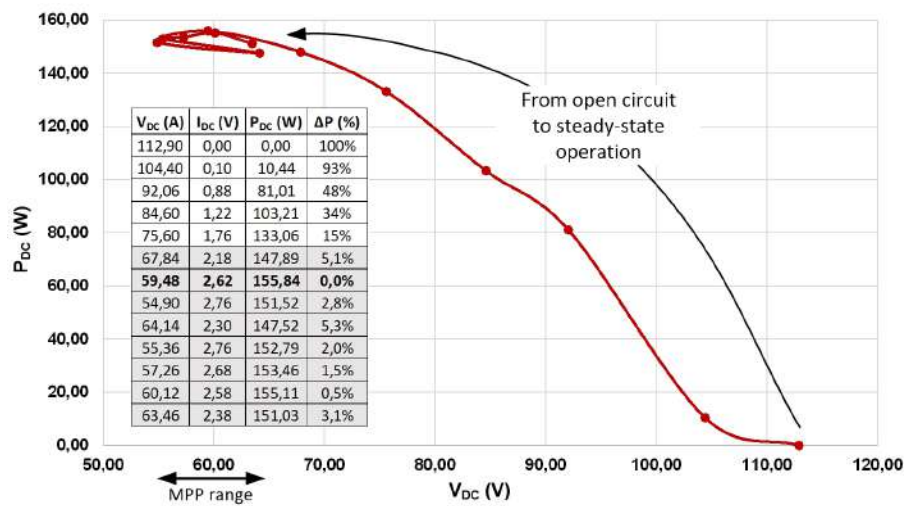


Fig. 15. P-V curve of water wheel connected to the microgrid with Solis700 PV inverter.

Table 4 shows the total and specific yield for a full year of PV generation. PV yield is far from the expected 1500 kWh/kWp for two reasons. First, the museum is awaiting for the authorization of energy injection into the utility grid. Because of this, energy injection into the utility grid is being limited to zero. In any case, if it is excessive, it is inevitably injected into the utility grid. Second, the museum was closed from March 16 to April 7 due to the pandemic. Thus, the PV generation was automatically limited. Moreover, it was even canceled, during the period of operation of the turbine, as can be seen in Fig. 16, during the day of March 23.

Table 4. Total and specific yield for a full year of PV generation.

2019				2020								Total first year
Sep	Oct	Nov	Dec	Jan	Feb	Mar	Apr	May	Jun	Jul	Aug	
504.4	446.0	266.1	188.7	238.0	363.1	223.8	406.6	297.2	542.8	612.8	659.0	4748 kWh
86.2	76.2	45.5	32.3	40.7	62.1	38.3	69.5	50.8	92.8	104.8	112.6	812 kWh/W _p

Table 5 shows the energy balance since the microgrid first commissioning on July 31, 2019, until September 9, 2020. From the analysis of Table 5, the autonomy rate is 52% and the direct consumption quota is 72%. These values will improve significantly with hydro generation, during the winter months, and

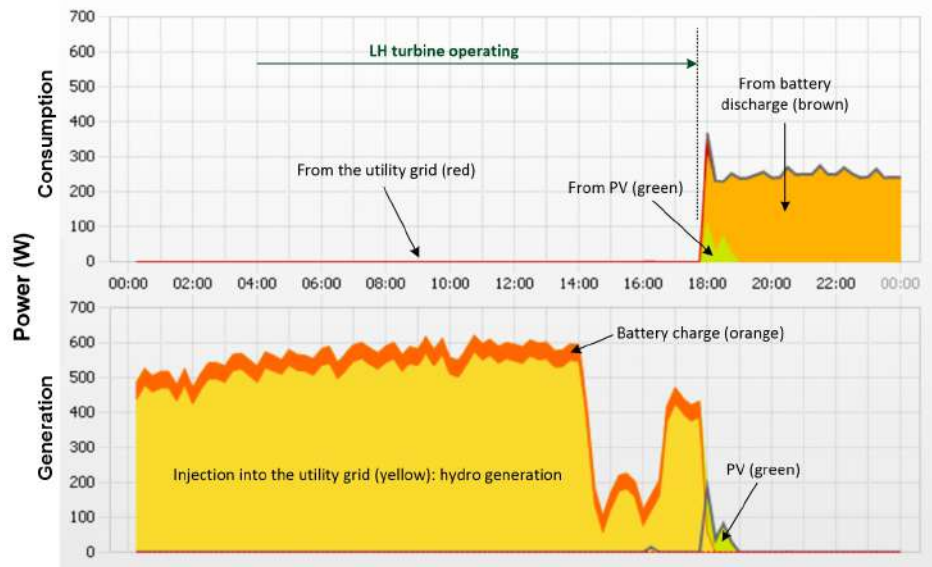


Fig. 16. Energy balance of March 23, 2020, when the LH turbine was stopped.

with the injection of energy into the utility grid. This is going to happen after the authorization of energy injection into the utility grid, even for free.

According to Table 1, the annual consumption (2014-2016) was 16271 kWh. During last year, from September 2019 to August 2020, the energy consumption from the utility grid was 4939 kWh. This means that utility grid consumption has dropped more than 2/3. During the winter months, hydro generation is expected to give an important contribution to reduce the consumption from the utility grid. After the authorization of energy injection into the utility grid, the House of Silk will be a sustainable museum in terms of electricity balance.

Table 5. Full energy balance (kWh), from July 31, 2019, to September 9, 2020.

Consumption	10371.55	Generation	5477.17
From the utility grid	5036.37	Direct consumption	3952.17
Battery discharge	1426.63	Battery charge	2188.95
Direct consumption	3952.17	Injection into the utility grid	146.76
Autonomy rate	52%	Direct consumption quota	72%

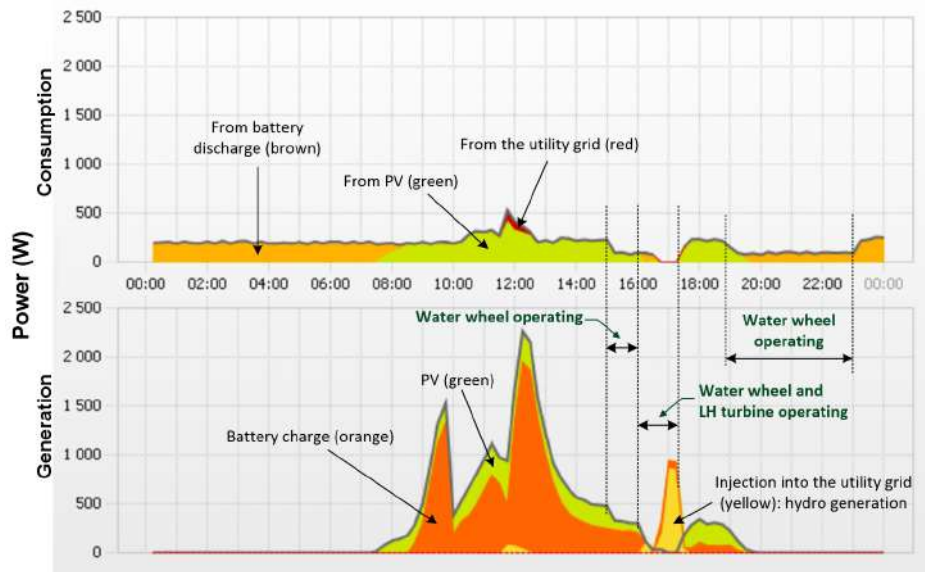


Fig. 17. Energy balance of September 7 when tests were carried out with the water wheel.

7 Conclusions

This paper presented a smart microgrid integrating two small-scale hydro systems: a low-head propeller turbine and an horizontal water wheel. It was implemented in the House of Silk (Casa da Seda), a small museum dedicated to science dissemination, integrated in the Bragança Ciência Viva Centre, located in Bragança, Portugal. This work was carried out under the project SilkHouse, funded by the Portuguese Foundation of Science and Technology. The project was aimed to transform the Silk House in a self-sustainable museum, in annual average terms, and contribute to the dissemination of renewable sources and new technologies for future buildings in smart cities.

The microgrid is based on the SMA Flexible Storage System with battery-backup with increased self-consumption. It is the museum's power system and integrates renewable generation and consumption (museum loads), energy storage in a battery bank, power control and energy management. It is connected to the utility grid and can operate in both grid-connected and islanded modes. The power control and energy management are carried out by the SMA Sunny Island battery inverters and Sunny Home Manager.

Power generation is achieved from two renewable sources available on site: solar photovoltaic and hydro. Taking advantage of Fervença river and an existing small dam, two pico-hydro turbines have been installed in a House of Silk gallery, where there was a mill. The two pico-hydro turbines are based on the low-

22 Vicente Leite

head propeller turbine LH400, from PowerSpout, and an horizontal water wheel manufactured on demand.

The LH400 turbine generates a maximum DC power of 1200 W for a head of 5 m and about 55 l/s. It was connected to the microgrid using an over-voltage protection circuit and the Solax 700 PV inverter.

The horizontal water wheel aims to recover the historical heritage of a former mill. It was manufactured on demand and is connected to the microgrid using the Solis 700 PV inverter with no need of over-voltage protection circuit. It operates as a grid connected very small-scale hydro turbine generating a maximum DC power of 160 W.

Further developments. According to the results obtained, when connecting hydro generators to the utility grid using PV inverters, it is important to investigate their operation in constant voltage mode, thus canceling the MPPT algorithm. After identifying the maximum power point and the corresponding DC voltage, with the tests performed, the PV inverter can be parameterized with this voltage value and starts to extract the maximum power, with constant voltage. However, many photovoltaic inverters may not have this functionality.

It is important to carry on additional tests using other PV inverters, with higher maximum input voltage, to connect the propeller turbine to the grid. The objective is to avoid the need of the over-voltage protection circuit.

As initially planned, the Municipality of Bragança will make an intervention in the galleries to improve the thermal and acoustic insulation.

Acknowledgments

The author would like to thank FCT (Foundation of Science and Technology, Portugal) for the financial support through the contract SACT-POL/24376/2016 (POCI-01-0145-FEDER-024376); Municipality of Bragança and Polytechnic Institute of Bragança for their support; and Bragança Ciência Viva Centre (BCCV) for the partnership in this project. Special thanks to Ivone Fachada and Estefânia Gonçalves of BCCV for their collaboration.

The author would also like to thank the following students for their contribution to the development of the project: Wellington Maidana, Paulo Araújo, Luís Figueiredo, Isabella Scotta, Gabriela Ribeiro, Iago Dalmarco, Henrique Quaresma and Marina Pietrobelli. Many thanks to colleagues Luís Queijo, Rui Oliveira, Ângela Ferreira for their collaboration and also to Vitor Gomes, José Batista, Abílio Marcelo and Jorge Paulo for their technical support.

References

1. IRENA: Global Energy Transformation: A roadmap to 2050, 2019 edn., International Renewable Energy Agency, Abu Dhabi (2019).

2. BP: Statistical Review of World Energy 2020. 69th edn., <http://www.bp.com/content/dam/bp/business-sites/en/global/corporate/pdfs/energy-economics/statistical-review/bp-stats-review-2020-full-report.pdf>. Last accessed 28 Jul 2020.
3. European Commission, <https://ec.europa.eu/info/research-and-innovation/research-area/energy-research-and-innovation/hydropower>. Last accessed 28 Jul 2020.
4. Leite, V., Ferreira, A., Couto, J., Batista, J.: Compatibility analysis of grid-connected pico-hydro systems using conventional photovoltaic inverters. In: 18th European Conference on Power Electronics and Applications (EPE), pp. 1–9, Karlsruhe, Germany (2016).
5. Basar, M.F., Ahmad, A., Hasim, N. Sopian, K.: Introduction to the pico hydro power and the status of implementation in Malaysia. In: IEEE Student Conference on Research and Development, pp. 283–288 (2011).
6. Tecnoturbines: Tecnoturbines powering water, <https://tecnoturbines.com/portfolio/comunidad-de-regantes-de-casinos-espana>. Last accessed 19 Aug 2020.
7. IEA: Small-scale hydro within a municipal water supply system. International Energy Agency. <https://sswm.info/node/4341>. Last accessed 19 Aug 2020.
8. Yadav, G. and Chauhan, A.K.: Design and Development of Pico Micro Hydro System by Using House Hold Water Supply. International Journal of Research in Engineering and Technology, Vol. 3, Special Issue 10, pp. 114–119, Jun 2014.
9. Ribeiro, G., Silva, W., Leite, V., Ferreira, A.: Grid Connection Approach for Very Small-Scale Pico-Hydro Systems Using PV Microinverters. In: 45th Annual Conference of the IEEE Industrial Electronics Society (IECON), Lisbon, Portugal (2019).
10. Scotta, I., Silva, W., Leite, V.: Over-voltage protection circuit for grid-connected pico-hydro generation using photovoltaic inverters, Revista Facultad de Ingeniería Universidad de Antioquia, <https://revistas.udea.edu.co/index.php/ingenieria/article/view/340689>.
11. Guerrero, J., Blaabjerg, F., Zhelev, T., Hemmes, K., Monmasson, E., Jemei, S., Comech, M., Granadino, R., Frau, J.: Distributed Generation: Toward a New Energy Paradigm. IEEE Industrial Electronics Magazine, Vol. 4, Issue 1, pp. 52–64 (2010).
12. Figueiredo, L.G., Maidana, W., Leite, V.: Implementation of a smart microgrid in a small museum: the Silk House. Springer Communications in Computer and Information Science book series, CCIS, Vol. 1152 (2020).
13. PowerSpout: Low Head Turbine Installation Manual, Sep 2015.
14. Dalmarco, I.: Conceção, fabrico e caracterização de plataforma para testes de um modelo de roda de água horizontal para a Casa da Seda. Master dissertation. Polytechnic Institute of Bragança, 2018.
15. Paish, O., 2002. Small hydro power: technology and current status. Renewable and Sustainable Energy Reviews 6, 537–556 (2002).
16. Sopian, K. and Razak, J.: Pico hydro: Clean power from small streams. 3rd WSEAS Int. Conf. on Renewable Energy Sources, pp. 414-419 (2009).
17. Pujol, T., Vashisht, A.K., Ricart, J., Culubret, D., Velayos, J.: Hydraulic efficiency of horizontal waterwheels: Laboratory data and CFD study for upgrading a western Himalayan watermill. Renewable Energy Vol. 83, pp. 576-586 (2015).
18. Leite, V., Figueiredo, T., Pinheiro, T., Ferreira, A., Batista, J.: Dealing with the Very Small: First Steps of a Picohydro Demonstration Project in an University Campus. In: International Conference on Renewable Energies and Power Quality (ICREPQ), (2012).
19. EC: Photovoltaic Geographical Information System (PVGIS). European Commission. https://re.jrc.ec.europa.eu/pvg_tools/en/#PVP. Last accessed August 2020.

24 Vicente Leite

20. Maidana, W., Leite, V., Ferreira, A., Queijo, L., Batista, J., Bonaldo, J., Golnçalves, E.: Design of a Self-sustainable System Based on Renewable Energy Sources for a Small Museum of Science Dissemination - the House of Silk. In: III Congresso Ibero-Americano de Empreendedorismo, Energia, Ambiente e Tecnologia, pp. 12-14, Bragança, Portugal (2017).
21. GNB: Handbook for Stationary Gel-VRLA Batteries. Part 2: Installation, Commissioning and Operation, edn. 17, GNB Industrial Power, 2012.
22. Molina, M., Pacas, M.: Improved power conditioning system of microhydro power plant for distributed generation applications. In: International Conference on Industrial Technology (ICIT), pp. 1733–1738 (2010).
23. Hofmeister, J., Krebs, S., Schickhuber, G., Scharfenberg, G.: Design and development of a pico hydro turbine system for the use in developing countries. In: 5th International Youth Conference on Energy (IYCE), pp. 1–7 (2015)
24. Anilkumar, T.T, Simon, S.P., Padhy, N.P.: Residential electricity cost minimization model through open well-pico turbine pumped storage system. Elsevier, Applied Energy, Vol. 195, pp. 23–35 (2017).
25. Koirala, N., Dhakal, R., Lubitz, D., Bhandari, S., Dev, G.P., Dhakal, Y., Uttam Niraula, U.: Review of Low Head Turbines System of Nepal for Rural Electrification. In: 6th International Conference on Renewable Energy Research and Applications (ICRERA), pp. 861–869 (2017).
26. Kerdtuad, P., Simma, T., Chaiamarit, K., Visawaphatradhanadhorn, S.: Establishment of a Pico Hydro Power Plant Using Permanent Magnet Synchronous Generator Supplied for AC Microgrid. In: 44th Annual Conference of the IEEE Industrial Electronics Society (IECON) (2018).
27. Powell, D., Ebrahimi, A., Nourbakhsh, S., Meshkaldini, M., Bilton, A.M.: Design of pico-hydro turbine generator systems for self-powered electrochemical water disinfection devices. Elsevier, Renewable Energy, Vol. 123, pp. 590–602 (2018).
28. Vasudevan, K.R., Ramachandaramurthy, V.K., Gomathi, V., Ekanayake, J.B., Tiong, S.K.: Modelling and simulation of variable speed pico hydel energy storage system for microgrid applications. Elsevier, Journal of Energy Storage, Vol. 24, pp. 1–14 (2019).
29. Titus, J., Ayalur, B.: Design and Fabrication of In-line Turbine for Pico Hydro Energy Recovery in Treated Sewage Water Distribution Line. Elsevier, Energy Procedia, 156, pp. 133–138 (2019).
30. Pali, B.S., Vadhera, S.: An Innovative Continuous Power Generation System Comprising of Wind Energy along with Pumped-Hydro Storage and Open Well. IEEE Transactions on Sustainable Energy, Vol. 11, N° 1, pp. 145–153 (2020).
31. Quaranta, E., Revelli, R.: Performance characteristics, power losses and mechanical power estimation for a breastshot water wheel. Elsevier, Energy, Vol. 87, No.1, pp. 315–325 (2015).
32. Helmizar: Turbine wheel - a hydropower converter for head differences between 2.5 and 5 m. Ph.D Thesis, University of Southampton, School of Civil Engineering and the Environment (20176).
33. Rynne, C.: The Technical Development of the Horizontal Water-Wheel in the First Millennium ad: Some Recent Archaeological Insights from Ireland. The International Journal for the History of Engineering and Technology, Vol. 85, No. 1, 70–93 (2015).
34. Quaranta, E.: Investigation and optimization of the performance of gravity water wheels. Ph.D Thesis, Politecnico di Torino (2017).
35. Quaranta, E.: Stream water wheels as renewable energy supply in flowing water: Theoretical considerations, performance assessment and design recommendations. Elsevier, Energy for Sustainable Development, Vol. 45, pp. 96–109 (2018).

Innovative Smart Microgrid Integrating Pico-hydro Systems 25

36. Leite, V., Couto, J., Ferreira, A., Batista, J.: A practical approach for grid-connected pico-hydro systems using conventional photovoltaic inverters. International Energy Conference (ENERGYCON), p.p. 1–6 (2016).
37. SMA: SMA Flexible storage system with battery-backup function – Planning Guidelines. <https://files.sma.de/downloads/SI-SBS-Backup-PL-en-26.pdf>. Last accessed 11 Sep 2020.
38. SMA: Guide SMA Flexible Storage System with Battery Backup Function – Installation - Quick Reference. <https://files.sma.de/dl/20472/Ersatzstrom-IS-en-33W.pdf>. Last accessed 11 Sep 2020.
39. SMA: Sunny Home Manager 2.0 – Operating Manual. <https://sol-distribution.com.au/SMA-Inverters/HM-20-BE-en-11.pdf>. Last accessed 11 Sep 2020.
40. SMA: Sunny Island 3.0M/4.4M/6.0H/8.0H and Sunny Remote Control – operating Manual. <https://files.sma.de/dl/17632/SI30M-44M-60H-80H-BE-en-33W.pdf>. Last accessed 11 Sep 2020

Economic Optimization of Photovoltaic Generation System with Hydrogen Storage

E. Alcover, R. Pujol-Nadal, V. Martínez-Moll, J.L. Rosselló and V. Canals

Department of Industrial Engineering and Construction, University of Balearic Islands, Palma,
Ctra. Valldemossa km 7.5, Campus UIB, Balearic Islands E-07122, Spain
enic.alcover@uib.cat, v.canals@uib.es

Abstract. This work aims to study the impact of the incorporation of a hydrogen-based storage system in grid-connected photovoltaic plants, located in a power-grid with low penetration of renewable sources. Consequently, a methodology is proposed as base of a numerical tool in charge to determine: the photovoltaic power generation every minute of PV plant and the cost of energy generated on a marginal market, such as the Iberian electricity system, model the generation of hydrogen by electrolysis of water, model its efficient storage and subsequent conversion back into electricity; using a proton exchange membrane (PEM) hydrogen fuel cell. The methodology evaluates a strategy for optimizing the energy flows of a PV plant in order to maximize the revenues of the property. Concretely, the methodology proposes to accumulate energy through the storage of hydrogen when the electricity market price, to then generate electricity through the fuel cell and sell it to the grid when the market price is higher. Finally, the methodology has been tested for a hypothetical 1 MW PV plant, located on the island of Mallorca, where less than 4 % of the installed generation power comes from renewable sources.

Keywords: Hydrogen storage, Fuel cells, Renewable energy, Solar energy, Photovoltaic systems.

1 Introduction

The current world electricity demand is still mostly covered by the combustion of fossil fuels in conventional plants (coal plants, CHP, ...). In turn, conventional electricity generation is one of the main sources of Greenhouse Gas (GHG) emissions worldwide, with the consequent environmental impacts and health problems related with these emissions [1]. As agreed in the United Nations Convention on Climate Change, 2015, held in Paris, this GHG emission should be reduced by 70% in 2050 compared to 2015. In order to tackle an energy transition of this magnitude, it will be necessary to develop a set of solutions ranging from power generation based on renewable sources (wind, photovoltaic, solar thermal ...), smart energy transport and storage. As part of a massive deployment of renewable energy, management of variability of solar and wind energy becomes a major issue, where the accumulation of energy is the key element, allowing displace generation in periods this is demanded, ie periods when

2

the market price of energy is higher. Among the various sources of renewable energy, photovoltaics is the one that has evolved over the last two decades [2], until today become a real alternative to conventional energy sources. However, its generation is characterized by a non-dispatchable and variable energy supply in time, due to the intermittency of the solar resource. In this scenario, the production of hydrogen by electrolysis and its accumulation can bring new capabilities to the PV plants, because the hydrogen can take different roles in the energy field, either as fuel for burning in combination with natural gas [3] or energy storage element for subsequent conversion into electric power by a fuel cell [4].

The methodology proposed in this work analyzes the impact would entail the incorporation of a storage system based on hydrogen in grid-connected photovoltaic systems, located in electrical networks partially isolated and low penetration of renewable energy. Specifically, the methodology states that when there is excess generation in a PV park or the market price is very low, the electrolyzer uses this energy to produce hydrogen, and when the market price of energy is adequate, the stored energy as hydrogen it can be used in a fuel cell to generate electricity again. Consequently, the combination of PV generation with accumulation in a photovoltaic park would make production more flexible, thus enabling optimal plant management based on the electricity market and demand. Although the use of hydrogen as an energy vector shows great potential to solve the variability of some of the renewable energy sources, in turn, there are important barriers that, a priori, prevent the widespread use of this technology. Such as the need for transport and distribution infrastructures in its immeasures (gas pipelines) and the cost of hydrogen storage technologies.

Finally, the proposed methodology is applied to analyze the operation of a 1MW photovoltaic plant located in Mallorca (Balearic Islands, Spain), where the energy produced by the photovoltaic plant can be injected into the electricity grid or released to the hydrogen plant depending on the market price of the electric power.

2 Materials and Methods

The proposed methodology focuses on analyzing the impact that the incorporation of a hydrogen-based storage system in photovoltaic plants connected to the grid would entail. The methodology has been implemented as a numerical tool in MATLAB®. In turn, this tool consists of five submodules, Fig 1, that implement specific parts of the developed methodology and incorporates a Monte Carlo algorithm in its nucleus, which allows a minute simulation minute generation PV, generation and accumulation H₂ for a time series of ten or more repetitions of the reference year (2017); from which the meteorological data and the marginal hourly price of electricity will be taken. Each of the sub-modules is presented below:

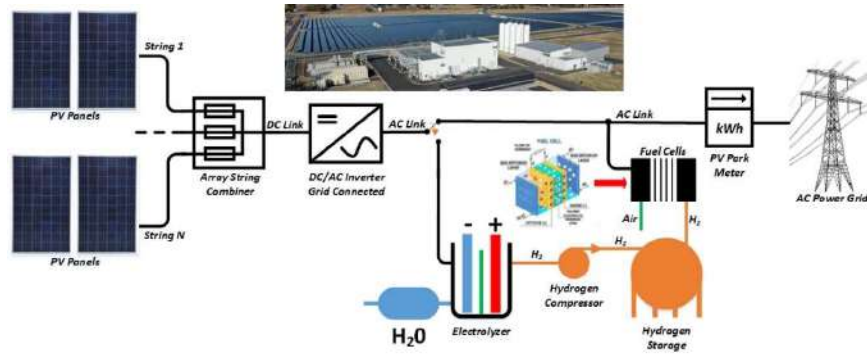


Fig. 1. Architecture of the PV plant with H₂ accumulation considered by the methodology

2.1 A Subsection Sample

In order to estimate the power output that can be generated in a PV park, it is indispensable to have a tool that simulates, from the characteristics of the solar park and the meteorological conditions of the facility's location, the energy generation at each given time interval during an evaluation period of at least one year. In the present work, the authors have developed a tool based on MATLAB[®] that is in charge of simulating the electrical generation, minute by minute, of a given PV park.

In order to obtain accurate results, it is essential to have quality meteorological data of the location or a nearby meteorological station, in this case it is obtained from the *Agencia Estatal de Meteorología* (AEMET) [5]. It is necessary to have the hourly global solar irradiance (*DGI*), the hourly diffuse solar irradiance (*DHI*) and the hourly direct normal irradiance (*DNI*), and also the ambient temperature from the reference year. This hourly radiation data is then converted to minute radiation, interpolating the missing values and using a random number generator based on the beta distribution, that simulates the presence of clouds along the day. Then the interpolated values are normalized to the hourly radiation detected by the AEMET sensors. The minute temperature values are also interpolated from hourly data and multiplied by a Gaussian based random number in order to simulate the fluctuations of the ambient temperature and then, obtain a minute temperature profile.

It is also fundamental to know the exact position of the sun along the year in order to calculate the amount of radiation that is reaching the oriented surface of the different photovoltaic modules that conform the PV installation. This is being calculated using the algorithm of the *Plataforma Solar de Almería* (PSA) [6]. This algorithm calculates the different sun angles (azimuth, declination, zenith angle and elevation) from the location and the date, in UTC, with high precision and huge computational efficiency.

The amount of irradiation (global and diffuse) reaching each panel depends on the slope and the azimuth of the panels and the sun coordinates. The direct irradiance over

4

the panel (ID) is calculated from the cosines of the panel normal angle respect the surface and the sun position, using the following equations:

$$\begin{aligned}
 \cos \gamma &= A + B + C + D + E \\
 A &= \sin \delta \cdot \sin \psi \cdot \cos \beta \\
 B &= -\sin \delta \cdot \cos \psi \cdot \sin \beta \cdot \cos \alpha \\
 C &= \cos \delta \cdot \cos \psi \cdot \cos \beta \cdot \cos h \\
 D &= \cos \delta \cdot \sin \psi \cdot \sin \beta \cdot \cos \alpha \cdot \cos h \\
 E &= \cos \delta \cdot \sin \beta \cdot \sin \alpha \cdot \sin h
 \end{aligned} \tag{1}$$

Where α is the panel azimuth, β is the panel slope, δ is the solar declination, ψ is the latitude and h is the solar angle. Then, the direct radiation reaching the panel surface is obtained by:

$$ID = DNI \cdot \cos \gamma \tag{2}$$

The total sky diffuse irradiance received by a surface tilted from the horizontal (ID_{if}) is calculated using the Perez model [7] that is based on the representation of the sky dome as anisotropic background superimposing a circumsolar and horizon effects.

$$ID_{if} = DHI \cdot [(1 - F1) \cdot \frac{(1 + \cos \beta)}{2} + F1 \cdot \frac{a}{b} + F2 \sin \beta] \tag{3}$$

Where $F1$ and $F2$ are coefficients expressing the degree of circumsolar and horizontal anisotropy respectively. The terms “ a ” and “ b ” are defined as:

$$\begin{aligned}
 a &= \max(0, \cos \gamma) \\
 b &= \max(0.087, \cos Z)
 \end{aligned} \tag{4}$$

The brightening coefficients $F1$ and $F2$ are modelled with a set of coefficients validated by data from different places on the world, the sun elevation and the air optical mass. This set of coefficients stored in a text file (*.csv), are read by the software and the following formula is applied:

$$\begin{aligned}
 F1 &= F11 + F12 \cdot \Delta + F13 \cdot Z \\
 F2 &= F21 + F22 \cdot \Delta + F23 \cdot Z
 \end{aligned} \tag{5}$$

Where $F11, F12, F13, F21, F22, F23$ are the Perez coefficients, Z is the azimuth and Δ is the optical path length (related to the optical mass).

Another factor that changes the amount of irradiance that can be used by the photovoltaic panel for generating electricity is the amount of this irradiance that is reflected by the protective cover. These effects can be significant for incidence angles greater than 65° . The effect of the absorption and reflection of radiation in function of the incident angle is expressed in function of the Incidence Angle Modifier (IAM), that is described as the ratio between the radiation absorbed by the panel at any incidence angle ($\tau(\gamma)$) divided by the absorption at normal incidence ($\tau(0)$).

$$IAM(\gamma) = \frac{\tau(\gamma)}{\tau(0)} \quad (6)$$

The absorption is also dependent on the glazing extinction coefficient (K) and the glazing thickness (L) that are read from a text file (*.csv) with descriptor of each panel/module. A good approximation of the transmission for the covering system, considering reflective losses and absorption inside the glass is:

$$\tau(\gamma) = e^{-\left(\frac{KL}{\cos r}\right)} \left[1 - \frac{1}{2} \left(\frac{\sin^2(\gamma_r - \gamma)}{\sin^2(\gamma_r + \gamma)} + \frac{\tan^2(\gamma_r - \gamma)}{\tan^2(\gamma_r + \gamma)} \right) \right] \quad (7)$$

And the angle of refraction is calculated using the Snell law as following expression:

$$\gamma_r = \arcsin(n \sin \gamma) \quad (8)$$

Where “ n ” is an effective index of refraction of the panel cover. A value of 4 m^{-1} for the extinction coefficient is reasonable for “water white” glass and a value of about 0.002 m is reasonable for most glass covered PV panels and, for the case of glass, n is 1.526.

The calculated IAM changes the amount of direct irradiance that is absorbed by the panel, and the effective direct irradiance absorbed by the photovoltaic panel is:

$$ID_{ef} = ID \cdot IAM(\gamma) \quad (9)$$

Finally, the total irradiance (IG) over the photovoltaic module is going to be the sum of the two components, the direct (ID_{ef}) and the diffusive ($IDif$), as is seen in the following expression:

$$IG = ID_{ef} + IDif \quad (10)$$

For a more accurate estimation on the power generated by each photovoltaic panel/module, is necessary to take into account the temperature effects, in this work the Sandia model [8] is implemented. This model takes into account two different ways of mounting the photovoltaic installation: roof mounting or open rack mounting. The type of mounting must be the same for all the installation modules/panels, because it is defined at the main descriptor of the software (at initialization file “init.xml”).

A thermal model based in local environmental conditions is required in order to predict the energy production of the modules. In this case we are using the data from the AEMET for calculating the cell temperature from an empirically-based thermal model developed by Sandia [9]. It is proved to be an adequate model for the photovoltaic systems with an accuracy of about $\pm 5^\circ\text{C}$ that results in less than 3% effect on power output.

$$T_m = E \cdot (e^{a+b \cdot WS}) + T_a \quad (11)$$

Where, T_m is the back-surface module temperature ($^\circ\text{C}$), T_a is the ambient air temperature ($^\circ\text{C}$), E is the solar irradiance on model surface (W/m^2), WS is the wind speed (m/s), “ a ” is an empirically-determined coefficient establishing the upper limit for mod-

6

ule temperature at low wind speeds and high solar irradiance, finally, “*b*” is an empirically determined coefficient establishing the rate at which module temperature drops as wind speed increases. The empirical coefficients “*a*” and “*b*” are found to be representatives of different mounting configuration and module type. In our tool is considered only one glass module type and two different mounting configurations, Table 1, open rack and roof mounting.

Table 1. PV panels mounting configuration parameters

Mounting configuration	<i>a</i>	<i>b</i>	ΔT (°C)
Open rack	-3.47	-0.0594	3
Roof mount	-2.98	-0.0471	1

The cell temperature can be related to the module back surface temperature through a simple relationship, based on the assumption of one-dimensional thermal heat conduction through the module materials behind the cell. It is then calculated as follows:

$$T_c = T_m + \frac{E}{E_0} \cdot \Delta T \tag{12}$$

Where *T_c* is the cell temperature (°C), *T_m* is the calculated back-surface temperature (°C), *E₀* is the reference solar irradiance on module (1000 W/m²). The increment on the cell temperature decreases the voltage generated by the solar cell, so the DC power generated will be lower as the temperature increases. The efficiency is assumed to decrease at linear rate as a function of temperature rise, governed by a temperature coefficient *γ* (%/°C) that depends on the cell model.

$$P_{dc} = \frac{I_{tr}}{1000} \cdot P_{dc0} \cdot \left(1 + \gamma \cdot (T_c - T_{ref}) \right) \tag{13}$$

Where *P_{dc}* is the power generated in Watts, the *I_{tr}* is the transmitted irradiance and *T_{ref}* is the reference temperature of 25°C.

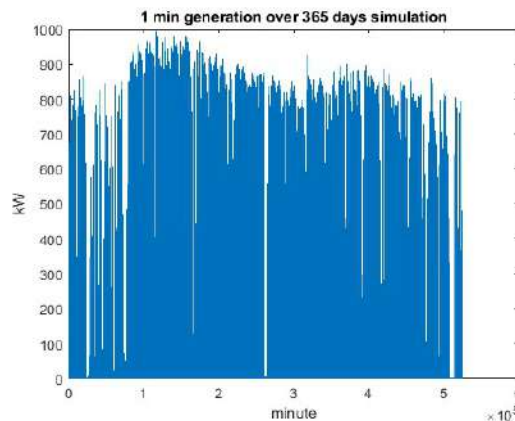
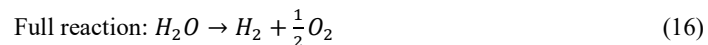
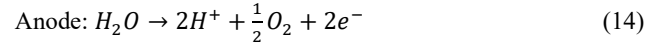


Fig. 2. Minute by minute power generated by a 1MW PV plant.

Finally, the power generated by each panel has to be ordered in an array of panels that are then connected to the inverter, Fig.2. The system also takes into account the resistivity of the wires and the losses due to the DC/AC conversion before obtaining the final power output (P_{AC}).

2.2 Hydrogen Generation by Electrolysis

The electrolysis of water is defined as the decomposition of water into oxygen (O_2) and hydrogen (H_2) gases by means of a continuous electric current connected to water by means of electrodes. This process, that has been widely studied by many authors, is already well known and, although there are different technologies that can be used, in the present work the Proton Exchange Membrane (PEM) electrolyser is proposed because of its capability of operate at high current densities, that can result in lower operational costs, mainly in systems coupled at dynamic sources as solar and wind. With PEM, water yields H^+ ions which cross a membrane to pick up electrons to become H atoms. The reaction taking place in the electrolyser can be explained as the sum of two half-cell reactions, on one side, the reaction taking place at the anode that is referred to as the Oxygen Evolution Reaction (OER), where the supplied water is oxidized to oxygen, protons and electrons; on the other side, the half-reaction taking place on the cathode is referred to as the Hydrogen Evolution Reaction (HER), where the supplied electrons and the protons that have traversed the membrane are combined to create hydrogen molecules in gaseous state [10].



These atoms then combine to make hydrogen molecules, this gas can be stored in tanks and be reconverted into electricity when there is a need of feeding the electric network, using a repowering unit such as a fuel cell or hydrogen gas turbine, that are technologies based on taking advantage of the following chemical reaction:



Energy can be converted into hydrogen by an electrolyser and stored for later use in a repowering unit such as a fuel cell or hydrogen gas turbine. Typical round-trip efficiency is around 40% ($\pm 70\%$ conversion efficiency from power to hydrogen and $\pm 60\%$ from hydrogen to power). The power required in order to obtain hydrogen by electrolysis is supplied by a set of photovoltaic panels, which make up what is known as the photovoltaic generator.

8

2.3 PEM electrolyzer

The amount of oxygen and hydrogen generated by the PEM electrolyzer can be evaluated by a simple model, that has been implemented in MATLAB. In the ideal case, the hydrogen production rate of an ideal electrolyzer is proportional to the charge transferred, according to the Faraday's law [11], can be expressed in $N \cdot m^3/h$ as:

$$f_{H_2} = \eta_f \cdot \frac{N_{Cell} \cdot I_{Cell}}{z \cdot F} \cdot \frac{22.41}{1000} \cdot 36000$$

$$f_{O_2} = \eta_f \cdot \frac{N_{Cell} \cdot I_{Cell}}{z \cdot F} \cdot \frac{17.36}{1000} \cdot 36000 \tag{18}$$

Where η_f is the faraday efficiency, defined as the ratio of ideal electric charge and the practical charge consumed by the device when a certain amount of hydrogen is generated, N_{Cell} is the number of cells in the PEM electrolyzer, I_{Cell} is the electric current, F is the Faraday's constant ($96,485 C \cdot mol^{-1}$) and "z" is the number of electron moles transferred, that per hydrogen mole is ($z = 2$) and for oxygen mole is ($z = 1$). Then, the specific energy consumption E ($kWh/N \cdot m^3$) for a given time interval Δt can be obtained by:

$$E = \frac{\int_0^{\Delta t} N_{cell} \cdot I_{cell} \cdot V_{cell} dt}{\int_0^{\Delta t} f_{H_2} dt} \tag{19}$$

Another important parameter that has to be determined is the electrolyzer efficiency, that represents the ratio between the energy contained in the hydrogen produced and the energy needed to electrolyze the water consumed during the process, it can be expressed as:

$$\eta_{EL} = \frac{HHV}{E} \cdot 100 \tag{20}$$

As seen in Table. 2, PEM technologies can modulate their power consumption easily, presenting a very huge hydrogen flow range (1-100%) making them very attractive for stabilizing power grids and delivering grid balancing or ancillary services, and for accumulating energy from a variable source as PV.

Table 2.

Number of cell stacks	10	Hydrogen flow range	1-100%
Nominal hydrogen flow	5000 Nm^3/h	Hydrogen purity	99.998%
Nominal input power	25 MW	Tap water consumption	<1.4 liters/ $N \cdot m^3 H_2$
AC power consumption	5.0-5.4 $kWh/N \cdot m^3$	Output Pressure	3MPa

2.4 Hydrogen Storage

In some cases, the power generated by renewable energy sources can be stored in order to balance its fluctuation and intermittence because of variable weather conditions[12]. Power-to-gas is a novel energy storage method that can also use the surplus

electricity from the grid during off-peak periods for converting it to hydrogen through a water electrolysis process. In the present work, hydrogen storage system will be implemented for performing an optimization strategy from an economic point of view.

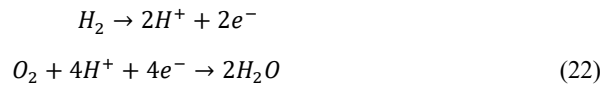
Usually, storage of the hydrogen as pressurised gas is theoretically simple but requires a compressor to increase the pressure of the gas produced by the electrolyser, the output pressure of the PEM electrolyzer used in this work is already 3MPa, so the compressor will be used for increasing this pressure until 30MPa. Then, the energy used by the compressor, considering an adiabatic compression process is:

$$P_{CP} = M_{H_2} \cdot C_p \cdot \frac{T_1}{\eta_C} \cdot \left[\left(\frac{p_2}{p_1} \right)^{\frac{k-1}{k}} - 1 \right] \cdot P_{EL} \quad (21)$$

Where M_{H_2} is the mass flow of hydrogen produced for every kW consumed by the electrolyzer. This amount of gas that can be stored in the tank until reaching its full capacity. The tank capacity proposed for the studied facility is of 10 m³ and is protected from direct solar radiation and placed in a dry, cool and ventilated environment.

2.5 Fuel Cells

Once the energy is stored as H₂, it can be used for producing electricity again by the means of a fuel cell system, that is an electrochemical device that transforms chemical energy into electrical energy in direct current. The hydrogen (H₂) and the oxidant (oxygen or air) reacts into the cell, obtaining direct current, water and heat, by the means of two different reactions, one at the anode and another at the cathode:



In order to obtain the desired power and voltage, several cells are arranged in series to form a stack. In this work, a PEM fuel cell is proposed, because of its advantages such as simplicity, low operating temperature, and easy maintenance [13]. This is going to be modeled by a zero-dimensional, isothermal and semi-empirical model [14]. The volume consumed by the fuel cell can be obtained from [15]:

$$V_{H_2} = \frac{E_{FC}}{\eta_{FC} \cdot pci_{H_2}} \quad (23)$$

Where E_{FC} is the energy delivered by the fuel cell, η_{FC} is the efficiency of the fuel cell and pci_{H_2} is the hydrogen calorific value $\left(3 \frac{kWh}{N \cdot m^3} \right)$.

3 Results

The proposed methodology focuses on analyzing the economic impact that the incorporation of a hydrogen-based storage system in a grid connected photovoltaic plant.

10

Specifically, in this work a hypothetical 1MW PV plant has been considered, located in the municipal district of Palma, on the island of Mallorca (Balearic Islands), Spain, with the minute power generation presented in Fig. 2.

The model proposed in this work is limiting the energy flows under certain conditions that increases the money incoming to the PV plant property. The different economic variables that will play an important role for determining the best energy flow are the market price of the electricity, that depends on the offer-demand of the market at each moment, and the oxygen market price, that allows us to sell the remaining oxygen generated with the electrolyzer. At the present work, the input market price for the simulation and the meteorological data of the same reference year (2017) will be used.

The electricity market price fluctuates due to the variability of the demand and consumption rates along the day. In this work, the data obtained from the OMIE web page [16] that specifies the hourly price of the MWh along the year as shown in Fig. 3.

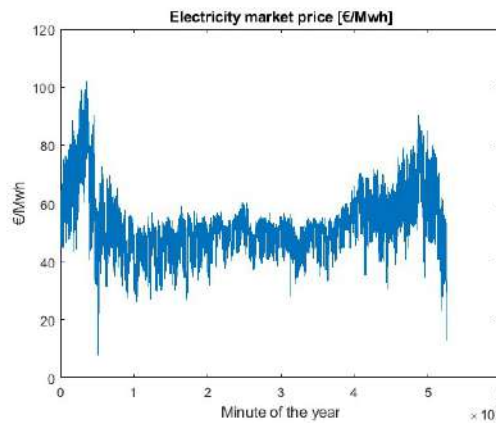


Fig. 3. Spanish marginal electricity market price along 2017 reference year.

The optimizing strategy proposed by the authors works as follows: when the market price of the energy produced is less than a 50% of the maximum electricity market price of the next 4 days, the electrolyzer is going to generate hydrogen from tap water and it is going to be accumulated in a tank with a capacity of 10 m³ at 300 bars. At the same time, the oxygen generated is going to be sold at the final price of 0,008 €/m³. Then, when the electricity market price reaches its maxim value of the next 4 days, the fuel cell is going to use the stored hydrogen to generate electricity and sell it to the grid in order to get the maximum profit of the PV-generated power.

Table 3. Hypothetical 1MW PV plant results, located at Palma of Majorca (Spain)

	With hydrogen storage	Without hydrogen storage
Annual Incomings [€]	95,527.98 €	92,523.27 €

After applying the proposed methodology, the annuals incomings of the power plant obtained for the two different scenarios, one with hydrogen storage and another without, are presented in the Table 3. It has to be noted that the historical data used in this work is from 2017, when the mean electricity market price in Spain was a 10% higher than in 2019.

4 Conclusions

Nowadays, the efficiency of modern photoconverters (i.e., photovoltaic) and electrolyzers is about 20 % and 70 %, respectively, then, the total efficiency of solar radiant energy transformed to chemical hydrogen energy is only nearly 16 % [9]. Consequently, the amount of energy that can be stored as hydrogen is not very high, and then, the different mechanisms that can convert this hydrogen to other usable energies have also a limited efficiency.

The economic results, Table. 3, show how the hydrogen-based storage facility in PV plants, where the penetration of renewables is very low and the energy demand is high, as in the Balearic Islands (<4%), does not make economic sense; as there is no technical restriction on generation.

Hydrogen accumulation can become an economically profitable strategy with an scenario of higher penetration of renewable sources, when the electricity market price is supposed to present higher variations along the day [17] due to its dependency on the meteorological conditions.

Acknowledgement

This work was supported in part by the Spanish Ministry of Economic Affairs and Digital Transformation (MINECO) and the EU with Regional European Development Funds under Grant TEC2017-84877-R. As well as by the *Ibero-American Program of Science and Technology for Development (CYTED)*, under the network project 518RT0558 entitled “*Fully Integrated, Efficient and Sustainable Smart Cities (CITIES)*”.

References

1. Perera F (2017) Pollution from Fossil-Fuel Combustion is the Leading Environmental Threat to Global Pediatric Health and Equity: Solutions Exist. *Int J Environ Res Public Health* 15:16 . <https://doi.org/10.3390/ijerph15010016>
2. Reichelstein S, Yorston M (2013) The prospects for cost competitive solar PV power. *Energy Policy* 55:117–127 . <https://doi.org/10.1016/j.enpol.2012.11.003>
3. Widera B (2020) Renewable hydrogen implementations for combined energy storage, transportation and stationary applications. *Therm Sci Eng Prog* 16:100460 . <https://doi.org/10.1016/j.tsep.2019.100460>

12

4. Clarke RE, Giddey S, Ciacchi FT, Badwal SPS, Paul B, Andrews J (2009) Direct coupling of an electrolyser to a solar PV system for generating hydrogen. *Int J Hydrogen Energy* 34:2531–2542 . <https://doi.org/10.1016/j.ijhydene.2009.01.053>
5. AEMET. <http://www.aemet.es>
6. Blanco-Muriel M, Alarcón-Padilla DC, López-Moratalla T, Lara-Coira M (2001) Computing the solar vector. *Sol Energy* 70:431–441 . [https://doi.org/10.1016/S0038-092X\(00\)00156-0](https://doi.org/10.1016/S0038-092X(00)00156-0)
7. Perez R, Ineichen P, Seals R, Michalsky J, Stewart R (1990) Modeling daylight availability and irradiance components from direct and global irradiance. *Sol Energy* 44:271–289 . [https://doi.org/10.1016/0038-092X\(90\)90055-H](https://doi.org/10.1016/0038-092X(90)90055-H)
8. King DL, Boyson WE, Kratochvil JA, King DL, Boyson WE, Kratochvil JA (2004) Photovoltaic Array Performance Model. In: Sandia National Laboratories. pp 2004–3535
9. King DL, Boyson WE, Kratochvil JA (2004) Photovoltaic array performance model. *Sandia Rep No 2004-3535* 8:1–19 . <https://doi.org/10.2172/919131>
10. Millet P, Ngameni R, Grigoriev SA, Mbemba N, Brisset F, Ranjbari A, Etiévant C (2010) PEM water electrolyzers: From electrocatalysis to stack development. *Int J Hydrogen Energy* 35:5043–5052 . <https://doi.org/10.1016/j.ijhydene.2009.09.015>
11. Ursúa A, Gandía LM, Sanchis P (2012) Hydrogen production from water electrolysis: Current status and future trends. *Proc IEEE* 100:410–426 . <https://doi.org/10.1109/JPROC.2011.2156750>
12. Park S, Shao Y, Liu J, Wang Y (2012) Oxygen electrocatalysts for water electrolyzers and reversible fuel cells: Status and perspective. *Energy Environ Sci* 5:9331–9344 . <https://doi.org/10.1039/c2ee22554a>
13. Barbir F (2013) PEM fuel cells: theory and practice. Elsevier 543 . <https://doi.org/10.1016/B978-0-12-387710-9.01001-8>
14. Mann RF, Amphlett JC, Hooper MAI, Jensen HM, Peppley BA, Roberge PR (2000) Development and application of a generalised steady-state electrochemical model for a PEM fuel cell. *J Power Sources* 86:173–180 . [https://doi.org/10.1016/S0378-7753\(99\)00484-X](https://doi.org/10.1016/S0378-7753(99)00484-X)
15. Marino C, Nucara A, Panzera MF, Pietrafesa M, Varano V (2019) Energetic and economic analysis of a stand alone photovoltaic system with hydrogen storage. *Renew Energy* 142:316–329 . <https://doi.org/10.1016/j.renene.2019.04.079>
16. OMIE. <https://www.omie.es/>
17. Hirth L (2013) The market value of variable renewables. *Energy Econ* 38:218–236 . <https://doi.org/10.1016/j.eneco.2013.02.004>

INBAL Solar Photovoltaic Electricity Generation and Consumption Reduction Programme

P.J. Escamilla-Ambrosio¹[0000-0003-3772-3651], M. Morales-Olea², O. Espinosa-Sosa¹, M.A. Ramírez-Salinas¹[0000-0002-9376-2893], A. Rodríguez-Mota¹[0000-0002-6133-1968], and Luis Hernández-Callejo³[0000-0002-8822-2948]

¹ Instituto Politécnico Nacional, Centro de Investigación en Computación, Ciudad de México, Mexico

² Fundación INBA A.C., Ciudad de México, Mexico

³ Universidad de Valladolid (UVa), Campus Duques de Soria, C.P. 42004, Soria, España
pescamilla@cic.ipn.mx

Abstract. Solar photovoltaic electricity generation systems along with electricity consumption reduction actions have been implemented at 10 academic units of Instituto Nacional de Bellas Artes y Literatura (INBAL). Such actions are part of an energy sustainability program intended to reduce the carbon footprint of this institution. These actions were implemented in accordance with recommendations proposed by environmental committees and considering the diagnoses of baseline energy consumption. This work reports the quantification of the savings generated by the implementation of operational measures of technological substitution and solar photovoltaic electric power generation. The foregoing includes a process of identification of the baseline of electricity consumption, the replacement of infrastructure and equipment of high energy consumption with equipment of low consumption and environmental impact, as well as the installation of technology for the generation of electrical energy by renewable sources. Ten solar photovoltaic systems were installed, replacement of luminaires, presence sensors and smart switches. It was found that on average the reduction in monthly electricity consumption is near 72% with the consequent economic savings. Regarding the reduction of the carbon footprint, the impact is on non-generation of tonnes of CO₂ equivalent to closer 60%, quantified compared to the generation before the implementation of the operational and power generation measures. This is equivalent to not having generated 19.10 tCO₂e per month. This work describes the activities carried out and the methodology used to calculate the savings found, both in energy consumption, economic, and in reducing the carbon footprint.

Keywords: Energy Sustainability, Solar Photovoltaic, Electricity Generation, Carbon Footprint.

1 Introduction

As part of the energy sustainability and carbon footprint reduction project at the Instituto Nacional de Bellas Artes y Literatura (INBAL, from the acronym in Spanish) [1],

a pilot program was implemented in 10 academic units, listed in Table 1. The project seeks to establish policies that facilitate the transition of the INBAL education system to a sustainable development model, which promotes the incorporation of innovations and technological developments in the area of equipment, furniture and work instruments, to reduce the impact on the environment of its daily operation and to reduce the consumption and dependence of electricity generated by fossil fuels.

Table 1. INBAL academic units involved in the project.

ID	Acronym	Academic Unit Name (in Spanish)	ID	Acronym	Academic Unit Name (in Spanish)
1	EART	Escuela de Artesanías	6	ENDF	Escuela Nacional de Danza Folklórica
2	CICO	Centro de Investigación Coreográfica	7	END-NyGC	Escuela Nacional de Danza Nellie y Gloria Campobello
3	CNM	Conservatorio Nacional de Música	8	ESMFL	Escuela Superior de Música "Fernández Leal"
4	EDIS	Escuela de Diseño	9	LAA	Laboratorio de Arte Alameda
5	EIA1	Escuela de Iniciación Artística No. 1	10	ELAU	Escuela de Laudería

The information of the results generated from the initial approach and corresponding monitoring of the project is presented, as well as the analysis of the data generated through the activation of the technological platform referred to as “Strategic System for Evaluation and Performance of Sustainability” (SEEDS, from Sistema Estratégico de Evaluación y Desempeño de la Sostenibilidad, in Spanish), implemented at 10 units of INBAL, which were equipped with the infrastructure that allows the use of alternative and sustainable energy.

2 Energy sustainability and carbon footprint reduction project implementation

The energy sustainability and carbon footprint reduction programme was implemented in the ten INBAL units considered, following these steps: a) activation of the SEEDS technology platform; b) installation of the electrical energy consumption monitoring networks; c) baseline of electricity consumption; d) replacement of equipment; d) installation of solar PV electricity generation systems, and e) quantification of savings, see Fig. 1. These actions are described in the following sections.

2.1 Activation of the SEEDS Technology Platform

SEEDS is a software platform designed to support decision makers and administrators in the transition towards a model of sustainable development in organizations. Through

programs developed for mobile and web environments, SEEDS allows to obtain the baseline of different sustainability variables, and evaluate performance in different intervention cycles. Furthermore, SEEDS allows entities the designing and monitoring of the effectiveness of improvement actions with respect to different sustainability variables, prioritizing the analysis of the consumption of electric energy and water usage, also as electricity energy generation. This software platform was installed in ten instances of INBAL to analyse and display information on the consumption of electricity and water, as energy generation, in real time, through an interactive web interface. The platform collects data through two systems:

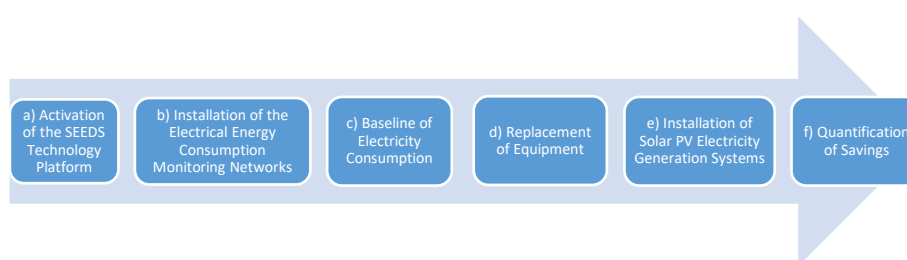


Fig. 1. Energy sustainability and carbon footprint reduction programme implementation steps.

1. Meters. The information is incorporated, from meters of electricity and water consumption, as electricity generation, in real time, to a database for processing and querying indicators in a web interface. This system has an API (Application Program Interface) to perform queries from other systems that have access permissions, for example, an Android application or other web system that request these data.
2. Logs. Module that allows to create logbooks with the information fields required to maintain a process of measuring the consumption of electricity and water, as well as electricity generation and the pattern of waste production.

SEEDS has a web interface for entering and consulting information. With the activation of SEEDS it was possible to integrate data that allow to know the pattern of resources consumption, in real time, identifying savings possibilities with the implementation of operational actions for the consumption of electric energy. By having data to define the quantification of electric power consumption, it was possible to establish indicators and goals related to the variables of sustainability based on a baseline of energy consumption. An example of the electricity consumption in a day at EART, as registered in the SEEDS platform, is shown in Fig. 2.

2.2 Installation of the Electrical Energy Consumption Monitoring Network

The installed monitoring network had seven basic components, 1) energy consumption meters, 2) water consumption meters, 3) analogue transmission antennas, 4) systems for data acquisition, 5) systems for information processing, 6). components for sending data and 7) Information display systems. The equipment that was installed in the ten INBAL instances seeks to innovate with the use of technological tools to facilitate

decision-making in projects focused on saving resources and improving the usage of energy. The general architecture of the monitoring network is shown in Fig. 3, while an example of the energy consumption meters installed at EART is shown in Fig. 4. The first step consisted of the installation of the electricity and water meters in the general connections, in the cases that were necessary, transmitting and receiving antennas were enabled to send the information to the data acquisition system. These meters were then connected to the data acquisition system to enable the reception and sending of the electric and water consumption records; data is sent according to the type of connection available (ethernet, Wi-Fi or 3G). A screen in the local monitoring system was installed so that general users could monitor the consumption of electricity and water in real time.

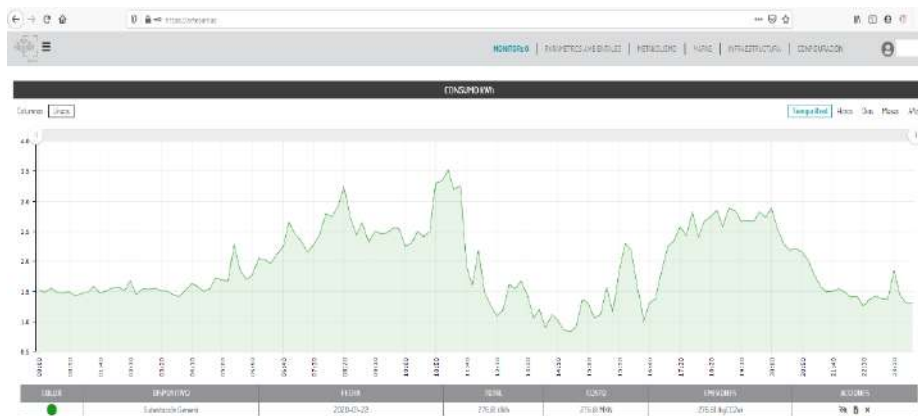


Fig. 2. Electricity consumption as registered in the SEEDS platform at EART on 2020-01-22.

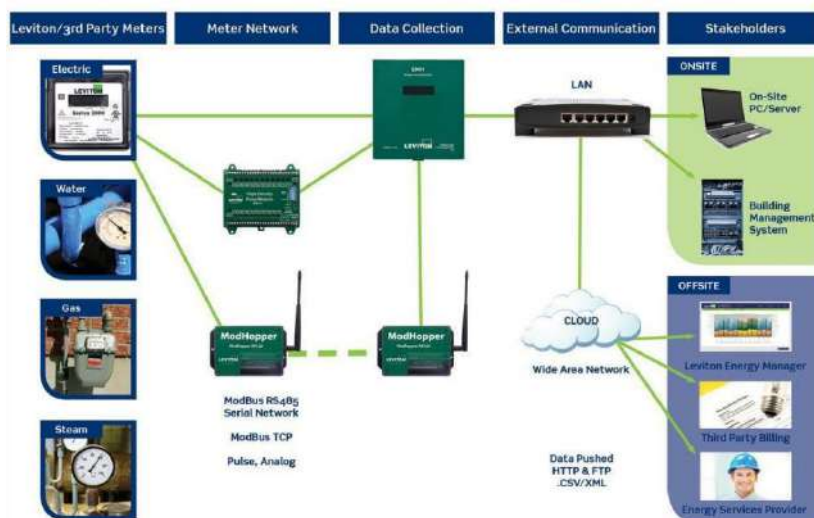


Fig. 3. Diagram of network architecture (source: Leviton, 2017 [2]).



Fig. 4. Energy consumption meters installed at EART.

2.3 Baseline of Electricity Consumption

The averaged electrical energy consumption (KWh) per month at the ten INBAL academic units considered were obtained using data collected by the installed monitoring network and registered in the SEEDS platform. The results obtained are summarized in Table 2. As can be seen, the most power-hungry instance at INBAL is EDIS.

Table 2. Averaged, monthly electricity consumption.

Instance	Averaged monthly electricity consumption (KWh)
EART	12,626.86
CICO	1355.36
CNM	15,409.47
EDIS	19,116.55
EIA1	2,207.44
ENDF	3,306.69
ENDNyGC	2,170.05
ESMFL	2,170.05
LAA	3,991.92
ELAU	1,430.50
TOTAL: 63,784.89	

2.4 Replacement of Equipment

The installation of energy saving equipment in each of the INBAL instances included replacement of high-energy consumption luminaires by low-energy consumption LED luminaires, replacement of switches with smart switches and presence sensors. A summary of the actions carried out in each instance is given in Table 3. A view of some of the installed equipment is shown in Fig. 5.

Table 3. Summary of the installed equipment.

Instance	Installed equipment	Instance	Installed equipment
EART	20 luminaires 2 switches	ENDF	28 presence sensors 2 switches
CICO	24 luminaires 6 switches	ENDNyGC	199 luminarias 16 presence sensors 2 switches
CNM	46 luminaires 8 switches 25 luminaires	ESMFL	64 luminaires 2 switches
EDIS	46 presence sensors 2 switches 92 luminaires	LAA	67 luminaires 8 switches
EIA1	10 switches	ELAU	74 luminaires 3 presence sensors 5 switches



Fig. 5. Replacement of luminaires in EART.

3 Installation of Solar PV Electricity Generation Systems.

In order to reduce the consumption of electric energy, and to reduce the carbon footprint, the company Greensun [3], carried out the design of the projects and performed the installation of ten solar PV electricity generation systems, one in each of the ten INBAL instances considered (EART, CICO, CNM, EDIS, EIA1, ENDF, ENDNyGC, ESMFL, LAA, ELAU). Table 4 presents a summary of the Installed solar PV systems. Figs. 6 to 8 show some views of the installed PV systems in each of the instances

considered. The total power generation capacity considering the ten FV systems is 126.72 KW, with a total of 352 PV panels and 36 inverters.

Table 4. Solar PV systems installed at 10 INBAL academic units.

Instance	Number of PV panels	Power of panel (Watts)	Total power Generation (Watts)	Inverters (Model Power in KW-quantity)
EART	70	360	25,200	Symo 15.0-3, Symo 10.0-3
CICO	8	360	2,880	Primo 3.8-1
CNM	28	360	10,080	Symo 10.0-3
EDIS	54	360	19,440	Symo 10.0-6
EIA1	28	360	10,080	Symo 10.0-3
ENDF	28	360	10,080	Symo 10.0-3
ENDNyGC	28	360	10,080	Symo 10.0-3
ESMFL	56	360	20,160	Symo 10.0-6
LAA	28	360	10,080	Symo 10.0-3
ELAU	24	360	8,640	Primo 3.8-1, Primo 5.0-1
TOTAL	352		TOTAL 126,720	



Fig. 6. Solar FV system installed at (a) EART, (b) CICO, (c) CNM, (d) EDIS.



Fig. 7. Solar FV system installed at (a) EIA1, (b) ENDF, (c) ENDNyGC, (d) ESMFL.



Fig. 8. Solar FV system installed at (a) LAA, (b) ELAU.

4 Quantification of Savings

In this section the quantification of electricity savings, cost savings and reduction of carbon footprint are presented. These savings are due to the implementation of operational measures including PV electricity generation and technological replacement of energy-hungry equipment. These savings were calculated using data of electricity consumption corresponding to the months of November 2019, December 2019, January 2020 and February 2020. The quantifications of the electricity savings in each instance considered are shown in Table 5. The quantifications of the corresponding economic savings in each instance considered are shown in Table 6. Finally, the quantification of the reduction of the carbon footprint in each instance considered are shown in Table 7. Notice that in the case of the carbon footprint, values are obtained in tonnes of carbon dioxide equivalent (tCO₂e) [4]. Also, it is necessary to specify that the carbon footprint and savings were calculated considering only the electricity consumption and electricity savings due to PV electricity generation and technology substitutions.

According to the data provided by the Energy Regulatory Commission (CER) of the Mexican Federal Public Administration as a regulatory body on energy matters and

with the opinion of the Secretary of Environment and Natural Resources (SEMARNAT), established that the National Electric System Emission Factor for 2017 is 0.527 tonnes of CO₂ / MWh.

Hence, the calculation of the reduction in the number of tonnes of CO₂ equivalent (tCO₂e) is a direct function of the total electricity consumption of the INBAL instances, specified in MegaWattsHora.

Table 5. Quantification of electricity savings at ten INBAL academic units.

Instance	Average monthly consumption before the implementation of savings measures (KWh)	Average monthly consumption after the implementation of savings measures (KWh)	Average monthly savings in KWh	% Average monthly electricity savings
EART	12,626.86	2,040.50	10,586.36	83.84
CICO	1,355.36	1,034.41	320.95	23.68
CNM	15,409.47	10,483.06	4,926.41	31.97
EDIS	19,116.55	8,210.56	10,905.99	57.05
EIA1	2,207.44	330.23	1,877.21	85.04
ENDF	3,306.69	626.95	2,679.74	81.04
ENDNyGC	2,170.05	-556.83	2,726.88	125.66
ESMFL	2,170.05	248.47	1,921.58	88.55
LAA	3,991.92	1,138.89	2,853.03	71.47
ELAU	1,430.50	407.69	1,022.81	71.5
TOTAL	63,784.89	23,963.93	39,820.96	71.98

Table 6. Quantification of economic savings at CIC, CIDETEC and ESCOM.

Instance	Average monthly cost for electricity consumption before the implementation of savings measures (MXN)	Average monthly cost for electricity consumption after the implementation of savings measures (MXN)	Average monthly economic savings in MXN	% Average monthly economic savings
EART	48,522.58	8,734.06	39,788.52	82.00
CICO	3,179.79	1,580.04	1,599.75	50.31
CNM	40,623.76	26,344.51	14,279.25	35.15
EDIS	25,402.68	18,589.68	6,813.00	26.82
EIA1	5,602.57	591.07	5,011.50	89.45
ENDF	8,267.36	3,160.61	5,106.75	61.77
ENDNyGC	6,861.19	497.44	6,363.75	92.75
ESMFL	8,449.04	2,887.04	5,562.00	65.83
LAA	9,990.00	5,244.75	4,745.25	47.5
ELAU	3,576.31	935.56	2,640.75	73.84
TOTAL	160,475.28	68,564.76	91,910.52	62.54

With the use of the monitoring network and through the SEEDS platform, the electricity consumption in MegaWatts / Month was obtained for the months of October, November and December 2019, as well as for the months of January, February and March of 2020, for the ten instances considered. In the months of April to December 2019, an

average estimated consumption value of the previous months measured with the monitoring network was used and the savings obtained due to operational measures of technological substitution and energy generation were subtracted, this is:

$$CME = \text{Average (CMA_SMT)} - \text{AED_LSAA} - \text{EGVPS} \tag{1}$$

where:

CME = Estimated Monthly Consumption

CMA_SMT = Previous Months consumption obtained through monitoring network

AED_LSAA = Estimated Savings LSAA Devices (Luminaires)

EGVPS = Energy Generated Via Solar Panels

Table 7 shows the results obtained, which are also plotted in Fig. 9. The global savings are summarised in Table 8.

Table 7. Quantification of carbon footprint reduction at ten INBAL academic units.

Instance	Average monthly emissions before the implementation of savings measures (tCO2e)	Average monthly emissions after the implementation of savings measures (tCO2e)	Average monthly emissions reduction (tCO2e)	% Average monthly emissions reduction (tCO2e)
EART	6.46	1.04	5.42	83.84
CICO	0.69	0.53	0.16	23.68
CNM	7.89	5.37	2.52	31.97
EDIS	9.79	4.20	5.58	57.05
EIA1	1.18	0.24	0.94	79.66
ENDF	1.74	0.78	0.96	55.17
ENDNyGC	1.45	0.22	1.23	84.83
ESMFL	1.14	0.16	0.98	85.96
LAA	2.1	1.27	0.83	39.52
ELAU	0.88	0.41	0.47	53.41
TOTAL	33.33	14.23	19.10	59.51

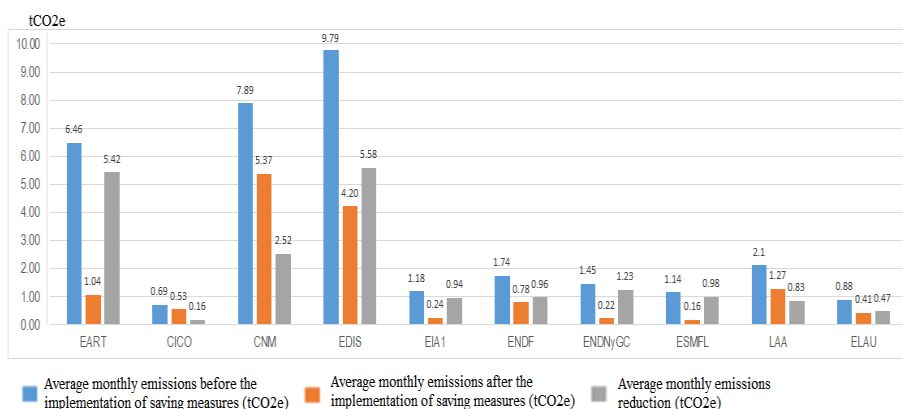


Fig. 9. Carbon footprint reduction at ten INBAL academic units.

Table 8. Global savings at ten INBAL academic units.

	Electricity consumption savings in KWh	Saving cost for electricity consumption in MXN	Reduction of emissions of tCO ₂
Overall monthly average savings	39,820.96	91,910.52	19.10
% Equivalent	71.98	62.54	59.51

5 Conclusions

Derived from the analysis of the information collected by the installed monitoring network and using the SEEDS platform, it was possible to perform the quantification of the savings generated by the operational measures of technological substitution and the implementation of PV systems for the generation of electricity from a renewable energy source in ten INBAL academic units, reducing the environmental impact, the carbon footprint and also reducing the consumption and dependence of electricity generated by fossil fuels.

The quantifications made indicate an average monthly savings in consumption of 39,820.96 KWh, corresponding to 71.98% of the average monthly electricity consumption. In economic terms, this is equivalent to an average monthly savings for electricity consumption costs of \$ 91,910.52 (MXN), equivalent to 62.54% of the average monthly total cost per electricity consumption in the ten INBAL instances. Finally, in terms of the reduction of the carbon footprint, expressed in the non-production of equivalent tonnes of CO₂ (tCO₂e), it corresponds to 19.10 tCO₂e, which represent 59.51% of the total generation of tCO₂e before the implementation of the measures of technological substitution and generation of electric energy from renewable sources.

The reduction in the consumption of electric energy, as well as the corresponding economic savings and reduction of equivalent CO₂ emissions quantified so far, and whose measurement is maintained in the temporality specified in this work, gives the guideline to continue monitoring the information through the SEEDS platform installed in ten INBAL instances. It will be necessary to obtain the statistics to ratify that the operational measures of technological substitution and electricity generation provide substantial savings to INBAL. If the trend of the figures obtained so far continues, then there will be enough information to recommend the route to improve the performance of other INBAL instances by the gradual incorporation of technologies for sustainable development.

Acknowledgments

This work was supported by Fondo Sectorial CONACYT-SENER Sustentabilidad Energética, under project grant 264087.

References

1. INBA Sustentable Homepage, <http://www.finba.mx/inbasustentable.php>, last accessed 2020/09/01.
2. Leviton Homepage, <https://www.leviton.com>, last accessed 2019/09/01.
3. Greensun Homepage, <http://www.greensun.com.mx>, last accessed 2019/09/01.
4. The Carbon Trust: Carbon footprintin, online at <https://www.carbontrust.com/resources/guides/carbon-footprinting-and-reporting/carbon-footprinting/#download-guide>, last accessed 2019/09/01.

Optimization of the capacity of photovoltaic arrays and modification of the geometry of a turbine-generator system to minimize dependence on the electricity grid

López-Meraz R. A. ¹[0000-0002-3236-3709], Hernández-Callejo L. ²[0000-0002-8822-2948],
Jamed-Boza L. O. ¹[0000-0002-6378-758X], Del Ángel-Ramos J. A.¹, Marín-Hernández J. J.¹
and Alonso-Gómez V. ²[000-0001-5107-4892]

¹ Universidad Veracruzana, Circuito Universitario Gonzalo Aguirre Beltrán s/n, 91000, Mexico

² Universidad de Valladolid, Campus universitario Duques de Soria s/n, 42004, Spain

meraz_raul@hotmail.com: R.L-M.; luis.hernandez.callejo@uva.es:
L.H-C.; lojb33@gmail.com: L.J-B.; jdelangel57@gmail.com: J.D-R.;
jmarin@uv.mx: J.M-H.; victor.alonso.gomez@uva.es: V.A-G.

Abstract. The main elements of microgrids are distributed energy sources, mostly renewable, and storage systems. Both generations try to cover the local demand, however, they are generally connected to the electricity grid of the utility company to ensure the delivery of energy to the loads. To be closer to self-sufficiency, this work proposes the adequate increase of the capacities of seven photovoltaic systems and the expansion of the alimentation characteristics of the turbine-generator backup of the microgrid of the Center for the Development of Renewable Energies (CEDER) belonging to the Center for Energy, Environmental and Technological Research (CIEMAT), which allows requesting less power from the external electrical system in the months of greatest demand. The methodology is based on the combination of the central composition design technique with the “lower is better” approach, taking as responses the mean requested power and the standard deviation, where the former is the primary solution. The results, with 20 years of simulation, show a significant saving of 82.26% of the demand if the changes in the solar arrays and the geometry of the hydraulic system are carried out.

Keywords: Dual Response, Power Reduction, Response Surface Methodology, Simulation.

1 Introduction

The evolution of the traditional electricity system, that is, unidirectional, towards a decentralized one is aimed at reducing the environmental impact, caused by the consumption of fossil fuels, and at improving the efficiency of the network, minimizing losses in transmission and distribution of electrical current to consumers. A relevant factor for this transition are the distributed generation units (DG) that take advantage of local

energy resources, mainly renewable (sun and wind), also helping to satisfy the growing demand for energy. From the DG arises the paradigm of microgrid that aims to manage various types of generation, storage and loads to obtain high reliability. They normally operate connected to the conventional network, but have the capacity to be self-sufficient [1].

One of the biggest challenges for GD and microgrids is finding mechanisms that determine the ideal capacity of generators and backup systems. In this sense [2] finds the appropriate magnitudes, among others, of a wind generator and hydrogen storage. On the other hand, [3] details different techniques, divided into intuitive analysis, numerical methods and artificial intelligence, to improve the sizing of photovoltaic and wind systems. In addition, [4] proposes with linear programming, the adequate power of a mixed wind-photovoltaic generation system, as well as the savings that could be achieved in billing. However, the experiment design tool, especially the response surface methodology (RSM), has been little used to optimize the sizing of energy systems. [5] proposes this technique in an autonomous system composed of the photovoltaic-wind binomial and with battery backup. Likewise, [6] uses the method of factorial experimental designs to optimize the parameters of a monocrystalline photovoltaic panel.

This work proposes the application of the central composition design (CCD), a branch of RSM, to minimize the power required from the supplier, in the months of greatest electricity demand, in the microgrid of the Center for the Development of Renewable Energies (CEDER). To achieve the objective, simulations developed in [7] were used, modifying the capacities of seven photovoltaic arrays and the power supply of the turbine-generator backup system. At the same time, the operability of productive systems was sought, adjusting them to the most appropriate parameter with the lowest variance, through their signal to noise [8], that is, the dual response technique was applied, simultaneously optimizing the mean and variance. The statistical analyzes were developed with the statistical application software JMP (version 8.0.2). The text is structured as follows: section two describes the components of the case study, then the methodology is presented where the analysis factors, the number of replications and, in general, the description of the CCD, the The next section, with the help of JMP, are the results of the months under study, and finally, the most relevant conclusions are presented.

2 Materials and methods

2.1 Case of study

CEDER is characterized by having various manageable components in the structure of its microgrid, Fig. 1 shows two of its components [9]. From the set of distributed elements, this work focuses on two types of generation: solar photovoltaic (PV) and mini-hydro. With regard to PV, there are 7 arrangements (AFV) of different technology, five of monocrystalline Silicon, one of polycrystalline Silicon and one of Cadmium Tellurium. The AFVs are as follows: FV1037 = 5 kW, FV1038 = FV1044 = 4.5 kW, FV2000 = 12 kW, FV2005 = 12.5 kW, FV2010 = 16 kW and FV4360 = 23.5 kW, in total a installed power of 78 kWp. On the other hand, the hydraulic plant is made up of a

double injector horizontal Pelton turbine, directly coupled to a three-phase asynchronous generator with a maximum power of 40 kW, delivering 400 V three-phase at a frequency of 50 Hz. A jump is used for its operation. It is close to 65 m and has two storage tanks with an approximate volume of 1637 m³ in the upper tank and 2206 m³ in the lower one, the distance between them is 700 m. The supply pipe is made of PVC with an internal diameter of 225 mm, it consists of two sections of different walls, one is 4 mm and the lower one is 6 mm in order to withstand water hammer.



Fig. 1. Photovoltaic turbine zone and Pelton turbine with 40 kW generator.

2.2 Design of experiments

The most efficient experimental designs are those that combine regressive effects on the response and allow the study of curvatures. The design that was originally called Box-Wilson [10] is known by the general name of CCD and has been shown to require fewer trials to obtain more reliable information. CCD is constructed from a full factorial augmented design with central and axial experimental points. The inclusion of central replicas favors the estimation of the general variance of the process of changes of values in the factors. Adding axial points, whose axial distance α can be defined by the researcher, gives qualities to the general profile of the variance, namely: (1) Axial distance on phase with $\alpha = 1$, generates a variance profile similar to that of full factorial design with an additional study level. (2) Rotatable axial distance with value $\alpha > 1$, creates a variance profile that tends to be constant as a function of the radius in the plane of a couple of factors studied. (3) Orthogonal axial distance with value $\alpha \geq 1$, produces a variance profile that tends to be uncorrelated with the quadratic effects under study. (4) Spherical axial distance with α value > 1 , generates a variance profile that tends to be constant as a function of the radius in a list of factors studied. Obviously, the number of replicas that the researcher decides will modify the values of these distances, except for the axial distance on phase, which is always $\alpha = 1$ [11].

To exemplify the above, Table 1 shows some values of the factors under study (f), factorial replicas (n), axial replicas (a) central replicas (c) (it is observed that $a \geq n$ y $c \geq a$ in all design CCD). For the case study, the axial distance $\alpha = \sqrt{2}$ was selected, with a rotatable characteristic to achieve the tendency to be a function of the radius from the center to the limit of the two-dimensional sample space (X_1, X_2). Where X_1 corresponds to the increase in the nominal power capacity of the 7 AFVs and X_2 is the increase in the geometry of the Turbine-Generator backup system. The increases allowed in the AFVs and the supply of the backup system, as well as the values studied, are presented in Table 2.

Table 1. Values of α for factor and replica conditions.

f	n	a	c	α_{rot}	α_{orto}	α_{esf}
2	1	1	1	1.414213562	1.000000	1.414213562
2	2	1	1	1.681792831	1.048341315	1.414213562
2	2	1	2	1.681792831	1.136442969	1.414213562
2	2	1	3	1.681792831	1.21541169	1.414213562
2	2	1	4	1.681792831	1.287188506	1.414213562
2	2	2	2	1.414213562	1.000000	1.414213562
2	2	2	3	1.414213562	1.040291787	1.414213562
2	2	2	4	1.414213562	1.07808982	1.414213562
3	1	1	1	1.681792831	1.21541169	1.732050808
3	2	1	1	2.000000	1.26161129	1.732050808
3	2	1	2	2.000000	1.340879924	1.732050808
3	2	1	3	2.000000	1.414213562	1.732050808
3	2	1	4	2.000000	1.482578506	1.732050808
3	2	2	2	1.681792831	1.21541169	1.732050808
3	2	2	3	1.681792831	1.252103974	1.732050808
3	2	2	4	1.681792831	1.287188506	1.732050808

Table 2. Nominal values, allowable increments and coded values.

Nominal Values				Values of x1 and x2				
Identifier	Min	Max	Var	-alfa	-1	0	1	alfa
FV1037	5	6.5	x1	5	5.22	5.75	6.28	6.50
FV1038	4.5	6		4.5	4.72	5.25	5.78	6.00
FV1144	4.5	6		4.5	4.72	5.25	5.78	6.00
FV2000	12	16		12	12.59	14	15.41	16.00
FV2005	12.5	16.5		12.5	13.09	14.5	15.91	16.50
FV2010	16	21		16	16.73	18.5	20.27	21.00
FV4360	23.5	30.5		23.5	24.53	27	29.47	30.50
Radio Upper Tank	12.5	15.5	x2	12.5	12.94	14	15.06	15.50
Upper Tank Height	3.3	4.13		3.3	3.42	3.715	4.01	4.13
Net Jump	65	70		65	65.73	67.5	69.27	70.00
% Increase in values				0.00%	14.64%	50.00%	85.36%	100.00%

RSM with dual response option in which the factorial experimental points are inscribed in an axial circle, allows simultaneously studying the primary response Y_1 (average daily power in each month) and the secondary response Y_2 (average standard deviation of Y_1 in each month), such that both can be minimized. The arrangement of experimental values used for both responses can be seen in Fig. 2. Where X_1 and X_2 are the factors under study given in percentage increments. The axial points are the extreme values of the circle and the square represents the factorial points. On the other hand, the geometry of the experimental points is presented in Table 3.

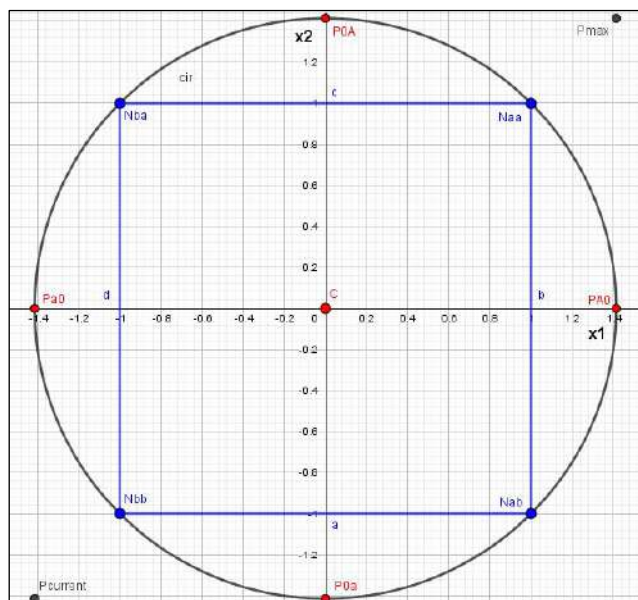


Fig. 2. Configuration of the CCD with 2 factors, 2 factorial replicas, 2 axial replicas, 4 central rotatable replicas.

Table 3. Location of factors and replicas of the CCD.

Point type	Point symbology	X1	X2
Pcurrent	Pc	-alfa	-alfa
axial	Pa0	-alfa	0
axial	POa	0	-alfa
axial	PA0	alfa	0
axial	POA	0	alfa
center	C	0	0
factorial	Nbb	-1	-1
factorial	Nba	-1	1
factorial	Nab	1	-1
factorial	Naa	1	1
Pmax	Pm	alfa	alfa

[12] formulates that this type of experimental design is based on the following approaches. Let $\hat{\mu}$ and $\hat{\sigma}$ be the response surfaces for the mean and standard deviation of the combined study process.

$$Y_1: \quad \hat{\mu} = b_0 + x'b + x'Bx \tag{1}$$

$$Y_2: \quad \hat{\sigma} = c_0 + x'c + x'Cx \tag{2}$$

Where B and C are matrices of size $k \times k$ containing the second order terms of the estimated coefficients of each response model; b and c are vectors of size $k \times 1$ with the first order terms of the estimated coefficients of each model; b_0 and c_0 are scalar additive constants and x is a $k \times 1$ vector of control or design variables. [13] details the general considerations for estimating models (1) and (2).

The answers Y_1, Y_2 were obtained by creating the experimental simulation of 24 years of operation, where 20 years correspond to the CCD, 2 years to the current condition of the CEDER (Pc) and the last 2 years to the maximum simultaneous increase of AFV and the storage geometry in the backup system. When obtaining the data for the 24 years, the number of days of power delivery (kW) in each month to the supplier's electrical network was counted. The categorical analysis directs the RSM study with dual response to the months where a greater participation of the supplier is required.

3 Results

In order to give a general overview of the responses in the 20 years that form the sample space, we obtained the averages and deviations for each condition analyzed. The above is presented in Table 4. It can be seen that the points POA, Naa and PA0 are the conditions with the least electrical dependence.

Table 4. Annual averages and deviations for each experimental condition.

Condition	Y1 avg	Y1 dev	Y2 avg	Y2 dev
Pa0	8.5964	12.8318	0.7197	0.6148
Pa0	8.4085	12.5356	0.7383	0.6299
Nbb	12.7210	21.0823	0.9790	1.0884
Nbb	10.4821	18.0221	0.8752	0.9324
Nba	4.7143	6.4099	0.5176	0.3030
Nba	5.4612	8.3533	0.5512	0.4085
POa	10.9462	18.2862	0.9358	1.0162
POa	10.1411	16.6696	0.8923	0.9177
C	5.0617	8.3925	0.5837	0.4369
C	4.6304	7.2770	0.5707	0.3837
C	5.5240	9.5407	0.5849	0.4947
C	4.8911	7.6152	0.5627	0.4023
POA	3.5222	5.4043	0.4542	0.2181
POA	2.5802	3.9445	0.4185	0.1715
Nab	6.5973	11.7398	0.7181	0.6597
Nab	7.7717	14.3192	0.7845	0.8084
Naa	2.8641	4.4255	0.4584	0.1828
Naa	2.4953	4.0501	0.4422	0.1645
PA0	2.5014	4.0598	0.4749	0.1980
PA0	3.4991	5.9659	0.5151	0.3002

On the other hand, Table 5 shows the years corresponding to the current situation of the CEDER and the permissible extent of modification of both the AFV and the turbine feed geometry. The difference in these extremes is visible.

Table 5. Annual averages and deviations in current and maximum condition.

Condition	Y1 avg	Y1 dev	Y2 avg	Y2 dev
Pc	16.2688	24.8376	1.1496	1.2514
Pc	13.9330	21.8388	1.0382	1.1078
Pm	2.2267	3.2979	0.4279	0.1110
Pm	2.2592	3.5489	0.4312	0.1118

The analysis of the days of power delivery to the external grid is summarized in Table 6. Under current conditions (Pc) the averages for November, December and January are the lowest, namely: 0, 0 and 2.5 kW, respectively. On the other hand, it is observed that in the same periods the sum of delivery days in the 24 simulations are the lowest. It is obvious that these months are the most dependent on the external network. The average daily monthly power calculated by the simulator in these months are: 54.2543, 58.9570 and 45.2519 kW/day. Table 7 shows the responses Y_1 and Y_2 at point Pc.

Table 6. Number of days of injection into the supplier's network.

Month	Number of days in kW daily delivery status per month																								Total Days	Daily Average	Daily Deviation
	Pc	Pc	Pa0	Pa0	POa	POa	C	C	C	C	POA	POA	PA0	PA0	Pm	Pm	Nbb	Nbb	Nba	Nba	Nab	Nab	Naa	Naa			
January	3	2	1	3	5	11	9	9	4	4	3	7	8	3	5	3	3	2	3	2	3	1	4	3	101	4.208	2.670
February	7	7	3	4	9	9	6	9	4	5	3	5	7	8	9	5	2	5	4	5	10	11	10	10	157	6.542	2.637
March	2	3	6	7	6	10	8	6	8	5	5	7	12	15	14	13	4	9	6	2	7	16	9	18	198	8.250	4.396
April	7	8	7	11	14	7	8	9	10	10	10	14	13	11	18	12	10	11	8	6	8	10	14	8	244	10.167	2.884
May	13	12	13	12	20	18	18	21	15	19	24	19	18	10	10	17	20	18	12	8	15	20	13	13	378	15.750	4.131
June	15	15	17	12	15	9	20	10	12	9	16	16	13	16	15	17	19	17	12	17	11	14	19	15	351	14.625	3.076
July	11	14	14	15	10	20	14	16	16	16	16	12	16	16	13	16	18	12	15	11	19	16	17	13	356	14.833	2.531
August	16	18	11	8	15	14	8	13	16	21	11	19	19	17	14	20	13	18	11	13	14	9	13	18	349	14.542	3.741
September	9	8	8	11	9	11	15	14	11	14	16	17	11	20	14	13	9	12	11	18	11	15	18	16	311	12.958	3.407
October	5	8	4	6	6	10	8	8	11	7	11	11	16	12	13	13	9	10	6	5	11	13	8	15	226	9.417	3.283
November	0	0	0	0	5	2	1	6	2	2	1	8	11	10	11	11	0	0	0	1	8	6	6	10	101	4.208	4.242
December	0	0	0	0	3	0	0	0	1	2	2	3	5	5	4	12	0	0	0	0	7	6	1	6	57	2.375	3.118

Table 7. Average daily demand.

Pc	Y1=kW/d avg	Y2=kW/d dev	CV=(S/xbar)100	Y1avg	Y2avg
November	55.0014	3.2799	5.9632	54.2543	3.2390
November	53.5071	3.1981	5.9769		
December	60.2180	3.1584	5.2449	58.9570	3.1090
December	57.6961	3.0596	5.3029		
January	55.6072	3.0724	5.5252	45.2519	2.5641
January	34.8965	2.0559	5.8914		

With the results obtained, it was decided to apply the RSM with dual response in the previous months where the savings are more significant. Statistical analyzes were done with [14]. However, this section only shows the graphs for the month of November. Figures 3 and 4 detail the behavior of the responses studied.

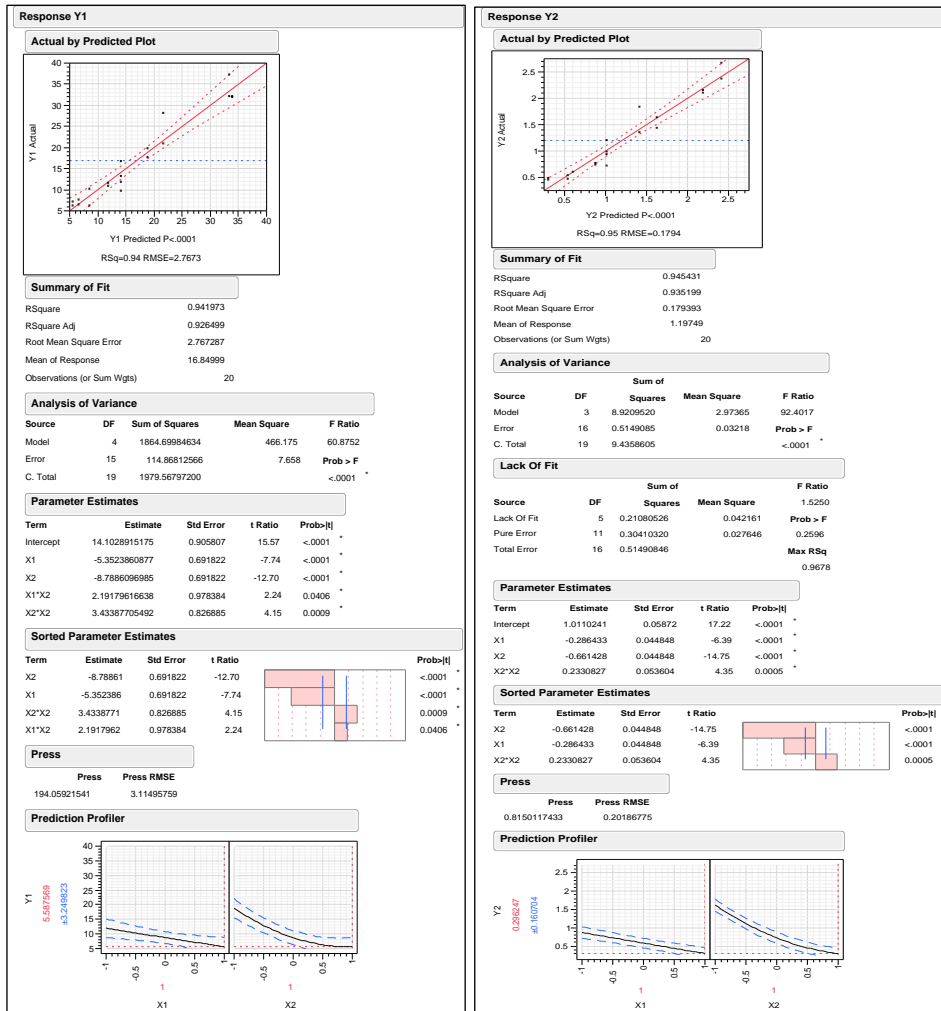


Fig. 3. Statistical analysis of the CCD with dual response for November.

November has a significant behavior of the variable Y_1 in the effects: X_1 , X_1X_2 , X_2 and X_2^2 which corresponds to the average demand. On the other hand, the variable Y_2 is significant in the effects X_2 , X_1 and X_2^2 , which corresponds to the standard deviation. The adjusted regressive model can be observed in the prediction profile section of Fig. 3. It should be noted that all statistical analyzes meet significant relationships with $\alpha \leq 0.05$.

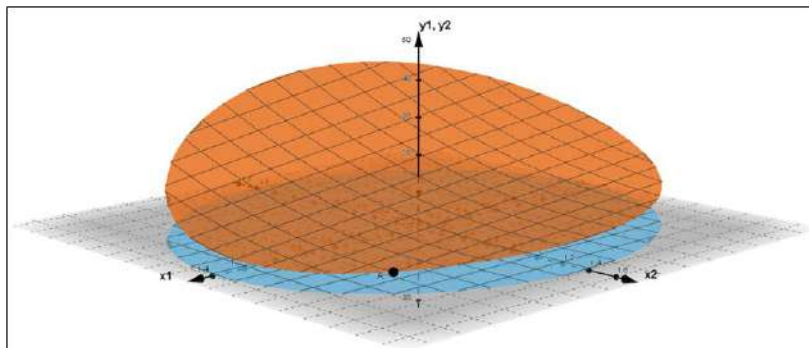


Fig. 4. Three-dimensional schematic of the fitted models of Y_1 and Y_2 .

The contour plot, Fig. 5., details the demand savings regions. The blue area represents the lowest demand section required. It is contained between the following points (x_1, x_2) : $(-0.5, 1.2)$; $(0, \alpha)$; $(1, 1)$; $(\alpha, 0)$; $(1.3, -0.2)$; $(0.7, 0)$; $(0.5, 0.5)$; $(0, 0.8)$ and $(-0.5, 1.2)$ the most recommended area is the first quadrant of $(x_1, x_2) \in E^2$.

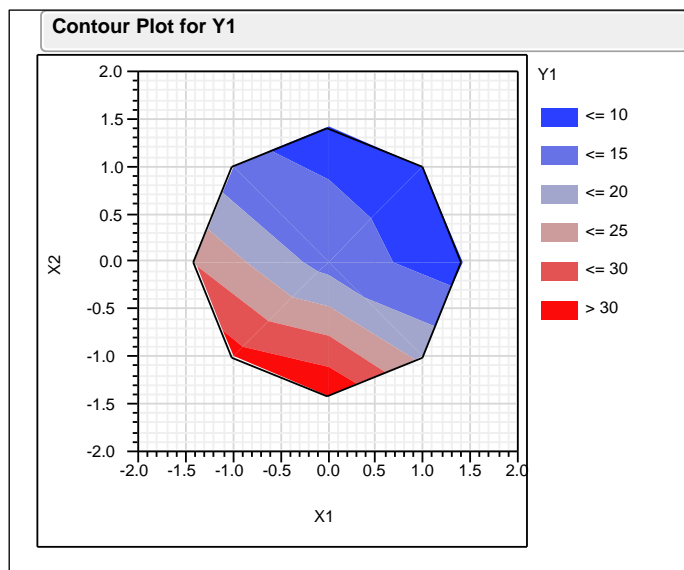


Fig. 5. Categories of possible savings in November.

In November, the region with the least required demand is intermediate in size, December covers a larger area and January presents a smaller savings section. If you want to achieve greater savings, it is recommended to locate the increase decisions in the smallest region (January), so the effect in the months of December and November will be greater and in January an acceptable one will be reached, on average. Fig. 6 splices the 3 previous zones.

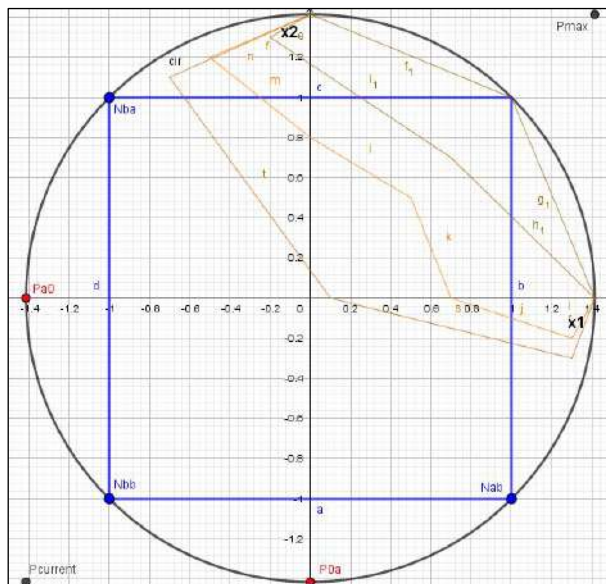


Fig. 6. Regions with the highest savings in the three months studied.

The most recommended area in all three cases is the proximity to point (1,1), that is, the first quadrant. Table 8 indicates the requested demand of the three months with the modification of X_1 and X_2 at that point.

Table 8. Increased state at point Naa (1,1).

Naa (1,1)	Y1=kW/d avg	Y2=kW/d dev	CV=(S/xbar)100	Y1avg	Y2avg
November	7.0454	0.4833	6.8599	6.5834	0.4626
November	6.1213	0.4420	7.2200		
December	10.8431	0.7432	6.8542	9.7125	0.6958
December	8.5819	0.6484	7.5558		
January	11.7550	0.8834	7.5151	11.7450	0.8771
January	11.7349	0.8708	7.4202		

The estimated average savings are: November (87.8657%), December (83.5261%) and January (74.0453%). Additionally, a significant decrease in the standard deviation is achieved. The relative increase in the coefficient of variation (CV) is due to the greater decrease in Y_1 compared to the decrease in Y_2 .

4 Conclusions

The combined effects of the AFVs and the turbine-generator backup power design are overall non-linear. This is the rationale behind the use of dual response option response surface experimental designs. The expected behavior when both factors increase is

found on the main diagonal whose direction is at the points: P_{current} , N_{bb} , C , N_{aa} and P_{max} . However, the analysis offers CEDER the possibility of increasing the local power in a given area where it is optimized, minimizing, the dependence on the supplier to approach energy autonomy. It is notable that the increase in AFV capacities provides better results than the increase in storage geometry.

5 Acknowledgments

We would like to thank the CEDER by providing information for the development of this work. The authors thank the CYTED Thematic Network “INTELLIGENT CITIES FULLY INTEGRAL, EFFICIENT AND SUSTAINABLE (CITIES)” n° 518RT0558.

References

1. Bordons, C., García-Torres, F and Valverde, J.: Gestión óptima de la energía en microrredes con generación renovable. *Revista Iberoamericana de automática e informática industrial* 12, 117-132 (2015).
2. Hakimi, S., Moghaddas-Tafreshi, S. M., Hassanzadehfard, H., Taylor, G. A., Alamuti, M. M.: Optimization of a reliable combined cooling, heat and power microgrid system. *Industrial Electronics Society, IECON 2013-39th Annual Conference of the IEEE* (2013).
3. Tamer, K., Azah, M., Sopian, K.: A review of photovoltaic systems size optimization techniques. *Renewable and Sustainable Energy Reviews* 22, 454-465 (2013).
4. Lamedica, R., Santini, E., Ruvio, A., Palag, L., Rossetta, I.: A MILP methodology to optimize sizing of PV - Wind renewable energy systems. *Energy*. Vol. 165, Part B, 15, 385-398 (2018).
5. Orhan, E., Banu, Y.: Size optimization of a PV/wind hybrid energy conversion system with battery storage using response surface methodology. *Applied Energy*. Vol. 85, 11, 1086-1101 (2006).
6. Kessaissia, F., Zegaoui, A., Aillerie, M., Arab, M., Boutoubad, M., Fares, C.: Factorial design and response surface optimization for modeling photovoltaic module parameters. *Energy reports* 6, 299-309 (2020).
7. Jamed, L., López, R: Programa simulador para la optimización de la generación solar FV con la integración del respaldo turbina-generador. Registro público del derecho de autor. Número de registro: 03-2018-082811402400-01 (2018).
8. Ranjit, R.: A primer on the Taguchi method. *Society of manufacturing engineers*. ISBN 13:978-0-87263-864-8. USA. p.10. (2010).
9. <http://www.ceder.es/instalaciones-redes> accessed on September 23, 2020.
10. Box, G., Wilson, K.: On the experimental attainment of optimum conditions. *Journal of the Royal Statistical Society*, B 13, 1-45 (1951).
11. Jamed, L.: La potencia prospectiva, una propuesta para su aplicación en el diseño de experimento. Tesis doctoral. La Habana, 30–31 (2009).
12. Köksoy, O., Doganaksoy, N.: Simultaneous Optimization of Mean and Standard Deviation in Response Surface Experimentation. *Journal of Quality Technology*, vol. 35, 3 (2003).
13. Myers, R., Montgomery, D.: *Response Surface Methodology*. John Wiley & Sons, (1996).
14. JMP 8.0.2 SAS Institute Inc. © 2009.

Preliminary evaluation of different underground hydrogen storage systems in Spain

Cristina Sáez Blázquez¹ [0000-0002-5333-0076], Ignacio Martín Nieto¹ [0000-0003-3984-7228], Miguel Ángel Maté-González^{1,2} [0000-0001-5721-346X], Arturo Farfán Martín¹ [0000-0002-1506-1207] and Diego González-Aguilera¹ [0000-0002-8949-4216]

¹ TIDOP Group, Department of Cartographic and Land Engineering, University of Salamanca, Higher Polytechnic School of Avila, Hornos Caleros 50, 05003 Avila, Spain
Department of Topographic and Cartography Engineering, Higher Technical School of Engineers in Topography, Geodesy and Cartography, Technical University of Madrid, Mercator 2, 28031 Madrid, Spain
u107596@usal.es

Abstract.

In the future energy system with a high share of renewable sources, the role of hydrogen will be essential to deal with the fluctuations in the electricity production. Hydrogen is understood as a system capable of storing energy for a later use in a controlled way. In this way, surplus electricity coming from renewable energies is used for generating hydrogen by the electrolysis process. Once produced, hydrogen is stored in one of the different underground storage structures to be used when needed. In this context, the aim of this research is to provide a preliminary evaluation about the potential for underground hydrogen storage in the country of Spain, considering the usual geological formations of these systems (deep aquifers, salt caverns and depleted hydrocarbon fields). The analysis of each alternative has allowed highlighting that Spain presents potential locations where future hydrogen storage could be feasible. Regarding salt caverns, this country has high onshore storage capacities, with a total of located 24 caverns. Furthermore, the Spanish potential of hydrogen storage in aquifers is also relevant especially in Tertiary sedimentary basins as the Ebro, Duero and Guadalquivir basins. The storage potential in depleted oil and gas fields is however reduced due to the limited hydrocarbon activity of the country.

Keywords: Renewable energies, Electricity production, Hydrogen, Underground storage, Spain.

1 Introduction

The reduction of fossil energy sources with the aim of meeting the climate protection International Agreements will inevitably require an increase in the generation of renewable energy [1-2]. The progressive growth in the share of variable renewable energy sources in the global energy mix brings to light the essential role of these sys-

2

tems in the future energy sector. However, the intermittency associated to these sources means an important obstacle that must be solved through storage technologies at different time scales (hourly, daily or seasonal). Energy storage systems will be then indispensable as renewable installations become the major source of energy. In this sense, Underground Hydrogen Storage (*UHS*) could mean an effective solution as large-scale storage of energy surplus to deal with seasonal demands [3]. Hydrogen can be produced by using the “Power to Gas” concept through electrolysis utilizing electricity coming from renewable sources [4]. This gas presents a high energy density and can be used in a wide range of applications such as methanation, fueling vehicles or re-electrification. In addition, hydrogen can be also fed into fuel cells to produce electricity in low generation periods (“Power to Power” concept).

As in the case of the natural gas, geological formations provide the required capacity to store the large volumes of hydrogen that could be used to cover the seasonal demands with a reasonable cost [5-6]. However, the properties and physical behavior of hydrogen are not the same of the natural gas or air. Under the same conditions hydrogen has inferior calorific value than the one of the natural gas, its molecular weight makes it more susceptible to leakage and its diffusion coefficient in air is four times greater than it is for natural gas at standard pressures and temperatures [7-8]. In this context, higher storage pressures are required to store the same mass and special preventive measures must be taken into account. It is also recommended to consider the chemical reactivity since hydrogen gas could affect the structural integrity of steel alloys and interact with clay or other minerals of the reservoir that could dissolve sulfate minerals, carbonates or feldspars, among others [9-10]. These phenomena must be also evaluated to avoid alterations in the reservoir quality such as primary flow paths or its preliminary porosity [11].

Geological formations usually considered for UHS are caverns in salt deposits (lined or unlined caverns in hard rock) and deep porous media such as depleted gas and oil fields and saline aquifers [12-13]. While there are numerous researches focused on the potential of UHS, practical experience for large-scale storage of hydrogen gas is limited to salt caverns in four locations worldwide (three of them are located in the United States and one in the United Kingdom [14-15]).

1.1 Underground gas storage in the world

As already mentioned, an underground gas storage system is an artificially accumulation of gas in the environment at a significant depth (hundreds of meters or more). The potential of these facilities derive from the advantages provided:

- The underground storage systems are easier to integrate with the landscape and the existing structures.
- These facilities are less susceptible to fire, military actions or terrorist attacks.
- The construction costs are much lower than the ones associated to surface structures with similar capacity.

- Suitable geological structures are commonly available in a large number of countries.

The above advantages have contributed to the global expansion of these storages. In this way, the number of underground gas storage structures and their capacity have grown considerably in the last 100 years, in special in those countries of the Northern Hemisphere. As shown in Figure 1, most of these facilities are located in depleted hydrocarbon deposits and then in aquifers and salt caverns.

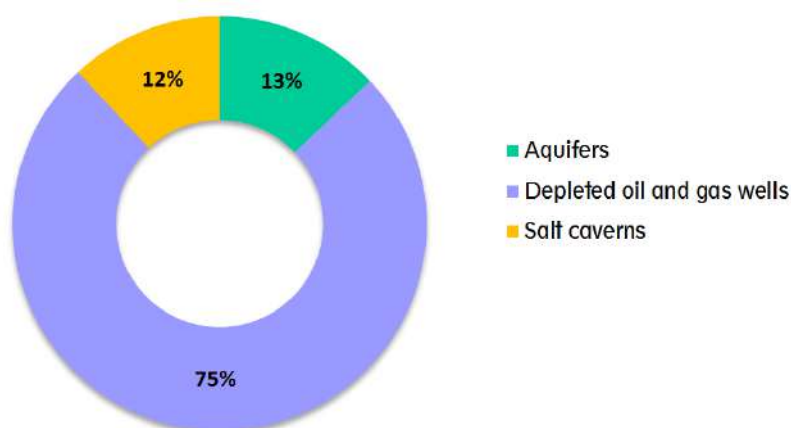


Fig. 1. Share of UGS by storage type in the world (2010) [16].

Additionally, Figure 2 presents the distribution of UGS by regions. As can be observed in the mentioned Figure 2, most UGSs are located in North America (USA and Canada) followed by Europe.

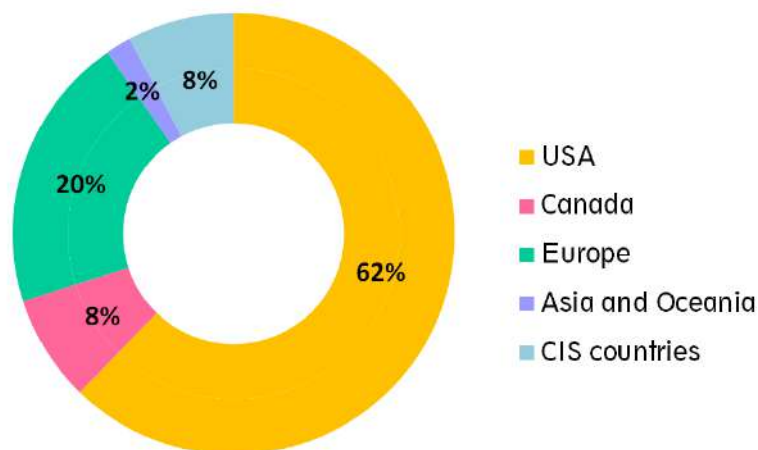


Fig. 2. Share of UGS by regions (2010) [16].

4

The development of the underground gas storages, especially the hydrogen systems considered in this research is quite limited in some European countries, such as Spain. For this reason, the aim of this work is to provide an overview of the possibilities of constituting effective underground hydrogen storages in Spain. Thus, each of the UHS alternatives will be evaluated to estimate the potential of the country within the hydrogen storage. The following sections include a description in terms of energy, geological, lithological and geotechnical information of Spain as well as the analysis of each type of underground structure in the country.

2 Description of the country under study

2.1 Energy perspectives in Spain

There is a current need among numerous countries of introducing governmental policies focused on the transformation of their energy systems. According to the European Union Energy and Climate Package, Europe is planned to increase the share of renewable generation from 28 % in 2015 to 36 % in 2020, exceeding 50 % in 2050 [17].

In Spain, the electricity sector is constituted by a reliable power generation mix in the frame of the fossil-renewable transition. The trend in the last ten years clearly shows a reduction in the contribution of fossil-based technologies leading to a growth of renewable sources, in special the wind and solar power production. This fact is in line with the objectives expressed in the Spain's National Renewable Energy Action Plan (2011-2020) [18].

Regarding the large power generation (nominal power ≥ 50 MW), Spanish coal-fired plants are now part of the Transitional National Plan (2016-2020) [19] that allows them to be exempt from complying with the emission limits of the Directive 2010/75/EU [20]. After the mentioned plan, all plants exceeding the limit values will be obliged to close down. In the context of the nuclear energy, five plants are in operation, being their licenses expired in the next 11 years.

Considering now the renewable sector, up to the year 2008, Spain was a global leader in the promotion of renewable energy. Wind energy systems progressively grew since the mid-1990s, while the number of photovoltaic (PV) installations remained low until 2004 [21]. After that, 2007 brought a boom in solar PV systems, rising from 103 MW in 2006 to 544 MW in 2007 and to 2708 MW in 2008. This increase caused the application of several amendments to the renewable energy scheme, paying special attention to the solar PV sector [22]. After years of standstill, Spain restarted the auctions of renewable electricity in 2017. The following Figure 3 describes the global electricity production by source for the period 1990-2018 in Spain.

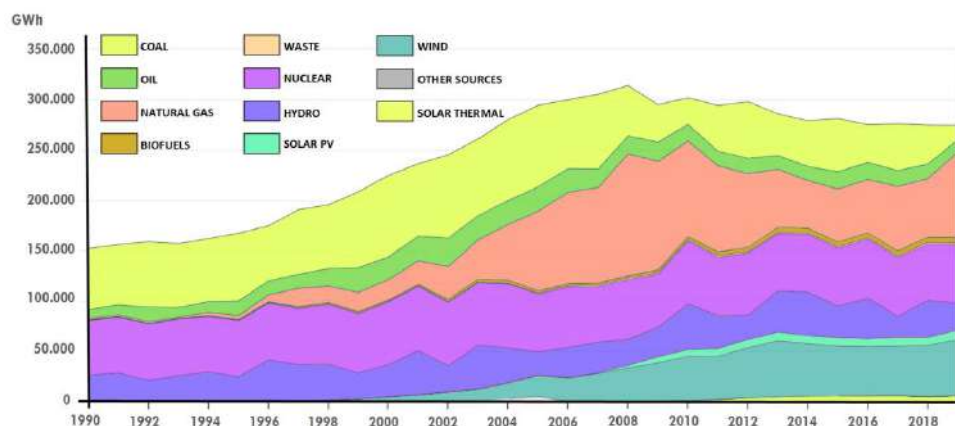


Fig. 3. Spanish electricity production by source during the period 1990-2018 [23].

In general terms, it can be assumed that Spain has significant overcapacity in its electricity system, that is to say, high installed capacity compared to the electricity demand. In addition, the Spanish electricity system constitutes an energy island with limited possibilities to export the produced energy. All the above causes that nearly all the power produced in the country has to be consumed on it.

In this sense, the management of surplus energy could be achieved in Spain by one of the possible alternatives of UHS systems. Focused on this aim, this research provides a preliminary overview of appropriate sites for UHS in Spain based on the available information.

2.2 Geology and seismic hazards

It can be assumed that the geology of Spain is hugely diverse, including one of the most complete Paleozoic sedimentary successions in Europe. These successions reveal a unique Iberian paleogeography influenced by the Atlantic Ocean and by events in the Tethys Ocean and Alpine-Himalayan orogeny. The underlying geology has been created by Cenozoic events linked to the Alpine orogeny. Apart from the mountainous northern and southern margins of Iberia, the center of Spain is dominated by two large Cenozoic basins, drained by the Duero River in the north and the Tajo River in the south [24].

An important concern when considering UHS is the seismic activities of the area which could compromise the integrity of the storage system. In Spain, Quaternary and Neogene volcanism has appeared in southern, south-central and eastern mainland Spain. The most remarkable phenomenon is the Canarias volcanoes which exposes one of the most known hot spot related ocean island chains. Beyond this, the seismic map of Spain presented in Figure 4 shows that most of the country fall into low hazard zones. However, the potential areas identified in this work must be submitted to an arduous analysis that ensures the technical viability of the future system.

6

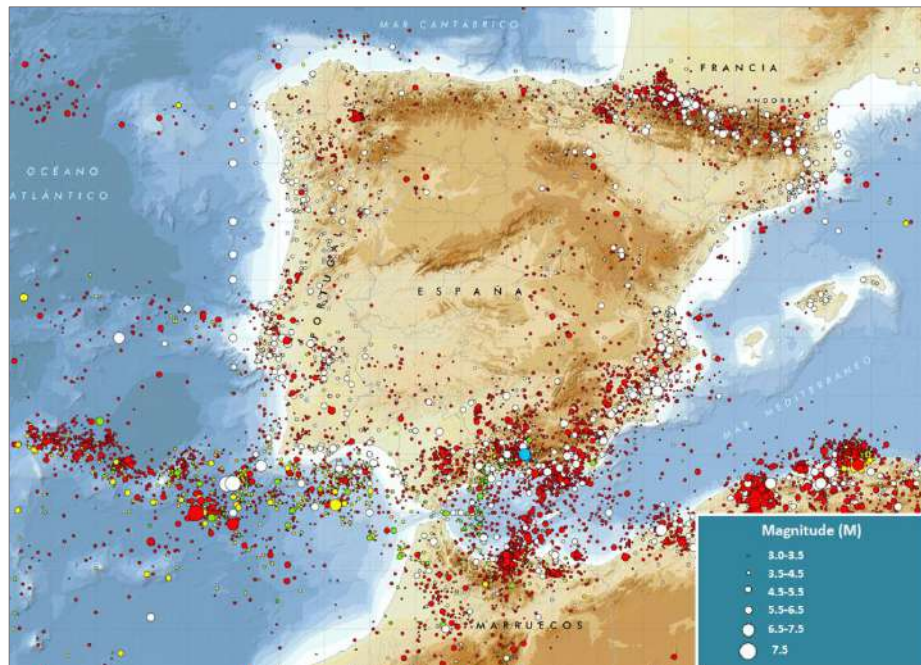


Fig. 4. Seismicity in the Iberian Peninsula and the vicinity areas [25].

3 Potential UHS structures

3.1 Salt caverns

Salt caverns are commonly considered the most promising underground storage option due to the low cushion gas requirement, the inter nature of the salt structure and the sealing capacity of the rock, which prevent the contamination of the stored hydrogen. As already mentioned in the introduction section, there are only a few sites being used for hydrogen storage in salt caverns (one in United Kingdom and three more in the United States). These projects have, however, proven for decades the technical feasibility of underground hydrogen storage systems.

Several authors have investigated the potential for hydrogen storage in underground formations such as the salt caverns, paying special attention to appropriate storage locations [26-27]. In particular, The *HyUnder project* addresses the study of caverns for hydrogen storages of 5 European countries; Germany, the Netherlands, the United Kingdom, Romania and Spain [28]. Focusing on the particular case of Spain, according to this project, this country presents four main locations for UHS. These sites were defined by considering the location near wind resources and electric and natural gas grids but also because of geological conditions and local hydrogen demand [29]. The following Figure 5 shows the potential areas selected in the project.



Fig. 5. Spanish salt cavern sites selected in the *HyUnder* project for underground hydrogen storage establishing a radio of utilization of 250 km [29].

Since the application of Power to Power or hydrogen re-electrification is not considered in the *HyUnder project*, this work also presents a general overview about the geological formations (salt caverns) that constitute the country under study and that could mean potential future UHS.

Spain is characterized by Mesozoic evaporite deposits covering large areas of the subsurface from the Betic Cordillera over the Iberian Range to the northern coast, up to the Bay of Biscay. Based on existing prospecting campaigns, the top salt of these deposits exceeds depths of 2000 m. Regarding Tertiary evaporitic formations; these can be found in the Ebro, Duero and Tagus Basin. The thickness of these halite beds is considerable but highly folded facies are present as well as high concentrations of anhydrite and gypsum.

When talking about storage potential of salt caverns, three main classifications are commonly established: onshore, onshore constrained and offshore. In this way, offshore caverns are placed in salt domes under the Sea; whereas the onshore ones are those located on land (once applied the eligibility constraints). The constrained caverns are defined considering a constraint of 50 km distance from shore. According to published report [28], the highest onshore storage potential is observed in Germany (9.45 PWh), followed by Poland (7.24 PWh) and Spain (1.26 PWh), constituting these three countries 77 % of the total potential. Hence, Spain has high onshore storage capacities, counting with a total of located 24 caverns. However, more than a half of these formations are placed less than 50 km from the coast.

The most important of all the Spanish salt caverns is known as the Salt Mountain of Cardona in Catalonia. It is in the shape of an elongated ellipse and has an area of 1.800 m long by 600 wide and an area of approximately 100 hectares. These caverns are constituted in some areas by a layer of salt of approximately 300 meters of thickness, constituting an excellent site for hydrogen storage.

The total storage capacity of Spain has been then estimated in 1.26 PWh of hydrogen, being all this potential onshore. In the case of offshore storage, Norway leads the European countries with 7.5 PWh-H₂ of storage potential for caverns in the high seas, all in the North Sea. The following Figure 6 summarizes the global cavern storage capacity for several European countries, including Spain.

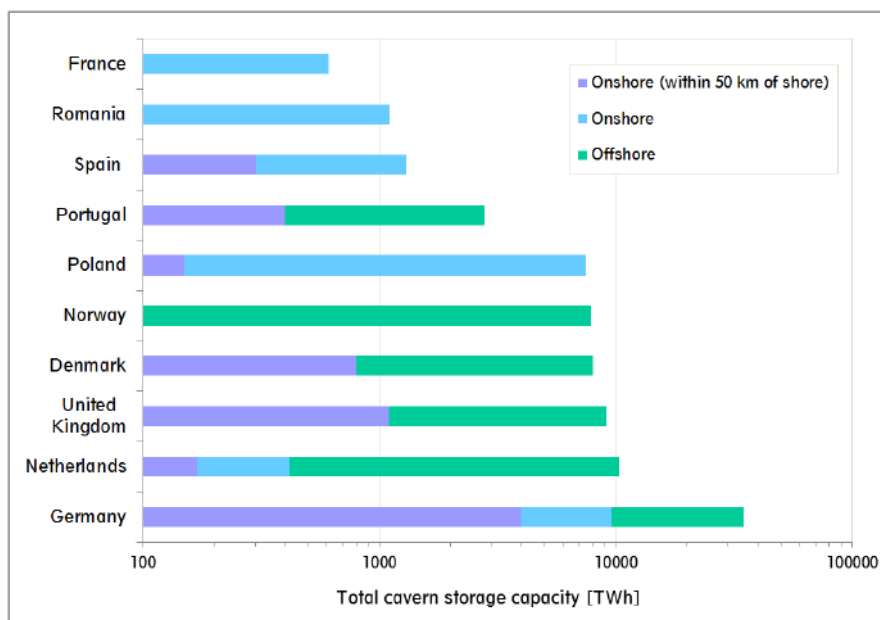


Fig. 6. Total cavern storage capacity for different European countries, including the one considered in this research [31].

3.2 Saline aquifers

Saline aquifers constitute geological structures distributed worldwide that present large potential storage capacity (around hundreds of Mm³). Despite these formations accumulate the majority of the natural gas storage in the subsurface, at date there are not pure hydrogen storages. Different aquifers are however being used to store town gas (with around 50 % of H₂ and 50 % of CH₄) in Germany, France and in the Czech Republic [32]. These experiences confirm that storage in deep aquifers is a cost-effective option and a promising alternative for seasonal hydrogen storage.

A potential underground storage formation must be constituted by impervious overlaying seal that ensure the confinement of the injected fluid and prevent the migration of the gas to the surface. The aquifer requires also having enough capacity and high permeability to allow the migration of the gas and to dissipate the pressure. The best situation is that in which the structure is located in appropriate tectonic traps such as domes to recovery the hydrogen in a high quality way.

When analysing the effective gas storage capacity of deep aquifers, the expression presented in Equation 1 can be used [33].

$$C_T = A \cdot h \cdot \emptyset \cdot \rho_G \cdot S_{eff} \quad (1)$$

Where:

C_T = total effective storage capacity (t)

A = area covered by regional aquifer (m²)

h = average height of aquifer · average net to gross ratio (m)

\emptyset = average reservoir porosity (%)

ρ_G = density of the gas at reservoir conditions (t/m³)

S_{eff} = storage efficiency (% of pores expected to be filled with the gas)

From Equation 1, the EU *GeoCacity project* estimated the gas storage capacity of different basins belonging to European countries, as Spain. This project was focused on the evaluation of three main areas [34]:

- *Iberian Massif*
Covering the Western part of Spain and almost the whole territory of Portugal, it is constituted by Palaeozoic materials affected by Hercinian tectonics. In this area, it is common to identify igneous and metamorphic rocks, along with faults, steep folding and compression. From the results of this analysis, this region was discarded as storage for CO₂ and therefore it will be probably rejected for storing hydrogen.
- *Alpine mountain ranges*
Three main mountains were formed during the Alpine movements: The Pyrenees and Cantabrian Mountains in the North with an E-W strike, the Iberian Mountains in central Spain with NW-SE strike and the Betican Chain on the Mediterranean coast with a SW-NE strike. This area has been considered appropriate for the gas storage, in special in those formations with sandstones and karstic carbonates.
- *Cenozoic Basins*
This kind of deposits is present in areas of great Iberian rivers (Ebro, Tajo, Duero and Guadalquivir). Prospecting analysis have shown that the thickness of sediments in some of these regions is over 5.000 m, including deposits of sands, sandstones and karstic carbonates filled with salty water. The characteristics and conditions of these deposits denote that the structures could constitute potential hydrogen storage.

In summary, in the case of Spain, the principal potential storage aquifers have been found in Tertiary sedimentary basins as the Ebro, Duero and Guadalquivir basins. In particular, in the Duero basin different structures have been identified for gas storage in previous carbon storage projects. The formations are located in the NW margin of the basin, close to the boundary with the Basque-Cantabrian basin. As described below, different Spanish projects and researches are addressing the evaluation of deep aquifers for CO₂ storage and could be the basis for the future UHS.

- In the north of Spain (Asturias), Palaeozoic sedimentary basins constituted by carbonated and siliciclastic aquifer formations are considered potential reservoirs of great thickness and suitable cap rocks in Carboniferous and Devonian materials [35].
- In the southeast of Spain, the Gañuelas-Mazarrón Tertiary basin hosts a deep saline CO₂-rich aquifer, being catalogued as a natural analogue for gas storage and recovery.
- The Utrillas formation (Teruel) in the San Pedro Dome saline aquifer has been numerically evaluated through computer simulations showing that the structure could be operated with optimal recovery ratios for seasonal energy demands. The formation is hosted by quartz-rich Albian sandstones, with high permeability ($1 \times 10^{-13} m^2$), high salinities (>50,000 ppm of total dissolved solids) and thickness up to 350 m in the top of the dome, being the porosity of the sandstones in the ranges of 13-20 %. On top of that, the formation is covered by low permeable rocks of Late Cretaceous age that ensure the isolation of the stored gas [36].
- Another Spanish CO₂ storage prospecting project in deep aquifers is The Hontomín URL led by the Fundación Ciudad de la Energía – CIUDEN. The Hontomín site (Burgos) is located in the southern sector of the Basque-Cantabrian Basin. The mentioned project has allowed defining the boundaries of the saline aquifer and identifying the most probable leakage pathways [37].

3.3 Depleted petroleum and gas fields

Depleted hydrocarbon deposits are geological structures usually adapted as gas storage facilities. These formations consist of a reservoir (hydrocarbons accumulated in the pore space of the rocks), a seal and an underlying aquifer.

Nowadays, depleted gas deposits are the most common option of underground storage sites. In this sense, costs may be reduced when adapting the deposits to the needs of underground hydrogen storage. The main advantage of these structures is that they were well recognised during the exploration and exploitation phases. Thus, as the original gas remained in the deposit for millions of year, its tightness is already guaranteed.

Regarding depleted oil deposits, they are not very common at underground gas storage facilities. The principal reason is that the large amounts of hydrogen could enter into chemical reactions with the residual oil. Hydrogen could, in this way, become converted into methane, dissolve in the oil and become irreversibly lost.

Focusing now in the country under study, first of all, it is important to highlight that Spain cannot be considered a prolific hydrocarbon country. Several deposits have been discovered, the first of which was oil, in 1964, in Ayoluengo (Burgos), and the later ones in the Mediterranean Sea, the Gulf of Valencia, the Cantabrian Sea, the Guadalquivir Valley and the Gulf of Cadiz.

The hydrocarbon exploration in Spain started in the early 20th century. In this context, 708 exploration wells have been drilled; 438 onshore and 270 offshore, 126 in the Mediterranean and 144 in the Atlantic. In spite of these exploration experiences, only 20 have been used for production.

There are currently five oil wells in production that contribute 0.15 % to the country's global demand. The production of these sites is progressively decreasing and is expected to be nil in the near future. Table 1 includes the production of the last twelve months of the five hydrocarbon wells currently operating in Spain.

Table 1. Spanish hydrocarbon wells currently in production.

Hydrocarbon well	Last 12 months production (kt)
Boquerón	17
Casablanca	45
Montanazo-Lubina	8
Rodaballo	2
Viura*	8
TOTAL PRODUCTION	80

* Mainly natural gas production

Additionally, in Figure 7 it is possible to observe the decreasing evolution of the hydrocarbon production in Spain for the period 1965-2015.

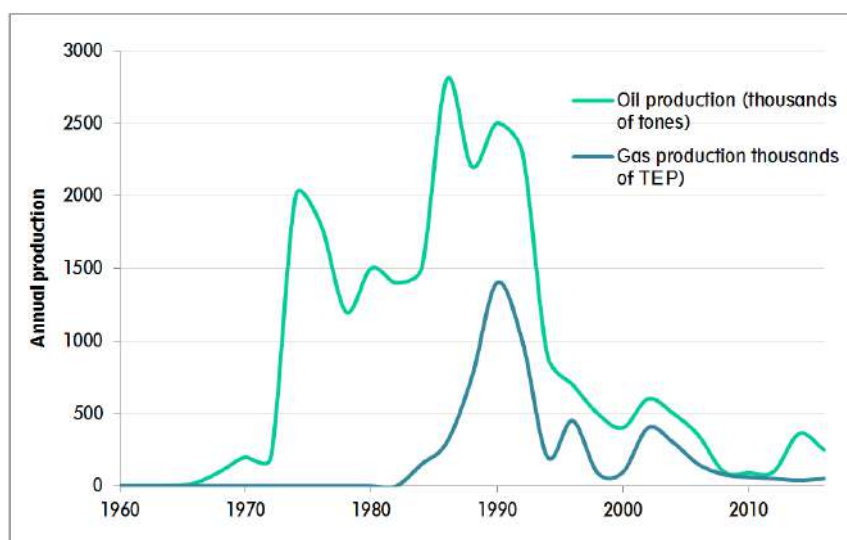


Fig. 7. Evolution of the gas and oil production in Spain 1960-2015 [38].

It is also important to mention that the new Spanish climate regulation prohibits the research and exploration activities of new hydrocarbon sites both in the marine and terrestrial subsoil. The prohibition of new permits does not affect, however, current applications in process.

4 Discussion

The analysis performed in the previous sections is crucial for identifying the real potential of the Spanish geological structures to become underground hydrogen storage. The experience of the country in storing other gases, such as the natural gas or the CO₂, means a valuable starting point to define the possibilities in the context of the hydrogen storage. Based on the information previously provided, the following statements can be deduced:

- The analysis of the energy perspectives in Spain shows that derived from the rising renewable electricity production, underground energy storages will be key for effective energy transition.
- From the existing experience in the natural gas storage, UHS is considered as a promising future option in the near future of the country.
- Among the geological structures considered as UHS, salt caverns and deep aquifers stand out in the country over the depleted hydrocarbon fields.
- Regarding the potential of storing hydrogen in salt caverns, previous works point out that Spain presents four principal locations for UHS, in the north, northeast, east and south of the country. On top of that, Spain is the third country with the highest onshore storage capacities in this kind of formations (counting with 24 caverns).
- Considering now the underground storage in saline aquifers, the most relevant potential of Spain has been found in Tertiary sediments basins, as the Duero, Ebro and Guadalquivir basins. However, other areas such as the formations of sandstones and karstic carbonates in the alpine mountain ranges could also constitute suitable gas storage structures. The high number of projects in the field of the CO₂ in the country lays the foundations for the future hydrogen storage in these formations.
- Concerning the depleted hydrocarbon fields, since Spain is not a prolific gas and petroleum country, the possibilities of using these structures as UHS is limited. Despite this fact, the wells that were in production (around 20) and are now depleted, constitute a promising structure with known storage conditions. In addition, the five fields currently operating in Spain are expected to be close down in the near future, so they will also constitute possible structures for the underground hydrogen storage.

5 Conclusions

The Spanish scenario for the year 2030 includes the replacement of a considerable amount of installed power from conventional sources with renewable energy systems. Derived from the generation of renewable electricity, the country will be obliged to face an important surplus of energy in spring and summer. Moreover, by the year 2050, the objective of Spain is to achieve 100 % renewable power generation. Having this information in mind, it is obvious that the seasonal energy storage will have to be complemented in order to avoid the need of importing so much natural gas in the cold months. In this sense, the use of hydrogen as underground energy storage will become essential in the near future of Spain.

This work analyzes the feasibility of UHS in the country of Spain by considering the usual geological structures (salt caverns, deep aquifers and depleted oil and natural gas deposits). Results clearly indicate that several rock structures in the country are favorable for the future storage of hydrogen. Numerous salt caverns are present with high onshore store capacities as well as the deep aquifers of the Tertiary sedimentary basins. Depleted hydrocarbon fields, although limited, could also constitute a defined reservoir for the underground hydrogen storage.

Further work is required in this field to study in-depth not only the geological and technical possibilities of the UHS but also the economic concern (proximity to renewable power installations and energy demand) that will ultimately define the global feasibility of the system.

This work highly contributes to the green environment and renewable energies development in the context of getting a sustainable future within the field of smart cities, the topic of the ICSC-CITIES 2020 Congress.

References

1. European Commission. "Energy 2020. A strategy for competitive, sustainable and secure energy." (2011).
2. UNITED NATIONS PUBLICATIONS. UNITED NATIONS TREATY SERIES. UN, (2016).
3. Tarkowski R.: Underground hydrogen storage: characteristics and prospects. *Renew Sustain Energy Rev* 105, 86-94 (2019).
4. Schiebahn S, Grube T, Robinius M, Tietze V, Kumar B, Stolten D.: Power to gas: technological overview, systems analysis and economic assessment for a case study in Germany. *Int J Hydrogen Energy* 40, 4285-94 (2015).
5. Taylor, J. B., Alderson, J. E. A., Kalyanam, K. M., Lyle, A. B., & Phillips, L. A.: Technical and economic assessment of methods for the storage of large quantities of hydrogen. *International Journal of Hydrogen Energy* 11(1), 5-22 (1986).
6. Carr, S., Premier, G. C., Guwy, A. J., Dinsdale, R. M., & Maddy, J.: Hydrogen storage and demand to increase wind power onto electricity distribution networks. *International journal of hydrogen energy*, 39(19), 10195-10207 (2014).
7. Crotofino F, Wasserstoff-Speicherung Hamelmann R. In: *Salzkavernen zur Glättung des Windstromangebots.*: KBB Underground Technologies GmbH; (2007).

14

8. Reitenbach V, Ganzer L, Albrecht D, Hagemann B.: Influence of added hydrogen on underground gas storage: a review of key issues. *Environ Earth Sci* 73(11), 6927-37 (2015).
9. Szummer A, Jezierska E, Lublinska K.: Hydrogen surface effects in ferritic stainless steels. *J Alloy Comp*, 293-295:356-60 (1999).
10. Kanazaki T, Narazaki C, Mine Y, Matsouoka S, Murakami Y.: Effects of hydrogen on fatigue crack growth behavior of austenitic stainless steels. *Int J Hydrogen Energy*, 33(10), 2604-19 (2008).
11. Henkel S, Pudlo D, Werner L, Enzmann F, Reitenbach V, Albrecht D.: Mineral reactions in the geological underground induced by H₂ and CO₂ injections. *Energy Proc* 63, 8026-35 (2014).
12. Lord, A. S.: Overview of geologic storage of natural gas with an emphasis on assessing the feasibility of storing hydrogen. SAND2009-5878, Sandia National Laboratory, Albuquerque, NM. (2009).
13. Ozarslan, A.: Large-scale hydrogen energy storage in salt caverns. *International Journal of Hydrogen Energy*, 37(19), 14265-14277 (2012).
14. Felseghi, R. A., Carcadea, E., Raboaca, M. S., Trufin, C. N., & Filote, C.: Hydrogen Fuel Cell Technology for the Sustainable Future of Stationary Applications. *Energies*, 12(23), 4593 (2019).
15. HyUnder. Overview on all known underground storage technologies for hydrogen. https://www.fch.europa.eu/sites/default/files/project_results_and_deliverables. (2018).
16. Gąska K, Hoszowski A, Gmiński Z, Kurek A. Monografia podziemnych magazynów gazu w Polsce. Stowarzyszenie Inżynierów i Techników Przemysłu Naftowego i Gazowniczego Oddział Warszawa II, Warszawa; (2012).
17. Capros, P., De Vita, A., Tasios, N., Siskos, P., Kannavou, M., Petropoulos, A., ... & Paroussos, L.: EU Reference Scenario 2016-Energy, transport and GHG emissions Trends to 2050, (2016).
18. Zeeshan Shirazi, S., & Mohammad Zeeshan Shirazi, S.: Review of Spanish renewable energy policy to encourage investment in solar photovoltaic. *Journal of renewable and sustainable energy*, 4(6), 062702 (2012).
19. Spanish Ministry of Agriculture, Fishing, Food and Environment. Spanish transitional national plan (TNP)-Directive 2010/75/EU-large combustion plants. Madrid: MAPAMA; (2016).
20. European Union. Directive 2010/75/EU of the European Parliament and of the Council of 24 November 2010 on industrial emissions (integrated pollution prevention and control). *Off J Eur Union*, L334:17-119 (2010).
21. Del Rio, P., & Mir-Artigues, P.: A cautionary tale: Spain's solar PV investment bubble. *International Institute for Sustainable Development* (2014).
22. Real Decreto 1578/2008, de 26 de septiembre, de retribución de la actividad de producción de energía eléctrica mediante tecnología solar fotovoltaica para instalaciones posteriores a la fecha límite de mantenimiento de la retribución del Real Decreto 661/2007, de 25 de mayo, para dicha tecnología. *Agencia Estatal Boletín Oficial del Estado (BOE)*, (2008).
23. IEA, International Energy Agency. *World Energy Balances, Database documentation* (2020).
24. Gibbons, W., & Moreno, T. (Eds.): *The geology of Spain*. Geological Society of London (2002).
25. IGN, Instituto Geográfico Nacional. *Seismic hazards map, general seismic map of the Iberian Peninsula* (2015).
26. Tarkowski R, Czapowski G.: Salt domes in Poland – potential sites for hydrogen storage in caverns. *Int J Hydrogen Energy*, 43, 21414-27 (2018).

27. Michalski J, Bünger U, Crotogino F, Donadei S, Schneider G-S, Pregger T, et al.: Hydrogen generation by electrolysis and storage in salt caverns: potentials, economics and systems aspects with regard to the German energy transition. *Int J Hydrogen Energy*, 42, 13427-43 (2017).
28. Assessment of the potential the A and RBC for LS and LTS of RE by HUS in E, editor. *HyUnder Project*, 18 (2014).
29. Simon, J., Ferriz, A. M., & Correas, L. C.: *HyUnder*-hydrogen underground storage at large scale: case study Spain. *Energy procedia*, 73, 136-144 (2015).
30. Gutiérrez, F., Calaforra, J. M., Cardona, F., Ortí, F., Durán, J. J., & Garay, P.: Geological and environmental implications of the evaporite karst in Spain. *Environmental Geology*, 53(5), 951-965 (2008).
31. Caglayan, D. G., Weber, N., Heinrichs, H. U., Linßen, J., Robinius, M., Kukla, P. A., & Stolten, D.: Technical potential of salt caverns for hydrogen storage in Europe. *International Journal of Hydrogen Energy*, 45(11), 6793-6805 (2020).
32. Panfilov, M., Gravier, G., & Fillacier, S.: Underground storage of H₂ and H₂-CO₂-CH₄ mixtures. In *ECMOR X-10th European conference on the mathematics of oil recovery* (pp. cp-23). European Association of Geoscientists & Engineers (2006).
33. Dalhoff, F., Vangkilde-Pedersen, T.: Storage capacity calculations in saline aquifers. *CO₂ Net Annual Seminar*, November 6-7 (2007).
34. Martínez, R., Suárez, I., Zapatero, M. A., Saftic, B., Kolenkovic, I., Car, M., ... & Donda, F.: The EU GeoCapacity project—saline aquifers storage capacity in group south countries. *Energy Procedia*, 1(1), 2733-2740 (2009).
35. Loredó, J., Cienfuegos, P., & Pendás, F.: OPPORTUNITIES FOR CO₂ GEOLOGICAL STORAGE IN CENTRAL COAL BASIN (NORTHERN SPAIN). *CO₂SC* (2006).
36. Sáinz-García, A., Abarca, E., Rubí, V., & Grandia, F.: Assessment of feasible strategies for seasonal underground hydrogen storage in a saline aquifer. *International Journal of Hydrogen Energy*, 42(26), 16657-16666 (2017).
37. Ogaya, X., Queralt, P., Ledo, J., Marcuello, Á., & Jones, A. G.: Geoelectrical baseline model of the subsurface of the Hontomín site (Spain) for CO₂ geological storage in a deep saline aquifer: A 3D magnetotelluric characterisation. *International Journal of Greenhouse Gas Control*, 27, 120-138 (2014).
38. CORES, Corporación de Derecho Público tutelada por el Ministerio para la Transición Ecológica y el Reto Demográfico (2020).

Errors in the design and execution of the well field of low enthalpy geothermal systems.

Ignacio Martín Nieto¹[0000-0003-3984-7228], Cristina Sáez Blázquez¹[0000-0002-5333-0076], Arturo Farfán Martín¹[0000-0002-1506-1207] and Diego González-Aguilera¹[0000-0002-8949-4216]

¹ Department of Cartographic and Land Engineering, University of Salamanca, Higher Polytechnic School of Avila, Hornos Caleros 50, 05003 Avila, Spain.

nachomartin@usal.es

Abstract. This work summarizes cases of defects in the design and execution process of low enthalpy geothermal systems. It is based on the research experience and the review and design of facilities and processes carried out in the TIDOP research group of the University of Salamanca during the last 4 years. A detailed report is presented of the observed cases as well as their frequency, also mitigation and remedial measures are proposed when this is possible. The importance of refining all the design and execution techniques of these systems to favor their large-scale implementation is also highlighted. This implementation is increasingly necessary in a scenario of electrification of heating/cooling systems to contribute to the reduction of greenhouse gases, taking into account the horizon set by the European Union for the coming years.

Keywords: Well Field Design, Cases, Geological Affection, Soil Depletion, Pipes and Grouting.

1 Introduction

A new emissions target for the year 2030 will be proposed by the European Union, it is expected that it is proposed to increase the reduction of greenhouse gases from the 40% currently proposed to at least 55% [1].

In this scenario, the emission reduction in the heating/cooling sector could play a very important role, taking into account that this sector is responsible of the 36% of the CO₂ emissions in the E.U. [2]. Here heat pump based cooling/heating systems could become the key in the decarbonization upcoming process.

It is expected to see an increasing growth in the spread of the low enthalpy geothermal systems thorough most of the European countries as well as the aerothermal energy installations (heat pump systems which extract energy from the surrounding air). So may be interesting to make a review of some different fail cases that could affect the performance of these systems. To make a short briefing about the things that can go wrong when designing this type of installations as well as during the construction phase.

When compiling the different possibilities described in this work, its nature, its observed frequency as well as its impact on the performance and operation of the facility

have been described. In addition, measures have been proposed to reduce the risk of appearance of the different failures, as well as ways to solve the problem when this is possible.

It will be noted that the percentages of frequencies in the different cases are sometimes given in an approximate manner. This is due to the fact that in most cases it has not been possible to carry out an exhaustive follow-up of the geothermal installations involved since it is in private areas with very limited access by the researchers. What has been collected is the fruit of the observations that have been made when it has been possible to get access to the installations or it's data.

The motivation of this work is to contribute in the development of policies of good practices that favor the reduction of the errors that are described here. It is necessary to reduce the percentage of low-enthalpy geothermal installations that fail in the first years of operation, as this is a brake on the popularization of these heating systems that will be important in the future.

2 Cases

Before entering the revision of the different possibilities founded in the designing process or in the construction step of the geothermal systems, it seems important to establish how is considered that a well-designed system looks like. The key in designing low enthalpy geothermal systems is to have accurate data about the thermal properties of the ground, after that the thermal needs to be provided by the ground are considered and then the dimensioning process of the ground heat exchanger is done through a simulation of the geothermal fluid temperature during no less than 25 years in order to discern if that temperature stabilizes above the minimum accepted temperature fixed by the designer. In fig. 1 a success case in the temperature stabilization can be observed.

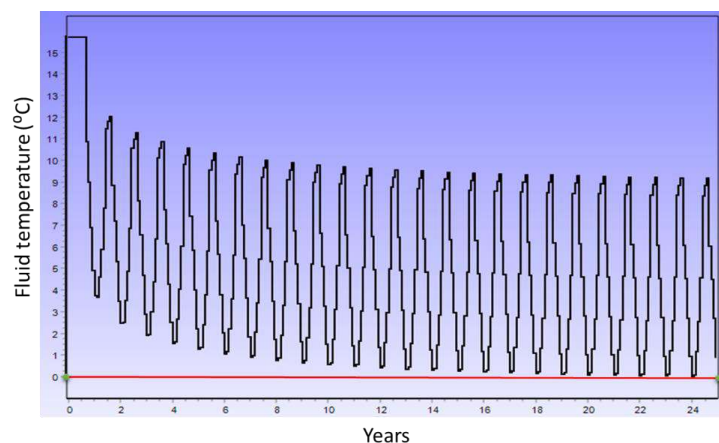


Fig. 1. Fluid temperature evolution (25 years). “Earth Energy Designer” (EED) software, developed by Blocon Software.

Notice in Fig. 1 that the temperature restriction for the fluid is 0 °C, hence the fluid does not surpass that lower limit and tends to stabilize above it.

Now, in Table 1 a summary of the different failure cases found during the years of investigation and in situ analysis of different low enthalpy geothermal systems. More critical fails are at the top and as the list goes down, the severity of the failures decreases.

Table 1. Different failures in low enthalpy geothermal systems.

Case	Description	Impact	Level of severity
A	Geological affection of the area	Local changes in the ground shape and properties	Very high
B	Loss of wells due to fluid leaks in geothermal pipes (with installation in operation phase).	From loss of efficiency in the heat pump to exhaustion of the soil by reducing the length of the effective heat exchanger.	From low to high
C	Well collapse during the drilling process	It can extend the duration of the drilling work as well as make it more expensive.	Medium-high
D	Failures concerning the overestimation of the thermal properties of the ground	Soil thermal depletion for under sizing of exchanger length	Medium-High
E	All failures concerning pipe installing and grouting. Including pressure tests.	Pipe replacing could be needed, bad grouting selection.	Medium
F	Failures concerning the underestimation of the thermal properties of the ground	Increase in initial investment costs. Reduction of energy consumption due to an increase in the COP of the heat pump.	Low

The frequency of appearance of the different events in table 1 can also be considered ascending from the rarities (case A) to the most common, and to a certain extent admitted, cases F.

3 Case discussion

In this section, a brief discussion of the different cases from Table 1 will be presented. Known and especially paradigmatic cases of each case considered will be cited and an estimate of the frequency of appearance will be made based on the experience of the research team.

3.1 Case A

The geological affection of the area due to geothermal drilling is an extremely rare event. There is only one case widely recognized by the scientific community dedicated to the research in the field of low enthalpy geothermal energy.

It is interesting to know the case of the city of Staufen im Breisgau, in the German Black Forest region, where geothermal perforations were made that were not filled quickly enough. There was a swelling of an anhydrite layer that encountered the water. This has produced changes in the terrain that have damaged more than 270 buildings in the historic city. Fig. 2. shows the situation of some buildings in the city as well as the geological scheme of the swelling.



Fig. 2. Staufen im Breisgau. Geological scheme. Situation of some buildings of the town.

As we can see, a study of the geology of the place where a geothermal catchment field is to be installed is of paramount importance. In addition to taking the proper precautions in terms of sealing times of the boreholes.

The frequency of events of this type is extremely low, considering that one has occurred in Europe among hundreds of thousands of installations [3].

3.2 Case B

In case B the loss of wells due to fluid leaks in geo-thermal pipes when the installation is in the operational phase could cause loss of efficiency in the heat pump in the less important of the cases. If a critical loss of length of the heat exchanger occurs, the exhaustion of the soil could happen. This is a critical fail of the well field.

As a guide to avoid the deterioration of the pipes throughout the useful life of the geothermal installation, we can recommend a series of measures. The materials used in the construction of the geothermal exchanger must be resistant to corrosion and adequate to the working pressures and temperatures. The AENOR UNE 100715-1: 2014 standard establishes a duration of the exchanger of at least 50 years. If we use polyethylene pipes, it is recommended that they have at least the characteristics of PE 100 PN 16 SDR 11.

It is highly recommended that geothermal probes should be made of a single piece, if at all except for the “U” or probe foot that must be factory-assembled and with its corresponding pressure test performed.

It is advisable to also require a PN 16 for buried sleeves, connections, and other accessories.

When installing vertical geothermal pipes, the lowering of the exchanger must be carried out with special care. This maneuver seems to be the source of all kinds of problems that are revealed later in the mandatory pressure tests. Not carrying out these pressure tests is a very serious irresponsibility towards the client, let us think that we are putting the well operation at risk. In general, a geothermal well that loses fluid is a problem that has no easy solution, beyond bridging that well.

It is strongly recommended to use a winch or similar device, which must have a brake mechanism to control the descent maneuver.



Fig. 3. Geothermal pipe-controlled descent. Comfortworks, Inc. Goldsby, Oklahoma, U.S.A.

Of the dozen geothermal facilities in operation reviewed by the research team in the region, one presented this type of failure after two years of operation. There was a loss of three of the four wells it had, the thermal performance of the installation was decreasing until it reached the operating limit of the heat pump.

In addition to following the recommendations of the UNE-EN standard mentioned above in the installation of the pipes and their manufacture, it is recommended to drill reserve wells if the budget and the size of the installation allow it.

3.3 Case C

The well collapse during the drilling process can extend the duration of the drilling work as well and make it more expensive.

The solution is a good geotechnical characterization of the ground in the phase prior to the selection of the drilling method.

Various geophysical methods have been proposed to overcome this obstacle. Perhaps the most complete solution is the production of a 3-D model of the whole well field for the selection of the drilling method, as well as the location of the boreholes [4].

With rare exceptions, this failure would not jeopardize the viability of the installation, but it can significantly increase its initial cost. We are not aware of this having happened when drilling for the geothermal facilities we have reviewed in the region.

3.4 Case D

Failures concerning the overestimation of the thermal properties of the ground may led to soil thermal depletion for under-sizing of the length of the ground heat exchanger.

Of all the magnitudes necessary for determining the thermal properties of the ground, the most important one is thermal conductivity when sizing the well field of low enthalpy geothermal facilities [5]. The ways of approaching the determination of this parameter are varied. From the consultation of geological maps and tables of properties of materials, for the most modest facilities, until the realization of geophysical prospections [6] and thermal response tests (TRT) of the terrain for the largest facilities that allow justifying a significant economic investment in this type of tests.

The standardization institutions in Europe recommend carrying out TRTs from installations greater than 70 kW of installed thermal power. For lower powers they provide tables with estimates of the thermal properties of different geologies to roughly derive the thermal conductivity there [7].

The errors in the determination of the thermal conductivity in the case of resorting to queries in databases on the geology of the place and tables with properties of the different materials are difficult to estimate. As for the deviations that we can commit when performing TRTs and geophysical tests, numerous studies have been done and here we present some results obtained (Table 2).

Table 2. Methods and devices for thermal conductivity testing and their correspondent errors.

Method/Device	Error (%)
Lab measurement of thermal conductivity on samples (KD2-PRO device)	10
Electrical Resistivity Tomography. 2d profile software processed (RES2DINV Geotomo Software, 2019).	16
Thermal response test (standard heat injection device) *	5

* Witte, H. J. (2013). Error analysis of thermal response tests. *Applied Energy*, 109, 302-311.

A series of design simulations of geothermal facilities of different sizes with different associated thermal conductivities of the ground will be carried out, to see how the variation of this parameter affects the length of the well field. This can give us an idea of the important deviation that we commit if we overestimate this parameter at the calculus stage of these facilities.

These series of simulations of the design of geothermal well fields have been carried out with the help of the newly developed GES-CAL software [8].

GES-CAL is a computer tool for assessing the technical calculation of closed-loop geothermal systems. It has been created in the Python IDE PyCharm, using the QT Designer framework by the TIDOP research group inside the cartographic and land engineering department of the university of Salamanca (Spain).

This software tool GES-CAL has evolved out of the previous background in the field of the research group developed through laboratory tests and experimental field works.

The calculation of the geothermal pipe length derives from the implementation of the expressions described in Equations 1 and 2, for heating and cooling mode respectively according to recommendations in designing these systems by the Spanish energy administration [9].

$$L_h = \frac{E_{dh} \cdot \frac{COP_h - 1}{COP_h} (R_p + R_s \cdot F_s)}{T_L - T_{MIN}} \quad (1)$$

$$L_c = \frac{E_{dc} \cdot \frac{COP_c - 1}{COP_c} (R_p + R_s \cdot F_s)}{T_{MAX} - T_H} \quad (2)$$

Parameters from Eq. 1 and 2 are as follow:

$$R_p = \frac{1}{2 \cdot \pi \cdot k_p} \cdot \left(\frac{D_0}{D_1} \right) \quad (3)$$

$$R_s = 1/4\pi\lambda E_i(-r^2/(4\alpha t)) \quad (4)$$

$$F_s = \frac{E_{dh} \text{ or } E_{dc}}{HP_{pw}} \quad (5)$$

$$T_L(X_s) = T_m - A_s \cdot e^{\left(-X_s \sqrt{\frac{\pi}{365 \cdot \alpha}}\right)} \quad (6)$$

$$T_H(X_s) = T_m + A_s \cdot e^{\left(-X_s \sqrt{\frac{\pi}{365 \cdot \alpha}}\right)} \quad (7)$$

Where:

L_h	Total pipe length in heating mode (m)
E_{dh}	Energy demand in heating mode (kWh)
COP_h	Heat pump coefficient of performance in heating mode
R_p	Pipes resistance factor
R_s	Ground resistance factor
F_s	Utilization factor
T_L	Ground minimum temperature (°C)
T_{MIN}	Inlet minimum temperature (°C)
L_c	Total pipe length in cooling mode (m)
E_{dc}	Energy demand in cooling mode (kWh)
COP_c	Heat pump coefficient of performance in cooling mode
T_{MAX}	Outlet maximum temperature (°C)
T_H	Ground maximum temperature (°C)
k_p	Thermal conductivity of the pipe material (W/m·K)

- D_0 External diameter of the pipe (m)
- D_I Internal diameter of the pipe (m)
- λ Ground thermal conductivity (W/m·K)
- E_i Exponential integral function
- α Ground thermal diffusivity (m²/s)
- r Pipe radius (m)
- t Operational period of the pipe (s)

As can be seen by the equations above, GES-CAL requires the introduction of some specific initial conditions of the shallow geothermal system. This required information refers to the space energy demand, the heat pump working properties, the ground thermal conductivity and the heat exchangers configuration selected (GESs-Cal is capable of working with many different geothermal systems like horizontal, helical, etc. Here only vertical well is going to be considered).

In Table 3 we have the different parameters introduced in GES-CAL and the correspondent lengths of the geothermal pipes calculated by the software.

Table 3. GES-CAL design of the different cases.

Installation	Thermal needs (MWh/year)	Design	Ground thermal conductivity (W·m ⁻¹ ·K ⁻¹)	Length of the geothermal pipe (m)
1	20	a	2.3	141
		b	1.7	183
2	45	a	2.3	305
		b	1.7	397
3	70	a	2.3	467
		b	1.7	607

As can be seen in Table 3, three facilities of different sizes (20, 45 and 70 MWh / year) have been selected, representing 3 common sizes of this type of installations (single-family house, small business and medium commercial building for example). It was considered that an investigation of the geology of the place and consultation of tables for the determination of the thermal conductivity of the ground would have yielded a result of 2.3 W / m·K, however, having carried out a TRT, the real conductivity would be 1.7 W / m·K (due to different factors such as rock fracturing, etc.). The different lengths for the geothermal exchanger in each case are shown in the last column. There we can see the differences.

In Figure 4 the results for case 1a as showed by GES-CAL are presented. Notice the different possibilities it offers for the design of the well field. All of them emerging from the pipe length calculated for these conditions.



Fig. 4. GES-CAL results output for case 1a.

In Figure 5 the graphic shows the different lengths for each one of the designs in Table 3.

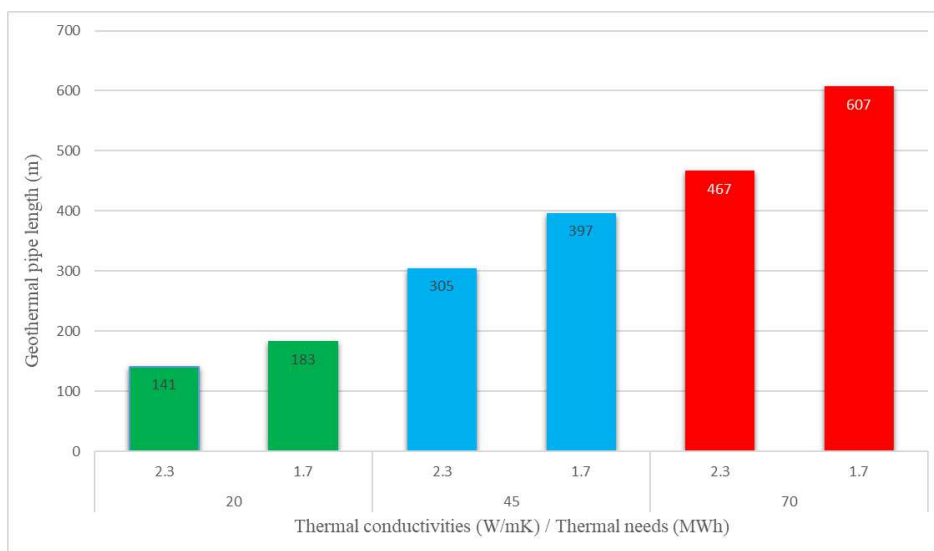


Fig. 5. Different lengths for the geothermal well fields in the different designs from Table 3.

For a 35% decrease in thermal conductivity, an increase of the order of 30% is observed in all cases in the design of the length of the geothermal exchangers.

A 30% difference in length is large enough to observe a drop in the performance of the geothermal installation, culminating in the final stoppage in the operation of the heat pump due to the plunge of the fluid's temperature beyond what admits the evaporator of the device.

This flaw in the design of low enthalpy heat pump geothermal systems could be much more common than we know now. This is due to the fact that most of the facilities that have been studied in the research group are too new to present total depletion of the ground, however in 20% of them some type of excessively marked loss of performance is already observed, which can make us think that insufficient dimensioning in the well field has occurred.

The solution for this type of failure is to carry out a TRT (or other similar tests) where the initial budget of the installation allows it, in addition to taking into account the possible error of these tests shown in Table 2. Once the installation is in operation and an excessively sharp drop in performance is observed that makes us suspect an error of the type that we are considering, the solution is to carry out new boreholes to increase the dimensioning of the well field in such a way that we avoid thermal depletion of the ground.

3.5 Case E

Failures concerning pipe installing and grouting considered in the construction phase of the well field are considered in this case, failures in geothermal pipes when the geothermal system is already in operation belong to case B. Some important defects found in the facilities that pertain to this case are failures in pressure tests, bad grouting selection and errors in the pipe descent process. Pipe and grout replacing could be needed.

Failure to do on-site pressure testing for geothermal pipes can be considered gross negligence in the process. Probe replacement implies a delay in the delivery of the finished installation and an increase in costs, but it is essential to guarantee the proper functioning of the installation in the long term.

Poor selection of borehole thermal grouting can negatively influence the energy performance of the facility. It cannot be considered a defect that puts the operation of the system at risk, but it entails long-term economic and environmental losses. There are customs among probe installers such as filling with water and bentonite, which should be banished in this sector due to its poor thermal performance [10].

According to our experience, the inadequate selection of the filling material occurs in 30% of the cases, the lack of in-situ pressure tests of the probes is not declared and the pressure failures in the pipes when installing them represents around 5 % of the cases.

3.6 Case F

Failures concerning the underestimation of the thermal properties of the ground are the most common of all. The increase in initial investment costs represents the main drawback, however, the reduction of energy consumption due to an increase in the COP of the heat pump somehow makes up for this.

If the oversizing of the length of the geothermal exchanger is not above 15%, this can be considered not as a design flaw, but rather as the installation being designed within the safety limits.

It is difficult to estimate the number of installations in which this oversizing can be considered a failure. The clue to suspect that this has happened is a heat pump's thermal performance well above expectations. This has not occurred in any of the facilities reviewed by the team.

4 Summary and Conclusions

An attempt has been made to provide a report with the faults found in real installations to promote good practices when making and designing this type of installations. Methods have been proposed to try to avoid these failures as well as ways to fix them when they occur (if this is possible).

Table 4 presents a summary of the casuistry found. It should be taken into account that the sample space is quite small, but on the other hand, the results have been collected first-hand and, in this type of facility, it is difficult to collect data of this type.

Table 4. Summary of the frequency found in the different cases.

Case	Description	Frequency found (%)
A	Geological affection of the area	Very low (one case known in Europe so far)
B	Loss of wells due to fluid leaks in geothermal pipes (with installation in operation phase).	8 %
C	Well collapse during the drilling process	---
D	Failures concerning the overestimation of the thermal properties of the ground	20 %
E	All failures concerning pipe installing and grouting. Including pressure tests.	30 % in grouting selection, 5 % in pipes replacement.
F	Failures concerning the underestimation of the thermal properties of the ground	---

All the failures described, perhaps with the exception of case F, have a very negative impact on the spread of this type of systems in the energy market for cooling/heating systems. The efforts made by the agents involved in the sector seem to be having a positive, albeit slow, effect on the dissemination of good practices for professionals in the sector.

With the good insights that are presented for this sector, it is important to refine as much as possible the design and installation techniques of these systems. It is hoped that this work will be useful as a reference to avoid the cases described in it in the future.

References

1. Frédéric Simon. LEAK: EU's 2030 climate plan makes case for 55% emissions cut. EURACTIV.com 14 sept. 2020.
2. Mastrucci, A.; Marvuglia, A.; Leopold, U.; Benetto, E. Life Cycle Assessment of building stocks from urban to transnational scales: A review. *Renew. Sustain. Energy Rev.* 2017, 74, 316–332
3. Lund, J., Sanner, B., Rybach, L., Curtis, R., & Hellström, G. (2004). Geothermal (ground-source) heat pumps: a world overview. *Geo-Heat Center Quarterly Bulletin*, 25(3).
4. Nieto, I. M., Martín, A. F., Blázquez, C. S., Aguilera, D. G., García, P. C., Vasco, E. F., & García, J. C. (2019). Use of 3D electrical resistivity tomography to improve the design of low enthalpy geothermal systems. *Geothermics*, 79, 1-13.
5. Kavanaugh, S. P. (2000). Field tests for ground thermal properties--methods and impact on ground-source heat pump design. Univ. of Alabama, Tuscaloosa, AL (US).
6. Sáez Blázquez, C., Martín Nieto, I., Farfán Martín, A., González-Aguilera, D., & Carrasco García, P. (2019). Comparative Analysis of Different Methodologies Used to Estimate the Ground Thermal Conductivity in Low Enthalpy Geothermal Systems. *Energies*, 12(9), 1672.
7. AENOR UNE 100715-1: 2014. Guide for the design, implementation, and monitoring of a geothermal system. Part 1: Vertical closed-circuit systems.
8. Blázquez, C. S., Nieto, I. M., Mora, R., Martín, A. F., & González-Aguilera, D. (2020). GES-CAL: A new computer program for the design of closed-loop geothermal energy systems. *Geothermics*, 87, 101852.
9. Instituto para la diversificación y ahorro energético, IDAE, Guía Técnica: Diseño de sistemas de intercambio geotérmico de circuito cerrado. Ahorro y eficiencia energética en climatización.
10. Blázquez, C. S., Martín, A. F., Nieto, I. M., García, P. C., Pérez, L. S. S., & González-Aguilera, D. (2017). Analysis and study of different grouting materials in vertical geothermal closed-loop systems. *Renewable Energy*, 114, 1189-1200.

Methane emissions and energy density of reservoirs of hydroelectric plants in Venezuela

Rhonmer Orlando Pérez Cedeño¹[0000-0003-4343-0935], Carmen Luisa Vásquez Stanescu¹[0000-0002-0657-3470], Leonardo Suárez-Matarrita²[0000-0002-6835-8362], Raquel Noemí Vásquez Stanescu³[0000-0002-8292-2601], William José Osal Herrera¹[0000-0002-7736-3745], Rodrigo Ramírez-Pisco⁴[0000-0001-8648-3805]

¹ Universidad Nacional Experimental Politécnica Antonio José de Sucre (UNEXPO), Barquisimeto, Venezuela

² Universidad Técnica Nacional y Universidad de Costa Rica, San José, Costa Rica

³ Doctorado de la Universidad Central de Venezuela (UCV), Caracas, Venezuela

⁴ Universidad de Barcelona (UNIBA) y Universidad Politécnica de Cataluña (UPC), Barcelona, España
rhonmerperez@gmail.com

Abstract. Venezuela is known as a country with great fossil resources and for its hydroelectric plants. Generally, greenhouse gas emissions are attributed to non-renewable sources. However, from the reports of the Intergovernmental Panel on Climate Change (IPCC) for the years 2007 and 2013, a methodology is derived to estimate methane gas emissions from flooded lands, which include the freshwater reservoirs used for the water reservoirs of these electric plants, since it has a greater global warming potential than CO₂. As of 2016, studies have been carried out in different reservoirs around the world, showing that the highest proportions of emissions are found in the tropical and temperate areas of Canada. This represents the first study for the country, which has nine water reservoirs. Emissions in water reservoirs are from three sources: diffusers, bubbles and degassing. For the present study, the diffusers are estimated, since the climate in the region is tropical dry or temperate humid, without the presence of ice in the year. In the methodology, the surfaces of the water reservoirs are estimated with the Google Earth tool. The results show that Guri, with a surface area of 417,620 ha, emits 44.9672 GgCH₄ / year. However, it is included among those with the lowest energy density (2.45 MW / km²). It is evident that the emissions are not strictly proportional to the surface, but rather depend significantly on its geographical location.

Keywords: Methane emissions, water reservoirs, Venezuela.

1 Introduction

The close relationship between the development of countries and the consumption of electricity makes its supply essential [1]. However, the generation of energy from fossil fuels and its environmental impacts has been questioned as a way of life in

society. The Fourth Report of the Intergovernmental Panel on Climate Change (IPCC) of 2007 [2] establishes that climate change is "unequivocal" and that it is mainly due to anthropogenic actions such as deforestation and the activities of the transport, power generation, industrial sectors and others. With a high degree of certainty, the cause of global warming and climate change is the increase in the concentration of greenhouse gases (GHG) in the Earth's atmosphere. These bring the rise in global average temperatures of the air and oceans, the widespread melting of snow and ice and the rise in sea levels. [2] [3] [4].

GHG and other gas emissions are generally attributed to fossil fuel power generation [5] [6] [7]. However, renewable and hydroelectric sources of supply are considered free of these emissions during their operation. But, for the first time, Appendix 3 of the 2006 IPCC report [8] warns of a future methodological development to estimate methane (CH₄) emissions from flooded lands. For 2013, the fifth IPCC report [9] indicates that 16% of anthropogenic emissions correspond to CH₄.

The CH₄ is considered a GHG with greater potential than CO₂ [10]. It is important to highlight that it is responsible for 90% of global warming, when the effect is estimated over a 20-year time horizon [11]. CH₄ is formed by various causes, one of them being the decomposition of organic matter in freshwater wetlands [12], hydroelectric reservoirs [13] [11] [14], rice crops [15] and others. Emissions depend on the age and depth of the reservoirs, land uses before the flood, climate and others [8] and, unlike CO₂, are variable both spatially and temporally.

In the case of the water reservoirs used for the reservoirs of hydroelectric power plants, three types of GHG are emitted, with an important impact on climate change, but generally ignored, CO₂, CH₄ and nitrous oxide (N₂O) [16]. CH₄ emissions depend mainly on the geographic location and climate where the water reservoir is located. Especially in power plants in tropical regions [17] [18] "*with the highest emission rates in the tropical Amazon region*" [13] and "*the temperate zone of Canada*" [16] additionally, it is being favored by the age of the water reservoir [14].

According to the International Commission of Large Water Reservoirs (ICOLD) [19], of 741 large hydroelectric plants greater than 10 MW, GHG emissions have been measured only in 18, in the tropics, that is, in the countries Australia, Brazil, France and Panama [17] [18]. Additionally the IDB report for 2016 shows estimates in the countries of Guatemala, Belize, El Salvador, Honduras, Nicaragua and Costa Rica and Panama [11]. Even in Colombia [17] and Ecuador [18] similar studies have been carried out to estimate similar water reservoirs. However, Venezuela is the country in the world that has the third largest water reservoir, after the Three Gorges in China and Itaipu in Paraguay, in addition to others, smaller, for a total of nine.

Venezuela has an installed capacity of 15,137 MW in hydroelectric generation, which represents 48.77% of the country's total installed capacity for the year 2015 [20]. For 2019, a total of 84.9 TWh of energy was consumed in the country, of which 0.56 exajoules is based on its hydroelectric resources [21].

Within this framework, the purpose of this work is to estimate CH₄ emissions from the nine reservoirs associated with the hydroelectric generation plants located in Venezuela. Additionally, it is pointed out that similar work has not been done in the country under study, making the information provided relevant with additional use as support material when establishing research with shared characteristics.

The article is organized as follows. The next section shows the concepts related to the water reservoirs of Venezuela and their general information such as the methane emissions. The applied methodology is described in Section 3 where the estimated areas of the water reservoirs of Venezuela are also shown. Section 4 presents the results about methane emissions, energy density and a graphical summary on a logarithmic scale of the hydroelectric reservoirs of Venezuela. Finally, Section 5 shows the conclusions and some suggestions for future work.

2 Development

2.1 Water Reservoirs in Venezuela

Venezuela is known for its fossil (oil and gas) and hydroelectric resources. It has an installed hydroelectric capacity of 15,137 MW [20]. The third largest hydroelectric plant in the world is located in this country with the name Simón Bolívar, previously known as Raúl Leoni. This hydroelectric plant began operating in 1983, and is located in the Guri water reservoir, artificially built on the Caroní River. During the closure of the water reservoir, there was a significant percentage of land flooded in the area, which led to the rescue of animals and other actions. It is still in operation and for 2019 it will supply about 56% of the energy consumed in the country [21]. The “El Niño” weather phenomenon, in 1999 and 2010, demonstrated the vulnerability of this highly concentrated energy supply scheme.

In addition to the Simón Bolívar Hydroelectric plant, the country has eight additional hydroelectric plants: Francisco de Miranda, Antonio José de Sucre, Manuel Palacios Fajardo, Manuel Piar, Fabricio Ojeda, José Antonio Páez, Leonardo Ruiz Pineda and José Antonio Rodríguez Domínguez, whose location and description are shown in Figure 1 and Table 1. This table shows that only the Caroní River has four hydroelectric plants along its route, demonstrating its enormous energy potential. This river is the second with the highest flow in the world.



Fig. 1. Geographical location of the Venezuelan hydroelectric reservoirs

Table 1. General information of the reservoirs for Hydroelectric purposes in Venezuela [25]

Water Reservoir	Name of the Electric Power Plant	River	Location		Execution Period of the Work	Installed capacity (MW)
			State	Coordinates		
Guri	"Simón Bolívar" Hydroelectric Plant	Caroní	Bolívar	7°46'10"N 62°59'19"O	1963 - 1986	10,235
Caruachi	"Francisco de Miranda" Hydroelectric Plant	Caroní	Bolívar	8°09'36"N 62°47'55"O	1997 - 2006	2,196
Macagua	"Antonio José de Sucre" Hydroelectric Plant	Caroní	Bolívar	8°18'09"N 62°40'46"O	1956 - 1961	3,152
Masparro	"Manuel Palacios Fajardo" Hydroelectric Plant	Masparro	Barinas	8°51'21"N 70°7'52"O	2005 - 2009	25
Tocoma	"Manuel Piar" Hydroelectric Plant	Caroní	Bolívar	7°54'25"N 63°01'35"O	2002 - 2020	2,160
La Vueltoza	"Fabricio Ojeda" Hydroelectric Plant	Camburito-Caparo	Mérida	7°49'45"N 71°26'32"O	2004 - 2011 (86%)	514
Santo Domingo	"José Antonio Páez" Hydroelectric Plant	Santo Domingo	Mérida	8°53'2"N 70°38'3"O	1970 - 1973	80
Uribante o La Honda	"Leonardo Ruiz Pineda" Hydroelectric Plant	Uribante	Barinas, Táchira y Mérida	7°57'2"N 71°42'34"O	1980 - 1986	1,260
Boconó-Tucupido	Central Hidroeléctrica "José Antonio Rodríguez Domínguez"	Boconó y Tucupido	Portuguesa y Barinas	9°0'0"N 70°0'0"O	1983 - 1986	80

2.2 Methane Emissions (CH₄)

The origin of methane emissions in water reservoirs is due to bacteria that decompose the organic matter of the sediments present at the bottom in fresh water with low oxygen content. The water layer has little oxygen in the deepest part of the water reservoirs. Only under these conditions does CH₄ have the peculiarity of oxidizing and turning into CO₂ when rising to the surface. In reservoirs located in tropical areas, with little amount of water, they do not allow the CH₄ bubbles to oxidize and, therefore, tend to contribute high emissions [13] [14] [15] [16]. Among the variables that affect the rate of decomposition of organic matter in a water reservoir are: depth, geographical location, age, temperature, residential time of the water, shape and volume and, finally, amount and type of flooded vegetation.

Among the most salient variables are the age of the reservoir, the type and amount of vegetation, since it has been shown that CH₄ emissions are increased in the period immediately after it has been created. Additionally, these tend to decrease later, causing the reduction rates according to the environmental policies initially established [23].

According to IPCC [8], CH₄ emissions in flooded lands can be due to:

- Diffusing emissions caused by molecular propagation through the air-water interface.
- Emissions of bubbles or gas from sediment through the water column in the form of bubbles. This being an important source of CH₄ emissions, especially in temperate and tropical regions. However, to estimate these emissions, country-specific factors are required.
- Degassing emissions as a consequence of a sudden change in hydrostatic pressure, as well as the increasing air / water exchange surface. This occurs when water flows through a turbine or any drainage path.

According to the methodology established by the IPCC [8], each of the emissions reflects a level. Level 1, 2 and 3 reflect the diffusing, bubble or gas emissions and, finally, refers to the entire approach, which includes the previous two plus the degassed, respectively. However, in level 2, bubble or gas emissions are applicable in temperate zones, where icy and ice-free seasons occur. Finally, the choice of the estimation method depends on the availability of the data and the emission factors of each country [8].

3 Methodology

According to the IPCC [8], the estimation of diffusing methane emissions is used in equation (1).

$$E(CH_4) \quad (1)$$

Where:

CH₄ emissions: total CH₄ emissions from flooded lands (Gg CH₄ / year)

P : Period without ice given in days / year (365 days, for our case study)
 $E (CH_4)_{dif}$: Daily average of diffusing emissions (kg of CH_4 $ha^{-1}day^{-1}$)
 $A_{inun_sup_total}$: Average total area of flooded surface (ha).

Tables 2 and 3 show the daily average of diffusing emissions and climate information from the areas where the water reservoirs are located, respectively. In these it can be seen that as the type of climate is tropical dry and, only in one case, temperate humid [8][24]. Being a climate of this type, at no time of the year is ice present in the water reservoirs and, therefore, emissions by bubbles or gas are not considered.

Table 2. Measured CH_4 emissions from flooded lands [8] [24]

Climate	Diffusing Emissions (kg of CH_4 $ha^{-1}day^{-1}$)		
	average	Minimum	Maximum
Polar/boreal very humid	0.086	0.011	0.3
Temperate cold humid	0.061	0.001	0.2
Temperate warm humid	0.150	-0.05	1.1
Temperate warm dry	0.044	0.032	0.09
Very humid tropical	0.630	0.067	1.3
Dry tropical	0.295	0.070	1.1

Table 3. Climate information and surface of the reservoirs for hydroelectric purposes of Venezuela [8][24] [25]

Water Reservoir	Type of Climatic Condition according to	
	Köppen-Geiger	IPCC [8]
El Guri	Aw	Dry tropical
Caruachi	Aw	Dry tropical
Las Macagua	Aw	Dry tropical
Masparro	Aw	Dry tropical
Tocoma	Aw	Dry tropical
La Vueltoza	Aw	Dry tropical
Santo Domingo	Cfb	Temperate cold humid
Uribante o La Honda	Aw	Dry tropical
Boconó-Tucupido	Aw	Dry tropical

To make comparisons of GHG emissions, the conversion factors to CO_2 equivalent (CO_2 -eq) are used. For this, the Global Warming Potential (GWP) of 21 for CH_4 is used [18]. Equation (2) shows the calculation of CO_2 -eq emissions [17].

$$(CH) \tag{2}$$

As an example, Figure 2 shows the Guri water reservoir, whose surface was estimated [25]. For this, the analysis of Google Earth images is used, which has shown adequate precision for similar studies [25] [26], with the nine water reservoirs. Table 4 shows areas estimated with this procedure.

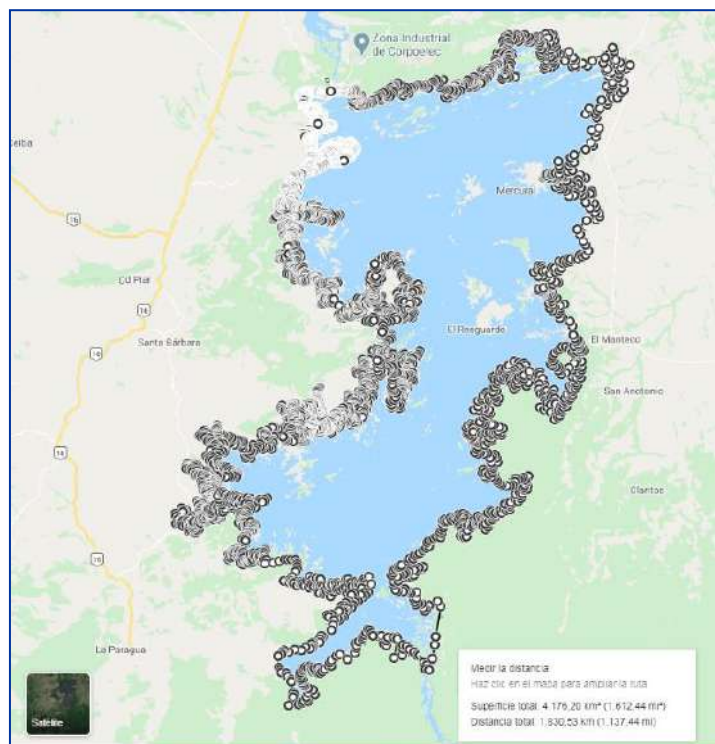


Fig. 2. Guri Water Reservoir surface, elaborated with [25]

Table 4. Estimated area surface for water reservoirs in Venezuela

Water Reservoir	Surface (ha)
El Guri	417,620
Caruachi	28,439
Las Macagua	5,766
Masparro	3,063
Tocoma	4,538
La Vueltoza	10,566
Santo Domingo	12
Uribante o La Honda	1,679
Boconó-Tucupido	9,567

4 Results

4.1 Emissions

Table 5 shows the CH₄ and CO₂-eq emissions per year for each water reservoir. Additionally, Figure 3 shows the proportion of CH₄ emissions per year, where it stands out that only the Guri water reservoir, for the year 2020, is 44.9672 GgCH₄.

Table 5. Diffuse emissions for hydroelectric reservoirs

Water reservoir	Gg CH ₄ /year	t CH ₄ /year	t CO ₂ -eq/year
El Guri	44.9672	44,967.23	944,311.90
Caruachi	3.0622	3,062.17	64,305.56
Las Macagua	0.6209	620.85	13,037.94
Masparro	0.3298	329.81	6,925.98
Tocoma	0.4886	488.63	10,261.21
La Vueltoza	1.1377	1,137.69	23,891.58
Santo Domingo	0.0003	0.26	5.55
Uribante o La Honda	0.1808	180.79	3,796.51
Boconó-Tucupido	1.0301	1,030.13	21,632.66

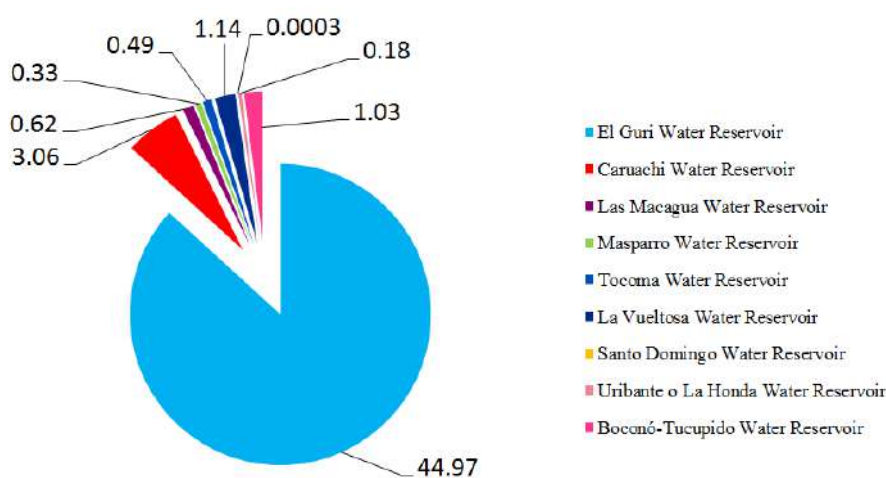


Fig. 3. CH₄ emissions (Gg CH₄/year) for hydroelectric reservoirs in Venezuela

4.2 Energy Density

Table 6 shows the surface data of each reservoir and the installed capacity of the hydroelectric plant as well as its energy density [27] [28] [29]. Additionally, figure 4 shows that the highest density is for the Santo Domingo water reservoir of the “José Antonio Páez” Hydroelectric Plant.

Table 6. Surface and Energy Density of the hydroelectric reservoirs of Venezuela

Water Reservoir	Surface (ha)	Installed capacity (MW)	Energy Density (MW/km ²)
El Guri	417,620	10,235	2.45
Caruachi	28,439	2,196	7.72
Las Macagua	5,766	3,152	54.67
Masparro	3,063	25	0.82
Tocoma	4,538	2,160	47.60
Vueltoza	10,566	514	4.86
Santo Domingo	11.88	80	673.40
Uribante o La Honda	1,679	1,260	75.04
Boconó-Tucupido	9,567	80	0.84

Figure 5 illustrates a summary graph in logarithmic scale with surface data, energy density and methane emissions for hydroelectric reservoirs in Venezuela. It is evident that methane emissions are proportional to the surfaces; graphically exceed the average values of the water reservoir areas. On the other hand, the energy density of the electricity generation plants is graphed in the same figure, where the installed capacity of the plant and the surface of the reservoir associated with it are considered, where a low average density is observed (less than 100 MW / km²) of all the reservoirs with the exception of the “José Antonio Páez” hydroelectric plant. The exponential trend lines of the graphs corresponding to the surfaces and emissions indicate the coefficients of determination (R²) showing different values between them.

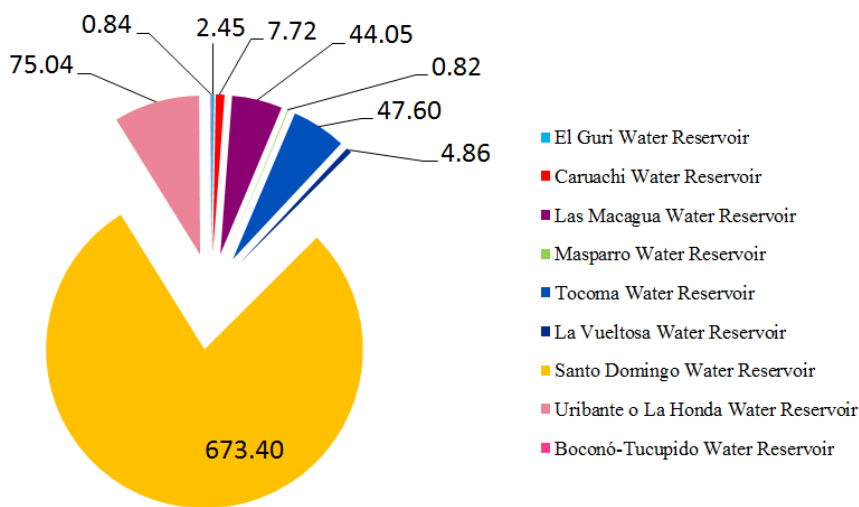


Fig. 4. Energy density (MW/km²) for the hydroelectric reservoirs of Venezuela

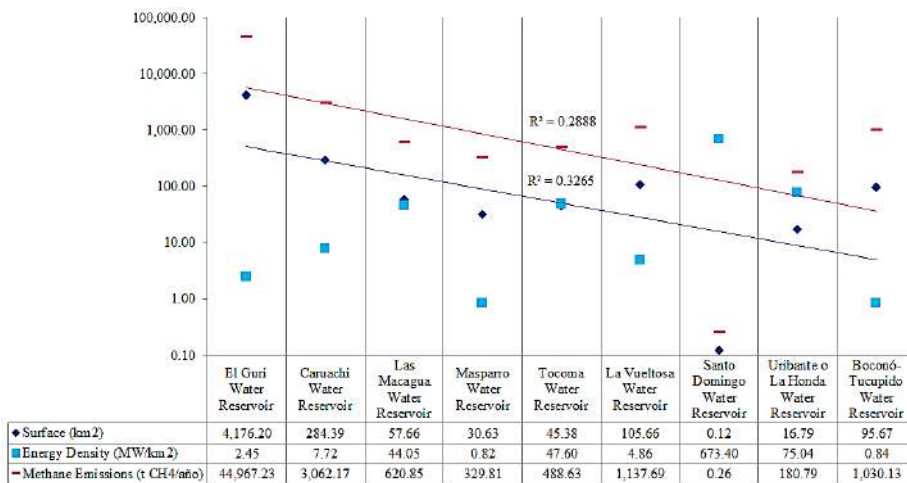


Fig.5. Data from the hydroelectric reservoirs of Venezuela.

5 Conclusions

Based on the bibliography consulted, a deficit of information has been observed regarding the sources of CH₄ emissions in the hydroelectric reservoirs of Venezuela, making a great contribution to the information provided in the present investigation for future works in the area.

By 2020, the high contribution of the Guri Water Reservoir in methane emissions is evident, generating 44.97 GgCH₄, which represents 86.78% of the total emissions from reservoirs for electricity generation purposes, followed for the Caruachi with 5.91%.

The energy density of the hydroelectric reservoirs illustrated in figure 4 indicates for the Guri water reservoir that, despite being the reservoir that houses the largest surface area of all, it has a low energy density being 2.45 MW / km². The highest density is found in the Santo Domingo water reservoir (“José Antonio Páez” Hydroelectric Plant) with 673.40 MW / km².

It is observed that, according to the coefficient of determination R² of the exponential trend lines, methane emissions are directly proportional to the surface of the water reservoir; however they do not meet the same pattern because there are other factors that influence emissions, among them the weather. From this idea it can be deduced that the methodology proposed can be used as a means of preliminary calculation for the estimation of emissions and with this, to determine the best location of the reservoir in the country's geography.

References

1. R. Pérez, «Metodología para la estimación de la emisión de gases de efecto invernadero en usuarios industriales.» Trabajo presentado como requisito parcial para optar al título de Ingeniero Electricista, Barquisimeto, 2018.
2. IPCC, «Cambio Climático 2007. Informe de Síntesis,» OMM/PNUMA, Ginebra, 2007.
3. Y. Zhang, «“El calentamiento del sistema climático es inequívoco”: Aspectos más destacados del Cuarto Informe de Evaluación del Grupo Intergubernamental de Expertos sobre el Cambio Climático,» ONU, [En línea]. Available: <https://www.un.org/es/chronicle/article/el-calentamiento-del-sistema-climatico-es-inequivocoaspectos-mas-destacados-del-cuarto-informe-de>. [Último acceso: 30 07 2020].
4. R. Pérez y W. Osal, «Gases de efecto invernadero por generación de electricidad en usuarios no residenciales de Venezuela 2006-2017,» *Publicaciones en ciencias y tecnología*, vol. 13, p. 30–40, 2019.
5. L. Sánchez, M. Lucena y C. Vásquez, «Emisiones de mercurio por uso de las lámparas fluorescentes compactas y por generación de energía eléctrica a base de combustibles fósiles,» *REVISTA CIENTÍFICA ECOCIENCIA*, vol. 4, n° 5, pp. 1-18, 2017.
6. L. Sánchez, C. Vásquez y A. Vilorio, «The data envelopment analysis to determine

- efficiency of Latin American countries for greenhouse gases control in electric power generation,» *International Journal of Energy Economics and Policy*, vol. 8, n° 3, pp. 197-208, 2018.
7. L. Sánchez, c. Vásquez y A. Vioria, «Políticas públicas en el sector suministro de energía e indicadores energéticos del desarrollo sostenible en Latinoamérica,» *Revista Científica Compendium*, vol. 21, n° 41, 2018.
 8. IPCC, «Apendice 3. Emisiones de CH₄ provenientes de tierras inundadas: Base para su futuro desarrollo metodológico,» 2006.
 9. IPCC, «Cambio climático 2013: la base de la ciencia física,» IPCC, Ginebra, 2013.
 10. V. Manrique, «Ciencias básicas sobre el efecto del metano sobre el cambio climático. Estado del arte y escenario de reducción,» *Innovación*, pp. 28-33.
 11. IDB, «VULNERABILIDAD AL CAMBIO CLIMÁTICO DE LOS SISTEMAS DE PRODUCCIÓN HIDROELÉCTRICA EN CENTRO AMERICA Y SUS OPCIONES DE ADAPTACIÓN,» IDB, 2016.
 12. M. Hernández y P. Moreno-Casanova, «Almacenes y flujos de carbono en humedales de agua dulce en México,» *Madera y bosques*, vol. 24, 2018.
 13. N. Barros, J. Cole y L. Tranvik, «Emisión de carbono de los embalses hidroeléctricos vinculada a la edad y latitud del embalse,» *Nature Geosci*, vol. 4, p. 593-596, 2011.
 14. V. Chanudet, J. Gaillard y J. Lambelain, «Emisión de gases de efecto invernadero de los reservorios hidroeléctricos templados franceses,» *Aquat Sci*, vol. 51, 2020.
 15. M. Cumpa, «REDUCCIÓN DE GAS METANO ATMOSFÉRICO UTILIZANDO TÉCNICAS DE RIEGO EN CULTIVO DE ARROZ EN CONDICIONES CLIMÁTICAS,» *Revista UCV-Scientia*, p. 130, 2017.
 16. L. Shibaoy, D. Weidong, T. Yao y G. Min, «Una revisión del impacto de los embalses hidroeléctricos en el cambio climático global,» *Ciencia del Medio Ambiente Total*, vol. 711, 2020.
 17. F. Mayor, «Estimación de la emisión histórica de gases de efecto invernadero por embalses hidroeléctricos en Colombia y su potencial impacto en el Factor de Emisión de la Generación Eléctrica,» UNAL, Bogotá, 2015.
 18. M. Samaniego y P. Amancha, «ESTIMACIÓN DE EMISIONES DE METANO PRODUCIDAS POR EMBALSES DE LAS CENTRALES HIDROELÉCTRICAS EN ECUADOR,» de *12º CONGRESO IBEROAMERICANO DE INGENIERÍA MECÁNICA*, Guayaquil, 2015.
 19. ICOLD, «Comité Nacional Español de Grandes Presas,» 2019. [En línea]. Available: <https://www.spancold.org/quienes-somos/>. [Último acceso: 01 07 2020].
 20. OLADE, «Informe de Estadísticas Energéticas,» OLADE, 2016.
 21. bp, «Statistical Review of World Energy/2020 69th edition,» bp, 2020.
 22. G. Maps, «Google Maps,» 2020. [En línea]. Available: <https://www.google.com/maps/@39.550051,-105.782067,6z?hl=es>. [Último acceso: 2020].
 23. W. Steinhurst, P. Knight y M. Schultz, «Hydropower Greenhouse Gas

- Emissions.» Synapse Energy Economics, Inc, Cambridge, 2012.
24. A. Strabler y A. Strabel, «Geografía Física. Edición Especial,» Barcelona, Omega, 2006.
 25. F. Contreras, F. Ferrelli y M. Piccolo, «IMPACTOS DE EVENTOS SECOS E CHUVOSOS NOS CORPOS DE ÁGUA PERIURBANOS SUBTROPICAIS;» *Finisterra*, pp. 3-22, 2020.
 26. C. Vigo, P. Juárez y M. Oliva, «Cosecha de agua de lluvia como tecnología de conservación de los manantiales amenazados, Chachapoyas,» *Revista de Investigación en Agroproducción Sustentable*, pp. 13-19, 2019.
 27. CORPOELEC, «Central Hidroeléctrica “Manuel Piar” en Tocomá,» CORPOELEC, 2014. [En línea]. Available: <http://www.corpoelec.gob.ve/proyectos/central-hidroel%C3%A9ctrica-manuel-piar-en-tocoma>. [Último acceso: 2020]
 28. E. La Marca, F. Silva Costa y M. Arriojas, «REPRESAS HIDROELÉCTRICAS EN LOS ANDES VENEZOLANOS: PROBLEMÁTICA AMBIENTAL, CRISIS ENERGÉTICA Y ENERGÍAS ALTERNATIVA,» Saber, Universidad del Oriente, vol. 30, pp. 582-598, 2018.
 29. MPPEE, «Anuario Estadístico 2013,» MPPEE, Caracas, 2013.

Technological architecture for synchrophasor measurement in power systems: an application for Colombia

Juan David Molina-Castro¹[0000-0002-7922-2276], Mauricio Alvarez-Alvarez¹, Luisa Buitrago-Arroyave¹, and Jaime Zapata Uribe²

¹ Colombia Inteligente, Medellín 050012, Colombia

² XM, Medellín 050022, Colombia

juandavid.molina@colombiainteligente.org

Abstract. Synchrophasor measurement is one of the main measurement technologies in electrical networks. Synchrophasor Measurement -SPM refers to the implementation of a set of technologies designed to improve the monitoring of the power system in large geographic areas to obtain an efficient response to power system disturbances and cascading blackouts, but new smartgrid applications have emerged at the transmission and distribution level. The Synchrophasor measurement process basically consists of comparing signals from different points in the system with a common time reference signal. The SPM process requires a series of standards so that each one of the domains of the SPM architecture can interact both inside them and outside with the other components of the power system. At the Colombian level, experiences and applications of flexible technologies aimed at grid stability, FACTS and storage, among other applications, were identified.

A technological architectural diagram was developed in which the actors, roles, interactions and information flows that should be considered for SPM are presented. At the same time, the standards and protocols are identified in the operation of the power system for the functionalities of synchrophasor measurement.

Keywords: Synchrophasor measurement, phasor measurement unit, TSO, DSO, FACTS, DER, technological architecture.

1 Introduction

Before exploring the topic of SPM, it is necessary to start with the concept of flexible operation of power systems. For this, the idea of what is understood as flexibility can be taken from different national and international entities, such as CIGRÉ [1], ISGAN [2], the IEEE, la ENTSO [3], IRENA, XM [4], among others. For this paper, the definition of XM (the Colombian market operator) regarding flexibility will be taken, which “refers to the ability of electrical power systems to respond to different conditions of change in the generation-demand balance, at all scales and time horizons” [4].

Due to the massive used of power electronics, microprocessors and communications, power systems, both at transmission and distribution levels, have undergone positive changes. This has led to a safer, more controllable and efficient operation of the electrical grid. On the other hand, the growing use of Distributed Energy Resources (DER) that include Distributed Generation (DG), Storage Systems (SS), Demand Response (DR) and Electric Vehicles (EV), is driving the need for greater coordination between Transmission System Operators (TSO), Distribution System Operators (DSO), prosumers, aggregators, and a variety of emerging players [1].

What has been described above makes up the smartgrid, within which are the support services such as synchrophasor measurement to carry out the supervision and control of the power q system.

2 Standard and protocols framework

Industry standards are approved by recognized standardization bodies to ensure consensus of subject matter experts. Without standardization, aspects of the electrical industry might not function or interact as expected. Furthermore, without standards, the products would not be economical for large-scale use, and could be risky to operate. Standardization of the electrical industry ensures consistency in accepted practices. These practices are essential to ensure quality, ecological sustainability, public and employee safety, financial responsibility, network reliability, infrastructure compatibility, utility interoperability, energy efficiency, and general effectiveness. When utilities and governments invest in standards development and enforcement several benefits can be reached.

Standards allow utilities to mitigate risk by adopting new technologies and allow the evolution and transition from obsolete technologies. Standards codify the latest technologies and facilitate their transfer; they are an invaluable source of knowledge, since they collect expert knowledge and make it widely available. In essence, standards and norms provide productivity tools that result in substantial cost savings for entities in the electrical industry, consumers, and the economy.

For the power system to function properly, a series of protocols and standards are required so that each one of the domains can interact within it as well as with the other domains that make up the technological architecture.

The protocols, norms and standards of SPM are developed by entities and groups that seek to normalize and establish the interoperability rules for the components and domains of the system. Within these entities are organizations such as IEEE [5], the International Electrotechnical Commission (IEC) [6]; the North American Electric Reliability Corporation (NERC), whose mission is to “Ensure the effective and efficient reduction of risks to the reliability and security of the network” [7], and the North American SynchroPhasor Initiative (NASPI), which is a collaboration between the electrical industry, NERC and the Department of Energy of the United States (DOE), to “advance the use of synchrophasor technology to improve network reliability and economics through measurement, monitoring and wide-area control” [8].

Table 1 describes the standards and protocols for the architectural domains of synchrophasor measurement.

Table 1.Standards and protocols for Synchrophasor Measurements.

Category	Standard	Description
Interoperability	IEC 61850	Defines international standards for communication between protection, control and measurement equipment within an automated substation. All aspects related to these topics are covered, such as design, operation and maintenance.
Time synchronization	IEEE 1588 PTP	Precision Time Protocol (PTP) is a packet-based bidirectional message exchange protocol for synchronizing clocks between nodes on a network, allowing for accurate distribution of time on a network.
Phasor data concentrator	IEEE C37.244	Functional, performance, and test guidelines for a phasor data concentrator are described in this guide. Supporting information is also provided.
Communication	IETF RFC-6272	Created to guide the reader in the proper use of the conceptual model of communication protocols via internet (Internet suite protocol) for applications related to smart grids. This document is mainly aimed at those natural or legal persons who are looking for a guide on how to manufacture or develop suitable profiles of these communication protocols via the Internet for smart grid applications.
Security	NERC CIP v06	NERC Standard which provides a cybersecurity framework for the identification and protection of critical cyber assets to support the reliable operation of the electrical system, which were taken in Colombia as a basis to guarantee the cybersecurity of electrical networks.
	NISTIR 7628 NIST SP 800	Presents an analytical work that organizations can use to develop effective cybersecurity strategies, tailored to their combination of smart grid-related characteristics, risks, and vulnerabilities.

Category	Standard	Description
	IEC 62351/62443 ISO/IEC 27002	Defines the expected security objectives, including the authentication of the transferred data through digital signatures, which allow the content to reach the expected recipient and thus avoid falsifications, intrusion interventions or loss of relevant information.
Synchronization	IEEE C37.238	Defines precision timing standards focused on power system protection, control applications, data automation using Ethernet architecture.
Data format	IEEE C37.239	Defines a common format for information files used in the exchange of event information, acquired from electrical power systems or models of power systems.
PMU Synchronization	IEEE C37.242	Provides a guide for the synchronization, calibration, testing and installation of PMU applied to the protection and control of the power system.
PDC functions and data	IEEE C37.247	Standard of functions that can be performed on synchrophasor data. Describes the PMU measurement network and indicates the location of the PDC in it. The standard defines the minimum functions that a PDC must perform.
Measurement	ANSI C12.1	Defines the parameters on which an acceptable performance of auxiliary equipment, measurement equipment, pulse equipment and demand recorders is assessed. Describes how the behavior of these devices should be when their performance is adequate
Meter	ANSI C12.20 IEC 145/185/687	Establishes acceptable performance criteria for electrical meters and encompasses designations of accuracy classes, current classes, and voltage and frequency ratings.

3 Flexible technology experiences in Colombia

Colombia has incorporated FACTS devices (SVC -Chinú, Tunal and Caño Limón-, STATCOM -Bacatá [9] - and SSSC -Red Valle de Aburrá), in order to provide a better quality of service, optimize resources as well as optimize existing infrastructures to

achieve a reliable and safe operation at efficient costs. There are also experiences in the analysis of flexible technology applications oriented to the use of SVC and STATCOM for grid stability, the use of storage to mitigate electrical restrictions, phase shifting transformers to mitigate congestion, HVDC for the integration of variable energies, among other applications (see Table 2).

Table 2. Studies of flexible technologies in Colombia

Technology	Description
SVC	Damping of oscillations by means of FACTS to prevent blackouts ¹ .
STATCOM	Bacatá STATCOM operating experience ²
SSSC	Distributed FACTS: Network transformation technology (Congestion management in the STN-STR Antioquia through Distributed FACTS) ³
Phase shifting transformer	Phase-shift transformer application ⁴ .
Storage	<ul style="list-style-type: none"> • Analysis of storage in the Atlantic area for congestion relief⁵. • Trends in energy storage in electrical systems⁶. • Reality check on energy storage⁷. • Battery energy storage systems - BESS and its applications⁸. • Implementation of storage systems as a timely solution for the operation of the National Interconnected System -SIN⁹. • Operation of wind farms with BESS¹⁰.

¹ <https://cnostatic.s3.amazonaws.com/cno-public/documentos/noticias/02.08-CNO-EEB-AmortiguamientoOscilaciones.pdf>

² https://cnostatic.s3.amazonaws.com/cno-public/archivosAdjuntos/verificacion_del_modelo_del_statcom_de_bacata.pdf

³ https://cnostatic.s3.amazonaws.com/cno-public/archivosAdjuntos/manejo_de_la_congestion_en_el_stnstr_antioquia_mediante_facts_distribuidos.pdf

⁴ https://cnostatic.s3.amazonaws.com/cno-public/archivosAdjuntos/21_a_jtt_2017_pst_epsa.pdf

⁵ https://cnostatic.s3.amazonaws.com/cnopublic/archivosAdjuntos/analisis_de_almacenamiento_en_el_area_atlantico_para_alivio_de_congestiones.pdf

⁶ <https://cnostatic.s3.amazonaws.com/cno-public/archivosAdjuntos/almacenamiento.pdf>

⁷ https://cnostatic.s3.amazonaws.com/cno-public/archivosAdjuntos/4_ramon_leon_isa.pdf

⁸ https://cnostatic.s3.amazonaws.com/cno-public/archivosAdjuntos/3_diego_tejada_u_comillas.pdf

⁹ https://cnostatic.s3.amazonaws.com/cno-public/archivosAdjuntos/5_edison_cardona_xm.pdf

¹⁰ https://cnostatic.s3.amazonaws.com/cno-public/archivosAdjuntos/0204.cno_-_bess_uniandes_isagen.pdf

Technology	Description
HVDC	<ul style="list-style-type: none"> • Cost estimation model for VSC-HVDC lines.¹¹. • HVDC technologies for connection of wind farms in Colombia¹². • Analysis of the connection of non-conventional renewable generation in La Guajira.¹³. • High voltage direct current transmission systems - HVDC.¹⁴.
SPM	Intelligent Supervision and Advanced Control Project –iSAAC [10].

From the bibliography consulted, several applications were identified in two types of technology already implemented in Colombia: the first one is the incorporation of SVC equipment in order to dampen oscillations of the system by means of FACTS, and the second one is the use of STATCOM, as a converter to modulate voltage, phase and frequency of the network.

In turn, the SIRENA-iSAAC project for synchronized phasor measurement was developed in Colombia by XM (in 2007 it began with the National Backup System project for large-scale events - SIRENA and in 2009 it incorporated WAMS into such project). XM implemented and tested a Wide Area Measurement System (WAMS), consisting of measurement equipment, telecommunications network, data processing platform and analysis tools, all with the aim of improving the quality, reliability, safety and situational awareness of Colombia's electrical system. In 2012, the SIRENA project was replaced by a larger project, Intelligent Supervision and Advanced Control (iSAAC), which was conceived to establish the foundations for future intelligent supervision and advanced control of the Colombian electricity system, through which achieve a natural evolution of traditional supervision [10]. Thus, in March 2018 there 70 PMUs were installed in 28 substations, 20 of which were developed by XM, and the other 50 belonging to other actors; of all the PMUs, 13 are for the supervision of generation units, 45 for transmission lines, 11 in transformers and 1 in an SVC [10].

In 2018 an advanced communication prototype was developed on which proofs of concept and use cases of the future network required for the iSAACnet [10] would be carried out. Due to this, XM makes the SPM by connecting to the synchrophasor data concentrators, PDCs, located in the National Dispatch Center (CND) for the application of supervision and control of the SIN, through a data network. The Control Center allows the integration of synchrophasors to the Energy Management System (EMS) through the SIGUARD® PDP platform and at the same time, accepts traditional measurements of the SCADA system, making it possible to incorporate these measures into operational supervision [10].

¹¹ https://cnostatic.s3.amazonaws.com/cno-public/archivosAdjuntos/modelo_de_estimacion_de_costos_de_lineas_vsc-hvdc.pdf

¹² https://cnostatic.s3.amazonaws.com/cno-public/archivosAdjuntos/hvdc_conexion_parque_eolicos.f.pdf

¹³ https://cnostatic.s3.amazonaws.com/cno-public/archivosAdjuntos/11_francisco_gafaro_xm.pdf

¹⁴ https://cnostatic.s3.amazonaws.com/cno-public/archivosAdjuntos/0103.cno_-_hvdc_uniandes_isagen.pdf

4 Technological architecture of synchrophasor measurement

Synchrophasor technology is being used for wide area monitoring and situational awareness, network model verification, event analysis, and analysis of a variety of network phenomena. Since the effective operation of synchrophasor technology requires highly accurate, fully reliable and secure monitoring, synchronization and communications systems are needed. Synchrophasor technology incorporates synchronization for successful smart grid deployment and coordination; it may become a critical service for power system operation and be in the early stages of use at the electrical distribution level [11].

Synchrophasor technology uses PMU to measure voltage and current waveforms, and to calculate phasors. Each measurement has a timestamp and is therefore synchronized with Coordinated Universal Time (CUT), using a time source such as GPS. PMU data is collected at a rate of 30 to 120 samples per second and is sent to data hubs and archives. Synchrophasor applications have one of the strictest precision timing and precision requirements of all timing uses in the electric power system, due to the high number of reports, the precision required for phasor and the extensive geographical distribution of PMUs.

The network is mainly managed using technologies associated with SCADA, provides quasi-static visibility at an update frequency of 4 to 6 seconds. As the level of distributed resources and bidirectional market operations make the overall system less predictable, the level and types of risk associated with maintaining the reliability and security of the network increase [11]. Synchronized time measurements are necessary to allow calculation and comparison of multiple phasors at different locations to obtain a view of the electrical network. Therefore, synchrophasor applications need reliable access to a stable time source such as CUT, to align the time data with the power system. Phasor data concentrators (PDC) are the systems that allow concentrating and correlating the data of the phasors acquired from multiple PMUs, with the aim of having a centralized way of managing the times of the PMU.

Thus, with the growing use of DER - DG, SS, DR and VE, it is driving the need for greater coordination between TSOs and DSOs to provide efficient and standardized services through an technological architecture that guarantees the flexible power system operation.

4.1 Services for flexible power system operation

Flexible operation services are basically composed of the flexible's technologies such as FACTS, Storage and HVDC; and within the support services are the SPM, Time Synchronization and Telecommunications Networks. These services are presented in Table 3.

Table 3. Flexible Operation Services.

	FACTS	Storage	HVDC
Network services	1. Reactive compensation.	1. Stability.	1. Stability
	2. Stability.	2. Spinning Reserve.	2. Power quality
	3. Flow control.	3. Frequency control.	3. Reduction of energy losses
	4. Voltage control.	4. Smoothing power variations.	4. Integration of systems and variable energies
	5. Power quality.	5. Peak shaving.	5. High power transmission over long distances
	6. Short circuit limitation.	6. Load shifting.	6. Active and reactive power control
		7. Island operation.	
	Synchrophasor measurement	Time Synchronization	Telecommunications Networks
Support services	1. Model validation	1. Precision of clocks	1. Wired
	2. Oscillation detection	2. Sampling rate	2. Wireless
	3. Event analysis	3. Measure report	
	4. Monitoring of frequency, voltage stability and phase angle.	4. Measurements in SCADA	
	5. Verification of the operational status of the equipment and situational awareness		

4.2 Support services

The power system uses precision timing for grid monitoring and situational awareness, to coordinate the operation and integration of a variety of grid assets, and for the protection and operation of the grid. As seen in Table 4, the subsystems to support flexible operation can be subdivided in three major blocks: the telecommunications system, which is transversal to the other systems, the time synchronization system with which all devices have the same clock reference, and a third system that corresponds to the Synchrophasor measurement system.

As mentioned, these three subsystems are interconnected by a data network. Previously, many different protocols were used for data transmission. Today almost all data networks operate based on the Internet protocol (IP). Data is shared on these networks by individual data packets that carry the destination and source addresses. Likewise, there are other wide area networks that can transport signals in real time such as voice or data, as in the case of clocks, and which also handle traffic priorities, an example of this type of technique is the Multiprotocol Label Switching (MPLS), used to connect devices and different domains of the technological architecture.

Table 4. Support services.

Type	Description
Telecommunications System.	<p>Telecommunications systems include wide coverage, local, wired and wireless networks that provide the capabilities for systems to communicate with each other or with users. A telecommunications system must comply with:</p> <ul style="list-style-type: none"> • Scalability • Network performance, speed • Availability • Costs • Security • Control <p>The telecommunications system can use wired or wireless technologies for communication such as:</p> <ul style="list-style-type: none"> • Wired technologies (Power Line Communication –PLC, o Digital Subscriber Line –xDSL o Fiber Optic –FO) • Wireless technologies (ZigBee (short range), WIFI (short range), Bluetooth (short range), Cellular networks (medium range), Low Power WAN –LPWAN (long range), Satellite or GPS (long range)
Time Synchronization	<p>The components of the network must be synchronized to obtain efficient services and avoid complications in the system. Incorrect timing can affect the power grid, cause damage, produce electrical transients and frequency alterations, among others. For example, phasor synchronization is the process of matching parameters such as voltage, frequency, phase angle, phase sequence, and waveform between the different parts of the system and the networks, and for this the system has to be synchronized in the weather.</p> <p>The following protocols are used for time synchronization:</p> <ul style="list-style-type: none"> • Simple Network Time Protocol –SNTP • Network Time Protocol –NTP • Precision Time Protocol –PTP • White Rabbit
Synchrophasor measurement	<p>SPM is the comparison of signals from different points in the system with a reference signal. The voltage and frequency signals are compared to produce synchrophasor measurements. The result of this measurement is the data that is sent through channels and processed at a central site by means of specialized software.</p>

4.3 Architecture Model

A technological architecture model is then proposed in which each of these domains is made up of a series of devices and functionalities that allow, through interfaces and communications, meet the objectives of electrical power systems, considering the integration of the smart grids, renewable energy and DER.

Fig. 1 shows some initiatives developed with the aim of building referential technological architectures for the electricity sector, mainly associated with the integration of smart grids and renewable energy sources as axes of the transformation of systems.

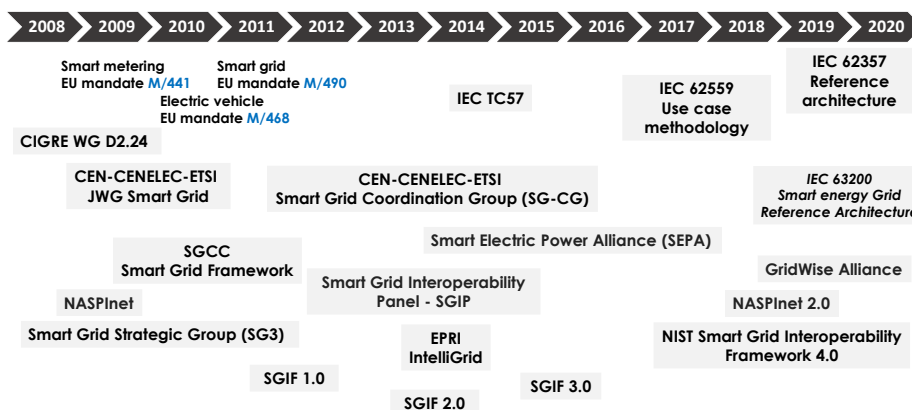


Fig. 1. Referential technological architectures
Source: Own elaboration

As previously stated, the challenges facing the Colombian power sector require having a benchmark technological architecture that allows the integration and deployment of new technological trends, while guaranteeing the provision of the electric power service, complying with the quality indicators established in the local context.

Fig. 2 depicts the different functionalities for each domain; however, according to the organizational structure and the services offered by the different companies that make up the Colombian power sector, it is possible that different interpretations of the reference architecture, as well as its systems and functionalities, may be presented. Taking into account the architecture presented in Fig. 2, each of these domains of operation, transmission, distribution, generation, and others, are interconnected by means of communication networks, which for the case is the transport network with the highest hierarchy or backbone network, such as an MPLS network mentioned earlier. Already within each domain are the domain's own subnets or backhaul networks, which can be of the WAN / NAN / LAN type. Finally, there are other types of access networks, such as networks that provide access to residential users or SMEs with LAN / HAN networks. It should be noted that communication networks are transversal to the architecture, being able to be networks of free or licensed use, but that at the same time they provide privacy and security models when using network functionalities such as virtual local area networks (VLAN), virtual private networks (VPN), and different forms of interconnection according to the type of network, such as Multi-Protocol Label Switch networks, which are networks with traffic prioritization functionalities, based on packet switching, which finally interconnect the aforementioned subnets.

The diagram of the use case, activity and sequence is presented in Fig. 3 to provide an understanding of the actors, interrelationships and processes of the SPM use case within the general architecture.

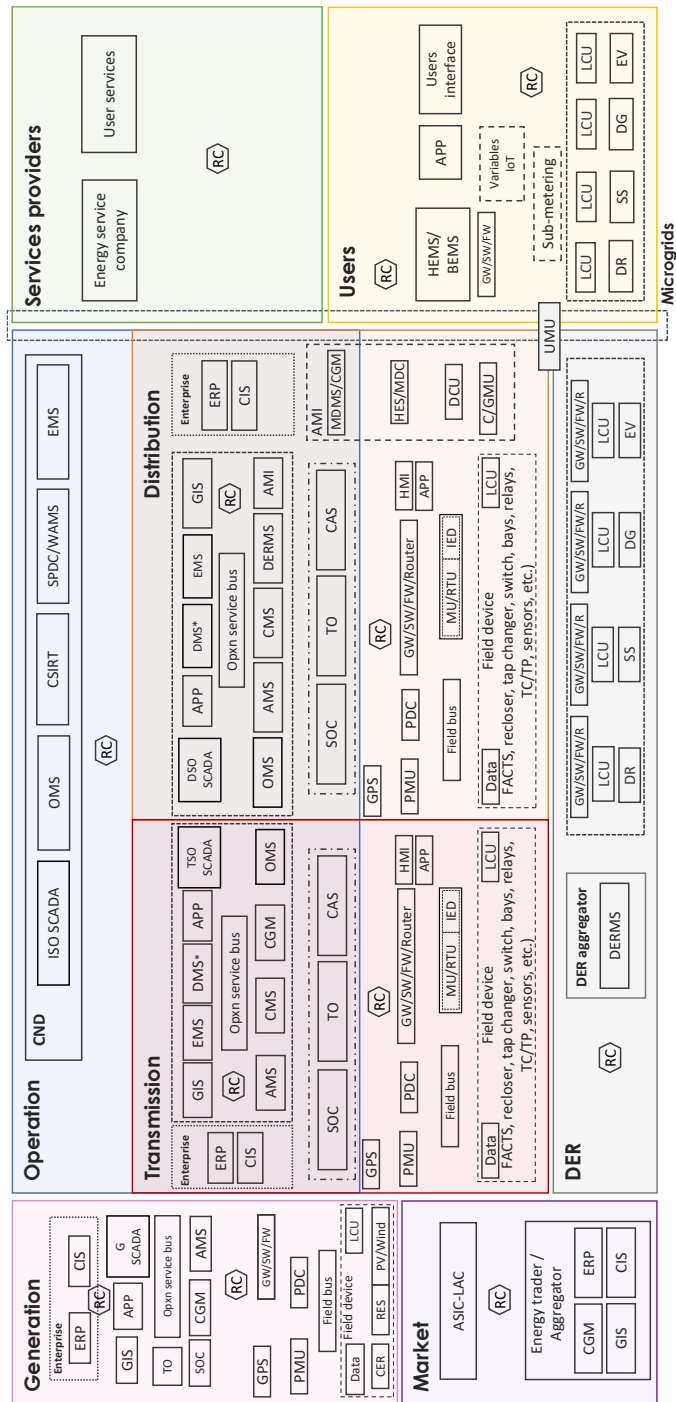


Fig. 2. Systems and functionalities of the referential architecture
 Source: Own elaboration

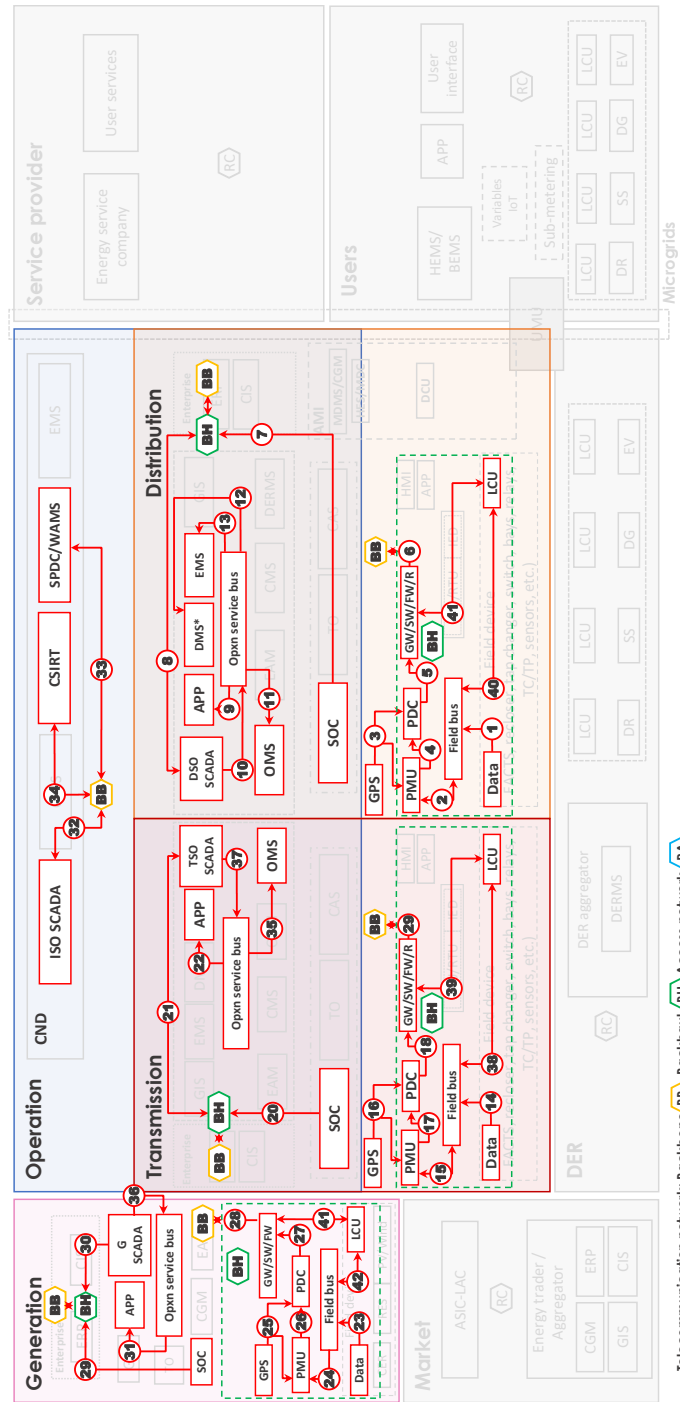


Fig. 3. Synchrophasor Measurement Diagram (actors and interrelationships)
Source: Own elaboration

According to what is presented in Fig. 2, the protocols and standards within the architecture of SPM are presented below in Table 5.

Table 5. Standard and protocols to SPM architecture

Fuente: Own elaboration. IEEE [12]

ID	Protocols / Standards
1, 2, 14, 15, 21, 22, 23, 24, 38,40, 42	IEC61850, IEEE C37.2392
3, 16, 25	IEEE 1588 PTP, IEEE C37.238
4, 5, 6, 17, 18, 19, 26, 27, 28, 39, 41	IEEE C37. 118.1/242/247 ANSI C12.20 2010, IEC 61850
7, 11, 20, 35	NERC-CIP, NISTIR 7628, IEC 61850/62351
8, 9, 10, 12, 13, 29, 30, 31, 32, 36, 37	IEC 60870/61850/62351, NERC-CIP / NISTIR 7628, IEEE C37.239
33	IEC 61850, IEEE C37.118.1
34	NERC-CIP, NISTIR 7628

5 Conclusions

In Colombia, there are several experiences with respect to flexible technologies through SVC and STATCOM for the stability of the electrical network; in the same way, there are experiences in bulk PMU network. The standards and protocols of SPM in the operation of the power system were presented; also, the functionalities and importance of SPM for the power system, regarding the support and operation of the network, were identified. The technical requirements and required criteria for the observability of the operation with the SPM were also established, and an architectural diagram was developed in which the actors, roles, interactions and information flows that should be considered for the SPM were presented.

In turn, standards and protocols are proposed in the operation of the power system for the functionalities of synchrophasor measurement.

The authors would like to thank the companies and member entities of the Colombia Inteligente collaborative network (RIAT Task Force).

References

- [1] International Smart Grids Action Network, «ISGAN,» 2019. [En línea]. Available: <https://es.slideshare.net/sustenergy/flexibility-needs-in-the-future-power-system>.

- [2] ENTSO, «Webinar on Flexibility Framework & Mapping,» 2019. [En línea]. Available: <https://www.entsoe.eu/events/2019/12/05/webinar-on-flexibility-framework-mapping/>.
- [3] J. A. Zapata, «Flexibilidad: Elemento clave para la transformación del sector,» de *II Foro XM: Por un sector en transformación para el usuario*, Medellín, 2019.
- [4] CIGRÉ, «System Operation Emphasizing DSO/TSO Interaction And Coordination.,» 2018.
- [5] IEEE, «IEEE definition,» 2020. [En línea]. Available: <https://techterms.com/definition/ieee>.
- [6] IEC, «International Electrotechnical Commission,» 2020. [En línea]. Available: <https://www.iec.ch/>.
- [7] NERC, «The North American Electric Reliability Corporation,» 2020. [En línea]. Available: <https://www.nerc.com/Pages/default.aspx>.
- [8] NASPI, «Summary of the North American SynchroPhasor Initiative (NASPI) Activity Area,» 2012. [En línea]. Available: <https://www.energy.gov/sites/prod/files/North%20American%20Synchrophasor%20Initiative%20%28NASPI%29%20Program%20Factsheet.pdf>.
- [9] N. Castrillón Gutiérrez, «XM - Verificación del Modelo STATCOM de Bacatá,» 2019. [En línea]. Available: https://cnostatic.s3.amazonaws.com/cnpublic/archivosAdjuntos/verificacion_d_el_modelo_del_statcom_de_bacata.pdf.
- [10] XM, «Propuesta Para Consolidar Y Extender La Medición Fasorial Sincronizada En Colombia,» 2018.
- [11] NASPI Technical Report, «The North American SynchroPhasor Initiative,» Mar 2017. [En línea]. Available: https://www.naspi.org/sites/default/files/reference_documents/tstf_electric_power_system_report_pnnl_263_31_march_2017_0.pdf.
- [12] IEEE Power & Energy, «IEEE Power & Energy,» 2019. [En línea]. Available: <https://ieeexplore.ieee.org/document/634216>.

New opportunities of Broadband Power Line Communications for the improvement of the Smart Grids

Noelia Uribe-Pérez¹ [0000-0001-6154-1087], Igor Fernández², David de la Vega², Asier Llano³, Ibon Arechalde¹ and Alexander Galarreta²

¹ TECNALIA, Basque Research and Technology Alliance (BRTA)
Parque Científico y Tecnológico de Bizkaia. Astondo Bidea, Edificio 700
E-48160 Derio (Bizkaia), Spain

² UPV/EHU, Dpt. Communications Engineering, University of the Basque Country
(UPV/EHU), Pz. Torres Quevedo s/n, E-48013, Bilbao, Spain

³ ZIV I+D Smart Energy Networks, Parque Científico y Tecnológico de Bizkaia, Edificio 210
E-48160 Derio (Bizkaia), Spain
noelia.uribe@tecnalia.com, igor.fernandez@ehu.eus, david.delavega@tecnalia.com,
asier.llano@zivautomation.com, ibon.arechalde@tecnalia.com
alexander.galarreta@ehu.eus

Abstract. The current efforts towards the improvement of the Smart Grid involves technologies able to deal with more strict requirements, i.e. cybersecurity and higher data rates capable of improving current services and introduce new demanding applications, while keeping low cost deployments and profitability. The roadmaps of the main electricity companies in Europe for the coming years include Broadband Power Line Communications (BPL) as a key player in this new scenario. Even though BPL has been widely used for in-home applications for more than a decade (internet distribution mainly) its behavior in the power grid is less known. Therefore, there is still work to be done prior to wide deployments of BPL in the power grid. The necessary research includes both theoretical and empirical work, since the power grid is a hostile medium for the communications and the performance of the technology remains poor documented in related works. In this context, the authors identify in this paper the main aspects to be addressed and the methodology to complete them, aiming at guaranteeing successful deployments of BPL. In addition, some lab trials are presented. This work is part of the BB-GRID project. First insights reveal BPL as a promising technology for the improvement of the Smart Grids and a perfect complement for already deployed infrastructures, such as the smart metering systems. Smart Cities will benefit greatly from these improvements, not only from the power grid perspective, but also considering management aspects, since the control of assets could be performed through BPL in real time while assuring cybersecurity and integrity of the data.

Keywords: Broadband Power Line Communications, Smart Grid, Electrical Grid, Transmission technologies.

1 Introduction

In the current process of digitization of the electrical networks, most of the European distribution companies have chosen the use of Power Line Communications (PLC) technologies. Despite the fact that this alternative presents high difficulties for the development of an efficient communication system, due to the high presence of interferences in the network and the influence of different assets connected to the network, PLC presents the advantage of offering control of the data transmitted over the network without the need to depend on third parties (mainly telecommunications operators, who offer turnkey solutions). This control of data is, and will continue to be, a compelling argument for electricity distribution companies to opt for the use of data transmission technologies over the electric cable, to the detriment of the use of wireless technologies already developed which are, indeed, technologically more powerful.

Unlike other transmission systems, these technologies were not developed using European or international standards, but by consortia of companies led by large electricity companies, which defined their own communications system and deployed their meters, in accordance with the technology developed. The main transmission technologies, along with power companies that have developed them are listed as follows:

- PoweRline Intelligent Metering Evolution (PRIME) [1]: Iberdrola - Spain, E.On - Germany, Naturgy - Spain, EDP - Portugal, Energa – Poland.
- Meters & More [2] : Enel - Italy, Endesa - Spain
- G3-PLC [3]: EDF – France.

These technologies belong to the Narrow Band Power Line Communications (NB-PLC) group, since they are narrow-band communications, which seek a high level of robustness against interference, at the cost of limiting the net data rate transmitted and providing very high response.

NB-PLC have contributed enormously to the success of the current digitalization of the electrical network, including the remote reading of meters and the monitoring of important aspects, such as the quality of supply and network overload. However, they show severe limitations for their use in advanced Smart Grids applications, especially those that require very low response times, high transmission rates or higher cybersecurity demands. This is the case of all those applications related to the remote monitoring and management of devices and subsystems connected to the network, which require very short response times, as all of them are limited by the high latency times of communications and, consequently, its implementation is not currently feasible. It is also the case of remote management of microgrids, distributed generation systems or remote management systems for electric car charging stations. These limitations led the electricity companies to raise the need for a new transmission technology that would offer the benefits required by future network management and control services: reduced latency times, higher transmission rates, greater bandwidth, greater stability. connection and improvements in cybersecurity. In this context, the role of Broadband Power Line Communications (BB-PLC or BPL) sounds promising. BPL uses higher frequency bands to deliver higher data rates with lower latencies.

The remaining work in this documented is grouped as follows: Section 2 introduces the fundamentals of the BPL technology; Section 3 highlights the benefits of BPL for

the coming smart grids; Section 4 describes current related work by BPL forums, Section 5 presents and describes the BB-GRID project, Section 6 presents first lab tests of BPL devices and, finally, Section 7 summarizes the main conclusions of this work.

2 Fundamentals of BPL

BPL, as any other PLC technology, uses the already existing power cables as the medium for data transmission. In contrast to widely deployed NB-PLC solutions, BPL utilizes higher bandwidth, typically in the frequency range between 2-30 MHz, which highly increases the data rate (up to hundreds of Mbps) and reduces the latency.

BPL technology has been used for in-home applications for more than a decade, hence it is well-understood in this context. G.hn and HomePlug were the primary PLC standards for home networking but since HomePlug have not announced any further technologies since 2016, G.hn seems to be the reference standard nowadays. G.hn is a standard endorsed by the International Telecommunications Union – Telecommunications (ITU-T). The ITU-T recommendation G.9960 (Specification of G.hn physical layer (PHY) and architecture) addresses PLC access and smart grid applications and specifies system architecture, most of the PHY and data-path related parts of MAC [4].

On the contrary, the use of BPL for access applications in Smart Grids is less known [5]. Despite very promising advantages, due to the benefits of using higher frequency ranges, one of the main drawbacks is the attenuation, which increases with distance and frequency. In addition, the coverage of BPL is limited to hundreds of meters, which makes the implementation of BPL for access networks difficult. This can be partially solved with the use of repeaters, at the cost of increasing the complexity of the network.

A typical structure of the BPL access network in the low voltage (LV) grid can be seen in Figure 1. In this scheme, the LV network is used for communication between the BPL subscribers and the substation. The access network is connected through the substation to a wide area network (WAN) by conventional communications technology. By implementing the BPL access technology, the LV grid can be considered as a tree topology, where the root is the transformer, the nodes of the tree are the street cabinets (mostly implemented on the roadsides) and each street cabinet is connected to different buildings, that are representing the BPL subscribers [5].

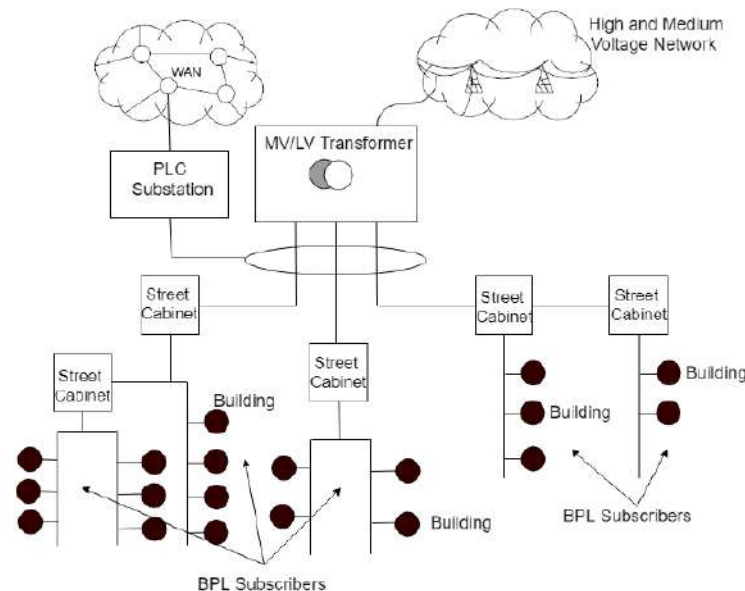


Figure 1. Typical structure of BPL access network [5].

3 Role of BPL within the Smart Grid context

NB-PLC technologies have been offering good connectivity for today's smart metering use cases. To date, smart meter networks have been able to operate while offering multiple services, such as hourly load curves, remote management of consumption and power contract, among others. Current data rates offered by NB-PLC technologies are usually around 20 Kbps, which is at its operational limit in most current applications; therefore, the margin for increasing the performance of the services in this band is certainly limited. Additionally, the usual response time of NB-PLC technologies is from a few seconds up to several minutes, limiting the number of applications that can be operated on these networks.

However, the natural benefits of the PLC technologies, i.e., a communication medium present in the entire electrical network without depending on the coverage provided by external operators, suggest a technological evolution of current NB-PLC towards higher bandwidths and lower latencies. BPL technology will allow, on the one hand, a much higher transfer data rate, being able to offer rates of up to hundreds of Mbps and, on the other hand, significantly shorter response times of less than 50 ms. The upgrading of these features cover an essential requirement to offer the necessary services for the smart networks of the future.

BPL technologies have been widely used since the beginning of the 21st century within homes for internet communications, as an alternative or complement to WiFi networks. Currently, these technologies offer speeds of one megabit per second (Mbps)

upstream and hundreds of Mbps downstream, for short distances within the home network. The extension of the use of BPL technologies to the rest of the electrical network is not immediate. BPL has been optimized for use of internet distribution within the home, in which the upwards/downwards data transmission is asymmetric, the distances between devices in the network are short (a few dozen meters of cable), the network topology is very simple (two or three communication nodes at most), the variability of the loads connected to the network is small and where the availability of the service, although important, is not critical. In addition, the data obtained from the electricity grid by the distribution company or by a power generation company using renewable energies is critical and they will circulate over a very wide network (several kilometers of cable and dozens of intermediate connectors), with very variable propagation conditions (due to changes in loads, impedances, noises ...) and with topologies of hundreds of communication nodes, which must adapt in real time to the environment and service conditions. Moreover, cybersecurity requirements that utilities and administrations are demanding for future services are considerably more challenging. The performance of all these characteristics must be evaluated in the field by means of use cases and pilots, like the trials planned by E.ON in Germany, in order to test the restrictive cybersecurity and efficiency requirements of German regulation [6].

Some electricity companies have already used BPL technologies in power grid automation but limited to the monitoring of the medium voltage (MV) section of the grid, with the purpose of collecting data from substations. Several companies have been using this for some time, although the existing solutions are proprietary solutions, dependent on specific manufacturers. These solutions for the MV sections do not entail the difficulties of the LV section since, on average, the network is much more stable (very stable impedances), the topologies are simpler (a lower number of nodes) and the propagation conditions are propitious (lower noise level and interferences).

For any other type of communication required for both LV and MV networks, the most common communications systems are based on radio frequency, mostly using mobile phone technologies such as GPRS, 3G, 4G and other similar protocols. The use of these communications has a high operational cost for electricity companies, this being the main cause that companies seek the development of a private communication network based on PLC. As it will be described in Section 4, international alliances that developed the NB-PLC solutions have already been working on the creation of a BPL standard applicable to smart LV electrical grids. The uses that are intended to be offered are diverse: the delivery of consumption and measurement data in real time to the users, the automation of LV distribution, the control and management of renewable generation plants in real time, the control and management of the MV network for the assurance of supply quality, the detection of isolated networks, the guarantee of cybersecurity aspects, the introduction of blockchain for the electricity market and future services, etc. For instance, related projects have reported raw data rate of several tens of Mbps achievable for links up to 500 m [7], which can be very positive for supporting and upgrading AMI applications, such as Demand Response (DR) [8]. DR allows utilities to increase the efficiency of their systems by adjusting the demand with the power supply on an instantaneous manner. The management of energy assets can also benefit from this increase of bandwidth, since more frequent and precise data can be transferred

in less time. Other smart services, such as the EV management or the cybersecurity over the power grid will be greatly improved with the higher data rates and low latency inherent to BPL. Smart Cities will benefit greatly from these improvements, not only from the power grid perspective, as described above, but also considering management aspects, since the control of assets such as public EV fleets, urban energy resources (e.g., district heating systems), traffic signaling, disposal management, etc. could be performed through BPL in real time while assuring cybersecurity and integrity of the data. For instance, Smart City Mannheim (moma), a research project set up under the German government funded programme 'E-Energy' was created to demonstrate how renewable energy can be optimally integrated into the grid as well as how the city can act as an energy store through the use of BPL [9].

Despite current efforts in the development of BPL systems, there is still few studies concerning the planning of BPL networks [7]. Therefore, the roll-out of large BPL networks needs deep research regarding the technology behaviour and the planning process.

4 Current work in related BPL Forums

Within the existing efforts towards the implementation of BPL, the PRIME Alliance [10] is one of the key drivers. PRIME (Powerline Intelligent Metering Evolution) is a mature, consolidated and global NB-PLC standard for smart metering or Advanced Metering Infrastructure (AMI), network control and monitoring applications, fulfilling the goal of establishing a set of open international PLC standards. One of the key challenges of PRIME has been to achieve interoperability between equipment and systems from different manufacturers and deployments of more than 20 million PRIME meters by utilities and solution providers across Europe with a recent expansion in the Middle East. Current PRIME solution is now being used and installed in more than 15 countries around the world [11].

The PRIME Alliance, promoted worldwide by Iberdrola and other utilities such as Naturgy, EDP, CEZ, Viesgo or Energa, created in 2019 a working group to develop a BPL standard able to address the delivery of consumption and measurement data in real time to the users, the automation of the LV distribution section, and the control and management of renewable generation plants in real time. Following the creation of this working group, E.on (German distribution company), Corinex (Canadian manufacturer of BPL devices for the home) and Devolo (German manufacturer of BPL devices for the home) also joined the PRIME Alliance. To these incorporations must also be added the active presence in the alliance of companies such as ST Microelectronics (Italy), Microchip (Spain), Renesas (Japan) or ZIV (Spain), which were relevant for the development of the NB-PLC standard in the Alliance. The working group analyzed in 2019 the different existing alternatives in the current use of BPL at home, such as HomePlug or Gh.n, to see how mature were the developments carried out by then and whether this solution could be adapted to the environment of the electrical distribution network. Some initial tests suggested that the ability of the Gh.n technology to be adapted to new scenarios can make it appropriate as the basis for the development of a PRIME-BPL

technology. Moreover, Gh.n is the proposed basis for the BPL solution presented in [2-1], with the aim of dealing with the security requirements recently announced by the German Federal Ministry for Economics and Technology in the development of their Smart Grids [12].

The PRIME Alliance has set a milestone by 2020-early 2021 to describe a full PRIME-BPL specification. This implies that laboratory and on-field tests will have to be developed. The laboratory tests will allow to check different implementations, for a first identification of relevant parameters and to get some feedback for the manufacturers. Field testing should ensure the performance of the devices both in controlled environments and in real-world situations where power line impedances, attenuations, and existing noise can limit the performance of the transmission technology. The specification must cover the physical layer, the MAC layer and a convergence layer, as it was defined in PRIME 1.3.6 and PRIME 1.4 NB-PLC specifications.

In addition, another relevant promoter of BPL is the Broadband Forum [13], an open, non-profit communications industry organization focused on accelerating broadband innovation, standards, and ecosystem development. Broadband Forum's projects span across 5G, connected homes, cloud, and access. Their working groups collaborate to define best practices for global networks and develop multi-service broadband packet networking specifications addressing architecture, device and service management, software data models, reference implementations, interoperability and certification in the broadband market. In fact, the Broadband Forum has developed a well-defined test bed and an established set of tests that enable a performance comparison between PLC products and technologies that can be independently verified, as described in Section 6.

In parallel, other associations, such as G3-PLC Alliance, promoted by EDF in France, is also addressing the increase of bandwidths and data rates to extend the uses of PLC communications.

5 Addressing BPL for the coming future: BB-GRID project

Considering the window of opportunity that currently exists for BPL technology, the BB-GRID project addresses the challenges and needs that a future deployment of BPL will require, mainly from the empirical perspective. The project counts on the support of some of the main European electricity companies and it is structured in the following main research topics:

1. Characterization of the LV section of the electrical network as a propagation medium for broadband data transmission. Given the lack of results about the behaviour of the propagation medium in higher frequency ranges and the absence of theoretical models, the first objective of the project will be the detailed characterization of the communication medium through extensive field measurements, in a set of network and cabling topologies that will be considered as representative of the most common scenarios of the LV network. In this sense, the definition of a measurement methodology and the implementation of a measurement system adapted to this frequency range will be also addressed.

2. Definition of a new technology for broadband data transmission in smart electrical grids (named PRIME-BPL), which meets the demanding requirements of future applications (low latency, high transmission rate, cybersecurity features, stability of connections and robustness against different types and interferences in the network).
3. Design and implementation of a development platform for the PRIME-BPL technology, which allows the testing of different configurations of the technology and the implementation of the necessary modifications, in an efficient and agile manner.
4. Laboratory and field tests of the new PRIME-BPL transmission technology, in order to test the performance of the technology in different scenarios, network topologies, transmission requirements and types of interference. The field tests will be developed in collaboration with an electricity company.
5. Proof of concept of transmission and reception of PRIME-BPL technology, with the aim of implementing the developed technology in an FPGA and testing it under laboratory conditions, including the conditions of the propagation medium.

5.1 Characterization of the LV section of the electrical network as a means of propagation for broadband data transmission

The characterization of the electrical network as a propagation medium for data transmission is essential for the subsequent design of a robust and efficient communication systems adapted to the environment. This characterization has been carried out empirically in recent years based on impedance and attenuation measurements of the network itself at the frequencies of interest, as well as the levels of emissions from the numerous devices connected to the grid. However, most studies carried out to date have been limited to frequencies below 150 kHz, only a few of them have extended the study only up to 500 kHz, which leads to a lack of results in the range of frequencies considered by BPL for distribution electrical grid (up to dozens of MHz). The behavior of the electrical network at frequencies above 150 kHz is, therefore, a question that must be resolved in order to implement the communications system that best suits the characteristics of the network.

On one hand, in terms of noise and interfering emissions in the LV electrical network, it has been shown that some devices connected to the network generate emissions in the frequency band from 2 to 150 kHz, a range commonly used by NB-PLC technologies [14]. Although these technologies consider the use of robust coding and modulation techniques, there are studies that show that these interfering emissions present in the transmission channel can severely affect communications [14-18].

These disturbances basically consist of radio noise and unwanted emissions generated by devices connected to the grid, which have been classified according to different criteria, such as frequency response and duration or periodicity as background noise, coloured noise, narrowband noise, harmonics of the switching frequency of the device connected to the grid and impulsive noise [19-21].

According to the European Committee for Electrotechnical Standardization (CENELEC), these types of noises and unwanted emissions are generated by a wide

variety of devices in the 2 to 150 kHz band [14]. The most relevant are: electronic devices that include small inverters for switching (power supplies, elevators, washing machines ...) [22-24], lighting equipment (compact bulbs, fluorescent and LEDs) [25-28] and distributed energy sources such as photovoltaic inverters (PV), battery chargers, hydraulic power systems or wind turbines [19-20], [24], [28-32]. As the number of renewable energy generators, electric vehicle (EV) chargers and energy-efficient devices is expected to increase in the coming years, the number and extent of unwanted emissions is also expected to increase considerably. The interest in the analysis of PV panels, battery chargers and other devices that contain inverters is that the inverters generally generate unwanted emissions in the harmonics of the switching frequency that interfere with PLC systems.

Due to the great variety of sources and types of unwanted emissions and the variable behaviour in time and frequency, their characterization has to be empirical, so it requires extensive field and laboratory measurement campaigns. This characterization must be carried out using a commonly accepted measurement methodology, which enables the analysis of the great temporal and frequency variability of the various types of noise. Moreover, since not many studies or measurement campaigns have been carried out at frequencies above 150 kHz, it is necessary to complete a detailed characterization of the electrical network in these terms at higher frequencies, to estimate whether the unwanted emissions could cause problems in communications in the frequency bands where BPL works.

In addition, the knowledge about the grid impedance of the LV section is limited, especially at frequencies above 9 kHz. However, the impedance has a significant impact on many aspects. First, the impedance of the electrical network affects the propagation of unwanted emissions, and therefore, it alters the possible interfering effects of these emissions on other electrical devices [14], [29-31]. Second, the impedance of a certain user device can present a low-impedance circuit at high frequencies and, therefore, it can cause high attenuation of the communications signal [14]. Additionally, the correct implementation of the power stages of the communication devices requires impedance mismatching in the operating frequency range, and for that, it is essential to estimate the impedance of the network at this frequency range. Therefore, it is important to investigate the typical values of the network impedance at higher frequencies. Since the access impedance depends on the network topology, type of cable and the connected loads, exhaustive measurement campaigns are needed in different scenarios, in order to carry out a statistical approximation that results in typical values of the network impedance [14], [33].

Finally, the characterization of the attenuation of the LV network is another of the key aspects to consider for the correct planning of communication services, given that high attenuation can lead to poor reception quality. As for the access impedance, there are few studies on this matter in the literature. Previous related work from the authors [34] showed that, added to the expected influence of the distance of the cable sections on the attenuation, the branches of the distribution network significantly increase the effects of the attenuation. In addition, it was concluded that there is a strong dependence of the attenuation with the frequency, without showing a common trend or pattern for different scenarios. The results corroborated the complexity of the electrical network

as a propagation medium for the data transmission, since the attenuation depends on the distance, the topology of the network and the frequency, but also on the impedance and the location of the different loads that can be connected to the network at all times.

Given the absence of theoretical models, the characterization must be carried out through field measurements, in a set of network topologies and cabling typology that are considered representative of the most common scenarios of the LV network. For the same reason, since there is no measurement methodology or measurement system adapted to this frequency range, it will be also designed as part of this work. Among the aspects to be investigated are the following: transmission losses, the influence of the topology of the electrical network and the type of cable and the effects of the loads connected to the network at all times. Likewise, it requires a detailed characterization of the typology of radioelectric noise and the interfering emissions present in the network in this frequency range, generated by the connected electronic devices. The nature and characteristics in the time and frequency domains of all these aspects will determine the most efficient set of techniques for communication to be robust against emissions of a certain nature, while allowing the maximization of the data bit rate and the scope of transmissions.

5.2 Definition of a new technology for broadband data transmission

Current uses of PLC technologies could suggest that the use of BPL technologies over the distribution network is immediate. However, the electrical distribution network presents very different characteristics with respect to the home networks. Within a home, the distance between two communication nodes (i.e., two computers connected to two sockets) is short, the impedance of the network within the home is very stable and, although there may be certain variations in terms of the number of phases or number of connection points and cable quality, this variety is very limited. Outside the home, the distance between the supply points and the substations is highly variable, ranging from a few dozen meters to a few kilometres, the impedances of the different points of the network vary depending on factors such as the connected loads accumulated at multiple supply points and cable types and network topologies can cause major inconveniences in the distribution of the communications signal.

Related researches carried out worldwide on broadband technologies for use in electricity distribution networks is also very limited. The search for a technology adapted for the electrical distribution network will entail the adaptation of the frequency bands currently defined for applications within the home and the optimization of the modulation schemes, as well as a more exhaustive analysis of the transmission medium, as described in Section 5.1.

The proposed definition of a new technology for broadband data transmission in smart electrical grids considered in this work does not intend to start from scratch, but rather to adapt the most successful technology used within the home and create a subset of parameters that allow the use of this technology in the electricity grid. This subset could include a limitation of the frequency bands used, an adaptation of the modulation schemes for its use in more extensive and varied networks, and a different management of the transmitted power than the method used in the standard within the home.

The first step to achieve the definition of the technology will be to analyse the differences in the environment in which the equipment will work for the required use versus the environment in which it had been used to date. Then, several performance levels to be met by the technology will be defined, in which the lowest level includes the minimum requirements that must be met. These minimum requirements must be met even in those cases in which the environmental conditions are more restrictive. The requirements must be defined in order to ensure the availability of communications in the network, limit the latency of communications, correctly manage the collisions that may occur and ensure the speed and flow necessary for the correct operation of the system in high-density networks of communication nodes.

Once these aspects are covered, the configuration of the physical (PHY) layer will be defined, taking the standard Gh.n as a starting point, that will most likely imply a limitation of the frequency bands. Another aspect to verify in the definition of the PHY layer will be the adequacy of a set of modulation configurations to be used in the wide variety of network topologies. Based on the experience of the NB-PLC deployment in the LV grids, the definition of a wide set of modulation configurations will be needed, in order to adjust the modulation scheme to the specific conditions of different scenarios. In addition, the definition of the maximum transmission power and the management of the transmitted power levels will be essential to achieve an efficient technological solution that complies with existing regulations, as there is a regulated limitation of the transmitted power in the radioelectric spectrum, both conducted and radiated. In defining this PHY layer, in addition to these regulatory aspects, it is very important to consider energy efficiency aspects, since the increase of the transmitted in a wide frequency range can lead to low efficiency rates in the transmission and/or to considerably technical losses in the electrical distribution network.

Finally, the relationship of the PHY layer with the upper layers will be considered. This is one of the most divergent aspects with respect to both the home broadband solutions and the NB-PLC grid technologies. Within the home, the solution is simple, since communication is limited to a few nodes (two or three) that establish a link at a specific time, which do not require changes in the network. In the NB-PLC deployments for electrical networks, a complex relationship between the PHY layer and the upper layers have to be addressed, given the number of nodes that could be connected, the variety of existing topologies and the variability of the topology over time. Each NB-PLC technology addresses this issue from different approach. The management of the MAC layer in Meters & More Association is closely related to the PHY layer and seeks the limitation of topology changes. On the contrary, the management of the MAC layer in the solutions of the PRIME Alliance or G3-PLC seeks a rapid adaptability of the networks by promoting the self-discovery of new nodes in the network. The approach selected in this task is closer to the solution carried out by the PRIME Alliance for NB-PLC. Taking the Gh.n standard as a starting point, this definition will be one of the critical aspects of the project.

5.3 Design and implementation of a development platform for the PRIME-BPL technology

Once the new technology is defined, a platform to develop and implement the new technology will be designed, in form of a user-friendly software platform that allows the introduction of multiple parameters in a simple way.

The definition of the technology described in the previous subsection will include both functionally and theoretically the technology to be implemented. However, there are many determining aspects derived from the technological implementation, as well as the need for subsequent diagnosis. During this stage, the bases of architectural issues, such as the definition of the system architecture, will be established, so that the tool can serve as an initial instrumentation implementation and later it can evolve to a commercial implementation. More detailed design issues will also be defined, such as the metrics to be obtained from the internal operation of the equipment for its diagnosis and operation, together with decisions of the high-level algorithms to be used in both transmitter and receiver blocks.

The software of the PRIME-BPL development platform will be developed in a modular way with a defined style guide, so that later, each one of the blocks can be replaced by optimized versions oriented to DSPs or specific algorithms in FPGAs. All the software development will be done on GIT revision control with unit tests. There will be a clear division between general-purpose signal processing routines and those that are developed specifically for the implementation of this BPL technology. All functional modules will have unit tests and their own diagnostic capacity.

Finally, as a first phase for the testing and evaluation of the technology, the implementation of the development platform must be validated at the laboratory. It is important to detect possible errors in the implementation, for which an isolated environment is required with respect to external sources of interferences. In addition, multiple possible options and configurations of the physical layer, considered for PRIME-BPL and implemented in the development platform (number of carriers, bandwidth, symbol time, modulation scheme, technical encoding, interlacing technique, etc.) must be also taken into consideration. Each module of the system must be tested individually, in order to guarantee that each one of the modules is correctly implemented. Furthermore, this validation methodology facilitates the identification and correction of possible implementation errors.

5.4 Laboratory and field tests of the new PRIME-BPL transmission technology

In this phase of the work, different configurations of the defined PRIME-BPL technology will be tested at two levels: first, in a controlled laboratory environment, in order to test the performance of the technology in presence of controlled sources of affection of the communication channel; second, at a set of locations on the power grid that are representative of typical distribution network topologies and cabling types.

The development platform described in the previous subsection will facilitate the testing of different configurations and options of the PRIME-BPL technology, allowing

the change from one to another in an agile and simple way, depending on the results obtained on-field.

As a previous step to the field tests, the performance of PRIME –BPL will be evaluated against different sources of interference over the propagation channel, controlled in amplitude, frequency and time of occurrence. In this way, the level of affection is clearly delimited and the response of the technology to each of the types of affection is precisely measured. The development of a laboratory workbench is proposed to carry out these tests. This workbench will allow the replication of representative scenarios of the grid. In addition, situations collected during the on-field measurements (subsection 5.1), such as attenuation levels, network impedance values for different frequencies and interfering emissions or noise levels, among others, will be replicated in the workbench. This will allow the replication of real scenarios present in the electricity network, in a controlled way, in the laboratory, to objectively measure the level of affection of each one of them in the quality of communications. Tests will be carried out against the following types of affections: narrow-band interfering emissions (single-frequency tones), interfering emissions composed of a set of harmonics of a reference frequency, white noise and colored noise of different levels and frequency patterns, replicas in NB-PLC emission frequency, different levels of channel attenuation, phase distortions, point fades, periodic noises and impulsive noises of different amplitude and duration. The metrics used for the evaluation of the technology will be the usual ones: SNR value for a threshold FER value, percentage of received frames, etc., for the different channel effects and for the different transmitted signal configurations. Once the first results are obtained, an iterative evaluation and correction work of the PRIME-BPL technology is proposed, so that all those aspects that are detected as susceptible to improvement, are implemented in the development platform and re-evaluated in the laboratory tests. This iterative process guarantees an improvement in the response of the technology to different channel effects and transmission requirements.

Then, a set of representative scenarios of the power grid, in terms of number of connected devices, network topology, type of cabling, sources of emissions and data transmission requirements, will be selected, in order to test the performance of the PRIME-BPL technology. In addition, representative situations of the future evolution of the electricity network will be included: microgrids, EV recharging points, renewable energy generation and storage systems (at the prosumer level and at the small producer level) and on-demand storage systems from the needs of the network. The selection of the scenarios and their corresponding access points will be carried out in collaboration with an electricity company, which has expressed its willingness to collaborate in this stage. These on-field measurements represent the key test to evaluate the technology developed. The response of PRIME-BPL, in terms of performance, robustness, latency times, connection stability and data transmission rate, in presence of different density of connected devices and of different types of interference, will be the definitive evaluation of the product developed.

Finally, once the first results from the measurements are obtained, an iterative evaluation and improvement process will be also conducted, so that all those aspects susceptible to improvement detected during the measurements can be applied to the PRIME-BPL development platform.

5.5 Proof of concept of transmission and reception of PRIME-BPL technology

In this stage, a proof of concept is developed with the objective of implementing the developed technology in an FPGA and testing it under laboratory conditions, including the conditions of the communication medium. Hence, the complete design of the proof of concept in FPGA format is considered, its implementation in the appropriate laboratory environment for this purpose and, finally, the evaluation of its performance, with the aim of validating the described BPL-PRIME technology in a practical way.

Throughout this task, the design of a proof of concept of the developed technology will be carried out, using the results obtained from the laboratory and on-field tests. During this design phase, the improvement proposals that will be defined in the previous stage will be used and will be integrated into the BPL development tool. The technically feasible improvements will be evaluated, taking into account their practical implementation to ensure an industrial future of the technology. Based on the results obtained, some parameters of the technology will be defined to reduce its parameterization, simplify its implementation and standardization, to ensure a design that is as simple as possible, facilitating its subsequent industrial viability. Additionally, a graphical interface will be designed to be able to use the tool dynamically, to ensure a simple diagnosis of its operation and a smooth transfer of technology to the business fabric.

Then, the implementation of the software previously designed will be carried out. Both the implementation of the enhancements and the graphical interface will contain unit tests. The software for the PRIME BPL tool and the graphical interface that allows diagnosing and configuring its use will be independent software with separate repositories, subtask management and unit tests. The design of the graphical interface will be done in C++ considering its portability to Windows and Linux environments. Existing AMI Manager tool from ZIV that already serves simpler NB-PLC systems and has been widely used in smart PLC systems will be used as a basis. During this task, tests will be carried out at the simulation and laboratory level of basic functions, in which the complete operation in presence of white and impulsive Gaussian noises will be tested. To do this, SNR-FER curves will be made and will be compared with other technologies, as well as with the theoretical limits.

Finally, both the measurements obtained in the work described in Subsections 5.2 and 5.4, respectively, will be used to test the demonstrator in representative Smart Grid environments. The tests will continue at the laboratory, now introducing the representative propagation characteristics obtained from the field trials. SNR-FER curves will be obtained for the operation of the technology as a function of the operating parameters. These SNR-FER curves will serve both to validate the technological implementation, but will also be used later to assist in the technological selection, in on-field deployments and in the configuration of the transmitter parameters of the adaptive algorithms for the management of the modulation schemes of the MAC layer.

6 Hands on BPL: lab tests and performance evaluation

First laboratory trials will be done following the last version of the “Performance Test Plan For In-Premises Powerline Communication Systems” published by the Broadband

Forum [35]. The document is aimed to provide industry, operators, and test labs with a well-defined test bed and an established set of tests that enable a performance comparison between PLC products and technologies that can be independently verified. Several categories of tests are included, such as throughput performances, noise immunity, topology, traffic, security and QoS, among others, thus, allowing the verification of a wide range of features of the BPL technology, which will provide a useful feedback for future deployments.

Below two main set-ups are described, corresponding to the throughput and Power Spectral Density (PSD) test performance. Figure 1 shows a proposed test set-up for the evaluation of the throughput and the performance against noise, aiming at testing the performance of BPL under different conditions. Several devices can be identified in this set-up [35]:

- Traffic generator/analyser: this block corresponds to a laptop that generates and analyses the traffic. Typically, iperf software is used. Iperf is a widely used tool for active measurements of the maximum achievable bandwidth on IP networks. It supports tuning of various parameters related to timing, buffers and protocols (TCP, UDP, SCTP with IPv4 and IPv6) [36]
- PLC adapter: this block corresponds to the BPL nodes. For the sake of this project, several BPL nodes from different vendors will be tested.
- UPLC: the Universal PLC splitter is an equipment that allows to transfer the PLC signal (transmitted either through 2 or 3 wires) that is being sent over a powerline cable into the three different coaxial conductors (corresponding to L, N and PE). A schematic of how such a device may be implemented can be seen in Figure 3.
- Channel emulator: this component allows to emulate the behavior of a real powerline channel. The channel emulator shall include a noise generator function. This noise generator function can be both activated and deactivated in the tests. A generic view of this device can be consulted in Figure 4.

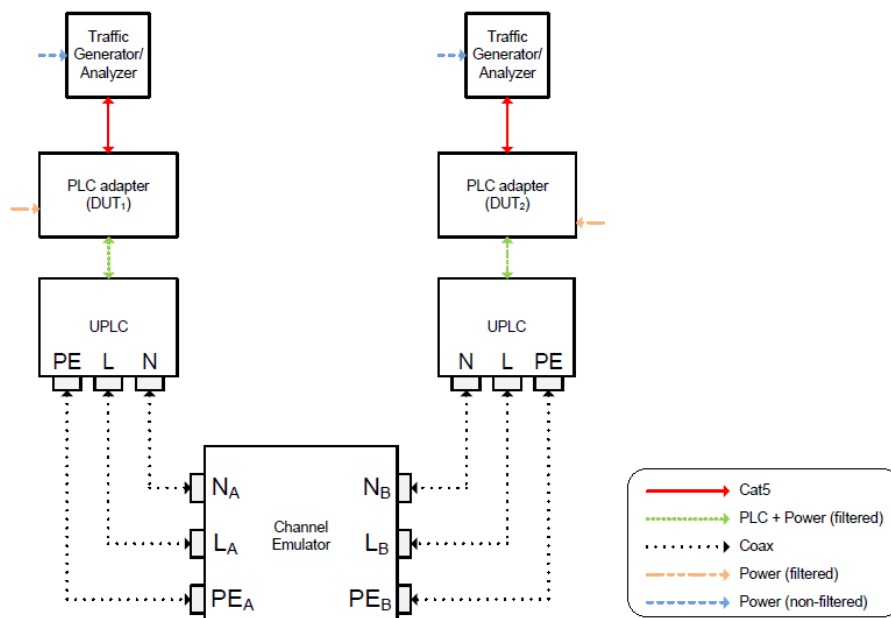


Figure 2. Test set-up for BPL evaluation - throughput [35].

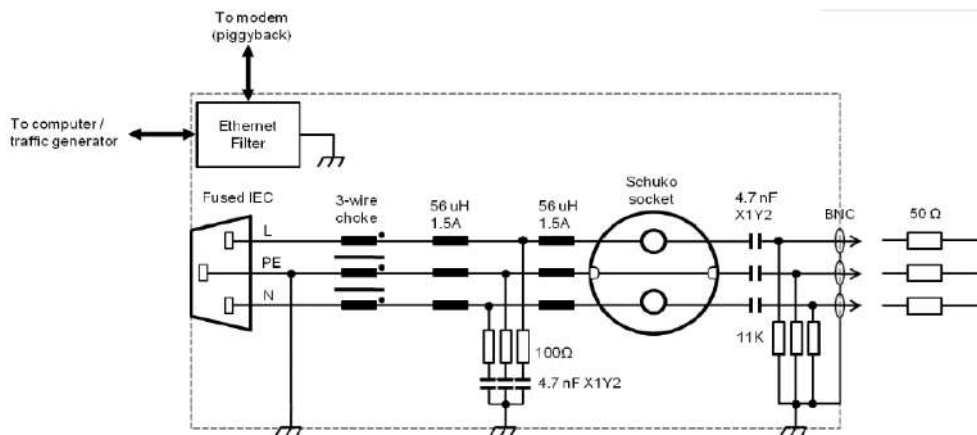


Figure 3. Universal PLC splitter schematic [35].

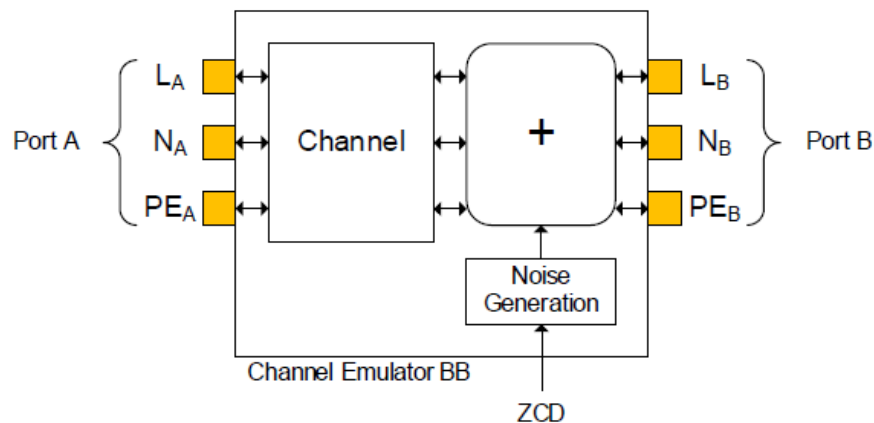


Figure 4. Generic schematic of the channel emulator [35].

Figure 5 shows the proposed set-up for the measurement of transmit PSD in-band and out of band for the system under test. In addition to the traffic generator, BPL node and UPLC blocks, as seen in the previous set-up, this configuration also includes:

- Spectrum analyser: this device will record the PSD measurements
- Splitter: for these tests, it is a 3dB power combiner/divider, ie, a passive device that connects three segments of a coaxial medium combining/dividing the power of the signals that pass through this device
- Att1, Att2 and Att3: corresponds to different values of attenuation for each line, according the test procedure.

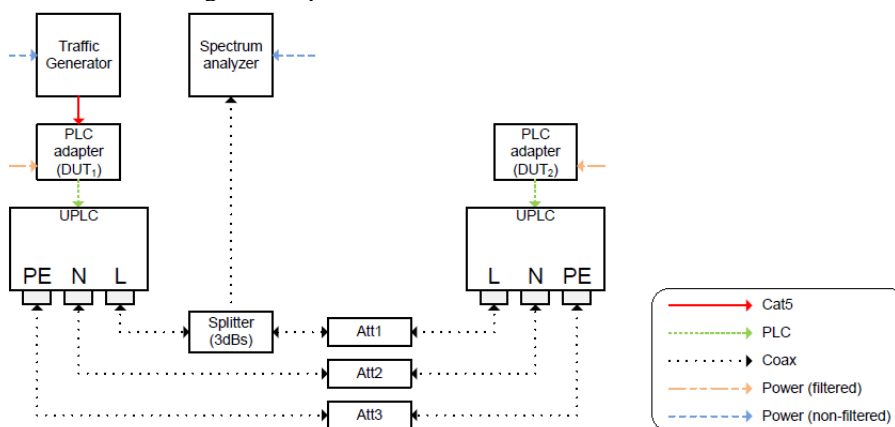


Figure 5. Test set-up for BPL evaluation - PSD [35].

7 Conclusions

This work presents the possibilities of BPL for the Smart Grid. The technology has been reviewed, as well as the current main drivers towards its introduction in future wide deployments. In addition, the BB-GRID project has been presented and some first lab trials with BPL devices have been introduced. BB-GRID intends to maximize the benefits of BPL for future improvement of the grid and new services through an extensive research and empirical work.

As an overall conclusion, BPL is a very promising technology for the enforcement of Smart Grids. Therefore, it should be seen not as a substitute of already deployed PLC technologies, such as NB-PLC, but as a necessary complement of these. Smart Cities will benefit greatly from these improvements, since beyond the power grid enhancement, management aspects can be also addressed with BPL in real time while guaranteeing data privacy and cybersecurity.

8 Acknowledgements

BB-GRID Project is partially funded by the Basque Government (Ref. KK-2020/00095). This work is also funded in part by the Spanish Government under the grant RTI2018-099162-B-I00 (MCIU/AEI/FEDER-UE).

References

1. PRIME Technology. Available online: https://www.prime-alliance.org/?page_id=6897
2. Meters & More Tecnology. Available online: <https://www.metersandmore.com/oursolution/>
3. G3-PLC Technology. Available online: <http://www.g3-plc.com/what-is-g3-plc/g3-plc-overview/>
4. Unified high-speed wire-line based home networking transceivers – system architecture and physical layer specification, ITU-T, Recommendation G.9960, 2011. Available online: <https://www.itu.int/rec/T-RECG.9960>.
5. G. Hallak, M. Berners and A. Mengi, "Planning Approach Towards Optimal Performance and Cost of G.hn Broadband PLC Access Networks," 2020 IEEE International Symposium on Power Line Communications and its Applications (ISPLC), Málaga, Spain, 2020, pp. 1-6, doi: 10.1109/ISPLC48789.2020.9115399.
6. G. Hallak, T. Frauenrath and A. Mengi, "Security Concepts Based on IEEE 802.1X for G.hn Broadband PLC Access Networks," 2020 IEEE International Symposium on Power Line Communications and its Applications (ISPLC), Málaga, Spain, 2020, pp. 1-6.
7. S. Dominiak, L. Andersson, M. Maurer, A. Sendin and I. Berganza, Challenges of Broadband PLC for Medium Voltage Smart Grid Applications. In Proceedings of the 6th Workshop on Power Line Communications, Rome, Italy, 20–21 September 2012, pp. 20–21.
8. A. Ikpehai, B. Adebisi and K. M. Rabie, Broadband PLC for clustered advanced metering infrastructure (AMI) architecture. *Energies*, 2016, 9(7), 569.
9. Moma – Smart City Mannheim Research Project. Available online: <https://www.ppc-ag.com/projekte/moma-smart-city-mannheim/>
10. PRIME Alliance. Available online: <https://www.prime-alliance.org>

11. PRIME Technology deployments. Available online: https://www.prime-alliance.org/?page_id=249
12. BSI: Protection Profile for the Security Module of a Smart Meter Gateway (Security Module PP), Version 1.03 – 11 December 2014.
13. Broadband Forum. Available online: <https://www.broadband-forum.org>
14. Electromagnetic Interference Between Electrical Equipment/Systems in the Frequency Range Below 150 khz, Standard CENELEC SC 205A, 2015.
15. N. Uribe-Pérez, L. Hernández, D. de la Vega, and I. Angulo, "State of the art and trends review of smart metering in electricity grids," *Appl. Sci.*, vol. 6, no. 3, p. 68, 2016
16. P. Pakonen, M. Pikkarainen, B. Siddiqui, and P. Verho, "Electromagnetic compatibility between electronic loads and automated meter reading systems using PLC," in *Proc. 22nd Int. Conf. Exhib. Electr. Distrib.*, Jun. 2013, pp. 1-4.
17. P. Pakonen, S. Vehmasvaara, M. Pikkarainen, B. A. Siddiqui, and P. Verho, "Experiences on narrowband powerline communication of automated meter reading systems" in *Proc. Electr. Power Qual. Supply Rel.*, Jun. 2012, pp. 1-6.
18. J. Matanza, S. Kiliccote, S. Alexandres, and C. Rodríguez-Morcillo, "Simulation of low-voltage narrow-band power line communication networks to propagate OpenAD signals," *J. Commun. Netw.*, vol. 17, no. 6, pp. 656-664, Dec. 2015.
19. G. López, J. I. Moreno, E. Sánchez, C. Martínez, and F. Martín, "Noise sources, effects and countermeasures in narrowband power-line communications networks: A practical approach," *Energies*, vol. 10, no. 8, p. 1238, 2017.
20. S. Hong and M. Zuercher-Martinson, "Harmonics and noise in photovoltaic (PV) inverter and the mitigation strategies," *Solaria Renew.*, to be published.
21. M. Gotz, M. Rapp, and K. Dostert, "Power line channel characteristics and their effect on communication system design," *IEEE Commun. Mag.*, vol. 42, no. 4, pp. 78-86, Apr. 2004.
22. S. K. Rönnberg, M. H. J. Bollen, H. Amaris, G. W. Chang, I. Y. H. Gu, H. Kocewiak, J. Meyer, M. Olofsson, P. F. Ribeiro, and J. Desmet, "On waveform distortion in the frequency range of 2 kHz_150 kHz Review and research challenges," *Electr. Power Syst. Res.*, vol. 150, pp. 1-10, Sep. 2017.
23. G. F. Bartak and A. Abart, "EMI of emissions in the frequency range 2 kHz_150 kHz," in *Proc. 22nd Int. Conf. Exhib. Electr. Distrib.*, Jun. 2013, pp. 1-4.
24. S. Rönnberg, "Emission and interaction from domestic installations in the low voltage electricity network, up to 150 khz," Ph.D. dissertation, Luleå Tekniska Univ., Luleå, Sweden, 2013.
25. E. O. A. Larsson and M. H. J. Bollen, "Measurement result from 1 to 48 fluorescent lamps in the frequency range 2 to 150 khz," in *Proc. 14th Int. Conf. Harmon. Qual. Power (ICHQP)*, Sep. 2010, pp. 1-8.
26. A. Larsson, "On high-frequency distortion in low-voltage power systems," Ph.D. dissertation, Luleå Tekniska Univ., Luleå, Sweden, 2011.
27. S. K. Rönnberg and M. H. J. Bollen, "Emission from four types of led lamps at frequencies up to 150 khz," in *Proc. IEEE 15th Int. Conf. Harmon. Qual. Power*, Jun. 2012, pp. 451-456.
28. S. Rönnberg, M. Bollen, and A. Gil-de-Castro, "Harmonic distortion from energy-efficient equipment and production in the low-voltage network," *Tech. Rep.*, 2014.
29. N. Uribe-Pérez, I. Angulo, L. Hernández-Callejo, T. Arzuaga, D. de la Vega, and A. Arrinda, "Study of unwanted emissions in the CENELEC-A band generated by distributed energy resources and their influence over narrow band power line communications," *Energies*, vol. 9, no. 12, p. 1007, 2016.

30. A. Nejadpak, A. Sarikhani, and O. A. Mohammed, "Analysis of radiated EMI and noise propagation in three-phase inverter system operating under different switching patterns," *IEEE Trans. Magn.*, vol. 49, no. 5, pp. 2213-2216, May 2013.
31. I. Fernandez, N. Uribe-Pérez, I. Eizmendi, I. Angulo, D. de la Vega, A. Arrinda, and T. Arzuaga, "Characterization of non-intentional emissions from distributed energy resources up to 500 kHz: A case study in Spain," *Int. J. Elect. Power Energy Syst.*, vol. 105, pp. 549-563, Feb. 2019.
32. M.A. Sonmez, M.A. Zehir, M. Bagriyanik, and O.Nak, "Impulsive noise survey on power line communication networks up to 125 kHz for Smart metering infrastructure in systems with solar inverters in turkey," in *Proc. Int. Conf. Renew. Energy Res. Appl. (ICRERA)*, Oct. 2013, pp. 705-710.
33. IEC/TR 60725:2012. Consideration of reference impedances and public supply network impedances for use in determining disturbance characteristics of electrical equipment having a rated current ≤ 75 A per phase.
34. I. Fernández, I. Angulo, A. Arrinda, D. de la Vega, I. Arechalde, N. Uribe-Pérez and T. Arzuaga, "Characterization of the frequency dependent transmission losses of the grid up to 500 kHz", *The 25th international conference and exhibition on electricity distribution (CIRED 2019)*, Madrid (Spain), 2019.
35. Broadband Forum. Performance Test Plan For In-Premises Powerline Communication Systems – TR-208. Technical Report. November 2019. Available online: https://www.broadband-forum.org/technical/download/TR-208_Issue-3.pdf
36. Iperf Tool. Available online: <https://iperf.fr>

Solid Oxide Fuel Cell Electric Vehicle: Cost Reduction Based on Savings in Fixed Carbon by Sugarcane

Danielle Rodrigues de Moraes^{1,2}[0000-0001-8259-7020], Vanessa de Almeida Guimarães^{1,2}[0000-0001-7662-3499], Luis Hernández-Callejo³[0000-0002-8822-2948], Bárbara de Noronha Gonçalves⁴[0000-0002-9012-7587] and Ronney Arismel Mancebo Boloy^{1,2}[0000-0002-4774-8310]

¹ Federal Centre of Technological Education Celso Suckow da Fonseca, Rio de Janeiro, Brazil

² Group of Entrepreneurship, Energy, Environment and Technology – GEEMAT

³ University of Valladolid, Campus Duques de Soria, Soria, Spain

⁴ Federal University of Rio de Janeiro, Rio de Janeiro, Brazil

danirdmoraes@gmail.com

Abstract. Carbon pricing is a cost-effective method for mitigating climate impacts, including in the transport sector. This article examines the life cycle cost and carbon dioxide (CO₂) emissions of the Solid Oxide Fuel Cell Electric Vehicle (SOFCEV) powered by Brazilian fuels. The potential for cost reduction of the SOFCEV dissemination was evaluated, considering the Brazilian productivity of sugarcane and the carbon fixed by these plantations through the mechanism of carbon credits sale. The fuels considered were sugarcane ethanol and gasoline C (73% gasoline and 27% anhydrous sugarcane ethanol). Three scenarios were outlined: a) Cost of investment in equipment, fuel production, and vehicle maintenance and operation in R\$/km, over a 10-year amortization period; b) Cost of CO₂ emissions of the SOFCEV from well-to-wheel added to cost (a); c) Cost of carbon fixed by hectares of sugarcane in Brazil necessary to supply the fuel demand of the SOFCEV subtracted from (b). Results showed that the SOFCEV fuelled with Brazilian sugarcane ethanol attend the carbon neutral cycle, since its avoided cost with carbon credits sale implementation is 3.6 times bigger than its emissions cost. Gasoline C showed similar results for the three scenarios, with an emissions cost 1.4 times bigger than the avoided cost by carbon fixation. Thus, it is expected to obtain economic and environmental indicators to encourage the use of biofuels in the Brazilian transport sector, specifically in electromobility.

Keywords: Life Cycle Cost, Carbon Credits, Solid Oxide Fuel Cell Electric Vehicle, Carbon Dioxide Emissions, Sugarcane Ethanol.

1 Introduction

In recent years, the actions resulting from economic and industrial activities have caused several negative impacts on the dynamics of ecosystems, particularly regarding the emission of greenhouse gases (GHG). Some of these impacts are: extreme weather conditions such as prolonged droughts, rising sea levels, increased forest

fires, changes in the rain regime and agricultural patterns, among others [1]. The world's energy matrix will have to undergo transformations to slow the increase in the global average temperature, this can be achieved by the adoption of green alternatives, until the level of zero net emissions can be reached. According to the International Renewable Energy Agency [2], in order to maintain global warming below 2°C until 2050, it is mandatory that, by 2030, the proportion of bioenergy in relation to global energy consumption be doubled, and triple the use of biofuels for the transport sector.

However, internal combustion engine vehicles (ICEV) dominate the Brazilian fleet of non-commercial light-duty vehicles (LDV) and, despite the success in using ethanol in flex vehicles, there is still a large share of inefficient ICEV with obsolete technologies that operate without remarkable fuel economy, and consequently with high exhaust emissions [3]. According to Souza et al. [4], it is estimated that LDV fuel consumption in Brazilian urban roads is around 3.77 MJ/km, while in the review made by Rosenfeld et al. [5], modern LDV have an average consumption of 1.60 MJ/km. Consequently, the main source of emissions in the Brazilian energy sector is transport, having been responsible for the emission of 200.2 million tons of carbon dioxide equivalent (CO₂ eq.) in 2018, which represents 49% of the total emitted [6].

Thus, it is understood that electromobility would play an important role in the decarbonization of the transport sector, as it combines technologies with low or zero exhaust emissions. The number of electric vehicles in circulation in early 2018 increased by 63% over the same period last year worldwide [7]. However, this increase is not uniform across the globe, with many countries lagging behind due to factors such as the lack of infrastructure and incentives for technologies that best serve a certain national scenario. In economic terms, the ICEV still has a more competitive selling price than electric and hybrid vehicles (around 40% more expensive), in addition to the high initial investment cost in local infrastructure for charging and adapting the electrical matrix [7].

According to the review conducted by Guimarães [8], some of the policies and actions can be adopted to mitigate emissions, especially in the transport sector, such as: (i) carbon emission regulation policies (e.g., carbon tax, carbon cap and carbon cap-and-trade); (ii) use of renewable fuels (i.e., biofuels); (iii) increased vehicle energy efficiency; (iv) emissions inventory; (v) actions in the transport infrastructure, vehicle technology and management, aiming to reduce these emissions. According to the World Bank [9], the carbon pricing policy represents the internalization of social costs resulting from GHG emissions, establishing a value for the ton of CO₂ eq. emitted. This social cost includes all expenses directed to society that may be related to climate change, such as the repair of territorial damage caused by floods or forest fires, and expenses resulting from damage to health caused by heat waves.

In addition, carbon pricing is a regulatory instrument that generates cost-effectiveness gains, i.e., it demonstrates mitigation potential by directing consumer demands and investments to services and technologies with a lower carbon footprint [10]. Carbon pricing in Brazil has been in development since 2011, with the establishment of the preliminary proposal to prepare the market for its implementation [11]. Regarding the transport sector, the National Biofuels Policy (RenovaBio) plays

an important role through the implementation of Decarbonization Credits (CBIO), which apply to Brazilian producers and importers of biofuels certified by RenovaBio. This instrument aims to value efficient agents in the biofuels market and generate incentives to reduce the carbon intensity of their production process each year [12]. According to projections by the International Council on Clean Transportation, the CBIO provide incentives for better performing sugarcane ethanol producers, with an emphasis on bagasse ethanol (i.e., second generation ethanol) producers which generates 95% carbon savings over fossil gasoline [13].

Among the cleanest electric vehicle technologies are the Battery Electric Vehicle (BEV) and the Hydrogen Fuel Cell Electric Vehicle (HFCEV), which have zero exhaust emissions. The commercially available HFCEV models operate with the Proton Exchange Membrane Fuel Cell, a low temperature fuel cell that must be fed directly with hydrogen and presents only water and heat as exhaust emissions. However, one of the biggest challenges for the mass adoption of HFCEV is the hydrogen supply infrastructure [14]. As an alternative, there is the Solid Oxide Fuel Cell Electric Vehicle (SOFCEV) which, due to the high operating temperature of its fuel cell, presents the possibility of internal production of hydrogen from the insertion of reformable fuels (e.g., ethanol and gasoline) in the vehicle.

Thus, it is believed that the SOFCEV could be adopted as an alternative to the Brazilian context, since it is a technology that values both the sugarcane ethanol produced in the country and the use of electromobility, without the requirement for significant changes in the local supply infrastructure. There is also the possibility of reducing costs based on obtaining and selling carbon credits, which tends to favor biofuel producers.

This article examines the life cycle cost and carbon dioxide (CO₂) emissions of the SOFCEV powered by Brazilian fuels. Thus, it is expected to obtain economic and environmental indicators to encourage the use of biofuels in the Brazilian transport sector, specifically in electromobility.

2 Methodology and Assumptions Adopted

The analysis was based on the life cycle cost (LCC) method for the SOFCEV, assuming capital investments (capital costs), vehicle manufacturing cost, maintenance and operating costs, fuel production cost and well-to-wheel (WTW) emissions cost. The fuels considered were Brazilian sugarcane ethanol and gasoline C (73% gasoline and 27% anhydrous sugarcane ethanol). The potential for the cost reduction was evaluated considering the cost avoided through the acquisition and sale of carbon credits, considering the Brazilian productivity of sugarcane and the carbon fixed by these plantations.

2.1 SOFCEV Operation and Specifications

Inside the SOFC with fuel processor several reactions occur, such as steam-reforming, water-gas shift, and electrochemical reactions. These reactions are designed to produce a gas mixture that mainly contains hydrogen (H₂), CO₂ and carbon monoxide

(CO). The hydrogen supplied after the fuel steam-reforming process via the anode side reacts with the atmospheric air from the cathode side to produce electricity and heat. The electricity produced charge the battery and the heat is recovered in the form of energy through the appropriate technology (e.g., gas turbine). This energy is taken to the fuel processor, where the internal production of hydrogen is restarted.

Fig. 1 shows a simplified SOFC scheme with a gas turbine. The model described by Facchinetti et al. [15] includes a fuel processor where partial steam-reforming of the fuel occurs, including auxiliary devices (i.e., pump and blowers) and excessive steam to guarantee a reduced rate of degradation of the SOFC. The use of heat exchangers is necessary to remove the extra energy generated during the operation of the system. Unused fuel is directed to a burner where it is oxidized. Finally, the expansion of the hot gases activates the turbine, ejecting the exhaust gases.

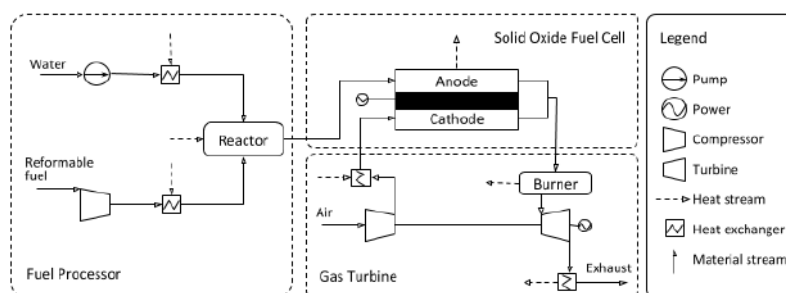


Fig. 1. Simplified Solid Oxide Fuel Cell Scheme with Gas Turbine [15].

The basic operation principle of the SOFC is based on three main reactions. These reactions are as follows:



The H₂ produced upstream is pumped to the fuel cell anode, where it is oxidized and separated into two hydrogen protons (H⁺) and two electrons (2e⁻), as described in Reaction 1 [16]. The oxygen (O₂) enters the fuel cell through the positive terminal, the cathode, where it is reduced forming two oxygen atoms (O²⁻), as in Reaction 2 [20,21]. Each O²⁻ attracts two H⁺ through the electrolyte, which combine to form the water molecule (H₂O) in an exothermic reaction (Reaction 3) [20,21]. These reactions together form an electron flow, as the electrons formed at the anode bypass the fuel cell electrolyte and return to the cathode, generating an electric current. This process can be resumed in an overall electrochemical cell reaction, as follows:



In addition, conventional vehicles (i.e., ICEV) operate with low efficiency, around 30-35% [18], while the efficiency observed by Facchinetti et al. [15] in Solid Oxide

Fuel Cell (SOFC) with gas turbines was between 60-72%. Therefore, it is expected that the SOFC vehicle application will meet increasingly restrictive efficiency and fuel economy standards.

2.2 SOFCEV Life Cycle Cost Calculation System

The vehicle LCC considers the financial expenses in stages such as preparing the infrastructure, manufacturing, producing the energy source (i.e., fuel or electricity), as well as the expenses resulting from its maintenance and operation, as explained in Fig 2. From WTW, there are essential expenses and GHG emissions intrinsic to the main stages of the SOFCEV dissemination: vehicle manufacture, generation and transportation of fuel, and circulation of the SOFCEV. The cost of manufacturing, preparation of infrastructure, as well as maintenance and operation of the SOFCEV were obtained through equations by different authors. The emissions inventory related to the cultivation of sugarcane, generation and transportation of fuel was prepared based on data available in the literature, specifically for the Brazilian scenario.

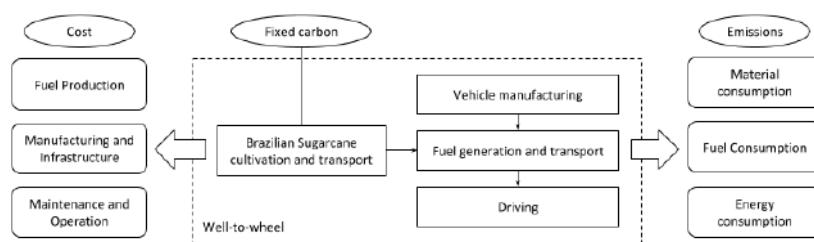


Fig. 2. Scope and calculation system.

Scenario A. This scenario includes the cost of investment in equipment, producing Brazilian fuels, manufacturing, maintaining and operating the vehicle. This cost will be presented in R\$/km, considering anhydrous sugarcane ethanol and gasoline C (73% gasoline and 27% anhydrous sugarcane ethanol) as fuel, during a 10-year amortization period.

The vehicle fuel flow was obtained through Eq. (1) from Braga [19], as follows:

$$\dot{m} = 3.6 \cdot \frac{P_{SOFC}}{\eta_{SOFC} \cdot \rho_f \cdot LHV_f} \tag{1}$$

Where \dot{m} is the fuel flow of the SOFCEV in m³/h; P_{SOFC} is the SOFC power in kW; η_{SOFC} is the average efficiency of the SOFC with heat recovery; ρ_f is the fuel density in kg/m³; LHV_f is the fuel lower heat value in MJ/kg.

Eq. (2) e Eq. (3) from [20,21] were used to estimate the manufacturing cost over a 10-year amortization period:

$$q = 1 + \frac{r}{100} \tag{2}$$

$$f = \frac{q^k \cdot (q - 1)}{q^k - 1} \quad (3)$$

Where r represents the annual interest rate of 3.75%, referring to the Selic rate for April 2020; f represents the annuity factor in 1/year; q represents the capital value; k represents the amortization period in years.

The manufacturing cost, fuel production cost, and the maintenance and operating cost are determined by Eq. (4), Eq. (5), and Eq. (6), below:

$$C_v = \frac{C_{SOFCEV}}{\Delta S} \cdot f \quad (4)$$

$$C_f = \frac{\dot{m} \cdot C_f'}{v} \quad (5)$$

$$C_{M\&O} = \%M\&O \cdot C_v \quad (6)$$

Where C_v represents the cost of vehicle equipment and components in R\$/km; C_{SOFCEV} represents the total manufacturing cost of the SOFCEV in R\$; ΔS represents the vehicle life cycle in km/year, considering a life cycle of 150,000 km in 10 years; C_f represents the fuel production cost in R\$/km; C_f' represents the fuel production cost in R\$/m³; v represents the average speed of LDV on urban roads as 40 km/h, according to the Brazilian Traffic Code [22]; $C_{M\&O}$ represents the portion referring to the cost of maintenance and operation in R\$/km; and $\%M\&O$ is the percentage of the vehicle equipment and components cost that represents the cost of maintenance and operation, adopted as 10% [23].

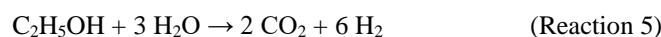
Therefore, adapting the methodology used by Braga [19] and Micena [23], the total cost of Scenario A is described by Eq. (7):

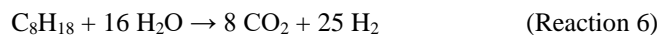
$$C_a = [1.23 \cdot (C_v + C_{M\&O})] + C_f \quad (7)$$

Where C_a represents the total cost of Scenario A over a 10-year amortization period. For a more realistic analysis the coefficient 1.23 was adopted, which includes additional expenses of 23% on investments in equipment, including land preparation (5%), design and engineering (10%), contingency (5%) and permission (3%) [23].

Scenario B. In this scenario the emissions cost is added to C_a . Thus, the social cost resulting from the negative effects of the anthropogenic GHG emissions is now internalized, i.e., from the carbon taxation mechanism, WTW emissions of the SOFCEV are accounted for and taxed, without acquisition of carbon credits. WTW emissions range from fuel production to vehicle circulation on urban roads.

Tank-to-wheel (TTW) emissions include the steps after the vehicle is supplied, i.e., the vehicle circulation and, eventually, the disposal or recycling of components. In this study, the TTW analysis includes only the exhaust emissions of the SOFCEV, obtained through Eq. (1) and the following global steam-reforming reactions for ethanol (C₂H₅OH) and the gasoline surrogate (C₈H₁₈):





From the chemical reactions described above it is possible to arrive at the CO₂ emission factor, in terms of kg of CO₂ eq. per kg of fuel, calculated by Eq. (8) [24]. Here, the CO₂ emissions are considered as CO₂ eq. emissions, since there are no emissions of methane, sulfur dioxide, nitrogen dioxide and particulates present in this simulated process.

$$f_{CO_2e} = \frac{n_{CO_2} \cdot M_{CO_2}}{n_f \cdot M_f} \quad (8)$$

Where f_{CO_2e} represents the steam-reforming emission factor in kg of CO₂ eq. per kg of fuel; n_{CO_2} and n_f represent the number of moles of CO₂ and fuel obtained from Reaction 5 and Reaction 6; M_{CO_2} and M_f are the molecular mass of CO₂ and fuel in g/mol. The values calculated from Eq. (8) for ethanol and gasoline surrogate were 1.91 kg CO₂ eq./kg and 3.08 kg CO₂ eq./kg, respectively.

The total cost of Scenario B is given by Eq. (9), as follows:

$$C_b = C_a + \left(R\$_{CO_2} \cdot \frac{\dot{m} \cdot f_{CO_2e} \cdot \rho_f}{v} \right) \quad (9)$$

Where C_b represents the total cost of Scenario B in R\$/km; $R\$_{CO_2}$ is the rate attributed to the kg of CO₂ emitted in R\$/kg CO₂; ρ_f is the fuel density in kg/m³.

Well-to-tank emissions (i.e., vehicle, battery, ethanol and gasoline production), as well as the estimate of TTW emissions (i.e., exhaust gas emissions) for the SOFCEV are explained in Table 1.

Table 1. Well-to-wheel emissions inventory.

Parameter	Value	Unit	Observations and Source
Well-to-Tank Emissions			
Vehicle production	0.0678	kg CO ₂ /km	Souza et al. [4] conducted a vehicle life cycle assessment in Brazil; value adapted for vehicle life cycle of 150,000 km.
Battery production	0.0052	kg CO ₂ /km	Value obtained by Souza et al. [4] and adapted for vehicle life cycle of 150,000 km.
Sugarcane ethanol production in Brazil	0.0117	kg CO ₂ /km	García & Sperling [25] estimated the average emission of 2,665 kg CO ₂ eq. per hectare of sugarcane, considering stages such as fertilization, harvest and transport, without carbon fixation; value adapted considering agro-industrial productivity, yield and fuel consumption.
Gasoline production in Brazil	0.0102	kg CO ₂ /km	Value obtained by Souza et al. [4] and adapted for vehicle life cycle of 150,000 km.
SOFCEV Tank-to-wheel Emissions			
Exhaust gas from ethanol	0.0488	kg CO ₂ /km	Obtained from the ethanol steam-reforming reaction, Eq. (1), Eq. (8), and the average speed of LDV on urban roads according to the Brazilian Traffic Code.
Exhaust gas from gasoline (without additions)	0.0393	kg CO ₂ /km	Obtained from the gasoline surrogate steam-reforming reaction, Eq. (1), Eq. (8), and the average speed of LDV on urban roads according to the Brazilian Traffic Code.

Scenario C. In this scenario the carbon fixed by sugarcane plantations will be counted when considering the Brazilian sugarcane ethanol pathway. Carbon fixation is the

photosynthetic reaction that occurs between atmospheric CO₂ and water to generate organic products needed by plants. Thus, Eq. (10) presents the adaptation of the methodology used by Neamhom et al. [26] and the United States Environmental Protection Agency [27] to estimate carbon fixation by sugarcane plantations:

$$CF = 0.4 \cdot \left(\frac{44 \text{ kg } CO_2}{12 \text{ kg } C} \right) \cdot Y \quad (10)$$

Where CF represents the carbon fixation per hectare of sugarcane in kg CO₂/ha; 0.4 is the conversion factor, which is a ratio of carbon in biomass in the photosynthetic reaction, as follows: $CO_2 + H_2O \rightarrow 4 CH_2O + O_2$; (44 kg CO₂/12 kg C) is the ratio of the molecular weight of carbon dioxide to carbon; Y is the sugarcane productivity per hectare in kg/ha.

To estimate the cost of fixed carbon when meeting the SOFCEV ethanol demand, Eq. (11) was used, as follows:

$$C_{fc} = R\$_{CO_2} \cdot \frac{CF \cdot V_f}{AP \cdot S} \quad (11)$$

Where C_{fc} represents the economy based on the carbon fixed by sugarcane plantations during the production of the ethanol needed to supply the SOFCEV demand in R\$/km; V_f represents the volume of ethanol consumed during the vehicle life cycle in m³; AP represents the agro-industrial productivity of Brazilian ethanol in m³/ha; S represents the vehicle life cycle in km.

Therefore, the total cost of Scenario C is determined by Eq. (12), as follows:

$$C_c = C_b - C_{fc} \quad (12)$$

Where C_c represents the total cost of Scenario C, considering the carbon fixed by sugarcane plantations during ethanol production in R\$/km. Through Eq. (12) the existence of a simplified market for the sale of carbon credits is considered. In this case, it would be possible to sell the credits referring to the fixed carbon value, and thus deduct from the total costs. However, it is assumed that there is no maximum emissions limit for the sector (cap). The additional costs resulting from the operation of the carbon market due to the lack of regulation worldwide have not been considered. In Brazil there are recent sectorial initiatives such as the Decarbonization Credits from RenovaBio, aimed at the certification of producers and importers of biofuels in the country [12].

2.3 Assumptions Adopted

The assumptions adopted to estimate the SOFCEV production cost, WTW emissions and carbon fixed by sugarcane plantations are shown in Table 2. The powertrain specifications were based on the Nissan prototype ethanol-powered “e-Bio Fuel-Cell”. Furthermore, the vehicle itself is based on the e-NV200, which has a 24-kWh capacity lithium-ion battery, a SOFC output in the order of 5 kW, a 30-liter fuel tank capacity, and an estimated range of 600 km or more [28].

Table 2. SOFCEV specifications, production cost and other assumptions adopted.

Parameter	Value	Unit	Source	Parameter	Value	Unit	Source
Electric engine power	40	kW	[18]	Anhydrous ethanol density	799.40	kg/m ³	-
Battery capacity	24	kWh	[28]	Gasoline surrogate density	737.00	kg/m ³	-
Car shell mass	1000	kg	[18]	Brazilian anhydrous ethanol LHV	28.26	MJ/kg	[29]
SOFCEV power	5	kW	[28]	Brazilian gasoline LHV	43.54	MJ/kg	[29]
Vehicle life cycle ¹	150,000	km	[18]	Ethanol production cost in Brazil	1930.00	R\$/m ³	[30]
Average speed on urban roads	40	km/h	[22]	Gasoline production cost in Brazil	1299.17	R\$/m ³	[31]
Electric engine cost ²	6,502.00	R\$	[18]	CO ₂ molecular mass	44.01	g/mol	-
Lithium-ion battery cost ²	78,024.00	R\$	[18]	C ₂ H ₅ OH molecular mass	46.07	g/mol	-
Car shell cost ²	72,576.41	R\$	[18]	C ₈ H ₁₈ molecular mass	114.23	g/mol	-
SOFCEV cost ²	42,439.01	R\$	[18]	Carbon tax	0.12	R\$/kg CO ₂	[32]
Fuel tank cost ²	411.79	R\$	[33]	Sugarcane yield in Brazil	74369.00	kg/ha	[34]
SOFCEV average efficiency	0.66	-	[15]	Ethanol agro-industrial productivity in Brazil ³	7.26	m ³ /ha	[35]

3 Results and Discussion

In the present study, the LCC assessment aimed to assess the possibility of the SOFCEV cost reduction based on the purchase and sale of carbon credits at a price equivalent to 0.12 R\$/kg of CO₂ emitted. According to Qiao et al. [36], it is estimated that the LCC of the BEV is 9% higher than that observed for the ICEV in 2020 in China, while in the same period, the GHG emissions of the BEV were 29% lower than that observed for an ICEV. This fact confirms the climatic benefits resulting from the advance of electromobility. The main reason for this cost difference is related to the high cost of production of the BEV, leading them to still depend on support policies and subsidies to encourage the increase of their representation in urban fleets.

Fig. 3 and Fig. 4 provide a comparison between the three scenarios considered in the study, which are: a) Cost of investment in equipment, fuel production, and vehicle maintenance and operation in R\$/km, over a 10-year amortization period; b) Cost of CO₂ emissions of the SOFCEV from WTW added to cost (a); c) Cost of carbon fixed by hectares of sugarcane in Brazil necessary to supply the fuel demand of the SOFCEV subtracted from (b). The SOFCEV fed with ethanol (Fig. 3) presented the lowest LCC in Scenario C, having benefited from the sale of carbon credits, consider-

¹ A vehicle life cycle of 150,000 km in 10 years of circulation was considered, without considering the cost of changing to a new cell after that period.

² For conversion purposes, the average price of the euro in 2020 until August was adopted as 5.42 R\$/€ [43].

³ Average agro-industrial productivity between first and second generation Brazilian ethanol was considered [35].

ing the avoided cost during fuel production from carbon fixation by plantations of sugarcane. Therefore, the greater the agro-industrial ethanol productivity, the greater the benefits of carbon pricing under the vehicle LCC, since the use of agricultural waste to produce second-generation ethanol increases the volume of ethanol produced per hectare of sugarcane. Gasoline C (Fig. 4) showed similar results in Scenarios A and C. Therefore, it can be said that the use of fossil fuels, even with the addition of biofuels, does not significantly benefit from the acquisition and sale of carbon credits. In addition, the carbon fixed by plantations equivalent to the 27% of sugarcane ethanol in gasoline C was responsible for making its LCC stable in Scenario C.

According to results obtained by Qiao et al. [36], the ICEV presented a LCC of 36,723.00 USD in 2020 under driving cycle in Beijing, and the BEV presented a LCC of 39,935.00 USD under the same conditions. When carrying out the necessary conversions, the ICEV and the BEV present a LCC of around 1.23 R\$/km and 1.34 R\$/km, respectively. Under a 10-year amortization period, the SOFCEV presented an average LCC of 2.22 R\$/km in Scenario C, which demonstrates a persistent lack of competitiveness compared to the vehicles analyzed by Qiao et al. [36]. The high LCC of the SOFCEV is strongly related to the high cost of its components, especially the SOFC and the lithium-ion battery, so that the acquisition and sale of carbon credits is not sufficient to overcome this economic barrier.

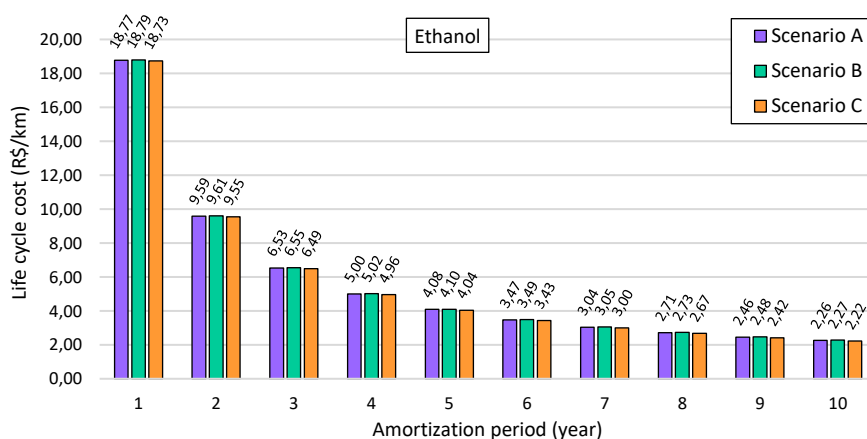


Fig. 3. Life cycle cost of the SOFCEV fuelled with Brazilian ethanol.

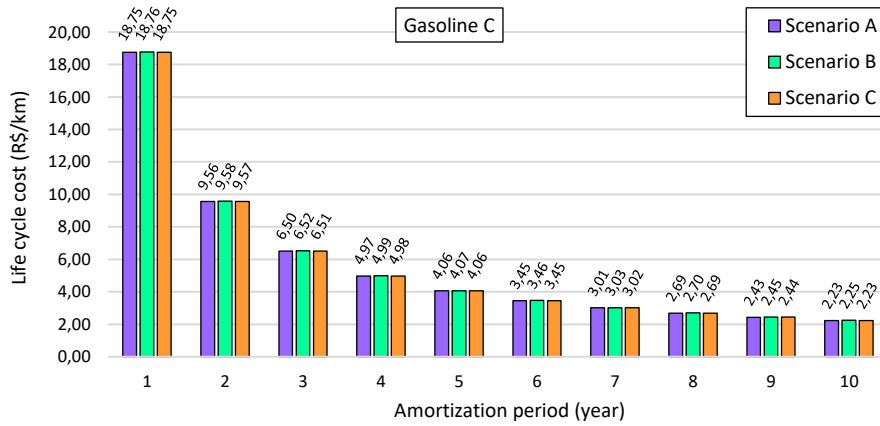


Fig. 4. Life cycle cost of the SOFCEV fuelled with Brazilian gasoline C.

Fig. 5 shows a comparison between the fuel production cost, the emissions cost and the avoided cost from carbon fixation in R\$/vehicle. It is possible to affirm that the SOFCEV fed with ethanol reaches neutrality in the carbon cycle, since the avoided cost from the fixed CO₂ emissions is 3.6 times higher than the cost of WTW emissions. The SOFCEV fed with gasoline C presented an emissions cost 1.4 times greater than the cost avoided by carbon fixation by sugarcane plantations. In 2019, the average production price of Brazilian ethanol was about 1.2 times higher than that observed for gasoline C in the country [28,29]. With the high avoided cost for ethanol (Fig. 5), the fuel becomes more competitive than gasoline C in a scenario of commercialization of carbon credits, having an ethanol production cost of around 3,011.79 R\$/vehicle over its entire life cycle. This new cost of ethanol production is 1.7 times lower than that observed for gasoline C.

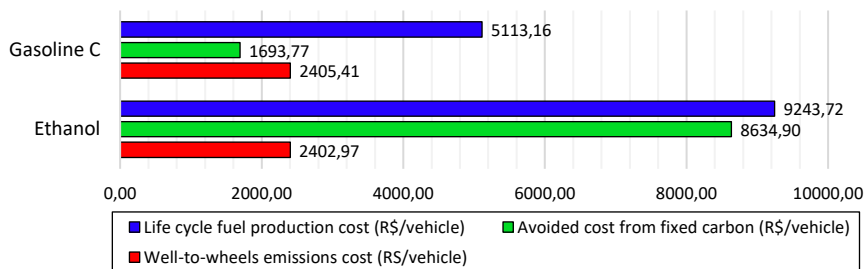


Fig. 5. Comparison between the SOFCEV life cycle production cost, emissions cost, and avoided cost from carbon fixation in R\$/vehicle.

Regarding TTW emissions, the SOFCEV with an average efficiency of 66% fed with ethanol and gasoline C was 48.75 g CO₂/km and 48.34 g CO₂/km, respectively. Such values are similar because the LHV of gasoline C is about 1.5 times greater than that observed for ethanol, causing the flow of gasoline C in the SOFCEV to be lower.

Thus, the exhaust emission presented by ethanol is comparable to that of gasoline C, even though the latter is a fuel of predominantly fossil origin. For the Brazilian context, according to Souza et al. [4], the ICEV on Brazilian urban roads presents TTW emissions around 191 g CO₂ eq./km and 162 g CO₂ eq./km when fed with regular gasoline and E25 gasoline (75% gasoline and 25% anhydrous ethanol), respectively [4]. For ICEV with more developed fuel economy, emissions are around 134 g CO₂ eq./km when fuelled with gasoline [5].

Within the electric vehicle category, the Hybrid Electric Vehicle (HEV) and the Plug-in Electric Hybrid Vehicle (PHEV) are the main models with exhaust emissions. Both HEV and PHEV have, at the same time, one electric engine and one engine powered by internal combustion. However, HEV uses a regenerative braking system to supply the electricity to the electric engine, whereas PHEV has the possibility to supply the electricity demand through external sources [37]. The light-duty HEV emits around 84 g CO₂ eq./km, while more modern models of light-duty PHEV have emissions in the order of 26 g CO₂ eq./km [5]. Therefore, TTW emissions from the SOFCEV exceed those from PHEV, but show a good result compared to TTW emissions from ICEV and HEV.

An analysis of WTW emissions is more extensive, also considering the steps that precede the supply and circulation of the vehicle. The ICEV under Brazilian conditions has WTW emissions in the order of 291 g CO₂ eq./km for E25 gasoline and 97 g CO₂ eq./km for hydrated ethanol (addition of 5% water) [4]. In the production stage of the ICEV, approximately 50% less emissions are generated than in the production of alternative vehicles (e.g., BEV). However, this situation tends to change with the optimization of processes and the wide insertion of these new technologies in the market [5]. Choi et al. [38] reported that, for the South Korean electric matrix based on coal and with 4% renewable sources, the average WTW emissions for the BEV are 109 g CO₂ eq./km. Meanwhile, for the Brazilian scenario, the BEV has emissions of around 18 g CO₂ eq./km [39]. According to the Brazilian Energy Balance of 2018, 83.2% of all national electricity produced came from renewable sources [40]. Therefore, what justifies such low WTW emissions for BEV in circulation in Brazil is the mostly renewable national electricity matrix with a reduced carbon footprint.

WTW emissions from HFCEV can be high depending on how hydrogen is obtained. In a WTW analysis, Yoo et al. [41] reported that, for the South Korean scenario, HFCEV emissions range from 50 to 388 g CO₂ eq./km, where hydrogen production from landfill gas generated the lowest emissions, while production by electrolysis generated the largest emissions due to the high emission factor of the national electric matrix. Nevertheless, in a scenario of high demand for hydrogen, the use of HFCEV becomes less favorable than the use of BEV, since the energy consumption of BEV in its life cycle will be lower, leaving more energy available for stationary uses [42]. Solutions such as the SOFCEV, with the insertion of fuel processor or the use of residual heat for internal reforming, could favor the dissemination of vehicles with fuel cell.

4 Conclusion and Further Work

An analysis of the SOFCEV LCC fuelled with Brazilian fuels was presented together with the estimate of the vehicle TTW and WTW emissions under national conditions, considering the Brazilian sugarcane ethanol pathway. Scenarios B and C, in which carbon taxation was applied, showed a small cost difference, but indicate a better performance of biofuels compared to fossil fuels, considering the avoided cost due to carbon fixation during the cultivation of sugarcane for ethanol production. Regarding exhaust emissions, the SOFCEV with Brazilian fuels showed better results than that observed for ICEV and HEV.

It was possible to state that the SOFCEV fed with sugarcane ethanol reaches neutrality in the carbon cycle, since the avoided cost from the fixed CO₂ emissions is 3.6 times greater than the cost of WTW emissions. The same is not true for the SOFCEV fuelled with gasoline C, where the emissions cost is 1.4 times higher than the cost avoided by carbon fixation by sugarcane plantations. In 2019, the average price of ethanol production surpassed that of gasoline C, in a scenario with a tax of 0.12 R\$/kg CO₂ emitted, the high avoided cost in the production of Brazilian ethanol made the fuel become more competitive than gasoline C, with a production cost of around 3,011.79 R\$/vehicle. This new cost of ethanol production is 1.7 times lower than that observed for gasoline C.

Therefore, the study suggests that carbon pricing tends to target consumer demand for less carbon-intensive products and services, considering the better economic performance of the SOFCEV supplied with ethanol from the acquisition and sale of carbon credits. The application of the carbon taxation mechanism presents the potential to favor the use of biofuels. However, under a 10-year amortization period, the sale of carbon credits was not able to generate sufficient advantages to make the SOFCEV competitive compared to vehicles already established in the market, such as BEV and ICEV, given the high cost of powertrain production.

For further work, the analysis is indicated considering the other carbon pricing mechanisms (e.g., carbon cap and carbon cap-and-trade), since carbon policies are still under development on a global scale [9], and, therefore, there is no consolidated database. In addition, the energy, economic and environmental analysis of the SOFCEV operating with other biofuels is also indicated.

Acknowledgment

The authors be very grateful to the financial support provided by the Institutional Program of Scientific Initiation Scholarships (PIBIC) from Federal Centre of Technological Education Rio de Janeiro – CEFET/RJ and the Iberoamerican Program of Science and Technology for Development (CYTED) with the project Smart Cities Totally Comprehensive, Efficient and Sustainable (CITIES). CODE: 518RT0557.

References

- [1] G. T. Farmer and J. Cook, *Climate Change Science: A Modern Synthesis - Vol.1*. Springer, 2012.
- [2] International Renewable Energy Agency (IRENA), *Global Renewables Outlook: Energy transformation 2050*. 2020.
- [3] C. A. Melo, G. de M. Jannuzzi, and P. H. de M. Santana, “Why should Brazil to implement mandatory fuel economy standards for the light vehicle fleet?,” *Renew. Sustain. Energy Rev.*, vol. 81, pp. 1166–1174, 2018.
- [4] L. L. P. Souza, E. E. S. Lora, J. C. E. Palacio, M. H. Rocha, M. L. G. Renó, and O. J. Venturini, “Comparative environmental life cycle assessment of conventional vehicles with different fuel options, plug-in hybrid and electric vehicles for a sustainable transportation system in Brazil,” *J. Clean. Prod.*, vol. 203, pp. 444–468, 2018.
- [5] D. C. Rosenfeld, J. Lindorfer, and K. Fazeni-Fraisl, “Comparison of advanced fuels—Which technology can win from the life cycle perspective?,” *J. Clean. Prod.*, vol. 238, p. 117879, 2019.
- [6] System Gas Emissions Estimation (SEEG), *Análise das Emissões Brasileiras de Gases de Efeito Estufa*. 2019.
- [7] International Energy Agency (IEA), *Global EV Outlook 2019: Scaling-up the transition to electric mobility*. 2019.
- [8] V. de Guimarães and Almeida, “Localização-alocação de centros de integração logística considerando critérios econômicos e ambientais,” UFRJ, Rio de Janeiro, Brazil, 2019.
- [9] World Bank, “Carbon Pricing Dashboard,” *What is Carbon Pricing?* [Online]. Available: <https://carbonpricingdashboard.worldbank.org/what-carbon-pricing>. [Accessed: 20-Jun-2020].
- [10] Brazilian Business Council for Sustainable Development (CEBDS), *Precificação de carbono: o que o setor empresarial precisa saber para se posicionar*. 2016.
- [11] Partnership for Market Readiness (PRM), “Implementing Country Participants: Brazil,” 2020. [Online]. Available: <https://www.thepmr.org/country/brazil-0>. [Accessed: 17-Aug-2020].
- [12] Brazilian Agency of Petrol Natural Gas and Biofuels (ANP), “RenovaBio,” 2020. [Online]. Available: <http://www.anp.gov.br/producao-de-biocombustiveis/renovabio>. [Accessed: 17-Aug-2020].
- [13] International Council on Clean Transportation (ICCT), “Opportunities and risks for continued biofuel expansion in Brazil,” 2019. [Online]. Available: <https://theicct.org/publications/biofuel-expansion-Brazil-portuguese>. [Accessed: 17-Aug-2020].
- [14] J. Wang, “Barriers of scaling-up fuel cells: Cost, durability and reliability,” *Energy*, vol. 80, pp. 509–521, 2015.
- [15] E. Facchinetti, D. Favrat, and F. Marechal, “Innovative hybrid cycle solid oxide fuel cell-inverted gas turbine with CO₂ separation,” *Fuel Cells*, vol. 11, no. 4, pp. 565–572, 2011.
- [16] T. Choudhary and Sanjay, “Thermodynamic assessment of SOFC-ICGT hybrid cycle: Energy analysis and entropy generation minimization,” *Energy*,

- vol. 134, pp. 1013–1028, 2017.
- [17] G. Lorenzo and P. Fragiacomio, “Energy analysis of an SOFC system fed by syngas,” *Energy Convers. Manag.*, vol. 93, pp. 175–186, 2015.
- [18] Z. Dimitrova and F. Maréchal, “Environomic design for electric vehicles with an integrated solid oxide fuel cell (SOFC) unit as a range extender,” *Renew. Energy*, vol. 112, pp. 124–142, Nov. 2017.
- [19] L. B. Braga, “Análise econômica do uso de célula a combustível para acondicionamento de ônibus urbano,” Universidade Estadual Paulista, Guaratinguetá, São Paulo, Brasil, 2010.
- [20] R. A. M. Boloy, M. E. Silva, A. E. Valle, J. L. Silveira, and C. E. Tuna, “Thermoeconomic analysis of hydrogen incorporation in a biodiesel plant,” *Appl. Therm. Eng.*, vol. 113, pp. 519–528, 2017.
- [21] R. A. M. Boloy, J. L. Silveira, C. E. Tuna, C. R. Coronado, and J. S. Antunes, “Ecological impacts from syngas burning in internal combustion engine: Technical and economic aspects,” *Renew. Sustain. Energy Rev.*, vol. 15, no. 9, pp. 5194–5201, 2011.
- [22] Brazil, “Federal Law no. 9,503, September 23, 1997. Disposes about the Brazilian Traffic Code,” 1997. [Online]. Available: http://www.planalto.gov.br/ccivil_03/leis/19503.htm. [Accessed: 12-Jun-2020].
- [23] R. P. Micena, “Estação de produção e abastecimento de hidrogênio solar: Análise técnica e econômica,” Universidade Estadual Paulista, Guaratinguetá, São Paulo, Brasil, 2020.
- [24] M. L. N. M. Carneiro and M. S. P. Gomes, “Energy-ecologic efficiency of waste-to-energy plants,” *Energy Convers. Manag.*, vol. 195, no. May, pp. 1359–1370, 2019.
- [25] J. C. C. Garcia and E. Von Sperling, “Greenhouse gas emissions from sugar cane ethanol: Estimate considering current different production scenarios in Minas Gerais, Brazil,” *Renew. Sustain. Energy Rev.*, vol. 72, pp. 1033–1049, 2017.
- [26] T. Neamhom, C. Polprasert, and A. J. Englande, “Ways that sugarcane industry can help reduce carbon emissions in Thailand,” *J. Clean. Prod.*, vol. 131, pp. 561–571, 2016.
- [27] United States Environmental Protection Agency (EPA), “Greenhouse Gases Equivalencies Calculator - Calculations and References,” 2020. [Online]. Available: <https://www.epa.gov/energy/greenhouse-gases-equivalencies-calculator-calculations-and-references>. [Accessed: 19-Aug-2020].
- [28] Nissan Motor Corporation, “Nissan announces development of the world’s first SOFC-powered vehicle system that runs on bio-ethanol electric power,” 2016. [Online]. Available: <https://global.nissannews.com/en/releases/>. [Accessed: 10-Jun-2020].
- [29] Brazilian Agency of Petrol Natural Gas and Biofuels (ANP), “RenovaCalc,” 2020. [Online]. Available: <http://www.anp.gov.br/producao-de-biocombustiveis/renovabio/renovacalc>. [Accessed: 10-Jun-2020].
- [30] Center for Advanced Studies in Applied Economics (CEPEA), “Etanol,” 2019. [Online]. Available: <https://www.cepea.esalq.usp.br/br/indicador/etanol.aspx>. [Accessed: 21-Aug-

- 2020].
- [31] Brazilian Agency of Petrol Natural Gas and Biofuels (ANP), *Anuário estatístico brasileiro*. 2019.
 - [32] Fusion Media Limited, “Future carbon credits - Dec, 2020,” 2020. [Online]. Available: <https://br.investing.com/commodities/carbon-emissions>. [Accessed: 21-Aug-2020].
 - [33] S. Bubeck, J. Tomaschek, and U. Fahl, “Perspectives of electric mobility: Total cost of ownership of electric vehicles in Germany,” *Transp. Policy*, vol. 50, no. 2016, pp. 63–77, 2016.
 - [34] Food and Agriculture Organization (FAO), “Food and Agriculture Data,” *FAOSTAT*, 2018. [Online]. Available: <http://www.fao.org/faostat/en/#data>. [Accessed: 21-Aug-2020].
 - [35] C. for S. S. and M. CGEE, *Second Generation Sugarcane Bioenergy & Biochemicals: Advanced Low-Carbon Fuels for Transport and Industry*. 2016.
 - [36] Q. Qiao *et al.*, “Life cycle cost and GHG emission benefits of electric vehicles in China,” *Transp. Res. Part D Transp. Environ.*, vol. 86, p. 102418, 2020.
 - [37] D. R. de Moraes, R. A. M. Boloy, and G. M. R. Vieira, “Electromobility: A Review on Electric Vehicle Technologies and Potentialities for the Brazilian Scenario,” in *II Ibero-american Congress of Smart Cities*, 2019, pp. 658–669.
 - [38] W. Choi, E. Yoo, E. Seol, M. Kim, and H. H. Song, “Greenhouse gas emissions of conventional and alternative vehicles: Predictions based on energy policy analysis in South Korea,” *Appl. Energy*, vol. 265, no. September 2019, p. 114754, 2020.
 - [39] A. C. R. Teixeira and J. R. Sodr e, “Impacts of replacement of engine powered vehicles by electric vehicles on energy consumption and CO2 emissions,” *Transp. Res. Part D Transp. Environ.*, vol. 59, no. February, pp. 375–384, 2018.
 - [40] Brazilian Energy Research Company (EPE), “Balanço Energético Nacional 2019 – Relatório Final,” 2019. [Online]. Available: <http://www.epe.gov.br/pt/publicacoes-dados-abertos/publicacoes/balanco-energetico-nacional-2019>.
 - [41] E. Yoo, M. Kim, and H. H. Song, “Well-to-wheel analysis of hydrogen fuel-cell electric vehicle in Korea,” *Int. J. Hydrogen Energy*, vol. 43, no. 41, pp. 19267–19278, 2018.
 - [42] M. F. Felgenhauer, M. A. Pellow, S. M. Benson, and T. Hamacher, “Economic and Environmental Prospects of Battery and Fuel Cell Vehicles for the Energy Transition in German Communities,” *Energy Procedia*, vol. 99, pp. 380–391, 2016.
 - [43] Brazilian Institute of Applied Economic Research (IPEA), “Data base,” 2020. [Online]. Available: <http://www.ipeadata.gov.br/>. [Accessed: 29-Aug-2020].

Battery Energy Storage System Dimensioning for Reducing the Fixed Term of the Electricity Access Rate in Industrial Consumptions

Jorge Nájera¹[0000-0002-3396-0062], Marcos Blanco¹[0000-0003-3641-1867], Gustavo Navarro¹[0000-0002-5169-9080] and Miguel Santos¹[0000-0002-5338-6336]

¹ CIEMAT, Government of Spain, 28040 Madrid, Spain
jorge.najera@ciemat.es

Abstract. Industrial buildings account for very few high peak of power demand that forces them to contract a high fixed electricity term to cover their demand. A more intelligent use of the energy in industrial buildings, together with an improved efficiency of the transmission and distribution of the energy along the electric power grid can be achieved by reducing the peak consumption of industrial buildings. Energy storage systems are one of the most promising devices for reducing this peak consumption. However, selecting the proper battery requires a dimensioning process in terms of energy and power which is not straightforward. This paper proposes a dimensioning methodology that takes into consideration both technical and economic terms, and applies it to a case example with real industrial consumption data, and a commercial battery. Results show that introducing batteries for reducing this peak consumption can lead to a cost-benefit improvement.

Keywords: Battery Energy Storage System, Industrial Consumption, Electricity Fixed Term.

1 Introduction

Electricity access rates, i.e. the fee that electricity consumers have to pay for the reliable and safe energy they use, is divided in two main terms in most European countries: the variable and the fixed term of the bill [1]. The variable term corresponds to the energy (kWh) consumed by the user, and the fixed term with the contracted power (kW), i.e. the maximum power available for consumption so the power-limit switch remains untriggered.

This fixed term is commonly over dimensioned, i.e. the usual consumption of a specific infrastructure may not be close to that power consumption limit, which is only reached at few specific moments along the day. This is specially relevant for industrial consumptions, which account for few high peak of power demand that forces them to contract a high fixed electricity term [2].

In order to enhance an intelligent use of the energy in industrial buildings, improve the efficiency of the transmission and distribution of the energy along the electric power

grid, and foster the “prosumer” behavior among industrial consumers, this situation where an industrial consumer has to pay a high electricity access fee due to a few moments of high-power demand must change. Different solutions have been proposed in the literature for achieving this goal. Introducing photovoltaic panels is presented as a promising solution in [3] and [4]. Nevertheless, the vast majority of studies that attempt to solve the aforementioned problem, include energy storage devices, as in [5], [6], or [7], among other studies.

Considering the energy storage devices found in a commercial level, battery energy storage systems (BESSs) for being connected in buildings and infrastructures, both industrial and residential, is one of the most prominent and leading uses [8]. Its benefits encompass the majority of the electricity value chain, including peak shaving and continuity of supply for residential and industrial customers, ancillary and power quality services for transmission and distribution system operators (TSOs & DSOs), and flexibility and curtailment minimization for renewable generation companies [9].

However, choosing a battery for being connected to an industrial consumption for diminishing the peak consumption is not a straightforward issue. Battery manufacturers offer a wide variety of solutions, and selecting an appropriate battery requires a dimensioning process that takes into account BESS energy, power, and cost.

In the literature, BESS dimensioning for reducing the electricity access fee in industrial buildings have been studied together with photovoltaic systems by using brute force calculations [10]. Moreover, a study considering incentives and selling prices conditions is published in [11], concluding that it could be economically viable to install BESS in industrial buildings without subsidies. At last, a stochastic model is applied in [12] for finding the optimal BESS investment for buildings, concluding that the stochastic model allows for a better decision making.

This work proposes a battery dimensioning methodology that focuses on reducing the fixed term of the electricity access rate in industrial consumptions. Moreover, this paper considers both technical and economic aspects for selecting the final solution, by means of a cost benefit analysis of the available technical BESS, and a detailed BESS ageing estimation. Hence, this approach is relevant for industrial consumers with an irregular consumption that includes several peaks of consumption, as well for BESS manufacturers aiming for specific developments for industrial consumptions. This methodology is applied for a case example for an existing industrial consumption, with a commercial battery, considering standard prices for the economic analysis.

The paper is organized as follows: Section 2 describes the BESS dimensioning methodology, including a description of the steps to be followed. Section 3 details the simulation models used during the methodology, including a grid model, and industrial consumption model, a power converter model, and a battery model. At last, section 4 includes a case example following the developed methodology, and conclusions are given in Section 5.

2 BESS dimensioning methodology

The BESS dimensioning methodology described in this section aims at reducing the fixed term of the electricity access rate by introducing a BESS that deals with the peaks of the industrial consumption. A few assumptions are taken by the authors for developing the BESS dimensioning methodology.

Firstly, both BESS (P_{BESS}) and the electrical grid (P_{GRID}) must cover the customers demand (P_{LOAD}) and the losses (P_{LOSS}):

$$P_{BESS} + P_{GRID} = P_{LOAD} + P_{LOSS} \quad (1)$$

Moreover, BESS must account for enough energy to cover the energy that is not delivered by the grid. Besides, BESS that are not able to fully recharge during low peak periods the energy they deliver during high peak periods, are not considered for the dimensioning process.

The methodology comprises a set of steps, as seen in the flow chart of Fig. 1.

Step 1. Parametrize models.

The first step consists of parametrizing the simulation models. These models must be parametrized based on the particular case under study. Parametrizing the models include calculating proper values for a grid, a BESS, and an industrial consumption.

Step 2. Define test cases.

The variable that define the test cases is the maximum fixed power that the grid can deliver (P_{LIMIT}). Reducing this power limit implies adding a greater contribution from the BESS, which yields to the different scenarios, which consequently will result in different BESS configurations and different BESS ageing.

Step 3. Simulate test case, calculate BESS requirements, and BESS configuration.

Once the scenarios have been defined, a simulation is performed for every value of P_{LIMIT} . Each scenario implies different necessities from the BESS, regarding power and energy. This requirements give different BESS configurations, in terms of number of cells in series and number of cells in parallel. The charge/discharge profile for the BESS is also obtained from the simulation.

Step 4. Calculate BESS ageing.

Once the minimum BESS configuration to satisfy the power and energy requirements is selected for each scenario, a BESS ageing analysis is performed, based on the BESS model, BESS configuration, and on the charge/discharge profile for each specific scenario. As a result of this step, the number of days until the BESS loses a 20% of capacity retention is obtained.

Step 5. Cost benefit analysis.

Prices and fees for both a BESS (as a function of the kW and kWh of the system) and the fixed access power are needed for introducing them in a cost function. BESS standard prices as well as Spanish fixed access rates are provided in Section 4, with a

case example. The cost can be computed yearly. The base scenario, i.e., when there is no BESS is then compared to the rest of scenarios in terms of cost, and the final solution can be obtained.

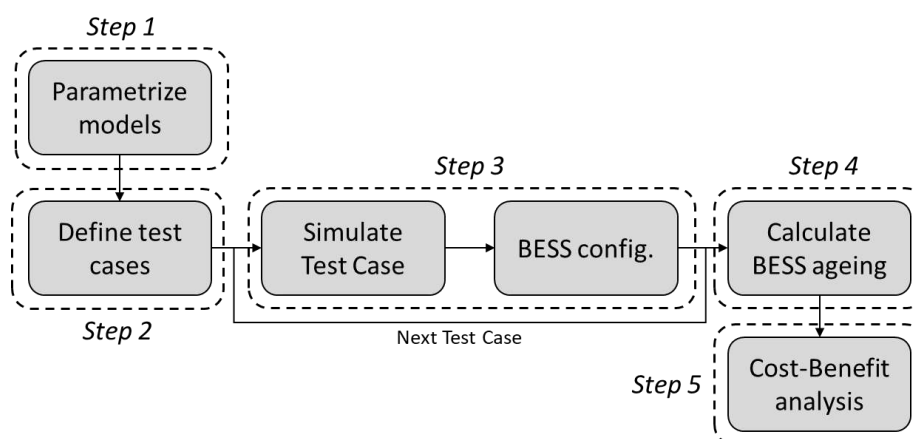


Fig. 1. Flow chart of the methodology.

3 Industrial consumption, BESS, and grid modelling

The mathematical and simulation models used in section 4 for performing a case example of the aforementioned methodology, are described along this section. Three main models are considered: an industrial consumption, a BESS, and a power grid. The BESS is connected to the same point as the industrial consumption, the point of common coupling (PCC), and both connected to the grid, as it can be seen in the general model diagram in Fig. 2. The complete model outputs several electrical variables time-series (P, Q, V, and I) for the three main components. Other electrical variables such as frequency or harmonic distortion are evaluated and calculated by the model, but the authors decided not to output them since they are not relevant for the purpose of this paper.

The models are developed with MATLAB Simulink, within the Simscape Electrical environment. When developing simulation models, a higher complexity and completeness usually implies a higher accuracy [13, 14]. However, complex models tend to require a substantial computational effort to run them, and a huge amount of information to parametrize them. Moreover, they are commonly valid for a specific device, making them non-generalizable [15, 16].

On the other hand, simplified models, usually composed by combination of resistors, inductors, and capacitors, are easily parametrized, they require low computational effort, and are valid for several devices with similar characteristics. Furthermore, even though they are not as accurate as complex models, they can mimic the behavior of the device with sufficient precision, so general conclusions can be drawn [17-19].

Hence, given the objective of this paper, the approach taken by the authors was to develop simplified models, that are generalizable and easily parametrized, which is sufficient for obtaining accurate general conclusions when dimensioning BESS.

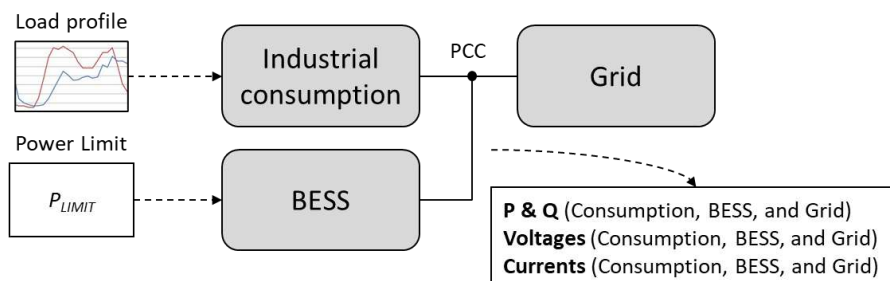


Fig. 2. General model diagram.

3.1 Industrial consumption model

The industrial consumption is modelled as a PQ load, i.e. it consumes the desired active and reactive power independently of the voltage at the PCC. Hence, it needs to be modelled as a controlled current source, as depicted in Fig. 3. The inputs of the model, named as P and Q in Fig. 3, correspond to the 24h active and reactive power profile on 1 second basis.

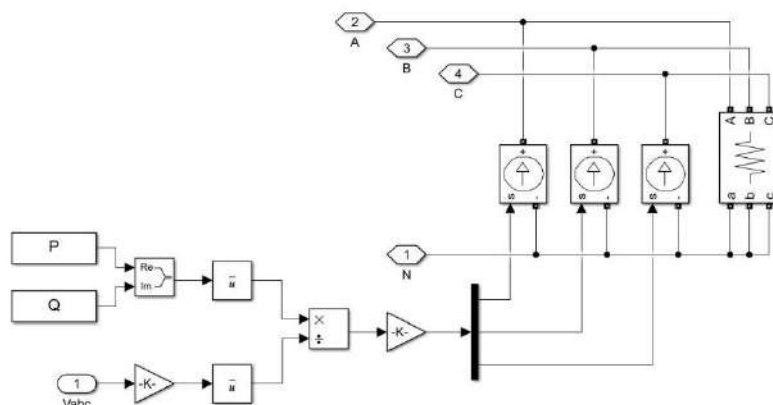


Fig. 3. Industrial consumption model in MATLAB Simulink.

3.2 BESS model

The BESS model includes both a battery model and a power electronic converter model, being the latter necessary to manage the battery behavior and to connect the battery to the AC grid.

Electronic converter model. For the purpose of this work there is no need to model the power electronic converter in detail, since neither efficiency nor power converter ageing are taken into consideration for the economic evaluation of the methodology. Thus, an ideal voltage source converter (VSC) has been selected, with no conduction or switching losses, and no power limitations, so the battery can dispatch as much power as required. As a result, the VSC is modelled as a controlled three-phase voltage source whose reference voltage is given by the converter control, which manages the power that flows in and out of the battery.

The control of a VSC can be modelled as explained in [20], consisting in two levels: a high-level control and a low-level control. The high-level control is in charge of selecting, based on a specific strategy, the power dispatched or consumed by the battery. Several strategies have been proposed in the literature, from those based on rules [21] to more complex strategies [22, 23]. For this paper, a simple strategy based on rules have been selected, which sets the reference power for the battery (P_{BATT}) based on the maximum power that the industrial consumption can absorb from the grid (P_{LIMIT}), the actual power that the industrial load is demanding (P_{LOAD}), and the battery state of charge (SoC_{BATT}). The flow diagram for the high-level control is shown in Fig. 4.

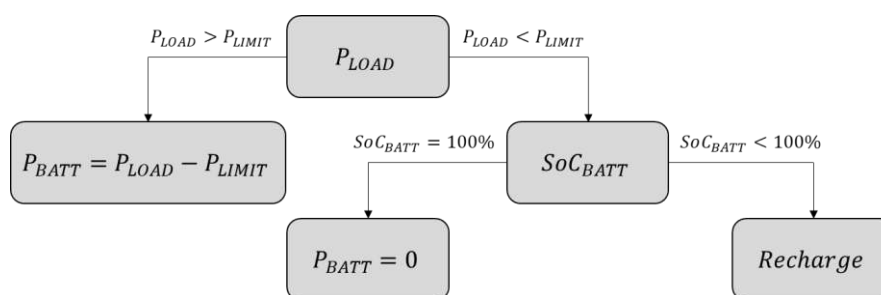


Fig. 4. Flow diagram for the VSC high-level control

BESS recharge profile has been defined as the minimum current that allows the BESS to recharge the same amount of energy as it has provided to the load along the day. Moreover, reactive power reference for the battery has been set to zero, so no contribution is expected from it.

On the other hand, the low-level control is in charge of setting the voltage at the VSC terminals so the power management commanded by the high-level control can be performed. The low-level control is a dq axis control, shown in Fig. 5, which has been developed based on [24]. The control is duplicated for P and Q, with minor variations. Each branch accounts for an outer PI loop control, which sets the battery power equal to the reference power coming from the high-level control, outputting a reference current. Then, there is an inner PI loop control that adjusts the current flowing through the VSC with the reference current, so a reference voltage is outputted. This voltage is finally regulated so it corresponds to the VSC voltage at its terminals. In order to properly control the VSC, the inner control must be considerably faster than the outer control. Detailed explanation about the implemented dq axis control for a VSC can be found in [20] and [24].

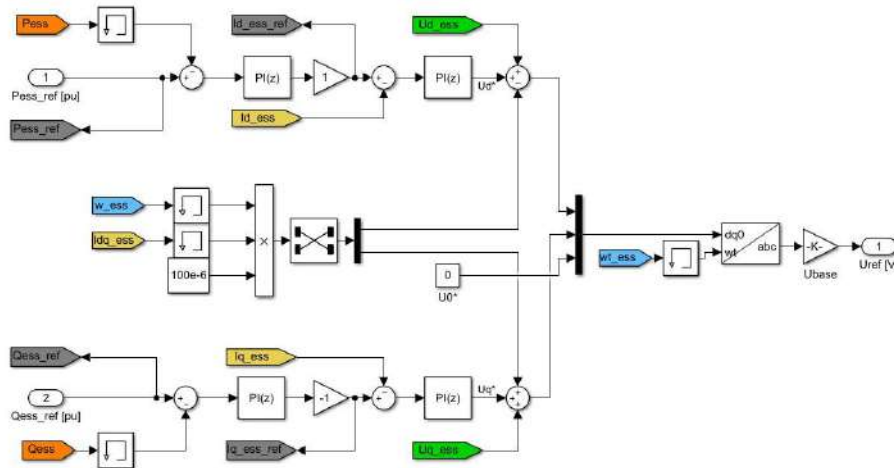


Fig. 5. VSC low-level control model in MATLAB Simulink.

Battery model. The battery model controlled by the VSC is represented as an equivalent circuit model which, as aforementioned, sacrifices accuracy in favor of generality. Nevertheless, equivalent circuit models account for errors lower than 5% [25], sufficient for obtaining general conclusions. The battery equivalent circuit is depicted in Fig. 6, where u is the instantaneous voltage of the battery [V], i is the battery current [A] ($i > 0$ discharging; $i < 0$ charging), I_{SELF} is the self-discharge current, R_{OHM} is the ohmic internal resistance [Ω], R_{POL} is the polarization internal resistance [Ω], and C_{POL} is the polarization capacitor [F].

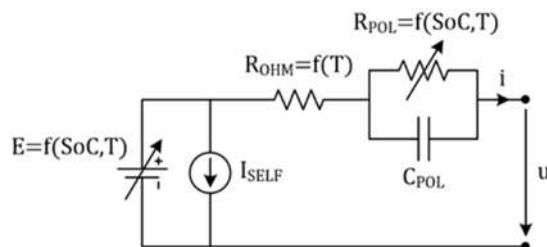


Fig. 6. Battery equivalent circuit model [R].

The selected battery model has been developed and validated by the authors in [14] and [26]. The model comprises three parts: a voltage/runtime model, a thermal model, and an ageing model.

Voltage/runtime and thermal model. The lithium-ion battery model used in this paper is a modification of the MATLAB Simulink model [27]. The battery equivalent circuit is based on the Shepherd equation [28], which was experimentally validated later in [29]. The Shepherd model keeps the error between 1% and 5% and it can be

parametrizable without testing the battery in laboratory; it suffices with the manufacturer datasheet information. The voltage/runtime equations that govern the model, considering thermal dependencies, can be written as follows:

$$E(SoC, T) = E_0(T) - K(T) \cdot Q_{MAX}(T) \cdot \left(\frac{100}{SoC} - 1\right) + A \cdot e^{-B \cdot Q_{MAX}(T) \cdot \left(1 - \frac{SoC}{100}\right)} \quad (2)$$

$$R_{POL-DISCHARGE}(SoC, T) = K(T) \cdot \frac{100}{SoC} \quad (3)$$

$$R_{POL-CHARGE}(SoC, T) = K(T) \cdot \frac{1}{1.1 - \frac{SoC}{100}} \quad (4)$$

$$E_0(T) = E_0(T_0) + \frac{dE}{dT} \cdot (T - T_0) \quad (5)$$

$$Q_{MAX}(T) = Q_{MAX}(T_0) + \frac{dQ}{dT} \cdot (T - T_0) \quad (6)$$

$$K(T) = K(T_0) \cdot e^{\alpha \left(\frac{1}{T} - \frac{1}{T_0}\right)} \quad (7)$$

$$R_{OHM}(T) = R_{OHM}(T_0) \cdot e^{\beta \left(\frac{1}{T} - \frac{1}{T_0}\right)} \quad (8)$$

where E is the open-circuit nonlinear voltage [V], E_0 is the open-circuit constant voltage [V], K is the polarization parameter [Ah⁻¹], Q_{MAX} is the maximum capacity [Ah], A is the exponential voltage constant [V], B is the exponential capacity constant [Ah⁻¹], T is the temperature [K], T_0 is the parameters reference temperature [K], and SoC is the state of charge [%].

The thermal model comprises two different parts: a heat generation model, and a heat evacuation model. The heat generation model can be expressed as follows [30]:

$$H = (E_0 - E) \cdot i + T \cdot \frac{dE}{dT} \cdot i + (R_{OHM} + R_{POL}) \cdot i^2 \quad (9)$$

where H is the generated heat [W], and $\frac{dE}{dT}$ the change of the equilibrium potential with temperature [V·K⁻¹].

The heat evacuation model occurs due to convection and radiation mechanisms, being the latter negligible [31]. Assuming that the temperature is uniform in the battery (reasonable approximation according to [35]), the following expression is obtained [31]:

$$H \approx m \cdot c_p \cdot \frac{dT}{dt} + \frac{1}{R_{OUT}} \cdot (T - T_0) \rightarrow R_{OUT} = \frac{1}{h \cdot Ar} \quad (10)$$

where m is the mass of the battery [kg], c_p is the specific heat capacity [J·kg⁻¹·K⁻¹], h is the convective heat transfer coefficient [W·m⁻²·K⁻¹], Ar is the external surface area [m²], and R_{OUT} is the equivalent thermal resistance with the ambient [K·W⁻¹].

Hence, the temperature variation can be calculated as:

$$T(s) = \frac{H \cdot R_{OUT} + T_0}{1 + m \cdot c_p \cdot R_{OUT} \cdot s} = \frac{H \cdot R_{OUT} + T_0}{1 + t_{th} \cdot s} \quad (11)$$

where t_{th} is the thermal time constant [s], and s is the Laplace complex frequency parameter.

Ageing model. The ageing estimator implemented in the battery model comprises two parts: a cycling ageing model, and a calendar ageing model. Cycling ageing is related to the capacity fade when the battery is subjected to charging and discharging cycles, i.e. when the current is flowing through the battery. It depends on several factors, among which C_{rate} , temperature, and DoD are the most relevant [32]. The cycling ageing model published in [33] for lithium-ion batteries has been implemented:

$$Q_{loss} = (a \cdot T^2 + b \cdot T + c) \cdot \exp((d \cdot T + e) \cdot C_{rate}) \cdot Ah \quad (12)$$

where Q_{loss} is the cycling loss capacity [Ah], Ah the Ah that have flown through the battery (in or out), and $a, b, c, d,$ and e are constants depending on the battery chemistry.

On the other hand, calendar ageing is related to the capacity fade in the battery because of the time passed from the moment it was manufactured. It is dependent on the *SoC* of the battery, the temperature, and the time [32]. The calendar ageing model published in [34] has been implemented:

$$Q_{loss} = a \cdot \exp(b \cdot SoC) \cdot \exp(c/T) \cdot t^z \quad (13)$$

where $a, b,$ and c are constant that depend on the battery chemistry, and z can take values between 0.5 and 1 and depend on the chemistry as well.

3.3 Grid model

The grid is modelled as an infinite power grid, so both the frequency and voltage are kept constant at the PCC. A Three-Phase Source model has been selected for this purpose, with a swing generator type, high short-circuit power, and low X/R ratio.

4 Case example

In order to illustrate how the described methodology could be implemented, a case example is provided. The models developed in Section 3 are used for performing the simulations. The same structure of steps defined in Section 2 is applied:

Step 1. Parametrize models.

At first, the simulations models need to be parametrized. For the grid model, the following parameters have been selected, so an almost infinite power grid can be implemented (**Table 1**).

The battery model can be parametrized following the methodology defined in [26] and [29]. A commercial lithium polymer battery cell from Kokam, model SLPB100255255HR2, has been selected for this case study, which is a standard lithium pouch cell [36]. The selected battery cell main parameters are listed in **Table 2**.

Table 1. Grid model parameters.

Parameter	Value
Reference voltage	400 V
Short-circuit ratio	25
X/R ratio	20

Table 2. Battery model parameters [36].

Parameter	Value	Remarks
Reference capacity	55 Ah	@0.2C, 23±3 °C
Energy density	140 Wh/kg	
Impedance	Max. 0.60 mΩ	AC @1kHz
Weight	Max. 1450 g	
Average voltage	3.7 V	
Lower limited voltage	2.7 V	
Upper limited voltage	4.2 V	
Max. current charge	165 A (3C)	@23±3 °C
Max. current discharge	660 A (12C)	@23±3 °C
Charging temperature	5 – 45 °C	
Discharging temperature	-20 – 55 °C	

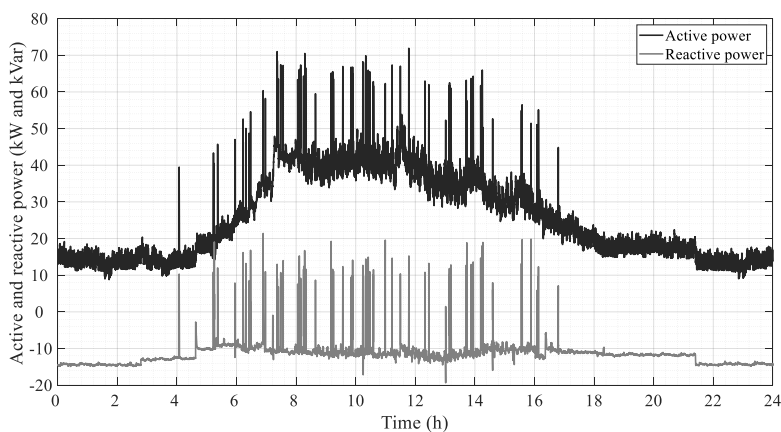


Fig. 7. Industrial consumption profile.

The load needs a power consumption profile as input. For this case example, a 24-hour profile on 1 second basis has been selected, corresponding to a typical day in an industrial building. The selected building is the CEDEX facility in Madrid, located at C/Julián Camarillo 30, 28037. For the analysis performed in this paper, the load

corresponds with a three-phase load with no unbalance between phases, whose active and reactive power profiles are shown in Fig. 7. The accumulative energy consumed by the load is shown in Fig. 8.

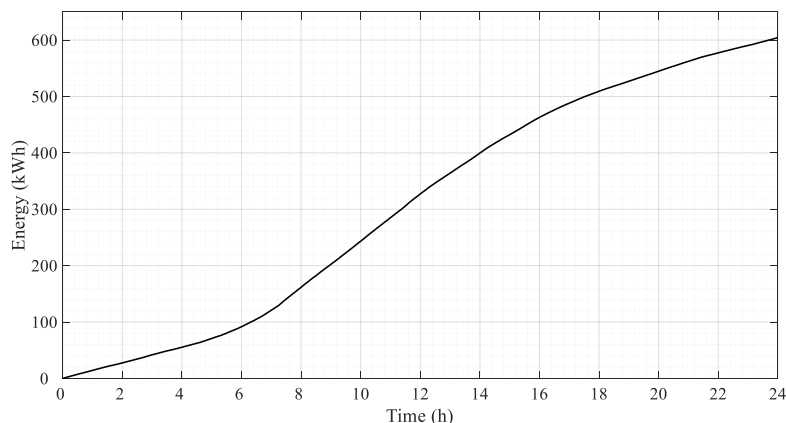


Fig. 8. Accumulative energy consumed by the load.

Step 2. Define test cases.

Test cases are defined by the BESS control parameter, which is the power limit that the load is allowed to consume from the grid (P_{LIMIT}). Hence, as P_{LIMIT} decreases, the battery will increase its contribution. SB corresponds to the base case scenario, which is the actual scenario, with a contracted power of 80 kW. Steps of 10 kW have been selected, so the following scenarios are defined:

Table 3. Scenarios defined for the case example.

Scenario	P_{LIMIT}
SB	80 kW
S6	60 kW
...	...
S2	20 kW
S1	10 kW

Step 3. Simulate scenarios and obtain BESS requirements and configuration.

As aforementioned in Section 2 and Section 3, BESSs that are not able to recharge as much energy as they have delivered along the day, are considered as not valid. Once the simulations are performed, BESS power profiles for the valid configurations are obtained. For the case example presented in this paper, valid BESS power profiles are shown in Fig. 9.

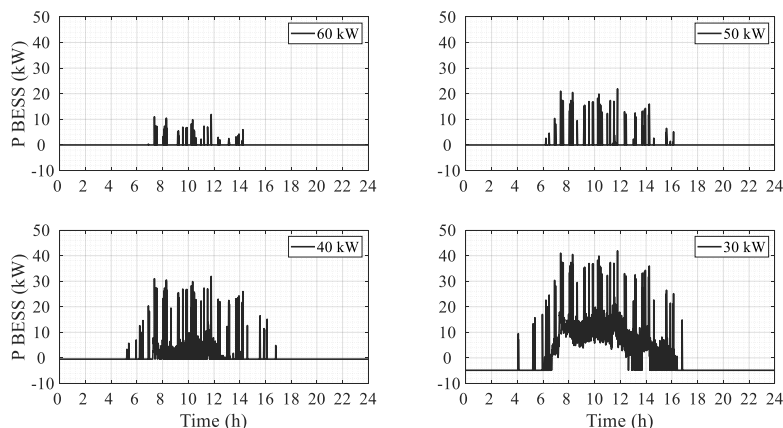


Fig. 9. BESS power profile for different values of P_{LIMIT} .

As expected, the lower the P_{LIMIT} the higher the contribution from the BESS. Since BESS deals with high demand peaks, it follows a similar distribution as the top part of the industrial load profile (Fig. 7). Scenario SN, i.e. when the grid delivers as much power as demanded by the load, implies no contribution from the BESS.

For P_{LIMIT} values below 30 kW, BESSs are not able to recharge the same amount of energy delivered during the high demand period. It must be noticed that P_{LIMIT} also affects the maximum power available for recharging, i.e. for a P_{LIMIT} value of 20 kW, the maximum power available for recharging is 20 kW since that recharging power is coming from the grid, which is not sufficient for the case example presented here.

Based on the BESS power profiles, the power and energy requirements ($P_{BESS-req}$ and $E_{BESS-req}$) for the valid scenarios are shown in **Table 4**.

Once the requirements are calculated, the most suitable BESS configuration must be selected for each scenario (number of cells connected in series and in parallel). Commercial three-phase inverters for 400 V grids demand 48 V in the DC side. Hence, based on the standard cell parameters (**Table 2**), the number of cells in series so the DC side voltage reaches 48 V equals:

$$\frac{48 \text{ V (DC side voltage)}}{3.7 \text{ V (Nominal cell voltage)}} \approx 13 \text{ cells in series} \tag{14}$$

The number of cells in parallel depends on the BESS energy requirements. Given that one branch of 13 cells accounts for:

$$13 \text{ cells} \cdot 3.7 \text{ V} \cdot 55 \text{ Ah} = 2.64 \text{ kWh} \tag{15}$$

the following table can be filled:

Table 4. BESS requirements for the different scenarios.

Scenario	P_{LIMIT}	$P_{BESS-req}$	$E_{BESS-req}$	Min. BESS config.
SN	80 kW	-	-	-
S6	60 kW	11.9 kW	0.08 kWh	13s1p
S5	50 kW	21.9 kW	0.31 kWh	13s1p
S4	40 kW	31.9 kW	10.41 kWh	13s4p
S3	30 kW	41.9 kW	74.51 kWh	13s29p

Scenarios S6 and S5 can satisfy their energy requirements with just one BESS branch in parallel. It must be noticed that, given the BESS configuration and the power demand shown in **Table 4**, the BESS in scenario S5 will be more demanded than in scenario S6, i.e. it will work with higher C rates.

Step 4. Calculate BESS ageing.

BESS ageing is closely related to its C rate and temperature (among other factors), as previously explained in Section 3. The higher the C rate, the higher the temperature augmentation in the battery. Hence, the BESS configuration has a huge influence in the BESS ageing, since batteries with a higher number of cells in parallel work with lower C rates, i.e. with less stress. This implies that “bigger” BESSs may last longer than “smaller” BESSs, which may be beneficial from a cost-benefit point of view.

Four configurations have been tested for each battery: the minimum number of cells so the energy requirements are satisfied, and three more configurations increasing one extra branch each time, so the C rate is decreased.

Commonly, a BESS is considered aged when it loses a 20% of capacity retention.

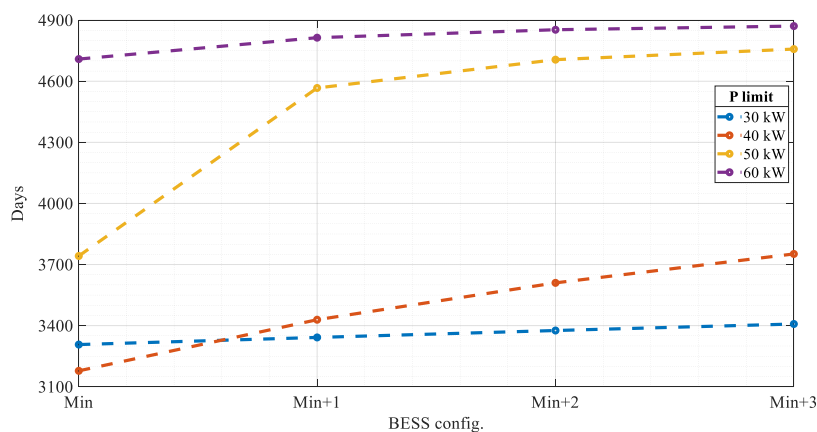


Fig. 10. Days until $\nabla Q = 20\%$ as a function of the BESS configuration.

Scenario S5 (50 kW) presents a very different behavior from the minimum configuration to the minimum plus one. This happens because the C rate is diminished to a half

when the branches in parallel are increased by one (from 1 to 2), which is a big difference according to the ageing model. A higher number of branches in parallel do not improve that much the behavior.

Scenarios S4 (40 kW) and S3 (30 kW) present the highest ageing, since they are working with a less intermittent profile (Fig. 9). This implies that temperature is higher during a cycle, and also the charging C rate is higher than the previous scenarios.

As it can be seen in Fig. 10, the number of days until the BESS losses a 20% of capacity retention increases for each battery as the number of cells in parallel increases from the minimum to the minimum plus three. Scenario S6 (60 kW) has a slight slope, and it lasts the longest even for the minimum configuration. This happens due to the C rate that the BESS is working with is low, and it works for very few periods of time (Fig. 9).

Step 5. Cost-benefit analysis.

Once the BESS ageing for different configurations has been calculated, a cost-benefit analysis must be performed, considering both BESS cost and fixed term energy cost. Among the different reports found in the literature that analyze energy storage costs, the one published in [37] has been selected as the most reliable study.

Moreover, electricity access fees for industrial consumptions for the regulated market in Spain can be found at [38]. Costs are summarized in **Table 5**.

The fixed term of the access fee considers three time periods of time-discrimination (P1, P2, and P3). For further information about the Spanish regulated market, and time discrimination periods, the authors recommend the work published in [24].

The variable term of energy is kept constant for every scenario, i.e. the BESS is recharged from the grid, and the BESS energy recharged from the grid plus the industrial load demand matches the total energy consumed by the industrial load in scenario SN, so the overall energy consumption remains constant. Hence, it is not included in the cost table.

Table 5. Summarized costs table.

Item	Cost
BESS cost (€/kW)	1876 €/kW
BESS cost (€/kWh)	469 €/kWh
P1	59.1734 €/kW and year
P2	39.4906 €/kW and year
P3	8.3677 €/kW and year

Considering this, the cost equation that needs to be optimized can be written as:

$$Cost \left(\frac{\text{€}}{\text{year}} \right) = (P1 + P2 + P3) \cdot P_{LIMIT} + BESS \text{ project cost} \tag{16}$$

The contracted power (P_{LIMIT}) is considered constant for the three time-discrimination periods (as usually happen for industrial consumptions). The yearly BESS project cost can be calculated as follows:

$$BESS \text{ project cost } \left(\frac{\text{€}}{\text{year}} \right) = (1876 \cdot P_{BESS} + 469 \cdot E_{BESS}) \cdot \frac{365}{\text{Days}} \quad (17)$$

where P_{BESS} is the maximum power to be delivered by the BESS for each scenario, E_{BESS} is the BESS energy for each case, calculated as $E_{BESS} = N_S \cdot N_P \cdot 3,7 \text{ V} \cdot 55 \text{ Ah}$ (N_S and N_P are the series and parallel cells of the BESS), and Days corresponds to the number of days that the BESS lasts until it loses a 20% of capacity retention (Fig. 10).

Hence, cost table in **Table 6** can be calculated.

Table 6. Cost table for the different scenarios.

Scenario	P_{LIMIT}	BESS config.	P_{BESS}	E_{BESS}	Fixed access fee	BESS project	Total
SN	80 kW	-	-	-	8562.53 €	-	8562.53 €
S6	60 kW	13s1p	11.9 kW	2.64 kWh	6421.91 €	1826.36 €	8248,27 €
		13s2p		5.29 kWh		1880.75 €	8302,66 €
		13s3p		7.93 kWh		1958.76 €	8380,67 €
		13s4p		10.58 kWh		2044.66 €	8466,57 €
S5	50 kW	13s1p	21.9 kW	2.64 kWh	5351.58 €	4128.20 €	9479,78 €
		13s2p		5.29 kWh		3481.79 €	8833,37 €
		13s3p		7.93 kWh		3474.99 €	8826,57 €
		13s4p		10.58 kWh		3532.35 €	8883,93 €
S4	40 kW	13s4p	31.9 kW	10.58 kWh	4281.26 €	7443,15 €	11724,41 €
		13s5p		13.22 kWh		7030,11 €	11311,37 €
		13s6p		15.87 kWh		6803,29 €	11084,55 €
		13s7p		18.51 kWh		6666,26 €	10947,52 €
S3	30 kW	13s29p	41.9 kW	76.71 kWh	3210.95 €	12646,57 €	15857,52 €
		13s30p		79.36 kWh		12649,86 €	15860,81 €
		13s31p		82.01 kWh		12656,83 €	15867,78 €
		13s32p		84.65 kWh		12670,61 €	15881,55 €

As it can be seen in **Table 6**, results indicate that introducing a BESS together with an industrial consumption for diminishing the fixed term of the electricity fee, can reduce the overall yearly cost. Moreover, this reduction can help to an intelligent use of the energy in industrial buildings, as well as improve the efficiency of the transmission and distribution of the energy along the electric power grid, since the consumption peaks are eliminated.

Table 6 shows that the minimum reduction in the fixed power limit is the best solution for this particular case example, from the point of view of the industrial consumer. Every configuration in scenario S6 reduces the yearly price of having a higher contracted power. The rest of the scenarios do not improve the price for this case example, although some interesting results are presented.

Scenario S5 shows that the minimum configuration might not be the optimal solution, since the configuration 13s3p provides a higher cost reduction than the minimum

configuration. This effect can be clearly seen in scenario S4, where a higher number of branches in parallel allow for a longer BESS life without increasing the cost severely, and even a higher number of branches in parallel would arise a greater cost reduction.

Scenarios S4 and S3 do not reduce the cost, since the BESS are dedicated not only to reduce the peak consumption, but to deal with an important part of the total demand. This causes the BESS to age faster than in previous scenarios, and indicates that a BESS may not be the best option for feeding an industrial infrastructure by itself since, even though is technically viable, it is costly.

5 Conclusions

This paper presents a BESS dimensioning methodology for reducing the fixed term of the electricity access fee for industrial consumptions, considering battery ageing and cost of the BESS and electricity access fees. By connecting a BESS together with a consumption, the power demand peaks can be reduced, so there is no need for contracting a high fixed term power to cover the high demand peaks.

The proposed methodology has potential interest for industrial consumers, since the cost-benefit analysis may reduce the yearly cost of their infrastructure, and also for TSOs and DSOs, since the peak reduction improves the efficiency of the transmission and distribution of the energy along the electric power grid. Moreover, BESS manufacturers could also find benefits in this methodology for the development of specific products related with this industrial demand peak and fixed term fee reduction.

Simulation models for grid, BESS, and industrial consumption are developed, described, and implemented.

A methodology of five steps to dimension a BESS is described, finishing with a cost-benefit analysis to make the final decision. The parameter that defines the different scenarios of the methodology is the power consumption limit from the grid.

A case example is performed, using the described methodology and the developed simulation methods. The case example considers a real industrial building consumption, as well as a commercial battery, and standard prices for both fixed term of electricity, battery, and power conversion system.

Results show that implementing a battery to limit the consumption peaks can lead to a cost reduction for the industrial consumer. This result include a battery ageing study, which indicates that over dimensioned batteries may have a higher reduction in the cost, since they work with lower C rates and lower temperatures, which make them last longer so the need for replacement is delayed, reducing the yearly cost of the project.

Future works include parametrizing the grid with frequency and voltage variations, so a further analysis considering BESS contributions to the grid in terms of frequency and voltage regulation can be performed. Moreover, a time discrimination pricing can be added to electricity energy prices, so the BESS can recharge during low price periods, providing an even higher reduction than the one shown in this work.

References

1. Eurostat, Statistics Explained. "Electricity price statistics." *Electricity prices for non-household consumers*. ISSN (2018): 2443-8219.
2. Jardini, José Antonio, et al. "Daily load profiles for residential, commercial and industrial low voltage consumers." *IEEE Transactions on power delivery* 15.1 (2000): 375-380.
3. Svetozarevic, Bratislav, et al. "Dynamic photovoltaic building envelopes for adaptive energy and comfort management." *Nature Energy* 4.8 (2019): 671-682.
4. Biyik, Emrah, et al. "A key review of building integrated photovoltaic (BIPV) systems." *Engineering Science and Technology, an International Journal* 20.3 (2017): 833-858.
5. Niu, Jide, et al. "Flexible dispatch of a building energy system using building thermal storage and battery energy storage." *Applied energy* 243 (2019): 274-287.
6. Lizana, Jesús, et al. "Advanced low-carbon energy measures based on thermal energy storage in buildings: A review." *Renewable and Sustainable Energy Reviews* 82 (2018): 3705-3749.
7. e Silva, Guilherme de Oliveira, and Patrick Hendrick. "Pumped hydro energy storage in buildings." *Applied energy* 179 (2016): 1242-1250.
8. Durand, Jean-Michel, Maria Joao Duarte, and Patrick Clerens. "European energy storage technology development roadmap towards 2030." *Int Energy Storage Policy Regul Work* 108 (2017).
9. EASE - Storage Applications. <http://ease-storage.eu/energy-storage/applications/>
10. Yassin, Mohammed AM, et al. "Battery capacity estimation for building integrated photovoltaic system: Design study for different geographical location (s)." *Energy Procedia* 142 (2017): 3433-3439.
11. Mulder, Grietus, et al. "The dimensioning of PV-battery systems depending on the incentive and selling price conditions." *Applied energy* 111 (2013): 1126-1135.
12. Pandžić, Hrvoje. "Optimal battery energy storage investment in buildings." *Energy and Buildings* 175 (2018): 189-198.
13. Fotouhi, Abbas, et al. "A review on electric vehicle battery modelling: From Lithium-ion toward Lithium-Sulphur." *Renewable and Sustainable Energy Reviews* 56 (2016): 1008-1021.
14. Zhang, Lei, et al. "A review of supercapacitor modeling, estimation, and applications: A control/management perspective." *Renewable and Sustainable Energy Reviews* 81 (2018): 1868-1878.
15. Amiribavandpour, Parisa, Weixiang Shen, and Ajay Kapoor. "Development of thermal-electrochemical model for lithium ion 18650 battery packs in electric vehicles." *2013 IEEE Vehicle Power and Propulsion Conference (VPPC)*. IEEE, 2013.
16. Rao, Venkat, et al. "Battery model for embedded systems." *18th International Conference on VLSI Design held jointly with 4th International Conference on Embedded Systems Design*. IEEE, 2005.
17. Lam, Long, Pavol Bauer, and Erik Kelder. "A practical circuit-based model for Li-ion battery cells in electric vehicle applications." *2011 IEEE 33rd International Telecommunications Energy Conference (INTELEC)*. IEEE, 2011.
18. Tremblay, Olivier, Louis-A. Dessaint, and Abdel-Allah Dekkiche. "A generic battery model for the dynamic simulation of hybrid electric vehicles." *2007 IEEE Vehicle Power and Propulsion Conference*. Ieee, 2007.
19. Chen, Min, and Gabriel A. Rincon-Mora. "Accurate electrical battery model capable of predicting runtime and IV performance." *IEEE transactions on energy conversion* 21.2 (2006): 504-511.

20. Fan, Lingling. *Control and dynamics in power systems and microgrids*. CRC Press, 2017.
21. Allègre, A. L., R. Trigui, and A. Bouscayrol. "Different energy management strategies of Hybrid Energy Storage System (HESS) using batteries and supercapacitors for vehicular applications." *2010 IEEE Vehicle Power and Propulsion Conference*. IEEE, 2010.
22. Laldin, Omar, Mazhar Moshirvaziri, and Olivier Trescases. "Predictive algorithm for optimizing power flow in hybrid ultracapacitor/battery storage systems for light electric vehicles." *IEEE Transactions on power electronics* 28.8 (2012): 3882-3895.
23. Zhou, Fang, et al. "Adaptive model predictive control-based energy management for semi-active hybrid energy storage systems on electric vehicles." *Energies* 10.7 (2017): 1063.
24. Yazdani, Amirnaser, and Reza Iravani. *Voltage-sourced converters in power systems: modeling, control, and applications*. John Wiley & Sons, 2010.
25. Concha, Pablo Moreno-Torres. *Analysis and Design Considerations of an Electric Vehicle Powertrain regarding Energy Efficiency and Magnetic Field Exposure*. Diss. Universidad Politécnica de Madrid, 2016.
26. Nájera, Jorge, et al. "Approach to hybrid energy storage systems dimensioning for urban electric buses regarding efficiency and battery aging." *Energies* 10.11 (2017): 1708.
27. Omar, Noshin, et al. "Lithium iron phosphate based battery—Assessment of the aging parameters and development of cycle life model." *Applied Energy* 113 (2014): 1575-1585.
28. Shepherd, Clarence M. "Design of primary and secondary cells: II. An equation describing battery discharge." *Journal of the Electrochemical Society* 112.7 (1965): 657.
29. Tremblay, Olivier, and Louis-A. Dessaint. "Experimental validation of a battery dynamic model for EV applications." *World electric vehicle journal* 3.2 (2009): 289-298.
30. Saw, L. H., et al. "Electro-thermal analysis of Lithium Iron Phosphate battery for electric vehicles." *Journal of Power Sources* 249 (2014): 231-238.
31. Chen, Yufei, and James W. Evans. "Three-dimensional thermal modeling of lithium-polymer batteries under galvanostatic discharge and dynamic power profile." *Journal of the Electrochemical Society* 141.11 (1994): 2947.
32. Redondo-Iglesias, Eduardo, Pascal Venet, and Serge Pelissier. "Calendar and cycling ageing combination of batteries in electric vehicles." *Microelectronics Reliability* 88 (2018): 1212-1215.
33. Wang, John, et al. "Degradation of lithium ion batteries employing graphite negatives and nickel-cobalt-manganese oxide+ spinel manganese oxide positives: Part 1, aging mechanisms and life estimation." *Journal of Power Sources* 269 (2014): 937-948.
34. Iglesias, Eduardo Redondo. *Étude du vieillissement des batteries lithium-ion dans les applications" véhicule électrique": combinaison des effets de vieillissement calendaire et de cyclage*. Diss. 2017.
35. Rao, Lin, and John Newman. "Heat-generation rate and general energy balance for insertion battery systems." *Journal of the Electrochemical Society* 144.8 (1997): 2697.
36. Kokam. "SLBP 55Ah high power superior lithium polymer battery." SLPB100255255HR2.
37. Mongird, Kendall, et al. *Energy storage technology and cost characterization report*. No. PNNL-28866. Pacific Northwest National Lab.(PNNL), Richland, WA (United States), 2019.
38. España, G. "Informe de precios energéticos regulados." (2019).

Sizing of Autonomous Microgrid Considering Life Cycle Emissions

Iván Jiménez-Vargas¹, German Osma-Pinto², Juan M. Rey³

Universidad Industrial de Santander, Bucaramanga, Colombia

¹ivan.jimenez@correo.uis.edu.co

²gealosma@uis.edu.co

³juanmrey@uis.edu.co

Abstract. This article presents a strategy for the optimal sizing of microgrids based on wind turbines, photovoltaic systems, diesel generation, and batteries. As optimization criteria, the reduction of life cycle emissions (LCE) and the net present cost (NPC) of the system were chosen, and a penalty-based combined economic-emissions dispatch (CEED) was implemented inside the energy management strategy (EMS). This strategy is compared to a diesel generation-based sizing and another based exclusively on the NPC. The results show that the system's hybridization allows reducing both costs (up to 29%) and LCEs (between 70 and -90%).

Keywords: Emissions, Life Cycle Assessment, Microgrid, Optimal sizing.

1 Introduction

Microgrid (MG) is an alternative concept to the traditional idea of power system, derived from hybrid energy systems. In general, an MG is an electrical energy distribution network containing distributed energy resources (DERs) capable of supplying local demand without using transmission networks. Likewise, they can include energy storage systems, hierarchical autonomous control systems, communications, and disconnection equipment capable of connecting or disconnecting it from other power networks [1]. Due to their renewable energies penetration capacity and management of renewable energies, MGs are considered a greener alternative to traditional systems [2]. However, MGs have some disadvantages compared to conventional distribution networks, such as high capital costs, complexity in operation, the need for robust control systems, communication equipment, and power quality issues, among others [3]. One of the main disadvantages is related to the high costs of initial investment and operation [4], which are the focus of the MGs sizing and planning problem.

1.1 Planning of MGs

Planning and sizing are tasks closely related and can become a challenge since the integration of DERs depends on several factors such as climatic conditions and load variability, making the nature of the problem non-deterministic [5]. Without the suitable techniques, MGs tend to be undersized or with high amounts of wasted energy. An optimal sizing approach is considered to overcome this and other challenges.

The optimal sizing consists of determining the optimal capacity of the MG's DERs, according to single or multiple optimization criteria [6]. This problem usually includes objectives, dispatch rules, or restrictions related to the system's future operation and planning. The goals of optimizing the MG design can be financial, technical, social, environmental, or a combination of them [6]. This problem is formulated and solved using optimization software such as GAMS, AMPL, and Matlab. Likewise, simulation software specialized in MGs allows us to carry out this task, such as HOMER Pro, HOMER Grid, HYBRID2, and IHOGA.

In the literature, there is abundant material on optimal sizing [4, 6, 7]. Authors have focused on the algorithms used to improve the runtime and accuracy of the solution [8]; or have studied the impact of considering the stochastic behavior of the load and the generation [9], as well as the inclusion of complex load prediction models [10] or demographic factors [11]. Some environmental impact analyzes have also been carried out, as will be discussed in the next section.

1.2 Environmental impacts of MGs implementation and operation

The integration of high amounts of DERs does not necessarily imply a reduction in environmental impact. Although wind and photovoltaic generation or batteries do not emit GHG in their operation, these systems' life cycle has an ecological cost that must be taken into account when quantifying these technologies' environmental impacts [12–14].

Although several studies have been carried out to consider the environmental component on the MGs sizing [16]–[20], it was identified that most of these address the problem of quantifying emissions only in the operation of the system [15–17]. Some works go beyond the operation and evaluate MG's performance using LCA methodologies, but this analysis is after implementing the MG [18]. Thus, no studies related to the formulation of the optimal sizing of the MG considering LCE were identified [7], except the work of Shi *et al.* [19]; however, its proposal is reduced to assume a typical day extended during the evaluation period without considering emissions due the power dispatch, and the purpose of including LCA in the formulation of the problem is just focused on reducing emissions due to the inclusion of a diesel generator in a PV/wind system while taking advantage of reliability provided by the diesel generator.

The absence of studies that analyze the MG's sizing considering life cycle emissions in the objective function and the dispatch strategy was identified. Therefore, this work's contribution focuses on filling this gap with the approach of a bi-objective optimal sizing strategy that considers economic and environmental factors, both in the objective function and energy management, and the analysis of their results through a case study. The next section presents the purpose of the contribution.

1.3 Objectives of the study

From the issues highlighted in the previous subsection, the problem that is the object of this paper is established from the following motivations:

- MGs are systems with great potential to positively impact the environment and reduce the electric power industry's GHG emissions.

- The optimal sizing of MGs is a current and relevant field of study to make these alternative systems viable and competitive.
- The literature does not show active efforts to plan hybrid energy systems that consider environmental impacts in the formulation of the sizing and energy management.
- LCA is a critical methodology for analyzing and evaluating the environmental impact of products and systems.

Therefore, this paper addresses the problem of the technical-economic-environmental design of MGs. An optimal sizing strategy for an MG is proposed by integrating financial, technical, and environmental components based on an LCA and optimization methodology. In particular, the inclusion of a multi-objective function is proposed to quantify the GHG emissions in the life cycle and the net present value of an MG, considering a proposed economic-environmental dispatch. The MG is composed of Photovoltaic systems (PV), Wind Turbines (WT), Diesel Generators (DG), and Battery Energy Storage Systems (BESS). This proposal is compared against two reference cases: the exclusively economic optimal sizing and a system powered only by diesel generators. This study aims to analyze the economic and environmental effects of considering LCA in planning hybrid energy systems.

This paper’s content is organized as follows: Section 2 presents data, models, and mathematical considerations about the sizing problem. Section 3 presents results and discussion. Finally, section 4 contains the conclusion of the study.

2 Modeling of the problem

The sizing problem can be formulated in multiple ways according to the dispatch approach, the objective function, constraints, and the solution method, among others. This section presents the considerations, mathematical models, and observations for the problem formulation and solution.

The dimensioned system corresponds to a configuration composed of PV/WT/DG/BESS due to its good relationship between reliability and economy [6] (see Fig. 1). The objectives are the net present cost (NPC) of the MG and the life cycle emissions (LCE) during the lifetime of the DERs. A rule-based energy management strategy (EMS) was chosen, including a stage of optimal combined economic-environmental dispatch (CEED) of the DG and the BESS in a five-year horizon.

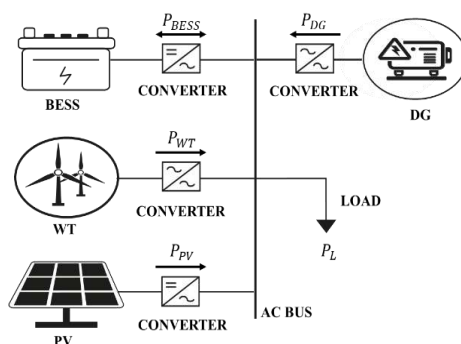


Fig. 1. Configuration of the microgrid for the study case.

2.1 Economic objective function

The economic indicator chosen as the objective was the NPC since it allows us to transform money flows from future years to their equivalent value in current currency. The system NPC is:

$$NPC = C_{IC} + C_{OM} + C_{FC} + C_{RE} + C_{SA} + C_{PE} \tag{1}$$

where C_{IC} is the initial capital, C_{OM} is the operation and maintenance costs, C_{FC} is the fuel consumption costs, C_{RE} is the replacement costs, C_{SA} is the salvage of the equipment at the end of the lifetime, and C_{PE} is the cost of GHG emissions penalties, all of them in USD. The annual costs were calculated as follows:

$$C_{IC_y} = \sum_G N_G PR_G \tag{2}$$

$$C_{OM_y} = \sum_{G \neq DG} (N_G OM_G) + N_{DG} OM_{DG} OH_{DG} \tag{3}$$

$$C_{FC_y} = PR_d FC_{DG} \tag{4}$$

$$C_{RE_y} = \sum_G 0.8 N_G PR_G \tag{5}$$

$$C_{SA_y} = - \sum_G 0.8 (1 - DE_G) N_G PR_G \tag{6}$$

$$C_{PE_y} = \sum_t \overline{PE}_{DG} P_{DG_t} \tag{7}$$

where G is the set of the four DERs, N_G is the quantity of each component of G , and PR_G is the capital price of DERs in USD/unit. OM_G and OM_{DG} are the cost of operation and maintenance of G in USD/unit and of DG in USD/h, and OH_{DG} is the time of operation of the DG in hours. PR_d is the price of diesel in USD/L, and DE_G is the percent of linear degradation of element G . FC_{DG} is the DG 's fuel consumption in L, \overline{PE}_{DG} is the average emission penalty factor [20] in USD/kWh, and P_{DG_t} the power generated by the DG in kWh.

Note that the costs represented by equations (2) to (7) are calculated annually, hence the subscript y . The following expression is used to convert the annual values to present value:

$$NPV = \sum_{y=1}^5 \frac{F_y}{(1 + i_f)^y} \tag{8}$$

where NPV is the present value of a cash flow F_y in the year y at a real discount rate i_f . Note that F_y represents the sum of costs of equations (2) to (7) in the year y , and the replacement costs only exist when equipment reaches the end of its useful life and salvage only occurs at year 5. Replacement and salvage costs are multiplied by 0.8 to consider that not all initial investment must be replaced or resold.

2.1 Environmental objective function

The environmental objective is to reduce GHG emissions during the system's life cycle, quantified using CO₂eq emissions. Regarding WT, PV, and BESS, emissions are concentrated in the pre-operational stage due to the extraction of raw material, manufacturing, transport, and installation [21–23]. In contrast, 95% of DG emissions are concentrated in diesel combustion [24]. CO₂eq emissions during the life cycle or LCEs of the MG are calculated as follows:

$$LCE = \sum_G GHE_G E_G \quad (9)$$

where GHE_G is the emissions of each element of G in kgCO₂eq/kWh and E_G is the energy generated by each generation source, or the total energy exchanged in BESS. This approach is appropriate because it allows associating the amount of emissions from renewable generators with the amount of use, since, in this study, an analysis horizon (5 years) was considered lower than the full useful life of the WT (10-20 years) and PV (20-30 years).

2.2 Constraints

The design variables are subject to technical restrictions associated with the generators' power limits, the maximum and minimum state of charge (SOC) of the BESS, and reliability. In this study was not considered the distribution system for simplicity. The capacity restrictions implemented were as follows:

$$N_G > 0 \quad (10)$$

$$0 \leq P_{DG}(t) \leq 1.1N_{DG}NC_{DG} \quad (11)$$

$$P_{BESS-min} \leq P_{BESS}(t) \leq P_{BESS-max} \quad (12)$$

$$SOC_{min} \leq SOC(t) \leq SOC_{max} \quad (13)$$

where $P_{DG}(t)$ is the power delivered by the diesel at time t in kW, and NC_{DG} is the rated power of the DG in kW. $P_{BESS-min}$ and $P_{BESS-max}$ are the maximum power delivered (or absorbed) by the BESS in kW. Finally, the state of charge $SOC(t)$ will be limited by a minimum value (SOC_{min}) and a maximum value (SOC_{max}), and it is expressed as a percentage.

The power balance of the MG must always be guaranteed, for which the following restriction is formulated:

$$P_{WT}(t) + P_{PV}(t) + P_{BESS}(t) + P_D(t) = P_L(t) \quad (14)$$

where $P_{WT}(t)$, $P_{PV}(t)$, $P_{BESS}(t)$, and $P_D(t)$ represent the power delivered by the WT, PV, BESS, and DG, respectively, while $P_L(t)$ is the demanded power.

In this kind of system, it is usual that all the demand cannot be met all the time, so a reliability restriction is added. It is required that at least 95% of the demanded power

be satisfied in all moment, so it was used as a reliability indicator based on the Loss of Power Supply Probability (LPSP) [25]:

$$\frac{\sum_t P_G(t)}{\sum_t P_{DG}(t)} > 0.05 \quad (15)$$

where $P_G(t)$ is the net power generated at time t and $P_{DG}(t)$ the power load in kW. To satisfy equations (14) and (15), a rule-based EMS was designed that guarantees the load's attention and, thus, a good system reliability, taking advantage of renewable resources and optimizing the dispatch between the BESS and the DG. This strategy is presented in the following subsection.

2.3 Rule-Based Energy Management Strategy

The rule-based EMS implemented allows us to take full advantage of generation from renewable sources and optimize DG and BESS's dispatch, considering emissions and their degradation. This strategy is executed once each hour of time of study (five years). The sequence of actions of the strategy is following described:

1. The data corresponding to a possible solution is loaded, that is, the number of WT / PV / BESS / DG.
2. The generation of renewables is calculated from the models in Subsection 2.4.
3. The difference between generation with renewables and demand is calculated.
4. For each instant interval t :
 - If the renewable generation is greater than the demand, the BESS is charged. The energy not supported by the BESS is counted as dump energy.
 - If the renewable generation is less than the demand, the power of the BESS and the DG is dispatched in such a way as to minimize the cost of energy, degradation, and the emissions penalty (see Subsection 2.4), in what is called CEED.
 - If the BESS's combined maximum capacity and the DG are not enough to meet the demand, the output power of this equipment will be set to its maximum, and an unattended load will be computed.
5. Once the iterative EMS process is finished, the reliability indicators, emissions, and costs about the possible solution are calculated.

2.4 Modeling of the microgrid components

This subsection presents the models that allow converting primary resources to output power for renewable sources, the model used for BESS, and the relationship between power demanded by the DG and its fuel consumption.

Wind Turbines. The calculation of the power generated by the WTs is made according to the wind speed and the cubic model with lower and higher cutting speeds [8]. Mathematically, this model is described like this:

$$P_{WT}(t) = \begin{cases} 0, & V < V_{C_{in}} \wedge V > V_{C_{out}} \\ N_{WT}NC_{WT} \left(\frac{V(t)^3 - V_{C_{in}}^3}{V_R^3 - V_{C_{in}}^3} \right), & V_{C_{in}} \leq V < V_R \\ N_{WT}NC_{WT}, & V_R \leq V < V_{C_{out}} \end{cases}, \quad (16)$$

where, NC_{WT} and V_R are the power in kW and nominal speed in m/s of the WT, respectively. $V(t)$, $V_{C_{in}}$ and $V_{C_{out}}$ is the wind speed at instant t , the lower cutting speed, and the upper cutting speed in m/s, respectively.

Photovoltaic system. The chosen model is a simplified model presented by Bukar *et al.* [8], which considers the manufacturer's parameters, irradiance, and temperature to calculate the power output thus:

$$P_{PV}(t) = N_{PV}\eta_{PV}A_{PV}I(t) \left(1 + \left(\frac{k_p}{100} \right) (T_c(t) - T_{STC}) \right) \quad (17)$$

where $P_{PV}(t)$, $I(t)$, and $T_c(t)$ represent the power generated in kW, the irradiance kW/m², and the temperature of the cell in °C [8] at an instant t . η_{PV} , A_{PV} , k_p , and T_{STC} are parameters that represent the efficiency, the effective area in m², the temperature constant in 1/°C, and the STC temperature of the panel in °C, respectively.

Battery Energy Storage System. As inferred from EMS, the battery's power input/output depends on their state of charge, power limits, and the EMS operation stage. Thus, the BESS can operate during:

Excess of renewables. If the generation produced by renewable sources exceeds the demand, that power will charge the batteries. This scenario is the only one in which BESS absorbs energy. This power injection will be limited by the SOC and the maximum battery charging power (see Subsection 2.4).

$$P_B(t) = -(P_{WT}(t) + P_{FV}(t) - P_L(t)) \quad (18)$$

Defect of renewables. If the generation of renewables is insufficient to satisfy the demand in an instant t , it will be decided to dispatch the batteries together with the diesel, minimizing the cost of generation at that instant. The cost of generating with batteries will be associated with their degradation, thus:

$$C_{BESS}(t) = \frac{PR_{BESS}}{ET_{BESS}} P_B(t), \quad P_B(t) > 0 \quad (19)$$

where PR_{BESS} is the capital price in USD, and ET_{BESS} is the energy throughput of the battery in kWh. This equation assigns a fee to the kWh delivered by the battery considering its useful life in terms of energy. This cost is not considered within the C_{OM} or C_{FC} component, since it is within the C_{SA} and C_{RE} calculation.

Diesel Generation. Like BESS, its dispatch depends on EMS. Additionally, the fuel consumption is used to calculate the cost of its dispatch and the component C_{FC} . The linear cost function of fuel consumption [26] chosen is presented below:

$$FC_{DG}(t) = 0.246P_{DG}(t) + 0.08415CN_{DG} \tag{20}$$

where CN_{DG} is the nominal capacity of the diesel generator in kW. For dispatch purposes, an additional factor that includes degradation due to use and a penalty factor for emissions was included. The dispatch cost function for the DG is:

$$C_{DG}(t) = PR_{DG}FC_{DG} + \overline{PE}_{DG}P_{DG}(t) + \frac{PR_{DG}}{ET_{DG}}P_{DG}(t) \tag{21}$$

where ET_{DG} is the total guaranteed energy that the DG can deliver during its entire useful life.

2.5 Study data

This section presents the primary resource and load profiles associated with the problem. The MG’s sizing was made for an isolated location in the north of Colombia, in La Guajira (12.154N, 72.063W), since it is a location with abundant solar and wind resources [27].

Load Profile. The load profile was generated from typical residential profiles in Colombia. The highest demand occurs at the beginning of the night (18:00 to 20:00) and is equal to 20 kW, on average. The profile contains a random variability of 15%. Figure 1 shows the power profile for two days.

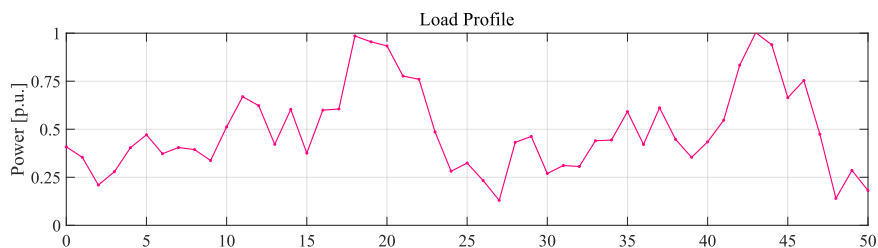


Fig. 2. Load profile for 50 hours of the evaluation period.

Primary energy resources. Energy resources are the climatic variables that affect renewable generation. For this work, irradiance, wind speed, and ambient temperature are considered. These data were obtained from the EU Science Hub. Figure 2 shows the irradiance profile, wind speed, and temperature for any two days.

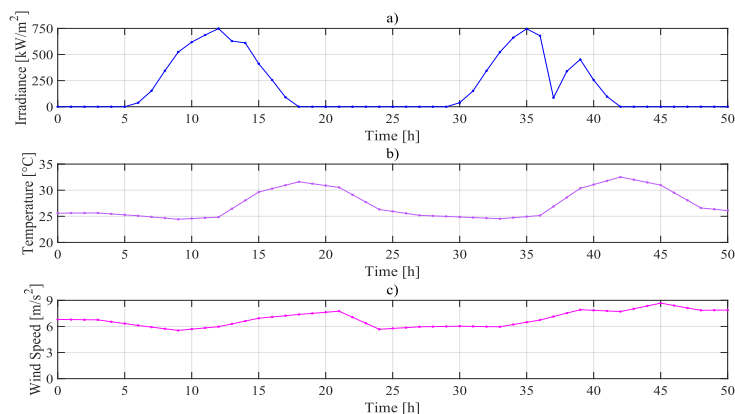


Fig. 3. Primary energy resources profiles. a) Solar radiation, b) temperature, and c) wind speed for 50 hours.

Parameters. Parameters are divided into three categories: economic, emissions, and technical parameters. The economic parameters are the values required for the cost calculations and are summarized in Table 1; the LCE function and the penalty in the CEDD information were collected in Table 2. Data associated with the mathematical models of the DERs and constraints is presented in Table 3.

Table 1. Economic parameters for system specification

Parameter	Value	Unit	Parameter	Value	Unit
PR_{DG}	5,000	USD/unit	OM_{WT}	450	USD/unit/year
PR_{WT}	40,000	USD/unit	OM_{PV}	10.21	USD/unit/year
PR_{PV}	714	USD/unit	OM_{BESS}	147	USD/unit/year
PR_{BESS}	3,057	USD/unit	i_f	6.6	%
OM_{DG}	0.17	USD/h	PR_d	0.7889	USD/L

Table 2. LCE parameters for system specification.

Parameter	Value	Unit	Parameter	Value	Unit
GHE_{WT} [21]	0.012	kgCO ₂ eq/kWh	GHE_{DG} [24]	20,203	kgCO ₂ eq/kWh
GHE_{PV} [22]	0.023	kgCO ₂ eq/kWh	\overline{PE}_{DG}	see [28]	USD/kWh
GHE_{BESS} [23]	0.040	kgCO ₂ eq/kWh	-	-	-

Table 3. Technical parameters for system specification.

Parameter	Value	Unit	Parameter	Value	Unit
C_{in}	3	m/s	SOC_{min}	40	%
C_{out}	20	m/s	SOC_{max}	100	%
CN_{WT}	10	kW	$P_{BESS-min}$	-3	kW
V_R	10	m/s	$P_{BESS-max}$	5	kW
η_{PV}	0.175	-	CN_{BESS}	9.8	kWh
A_{PV}	1.944	m ²	ET_{BESS}	30,000	kWh
k_p	-0.35	-	LT_{DG}	15,000	h

T_{STC}	25	°C	ET_{DG}	63,750	kWh
CN_{PV}	0.34	kW	CN_{DG}	5	kW

2.6 Solution method

It was used Matlab software and the parallel computing toolbox to solve the problem. An algorithm based on an exhaustive search was implemented since it was also interesting to observe all combinations' affectation. The search space comprised 405,720 combinations, and limits of the amounts of DG, WT, PV, and BESS are 1 to 4 DGs, 0 to 20 WTs, 0 to 160 PV, and 1 to 30 BESS. Total solution time was less than 8 minutes on a PC with an Intel (R) Core™ i7-3770 CPU @ 3.40GHz Quadra-core.

3 Results and Discussion

This section presents the results for the three proposed interest cases. The general results of the three points are shown in Table 4. Between the worst configuration used to meet demand (Case 1) and the most economical (Case 2), there is a set of financially viable possibilities that present reductions in LCEs, called Pareto front. One interesting solution of case 3 is the 'Best' solution with the better relation between NPC and LCEs, namely, the solution closer to the ideal value (NPC = 0, LCE = 0).

Table 4. The best solution for each case studied.

Case	Solution				NPC [USD]	LCE [tCO ₂ eq]
	N_{DG}	N_{WT}	N_{PV}	N_{BESS}		
1	4	0	0	0	154 K	605
2	2	2	54	3	107 K	173
3	1	1	105	20	127 K	68

3.1 Case 1: DG-based sizing. Meeting the load exclusively with DGs requires four units with a LPSP₁ of 0.28%. This configuration has an NPC₁ of \$153,932 and emits 605.5 tCO₂eq, making it the most expensive and less environmentally friendly option.

3.2 Case 2: Economic-based sizing. Economical solution features an NPC₂ of \$107,525 due to 2 DG, 2 WT, 54 PV, and 3 BESS with an LPSP₂ of 4.81%. The LCEs are equal to 173.7 tCO₂eq. This case is the less expensive option, and a reduction of three times was obtained in the total emissions compared with Case 1.

3.3 Case 3: LCA-CEED-based sizing. The inclusion of CEED and LCE produces the Pareto front of Figure 3. On this front, the NPC of the previous cases stand out, establishing the limits between the cheapest option possible (NPC_2) and the most expensive option (NPC_1). The Figure reveals that there are solutions up to 29% less expensive than Case 1. The variations of LCE with respect to case 1 (ΔLCE) were calculated and plotted in the right axis; this second plot shows emission reductions from 71% to more than 90%. Finally, the ‘Best’ solution is 17% cheaper and emits 89% less tCO₂eq than case 1.

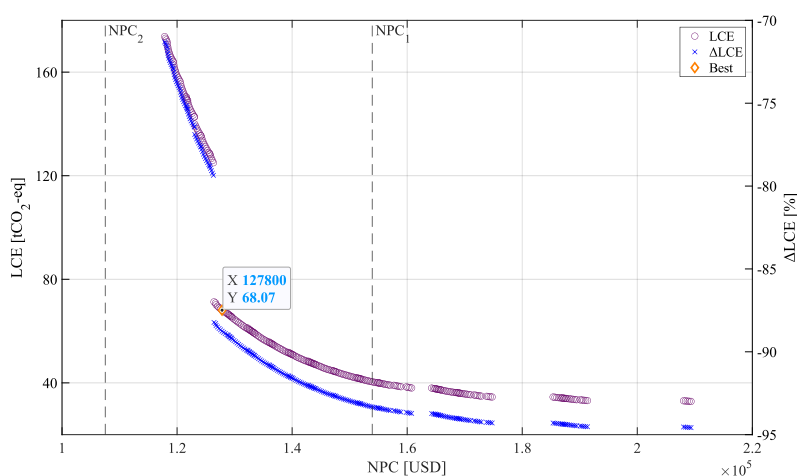


Fig. 4. Pareto front for case 3. The left axis represents LCEs, and the right axis represents variation of LCEs with respect to case 1.

Effects of CEED. Considering CEED has an economic impact on the solution does not necessarily guarantee lower emissions. In this study, considering the penalty cost (C_{PE}) only has adverse economic effects since it can be seen how the entire Pareto front “shift” horizontally to the right, that is, all solutions become slightly more expensive in proportion to this penalty, as shown in Figure 4.

The explanation is as follows: the rule-based EMS optimizes the dispatch cost every time the renewable generation is insufficient. Since the cost function is linear, the solution will always maximize the cheaper component’s power production. In the dispatch cost function (see Equation 20), the most affordable element is always BESS (0.10 USD / kWh) compared to DG (> 0.20 USD / kWh), so adding the penalty factor makes DG more expensive (and therefore, the solution). However, this does not significantly affect the power dispatch (compared to the case without CEED) and, consequently, the total emissions.

The most affected solutions on the Pareto fronts will be those with the highest DG penetration, as shown in the group of solutions demarcated by the blue rectangle in Figure 4. This set of solutions requires 2 DGs, and thus, diesel generation has a remarkable impact on its operation compared with those that operate with only 1 DG. This fact

also reveals the inverse relationship between the DG penetration level and the amount of LCEs.

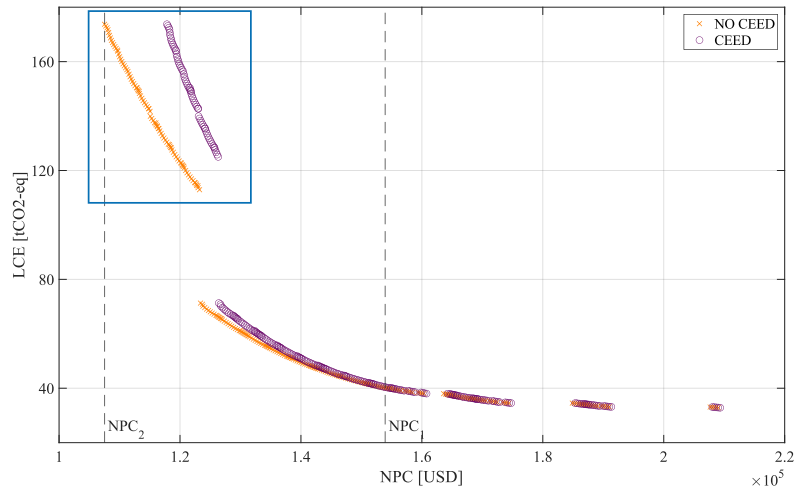


Fig. 5. Pareto front with (o-mark) and without (x-mark) CEED.

Relationship between solutions and emissions. Figure 5 relates the number of DERs with the LCEs of the solution. As expected, an increase in DG penetration produces an increase in the total emissions (Figure 5.a). At the same time, the reduction in LCEs is associated with greater penetration of PV and BESS (Figure 5.b and 5.d). However, WTs are directly related to higher emission levels since wind turbines provide a stable generation (according to the wind profile) throughout the day that integrates very well with diesel generation.

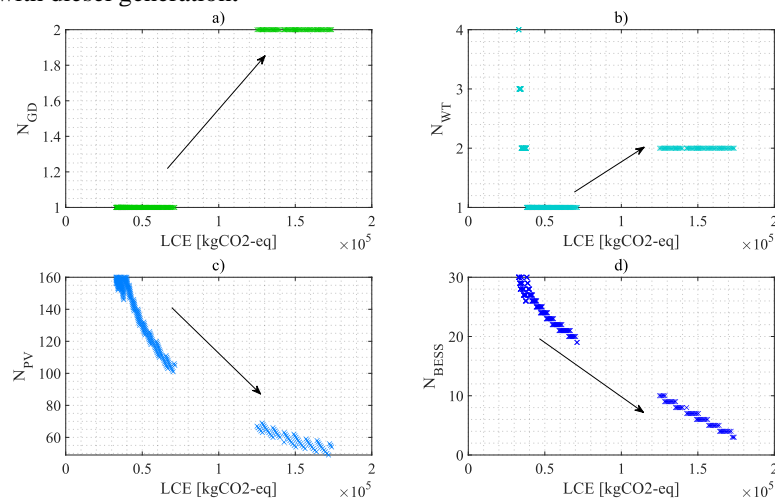


Fig. 6. Correlation between the number of DERs and LCEs. a) DG, b) WT, c) PV, and d) BESS.

3.4 Discussion

The sizing and planning of MGs with reduced LCEs are economically feasible. The case studies show that there are multiple solutions with lower emissions and less expensive than the solution based exclusively on diesel generators. This fact confirms that the hybridization of MG is an excellent alternative in economic and environmental terms.

On the other hand, it can be observed that implementing a CEED approach on the ruled-based EMS does not necessarily have a positive impact on the total emissions of the system. The results show that the inclusion of an emission charge makes the DG operation more expensive but does not significantly affect the power dispatch. For this reason, at least in terms of emissions, the results are quite similar with or without CEED.

Finally, it was found that the increase in penetration of PV and BESS systems is correlated with the decreases in LCEs. However, it is not the case with WT, although it is a type of renewable generation. The reason for this is strongly linked with the wind resource profile of the case study, which generates a strong correlation between the use of WT and DGs.

4 Conclusion

This paper presents a strategy for the optimal sizing of MGs, which considers LCA in the design and planning. The economic impact of LCE inclusion was calculated, concluding that hybrid MGs can have lower emissions and can be less expensive than systems based exclusively on diesel generators. The effect of increase the penetration of DERs and consider a combined economic-environmental dispatch was simulated on a case study, analyzing its variations on costs and GHG emissions. Future works will be focused on including the quantification of environmental indicators such as embedded energy, soil acidification, water consumption, among others.

References

1. Brandt, S.: Smart microgrids. In: From Design to Laboratory-Scale Implementation. Routledge, Abingdon, Oxon; New York, NY: Routledge, 2018. (2018). <https://doi.org/10.4324/9781351174824-26>.
2. Hirsch, A., Parag, Y., Guerrero, J.: Microgrids: A review of technologies, key drivers, and outstanding issues. *Renew. Sustain. Energy Rev.* 90, 402–411 (2018). <https://doi.org/10.1016/j.rser.2018.03.040>.
3. Parhizi, S., Lotfi, H., Khodaei, A., Bahramirad, S.: State of the art in research on microgrids: A review. *IEEE Access.* 3, 890–925 (2015). <https://doi.org/10.1109/ACCESS.2015.2443119>.
4. Luna-Rubio, R., Trejo-Perea, M., Vargas-Vázquez, D., Ríos-Moreno, G.J.: Optimal sizing of renewable hybrids energy systems: A review of methodologies. *Sol. Energy.* 86, 1077–1088 (2012). <https://doi.org/10.1016/j.solener.2011.10.016>.
5. Ghasemi, A., Enayatzare, M.: Optimal energy management of a renewable-based

- isolated microgrid with pumped-storage unit and demand response. *Renew. Energy*. (2018). <https://doi.org/10.1016/j.renene.2018.02.072>.
6. Al-falahi, M.D.A., Jayasinghe, S.D.G., Enshaei, H.: A review on recent size optimization methodologies for stand-alone solar and wind hybrid renewable energy system. *Energy Convers. Manag.* 143, 252–274 (2017). <https://doi.org/10.1016/j.enconman.2017.04.019>.
 7. Lian, J., Zhang, Y., Ma, C., Yang, Y., Chaima, E.: A review on recent sizing methodologies of hybrid renewable energy systems. *Energy Convers. Manag.* 199, 112027 (2019). <https://doi.org/10.1016/j.enconman.2019.112027>.
 8. Bukar, A.L., Tan, C.W., Lau, K.Y.: Optimal sizing of an autonomous photovoltaic/wind/battery/diesel generator microgrid using grasshopper optimization algorithm. *Sol. Energy*. 188, 685–696 (2019). <https://doi.org/10.1016/j.solener.2019.06.050>.
 9. Shaabani, Y. ali, Seifi, A.R., Kouhanjani, M.J.: Stochastic multi-objective optimization of combined heat and power economic/emission dispatch. *Energy*. 141, 1892–1904 (2017). <https://doi.org/10.1016/j.energy.2017.11.124>.
 10. Niknam, T., Azizpanah-Abarghoee, R., Narimani, M.R.: An efficient scenario-based stochastic programming framework for multi-objective optimal micro-grid operation. *Appl. Energy*. 99, 455–470 (2012). <https://doi.org/10.1016/j.apenergy.2012.04.017>.
 11. Tito, S.R., Lie, T.T., Anderson, T.N.: Optimal sizing of a wind-photovoltaic-battery hybrid renewable energy system considering socio-demographic factors. *Sol. Energy*. 136, 525–532 (2016). <https://doi.org/10.1016/j.solener.2016.07.036>.
 12. Asdrubali, F., Baldinelli, G., D'Alessandro, F., Scrucca, F.: Life cycle assessment of electricity production from renewable energies: Review and results harmonization. *Renew. Sustain. Energy Rev.* 42, 1113–1122 (2015). <https://doi.org/10.1016/j.rser.2014.10.082>.
 13. Wong, J.H., Royapoor, M., Chan, C.W.: Review of life cycle analyses and embodied energy requirements of single-crystalline and multi-crystalline silicon photovoltaic systems. *Renew. Sustain. Energy Rev.* 58, 608–618 (2016). <https://doi.org/10.1016/j.rser.2015.12.241>.
 14. Torabi, F., Ahmadi, P.: Battery technologies. In: *Simulation of Battery Systems*. pp. 1–54. Elsevier (2020). <https://doi.org/10.1016/B978-0-12-816212-5.00005-2>.
 15. Mahdi, F.P., Vasant, P., Kallimani, V., Watada, J., Fai, P.Y.S., Abdullah-Al-Wadud, M.: A holistic review on optimization strategies for combined economic emission dispatch problem, <http://dx.doi.org/10.1016/j.rser.2017.06.111>, (2018). <https://doi.org/10.1016/j.rser.2017.06.111>.
 16. Dey, B., Roy, S.K., Bhattacharyya, B.: Solving multi-objective economic emission dispatch of a renewable integrated microgrid using latest bio-inspired algorithms. *Eng. Sci. Technol. an Int. J.* 22, 55–66 (2019). <https://doi.org/10.1016/j.jestch.2018.10.001>.
 17. Elattar, E.E.: Modified harmony search algorithm for combined economic emission dispatch of microgrid incorporating renewable sources. *Energy*. 159, 496–507 (2018). <https://doi.org/10.1016/j.energy.2018.06.137>.
 18. Zhang, D., Evangelisti, S., Lettieri, P., Papageorgiou, L.G.: Optimal design of CHP-based microgrids : Multi-objective optimisation and life cycle assessment. *Energy*. 85, 181–193 (2015). <https://doi.org/10.1016/j.energy.2015.03.036>.

19. Shi, B., Wu, W., Yan, L.: Size optimization of stand-alone PV/wind/diesel hybrid power generation systems. *J. Taiwan Inst. Chem. Eng.* 73, 93–101 (2017). <https://doi.org/10.1016/j.jtice.2016.07.047>.
20. Krishnamurthy, S., Tzoneva, R.: Impact of price penalty factors on the solution of the combined economic emission dispatch problem using cubic criterion functions. In: *IEEE Power and Energy Society General Meeting* (2012). <https://doi.org/10.1109/PESGM.2012.6345312>.
21. Dolan, S.L., Heath, G.A.: Life Cycle Greenhouse Gas Emissions of Utility-Scale Wind Power. *J. Ind. Ecol.* 16, S136–S154 (2012). <https://doi.org/10.1111/j.1530-9290.2012.00464.x>.
22. Hsu, D.D., O'Donoghue, P., Fthenakis, V., Heath, G.A., Kim, H.C., Sawyer, P., Choi, J.-K., Turney, D.E.: Life Cycle Greenhouse Gas Emissions of Crystalline Silicon Photovoltaic Electricity Generation. *J. Ind. Ecol.* 16, S122–S135 (2012). <https://doi.org/10.1111/j.1530-9290.2011.00439.x>.
23. Peters, J.F., Baumann, M., Zimmermann, B., Braun, J., Weil, M.: The environmental impact of Li-Ion batteries and the role of key parameters – A review. *Renew. Sustain. Energy Rev.* 67, 491–506 (2017). <https://doi.org/10.1016/j.rser.2016.08.039>.
24. Sothea, K., Kim Oanh, N.T.: Characterization of emissions from diesel backup generators in Cambodia. *Atmos. Pollut. Res.* 10, 345–354 (2019). <https://doi.org/10.1016/j.apr.2018.09.001>.
25. Vergara, P.P., Rey, J.M., da Silva, L.C.P., Ordóñez, G.: Comparative analysis of design criteria for hybrid photovoltaic/wind/battery systems. *IET Renew. Power Gener.* 11, 253–261 (2017). <https://doi.org/10.1049/iet-rpg.2016.0250>.
26. Lujano-Rojas, J.M., Monteiro, C., Dufo-López, R., Bernal-Agustín, J.L.: Optimum load management strategy for wind/diesel/battery hybrid power systems. *Renew. Energy.* 44, 288–295 (2012). <https://doi.org/10.1016/j.renene.2012.01.097>.
27. Pasqualino, J., Cabrera, C., Chamorro, M.V.: The environmental impacts of folic and solar energy implementation in the Colombian Caribe. 13, 68–75 (2015). <https://doi.org/10.15665/rp.v13i1.361>.
28. Trivedi, I.N., Jangir, N., Jangir, P., Pandya, M.H., Bhesdadiya, R.H., Kumar, A.: Price penalty factors based approach for emission constrained economic dispatch problem solution using whale optimization algorithm. In: *1st IEEE International Conference on Power Electronics, Intelligent Control and Energy Systems, ICPEICES 2016*. Institute of Electrical and Electronics Engineers Inc. (2017). <https://doi.org/10.1109/ICPEICES.2016.7853284>.

The Profile of Studies on Renewable Energy in Sustainable Supply Chain

Eduardo do Carmo Marques^{1,2}[0000-0002-1731-6998] Maxwel de Azevedo-Ferreira³[0000-0002-8790-6483] Luis Hernández-Callejo⁴[0000-0002-8822-2948] Ronney Mancebo Boloy²[0000-0002-4774-8310] Vanessa de Almeida Guimarães²[0000-0001-7662-3499]

¹ Instituto Politécnico de Bragança, Campus de Santa Apolónia, Bragança, Portugal

² Centro Federal de Educação Tecnológica Celso Suckow da Fonseca, Rio de Janeiro, Brazil

³ Instituto Federal de Educação, Ciência e Tecnologia do Rio de Janeiro, Niterói, Brazil

⁴ Universidad de Valladolid, Campus Universitario Duques de Soria, Soria, Spain

eduardo.marques@aluno.cefet-rj.br
maxwel.ferreira@ifrj.edu.br
luis.hernandez.callejo@uva.es
ronney.boloy@cefet-rj.br
vanessa.guimaraes@cefet-rj.br

Abstract. Over the years, has been growing policies aiming to reduce the greenhouses gases emissions – GHG, which lead for the searching of sustainable alternative solutions. One way mitigates the GHG emissions is the use of renewable energy sources. Nevertheless, for the use of such resources there are a series of processes inherent to the energy production and consumption, being the supply chain one of the principals. Based on this, the main objective of present article is to map the role of renewable energies inside the context of sustainable supply chain, observing how the studies have been developed, looking for the main researchers, organizations and collaboration networks, being at final a mapping of the 15 most cited studies in area. The research was carried out with the papers published at Web of Science database, using VantagePoint software to quantify the information's, including the evolution of studies over time until 2019. It was possible to perceive that the research has been growing since 2010, moreover, subjects related to biomass, biofuels and photovoltaic energy were the most recurrent at the most cited. However, within this framework, the theme presented itself as new and that there are still great potentials to be explored.

Keywords: Renewable energies, supply chain, sustainable.

1 Introduction

Nowadays, the concern about the global warming and carbon emission is increasing more over [1], [2]. It is scientific knowledge that the global warming is caused by GHG emissions, mainly for carbon dioxide (CO₂), which is also generated by fossil fuel combustion processes [3]–[5]. According to Fang et al [6], the industrial sector contributes

with one-half of the global energy consumption. Within this context, the supply chain it is a process that involves different layers (from raw material, to manufacturing and delivering the products for clients – sometimes, even the recycling and disposal) and process (as manufacturing, transportation, storage and so on) that are intensive in energy consumption.

Therefore, one of the solutions that has been studied and implement over the years is the use of renewable energies [7], [8], that covers a wide use of different resources, such as, photovoltaic energy [9], hydrogen [10], wind energy [11], biogas for cogeneration [12] and many others [13]–[15].

According to Eurostat data (September of 2020) [16] in Fig. 1, the energy balance of renewable sources has increased by almost 6% in all European Union in the last 10 years, highlighting Portugal as one of main growing countries from renewable sources. Another important fact to highlight, is the growth of renewable energies in emerging countries, such as Brazil, with according to data from the Ministry of Mines and Energy [17], renewable energy sources, which include hydro, wind, solar and bioenergy, reached 46.1% of participation in the 2019 total energy demand matrix, increasing 0.6 percentage point in relation to the 2018 indicator.

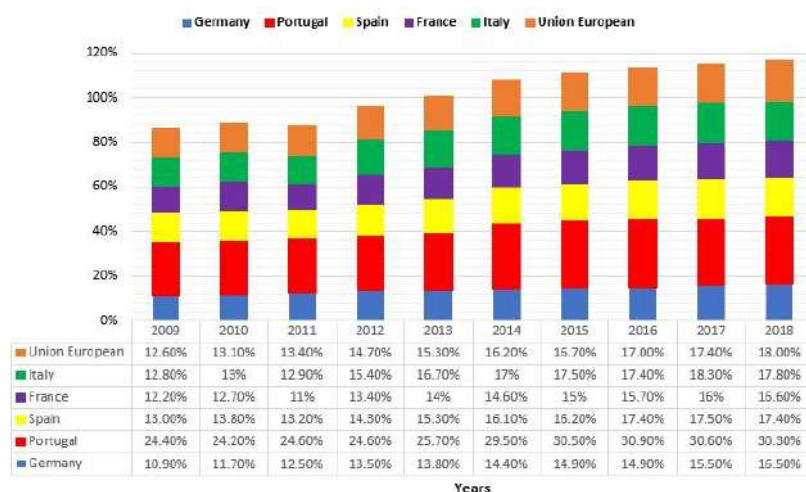


Fig. 1. Energy balance from renewable sources for European Union and other countries (2020) (Source: Eurostat adapted by the authors [16]).

Furthermore, an increasing the consumption of renewable energy can also decrease the dependence on fossil energy sources, promoting a sustainable development [18], [19]. However, for sustainable development it is necessary attend to social and environmental scenario, where in most of the time they are not even take account [20].

Still within the concept of sustainable development, an area that has grown up the studies is the design of sustainable supply chains. In general, the design of supply chains

is crucial to integrate several flows of raw materials, goods, and products at the end of their useful lives, that are some relevance for industrial processes [21].

As global demand has accrete dramatically (according to data from Energy Information, 30% of energy consumption will increase between 2020 and 2050) [22], the business sector has focused much of the efforts with the economic aspect, often leaving aside social and environmental aspects [23].

It is important to emphasize that quantifying these aspects is not always easy, bringing greater complexities in the development of mathematical models that support decision making regarding the design of supply chains [24]. In this sense, some authors point out that the incorporation of environmental and social aspects is a challenge in the area for the next years [25], [26], making it possible to visualize the recent efforts of researchers that have brought these dimensions for the literature [27]–[29].

With this, researchers observed that improvements can be achieved by two different ways: advanced programming research and operational strategies [30]. Based on this, this article aims to understand the role of renewable energy within the context of sustainable supply chain, performing the following questions, (i) Who are the main researchers in the field? (ii) How countries and institutions have worked to promote these studies? and (iii) How have studies grown in area and what are the most relevant thematic areas in this subject? Raising these questions, the next sections will discuss the methodological procedures to answer that, as well the results and discussion followed by conclusion.

2 Methodological Procedures

The methodological procedures used in this study involves a qualitative analysis of the literature and, the use of statistical techniques. Through a datamining process, the articles were obtained from the Web of Science (Wos) database, due to its scope and coverage [31]. Table 1 shows the parameters of search performed.

Table 1. Description of search in the Web of Science database

Criterion	Description
Topic 1	TS1 = (“SUPPLY CHAIN*”) OR “SUPPLY NETWORK*”))
Topic 2	TS2 = (“SUSTAINAB*”))
Combination	TS3 = (“TS1” AND “TS2”)
Data base	Web of Science
Refinement	Only Articles
Data	March 20, 2020 - 16:20 GMT-3

In a first time, the study had not included any keyword related to renewable energy sources, since decided to gather all the papers published about the subject and then, select for a frame of analysis. By doing that, the associated error was reduced with the

elimination of papers that could be related to the theme but does not use a specific keyword as the indexation terms.

Therefore, with the results from the search performed accordingly Table 1, was selected those papers that had keywords related to any kind of renewable energy. In Table 2 are listed the main categories used to select those papers. It is important to point that were found 260 keywords related to renewable energy.

Table 2. Categories and some keywords used for cutout in Wos database

Category	Keywords
Energy	Energy Renewable Energy Energy Efficiency Energy Consumption Exergy Sustainable Energy Electricity
Renewable Energy	Wind Energy Solar Energy Wind and Solar Power Solar Photovoltaic Off-Grid Solar Thermal Energy
Bioenergy	Biomass Bioenergy Biofuel Palm Oil Biogas Ethanol Forest Biomass Woody Biomass
Supply Chain	Biomass Supply Chain Bioethanol Supply Chain Hydrogen Supply Chain Biorefinery Supply Chain Thermal Coal Supply Chain
Systems	Biocatalysis C-Si Photovoltaic Panel Hybrid Generation Heat Recovery Hydrogen System
Others	Biomethane Cellulosic Biofuels

Another way to visualize the quantification of words is by the graph illustrate in Fig. 2, where is possible to view the frequency of each category of words referring to

renewable energies, in which the largest amount is represented by biomass followed by biofuel, ethanol, solar, photovoltaic and hydrogen.

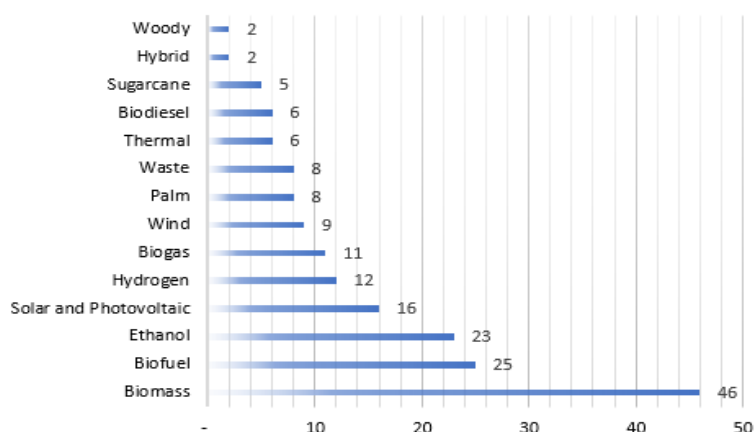


Fig. 2. Most recurrent words of 260 for clipping inside the Wos database from Table 1 (Source: The authors)

After this step of segregating words related to renewable energies, the study was carried out from VantagePoint, in which the main results and discussions will be presented in the next section.

3 Results and discussion

As discussed in the methodological procedures, the first step was to perform the search according to the criteria presented in Table 1. Where in all time (1900-2019), 9558 studies were found, being 6984 indexed scientific articles (Table 3).

Based on these results, the database for this study was created, focusing on the 6984 indexed journals. Therewith, the next step is understanding the role of renewable energies within this context. For this, the keywords that involved areas and categories related to renewable energy sources were cutout according to the search criteria established by Table 2, in which a total of 547 studies were found.

The first result analyzed was how the studies that relate renewable energy in sustainable supply chain have been developed over the years (Fig 3). In Fig. 3 the green line shows the records in function of the years and the blue one is the tendency line. Fig. 3 shows that the interest in this subject is recent (first paper published in 2002), with an accentuated growth from 2010.

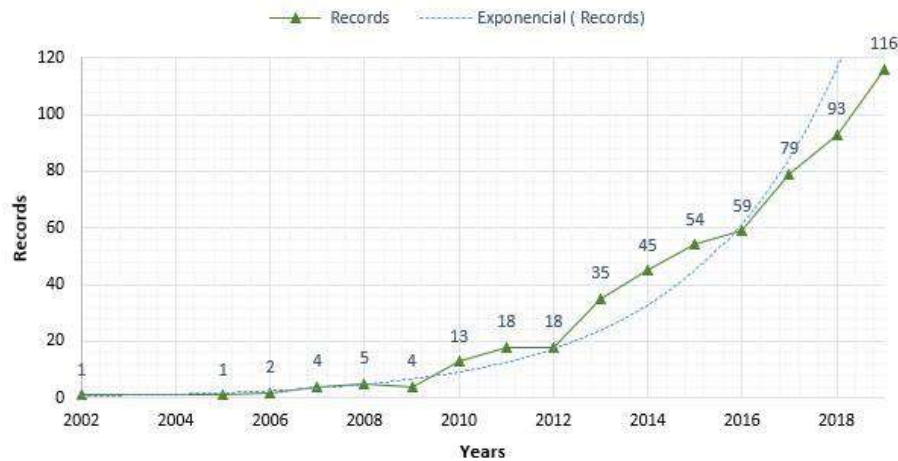


Fig. 3. Evolution of sustainable supply chain and renewable energies records in function of years (Source: VantagePoint and the authors)

The second analysis sought to understand the collaboration network among the main authors. A total of 1777 authors were found, which the 10 largest authors in the database were (records) respectively; You, FQ (12), Bezzo, F (7), Faaij, APC (7), Junginger, M (7), Ponce-Ortega, JM (7), Zhang, J (7), Cucchiella, F (6), D'Adamo, I (6), Lam, HL (6) and Osmani, A (6). The collaboration network is presented by Fig. 4, in which it is possible to observe, at least, 10 contribution networks composed by 3 authors or more.

To clarify the visualization of the main authors that publish about sustainable supply chain and renewable energy, Table 3 lists 28 authors with at least 4 publications. Where can be seen some collaboration network, among the main authors, You, FQ is between two networks, being made up of Yue, Dj and Ponce-Ortega, JM, besides this, it stands out Cucchiella and D'Adamo working together, Lam, Zhang, Y and Khan, SAR, among other authors with great importance in the area.

The next analysis carried out was to understand the main organizations and institutions that have published most in the thematic area of this article. The main results led to: Imperial College of Science, Technology and Medicine (with 16 records), University of Padua (14), Iran University Science and Technology (12), University of Utrecht (11), Wageningen University (11), University of Groningen (10), Northwestern University (9), Oak Ridge National Laboratory (9), University of California (9), University of Manchester (9).

Table 3. The 28 more recurrent authors with most records in database for sustainable supply chain and renewable energy (Source: The authors)

Position	Author	Records
1°	You, FQ	12
	Bezzo, F	7
2°	Faaij, APC	7
	Junginger, M	7
	Ponce-Ortega, JM	7
	Zhang, J	7
	Cucchiella, F	6
3°	D'Adamo, I	6
	Lam, HL	6
	Osmani, A	6
	Azapagic, A	5
4°	Dale, VH	5
	Hilliard, MR	5
	Khan, SAR	5
	Pishvaei, MS	5
	Santibanez-Aguilar, JE	5
	Sarkar, B	5
	Shah, N	5
	Efroymsen, RA	4
5°	Elkamel, A	4
	Garcia, DJ	4
	Gonela, V	4
	Guillen-Gosalbez, G	4
	Jaber, MY	4
	Jeswani, HK	4
	Murphy, RJ	4
	Yue, DJ	4
	Zhang, Y	4

The main Brazilian institutions that appear in the database are Federal Fluminense University – UFF (4), Federal University of Rio de Janeiro – UFRJ (3), São Paulo University – USP (3) and Federal Technological University of Paraná – UTFPR (2).

Regarding the countries that published the most about the subject, we highlight the top 10: USA (with 145 records), UK (67), Italy (63), Netherlands (45), Germany (34), China (30), Australia (26), Canada (25), Brazil (24) and Malaysia (24). Fig. 5 shows the map of countries with different colors for the number of publications.

It is also important to note that, it is well known that some countries on the African continent, the Middle East, and a small number of countries in Latin America have not contributed to the research area. However, it is a topic that been studied widely in a global scale.

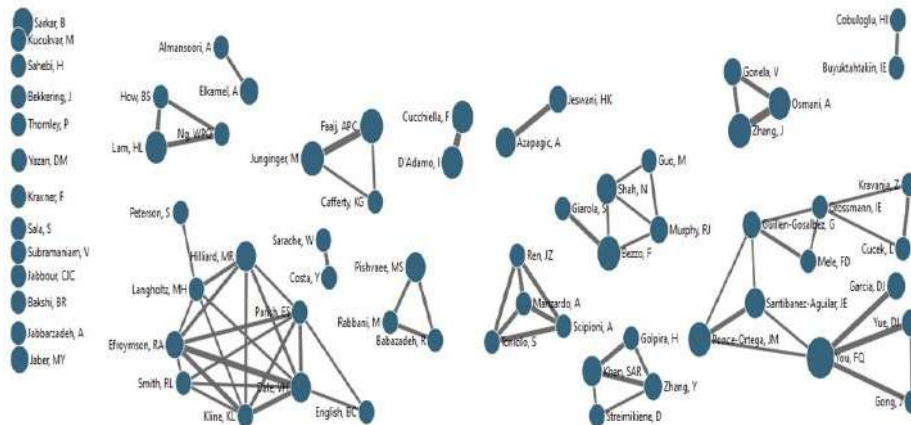


Fig. 4. Collaboration networks and micro-networks between the various authors found in the database (Source: VantagePoint and the authors).

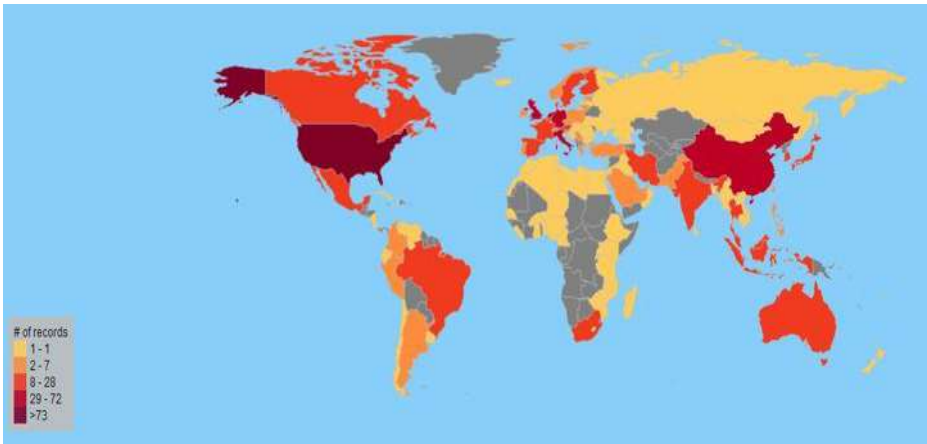


Fig. 5. Global map presenting the number of records for countries (Source: VantagePoint and the authors).

After analyzing the main authors involved and their networks, organizations and countries, the next step was to understand what the main areas of research are related to sustainable supply chains and renewable energies (Fig. 6). As expected the main results are related to the areas energy, engineering and technology, as follow: Energy & Fuels (with 221 records), Engineering (213), Environmental Sciences & Ecology (201), Science & Technology - Other Topics (157), Biotechnology & Applied Microbiology (70), Agriculture (57), Business & Economics (46), Thermodynamics (33), Computer Science (28) and Operations Research & Management Science (27).

In addition, it was observed the appearance of other areas not very close to renewable energies but that involve decision-making process, leading to a conclusion that the different industrial segments are looking for sustainable alternatives to minimize the environmental impacts in the supply chain.

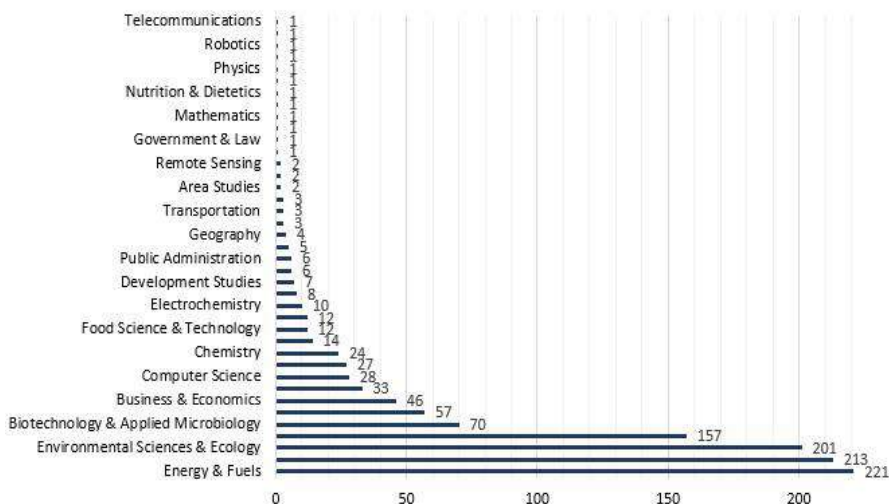


Fig. 6. Research areas and the number of records (Source: The authors)

Finally, the last analysis consisted of understanding which keywords are most present in the studies, Fig. 7 shows the words with the highest record within the base of data. As can be seen, the most frequent words are bioenergy, biofuel, bioethanol, biogas, renewable energy, palm oil, among others. It is possible to view different sources of energy presents that more recurrent.

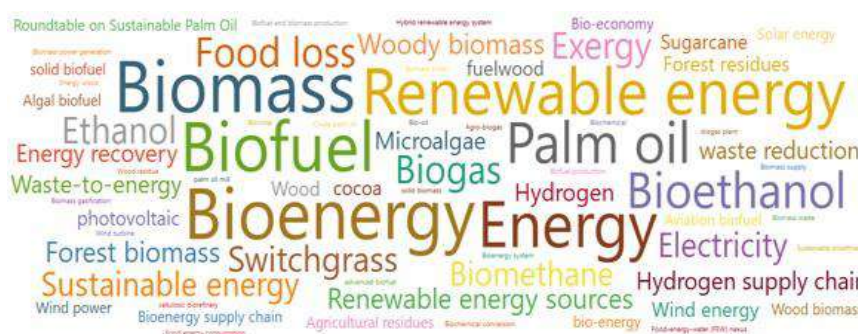


Fig. 7. Word cloud with the most frequently keywords in database (Source: VantagePoint and the authors).

Finally, a mapping with the 15 most cited works in the area is presented according to Table 4, which represents a total of approximately 2.74% of all works. Scientific publications were ordered by citation recurrence and categorized by author (year), objective of the work, source of energy, supply chain and which sustainable criteria were presented.

Table 4. Mapping of the most cited works in area (Source: The authors)

Author	Objective	Energy Source	Supply Chain	Sustainable Criteria
You et al. (2011) [32]	Design of cellulosic ethanol supply chain under sustainable criteria	Biomass (switchgrass and miscanthus)	Cellulosic ethanol supply chain	<ul style="list-style-type: none"> • Emissions of GHG • Job creation • Cost
Yue, You and Snyder (2014) [33]	Describes the key challenges and opportunities in optimization of biomass-to bioenergy supply chains	Biomass (algae) (agricultural/forest)	Biofuel/bioenergy supply chain	<ul style="list-style-type: none"> • Emissions of GHG • Emissions of CO₂ • Job creation • Cost
Gold and Seuring (2011) [34]	Literature review about bio-energy production	Biomass	Bio-energy supply chain	<ul style="list-style-type: none"> • Emissions of CO₂ • Transport Traffic congestion • Cost
Choudhary and Shankar (2012) [35]	STEER-fuzzy AHP-TOPSIS based framework for evaluation and selection of locations for TPPs	Coal	TPP supply chain**	<ul style="list-style-type: none"> • Environmental impact • Cost
Goodrich et al. (2013) [36]	Analysis of manufacturing costs for wafer-based monocrystalline PV module supply chain	PV	PV module supply chain	<ul style="list-style-type: none"> • Cost • Energy Efficiency
Ahmad and Tahar (2014) [37]	Review and selection of a RE source in Malaysia	Hydropower, Wind, PV, Biogas and Biomass	Energy generation supply chain	<ul style="list-style-type: none"> • Emissions of CO₂ • Environmental impact • Job creation • Public acceptance • Cost
Mccormick and Kaberger (2007) [38]	Analysis, and discussion of barriers for bioenergy in the EU	Biomass and Biogas	Bioenergy supply chain	<ul style="list-style-type: none"> • Emissions of GHG • Job creation • Cost
Scott et al (2012) [39]	Review of problems in bioenergy sector using MCDM	Biomass, PV Wind, Hydrogen	Biomass/Biofuel Supply Chain	<ul style="list-style-type: none"> • Emissions of GHG • Emissions of CO₂ • Environmental impact • Job creation • Public acceptance • Cost
Zangh et al (2013) [40]	Mathematical model to determine the optimal supply chain/logistics decisions of SBSC	Biomass (Switchgrass)	Bioethanol Supply Chain	<ul style="list-style-type: none"> • Energy consumption • Cost
Cucchiella and D'Adamo (2013) [41]	Literature review of supply chain and RE	Biomass, hydrogen, PV and Wind power.	RE supply chain/supply chain management	<ul style="list-style-type: none"> • Emissions of GHG • Job creation

				Cost
Corsano et al. (2011) [42]	MINLP optimization model for a sustainable design and behavior analysis of sugar/ethanol supply chain (SC).	Biomass (Sugarcane)	Sugar/ethanol supply chain	<ul style="list-style-type: none"> • Cost • Environmental impact
Cucchiella et al. (2015) [43]	Environmental and economic analysis of building integrated photovoltaic systems in Italian regions	PV	PV supply chain**	<ul style="list-style-type: none"> • Emissions of CO₂ • Energy Efficiency • Energy consumption • Cost
Stokes et al. (2011) [44]	Quantifying the life-cycle energy consumption and associated air emissions from water supply, treatment, and distribution	Natural Gas	Water distribution and treatment supply chain	<ul style="list-style-type: none"> • Emissions of CO₂ • Emissions of GHG • Energy consumption
Chiaroni et al. (2014) [45]	Debate concerning self-consumption to support the economic sustainability of photovoltaic facilities	PV	PV supply chain	<ul style="list-style-type: none"> • Cost • Energy Efficiency
Khan et al. (2018) [46]	Examine the relationship between green logistics operations and energy demand, economic growth and environmental sustainability for 43 countries	Biomass	Industrial/biofuel supply chain management	<ul style="list-style-type: none"> • Emissions of CO₂ • Emissions of GHG • Cost

*TPP – Thermal Power Plant, PV – Photovoltaic, RE – Renewable Energy, EU – Europe Union, MCDM – Multi-Criteria Decision-Making, SBSC – switchgrass-based bioethanol supply chain.

** Supply chains not explicit by the authors

Most of the authors found in the database as the main ones listed of the most cited, being them, You, Lam, Yue, Zangh, Cucchiella, D'Adamo and Khan. Moreover, biomass and photovoltaic was the most recurrent source energy, cost and emissions of CO₂ and GHG was sustainable criteria more recurrent and biofuel and bioenergy was supply chain most recurrent.

4 Conclusion

This paper showed that the renewable energies theme in supply chain still young, being started to have grown from 2010, which can be noted in the most cited works (where only one is before 2010). Furthermore, it was seen that a lot of countries and institutions of all words is searching solutions to implement renewable energies in supply chain, justified by the global map of publications, where only a small portion of the Middle East and some countries on the African continent did not respond. Another important conclusion is to see how the different industrial sectors have implemented

research in this area, which includes sector ranging from the pharmaceutical to food for example. Inside the area, the themes that presented high research were related to biomass, biofuels, and bioenergy, followed by photovoltaic, wind energy and biogas, however, many studies involved other areas was founded in database such as thermal, cogeneration, hybrid system, but not presenting the same recurrence as the main. Regarding the observed sustainable criteria, much is looked at the cost and GHG emissions, however, the social factors were the least pointed out. This study demonstrated the effectiveness of the VantagePoint for the presentation of results from the database, in addition, as limitations of this research, we have the low number of mapped articles (about 2.74% of the entire database) and not considering studies from the database from 2020 (considering that it is the current year). As a suggestion for futures works, a greater analysis of scientific articles could more clearly validate the information taken from the database, in addition to a more critical assessment for the social and environmental scenarios.

Acknowledgment

The authors would like to thank CNPq by the scholarship awarded, IFRJ for the availability of VantagePoint software and the project “Ciudades Inteligentes, totalmente integrales, eficiente y sostenibles (CITIES), n. de processo: 518RT0557”.

References

- [1] J. Y. Ding, S. Song, and C. Wu, “Carbon-efficient scheduling of flow shops by multi-objective optimization,” *Eur. J. Oper. Res.*, vol. 248, no. 3, pp. 758–771, 2016.
- [2] E. Mastrocinque, F. J. Ramírez, A. Honrubia-Escribano, and D. T. Pham, “An AHP-based multi-criteria model for sustainable supply chain development in the renewable energy sector,” *Expert Syst. Appl.*, vol. 150, p. 113321, 2020.
- [3] S. E. Hosseini, “An outlook on the global development of renewable and sustainable energy at the time of COVID-19,” *Energy Res. Soc. Sci.*, vol. 68, no. April, p. 101633, 2020.
- [4] E. Huang *et al.*, “Multi-objective optimization for sustainable renewable jet fuel production: A case study of corn stover based supply chain system in Midwestern U.S.,” *Renew. Sustain. Energy Rev.*, vol. 115, no. March, p. 109403, 2019.
- [5] C. J. C. Jabbour, A. B. L. de S. Jabbour, J. Sarkis, and M. G. Filho, “Unlocking the circular economy through new business models based on large-scale data: An integrative framework and research agenda,” *Technol. Forecast. Soc. Change*, vol. 144, no. June, pp. 546–552, 2019.
- [6] K. Fang, N. Uhan, F. Zhao, and J. W. Sutherland, “A new approach to scheduling in manufacturing for power consumption and carbon footprint reduction,” *J. Manuf. Syst.*, vol. 30, no. 4, pp. 234–240, 2011.

- [7] J. Maroušek, S. Hašková, R. Zeman, J. Váchal, and R. Vaníčková, “Assessing the implications of EU subsidy policy on renewable energy in Czech Republic,” *Clean Technol. Environ. Policy*, vol. 17, no. 2, pp. 549–554, 2015.
- [8] A. Kuriqi, A. N. Pinheiro, A. Sordo-Ward, and L. Garrote, “Influence of hydrologically based environmental flow methods on flow alteration and energy production in a run-of-river hydropower plant,” *J. Clean. Prod.*, vol. 232, pp. 1028–1042, 2019.
- [9] L. Hernández-Callejo, S. Gallardo-Saavedra, and V. Alonso-Gómez, “A review of photovoltaic systems: Design, operation and maintenance,” *Sol. Energy*, vol. 188, no. March, pp. 426–440, 2019.
- [10] J. G. F. Madeira, R. A. M. Boloy, A. R. S. Delgado, F. R. Lima, E. R. Coutinho, and R. de C. Pereira Filho, “Ecological analysis of hydrogen production via biogas steam reforming from cassava flour processing wastewater,” *J. Clean. Prod.*, vol. 162, pp. 709–716, 2017.
- [11] S. Deep, A. Sarkar, M. Ghawat, and M. K. Rajak, “Estimation of the wind energy potential for coastal locations in India using the Weibull model,” *Renew. Energy*, vol. 161, pp. 319–339, 2020.
- [12] Y. A. de Oliveira Chaves, M. Val Springer, R. A. M. Boloy, O. M. de Castro Ferreira Soares, and J. G. F. Madeira, “Performance Study of a Microturbine System for Cogeneration Application Using Biogas from Manipueira,” *Bioenergy Res.*, vol. 13, no. 2, pp. 659–667, 2020.
- [13] P. E. Escamilla-García, R. H. Camarillo-López, R. Carrasco-Hernández, E. Fernández-Rodríguez, and J. M. Legal-Hernández, “Technical and economic analysis of energy generation from waste incineration in Mexico,” *Energy Strateg. Rev.*, vol. 31, 2020.
- [14] L. Samylingam *et al.*, “Thermal and energy performance improvement of hybrid PV/T system by using olein palm oil with MXene as a new class of heat transfer fluid,” *Sol. Energy Mater. Sol. Cells*, vol. 218, no. January, p. 110754, 2020.
- [15] B. Koçak, A. I. Fernandez, and H. Paksoy, “Review on sensible thermal energy storage for industrial solar applications and sustainability aspects,” *Sol. Energy*, vol. 209, no. September, pp. 135–169, 2020.
- [16] Eurostat, “Estatísticas das Energias Renováveis,” 2020. [Online]. Available: https://ec.europa.eu/eurostat/statistics-explained/index.php?title=Renewable_energy_statistics/pt. [Accessed: 17-Sep-2020].
- [17] Ministério de Minas e Energia, “Fontes renováveis sobem 0,6 ponto percentual na Matriz Energética,” 2020. [Online]. Available: http://www.mme.gov.br/todas-as-noticias/-/asset_publisher/pdAS9IcdBICN/content/fontes-renovaveis-sobem-0-6-ponto-percentual-na-matriz-energetica. [Accessed: 24-Sep-2020].
- [18] A. Alper and O. Oguz, “The role of renewable energy consumption in economic growth: Evidence from asymmetric causality,” *Renew. Sustain. Energy Rev.*, vol. 60, pp. 953–959, 2016.
- [19] Q. Wang and L. Zhan, “Assessing the sustainability of renewable energy: An

- empirical analysis of selected 18 European countries,” *Sci. Total Environ.*, vol. 692, pp. 529–545, 2019.
- [20] E. Marques and V. Guimarães, “The Influence of Facility Location on the Sustainability of Smart Cities: Current Literature Analysis,” in *In Efficient, Sustainable, and Fully Comprehensive Smart Cities: II Ibero-American Congress of Smart Cities (ICSC-CITIES 2019)*, L. Hernández Callejo and C. Liliana Zuñiga Cañón, Eds. Soria: Universidad Santiago de Cali, 2020, 2020, p. 889.
- [21] F. L. E. Viana, J. de P. Barros Neto, and M. E. M. Añez, “Gestão da cadeia de suprimento e vantagem competitiva relacional nas indústrias têxtil e de calçados,” *Gestão & Produção*, vol. 21, no. 4, pp. 836–852, 2014.
- [22] A. Kahan, “EIA projects nearly 50% increase in world energy usage by 2050, led by growth in Asia,” 2019. [Online]. Available: <https://www.eia.gov/todayinenergy/detail.php?id=41433>. [Accessed: 31-Aug-2020].
- [23] C. Gahm, F. Denz, M. Dirr, and A. Tuma, “Energy-efficient scheduling in manufacturing companies: A review and research framework,” *Eur. J. Oper. Res.*, vol. 248, no. 3, pp. 744–757, 2016.
- [24] R. Z. Farahani, M. SteadieSeifi, and N. Asgari, “Multiple criteria facility location problems: A survey,” *Appl. Math. Model.*, vol. 34, no. 7, pp. 1689–1709, 2010.
- [25] A. B. Arabani and R. Z. Farahani, “Facility location dynamics: An overview of classifications and applications,” *Comput. Ind. Eng.*, vol. 62, no. 1, pp. 408–420, 2012.
- [26] S. Luthra, K. Govindan, D. Kannan, S. K. Mangla, and C. P. Garg, “An integrated framework for sustainable supplier selection and evaluation in supply chains,” *J. Clean. Prod.*, vol. 140, pp. 1686–1698, 2017.
- [27] S. A. Yawar and S. Seuring, “Management of Social Issues in Supply Chains: A Literature Review Exploring Social Issues, Actions and Performance Outcomes,” *J. Bus. Ethics*, vol. 141, no. 3, pp. 621–643, 2017.
- [28] D. R. Krause, S. Vachon, and R. D. Klassen, “Special topic forum on sustainable supply chain management: introduction and reflections on the role of purchasing management,” *J. Supply Chain Manag.*, vol. 45, no. 4, pp. 18–25, 2009.
- [29] C. R. Carter and D. S. Rogers, “A framework of sustainable supply chain management: moving toward new theory,” *Int. J. Phys. Distrib. Logist. Manag.*, 2008.
- [30] R. Drake, M. B. Yildirim, J. Twomey, L. Whitman, J. Ahmad, and P. Lodhia, “Data collection framework on energy consumption in manufacturing,” *2006 IIE Annu. Conf. Exhib.*, 2006.
- [31] X. Chen, “The declining value of subscription-based abstracting and indexing services in the new knowledge dissemination era,” *Ser. Rev.*, vol. 36, no. 2, pp. 79–85, 2010.
- [32] F. You, L. Tao, D. J. Graziano, and S. W. Snyder, “Optimal design of sustainable cellulosic biofuel supply chains: multiobjective optimization

- coupled with life cycle assessment and input–output analysis,” *AIChE J.*, vol. 58, no. 4, pp. 1157–1180, 2012.
- [33] D. Yue, F. You, and S. W. Snyder, “Biomass-to-bioenergy and biofuel supply chain optimization: Overview, key issues and challenges,” *Comput. Chem. Eng.*, vol. 66, pp. 36–56, 2014.
- [34] S. Gold and S. Seuring, “Supply chain and logistics issues of bio-energy production,” *J. Clean. Prod.*, vol. 19, no. 1, pp. 32–42, 2011.
- [35] D. Choudhary and R. Shankar, “An STEEP-fuzzy AHP-TOPSIS framework for evaluation and selection of thermal power plant location: A case study from India,” *Energy*, vol. 42, no. 1, pp. 510–521, 2012.
- [36] A. Goodrich *et al.*, “A wafer-based monocrystalline silicon photovoltaics road map: Utilizing known technology improvement opportunities for further reductions in manufacturing costs,” *Sol. Energy Mater. Sol. Cells*, vol. 114, pp. 110–135, 2013.
- [37] S. Ahmad and R. M. Tahar, “Selection of renewable energy sources for sustainable development of electricity generation system using analytic hierarchy process: A case of Malaysia,” *Renew. Energy*, vol. 63, pp. 458–466, 2014.
- [38] K. McCormick and T. Käberger, “Key barriers for bioenergy in Europe: Economic conditions, know-how and institutional capacity, and supply chain co-ordination,” *Biomass and Bioenergy*, vol. 31, no. 7, pp. 443–452, 2007.
- [39] J. A. Scott, W. Ho, and P. K. Dey, “A review of multi-criteria decision-making methods for bioenergy systems,” *Energy*, vol. 42, no. 1, pp. 146–156, 2012.
- [40] J. Zhang, A. Osmani, I. Awudu, and V. Gonela, “An integrated optimization model for switchgrass-based bioethanol supply chain,” *Appl. Energy*, vol. 102, pp. 1205–1217, 2013.
- [41] F. Cucchiella and I. D’Adamo, “Issue on supply chain of renewable energy,” *Energy Convers. Manag.*, vol. 76, pp. 774–780, 2013.
- [42] G. Corsano, A. R. Vecchiotti, and J. M. Montagna, “Optimal design for sustainable bioethanol supply chain considering detailed plant performance model,” *Comput. Chem. Eng.*, vol. 35, no. 8, pp. 1384–1398, 2011.
- [43] F. Cucchiella, I. D’Adamo, and S. C. Lenny Koh, “Environmental and economic analysis of building integrated photovoltaic systems in Italian regions,” *J. Clean. Prod.*, vol. 98, pp. 241–252, 2015.
- [44] J. R. Stokes and A. Horvath, “Sustainability of Natural Hazard Risk Mitigation: Life Cycle Analysis of Environmental Indicators for Bridge Infrastructure,” *J. Infrastruct. Syst.*, vol. 17, no. December, pp. 395–408, 2013.
- [45] D. Chiaroni, V. Chiesa, L. Colasanti, F. Cucchiella, I. D’Adamo, and F. Frattini, “Evaluating solar energy profitability: A focus on the role of self-consumption,” *Energy Convers. Manag.*, vol. 88, pp. 317–331, 2014.
- [46] S. A. Rehman Khan, Y. Zhang, M. Anees, H. Golpîra, A. Lahmar, and D. Qianli, “Green supply chain management, economic growth and environment: A GMM based evidence,” *J. Clean. Prod.*, vol. 185, pp. 588–599, 2018.